

THE SCIENCE AND TECHNOLOGY OF INDUSTRIAL WATER TREATMENT

Edited by
ZAHID AMJAD

IWA
Publishing
London • New York



CRC Press
Taylor & Francis Group

**THE SCIENCE
AND TECHNOLOGY
OF INDUSTRIAL
WATER TREATMENT**

THE SCIENCE AND TECHNOLOGY OF INDUSTRIAL WATER TREATMENT

**Edited by
ZAHID AMJAD**



Publishing
London • New York



CRC Press

Taylor & Francis Group

Boca Raton London New York

CRC Press is an imprint of the
Taylor & Francis Group, an **informa** business

Co-published by IWA Publishing, Alliance House, 12 Caxton Street, London SW1H 0QS, UK
Tel. +44 (0) 20 7654 5500, Fax +44 (0) 20 7654 5555
publications@iwap.co.uk
www.iwapublishing.com
ISBN 1843393115
ISBN13 9781843393115

MATLAB® is a trademark of The MathWorks, Inc. and is used with permission. The MathWorks does not warrant the accuracy of the text or exercises in this book. This book's use or discussion of MATLAB® software or related products does not constitute endorsement or sponsorship by The MathWorks of a particular pedagogical approach or particular use of the MATLAB® software.

CRC Press
Taylor & Francis Group
6000 Broken Sound Parkway NW, Suite 300
Boca Raton, FL 33487-2742

© 2010 by Taylor and Francis Group, LLC
CRC Press is an imprint of Taylor & Francis Group, an Informa business

No claim to original U.S. Government works

Printed in the United States of America on acid-free paper
10 9 8 7 6 5 4 3 2 1

International Standard Book Number-13: 978-1-4200-7145-0 (Ebook-PDF)

This book contains information obtained from authentic and highly regarded sources. Reasonable efforts have been made to publish reliable data and information, but the author and publisher cannot assume responsibility for the validity of all materials or the consequences of their use. The authors and publishers have attempted to trace the copyright holders of all material reproduced in this publication and apologize to copyright holders if permission to publish in this form has not been obtained. If any copyright material has not been acknowledged please write and let us know so we may rectify in any future reprint.

Except as permitted under U.S. Copyright Law, no part of this book may be reprinted, reproduced, transmitted, or utilized in any form by any electronic, mechanical, or other means, now known or hereafter invented, including photocopying, microfilming, and recording, or in any information storage or retrieval system, without written permission from the publishers.

For permission to photocopy or use material electronically from this work, please access www.copyright.com (<http://www.copyright.com/>) or contact the Copyright Clearance Center, Inc. (CCC), 222 Rosewood Drive, Danvers, MA 01923, 978-750-8400. CCC is a not-for-profit organization that provides licenses and registration for a variety of users. For organizations that have been granted a photocopy license by the CCC, a separate system of payment has been arranged.

Trademark Notice: Product or corporate names may be trademarks or registered trademarks, and are used only for identification and explanation without intent to infringe.

Visit the Taylor & Francis Web site at
<http://www.taylorandfrancis.com>

and the CRC Press Web site at
<http://www.crcpress.com>

Contents

Preface.....	ix
Editor	xi
Contributors	xiii
Chapter 1 Mineral Scales and Deposits: An Overview	1
<i>Zahid Amjad and Peter G. Koutsoukos</i>	
Chapter 2 Crystal Growth Inhibition of Calcium Sulfate and Calcium Oxalates in Aqueous Systems	21
<i>Mualla Oner</i>	
Chapter 3 Calcium Carbonate Scale Control in Industrial Water Systems	39
<i>Peter G. Koutsoukos</i>	
Chapter 4 Calcium Carbonate: Polymorph Stabilization in the Presence of Inhibitors	61
<i>Peter G. Koutsoukos and Tao Chen</i>	
Chapter 5 Scale and Deposit Control Polymers for Industrial Water Treatment.....	81
<i>Robert W. Zuhl and Zahid Amjad</i>	
Chapter 6 New Models for Calcium Phosphate Scale Formation and Dissolution	105
<i>Lijun Wang, Patrick P. Emmerling, Zachary J. Henneman, and George H. Nancollas</i>	
Chapter 7 Design and Applications of Cooling Water Treatment Programs.....	113
<i>Libardo A. Perez, Gary E. Geiger, and Charles R. Ascolese</i>	
Chapter 8 Latest Developments in Oilfield Scale Control	129
<i>Mingdong Yuan</i>	
Chapter 9 Control of Silica Scaling in Geothermal Systems Using Silica Inhibitors, Chemical Treatment, and Process Engineering	155
<i>Darrell L. Gallup and Paul N. Hirtz</i>	
Chapter 10 Recent Developments in Controlling Silica and Magnesium Silicate Foulants in Industrial Water Systems	179
<i>Konstantinos D. Demadis</i>	

Chapter 11	Phosphate Containing Scale Formation in Wastewater	205
	<i>Peter G. Koutsoukos and Aikaterini N. Kofina</i>	
Chapter 12	New Developments in Membrane-Based Processes for Industrial Applications.....	227
	<i>Peter S. Cartwright</i>	
Chapter 13	Reverse Osmosis Membrane Fouling Control	247
	<i>Jane Kucera</i>	
Chapter 14	Scale Formation and Control in Thermal Desalination Systems.....	271
	<i>Faizur Rahman and Zahid Amjad</i>	
Chapter 15	Boiler Water Treatment	297
	<i>Bruce T. Ketrick, Sr.</i>	
Chapter 16	Corrosion Control in Industrial Water Systems	319
	<i>Mel J. Esmacher</i>	
Chapter 17	Interactions of Polyelectrolytes with Particulate Matter in Aqueous Systems	343
	<i>P. Somasundaran and Venkataramana Runkana</i>	
Chapter 18	Mechanistic Aspects of Heat Exchanger and Membrane Biofouling and Prevention.....	365
	<i>Luis F. Melo and Hans-Curt Flemming</i>	
Chapter 19	Biocides: Selection and Application.....	381
	<i>Christopher J. Nalepa and Terry M. Williams</i>	
Chapter 20	<i>Legionella</i> in Water Systems.....	411
	<i>Yusen E. Lin</i>	
Chapter 21	Analytical Techniques for Identifying Mineral Scales and Deposits	425
	<i>Valerie P. Woodward, Robert C. Williams, and Zahid Amjad</i>	
Chapter 22	Deposit Control Polymers: Types, Characterization, and Applications.....	447
	<i>Zahid Amjad, Robert W. Zuhl, and Strong Huang</i>	

Contents	vii
Chapter 23 Applications of Cationic Polymers in Water Treatment.....	465
<i>Logan A. Jackson</i>	
Chapter 24 Recent Development in Water Treatment Chemicals Monitoring	481
<i>Vadim Malkov and Phil Kiser</i>	
Index	505

Preface

The use of natural hard waters in industrial water systems (e.g., cooling, boilers, desalination, oil production, etc.) can cause severe scaling and corrosion of equipment surfaces, and pose serious technical and economic challenges. The scales commonly encountered are sulfates, carbonates, and phosphates of calcium, magnesium, and barium. The precipitation and deposition of scales on equipment surfaces are influenced by various factors, including feed and recirculating water chemistry, pH, temperature, flow velocity, heat exchanger metallurgy, and the types of additives used in the water treatment formulation. Such scale deposits significantly reduce heat transfer efficiency, constrict flow, increase the operating pressure of pumps, and enhance the probability of corrosion damage. In many cases, the removal of deposits leads to the discontinuous operation of the system, resulting in higher operating costs.

The crystallization of sparingly soluble salts is also of primary importance in biological systems. Tartar, or dental calculus, primarily consists of salts of calcium, phosphate, and carbonate. Calcium oxalates are the main components of pathological deposits in the urinary tract. Calcium phosphate deposits have been observed during the pasteurization of milk. Interestingly, calcium oxalates are common deposits in the brewing industry. Thus, the physicochemical processes (adsorption, desorption, precipitation, dissolution, inhibition, adhesion, kinetics, etc.) involved in water treatment applications are similar to those encountered in other industries.

Investigators have proposed several options for controlling scale formation including the use of acids, chelants, or the addition of scale inhibitors and dispersants. The most promising method is the addition of water-soluble additives at very low concentrations such as few parts per million (ppm). Additives commonly used for scale control include phosphonates and homo- and copolymers of acrylic and maleic acids. Mineral scale deposits are not the only challenges that adversely affect the operation of industrial water systems. Corrosion, suspended matter, and microbiological growth are equally important factors that have to be controlled along with scale formation. The deposition of suspended matter is typically controlled by the incorporation of a dispersant in the treatment formulation. To prevent the formation of biofilms and to achieve optimum system efficiency, microbiological growth within the water system must be controlled. Generally, biofilm formation is controlled by the addition of biocides, biostats, and biodispersants to the water system.

Research on understanding the mechanisms of scale formation, corrosion, and biofilm has attracted considerable attention in the past three decades. Additionally, significant progress has been made not only in developing new water treatment additives but also in the application of these additives under stressed operating conditions, online monitoring of chemicals used, and system parameters. During this period, numerous papers have been published in professional journals and trade magazines, thousands of patents have been granted, and a large number of new additives have been introduced in the water treatment market.

This book is designed to provide a comprehensive discussion on both the fundamental and practical aspects of industrial water treatment. The authors were selected from academia and industries because they are specialists in their particular fields, possessing fundamental and practical experience, and are able to analyze recent results and relate them to their respective areas of expertise. New information, as well as review of current concepts, generally highlights the individual contributions.

The book starts with an overview (Chapter 1) of water chemistry and covers the characteristics of commonly encountered mineral scales. Chapters 2 through 11 address both the formation and the control of different scales in various systems including cooling, geothermal, oil field, and wastewater systems. Chapters 12 through 14 cover new developments in membrane-based separation

processes followed by a detailed account on the operational challenges of reverse osmosis systems and scale control in thermal distillation processes. Chapters 15 and 16 present corrosion control in cooling, boiler, geothermal, and desalination systems. Chapter 17 discusses interactions of polyelectrolytes with suspended matter.

Microbiological fouling is a frequent cause of performance deterioration in both cooling and membrane-based systems and is poorly understood. Chapters 18 and 19 present a comprehensive discussion of bacterial species commonly encountered in water supplies, the mechanisms of biofouling, approaches to control biofouling, and criteria for selecting biocides for water treatment applications. Chapter 20 deals with *Legionella* in water systems. Chapter 21 describes the various analytical techniques for identifying mineral scales and deposits. Chapters 22 and 23 deal with applications of polymers for treating industrial and wastewater systems. Finally, Chapter 24 gives an account on analytical approaches to monitor various operational parameters and chemicals used to treat industrial water systems.

Considering the general interest in the science and technology of industrial water treatment, this book is intended for academic researchers in the fields of biology, chemistry, dentistry, geology, chemical engineering, environmental engineering, and medicine. It will also be useful for technology-focused researchers in the industry whose interests might be directly or indirectly related to different types of mineral scales.

It is hoped that this handy reference will prove to be a valuable addition to the library of academic researchers. It should also prove useful to scientists, technologists, process and design engineers, operations personnel, and plant managers working in the water treatment industry, and to researchers in other industries including petroleum, textile processing, high-purity water production, semiconductor, food and beverage production, pharmaceutical, and industrial effluent cleaning.

I thank the editorial staff at Taylor & Francis for their patience and invaluable help. I also acknowledge the support of my colleagues and management at Lubrizol Advanced Materials, Inc., Cleveland, Ohio. Special thanks also go to all the contributors of this book not only for sharing their extensive expertise but also for patiently enduring the unavoidable delays of a multiauthored book. Finally, I want to thank my wife, Rukhsana, who has contributed to the completion of this book in more ways than I can mention.

MATLAB® is a registered trademark of The MathWorks, Inc. For product information, please contact:

The MathWorks, Inc.
3 Apple Hill Drive
Natick, MA 01760-2098 USA
Tel: 508 647 7000
Fax: 508-647-7001
E-mail: info@mathworks.com
Web: www.mathworks.com

Zahid Amjad

Editor

Zahid Amjad received his MSc in chemistry from Punjab University, Lahore, Pakistan, and his PhD in chemistry from Glasgow University, Glasgow, Scotland. Dr. Amjad was a lecturer at the Institute of Chemistry, Punjab University, and an assistant research professor at the State University of New York at Buffalo. He began his professional career as an R&D scientist. During his more than 30 years at Calgon Corporation, Pittsburgh, Pennsylvania, and Lubrizol Advanced Materials, Inc., Cleveland, Ohio, he has worked in various fields including cosmetics, home care, oral care, pharmaceutical, water treatment, and related areas. His areas of research include the development and application of water-soluble/swellable polymers, inhibition of mineral scale formation, water purification, and interactions of polymers with different substrates (i.e., heat exchanger, membrane, tooth enamel, hair, fabric, pigments). He has published over 140 technical papers, holds 30 patents, and has edited 5 books. He was inducted into the National Hall of Corporate Inventors and is listed in *American Men and Women of Sciences*, *Who's Who in Technology*, and *Who's Who of American Inventors*. Dr. Amjad was the 2002 recipient of the Association of Water Technologies' Ray Baum Memorial Water Technologist of the Year award. He is currently a technical consultant to Lubrizol Advanced Materials, Inc., Cleveland, Ohio, and the owner of Aqua Science and Technology LLC, Columbus, Ohio, which provides consulting services for industrial water treatment, separation processes, and related technologies.

Contributors

Zahid Amjad

Lubrizol Advanced Materials, Inc.
Cleveland, Ohio

Charles R. Ascolese

GE Water & Process Technologies
Trevose, Pennsylvania

Peter S. Cartwright

Cartwright Consulting Company
Minneapolis, Minnesota

Tao Chen

Champion Technologies Ltd
Aberdeen, United Kingdom

Konstantinos D. Demadis

Crystal Engineering, Growth
and Design Laboratory
Department of Chemistry
University of Crete
Heraklion, Greece

Patrick P. Emmerling

Department of Chemistry
University at Buffalo
Buffalo, New York

Mel J. Esmacher

GE Water & Process Technologies
The Woodlands, Texas

Hans-Curt Flemming

Faculty of Chemistry
Biofilm Centre
University of Duisburg-Essen
Duisburg, Germany

Darrell L. Gallup

Chevron Energy Technology Company
Oilfield Chemistry and Field
Applications
Houston, Texas

Gary E. Geiger

GE Water & Process Technologies
Trevose, Pennsylvania

Zachary J. Henneman

Department of Chemistry
University at Buffalo
Buffalo, New York

Paul N. Hirtz

Thermochem, Inc.
Santa Rosa, California

Strong Huang

Lubrizol Advanced Materials, Inc.
Cleveland, Ohio

Logan A. Jackson

Kemira Chemicals, Inc.
Atlanta, Georgia

Bruce T. Ketrick, Sr.

Guardian CSC
York, Pennsylvania

Phil Kiser

Hach Company
Loveland, Colorado

Aikaterini N. Kofina

Department of Chemical Engineering
and FORTH-ICEHT
University of Patras
Patras, Greece

Peter G. Koutsoukos

Department of Chemical Engineering
and FORTH-ICEHT
University of Patras
Patras, Greece

Jane Kucera

Nalco Company
Naperville, Illinois

Yusen E. Lin

Center for Environmental Laboratory Services
Graduate Institute of Environmental Education
National Kaohsiung Normal University
Kaohsiung, Taiwan

Vadim Malkov

Process Instruments Business
Unit
Hach Company
Loveland, Colorado

Luis F. Melo

Laboratory for Process, Environmental
and Energy Engineering
Department of Chemical Engineering
Faculty of the University of Porto
University of Porto
Porto, Portugal

Christopher J. Nalepa

Albemarle Corporation
Baton Rouge, Louisiana

George H. Nancollas

Department of Chemistry
University at Buffalo
Buffalo, New York

Mualla Oner

Department of Chemical Engineering
Yildiz Technical University
Istanbul, Turkey

Libardo A. Perez

GE Water & Process Technologies
The Woodlands, Texas

Faizur Rahman

Research Institute
King Fahd University of Petroleum
and Minerals
Dhahran, Saudi Arabia

Venkataramana Runkana

Tata Consultancy Services
Pune, Maharashtra, India

P. Somasundaran

National Science Foundation Industry/
University Cooperative Research Center
for Advanced Studies in Novel Surfactants
School of Engineering and Applied Science
Columbia University
New York, New York

Lijun Wang

Department of Chemistry
University at Buffalo
Buffalo, New York

Robert C. Williams

Lubrizol Advanced Materials, Inc.
Cleveland, Ohio

Terry M. Williams

Rohm and Hass Company
Philadelphia, Pennsylvania

Valerie P. Woodward

Lubrizol Advanced Materials, Inc.
Cleveland, Ohio

Mingdong Yuan

Baker Hughes, Inc.
Baker Petrolite
Sugar Land, Texas

Robert W. Zuhl

Lubrizol Advanced Materials, Inc.
Cleveland, Ohio

1 Mineral Scales and Deposits: An Overview

Zahid Amjad and Peter G. Koutsoukos

CONTENTS

1.1	Introduction	2
1.2	Water Cycle.....	2
1.3	Water Sources	3
1.3.1	Seawater.....	3
1.3.2	Lake Water.....	4
1.3.3	Surface Water	4
1.3.4	Subsurface Water	4
1.4	Water Chemistry.....	5
1.4.1	Physical Characteristics.....	5
1.4.1.1	Color	5
1.4.1.2	Detergency.....	5
1.4.1.3	Odor.....	5
1.4.1.4	Temperature.....	5
1.4.1.5	Turbidity	5
1.4.2	Chemical Characteristics.....	6
1.4.2.1	Aluminum.....	6
1.4.2.2	Barium	6
1.4.2.3	Calcium.....	7
1.4.2.4	Copper	7
1.4.2.5	Chromium.....	7
1.4.2.6	Iron	7
1.4.2.7	Magnesium	7
1.4.2.8	Manganese.....	7
1.4.2.9	Sodium.....	7
1.4.2.10	Potassium.....	7
1.4.2.11	Silica	7
1.4.2.12	Selenium	8
1.4.2.13	Strontium	8
1.4.2.14	Zinc.....	8
1.4.2.15	Bicarbonate.....	8
1.4.2.16	Carbonate.....	8
1.4.2.17	Chloride	8
1.4.2.18	Fluoride.....	8
1.4.2.19	Sulfate.....	8
1.4.2.20	Carbon Dioxide	9
1.4.2.21	Hydrogen Sulfide.....	9
1.4.2.22	Oxygen.....	9
1.4.2.23	Organic Chemicals.....	9

1.5	Importance of Feed Water Analysis for Industrial Systems.....	9
1.6	Mineral Scales and Deposits	10
1.6.1	Scaling	10
1.6.1.1	Calcium Carbonate Deposits	11
1.6.1.2	Metal Sulfate Scale Deposits	11
1.6.1.3	Calcium Phosphate Scale Deposits.....	13
1.6.1.4	Calcium Fluorides.....	14
1.6.1.5	Calcium Oxalates.....	14
1.6.1.6	Silica/Metal Silicates	14
1.6.1.7	Iron-Based Scales	16
1.6.2	Biofouling	17
1.6.3	Colloidal Fouling	17
1.6.4	Corrosion-Related Fouling	17
1.7	Summary	18
	References.....	18

1.1 INTRODUCTION

Water is the wellspring of life. It is the most important liquid in the world for maintaining plant and animal life. It fills lakes, streams, and vast oceans, and flows under the ground. The distribution of water on earth is 97.23% in the oceans, 2.14% in ice caps and glaciers, 0.61% in groundwater, 0.01% in freshwater lakes, and 0.01% in various other formations. Most of the freshwater is frozen at the North and South Poles and about a third of the freshwater is in aquifers, rivers, streams, and springs. It has been reported that 99% of all water (oceans, seas, ice, most saline water, and atmospheric water) is not available for our uses. And even much of the remaining fraction of 1% is out of reach. On the basis of the total water available, it is estimated that surface water sources (such as rivers) constitute only about 0.0067% of the total water, yet rivers are the source of most of the water that people use.

Pure water (H_2O) is colorless, odorless, and tasteless. It is composed of hydrogen and oxygen. Because water becomes contaminated by the substances with which it comes into contact, it is not available for use in its pure state. To some degree, water can dissolve every naturally occurring substance on the earth. Because of this property, water has been termed as the “universal solvent.” Although beneficial to mankind, the solvency power of water can pose a major threat to industrial equipments. In virtually all domestic and industrial processes in which untreated water is heated, the fouling of equipment is the single-most serious problem encountered. The affected application areas include laundry, dairy, dishwashing, cooling, boilers, geothermal, power generation, semiconductor manufacturing, and many other production processes [1]. A significant operating cost factor of a reverse osmosis (RO) system is the membranes themselves, a factor often increased unnecessarily through fouling by deposits of unwanted materials on RO membrane surfaces [2]. A mineral scale is defined as a deposit of certain sparingly soluble salts, such as calcium carbonates, calcium phosphates, and calcium sulfates, from the process fluids after precipitation onto the tubing and other process surfaces. A deposit generally includes various foulants, i.e., corrosion products and microbiological, colloidal, or suspended matter. The fouling of heat exchangers and RO membranes is a complex phenomenon involving the deposition of several different, but related types of foulants. This chapter addresses the quality of feed water available for industrial applications and the impact of water chemistry on system performance. In addition, the causes and types of various mineral scales and deposits commonly encountered in industrial water systems are reviewed.

1.2 WATER CYCLE

The water cycle, also known as the hydrologic cycle, includes the processes of condensation, evaporation, precipitation, and transpiration. Due to the heat of the sun, water vaporizes (evaporates) from lakes, rivers, streams, reservoirs, and oceans into the atmosphere. Plants, too, are heated

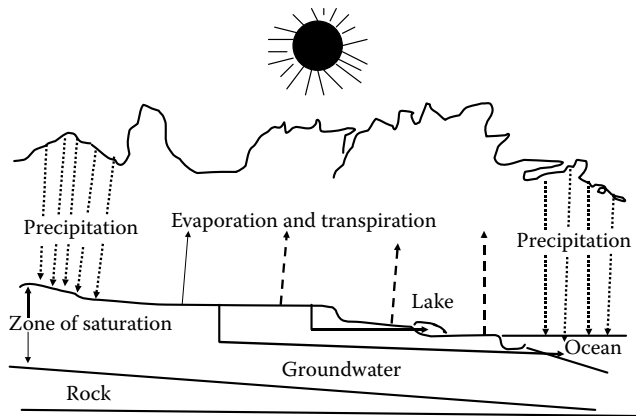


FIGURE 1.1 The water cycle.

by the sun, and release water molecules into the atmosphere through their leaves (transpiration). These water molecules form clouds. When millions of vapor particles unite, they form droplets of moisture. As these increase in size, they finally become heavy enough to fall to earth as precipitation in such varied forms as rain, snow, hail, and dew. This recycling of water—from surfaces to vapor to falling again—is the hydrologic cycle, and is shown pictorially in Figure 1.1. On passing from the liquid state to the vapor state, only water molecules leave the surface, leaving most impurities behind. However, when water returns to the earth as rain, it comes into contact with not only dust particles but also gases, including carbon dioxide, sulfur dioxide, and oxides of nitrogen. These gases when dissolved in water contribute to what is known as acid rain [3].

The precipitation that does not quickly evaporate either seeps deep into the soil or finds its way into lakes and rivers, and eventually flows into oceans. Various factors that contribute to the distribution of water after precipitation include surface topography, porosity of the soil, degrees of its saturation at the time of the rainfall, surface vegetation, and atmospheric conditions. Water's solvent action that permits it to have a cleansing action on the atmosphere continues after it reaches the earth. A certain percentage of precipitation generates a surface runoff. In this process, it acquires further amounts of hardness from minerals in addition to ample quantities of clay, silt, and decayed animal and vegetable matter. Further, when water percolates into the ground, it loses some of the impurities it absorbed from the air and the ground. But while the soil structure filters out certain impurities, it provides ample opportunities for water to dissolve large amounts of earth minerals. These, of course, increase the hardness and iron content of water, among other impurities.

1.3 WATER SOURCES

The sources of water that are potentially useful to humans fall into four categories, namely, oceans, lakes, surfaces, and subsurfaces. The water from these sources is used for agricultural, industrial, domestic, recreational, and environmental activities. A brief discussion of water sources is presented below.

1.3.1 SEAWATER

The solids in seawater come from two sources: the chemical weathering of rocks washed into the seas by the rivers and water circulation through hydrothermal vents (hot springs). The major dissolved constituents of seawater are the same as those encountered in natural waters. The average

salinity of seawater is 35%. The gases dissolved in seawater are in constant equilibrium with the atmosphere, but their relative concentrations depend on each gas' solubility, which also depends on salinity and temperature.

1.3.2 LAKE WATER

Lakes are a major source of freshwater. They are of particular importance in North America, especially in the Great Lakes region. The composition of lake water is generally affected by seasonal changes and sometimes daily due to variations in weather conditions. Although most of the dissolved mineral constituents may not be greatly affected by seasons and weather, various factors, such as dissolved oxygen, temperature, suspended solids, turbidity, and carbon dioxide, may be influenced by biological activity [3].

1.3.3 SURFACE WATER

Surface water is one of the most valuable natural resources. Contaminants in the surface water depend on the nature of the terrain over which it flows. In areas consisting of hard-packed clay, very little water penetrates the ground. In these cases, the water generates a runoff. Several factors can affect a surface runoff. The extent of runoff is a function of rock and soil types, climate, precipitation, saturation, vegetation, and time. A porous material (sand, gravel, and soluble rock) absorbs water far more readily than does fine-grained, dense clay, or unfractured rock. A poorly drained material (nonporous) has a higher runoff potential, resulting in greater drainage density. Rivers carry the dissolved ions they receive from ground and surface runoff to the sea. These dissolved ions include Na^+ , K^+ , Ca^{2+} , Mg^{2+} , HCO_3^- , CO_3^{2-} , PO_4^{3-} , and Cl^- . Total dissolved solids in rivers are about 100mg/L. Rivers also carry small particles of rock and minerals. Many surface water supplies also contain organic materials, which may occur naturally or as a result of human intervention. Tannins and lignins resulting from the decomposition of vegetation are colloidal suspensions and/or dissolved compounds present in surface water. The concentration of these compounds usually varies seasonally.

1.3.4 SUBSURFACE WATER

Subsurface water, or groundwater, is freshwater located in the pore space of soils and rocks. It is generally recognized that underground water usually moves very slowly. Its flow is measured in feet per year; compare this with surface streams, where velocities are in the feet-per-second range. Because of this slow movement, the composition of any one well is usually quite constant. Although shallow wells may vary seasonally in temperature, most wells are also constant in temperature, usually in the range of 50°F–60°F (10°C–16°C) [3]. Since the water has passed through miles of porous rock formations, it is invariably clear if the well has been properly developed to keep fine sand from entering the casing. Since the water chemistry is related to the composition of the geological formations through which the water has passed, water from wells drilled into different strata have different chemistries. Some aquifers are so large that they may cover several states in their total area, and wells drilled into such aquifers produce water of a similar composition. As water filters through the ground, soil organisms consume dissolved oxygen and produce carbon dioxide, one of the principal corrosive agents in dissolving the minerals from the geological structures [4]. It is common to find iron and manganese in waters that are devoid of oxygen if they have been in contact with iron-based minerals. Shallow wells containing oxygen are generally free of iron. It should be remembered that although the water chemistry of wells remains essentially constant, great care, however, should be exercised in mixing waters from different wells even in the same vicinity, as water chemistry may vary significantly and cause incompatibility issues.

1.4 WATER CHEMISTRY

Water, being a universal solvent, normally contains many impurities that it picks up from its surroundings. These impurities can be classified into five broad categories:

1. Dissolved inorganic compounds, such as bicarbonates, carbonates, sulfates, and fluorides of calcium, magnesium, barium, and strontium, and small amounts of iron, manganese, aluminum, and other substances.
2. Dissolved organic compounds, such as humic acid, fulvic acid, and tannins; insoluble organic matter, such as leaves, dead bacteria, and other biological products and industrial wastes.
3. Gases, such as oxygen, nitrogen, carbon dioxide, sulfur dioxide, hydrogen sulfide, and methane, absorbed from the atmosphere and subsurface sources.
4. Suspended matter, such as clay, silt, oil, fat, and grease.
5. Microorganisms, such as bacteria, algae, and fungi.

The types and quantities of impurities present determine the quality of water and the subsequent problems that can arise from its use in industry [4].

1.4.1 PHYSICAL CHARACTERISTICS

The physical characteristics of water include color, detergency, odor, temperature, and turbidity.

1.4.1.1 Color

Dissolved organic materials from decaying vegetation and certain dissolved inorganic compounds can cause color in water. Although color itself is not usually objectionable, its presence due to certain dissolved impurities may interfere with water treatment program.

1.4.1.2 Detergency

Many natural and synthetic substances will cause foam when water is agitated. The major cause of foaming is surfactants, which are synthetic chemicals used in detergents. Water with a high detergency should be analyzed to determine what treatment is required to discover the origin of contamination. Foaming substances may interfere with the performance of chemicals used in water treatment formulations. Foaming substances can be removed by a conventional treatment consisting of sedimentation, coagulation/flocculation, and filtration, or activated carbon.

1.4.1.3 Odor

Odor in water can be caused by foreign matter such as organic compounds, inorganic salts, and dissolved gases. These impurities may come from natural, agricultural, or industrial sources. Water should be free from any objectionable color as it may interfere with the analysis of chemicals used in water treatment formulations.

1.4.1.4 Temperature

Temperature is important in determining the rate at which scale-forming salts will precipitate on heat exchanger, RO membrane, and equipment surfaces, and, thus, to the extent to which these salts could become a major fouling problem. In desalination by RO, temperature is important in determining the pressure drop through the membrane at the intended flux rate.

1.4.1.5 Turbidity

Turbidity in water is due to the presence of suspended solids dispersed throughout the water and is a measure of the extent to which light is scattered by the suspended solids, such as clay, silt, and organic matter, and by plankton and other microscopic organisms that interfere with the passage

of light through water. Turbidity is closely related to the total suspended solids, but also includes plankton and other organisms, and is measured in nephelometric turbidity units (NTU). The turbidity of natural waters tends to increase during runoffs as a result of increased overland flow, stream flow, and erosion. Turbidity in excess of 5 NTU is easily detected in a glass of water and is usually objectionable for aesthetic reasons. Water containing suspended matter is a problem for several reasons, including the following: (a) it protects the microorganisms from chlorine and other biocides, (b) it interferes with the test for coliform bacteria, (c) it interferes with the maintenance of residual chlorine, and (d) it acts as a food source for microorganisms, allowing them to survive and multiply. Excessive turbidity must be removed by filtration.

1.4.2 CHEMICAL CHARACTERISTICS

The chemical characteristics of water include dissolved minerals, organic substances, dissolved gases, and microbiological contaminants [5]. In industrial water applications, the quality of feed water is generally expressed as shown in Table 1.1. High-purity water includes ultrapure water and pure water. The definition of ultrapure water differs from pure water or deionized water. Ultrapure water refers to water that is free of “all” impurities. Power plants are the single-largest users of high-purity water. Other industrial users of high-purity water include beverage industries, research laboratories, microelectronics, and pharmaceuticals. Pure water, on the other hand, refers to the water that meets specific needs of a given process or product. For example, in textile washing, the removal of calcium, magnesium, iron, and manganese is essential, whereas in pharmaceuticals, the removal of organisms or pyrogenic substances is of utmost importance.

1.4.2.1 Aluminum

Aluminum-based compounds, such as sodium aluminate and aluminum sulfate, have been used for years as coagulant aids to clarify industrial and municipal waters. These flocculating agents hydrolyze to form insoluble hydroxides and neutralize the charge of turbidity particles in water. In most cases, these large particles are removed via settling in a clarifier and are collected as sludge. Time-to-time fluctuations in pH at the water treatment plant, however, cause excessive amounts of aluminum to pass into the distribution system, usually in the dissolved form. Under proper circumstances, the aluminum precipitates formed in the water treatment plants are completely filtered out, and thus are not present in the treated water. Aluminum is amphoteric, with Al^{3+} present at low pH values and aluminate anion existing at higher pH values, and exhibits minimum solubility at about pH 6.6. Further, if pH adjustment is required to control calcium carbonate scaling, aluminum hydroxide may precipitate and deposit on heat exchanger and RO membrane surfaces.

1.4.2.2 Barium

Barium is a divalent ion, which forms insoluble salts with sulfate ions, that is soluble to the level of less than 1 mg/L. Like calcium ions, barium ions also form insoluble salts with fluoride ions.

TABLE 1.1
Classification of Feed Water

Classification	Hardness (ppm)	Hardness (Grains per
		U.S. Gallons)
Soft	1–65	0–3.8
Slightly hard	66–125	3.9–7.3
Hard	126–200	7.4–11.7
Very hard	>200	>11.7

1.4.2.3 Calcium

Calcium is always present as divalent ions that form insoluble salts with various anions, such as carbonate, fluoride, oxalate, phosphate, and polyphosphate. Further, under certain conditions, calcium ions also form insoluble salts with organophosphonate compounds and acrylic and maleic acid-based polymers commonly used to prevent the precipitation of calcium-based salts in industrial water systems.

1.4.2.4 Copper

Copper is found in some natural waters, particularly in areas where copper has been mined. The presence of copper, especially in recirculating water, may be due to the corrosion of copper and copper-based alloys used in pipes.

1.4.2.5 Chromium

Many chromium compounds are relatively water insoluble. The metal industry mainly discharges trivalent chromium. Hexavalent chromium in industrial wastewater mainly originates from tanning and painting. Chromium in seawater varies strongly, and is usually 0.2–0.5 parts per billion (ppb). Rivers contain approximately 1 ppb of chromium, although strongly increased concentrations are possible.

1.4.2.6 Iron

Among the various dissolved impurities in natural waters, iron-based compounds cause the most serious problems in the efficient operation of industrial water systems. In the reduced state, iron (II) or ferrous (Fe^{2+}) ions are very soluble and pose no serious problems, especially at low pH values. However, upon contact with air, Fe^{2+} ions are oxidized to a higher valence state (Fe^{3+}) and readily undergo hydrolysis to form insoluble hydroxide. Further, iron at low concentrations exhibits a negative influence on the performance of scale inhibitors [6].

1.4.2.7 Magnesium

Magnesium forms sparingly soluble salts, such as magnesium silicate and, under high pH conditions, magnesium hydroxide. Both are common in cooling and boiler systems.

1.4.2.8 Manganese

Manganese is usually present below 0.5 mg/L in public water supplies. Private water supplies often contain higher manganese levels, mostly in a dissolved form that precipitates as hydroxides on exposure to oxygen. A well water supply containing manganese should be pretreated for manganese removal, or steps should be taken to eliminate contact with air or oxidants to assure that the manganese remains soluble. Manganese water chemistry is very complex. Manganese exists in several oxidation states among which Mn^{2+} and Mn^{4+} are the most important with respect to water problems.

1.4.2.9 Sodium

Because a sodium ion is monovalent, it forms relatively soluble salts with most anions, including bicarbonate, carbonate, sulfate, and chloride, and, thus, seldom presents a scaling problem in desalination and cooling water systems.

1.4.2.10 Potassium

Although chemically similar to sodium, potassium is not likely to be present in appreciable amounts in a water supply. No operating or scaling problems are caused by potassium ions in industrial water systems.

1.4.2.11 Silica

Silica very often limits the extent to which water can be used in cooling and RO systems. Although the true solubility level of silica is affected by various factors, such as pH, temperature, and TDS, the maximum silica concentration is customarily given as 150 mg/L. However, silica in excess of

180 mg/L presents a potential problem, especially in the presence of polyvalent metal ions. Silica solution chemistry is very complex and difficult to predict. In industrial water systems, silica can exist in three different forms, namely, dissolved or monomeric silica, polymerized or colloidal silica, and particulate silica.

1.4.2.12 Selenium

Selenium is a metal found in natural deposits as ores containing other elements. The greatest use of selenium compounds is in electronic and photocopier components. The levels of selenium in surface water and groundwater vary from 0.06 to 400 ppb and in drinking water supplies are usually 10 ppb.

1.4.2.13 Strontium

Strontium is a divalent ion found in some water supplies. Like calcium and barium, it also forms insoluble salts with sulfate ions.

1.4.2.14 Zinc

Zinc is found in some natural waters, particularly in areas where zinc has been mined. Zinc at low concentrations (few ppm) may not pose any problems, but at higher concentrations, it may delay calcium phosphate [7] precipitation and may also form insoluble salts with hydroxide ions [8].

1.4.2.15 Bicarbonate

Bicarbonate ions do not form insoluble salts; however, a portion of bicarbonate on exposure to a high pH and temperature, and under conditions of high cycle of concentrations can be converted to carbonate ions, resulting in calcium carbonate. Such cases require the addition of an acid or a scale inhibitor to prevent the precipitation and deposition of calcium carbonate on equipment surfaces.

1.4.2.16 Carbonate

Carbonate forms insoluble salts with calcium and iron ions, which, as discussed above, can precipitate and form scale deposits on RO membrane and heat exchanger surfaces. Carbonate-based deposits are normally controlled by reducing the water pH or adding a scale inhibitor to the feed water.

1.4.2.17 Chloride

Most waters contain chloride. It can be caused by the leaching of marine sedimentary deposits and by pollution from seawater, brine, or industrial wastes. An increase in chloride content may indicate possible pollution from sewage sources, particularly if the normal chloride content is known to be low. Chloride is relatively safe—it has neither any negative effect on the life of RO membranes, nor does it generate insoluble salts.

1.4.2.18 Fluoride

Fluoride levels in water vary according to the source, with seawater > groundwater > surface water. Fluoride ions do not directly affect either an RO membrane or a heat exchanger, but form insoluble salts with barium, calcium, magnesium, and strontium. The precipitation of fluoride-based salts should be carried out by adding a scale inhibitor to the feed water.

1.4.2.19 Sulfate

Waters containing high levels of sulfate caused by the leaching of natural deposits of magnesium sulfate or sodium sulfate may cause scaling problems due to the formation of insoluble salts with calcium, barium, and strontium.

1.4.2.20 Carbon Dioxide

Carbon dioxide does not play a major role in RO fouling. However, it does pass readily through any RO membrane, equilibrating on both sides. Under some circumstances, it is the major dissolved constituent of the permeate.

1.4.2.21 Hydrogen Sulfide

Hydrogen sulfide is a gas present in some waters. There is never any doubt as to when it is present due to its offensive “rotten egg” odor. This characteristic odor is sometimes apparent in concentrations below 1 mg/L. Occasionally, the amount goes as high as 50–75 mg/L. Hydrogen sulfide is more common to well waters than to surface water supplies. Under the right conditions, hydrogen sulfide forms sulfur particles and contributes to the fouling of ion exchange resin beds and also RO membranes. Further, hydrogen sulfide promotes corrosion due to its activity as a weak acid.

1.4.2.22 Oxygen

Waters void of oxygen are likely to contain soluble iron, manganese, and hydrogen sulfide. Upon exposure of these waters to oxygen, precipitates are likely to form and may cause serious operational problems.

1.4.2.23 Organic Chemicals

Organic chemicals include pesticides, herbicides, trihalomethanes, and volatile synthetic organics. Maximum contaminant levels for several common pesticides and herbicides have been established.

1.5 IMPORTANCE OF FEED WATER ANALYSIS FOR INDUSTRIAL SYSTEMS

As discussed above, each water source offers a unique water chemistry, and it is, therefore, very important to get a complete analysis of the feed water for selecting an appropriate treatment program for an industrial water system. For example, maintaining membrane performance guarantees in an RO system requires periodic water analyses. Newly installed RO systems require complete monthly water analyses. Even older systems, which have a complete performance and operational history, can benefit from frequent water analyses as a method of monitoring changes in the water quality. In addition to providing analyses of the feed, the product, and the brine streams, a really useful analysis will also compute the rejection and recovery of the principal components (e.g., Ca, Mg, Na, Cl, and SO_4) and calculate the scaling potential of the brine stream. These parameters are essential in predicting the cause of a performance decline in boiler, cooling, geothermal, and RO systems. Operators of these systems can benefit greatly from accurate water analyses of feed and recirculating water by tracking the performance of their systems and identifying downward trends. Thus, in many cases, the replacement of expensive equipments (i.e., heat exchangers, pipes, pumps, and RO membranes) can be avoided [5].

Since different sources of water offer a wide range of potential problems in industrial systems, care should be exercised in mixing different feed water sources. If incompatible constituents are present in different feed water sources, mixing of these feed waters could lead to new scaling problems. Temperature changes, turnovers, and intrusions or upsets into water sources, all have an effect on the successful operation of the systems. For example, if flocculants or coagulants of inorganic or organic type are used to clarify feed water, it is important to keep the residual clarifying agents to very low levels (<0.1 ppm). It has been well documented that trace levels of aluminum, iron, and cationic polymer exhibit marked antagonistic effects on the performance of deposit control polymers used in treatment formulations [6,9]. Similarly, an analysis of recirculating water is important for a

complete mass balance and to avoid the precipitation of treatment chemicals with the hardness ions. Computer models are presently used by engineers and operators to project fouling tendencies based on water chemistry. Water analyses that accurately represent the feed water are imperative to ensure the proper use of this valuable tool. Inaccurate analyses or misinformation can be more dangerous than a lack of information [5].

The cost of water analysis can vary, based on the number of the constituents to be analyzed and the laboratory chosen to perform the analysis. Membrane manufacturers, service companies, and chemical supply companies often offer supporting water analysis. Environmental laboratories also perform water analyses. The typical cost to perform an individual water analysis varies from \$250 to \$400 per sample. This is a minor cost to ensure the proper operation of the industrial water system [5].

1.6 MINERAL SCALES AND DEPOSITS

Foulants commonly encountered in industrial water systems are of two types:

- Mineral scales, which are hard, dense, crystalline precipitates of calcium carbonate, calcium sulfate, barium sulfate, calcium fluoride, calcium phosphate, etc.
- Deposits, such as colloidal and suspended matter, biological growth, corrosion products, etc.

Understanding the distinction between scaling and deposit formation is very important in choosing the water treatment program. A brief discussion of mineral scales and deposits is presented below.

1.6.1 SCALING

The physicochemical prerequisite for the formation of any mineral solid deposit is the excess of mineral solubility in the respective fluid. Mineral scale deposits do form in practically all processes using water. Typical examples are boilers; heat exchangers; cooling towers; pipes, especially those handling turbulent water; and RO membranes. Figure 1.2 shows typical scale deposits formed in a boiler, from the water side. In Figure 1.3, calcium carbonate scale deposits formed in a tubular heat exchanger are shown. Ionic salts form most often on layers of miscellaneous deposits, following changes either in fluid flow or temperature. The variation of the deposit layers may be seen in a deposit formed in PVC pipes by flowing water mixed with organic waste, as shown in Figure 1.4. As can be seen (Figure 1.4), the texture of the deposits is laminar, showing on the external side an organic crust followed by formations of calcium carbonate. The identification of the cause of solid formations can be done through combinations of analyses of the aqueous phase and of the solid deposits.



FIGURE 1.2 Boiler scale deposits formed on the water side.

1.6.1.1 Calcium Carbonate Deposits

One of the most typical examples of crystallization fouling is the formation of crystalline deposits of calcium carbonate. The nature of the calcium carbonate polymorphs deposited on solid substrates depends strongly not only on the presence of inorganic and/or organic ions in the aqueous medium but also on other parameters, including solution temperature; the flow rate and pH are detrimental for the stabilization of transient polymorphic phases [10]. Scale deposits formed at rather low temperatures consist of calcite, while at temperatures exceeding 50°C, aragonite prevails. Calcium carbonate scale deposits are encountered in heat exchangers, cooling water towers, water transfer pipes, the low-enthalpy geothermal energy fluid-handling equipment, water desalination processes using RO or water evaporation, petroleum production, etc. In carbonate-rich geothermal fluids, the formation of calcium carbonate causes significant problems in the operation of pumps or in the clogging of pipes. In Figure 1.5, typical aragonite scale deposits from the geothermal field of Soussaki are shown. Figure 1.6 presents calcium carbonate deposits formed in an ammonia cooling tower at an industrial unit processing frozen seafood.

The formation of calcium carbonate deposits also depends strongly on the substrate [11,12]. It is interesting that strongly adhering calcium carbonate forms even in PVC pipes used for the transport of drinking water, as shown in Figure 1.7. The increased calcium and carbonate concentration levels are responsible for the formation of scale deposits on the RO membrane fibers [13], as shown in Figure 1.8.

1.6.1.2 Metal Sulfate Scale Deposits

Sulfate-containing scales formed in the presence of alkaline earth metals include gypsum ($\text{CaSO}_4 \cdot 2\text{H}_2\text{O}$), anhydrite (CaSO_4), barite (BaSO_4), and celestite (SrSO_4). These scales are commonly encountered in oil field operations [14]. Calcium sulfate can exist in six different solid phases: three anhydrites, two hemihydrates, and one dihydrate. Gypsum ($\text{CaSO}_4 \cdot 2\text{H}_2\text{O}$), hemihydrate ($\text{CaSO}_4 \cdot \frac{1}{2}\text{H}_2\text{O}$), and anhydrite III and anhydrite II can exist at room temperatures, whereas anhydrite I only exists above 1180°C [15]. The connate brines present in oil reservoirs are enriched in the ions constituting the solid precipitates because of equilibration with their surrounding geological formations. Moreover, the activity of sulfate-reducing bacteria enriching solutions with sulfate

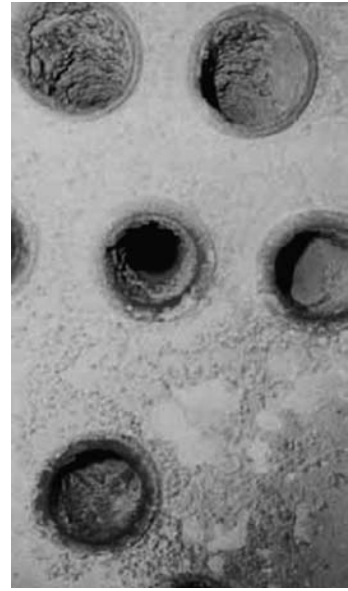


FIGURE 1.3 Calcium carbonate scale deposits formed in a tubular heat exchanger.

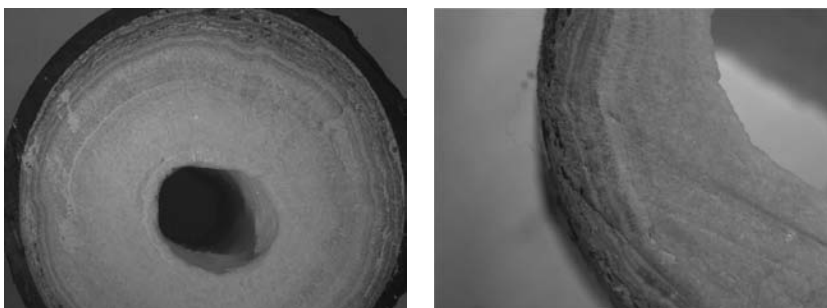


FIGURE 1.4 Calcium carbonate scale deposits formed in wastewater pipes. Layer overgrowth on slit (external black crust).

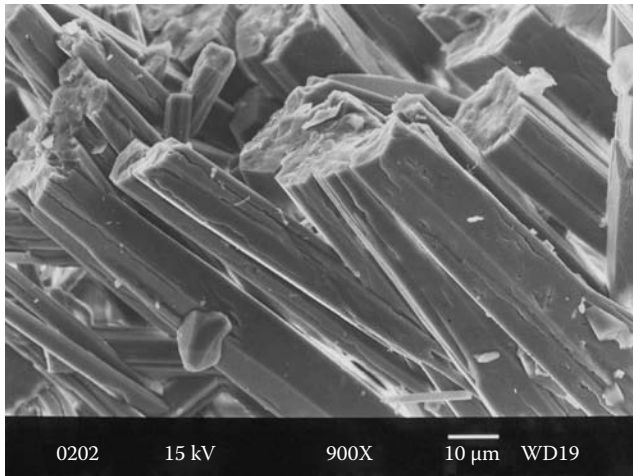


FIGURE 1.5 Aragonite scale deposits in pipes handling geothermal water from the Soussaki geothermal field, Greece.



FIGURE 1.6 Calcium carbonate deposits in an ammonia cooling tower.



FIGURE 1.7 Cemented calcium carbonate deposits formed in a PVC drinking water transport pipe.

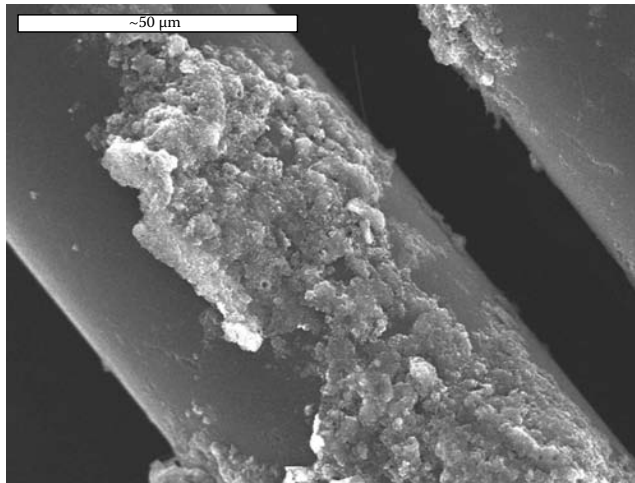


FIGURE 1.8 Biofoulants and carbonaceous deposits formed on hollow fibers used in water desalination.



FIGURE 1.9 Barium sulfate scale deposit in an oil field pipeline.

anions has been held responsible for the increased sulfate concentrations of injected water in oil wells [16]. Calcium sulfate scaling is also a serious impediment for water desalination with RO systems [17]. Barium sulfate, on the other hand, is a salt commonly encountered in the production of oil in offshore wells [18]. Figure 1.9 shows a barium sulfate scale deposit in an oil field pipeline.

1.6.1.3 Calcium Phosphate Scale Deposits

Calcium phosphates are important from the industrial water systems point of view because they occur as deposits on heat exchanger and RO membrane surfaces. In more recent times, the increase in phosphate concentrations in lakes and rivers near heavily populated areas has been the major factor in the resurgence of interest in the physicochemical processes of precipitation and dissolution of phosphate salts. Despite the continuous transport of phosphate ions into lakes, the phosphate concentration of the lakes does not increase proportionally, indicating that at least some phosphate is removed by precipitation.

Calcium phosphates of interest include dicalcium phosphate dihydrate ($\text{CaHPO}_4 \cdot 2\text{H}_2\text{O}$), dicalcium phosphate anhydrous (CaHPO_4), octacalcium phosphate ($\text{Ca}_8\text{H}_2(\text{PO}_4)_6 \cdot 5\text{H}_2\text{O}$), tricalcium phosphate ($\text{Ca}_3(\text{PO}_4)_2$), and hydroxyapatite ($\text{Ca}_5(\text{PO}_4)_3\text{OH}$). Among the various calcium phosphates, tricalcium phosphate and hydroxyapatite are the most commonly encountered scales in cooling and

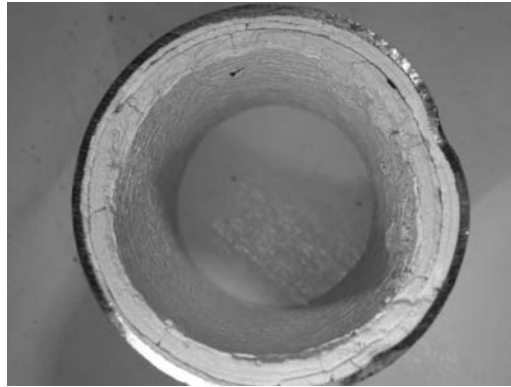


FIGURE 1.10 Apatitic deposit formed in a stainless steel pipe used in the pasteurization process of milk.

boiler systems [19]. Calcium phosphate deposits have also been encountered during the pasteurization of milk. Figure 1.10 shows an apatitic deposit formed in a stainless steel pipe used in the pasteurization process of milk.

1.6.1.4 Calcium Fluorides

Calcium fluoride (CaF_2) scale deposits form, although not very often, in RO water treatment systems when the fluoride concentration levels in the water are significant. The examination of scale deposits in boilers and tubing in coal gasification installations was shown to consist mainly of iron sulfides, sodium chloride, and calcium fluoride [20]. The CaF_2 crystallites may form either by a reaction of gaseous HF during coal gasification with volatilized calcium or directly during gasification. It is interesting to note that calcium fluoride scale deposits have been found in high-pressure, high-temperature oil wells during production using the water-flooding approach [21]. In oil wells in sandstone reservoirs, acidification is often done using hydrofluoric acid solutions, which, with the dissolving calcium, result in calcium fluoride formations.

1.6.1.5 Calcium Oxalates

Calcium oxalate forms in three different hydrates: calcium oxalate monohydrate (COM), calcium oxalate dehydrate (COD), and calcium oxalate trihydrate (COT), in the order of decreasing thermodynamic stability (increasing solubility). COT hydrolyzes directly to COM, except for the case in which certain impurities present stabilize the intermediate COD [22]. Calcium oxalate scales (both COM and COD) have been identified in sugar mill evaporators [23]. Moreover, the turbidity in white sugar found in beet sugar processing was due to the formation of thin crystals of COD [24]. Figure 1.11 shows COM crystals formed by spontaneous precipitation.

Calcium oxalate scale deposits form in pulp mills because of the use of recycled washer filtrates implemented to reduce the effluent volume. Moreover, the use of chlorine dioxide in the first stage decreases the ability of the bleach plant to remove calcium and barium. As a result, calcium oxalate and barium sulfate scale deposits form in the first chlorine dioxide bleach stage, while calcium carbonate deposits form in the first extraction stage. In particularly severe cases, calcium oxalate also forms in later bleach stages [25].

1.6.1.6 Silica/Metal Silicates

The markedly different solubilities between amorphous and crystalline silica in neutral pH is the main factor responsible for supersaturation with respect to silicate and metal silicate salts [26].

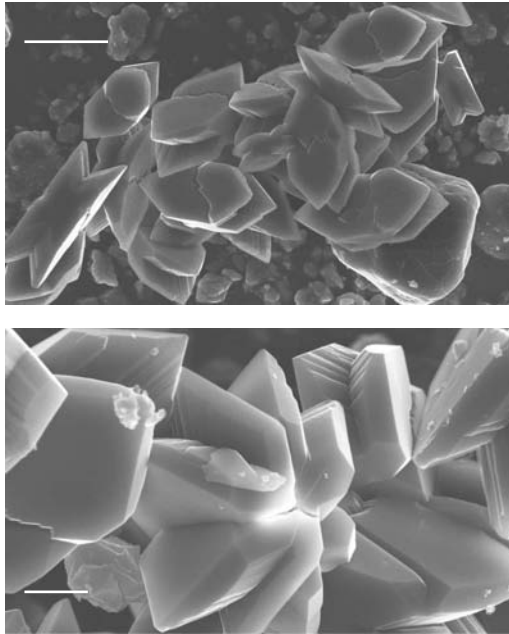


FIGURE 1.11 COM crystals formed by spontaneous precipitation. Upper bar 10 μm; lower bar 2 μm.

The silicate-based scale deposits in cooling water systems consist mainly of silica, calcium, magnesium, and aluminosilicates [27]. If magnesium is present in high-enough concentrations, magnesium silicate scaling will occur at a pH of 8.5. Silica-scale formation in water desalination systems by RO and also in water treatment processes as silicate ions cannot be removed through an ion exchange treatment. The presence of cations like manganese and nickel has been suggested to play a catalytic role in the polymerization of silica, resulting in the fouling of RO membranes. The fouling of ultrafiltration systems used for drinking water purification has been shown to contain scales rich in calcium and silicate deposits [28]. Colloidal silica was also responsible for membrane fouling during the RO treatment of municipal wastewater [29]. Figure 1.12 shows the scanning electron micrograph of an RO membrane fouled with amorphous silica.

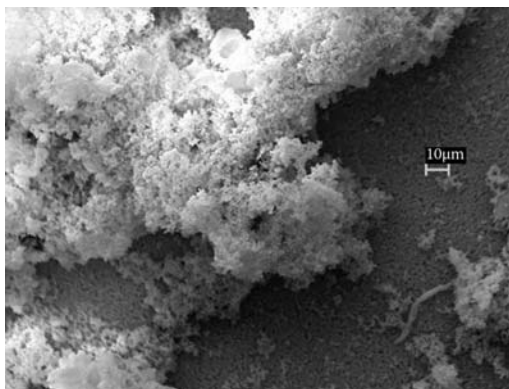
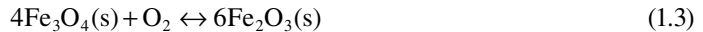
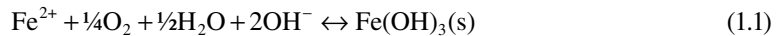


FIGURE 1.12 Scanning electron micrograph of an RO membrane fouled with amorphous silica.

1.6.1.7 Iron-Based Scales

Iron-containing scales are often encountered coupled with the corrosion of metallic surfaces and components [30]. Dissolved oxygen in water contributes to the oxidation of ferrous iron (Fe^{2+}) or iron scales:



The rate of corrosion of the iron metal has little relationship to the amount of iron that actually goes into the water, primarily due to the deposition of oxidized iron or other compounds into a scale that serves as a large reservoir of corrosion by-products. Iron scales are very heterogeneous, consisting of a large variety of compounds. Examples of these types of compounds are given below.

1.6.1.7.1 Siderite

Siderite (FeCO_3) scales form as a result of the presence of reduced iron species. It is interesting, however, to note that siderite provides a more protective scale than oxidized ferric scales, such as goethite (FeOOH) and hematite (Fe_2O_3) [31]. The presence of siderite has been identified in a large number of iron scales [32]. However, it is interesting to note a discrepancy regarding siderite in studies of pure iron in high carbonate solutions (not drinking water). Two such studies concluded that siderite was the key to forming a protective scale [33,34].

1.6.1.7.2 Green Rust

“Green rust” is the generic name given to iron compounds containing both ferrous and ferric iron, as well as other ions, such as carbonate, chloride, and sulfate [35,36]. Green rusts have been identified in the corrosion products on iron and steel [37]. The composition of iron-containing scales depends on the chemistry of the aqueous fluids in contact with metallic surfaces. Geothermal fluids for example, in some cases, contain high concentrations of hydrogen sulfide [38]. The problem is attenuated by elevated temperatures and by the presence of chloride and bicarbonate ions. The nature, the stoichiometry of the iron sulfides, and their quantity depend strongly on the operational parameters of the respective geothermal field [39]. The presence of iron (II) in groundwater often causes problems in water treatment using membranes because of precipitation of oxides like FeOOH , which, in the presence of chlorine, oxidize and yield hematite, Fe_2O_3 [40]. Deposits of iron sulfide and copper sulfide on an RO membrane are shown in Figure 1.13.

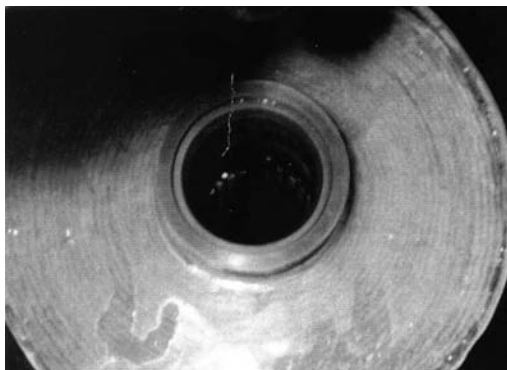


FIGURE 1.13 Deposits of iron sulfide and copper sulfide on an RO membrane.



FIGURE 1.14 Fungus growth on an RO membrane.

1.6.2 BIOFOULING

Fouling by microbiological slimes is a constant threat to the efficient operation of cooling water and RO systems. Microorganisms, which cause the slime deposits, are living organisms capable of exceeding rapid reproduction. Biological fouling can occur when the feed and recirculating waters contain sufficient nutrients to sustain a rapid growth of organisms. Because microorganisms adhere to the RO membrane, heat exchanger, and other metal surfaces, especially in the low water flow areas, these are ideal conditions for optimum growth. In most recirculating water and RO systems, a thin biofilm is formed on the heat exchanger and RO surfaces that does not interfere with short-term performance. However, during long periods of operation, the biofilm accumulates, thereby affecting system performance. In addition, microbiological fouling may influence under deposit corrosion. Figure 1.14 shows the growth of fungus in a low-flow region of a scaled RO membrane.

1.6.3 COLLOIDAL FOULING

The fouling of heat exchanger and membrane surfaces by suspended matter (i.e., silt, clay, organic debris, etc.) is of critical concern to water technologists and plant operators. Certain feed waters, especially surface waters, require a far more extensive pretreatment than other sources, such as deep wells. Changes in feed water composition can occur because of seasonal variations in the water supply. Feed waters containing suspended matter are typically treated with inorganic and organic clarification agents. The effectiveness of a surface treatment to reduce suspended matter is dependent upon the proper selection and concentration of clarifying agents, pH, mixing, and residence time. Commonly used water clarification agents include aluminum chloride, ferric chloride, and cationic polymers (e.g., diallyldimethyl ammonium chloride and hydrolyzed polyacrylamide). In some cases, residual clarification agents have been reported to foul the membrane surface, resulting in decreased system performance. Figure 1.15 shows the photograph of an RO membrane fouled with colloidal matter (e.g., silt and clay).

1.6.4 CORROSION-RELATED FOULING

Corrosion is defined as the deterioration of metal by a chemical or electrochemical reaction with its environment. In industrial water systems, the corrosion of metal-based equipment, if not properly controlled, could lead to several operational challenges. Numerous factors, such as metallurgy,

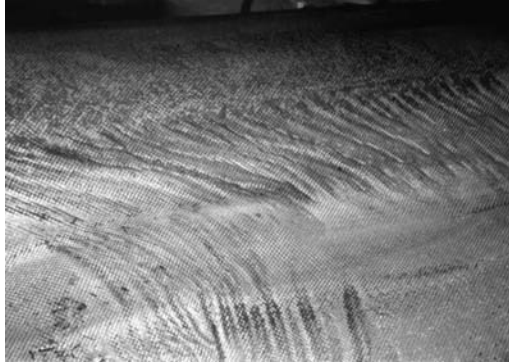


FIGURE 1.15 An RO membrane fouled with colloidal matter.

water chemistry, temperature, pH, and water flow rate, influence corrosion. Foulants resulting from the industrial water system corrosion include oxides of iron, copper, and zinc.

1.7 SUMMARY

Water is used in more processes than any chemical known to man. It is also the most important liquid in the world to maintain human, plant, and animal life. Additionally, high population growth, rapid urbanization, phenomenal industrial growth, and agricultural development make water one of the most precious resources in the world. Water quality plays an important role in the efficient operation of industrial water systems. In many cases, the quality of water available for industrial applications is extremely poor. Unfavorable water-quality characteristics coupled with a lack of poor system design and inadequate treatment programs often results in the buildup of undesirable deposits, such as mineral scales, colloidal matter, corrosion products, and biological growth on heat exchanger and RO membrane surfaces, pipes, and pumps. In several instances, the removal of deposits leads to a discontinuous operation of the system, resulting in higher operating costs.

Water hardness and alkalinity in combination with elevated temperatures involved in a number of industrial processes result in the formation of tenaciously adhering carbonate deposits, consisting mainly of calcium carbonate polymorphs associated with other divalent metal carbonates and/or silicates. These types of deposits are a serious impediment on the exploitation of geothermal energy sources. Treatment of water sources by additives like the successfully employed phosphonic acid derivatives may result in the formation of calcium phosphonate scale deposits. The presence of residual orthophosphates in treated water or during the processing of foodstuff (e.g., milk processing and sugar production) results often in the formation of calcium phosphate and calcium oxalate scale deposits. Finally, fouling of RO membranes or of equipment used for the treatment of both low- and high-enthalpy geothermal fluids, through the formation of transition metal sulfides (iron sulfide, copper sulfide, etc.), is a serious threat for the performance of the respective processes, and calls for special attention. Considerable amelioration may be done provided that a good knowledge between water chemistry and scale deposits is acquired.

REFERENCES

1. Amjad, Z. Scale inhibition in desalination applications: An overview. CORROSION/96, Paper No. 230, NACE International, Houston, TX (1996).
2. Amjad, Z. (Ed.) *Reverse Osmosis: Membrane Technology, Water Chemistry, and Industrial Applications*, Van Nostrand Reinhold, New York (1993).
3. Hamonn, H. Water and its chemistry, Flex Notes, 1(3), Arrowhead Industrial Water Inc., Lincolnshire, IL (July 1993).

4. Kemmer, F. R. and McCallion, J. (Eds.) *The Nalco Water Handbook*, McGraw-Hill Book Company, New York (1979).
5. Hooley, J. H., Pittner, G. A., and Amjad, Z. The importance of water analysis for reverse osmosis design and operation. In *Reverse Osmosis: Membrane Technology, Water Chemistry, and Industrial Applications*, Amjad, Z. (Ed.), Van Nostrand Reinhold, New York (1993), Chapter 5.
6. Wilson, D. Influence of molecular weight on selection and application of polymeric scale inhibitors. CORROSION/98, Paper No. 48, NACE International, Houston, TX (1998).
7. Amjad, Z., Butala, D., and Pugh, J. The Influence of recirculating water impurities on the performance of calcium phosphate inhibiting polymers. CORROSION/99, Paper No. 118, NACE International, Houston, TX (1999).
8. Amjad, Z. Controlling metal ions fouling in industrial water systems. *Ultrapure Water* 14, 31–40 (2000).
9. Amjad, Z., Zuhl, R. W., and Zibrida, J. F. The effect of biocides on deposit control polymer performance. In *Proceedings of the 12th Annual Convention*, Association of Water Technologies, Honolulu, HI (2000).
10. Chen, T., Neville, A., and Yuan, M. Assessing the effect of Mg^{2+} on $CaCO_3$ scale formation-bulk precipitation and surface deposition. *J Cryst Growth* 275, 1341–1347 (2005).
11. Neville, A. Calcium carbonate scale formation-assessing the initial stages of precipitation and deposition. *J Petrol Sci Eng* 46, 185–194 (2005).
12. Wua, Z., Francis, L. F., and Davidson, J. H. Scale formation on polypropylene and copper tubes in mildly supersaturated tap water. *Solar Energy* 83(5), 636–645, doi:10.1016/j.solener.2008.10.012 (2008).
13. Tzotzi, C., Pahiadaki, T., Yiantsios, S. G., Karabalis, A. J., and Andritsos, N. A study of $CaCO_3$ scale formation in RO and NF membrane processes. *J Membr Sci* 296, 171–184 (2007).
14. Atkinson, G. and Mecik, M. The chemistry of scale prediction. *J Petrol Sci Eng* 17, 113–121 (1997).
15. Wirching, F. and Gipswerke, G. K. W. Calcium sulfate. In *Ullmann's Encyclopedia of Industrial Chemistry*, Gerhartz, W., Yamamoto, Y. S., Campbell, F. T., Pfeirkorn, R., and Roundsaville, J. F. (Eds.), 5th edn., Vol. 4, pp. 556–558, VCH Verlagsgesellschaft, Weinheim, Germany (1985).
16. Nasr-El-Din, H. A., Al-Saiari, H. A., and Al-Ruwaily, A. A. Removal and mitigation of calcium carbonate scale in a sandstone reservoir in Saudi Arabia: Long term field monitoring, paper SPE 102863. In *SPE Annual Technical Conference and Exhibition*, San Antonio, TX (2006).
17. Amjad, Z. Applications of antiscalants to control calcium sulfate scaling in reverse osmosis systems. *Desalination* 54, 263–276 (1985).
18. Amjad, Z. Inhibition of barium sulfate precipitation: Effect of additives, solution pH, and supersaturation. *Water Treat* 9, 47–56 (1994).
19. Amjad, Z. (Ed.) *Calcium Phosphates in Biological and Industrial Systems*, Kluwer Academic Publishers, Boston, MA (1998).
20. Brooker, D. Chemistry of deposit formation in a coal gasification syngas cooler. *Fuel* 72, 665–670 (1993).
21. Adeniyi, O. D., Nwalor, J. U., and Ako, C. T. A review on waterflooding problems in Nigeria's crude oil production. *J Disp Sci Technol* 29, 362–365 (2008).
22. Gardner, G. L. Kinetics of the dehydration of calcium oxalate trihydrate crystals in aqueous solution. *J Colloid Interface Sci* 54, 298–310 (1976).
23. Doherty, W. O. S., Crees, O. L., and Senogles, E. The effect of polymeric additives on the crystallization of compounds found in evaporator scales of Australian sugar mills. *Cryst Res Technol* 28, 603–613 (1993).
24. Bensouissi, A., Rousse, C., Roge, B., Douglade, J., and Mathlouthi, M. Isolation and characterization of scale and turbid particles in beet sugar processing and the quality of granulated sugar. *Food Chem* 114(4), 1570–1575, doi:10.1016/j.foodchem.2008.11.089 (2009).
25. Dexter, R. J. and Wang, X. H. The formation and control of bleach plant scale as a result of water minimization. In *Proceedings of TAPPI Pulping Conference*, Atlanta, GA, pp. 1341–1347 (1998).
26. Scachachiyunta, P., Koo, T., and Sheikholeslami, R. Effect of several inorganic species on silica scale fouling in RO membranes. *Desalination* 144, 373–378 (2002).
27. Szymura, T. Deposits in water-based cooling systems. *Physicochem Probl Miner Process* 42, 131–140 (2008).
28. Mosqueda-Jimenez, D. B., Huck, P. M., and Basu, O. D. Fouling characteristics of an ultrafiltration membrane used in drinking water treatment. *Desalination* 230, 79–91 (2008).
29. Ning, R. Y. and Troyer, T. L. Colloidal fouling of RO membranes following MF/UF in the reclamation of municipal wastewater. *Desalination* 208, 232–237 (2007).
30. Sarin, P., Snoeyink, V. L., Lytle, D. L., and Kriven, W. M. Iron corrosion scales: Model for scale growth, iron release and colored water formation. *J Environ Eng* 130, 364–373 (2004).

31. Sontheimer, H., Kollé, W., and Snoeyink, V. L. The siderite model of the formation of corrosion-resistant scales. *J Am Water Works Assoc* 73, 572–577 (1981).
32. Mishra, B., Olson, D. L., Al-Hassan, S., and Salama, M. M. Physical characteristics of iron carbonate scale formation in line pipe steels, Paper No. 13, CORROSION/92, NACE International, Houston, TX (1992).
33. Blengino, J. M., Labbe, J. P., and Robbiola, L. Physico-chemical characterization of corrosion layers formed on iron in sodium carbonate-bicarbonate containing environment. *Corros Sci* 37, 621–643 (1995).
34. Simpson, L. J. and Melendres, C. A. Surface-enhanced Raman spectrochemical studies of corrosion films on iron in aqueous carbonate solution. *J Electrochem Soc* 143, 2146–2152 (1996).
35. Simon, L., Genin, J. M., and Refait, P. Standard free enthalpy formation of Fe(II)-Fe(III) hydroxysulfite green rust one and its oxidation into hydroxysulfate green rust two. *Corros Sci* 39, 1673–1685 (1997).
36. Genin, J. M., Bourrie, G., Trolard, F., Abdelmoula, M., Jaffrezic, A., Refiat, P., Maitre, V., Humbert, B., and Herbillon, A. Thermodynamic equilibria in aqueous suspensions of synthetic and natural Fe(II)-Fe(III) green rusts: Occurrences of the mineral in hydrophobic soils. *Environ Sci Technol* 32, 1058–1068 (1998).
37. McGill, I. R., McEnaney, B., and Smith, D. C. Crystal structure of green rust formed by corrosion of cast iron. *Nature* 259, 200–201 (1976).
38. Philips, S. L., Mathus, A. K., and Garrison, W. *Special Technical Publication 717*, ASTM, Washington, DC (1980).
39. Amalhay, M., Gauthier, B., and Ignatiadis, I. The influence of some physicochemical parameters and exploitation conditions on corrosion and scaling in geothermal wells in the Paris basin. In *Proceedings of the International Symposium, Geothermics 94 in Europe*, Document BRGM No. 230, Orleans, France (1994).
40. Liu, H., Guo, H., Li, P., and Wei, Y. Transformation from δ -FeOOH to hematite in the presence of trace Fe(II). *Journal of Physics and Chemistry of Solids* 70[1], 186–191 (January 2009).

2 Crystal Growth Inhibition of Calcium Sulfate and Calcium Oxalates in Aqueous Systems

Mualla Oner

CONTENTS

2.1	Introduction	21
2.2	Scale Formation	22
2.2.1	Classification of Inhibitors.....	23
2.3	Mechanism of the Inhibition of Mineral Precipitation.....	23
2.3.1	Growth Rate Retardation.....	24
2.3.2	Nucleation Delay.....	24
2.3.3	Crystal Morphology Modification.....	25
2.4	Theory of Crystal Growth Inhibition	26
2.4.1	Kink Blocking	27
2.4.2	Step Pinning.....	27
2.4.3	Incorporation of Impurities	27
2.4.4	Step Edge Adsorption.....	28
2.5	Calcium Sulfate Crystallization.....	29
2.5.1	Calcium Sulfate Kinetic Models	30
2.6	Calcium Oxalate Crystallization	32
2.6.1	Effect of Additives on Calcium Oxalate Crystallization.....	34
2.7	Summary	35
	References.....	35

2.1 INTRODUCTION

The crystallization of solid material from solution is one of the most frequently used unit operation and one of the oldest separation and purification operations employed in chemical industries. Crystallization determines chemical purity and physical properties of substances including crystal habit, crystal size distribution, crystal structure, and the degree of crystal imperfection. It serves not only to separate and purify substances, but also to produce crystals with the required shape. Models for the growth of crystals by condensation from the vapor are well established, but crystal growth and dissolution from solution is much more complicated. Despite its almost universal applicability, the mechanism involved in many crystallization processes is still not completely understood. Nevertheless, the elucidation of the mechanisms controlling these reactions is extremely important because of their involvement in both industrial and biological processes [1]. Calcium-containing minerals are the most abundant because of their relatively low solubility with ions such as oxalates, sulfates, phosphates, and carbonates [2]. The precipitation of calcium sulfate onto the walls of water-handling equipment, e.g., boilers and heat exchangers, is a serious problem encountered in many industrial processes [3a,b,c,d]. These deposits are formed from salts that are dissolved in the

process feed water. During the process, the process water becomes supersaturated with respect to these salts, which then precipitate out onto equipment walls. The supersaturation of process water usually arises from an increase in temperature or from an accumulation of dissolved salts in recycling stream. These deposits lead to a loss of heat transfer efficiency, to partial or even total blockage of water flow, and are the cause of boiler cracking and boiler explosions [4].

Calcium oxalate monohydrate (COM, $\text{CaC}_2\text{O}_4 \cdot \text{H}_2\text{O}$), the most thermodynamically stable form of calcium oxalate (CaOx) crystals, is the primary constituent of the majority of human kidney stones [5]. Although normal urine is often supersaturated with respect to calcium oxalate, human kidney stone formation is usually suppressed by urinary inhibitors [6]. On the other hand, COM is recognized as a major component of scales formed on the calandria tubes in many cane sugar mill evaporators [7]. The formation of these compounds during the concentration of juice reduces the heat transfer coefficient of the evaporator station.

Several techniques are commonly used to prevent or control scale deposition. These are lowering the pH of the water by adding acids and thus increasing the solubility of scales, pretreating the water with ion-exchange resins, or adding certain chemical substances that inhibit the growth of scale-forming minerals at very low concentrations, such as organic polyphosphonates, inorganic polyphosphates, proteins and polycarboxylates, and polyacrylates [8]. These chemical substances are widely used in industry to control scale because they are relatively inexpensive, or very small quantities are needed. They prevent the buildup of mineral scales by preventing mineral crystals from growing, and therefore are also called inhibitors. This review discusses the principal features of crystallization in relation to the controlled scale formation and crystal growth inhibition of calcium sulfate and calcium oxalates in aqueous systems.

2.2 SCALE FORMATION

Scaling may be defined as solid layer deposition on a surface that arises primarily from the presence of dissolved inorganic salts in the flowing solution that exhibit supersaturation under the process conditions. Scale is formed when hard water is heated or cooled in heat transfer equipment such as heat exchangers, condensers, evaporators, cooling towers, boilers, and pipe walls. The type of scale differs depending on the mineral content of the available water. Many waters contain alkaline earth metal cations (such as barium, strontium, calcium, and magnesium) and anions (such as sulfate, bicarbonate, carbonate, phosphate, and fluoride). When combinations of these anions and cations are present in concentrations that exceed the solubility product of the various species, precipitates form until the respective solubility products are no longer exceeded. Solubility products exceed for various reasons, such as the evaporation of the water phase; change in pH, pressure, or temperature; and the introduction of additional ions that can form insoluble compounds with the ions already present in the solution. As these reaction products precipitate on the surfaces of the water-containing system, they form adherent scales. Scaling presents one of the major fouling problems in almost all chemical industries such as paper mills, food processing plants, electricity generation plants, etc. Water hardness salts such as calcium sulfate and calcium carbonate are the main fouling species during water cooling applications. When the hard water is heated inside heat transfer equipment, the calcium ions precipitate due to the change in solubility, forming hard scale on the heat transfer surfaces and clogging pipes and manifolds [9a,b,c].

In saline water distillation plants, the precipitation of calcium sulfate present in seawater is very common. During water desalination by reverse osmosis membranes, calcium sulfate blocks the membranes [10]. Even small quantities of these salts in the boiler feed water cause a significant increase in power consumption. Scale formation is a big problem in the petroleum industry because water constantly dissolves and deposits solids. The economic loss due to fouling is one of the biggest problems in all industries dealing with heat transfer equipment [11]. Scales are responsible for many equipment failures, production losses, costly repair, and maintenance shutdowns. In some industries, the periodic cleaning of heat transfer surface is routinely practiced, leading to high operating

cost. Periodic descaling has an adverse effect on the process economics and equipment involved. Tens of millions of dollars are spent every year to prevent the formation of mineral scales or to remove them once they have occurred in the field. Therefore, effective methods of prevention and control will require specialized mechanical and chemical treatment techniques and better knowledge of the causes of scaling.

2.2.1 CLASSIFICATION OF INHIBITORS

The crystallization processes are influenced by a variety of factors such as the supersaturation, solution temperature, stirring rate, and presence of additives. Among the many factors affecting the process of crystallization, impurities often exhibit the most pronounced effect. Early studies established that although a large number of inorganic and organic compounds have no effect on crystallization, there are several groups of chemicals that are effective in varying degrees. The compounds included (a) a few low molecular weight chemicals such as free acids or bases, including boric, succinic, citric, and tartaric acids (acids or bases most frequently used usually have a common ion with the crystallizing substance); (b) inorganic inhibitors such as polyvalent cations (e.g., Fe^{3+} , Cr^{3+} , Al^{3+} , Cd^{2+} , Pb^{2+}) and anions (e.g., WO_4^{2-} , PO_4^{3-}); (c) organic additives such as surface-active substances or organic dyestuffs; (d) protein-type materials including gelatin and keratin; and (e) long-chain polymers with carboxyl side chains, such as alginic acid, carboxymethylcellulose, polyacrylic acid, and polymethacrylic acid. The charge on the functional groups was discovered to be of key importance. Anionic polyelectrolytes were often found to be effective inhibitors, uncharged polymers (such as polyacrylamide) much less effective, and cationic polymers completely ineffective [8].

2.3 MECHANISM OF THE INHIBITION OF MINERAL PRECIPITATION

A well-established fact in crystallization is that the presence of additives or some foreign ions and molecules can profoundly affect nucleation and measured crystal growth rate, as well as crystal morphology, without significant changes in the solubility. Even if the additives are present in such low concentrations, their effect may still be significant. It is generally agreed that the presence of effective additives tends to reduce the crystal growth rate, and various index faces may be affected differently and may lead to a modification of crystal habit. However, the effects of additives on crystal morphology and nucleation rate are not easily predictable. In all cases, a required first step of interaction between additives and the crystallizing species is the adsorption of the additives on the surfaces of crystal or pre-nuclear cluster.

Additives can influence the rate of crystal growth in a number of ways. The marked effect of inhibitors on the crystal growth from supersaturated solution has been explained in terms of the following factors [12a,b,c,d]: (a) They can change solution properties, such as changing of the ionic strength of the solution. (b) The equilibrium saturation concentration and hence the supersaturation. The inhibitors may form stable complexes with one or more lattice ions of the potential scale-forming salt, thus reducing the effective concentration of free ions necessary for crystallization. This mechanism requires relatively large amounts of the inhibitors. (c) The adsorption of the inhibitor on the crystal surfaces, either generally or at the growth sites. The characteristics of the adsorption layer at the crystal–solution interface affects the integration of growth units. This surface poisoning effectively prevents or slows further growth of the crystallites so they never reach critical size and consequently will eventually redissolve. (d) The outer crystal surface property if they incorporate into the growing crystals.

Generally, the effective crystallization inhibitors retard precipitation by the third process, by adsorption. This is shown by the extremely small amounts of these chemicals that are required to prevent nucleation and/or growth. It is not necessary for the impurity to cover the whole surface. Large reductions in crystal growth may still occur if these sites are selectively “poisoned” by adsorbed impurities. The small degree of crystallite surface coverage by inhibitor molecules

for effective inhibition has been documented by Nancollas and Zawacki [2b] who found that 5% coverage of gypsum seeds by hydroxyethylidene diphosphonic acid completely prevented growth on the seeds. The small amount of additive required to prevent nucleation suggests that sequestering is not the inhibiting process because much larger amounts of sequestering agent would be required. Experiments have shown that adsorption is often on specific sites; for example, experiments with calcite growth have shown that growth is completely prevented by inhibitor concentration in which less than 1% of the crystal surfaces would be covered by the additive [2a]. Several workers have suggested that additive molecules prevent crystal growth by being adsorbed firmly at growth by lateral movement. Therefore, very small amounts of strongly adsorbed substances could retard or prevent growth by affecting the motion of the growth steps [13].

2.3.1 GROWTH RATE RETARDATION

The effects of additives on crystallization rate are variable. They can retard crystal growth or increase crystal growth rates [14]. Furedi-Milhofer and Walton [15] wrote that crystal growth is inhibited when the adsorption kinetics are slower than the molecular exchange between the crystal and the mother liquor. On the other hand, for weak adsorption, when interaction between the adsorbate and the solution is faster than between substrate molecules and the environment, additives do not actually block the surface but lower the surface free energy of the nucleus or crystal face. As a consequence of lowering surface energy, the activation energy for nucleation or growth should decrease and the rate of the respective process increases on additive adsorption. It was reported that the additive both promotes growth (at low concentrations) and retards growth (at higher concentrations) in the same system [16]. In most cases, however, the presence of additive reduces the overall crystal growth rate.

In three-dimensional nucleation crystal growth is inhibited by additive adsorption because the kinetic factors decrease more rapidly than the thermodynamic factors. Additives may also decrease the growth of crystal faces by partially blocking the surface and hindering the approach and incorporation of growth molecules. While additives may be effective at extremely low concentrations, they are generally more effective at increased concentrations and also at decreasing supersaturation [17,18].

A way to think about crystal growth rate retardation by additives is to envision the phenomenon of surface adsorption of the additives, which reduces the area of crystal surface available for growth. An alternative view is that the adsorption of additives on various sites on a crystal face impedes the flow of growth layers and thus reduces the overall growth rate. The rates of additive adsorption and desorption relative to the deposition rate of crystallizing molecules are important considerations when studying the retardation effect. The ratio of additive adsorption rate to additive desorption rate is a measure of additive affinity on a particular surface. For relatively weak adsorption, the crystal growth rate is retarded, but no additive incorporation occurs according to Mullin [16]. When adsorbed, the additives retard crystal growth temporarily, but they soon desorb, and normal growth resumes. This sequence of additive adsorption and desorption contributes to intermittent crystal growth retardation.

2.3.2 NUCLEATION DELAY

Impurities may either enhance nucleation or suppress it by interfering with the formation of stable embryos. The parameter generally used to quantitate nucleation efficiency is the nucleation rate. Any significant change in the nucleation rate is usually viewed as evidence of additive action. Rodriguez-Hornedo [19] cites two possible processes by which additives affect nucleation through adsorption. Adsorption of additives on the surface of pre-nuclear clusters or embryos reduces the rate at which they pass through the critical size barrier, thereby decreasing the nucleation rate. However, adsorption also reduces the solid-liquid interfacial tension, which enhances the rate of embryo formation,

and hence increases the nucleation rate. The presence of foreign particles in a melt decreases the free energy of formation of a critical nucleus. As a result, the rate of nucleation should increase [20]. It is difficult to assess the combined effect of these two processes. Thus, the effect of impurities is complex and unpredictable. Several experimental investigations have been undertaken to clarify this situation [21] but no quantitative model has been proposed to predict these impurity effects on the nucleation process.

The measurement of nucleation rate is difficult. A more common method to evaluate the effect of additives on nucleation is to measure their abilities to affect the induction period of nucleation. Nucleation kinetics is experimentally determined through experimental measurements of nucleation rates, induction times, or metastability zone widths (i.e., supersaturation necessary for spontaneous nucleation) as a function of initial supersaturation. There is usually a period of time that elapses between the achievement of supersaturation and the observation of the first nuclei or crystals, which is often referred to as the induction or the initiation period [22]. Crystal nuclei are in the nanometer range, and therefore the precise onset of nucleation is difficult to detect. Induction time is a measure of the effectiveness of an additive in inhibiting crystallization [23].

2.3.3 CRYSTAL MORPHOLOGY MODIFICATION

The ability to produce crystals with the desired morphology is very important in industrial crystallization. Certain characteristics of crystal morphology are considered undesirable for commercial purposes due to poor appearance, poor flow property, and handling difficulty. In most cases, crystals possessing granular or prismatic shape are desirable, but occasionally needlelike or platelike crystals are wanted. Monitoring the changes in morphology by visual examination can be a powerful tool when troubleshooting crystallization problems. The appearance of crystals with a different morphology is indicative of changes in the processing conditions such as the degree of supersaturation, rate of heating or cooling, or the presence of impurities.

The observation of crystals grown from solution is often quite different from the prediction by the model. For crystals grown in solution, their shape will depend on kinetic factors that are affected by crystal defects, surface roughening, solvent type, supersaturation temperature, impurities in the solvent, and other solution conditions. These environmental conditions affect the growth of a given face. The external shape or morphology of a crystal is a consequence of the relative growth rates of the faces, and reveals the molecular events occurring at the solid–liquid interfaces during growth. The morphological importance of a crystal's face is inversely proportional to its growth rate. Based on these concepts, a standard way of identifying the influence of additives on nucleation or growth is to investigate the relationship between crystal morphology and the growth conditions.

The morphology of some crystals can be modified by introducing selective additives to the crystallizing medium. The basis of the additive action is contingent on the adsorption of the additive on specific crystal faces that results in growth hindrance of the affected faces. Crystal morphology modification can thus be achieved through deliberate growth suppression of selective crystal faces. Crystal morphology modification by selective additive adsorption is essentially a surface phenomenon. Due to lattice orientation, different crystal faces may possess different surface groups that impart different surface properties to each face. Therefore, the adsorption affinity for an additive may vary with each face. If an additive or impurity selectively adsorbs to a crystal face, the growth rate of that face will be altered, resulting in a change in crystal morphology. There has been work exploiting the selective interaction of additives with crystal faces in order to tailor the crystal morphology to a more favorable crystal habit [24]. Berkovitch-Yellin et al. [24] used tailor-made additives to probe the surface chemical structure of organic compounds by studying their effects on crystal morphology.

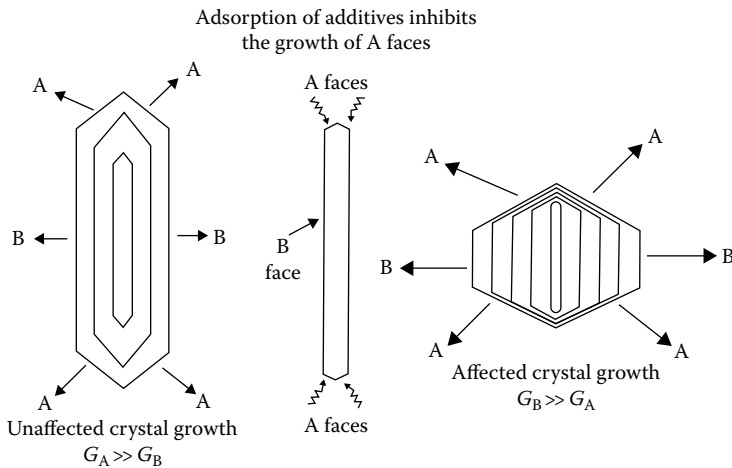


FIGURE 2.1 Effect of additive adsorption on crystal morphology.

The most elegant and thorough studies on this subject were carried out by a solid-state group at the Weizmann Institute [25]. A series of small molecule inhibitors were systematically designed to illustrate the crystal inhibitor recognition at the molecular level. Such inhibitors were adsorbed on specific crystal planes at lattice sites where part of the molecule that is identical to the substrate molecule could fit into the regular arrangement of the surface layer (Figure 2.1). The remainder of the inhibitor molecule, which did not fit into the lattice site, stuck out of the surface and acted as a barrier to disrupt the regular deposition of the subsequent layer, thereby slowing growth in this direction. Since crystal habit is determined by the relative growth rates of the crystal along different directions, this provides a powerful way to engineer crystal morphology. Conversely, information about the crystal planes specifically interacting with inhibitors can also be deduced by the analysis of the morphological change by the inhibitors [26].

2.4 THEORY OF CRYSTAL GROWTH INHIBITION

Although the effect of inhibitors on crystal growth has been known for a long time, the theoretical framework for the crystal growth inhibition is only slightly developed [16,27]. Few rate laws for crystal growth in the presence of inhibitors are actually used by experimentalists to describe their rate data. Furthermore, most of the experimental work is qualitative.

In many instances, small amounts of impurities can have dramatic effects on crystal growth, morphology, and nucleation. To explain the large effect of some impurities at the part per million levels on nucleation and crystal growth, the presence of key growth sites dominating the growth process on the surface must be invoked. The process of crystal growth is a phase transition, the ions or molecules that the crystal is made of are going from one state (the fluid phase) where they are dissolved in a fluid to another state (the solid phase) where they are part of the crystal lattice. This process takes place at the interface between the crystal and the fluid, which is called the surface of the crystal. Kossel [28] was one of the first investigators to recognize the importance of atomic inhomogeneities of crystalline surfaces and its relevance to the growth process. As illustrated in Figure 2.2, the Kossel model divides the crystal interface into three regions: (a) flat surfaces, or terraces, which are atomically smooth, the relatively large and flat areas between steps, (b) steps, which are the terminations of one or more monolayers of the crystal lattice on the crystal surface and separate terraces, and (c) kinks, which are the terminations of individual rows of lattice ions in steps.

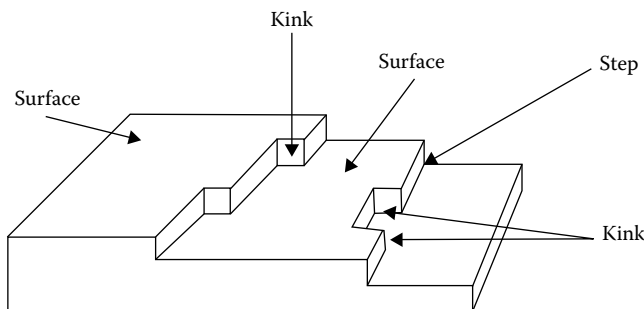


FIGURE 2.2 Kossel's model of a growing crystal surface showing energetically favorable sites for integration.

During crystal growth, the lattice ions or molecules (also called growth units) have to undergo a sequence of consecutive steps [29]. Dove et al. [30] proposed four mechanisms by which ions or molecules can modify or inhibit growth hillocks: (a) kink blocking, (b) step pinning, (c) incorporation, and (d) step edge adsorption (needs clarification of surfactant). Each of these mechanisms shows a characteristic dependence of step speed on supersaturation and impurity concentration.

2.4.1 KINK BLOCKING

Kink blocking occurs when an impurity adsorbs to a kink site, leading to a reduction in kink density. Kossel hypothesized that kink sites present the most probable position for solute integration due to the higher bonding energy associated with integration. The effect is highly dependent on step-impurity interactions and can result in a change in crystal shape.

2.4.2 STEP PINNING

The inhibitor molecules or ions adsorb onto terrace sites or directly onto step sites of a growing crystal where they impede the advancement of that step. Steps correspond to the intermediate binding energy and terrace the lowest, and as the result are energetically less probable sites for incorporation. The step, however, is able to move around and squeeze through neighboring inhibitors as long as the distance between adsorbed inhibitors is larger than a critical radius for the step (critical radius in this case being the smallest amount of linear area in which the step can continue to grow). Step pinning is highly dependent on details of impurity-step interactions. Therefore, ions or molecules that may block one step may have no effect on the other steps. It is in this way that step pinning can lead to a drastic change in the hillock and overall crystal shape. Since the growth process consists of a surface diffusion of solute, diffusion along the step to a kink, and incorporation into the lattice at the kink site, the concentration of the kinks and steps become a fundamental quantity in the growth process [31]. It has been observed that the sources of steps are nearly always present on the crystal surface when crystals grow at exceedingly small supersaturations. This problem of the creation of steps was solved by Burton et al. [32] who proposed the existence of crystal dislocations that can provide a continuous source of steps on the surface. The resulting layer growth model considers two simultaneous processes at the surface: (a) the continuous creation of steps at the source of dislocation sites and (b) motion of steps away from the source [31]. Based on the layer growth model, the impurity adsorption, even at low concentrations but still high enough to poison kinks, can have a dramatical influence on the growth of crystals [23].

2.4.3 INCORPORATION OF IMPURITIES

Impurities adsorbed on the crystalline interface can reduce the growth rate by reducing or hindering the movement of steps on the crystal surface. Depending on the amount and strength of adsorption, impurities can be completely immobile to completely mobile on the crystal surface. The strength

of bonds between the lattice molecules and the impurity determines the relative mobility of the impurity. In general, strongly adsorbing impurities are expected to have a much greater effect on the growth rate of crystals than impurities that tend to be less strongly bound.

Immobile impurities impede the movement of steps and may become incorporated as steps move around and pass them. Incorporation occurs when ions or molecules become captured by advancing steps or are incorporated into kink sites to become part of a growing crystal. However, incorporation does not always lead to an inhibition in growth rates; at sufficiently low concentration, growth can be promoted. This is because the impurity always increases the entropy of the solid, making the solid more stable and thus decreasing its solubility. Incorporation mechanisms can change crystal shapes when they incorporate into adjacent steps at different rates. The result is a crystal with sharp divisions in impurity content at the boundaries of two different step directions. These variations lead to a lowering of effective supersaturation and thus inhibit growth.

2.4.4 STEP EDGE ADSORPTION

Adsorption of surfactants to the crystal surface can modify many aspects of the crystal surface by lowering the interfacial energy between the solid and the surrounding liquid. Impurities that adsorb to step edges have similar effects, inhibiting the growth of steps by lowering the step-edge energy. Orme et al. [33] showed that the shapes of the growth hillocks are altered in the presence of citrate. This result provides evidence for the lowering of interfacial energy. The advent of atomic force microscopy (AFM) shows great promise in providing direct insights into crystal growth processes. It will provide information needed to refine existing theories and lays a foundation for new theories based on the experimental observation of actual crystal faces [33]. The classical theory of crystal growth is based on some fundamental ideas advanced several decades ago mainly by Burton, Cabrera, and Frank. In spite of the ever-increasing research effort, however, no new basic concepts have been introduced since that time. A more detailed description and derivation of this concept can be found in Davey [23], Davey [34], Sears [35], and Cabrera and Vermileya [36].

The growth rate in the presence of inhibitors is assumed to be proportional to the number of active growth sites that are not blocked. The fraction of growth sites that are blocked by the inhibitor is obtained using the Langmuir isotherm. This approach to describe crystal growth inhibition is often used by researchers to model their rate data. The rate of crystal growth in the presence of inhibitors thus obtained is

$$\frac{R_0}{R_0 - R_i} = 1 + \frac{k_{\text{des}}}{k_{\text{ads}}} \frac{1}{C_i} \quad (2.1)$$

where

R_0 and R_i are the growth rates in the absence and presence of inhibitors, respectively

C_i is the inhibitor concentration

$k_{\text{ads}}/k_{\text{des}}$ can be considered as a measure for the adsorption affinity of the inhibitor for the crystal surface

The rate law for crystal growth in the presence of inhibitors in its simplest form is [36]

$$\frac{v_i}{v_0} = \left[1 - r_c (\theta_i n_{\text{max}})^{1/2} \right]^{1/2} \quad (2.2)$$

where

v_i and v_0 are the step velocities on the crystal face in the absence and presence of inhibitors

r_c is the critical radius of the 2D nucleus and corresponds to the critical distance

n_{max} is the number of sites available for adsorption per unit area

θ_i is the coverage of adsorption-active sites and is a function of inhibitor concentration in solution

Variations of crystal growth inhibition can be found in Cabrera and Vermileya [36], Van der Leeden et al. [37], Ohara and Reid [38], and Füredi-Milhofer and Sarig [39]. More recently, Kubota and Mullin developed a new kinetic model for crystal growth in the presence of impurities [40]. The model describes the adsorption of an impurity along steps. It assumes that the step velocity decreases linearly with increasing surface coverage by impurities adsorbed on the growing crystal and introduces an impurity effectiveness factor, α , for the impurity adsorption.

In the case of a spiral growth mechanism, the relationship between the relative growth rate, R_i/R_0 , and the fraction coverage, θ_i , of the surface in the presence of an impurity may be given by [40]

$$\left(\frac{R_0 - R_i}{R_0}\right)^n = \alpha^n \theta_i \quad (2.3)$$

The exponent $n = 1$ represents the case at which impurity adsorption occurs at kinks in step edges as in the Kubota–Mullin model and $n = 2$ represents adsorption on surface terrace as in the Cabrera–Vermileya model. θ_i is the coverage of adsorption-active sites, and may be described by the Langmuir adsorption isotherms:

$$\theta_i = \frac{KC_i}{1 + KC_i} \quad (2.4)$$

In Equation 2.4, K is the Langmuir constant given by [41]

$$K = \exp Q_{\text{diff}}/RT \quad (2.5)$$

where Q_{diff} is the differential heat of adsorption corresponding to impurity coverage θ_i of the available adsorption sites.

Using Equation 2.3 in combination with the Langmuir isotherm Equation 2.4 we can write the following equation, linear in $(1/C_i)$:

For $n = 1$

$$\left(\frac{R_0}{R_0 - R_i}\right) = \frac{1}{\alpha} \left(1 + \frac{1}{KC_i}\right) \quad (2.6)$$

For $n = 2$

$$\left(\frac{R_0}{R_0 - R_i}\right)^2 = \frac{1}{\alpha^2} \left(1 + \frac{1}{KC_i}\right) \quad (2.7)$$

Recently, the data on the growth kinetics of COM crystals in the presence of polyelectrolytes were examined by using Equations 2.6 and 2.7 [42]. It was found that Langmuir adsorption isotherm do not differ substantially when impurity adsorption is considered at kinks (Kubota–Mullin model) and on the surface terrace (Cabrera–Vermileya model).

2.5 CALCIUM SULFATE CRYSTALLIZATION

The growth of calcium sulfate dihydrate or gypsum is of considerable importance since it is frequently encountered both in nature and in industrial processes. Large quantities of gypsum are produced as a by-product in the production of phosphoric acid. The problem of scale formation on

the heat exchanger, reverse osmosis membrane surface, and equipment surface is a persistent and an expensive problem in cooling water systems, boilers, and secondary oil recovery utilizing water-flooding techniques, desalination by evaporation, and reverse osmosis methods [43]. The effectiveness of a number of additives in preventing or reducing the crystallization of calcium sulfate from supersaturated solution has been the subject of numerous investigations [44,45]. The first recorded use of chemicals for calcium sulfate scale suppression was reported by Rosenstein [46]. Some 30 years later, McCartney and Alexander [47] have examined the number of polyelectrolytes on the growth rate of calcium sulfate dihydrate. It was found that polymers containing carboxyl ($-\text{COOH}$) groups such as carboxymethyl cellulose, aliginic acid, polymethacrylic acid, and polyacrylic acid were the most active inhibitors due to their ability to preferentially adsorb on the active growth sites of gypsum crystal faces, while polyacrylamide had little effect, and polycationic additives had no effect at all. The precipitation of $\text{CaSO}_4 \cdot 2\text{H}_2\text{O}$ in the presence of trace amounts of polyphosphates and phosphonates has been studied by Liu and Nancollas [12a]. It was reported that trace amounts of phosphonates can stabilize supersaturated calcium sulfate solutions and lengthen the induction period before the onset of crystallization. The precipitation of gypsum in the presence of polyglutamic acid (PGA) and polyvinyl sulfonate (PVS) has been investigated by Sarig et al. [48]. These authors concluded that PGA was more effective than PVS as a gypsum growth-retarding agent because the carboxylic functional groups in PGA is structurally more compatible with $\text{CaSO}_4 \cdot 2\text{H}_2\text{O}$ than the sulfonic groups in PVS. It was concluded that the most efficient crystal growth inhibitor will be an inhibitor that is structurally well fitted to the crystal lattice of the growing crystals. Subsequent studies on the use of chemical additives for the inhibition of mineral salt crystal formation have demonstrated the relative efficiency of various polyelectrolytes on the retardation of crystal growth. For gypsum it has been measured that a surface coverage of only a few percent with phosphonate-inhibitor ions is already sufficient to achieve total blockage of the crystal growth process [49a,b]. Prisciandaro et al. [50a] have studied the effect of nitrilotrismethylene phosphonic acid (NTMP) on calcium sulfate dihydrate nucleation at 25°C in a batch crystallizer. They found that NTMP is more effective retarding gypsum nucleation than citric acid. Moreover, the addition of NTMP modifies the crystal habit from the needlelike form to a less elongated one. El-Shall et al. [51] studied the effect of NTMP on gypsum nucleation and found that NTMP increases the induction time at all studied supersaturation ratios. A number of papers reported that the calcium sulfate dihydrate formation is reduced in the presence of additives such as polyelectrolytes [3a,52], citric acid [50b], and organophosphorus compounds [53]. Klepetsanis and Koutsoukos [54] found that the rate of precipitation was reduced by 90% at a concentration below $1\ \mu\text{M}$ of organophosphorus compounds. Oner et al. [52a,b] reported that the adsorption of polyelectrolytes depends on the sign of the charge on the polyelectrolytes and on the solid surface. The larger number of negatively charged functional groups increases the attraction between the adsorbate and the positive sites at the precipitate solution interface. Weijnen et al. [49c] found that the presence of sulfonic or phenylsulfonic acid groups in a polymer reduces the inhibitory function of the polyelectrolytes on the crystal growth of gypsum.

2.5.1 CALCIUM SULFATE KINETIC MODELS

The kinetics and mechanism of calcium sulfate crystallization have been studied extensively over the years by a number of researchers. Despite this growing body of literature there is significant uncertainty regarding the order of the crystal growth kinetics. Schierholtz [55] conducted spontaneous crystallization studies by mixing equimolar amounts of calcium hydroxide and sulfuric acid at 10°C , and raised the experiment temperature of the solution to 25°C whereby precipitation occurred. Schierholtz reported a first-order growth rate, $n = 1$, suggesting diffusion controlled growth but the plot of his experimental results showed considerable deviations from linearity. McCartney and Alexander's results [47] gave second-order plots for part of the crystallization range. Packter [56] conducted homogeneous crystallization experiments using equivalent calcium nitrate solution and

sodium sulfate solutions at 0.02–0.24 M under constant stirring at 100 rpm at 22°C and obtained a rate order of $n = 9–10$. Nancollas [57] argued that spontaneous crystallization studies conducted using the above method for sparingly soluble salts were difficult to reproduce, and demonstrated that by using the seeded growth technique for gypsum crystallization, excellent reproducibility was obtained suggesting that $n = 2$. Tadros and Mayes [58] studied the structure of forming gypsum crystals with Polaroid photomicrographs, in the presence of carboxylic and phosphonic acid derivatives by mixing sodium sulfate and calcium chloride. They concluded that gypsum crystallization followed second order with respect to concentration ($n = 2$), which they suggested was indicative of a polynuclear layer reaction-controlled growth mechanism. Klepetsanis and Koutsoukos [59] studied the precipitation of calcium sulfate dihydrate at constant activity. The kinetics of precipitation was found to be independent of pH, and the order of reaction of $n = 4$ for the precipitation process was found from the kinetics based on the initial rates. He et al. [60] studied the seeded crystal growth rate of calcium sulfate dihydrate. They found that the growth followed a second-order parabolic rate law. Attempts to model gypsum precipitation, as discussed above, showed that the reaction-rate order seemed to be specific to the experimental system and the experimental conditions employed in the study.

Smith and Sweett [13] studied the bulk crystallization of calcium sulfate dihydrate from aqueous solutions at 30°C in the absence of added seed crystals by using a dilatometer, and indicated that nucleation was heterogeneous. It was found that the growth rate was proportional to the crystal surface area and to the square of the supersaturation. It was observed that nucleation is complete in a very short time after solution preparation, which suggests heterogeneous rather than homogeneous nucleation. They performed seeded experiments at a range of temperatures from 50°C to 90°C, and based on the extracted reaction rate constant results a value of 63 kJ/mol was reported for the activation energy of crystallization process. They pointed out that in general, whenever the surface area of the crystals changes significantly during the growth, it is necessary to incorporate its effect. They adopted a model to consider the crystal surface area changes during the crystallization process. The model starts with the following equation:

$$S_c = S_0(M/M_0)^{2/3} \quad (2.8)$$

where

M and M_0 correspond to the mass of crystals at any time t and the initial mass of the crystals, respectively

S_c and S_0 correspond to the surface area of crystals at any time t and the initial surface area of the crystals, respectively

It was assumed that the shape of the growing crystals remains invariant during the growth process. They incorporated Equation 2.8 into a variety of kinetic models

The crystallization of calcium sulfates on the addition of seed crystals to stable supersaturated solutions has been investigated by Nancollas [57]. It was concluded that a sufficient number of growth sites must be provided initially for uncomplicated second-order growth, otherwise new sites must be generated by nucleation. A geometric mean model that is based on the geometric mean of the concentrations of the ions was proposed:

$$-r_A = A_c k_R \{ [Ca^{2+}]^{1/2} [SO_4^{2-}]^{1/2} - K'_s \}^2 \quad (2.9)$$

where A_c and k_R are the total crystal surface area and reaction rate constant, respectively. K'_s , the ionic solubility product based on concentration, can be expressed as

$$K'_s = [Ca^{2+}]_s \cdot [SO_4^{2-}]_s \quad (2.10)$$

If depositing species are in stoichiometric proportions, then

$$-r_A = A_c k_R (C_A - C_S)^2 \quad (2.11)$$

Hasson [61] discussed an ionic product model for calcium sulfate precipitation. The model considers the following crystallization reaction:



By analogy to an elementary reversible chemical reaction that can be expressed as

$$-r_A = A_c k_R \{ [\text{Ca}^{2+}] \cdot [\text{SO}_4^{2-}] - K'_s \} \quad (2.13)$$

when the depositing species are in stoichiometric proportions, then

$$-r_A = A_c k_R (C_A^2 - C_S^2) \quad (2.14)$$

Konak [62] proposed a different model for surface-reaction-controlled growth of crystals from solution. It was based on a concept of “traveling” steps instead of surface diffusion of adsorbed growth units. He concluded that the growth rate is a function of supersaturation, $(C_A - C_S)$, rather than of supersaturation concentration, C_A , itself, and in almost all cases measured growth rates can be satisfactorily correlated by an equation of the form

$$\text{Rate} = K(C_A - C_S)^n \quad (2.15)$$

It was shown how to take into account the mass transfer effects in the general case of solution growth. He used a power law model in the form

$$-r_A = A_c k_R (C_A - C_S)^P \quad (2.16)$$

where P is an experimentally fitted parameter, and for calcium sulfate precipitation, it can be written as

$$-r_A = A_c k_R (C_A - C_S)^2 \quad (2.17)$$

which is in agreement with Nancollas [57]. Many researchers have integrated the above expression for batch systems, which yields a simple linear relationship between $(C_A - C_S)^{-1}$ and time t , and is useful for kinetic parameter evaluation.

2.6 CALCIUM OXALATE CRYSTALLIZATION

Crystallization studies of calcium oxalate (CaC_2O_4 , CaOx) have been of interest to engineers and urologists for several years [63]. Its precipitation is of particular dual interest to the biomineralization community [64] and also to industrial crystallization applications' area [65]. Calcium oxalate is a naturally occurring mineral found in fossils [66], plants [67], and mammal urinary calculi [68], and is a by-product in some processes such as paper [69], food [70], and beverage processing [71]. In water-related industries, calcium oxalate forms scale deposits on critical industrial equipment, such as heat exchangers, boilers, and reverse osmosis membranes. Calcium oxalate monohydrate (COM) and calcium oxalate dihydrate (COD) are found to be the main components of the composite scale formed in the multi-effect evaporator during juice concentration [7].

Urolithiasis, the formation of urinary calculi, is one of the oldest documented diseases known to man. CaC_2O_4 forms as a crystalline material in the urinary tract, and is the majority constituent in kidney, gall, and bladder stones [72,73]. Although normal urine is often supersaturated with respect to calcium oxalate, the formation of human kidney stones is strongly prevented by acid-rich urinary proteins [74] and naturally occurring citrate [75], magnesium [76], osteopontin [77], Tamm-Horsfall protein [78], a plethora of polycarboxylic acids [79], copolymers of polyacrylic acid [80], phosphonates [81], or even unidentified biomacromolecules [82].

Calcium oxalate is known to crystallize in three hydrated forms: thermodynamically stable monoclinic monohydrate (COM) ($\text{CaC}_2\text{O}_4 \cdot \text{H}_2\text{O}$, whewellite); metastable tetragonal dihydrate (COD) ($(\text{CaC}_2\text{O}_4 \cdot (2+x)\text{H}_2\text{O}, x < 0.5)$, weddellite); and triclinic trihydrate (COT) ($\text{CaC}_2\text{O}_4 \cdot x\text{H}_2\text{O}, 3 > x > 2.5$; COT). COM is thermodynamically the most stable phase, and has the strongest affinity for renal tubule cell membranes among the three kinds of crystals [83]. COM is easy to form urinary stones because it is more difficult to be ejected out along with urine than COT or COD. COD is also found frequently in kidney stones, plants, and fossils, although usually in lesser quantities [84]. While COT has never been observed in a renal stone, it may act as an important precursor-nucleating phase for the initiation of calculus formation [85]. The transformation reactions of the metastable COD and COT phases into the thermodynamically stable COM may be of extreme importance in urolithiasis, since in many cases, kinetic factors, rather than thermodynamic stabilities, determine the phase that initially precipitates in the solution. Hence, an in-depth understanding of CaOx crystallization processes is essential for urologists, and may augment an effort to develop effective therapeutic agents against stone formation.

Several studies have shown that COM, COD, and COT differ substantially in solubility, structure, morphology, and specific surface area [86a,b,c]. COM, or whewellite, is the thermodynamically most stable calcium oxalate phase. The hydrate content is fixed at one water molecule per calcium, and is not found to vary in synthetic or natural samples. The crystal habit of the monohydrate is given in Figure 2.3. Whewellite crystallizes in a monoclinic structure, space group $P2_1/c$. COD, or weddellite, is a major constituent of urinary crystallites and calcium oxalate renal calculi [87]. COD has a tetragonal structure with a space group of $I4/m$ and a crystal habit that can be best described as tetragonal bipyramidal [88]. Crystallographic data indicate that weddellite has a basic hydrate content of 2 mol of water per mole of calcium [89]. An additional amount of water, up to 0.50 moles (per calcium) may be held zeolitically. As a result, the total water content of COD may vary between 2 and 2.5 per mole of calcium. In comparison to whewellite, calcium is bound to one less oxalate group and one more water molecule. If calcium dehydration and the subsequent oxalate coordination

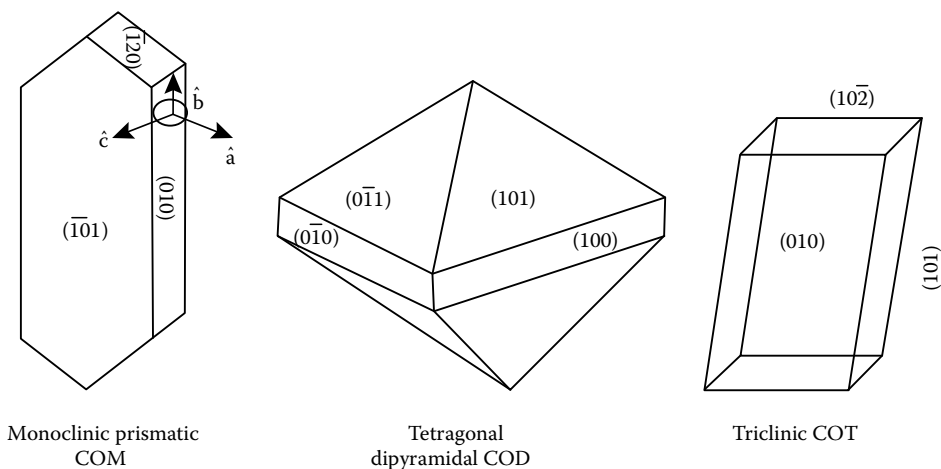


FIGURE 2.3 Crystal habits of calcium oxalates.

are considered as important steps in the calcium oxalate precipitation reaction, then the dihydrate could be considered as a precursor to monohydrate, due to its incomplete dehydration. The dihydrate is considerably more soluble in aqueous solutions than COM, and forms much smaller crystallites during precipitation. In solutions free from inhibitors, COD rapidly undergoes transformation to COM. The mechanism of stabilization of weddellite by synthetic and natural inhibitors may be of extreme importance in urolithiasis, and is currently the subject of considerable research interest.

A number of natural and synthetic molecules have been shown to promote the precipitation of COD from *in vitro* supersaturated solutions. COT is the least stable hydrate phase of calcium oxalate in solution. While COT has never been observed in renal stone, it may act as an important precursor-nucleating phase for the renal calculi. Many natural and synthetic molecules have previously been observed to stabilize COT precipitation in supersaturated solutions *in vitro* [90]. If COT initiates stone formation, it unquestionably transforms to COM rapidly *in vivo*, thus making its identification as a stone precursor difficult. The crystal habit of CaOx is given in Figure 2.3.

2.6.1 EFFECT OF ADDITIVES ON CALCIUM OXALATE CRYSTALLIZATION

Earlier work on the kinetics of calcium oxalate precipitation by Nielsen [91] suggested that the rate-determining step in the precipitation of calcium oxalate is a reaction in the surface of the crystals at a concentration below 1 mM. The reaction order was found to be between 3.0 and 3.5. It was reported that the rate is determined by diffusion at a concentration above 1 mM. Nancollas [92] studied the growth of COM crystals in stirred suspensions by following the changes in ionic conductivity in supersaturated solutions. The quadratic expression for the rate of growth of calcium oxalate in supersaturated solutions was used to describe the results of the experiments. Tomazic and Nancollas [86b] discussed the kinetics of crystallization of COM, COD, and COT in calcium oxalate supersaturated solutions. It was found that the rate of crystallization is proportional to the square of the relative supersaturation for all three hydrate phases. Rizkalla and Moawad [93] studied the kinetics of precipitation of COM conductometrically for both spontaneous and seeded growth systems. It was found that the rate of growth follows a quadratic dependence upon the relative supersaturation, which suggests a surface-controlled mechanism. Singh et al. [94] investigated the kinetics of crystal growth of COM on seed crystals by using constant composition method. The initial linear growth curves were analyzed in terms of a parabolic rate law. It was suggested that the applicability of the parabolic rate law indicates a spiral dislocation mechanism.

A large number of reports have appeared in the literature on the effects of various additives on calcium oxalate crystallization. These researchers include maleic acid copolymers [95], polyaspartic and polyglutamic acids [96], acrylic polymers [97], poly-(styrene-*alt*-maleic acid) [98], tartrates [99], diisooctyl sulfosuccinate [100], uric acid [101], and poly(sodium 4-styrene-sulfonate) [102]. The effect of pyrophosphate and phosphonate anions on the spontaneous formation of COM, COD, and COT has been studied in supersaturated solutions [103]. The rate of crystal growth in the presence of these additives was found to be dependent on the square of the solution supersaturation. The influence of histidine, serine, tryptophan glutamic acid, and ornithine on the formation and transformation of calcium oxalate crystals has been investigated by Brecevic and Kralj [104]. Tryptophan and histidine promote the formation of COD over COM. Manne et al. [105] studied the effect of anionic polyelectrolytes on the crystallization of calcium oxalate hydrates. They found that regardless of the character of the polyelectrolytes (carboxylate or sulfonate), as the polymer concentration increases there is shift from monohydrate to trihydrate and to dihydrate. The effect of ethylene diammine tetracetic acid, citrate, and phytate on the growth kinetics of COM has been studied by Millan et al. [106]. Phytate has been confirmed as a powerful inhibitor of COM, EDTA acts at the bulk level, and citrate shows weak effect at bulk and crystal surface levels. Öner et al. found [107] that the high binding affinity of the biopolymer molecules resulted in morphological transition of COD crystals from tetragonal bipyramids dominated by the (101) faces to elongated tetragonal prisms dominated by the (100) faces.

A number of important observations point to the way carboxylate-containing macromolecules may affect CaOx crystallization. Elegant works by Ward et al. (with AFM) [108] and by Kim et al. (with scanning electron microscopy and x-ray diffraction) [109] have focused on studying the interactions of polymers with pendant carboxylate groups (polyacrylate, polyaspartate, and polyglutamate), with various crystallographic planes of COM crystals. These studies revealed the importance of cooperative binding of the polymer carboxylate groups to Ca²⁺ sites on the crystal surfaces of the “steps.” Specifically, when growth of the (001) and (021) hillocks was studied, it was documented that the ranking of polymeric inhibitors was polyacrylate > polyaspartate > polyglutamate. Polyacrylate was also a potent inhibitor of growth on the (021) and $12\bar{1}$ planes. Data also revealed that polyglutamate was more effective than polyaspartate for both (021) and $12\bar{1}$ planes. However, polyaspartate was more effective than polyglutamate in inhibiting the growth of (010) hillocks. Overall, the binding behavior of carboxylate-containing macromolecules to several crystal faces is clearly complex.

2.7 SUMMARY

Additives are a very important and useful independent variable in crystallization. It is clear from this review of the influence of inhibitors on crystal growth and inhibition that many factors have to be taken into account in precipitation. The design of meaningful experiments for the quantitative studies of the additive effects in crystallization is important in order to study factors such as growth rates, nucleation rates, the influence of supersaturation, the extent of adsorption, and habit modification.

REFERENCES

- (a) Nancollas, G. H. The nucleation and growth of scale crystals. In *Fouling of Heat Exchanger Surfaces*, ed. R. W. Bryers. New York: United Engineering Trustees Inc. (1983); (b) Nancollas, G. H. *Adv. Colloid Interface Sci.* 10, 215–252 (1979).
- (a) Nancollas, G. H. and Reddy, M. M. Crystal growth kinetics of minerals encountered in water treatment processes. In *Aqueous-Environmental Chemistry of Metals*, ed. A. J. Rubin, pp. 219–253. Ann Arbor, MI: Ann Arbor Science Publishers (1974); (b) Nancollas, G. H. and Zawacki, S. J. Inhibitors of crystallization and dissolution. In *Industrial Crystallization*, eds. S. J. Jancic and E. J. De Jong, pp. 51–59. New York: Elsevier Publ. Co. (1984).
- (a) Amjad, Z. *Tenside Surf. Deterg.* 41, 214–219 (2004); (b) Amjad, Z. and Hooley, J. J. *Colloid Interface Sci.* 111, 496–503 (1986); (c) Amjad, Z. *Can. J. Chem.* 66, 1529–1536 (1988); (d) Amjad, Z. *J. Colloid Interface Sci.* 123, 523–536 (1988).
- (a) Amjad, Z. *Mater Perform* 28, 52–55 (1989); (b) Austin, A. E., Miller, J. F., Vaughan, D. A., and Kircher, J. F. *Desalination* 16, 345–357 (1975); (c) Adams, J. F. and Papangelakis, V. G. *Can. Metall. Q.* 39, 421–432 (2000).
- (a) Ouyang, J. M. and Deng, S. P. *Colloids Surf. A—Physicochem. Eng. Asp.* 257–258, 395–400 (2005); (b) Deng, S. P. and Ouyang, J. M. *Colloids Surf. A—Physicochem. Eng. Asp.* 257–258, 47–50 (2005).
- (a) Weaver, M. L., Qiu, S. R., Hoyer, J. R. et al. *J. Cryst. Growth* 306, 135–145 (2007); (b) Sidhu, H., Gupta, R., Thind, S. K., and Nath, R. *Urol. Res.* 14, 299–303 (1986); (c) Bek-Jensen, H., Fornander, A. M., Nilsson, M. A., and Tiselius, H. G. *Urol. Res.* 24, 67–71 (1996).
- Yu, H., Sheikholeslami, R., and Doherty, W. O. S. *J. Cryst. Growth* 265, 592–603 (2004).
- Nyvtl, J. and Ulrich, J. *Admixtures in Crystallization*. Weinheim, Germany: VCH nmH (1995).
- (a) Alimi, F. and Gadri, A. *Desalination* 166, 427–434 (2004); (b) Amathieu, L. and Boistelle, R. *J. Cryst. Growth* 88, 183–192 (1988); (c) Budz, J., Jones, A. G., and Mullin, J. W. *J. Chem. Tech. Biotech.* 36, 153–161 (1986).
- (a) Hasson, D. and Zahavi, J. *I&EC Fundam.* 9, 1–10 (1970); (b) Hasson, D., Drak, A., and Semat, R. *Desalination* 157, 193–207 (2003); (c) Rahardianto, A., Shih, W. Y., Lee, R. W., and Cohen, Y. *J. Membr. Sci.* 279, 655–668 (2006); (d) Najibi, S. H., Muller-Steinhagen, H., and Jamialahmadi, M. *Chem. Eng. Sci.* 52, 1265–1283 (1997).
- (a) Muller-Steinhagen, H. Cooling water fouling in heat exchangers. In *Advances in Heat Transfer*, ed. J. P. Hartnett, Vol. 33, pp. 415–496. New York: Academic Press (1999); (b) Parsons, S. A., Judd, S. J., Stephenson, T., Udol, S., and Wang, B. L. *Inst. Chem. Eng.* 75, 98–104 (1997).

12. (a) Liu, S. T. and Nancollas, G. H. *J. Colloid Interface Sci.* 44, 422–429 (1973); (b) Liu, S. T. and Nancollas, G. H. *J. Colloid Interface Sci.* 52, 593–601 (1975); (c) Liu, S. T. and Nancollas, G. H. *J. Cryst. Growth* 6, 281–289 (1970); (d) Liu, S. T. and Nancollas, G. H. *Talanta* 20, 211–216 (1973).
13. Smith, B. R. and Sweett, F. J. *Colloid Interface Sci.* 37, 612–618 (1971).
14. Eidelman, N., Azoury, R., and Sarig, S. *J. Cryst. Growth* 74, 1–9 (1986).
15. Furedi-Milhofer, H. and Walton, A. G. Principles of precipitation of fine particles. In *Dispersion of Powders in Liquid*, ed. G. D. Parfitt. London, U.K.: Applied Science Publishers (1981).
16. Mullin, J. W. *Crystallization*, 4th edn. Oxford, U.K.: Butterworth-Heinemann (2001).
17. Gilmer, G. H. *J. Cryst. Growth* 36, 15–28 (1976).
18. Kofina, A. N., Demadis, K. D., and Koutsoukos, P. G. *Cryst. Growth Des.* 7, 2705–2712 (2007).
19. Rodriguez-Hornedo, N. and Carstensen, J. T. *J. Pharm. Sci.* 75, 552–558 (1986).
20. Garside, J. and Davey, R. J. *Chem. Eng. Commun.* 4, 394–424 (1980).
21. Nyvlt, J., Söhnel, O., Matuchová, M., and Broul, M. *The Kinetics of Industrial Crystallization*. Prague, Czech Republic: Academia Press (1985).
22. (a) Söhnel, O. and Garside, J. *J. Cryst. Growth* 89, 202–208 (1988); (b) Nyvlt, J. *Collect. Czechos. Chem. Commun.* 48, 1977–1983 (1983); (c) Grand, D. J. W. and Hendricksen, B. A. *J. Cryst. Growth* 156, 252–260 (1995).
23. Davey, R. J. *J. Cryst. Growth* 34, 109–119 (1976).
24. Berkovitch-Yellin, Z., Van Mil, J., Addadi, L. et al. *J. Am. Soc.* 107, 3111–3122 (1985).
25. (a) Addadi, L., Berkovitch-Yellin, Z., Weissbuch, I. et al. *Angew. Chem. Int. Ed. Engl.* 24, 466–485 (1985); (b) Addadi, L. and Weiner, S. *Proc. Natl. Acad. Sci. U.S.A.* 82, 4110–4114 (1985); (c) Addadi, L., Moradian, J., Shay, E., Maroudas, N. G., and Weiner, S. *Proc. Natl. Acad. Sci. U.S.A.* 84, 2732–2736 (1987).
26. Sinclair, B. D. Interpreting changes in nucleation and crystal morphology of carbamazepine dehydrate by probing the intermolecular interactions between additives and crystal surfaces. PhD dissertation, University of Michigan, Ann Arbor, MI (2000).
27. Buckley, H. E. *Crystal Growth*. New York: Wiley (1951).
28. Kossel, W. *Ann. Phys.* 21, 457–480 (1934).
29. Mersmann, A. *Crystallization Technology Handbook*. Boca Raton, FL: Routledge (2001).
30. Dove, P. M., Davis K. J., and De Yoreo, J. J. Inhibition of CaCO₃ crystallization by small molecules the magnesium example. In *Solid-Fluid Interfaces to Nanostructural Engineering*, eds. X. Y. Liu and J. J. Yoreo. New York: Kluwer/Plenum Academic Press (2005).
31. Gilmer, G. H., Ghez, R., and Cabrera, N. *J. Cryst. Growth* 8, 79–93 (1971).
32. Burton, W. K., Cabrera, N., and Frank, F. C. *Philos. Trans. R. Soc. Lond.* 243, 299–358 (1951).
33. Orme, C. A., Noy, A., Wierzbicki, A. et al. *Nature* 411, 775–779 (2001).
34. Davey, R. J. *J. Cryst. Growth* 29, 212–214 (1975).
35. Sears, G. W. *J. Chem. Phys.* 29, 1045–1048 (1958).
36. Cabrera, N. and Vermileya, D. A. The growth of crystals from solution. In *Growth and Perfection of Crystals*, eds. R. H. Doremus, B. W. Roberts, and D. Turnbull. New York: Wiley (1958).
37. Van der Leeden, M. C., Kashchiev, D., and Van Rosmalen, G. M. *J. Colloid Interface Sci.* 152, 338–350 (1992).
38. Ohara, M. and Reid, R. C. *Modelling Crystal Growth Rates from Solution*. Englewood Cliffs, NJ: Prentice Hall (1973).
39. Furedi-Milhofer, H. and Sarig, S. *Prog. Cryst. Growth Charact. Mater.* 32, 45–74 (1996).
40. Kubota, N. and Mullin, J. W. *J. Cryst. Growth* 152, 203–208 (1995).
41. (a) Sangwal, K. *J. Cryst. Growth* 203, 197–212 (1999); (b) Sangwal, K. *Prog. Cryst. Growth Charact.* 36, 163–248 (1998).
42. Akyol, E. and Öner, M. *J. Cryst. Growth* 307, 137–144 (2007).
43. Van Rosmalen, G. M., Daudey, P. J., and Marchee, W. G. J. *J. Cryst. Growth* 52, 801–811 (1981).
44. Solomon, D. H. and Rolfe, P. E. *Desalination* 1, 260–266 (1966).
45. Rolfe, P. F. *Desalination* 1, 359–366 (1966).
46. Rosenstein, L. Process of treating water. U.S. Patent No. 2038316 (1936).
47. McCartney, E. R. and Alexander, A. E. *J. Colloid Sci.* 13, 383–396 (1958).
48. Sarig, S., Kahana, F., and Leshem, R. *Desalination* 17, 215–229 (1975).
49. (a) Weijnen, M. P. C. and Van Rosmalen, G. M. *J. Cryst. Growth* 79, 157–168 (1986); (b) Weijnen, M. P. C., Van Rosmalen, G. M., Bennema, P., and Rijpkema, J. J. M. *J. Cryst. Growth* 82, 509–527 (1987); (c) Weijnen, M. P. C. and Van Rosmalen, G. M. *Desalination* 54, 239–261 (1985).

50. (a) Prisciandaro, M., Olivieri, E., Lancia, A., and Musmarra, D. *Ind. Eng. Chem. Res.* 45, 2070–2076 (2006); (b) Prisciandaro, M., Lancia, A., and Musmarra, D. *Ind. Eng. Chem. Res.* 42, 6647–6652 (2003).
51. El Shall, H., Rashad, M. M., and Abdel-Aal, E. A. *Cryst. Res. Technol.* 37, 1264–1273 (2002).
52. (a) Öner, M., Doğan, Ö., and Öner, G. *J. Cryst. Growth* 186, 427–437 (1998); (b) Doğan, Ö., Akyol, E., and Öner, M. *Cryst. Res. Technol.* 39, 1108–1114 (2004); (c) Lioliou, M. G., Paraskeva, C. A., Koutsoukos, P. G., and Payatakes, A. C. *J. Colloid Interface Sci.* 303, 164–170 (2006).
53. Amathieu, L. and Boistelle, R. *J. Cryst. Growth* 79, 169–177 (1986).
54. Klepetsanis, P. G. and Koutsoukos, P. G. *J. Cryst. Growth* 193, 156–163 (1998).
55. Schierholtz, O. J. *Can. J. Chem.* 36, 1057–1063 (1958).
56. Packter, A. *J. Cryst. Growth* 21, 191–194 (1974).
57. Nancollas, G. H. *J. Cryst. Growth* 3–4, 335–339 (1968).
58. Tadros, M. E. and Mayes, I. *J. Colloid Interface Sci.* 72, 245–254 (1979).
59. Klepetsanis, P. G. and Koutsoukos, P. G. *J. Cryst. Growth* 98, 480–486 (1989).
60. He, S., Oddo, J. E., and Thomson, M. B. *J. Colloid Interface Sci.* 163, 372–378 (1994).
61. Hasson, D. Precipitation fouling. In *Fouling of Heat Transfer Equipment*, eds. E. F. C. Somerscales and J. G. Knudsen, pp. 527–568. New York: Hemisphere (1981).
62. Konak, A. R. *Chem. Eng. Sci.* 29, 1537–1543 (1974).
63. (a) Ajavi, L., Jaeger, P., Robertson, W., and Unwin, R. *Medicine* 35, 415–419 (2007); (b) Webber, D., Rodgers, A. L., and Sturrock, E. D. *J. Cryst. Growth* 259, 179–189 (2003).
64. Sikiric, M. D. and Furedi-Milhofer, H. *Adv. Colloid Interface Sci.* 128–130, 135–158 (2006).
65. Yu, H., Sheikholeslami, R., and Doherty, W. O. S. *Powder Technol.* 160, 2–6 (2005).
66. Franceschi, V. R. and Horner, H. T. *Botan. Rev.* 46, 361–427 (1980).
67. Pennisi, S. V., McConnell, D. B., Gower, L. B., Kane, M. E., and Lucansky, T. *New Phytol.* 150, 111–120 (2001).
68. Nakagawa, Y., Abram, V., and Coe, F. L. *Am. J. Physiol. Ren. Physiol.* 247, F765–F772 (1984).
69. Potter, S., Reath, S., Hussein, A. et al. *Wood Sci. Technol.* 37, 321–329 (2003).
70. Perera, C. O., Hallett, I. C., Nguyen, T. T., and Charles, J. C. *J. Food Sci.* 55, 1066–1069 (1990).
71. Masár, M., Zuborová, M., Kaniánsky, D., and Stanislawski, B. *J. Sep. Sci.* 26, 647–652 (2003).
72. (a) Schwarz, R. D. and Dwyer, N. T. *Urology* 67, 812–816 (2006); (b) Asplin, J. R. and Coe, F. L. *J. Urol.* 177, 565–569 (2007).
73. Schoenfield, L. J. and Marks, J. W. *Am. J. Surg.* 165, 427–430 (1993).
74. Garti, N., Tibika, F., Sarig, S., and Perlberg, S. *Biochem. Biophys. Res. Commun.* 97, 1154–1162 (1980).
75. (a) Weaver, M. L., Qiu, S. R., Hoyer, J. R. et al. *J. Cryst. Growth* 306, 135–145 (2007); (b) Sidhu, H., Gupta, R., Thind, S. K., and Nath, R. *Urol. Res.* 14, 299–303 (1986); (c) Bek-Jensen, H., Fornander, A. M., Nilsson, M. A., and Tiselius, H. G. *Urol. Res.* 24, 67–71 (1996); (d) Qiu, S. R., Wierzbicki, A., Salter, E. A. et al. *J. Am. Chem. Soc.* 127, 9036–9044 (2005).
76. Wunderlich, W. *Urol. Res.* 9, 157–161 (1981).
77. (a) Wang, L., Zhang, W., Qiu, S. R. et al. *J. Cryst. Growth* 291, 160–165 (2006); (b) Konya, E., Umekawa, T., Iguchi M., and Kurita, T. *Eur. Urol.* 43, 564–571 (2003).
78. (a) Gokhale, J. A., Glenton, P. A., and Khan, S. R. *J. Urol.* 166, 1492–1497 (2001); (b) Ganter, K., Bongartz, B., and Hesse, A. *Urology* 53, 492–495 (1999).
79. (a) Cody, A. M. and Cody, R. D. *J. Cryst. Growth* 135, 235–245 (1994); (b) Azoury, R., Randolph, A. D., and Drach, G. W. *J. Cryst. Growth* 64, 389–392 (1983); (c) Ouyang, J. and Deng, F. *Mat. Sci. Eng. C* 26, 688–691 (2006).
80. Akyol, E., Bozkurt, A., and Öner, M. *Polymers Adv. Technol.* 17, 58–65 (2006).
81. Meyer, J. L., Lee, K. E., and Bergert, J. H. *Calcif. Tissue Res.* 28, 83–86 (1977).
82. Sorensen, S., Hansen, K., Bak, S., and Justesen, S. *J. Urol. Res.* 18, 373–379 (1990).
83. Rabinovich, Y. I., Esayanur, M., Daosukho, S. et al. *J. Colloid Interface Sci.* 300, 131–140 (2006).
84. (a) Wesson, J. A., Worcester, E. M., and Kleinman, J. G. *J. Urol.* 163, 1343–1348 (2000); (b) Joshi, V. S., Parekh, B. B., Joshi, M. J., and Vaidya, A. B. *J. Cryst. Growth* 275, 403–408 (2005).
85. Heijnen, W. M. M. *J. Cryst. Growth* 57, 216–232 (1982).
86. (a) Tomazic, B. and Nancollas, G. H. *J. Colloid Interface Sci.* 75, 149–160 (1980); (b) Tomazic, B. and Nancollas, G. H. *J. Cryst. Growth* 46, 355–361 (1979); (c) Tomazic, B. and Nancollas, G. H. *Invest. Urol.* 18, 97–101 (1980).
87. Elliot, J. S. and Rabinowitz, I. N. *J. Urol.* 123, 324–327 (1980).
88. Tazzoli, V. and Domeneghetti, C. *Am. Mineral.* 65, 327–334 (1980).
89. Sterling, C. *Acta Crystallogr.* 18, 917–921 (1965).
90. Rodgers, A. and Garside, J. *Invest. Urol.* 18, 484–488 (1981).

91. Nielsen, A. E. *Acta Chem. Scand.* 14, 1654–1659 (1960).
92. Nancollas, G. H. and Gardner, G. L. *J. Cryst. Growth* 21, 267–276 (1974).
93. Rizkalla, E. N. and Moawad, M. M. *J. Chem. Soc. Faraday Trans.* 1 80, 1617–1629 (1984).
94. Singh, R. P., Gaur, S. S., Sheehan, M. E., and Nancollas, G. H. *J. Cryst. Growth* 87, 318–324 (1988).
95. Bouropoulos, K., Bouropoulos, N., Melekos, M. et al. *J. Urol.* 159, 1755–1761 (1998).
96. Campbell, A. A., Ebrahimpour, A., Perez, L., Smesko, S. A., and Nancollas, G. H. *Calcif. Tissue Int.* 45, 122–128 (1989).
97. Öner, M. and ve Calvert, P. *Mat. Sci. Eng. C* 2, 93–101 (1994).
98. Yu, J., Tang, H., Cheng, B., and Zhao, X. *J. Solid State Chem.* 177, 3368–3374 (2004).
99. Ouyang, J. M., Deng, S. P., Zhou, N., and Tieke, B. *Colloids Surf. A—Physicochem. Eng. Asp.* 256, 21–27 (2005).
100. Tunik, L., Furedi-Milhofer, H., and Garti, N. *Langmuir* 14, 3351–3355 (1998).
101. Frincu, M. C., Fogarty, C. E., and Swift, J. A. *Langmuir* 20, 6524–6529 (2004).
102. Yu, J., Tang, H., and Cheng, B. *J. Colloid Interface Sci.* 288, 407–411 (2005).
103. Gardner, G. L. *J. Phys. Chem.* 82, 864–870 (1978).
104. Brecevic, L. and Kralj, D. *J. Cryst. Growth* 79, 178–184 (1986).
105. Manne, J. S., Biala, N., Smith, A. D., and Gryte, C. C. *J. Cryst. Growth* 100, 627–634 (1990).
106. Millan, A., Pavelkova, M., Sohnel, O., and Grases, F. *Cryst. Res. Technol.* 33, 777–786 (1998).
107. Akin, B., Öner, M., Bayram, Y., and Demadis, K. *Crystal Growth and Design.* 8, 1997–2005 (2008).
108. (a) Jung, T., Sheng, X., Choi, C. K. et al. *Langmuir* 20, 8587–8596 (2004); (b) Guo, S. W., Ward, M. D., and Wesson, J. A. *Langmuir* 18, 4284–4291 (2002); (c) Sheng, X., Jung, T., Wesson, J. A., and Ward, M. D. *Proc. Natl. Acad. Sci.* 102, 267–272 (2005).
109. Jung, T., Kim, W. S., and Choi, C. K. *J. Cryst. Growth* 279, 154–162 (2005).

3 Calcium Carbonate Scale Control in Industrial Water Systems

Peter G. Koutsoukos

CONTENTS

3.1 Introduction.....	39
3.2 Thermodynamics of Formation of Scale Deposits.....	40
3.3 Kinetics of Precipitation	44
3.4 Control of the Scale Deposits	50
3.5 Summary	56
References.....	57

3.1 INTRODUCTION

Fouling in water-intensive industrial applications is one of the most severe problem-causing situations as it often leads to shorter or longer shutdowns of the units with concomitant increase in process cost. Several types of fouling have been identified, depending on the respective cause of development. Despite the fact that all these types deserve special attention, crystallization fouling is considered to be most detrimental to the industrial processes worldwide. This type of fouling is defined as the process in which dissolved ionic components of salts crystallize and eventually deposit at the water/solid interface involved in the process. Salts with inverse solubility tend to cause fouling of heated metallic surfaces, while more soluble salts crystallize on cold or cooled surfaces. Water-formed scale deposits, even in cases in which their composition is not complex, depend on a number of factors, including the ion speciation in the aqueous medium, the properties and the characteristics of the surfaces in contact with the aqueous phase, the fluid dynamics, and the heat-transfer parameters of the process. Calcium carbonate deposits have been identified in water-carrying pipes from antiquity, as may be seen from outdoor exhibits at the archeological museum of Naxos, Greece, as shown in Figure 3.1.

Because of the polymorphism it exhibits, the system of calcium carbonate shows peculiarities upon formation. The three polymorphic phases, vaterite, aragonite, and calcite, in the order of increasing thermodynamic stability have different solubility, morphological, and crystallographic characteristics [1,2]. Depending on the fluid conditions (composition, temperature, fluid dynamics, and substrate), less stable polymorphs or hydrated phases may be stabilized and/or converted into the thermodynamically most stable calcite. Moreover, the formation of amorphous calcium carbonate has been reported as a precursor phase, forming upon the development of the appropriate conditions (high pH and high calcium and carbonate concentrations) [3,4]. Water used in the industry for most of the cases is characterized by increased hardness. Water hardness is mainly due to the presence of calcium and carbonate ions. The distribution of the carbonic species depends in turn on the solution pH. For a system closed to the atmosphere, the carbonate species present include $\text{CO}_2(\text{aq})$, H_2CO_3 , HCO_3^- , and CO_3^{2-} . Over a wide pH range around the neutral, the bicarbonate, HCO_3^- , is

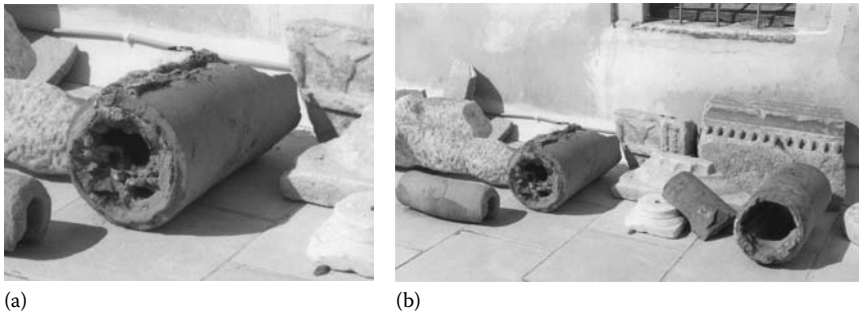


FIGURE 3.1 (a and b) Scale deposits formed inside ceramic water-carrying pipes, exhibited in the archeological museum of Naxos, Greece.

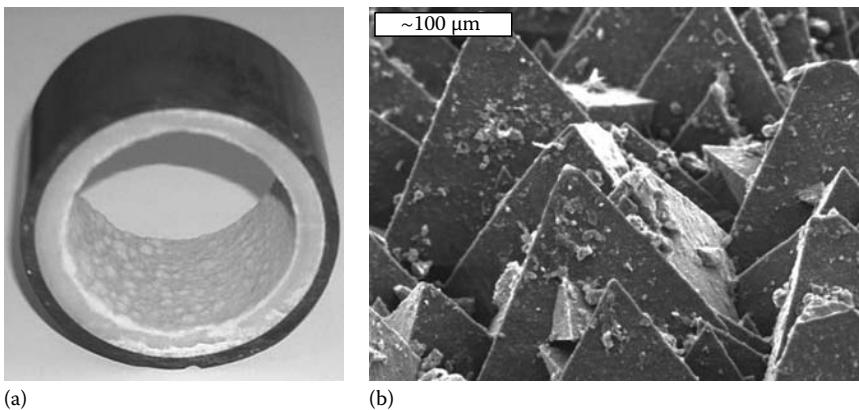
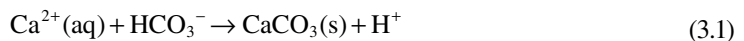


FIGURE 3.2 (a) calcium carbonate deposits in a pipeline for the transport of geothermal water in Therma, Nigrita, Greece; (b) SEM of scale deposits from the same field. (Courtesy of Prof. N. Andritsos, University of Thessaly, Volos, Greece.)

the dominant species. The formation of calcium carbonate takes place according to Equation 3.1, provided that the concentration of the calcium ions present is sufficiently high:



According to Equation 3.1, provided that the precipitation of the solid phase is initiated, it shall proceed until equilibrium is reached. Examples of calcium carbonate scale deposits are shown in Figure 3.2.

Except for the precipitation, during which crystallites of the scale deposits are generated, secondary processes, including ageing and agglomeration, contribute to the formation of adhering deposits. A schematic representation of the physical processes taking place in an aqueous medium and leading to the formation of tenaciously adhering calcium carbonate deposits is shown in Figure 3.3. It is interesting to note that the calcitic scale was deposited and adhered strongly on a polymeric (PVC) tube, as shown in Figure 3.3.

3.2 THERMODYNAMICS OF FORMATION OF SCALE DEPOSITS

The thermodynamic driving force behind the formation of calcium carbonate in a complex aqueous medium containing calcium and carbonate ionic species is described qualitatively as the distance of this solution from equilibrium. This “distance” may be expressed in a quantitative manner as the

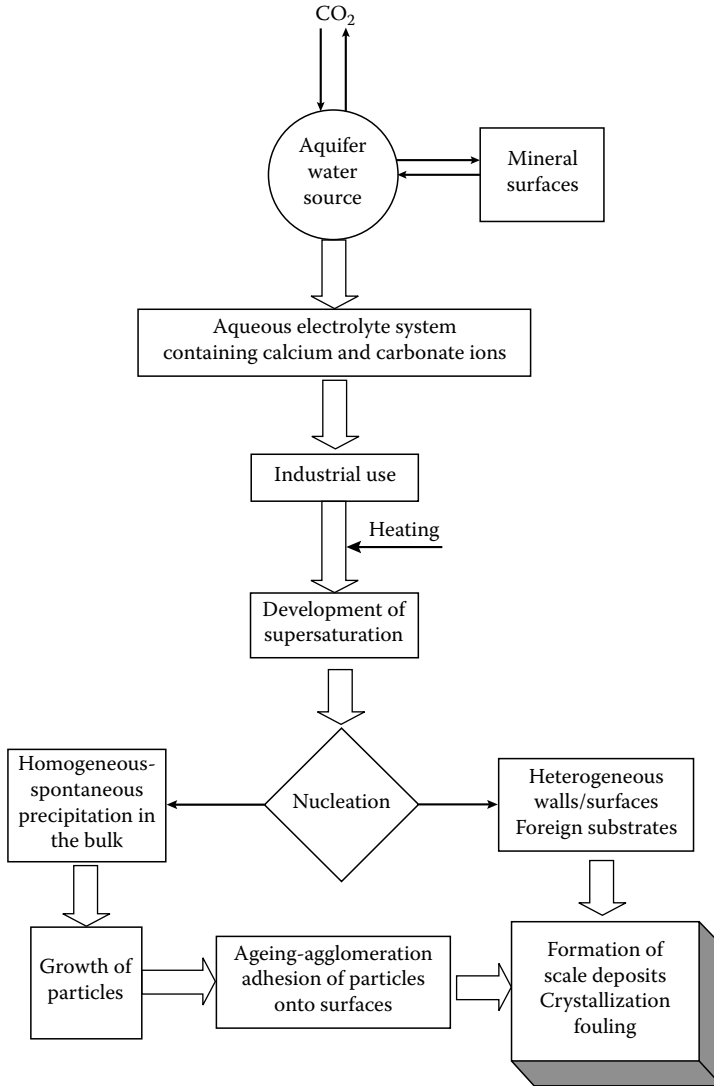


FIGURE 3.3 Physical processes taking place in industrial operations, leading to the formation of calcium carbonate scale deposits.

difference between the chemical potentials of the solute species (calcium carbonate) and the respective values at equilibrium [5]:

$$\begin{aligned} \Delta\mu &\equiv \left(\frac{\partial G_{\text{CaCO}_3, \text{equilibrium}}}{\partial n_{\text{CaCO}_3, \text{equilibrium}}} \right)_{T,P} - \left(\frac{\partial G_{\text{CaCO}_3, \text{solution}}}{\partial n_{\text{CaCO}_3, \text{solution}}} \right)_{T,P} = \mu_{\text{equilibrium}} - \mu_{\text{solution}} \\ &= -RT \{ \ln \alpha_{\pm, \text{solution}} - \ln \alpha_{\pm, \text{equilibrium}} \} \end{aligned} \tag{3.2}$$

Considering mean ionic activities, the thermodynamic driving force becomes

$$\Delta\mu = -\frac{RT}{2} \ln \frac{\{ \alpha_{\text{Ca}^{2+}, \text{solution}} \alpha_{\text{CO}_3^{2-}, \text{solution}} \}}{\{ \alpha_{\text{Ca}^{2+}, \text{equilibrium}} \alpha_{\text{CO}_3^{2-}, \text{equilibrium}} \}} \tag{3.3}$$

where

R is the gas constant

T is the temperature

α is the activities of the respective ions at the state indicated by the subscripts

The numerator in Equation 3.3 is the ion activity product of calcium carbonate in the aqueous medium, and the activity product at equilibrium shown in the denominator is the thermodynamic solubility product. The ratio in the logarithmic term is defined as the supersaturation ratio, S :

$$S = \frac{\{\alpha_{\text{Ca}^{2+},\text{solution}} \alpha_{\text{CO}_3^{2-},\text{solution}}\}}{\{\alpha_{\text{Ca}^{2+},\text{equilibrium}} \alpha_{\text{CO}_3^{2-},\text{equilibrium}}\}} \quad (3.4)$$

The relative supersaturation, σ , with respect to the solid precipitating is

$$\sigma = S^{1/2} - 1 \quad (3.5)$$

Using Equations 3.3 through 3.5, it is possible to obtain quantitative estimates of the deviation from a given value of the equilibrium constant, which is different for every polymorphic phase of calcium carbonate. Depending on the deviation from equilibrium, different processes may take place in a solution which tends to return to equilibrium ($\Delta\mu = 0$). These processes are schematically shown in Figure 3.4. Positive values of σ correspond to supersaturated solutions and negative values to undersaturated solutions. The zero value corresponds to saturation (equilibrium). As may be seen, the supersaturation domain includes two regions: the stable and the labile. In the stable region, the supersaturated solutions are practically stable (no precipitation is observed for very long periods of time). The growth of calcium carbonate with subsequent transition into the saturated state may take place upon the introduction of a foreign substrate with specific affinity for this salt. The specific case in which crystal growth is initiated by seeding the supersaturated solutions with calcium carbonate seed crystals is the *seeded growth technique*, a method used for the preparation of crystals or for the investigation of crystal growth processes [6,7].

Alternatively, the presence of foreign substrates that favor the accommodation of the calcium carbonate crystallite structures may also result in the formation of mixed substrate-calcium carbonate

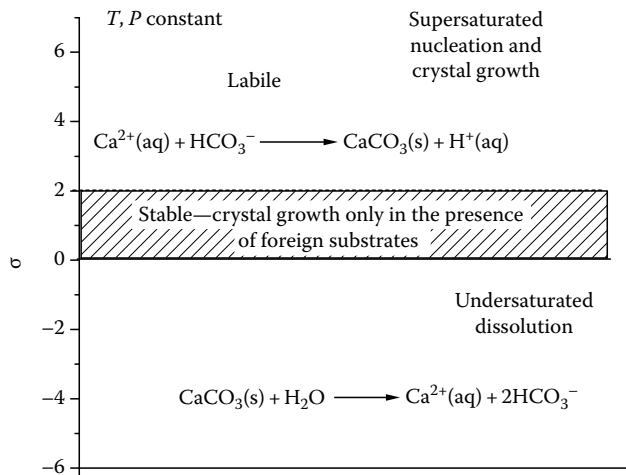


FIGURE 3.4 Schematic diagram of the processes taking place in an aqueous calcium carbonate solution as a function of the relative saturation.

products. Early studies have presented results in which river clay particles accelerated the rates of calcium carbonate scale formation [8]. In the case of crystalline substrates, crystal lattice matching is a sufficient, but not necessary, condition for the oriented overgrowth of calcium carbonate [9–12]. On heat-transfer surfaces, calcium carbonate scale formation is believed to be initiated at three phases: CO₂ gas, metal surface, and water boundary [13,14]. At lower temperatures (below 30°C), in the absence of gas bubbles, it was suggested that the calcite crystallites formed adhere onto the substrate where they subsequently outgrow, forming compact layers which have a dramatic effect on their morphology [15]. In desalination processes, either by thermal methods or using membranes, the solution concentration past the solubility limits is the primary cause for calcium carbonate scale formation [16,17]. Throughout the relevant literature, there is a general agreement that one of the most important factors influencing calcium carbonate scale formation is the concentration level of the constituent ions [18]. The evaluation of the scaling potential should be done on the basis of equations such as Equation 3.3, taking into consideration salinity, activity coefficients, and ion interactions in the complex ionic media [19–21]. The computation of the activities of the free ions, taking into consideration all equilibria involved in a complex system such as the industrial water, may be done with free energy-minimization programs [22–24]. In water industry, a number of indices are used by technologists for the qualitative evaluation of the scaling potential of the water used. These indices are, in essence, thermodynamic but they may be used only for rough estimates because the underlying thermodynamics are oversimplified. These indices include the Langelier index (LI), the Ryznar solubility index (RSI), and the Stiff and Davis index (SDI). The LI is defined (Equation 3.6) as the difference between the measured solution pH and the respective value at saturation, denoted by subscript s:

$$LI = \text{pH} - \text{pH}_s \quad (3.6)$$

where

$$\text{pH}_s = \text{pCa} + \text{pAlk} + \text{TDS} \quad (3.7)$$

In equation 3.7:

pCa is the negative logarithm of the calcium hardness

pAlk is the alkalinity

TDS is the total dissolved solids

All terms are expressed as ppm of CaCO₃ at the water temperature. The saturation pH value is a calculated value.

When the measured pH is equal to the saturation pH_s, LI is zero and the water is at a saturation state. As a result, no scale is anticipated while corrosion is expected to be negligible. For pH values > pH_s, LI > 0, the water is supersaturated with respect to calcium carbonate. On the other hand, for pH < pH_s, LI < 0, calcium carbonate scale does not deposit, or if present, it shall dissolve. However, in this case, water has a tendency to cause corrosion of the metal surfaces in contact. Examples of the meaning of the values of the LI in industrial waters are shown in Table 3.1.

The RSI is defined as

$$RSI = 2\text{pH}_s - \text{pH} \quad (3.8)$$

The predictive significance of the values for this index is summarized in Table 3.2.

The SDI is a modification of the LI to take into account the effect of high levels of dissolved solids on the solubility of calcium carbonate. The SDI was developed for use in oil fields, where highly

TABLE 3.1
Values of the LI and the Respective Meaning
for Water Used in Industrial Processes

Value of LI	Water Characteristics
+2.0	Scale-forming—noncorrosive
+0.5	Slightly scaling and noncorrosive
0.0	Balanced but pitting corrosion possible
-0.5	Slightly corrosive and non-scale-forming
-2.0	Highly corrosive

TABLE 3.2
Values of the RSI and the Respective Meaning
for Water Used in Industrial Processes

Value of RSI	Water Characteristics
4.0–5.0	Significant scale formation
5.0–6.0	Scaling to small extent
6.0–7.0	Little scaling, slightly corrosive
7.0–7.5	Corrosive
7.5–9.0	Intensively corroding
9.0 and higher	Destructive corrosion

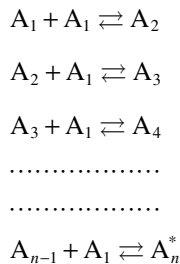
saline waters or brines are produced. This index is also useful in cases where recovered wastewater is used for makeup water in large quantities. The SDI is defined as

$$SDI = pH_p - pCa - pAlk - I \tag{3.9}$$

where *I* is a constant, dependent on the temperature and the ionic strength of the water.

3.3 KINETICS OF PRECIPITATION

The development of supersaturation is a prerequisite for the formation of calcium carbonate. In a supersaturated solution, the nucleation process may be thought as a sequence of bimolecular reactions between growth units, A_1 , and clusters, A_m , made up of *m* units, according to the scheme



As shown in the scheme above, during the nucleation stage, the growth unit clusters keep increasing until they reach a critical size. The critical size nucleus, A_n^* , once it is formed, grows as a macroscopic crystal, which may be characterized by physical–chemical methods [25]. The time needed for the

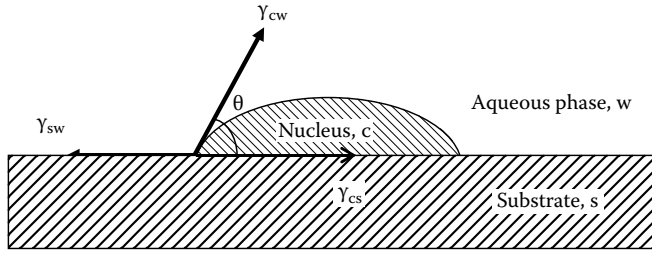


FIGURE 3.5 Schematic diagram of the partial surface tension vectors for a nucleus formed on a solid surface from an aqueous supersaturated solution.

formation of the critical nucleus is defined as the *incubation* or the *induction time*, τ . The nucleation process may take place either homogeneously in the bulk solution or heterogeneously on foreign substrates which may be particles or surfaces. The latter is the most common in practical cases. It is obvious that in the case of heterogeneous nucleation, the energy barrier needed to be overcome for the nucleation is lower than the corresponding in the case of homogeneous nucleation:

$$\Delta G_{\text{heterogeneous}} = \varphi \Delta G_{\text{homogeneous}} \tag{3.10}$$

where, $0 < \varphi < 1$. The factor φ is related to the wetting of the substrate by the nucleus. The formation of the new nucleus is schematically shown in Figure 3.5.

From the vector balance shown in Figure 3.3, contact angle θ is

$$\cos \theta = \frac{\gamma_{sw} - \gamma_{cs}}{\gamma_{cw}} \tag{3.11}$$

The value of the angle θ is a measure of the affinity of the deposit with the substrate. The induction time is interpreted as the time lapsed for the formation of the critical size nucleus and depends on the solution supersaturation:

$$\ln \tau = B \frac{\gamma_s^3 f(\theta)}{T^3 (\ln S)^2} + C \tag{3.12}$$

where, γ_s is the surface energy of the nucleating solid and the constant B is

$$B = \frac{\beta v^2}{(2.3k)^3 v^2} \tag{3.13}$$

where

- β is a shape factor
- v is the molecular volume of the precipitating salt
- k is the Boltzmann's constant
- v is the number of ions in the calcium carbonate formula (=2)

The function $f(\theta)$ is

$$f(\theta) = \frac{2 - 3 \cos \theta + \cos^3 \theta}{4} \tag{3.14}$$

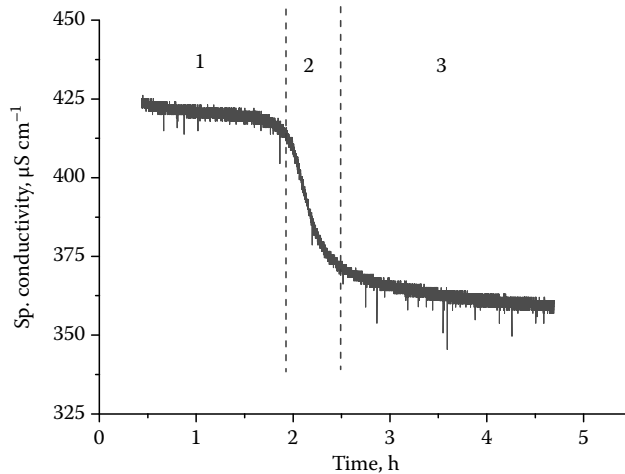


FIGURE 3.6 Variation of specific conductivity of tap water in contact with a stainless steel tube at 70°C during the course of calcium carbonate scale formation.

For a solid phase completely not wet by the overgrowth $\theta = 180^\circ$, $f(\theta) = 1$. For $\theta < 180^\circ$, $f(\theta) < 1$. The constant C in Equation 3.12 is a preexponential factor, associated with the nucleation of the solid phase. As may be seen from Equation 3.12, the induction time preceding the formation of calcium carbonate precipitates on a foreign surface is predicted to be inversely proportional to the solution supersaturation. The higher the supersaturation, the shorter the induction times, that is, the time periods lapsed before the onset of the calcium carbonate scale formation. A typical profile of the progress of the development of calcium carbonate encrustation is shown in Figure 3.6. The data provided are concerned with monitoring a parameter (in this case, the specific conductivity of the aqueous phase), which changes with the progress of the precipitation process.

In Figure 3.6, three distinct regions may be seen. In region 1, no scale deposit is observed, and the specific conductivity of water remained practically constant. Past an induction time of approximately 2 h, however, calcium carbonate scale started to deposit on the stainless steel surface of the laboratory heat exchanger. The mainly linear part of the curve in region 2 corresponds to the growth of the crystalline deposit layer, accompanied with solution desupersaturation. This linear growth of scale deposits has been reported in the literature [26]. In region 3, the solution desupersaturation has sufficiently advanced and it gradually approaches equilibrium. The dependence of the induction times preceding the formation of calcitic deposits on heated metal surfaces is demonstrated in Figure 3.7 [27].

The predominantly heterogeneous nature of this process is demonstrated in Figure 3.8 in which the variation of the induction times depending on the material of the substrate is demonstrated.

As may be seen, the glass-coated substrate yielded the longest induction times and the aluminum material the shortest, for each supersaturation tested. This result may be explained by the fact that in the presence of chloride, aluminum shows pitting corrosion, resulting in the formation of pits on its surface. Sites of this type on a substrate are expected to promote heterogeneous nucleation [28].

Once the nuclei grow to the critical size, they undergo crystal growth through the incorporation of growth units in their lattice. As a result, the supersaturation in the mother liquor is reduced until the limit of equilibrium is reached. Monitoring the variation of parameters (physical and/or chemical) associated with the formation of calcium carbonate scale deposits yields valuable information concerning the kinetics of scale formation. It is thus possible to quantitatively evaluate the effect of various parameters on the kinetics, including supersaturation, the presence of foreign ions, and/or compounds, etc.

The measurement of calcium carbonate kinetics is of paramount significance because of the polymorphism of the system. Less stable than calcite phases, it is possible that they stabilize

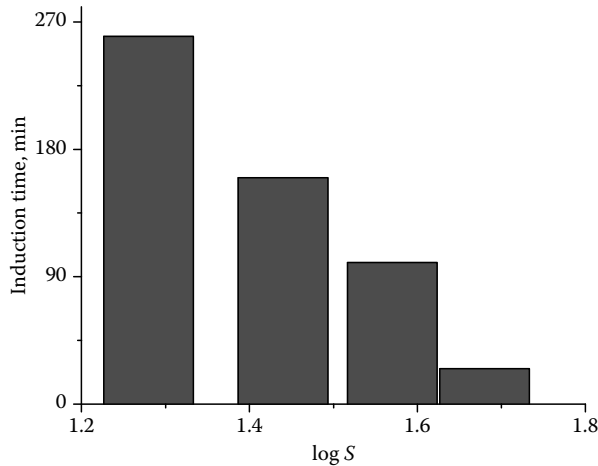


FIGURE 3.7 Effect of the supersaturation with respect to calcite on the induction time preceding precipitation of calcium carbonate on stainless steel tube. (Recalculated from Dalas, E. and Koutsoukos, P.G., *Desalination*, 78, 403, 1990.)

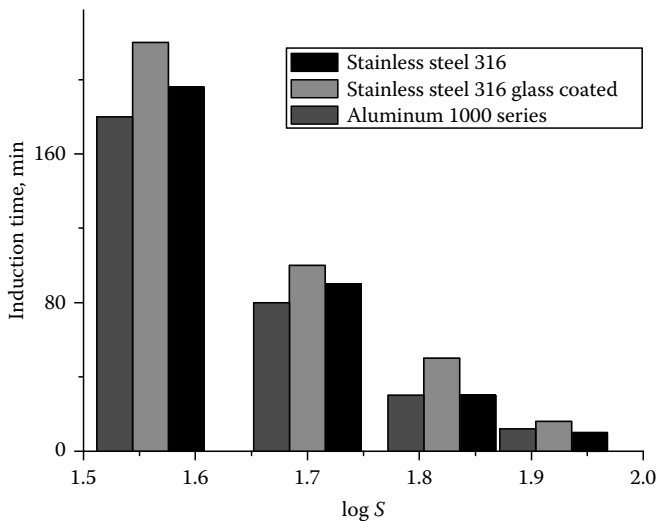


FIGURE 3.8 Dependence of the induction time preceding the precipitation of calcium carbonate deposits on tubes heated at 80°C at various supersaturations on the tube material; pH 8.50. (Recalculated from Dalas, E. and Koutsoukos, P.G., *Desalination*, 78, 403, 1990.)

kinetically [29]. Early kinetics studies were done from desupersaturation measurements [30,31]. Although it is possible to estimate crystal growth parameters from the desupersaturation curves [32], the rapid change of supersaturation may cause fast transformation of the less stable polymorphic phases of calcium carbonate into the most stable calcite [33]. Despite the fact that sensitive methods based on labeled elements have been developed to monitor scale deposition [34], the determination of the initial rates at experimental conditions in which several parameters (e.g., ion concentrations, solution pH, particle density, or solid/solution ratio) change during the course of the solid phase formation shows reduced precision. The development of the pH-stat method allowed for investigations at constant solution pH, and the precision and reproducibility measurements of the crystal growth process were improved [35,36]. A better control of the metastable phases was reported using a constant CO₂ supply in combination with constant pH [37]. However, the problems associated

with the rapid changes in the solution supersaturation were overcome at conditions of controlled solution supersaturation [38]. At these conditions, it was possible to investigate the process of crystal growth, both at very low and even at very high supersaturations where crystallization took place upon inoculation with calcite seed crystals and by spontaneous precipitation, respectively [39]. The advantage of this methodology is the maintenance of pseudo-steady-state conditions where not only the rates of crystal growth can be measured accurately but also the transformation of the unstable intermediate polymorphic phases of calcium carbonate may be monitored, mainly through the characterization of the solid phase collected at various time intervals. Sufficient time is provided through the maintenance of the solution supersaturation, even if the $\text{Ca}:\text{CO}_3$ stoichiometry in the solid and in the solution do not change. The method was applied successfully in systems in which the supersaturated solutions contact heated metal surfaces on which scale is deposited [27]. In this case, the supersaturation control is done in the feed solution so that a steady-state supersaturation is established on the surface of the heat exchanger or the surface tested for encrustation. The rate of calcium carbonate formation has been shown to have a second-order dependence on the relative supersaturation with respect to the polymorph investigated [40,41]. The kinetic equation widely used in the literature is

$$R_g = k_g f(A) \sigma^2 \quad (3.15)$$

where, k_g is the rate constant and $f(A)$ a function of the active sites of the substrate for the overgrowth of calcium carbonate, often taken as equal to the total surface area [for polycrystalline materials, it is the $\text{mass}(g) \times \text{BET-specific surface area} (\text{m}^2 \text{g}^{-1})$]. From the mechanistic point of view, the information obtained from the satisfactory fitting of the measured rates of crystal growth over a range of relative supersaturation is that the rate-determining step in the crystal growth process is the surface diffusion of the growth units onto the active sites with the least energy. Schematically, the steps involved in the growth of a crystal from supersaturated solutions are shown in Figure 3.9. Step 1 includes the transport of the growth unit to the surface of a crystal with imperfections. The crystal imperfections include terraces, steps, holes, and kinks. The surface reaction processes in the case of calcite take place at kinks, which are generally characterized by lower energy content [42–44]. The presence of kinks is important because the growth units that attach at these sites can make more bonds to neighboring units in comparison with the units bound to other types of imperfections. The second-order dependence shown in Equation 3.15 was verified both with different seed crystal

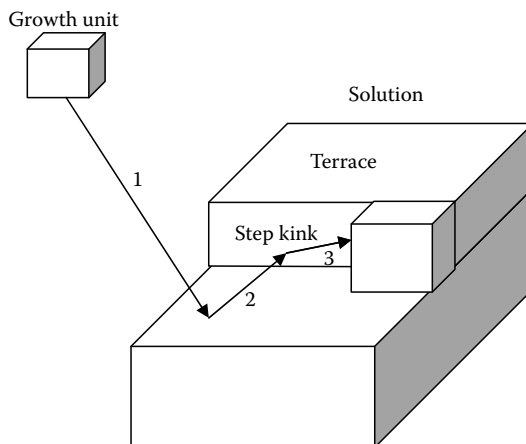


FIGURE 3.9 Steps involved in the crystal growth from solution. Step 1: diffusion from the bulk solution, partial dehydration adsorption on a terrace. Step 2: diffusion to a step followed by additional partial dehydration. Step 3: further dehydration and attachment to a kink site.

preparations and with fitting of literature data [38]. However, in cases where the precipitation of calcium carbonate takes place spontaneously or in the presence of complex aqueous media, such as seawater, apparent orders >2 have been reported [41,45]. This may be interpreted either as a polynuclear mechanism or by the formation of different polymorphic phases at different supersaturation values which may develop with pH changes [46]. The transient formation of aragonite and vaterite was confirmed for calcium carbonate by in situ probing using wide-angle x-ray scattering (WAXS) at ambient and elevated temperatures [47].

In the case of scale deposition in pipes heated isothermally, the supersaturation in the turbulent bulk fluid is practically constant, and the formation of calcium carbonate may take place either spontaneously in the bulk solution (in case where the supersaturation is very high) or on the walls by heterogeneous nucleation and crystal growth. Tube walls may provide for the active growth sites necessary for the development of new calcium carbonate nuclei. It is thus anticipated that in most cases, the precipitates form on the tube walls [48] a supersaturation gradient is established, as can be seen in Figure 3.10.

As shown in Figure 3.10, C_i is the concentration of calcium carbonate next to the adsorption layer of thickness Δ , corresponding to the thickness of one growth unit, and δ the diffusion layer thickness. When the surface diffusion processes described above are very fast, the rate-determining process is anticipated to be the diffusion from the bulk solution to the surface of the substrate on which the nuclei grow to macroscopic crystals. The flux of the growth unit is related to the concentration gradient by Fick's first law [49]:

$$\text{Flux} \equiv J = -D \frac{dC}{dx} = -D \frac{(C_i - C_{\text{bulk}})}{\delta} \approx k_d (C_s - C_{\text{bulk}}) \tag{3.16}$$

In Equation 3.16, it is assumed that the concentration near the surface may be set equal to the surface concentration, provided that surface reactions are sufficiently fast and

$$k_d = \frac{D}{\delta} \tag{3.17}$$

The constant k_d is the convective mass transfer coefficient and can be estimated from the Linton–Sherwood equation:

$$k_d = 0.023 U S c^{-2/3} Re^{-0.17} \tag{3.18}$$

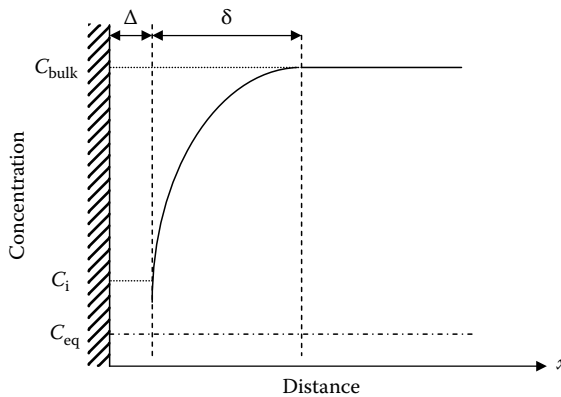


FIGURE 3.10 Concentration profile adjacent to the walls of a tube in which calcium carbonate scale is deposited as a function of distance x from its surface.

where

U is the flow velocity

$Sc (=v_s/D)$ and $Re (=Ud/v_s)$, the Schmidt and Reynolds numbers, respectively

v_s is the kinematic viscosity of the fluid

d is the tube diameter

Since calcium carbonate is an ionic compound, an expression for the rate of scale deposition in pipes, which takes into account both diffusion and surface reactions expressed by the respective rate constants k_d and k_r were developed by Andritsos et al. on the basis of the model developed by Hasson et al. [50,51]:

$$R_g = \frac{k_d}{2} \left([Ca^{2+}] + [CO_3^{2-}] + \frac{k_d}{k_r} \right) \left\{ 1 - \sqrt{1 - \frac{[Ca^{2+}][CO_3^{2-}] - K_s^0}{1}} \right\} \quad (3.19)$$

$$\sqrt{4 \left([Ca^{2+}] + [CO_3^{2-}] + \frac{k_d}{k_r} \right)^2}$$

The rate expression (3.19) was used to fit the experimental data at high pH (>9) and very high supersaturations. It was concluded that at these conditions, there is a mechanism change from surface diffusion, predominant at lower pH values and supersaturations, to bulk diffusion controlled. Mechanistic information is of paramount importance for understanding the process operative in each case of scale formation. It is very important, especially in the case of calcite scale formation, to identify the polymorphs that form at the initial stages of precipitation, not only because of their solubility and morphological differences but also because of differences in surface charge, which in turn affect particle adhesion properties. In general, however, the electric charge cancels at equilibrium, while in supersaturated solutions calcite and aragonite have been shown to exhibit high negative ζ -potential values [52]. It should be noted that the potential-determining ions, Ca^{2+} and CO_3^{2-} , play a dominant role in the value of the electrical charge on the surface of the calcium carbonate crystallites. Moreover, it has been suggested that the presence of $\equiv CO_3^-$ and $\equiv CaCO_3^-$ on the surface (denoted by \equiv) of the substrate catalyzes the precipitation of calcite [53].

3.4 CONTROL OF THE SCALE DEPOSITS

The progressively more intense scarcity of freshwater supplies and the more stringent environmental regulations have promoted the need for larger number of cycles of water reuse in cooling waters involved in numerous processes. The implementation of this task, however, is limited by the precipitation and scale deposits formation consisting of calcium carbonate. Several methods are used for the control of calcitic scale, including pH adjustment, removal or reduction of scale-forming species, use of chemical additives acting as inhibitors of scale formation, and removal by mechanical and/or chemical means. Moreover, control methods include the prevention of particle adhesion on the walls of the equipment on which deposits are formed. Finally, it should be mentioned that there is considerable interest in the application of physical methods, including magnetic and electric treatment of water aiming at preventing scale formation [54–56].

The use of mineral acids, under certain circumstances, may be the only method to remove calcium carbonate but the concomitant corrosion problems should be taken care of with the simultaneous use of anticorrosion inhibitors. Moreover, acid injection downhole in geothermal wells or with formation water in oil production either in the form of mineral acids or as pressurized CO_2 [57] results in the reduction of the activity of the free carbonate ions and therefore of the supersaturation with respect to calcium carbonate. The use of chelants for the removal of calcium carbonate scale

deposits is not recommended as they are slow in action while almost stoichiometric quantities are needed. The calcium carbonate deposits consist largely of calcite or of aragonite under certain circumstances, depending on the solution supersaturation and on the presence of magnesium in water [58–60]. The most important approach in practice for the prevention and control of calcium carbonate scale formation is the use of water-soluble compounds which have the potential of interference with the processes of nucleation and crystal growth. Inhibition of the formation of crystals at the nucleation stage due to the presence of additives in the aqueous medium is known as *threshold inhibition* and the respective compounds *threshold inhibitors*. The first investigations were concerned with the inhibition of calcium carbonate in the presence of polyphosphates. Their effect was explained by the formation of small nuclei which were unstable and redissolved, thus retarding or canceling nucleation and the subsequent crystal growth [61]. In general, scale inhibitors are water-soluble compounds of relatively large size in comparison with the small ions, which through the ionizable functional groups they possess, are capable of adsorption onto the crystal growth active sites present at the various faces of the first crystallites that form once the nucleation barrier is overcome and the nuclei have grown over the critical size. Besides their effect on the retardation of kinetics, the presence of inhibitors in scale deposits affects the morphology of the crystals forming [62,63]. Besides acting on the retardation of the onset of precipitation, inhibitors may cause other effects, namely crystal distortion, where the effect of the inhibitors is expressed in the development of rounded surfaces with rather poor adhesion on the scaling surfaces. Another mode of action of the inhibitors is dispersion. In this case, the presence of the inhibitor results in the development of electric charge on the particles of the same sign as the respective charge of the walls. The electrostatic repulsion between the crystals of the same charge and the walls results in the reduction of deposition on the surfaces. There are several reports of the fact that the presence of additives like organophosphorus compounds and polyphosphates stabilize kinetically transient phases [64]. Finally, inhibitors may act through sequestration or chelation, binding calcium and/or other ions to form soluble complexes.

In the case that the rates of crystal growth are determined by the surface diffusion of the growth units, adsorption of the inhibitor molecules onto the active sites and more specifically at kinks may retard or even cancel the crystal growth process by blocking motion of the crystal growth units. The presence of metal ions has been associated not only with habit changes but also with retardation of the induction time preceding the formation of the calcium carbonate polymorph [65,66]. Based on the assumption that at conditions of surface-diffusion-controlled crystal growth processes, the inhibitors act by adsorption onto the active growth sites, it is possible to relate the adsorption characteristics with the kinetics of inhibition. The description of adsorption of the inhibitor on calcite by a thermodynamic model like the Langmuir model is given by Equation 3.20:

$$\theta = \frac{\Gamma_i}{\Gamma_m} = \frac{k_{ad} \cdot C_{eq}}{k_{des} + k_{ad} \cdot C_{eq}} \quad (3.20)$$

where

θ is the fraction of the sites on the surface occupied by the additive

Γ_i and Γ_m are the surface concentrations of the adsorbate corresponding to the solution conditions and at monolayer coverage, respectively

k_{ad} and k_{des} are the specific rate constants for adsorption and desorption, respectively

C_{eq} is the equilibrium concentration in the solution

Equation 3.20 upon rearrangement gives

$$\theta = \frac{\frac{k_{ad}}{k_{des}} \cdot C_{eq}}{1 + \frac{k_{ad}}{k_{des}} \cdot C_{eq}} \quad (3.21)$$

The ratio k_{ad}/k_{des} is referred to as the affinity constant, k_{aff} , and is a measure of the affinity of the adsorbate for the adsorbent [67,68]. Equation 3.20 may be rewritten as

$$\theta = \frac{\Gamma_i}{\Gamma_m} = \frac{k_{aff} \cdot C_{eq}}{1 + k_{aff} \cdot C_{eq}} \quad (3.22)$$

The rate of crystal growth in the presence of foreign compounds i , $R_{g,i}$, is related to the fraction of the unoccupied sites on the surface of the growing scale crystals, and to the rate of crystal growth in the absence of inhibitors, $R_{g,0}$, as shown in Equation 3.23:

$$R_{g,i} = R_{g,0} (1 - b\theta) \quad (3.23)$$

The rearrangement of Equation 3.23 and substitution of θ from Equation 3.21 yields [67]

$$\frac{R_0}{R_0 - R_i} = \frac{1}{b} + \frac{1}{b \cdot k_{aff}} \cdot \frac{1}{C_i} \quad (3.24)$$

where

b is a constant ($0 < b \leq 1$)

C_i the inhibitor concentration in the supersaturated solutions

Equation 3.24 has been widely applied to crystal growth and scale formation kinetics data and despite the fact that it is based on oversimplifications like the mostly unproven Langmuir-type adsorption, it provides a means for the comparison of various inhibitors tested with respect to their efficiency in the retardation of calcium carbonate formation [69]. Intensive research has been addressed to the development of novel polymeric products which may act as scale inhibitors. Important aspects of their activity include interactions with hardness ions (Ca, Mg, Ba), method of preparation, and the physicochemical characteristics of the monomers. It has been reported that terpolymers are more tolerant with respect to the hardness ions in comparison with homo- and copolymers [70]. The divalent ions may also change the conformation of the polymeric ions and control the morphology of the precipitating calcium carbonate [71]. Polymeric compounds with ionizable functional groups, including $-\text{COOH}$, PO_3H_2 , $-\text{SO}_3\text{H}$, and amino groups are the most commonly employed commercial scale inhibitor products. The investigation of a series of polymeric compounds containing carboxylic groups (polyacrylic acid, PAA) and carboxyl and amino groups containing poly-aspartic acid (P-AS) were shown to retard the onset of spontaneous precipitation of calcium carbonate, as can be seen in Figure 3.11 [72].

The presence of phosphonic groups in the water additives inhibited the precipitation of calcium carbonate and stabilized the formation of the unstable vaterite, as can be seen in Figure 3.12 [73].

The comparison of a series of phosphonates with respect to their inhibition of calcium carbonate has shown that these compounds are both threshold inhibitors, as can be seen in Figure 3.13.

These compounds also act as retardants, decreasing the rates of nucleation and growth of calcium carbonate from supersaturated solutions, as shown in Figure 3.14.

Tomson and coworkers [74] have developed a semiempirical model, based on the nucleation theory and experimental observations. A nucleation inhibitor index was thus developed for the prediction of the induction period in the presence of inhibitors. According to this evaluation, 1-hydroxy ethylidene-1,1-diphosphonic acid (HEDP) was found to be the most effective inhibitor on the weight basis. Provided that the activity of the inhibitors is due to their adsorption onto the developing crystals, both the type of the functional groups (pKs) and their geometry are important factors playing decisive role in their efficiency. Comparison of different polymeric inhibitors with respect to their

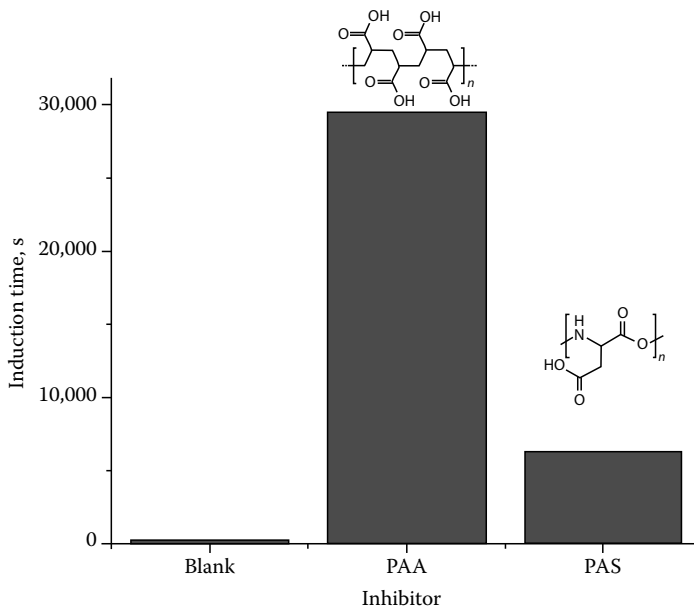


FIGURE 3.11 Effect of the presence of 0.5 ppm of inhibitor on the induction time preceding the precipitation of calcium carbonate: Total calcium = Total carbonate = 5.5 mM, NaCl 150 mM, pH 8.50, 35°C. (From Amjad, Z., *Tenside Surf. Deterg.*, 36, 162, 1999.)

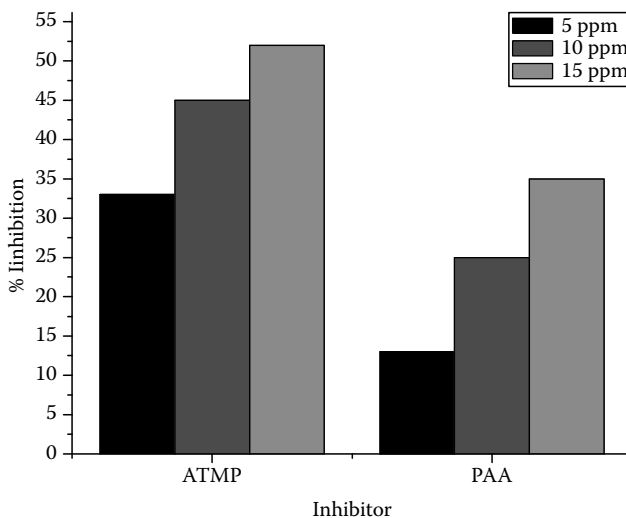


FIGURE 3.12 Comparison of inhibition efficiency of PAA and of aminotrimethylene phosphonic (ATMP) acid. Total calcium 6.4 mM, total carbonate 12 mM, CO₂ bubbling (80L/h) for 5 h, 60°C. (From Tang, Y. et al., *Desalination*, 229, 55, 2008.)

efficiency in the retardation of calcium carbonate precipitation has shown that PAA homopolymers were more efficient in comparison with poly(acrylic acid:2-acrylamido-2-methyl propane sulfonic acid) (PAS) and even more efficient than poly(acrylic acid:2-acrylamido-2-methyl propane sulfonic acid: sulfonated styrene) (PSS) [75]. Similar correlation of the inhibitory efficiency has also been reported for copolymers that contained maleic acid, the presence of which improved the activity of the inhibitor with respect to the nucleation and crystal growth of calcium carbonate [76].

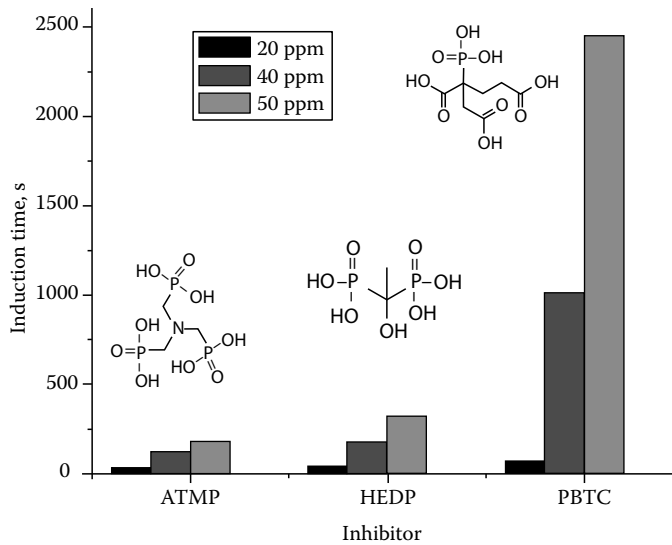


FIGURE 3.13 Effect of the presence of phosphonate inhibitors on the induction time preceding the precipitation of calcium carbonate: 223 \times calcite supersaturation, pH 9.0, 50°C. (From Amjad, Z. and Zuhl, R.W., Kinetic and morphological investigation on the precipitation of calcium carbonate in the presence of inhibitors, Corrosion/2006, Paper No. 6385 NACE International, Houston, TX, 2006.)

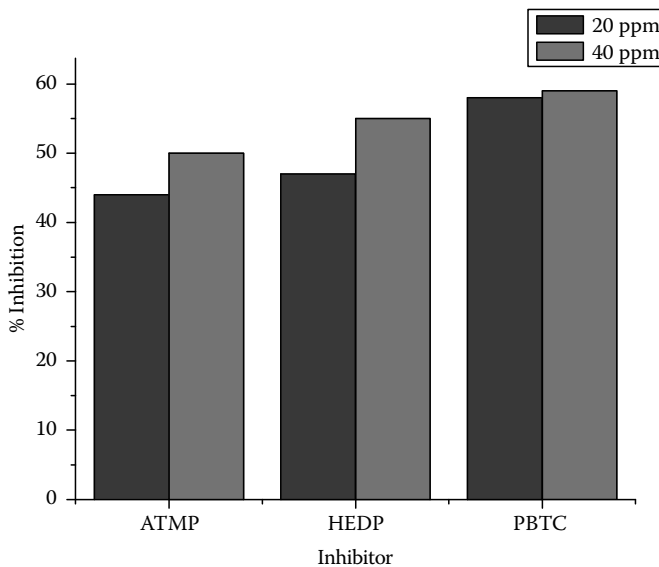


FIGURE 3.14 Percent inhibition of calcium carbonate precipitation in the presence of phosphonate inhibitors: 223 \times calcite supersaturation, pH 9.0, 50°C. (From Amjad, Z. and Zuhl, R.W., Kinetic and morphological investigation on the precipitation of calcium carbonate in the presence of inhibitors, Corrosion/2006, Paper No. 6385 NACE International, Houston, TX, 2006.)

The molecular weight of the polymeric inhibitors is an important issue. Investigations on the efficiency of PAA have concluded that relatively low-molecular-weight polyacrylates are more efficient inhibitors of calcium carbonate formation [77]. The differences obtained were attributed to differences in the adsorption of the polymers onto the active sites of the growing crystals. Similar results have been reported for the inhibition of calcium phosphates by polycarboxylates [78].

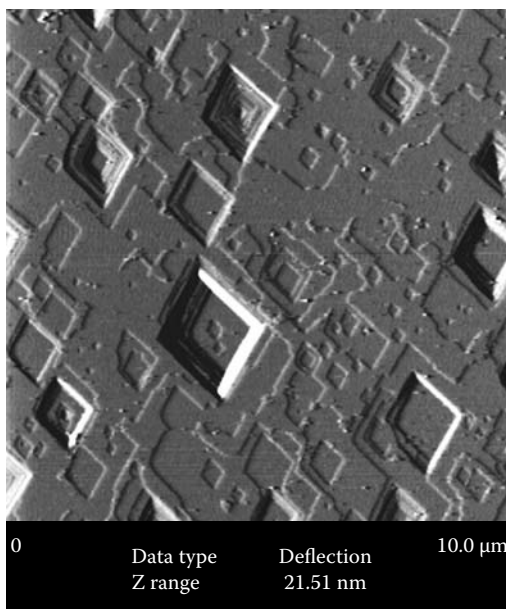


FIGURE 3.15 Dissolution of single crystal of calcite under flow conditions; pH 8.1, 25°C, 0.66 mL min⁻¹.

The dissolution of calcium carbonate scale at conditions far from equilibrium is believed to follow a mass transport-controlled mechanism. Such conditions are prevalent in the low pH range [79]. The dissolution of calcite crystals results in the formation of steps and etch pits which are the active sites for dissolution. Typical surface morphology of a natural calcite single crystal is shown in Figure 3.15. The picture was taken with an atomic force microscope (AFM) with an open cell under flow of undersaturated solution (0.66 mL min⁻¹). Deep etch pits and rising steps are clearly shown. The application of inhibitors interacts with these sites, resulting in slower step recession.

The work on calcite dissolution published by Plummer et al. [80,81] showed that the surface-controlled mechanism is important at conditions of higher pH (and closer to equilibrium). In this case, the surface activities of species like Ca²⁺, H⁺, HCO₃⁻, and H₂CO₃⁰ play an important role. However, the validity of this model was questioned with respect to applicability in natural materials for which the rates of dissolution were significantly lower. This effect was attributed to the adsorption of foreign substances on the active dissolution sites [82]. A comprehensive review on the formation and dissolution mechanisms of calcium carbonate has recently been published by Morse et al. [83]. The results obtained for naturally occurring samples are very interesting for calcitic scale deposits which grow in the presence of impurities included in the aqueous media that include both metal ions and ionized organic compounds. A typical demonstration of this fact may be seen in the different kinetics obtained in the case of two different calcitic marbles, Pentelic and Carrara. These materials consist exclusively of calcite (>98%) but they contain different amounts of manganese and magnesium ions, in addition to silica inclusions. The results are shown in Figure 3.16 in which data from dissolution experiments in solutions undersaturated with respect to calcite and inoculated with powdered marbles of the two types examined are plotted [84,85].

Dissolution of calcite deposited due to contact of water with solid substrates proceeds in a way which is the reverse process of the crystal growth. Surface diffusion from the kink sites to steps and terraces and finally to the bulk solution are the elementary steps of importance to the dissolution process of interest to the scale formed from water use in industrial applications. AFM studies have shown that the reactivity of the calcite surfaces increases through the increase in the step density and in the step edges roughness [42]. Dissolution of calcium carbonate may be promoted by the presence of additives which are able to form complexes with the calcium ions on the surface of the

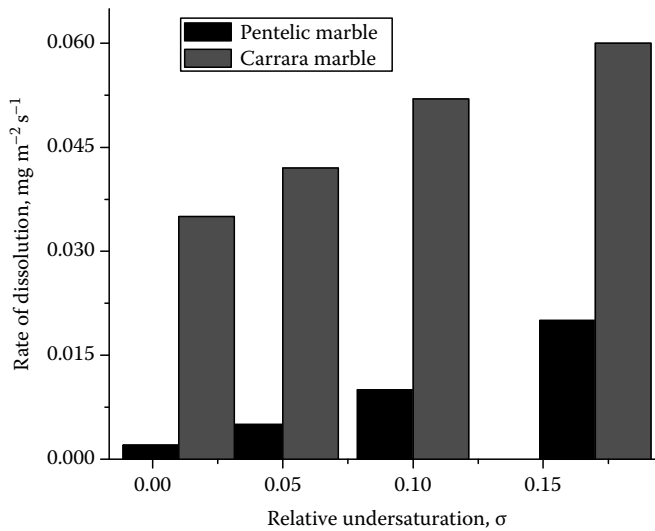


FIGURE 3.16 Dissolution rates as a function of the relative undersaturation for two types of calcitic marble. 25°C, pH 8.25.

deposits [86]. On the other hand, at low concentrations inhibitors may adsorb onto the active sites of calcite for dissolution and thus reduce the rates of dissolution [85,87,88].

It should be noted that surface speciation is important for understanding the effect of the action of the water-soluble inhibitors on the kinetics of dissolution. Spectroscopic studies provide evidence that the surface calcium and carbonate ions at the calcite/water interface are hydrolyzed, forming the species $\equiv\text{CaOH}^0$ and $\equiv\text{CO}_3\text{H}^0$ (\equiv represents the calcite surface) with a 1:1 stoichiometry [89–92]. The additives present in the aqueous solutions interact with both these surface groups, but there are also considerable lateral interactions between the adsorbed molecules, which are located at the inner Helmholtz plane of the electrical double layer at the calcite/water interface [93].

The rates of dissolution can be monitored in a similar way as the precipitation rates. A number of interesting methods have been suggested for monitoring the deposition and/or dissolution of the calcium carbonate deposits based on acoustic and electrochemical methods and/or combinations [94]. The rate equations relating the measured rates of dissolution as a function of the relative solution undersaturation for the various mechanisms possible (surface diffusion and volume diffusion) are the same as the respective equations for the crystal growth [49].

3.5 SUMMARY

The formation of tenaciously adhering calcium carbonate scale in installations and equipment in contact with water is a persistent problem in the industry. Understanding the mechanism of formation of calcium carbonate scale is essential, and among the prerequisites to reach this understanding is the thermodynamics analysis of the fluid aqueous phase in contact with water. The ionic composition of the aqueous medium, including pH and temperature, determines the degree of deviation of the system from equilibrium. The thermodynamic driving force for the formation of scale deposits can be calculated from the equilibria involved and the mass-balance equations. Kinetics of scale formation is a strong function of the driving force but the transient formation of unstable intermediate phases complicates the overall picture. In industrial applications, scale formation is heterogeneous as a rule and the prevalent mechanism depends on the local conditions of supersaturation and fluid dynamics. Prevention and control of the scale deposits is a challenge, and several attempts involving widely different approaches and methods are employed. The most common approach, however, is the use of water-soluble inhibitors which interfere either with nucleation or with crystal

growth or with both, slowing down the respective processes. Threshold inhibitors extend the induction times and in some cases cancel scale formation, while in most cases, adsorption of the inhibitors on the active sites of the first nucleating crystallites reduces or stops their further growth to form undesirable deposits. The surface of the deposits, which depends on the type and concentration of the functional groups present, plays a decisive role in the interactions of the additives with the substrates. Kinetic laws are helpful in understanding the deposit formation mechanisms and to design the most appropriate scale prevention strategy. Low-molecular-weight inhibitors are more effective probably because of their more efficient adsorption onto the developing crystallites. Finally, the dissolution of the calcium carbonate deposits is a process reverse to crystal growth and may be described both mechanistically and in terms of rate laws in a similar way as crystal growth. The role of additives in dissolution may be dual, either accelerating dissolution through complex formation or inhibiting it through the blockage of the active sites for dissolution.

REFERENCES

1. Kitano, Y. A study of the polymorphic formation of calcium carbonate in thermal springs with emphasis on the temperature. *Bull Chem Soc Jpn*, 35, 1980–1985 (1962).
2. Carlson, W. D. The polymorphs of CaCO_3 and the aragonite-calcite transformation. In *Reviews in Mineralogy*, Vol. 11, pp. 191–225, Ribbe, P. H. (Ed.), Mineralogical Society of America, Chelsea, MI (1983).
3. Brecevic, L. and Nielsen, A. E. Solubility of amorphous calcium carbonate. *J Cryst Growth*, 98, 504–510 (1989).
4. Dorfmueller, G. Action of carbonic acid on lime-water and sugar-lime solutions and of alkali carbonates on solutions of calcium salts. *Deut Zuckerind*, 63, 1217–1220 (1938).
5. Robinson, R. A. and Stokes, R. H. *Electrolyte Solutions*, Butterworths, London, U.K. (1959).
6. Donnet, M., Bowen, P., Jongen, N., Lemaître, J., and Hofmann, H. Use of seeds to control precipitation of calcium carbonate and determination of seed nature. *Langmuir*, 21, 100–110 (2005).
7. Klepetsanis, P., Kladi, A., Ostvold, T., Kontoyiannis, C. G., Koutsoukos, P. G., Amjad, Z., and Reddy, M. M. The inhibition of calcium carbonate formation in aqueous supersaturated solutions. Spontaneous precipitation and seeded crystal growth. In *Advances in Crystal Growth Inhibition Technologies*, Amjad, Z. (Ed.), Kluwer Academic Press, Boston, MA (2000).
8. Lee, S. H. and Knudsen, J.G. Scaling characteristics of cooling tower water. *ASHRAE Trans*, 85(1), 281–302 (1989).
9. Miyazaki, H., Mizutani, M., Yamashita, T., Aoyama, H., Seue, H., and Ota, T. Growth of calcium carbonate crystal imitating stalagmite growth in nature. *Mater Res Bull*, 41, 1272–1278 (2006).
10. Singh, R. P. Carbonate precipitation on sand (α -quartz). In *Fundamentals and Applications of Anion Separations*, pp. 325–339, Moyer, B. A. and Singh, R. P. (Eds.), Kluwer Academic Publishers, New York (2004).
11. Baer, D. R., Liang, Y., Lea, A. S., Amonette, J. E., and Colton, N. G. Scanning-force microscopy measurements of dissolution and growth processes: CaCO_3 examples. In *State-of-the-Art Application of Surface and Interface Analysis Methods to Environmental Material Interactions*, Baer, D. R., Clayton, C. R., Halada, G. P., and Davis, P. V. (Eds.), The Electrochemical Society Proceedings Series, Pennington, NJ (2001).
12. Kralj, D. and Vdovic, N. The influence of some naturally occurring minerals on the precipitation of calcium carbonate minerals. *Water Res*, 34, 179–184 (2000).
13. Kim, W. T. and Cho, W. I. A study of the scale formation around air bubble attached on a heat-transfer surface. *Int Commun Heat Mass Transfer*, 29, 1–14 (2002).
14. Bramson, D., Hasson, D., and Semiat, R. The roles of gas bubbling, wall crystallization and particulate deposition in CaSO_4 scale formation. *Desalination*, 100, 105–113 (1995).
15. Andritsos, N., Karabelas, A. J., and Koutsoukos, P. G. Morphology and structure of CaCO_3 scale layers formed under isothermal conditions. *Langmuir*, 13, 2873–2879 (1997).
16. Hasson, D. and Semiat, R. Scale control in saline and wastewater desalination. *Isr J Chem*, 46, 97–104 (2006).
17. Karabelas, A. J. Scale formation in tubular heat exchangers-research priorities. *Int J Thermal Anal*, 41, 682–692 (2002).
18. Khan, J. R. and Zubair, S. M. An improved design and rating analyses of counterflow wet cooling towers. *Trans ASME J Heat Transfer*, 123, 770–778 (2001).
19. Nancollas, G. H. *Interactions in Electrolyte Solutions*, Elsevier, Amsterdam, the Netherlands (1966).

20. Sheikholeslami, R. Scaling potential index (SPI) for CaCO_3 based on Gibbs free energies. *AIChE J*, 51, 1782–1789 (2005).
21. Sheikholeslami, R. Mixed salts—Scaling limits and propensity. *Desalination*, 154, 117–127 (2003).
22. Nordstrom, D. K., Plummer, L. N., Wigley, T. M. L., Wolery, T. J., Ball, J. W., Jenne, E. A., Basset, R. L., Crerar, D. A. et al. A comparison of computerized chemical models for equilibrium calculations in aqueous systems. In *Chemical Modeling in Aqueous Systems, Speciation, Sorption, Solubility, and Kinetics*, pp. 857–892, Jenne, E. A. (Ed.), Series 93, American Chemical Society, Washington DC (1979).
23. Plummer, L. N., Parkhurst, D. L., Fleming, G. W., and Dunkle, S. A. A computer program incorporating Pitzer's equations for calculation of *geochemical* reactions in brines. U.S. Geological Survey Water-Resources Investigations Report 88-4153, 310, Denver, CO (1988).
24. David, L., Parkhurst, D. L., and Appelo, C. A. J. PHREEQC. A computer program for speciation, batch-reaction, one-dimensional transport, and inverse geochemical calculation. USGS, Denver, CO (1999).
25. Söhnel, O. *Precipitation*, Butterworth-Heinemann, Oxford, U.K. (1992).
26. Hasson, D., Semiati, R., Bramson, D., Busch, M., and Limoni-Relis, B. Suppression of CaCO_3 scale deposition by anti-scalants. *Desalination*, 118, 285–296 (1998).
27. Dalas, E. and Koutsoukos, P. G. Calcium carbonate scale formation and prevention in a flow-through system at various temperatures. *Desalination*, 78, 403–416 (1990).
28. Mullin, J. W. *Crystallization*, 3rd edn., Butterworths-Heinemann, Oxford, U.K. (1993).
29. Ogino, T., Suzuki, T., and Sawada, K. The formation and transformation mechanism of calcium carbonate in water. *Geochim Cosmochim Acta*, 51, 2757–2767 (1988).
30. Nancollas, G. H. and Reddy, M. M. The crystallization of calcium carbonate II. Calcite growth mechanism. *J Colloid Interface Sci*, 37, 824–830 (1971).
31. Nancollas, G. H. and Reddy, M. M. The kinetics of crystallization of scale forming minerals. In *SPE 4360, SPE-AIME Oilfield Chemistry Symposium*, pp. 117–126, Denver, CO, May 24–25 (1973).
32. Garside, J., Gibilaro, L. G., and Tavare, N. S. Evaluation of crystal growth kinetics from a desupersaturation curve using initial derivatives. *Chem Eng Sci*, 37, 1625–1628 (1982).
33. Spanos, N. and Koutsoukos, P. G. The transformation of vaterite to calcite: Effect of the conditions of the solutions in contact with the mineral phase. *J Cryst Growth*, 191, 783–790 (1998).
34. Stamatakis, E., Stubos, A., Palyvos, J., Chatzichristos, C., and Muller, J. An improved predictive correlation for the induction time of CaCO_3 scale formation during flow in porous media. *J Colloid Interface Sci*, 286, 7–13 (2005).
35. Nancollas, G. H. and Mohan, M. S. The growth of hydroxyapatite crystals. *Arch Oral Biol*, 15, 731–740 (1970).
36. Gutjahr, A., Dabringhaus, H., and Lacmann, R. Studies of the growth and dissolution kinetics of the CaCO_3 polymorphs calcite and aragonite I. Growth and dissolution rates in water. *J Cryst Growth*, 158, 296–309 (1996).
37. Chen, P. C., Tai, C. Y., and Lee, K. C. Morphology and growth rate of calcium carbonate crystals in a gas-liquid-solid reactive crystallizer. *Chem Eng Sci*, 52, 4171–4177 (1997).
38. Kazmierczak, T. F., Tomson, M. B., and Nancollas, G. H. Crystal growth of calcium carbonate. A controlled composition kinetic study. *J Phys Chem*, 86, 103–107 (1982).
39. Spanos, N. and Koutsoukos, P. G. Kinetics of precipitation of calcium carbonate in alkaline pH at constant supersaturation. Spontaneous and seeded growth. *J Phys Chem B*, 102, 6679–6684 (1998).
40. Nancollas, G. H. The growth of crystals in solution. *Adv Colloid Interface Sci*, 10, 215–252 (1979).
41. Sabbides, Th. G. and Koutsoukos, P. G. The crystallization of calcium carbonate in artificial seawater: Role of the substrate. *J Cryst Growth*, 133, 13–22 (1993).
42. De Guidici, G. Surface control vs. diffusion control during calcite dissolution: Dependence of step-edge velocity upon solution pH. *Am Mineral*, 87, 1279–1285 (2002).
43. Zieba, A., Sethuraman, G., Perez, F., Nancollas, G. H., and Cameron, D. Influence of organic phosphonates on hydroxyapatite crystal growth kinetics. *Langmuir*, 12, 2853–2858 (1996).
44. Sushko, P. V., Gavartin, J. L., and Shluger, A. L. Electronic properties of structural defects at the MgO (001) surface. *J Phys Chem B*, 106, 2269–2276 (2002).
45. Xyla, A. G., Mikroyannidis, J., and Koutsoukos, P. G. The inhibition of calcium carbonate precipitation in aqueous media by organophosphorus compounds. *J Colloid Interface Sci*, 153, 537–551 (1992).
46. Tai, C. Y. and Chen, F. B. Polymorphism of CaCO_3 precipitated in a constant composition environment. *AIChE J*, 44, 1790–1798 (1998).
47. Chen, T., Neville, A., Sorbie, K., and Zhong, Z. Using in situ synchrotron radiation wide angle X-ray scattering (WAXS) to study CaCO_3 scale formation at ambient and elevated temperatures. *Faraday Discuss*, 136, 355–365 (2007).

48. Hasson, D., Bramson, D., Limoni-Relis, B., and Semiat, R. Influence of the flow system on the inhibitory action of CaCO₃ scale prevention additives. *Desalination*, 108, 67–79 (1996).
49. Zhang, J. W. and Nancollas, G. H. Mechanisms of growth and dissolution of sparingly soluble salts. In *Reviews in Mineralogy*, Vol. 23, pp. 365–396, Hochella, M. F. and A. F. White (Eds.), Mineralogical Society of America, Washington DC (1990).
50. Andritsos, N., Kontopoulou, M., Karabelas, A. J., and Koutsoukos, P. G. Calcium carbonate deposit formation under isothermal conditions. *Can J Chem Eng*, 74, 911–919 (1996).
51. Hasson, D., Sherman, H., and Biton, M., Prediction of calcium carbonate scaling rates. In *Proceedings of the 6th International Symposium on Fresh Water from the Sea*, pp. 193–199, Delyannis A. and Delyannis, E. (Eds.), European Federation of Chemical Engineers, Las Palmas, Gran Canaria, Spain (1978).
52. Moulin, P. and Roques, H. Zeta potential measurement of calcium carbonate. *J Colloid Interface Sci*, 261, 115–126 (2003).
53. Lin, Y. P. and Singer, P. C. Effects of seed material and solution composition on calcite precipitation. *Geochim Cosmochim Acta*, 69, 4495–4504 (2005).
54. Baker, J. S. and Judd, S. J. Magnetic amelioration of scale formation. *Water Res*, 30, 247–260 (1996).
55. Lipus, L. C., Krope, J., and Crepinsek, L. Dispersion destabilization in magnetic water treatment. *J Colloid Interface Sci*, 236, 60–66 (2001).
56. Gabrielli, C., Maurin, G., Francy-Chausson, H., Thery, P., Tran, T. I. M., and Tlili, M. Electrochemical water softening: Principle and application. *Desalination*, 201, 150–163 (2006).
57. Paul, J. M. Method for scale removal in a wellbore. U.S. Patent No. 5,146,988 (1992).
58. Sabbides, Th., Giannimaras, E., and Kutsoukos, P. G. The precipitation of calcium carbonate in artificial seawater at sustained supersaturation. *Environ Technol*, 13, 73–80 (1992).
59. Wray, J. L. and Farringtondoanni, E. L. S. Precipitation of calcite and aragonite. *J Am Chem Soc*, 79, 2031–2034 (1957).
60. Turner, C. W. and Smith, D. W. Calcium carbonate scaling kinetics determined from radiotracer experiments with calcium-47. *Ind Eng Chem Res*, 37, 439–448 (1998).
61. Cooper, K. G., Hanlon, L. G., Smart, G. M., and Talbot, R. E. The threshold inhibition phenomenon. *Desalination*, 31, 257–266 (1979).
62. Amjad, Z. and Zuhl, R. W. Kinetic and morphological investigation on the precipitation of calcium carbonate in the presence of inhibitors. Corrosion/2006, Paper No. 6385 NACE International, Houston, TX (2006).
63. GuiCai, Z., JiJiang, G. MingQin, S., BinLin, P., Tao, M., and ZhaoZheng, S. Investigation of scale inhibition mechanisms based on the effect of scale inhibitor on calcium carbonate crystal forms. *Sci China Ser B Chem*, 50, 114–120 (2007).
64. Gal, J.-Y., Bollinger, J. C., Tolosa, H., and Gache, N. Calcium carbonate solubility: A reappraisal of scale formation and inhibition. *Talanta*, 43, 1497–1509 (1996).
65. Sohnel, O. and Mullin, J. W. Precipitation of calcium carbonate. *J Cryst Growth*, 60, 239–250 (1982).
66. Chen, T., Neville, A., and Yuan, M. Influence of Mg²⁺ on CaCO₃ formation-bulk precipitation and surface deposition. *Chem Eng Sci*, 61, 5318–5327 (2006).
67. Nancollas, G. H. and Zawacki, S. J. Inhibitors of crystallization and dissolution. In *Industrial Crystallization* 84, pp. 51–59, Jancic, S. J., and de Jong, E. J. (Eds.), Elsevier, Amsterdam, the Netherlands (1984).
68. Amjad, Z., Pugh, J., and Reddy, M. M. Kinetic inhibition of calcium carbonate crystal growth in the presence of natural and synthetic organic inhibitors, In *Water Soluble Polymers. Solution Properties and Applications*, pp. 131–147, Amjad, Z. (Ed.), Plenum Press, New York (1998).
69. Koutsoukos, P. G., Klepetsanis, P., Spanos, N., and Kanellopoulou, D. G. Calcium carbonate crystal growth and dissolution inhibitors. Corrosion/2007, Paper No. 7052 NACE International, Houston, TX (2007).
70. Amjad, Z. Interactions of hardness ions with polymeric scale inhibitors in aqueous systems. *Tenside Surf Deterg*, 42, 71–77 (2005).
71. Pai, R. K. and Pillai, S. Divalent cation-induced variations in polyelectrolyte conformation and controlling calcite morphologies: Direct observation and phase transition by atomic force microscopy. *J Am Chem Soc*, 130, 13074–13078 (2008).
72. Amjad, Z. Precipitation of calcium carbonate in aqueous systems. *Tenside Surf Deterg*, 36 162–167 (1999).
73. Tang, Y., Yang, W., Yin, X., Liu, Y., Yin, P., and Wang, J. Investigation of CaCO₃ scale inhibition by PAA, ATPM and PAPEMP. *Desalination*, 229, 55–60 (2008).
74. He, S., Kan, A. T., and Tomson, M. B. Inhibition of calcium carbonate precipitation in NaCl brines from 25 to 90°C. *Appl Geochem*, 14, 17–25 (1999).

75. Amjad, Z., Klepetsanis, P. G., and Koutsoukos, P. G. Precipitation and crystal growth of calcium carbonate in the presence of acrylic acid copolymers. In Paper No. 267, *15th International Symposium on Industrial Crystallization*, Sorrento, Italy, September 15–18 (2002).
76. Klepetsanis, P. G., Koutsoukos, P. G., Chitanu, G. C., and Karpov, A. The inhibition of calcium carbonate formation by copolymers containing maleic acid. In *Water Soluble Polymers. Solution Properties and Applications*, Amjad, Z. (Ed.), Plenum Press, New York, (1998).
77. Jada, A., Ait Akbour, R., Jacquemet, C., Suau, J. M., and Guerret, O. Effect of sodium polyacrylate molecular weight on the crystallogenesis of calcium carbonate. *J Cryst Growth*, 306, 373–382 (2007).
78. Howie-Meyers, C. L., Yu, K., Elliot, D., Vasudevan, T., Aronson, M. P., Ananthapadmanabhan, K. P., and Somasundaran, P. Crystal growth inhibition of hydroxyapatite by polycarboxylates. In *Mineral Scale Formation and Inhibition*, Amjad, Z. (Ed.), Plenum Press, New York (1995).
79. Berner, R. A. and Morse, J. W. Dissolution kinetics of calcium carbonate in seawater: IV. Theory of calcite dissolution. *Am J Sci*, 274, 108–134 (1974).
80. Plummer, L. N., Wigley, T. M. L., and Parkhurst, D. L. The kinetics of calcite dissolution in CO₂ water systems at 5°C–60°C and 0.0–1 atm CO₂. *Am J Sci*, 278, 179–216 (1978).
81. Plummer, L. N., Wigley, T. M. L., and Parkhurst, D. L. Critical review of the kinetics of calcite dissolution and precipitation. In *Chemical Modeling in Aqueous Systems*, pp. 537–572, Jenne, E. A. (Ed.), American Chemical Society Symposium Series 93, Washington DC (1979).
82. Svensson, U. and Dreybrodt, W. Dissolution kinetics of natural calcite minerals in CO₂–water systems approaching calcite equilibrium. *Chem Geol*, 100, 129–145 (1992).
83. Morse, J. W., Arvidson, R. S., and Lüttge, A. Calcium carbonate formation and dissolution. *Chem Rev*, 107, 342–381 (2007).
84. Orkoula, M. G., and Koutsoukos, P. G. Dissolution of Pentelic marble in alkaline pH. *Langmuir*, 16, 7623–7267 (2000).
85. Kanellopoulou, D. G. and Koutsoukos, P. G. The calcitic marble/water interface: Kinetics of dissolution and inhibition with potential implications in stone conservation. *Langmuir*, 19, 5691–5699 (2003).
86. Demadis, K., Lykoudis, P., Raptis, R., and Mezei, G. Phosphonocarboxylates as chemical additives for calcite scale dissolution and metallic corrosion inhibition based on a calcium-phosphonocarboxylate organic-inorganic hybrid. *Cryst Growth Des*, 6, 1064–1067 (2006).
87. Compton, R. G. and Brown, C. A. The inhibition of calcite dissolution/precipitation: Mg²⁺ cations. *J Colloid Interface Sci*, 165, 445–449 (1994).
88. Compton, R. G. and Brown, C. A. The inhibition of calcite dissolution/precipitation: 1,2-Dicarboxylic acids. *J Colloid Interface Sci*, 170, 586–590 (1995).
89. Stipp, S. L., Eggleston, C. M., and Nielsen, B. S. Calcite surface structure observed at microtopographic and molecular scales with atomic force microscopy (AFM). *Geochim Cosmochim Acta*, 58, 3023–3033 (1994).
90. Van Cappellen, P., Charlet, L., Stumm, W., and Wersin, P., A. A surface complexation model of the carbonate mineral-aqueous solution interface. *Geochim Cosmochim Acta*, 57, 3505–3518 (1993).
91. Schindler, P. W. and Stumm, W. The surface chemistry of oxides and hydroxides and oxide minerals. In *Aquatic Surface Chemistry*, pp. 83–110, Stumm, W. (Ed.), John Wiley & Sons, New York (1987).
92. Fenter, P., Uhler, P. G., Dimasi, E., Srajer, G., Sorensen, L. B., and Sturchio, N. C. Surface speciation of calcite observed in situ by high resolution x-ray reflectivity. *Geochim Cosmochim Acta*, 64, 1221–1228 (2000).
93. Spanos, N., Kanellopoulou, D. G., and Koutsoukos, P. G. The interaction of diphosphonates with calcitic surfaces: Understanding the inhibition activity in marble dissolution. *Langmuir*, 22, 2074–2081 (2006).
94. Ramadan, S. and Idrissi, H. In situ monitoring of deposition and dissolution of calcium carbonate by acoustic emission techniques associated to electrochemical measurements. *Desalination*, 219, 358–366 (2008).

4 Calcium Carbonate: Polymorph Stabilization in the Presence of Inhibitors

Peter G. Koutsoukos and Tao Chen

CONTENTS

4.1	Introduction.....	61
4.2	Calcium Carbonate Polymorphs	62
4.2.1	Scale Inhibitors	63
4.2.2	Effect of Inorganic Ions	63
4.2.3	Effect of Organic Compounds on the Kinetics and the Characteristics of Calcium Carbonate Scale	67
4.2.4	Effect of DETPMP on Scale Formation at 80°C	71
4.3	Summary	77
	References.....	77

4.1 INTRODUCTION

Calcium carbonate is a common scale component in water-intensive processes primarily because of the inverse solubility of this salt [1–3]. The relatively high calcium and carbonate concentration levels in natural waters result from the composition of geological formations with the aquifer [3]. The calcium carbonate scaling problem depends not only on the solution composition (pH, calcium, and carbonate concentrations), but also on the crystal morphology of the precipitated phase. The polymorphism of the calcium carbonate system is responsible for the formation of particles of various shapes and sizes [4–6]. Some crystal shapes will pack together and form tenaciously adhering scale deposits, whereas others can be readily swept away in the stream of salt solution in contact with the surface [7]. Depending on the experimental conditions and/or on the presence of foreign compounds or metal ions in the aqueous medium in which scale deposits are formed, three calcium carbonate polymorphs may be formed: calcite, aragonite, and vaterite [8]. The formation of amorphous calcium carbonate has been reported [9,10] in addition to the two hydrate forms of calcium carbonate: monohydrate or monohydrocalcite and hexahydrate or ikaite [11,12].

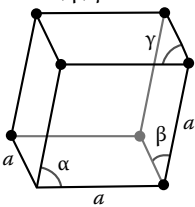
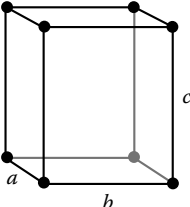
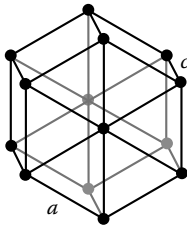

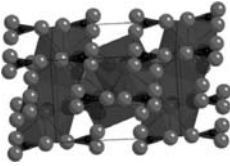
Calcite is the most stable polymorph of calcium carbonate. Calcite is trigonal–rhombohedral, though actual calcite rhombohedra are rare as natural crystals. However, they show a remarkable variety of habits, including acute to obtuse rhombohedra, tabular forms, prisms, or various scale-nohedra. Calcite exhibits several twinning types, adding to the variety of observed forms. It may occur as fibrous, granular, lamellar, or compact [13–16]. Aragonite is one of the naturally occurring polymorphs of calcium carbonate but also frequently encountered in scale deposits formed at temperatures exceeding 50°C [17,18]. Vaterite, like aragonite, is a metastable phase of calcium carbonate and forms rather rarely on the surface of the earth at ambient conditions [19], in coal liquefaction [20], and in cold waters where it forms cementitious deposits [21]. In scale deposits,

vaterite is reported to form as a transient phase, which may be stabilized at specific experimental conditions, including the application of electric field [22,23], the presence of ions like magnesium [24], and various types of organic compounds dissolved in the aqueous medium in which calcium carbonate is formed [25,26].

4.2 CALCIUM CARBONATE POLYMORPHS

The main polymorphic crystalline forms of calcium carbonate are presented in Table 4.1. In heterogeneous deposition cases, vaterite crystals are generally observed in direct contact with the substrate [27]. Only calcite or aragonite crystals were observed on the top layer, depending on the experimental conditions. It was found that calcite nucleates either on the substrate surface beside vaterite or on the top of the previously formed vaterite crystals [28]. There is considerable evidence that in the calcium carbonate system, crystal growth takes place through the formation of metastable intermediates, which initially are favored kinetically but which rapidly transform to the thermodynamically stable phases typically observed in the field after equilibrium has been reached [29–32].

TABLE 4.1
Crystallographic Description of the Main Polymorphic
Forms of Calcium Carbonates

Parameter	Calcite	Aragonite	Vaterite
Crystal system	Hexagonal–rhombohedral $\alpha, \beta, \gamma \neq 90^\circ$	Orthorhombic $a \neq b \neq c$	Hexagonal $a \neq c$
			
Unit cell			—
Crystal morphology	Cubic to rhombohedral	Needlelike or elongated prisms	Spherical or disklike
Parameter	$a = 4.89$ $c = 17.062$	$a = 4.9623$ $b = 7.968$ $c = 5.744$	$a = 7.147$ $c = 16.917$
Density (g/cm ³)	2.71	2.93	2.66

Note: a , b , and c represent the lattice parameter according to the three spatial directions.

The thermodynamically unstable vaterite tends to transform naturally into aragonite or calcite. The formation of aragonite from the less-stable formations follows a two-step process. First, the unstable vaterite kernels undergo a phase transformation to aragonite without change in their external habit. In the second step, the characteristic aragonite prismatic crystallites grow on the extremities of the kernel. It has been shown that the formation of aragonite on a vaterite crystal is a transformation of the vaterite structure and not a further crystallization of this polymorph upon vaterite crystals [29–32]. In the presence of fluid, the polymorph transitions from aragonite to calcite and from vaterite to calcite or aragonite are fast [33]. A number of factors play a controlling role in the regulation of the stability of various calcium carbonate polymorphs. Among these factors, the fluid pH [34], temperature [35], supersaturation [29], and the presence of additives are the most important [36,37]. It should be stressed, however, that changes in parameters such as temperature, pH, ionic strength, and/or concentration of the component ions ultimately affect the solution supersaturation, which is the most important factor affecting the formation and transformation of calcium carbonate polymorphs.

The polymorphic phase forming on heat-transfer surfaces depends on the degree of supersaturation. Calcite crystals were observed when the supersaturation ratio at the temperature of the heat-transfer surface was relatively moderate, whereas aragonite was observed when the supersaturation was relatively high. There was no sharp boundary between the regimes where calcite and aragonite were the dominant crystalline phases [38]. Of particular interest is the effect of the presence of impurities on the formation of the various calcium carbonate polymorphs and/or the stabilization of transient phases in the presence of either inorganic or organic compounds dissolved in the aqueous medium.

4.2.1 SCALE INHIBITORS

The use of scale inhibitors has been a standard industrial practice for the inhibition of calcium carbonate scale for several decades already. Inhibitors retard the nucleation and growth of scale, depending on their specific functionality. The inhibitors are water-soluble compounds and inhibit scale formation through their interaction with the developing nuclei at different stages (i.e., nucleation, crystal growth, and/or processes such as ageing, agglomeration, etc.). The influence of inhibitors on the formation of various CaCO_3 polymorphs has been the subject of numerous investigations. Substances that are able to inhibit the formation of calcium carbonate scale include both inorganic ions and water-soluble organic and/or polymeric compounds.

4.2.2 EFFECT OF INORGANIC IONS

The presence of dissolved iron ions in a supersaturated solution can considerably affect the rate of CaCO_3 scaling and the morphology of the deposit. The available data, obtained for the most part from studies of CaSO_4 and CaCO_3 scale formation, suggested that the presence of dissolved iron ions may either enhance or reduce the CaCO_3 scale deposition process. The presence of dissolved ions, such as Mg^{2+} and Zn^{2+} , upon adsorption onto the active crystal growth sites of the developing crystals, resulted in a significant reduction in the rates of formation of the crystalline deposits. The effect of the magnesium ion on the precipitation of CaCO_3 has been the subject of intensive research efforts over the past decade. In the presence of magnesium ions, the calcite crystal growth rate in supersaturated solutions was greatly reduced, while the growth of aragonite was not influenced. In the solutions where spontaneous precipitation occurred, aragonite rather than the thermodynamically stable calcite precipitated in the presence of magnesium ions [39]. The presence of magnesium in the bulk solution results in the inhibition of the transformation of vaterite and aragonite to calcite [40,41]. This behavior may be related to the fact that Mg^{2+} and Zn^{2+} ions are rather easily incorporated into the crystal

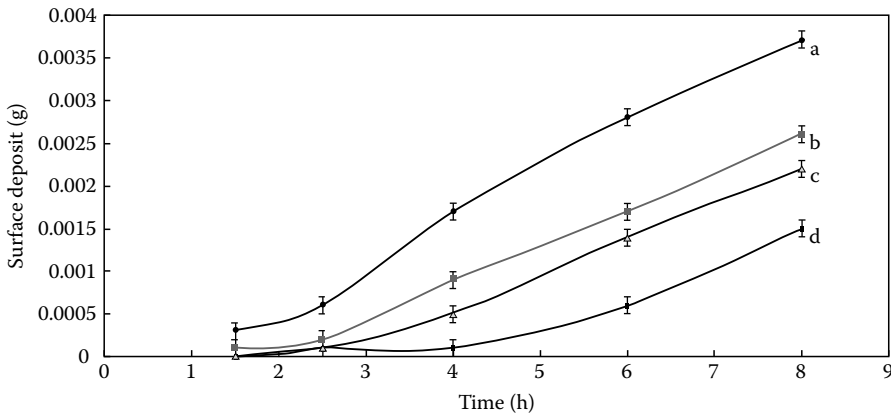


FIGURE 4.1 Effect of Mg^{2+} on calcium carbonate surface deposition. 25°C, saturation ratio with respect to calcite = 17.8. Magnesium concentration: (a) 0 ppm; (b) 200 ppm; (c) 400 ppm; and (d) 600 ppm. (From Chen, T., et al., *J Cryst Growth*, 275, 1343, 2005. With permission.)

lattice of calcite [42]. Dragonne and Cailleau [43] have shown the transformation from a crystalline mixture containing well-formed cubic calcite and vaterite in the absence of Mg^{2+} to needlelike aragonite in the presence of increasing Mg^{2+} concentration. It has also been reported that calcite nucleation was completely suppressed and only aragonite was formed in the presence of Mg^{2+} ions at concentrations exceeding 1000 ppm [41,43]. The presence of the larger Sr^{2+} , which cannot easily be incorporated into the calcite lattice according to quantum mechanical calculations [42], favors the formation of aragonite in solutions supersaturated with respect to the calcium carbonate polymorphs [44]. Clearly, the relative proportion of the foreign ions present in the supersaturated solution with respect to the calcium ions is a decisive factor for the intensity of the respective effects. In formation and injection waters under downhole conditions in oil and gas production, the Mg/Ca ratio is normally below 0.5. Experiments in which this ratio varied between 0 and 0.667 have shown that in all cases the presence of magnesium ions in the supersaturated solutions resulted in the inhibition of the formation of deposits, as can be seen in Figure 4.1.

It is evident from Figure 4.1 that the amount of surface deposits decreased with increasing Mg^{2+} concentration. The effect of the presence of magnesium ions on the morphology of the precipitated crystals is depicted in the micrographs shown in Figure 4.2. The morphology of the $CaCO_3$ crystals grown over a time period was monitored by scanning electron microscopy (SEM). The deposits were collected past 8 h of scale formation.

As can be seen in the micrographs shown in Figure 4.2, two types of crystal morphologies were observed: the “apricot” vaterite and the “cubical or rhombohedral” calcite. In the absence of Mg^{2+} ions, the precipitate consisted almost exclusively of vaterite with a few calcite crystals. With increasing Mg^{2+} ions in the bulk solution, the ratio of the amount of vaterite to calcite decreased. In the presence of 600 ppm Mg^{2+} , calcite crystals were found as the major constituent of the solid deposit. The morphology of the vaterite crystals formed in the presence of various concentrations of Mg^{2+} was also affected, as can be seen from the micrographs shown in Figure 4.3.

It is evident that the size of the vaterite crystallites formed decreased with increasing magnesium concentration, while the surface roughness showed the reverse trend. The presence of magnesium in the precipitating fluid affected the morphology of the calcite crystals formed, as can be seen from the series of electron micrographs shown in Figure 4.4.

As shown in Figure 4.4, two distinct forms of calcite crystals were found: the well-shaped rhombohedra calcite and distorted crystals. In the absence of magnesium, the calcite crystals were well-shaped. The relative amount of distorted calcite crystals increased with increasing magnesium

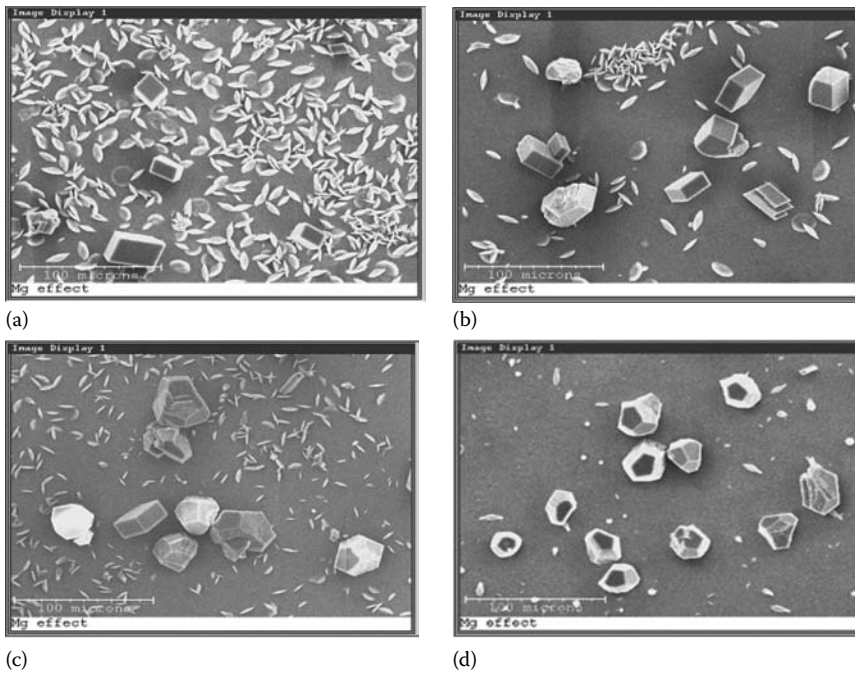


FIGURE 4.2 Scanning electron micrographs of scale formed in the presence of different Mg^{2+} concentrations (bar = 100 microns). (a) 0 ppm; (b) 200 ppm; (c) 400 ppm; and (d) 600 ppm. (From Chen, T., et al., *Chem Eng Sci*, 61, 5321, 2006. With permission.)

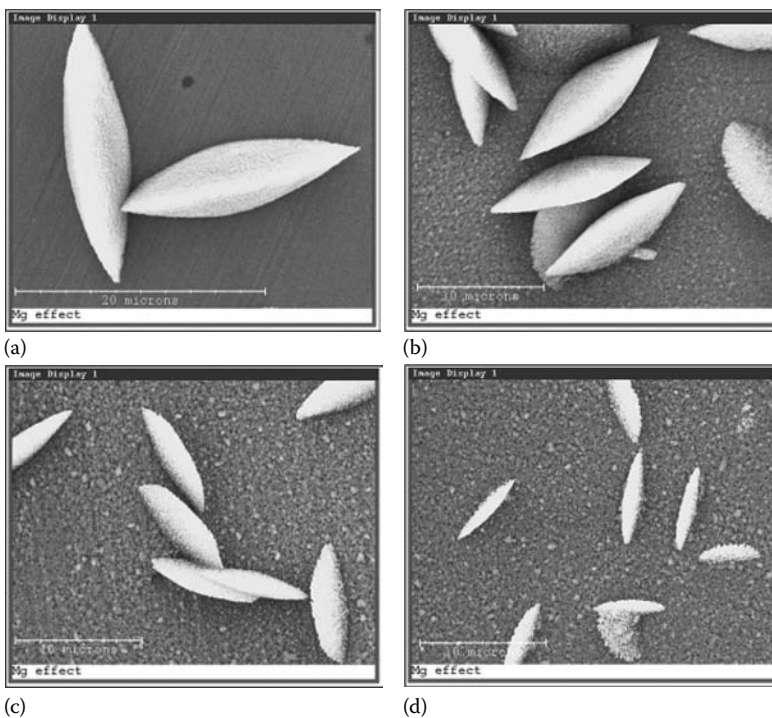


FIGURE 4.3 Scanning electron micrographs showing vaterite scale crystals formed in the presence of various Mg^{2+} concentration levels. (a) 0 ppm; (b) 200 ppm; (c) 400 ppm; and (d) 600 ppm. (From Chen, T., et al., *Chem Eng Sci*, 61, 5322, 2006. With permission.)

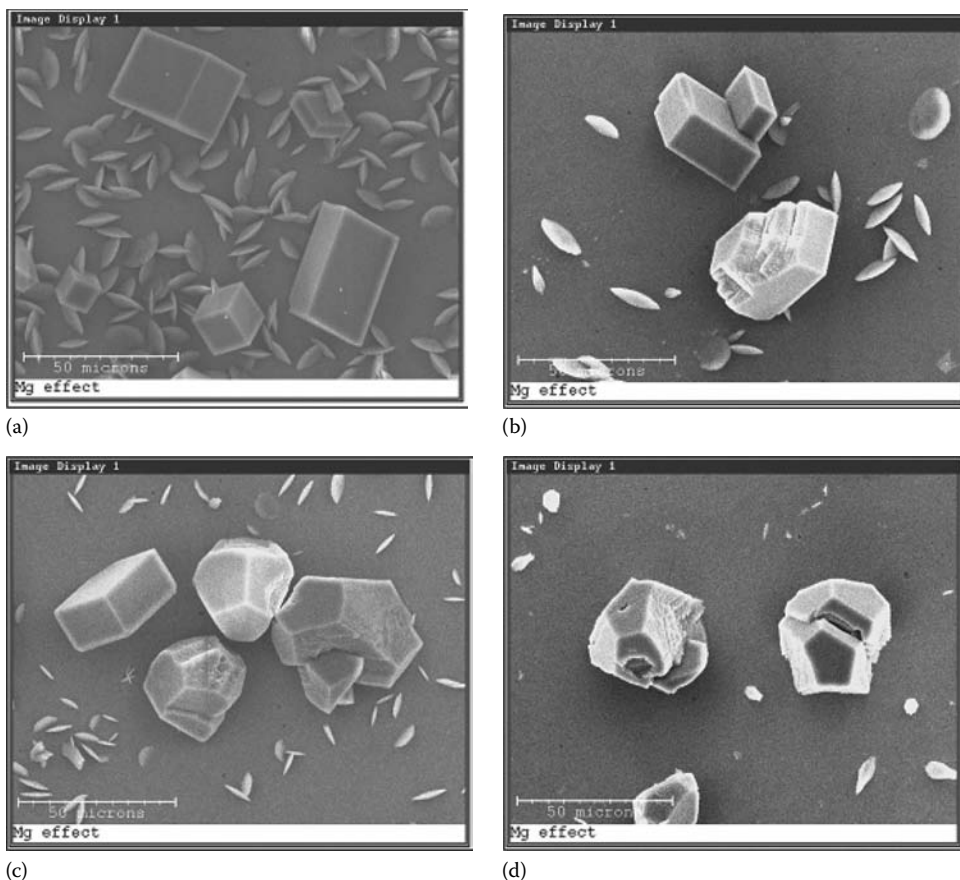


FIGURE 4.4 Scanning electron micrographs showing calcite crystals in scale deposits in the presence of various Mg^{2+} concentration levels. (a) 0 ppm; (b) 200 ppm; (c) 400 ppm; and (d) 600 ppm. (From Chen, T., et al., *Chem Eng Sci*, 61, 5322, 2006. With permission.)

concentration. It is interesting to note that in the presence of 600 ppm Mg^{2+} the calcite crystals formed were distorted. The effect of the presence of increasing magnesium concentration on the surface roughness of the calcite crystallites was similar to the respective trend of vaterite, as can be seen from the electron micrographs shown in Figure 4.5.

In the Mg-free solutions, the spontaneously precipitated calcite crystals showed a well-shaped rhombohedral habit. Adsorption of Mg^{2+} ions onto calcite, probably due to the incorporation of these ions into the calcite lattice [42], promotes the surface formation of magnesian calcites heterogeneously [45–47]. It was suggested by Zhang et al. [48] that Mg^{2+} is incorporated into the calcite crystal surface in a nonuniform mode and develops new crystal surfaces, with higher Mg^{2+} density and lower growth rate than that on the original calcite seed surfaces. New faces appeared on the edges of rhombohedral calcite seed crystals when Mg^{2+} was present in the solution. Paquette et al. [49] observed similar morphological changes as the result of the presence of Mg^{2+} . Paquette and Reeder [50] suggested that the new surface is developed at the corners and edges of calcite seeds. Mg^{2+} has a higher affinity for some of these sites, and it is adsorption or perhaps dehydration during incorporation that preferentially slows down growth in specific directions, for example, toward the edges and corners. As a consequence of the inhibition by Mg^{2+} , new crystal faces develop, and the type of surface sites for which Mg^{2+} has a higher affinity dominates these faces, eventually affecting the crystal morphology.

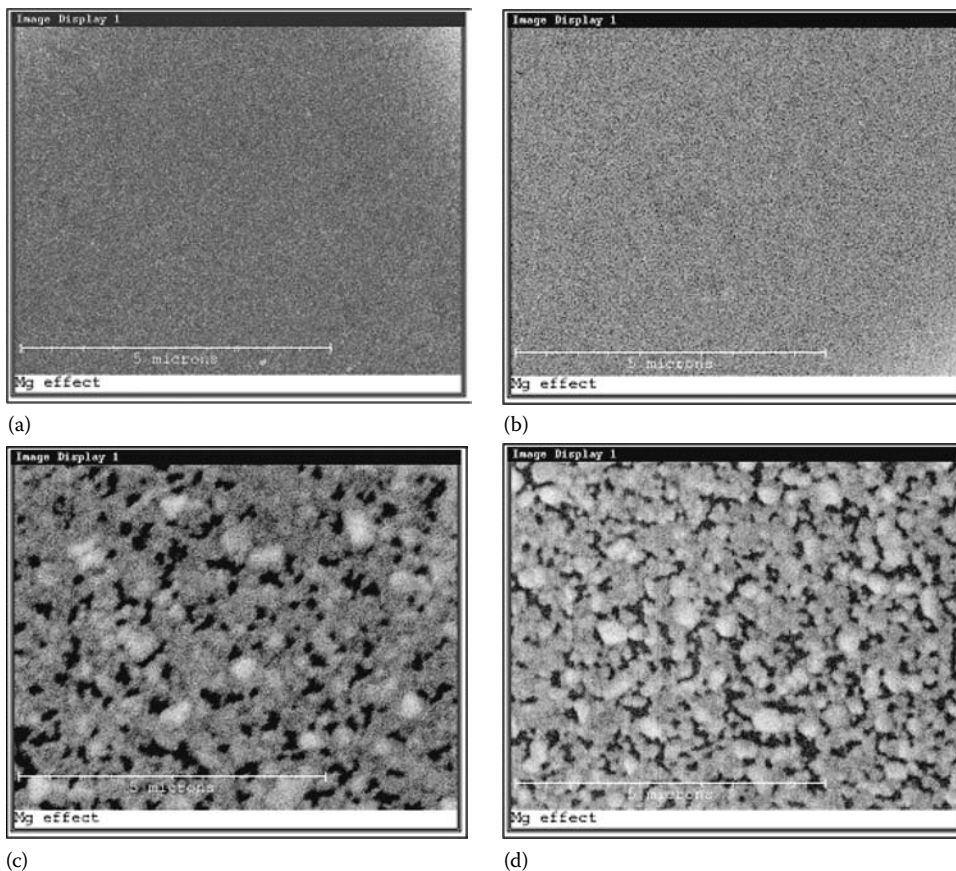


FIGURE 4.5 Effect of Mg^{2+} concentration on the surface roughness of the calcite crystals found in the scale deposits. (a) 0 ppm; (b) 200 ppm; (c) 400 ppm; and (d) 600 ppm. (From Chen, T., et al., *Chem Eng Sci*, 61, 5323, 2006. With permission.)

4.2.3 EFFECT OF ORGANIC COMPOUNDS ON THE KINETICS AND THE CHARACTERISTICS OF CALCIUM CARBONATE SCALE

Organic phosphonates are used extensively in numerous applications, including chemical water treatment for the prevention and control of scale deposits consisting of alkaline earth metal insoluble salts (phosphates, sulfates, and carbonates) [51–54]. Polyphosphonocarboxylic acid (PPCA) and diethylenetriaminepenta (methylenephosphonic acid) (DETPMP) are two common commercial scale inhibitors used to control mineral scaling in the oil and gas industry. The effects of these compounds on the inhibition of calcium carbonate scale formation at elevated temperature ($80^{\circ}C$) have been demonstrated [52,53]. PPCA and DETPMP inhibited the formation of calcium carbonate on metal surfaces [55]. The $CaCO_3$ scale formation experiments were carried out at $80^{\circ}C$. The composition of the $CaCO_3$ scaling solutions are shown in Table 4.2. The supersaturation ratio (SR) of calcium carbonate was calculated equal to 77.6 at $80^{\circ}C$, a value representative of a typical severe scaling solution in the oil and gas industry.

The molecular mass of PPCA is 3800 g/mol and the activity is 42%. The molecular mass of DETPMP is 573 g/mol and the activity is 45%. The structures of PPCA and DETPMP are shown in Figure 4.6. The effect of PPCA on the kinetics of calcium carbonate scale formation is shown in Figure 4.7.

TABLE 4.2
Composition of the CaCO₃ Scaling Solutions Used to Study the Effect of Inhibitor on Scale Formation

Ca ²⁺ (ppm)	HCO ₃ ⁻ (ppm)	Na ⁺ (ppm)	Cl ⁻ (ppm)
1,440	2,196	6,873	11,871
SR	80°C	77.6	

Note: SR, supersaturation ratio.

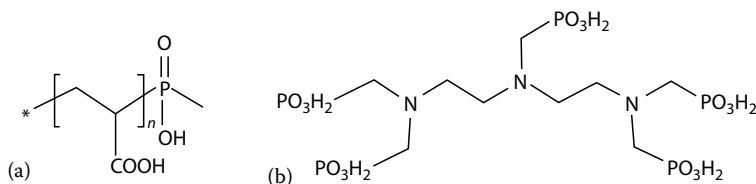


FIGURE 4.6 Molecular formulae for (a) PPCA and (b) DETPMP.

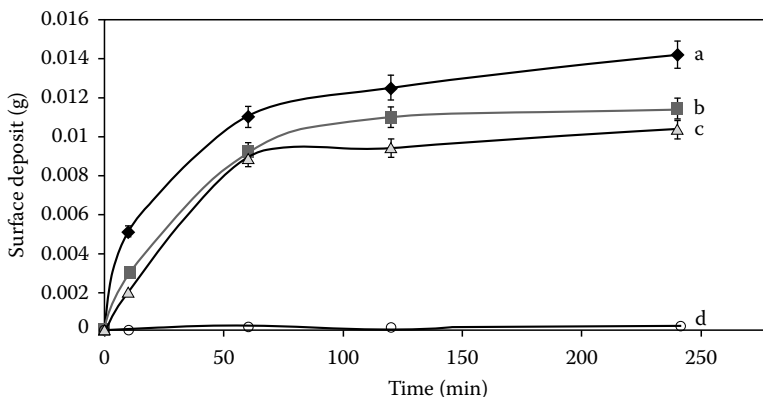


FIGURE 4.7 Effect of PPCA inhibitor on calcium carbonate scale formation at 80°C (see Table 4.2). Plot of the calcium carbonate deposited as a function of time: (a) 0 ppm; (b) 1 ppm; (c) 2 ppm; and (d) 4 ppm.

As can be seen, complete inhibition was achieved at a concentration of 4 ppm. The effect of PPCA on the morphology of the calcium crystals formed in the absence and in the presence of the inhibitor tested and for various times of scaling is shown in Figures 4.8 and 4.9.

It is evident from the micrograph of Figure 4.8a that the surface deposit contained to a large extent leaflike vaterite, cubic calcite, and needlelike aragonite. The size of the vaterite crystals was up to 60 microns and the cubic calcite was about 10–20 microns in size. It seems that calcite crystals adhere to the metal surface tightly while vaterite and aragonite crystals seem to be attached rather loosely. With the progress of scale deposition (Figure 4.8b through d), the deposit was enriched in aragonite and calcite and the vaterite leaflets were significantly reduced. In Figure 4.9a, it may be seen that the deposit consisted of leaflike vaterite which adheres to the surface loosely and of cubic calcite which adheres to the surface tightly. No needlelike aragonite crystallites were observed for the first 10 min of scale formation. The sizes of the vaterite and calcite crystallites were the same as in the absence of PPCA. At later stages of scale formation (Figure 4.9b through d), needlelike aragonite crystallites appeared past 1 h from the onset of

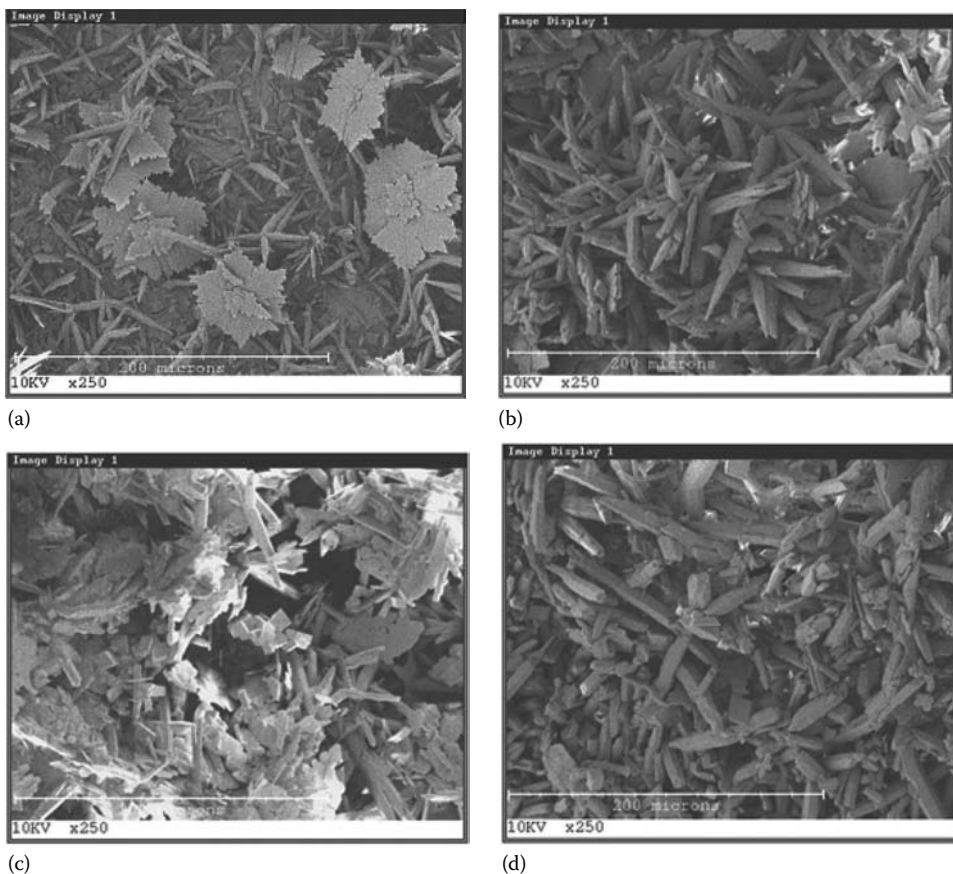


FIGURE 4.8 Scanning electron micrographs of calcium carbonate deposits formed on metal surfaces at 80°C in the absence of PPCA (conditions as in Table 4.2). (a) 10 min; (b) 1 h; (c) 2 h; and (d) 4 h.

precipitation. This polymorph was dominant past 4 h of scale formation on the metal surface. In the presence of 2 ppm PPCA past 10 min, the presence of leaflike, loosely adhering vaterite was dominant with a smaller amount of strongly adhering calcite crystallites. Vaterite remained the dominant polymorph for the rest of the duration of the scaling process, changing from the leaflike habit to kernel-like. The morphology of the crystals of the calcium carbonate scale formed at various times is shown in Figure 4.10.

At 4 ppm PPCA, the number of crystals formed was drastically reduced in agreement with the kinetics results. The crystals consisted of leaflike vaterite which changed to kernel-like habit with the progress of the scale formation up to 4 h. It is important to note that the presence of the organophosphorus compound, PPCA, not only reduced the rates of calcium carbonate formation but also resulted in the stabilization of vaterite, the morphology of which was also affected probably because of the selective blockage of specific crystal faces of the growing scale crystallites through adsorption. Molecules like PPCA that contain carboxyl and phosphonic functional groups which are ionized may interact with the positively charged sites of ionic crystals like calcium carbonate and form surface complexes [56]. The identification of the mineral phases present in the scale deposits is shown in Figure 4.11.

In the absence of PPCA, the crystals consisted mainly of aragonite and calcite. In the presence of 1 ppm PPCA, aragonite and calcite were again predominant. A small reflection at $2\theta = 24.9^\circ$ suggested the presence of vaterite. In the presence of 2 ppm PPCA, vaterite is the main polymorph in the scale deposit. The low intensity of the various reflections in the diffractogram obtained in the

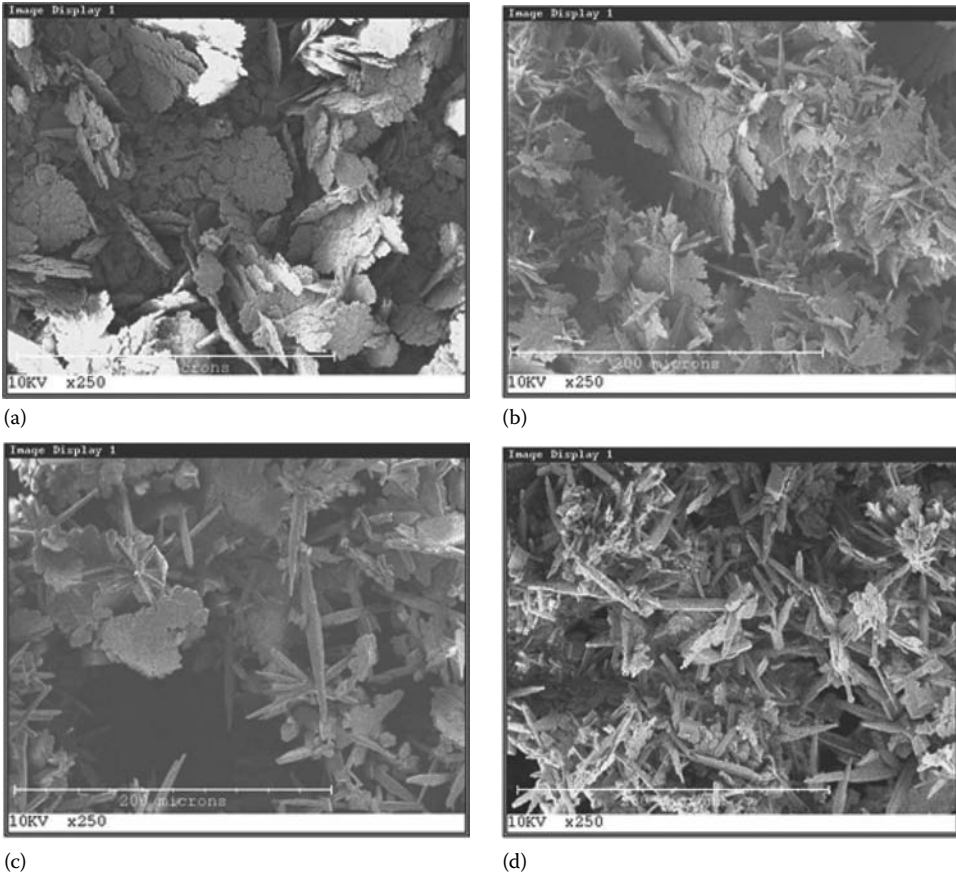


FIGURE 4.9 Scanning electron micrographs of calcium carbonate deposits formed on metal surfaces at 80°C in the presence of 1 ppm PPCA (conditions as in Table 4.2). (a) 10 min; (b) 1 h; (c) 2 h; and (d) 4 h.

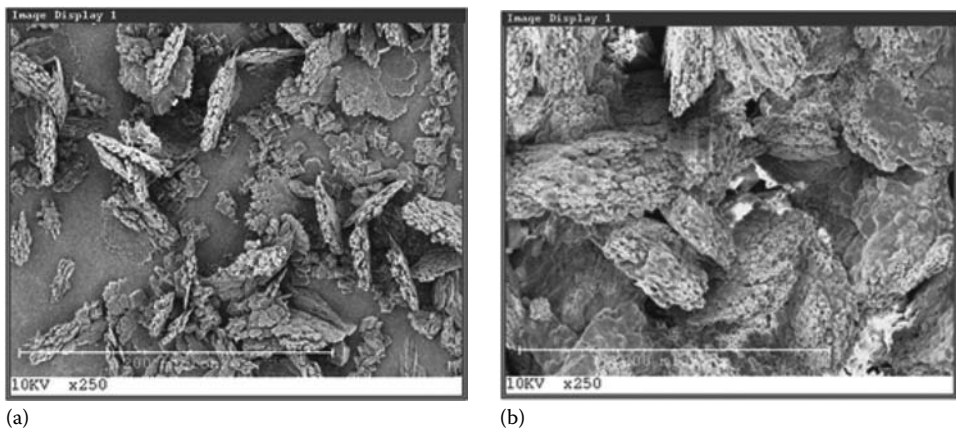


FIGURE 4.10 Morphology of calcium carbonate scale formed in the presence of 2 ppm PPCA at 80°C (conditions as in Table 4.2). (a) 10 min; (b) 1 h;

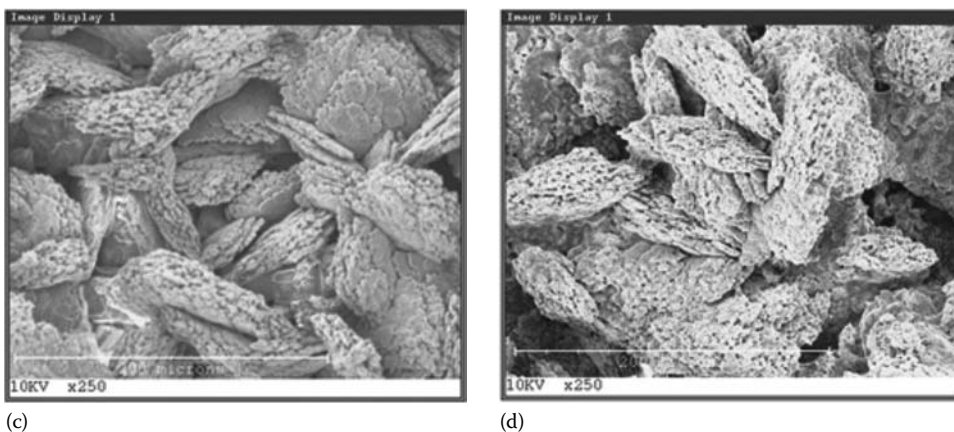


FIGURE 4.10 (continued) (c) 2 h; and (d) 4 h.

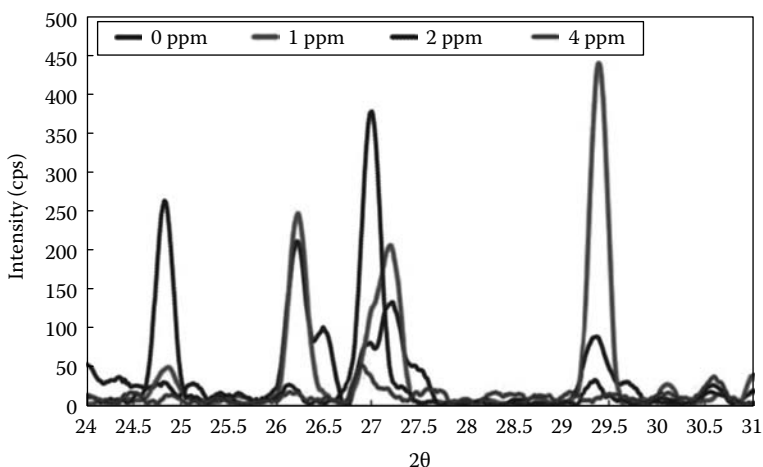


FIGURE 4.11 X-ray diffraction (XRD) of calcium carbonate scale formed in the presence of PPCA past 4 h of scale formation at 80°C (solution conditions as in Table 4.2).

presence of 4 ppm PPCA is due to the fact that the amount of scale deposited on the metal surface past 4 h was not enough for XRD analysis. The results of the mineralogical analysis by XRD of the scale deposits formed in the presence of PPCA confirmed that the presence of this compound in the supersaturated solutions suppressed the formation of aragonite and calcite in favor of vaterite. The effect of PPCA on the calcium carbonate scale deposited on the metal surface detected by XRD was consistent with the morphological analysis.

4.2.4 EFFECT OF DETPMP ON SCALE FORMATION AT 80°C

DETPMP was tested with respect to the kinetics of calcium carbonate scale formation at the same conditions as PPCA on the calcium carbonate surface deposition. The results of the kinetics of scale deposition experiments are summarized in Figure 4.12.

As can be seen in Figure 4.12, past 2 and 4 h of scale deposition, the inhibition effect in the presence of 1 ppm DETPMP is practically eliminated. Efficient inhibition of calcium carbonate scale formation was obtained at 2 and 4 ppm concentration levels of the inhibitor. The morphology of the crystals of the deposits can be seen in Figure 4.13, for scale deposition duration up to 4 h.

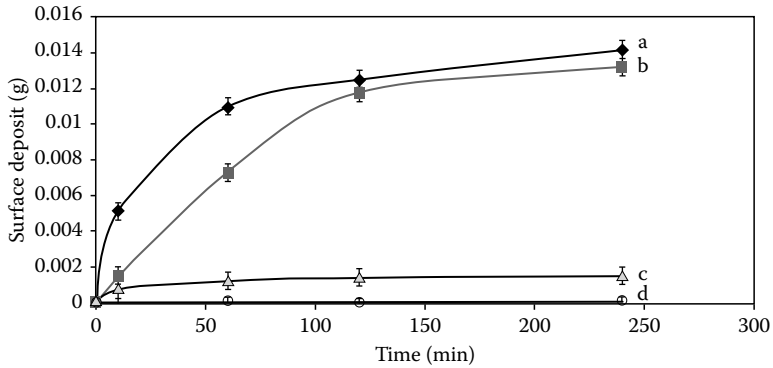


FIGURE 4.12 Effect of the presence of DETPMP in solutions (see Table 4.2) on the deposition of calcium carbonate scale at 80°C at various DETPMP concentrations: (a) 0 ppm; (b) 1 ppm; (c) 2 ppm; and (d) 4 ppm.

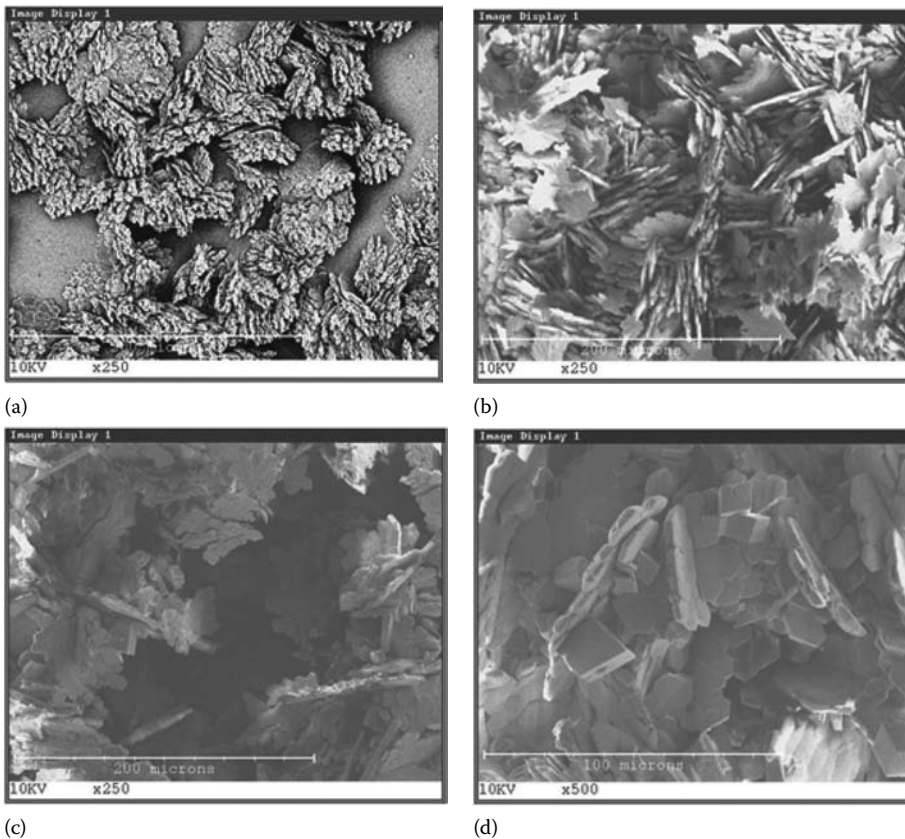


FIGURE 4.13 Scale deposits formed in the presence of 1 ppm DETPMP on metal surfaces in contact with solutions supersaturated with respect to calcium carbonate (conditions as in Table 4.2) at 80°C. (a) 10 min; (b) 1 h; (c) 2 h; and (d) 4 h.

Figure 4.14a shows an image of surface deposit in the presence of 1 ppm DETPMP inhibitor at 80°C after 10 min. The surface deposit mainly comprised leaflike vaterite. In the presence of higher concentration (2 ppm) of DETPMP, the scale deposits consisted mainly of agglomerated leaflike vaterite crystals.

In the presence of 4 ppm DETPMP, the number of crystals was very limited and consisted as before of distorted and agglomerated vaterite. The powder x-ray diffractogram of the scale

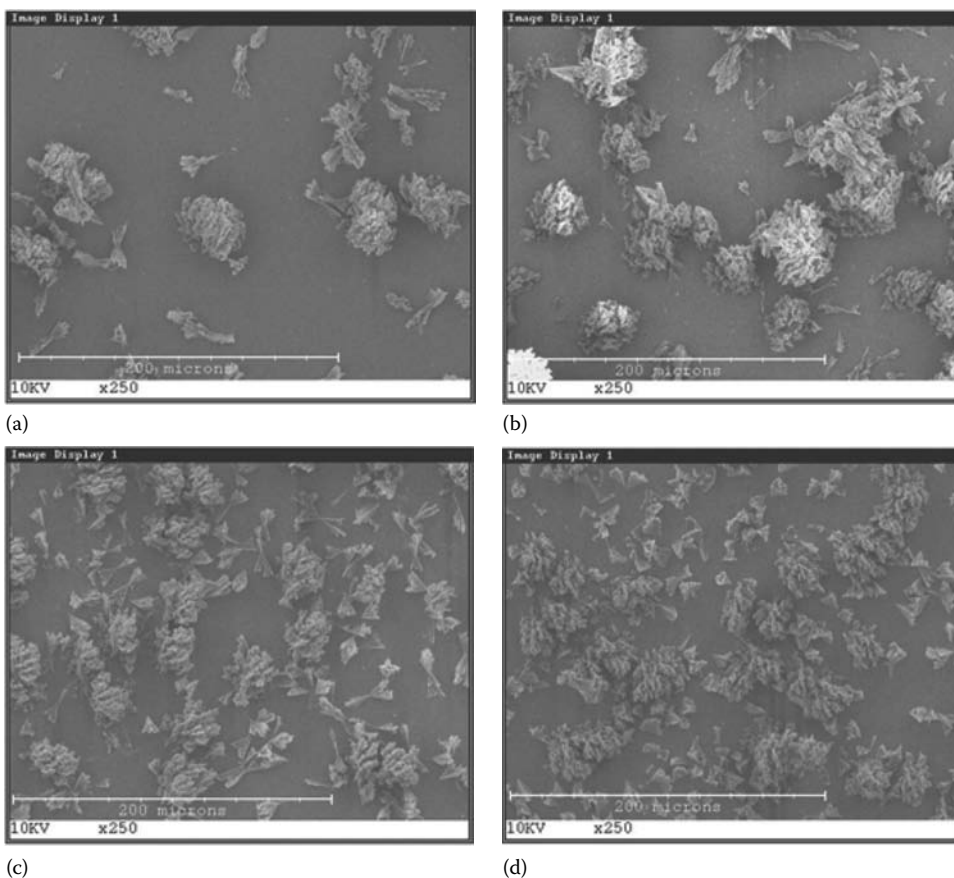


FIGURE 4.14 Scale deposits formed in the presence of 2 ppm DETPMP on metal surfaces in contact with solutions supersaturated with respect to calcium carbonate (conditions as in Table 4.2) at 80°C. (a) 10 min; (b) 1 h; (c) 2 h; and (d) 4 h.

deposits in the presence of DETPMP is shown in Figure 4.15. In the absence of inhibitor, the scale deposits consisted mainly of aragonite and calcite. In the presence of 1 ppm DETPMP, the aragonite reflection at $2\theta = 27.2^\circ$ disappeared and the respective integrated area under the reflection at $2\theta = 26.2^\circ$ decreased. On the contrary, the vaterite reflections at $2\theta = 24.9^\circ$ and 27.1° showed up and the integrated area corresponding to the reflection of calcite at $2\theta = 29.4^\circ$ increased. It is clear that the presence of 1 ppm DETPMP in the supersaturated solutions, besides their kinetics effect, suppressed the formation of the aragonite crystals in favor of vaterite. At concentration levels of 2 ppm DETPMP, vaterite and calcite were the dominant polymorphs. In the presence of 4 ppm DETPMP, the amount of scale deposited on the metal surface at 4 h was too small for XRD analysis.

The characterization of CaCO_3 scale deposits and the mechanism involved in their formation was further confirmed using a novel in situ wide-angle x-ray scattering (WAXS) methodology. WAXS measurements were made at the facilities of the Brookhaven National Laboratory in the United States. The investigation was done by the development of an appropriate cell in order to conduct measurements in situ at 80°C, both in the presence and in the absence of inhibitors. The in situ flow cell developed may be operated at elevated temperatures up to 250°C and pressures up to 340 MPa in conjunction with synchrotron radiation (WAXS). Calcium carbonate was precipitated spontaneously in the CaCO_3 scale solutions in the in situ cell for WAXS measurements at high temperature and pressure, as shown in Figure 4.16.

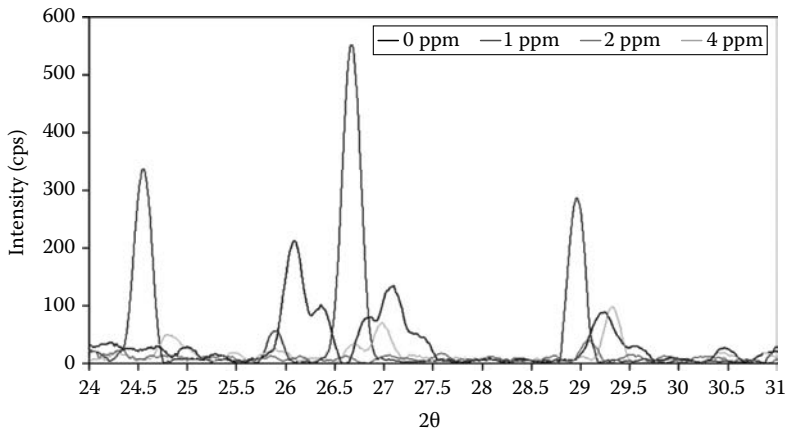


FIGURE 4.15 XRD of calcium carbonate scale formed in the presence of PPCA past 4 h of scale formation at 80°C (solution conditions as in Table 4.2).

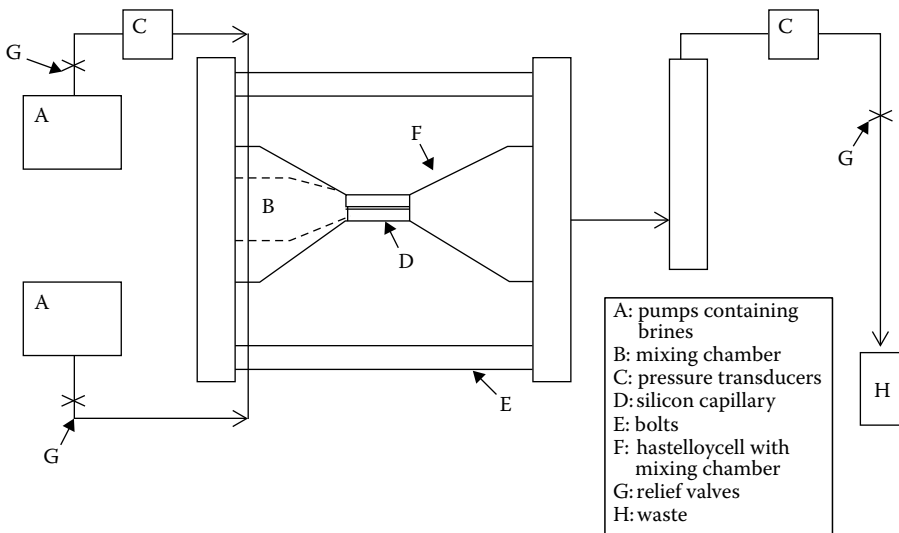


FIGURE 4.16 In situ cell for WAXS measurements of formation of scale deposits at high temperatures and pressures. (From Chen, T. et al., 2008. With permission.)

Calcium carbonate crystals deposit on the surface of capillary cell and precipitate in the bulk solution. The high-energy x-ray beamline goes through the calcium carbonate crystal and is diffracted, thus giving structural information on the CaCO_3 crystals. The most commonly chosen 2θ range for calcium carbonate for the X17B1 beamline with a x-ray energy of 67 keV and wavelength of 0.368 Å is approximately 5°–10.5°, which is equivalent to approximately 18°–45° for $\lambda = 1.54$ Å. The growth of calcium carbonate crystals at 80°C is shown in Figure 4.17.

The initial phase of crystallization is characterized by instability before 6 min, with individual planes from various polymorphs emerging and subsequently disappearing under the hydrodynamic conditions (i.e., a peak appears and then disappears at the next frame due to crystals in bulk precipitate or crystals on the surface being flushed away). The majority of these planes can be assigned to the aragonite polymorphs. For example, the peak that appears after 4 min at $2\theta = 5.697^\circ$ is aragonite (110) plane, and the peak that appears after 6 min at $2\theta = 6.104^\circ$ is aragonite (111) plane. After the initial unstable phase characterized by the presence of aragonite, the crystal

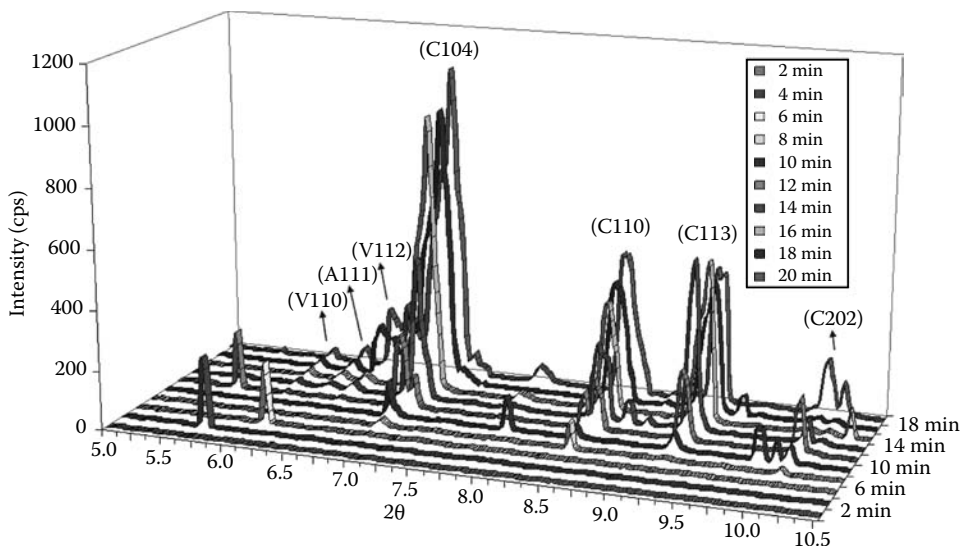


FIGURE 4.17 The growth of calcium carbonate crystals at 80°C monitored by synchrotron radiation (WAXS) in the absence of additives. Peaks for all the three polymorphs are distinguished. V: vaterite; A: aragonite; and C: calcite. (From Chen, T. et al., 2008. With permission.)

planes to attach to the surface and then grow on the surface are the calcite (104) and (110) planes past 8 min (i.e., a peak is present and then the intensity and integrated area of this peak increase at the next frame due to growth of surface deposit). The next plane to emerge is the (113) plane of calcite after 10 min. Another three peaks attach to the surface and grow on the surface after 14 min, which represent for (110) and (112) planes of vaterite and (111) plane of aragonite. As the experiment progresses, the growth of calcite (104), (110), and (113) planes is apparent. The calcite (202) plane is observed after 8 min, disappears after 14 min, and appears again after 20 min. It shows an unstable adherence. The other calcite planes (102) and (006) are hardly detectable after 20 min. In addition, various planes from the vaterite and aragonite polymorphs start appearing again, as in the initial stage of the experiment, but they are flushed out of the cell or possibly transformed by the time. However, after 14 min, the first stable vaterite (110) and (112) planes and aragonite (111) plane emerge. This time they stick to a surface rather than being flushed out of the cell or transformed into calcite planes.

In the presence of 4 ppm of the inhibitor PPCA, the growth of calcium carbonate crystals monitored by synchrotron radiation (WAXS) is shown in Figure 4.18. The initial phase of crystallization is characterized by instability before 8 min, with individual planes from various polymorphs emerging and subsequently disappearing under the hydrodynamic conditions. The majority of these planes can be assigned to the vaterite polymorphs. For example, the peak that appears after 4 min at $2\theta = 8.127^\circ$ is vaterite (016) plane and the peak that appears after 8 min at $2\theta = 6.104^\circ$ is vaterite (022) plane. After the initial unstable phase with vaterite, the first crystal plane to attach to the surface and then grow on the surface is the (104) plane of calcite after 12 min. Another two peaks attaching to the surface and then growing on the surface are detected after 16 min, which represent (110) plane of vaterite and (113) plane of calcite. After 24 min, the growth of the (112) plane of vaterite and (110) and (006) planes of calcite are observed. The (006) plane of calcite usually gives rise to weak diffractions and is therefore not regarded as a major plane. As the experiment progresses, the growth of calcite (104) and (113) planes are apparent. The calcite (006) and (110) planes are observed after 24 min. The other calcite plane (102) is hardly detectable after 30 min. In addition, various planes from the vaterite polymorphs start appearing again, as in the initial stage of the experiment, but they are flushed out of the cell or possibly transformed by the time. However, after 16 min, the first stable vaterite (110) emerges.

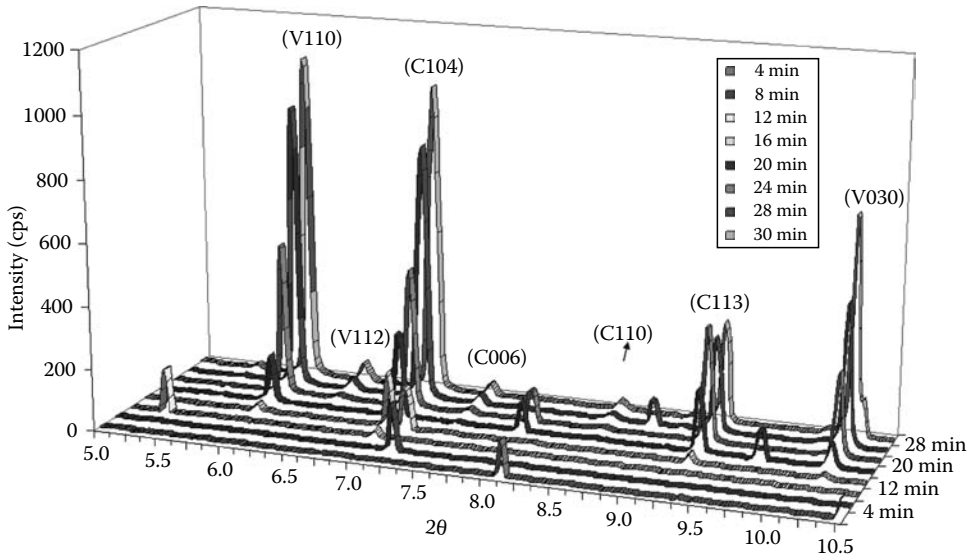


FIGURE 4.18 The growth of calcium carbonate crystals in the presence of 4 ppm PPCA at 80°C detected by synchrotron radiation (WAXS). V: vaterite; A: aragonite; and C: calcite. (From Chen, T. et al., 2008. With permission.)

The effect of the presence of DETPMP in the supersaturated solutions was also investigated with the synchrotron radiation and the scale formation process was monitored, as can be seen in Figure 4.19. In the presence of 4 ppm DETPMP, the main peaks of calcium carbonate scale from both calcite and vaterite crystals were observed: calcite (104), (110), and (113), and vaterite (110) and (030). The presence of 10 ppm DETPMP in the supersaturated solutions resulted in the complete suppression of the formation of calcite crystals adhering to the surface. In this case, the formation of vaterite was favored.

In the absence of inhibitor, calcite (104), (113), and (110) planes were the main planes observed. The cell was blocked after 20 min. In the presence of 4 ppm PPCA and DETPMP, the cell was

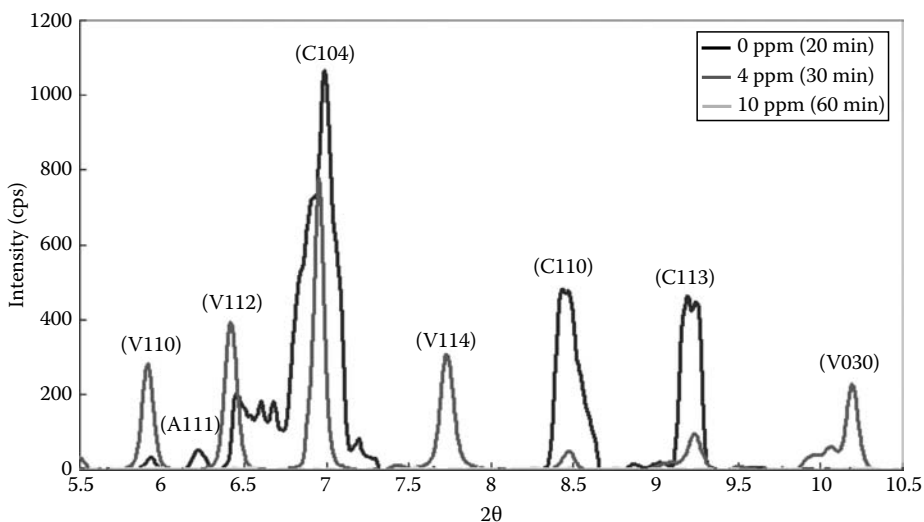


FIGURE 4.19 Formation of calcium carbonate scale deposits characterized in situ with synchrotron radiation in the absence and in the presence of DETPMP, 80°C. V: vaterite; A: aragonite; and C: calcite. (From Chen, T. et al., 2008. With permission.)

blocked after 30 min. However, no blockage was found after 60 min for concentration levels 10 ppm PPCA and DETPMP. Despite the fact that the two phosphonate compounds tested showed similar inhibition, the mechanism corresponding to each compound was different. More specifically, PPCA and DETPMP favor different crystal plane formation at certain concentrations. At 4 ppm, PPCA favors the formation of vaterite (110) plane and suppresses the vaterite (112) plane. Vaterite (110) is the main plane observed in the presence of 4 ppm PPCA and a small amount of vaterite (112) appeared at this condition. However, both vaterite (110) and (112) planes are the main planes observed at 4 ppm DETPMP. In the presence of 10 ppm DETPMP past 60 min, the mineral phase formed was characterized by instability, with individual planes from various polymorphs emerging and subsequently disappearing under the hydrodynamic conditions of the flow cell. On the contrary, in the presence of 10 ppm PPCA 60 min past the onset of scale deposit formation, the stable crystals were observed to stick onto the surface. It was thus concluded that DETPMP was a more efficient inhibitor of the calcium carbonate deposition at 80°C in comparison with the performance of PPCA under the same fluid conditions.

4.3 SUMMARY

Polymorphism of the calcium carbonate system is very important for understanding the mechanism of scale formation and adhesion on surfaces. The anhydrous polymorphs of calcium carbonate, vaterite, aragonite, and calcite, have different solubility and distinct morphologies. In the absence of additives and over a range of temperatures up to 80°C, a mixture of all the three polymorphs is obtained. The presence of magnesium ions favors the stabilization of aragonite, while organic compounds, including organophosphorus compounds, besides their retardation effect, tend to stabilize the formation of vaterite. Calcite crystals have been shown to adhere tenaciously to metal surfaces while vaterite and aragonite are rather loosely held. Organophosphorus compounds with more than one phosphonic group in their molecule at concentration levels up to 10 ppm retarded the formation of calcium carbonate scale and at concentrations of 4 ppm at 80°C were able to completely suppress the mineral deposition. Higher levels of concentration of the additives tested induced increased surface roughness. The stabilization of vaterite in the presence of organic water-soluble compounds and of aragonite in the presence of magnesium was confirmed with powder XRD and SEM. Moreover, the scale formation process was monitored by synchrotron radiation, both in the absence and in the presence of organophosphorus inhibitors, and the conclusions drawn concerning the stability of the transient polymorphs of calcium carbonate were confirmed. Synchrotron radiation allowed for a better time-resolved understanding of the scale formation process and of the adhesion of the particles formed on metal surfaces.

REFERENCES

1. Ellis, A. J. The solubility of calcite in sodium chloride at high temperatures. *Am J Sci*, 261, 259–266 (1963).
2. Newton, R. C. and Manning, C. E. Experimental determination of calcite solubility in H₂O-NaCl solutions at deep crust/upper mantle pressures and temperatures: Implications for metasomatic processes in shear zones. *Am Mineral*, 87, 1401–1409 (2002).
3. Cowan, J. C. and Weintritt, D. J. *Water Formed Scale Deposits*. Gulf Publishing Co., Houston, TX, pp. 93–132 (1976).
4. Koutsoukos, P. G. Polymorphism in the calcium carbonate system. In *12th Symposium on Industrial Crystallization*, Ed. Z. H. Rojkowski, pp. 115–121. Warsaw, Poland (1993).
5. Kitano, Y. A study of the polymorphic formation of calcium carbonate in thermal springs with emphasis on the temperature. *Bull Chem Soc Jpn*, 35, 1980–1985 (1962).
6. Carlson, W. D. The polymorphs of CaCO₃ and the aragonite-calcite transformation. In *Reviews in Mineralogy*, Vol. 11, Ed. P. H. Ribbe, pp. 191–225, Mineralogical Society of America, Washington, DC (1983).
7. Nancollas, G. H. and Reddy, M. M. The kinetics of crystallization of scale-forming minerals. In *SPE-AIME Oilfield Chemistry Symposium*, Denver, CO, SPE 4360, May 24–25 (1973).

8. Chakraborty, D., Agarwal, V. K., Bhatia, S. K., and Bellare, J. Steady-state transitions and polymorph transformations in continuous precipitation of calcium carbonate. *Ind Eng Chem Res*, 33, 2187–2197 (1994).
9. Brecevic, L. and Nielsen, A. E. Solubility of amorphous calcium carbonate. *J Cryst Growth*, 98, 504–510 (1989).
10. Gorna, K., Hund, M., Vučak, M., Gröhn, F., and Wegner, G. Amorphous calcium carbonate in form of spherical nanosized particles and its application as fillers for polymers. *Mat Sci Eng A*, 477, 217–225 (2008).
11. Coleyshaw, E. E., Crump, G., and Griffith, W. P. Vibrational spectra of hydrated carbonate minerals ikaite, monohydrocalcite, lansfordite and nesquehonite. *Spectrochim Acta A Mol Biomol Spectrosc*, 59, 2231–2239 (2003).
12. Sala, M., Delmonte, B., Frezzotti, M., Proposito, M., Scarchilli, C., Maggi, V., Artioli, G., Dapiaggi, M., Marino, F., Ricci, P. C., and De Giudici, G. Evidence of calcium carbonates in coastal (Talos Dome and Ross Sea area) East Antarctica snow and firn: Environmental and climatic implications. *Earth Planet Sci Lett*, 271, 43–52 (2008).
13. Chen, T., Neville, A., and Yuan M. Assessing the effect of Mg^{2+} on $CaCO_3$ scale formation–bulk precipitation and surface deposition. *J Cryst Growth*, 275, 1341–1347 (2005).
14. Fernandez-Díaz, L., Astilleros, J. M., and Pina, C. M. The morphology of calcite crystals grown in a porous medium doped with divalent cations. *Chem Geol*, 225, 314–321 (2006).
15. Mao, Z. and Huang, J. Habit modification of calcium carbonate in the presence of malic acid. *J Solid State Chem*, 180, 453–460 (2007).
16. Henderson, G. E., Murray, B. J., and McGrath, K. M. Controlled variation of calcite morphology using simple carboxylic acids. *J Cryst Growth*, 310, 4190–4198 (2008).
17. Lipus, L. C. and Dobersek, D. Influence of magnetic field on the aragonite precipitation. *Chem Eng Sci*, 62, 2089–2095 (2007).
18. Andritsos, N. and Karabelas, A. J. Calcium carbonate scaling in a plate heat exchanger in the presence of particles. *Int J Heat Mass Transfer*, 46, 4613–4627 (2003).
19. Grasby, S. Naturally precipitating vaterite (μ - $CaCO_3$) spheres: Unusual carbonates formed in an extreme environment. *Geochim Cosmochim Acta*, 67, 1659–1666 (2003).
20. Brunson, R. J. and Chabak, J. J. Vaterite formation during coal liquefaction. *Chem Geol*, 25, 333–338 (1979).
21. Rao, C. P. and Adabi, M. H. Carbonate minerals, major and minor elements and oxygen and carbon isotopes and their variation with water depth in cool, temperate carbonates, Western Tasmania, Australia. *Mar Geol*, 103, 249–272 (1992).
22. Gabrielli, G., Maurin, G., Franchy-Chausson, H., They, P., Tran, T. T. M., and Tlili, M. Electrochemical water softening: Principle and application. *Desalination*, 201, 150–163 (2006).
23. Simpson, L. J. Electrochemically generated $CaCO_3$ deposits on iron studied with FTIR and Raman spectroscopy. *Electrochim Acta*, 43, 2543–2547 (1998).
24. Chen, T., Neville, A., and Yuan, M. Influence of Mg^{2+} on $CaCO_3$ formation–bulk precipitation and surface deposition. *Chem Eng Sci*, 61, 5318–5327 (2006).
25. Manoli, F. and Dalas, E. Calcium carbonate crystallization in the presence of glutamic acid. *J Cryst Growth*, 222, 293–297 (2001).
26. Manoli, F., Kanakis, J., Malkaj, P., and Dalas, E. The effect of aminoacids on the crystal growth of calcium carbonate. *J Cryst Growth*, 236, 363–370 (2002).
27. Gabrielli, C., Jaouhari, R., Keddad, M., and Maurin, G. An electrochemical method for testing the scaling susceptibility of insulating materials. *J Electrochem Soc*, 148, B517–B521 (2001).
28. Gabrielli, C., Jaouhari, R., Joiret, S., and Maurin, G. In situ Raman spectroscopy applied to electrochemical scaling. Determination of the structure of vaterite. *J Raman Spec*, 31, 497–501 (2000).
29. Spanos, N. and Koutsoukos P. G. Kinetics of precipitation of calcium carbonate in alkaline pH at constant supersaturation. Spontaneous and seeded growth. *J Phys Chem B*, 102, 6679–6684 (1998).
30. Todd, A. C. and Yuan, M. D. Barium and strontium sulfate solid-solution scale formation at elevated temperatures. *SPE Prod Eng*, 7, 85–92 (1992).
31. Elfil, H. and Roques, H. Role of hydrate phases of calcium carbonate on the scaling phenomenon. *Desalination*, 137, 177–186 (2001).
32. Roques, H. (Ed.), *Chemical Water Treatment: Principles and Practice*, VCH, Weinheim, Germany, p. 688 (1995).
33. Zhou, G. and Zheng, Y. Chemical synthesis of $CaCO_3$ minerals at low temperatures and implication for mechanism of polymorphic transition. *N Jb Miner Abh*, 176, 323–343 (2001).
34. Chen, J. and Xiang, L. Controllable synthesis of calcium carbonate polymorphs at different temperatures. *Powder Technol*, 6, 4 (2008).

35. Andritsos, N., Karabelas, A. J., and Koutsoukos, P. G. Morphology and structure of CaCO_3 scale layers formed under isothermal flow conditions. *Langmuir*, 13, 2873–2879 (1997).
36. Neville, A. and Morizot, A. P. A combined bulk chemistry/electrochemical approach to study the precipitation, deposition and inhibition of CaCO_3 . *Chem Eng Sci*, 55, 4737–4744 (2000).
37. Kladi, A., Klepetsanis, P. G., Østvold, T., Kontoyannis, C. G., and Koutsoukos, P. G., Crystal growth of calcium carbonate in seawater. The effect of temperature and of the presence of inhibitor. In *Advances in Crystal Growth Inhibition Technologies*, Ed. Z. Amjad, pp. 85–106, Kluwer Academic Publisher, New York (2000).
38. Turner, C. W. and Smith, D. W. Calcium carbonate scaling kinetics determined from radiotracer experiments with calcium-47. *Ind Eng Chem Res*, 37, 439–448 (1998).
39. Park, W. K., Ko, S. J., Lee, S. W., Cho, K. H., Ahn, J. W., and Han, C. Effects of magnesium chloride and organic additives on the synthesis of aragonite precipitated calcium carbonate. *J Cryst Growth*, 310, 2593–2601 (2008).
40. Berner, R. A. The role of magnesium in the crystal growth of calcite and aragonite from sea water. *Geochim Cosmochim Acta*, 39, 489–494 (1975).
41. Kitamura, M. Crystallization and transformation mechanism of calcium carbonate polymorphs and the effect of magnesium ion. *J Colloid Interface Sci*, 236, 318–327 (2001).
42. Menadakis, M., Maroulis, G., and Koutsoukos, P. G. A quantum chemical study of doped CaCO_3 (calcite). *Comput Mater Sci*, 38, 522–525 (2007).
43. Cailleau, P. Importance de l'ion Mg^{2+} sur la croissance cristalline des carbonates de calcium en milieu libre, PhD thesis, University Montpellier, Montpellier (1978).
44. Nancollas, G. H. and Zieba, A. Constant composition kinetics studies of the simultaneous crystal growth of some alkaline earth carbonates and phosphates. In *Mineral Scale Formation and Inhibition*, Ed. Z. Amjad, Plenum Press, New York (1995).
45. Sastri, C. S. and Möller, P. Study of the influence of Mg^{2+} ions on Ca^{45}Ca isotope exchange on the surface layers of calcite single crystals. *Chem Phys Lett*, 26, 116–120 (1974).
46. Möller, P. Determination of the composition of surface layers of calcite in solutions containing magnesium (2+). *J Inorg Nucl Chem*, 35, 395–401 (1973).
47. Pai, R. and Pillai, S. Divalent cation-induced variations in polyelectrolyte conformation and controlling calcite morphologies: Direct observation of the phase transition by atomic force microscopy. *J Am Chem Soc*, 130, 13074–13078 (2008).
48. Zhang, Y. and Dawe R. A. Influence of Mg^{2+} on the kinetics of calcite precipitation and calcite crystal morphology. *Chem Geol*, 163, 129–138 (2000).
49. Paquette, J., Vali, H., and Mucci, A. TEM study of Pt-C replicas of calcite overgrowths precipitated from electrolyte solutions. *Geochim Cosmochim Acta*, 60, 4689–4699 (1996).
50. Paquette, J. and Reeder, R. J. Relationship between surface structure, growth mechanism, and trace element incorporation in calcite *Geochim Cosmochim Acta*, 59, 735–749 (1995).
51. Sweeney, F. M. and Cooper, S. D. The development of a novel scale inhibitor for severe water chemistries. In *Society of Petroleum Engineers International Symposium on Oilfield Chemistry*, New Orleans, LA, March 2–5, paper SPE 25159 (1983).
52. Demadis, K. D. and Baran, P. Chemistry of organophosphonate scale growth inhibitors: Two-dimensional, layered polymeric networks in the structure of tetrasodium 2-hydroxyethyl-amino-bis(methylenephosphonate). *J Solid State Chem*, 177, 4768–4776 (2004).
53. Amjad, Z. and Hooley, J. P. Effect of antiscalants on the precipitation of calcium carbonate in aqueous solutions. *Tens Surf Deter*, 31, 12–17 (1994).
54. Pastero, L., Costa, E., Bruno, M., Rubbo, M., Sgualdino, G., and Aquilano, D. Morphology of calcite (CaCO_3) crystals growing from aqueous solutions in the presence of Li^+ ions. Surface behaviour of the {0001} form. *Cryst Growth Des*, 4, 485–490 (2004).
55. Chen, T., Neville, A., and Yuan, M. Effect of PPCA and DETPMP inhibitor blends on CaCO_3 scale formation. In *International Symposium on Oilfield Scale*, SPE 87442, Society of Petroleum Engineers, Aberdeen, Scotland, May 2004.
56. Pokrovsky, O. S., Mielczarski, J. A., Barres, O., and Schott, J. Surface speciation models of calcite and dolomite/aqueous solution interfaces and their spectroscopic evaluation. *Langmuir*, 16, 2677–2688 (2000).
57. Chen, T., Neville, A., Sorbie, K., and Zhong, Z. In-situ monitoring the inhibiting effect of polyphosphinocarboxylic acid on CaCO_3 scale formation by synchrotron x-ray diffraction, accepted (2008).
58. Chen, T., Neville, A., Sorbie, K., and Zhong, Z. In-situ monitoring the inhibiting effect of DETPMP on CaCO_3 scale formation by synchrotron x-ray diffraction, NACE, paper 07053 (2007).

5 Scale and Deposit Control Polymers for Industrial Water Treatment

Robert W. Zuhl and Zahid Amjad

CONTENTS

5.1	Introduction	81
5.2	Deposit Control Polymer Evaluation Process: An Overview	82
5.3	Deposit Control Polymer Performance Evaluation.....	85
5.3.1	Inhibitor Interactions	85
5.3.1.1	Calcium–Polymer Interactions	85
5.3.1.2	Calcium–Phosphonate Interactions	87
5.3.1.3	Polymer–Polymer Interactions.....	88
5.3.2	Scale Inhibition.....	90
5.3.2.1	Calcium Phosphate.....	90
5.3.2.2	Calcium Carbonate	92
5.4	Polymer Architecture Influence on Dispersing Particulate Matter	98
5.4.1	Iron Oxide Dispersion	99
5.4.2	Iron (III) Stabilization	100
5.5	Summary	101
	References.....	102

5.1 INTRODUCTION

The accumulation of unwanted deposits on equipment surfaces is a phenomenon that occurs in virtually all processes in which untreated water is heated. The deposits commonly encountered may be categorized into the following five groups: (a) mineral scales (e.g. CaCO_3 , $\text{CaSO}_4 \cdot 2\text{H}_2\text{O}$, BaSO_4 , $\text{Ca}_3(\text{PO}_4)_2$, CaF_2 , SiO_2), (b) suspended matter (e.g. mud or silt), (c) corrosion products (i.e., Fe_2O_3 , Fe_3O_4 , ZnO , CuO), (d) microbiological, and (e) metal-inhibitor salts. The deposition of these materials, especially on heat exchanger surfaces in cooling, boiler, geothermal, and distillation systems, can cause a number of operational problems such as plugging of pipes and pumps, inefficient water treatment chemical usage, increased operation costs, lost production due to system downtime, and ultimately heat exchanger failure. Greater water conservation has been a driver for operating industrial water systems at higher cycles of concentrations, thereby increasing the potential for deposit buildup on heat exchanger surfaces. Operating industrial water systems under stressed conditions demands a better understanding of system (feed and recirculating) water chemistry as well as the development of new and innovative agents for controlling scale/deposit, corrosion, and biofouling.

Researchers have proposed several chemical addition options for controlling scale formation including the use of acids, chelants, or inhibitors. The most promising scale control method involves

adding substoichiometric dosages, typically a few parts per million, to the feed water either nonpolymeric (e.g., polyphosphates, phosphonates, phosphonocitric acid) or polymeric (e.g., the homopolymers of acrylic acid (AA), maleic acid, aspartic acid, and copolymers containing monomers of different functional groups) water-soluble additives.

For carboxylic acid containing polymers, it appears that the precipitation inhibition of scale-forming salts is dependent on (a) polymer architecture (e.g., ionic charge, monomer size, monomer ratio, molecular weight [MW]) and (b) the scaling salt being formed. In addition, various factors (e.g., water chemistry; types and concentrations of flocculants, biocides, phosphonates, and deposit control polymers used as components of treatment programs; as well as a deposit control polymer's hydrolytic and thermal stability) also play important roles in the efficient operation of industrial water systems [1–4].

The use of synthetic polymers [e.g., poly(acrylic acids), poly(methacrylic acid), hydrolyzed polyacrylamides, acrylic acid/acrylamide copolymers] dates back to the 1950s. Researchers have shown that polymer MW is an important consideration relative to performance [5,6]. Eventually, copolymers of acrylic acid, methacrylic acid, and/or maleic acid with a variety of other comonomers [e.g., sulfonated styrene (SS), 2-acrylamido-2-methylpropane sulfonic acid (SA), acrylamides, acrylate esters, and so on] were found to provide improved performance characteristics in various applications including, boiler, cooling, geothermal, oil field, and desalination (thermal and membrane based) processes [7,8].

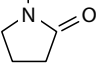
The impact of solution pH on corrosion rate and scaling tendency has been studied. It is well known that alkaline pH and high alkalinity generally reduce corrosion rates. However, a system water pH increase, especially in phosphate-based cooling water treatment (CWT) program can increase the scaling potential, thereby necessitating the use of a high-performance calcium-phosphate-inhibiting polymer. The influence of soluble impurities (i.e., Fe^{3+} , polymeric flocculant, cationic biocides, and so on) on the performance of calcium phosphate inhibitors has been investigated. The results of these studies reveal that polymeric impurities, when present at low concentration (<1 ppm), exhibit antagonistic effect on the performance of calcium-phosphate-inhibiting polymers [9,10]. Other factors that impact the selection of polymers as scale inhibitor and/or dispersant include compatibility with formulation ingredients, water hardness, polymer stability under harsh conditions, and environmental acceptability. Polymer performance retention under heat-stressed conditions is also an important property in high-temperature applications (e.g., geothermal and boiler). The data reviewed in this chapter provide water technologists a basis to select deposit control polymers that deliver performance under a variety of stressed operating conditions. The chapter is divided into two sections: (a) an overview of a deposit control polymer evaluation process and (b) an evaluation of deposit control polymer performance data using a variety of laboratory screening tests. Table 5.1 shows the structures of polymeric and nonpolymeric additives tested.

5.2 DEPOSIT CONTROL POLYMER EVALUATION PROCESS: AN OVERVIEW

A large variety of polymeric and nonpolymeric additives are available to water technologists for developing new and improved formulations for handling different challenges in treating industrial water systems. Water technologists typically use a combination of laboratory screening, small-scale or dynamic pilot testing, and field testing to evaluate and optimize the performance of deposit control polymers and/or water treatment formulations. Table 5.2 lists the commonly used methods to screen deposit control polymers for a variety of properties [e.g., scale inhibition, particulate dispersion, metal-ion stabilization, the prevention of scale deposition on equipment surfaced (heat exchangers and/or reverse osmosis membranes), the impact of soluble and suspended impurities on polymer performance, and the type of metallurgy]. The test methods listed in Table 5.2 provide a basis for comparing the performance of competitive polymers.

After selecting the deposit control polymer(s) that provide the best cost performance for a given application, the next step in the polymer evaluation process involves pilot testing of formulated

TABLE 5.1
Polymeric and Nonpolymeric Additives Tested

Polymer	Structure	Mol. Wt.	Acronym
Poly(acrylic acid)	$-(\text{CH}_2-\text{CH})_n-$ COOH	800	P1
Poly(acrylic acid)	$-(\text{CH}_2-\text{CH})_n-$ COOH	2,000	P2 ^a
Poly(acrylic acid)	$-(\text{CH}_2-\text{CH})_n-$ COOH	6,000	P3 ^a
Poly(acrylic acid)	$-(\text{CH}_2-\text{CH})_n-$ COOH	7,000	P4 ^b
Poly(acrylic acid)	$-(\text{CH}_2-\text{CH})_n-$ COOH	100,000	P5
Poly(acrylic acid)	$-(\text{CH}_2-\text{CH})_n-$ COOH	<10,000	P6 ^c
Poly(methacrylic acid)	$-(\text{CH}_2-\text{CH})_n-$ COOH CH ₃	5,000	P7
Poly(maleic acid)	$-(\text{CH}-\text{CH})_n-$ COOH COOH	<1,000	P8
Poly(acrylamide)	$-(\text{CH}_2-\text{CH})_n-$ CONH ₂	<10,000	P9
Poly(vinyl pyrrolidone)	$-(\text{CH}_2-\text{CH})_n-$ 	PVP	P10
Poly(2-acrylamido-2-methylpropane sulfonic acid)	$-(\text{CH}_2-\text{CH})_n-$ CO NH H ₃ C-C-CH ₃ CH ₂ SO ₃ H	7,000	P11
Poly(maleic acid:acrylic acid)	$-(\text{CH}-\text{CH})_n-(\text{CH}_2-\text{CH})_m-$ COOH COOH COOH	<10,000	P12
Poly(acrylic acid:hydroxypropyl acrylate)	$-(\text{CH}_2-\text{CH})_n-(\text{CH}_2-\text{CH})_m-$ COOH CO H ₃ C-CH-CH ₂ OH	7,000	P13

(continued)

TABLE 5.1 (continued)
Polymeric and Nonpolymeric Additives Tested

Polymer	Structure	Mol. Wt.	Acronym
Poly(acrylic acid:2-acrylamido-2-methylpropane sulfonic acid)	$\begin{array}{c} \text{---}(\text{CH}_2\text{---CH})_n\text{---}(\text{CH}_2\text{---CH})_m\text{---} \\ \qquad \qquad \qquad \\ \text{COOH} \qquad \qquad \text{CO} \\ \\ \text{NH} \\ \\ \text{H}_3\text{C---C---CH}_3 \\ \\ \text{CH}_2\text{SO}_3\text{H} \end{array}$	<15,000	P14
Poly(acrylic acid:2-acrylamido-2-methylpropane sulfonic acid:sulfonated styrene)	$\begin{array}{c} \text{---}(\text{CH}_2\text{---CH})_n\text{---}(\text{CH}_2\text{---CH})_m\text{---}(\text{CH}_2\text{---CH})_p\text{---} \\ \qquad \qquad \qquad \qquad \qquad \qquad \\ \text{COOH} \qquad \qquad \text{CO} \qquad \qquad \text{C}_6\text{H}_4\text{---} \\ \qquad \qquad \qquad \qquad \qquad \qquad \\ \text{NH} \qquad \qquad \qquad \text{SO}_3\text{H} \\ \\ \text{H}_3\text{C---C---CH}_3 \\ \\ \text{CH}_2\text{SO}_3\text{H} \end{array}$	<15,000	P15
Poly(acrylic acid:2-acrylamido-2-methylpropane sulfonic acid: <i>t</i> -butyl acrylamide)	$\begin{array}{c} \text{---}(\text{CH}_2\text{---CH})_n\text{---}(\text{CH}_2\text{---CH})_m\text{---}(\text{CH}_2\text{---CH})_p\text{---} \\ \qquad \qquad \qquad \qquad \qquad \qquad \\ \text{COOH} \qquad \qquad \text{CO} \qquad \qquad \text{CO} \\ \qquad \qquad \qquad \qquad \qquad \qquad \\ \text{NH} \qquad \qquad \qquad \text{NH} \\ \qquad \qquad \qquad \qquad \qquad \qquad \\ \text{H}_3\text{C---C---CH}_3 \quad \text{H}_3\text{C---C---CH}_3 \\ \qquad \qquad \qquad \qquad \qquad \qquad \\ \text{CH}_2\text{SO}_3\text{H} \qquad \text{CH}_3 \end{array}$	<15,000	P16
Poly(diallyldimethyl ammonium chloride)	$\begin{array}{c} \text{---}(\text{CH}_2\text{---CH---CH---CH}_2\text{---})\text{---} \\ \qquad \qquad \\ \text{H}_3\text{C} \qquad \text{CH}_3 \\ \diagdown \qquad / \\ \text{N}^+ \\ / \qquad \diagdown \\ \text{H}_3\text{C} \qquad \text{CH}_3 \end{array} \quad \text{Cl}^-$	1,000,000	P17
Amino tris (methylene phosphonic acid)	$\begin{array}{c} \text{CH}_2\text{PO}_3\text{H}_2 \\ / \\ \text{N} \\ \backslash \\ \text{CH}_2\text{PO}_3\text{H}_2 \\ / \\ \text{CH}_2\text{PO}_3\text{H}_2 \end{array}$	206	AMP
Hydroxyethylidene-1,1-diphosphonic acid	$\begin{array}{c} \text{OH} \\ \\ \text{H}_2\text{O}_3\text{P---C---PO}_3\text{H}_2 \\ \\ \text{CH}_3 \end{array}$	299	HEDP
2-Phosphonobutane-1,2,4-tricarboxylic acid	$\begin{array}{c} \text{PO}_3\text{H}_2 \quad \text{H} \quad \text{H} \\ \qquad \qquad \\ \text{H}_2\text{C---C---C---C---H} \\ \qquad \qquad \qquad \\ \text{COOH} \quad \text{COOH} \quad \text{H} \quad \text{COOH} \end{array}$	270	PBTC

^a Organic solvent polymerized.

^b Water polymerized.

^c Contains phosphinate group.

product(s). The pilot testing enables water technologists to study the performance of formulated product under small-scale simulated field conditions and evaluate potential operating conditions. Upon completion of pilot testing, including performance optimization, water technologists select suitable customer sites to conduct field trials to confirm treatment program performance.

5.3 DEPOSIT CONTROL POLYMER PERFORMANCE EVALUATION

5.3.1 INHIBITOR INTERACTIONS

5.3.1.1 Calcium–Polymer Interactions

Scale inhibitors (polymeric and nonpolymeric) used in water treatment formulations may form insoluble salts with hardness ions under conditions frequently encountered in cooling water systems. The trend toward the operation of cooling water systems under increasingly severe operating conditions (e.g., high hardness, high alkalinity, and higher pH and temperature) has increased the potential for the formation of insoluble calcium-inhibitor salts. For this reason, “Ca ion tolerance” or the ability of an inhibitor to remain soluble in the presence of high hardness ions is of increasing importance. *Ca ion tolerance* is defined as the maximum amount of the deposit control polymer that can be added to the water system without the significant precipitation of calcium polymer salt. When polymers form an insoluble salt with Ca ion, it causes both additional scaling problems and decreases the effective concentration of polymer thereby leading to additional scaling problem.

Figure 5.1 illustrates turbidity (100-%T), where “%T” is “% transmittance,” as a function of P3 (polyacrylic acid, MW 6000 Dalton, hereafter “Da”) concentration and shows good reproducibility ($\pm 7\%$). The inflection point in

TABLE 5.2
Laboratory Screening Tests for Evaluating Deposit Control Polymers

1. Threshold inhibition
 - a. Calcium carbonate
 - i. Static moderate conditions
 - ii. Stirred severe conditions
 - b. Calcium sulfate
 - c. Barium sulfate
 - d. Calcium phosphate
 - e. Calcium phosphonate
 - f. Silica polymerization
2. Dispersancy
 - a. Iron oxide
 - b. Hydroxyapatite
 - c. Kaolin clay
3. Metal ion stabilization
 - a. Iron
 - b. Zinc
4. Deposit control
 - a. Calcium carbonate
 - b. Calcium sulfate
5. Product use considerations
 - a. Calcium ion tolerance
 - b. Chlorine compatibility
 - c. Hydrolytic stability
 - d. Thermal stability
 - e. Total solids

Source: Lubrizol Advanced Materials, Inc. product bulletin, “Test procedures for evaluating deposit control polymers,” CBS-TPEDCPP (Oct. 2007).

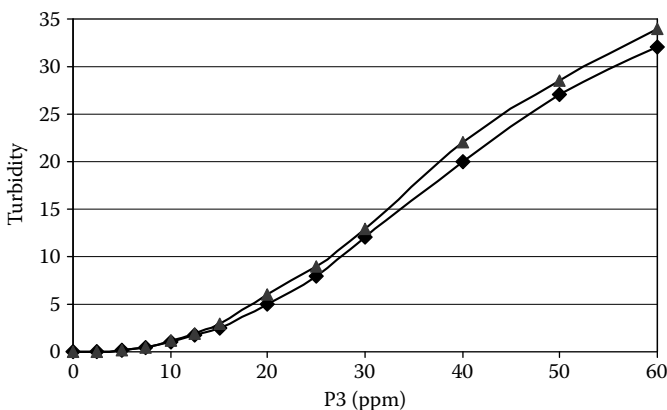


FIGURE 5.1 Calcium ion interactions with poly(acrylic acid), P3. Plots of turbidity versus P3 concentrations at pH 9.0, 25°C, and 1000 mg/L Ca.

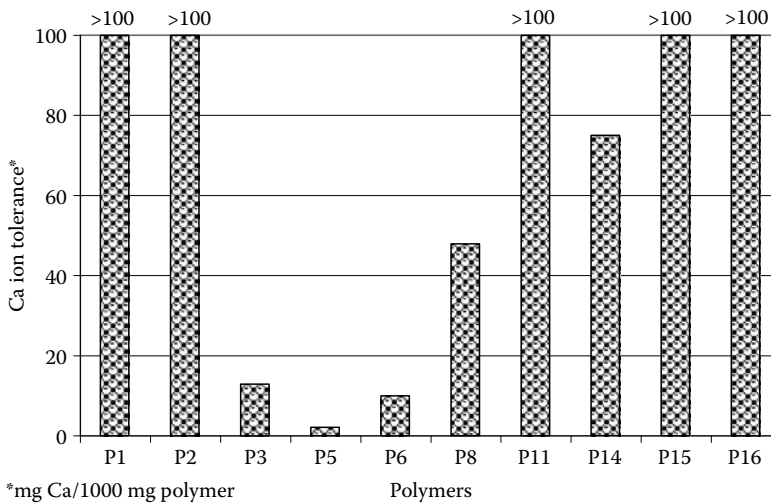


FIGURE 5.2 Calcium ion tolerance of homo-, co-, and terpolymers at pH 9.00, 25°C, 1000 mg/L Ca.

the turbidity versus P3 concentration profile was used to calculate the point of onset of turbidity. The tolerance value calculated for P3 is 13 ± 1 ppm per 1000 mg/L Ca. Figure 5.2 presents Ca ion compatibility data for several homo-, co-, and terpolymers that indicate the following:

- The Ca ion compatibility of P-AA decreases with increasing polymer MW.
- Among homopolymers, P10 (polysulfonic acid, MW 7000 Da) is more tolerant to Ca ion than homopolymers of acrylic acid and maleic acid. This may be attributed to the weak interactions of Ca ions with SO_3H (SA) group versus COOH group.
- Replacing the portion of acrylic acid (AA) with sulfonic acid (SA) results in the improved tolerance of copolymer (e.g., P14).
- AA:SA copolymers incorporating either nonionic (P16) or sulfonated styrene (P15) monomer groups exhibit excellent Ca ion tolerance.

The calcium ion tolerance of several polymers exposed to thermal stress (200°C, 20 h) is presented in Figure 5.3. The data presented in Figure 5.3 indicate that the thermal treatment of acrylic

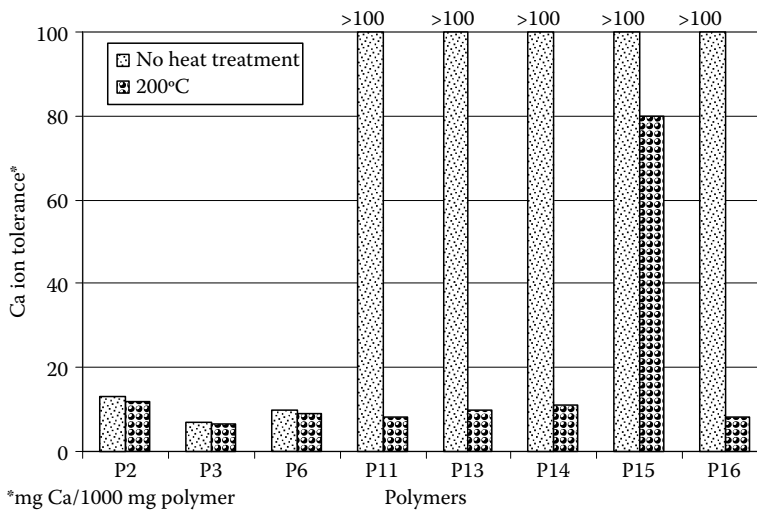


FIGURE 5.3 Effect of heat treatment on calcium ion tolerance of homo-, co-, and terpolymers.

acid homopolymers (i.e., P2, P3, and P4) does not significantly impact the compatibility of these polymers with calcium ion. These data also reveal that all SA containing homo-, co-, and terpolymers are affected by thermal treatment [11]. With the exception of terpolymer P15, all co- and terpolymers became significantly less tolerant to Ca. For example, the Ca ion tolerance values obtained for both P13 (AA:HPA) and P14 (AA:SA) were >100 ppm polymer/1000 mg/L Ca before thermal stress compared to <2 ppm after being subjected to thermal stress (200°C, 20h). Because the resultant polymer is a P-AA, the poor compatibility obtained for both polymers is consistent with high MW P-AA [12]. The improved calcium ion compatibility of P15 versus P16 may contribute to the thermal stability of SS in the P16. Thus, from a practical viewpoint, polymers that exhibit high Ca tolerance should be favored for use in systems operating under higher cycles of concentrations.

5.3.1.2 Calcium–Phosphonate Interactions

Organophosphonate compounds are a broad family of chemicals used in a variety of industrial process applications, including crude oil production, pigment dispersion, electroplating, paper and pulp slurries, scale removal, and industrial water treatment. Organophosphonates differ structurally from polyphosphates in that they have a P–C bond rather than a P–O bond and these structural differences account for the superior stability of organophosphonates versus polyphosphates under pH and temperature extremes. In water treatment processes, phosphonates are used for a variety of reasons but primarily for inhibiting the formation of scale-forming salts and inhibiting steel corrosion (as cathodic inhibitors). Phosphonates are key components of most CWT programs and play an important role in protecting heat exchangers from corrosion and calcium carbonate scale formation. It is well documented that phosphonates, under stressed operating conditions (e.g., high hardness, high pH, and/or high temperature), can react stoichiometrically with the calcium ion leading to calcium phosphonate precipitation. In addition, solution phosphonate concentration can be depleted due to calcium phosphonate precipitation, thereby causing severe corrosion and calcium carbonate scaling [13–15].

Although there are several types of phosphonates available, the three most commonly used phosphonates (see Table 5.1) in deposit control water treatment are (a) amino tris (methylenephosphonic acid), AMP, (b) hydroxyethylidene 1,1-diphosphonic acid, HEDP, and (c) 2-phosphonobutane-1,2,4 tricarboxylic acid, PBTC. Figure 5.4 presents turbidity data as a function of various concentrations of AMP, HEDP, and PBTC. As illustrated, all phosphonates form insoluble salts with Ca ions.

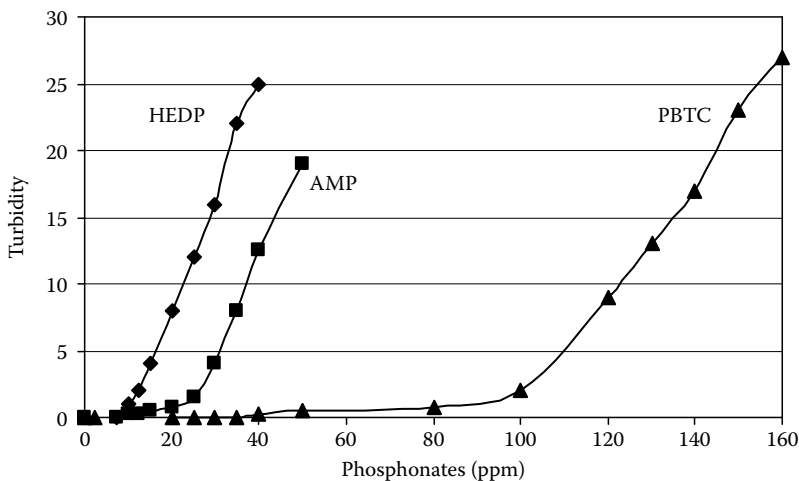


FIGURE 5.4 Calcium ion interactions with phosphonates. Plots of turbidity versus phosphonate concentration at pH 9.50, 250 mg/L Ca, 25°C.

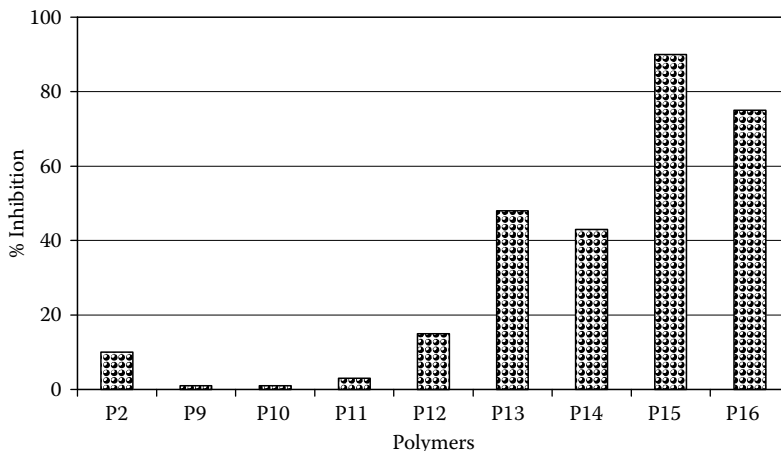


FIGURE 5.5 Ca-HEDP inhibition by polymers (150 mg/L Ca, 15 mg/L HEDP, 10 ppm polymer, pH 8.50, 50°C, 20h).

Based on the compatibility data (250 mg/L Ca ions, pH 9.50, 25°C, 30 min), these phosphonates can be ranked (in the descending order) as follows:

PBTC (98 ppm) >> AMP (26 ppm) >> HEDP (12 ppm)

The influence of polymers on the precipitation of Ca-phosphonates has been the subject of numerous investigations. Boffardi and Schweitzer [16] reported that the relatively poor calcium tolerance of phosphonates could be overcome by adding an acrylic acid:2-acrylamido-2-methylpropane sulfonic acid copolymer. Smyk et al. [17], in their investigations, showed that acrylic-based terpolymers performed better than the homopolymers of acrylic acid and a copolymer of acrylic acid and hydroxylpropyl acrylate (AA:HPA). Figure 5.5 presents results on the performance of various polymers as Ca-HEDP inhibitors. Under the experimental conditions employed (150 mg/L Ca, 15 mg/L HEDP, 10 ppm polymer, pH 8.50, 50°C, 20h), the data indicate that P2 [2000MW poly(acrylic acid), homopolymer containing COOH group] performs better than other homopolymers containing either nonionic groups (i.e., P9 and P10) or a sulfonic group (P11). The data presented in Figure 5.5 also reveal that terpolymers (i.e., P15 and P16) perform better than copolymers with only two functional groups (i.e., P12, P13, and P14). Based on the inhibition data presented, the polymers can be ranked (in terms of descending order) as

Terpolymers > Copolymers > Homopolymers

5.3.1.3 Polymer-Polymer Interactions

Cationic polyelectrolytes have been used for decades as flocculants/coagulants to isolate and separate colloidal particles from water streams. Commonly used polyelectrolytes include aluminum- and iron-containing compounds (e.g., alum, ferric chloride, and ferric sulfate). These polyelectrolytes hydrolyze to form insoluble precipitates, neutralize the charge of the colloidal particles in the water, and entrap additional particles. In most cases, these large particles (flocs) are removed via settling in a clarifier and are collected as sludge. Occasionally, clarifier upsets cause metal containing flocs to “carry over,” which may lead to the formation of aluminum- and iron-based deposits on heat exchangers. Although aluminum- and iron-based compounds can exhibit positive effects in terms of clarifying the water, the optimum performance of these compounds is very sensitive to water pH and alkalinity. A variety (e.g., linear, branched, and lightly cross-linked) of more versatile synthetic polyelectrolytes (linear, branched, and lightly cross-linked) have been developed. Among the commercial cationic polyelectrolytes, a diallyldimethyl ammonium chloride homopolymer (P17) is frequently the choice due to its high performance and reasonable cost.

It has been reported that pairs of opposite-charged polymers typically form complexes (soluble and insoluble) in aqueous solution [18,19]. Depending primarily on MW and linear-charge densities, these complexes may be amorphous solid or soluble (colloidal) aggregates. The forces driving the formation of these complexes are primarily electrostatic, and therefore parameters such as polymer charge density, solution pH, and ionic strength are particularly important.

The interactions between anionic polymers (APs) commonly used in water treatment applications and a cationic polymer (CP, diallyldimethyl ammonium chloride, P17, MW >1 MM Da) were investigated using a turbidimetric method. The test conditions employed (100 mg/L Ca, 100 mg/L Mg, 110 mg/L Na, 470 mg/L Cl, 150 mg/L SO₄, 100 mg/L HCO₃, pH 8.0) involved mixing 5 ppm CP with 5 ppm APs. The solutions were stirred at 25°C and the progress of reaction was monitored by measuring turbidity at 30 min. Higher turbidity indicates the poor compatibility of APs with CP. Figure 5.6 presents the compatibility data of CP with APs, leading to the following observations regarding anionic polymer: (a) MW: the compatibility of CP with P-AAs depends on polymer MW (e.g., low MW P1 is more compatible than high MW P2); (b) ionic charge: among the homopolymers tested, P2, P3, and P8 are less compatible than nonionic polymers (i.e., P9 and P10); and (c) composition: the incorporation of hydrophobic and bulkier groups increases the compatibility of co- and terpolymers. It has been shown that polymeric and nonpolymeric scale inhibitors, when present at low concentrations in recirculating water, form insoluble complexes/salts with cationic-charged polymeric flocculants/coagulants and/or biocides.

The data presented in Figure 5.6 show that cationic-charged polymeric flocculants/coagulants form insoluble complexes/salts with anionic polymers present at low concentrations in recirculating water. The driving forces in the formation of such insoluble complexes between cationic and anionic additives are electrostatic in nature. Therefore, water technologists must understand the system water chemistry and take appropriate actions to avoid the formation of AP-CP salts in recirculating waters. This could be achieved by ensuring that proper pretreatment is applied and the concentration of CP is maintained extremely low (<0.1 ppm).

As discussed above, water chemistry, formulation components, and polymer architecture all impact the deposit control performance in cooling water applications. For example, it was shown that the tendency of CWT formulation components (i.e., deposit control polymer and phosphonates) to form insoluble salts with Ca ion increases with increasing Ca concentration, increasing pH, and increasing temperature [20,21]. In addition, it was also shown that cationic polymeric biocides and flocculating agents form insoluble salts with anionic polymers commonly used in water treatment applications.

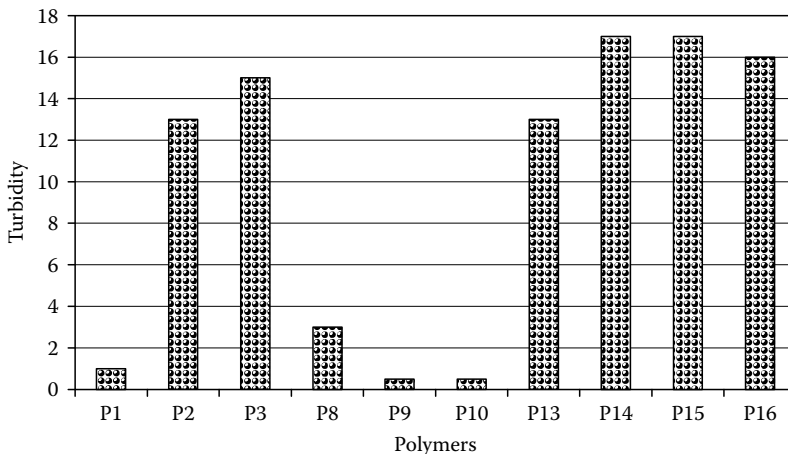


FIGURE 5.6 Plots of turbidity for the interaction of anionic polymers (5 ppm) with 5 ppm cationic polymer (100 mg/L Ca, 100 mg/L Mg, 110 mg/L Na, 470 mg/L Cl, 150 mg/L SO₄, pH 8.0, 25°C).

5.3.2 SCALE INHIBITION

5.3.2.1 Calcium Phosphate

Over the years, many different treatment programs have been developed for open recirculating cooling water systems. These treatment programs include (a) “soft” phosphate or dispersant, (b) “stabilized” phosphate, (c) “all organic,” (d) molybdate, (e) alkaline zinc, and (f) chromate/zinc. The incorporation of multifunctional deposit control polymers is critical to the success of these CWT programs. Since the 1960s, molybdates, silicates, polyphosphates/phosphates, phosphonates, and zinc salts are among the more environmentally acceptable mild steel corrosion inhibitors that have displaced chromates. Phosphates, from the perspective of versatility, cost, and performance, have become a new performance standard. However, phosphate-based CWT programs require more careful system parameter control than do chromate programs, mainly because they rely on relatively high phosphate levels for corrosion protection. These high phosphate levels, and especially cooling systems operating at alkaline pH and high calcium hardness water, can lead to calcium phosphate precipitation and heat exchanger fouling. The key to the successful use of phosphate-based CWT program lies in the proper selection of polymeric calcium phosphate inhibitor that has a dual role: (a) controls the thickness of the calcium phosphate film on the metal surface and (b) prevents precipitation of the calcium phosphate in the recirculating water.

Currently, a variety of deposit control polymers are commercially available for developing water treatment formulations. However, it is recommended that water technologists consider the following criteria in selecting polymer(s) for optimizing the performance of systems operating under stressed conditions: (a) calcium phosphate inhibition, (b) tolerance to hardness ions, (c) compatibility with organic cationic flocculant, (d) tolerance to thermal stress, (e) retention of performance in the presence of inorganic and organic flocculant, (f) retention of activity in the presence of cationic biocides, (g) environmental acceptability, (h) formulation flexibility in a wide pH range, and (i) compatibility with oxidizing biocides.

5.3.2.1.1 Polymer Composition

Figure 5.7 shows performance data for several deposit control polymers before and after heat treatment at 200°C. It is evident from Figure 5.7 that heat treatment exposure has varying effects on deposit control polymer performance. For example, the heat treatment of carboxylic acid

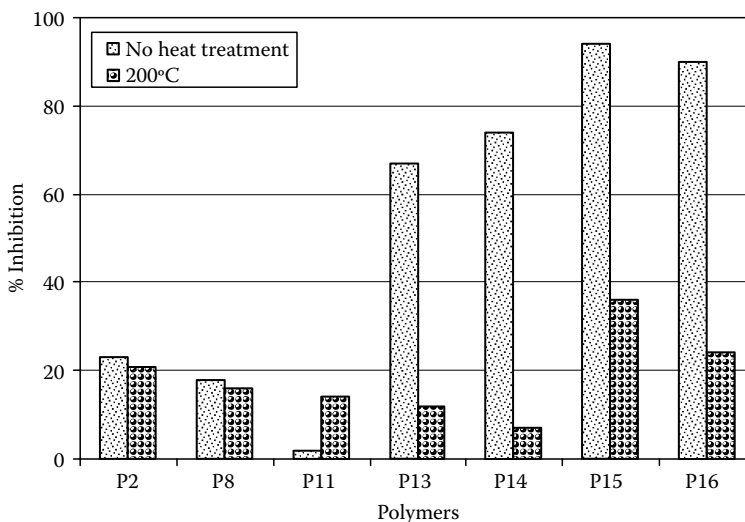


FIGURE 5.7 Calcium phosphate inhibition by heat-treated and non-heat-treated polymers (140 mg/L Ca, 9.0 mg/L PO₄, 10 ppm polymer, pH 8.50, 50°C, 22 h).

containing homopolymers (i.e., P2 and P8) shows no negative impact on the performance of these polymers, indicating that there is no significant loss of carboxylic acid group. However, for the copolymers containing carboxylic acid and either acrylate ester or sulfonic acid groups (i.e., P13 and P14), the situation is dramatically different; these copolymers lost ~90% inhibitory power upon heat treatment. This suggests that the SA and ester components of the AA:SA (P14) and AA:HPA (P13) copolymers underwent essentially complete degradation, leading to the formation of P-AA. The poor performance (<10% calcium phosphate inhibition) exhibited by thermally treated copolymers is consistent with the performance of high (>10,000) MW P-AA [22]. Figure 5.7 also presents calcium phosphate inhibition data for the two terpolymers (i.e., P15 and P16). As shown in Table 5.1, the primary difference between these two terpolymers is the third monomer [i.e., sulfonated styrene (SS) for P15 and nonionic for P16]. It is interesting to note that P16 lost more inhibitory power (~73%) compared to ~60% loss for P15, indicating that SS is more thermally stable than the nonionic monomer present in P16.

5.3.2.1.2 Polymer Dosage

The impacts of thermal stress shown in Figure 5.7 are amplified in Figure 5.8 wherein P15 dramatically outperforms both the P14 copolymer and the P16 terpolymer at the baseline 10 ppm dosage and to a greater extent as polymer dosage increases to 20 ppm. The excellent performance shown by the heat-treated P15 may be attributed to the superior thermal stability of the SS component.

5.3.2.1.3 Polymer Solution Temperature

Figure 5.9 presents the calcium phosphate inhibition performance data for the two terpolymers (i.e., P15 and P16) before and after various levels of thermal stress. As shown in Figure 5.9, P14, compared to P15, is a more effective calcium phosphate inhibitor after heat treatment (at 150°C, 200°C, and 240°C).

5.3.2.1.4 Effect of Iron (III)

The presence of iron in the recirculating water, whether originating from the feed water as a result of the carryover from the clarifier operating on iron-based flocculating agents or as a result of the corrosion in the system, may influence the performance of calcium-phosphate-inhibiting polymer and the CWT program. Figure 5.10 shows results for iron sensitivity testing for several

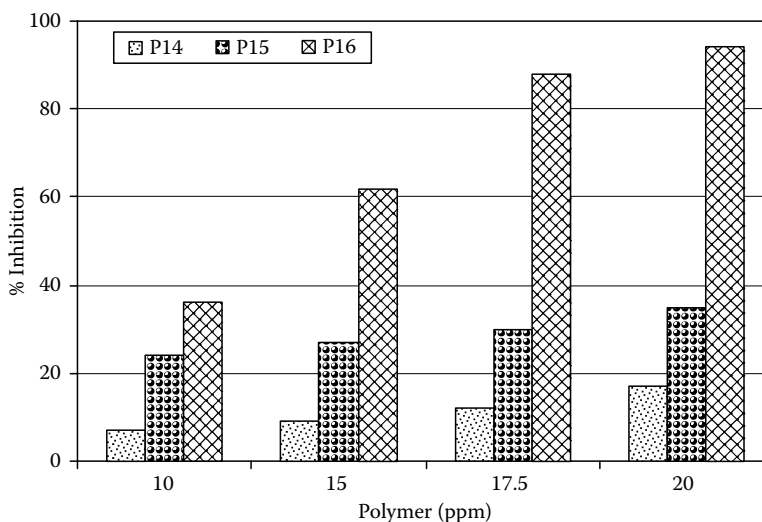


FIGURE 5.8 Calcium phosphate inhibition by thermally stressed (200°C, 20h) polymers versus dosage (140 mg/L Ca, 9.0 mg/L PO₄, 10 ppm polymer, pH 8.50, 50°C, 22h).

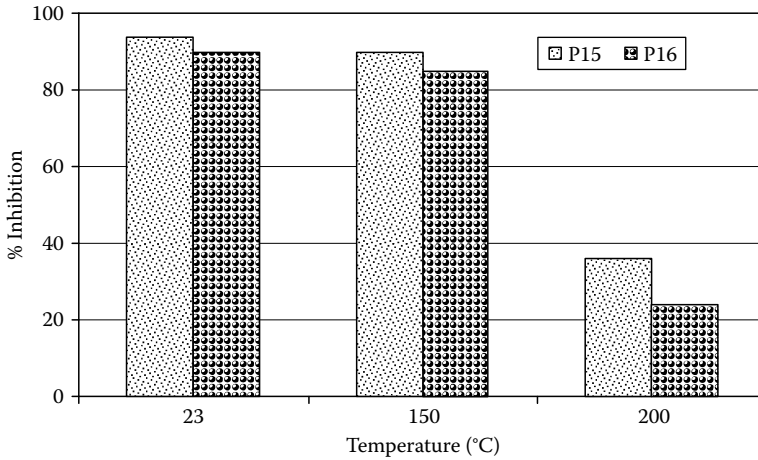


FIGURE 5.9 Calcium phosphate inhibition by thermally stressed terpolymers (140 mg/L Ca, 9.0 mg/L PO₄, 10 ppm polymer, pH 8.50, 50°C, 22h).

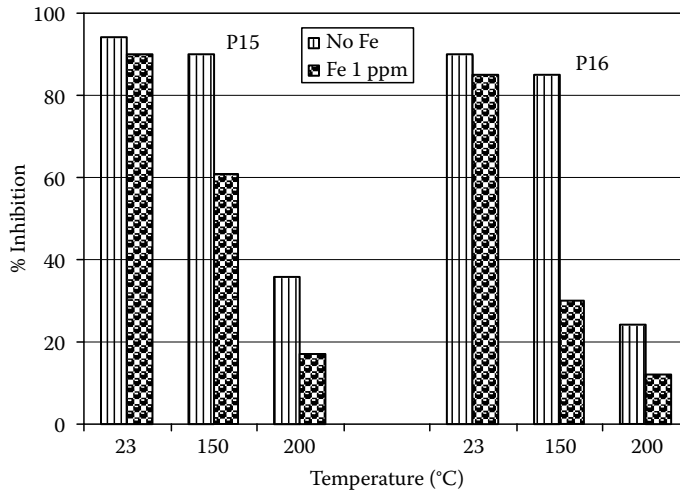


FIGURE 5.10 Calcium phosphate inhibition in the presence of 0 and 1 ppm Fe (III) by thermally stressed terpolymers (140 mg/L Ca, 9.0 mg/L PO₄, 10 ppm polymer, pH 8.50, 50°C, 22h).

calcium-phosphate-inhibiting polymers in the presence of 0 and 1.0 ppm Fe (III). As shown, terpolymer P15 exhibits better tolerance to iron than the terpolymer P16. In addition to inhibiting calcium phosphate precipitation and dispersing iron oxide, the ability to resist the negative effects of iron should be a part of the deposit control polymer selection criteria for effective CWT programs. Polymer thermal stability is a key consideration to ensure the optimum performance of boiler water treatment programs.

5.3.2.2 Calcium Carbonate

Calcium carbonate (CaCO₃) is one of the most commonly encountered scale deposits. CaCO₃ is found in different crystalline forms in the following order of increasing solubility: calcite, aragonite, vaterite, CaCO₃ monohydrate, and CaCO₃ hexahydrate. Calcite, the thermodynamically most stable polymorph of CaCO₃, forms tenaciously adhering, hard mineral deposits. The precipitation and stabilization of CaCO₃ polymorphs depend on the precipitation conditions (i.e., supersaturation level, pH, temperature, pressure, and the concentration and architecture of the additives).

The influence of polymeric and nonpolymeric additives such as CaCO_3 inhibitors has been of great interest to both academic researchers and industrial technologists. Common nonpolymeric inhibitors evaluated include organophosphonates, polyphosphates, polycarboxylic acids, and fulvic acids. It has been reported that these inhibitors, when present at low concentrations, markedly inhibit the CaCO_3 precipitation from supersaturated solutions. A surface adsorption method involving a simple Langmuir adsorption model has been proposed to account for the inhibition of CaCO_3 crystal growth. Among the polymeric inhibitors evaluated were P-AA; P-MA; and copolymers comprising AA, MA, and other monomers containing different functional groups. This section discusses the performance of various polymers exposed to different heat treatment. In addition, results are presented on the efficacy of polymers, phosphonates, and polymer/phosphonate blends as calcium carbonate scale inhibitor under varying calcite super-saturations.

5.3.2.2.1 Polymer Dosage

Figure 5.11 presents CaCO_3 % inhibition data as a function of P-AA (P3) dosage [560 mg/L Ca, 630 mg/L HCO_3^- , 30 mg/L CO_3^{2-} (all expressed as CaCO_3), pH 8.25, 67°C, 24 h]. Figure 5.11 shows that adding relatively small amounts of P3 significantly inhibits CaCO_3 precipitation: 1.0 ppm inhibits precipitation by 35%, increasing P3 to 3 ppm increases inhibition $\sim 2\times$ (to 67%), and increasing the P3 dosage to 5.0 ppm results in a 75% inhibition value.

5.3.2.2.2 Heat Treatment of Homopolymers

Figure 5.12 presents the performance comparison of homopolymers with and without heat treatment at 200°C. It is evident from Figure 5.12 that the exposure of aqueous solutions of carboxylic acid containing homopolymers (i.e., P-AAs, P-MAA, and P-MA) to heat treatment has varying effects on polymer performance. For example, the heat treatment of polymers (i.e., P3, P6, and P7) has no negative impact on their performance, indicating that under the experimental conditions employed there is no significant loss of carboxylic acid group. Furthermore, neither of the P-AAs (i.e., P3 and P6) made in different solvents (i.e., organic and water, respectively) and with different end group (i.e., phosphonate for P6) appears to be impacted by heat treatment. Similarly, no significant loss in performance was observed for P7 or the P-MAA whose composition differs from the P3 and P6 primary because the hydrogen in acrylic acid was replaced with a methyl group. However, for the P-MA (P8), containing two carboxylic acid groups on the adjacent carbons, the situation is significantly different; P8 lost $\sim 12\%$ inhibitory power. This suggests that the maleic acid component of P8 underwent more severe degradation than the acrylic acid or methacrylic acid in P3 and P7.

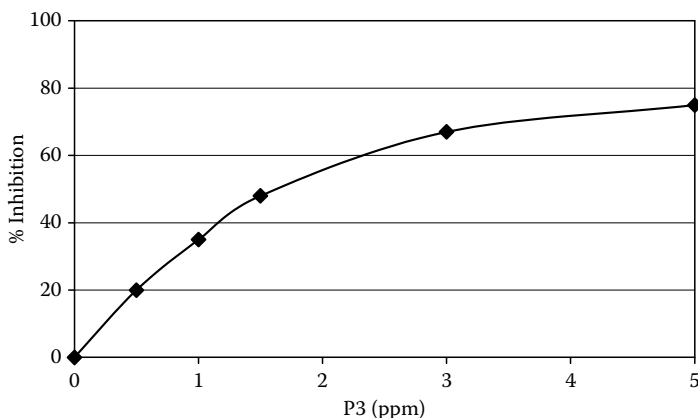


FIGURE 5.11 Calcium carbonate inhibition by poly(acrylic acid), P3 (560 mg/L Ca, 630 mg/L HCO_3^- , 30 mg/L CO_3^{2-} , pH 8.25, 67°C, 24 h).

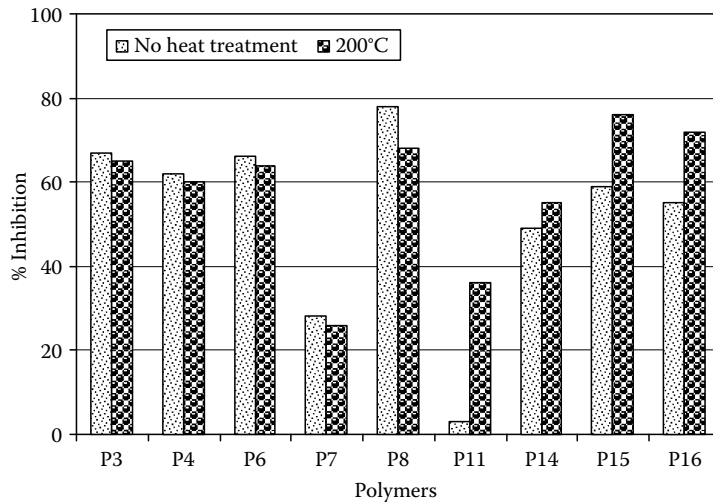


FIGURE 5.12 Calcium carbonate inhibition by thermally stressed homo-, co-, and terpolymers (560 mg/L Ca, 630 mg/L HCO_3^- , 30 mg/L CO_3^{2-} , 3 ppm polymer, pH 8.25, 67°C, 24 h).

Masler [23], in his investigation on the effect of the thermal treatment (250°C, 18 h, pH 10.5) of several homopolymers, reported that P-MAA lost slightly less MW than P-AA which lost considerably less MW than P-MA. In terms of decarboxylation, P-AA decarboxylated less than P-MAA, which decarboxylated less than P-MA. In addition, it was reported that P-MA lost ~40% activity as a CaCO_3 inhibitor after heat treatment. It is interesting to note that under similar experimental conditions, P-AA and P-MAA lost only ~5% to 8% inhibitory activity, thus suggesting that carboxyl content in the polymer plays an important role in inhibiting the precipitation of calcium carbonate. The inhibition data presented in Figure 5.12 suggest that there was insignificant loss of inhibitory activity or carboxyl content for P3 and P6 under the experimental conditions employed in the present conditions.

Figure 5.12 also presents inhibition data collected in the presence of 3 ppm P11 (P-SA) and shows that P11, without heat treatment, exhibits poor inhibitory activity (<5% inhibition). This suggests that SO_3H group present in P11, compared to COOH in P3, shows weak interaction with calcium ions. However, after heat treatment, the P11 inhibition value increases (from 3% to 36%) may be attributed to the formation of P-AA during heat treatment process. The influence of polymer MW on the precipitation of scale-forming salts has been the subject of numerous investigations [24–26]. The results of these studies reveal that especially for P-AA, the optimum performance is obtained with ~2000 MW. The poor performance of heat-treated P11 (36%) compared to P2 (67%), as observed in the present investigation, is consistent with previous studies on the influence of polymer MW in inhibiting calcium carbonate precipitation.

5.3.2.2.3 Heat Treatment of Co- and Terpolymers

Comparative inhibition data on several co- and terpolymers are depicted in Figure 5.12. As shown, both the co- and terpolymers in the absence of thermal stress exhibit mediocre (<60%) CaCO_3 inhibition. However, heat treatment (200°C, 20 h) results in varying performance changes. For example, % CaCO_3 inhibition values obtained for the AA:SA copolymer (P14) before and after heat treatment were 49% and 55%, respectively. The slight improvement in the inhibitory power of heat-treated P14 may be attributed to changes in MW and the loss of SA to form COOH .

CaCO_3 inhibition data for terpolymers (i.e., P15 and P16) are shown in Figure 5.12 and indicate that both terpolymers in the absence of heat treatment show mediocre (<60%) inhibitory power. It is evident from Figure 5.12 that both terpolymers had significant CaCO_3 inhibition improvement following heat treatment (200°C, 20 h); % inhibition values obtained for P15 and P16 before heat

treatment were 59% and 52% compared to 72% and 76%, respectively, for heat-treated terpolymers. As shown in Table 5.1, the key structural difference between P15 and P16 is the dissimilar third monomer [i.e., sulfonated styrene (SS) in P15 versus nonionic monomer in P16]. From the data presented in Figure 5.12, it's clear that upon subjecting the terpolymers to heat treatment, P15 and P16 gained more inhibitory power compared to P14. The observed increase in performance between these two terpolymers and P14 may be attributed to the difference in MW (<10,000 for terpolymers vs. <40,000 for copolymer). It is worth noting that both terpolymers showed performance improvement in this testing, whereas these terpolymers have been shown to lose performance as calcium phosphate inhibitors when they were exposed to heat treatment (200°C, 20 h).

5.3.2.2.4 Effect of Temperature

The performance data presented in Figure 5.13 illustrate excellent thermal stability for the P-MAA (P7) and two P-AAs (i.e., P2 and P3) evaluated at 150°C, 200°C, and 240°C. However, for P8, the situation is markedly different. As shown in Figure 5.13, increasing the temperature (from 150°C to 200°C to 240°C) results in gradual and significant decrease in P8 performance. The drop in inhibitory activity may be attributed to loss in MW and increased decarboxylation with increasing solution temperature. Figure 5.13 also shows a comparison of the terpolymers that have the same baseline performance before heat treatment. However, as the terpolymers are exposed to thermal stress, a marked increase in polymer performance is observed. For example, % inhibition values for P15 and P16 without heat treatment are 59% and 55% compared to 76% and 70%, respectively, for heat-treated (200°C, 20 h) terpolymers. As noted in Figure 5.13, increasing the solution temperature from 200°C to 240°C results in further (~5%) inhibition improvement. The performance data presented in Figure 5.13 suggest that essentially all of SA and nonionic monomers present in P15 and P16 are degraded to form P-AA or create a copolymer of acrylic acid and SS.

5.3.2.2.5 Phosphonates, Polymers, and Phosphonate/Polymer Blends

The performance of phosphonates as CaCO₃ inhibitors has been the subject of numerous investigations [27–29]. It is generally agreed that conventional phosphorus-based and polymeric CaCO₃ scale inhibitors are effective up to a maximum of 100× to 125× calcite saturation (equivalent to a LSI of +1.9 to 2.2). As previously discussed, phosphonate tolerance to Ca ions plays an important role in cooling water systems operating under stressed conditions. Good performance demands that phosphonates remain in solution and be available to prevent CaCO₃ precipitation and deposition on heat exchangers.

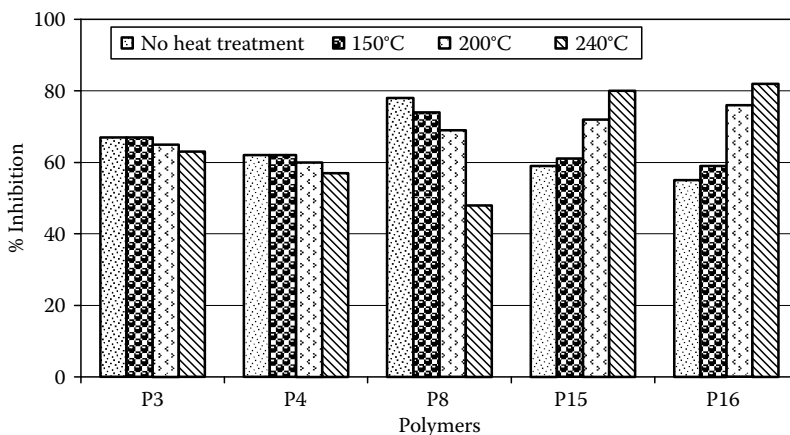


FIGURE 5.13 Calcium carbonate inhibition by thermally stressed (150°C, 200°C, and 240°C) homo-, co-, and terpolymers (560 mg/L Ca, 630 mg/L HCO₃, 30 mg/L CO₃, 3 ppm polymer, pH 8.25, 67°C, 24 h).

Figures 5.14 and 5.15 present CaCO₃ inhibition data in the presence of varying concentrations of phosphonates at two different water chemistries (i.e., 180× and 223× calcite saturation). Results obtained for both water chemistries (see Table 5.3) suggest that CaCO₃ inhibition increases as the phosphonate concentration is increased from 5 to 40 ppm. As illustrated, the CaCO₃ inhibition is rapid up to 5 ppm for both AMP and HEDP, then begins to level off, and finally reaches a plateau at ≥20 ppm for both phosphonates. However, the PBTC performance increases gradually as the concentration of PBTC is increased from 5 to 40 ppm. It should be noted that 100% CaCO₃ inhibition was not obtained for either water chemistry A or B (see Table 5.3) up to 40 ppm phosphonate concentrations. The data clearly indicate that the three phosphonates (i.e., AMP, HEDP, and PBTC) evaluated cannot completely prevent the precipitation of CaCO₃. Based on the results collected under both water chemistries A and B, CaCO₃ scale inhibition using 5 ppm phosphonate has the following order of effectiveness: HEDP ≥ AMP ≥ PBTC. However, at a 40 ppm phosphonate dosage, the performance-based ranking changes to PBTC ≥ HEDP ≥ AMP. This trend observed for phosphonate as CaCO₃ inhibitor is consistent with the trend noted above for phosphonate tolerance to Ca ions. Thus, it is clear from the data presented in Figures 5.14 and 5.15 that PBTC performs better than both AMP and HEDP in waters containing high calcite saturations.

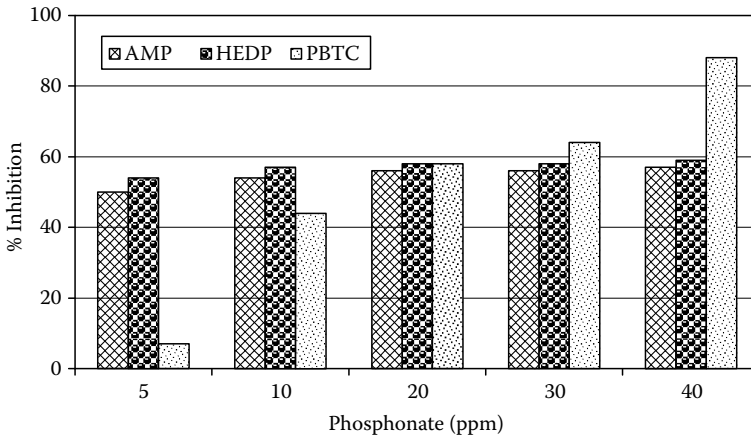


FIGURE 5.14 Calcium carbonate inhibition at 180× calcite saturation by varying dosages of phosphonates.

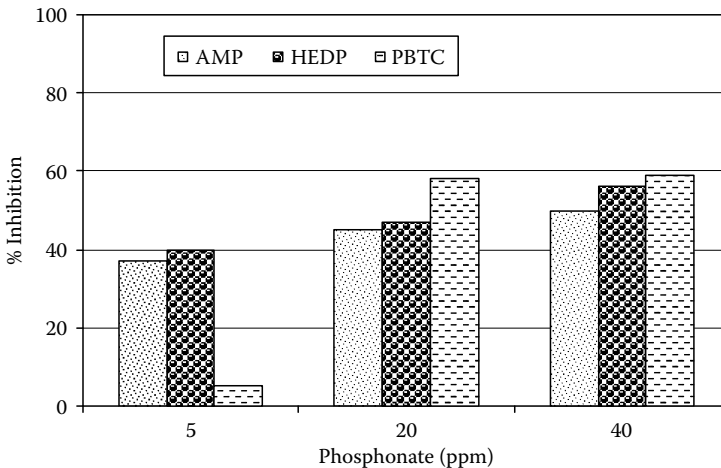


FIGURE 5.15 Calcium carbonate inhibition at 223× calcite saturation by varying dosages of phosphonates.

TABLE 5.3
Water Chemistries Used in Calcium
Carbonate Inhibition

Parameter	Condition A	Condition B
LSI	2.89	2.76
Calcite saturation	223	180
Calcium (mg/L as Ca)	250	210
Magnesium (mg/L as Mg)	75	63
Sodium (mg/L as Na)	240	228
Bicarbonate (mg/L as bicarbonate)	450	380
Carbonate (mg/L as carbonate)	100	100
Chloride (mg/L as chloride)	626	558
pH	9.00	9.00
Temperature (°C)	50	50

Figure 5.16 shows the CaCO_3 inhibition data for several deposit control polymers of varying compositions (Table 5.1) commonly used as the components of CWT formulations. It can be seen that P3 (P-AA) performs better than P8 (P-MA). Although, P8 contains two carboxylic acid groups compared to one carboxylic acid group present in P-AA, the poor performance shown by P-MA may be attributed to the lower MW of P-MA and/or the poor Ca ion compatibility of P-MA. Among the copolymers tested, P14 (AA:SA) exhibits better CaCO_3 inhibition than P12 (AA:MA), which may be attributed to the poor calcium ion compatibility of P12. In addition, P15 is a slightly better CaCO_3 inhibitor than P16 which may be attributed to polymer MW and polymer composition differences.

Figure 5.17 shows the performance of polymer/PBTC (3:1) blends as a function of dosage (10 to 40 ppm) at $180\times$ calcite saturation as CaCO_3 inhibitors. It is clear from Figure 5.17 that the performance of PBTC and polymer/PBTC blends increases with increasing inhibitor dosages. Among the various polymer/PBTC blends evaluated, the P15/PBTC blend is the most effective.

Figure 5.18 shows the CaCO_3 inhibition for several polymer/HEDP (3:1) blends at 30 ppm dosage and at $180\times$ calcite saturation and indicates the following order of effectiveness: P15/HEDP > P16/HEDP > P-AA/HEDP. As illustrated, all of the polymer/HEDP blends provide better CaCO_3 inhibition than HEDP alone. Consistent with the observations for the P15/PBTC blend, the P15/HEDP blend provides the best performance.

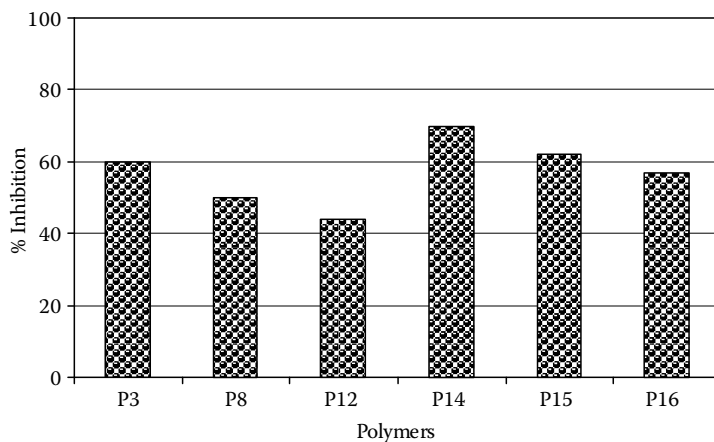


FIGURE 5.16 Calcium carbonate inhibition at $180\times$ calcite saturation by homo-, co-, and terpolymers.

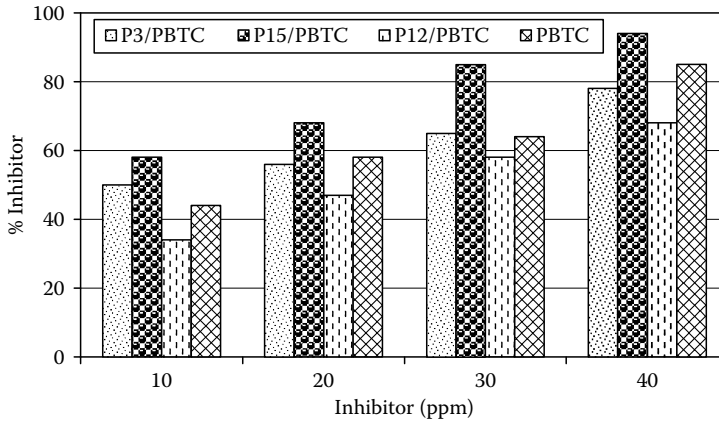


FIGURE 5.17 Calcium carbonate inhibition at 180 \times calcite saturation by varying dosages of polymer/PBTC (3:1) blends.

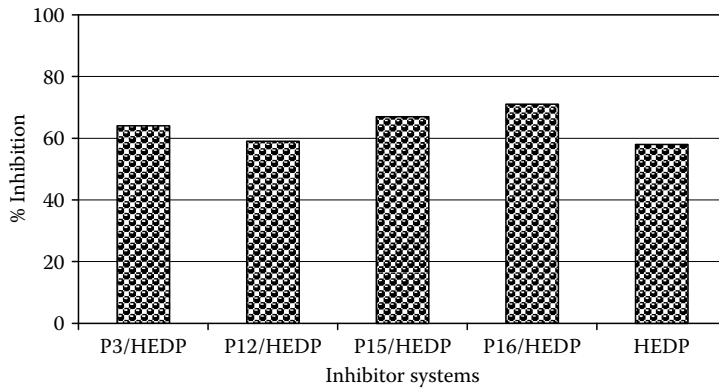


FIGURE 5.18 Calcium carbonate inhibition at 180 \times calcite saturation in the presence of 30 ppm of polymer/HEDP (3:1) blends.

5.3.2.2.6 Calcium Carbonate Crystal Morphology

Crystals formed during the CaCO_3 precipitation experiments in the absence (control) and presence of the inhibitor P15/PBTC (3:1) blend are shown in Figures 5.19 and 5.20, respectively. Figure 5.20 illustrates that CaCO_3 crystals are <10 microns and have regular shapes (major: calcite, minor: aragonite). Whereas the CaCO_3 crystal structures in Figure 5.20 (inhibited system) are fewer in number, most are >10 microns, spherically shaped, significantly distorted, and are all calcite.

5.4 POLYMER ARCHITECTURE INFLUENCE ON DISPERSING PARTICULATE MATTER

Suspended and colloidal matter causes turbidity in water. The type, size, and concentration of particles affect their behavior in the industrial water system. Examples of the types and sources of feed water particulates that impact industrial water systems include: (a) inorganic (i.e., silt, clay, asbestos, corrosion products, and calcium phosphates), (b) coagulant/flocculating agents by-products, and (c) organic (i.e., humic acid, tannic acid, and debris from dead organisms). The suspended particles typically encountered in industrial water applications generally carry a slight negative charge. Therefore, anionic polymers that increase negative surface charge and

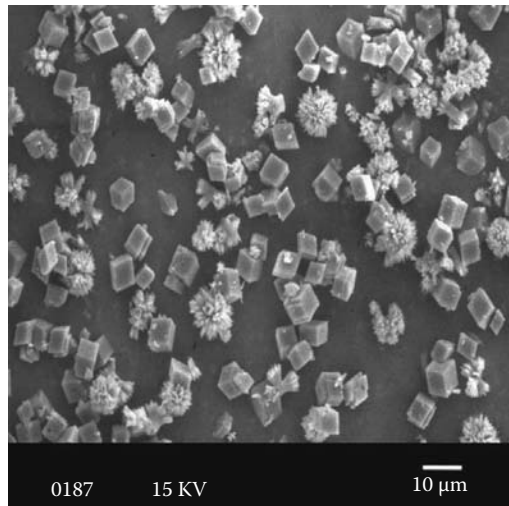


FIGURE 5.19 CaCO₃ (control).

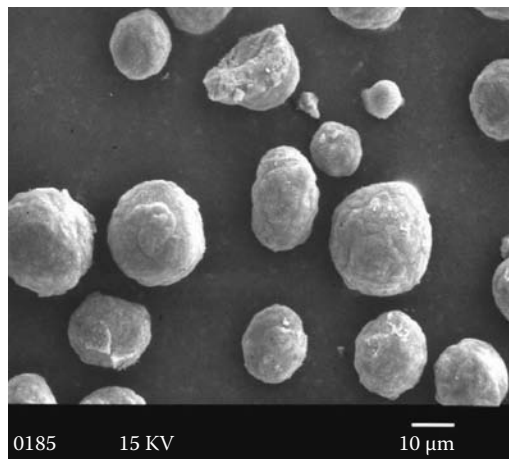


FIGURE 5.20 CaCO₃ in presence of P15/PBTC (3:1) blend.

keep particle in suspension are normally the most efficient dispersants. Cationic polymers can be used as dispersants, but this requires relatively high polymer concentrations in order to first neutralize the negative surface charges and then to transfer cationic charge to particles for efficient dispersion.

5.4.1 IRON OXIDE DISPERSION

Among many dissolved impurities present in natural waters, the iron-based compounds present one of the most serious problems in the efficient operation of industrial water systems. The sources of iron-ion impurities include boiler condensate, corrosion products (from heat-transfer equipment, pipelines, pumps, and so on), biological activity (the transformation of iron during bacterial processes), and water treatment residuals or by-products (e.g., excess iron-based flocculating agents). Regardless of the source, soluble iron can and does precipitate under certain conditions to form troublesome scales and deposits (e.g., Fe₂O₃, Fe₃O₄, Fe(OH)₃, FePO₄). For this reason, deposit control polymers are used to keep iron oxide particles dispersed and transported

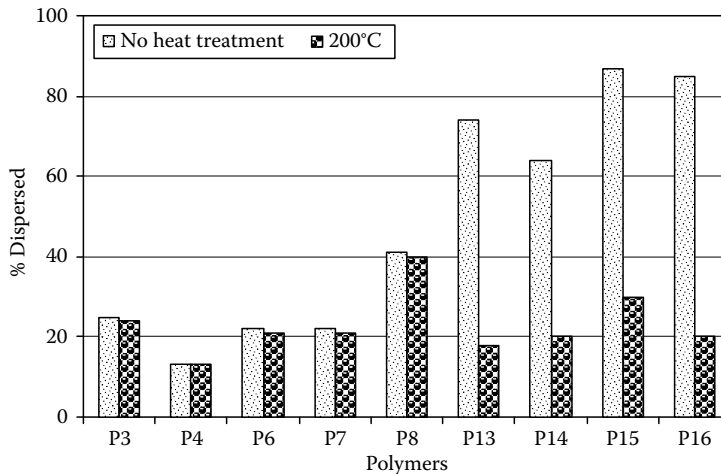


FIGURE 5.21 Iron oxide dispersion by thermally stressed polymers (100 mg/L Ca, 30 mg/L Mg, 314 mg/L Na, 200 mg/L SO_4 , 561 mg/L, 60 mg/L HCO_3 , 200 ppm iron oxide, 1 ppm polymer, 23°C, 3 h).

in boiler water systems. This dispersion activity results from the adsorption of polymer onto the surface of iron oxide particles, thereby changing particle charge characteristics and minimizing agglomeration.

Figure 5.21 presents performance data for several polymers under standard test conditions (200 ppm iron oxide, 1 ppm active polymer, 3 h, 7.8 pH, 100 mg/L Ca, 30 mg/L Mg, 314 mg/L Na, 200 mg/L sulfate, 571 mg/L Cl, 60 mg/L bicarbonate, 23°C). As shown, the homopolymers (P3, P4, P6, and P7) before thermal treatment provide relatively poor (<45%) iron oxide dispersion. Furthermore, the iron oxide dispersion values are very similar for both heat-treated and nonheat-treated homopolymers. This indicates that thermal stress has a negligible detrimental effect on the dispersing ability of these homopolymers. Although the absolute performance levels of these homopolymers are poor, it is interesting to note that the solvent polymerized P-AA (P3) performs better than the water polymerized P-AA (P4) and is comparable to P6 that is promoted in boiler water applications for iron stabilization.

Figure 5.21 also presents comparative dispersion data for several copolymers (P13 and P14) and terpolymers (P15 and P16). As illustrated, both the co- and ter-polymers in the absence of thermal stress exhibit excellent (>75%) iron oxide dispersion. However, when these co- and ter-polymers are exposed to thermal stress (200°C, 20 h), the iron oxide dispersion decreases drastically (by a factor 4). For example, % iron oxide dispersion values obtained for P15 and P16 before heat treatment were both >85% compared to 26% and 18%, respectively, after thermal stress. The data indicate that the performance of heat-treated terpolymers is similar to that obtained for homopolymers. As illustrated in Figure 5.21, the performance of copolymers is drastically affected by heat treatment.

5.4.2 IRON (III) STABILIZATION

Iron exists in two oxidation states: Fe^{2+} (ferrous) and Fe^{3+} (ferric). The chemistry of iron compounds is considerably more complex than carbonate- and sulfate-containing scales. When these two iron oxidation states (Fe^{2+} and Fe^{3+}) combine with the same anion, the result is usually the formation of compounds with significant differences in solubility. Iron deposits typically are in the form of FeO , FeS , Fe_2O_3 , iron silicate, and so on, and frequently include traces of manganese. Iron-based scale deposition on heat exchanger surfaces occurs as a result of corrosion processes throughout the systems. Thus, it is very important to implement a good corrosion control program. Iron fouling sometimes occurs in cooling waters as a result of high incoming iron levels from the feed water (e.g., some

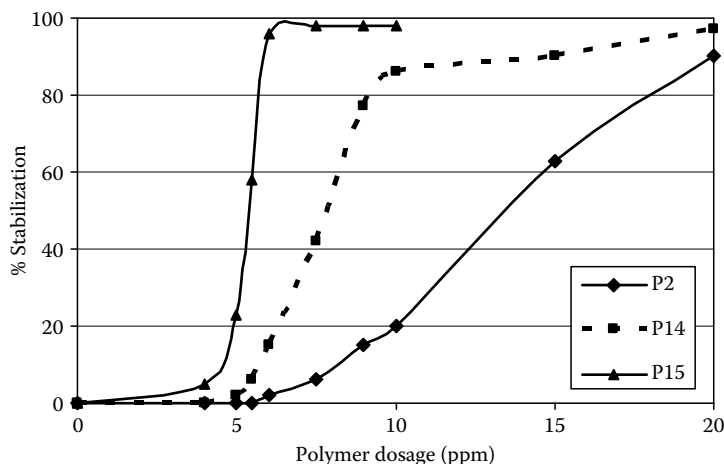


FIGURE 5.22 Stabilization of Fe^{3+} by homo-, co-, and terpolymers (104 mg/L Ca, 31 mg/L Mg, 361 mg/L Na, 202 mg/L SO_4 , 600 mg/L Cl, 146 mg/L HCO_3 , 3 ppm Fe^{3+} , pH 7.0, 23°C).

well waters or carryover from clarifiers where iron salts may be used as coagulants). Iron levels ≥ 2 ppm in the recirculating water typically can be controlled through the use of iron dispersants or deposit control agents. The use of an iron dispersant is strongly recommended to avoid major equipment failure problems. In cooling waters, Fe_2O_3 (hematite) and FeO are the most common deposits. Magnetite (Fe_3O_4) is rarely found in cooling systems; it needs high temperatures and/or anaerobic conditions. The formation of iron sulfide scale on equipment surfaces has been reported during oil and gas production from the formations containing large amounts of hydrogen sulfide. Sulfate-reducing bacteria (*Desulfovibrio*) are a major source of hydrogen sulfide in natural subsurface water. Iron carbonate or siderite is another type of iron scale, which occurs in oil and gas production.

Figure 5.22 compares the performance of homo-, co-, and terpolymers as Fe^{3+} ions stabilizing agents. The stabilization data indicate that performance increases with increasing deposit control polymer concentration. It is also evident that sulfonic acid groups (SA or both SA and SS), in combination with acrylic acid, exhibit a positive influence on the performance of co- and terpolymers. For example, % stabilization values obtained in the presence of 7.5 ppm P2, P14, and P15 are 6%, 42%, and 98%, respectively. Thus, the partly substitution of acrylic acid in P-AA with two sulfonated monomers (i.e., SA and SS) markedly improves the performance of terpolymer.

5.5 SUMMARY

Currently, a wide variety of chemicals (e.g., flocculants, coagulants, scale inhibitors, biocides, corrosion inhibitors, and so on) with different ionic charges and molecular architecture are available to water technologists to develop formulations capable of achieving desired performance objectives of the water treatment programs. The results reviewed in this chapter show that the performance of polymeric and nonpolymeric additives depends on both the water chemistry and inhibitor architecture. It has been shown that deposit control polymer performance as scale inhibitor, dispersant, and metal ions stabilization increases with increasing polymer concentration. The calcium ion compatibility exhibited by the polymers tested ranged from poor for the homopolymers to excellent for the sulfonic acid containing co- and ter-polymers. However, thermal stress profoundly impacts the calcium ion compatibility of all the copolymers. Test data suggest that the blends of PBTC with a high-performance terpolymer (i.e., AA:SA:SS, P15) exhibit synergistic influence on calcium carbonate precipitation inhibition. In addition, when selecting deposit control polymers as a component of boiler and cooling water treatment programs, it is important to understand the operating conditions of the system, water chemistry, the type and level of impurities, and the thermal stability of the polymers.

REFERENCES

1. Amjad, Z. The design and application of calcium phosphate inhibiting polymers in industrial water systems. *Phosphorus, Sulfur and Silicon and the Related Elements* 144, 144–146 (1999).
2. Klepetsanis, P. G., Kladi, A., Koutsoukos, P. G., and Amjad, Z. The interaction of water soluble polymers with solid substrates. Implications on the kinetics of crystal growth. *Progress in Colloid and Polymer Science* 115, 1006–1011 (2000).
3. Gill, J. S. and Yorke, M. A. Calcium carbonate control in highly supersaturated aqueous environment. CORROSION/94, Paper No. 195, NACE International, Houston, TX (1994).
4. Amjad, Z., Zuhl, R. W., and Zibrida, J. F. The effect of biocides on deposit control polymer performance. *Proceedings of the 12th Annual Convention*, Association of Water Technologies, Honolulu, HI (2000).
5. Amjad, Z. Effect of antiscalants on the precipitation of calcium carbonate in aqueous solutions. *Tenside Surfactants Detergents* 31, 12–16 (1994).
6. Wilson, D. Influence of molecular weight on selection and application of polymeric scale inhibitors. CORROSION/98, Paper No. 48, NACE International, Houston, TX (1998).
7. Amjad, Z., Zibrida, J. F., and Zuhl, R. W. Performance of polymers in industrial water systems: The influence of process variables. *Material Performance* 36, 32 (1997).
8. Boffardi, B. P. and Schweitzer, G. W. Advances in the chemistry of alkaline cooling water treatment. CORROSION/85, Paper No. 132, NACE International, Houston, TX (1985).
9. Kessler, S. M. Advanced scale control technology for cooling water systems CORROSION/2002, Paper No. 02402, NACE International, Houston, TX (2002).
10. Amjad, Z. Precipitation of calcium phosphate in the presence of anionic polymers: The influence of cationic polymeric materials. *Phosphorus Research Bulletin* 9, 31–40 (1999).
11. Amjad, Z. and Zuhl, R. W. Factors influencing the precipitation of calcium-inhibitor salts in industrial water systems. *2003 Annual Convention*, Association of Water Technologies, Phoenix, AZ (2003).
12. Amjad, Z. Interactions of hardness ions with polymeric scale inhibitors in aqueous systems. *Tenside Surfactants Detergents* 42, 71–77 (2005).
13. Amjad, Z. Performance of polymers as precipitation inhibitors for calcium phosphonate. *Tenside Surfactants Detergents* 34, 102 (1997).
14. Ashcraft, R. H. Scale inhibition under harsh conditions by 2-phosphonobutane 1,2,4-tricarboxylic acid. CORROSION/85, Paper No. 132, NACE International, Houston, TX (1985).
15. Amjad, Z. Influence of cationic polymers on the performance of anionic polymers as precipitation inhibitors for calcium phosphonates. *Phosphorus Research Bulletin* 13, 59–65 (2002).
16. Geiger, G. and Sui, C. Improved calcium phosphate control for stressed systems. *CTI Journal* 29, 42–48 (2008).
17. Smyk, E. B., Hoots, J. E., Fivizzani, K. P., and Fulks, K. E. The design and application of polymers in cooling water programs. Paper No. 14, CORROSION/88, NACE International, Houston, TX (1988).
18. Dubin, P., Rigsbee, D. R., Gang, L. M., and Fallon, M. A. Equilibrium binding of mixed micelles to oppositely charged polyelectrolytes. *Macromolecules* 21, 2555–2559 (1988).
19. Dubin, P., Ross, T. D., Sharma, I., and Yegerlehner, B. E. Coacervation of polyelectrolyte-protein complexes. Chapter No. 8, *ACS Special Symposium Series* No. 342, W. L. Hinze and D. W. Armstrong, Eds. American Chemical Society, Washington, DC (1987).
20. Masler, W. F. and Amjad, Z. Advances in the control of calcium phosphonate with a novel polymeric inhibitor. CORROSION/88, Paper No. 11, NACE International, Houston, TX (1988).
21. Amjad, Z. and Zuhl, R. W. The use of polymers to improve control of calcium phosphonate and calcium carbonate in high stressed cooling water systems, 2004 Annual Convention, Association of Water Technologies, Nashville, TN (2004).
22. Amjad, Z. Effect of precipitation inhibitors on calcium phosphate scale formation. *Canadian Journal of Chemistry* 67, 850–856 (1989).
23. Masler, W. F. Characterization and thermal stability of polymers for boiler water treatment. *43rd Annual Meeting, International Water Conference*, Pittsburgh, PA, (1982).
24. Oner, M., Dogan, O., and Oner, G. The influence of polyelectrolytes architecture on calcium sulfate dihydrate growth retardation. *Journal of Crystal Growth* 186, 427–437 (1998).
25. Amjad, Z. Inhibition of calcium fluoride crystal growth by polyelectrolytes *Langmuir* 7, 2405–2408 (1991).
26. Amjad, Z. Inhibition of barium sulfate precipitation: Effect of additives, solution pH, and supersaturation. *Water Treatment* 9, 47–56 (1994).

27. Sherwood, N. Novel calcium carbonate for maximum acid-free cooling water reuse. CORROSION/94, Paper No. 453, NACE International, Houston, TX (1994).
28. Amjad, Z. Precipitation of calcium carbonate in aqueous systems. *Tenside Surfactants Detergents* 36, 162–169 (1999).
29. Perez, L. A. and Freese, D. T. Scale prevention at high LSI, high cycles, and high pH without the need for acid feed. CORROSION/97, Paper No. 174, NACE International, Houston, TX (1997).

6 New Models for Calcium Phosphate Scale Formation and Dissolution

*Lijun Wang, Patrick P. Emmerling,
Zachary J. Henneman, and George H. Nancollas*

CONTENTS

6.1	Introduction	105
6.2	Theory on Crystallization/Dissolution	105
6.3	Experimental Procedure	107
6.4	Results and Discussion	107
6.4.1	New Dissolution Model: Critical Pit Size.....	107
6.4.2	Inhibitors: The Bisphosphonates	110
6.5	Summary	111
	Acknowledgment	111
	References.....	111

6.1 INTRODUCTION

Scale inhibitors are usually evaluated by performing empirical precipitation tests and by assessing the resulting change in the mass of scale formed. Little attention is usually paid to the molecular events that result in the observed inhibition with a reduction in the crystal nucleation, growth, or dissolution of these sparingly soluble minerals. Recently, there has been considerable activity in studies aimed at elucidating the mechanisms of these reactions. Using a thermodynamic approach together with atomic force microscopy (AFM), new light has been shed on the ways in which ions and water molecules can assemble to form complex crystals. Scale inhibitors may influence the growth and dissolution of different crystal faces, resulting in marked changes in morphology that can influence crystal adherence to scaling surfaces. In the dispersal of scale crystals by dissolution, a newly developed model reveals that when crystals are sufficiently small, the surfaces may be unable to support etch pits of sufficient size, thus inhibiting the dissolution process. Crystals then resist dissolution even when the aqueous phases are undersaturated. These new models and their applicability to scale formation are discussed in this chapter.

6.2 THEORY ON CRYSTALLIZATION/DISSOLUTION

It is well known that both the precipitation and the dissolution of crystals are highly dependent on the thermodynamic driving force, usually expressed in terms of supersaturation, S :

$$S = C / C_s \tag{6.1}$$

where, C and C_s are the solute concentrations and the values in saturated solutions, respectively. A typical solubility isotherm for salt AB can be divided into three distinct regions: $S > 1$, $S = 1$, and $S < 1$ corresponding to supersaturation, equilibrium, and undersaturation, respectively. The supersaturated region can be further divided into metastable ($1 < S < S_C$) and labile ($S > S_C$) parts, where S_C is the critical supersaturation. In the former, solutions may not precipitate immediately unless seeded, whereas in the labile region, spontaneous precipitation may occur. The existence of a metastable region has been attributed to the need to provide the interfacial energy of the nucleating solid phases [1]. In the nucleation stage, critical-sized nuclei are formed resulting from overcoming the nucleation barrier during the fluctuation and growth of embryos (embryos are metastable clusters of structural units with a broad distribution in size). The molecular process of nucleation can be regarded as follows: the constituent atoms or molecules in the ambient phase may, on collision, join into assemblies of two or more particles, forming dimers, trimers, tetramers, and so on. Before the embryos can reach a critical radius, r_c , they are unstable even when a positive thermodynamic driving force, $\Delta\mu/k_B T$, is applied ($\Delta\mu = \mu^f - \mu^s$, where μ^f and μ^s are the chemical potentials of the solute molecules in the fluid phase and in the solid phase, respectively; k_B is the Boltzmann constant; and T is the temperature). To reach r_c , an energy barrier, the so-called nucleation barrier, ΔG^* , must be overcome, following which the second stage of the phase transition begins: growth [2].

The above process can be described in terms of the Kelvin–Gibbs equation, expressing the dependence of the energy of formation of nucleated droplet radius, r , and surface tension, γ_{SL} :

$$\Delta G_S = 4\pi r^2 \gamma_{SL} \quad (6.2)$$

where, ΔG_S , the excess free energy required for solid/liquid interface formation, is balanced by a favorable ΔG_V , describing the spontaneous tendency of a supersaturated solution to undergo deposition. This process reduces the Gibbs free energy of the system, as shown in the following equation:

$$\Delta G_V = -\frac{4\pi r^3}{3\Omega} kT \ln S \quad (6.3)$$

where

k is the Boltzmann constant

Ω is the volume occupied by each growth unit

The overall free energy change for nucleation, ΔG_N , is the sum of ΔG_S and ΔG_V , which illustrates the free energy balance between the formation of the solid phase and the solution depletion. ΔG_N passes through a maximum at a critical size, r^* , the value of which is determined by differentiating ΔG_N with respect to r , resulting in

$$r^* = \frac{2\gamma_{SL}\Omega}{kT \ln S} \quad (6.4)$$

It follows that spontaneous crystallization does not occur until critical conditions are reached, or the driving force (supersaturation) is sufficiently high ($S > S_C$). Rather, a metastable equilibrium condition persists during an “induction period,” τ , prior to crystal formation. If the simplifying assumption is made that τ is concerned with classical nucleation, we can use the following equation:

$$\ln \tau \propto \left[C_1 + C_2 \frac{\gamma_{SL}^3}{k^3 T^3 (\ln S)^2} \right] \quad (6.5)$$

in which C_1 and C_2 are independent constants.

When $S < 1$, the solution is undersaturated and, in the traditional theories of dissolution, spontaneous reaction should continue until equilibrium is reached or all crystallites are dissolved. It also requires that solid solute must be dissolving in this zone, and no solid phase can be stabilized in the undersaturated region. These theories assume that dissolution is a process of crystallite size reduction so that the solid/solution interfacial areas and the corresponding surface energy term, ΔG_S , must decrease as the reaction proceeds, as well as the value of ΔG_V . Thus, there is no energy barrier for dissolution similar to the free energy change, ΔG_N , for nucleation. These dissolution theories also imply that dislocations on the crystal surfaces and the edges of crystals provide natural dissolution sites without the necessity to create new active sites to initiate the reaction. Consequently, neither critical conditions nor metastable zones are part of the traditional interpretation of dissolution.

6.3 EXPERIMENTAL PROCEDURE

Constant composition (CC) crystal growth and dissolution experiments were conducted in magnetically stirred double-walled Pyrex vessels. The super/undersaturated reaction solutions (200 mL) were prepared by mixing calcium chloride and potassium dihydrogen phosphate with sodium chloride to maintain the ionic strength, I , at 0.15 mol L^{-1} . The pH was adjusted to the desired values, 7.40 for growth and 4.50 for dissolution. Nitrogen, saturated with water vapor at 37°C , was purged through the reaction solutions to exclude carbon dioxide. The reactions were initiated by the introduction of apatite seed crystallites (10.0 mg). Titrant addition was potentiometrically controlled by glass and Ag/AgCl reference electrodes. During growth/dissolution, the electrode potential was constantly compared with a preset value and the difference, or error signal, activated motor-driven titrant burets. Thus, a constant thermodynamic growth/dissolution driving force was maintained.

In situ AFM images of brushite surfaces were collected in contact mode by using a Digital Instruments Nanoscope III microscope. All images were acquired in height and deflection modes by using the lowest tip force possible to reduce tip–surface interactions. The crystals were anchored inside the fluid cell and undersaturated solution was passed through while the images were taken.

6.4 RESULTS AND DISCUSSION

6.4.1 NEW DISSOLUTION MODEL: CRITICAL PIT SIZE

The development of AFM has enabled the real-time observation and measurement of both growth and dissolution processes for crystals in solution [3], which has enabled crystal growth and dissolution theories to be developed in terms of molecular events at the crystal surfaces. The demonstrated importance of pit formation during dissolution has markedly changed our understanding of this process [4]. Microscopic pit formation and the spreading of stepwaves have been studied experimentally at a molecular level. For example, the in situ AFM studies of brushite (dicalcium phosphate dihydrate, $\text{CaHPO}_4 \cdot 2\text{H}_2\text{O}$, DCPD) dissolution show that the reaction is dominated by the creation and development of pits on the crystal surfaces. The immediate appearance of numerous triangular pits on brushite (010) faces was observed when seed crystals were exposed to an undersaturated solution. These pits provided dissolution sites, and the entire reaction proceeded via nucleation and growth of triangular pits accompanying step flow. Neither significant dissolution from edges nor spiral dissolution was observed directly [5]. Figure 6.1 shows the relationship between the expanding velocities of (201) and (001) steps and their sizes on dissolving (010) brushite faces, as measured by AFM [6]. The lines are plotted according to our new dissolution theory. There is a direct relationship between the dissolution rate and the length of the dissolution step, which is shown at the micron level.

Recent CC dissolution studies of synthetic hydroxyapatite (HAP, $\text{Ca}_5(\text{PO}_4)_3\text{OH}$), a phase often involved in scale formation (Figure 6.2), have confirmed this interesting and unusual

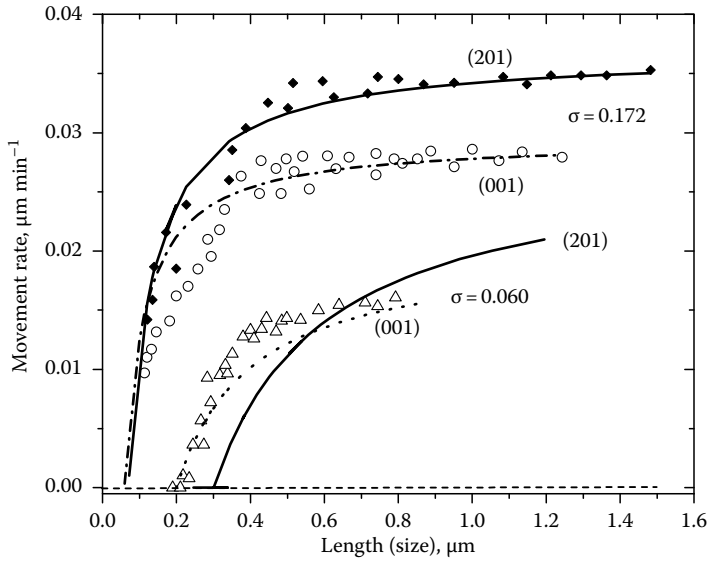


FIGURE 6.1 Step displacement rates as a function of size for (201) and (001) steps at relative undersaturations of $\sigma = 0.060$ and 0.172 , respectively. The lines are plotted according to our new dissolution theory. There is a direct relationship between the dissolution rate and the length of dissolution step, which is observed at the micron level.

behavior in that dissolution rates decreased, eventually resulting in effective suppression, when crystal sizes were reduced to a critical length scale—always at the nanoscale [7]. Figure 6.2a showed CC plots of titrant volume against time at different undersaturations. The red lines indicate the titrant volumes for full dissolution of the added seeds. Only at very high undersaturation ($S = 0.02$) does the dissolution go to completion. The dissolution rates, represented by the slopes of the curves, decrease with time and eventually only a fraction of the added seeds undergo dissolution before the rates approach zero. Near equilibrium ($S = 0.828$), no dissolution can be detected in the undersaturated solutions. For the smaller hydroxyapatite seeds (length, 200–300 nm, and width, 50–80 nm), no CC dissolution can be detected at an even higher undersaturation of $S \geq 0.720$. Figure 6.2b through d showed that SEMs of seed crystals (Figure 6.2b) and crystallites remaining at the end of dissolution experiments at $S = 0.580$ (Figure 6.2c) and $S = 0.315$ (Figure 6.2d).

Clearly, this dissolution termination is a kinetic phenomenon that can be explained in terms of a model that incorporates particle size considerations. Analogous to the formation of two-dimensional nuclei/hillocks for crystal growth, in dissolution, the rate of step movement from a pit of radius r can be obtained from treatments similar to the model of Burton, Cabrera, and Frank for the corresponding crystal growth processes [8]:

$$R(r) = R_{\infty} \left[1 - \frac{e^{(1-S)r^*/r-1}}{e^{1-S} - 1} \right] \approx R_{\infty} \left(1 - \frac{r^*}{r} \right) \quad (6.6)$$

where r^* , the critical radius for the formation of a two-dimensional pit/dissolution step, is given by

$$r^* = \frac{\gamma_{SL}\Omega}{|\Delta G|} \quad \text{and} \quad \Delta G = kT \ln S \quad (6.7)$$

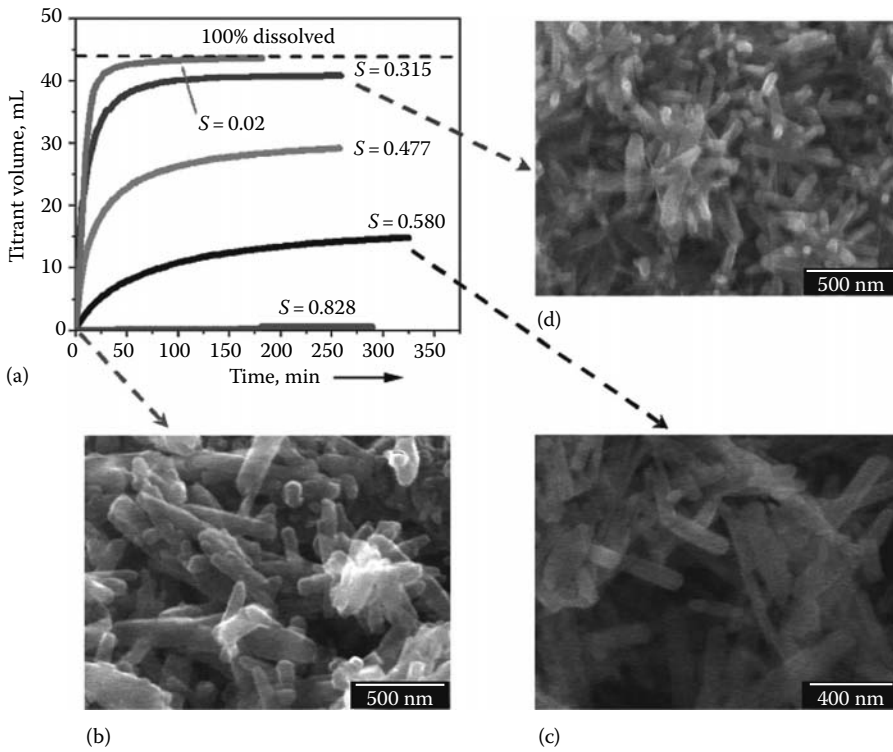


FIGURE 6.2 In vitro CC dissolution of synthetic hydroxyapatite. (a) CC plots of titrant volume against time at different undersaturations. Only at very high undersaturation ($S = 0.02$) does the dissolution proceed to completion, indicated by the dotted line. Dissolution rates, represented by the slopes of the curves, decrease with time, and eventually only a fraction of the added seeds undergo dissolution before the rates approach zero. Near equilibrium ($S = 0.828$), no dissolution can be detected in the undersaturated solutions. For the smaller hydroxyapatite seeds (length, 200–300 nm and width, 50–80 nm), no CC dissolution can be detected at an even higher undersaturation of $S \geq 0.720$. (b) SEM micrographs of seed crystals. (c) Crystallites remaining at the end of dissolution experiments at $S = 0.580$ and (d) $S = 0.315$.

where

γ_{SL} is the interfacial tension

k is the Boltzmann constant

Ω is the volume per dissolution unit

ΔG is the Gibbs free energy change for dissolution

In Equation 6.6, R_{∞} is the velocity of dissolution steps as $r \rightarrow \infty$. It has been shown that only pits that are larger than r^* provide the active dissolution sites that contribute to dissolution. When r is closer to r^* , there is no fast movement of its stepwave and the dissolution rate approaches zero (Equation 6.6). The critical size of pits, r^* , is a function of undersaturation (Equation 6.7). When the dimensions of the crystallites (l) are of the same order as r^* during the dissolution (e.g., l becomes less than $20 r^*$), the formation of active pits is more difficult since their sizes are restricted to those of the small crystallites. As shown in Equation 6.6, $R(r)$ is strongly dependent on pit size. Correspondingly, the macroscopic CC dissolution rate decreases with the extent of dissolution. Residues of these nanoparticles, collected at the end of dissolution reactions, are stabilized due to the lack of surface defects/pits, and are thus able to resist dissolution [9]. In addition, since traditional solution theories are based on experiments involving soluble salts, these phenomena are not observed since the

critical conditions would be outside the range of the experimental techniques employed. If other sparingly soluble scale crystals also show this dissolution termination when the sizes are reduced to a critical value, scale dissolution and dispersion process will be strongly affected.

6.4.2 INHIBITORS: THE BISPHOSPHONATES

Originally derived from pyrophosphate, bisphosphonates (BPs) have been used to inhibit the precipitation of scale in washing powders in water and in oil brines. They also bind strongly to calcium phosphates (Ca-P) *in vivo*, influencing both the formation and the dissolution of Ca-P crystals in ectopic calcification. Unfortunately, the low resistance of pyrophosphate to hydrolytic and enzymatic breakdown proved problematic, and this was corrected by the substitution of the P-O-P backbone by P-C-P, allowing additional functional groups to be added to increase inhibitory effectiveness.

One of the most widely used BPs for industrial scale prevention has been 1-hydroxyethylidene diphosphonic acid (HEDP) and its tetrasodium salt (Figure 6.3). The introduction of the hydroxyl group greatly increases the binding affinity of the molecule, allowing for multidentate chelation with cationic species in solution, such as Ca^{2+} , Mg^{2+} , and Ba^{2+} , which are typically found in deposited boiler scale. Strikingly, concentrations as low as $2.5 \times 10^{-6} \text{ mol L}^{-1}$ have been found to cause upward of 50% inhibition of scale formation [10].

The popularity of BPs for treating osteoporosis and other skeletal disorders has eclipsed their original purpose as antiscaling additives [11]. The substitution of the methyl group for a *N*-containing

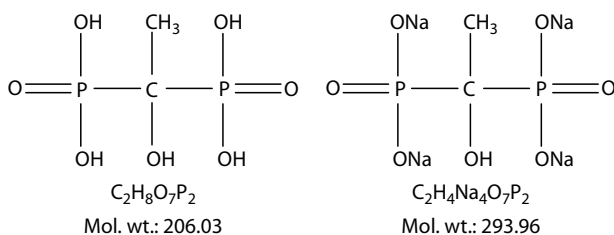


FIGURE 6.3 Chemical structures of HEDP and Na_4 -HEDP.

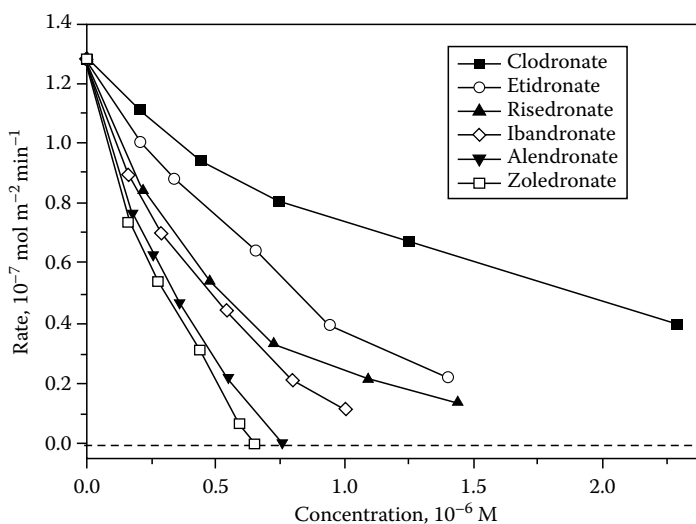


FIGURE 6.4 HAP growth rate plotted against inhibition concentration for five different bisphosphonates at pH 7.4, demonstrating the effectiveness of BPs in inhibiting HAP growth ($S = 8.40$; control growth rate = $1.28 \times 10^{-7} \text{ mol m}^{-2} \text{ min}^{-1}$).

side chain has led to the development of alendronate (alkyl primary amine), ibandronate (alkyl tertiary amine), risedronate (pyridine), and zoledronate (imidazole), which have proven to be 100–10,000 times more effective than HEDP *in vivo* for inhibiting the progression of osteoporosis. This additional potency has been ascribed to the *N*-containing side chains, which have been shown to adversely influence the cellular processes necessary for osteoclast proliferation. It will be particularly interesting to investigate the effectiveness of this broader family of bisphosphonates as scale inhibitors; Figure 6.4 demonstrates the effectiveness of BPs in inhibiting hydroxyapatite growth at pH 7.4, $S = 8.40$; the control growth rate = $1.28 \times 10^{-7} \text{ mol m}^{-2} \text{ min}^{-1}$, which showed them to be remarkably effective in inhibiting hydroxyapatite growth from supersaturated solution [12]. A molecular picture of their binding to the mineral surfaces will enable tailor-made BP molecules to be developed for specific scaling problems.

6.5 SUMMARY

The growth and dissolution kinetics of hydroxyapatite, as a model for scale minerals, was investigated using nanomolar-sensitive CC and *in situ* AFM under simulated scale formation conditions. The dissolution rate decreased as the reaction proceeded in accordance with our recently proposed crystal dissolution model, resulting in nanosized crystallites that were resistant to further dissolution. This study showed that CC dissolution of hydroxyapatite in acidic medium follows this new model that can be used to mimic scale dissolution. In addition, we discussed the effectiveness of bisphosphonates as scale formation inhibitors, and their effectiveness in inhibiting hydroxyapatite growth from supersaturated solution.

ACKNOWLEDGMENT

This work was supported by the National Institutes of Health (NIDCR DE03223).

REFERENCES

1. Hartman, P. *Crystal Growth: An Introduction*. North-Holland: Amsterdam (1975).
2. Jia, Y. and Liu, X. Y. From surface self-assembly to crystallization: Prediction of protein crystallization conditions. *J Phys Chem B* 110, 6949–6955 (2006).
3. Land, T. A., Malkin, A. J., Kuznetsov, Y. G., McPherson, A., and De Yoreo, J. J. Mechanisms of protein crystal growth: An atomic force microscopy study of canavalin crystallization. *Phys Rev Lett* 75, 2774–2777 (1995).
4. Tang, R., Nancollas, G. H., and Orme, C. A. Mechanism of dissolution of sparingly soluble electrolytes. *J Am Chem Soc* 123, 5437–5443 (2001).
5. Tang, R., Orme, C. A., and Nancollas, G. H. A new understanding of demineralization: The dynamics of brushite dissolution. *J Phys Chem B* 107, 10653–10657 (2003).
6. Tang, R., Orme, C. A., and Nancollas, G. H. Dissolution of crystallites: Surface energetic control and size effects. *Chem Phys Chem* 5, 688–696 (2004).
7. Tang, R., Wang, L. J., Orme, C. A., Bonstein, T., Bush, P. J., and Nancollas, G. H. Dissolution at the nanoscale: Self-preservation of biominerals. *Angew Chem Int Ed* 43, 2697–2701 (2004).
8. Burton, W. K., Cabrera, N., and Frank, F. C. The growth of crystals and the equilibrium structure of their surfaces. *R Soc Lond Philos Trans A* 243, 299–358 (1951).
9. Wang, L. J., Tang, R., Bonstein, T., Orme, C. A., Bush, P. J., and Nancollas, G. H. A new model for nano-scale enamel dissolution. *J Phys Chem B* 109, 999–1005 (2005).
10. Van Rosmalen, G. M., Van der Leeden, M. C., and Gouman, J. The influence of inhibitors on the growth of barium sulfate crystals in suspension: Scale prevention (II). *Kristall und Technik* 15, 1269–1277 (1980).
11. Fleisch, H. *Bisphosphonates in Bone Disease*, 4th edn. Academic Press, San Diego, CA (2000).
12. Nancollas, G. H., Tang, R., Phipps, R. J., Henneman, Z., Gulde, S., Wu, W., Mangood, A., Russell, R. G. G., Ebetino, F. H. Novel insights into actions of bisphosphonates on bone: Differences in interactions with hydroxyapatite. *Bone* 38, 617–627 (2006).

7 Design and Applications of Cooling Water Treatment Programs

Libardo A. Perez, Gary E. Geiger, and Charles R. Ascolese

CONTENTS

7.1	Introduction	113
7.2	Designing a Chemical Treatment Program	114
7.2.1	Deposit Control.....	114
7.2.2	Corrosion Control	116
7.2.3	Biological Control.....	118
7.2.3.1	The Need for Biological Control.....	118
7.2.3.2	What Are the Organisms That Must Be Controlled?	118
7.2.3.3	Areas of the Cooling System That Require Special Attention	119
7.2.3.4	Essential Tools for Biocontrol.....	121
7.2.3.5	Biomonitoring	123
7.3	Applying a Designed Treatment Program	124
7.3.1	Control of Chemical Feed.....	124
7.3.2	Monitoring System	124
7.3.3	Data Management.....	126
7.4	Summary	126
	References.....	126

7.1 INTRODUCTION

Cooling water systems play an important role in keeping industrial plants running continuously and at full capacity. Most cooling systems consume large amount of waters, which make this system an excellent target for water conservation. As a consequence, the use of poor-quality water, the need for increasing cycles of concentrations, and the need to implement water reuse as a culture to conserve water have called for improvements on water treatment programs that are able to perform under these more stressful conditions.

It has been pointed out that for the proper operation of a cooling system, the focus should be on system performance and cost optimization [1] that allows (a) to control problems related to corrosion, scale, fouling, and microbiological growth; (b) to maintain proper dosage of chemicals and keep all operational parameters in the recommended range (this can be achieved by implementing control equipments and software that are able to monitor and manage received data to identify, automatically make corrections, and report any problem affecting system performance); (c) to operate the system in a cost-effective manner that takes into consideration both total water system capital and operating costs, as well as the impact on plant productivity; and (d) to operate the system in a healthy, safe, and environmentally acceptable way.

The chemical program applied to a system must be online with the four requirements described above. It should be recognized that there is no universal treatment program capable of treating all the varieties of makeup water sources. Formulations for a given treatment program must take into account the actual system conditions as well as the potential problems/contaminations that the system may undergo under normal operational conditions.

7.2 DESIGNING A CHEMICAL TREATMENT PROGRAM

In order to design an effective chemical treatment program, the system's operating parameters, the type of metallurgy and other surfaces to be in contact with the cooling water, as well as the water quality being used must be taken into account. The use of different sources of water also needs to be considered, especially in today's world in which the types of water that were considered as unusable in the past are becoming part of the makeup water for the cooling system as a result of water scarcity, water cost, and the trend to save water [2]. The design treatment also needs to be environmentally friendly to reduce environmental impact. In addition, the program has to be able to control deposition, corrosion, and biological growths, which are the three main problems affecting a cooling system's performance. It is important that all chemical components used in the chemical treatment program are compatible among themselves to prevent negative interactions, which could result in poor performance.

7.2.1 DEPOSIT CONTROL

The designed chemical treatment program must be capable of controlling deposition under all potential scaling and fouling tendencies under the system operating conditions. A poor control of deposition could result in lower plant production due to problems associated with reduced heat transfer, under-deposit corrosion, and higher cleaning frequency. The formulation of the chemical components of the treatment program to be used need to be developed considering the potential scaling tendencies of all potential scale former salts; calculation of these tendencies can be achieved by using software that are capable of making these predictions combined with expertise on controlling the precipitation of all potential scale formers. The type of scale will depend on the chemical composition of the makeup water. For this reason, when designing a treatment program it is important to conduct a water analysis of all potential sources of waters to be used alone or in combination with each other. The most common cooling system scale formers are calcium carbonate, calcium phosphate, zinc phosphate, silica, silicates, and iron and manganese oxides.

Deposition due to scaling is normally eliminated/minimized by the use of scale inhibitors, which can be simple molecules, for example, phosphonates, to more complex polymeric structures. These inhibitors are designed by taking into account parameters such as the ability of the inhibitors to interact with the surface-active sites of the potential scale former, the geometry and orientation of the inhibitor when approaching the surface, and the inhibitor molecular size [3].

Parameters such as pH, temperature, chlorine levels, calcium concentration, suspended solids levels, and aluminum and iron levels can impact the performance of scale inhibitors. When choosing treatment components, the effect of these parameters on the scale inhibitors need to be considered. Molecules, for example, the phosphonates, are limited in their performance due to relatively poor stability to chlorine levels normally used in cooling systems in addition to other problems associated with their tolerance to calcium and iron levels [4]. These limitations greatly reduce the phosphonates' performance and prevent their use when considering increasing cycles of concentrations, or in systems where poor water quality may require relatively high levels of continuous chlorination for microbiological control, or in systems in which the characteristic of the makeup source is constantly changing the concentration of cations (calcium, iron, aluminum, etc.) and/or suspended solids.

The limitations presented by phosphonates-based treatments to prevent calcium carbonate deposition can be overcome by using an inhibitor that has proven to be stable in the presence of chlorine,

and which is able to tolerate high levels of calcium and iron. Recently, a new halogen-stable inhibitor, alkyl epoxy carboxylate (AEC) was developed; this new inhibitor is capable of handling higher cycles of concentrations under very stressful conditions [5,6]. This inhibitor not only offers the stability advantage but also is more environmentally friendly since it does not contain phosphorus in its chemical structure as the phosphonates do. In addition, unlike the phosphonates, AEC is very calcium tolerant. Typical phosphonates such as the hydroxyethylidenediphosphonic acid (HEDP) and other aminophosphonates have relatively low calcium tolerance, and degrade to chlorinated organic compounds in the presence of chlorine, which makes them less effective. In addition, the use of phosphonates increases environmental concerns due to their eutrophication potential. The AEC's higher performance, even under the most stressful conditions, and its chlorine tolerance has made it the industrial standard to prevent calcium carbonate scale formation in water cooling systems.

The presence of phosphate in the makeup water is becoming a more common phenomenon as the practice of using reuse water and gray water as makeup in a cooling system increases. This together with the necessity to increase concentration cycles in order to reduce water consumption and discharge have resulted in very stressful operating conditions, which has made traditional metal-phosphate scale inhibitors not cost effective. A new terpolymer able to control metal-phosphate scale inhibition under stressful conditions of cooling system was developed. This new stress-tolerant polymer (hereafter referred to as STP) is able to control calcium phosphate under severe conditions even in the presence of other metals ions such as iron and aluminum at the normal levels present in a cooling system. STP has shown to be twice as effective as traditional commercially available polymeric calcium phosphate inhibitors, which makes it cost effective. This cost-effectiveness together with its chlorine stability make it possible to run cooling systems at higher cycles even in water with high calcium and phosphate concentrations, which results in saving on operation costs [7].

The relative calcium phosphate inhibition performance of STP to commonly used commercial copolymers and terpolymers is illustrated in Figures 7.1 and 7.2, respectively. Figure 7.1 compares the relative abilities of the polymers to prevent calcium phosphate precipitation in the cooling water in the absence of contaminants. Figure 7.2 shows the performance when low levels of soluble iron (3 ppm) are present. Soluble iron is known to "poison" polymeric dispersants causing a reduction in precipitation inhibition and particulate dispersion, both of which can lead to increased system fouling. As can be seen from the graphs, the use of an STP provides better overall calcium phosphate precipitation inhibition in the presence or absence of soluble iron. This performance advantage can reduce both cooling system fouling and the cost associated with the chemical treatment program (i.e., lower polymer usage).

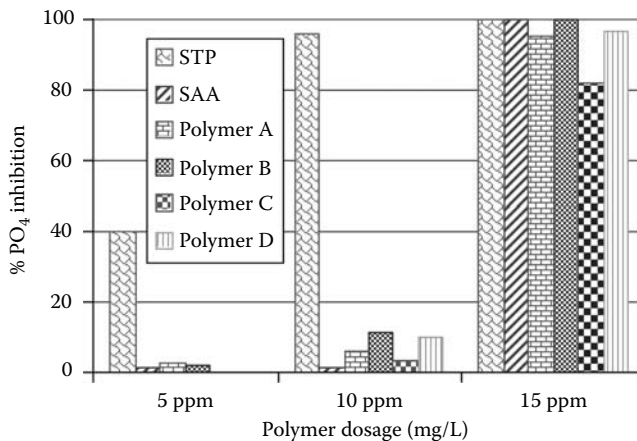


FIGURE 7.1 Calcium phosphate precipitation inhibition study at 400 ppm calcium hardness as CaCO_3 , pH 8.2, 10 ppm PO_4^{3-} , 160°F (70°C).

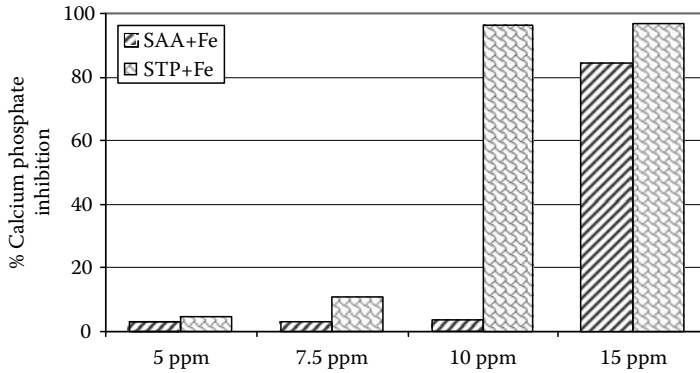


FIGURE 7.2 Calcium phosphate inhibition study in the presence of low levels of soluble iron at 400 ppm calcium hardness as CaCO_3 , pH 8.2, 10 ppm PO_4^{3-} , 3 ppm Fe^{3+} , 160°F (70°C).

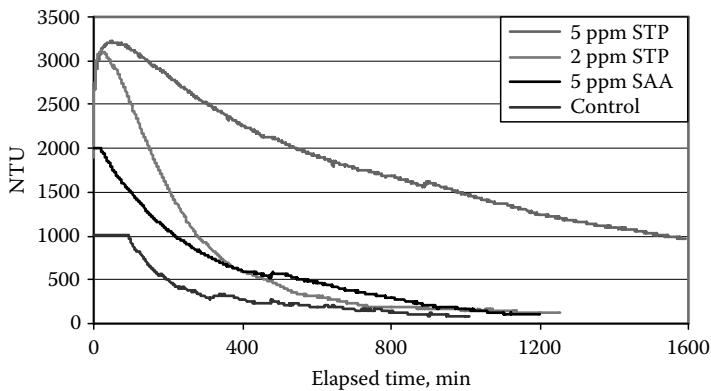


FIGURE 7.3 Dispersion of iron oxide at 500 ppm calcium hardness as CaCO_3 , 200 ppm magnesium hardness as CaCO_3 , pH 7.5, 750 ppm Fe_2O_3 , 77°F (25°C).

Fouling of cooling system surfaces is the result of the settling of suspended solids. Fouling can be prevented by using dispersants and surfactants, which adsorb on the solid surface modifying surface charges and causing repulsion among particles. Multifunctional polymers, such as STP, have proved to be excellent dispersant agents in addition to being excellent calcium phosphate inhibitors. Dispersion of suspended solids such as silt, mud, and corrosion products should be considered when designing a cooling water treatment program to ensure fouling is prevented. Figures 7.3 and 7.4 compare the efficacy of STP versus another commercially available sulfonated polymer. In these graphs, the polymers tested represent the state-of-the-art calcium phosphate inhibitors that have been developed over the past 20 years. SAA is a sulfonated acrylic acid copolymer, and is the most commonly used phosphate scale control. In this dynamic testing, the higher the turbidity the better is the dispersion property of the polymer. Having a polymer with higher dispersion efficacy reduces the potential for deposition of suspended solids on the surfaces of the cooling system, which improves system reliability.

7.2.2 CORROSION CONTROL

Corrosion can be maintained under control by using inhibitors, which are selected based upon the type of metallurgy. All types of metals under stressful operating conditions can be corroded and be susceptible to deposition by scale formation, fouling, and microbiological attack. Different

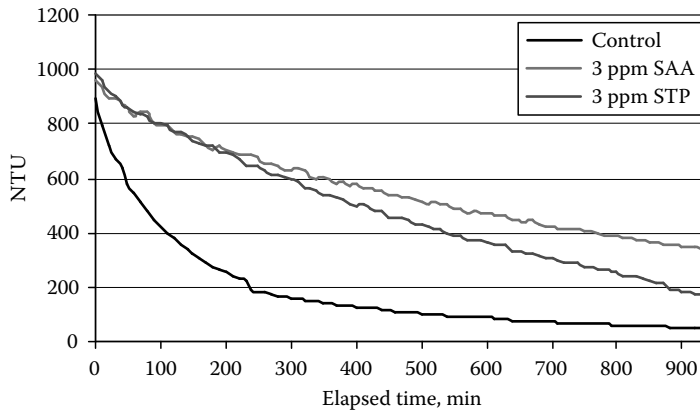


FIGURE 7.4 Dispersion of clay at 500ppm calcium hardness as CaCO_3 , pH 9.0, 1000ppm clay.

types of metals will corrode for different reasons. Because of this, it is important to know the metallurgy present in the system in a way that the designed treatment program contains inhibitors that are able to maintain under control all potential corroding surfaces.

Copper and its alloys are susceptible to corrosion from ammonia as well as the high content of dissolved solids and deposits that may form on the surface. Ammonia can cause cracking on admiralty brass, severe corrosion on all copper alloys, and contribute to biomass, which can create the right conditions for under-deposit corrosion. In the case of copper or its alloys, the most used inhibitor is the tolyltriazole (TTA) followed by benzotriazole (BZT). However, TTA and BZT efficacy is limited by the use of chlorine, which is the most widely used biocide because of its efficacy and low cost. In the presence of chlorine, TTA and BZT degrade, and the protective film formed on the metal surface is damaged reducing the capacity to prevent corrosion. Copper corrosion will release copper ions into the water, which will induce galvanic corrosion on mild steel surfaces. In addition, this degradation increases the chlorine demand, which not only increases costs due to the use of larger amounts of chlorine but also increases the corrosiveness in the system.

To avoid problems associated with TTA and BZT degradation, a new family of azoles that do not degrade in the presence of chlorine has been reported. One of these new azoles is the HRA (halogen-resistant azole, which is a modified azole), which when fed to the cooling system forms a stronger film than TTA and BZT. In addition, the film is not damaged by the addition of chlorine. Since HRA is not degraded by chlorine, HRA does not increase chlorine demand resulting in lower costs than when TTA or BZT is applied as the copper corrosion inhibitor.

From the environmental point of view, HRA also offers advantages in comparison to TTA and BZT. Degradation of TTA produces chlorinated compounds, which produce a smell that could cause nausea in people close to the cooling system. Furthermore, because of the fact that HRA does not degrade and form a stronger film on the metal surface, a lower dosage is needed compared to TTA or BZT to obtain similar corrosion inhibition. As a consequence, the amount of chemical discharged to the environment is significantly reduced [8,9].

Waters having high total dissolved solids, which is worst when chloride is present at high levels, accelerate mild steel corrosion. In addition, any deposit formed on the mild steel surface from suspended solids, biomass, scale, and/or any contaminant will also induce mild steel corrosion. A common problem could be galvanic corrosion due to copper deposition on the mild steel surface.

Use of an effective water treatment program and operational changes can eliminate or minimize mild steel corrosion. Using cathodic and/or anodic corrosion inhibitors normally does control mild steel corrosion. Phosphate is widely used as a mild steel corrosion inhibitor. Depending on the aggressiveness of the water and the operating conditions, phosphate may be used in combination with pyrophosphate or zinc to eliminate/reduce pitting corrosion, which is perhaps one of the most

detrimental types of corrosion. Choosing a polymer capable of maintaining the metal-phosphate corrosion-protecting film without allowing metal-phosphate scale formation is a key issue in the application of phosphate and zinc-based corrosion inhibition. The efficacy of the polymer to act as an inhibitor is associated with the types of functional groups present in the polymer chain, size of the polymer, and the geometrical configuration of the polymer when they interact with the surface, rather than if the polymer is a co- or terpolymer.

Stainless steel corrodes at much lower rates than mild steel. However, chloride ions can cause stress corrosion cracking or severe pitting. Chloride levels present in the water must be considered when selecting the type of stainless steel to be used. Biomass deposits, mainly from sulfate-reducing bacteria (SRB) and iron deposit bacteria can very rapidly induce pitting. An effective chemical water treatment program can minimize/eliminate the pitting problem.

Microbiologically induced corrosion (MIC) is also one of the types of corrosion that could create severe damage to the system metallurgy. Implementing an effective microbiological growth control program is a must to prevent MIC.

7.2.3 BIOLOGICAL CONTROL

Effective biological control programs for cooling water systems will (a) treat the system not just the water; (b) address the range of organisms posing threats to the cooling system; (c) control both planktonic and sessile microbes; (d) treat all areas of the cooling system including key areas such as tower deck, tower plenum, tower fill, heat exchanger equipment, and bulk water; (e) utilize a range of complementary biocontrol agents such as oxidizing biocides, nonoxidizing biocides, and biocides; (f) be supported by monitoring that tracks bioactivity levels and program performance; and (g) be applied consistently with regulations governing product use (e.g., labeling) discharge.

7.2.3.1 The Need for Biological Control

Biological control is as important as corrosion and deposit control for the successful treatment and protection of cooling systems. If cooling system biology is not effectively managed, efforts to control corrosion and deposition resulting from nonbiological sources will also be compromised. Organisms colonizing wetted and submerged surfaces form communities of organisms called biofilms. A biofilm is effectively a living tissue consisting of the cells of various organisms and extracellular polymers produced by these organisms. When left uncontrolled, biofilms form fouling deposits on surfaces that reduce heat transfer and increase corrosion rates. The polymers associated with the biofilm are hydrated and effectively increase the water film thickness at heat transfer surfaces. Since water conducts heat much less efficiently than metal, heat transfer rates across biofouled heat transfer areas suffer compared to rates across unfouled metal surfaces. Polymers also adsorb suspended solids from the bulk water thereby increasing the mass of fouling deposits. Biofilms prevent corrosion inhibitors from reaching and protecting colonized surfaces. Further, metabolic activity in the biofilm can generate by-products and create conditions that promote or enhance corrosion (i.e., microbiologically induced corrosion; MIC).

In addition to their impact on corrosion and deposition, biofilms can contribute to a higher risk for disease by supporting growth of waterborne pathogens, including the bacteria that cause Legionnaires' disease. Cooling water treatment programs designed to ensure biological control as well as nonbiological corrosion and deposit control are essential to protect capital equipment, realize unit availability and reliability goals, and to ensure safe, efficient, and profitable operations.

7.2.3.2 What Are the Organisms That Must Be Controlled?

An enormous range of organisms can be found in cooling water systems. Various mollusks, as well as sponges, bryozoa and hydrozoa, are examples of macroscopic life forms that are often encountered—especially in once-through cooling systems and, in particular, those using seawater. Fouling by these larger organisms can block heat exchanger tubes, and reduce or interrupt water flow in transfer lines. Mollusks such as Asiatic clams and Zebra mussels can occasionally cause mechanical damage.

Nematodes, protozoa, algae, fungi, and bacteria are but a few of the microscopic forms encountered in cooling systems of all sorts. In open recirculating cooling systems, algae, fungi, and bacteria are the microbiological foulants that are most commonly of primary concern.

An effective cooling water treatment program must address organisms present in the bulk water, but more importantly, the program must address organisms attached to submerged and wetted surfaces. These sessile organisms cause the problems associated with biofouling—reduced heat transfer, MIC, and increased health risk. The accumulation of biological fouling material in film-type tower fill can result in weight loads that exceed design specifications and lead to mechanical failure and collapse of the fill.

Planktonic or free-floating organisms present in the bulk water reflect water quality, but targeting these organisms alone will not guarantee an effective biological control program. This is not to say the control of organisms in the bulk water can be ignored. For example, most community-acquired cases of Legionnaires' disease are associated with the inhalation of contaminated aerosols. While a correlation between microbial levels in the bulk water and recovery of *Legionella* bacteria has not been found, it is obvious that effective bulk water treatment is essential to prevent the dissemination of *Legionella*-infested aerosols from the cooling system.

The same types of organisms can be found in either phase (in the bulk water or on surfaces); however, the significance of these populations will differ. The SRB can be used to illustrate this point. These anaerobic organisms are killed by prolonged exposure to oxygen yet can be recovered from the fully aerated bulk water of the cooling system. Barring use of a heavily polluted makeup water source, finding them in the bulk water on a consistent basis suggests there are anaerobic deposits in the cooling system. Aerobic organisms in the biofilm consume oxygen faster than it diffuses into the film. The lower regions of the biofilm become oxygen depleted providing an environment that supports growth of anaerobes such as the sulfate reducers. Controlling only bulk water SRB will not address the true source of these organisms—the biofilm. Since the SRB are often associated with MIC and severe localized corrosion, the cooling water disinfection program must address sessile SRB and the biofilm supporting them to avoid such damage.

Planktonic organisms typically enter the cooling system with the makeup water or are scrubbed out of the air by the cooling tower. Low concentrations (<1.0 ppm free residual as Cl_2) of common disinfectants such as chlorine are commonly used to control such organisms. Low levels of oxidizing disinfectants are not always effective in penetrating biofilms and controlling sessile organisms, however. Organisms in the biofilm are protected from the effects of disinfectants compared to planktonic organisms. The extracellular polymers they produce can act as nonliving demand-depleting residuals of oxidizing biocides within the film. Metabolic by-products such as reduced sulfur compounds and reduced conditions in the film will also deplete oxidizing residuals. Further, slow diffusion processes play a greater role in the transport of disinfectants within the biofilm compared to rapid, convective, mechanically aided transport through the bulk water. As a result, to effectively control biofilms, oxidizers should be supplemented with nonoxidizing biocides and/or biodispersants.

An effective cooling water treatment program must manage the range of species that represent the most significant threat(s) to safe and efficient operations. Generally, cooling water treatment programs should be designed to provide routine, day-to-day control of algae, fungi, and bacteria. Some control of macrofouling species may be achieved as a result of this same general, day-to-day microbiological control program, but often control of these organisms will require more specialized, periodic (e.g., seasonal) treatments.

7.2.3.3 Areas of the Cooling System That Require Special Attention

Bacteria are widespread throughout cooling systems and can be found on most wetted and submerged surfaces. Since bacteria are often the numerically dominant microbial form in biofilms, an effective biological control program must target bacteria and sessile bacteria in particular to protect heat exchangers and other critical cooling equipment.

High efficiency, film-type cooling tower fill deserves special attention since it is very prone to biofouling. The coatings used on such fill appear to be readily colonized by microorganisms. Once colonized, the fill accumulates suspended solids due to the “sticky” nature of polymers produced by biofilm organisms. Biofouling will interrupt water flow, change the liquid:gas ratio in the tower, and reduce cooling efficiency. Fouling makes it difficult to deliver treatment to affected areas since water flow within the affected area is blocked. In extreme cases, such fouling has led to fill collapse.

Owners of cooling towers, especially those using surface water with seasonal, high-suspended solids or with processes that contribute suspended solids to the cooling water, are advised to monitor fill weight on a regular basis. Periodic feed of biocides to tower return risers can be an effective means for targeting microbes in the fill before they cause problems. Hydrogen peroxide has been found to provide advantages over chlorine for mitigating biofouled tower fill. A recently available cleaner for biofouled surfaces is now available. This non-biocidal agent is to be used with either oxidizing or non-oxidizing biocides. It is highly effective and provides rapid cleaning of biofilm and adsorbed solids. In addition, compared to other biodispersant-type products previously available, it is non-foaming.

Compared to the bacteria, the nutrient requirements of fungi and algae tend to limit their distribution in the cooling system, yet achieving control of these types of organisms can present special problems for the cooling system treatment program. Fungi can attack both the exterior and interior of wood tower components. External, surface attack causes soft rot on wet and flooded wood surfaces. Internal fungal attack causes deep rot, and is the more serious problem. It is harder to detect and can result in severe weakening of affected members and tower collapse in extreme cases. Deep rot occurs in wood located in non-flooded, high-humidity areas of the tower such as the plenum.

Typical low residuals of halogens like chlorine or bromine used for cooling water disinfection will be effective against fungi in the bulk water. However, nonoxidizing biocides should be used to enhance control of fungi on submerged wood surfaces. Fungi growing in the plenum or on other non-flooded wood surfaces are not contacted by biocides added to the recirculating water and are therefore not controlled by such treatments.

To control organisms in the plenum and elsewhere in the tower, wood that has been pressure treated with preservative is often used to construct the tower, but pressure-treating lumber provides limited protection against fungal attack; temporary protection from surface attack, at most. Pressure treating, even if wood is incised, drives the preservative only a few millimeters into the wood, and this protection can be breached. Saw cuts, drill holes, or cracks in tower members expose unprotected interior wood thereby providing avenues for penetration leading to fungal growth inside treated lumber.

Periodic spray application of approved biocides to wood surfaces in the plenum and elsewhere is of some limited benefit. It may be most helpful after repairs have been made in towers that experienced severe fungal attack. A prominent cooling tower manufacturer has advocated this approach to reduce residual fungal contamination levels after removal of decayed lumber and to help protect newly installed lumber. From a water treatment point of view, little can be done to prevent fungal attack in the plenum and other non-flooded areas of the tower. Since internal fungal attack can have severe consequences, inspections of tower wood should be part of the cooling system treatment program. Cooling tower owners are advised to use third party companies to conduct periodic tower inspections (e.g., every 3–5 years) and the services of a spray treatment company to apply approved biocides perhaps every 1–2 years depending on inspection history.

Algae are photosynthetic organisms. They use light to generate chemical energy required to support metabolic processes. As a result they are found primarily on sunlit areas of the tower. Algae-related problems are often due to their growth on the open decks of cross-flow cooling towers where they can block distribution nozzles, upset water balance, and decrease cooling efficiency. Algae can produce copious amounts of “slime” that helps protect them from oxidizing biocides. Uncontrolled algae growth will contribute organics that feed other microorganisms and further deplete oxidizing biocide residuals. Algae are associated with the growth of *Legionella* bacteria, and algae mats can provide anaerobic niches for the growth of SRB.

Algae growths are not well controlled by oxidizing biocides at typical-use levels. Nonoxidizing biocides are essential for managing algae in cooling systems. Nonoxidizing biocides based on surface-active ingredients have been found to be very effective. As for protection of tower fill, periodic injection of biocides to the return risers of cooling towers with open decks can enhance algae control. Algae control products are available. Such products, known as “algistats,” do not kill quickly but rather interrupt photosynthesis and slowly starve algae. An algistat can be highly effective but requires careful, consistent application over several weeks since a lapse in treatment over this time can allow algae to recover.

7.2.3.4 Essential Tools for Biocontrol

Oxidizing biocides like chlorine from gas or sodium hypochlorite (liquid chlorine bleach) should be the backbone of an effective cooling system biocontrol program. Chlorine is proven, widely available, and a very cost-effective disinfectant, especially for cooling system bulk water. It is widely recommended for use in Legionella risk-mitigation programs. When biological control achieved by chlorine is inadequate, consider bromine. Bromine may enhance biocontrol under conditions of high pH (e.g., ≥ 8.0), especially when contact time is limited, and in the presence of ammonia contamination. Since bromine will almost always add to biocontrol costs compared to those of chlorine from gas or bleach, it is important to first evaluate results by feeding chlorine at higher residuals. The development of halogen-stable cooling water treatment chemicals enables chlorine to be safely used at levels higher than historical norms (i.e., 0.5–1.0 ppm free residual chlorine vs. 0.1–0.5 ppm FRC_{l₂}).

Bromine is available in a number of different forms. Liquid sodium bromide salt products are the lowest cost sources but must be activated by co-feeding with chlorine. Bulk-storage-related feed equipment should be considered when evaluating total costs of this approach. Bromine is also available in the form of hydantoin-based, solid halogen donor products. These products release active bromine when dissolved. Because of the relatively low solubility of hydantoins, specialized feeders are required to apply these products. Liquid, “stabilized” bromine products represent another option. These products deliver active bromine as fed, and typically incorporate a small amount of sulfamic acid (NH₂SO₃) as stabilizer. The nitrogen acts as a stabilizer by forming a complex with the active bromine based compound. They claimed to extend the life of the halogen residual in the cooling water and also enhance product performance. These liquid, active bromine products can be fed with a simple chemical pump.

Continuous feed of oxidizing biocides is preferred though not always possible. Continuous feed allows for more consistent residual control and provides “infinite” contact time thereby ensuring good disinfection efficacy (at least in the bulk water) and unbroken protection. Intermittent application may be required to meet discharge requirements or to manage water treatment costs. Intermittent feed reduces contact time, and this can compromise protection. Intermittent feed also requires more attention to product feed rates. At the start of the feed period the hydraulic and chemical demand in the system must be met, and this can require an increased feed rate. Once the system demand is met, the feed rate must be decreased to avoid exceeding the target control range.

To ensure adequate biocontrol when oxidizers are applied intermittently, use of biodispersants or nonoxidizing biocides should be considered. Use of oxidizing biocides can be limited for various other reasons. For example, concerns about chloride contribution and potential effects on stainless steel may limit the amount of chlorine fed. Chlorine and other oxidizers cannot be used in closed cooling systems treated with nitrite for mild steel corrosion protection. In such systems, an oxidizer would convert nitrite to ineffective nitrate and eliminate its ability to protect mild steel. Where operating conditions or system requirements limit oxidizing biocides, nonoxidizing biocides are recommended. Although oxidizers are highly effective against bulk water organisms at low residuals, they will not deliver equivalent performance against biofilm organisms at these same levels (as discussed previously). Use nonoxidizers to ensure effective control of biofilms. The same factors associated with biofilms (diffusion-based transport, reduced conditions, and nonliving chemical demand)

that adversely affect oxidizing biocide performance can also be encountered in low-flow shell-side cooling equipment, in open distribution decks colonized by algae, and in high-efficiency film-type tower fill. Nonoxidizing biocides should be used to ensure biocontrol in systems with these conditions and components.

A number of nonoxidizing biocide active ingredients are used for treatment of cooling systems. Some examples of the most common types of actives are bronopol, DBNPA, glutaraldehyde isothiazolin, methylene-bis-thiocyanate, and quaternary ammonium salts. Typically, commercially available cooling biocide products are formulated with a single active ingredient. There are, however, various blended nonoxidizing biocides that exhibit synergy, that is, the combination of actives produces a reduction in target microbial populations greater than the sum of the reductions produced by the individual actives applied separately. Identifying synergistic blends require extensive developmental research to discover the proper ratio of actives displaying this property. The U.S. Patent Office has recognized the uniqueness of certain combinations and awarded patents based on a demonstration of synergy. When the nonoxidizing biocide blend is also found to be synergistic with oxidizing biocides, a highly effective antimicrobial agent control can be produced. Significant benefits derived from use of such synergistic blends include (a) better biocontrol at a lower dosage and treatment cost; (b) reduced environmental impact; (c) resistant populations are “selected out” at a reduced rate; (d) the useful life of the product at a given site is extended; and (e) administrative costs associated with management of change processes for biocide “switch outs” are reduced.

Given there are many potential nonoxidizing biocide products that might be used, and since they do not demonstrate the same activity against all microbial types, design of the biocontrol segment of the cooling system treatment program should include a process to help identify the product best suited for use in a given system. This process should cover the following points: (a) consider the type of organism to be controlled, such as algae, fungi, aerobic bacteria, and anaerobic sulfate reducers; (b) biocide efficacy is a function of the concentration fed and the contact time with the target population; (c) understand various system parameters that will influence product performance, such as pH, retention time, chlorine compatibility, etc.; (d) evaluate the discharge environment. Will cooling tower blowdown or other treated water go direct to a river, lake, or stream? Or will the treated water go to a waste treatment plant, either an on-site or an off-site Publicly owned treatment works (POTW)? How will use of a given product affect any government-issued discharge permit? (e) check candidate product labels to ensure they are registered for use in the type of water system to be treated. Determine whether products have any other necessary government approvals for use in the system; and (f) perform a toxicant evaluation. This evaluation will screen the antimicrobial activity of candidate products at various dosages against organisms (typically, bacteria) taken from the system. It will help identify those products that have the best chance of working in the system. Toxicant evaluations can be performed against planktonic bacteria as well as sessile bacteria. Testing against sessile bacteria will require use of a specialized sampling device, a “modified Robbins device.” Products that deserve further consideration are those effecting a 90% or greater reduction in microbial levels compared to untreated controls.

Generally, shot feed (slug) nonoxidizing biocides to the volume of the system. Application of biocide to hot return risers can be helpful when combating algae on the tower deck or biofouling in the tower fill. Continuous low-level applications are less common due to concerns about the efficacy of low nonoxidizer residuals. When shot feeding biocides, product addition should be made as quickly as possible to ensure a maximum concentration from a given volume of water, and that product is not unnecessarily wasted by discharge with the tower blowdown during a prolonged feed. To maximize the concentration achieved and reduce the amount of product required (a) apply biocides during periods of low heat load; (b) drop the water level in the tower basin (if this can be done safely); (c) reduce cycles; and (d) block in blowdown.

Base dosage and frequency of nonoxidizing biocide applications on the needs of the system and biomonitoring results. Factors such as the rate of microbial growth, the system pH, the system retention time, and the discharge environment will influence the decision. If a choice must

be made between dosage and frequency, a high dose applied less frequently is preferable to a low, potentially ineffective dose applied more often. Label dosage limits and the potential aquatic toxicity in direct discharge situations must be considered whatever decision is made about the biocide feed schedule.

Biodispersants represent a third and increasingly useful class of tools for biocontrol. They are not substitutes for biocides, but are used with biocides to improve results achieved by a given oxidizer/nonoxidizer-based biocontrol program. Since biodispersants are not biocides, the improved biocontrol they enable is achieved without resorting to higher levels of toxic materials. Their use can help reduce the environmental impact of the overall biocontrol program. Biodispersants are commonly described as aiding penetration of biocides into biofilms and into individual microbial cells. Some types appear to slow the rate at which surfaces foul. Recently, a new type of cleaner for biofouled surfaces has been identified. This material, used in conjunction with other biocides, exhibits an unprecedented level of activity removing biological and other foulants from cooling system surfaces. A unique feature of this product, compared to conventional biodispersants that are highly surface active, is that it does not foul—even if applied at high concentrations.

7.2.3.5 Biomonitoring

Conduct biological monitoring to assess system cleanliness and performance of the biocontrol program. A range of biomonitoring tools are available. These can be grouped in three main categories: (a) culture based; (b) biochemical markers; and (c) performance indicators.

Culture-based methods rely on growth of organisms on or in nutrient media. These are traditional methods as exemplified by the Standard Method Plate Count, 3M's Petrifilm, Dipslides, and serial dilution vials. Serial dilutions of an aliquot of cooling water are applied to the surface of the growth medium or injected into nutrient broth. After a period of incubation (2–7 days, depending on the type of organism) microbes present in the original sample grow and form visible colonies on solid media or turbidity in nutrient broths. Results are expressed as CFU (colony forming units) per milliliter, and can be quantitative or semiquantitative. These techniques are commonly used to quantify total aerobic heterotrophic bacteria, molds and yeast (fungi), and anaerobic SRB. However, no one medium or set of incubation conditions can provide suitable growth conditions for all the microbes present in a cooling system. Even using a range of media to detect aerobic and anaerobic bacteria as well as fungi, growth-based techniques still grossly underreport total numbers of microorganisms in the system. Some researchers believe culture-based methods report as little as 1% of the total microbes present. Consequently, culture-based methods provide only a very narrow and limited window on the total possible range of bioactivity that can be occurring in the cooling system. In addition, because of incubation time requirements, several days will elapse before biomonitoring results are available. This greatly delays deciding whether the biocontrol program needs to be adjusted.

Biochemical markers such as adenosine triphosphate (ATP), DNA, RNA, or NAD can also be used to assess levels of microorganisms in cooling systems. Methods based on tracking such molecules generally require complex sample processing techniques, sophisticated and relatively expensive lab equipment, and a high level of training for the analyst. In addition, it can be difficult to relate levels of these biochemicals to actual numbers of viable microbes.

ATP-based biomonitoring represents the exception to these generalizations. ATP is the “energy currency” found in all living things. Measuring ATP levels has been greatly simplified over the last 10–20 years, and the cost for ATP-based biomonitoring systems has decreased as well. Easy-to-use, relatively stable pen-based reagent systems based on the same chemistry as found in the firefly are commercially available. An unknown amount of ATP extracted from organisms in a water sample causes light to be produced when mixed with an enzyme/substrate reagent system. A luminometer is used to measure the amount of light produced and reports this as “relative light units.” Because reagents are in excess compared to ATP, the amount of light released is a function of ATP levels that in turn are a function of the amount of biological activity in the water sample. ATP-based

biomonitoring has the virtue of providing an assessment of a cooling system's total bioactivity levels in just a few minutes. Since all living things contain ATP, this assessment is not limited to one segment of the total population. While some operator training is required, and though ATP from nonmicrobial sources (e.g., plants and insects) can complicate interpretation of results, when ATP-based biomonitoring data is trended and related back to equipment performance, a real-time basis for assessing and adjusting the biocontrol program is provided.

Calculate and track performance parameters such as U coefficients, approach temperatures, condenser backpressure, or chiller efficiency for key cooling system equipment. Plot biomonitoring results based on ATP or culture-based methods against relevant equipment operating parameters. This process can help identify correlations between bioactivity levels and effects on system operations. Use such correlations to interpret biomonitoring data and set action points for managing the biocontrol program.

7.3 APPLYING A DESIGNED TREATMENT PROGRAM

7.3.1 CONTROL OF CHEMICAL FEED

Despite the importance of properly functioning cooling tower systems, operational control of cooling water treatment programs frequently is neglected, and thus is the single most common cause of program failure. The best possible combination of corrosion, scale, and deposition control chemicals, with effective biocides, is completely worthless if not consistently and correctly applied to the cooling water.

Best practice for proper feed control is achieved through an automatic feed control system. The controller must (a) provide optimum treatment federates in an automatic and continuous manner. It should respond to changes in process conditions in a way that the required chemical active levels could be maintained; (b) ensure feed accuracy of each product by automatically verifying the exact amount of chemical being fed; (c) be able to accurately feed chemical directly from bulk storage, avoiding chemical handling and in this way enhance employee health and safety; (d) provide comprehensive information management and reporting capabilities to meet customer needs; and (e) be able to control blowdown and monitor makeup in a way that chemicals being fed can be adjusted according to changes in blowdown or makeup flows.

Controlling feed rate based upon mass balance of each product being fed is the most effective form of controlling treatment feed rate. Controlling product feed rate based upon adjustment on the monitoring of a tagged component is not enough. Knowing that the tagged component is present in the system does not mean that the other components are also present at the required dosage. This is true when some of the components may precipitate with calcium or other metal or degrade in the presence of halogen, as is the case of the phosponates and the TTA.

7.3.2 MONITORING SYSTEM

A monitoring and maintenance program is essential to ensure high system performance. A preventive monitoring and maintenance schedule should be implemented under the supervision of an industrial water treatment specialist. There are a number of good reasons for continuous performance monitoring of cooling systems including (a) changes in makeup water chemistry; (b) changes in temperature due to seasonal variations; (c) changes in system heat load due to production level changes; (d) changes in biological control requirements due to seasonal variations; (e) treatment chemical quality control problems; (f) system feed and control problems; and (g) system contamination from atmospheric or process leaks. Routine chemical testing of both recirculating and makeup water is important for getting target results. Chemical tests should include but not be limited to total and calcium hardness, alkalinity, silica, conductivity, phosphate, zinc, copper, iron, chlorides, pH, ammonia, phosphate, and biological activity. Chemical test frequency must be established based

upon system operating conditions. Test results must be compared with target conditions as well as with past results to be able to evaluate any change that may have happened. Using an online totalizer for daily flow rate and a rotameter for instantaneous flow rate can monitor makeup water volume. A magnetic flow meter can be used to measure flow rate in piping. All of these devices must be calibrated to prevent errors. In-line flow meters can clog due to deposition and biofouling, and as a consequence provide inaccurate flow value.

Monitoring units such as DAT and MonitAll [10] units are able to simulate deposition that could be occurring in the heat exchangers. However, direct monitoring of the heat exchanger, if it is possible, is the best way to know how clean the heat exchanger surface is. Determination and follow-up of the U -coefficient is a very good way of knowing the heat exchanger performance. A newly developed monitoring tool called CheX is a comprehensive tool, which monitors, predicts, and diagnoses the heat exchanger performance [11]. The unique features of this advanced technology include numerous data cleaning steps to improve data quality and isolate a net fouling trend, an adaptive model that learns from the past to predict performance 3 years in advance, and knowledge-based diagnostics that identify the probable cause(s) of fouling and recommend corrective actions.

Corrosion monitoring employs a variety of techniques to determine how corrosive the environment is and at what rate metal loss is being experienced. Corrosion measurement is the quantitative method by which the effectiveness of corrosion control and prevention techniques can be evaluated, and provides the feedback to enable corrosion control and prevention methods to be optimized. The rate of corrosion dictates how long any process plant can be usefully and safely operated. The measurement of corrosion and the action to remedy high corrosion rates permits the most cost-effective plant operation to be achieved while reducing the life-cycle costs associated with the operation.

Corrosion-monitoring techniques can help in several ways by (a) providing an early warning that damaging process conditions exist that may result in a corrosion-induced failure; (b) studying the correlation of changes in process parameters and their effect on system corrosivity; (c) diagnosing a particular corrosion problem, identifying its cause and the rate controlling parameters, such as pressure, temperature, pH, flow rate, etc.; (d) evaluating the effectiveness of a corrosion control/prevention technique such as chemical inhibition, and the determination of optimal applications; and (e) providing management information relating to the maintenance requirements and ongoing condition of plant,

The following list details the most common techniques that are used in industrial applications:

- Corrosion coupons (weight loss measurements)
- Electrical resistance (ER)
- Linear polarization resistance (LPR)
- Electrochemical noise (ECN)
- Galvanic (ZRA)/potential
- Hydrogen penetration
- Microbial
- Sand/erosion

Monitoring techniques to be used depend upon the system operating conditions, system metallurgy, and water quality. The ATP method can monitor the levels of microbiological organisms in cooling water. This is an easy and quick way to know microbiological activity. ATP measurement offers the advantage that is a real-time measurement and allows for immediate corrective actions. Test strips and dip slide can also be used; however, these are more time-consuming techniques, and results are obtained after several days needed for incubation.

Testing for SRB is essential. SRB are detrimental to all metallurgies since these bacteria can induce pitting corrosion. Total bacteria test will not identify Legionella bacteria. It is recommended to send cooling water samples to a specialized laboratory for Legionella detection.

A biofouling tube tracking device is also very important for biofouling monitoring. This is a piece of stainless steel tube with pressure-monitoring devices at each end. If biofouling starts to take place, a change in pressure can be detected.

7.3.3 DATA MANAGEMENT

A monitoring and diagnostics system that enables effective management of overall plant water and process systems' performance through remote data acquisition and analysis is essential for managing the cooling system. The system should have reporting capabilities to allow plant personnel and other service teams to focus on maximizing energy efficiency, production throughput, and equipment life expectancy with minimal personnel time.

The system should be able to collect data from (a) chemical feed controllers; (b) plant data system; (c) operators logs; and (d) system monitoring tools. In addition, the system should have other capabilities including the following: (a) provide data tables; (b) provide trends of raw data; (c) develop technical performance scorecards; (d) be able to perform statistical analysis and process control charts; and (e) send electronic alarm notification via e-mail or telephone.

Data management systems, such as GE W&PT Insight system, have proven to be important to customers to gather information on multiple systems, locations, and data sources, using a simple mechanism via the Web and the e-mail. This allows taking corrective action immediately and keeping people informed on system performance 24 h a day.

7.4 SUMMARY

The function of a cooling water system is to remove heat from a process or equipment. In order for the system to be efficient, all potential problems due to deposition, corrosion, and microbiological growth must be maintained under control. Each system requires a unique approach as far as designing a water treatment program capable of maintaining system performance and ensure

- Plant reliability
- Productivity
- Asset protection
- Health and safety
- Profitability

Understanding the mode of action of each component helps in choosing of the cooling program. This combined with the knowledge of the system to be treated and its influence on the environment permits a proper and cost-effective cooling treatment program. When choosing the correct treatment program, one must consider the chemical characteristic of the water sources(s) used as makeup as well as the type of metallurgy and other surfaces present in the cooling system. Each chemical component of the treatment program needs to be checked for its stability under the operating conditions: chlorine, tolerance to calcium, pH, compatibility with other components of the treatment program, environmental impact, and safety of the people handling the product or that are close to the vicinity of the system. Controlling the feed of the program to the system as well as monitoring its performance and managing the results is a key to the successful application of any designed treatment program.

REFERENCES

1. Perez, L. A. and Post, R. Managing a seawater cooling system: Water treatment program and monitoring optimization. In *Proceedings of the International Desalination Conference*, Aruba (2007).
2. Perez, L., Walterick, G., Hendel, R., and Irwin, K. Best practices for deposit control in RO seawater desalination. In *AMTA Desalination Conference*, Anaheim, CA (2006).

3. Shimabayashi, S. and Uno, T. Crystal growth of calcium phosphate in the presence of polymeric inhibitors. In *Calcium Phosphate in Biological and Industrial Systems*, Amjad, Z. (Ed.), pp. 193–215. Kluwer Academic Publishers, Boston, MA (1998).
4. Perez, L. A. and Zidovec, D. Scale control by using a new non-phosphorus, environmentally friendly scale inhibitor. In *Mineral Scale Formation and Inhibition*, Amjad, Z. (Ed.), pp. 47–61. Plenum Press, New York (1994).
5. Geiger, G. and Ertel, J. Advances in alkaline cooling water treatment technology. Corrosion/94, Paper No. 320, NACE International, Houston, TX (1994).
6. Brown, J. M., Carey, W. S., and McDowell, J. F. Development of an environmentally acceptable cooling water treatment program; non-phosphorus scale inhibitor, Corrosion/93, Paper No. 463, (1993), NACE International, Houston, TX (1993).
7. Holliday, R. and Kessler, S. Development and testing of a novel polymer for cooling water applications. Available at www.gewater.com, Trevese, PA (2004).
8. Given, K. M., May, R. C., and Pierce, C. C. A new halogen resistant (HRA) for copper corrosion inhibition. Available at <http://www.gewater.com>, Trevese, PA (2005).
9. May, R. C. Application of a new corrosion inhibitor for copper alloys at the Harris nuclear plant. Available at www.gewater.com, Trevese, PA (2004).
10. Cooling monitoring tools. Available at <http://www.gewater.com>, Trevese, PA.
11. Prasad, V. Predictive heat exchanger efficiency monitoring. In *Proceedings of HT2005 2005 ASME Summer Heat Transfer Conference*, July 17–22, San Francisco, CA (2005).

8 Latest Developments in Oilfield Scale Control

Mingdong Yuan

CONTENTS

8.1	Introduction	129
8.2	Viscosified Fluids for Improvement of Scale Inhibitor Placement.....	130
8.3	Nonaqueous Scale Inhibitors for Squeeze Treatments	131
8.4	Development and Use of New Chemical Inhibitors	132
8.4.1	Environmentally Acceptable Inhibitors.....	132
8.4.2	Inhibitors with Enhanced Functionality	133
8.5	Sulfate Removal from Injection Seawater	133
8.6	Brine Mixing, Ion Exchange, and Scale Precipitation Inside Oil Reservoirs	136
8.7	Impact of Hydrate Inhibitors	137
8.8	Fundamental Studies on Scale Formation, Inhibition, and Inhibitor–Rock Interactions.....	140
8.8.1	Scale Formation, Precipitation, and Deposition	141
8.8.2	Scale Inhibition.....	143
8.8.3	Scale Inhibitor Interactions and Reactions with Rock Substrates	146
8.9	Miscellaneous Developments	148
8.10	Summary	148
	Acknowledgments.....	149
	References.....	149

8.1 INTRODUCTION

There are a number of new developments and trends in the oil and gas industry that impact how mineral scales are formed and prevented, namely, (a) the production of oil and gas (and water) from deepwater and ultra deepwater, especially from subsea satellite fields that are tiebacks to a main production platform or a floating production, storage, and offloading (FPSO) vessel; (b) production from high-pressure, high-temperature (HPHT) reservoirs, some of which contain high-salinity (HS) formation brines; (c) production from long-reach horizontal wells and complex wells in complex reservoir formations; (d) the minimization of environmental impact from chemical products to meet more stringent regulatory requirements; and (e) gas hydrate formation and the use of hydrate inhibitors. In response to these operational and environmental challenges, significant technological advances have recently been made in oilfield scale control. This chapter therefore intends to review and discuss some of these major developments and advances in the last few years, namely, (a) the use of viscosified fluids to improve chemical placement into targeted formation zones in horizontal wells, complex wells, and complex formations; (b) the use of nonaqueous inhibitor solutions and treatment packages to minimize potential formation damages resulting from scale inhibitor squeeze treatments; (c) the development and selection of chemical inhibitors that are more environmentally acceptable or that are with enhanced functionality or improved secondary properties; (d) alternative

approaches to scale inhibition by reducing/removing sulfate ions in the injection seawater; (e) the mapping of ions and scale precipitation throughout oil reservoirs; and (f) the impact of gas hydrate inhibitors on scale formation and inhibition. Furthermore, this chapter attempts to review some of the recent fundamental studies on scale formation, inhibition, and inhibitor–rock interactions, and transport. Instead of attempting to critique the soundness and validity of the referenced studies, this chapter intends to keep readers abreast of the recent major developments in oilfield scale and the resulting key findings, and serve as a source of literature references for further reading.

8.2 VISCOSIFIED FLUIDS FOR IMPROVEMENT OF SCALE INHIBITOR PLACEMENT

In offshore deepwater production, owing to the high cost of the scale-formation squeeze treatment and the significant disruptions to normal oil and gas production, there is an emphasis on improving the reliability, the effectiveness, and the treatment lifetime of an inhibitor squeeze application. In this regard, inhibitor placement in long-reach horizontal wells, complex wells, and heterogeneous formations is a key to ensure the scale inhibitor will be present in the formation zone(s) and producing wellbore section(s) where there is a potential for waterborne scaling.

With this in mind, there have been a large amount of recent laboratory and field studies that have advanced the inhibitor placement technology [1–9]. Chemical diverters have been developed or identified to help place the scale inhibitor in the targeted formation zones. The most recent developments on scale inhibitor diversion have been focused on self-diversion treatments via bull-heading by using viscosified fluids. On the one hand, bullheading of viscosified fluids is cost effective and practical in increasing inhibitor placement into the toe section of the formation. On the other hand, they do not usually cause complications to the treatment operation, production formations, and scale inhibitor performance. As a viscosified fluid enters an upper formation zone (the heel), the increased fluid viscosity starts to create resistance to the fluid penetration and further propagation into the formation, which then forces the fluid (scale inhibitor solution) inside the wellbore to be pumped further down to the lower (toe) section and be forced into the bottom formation zone [3–5]. Aqueous, homogenous shear-thinning non-Newtonian and linear-viscosity Newtonian fluids as well as emulsified viscous fluids have been studied and applied in the field as a diverter. The additives used to make these viscous solutions are typically synthetic polymers, such as polyacrylamide (PAM), or biopolymers such as hydroxyethylcellulose (HEC) and Xanthan and Guar gums [1,9].

The recent advances in this area have been achieved through both laboratory experimental studies [1,4,8,9] and computer simulation [2–5] of the effects of viscous fluids on diverting scale inhibitor into multiple heterogeneous formation zones. Shear-thinning fluids are generally found to be more effective than the simple Newtonian fluids. This is because while being pumped down the wellbore, a shear-thinning fluid at a relatively high velocity has a much lower viscosity, thus allowing it to travel further down the wellbore with less resistance, but it becomes increasingly more viscous as it enters the top formation zone and propagates further away from the wellbore where the velocity dramatically reduces. A viscosified fluid can be applied as a pretreatment (preflush) ahead of the scale inhibitor main pill, or the scale inhibitor pill can be viscosified to become self-diverting. In addition, overflush fluid may be viscosified to chase the scale inhibitor and reduce viscous fingering inside the formation of the overflush fluid through the inhibitor solution.

Although it is widely agreed that viscosified fluids help scale inhibitor placement into formation layers of permeability and pressure contrast, there is however a disagreement as how significant this effect can be. Whereas one model predicts a very significant positive diverting effect from a viscous shear-thinning fluid [4], a different model indicates such an impact is more moderate in a radial flow system such as that of a near-wellbore formation [3], and any improvement of shearing thinning on viscous Newtonian fluid in inhibitor placement is marginal [5].

Several field applications of viscosified self-diverting treatments using shear-thinning fluids have recently been reported [2,4,7,9]. These applications were mostly successful as far as scale inhibitor placement and scale inhibitor return are concerned, although two treatments reportedly caused an upset to the fluid separation during initial flow backs and one application resulted in well productivity decline [2,9]. One successful application was a squeeze treatment using Xanthan viscosified scale inhibitor solution in a long-reach horizontal well in the Nelson field in the North Sea. This treatment resulted in scale inhibitor return at above 10 ppm for more than 5 million barrels of produced water, which was more than double the treatment lifetimes that were obtained with conventional squeezes in the same well.

8.3 NONAQUEOUS SCALE INHIBITORS FOR SQUEEZE TREATMENTS

Since a squeeze treatment is intended to arrest well production decline that otherwise would occur as a result of scale deposition in the near-wellbore formation and/or in the production tubular, any loss of well productivity resulting from a squeeze treatment would defeat the purpose of such a treatment. Formation damages from wettability change, water blocking, clay swelling, and mineral dissolution may potentially arise from a conventional, aqueous squeeze treatment in low water-cut and water-sensitive formations. With this in mind, most recent studies and developments in avoiding or minimizing squeeze-induced damages have been focused on nonaqueous inhibitor treatments as an alternative to the conventional, aqueous treatments [10–20]. There are several types of nonaqueous scale inhibitor solutions that have been developed for squeeze applications: (a) truly oil-soluble (or completely water free) scale inhibitor solution [10,11,15], (b) oil-soluble scale inhibitor solution (with the intrinsically water-soluble inhibitor formulated into an oil-soluble solution package) [14,16,20], (c) water-soluble scale inhibitor formulated into amphiphilic/mutual solvents [12,14,16], and (d) scale inhibitor formulated into oil-continuous emulsions or microemulsions [11,17]. A detailed review and description of these different systems can be found in a reference paper [13].

Although many of the nonaqueous squeeze treatments were reportedly successful, causing no formation damages or even resulting in increased oil productivity following each treatment [12,13], they are however not fool-proof as far as formation damage is concerned. This is because there are other damage mechanisms that could be induced by a nonaqueous solution and the additives therein, such as emulsion formation or precipitation of the inhibitor and/or additives in situ. For instance, two squeeze treatment failures (formation damages) were reported with use of oil-soluble scale inhibitors [13], and slight productivity declines were reported following two other squeeze treatments using amphiphilic-solvent-based nonaqueous inhibitor [12].

Most of the nonaqueous squeeze treatments were reported to, when compared to the aqueous treatments, have resulted in enhanced inhibitor retention or extended inhibitor squeeze lifetimes at a given minimum inhibition concentration (MIC) [11,12,17,18], even though there were also reports that nonaqueous squeezes did not provide any improvement in inhibitor return or even gave somewhat shorter treatment lifetimes [16]. In one carefully controlled laboratory experimental study [14,16], three inhibitor solutions were formulated by using the same phosphonate scale inhibitor: one an aqueous solution, another a mutual-solvent-based nonaqueous solution, and the third an oil-soluble solution. These three inhibitor solutions were then applied in three identical core floods to simulate inhibitor squeeze treatments. Both the mutual-solvent-based and oil-soluble inhibitor solutions in these core floods resulted in similar inhibitor returns (squeeze lifetimes) to that from the aqueous solution core flood, as shown in Figure 8.1.

Although a majority of the reported studies on nonaqueous inhibitors focused on practical aspects (such as permeability changes and inhibitor returns), a few studies investigated the more fundamental aspects of these solutions, such as phase behavior, kinetics, and adsorption/desorption processes, which were carried out by experiments [13,14,20] as well as computer modeling [14,16,19,20].

When compared to conventional aqueous squeeze treatments, the total number of scale squeezes using nonaqueous scale inhibitor technologies are still relatively small [13]. This limited acceptance

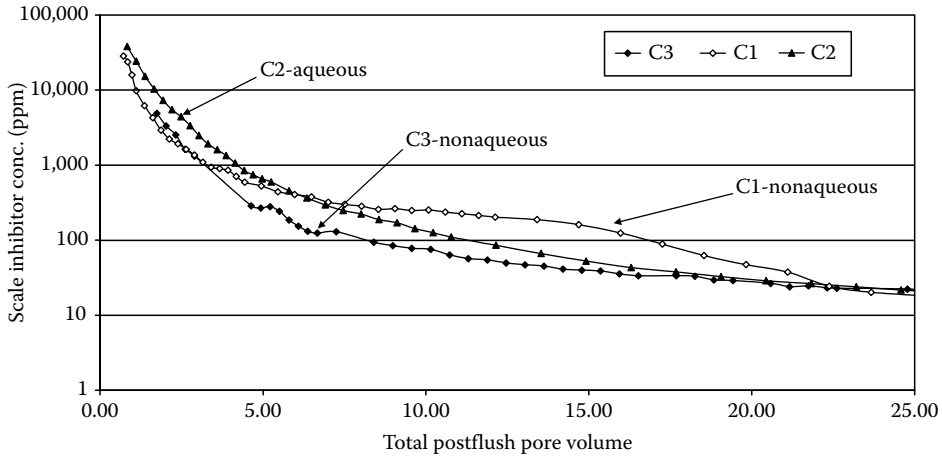


FIGURE 8.1 Scale inhibitor return during early postflush (>20 ppm). (From Guan, H. et al., *SPE Prod. Oper.*, 21, 419, 2006. With permission.)

by the industry is likely due to a multitude of factors, such as relatively higher costs of nonaqueous products than aqueous-based products, additional complexity of the treatment procedures, and potential product instability that may be associated with some nonaqueous technologies [13,18]. Besides, nonaqueous scale squeeze technologies are competing with conventional aqueous technologies that are suitable for squeezing in a majority of oil and gas wells. Furthermore, there have been successful scale inhibitor squeeze treatments in low water-cut and water-sensitive formations by combining nonaqueous preflush and overflush (e.g., mutual solvent or diesel) with aqueous main-scale inhibitor pill [6,21]. These “hybrid” inhibitor squeezes seem to expand the applicability of aqueous scale inhibitors in low water-cut and water-sensitive formations.

8.4 DEVELOPMENT AND USE OF NEW CHEMICAL INHIBITORS

A substantial amount of recent advances has centered on the development, evaluation, and application of environmentally more acceptable inhibitor chemistries and products, while other efforts have also been made to improve inhibitor functionality (lower MIC and/or improved inhibitor retention) as well as their secondary properties that enable their use in harsh conditions (e.g., higher thermal stability and better brine compatibility).

8.4.1 ENVIRONMENTALLY ACCEPTABLE INHIBITORS

In order to meet more stringent environmental regulations [22–24], more environmentally friendly scale inhibitors were developed or identified that would minimize their impact when discharged into the environment such as the ocean. There have been a number of reports of new chemistries and products that are more environmentally acceptable and that have been studied in the laboratory and/or applied in the field [17,22,24–30]. One particular “green” chemistry class, carboxy methyl inulins (CMIs), was widely studied [17,24,26,31]. It is reported to be inherently biodegradable [17,26]. Figure 8.2 shows

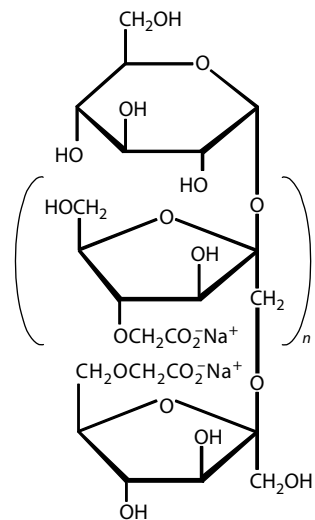


FIGURE 8.2 Carboxy methyl inulin. (From Romero, C. et al., *SPE Prod. Oper.*, 22, 191, 2007. With permission.)

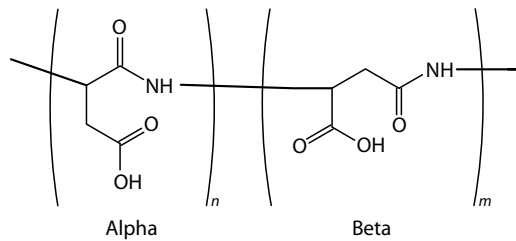


FIGURE 8.3 Poly-alpha, beta-D,L-aspartate. (From Inches, C.E. et al., Green inhibitors: Mechanisms in the control of barium sulfate scale, Paper 06485 presented at *NACE Annual Corrosion Conference & Exposition*, San Diego, CA, 2006. With permission.)

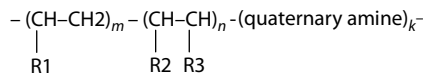


FIGURE 8.4 Structure of a new polymer scale inhibitor (R1 = R2 = R3 = carboxylic function group). (From Chen, P. et al., A scale inhibitor chemistry developed for downhole squeeze treatments in a water sensitive and HTHP reservoir, Paper presented at the *International Oil Field Chemistry Symposium*, Geilo, Norway, 2008. With permission.)

the chemical structure of a CMI. CMIs are found to be effective barium sulfate and calcium carbonate inhibitors, and have good adsorption and desorption properties on limestone substrates. Another “green” chemistry that has been widely studied is polyaspartic acids (polyaspartates) [24,26,31]. A molecular structure of polyaspartates is shown in Figure 8.3.

A comparative laboratory study was carried out on conventional scale inhibitors and environmentally friendly scale inhibitors (referred to as “green” scale inhibitors or GSIs in the referenced paper) [24], and it concluded that (a) “currently available GSIs do work under certain test conditions and would be suitable in terms of inhibition efficiency (IE) to tackle specific milder barium sulfate scaling problems,” and (b) “the GSIs tested do appear to fit into the mechanistic schemes proposed for conventional scale inhibitors. As expected, they generally lie in the polymer region, and operate principally as nucleation inhibition species like PVS and PPCA.”

8.4.2 INHIBITORS WITH ENHANCED FUNCTIONALITY

Several new inhibitor chemistries were reported that provide improvement on inhibitor retention in the formations or squeeze lifetimes [29,32–34]. Two of the papers [32,33] reported successful squeeze treatments using a new polymeric scale inhibitor in an oilfield with severe barium sulfate scaling, where the inhibitor squeeze lifetimes almost doubled over the incumbent inhibitors. Unfortunately, no details were revealed about this inhibitor chemistry. Two other papers [29,34] reported successful squeeze applications of new co-polymer and ter-polymer inhibitors that contain both a carboxylic acid functional group and a quaternary amine monomer. Figure 8.4 shows a schematic drawing of such a ter-polymer. It is very interesting and highly uncommon that one scale inhibitor molecule contains both anionic and cationic groups, especially considering that conventional scale inhibitors are anionic in nature. The authors claim that the positively charged amine group would help the inhibitors to adsorb on the negatively charged sandstone formations.

8.5 SULFATE REMOVAL FROM INJECTION SEAWATER

In offshore production, seawater is commonly injected into petroleum reservoirs to maintain or increase oil recovery. However, with seawater injection, as soon as the injection water breaks through into the production side, barium sulfate scale deposition often becomes a major production problem in the near-wellbore producing formations, production tubulars, and flowlines. This is

a result of commingling of formation brines that are rich in barium ions (typically from 10s to 100s mg/L) and seawater that contains excessive sulfate ions (in high 2000s mg/L).

Conventionally, scale prevention and, to a lesser extent, scale removal on the production side have been the norm of the oilfield scale control measures. However, as the consequence of scale-related operational failure or production loss can be unbearable in deepwater subsea systems and scale-related well interventions are disruptive and often cost-prohibitive, sulfate ion removal from the source injection water has become a more attractive alternative scale prevention strategy [35–40]. Furthermore, the advent in sulfate removal technology has made this alternative strategy more economical and effective.

The common sulfate removal or reduction technology is based on nano-filtration membranes that retain larger ions such as sulfate ions [36,39]. The sulfate-reduced water is then injected into the reservoir [36]. Figure 8.5 provides schematic diagrams of the conventional membrane sulfate removal process. The other sulfate removal technology is based on a reverse osmotic process, but it is more expensive than the membrane technology [36,37].

Since the first commercial implementation of a sulfate removal plant on the Brae field in the North Sea in the early 1980s, this technology has been improved over the years in terms of the extent of sulfate reduction in the seawater [39]. While the first generation of the sulfate removal technology reduced sulfate ions in seawater to about 100 ppm [39], the newer sulfate removal technology on several projects under operation reduces sulfate concentration in seawater to about 40 ppm [36,37]. Today, the technology can routinely reduce sulfate to 20 ppm [39] and it can go lower further almost completely by changing the processing array setup while utilizing the standard membranes [36,39]. By removing the vast majority of the sulfate ions from injection seawater, it either eliminates or dramatically reduces the supersaturation and deposition of barium sulfate in the mixed injection

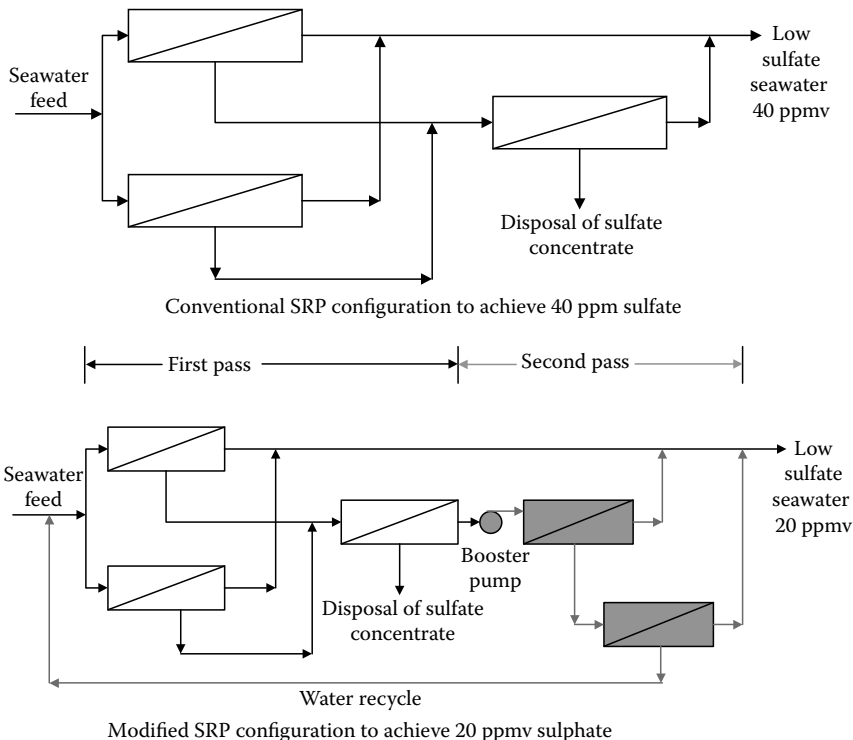


FIGURE 8.5 Schematic diagrams of the conventional 1-pass SRP nano-filtration configuration (sulfate reduction to 40 ppm) compared with 2-pass configuration to achieve 20 ppm. (From Collins, I.R. et al., sulfate removal for barium sulfate scale mitigation in a deepwater subsea production system, Paper SPE87465 presented at the *SPE International Symposium on Oilfield Scale*, Aberdeen, U.K., 2004. With permission.)

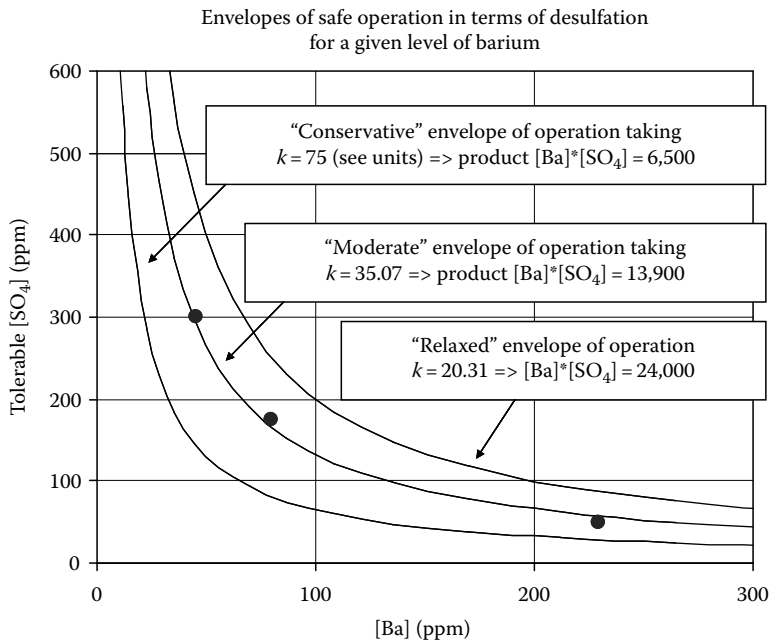


FIGURE 8.6 Envelope of tolerable levels of $[SO_4^{2-}]$ by desulfation for given levels of barium concentration based on the acceptable rate of barium loss from a solution. (From Boak, L.S. et al., what level of sulfate reduction is required to eliminate the need for scale-inhibitor squeezing? Paper SPE95089 presented at the *SPE International Symposium on Oilfield Scale*, Aberdeen, U.K., 2005. With permission.)

water and formation water, and hence the requirement for scale inhibition accordingly. For example, a particular formation brine (containing 170 mg/L barium ions) when mixed with seawater without desulfation would have a severe barium sulfate scaling potential (a saturation index as high as 1.7 and precipitation as much as 230 mg/L) [40]. In contrast, when sulfate is reduced to 20 ppm in the seawater, barium sulfate would become undersaturated across the entire mixing range between the formation brine and seawater.

Modeling and lab studies were carried out to correlate crystal nucleation induction time [39] and deposition kinetics [37] with respect to sulfate reduction in seawater. One study, by coupling laboratory experiments with modeling of barium sulfate deposition kinetics [37], produced envelopes of “safe operation” that correlate the required level of desulfation at any given level of barium ions. Such “safe operation” envelopes are illustrated in Figure 8.6. A separate study [39] developed a relationship of sulfate reduction required to meet a target induction time at a given level of barium ions, with an example shown in Figure 8.7. Although sulfate reduction to a very low level reduces barium sulfate scaling tendency significantly, scale inhibition may still be needed, albeit at a much lower inhibitor concentration [36,37,39]. One experimental study [39] found that a trace level of scale inhibitor might extend the safe range of SO_4^{2-} in the injection water enormously.

There have been studies assessing the cost-effectiveness of installing and operating a sulfate removal facility on an offshore platform or FPSO versus conventional periodic scale inhibition treatments [35,36]. For example, for the Greater Plutonio deepwater project offshore Angola, economic analysis concluded that it would cost the project less over its lifetime by having a sulfate removal plant that reduces seawater sulfate ions to about 40 ppm, and a further economic analysis indicated that by reducing sulfate ions to 20 ppm, it would save the overall project cost by another \$30 million, because at 20 ppm SO_4^{2-} it would eliminate all the scale-related well interventions from the field operating cost [36]. For a specific project, whether to implement a sulfate removal plant for injection seawater or adopt more conventional scale prevention approach should

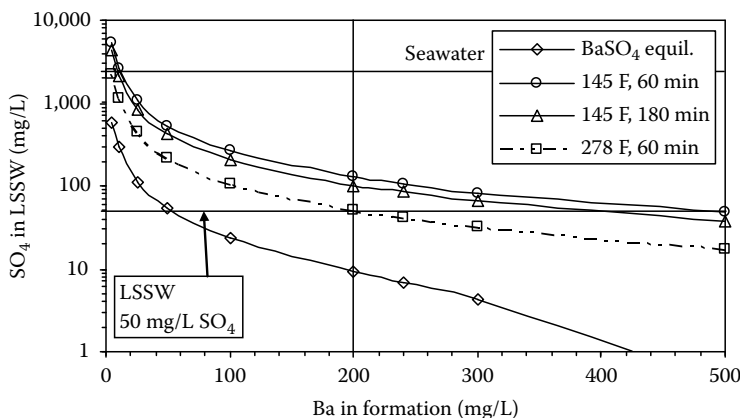


FIGURE 8.7 Plot of Ba^{2+} versus SO_4^{2-} concentration isopleths that (a) is at equilibrium with respect to barite; (b) precipitates after the brine mixed for 60 min at 145°F and 278°F ; and (c) precipitates after the brine mixed for 180 min at 145°F . (From McElhiney, J.E. et al., Design of low-sulfate seawater injection based upon kinetic limits, Paper SPE100480 presented at the *SPE International Symposium on Oilfield Scale*, Aberdeen, U.K., 2006. With permission.)

be determined based on an economic analysis that considers a multitude of factors including field configuration, recovery method, well and flow line construction, potential capital and operating costs, etc. [35,36,38].

8.6 BRINE MIXING, ION EXCHANGE, AND SCALE PRECIPITATION INSIDE OIL RESERVOIRS

Of the recent effort to understand potentials of mineral scaling and their consequences, the most insightful work has been the development of an understanding of brine mixing, ion exchange, and scale precipitation deep inside the oil reservoirs [6,38,41–43]. In produced water containing mixed formation brine and injection water, one would expect the concentration of an ion (e.g., barium, sulfate, or magnesium) in it to change with the injection water fraction in the produced water, namely, the concentration of a particular ion plotted as a function of the injection water fraction would simply following the linear, ideal dilution line from 100% formation brine to 100% injection water. In reality, concentrations of some ions in a produced water would markedly deviate from the ideal dilution line as injection water fraction increases. Figure 8.8 provides a case in point for barium sulfate ions in the produced water from a reservoir formation that contains 180 mg/L Ba^{2+} on average in the native formation water but has since been flooded with seawater. It is clear that the barium concentration in the produced water was only a small fraction of what would be expected based on the ideal dilution line. It turns out that the reduction of barium ions in the produced waters with seawater injection is mainly caused by in situ precipitation of barium sulfate (or barium stripping by sulfate ions) inside the reservoir as the injection water mixes with the native formation water on its way to the production side [6,38,41,42]. In comparison, sulfate ion concentration change often would simply follow the ideal dilution line, which is because SO_4^{2-} in the seawater are usually orders of magnitude higher than $[\text{Ba}^{2+}]$ in the formation water, and the reduction of SO_4^{2-} from precipitation with barium hence was often negligible. However, in a reservoir rich in calcite and with a formation brine high in $[\text{Ca}^{2+}]$, the main scale can be calcium sulfate and sulfate stripping could occur as a consequence [43]. In such a calcium-rich reservoir environment, ion exchange between magnesium ions in the injection seawater and the calcium ions on the calcite solid phase in the reservoir may also take place, which would then result in the depletion of $[\text{Mg}^{2+}]$ and an increase in $[\text{Ca}^{2+}]$ in the produced water [43].

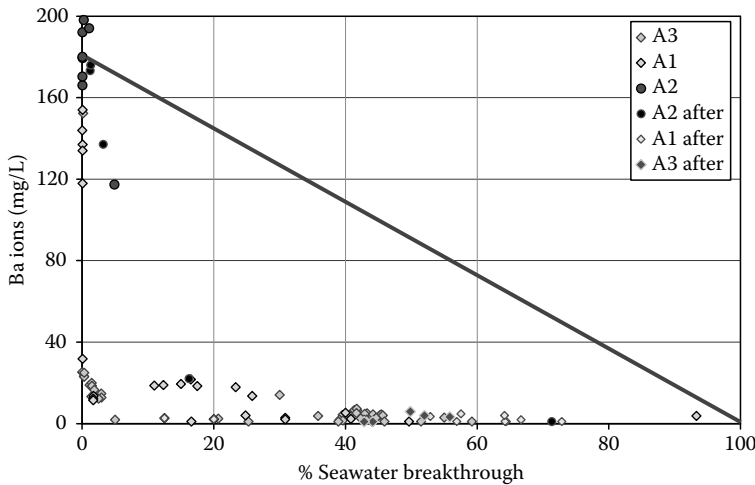


FIGURE 8.8 Barium ion concentration in produced water as a function of calculated seawater cut. The ideal dilution line (—) for barium ions is shown from 100% formation water to 100% seawater. Barium ion concentrations from wells prior to and after scale squeeze treatments are presented. (From Bogaert, P. et al., *SPE Prod. Oper.*, 23, 451, 2007. With permission.)

This cation exchange may exacerbate the sulfate stripping because it makes additional calcium ions available into the aqueous phase. Various computer software programs have been developed and/or used to simulate and predict these processes of brine mixing, ion exchange, and scale precipitation [6,38,41–43]. The simulation studies usually use modified reservoir simulators coupled with near-wellbore, localized models to describe the multiphase fluid flow, brine mixing, reaction, and transport of the ions. However, as there are many factors that can affect the accuracy of a simulation or prediction, care and caution should be taken in using such data when planning scale control options [6,41].

Overall, these recent studies have provided a valuable insight into why scale ion concentrations in the production water vary over time and why they often deviate from the expected “norm.” Such information is useful in forecasting produced water chemistry change, assessing scale risks, planning for scale inhibition treatments, and determining minimum inhibitor requirement.

8.7 IMPACT OF HYDRATE INHIBITORS

Gas hydrates often impose a flow assurance risk in offshore oil and gas production, and gas hydrate formation is often prevented by injecting into the produced fluids large quantities of thermodynamic hydrate inhibitors (THIs) such as methanol and glycols (ethylene glycol and triethylene glycol), or low dosage hydrate inhibitors (LDHIs) such as anti-agglomerants and kinetic hydrate inhibitors. Since THIs are typically dosed at percentage levels (as much as 50%, v/v) in the produced water, it is of great interest and importance to know whether these hydrate inhibitors would affect (a) salt and mineral scale solubility in the produced waters, (b) kinetics of salt and scale precipitation, and (c) scale inhibitor performance against salt and scale precipitation. In the last few years, there has been a substantial amount of research work carried out focusing on the effects of THIs, such as methanol and glycols [44–48]. Methanol, even at only a few volume percent in an oilfield brine, drastically reduces the solubilities of common scale minerals, such as barite, calcite, and gypsum [44,45,48,49]. It has a similar adverse effect on common salts in oilfield brines, such as halite, sylvite, and antarcticite [44,45]. In comparison, glycols have less adverse effects on salt and scale solubilities [44–46,48]. Figure 8.9 shows the effects of methanol present in salt solutions on common sulfate minerals, and Figure 8.10 compares the effects of methanol and glycols on barite solubility.

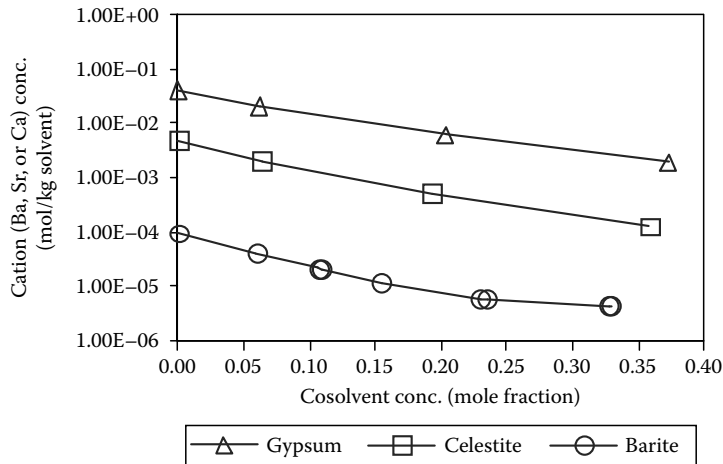


FIGURE 8.9 Plot of Ba, Sr, and Ca concentrations versus methanol concentrations. The Ba, Sr, and Ca concentrations were measured in solutions of dissolution experiments where barite, celestite, and gypsum solids were dissolved in methanol/NaCl (1 M)/H₂O solutions at 25°C and at various methanol concentrations. (From Tomson, M.B. et al., *SPE J.*, 11, 248, 2006. With permission.)

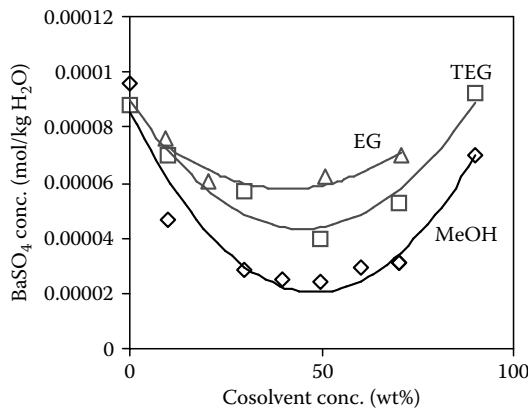


FIGURE 8.10 Plot of barite solubilities in three different hydrate inhibitors/brine combinations. The three types of solution matrices are (1) NaCl-BaSO₄-H₂O-Methanol, (2) NaCl-BaSO₄-H₂O-MEG, and (3) NaCl-BaSO₄-H₂O-TEG. All experiments were done in 1 M NaCl, 25°C. (From Tomson, M.B. et al., *SPE J.*, 10, 256, 2005. With permission.)

Figure 8.11 shows the halite solubilities in the presence and absence of methanol over a range of temperature. In another study [46], solubilities of calcium carbonate and calcium sulfate (both gypsum and anhydrite) in NaCl solutions were experimentally measured as a function of monoethylene glycol concentration.

The recent experimental studies also determined the nucleation induction times of barite scale in the presence of methanol and glycols [45,47,48]. As shown in Figure 8.12, barite nucleation is significantly accelerated by as little as 5% (wt) methanol, and this effect becomes more pronounced at higher methanol concentrations. Similar to their effects on barite solubility, glycols have less adverse effects than methanol on barite induction time. To varied degrees, all the hydrate inhibitors reduce barite nucleation time because of the increase in barite supersaturation and a change in crystal/solution interfacial energy in the presence of the hydrate inhibitors [45,47,48].

Accompanying the experimental studies, mathematical expressions and/or models were developed to calculate or predict the effects of hydrate inhibitors on salt and scale solubilities and precipitation.

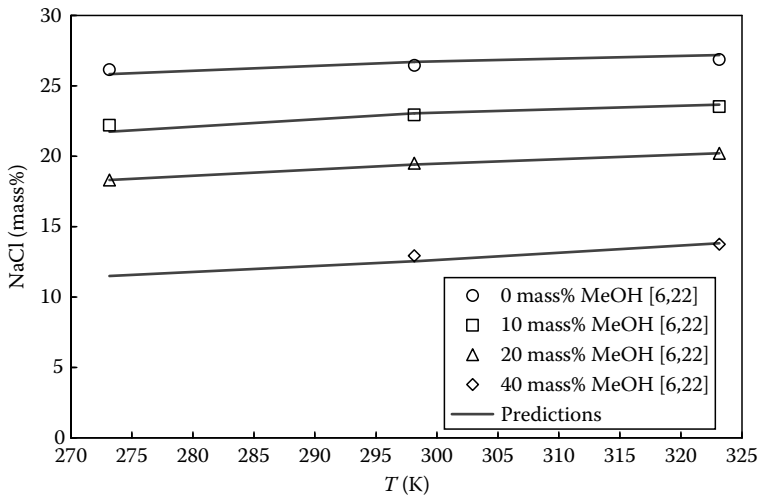


FIGURE 8.11 Experimental and calculated maximum soluble mass of NaCl in aqueous methanol solutions as a function of temperature and MeOH concentrations. MeOH concentrations are shown on a salt-free basis. (From Masoudi, R. et al., *SPE Prod. Oper.*, 21, 182, 2006. With permission.)

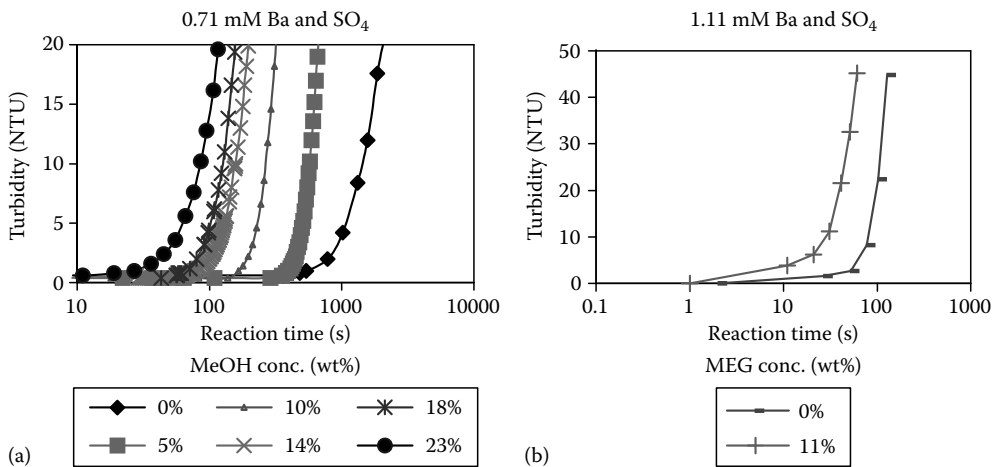


FIGURE 8.12 Effect of (a) methanol and (b) MEG on nucleation rate of barite at 25°C. For the methanol experiments, the solutions contained 1 M NaCl, 0.1 M CaCl₂, 0.71 mM of Ba²⁺ and SO₄²⁻ and 5 mM PIPES buffer at pH 6.42 and various concentrations of methanol. For the MEG experiments, the solutions contained 1 M NaCl, 1.116 mM of Ba²⁺ and SO₄²⁻ and 0 and 11 wt% of MEG. (From Tomson, M.B. et al., *SPE J.*, 10(3), 256, 2005. With permission.)

An activity model was developed to predict salt and mineral solubilities in hydrate inhibitors/water/salt solutions, which uses the Pitzer theory of ion interactions to model the salt effect and the Born equation to model methanol effect on the salt and mineral solubilities [45,48]. The impact of hydrate inhibitors on the nucleation rates of barite can be predicted by semiempirical equations of classical nucleation theory [45,47,48]. Another thermodynamic model was developed to predict salt formation in multi-salt systems with or without hydrate inhibitors, which is based on the equality of the fugacities of salt in solid phase and in aqueous phase where an equation of state is used to calculate the salt fugacities [44]. In a separate research study [46], a scale prediction model was upgraded to simulate the effects of ethylene glycol on CO₂ equilibria, solution pH, and solubilities of common scales. The model is based on a semiempirical approach that combines an ion activity model and curve fitting of the solubility data.

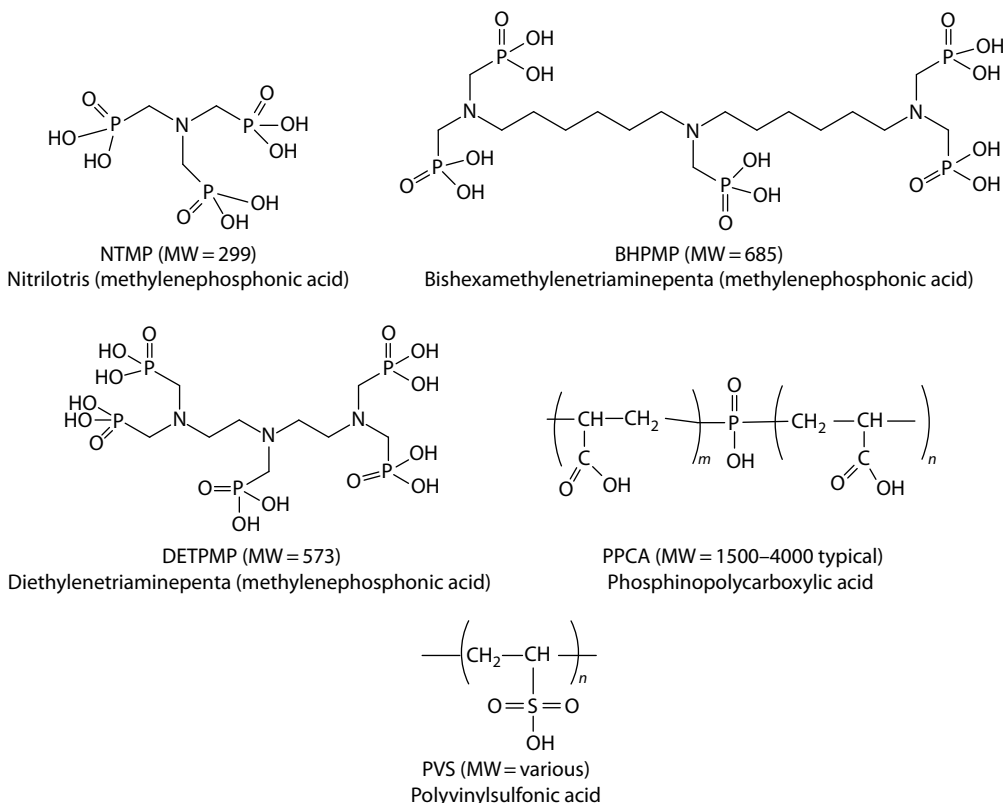


FIGURE 8.13 Common oilfield scale inhibitors.

Laboratory experiments were also carried out to study hydrate inhibitor's effects on scale inhibitor performance, as measured by the nucleation induction rates of barite [45,47,48]. Several scale inhibitors were examined, including bishexamethylenetriaminepenta (methylenephosphonic acid) (BHPMP), nitrilotris (methylenephosphonic acid) (NTMP), and phosphinopolycarboxylic acid (PPCA) [45,47,48]. The molecular structures of these common oilfield inhibitors are shown in Figure 8.13. It was found that scale inhibitor efficiency was severely impaired by methanol. For example, in a 20% methanol solution, the MIC of BHPMP is increased by a factor of 6 when compared to its MIC in a methanol-free solution [47]. At high methanol concentrations, due to a combination of increased supersaturation and possible formation of phosphonate metal salts, barite scale inhibition by phosphonates may become impossible [47,48]. Compared to methanol, glycols exhibited less adverse effects on the scale inhibitor performance [45,47,48]. In these studies, the authors also used a semiempirical nucleation inhibition model to predict the effects of hydrate inhibitors on scale inhibitor efficiency, expressed in terms of barite nucleation induction time and scale inhibitor's MIC. These research findings highlight a need to consider the potentially dramatic impact of thermodynamic hydrate inhibitors on scale formation and inhibition. Neglect or underestimate of such effects could have catastrophic consequences [49].

8.8 FUNDAMENTAL STUDIES ON SCALE FORMATION, INHIBITION, AND INHIBITOR–ROCK INTERACTIONS

Parallel to developing practical application technologies and inhibitor products, there has been a substantial amount of fundamental and mechanistic studies over a wide range of scale topics in recent years. Of these studies, the majority of the work can be captured in three topical areas: (a) scale

formation (nucleation, precipitation, and deposition), (b) scale inhibition, and (c) scale inhibitor interactions and reactions with rock substrates and minerals.

8.8.1 SCALE FORMATION, PRECIPITATION, AND DEPOSITION

A number of researchers have investigated scale nucleation induction, crystal growth and morphology, and various influencing factors such as ion composition, supersaturation, and temperature [50–60]. Several rather insightful and interesting studies focused on the simultaneous bulk solution precipitation and surface deposition processes of scale formation by using two novel and powerful techniques. One is based on a rotating disk crystallizer (RDC), which is also called the rotating disk electrode (RDE) [50–54], and the other utilizes synchrotron radiation wide angle x-ray scattering (WAXS) technique, which is also referred to as synchrotron XRD (SXRD) [55,57,58,60]. The detailed descriptions of the RDC and SXRD instruments and the corresponding experimental setups can be found in the referenced papers.

As bulk solution precipitation in a clean, filtered brine is a homogeneous process and surface deposition is a heterogeneous process where the metal surface acts as the nucleation sites, the recent study using an RDC [52] confirms that bulk solution precipitation and surface deposition have different dependencies on the index of supersaturation. The scale nucleation and crystal growth at low supersaturation indexes are found to be rapid on the metal surface, while bulk nucleation and crystal growth appear slow. It is also found that submicron-size particles formed in the initial nucleation period are the main contribution to the coverage in the initial stages of surface scale formation. Crystals formed on the surface are larger than those formed in the bulk solution, as heterogeneous conditions promote crystal growth.

Since magnesium ions are a common ion species in both oilfield formation waters and injection waters, studies were carried out to investigate their effect on the precipitation and deposition of calcium carbonate scale by using the RDC technique [50,51,53,54]. Several interesting findings emerged from this investigation. Mg^{2+} adsorbs on the deposited scale crystals. Mg/Ca ratio in the deposit on the metal surface is proportional to the $[Mg^{2+}]/[Ca^{2+}]$ ratio in the scaling water (as shown in Figure 8.14), but the distribution coefficient in the surface deposition and in the bulk solution is a constant, independent of $[Mg^{2+}]$ in the bulk solution. Magnesium accelerates crystal transformation from vaterite to calcite. Magnesium ions adsorbed on calcium carbonate crystals increase the crystal surface roughness as well as distort crystals (as presented in Figure 8.15). Magnesium ions appear to inhibit both bulk precipitation and surface deposition of calcium carbonate, as both the

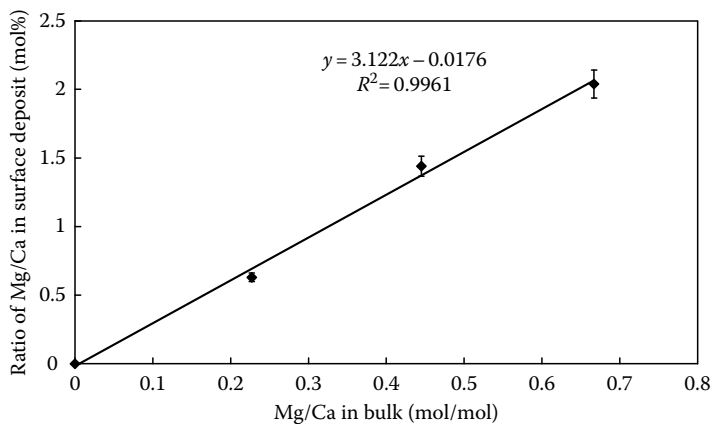


FIGURE 8.14 Ratio of Mg^{2+} incorporated in the scale formed on the metal surface under 1500rpm RDE condition for 8 h at 20°C. (From Chen, T. et al., *Chem. Eng. Sci.*, 61, 5318, 2006.)

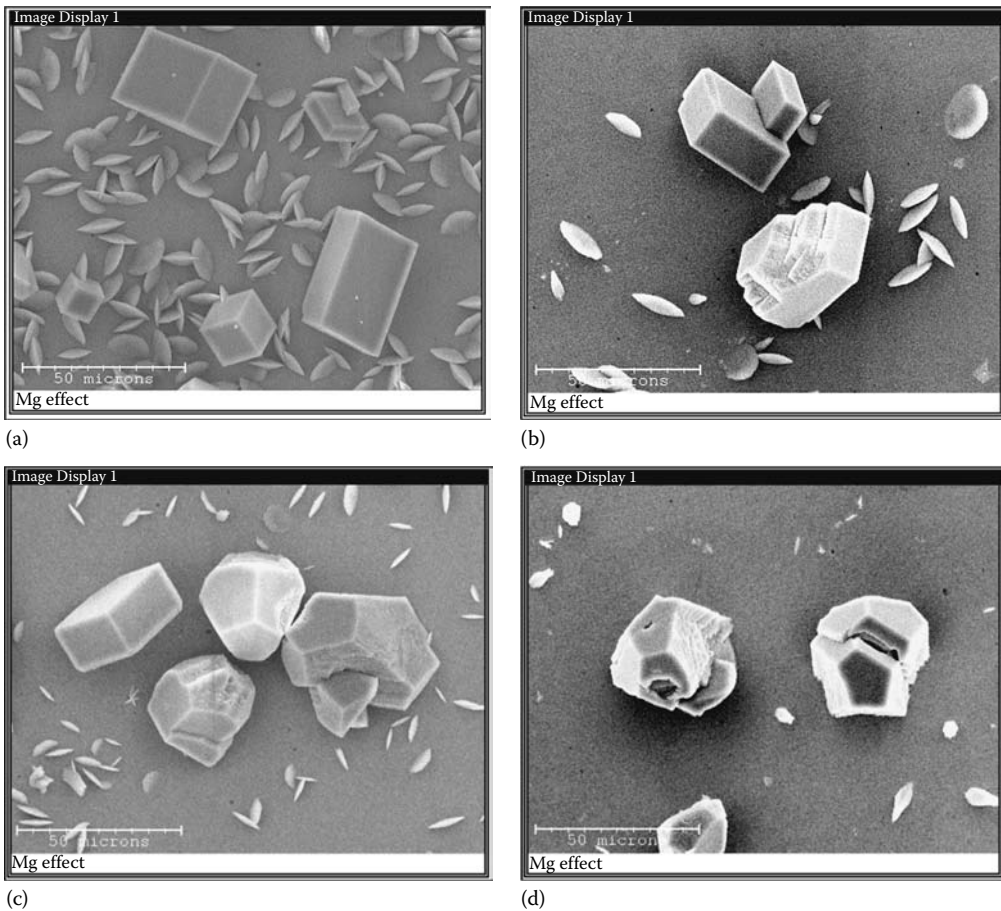


FIGURE 8.15 Microscopy of calcite formed under different Mg^{2+} concentration scale formation solutions at 8 h under static conditions with RDE at $20^{\circ}C$: (a) 0 ppm Mg^{2+} ; (b) 200 ppm Mg^{2+} ; (c) 400 ppm Mg^{2+} ; and (d) 600 ppm Mg^{2+} . (From Chen, T. et al., *Chem. Eng. Sci.*, 61, 5318, 2006.)

quantity and the number of crystals of scale deposit and bulk precipitate decrease with increase of $[Mg^{2+}]$ in the solution, and calcite induction time increases considerably with increased $[Mg^{2+}]/[Ca^{2+}]$ ratio in the solution.

The SXRDR technique allows the study of both bulk precipitation and surface deposition in the same system. It takes only about 10 s to analyze a scale sample, thus this technique provides a powerful tool for in situ, real-time measurement of crystal nucleation, crystal growth, crystal polymorphs, and the evolution of their individual planes. Most of the SXRDR study is focused on the growth of various calcareous polymorphs and the evolution of their individual crystal planes as calcium carbonate scaling brine flows through the scaling capillary [55,57,58]. In a silicon reaction cell, the initial phase of crystallization of $CaCO_3$ is characterized by instability with individual planes from various vaterite and aragonite polymorphs emerging and subsequently disappearing (flushed out) under hydrodynamic conditions. After the initial unstable phase, various calcium carbonate crystal planes (mainly calcite) begin to adhere, then grow on the surface, and various planes from the vaterite and aragonite polymorphs appear again as calcite growth appears to stimulate the adherence of vaterite and aragonite. Figure 8.16 shows an example of SXRDR detection of calcium carbonate crystal growth over time. The main planes of crystals are found to depend on temperature, as temperature elevation increases the surface growth of calcium carbonate crystals.

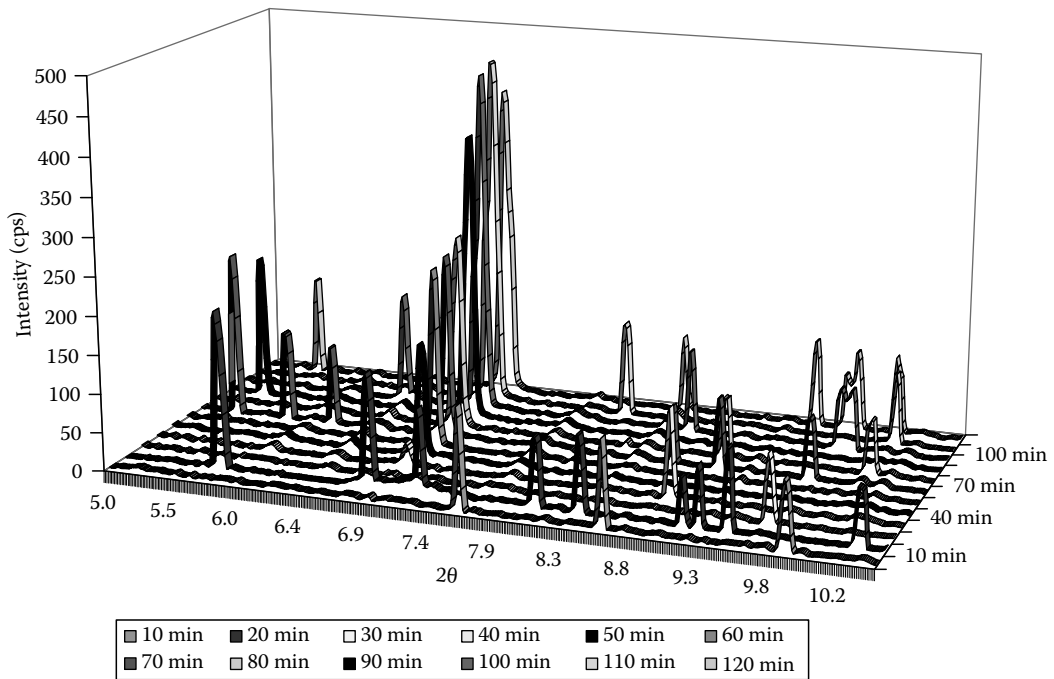


FIGURE 8.16 The growth of calcium carbonate crystals at 25°C detected by SXR. (From Chen, T. et al., *Faraday Discuss.*, 1361, 2007. With permission.)

A subsequent study by the same authors used a metal (stainless steel) reaction cell instead of the silicon reaction cell [60]. Different results in terms of crystal phases and their stability are found between the steel substrate and the silicon substrate. On the steel surface, all the calcium carbonate plane peaks are almost stable from the initial spectra at 2 min, which is contrary to the results obtained with the silicon substrate. It appears that the crystals adhere to the stainless steel cell and they are stable after very short times. The main peaks are mostly vaterite and aragonite, and only one is characteristic of calcite. By comparison, when the silicon substrate was used, the calcite planes were the most abundant. One important difference between the silicon and the stainless steel substrates is the peak intensity. For example, the greatest intensity is observed with the calcite (104) plane on the silicon substrate but with the vaterite (110) plane on stainless steel.

Besides the work using RDC and SXR techniques, other experimental studies on scale formation concentrated on the kinetics of barium sulfate (barite) precipitation, deposition, and dissolution [56,59]. One study [56] shows that at higher concentrations of both barium and sulfate ions, the barite precipitate rate is rapid but it slows down considerably as the concentration of one of the ions is reduced to a sufficiently low level. The experimental deposition rate data is broadly consistent with a simple rate law. The experiments demonstrate that seeding the tests with barite or sand particles accelerates the approach to barite saturation equilibrium, especially in the presence of excess of fine barite particles. The other experimental study [59] examines the kinetics of both barite precipitation and dissolution processes. It is found that, on the one hand, the dissolution reaction is normally very fast going from undersaturation to saturation; on the other hand, the precipitation reaction is often slow going from supersaturation to saturation.

8.8.2 SCALE INHIBITION

The RDC and SXR techniques were also used by the researchers to study scale inhibition by two common oilfield scale inhibitors, phosphinopolycarboxylic acid (PPCA) and diethylenetriaminepenta

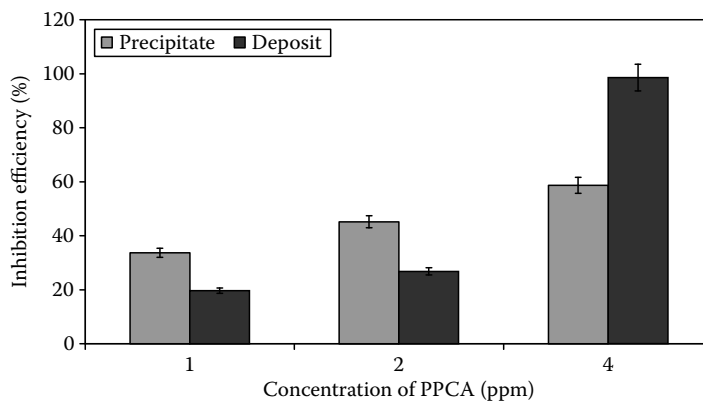


FIGURE 8.17 Comparison of inhibition efficiency of PPCA on bulk precipitation and surface deposition at 80°C after 4 h. (From Chen, T. et al., *Prog. Nat. Sci.* (special issue), 35, 2005.)

(methylenephosphonic acid) (DETPMP) as well as their blends [55,57,60–62]. In the study on calcium carbonate inhibition at 80°C using the RDC technique [61,62], PPCA delays the nucleation and growth of both bulk precipitation and surface scaling of CaCO_3 especially in the initial stages. PPCA has a profound effect on the kinetics and morphology of CaCO_3 scale formation. PPCA suppresses calcite and aragonite crystal formation and results in less-stable vaterite crystals dominating the scale. Calcite crystals appear to adhere on the surface tightly while vaterite and aragonite crystals only loosely. Although PPCA inhibits both bulk precipitation and surface deposition, it varies from bulk to surface to a different degree. For example, Figure 8.17 shows that, at 4 ppm, PPCA IE of surface deposition is greater than that of bulk precipitation, but the opposite is true at 1 and 2 ppm. It is proposed that the inhibitor forms a film on the metal surface that prevents the adhesion of scale crystals onto the surface. Inhibitors increase the nucleation time of calcium carbonate in bulk precipitation by the following ranking: PPCA > Blends > DETPMP. The blends, however, have a greater inhibiting efficiency than PPCA or DETPMP alone for surface deposition at the concentrations studied (0.02, 0.04, and 0.08 ppm). It is postulated that a combination of larger PPCA molecules and smaller DETPMP molecules could form a denser, less porous film on the surface than that formed by PPCA alone, which thus provides more effective inhibition of calcium carbonate deposition.

In the calcium carbonate scale inhibition experiments using SXRD [57], PPCA is shown to inhibit surface deposition on the silicon substrate. Similar to what is seen on the RDC metal surface [61,62], it suppresses calcite formation and results in a vaterite-dominated scale. PPCA has a profound effect on the induction time of surface deposition. The induction time of surface deposition increases with an increase of PPCA concentration in the scaling solution. Figure 8.18 illustrates the effect of PPCA on the crystal planes. In a parallel study on the effect of DETPMP on calcium carbonate scale inhibition [55], DETPMP similarly shows a profound effect on the induction time of scale deposit by inhibiting scale crystal adhesion on the surface, even though bulk precipitation is occurring. It exhibits different inhibition mechanisms for bulk precipitation and surface deposition inhibition. Similar to PPCA, DETPMP suppresses calcite formation and results in the least stable vaterite crystal formation on the surface. In a follow-up study using a metal (stainless steel) reaction cell [60], PPCA inhibitor is shown to promote the growth in intensity of certain CaCO_3 crystal faces, which is consistent with what was found on the silicon substrate. While aragonite is the most abundant CaCO_3 polymorph on the metallic substrate in the absence of scale inhibitor, the scale formed in the presence of PPCA is vaterite/aragonite dominated. In comparison, the scale deposited on the silicon substrate was vaterite/calcite (inhibited) and calcite (uninhibited).

Several other studies [63–66] attempted to develop further understanding of scale inhibition mechanisms by investigating solution chemistry, scale inhibitor speciation, inhibitor–crystal interactions,

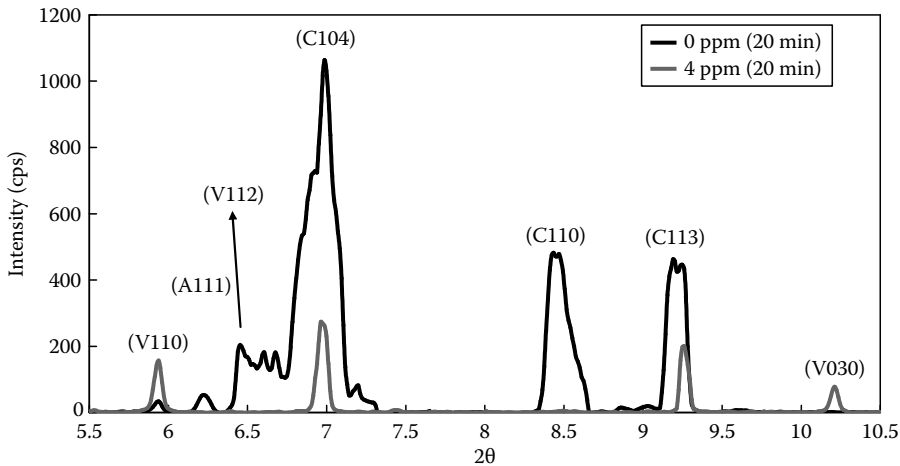


FIGURE 8.18 Comparison of calcium carbonate scales formed in the absence of PPCA and in the presence of 4 ppm PPCA after 20 min. (From Chen, T. et al., *CORROSION/06* Paper 06386 presented at *NACE Annual Corrosion Conference & Exposition*, San Diego, CA, 2006. With permission.)

and various influencing factors such as temperature, solution pH, $[Ca^{2+}]$, and $[Mg^{2+}]$, the key findings of which are summarized in the following section.

In one experimental study [63], phosphonate scale inhibitors are found to adsorb similarly on scale surfaces regardless of scale mineral type, and the scale inhibitors show similar inhibition efficiencies on different types of scales. It requires 16% surface coverage by a scale inhibitor to reach maximum inhibition. Excessive sulfate ions in the solution are seen to drastically reduce phosphonate adsorption on barite. These authors propose that scale inhibitor adsorption on a mineral surface is driven by the macro-neutral molecule's hydrophobic repulsion from the solution rather than the mineral surface attraction. In a different study [65], however, the researchers observed no direct correlation between scale inhibitor adsorption on barite and their IE. Those researchers instead postulated that scale inhibitor molecules are incorporated into the scale crystal lattice. They also reported that only deprotonated scale inhibitor molecules inhibit barite. Furthermore, via a series of static jar tests and tube-blocking flow tests, they compared three scale inhibitors, DETPMP, PPCA, and PVS (polyvinylsulfonic acid), in relation to their relative sensitivities to solution pH, temperature, $[Ca^{2+}]$, and $[Mg^{2+}]$. Their previous findings on how different inhibitors work are reaffirmed, namely, PVS is predominantly a nucleation inhibitor, DETPMP on the contrary is primarily a crystal growth inhibitor, and PPCA exhibits an "intermediate" behavior. With respect to temperature, DETPMP IE correlates to barite supersaturation ratios at different temperatures (i.e., higher temperatures (faster kinetics) \rightarrow lower supersaturation \rightarrow higher IE); PVS IE instead follows the nucleation kinetics (lower temperatures (higher supersaturation but slower kinetics) \rightarrow slower nucleation \rightarrow higher IE); and PPCA shows an "intermediate" behavior. Since only the deprotonated inhibitor molecules are effective at scale inhibition, PVS will inhibit scale down to a much lower pH than DETPMP does, owing to its having a much lower "mean" pK_a (~ 3.0) than that of DETPMP (~ 4.5). There is a significant amount of calcium ion (4%–12%) inclusion in the barite lattice, but there is no magnesium inclusion. Calcium inclusion decreases the lattice parameter (a -axis), which retards the lattice growth or makes growth easier to inhibit. At relatively high $[Ca^{2+}]/[Mg^{2+}]$ ratios, calcium ions enhance DETPMP IE by complexing the inhibitor first then incorporating it in the barite lattice to disrupt the crystal growth. In contrast, magnesium ions "poison" DETPMP IE as follows: as magnesium ions compete with calcium ions for DETPMP in the solution via complexation, magnesium reduces the number of DETPMP molecules available for calcium complexation, hence their subsequent inclusion in the barite lattice. Calcium ions only show modest enhancement on barite IE of

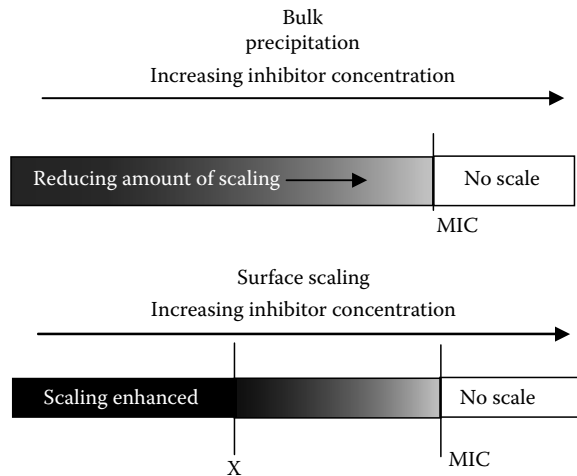


FIGURE 8.19 Schematic diagram of surface and bulk scaling scenarios. (From Graham, A.L. et al., *SPE Prod. Oper.*, 21, 19, 2006. With permission.)

PVS and PPCA, as these inhibitors mainly operate through nucleation inhibition rather than crystal growth retardation. For the same reason, magnesium ions show little effect on PVS and PPCA IE.

Another laboratory investigation examined the effects of PPCA scale inhibitor on barite scale bulk precipitation and surface deposition when its concentration in the solution is less than the MIC required for bulk precipitation [64,66]. It finds that the presence of a scale inhibitor at marginally below the MIC actually enhances scale growth on a metal surface over a range of temperatures typically encountered in production systems (5°C, 50°C, and 95°C). In other words, this result suggests that inhibitor concentration falling below MIC will still reduce bulk precipitation, but it could promote surface scaling. This phenomenon is illustrated in Figure 8.19.

8.8.3 SCALE INHIBITOR INTERACTIONS AND REACTIONS WITH ROCK SUBSTRATES

Recent studies in this area have focused on calcite and calcite-rich rocks. A series of experiments were carried out to investigate reactions between calcite and calcite-rich formation rocks and several common phosphonate scale inhibitors, NTMP, DETPMP, and BHPMP, as well as a polymeric inhibitor, PPCA [67–71]. The researchers conclude that, other than rock mineralogy, inhibitor and solution chemistry is also an important determinant for inhibitor retention and release, and adsorption/precipitation of phosphonates to calcite-rich formation rock material is essentially identical to the adsorption/precipitation of phosphonates to pure calcite after normalizing the rock surface by calcium content [68,70]. It is proposed that an acidic scale inhibitor solution goes through a series of reactions with calcite: acid dissolution of calcite, phase separation, formation of a crystalline Ca–phosphonate layer at the solid–liquid interface, slow dissolution of calcite, and formation of several different Ca–phosphonate solid phases [68]. The inhibitor concentrations are determined by adsorption mechanisms at low concentrations and precipitations at high concentrations [67]. At low inhibitor concentrations (<1 μmol/L NTMP), the reaction proceeds like a Langmuir-type adsorption, followed by crystal growth of a low-solubility calcium salt at the calcite–water interface (4–5 layers of Ca–phosphonate solid phase with stoichiometry of Ca_{2,5}HNTMP) [68,69]. At high inhibitor concentrations, the inhibitor/calcite reaction is limited by solution phase [Ca²⁺] due to surface inhibition controlling calcite dissolution. For example, only about 8% of the surface is covered with NTMP before reaching maximum adsorption. In the solution the high concentrations of phosphonate and dissolved calcium induce the formation of more soluble, less crystalline mixed solid phases of Ca–phosphonate salts [68,69]. Apparently the inhibitor adsorption occurs at the kink sites or step

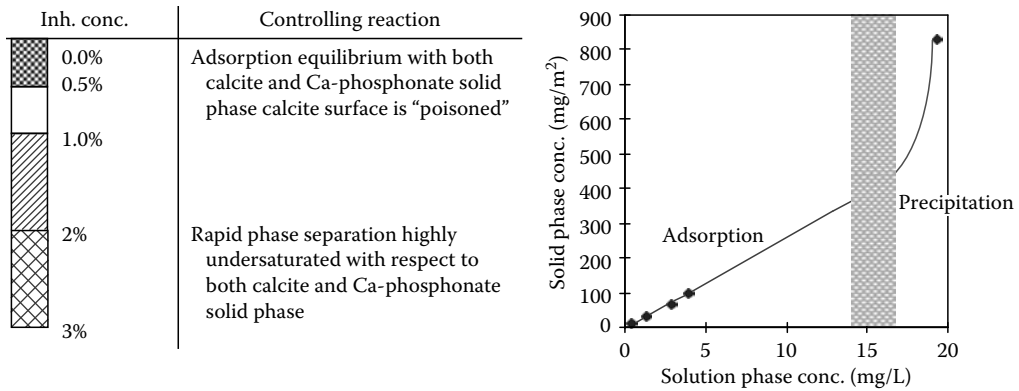


FIGURE 8.20 Summary of observations on inhibitor/core reactions. (From Kan, A.T. et al., *SPE J.*, 9, 280, 2004. With permission.)

edges on calcite solid phase. Figure 8.20 schematically summarizes the key observations on the inhibitor/core material reactions. These authors postulate that two reactions are central to inhibitor retention in a Ca-rich formation [67]: (a) calcite surface poisoning by Ca-inhibitor coating leading to reduction of calcite dissolution, and (b) precipitation of solid with either low or high Ca stoichiometry. For example, an acidic Ca-NTMP salt is formed in a low pH environment, and additionally two crystalline phases and one amorphous Ca-NTMP salt may form. It is found that different inhibitors at similar weight percent concentrations exhibited different surface poisoning effects, which is perhaps responsible for their varied behaviors during inhibitor squeeze applications. Calcite poisoning limits the release of base (HCO_3^-), thus keeping the solution more acidic and allowing more soluble Ca-phosphonate solid phase to form.

In a further experimental study of NTMP and calcite reactions in calcite packed columns that simulate scale inhibitor squeeze injection and back flow, these authors found that three Ca-NTMP solid phases, one amorphous and two crystalline, are particularly important for the inhibitor retention [70]. For an acidic pill, approximately 78% of the phosphonate precipitated mostly near the injection port. In contrast, for a neutralized pill, about 50% of the SI precipitated at the rear end of the column. Figure 8.21 shows precipitated phosphonate distribution in the column versus inhibitor neutralization. A portion of the phosphonate was retained as a crystalline salt (Ca_2HNTMP , $\text{p}K_a$ 24.2) and another portion as more soluble salts ($\text{p}K_a$ 22.6 and $\text{p}K_a$ 21.3). The long-term phosphonate return

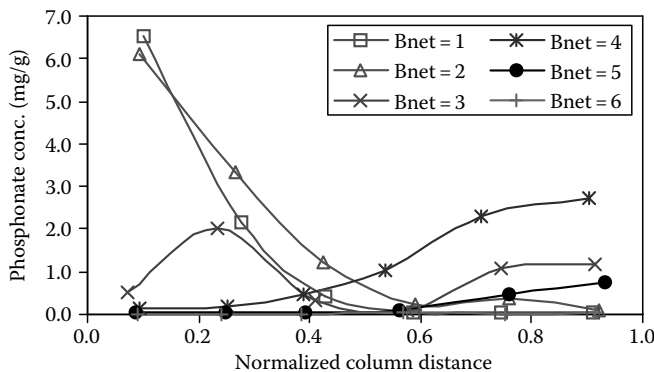


FIGURE 8.21 Plot of solid-phase phosphonate distribution versus normalized column length for Experiments 8 through 10 and 12 through 14, where the phosphonate concentrations were 4% and the inhibitor pills were neutralized to different degrees (Bnet = 1–6). (From Tomson, M.B. et al., *SPE J.*, 11, 283, 2006. With permission.)

was controlled by the pK_a 22.6 phase that gives a 23 mg/L return concentration, and the final returned phosphonate concentration always drops to 0.3 mg/L, resulting from the pK_a 24.2 phase. This study proposes that the scale inhibitor forms a monomolecular coverage on calcite, which “poisons” the calcite surface and limits calcite dissolution, which is inconsistent to the early findings by the same authors that indicate four to five NTMP layers form at the liquid/calcite solid [68,69]. Neither a Langmuir-type adsorption (or desorption) at very low inhibitor concentrations was mentioned in these more recent studies, as compared to their earlier publications.

Other researchers [72,73] investigated DETPMP inhibitor interactions with carbonate rocks by carrying out a series of core flooding experiments using consolidated carbonate cores comprised of almost pure calcite. One set of the core floods [72] used short cores (2.5 in. in length). Into each core, more than *10 pore volumes* (PVs) of an inhibitor pill (5000 ppm DETPMP in a synthetic seawater) was injected that fully saturated the core with inhibitor. After a shut-in, the core was continuously injected in the same direction with a synthetic seawater as postflush brine until inhibitor residuals in the effluent samples dropped to a low concentration (around 10 ppm). These core floods focused on the effect of the solution pH on the inhibitor–rock interactions by using three inhibitor/postflush brine pHs, 5.81, 4.0, and 2.0, respectively. These core floods find more carbonate dissolution and higher phosphonate retention at pH 4 than at pH 5.81. The effluent solutions from pH 4 and pH 5.81 floods have become neutralized by carbonate dissolution in the cores, reaching about pH 7. With pH 2 inhibitor solution and postflush brine, a “wormhole” was created throughout the length of the core, as a result of dissolution of a large quantity of calcite by the acidic solution.

The same researchers went on to conduct core floods in long (12 in. in length) “contained” cores [73]. In such a core flood, the core was injected with *only one pore volume* of DETPMP solution of 5,000 or 10,000 ppm at pH 4 or 25,000 ppm at pH 2. After a shut-in, the core was injected with a pH 6 postflush brine in a *reversed* direction. Compared to the earlier core floods with short cores with multipore volume inhibitor injection and unidirectional postflush, this new experimental setup provides better resemblance to an actual scale inhibitor squeeze application. From these core floods, DETPMP was found to be strongly bound to magnesium and calcium ions. Calcium dissolution occurred during inhibitor injection and shut-in, which more than compensated for calcium depletion from solution by Ca–phosphonate complexation. Core permeability after floods increased as a result of calcite dissolution. Phosphonate salts were found in the pore voids, more so at a high inhibitor concentration and a lower solution pH.

8.9 MISCELLANEOUS DEVELOPMENTS

Although this review article endeavors to capture as much of the latest oilfield scale research and development work as possible, the limited knowledge and research of the subject on the author’s part has undoubtedly failed to present some other important developments in oilfield scale control in this chapter. For those readers who would like to explore additional topics, references to some of the other new developments are briefly listed as follows: prevention and control of unconventional (exotic) scales [74–80], combination products [22,81,82], scale and inhibitor detection techniques [28,83–85], scale prediction [46,86], scale removal [30,77,87], inhibitor tagging [83], and scale inhibitors products based on nanotechnology [88,89].

8.10 SUMMARY

Although oilfield scale has been a mature production problem, many new developments in the oil and gas industry such as deepwater subsea fields and complex horizontal wells and the need for maximizing production and reducing cost have presented new challenges and opportunities to advance mineral scale control products, application techniques, and the fundamental understanding of scale formation, deposition, and inhibition. With this background, this chapter summarizes the latest developments in oilfield scale control and, in particular their impacts on oil and gas

production from offshore deepwater or subsea production systems and/or complex production wells. Specifically, this chapter reviews the following pertinent areas of recent advances in scale control technology, namely, (a) viscosified fluids for improving scale inhibitor squeeze placement, (b) non-aqueous scale inhibitor squeeze treatments for minimizing formation damages, (c) new inhibitors for enhanced functionality, improved secondary properties or improved environmental profile, (d) sulfate ion removal from injection seawater as an alternate scale control technique, (e) brine mixing, ion exchange, and their implications on produced water chemistry and scale deposition, and (f) the effect of hydrate inhibitors on scale formation and inhibition. In addition, this chapter also presents a review of the recent advances in mechanistic understanding of scale nucleation, precipitation, and deposition, scale inhibition, and scale inhibitor–rock interactions.

ACKNOWLEDGMENTS

The author would like to acknowledge many of his peers in the oilfield scale community, who kindly provided copies of their publications for the author to review. The scientists and engineers working in this field deserve all the credits for the recent technological advances and breakthroughs in oilfield scale control. The author would also like to thank Baker Petrolite Division of Baker Hughes Incorporated for its permission to publish this chapter.

REFERENCES

1. Stalker, R., Graham, G. M., Oliphant, D., and Smillie, M. Potential application of viscosified treatments for improved bullhead scale inhibitor placement in horizontal wells—a theoretical and laboratory examination. In: Paper SPE87439 presented at the *SPE International Symposium on Oilfield Scale*, Aberdeen, U.K. (2004).
2. James, J. S., Frigo, D. M., Townsend, M. M., Graham, G. M., Wahid, F., and Heath, S. M. Application of a fully viscosified scale squeeze for improved placement in horizontal wells. In: Paper SPE94593 presented at the *SPE International Symposium on Oilfield Scale*, Aberdeen, U.K. (2005).
3. Sorbie, K. S. and Mackay, E. J. Scale inhibitor placement: Back to basics—theory and examples. In: Paper SPE95090 presented at the *SPE International Symposium on Oilfield Scale*, Aberdeen, U.K. (2005).
4. Stalker, R., Graham, G. M., and Wahid, F. Stimulating chemical placement in complex heterogeneous wells. In: Paper SPE100631 presented at the *SPE International Symposium on Oilfield Scale*, Aberdeen, U.K. (2006).
5. Sorbie, K. S., Mackay, E. J., Collins, I. R., and Wat, R. Placement using non-Newtonian scale inhibitor slugs: The effect of shear thinning. *SPE Production & Operations*, 22(4), 434–441 (2007).
6. Bogaert, P., Berredo, M. C., Toschi, C., Jordan, M. M., Frigo, D. M., Morgenthaler, L., Bryson, B., and Alfonso, M. Scale inhibitor squeeze treatments deployed from a FPSO in deepwater, subsea fields in the Campos Basin. *SPE Production & Operations*, 22(4), 451–471 (2007).
7. Stalker, R., Butler, K., Graham, G. M., and Wahid, F. Maximizing chemical placement in complex wells. In: Paper SPE106498 presented at the *SPE International Symposium on Oilfield Chemistry*, Houston, TX (2007).
8. Stalker, R., Butler, K., Graham, G. M., Wat, R., Hauge, L.-E., and Wennberg, K. E. Evaluation of polymer gel diverters for a high-temperature field with special focus on the formation shape factor — an important parameter for enhancing matrix placement of stimulation chemicals. In: Paper SPE107806 presented at the *European Formation Damage Conference*, Scheveningen, the Netherlands (2007).
9. Selle, O. M., Springer, M., Auflem, I. H., Chen, P., Matheson, R., Mebratu, A., and Glasbergen, G. Gelled scale inhibitor treatment for improved placement in long horizontal wells at Norne and Heidrun fields. In: Paper SPE112464 presented at the *SPE International Symposium and Exhibition on Formation Damage Control*, Lafayette, LA (2008).
10. Wylde, J. J. and McAra, E. K. Optimization of an oil soluble scale inhibitor for minimizing formation damage: Laboratory and field studies. In: Paper SPE86477 presented at the *SPE International Symposium and Exhibition on Formation Damage Control*, Lafayette, LA (2004).
11. Heath, S. M., Wylde, J. J., Archibald, M., and Sim, M. Development of oil soluble precipitation squeeze technology for application in low and high water cut wells. In: Paper SPE87451 presented at the *SPE International Symposium on Oilfield Scale*, Aberdeen, U.K. (2004).

12. Chen, P., Hagen, T., Bourne, H., Turner, K., Nielsen, F. M., Rian, M., and Haldoupis, A. The challenge of squeezing a water sensitive HP/HT reservoir: Lab and field experiences with a novel non aqueous inhibitor/enhancer package. In: Paper SPE87435 presented at the *SPE International Symposium on Oilfield Scale*, Aberdeen, U.K. (2004).
13. Miles, A. F., Vikane, O., Healey, D. S., Collins, I. R., Saeten, J., Bourne, H. M., and Smith, R. G. Field experiences using "oil soluble" non-aqueous scale inhibitor delivery systems. In: Paper SPE87431 presented at the *SPE International Symposium on Oilfield Scale*, Aberdeen, U.K. (2004).
14. Guan, H., Sorbie, K. S., Yuan, M., and Smith, K. Non-aqueous squeeze treatments in sandstones: Core flood studies and modeling. In: Paper 04386 presented at *NACE Annual Corrosion Conference & Exposition*, New Orleans, LA (2004).
15. Wyld, J. J. The advent of a truly oil soluble scale inhibitor. In: Paper 04384 presented at *NACE Annual Corrosion Conference & Exposition*, New Orleans, LA (2004).
16. Guan, H., Sorbie, K. S., and Mackay, E. J. The comparison of nonaqueous and aqueous scale-inhibitor treatments: Experimental and modeling studies. *SPE Production & Operations*, 21(4), 419–429 (2006).
17. Romero, C., Bazin, B., Zaitoun, A., and Leal-Calderon, F. Behavior of a scale inhibitor water-in-oil emulsion in porous media. *SPE Production & Operations*, 22(2), 191–201 (2007).
18. Jordan, M., Sørhaug, E., Elrick, M., and Marlow, D. The development of a scale management and monitoring program for a high temperature oil field during the production-decline phase of the life cycle. In: Paper SPE106134 presented at the *SPE International Symposium on Oilfield Chemistry*, Houston, TX (2007).
19. Vasquez, O., Mackay, E. J., and Sorbie, K. S. Modeling of non-aqueous and aqueous scale inhibitor squeeze treatments. In: Paper SPE106422 presented at the *SPE International Symposium on Oilfield Chemistry*, Houston, TX (2007).
20. Shields, R. A., Sorbie, K. S., Singleton, M. A., and Guan, H. Analysis of the mechanism of transport and retention of nonaqueous-scale-inhibitor treatments in cores using novel tracer techniques. *SPE Production & Operations*, 23(1), 56–62 (2008).
21. Bogaert, P., Berredo, M. C., Toschi, C., Bryson, B., Jordan, M. M., Frigo, D. M., and Alfonso, M. Modeling formation damage risk from scale inhibitor squeeze treatments in deepwater subsea fields in Campos Basin. In: Paper SPE107633 presented at the *European Formation Damage Conference*, Scheveningen, the Netherlands (2007).
22. McNaughtan, D., Winning, I. G., and Sim, M. The evaluation of a new environmentally friendly combined product for application in the North Sea for effective scale and corrosion control. In: Paper 90444 presented at the *SPE Annual Technical Conference and Exhibition*, Houston, TX (2004).
23. Stiegler Øye, K. M., Hustad, B. M., and Wat, R. Challenges in qualifying environmental acceptable chemicals for a HPHT field. In: Paper presented at the *International Oil Field Chemistry Symposium*, Geilo, Norway (2006).
24. Inches, C. E., Sorbie, K. S., and El Doueiri, K. Green inhibitors: Mechanisms in the control of barium sulfate scale. In: *CORROSION/06, Paper No. 06485*, presented at *NACE Annual Corrosion Conference and Exposition*, San Diego, CA (2006).
25. Kohler, N., Bazin, B., Zaitoun, A., and Johnson, T. Green scale inhibitors for squeeze treatments: A promising alternative. In: *CORROSION/04, Paper No. 04537*, presented at *NACE Annual Corrosion Conference and Exposition*, New Orleans, LA (2004).
26. Bazin, B., Kohler, N., Zaitoun, A., Johnson, T., and Raajimakers, H. A new class of mineral scale inhibitors for squeeze treatments. In: Paper SPE87453 presented at the *SPE International Symposium on Oilfield Scale*, Aberdeen, U.K. (2004).
27. Chen, P., Hagen, T., Montgomerie, H., Berge, T., Haaland, T., Matheson, R., Sæten, J. O., et al. Field experiences in the application of an inhibitor/additive package to extend an inhibitor squeeze lifetime. In: Paper SPE100466 presented at the *SPE International Symposium on Oilfield Scale*, Aberdeen, U.K. (2006).
28. Jones, C. R., Hails, M. J., and Downward, B. L. New convenient analytical method for biodegradable squeeze scale inhibitors. In: *CORROSION/07, Paper 07062*, presented at *NACE Annual Corrosion Conference and Exposition*, Nashville, TN (2004).
29. Montgomerie, H., Chen, P., Hagen, T., Vikane, O., Berge, T., Matheson, R., Leirvik, V., Frøylog, C., and Sæten, J. O. Development of a new polymer inhibitor chemistry for downhole squeeze applications. In: Paper SPE113926 presented at the *SPE International Oilfield Scale Conference*, Aberdeen, U.K. (2008).
30. Wat, R., Sandengen, K., Sletfjerding, E., Mjaaland, S., Chen, P., and Matheson, R. Åsgard scale control – a journey that began in 1998. In: Paper presented at the *International Oil Field Chemistry Symposium*, Geilo, Norway (2007).

31. Inches, C. E., Sorbie, K. S., Christophe, C., and Papirer, L. Thermal stability of selected green scale inhibitors. In: Paper presented at the *International Oil Field Chemistry Symposium*, Geilo, Norway (2007).
32. Wyld, J. J., Williams, G. D. M., Careil, F., Webb, P., and Morris, A. A new type of super-adsorption, high-desorption scale squeeze chemistry: Doubling treatment life on Miller wells. In: Paper SPE92833 presented at the *SPE International Symposium on Oilfield Scale*, Aberdeen, U.K. (2005).
33. Wyld, J. J., Williams, G. D. M., and Careil, F. Innovative, integrated, and cost effective chemical management on the Miller platform. In: Paper SPE 92834 presented at the *SPE Middle East Oil & Gas Show and Conference*, Bahrain (2005).
34. Chen, P., Hagen, T., Montgomerie, H., Matheson, R., Haaland, T., Juliussen, B., and Benvie, R. A scale inhibitor chemistry developed for downhole squeeze treatments in a water sensitive and HTHP reservoir. In: Paper presented at the *International Oil Field Chemistry Symposium*, Geilo, Norway (2008).
35. Mota, R. O., Bezerra, M. C. M., Rosario, F. F., and Prais, F. Forecasts and alternative analysis for sulfate removal or chemical treatments for barium and strontium scale deposition—offshore Brazil. In: Paper SPE87464 presented at the *SPE International Symposium on Oilfield Scale*, Aberdeen, U.K. (2004).
36. Collins, I. R., Stalker, R., and Graham, G. M. Sulfate removal for barium sulfate scale mitigation in a deepwater subsea production system. In: Paper SPE87465 presented at the *SPE International Symposium on Oilfield Scale*, Aberdeen, U.K. (2004).
37. Boak, L. S., Al-Mahrouqi, H., Mackay, E. J., Inches, C. E., Sorbie, K. S., Bezerra, M. C. M., and Mota, R. O. What level of sulfate reduction is required to eliminate the need for scale-inhibitor squeezing? In: Paper SPE95089 presented at the *SPE International Symposium on Oilfield Scale*, Aberdeen, U.K. (2005).
38. Jordan, M. M., Collins, I. R., and Mackay, E. J. Low-sulfate seawater injection for barium sulfate scale control: A life-of-field solution to a complex challenge. In: Paper SPE98096 presented at the *SPE International Symposium and Exhibition on Formation Damage Control*, Lafayette, LA (2006).
39. McElhiney, J. E., Mason, T. B., and Kan, A. T. Design of low-sulfate seawater injection based upon kinetic limits. In: Paper SPE100480 presented at the *SPE International Symposium on Oilfield Scale*, Aberdeen, U.K. (2006).
40. Chen, H. J., Hinrichsen, C. J., Burnside, C. A., and Widener, M. A. Assessing barite scaling potentials, sulfate removal options, and chemical treating strategies for the Tombua-Landana development. In: Paper SPE106480 presented at the *SPE International Symposium on Oilfield Chemistry*, Houston, TX (2007).
41. Mackay, E. J., Jordan, M. M., Feasey, N. D., Shah, D., Kumar, P., and Ali, S. A. Integrated risk analysis for scale management in deepwater developments. *SPE Production & Facilities*, 20(2), 138–154 (2005).
42. Mackay, E. J. and Jordan, M. M. Impact of brine flow and mixing in the reservoir on scale control risk assessment and subsurface treatment options: Case histories. *Journal of Energy Resources Technology*, 127, 1–13 (2005).
43. Mackay, E., Sorbie, K., Kavle, V., Sørhaug, E., Melvin, K., Sjørsæther, K., and Jordan, M. Impact of sulfate stripping on scale management in the Gyda field. In: Paper SPE100516 presented at the *SPE International Symposium on Oilfield Scale*, Aberdeen, U.K. (2006).
44. Masoudi, R., Tohidi, B., Danesh, A., Todd, A. C., and Yang, J. Measurement and prediction of salt solubility in the presence of hydrate organic inhibitors. *SPE Production & Operations*, 21(2), 182–187 (2006).
45. Tomson, M. B., Kan, A. T., Fu, G., Al-Thubaiti, M., Shen, D., and Shipley, H. J. Scale formation and prevention in the presence of hydrate inhibitors. *SPE Journal*, 11(2), 248–258 (2006).
46. Kaasa, B., Sandengen, K., and Østvold, T. Thermodynamic predictions of scale potential, pH and gas solubility in glycol containing systems. In: Paper SPE95075 presented at the *SPE International Symposium on Oilfield Scale*, Aberdeen, U.K. (2005).
47. Tomson, M. B., Kan, A. T., and Fu, G. Inhibition of barite scale in the presence of hydrate inhibitors. *SPE Journal*, 10(3), 256–266 (2005).
48. Shipley, H. J., Kan, A. T., Fu, G., Shen, D., and Tomson, M. B. Effect of hydrate inhibitors on calcite, sulfates, and halite scale formation. In: Paper SPE100522 presented at the *SPE International Symposium on Oilfield Scale*, Aberdeen, U.K. (2006).
49. Yuan, M., Smith, J. K., Cooley, C., and Williamson, D. A. Effective mineral scale control in Canyon Express, Gulf of Mexico. In: Paper SPE87429 presented at the *SPE International Symposium on Oilfield Scale*, Aberdeen, U.K. (2004).
50. Chen, T., Neville, A., and Yuan, M. Influence of Mg^{2+} on initial stages of $CaCO_3$ scale formed on metal surface. *Chemical Research in Chinese Universities*, 20, 381–385 (2004).

51. Chen, T., Neville, A., and Yuan, M. Influence of Mg^{2+} on the kinetics and crystal morphology of $CaCO_3$ scale formation on the metal surface and in bulk solution. In: *CORROSION/04, Paper No. 04393, NACE Annual Corrosion Conference and Exposition*, New Orleans, LA (2004).
52. Chen, T., Neville, A., and Yuan, M. Calcium carbonate scale formation—assessing the initial stages of precipitation and deposition. *Journal of Petroleum Science and Engineering*, 46, 185–194 (2005).
53. Chen, T., Neville, A., and Yuan, M. Assessing the effect of Mg^{2+} on $CaCO_3$ scale formation—bulk precipitation and surface deposition. *Journal of Crystal Growth*, 275, e1341–e1347 (2005).
54. Chen, T., Neville, A., and Yuan, M. Influence of Mg^{2+} on $CaCO_3$ formation—bulk precipitation and surface deposition. *Chemical Engineering Science*, 61, 5318–5327 (2006).
55. Chen, T., Neville, A., Sorbie, K., and Zhong, Z. Using synchrotron radiation Wide Angle X-ray Scattering (WAXS) to study the inhibition effect of diethylenetriaminepenta (methylene phosphonic acid) (DETPMP) on $CaCO_3$ scale formation. In: Paper SPE100440 presented at the *SPE International Symposium on Oilfield Scale*, Aberdeen, U.K. (2006).
56. Boak, L. S. and Sorbie, K. S. The kinetics of sulfate deposition in seeded and unseeded tests. In: Paper SPE100513 presented at the *SPE International Symposium on Oilfield Scale*, Aberdeen, U.K. (2006).
57. Chen, T., Neville, A., Sorbie, K., and Zhong, Z. Using synchrotron radiation Wide Angle X-ray Scattering (WAXS) to study the inhibiting effect of polyphosphinocarboxylic acid (PPCA) on $CaCO_3$ scale formation. In: *CORROSION/06, Paper No. 06386*, presented at *NACE Annual Corrosion Conference and Exposition*, San Diego, CA (2006).
58. Chen, T., Neville, A., Sorbie, K., and Zhong, Z. Using in situ synchrotron radiation Wide Angle X-ray Scattering (WAXS) to study $CaCO_3$ scale formation at ambient and elevated temperatures. *Faraday Discussions*, 1361–11 (2007).
59. Shen, D., Fu, G., Al-Saiari, H., Kan, A. T., and Tomson, M. B. Seawater injection, inhibitor transport, rock-brine interactions, and $BaSO_4$ scale control during seawater injection. In: Paper SPE114062 presented at the *SPE International Oilfield Scale Conference*, Aberdeen, U.K. (2008).
60. Martinod, A., Neville, A., Sorbie, K., and Zhong, Z. Assessment of $CaCO_3$ inhibition by the use of SXRD on a metallic substrate. In: *CORROSION/08, Paper No. 08351*, presented at *NACE Annual Corrosion Conference and Exposition*, New Orleans, LA (2008).
61. Chen, T., Neville, A., and Yuan, M. Effect of PPCA and DETPMP inhibitor blends on $CaCO_3$ scale formation. In: Paper SPE87442 presented at the *SPE International Symposium on Oilfield Scale*, Aberdeen, U.K. (2004).
62. Chen, T., Neville, A., Yuan, M., and Sorbie, K. S. Influence of PPCA inhibitor on $CaCO_3$ scale surface deposition and bulk precipitation at elevated temperature. *Progress in Natural Science (special issue)*, 35–41 (2005).
63. Tomson, M. B., Fu, G., Watson, M. A., and Kan, A. T. Mechanisms of mineral scale inhibition. *SPE Production & Facilities*, 18(33), 192–199 (2003).
64. Graham, A. L., Vieille, E., Neville, A., Boak, L. S., and Sorbie, K. S. Inhibition of $BaSO_4$ at a Hastelloy surface and in solution: The consequences of falling below the minimum inhibitor concentration (MIC). In: Paper SPE87444 presented at the *SPE International Symposium on Oilfield Scale*, Aberdeen, U.K. (2004).
65. Sorbie, K. S. and Laing, N. How scale inhibitors work: Mechanisms of selected barium sulfate scale inhibitors across a wide temperature range. In: Paper SPE87470 presented at the *SPE International Symposium on Oilfield Scale*, Aberdeen, U.K. (2004).
66. Graham, A. L., Boak, L. S., Neville, A., and Sorbie, K. S. How minimum inhibitor concentration (MIC) and sub-MIC concentrations affect bulk precipitation and surface scaling rates. *SPE Production & Operations*, 21(1), 19–25 (2006).
67. Kan, A. T., Fu, G., Tomson, M. B., Al-Thubaiti, M., and Xiao, A. Factors affecting scale inhibitor retention in carbonate-rich formation during squeeze treatment. *SPE Journal*, 9(3), 280–289 (2004).
68. Kan, A. T., Fu, G., and Tomson, M. B. Reactions of phosphonates and phosphinopolycarboxylate in the subsurface. In: *Biogeochemistry of Chelating Agents*. Nowack, B. and VanBriesen, J. M. (Eds.), Oxford University Press, New York, pp. 248–262 (2005).
69. Kan, A. T., Fu, G., and Tomson, M. B. Adsorption and precipitation of an aminoalkylphosphonate onto calcite. *Journal of Colloid and Interface Science*, 281, 275–284 (2005).
70. Tomson, M. B., Kan, A. T., and Fu, G. Control of inhibitor squeeze through mechanistic understanding of inhibitor chemistry. *SPE Journal*, 11(3), 283–293 (2006).
71. Tomson, M. B., Kan, A. T., Fu, G., Shen, D., Nasr-El-Din, H. A., Al-Saiari, H., and Al-Thubaiti, M. Mechanistic understanding of rock/phosphonate interactions and the effect of metal ions on inhibitor retention. In: Paper SPE100494 presented at the *SPE International Symposium on Oilfield Scale*, Aberdeen, U.K. (2006).

72. Baraka-Lokmane, S. and Sorbie, K. S. Scale inhibitor core floods in carbonate cores: The influence of pH on phosphonate-carbonate interactions. In: Paper SPE87448 presented at the *SPE International Symposium on Oilfield Scale*, Aberdeen, U.K. (2004).
73. Baraka-Lokmane, S. and Sorbie, K. S. Scale inhibitor core floods in carbonate cores: Chemical interactions and modeling. In: Paper SPE100515 presented at the *SPE International Symposium on Oilfield Scale*, Aberdeen, U.K. (2006).
74. Yuan, M., Williamson, D. A., Smith, J. K., and Lopez, T. H. Effective control of exotic mineral scales under harsh system conditions. In: Paper SPE80234 presented at the *SPE International Symposium on Oilfield Chemistry*, Houston, TX (2003).
75. Lopez, T. H., Fielder, G. D., Yuan, M. SPE; Williamson, D. A., and Przybylinski, J. L. Comparing efficacy of scale inhibitors for inhibition of zinc sulfide and lead sulfide scales. In: Paper SPE95097 presented at the *SPE International Symposium on Oilfield Scale*, Aberdeen, U.K. (2005).
76. Dyer, S., Orski, K., Menezes, C., Heath, S., MacPherson, C., Simpson, C., and Graham, G. Development of appropriate test methodologies for the selection and application of lead and zinc sulfide inhibitors for the Elgin/Franklin field. In: Paper SPE100627 presented at the *SPE International Symposium on Oilfield Scale*, Aberdeen, U.K. (2006).
77. Orski, K., Grimbert, B., Menezes, C., and Quin, E. Fighting lead and zinc sulfide scales in a North Sea HP/HT field. In: Paper SPE107745 presented at the *European Formation Damage Conference*, Scheveningen, the Netherlands (2007).
78. Okocha, C., Sorbie, K. S., and Boak, L. S. Inhibition mechanisms for sulfide scales. In: Paper SPE112538 presented at the *SPE International Symposium and Exhibition on Formation Damage Control*, Lafayette, LA (2008).
79. Smith, J. K., Hammons, J., Boyd, G., and Fu, Q. Performance of scale inhibitors under carbonate and sulfide scaling conditions. In: Paper SPE114075 presented at the *SPE International Oilfield Scale Conference*, Aberdeen, U.K. (2008).
80. Wyld, J. J., Duthie, A. W., and McAllister, H. Root cause failure analysis, removal and mitigation of iron sulfide scale deposition in the BP Bruce produced water reinjection plant. In: *CORROSION/08, Paper No. 08350*, presented at *NACE Annual Corrosion Conference and Exposition*, New Orleans, LA (2008).
81. Feasey, N. D., Budge, M., Jordan, M. M., and Robb, M. Development and deployment of improved performance “green” combined scale/corrosion inhibitor for subsea and topside application, North Sea Basin. In: *CORROSION/06, Paper No. 06481*, presented at *NACE Annual Corrosion Conference and Exposition*, San Diego, CA (2006).
82. Leontieff, A., Collins, J. A., and Edwards, C. L. Development of biodegradable combination scale/corrosion inhibitors for subsea applications via umbilical. In: Paper presented at the *International Oil Field Chemistry Symposium*, Geilo, Norway (2008).
83. Leontieff, A., Poynton, N., Dugue, D. D., Green, S. A., and Williams, J. Development of a phosphorus tagged polymeric scale inhibitor to enable squeeze and topside scale control via the same inhibitor chemistry. In: Paper SPE SPE94866 presented at the *SPE International Symposium on Oilfield Scale*, Aberdeen, U.K. (2005).
84. Ohen, H. A., Williams, L. E., Lynn, J. D., and Ali, L. Assessment and diagnosis of inorganic-scaling potential using near-infrared technology for effective treatment. *SPE Production & Facilities*, 20, 245–252 (2004).
85. Ramstad, K., Rohde, H. C., Tydal, T., and Christensen, D. Scale squeeze evaluation through improved sample preservation, inhibitor detection and minimum inhibitor concentration monitoring. In: Paper SPE114085 presented at the *SPE International Oilfield Scale Conference*, Aberdeen, U.K. (2008).
86. Ramstad, K., Tydal, T., Askvik, K. M., and Fotland, P. Predicting carbonate scale in oil producers from high temperature reservoirs. In: Paper SPE87430 presented at the *SPE International Symposium on Oilfield Scale*, Aberdeen, U.K. (2004).
87. Wat, R., Wennberg, K., Holden, R., Hustad, B., Heath, S., Archibald, M., and Singdahlsen, K. The challenge associated with performing and combining scale dissolver and squeeze treatments in Kristin—a subsea HP/HT gas condensate field. In: Paper SPE114079 presented at the *SPE International Oilfield Scale Conference*, Aberdeen, U.K. (2008).
88. Del Gaudio, L., Bortolo, R., and Lockhart, T. Nanoemulsions: A new vehicle for chemical additive delivery. In: Paper SPE106016 presented at the *SPE International Symposium on Oilfield Chemistry*, Houston, TX (2007).
89. Shen, D., Zhang, P., Kan, A. T., Fu, G., Farrell, J., and Tomson, M. B. Control placement of scale inhibitors in the formation with Ca-DTPMP nanoparticle suspension and its transport in porous media. In: Paper SPE114063 presented at the *SPE International Oilfield Scale Conference*, Aberdeen, U.K. (2008).

9 Control of Silica Scaling in Geothermal Systems Using Silica Inhibitors, Chemical Treatment, and Process Engineering

Darrell L. Gallup and Paul N. Hirtz

CONTENTS

9.1	Introduction	155
9.2	The Geochemistry of Silica.....	156
9.2.1	Silica Deposition.....	158
9.3	Silica Precipitation Kinetics	159
9.4	General Techniques for Silica/Silicate Scale Inhibition.....	160
9.5	Current Scale Control Techniques at High Supersaturation.....	163
9.6	Case Study for Scale Control in a Hybrid Plant Design.....	168
9.7	Scale Control Using New Inhibitors and Dispersants	171
9.7.1	Early Studies of Organic Additives	172
9.7.2	Later Studies of Organic Additives	172
9.7.3	Geogard SX and Other Inhibitors.....	174
9.8	Summary	175
	References.....	175

9.1 INTRODUCTION

Worldwide output from geothermal sources has increased significantly over the past three decades. A total of 75% of the worldwide capacity increase is produced from about 20 sites with more than 100MWe of installed generating capacity. These geothermal power projects convert the energy contained in hot rocks into electricity by using water to adsorb the heat from the rock and transport it to the earth's surface, where it is converted to electrical energy through turbine generators. It is estimated that more than 97% of the current geothermal reservoir production is from magmatically driven reservoirs. Geothermal reservoirs may also develop outside regions of recent volcanic activity, where deeply penetrating faults allow groundwater to circulate to depths of several kilometers and become heated by the geothermal gradient [1].

More than 90% of exploited fields are "liquid dominated" under pre-exploitation conditions with reservoir pressures increasing with depth in response to liquid-phase density. "Vapor-dominated" systems, such as The Geysers in California, have vertical pressure gradients controlled by the density of steam. In vapor-dominated systems, steam is cleaned and then passed directly into low-pressure turbines. Typically, water from high-temperature (>240°C) reservoirs is partially flashed to steam.

Heat is converted to mechanical energy by passing steam through low-pressure steam turbines. A small fraction of geothermal generation worldwide is generated using a heat exchanger and secondary working fluid to drive turbines [2].

The development and execution of technology have made it possible to exploit geothermal resources that might not have otherwise been accomplished. A major focus of production chemistry and engineering in the geothermal energy industry has been to control scale deposits and corrosion from the geothermal fluids. The primary scale encountered in geothermal resource production and power generation facilities has been amorphous silica or poorly crystalline silicates. This chapter discusses the fundamental and practical aspects of precipitation, dissolution, and inhibition of silica and silicate scale.

9.2 THE GEOCHEMISTRY OF SILICA

The concentration of silica (SiO_2) in geothermal waters in reservoirs is usually controlled by the dissolution of quartz from the geological strata of the reservoirs.



Silica solubility at reservoir temperatures (above about 185°C) is controlled by quartz; solubility at surface facility temperatures (usually less than about 185°C) is controlled by amorphous silica or metal silicates. The deposition of silica or silicate as a scale, however, is primarily controlled by its polymerization and precipitation as amorphous silica or poorly crystalline silicates, *vide post*, which is more soluble than quartz. The solubility of quartz and amorphous silica as a function of temperature in pure water is illustrated in Figure 9.1. Equations to calculate the solubility of quartz and amorphous silica in pure water are available from various sources [3–5]. Quartz deposition is negligible under most geothermal production conditions due to its slow precipitation kinetics compared with amorphous silica or poorly crystalline silicates. The precipitation of silica may occur immediately or sometime after cooling depending on the pH and supersaturation ratio, but the precipitate that forms will be amorphous silica or metal silicates rather than quartz.

Although quartz is thermodynamically more stable than amorphous silica, extreme conditions of temperature, pressure, and/or alkalinity are required for the growth of quartz at measurable rates in aqueous solutions. The greater solubility of amorphous silica relative to quartz is a distinct advantage for geothermal resource production facilities because it limits the precipitation of silica from produced

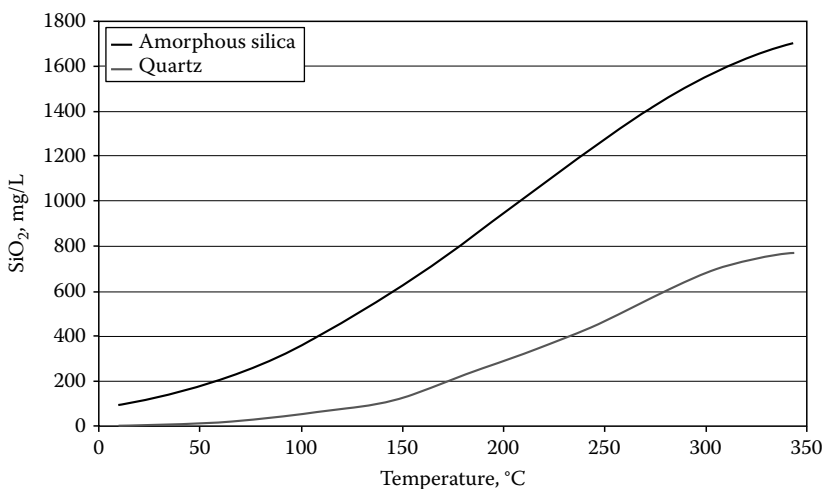


FIGURE 9.1 Solubilities of amorphous silica and quartz in pure water as a function of temperature.

waters. Dissolved salts and pH also affect the solubility of silica in aqueous solutions. Fournier and Marshall [6] have developed equations to calculate the solubility of amorphous silica at circum-neutral pH from 25°C to 300°C using the concept of effective density of water and the “salting out” effects of mixed electrolytes. Cations exhibiting elevated “hydration numbers,” such as the alkaline-earths, depress the solubility of amorphous silica more than cations exhibiting low “hydration numbers” due to “free” water available for solvation. The effect of NaCl molality and temperature on amorphous silica and quartz solubility is shown in Figures 9.2 and 9.3, respectively. The solubility of silica is substantially independent of pH until the pH level increases into the alkaline range.

Goto [7] examined the effect of pH on the solubility of amorphous silica from 0°C to 200°C from pH 5.5 to 10.0. As expected, the solubility of amorphous silica increased with increasing temperature, while solubilities remained relatively constant over the pH range of about 5.5–8.5. Above pH 8.5, the solubility increased significantly:

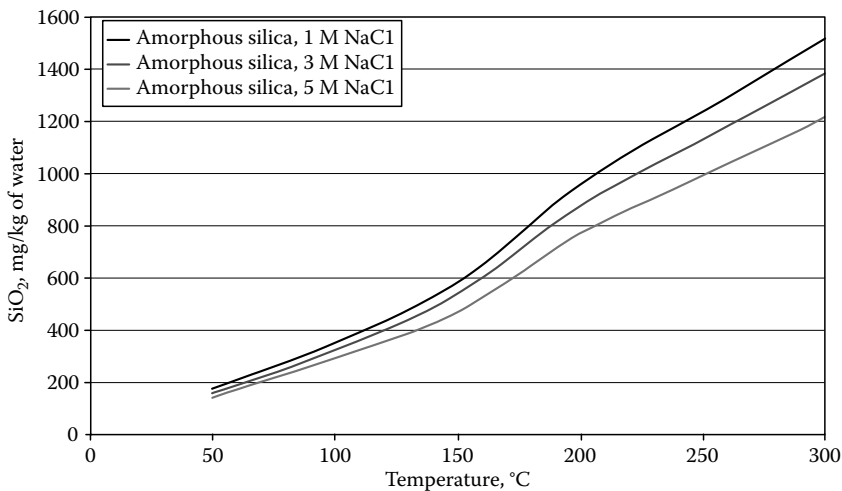
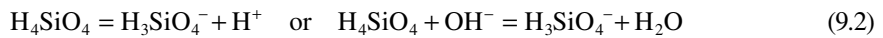


FIGURE 9.2 Effect of NaCl on amorphous silica solubility.

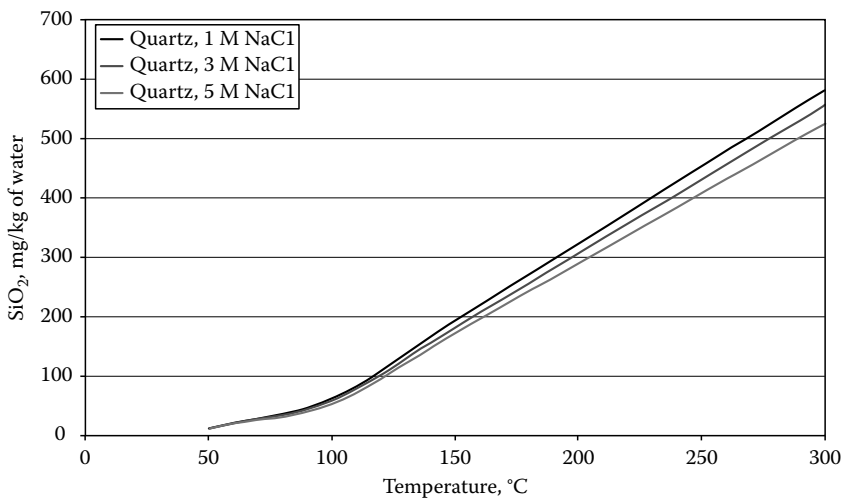


FIGURE 9.3 Effect of NaCl on quartz solubility.

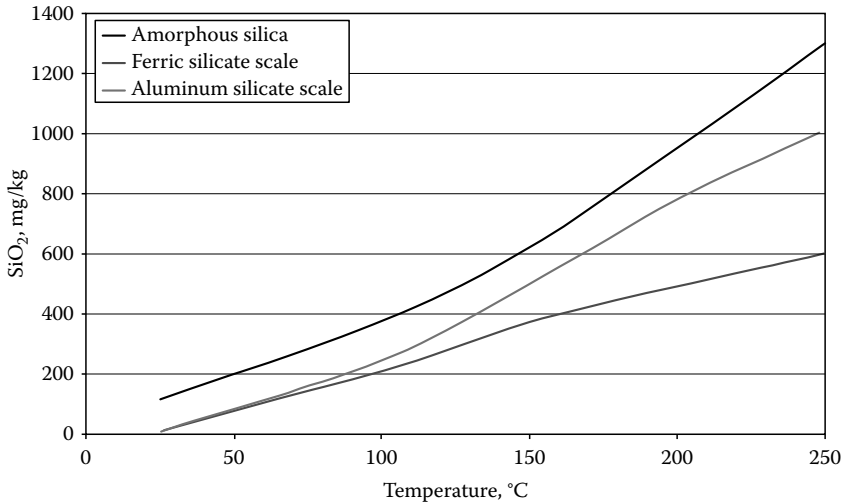


FIGURE 9.4 Solubility of silicates in pure water.

The first ionization constant for monomeric silicic acid is given as $K_1 = 10^{-9.7}$ at 25°C by Wahl [8]. The ionization constant can be calculated at higher temperatures using the following equation:

$$\ln K_1 = -16.76 - \frac{1661}{T} \quad (9.3)$$

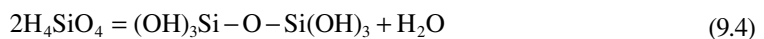
where T is the temperature, K. The effect of pH on the equilibrium solubility of monomeric silica is generally of little practical significance under typical geothermal water conditions where the pH level usually ranges from 5 to 9.

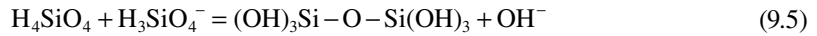
Non-alkali and alkaline-earth cations present in geothermal conditions may react directly with silicic acid to form metal silicates. These silicates are usually poorly crystalline; their x-ray diffraction patterns exhibit broad humps that are shifted from the normal opal-A hump centered near 23° 2 θ [9–11]. X-ray absorption spectroscopic studies showed that the silicates exhibit Si–O–M bonding and are not simply mixtures of silica and metal oxides/hydroxides. These metal silicates are not as soluble in pure water or aqueous solutions as pure amorphous silica as shown in Figure 9.4.

9.2.1 SILICA DEPOSITION

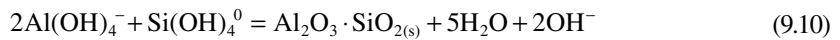
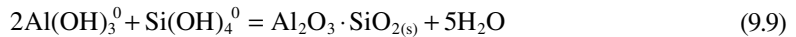
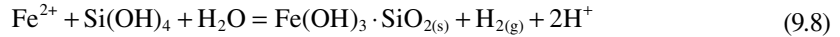
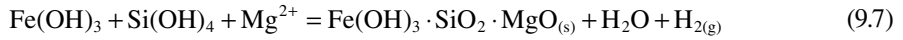
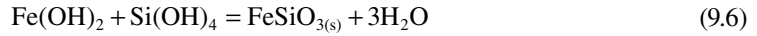
Amorphous silica scale deposition may occur via two mechanisms: the formation and growth of a colloid or the direct deposition of a monomer on a surface. Colloidal precipitates are softer and less adhesive, while monomer precipitates are very hard, vitreous, and difficult to remove. Precipitation of amorphous silica is much slower when the silica is in the form of colloids vs. monomers. The metal silicates behave similar to monomeric deposition forming quickly in the form of hard, glassy solids. For example, a manganese silicate scale adhered extremely tightly to a variety of steels and corrosion-resistant alloys, an iron silicate scale adhered tightly to carbon steel, but not to corrosion resistant alloys, and a rather pure amorphous silica scale adhered less tightly to carbon steel and not at all to alloys [12].

The primary reactions responsible for silica deposition from geothermal waters are the condensation (polymerization) reaction of silicic acid and the reaction of the silicic acid with the silicate anion, respectively:





In the case of the metal silicates, a number of reactions may be responsible for deposition, e.g.,



9.3 SILICA PRECIPITATION KINETICS

As mentioned above, various factors affect the rate at which silica polymerizes and precipitates from solution. The kinetics of silica polymerization is influenced by the degree of supersaturation, temperature, catalysts (fluoride), and nucleation site availability. The maximum rate of silica precipitation occurs at a temperature of 25°C–50°C below the silica saturation temperature as geothermal water or brine cools by flashing steam or by natural heat loss. As a rule, once the supersaturation ratio nears 2, silica precipitation commences without delay. Weres et al. [4] postulated that the silica precipitation process consists of the following steps:

1. Formation of silica polymers of less than the nucleus size
2. Nucleation of an amorphous silica phase in the form of colloidal particles
3. Growth of supercritical amorphous silica particles by further chemical deposition of silicic acid on their surfaces
4. Coagulation or flocculation of colloidal particles to give either a precipitate or a semisolid material
5. Cementation of the particles in the deposit by chemical bonding and further deposition of silica
6. Growth of a secondary phase in the interstices between the amorphous silica particles (occurs rarely)

A solid surface in contact with a supersaturated solution of amorphous silica may have a layer of amorphous silica on it and further deposition may proceed by Step 3 alone. If colloidal amorphous silica particles form in the supersaturated solution, these may adhere to the surface (Steps 4 and 5), while Step 6 may follow. The formation of amorphous silica colloidal particles from a supersaturated solution is often referred to as homogeneous nucleation, which is the dominant process at high initial supersaturation ratios required for rapid polymerization of amorphous silica. Heterogeneous nucleation applies to the deposition of amorphous silica on preexisting colloidal amorphous silica particles, but it is not actually a nucleation process. Nucleation by other scale particles can also occur to provide surfaces for amorphous silica deposition [13].

The nucleation process frequently includes an induction time during which the concentration of molecular silicic acid remains constant. After some period of time, the concentration of molecular

silicic acid begins to decrease, which indicates that nucleation is occurring. This induction time phenomena has been interpreted in two ways. First, the approximate time required for subcritical clusters of amorphous silica to grow to critical nucleus size and slightly beyond it is considered to be the induction time. The induction time is longer at lower saturation ratios because the critical nucleus size is larger at these ratios.

An alternative interpretation views the induction time as simply the length of time required for enough particles to nucleate and grow to a point where the concentration of molecular silicic acid decreases. Rapid attainment of steady-state nucleation is implicit in this interpretation. Therefore, an initially slower nucleation rate may be ignored for practical purposes. This interpretation applies to induction times observed for both homogeneous and heterogeneous nucleation. Furthermore, a threshold value for amorphous silica supersaturation may be necessary to achieve nucleation. Similar to the dissolution of quartz or amorphous silica, temperature, degree of supersaturation, pH, dissolved salt concentration, and fluoride ions can affect the rate of silica nucleation [14]. Both Iler [14] and Weres et al. [4] report that the rate of silica deposition is proportional to the sodium ion concentration, i.e., dissolved NaCl or other electrolytes may promote a faster solubility equilibrium. They also report a 10-fold increase in deposition rates upon increasing the water pH level from 5 to 6, and that fluoride catalyses the silica polymerization reaction. Conversely, the kinetics of silica deposition slows dramatically as the pH is lowered into the acid range, *vide post*.

9.4 GENERAL TECHNIQUES FOR SILICA/SILICATE SCALE INHIBITION

Silica deposition is found in almost all high enthalpy, liquid-dominated geothermal operations to some extent. Initiation of silica precipitation can occur within minutes or hours after supersaturation is reached [15]. The most common methods used in the geothermal industry to control silica/silicate scaling include (a) processing water or brine at temperatures at or above silica/silicate saturation; (b) diluting brine with freshwater; (c) reducing the pH of the water; (d) treating the water with reducing, complexing, and sequestering agents; (e) removing silica from water by lime or similar softening; (f) controlled precipitation of silica in water with metals or cationic surfactants; (g) controlled precipitation of silica in ponds or crystallizer-clarifiers; (h) cooling or rapid thermal quenching of geothermal brine; and (i) treating the water with silica scale inhibitors/dispersants [16]. Combinations of these control methods have also been used and are generally site (reservoir geochemistry) specific.

A. A few geothermal fields flash steam from hot water and then dispose of the water at the surface. Some fields located near coastlines were or are operated with the discharge of fluids into the ocean or other waterways under significant environmental scrutiny [17]. However, this practice has potential environmental impacts due to the presence of salinity, heavy metals, and other toxic species such as arsenic, boron, and ammonia. Due to environmental concerns, reinjection of water/brines, cooling tower waters, and excess steam condensate has been applied. The principal advantage of reinjection is that the net withdrawal of mass from the geothermal system is greatly reduced. Reservoir pressure is supported, so that production well outputs can be maintained for a longer time [2]. The principal disadvantage of reinjection is that the cool brine may flow directly to certain production wells before it has been in contact with hot rock long enough to reheat, causing a reduction in steam output from the production wells. This is a common problem and challenge for geothermal energy production because a strong pressure difference builds up between the injectors and the producers. The fractured nature of the rocks in geothermal systems often allows an unpredictable, highly permeable path from the injector to the producer. This problem is usually mitigated by increasing the distance between the injection and production wells. A technology that has been successfully employed in fields to understand the communication between injectors and producers is stable tracers. These tracers may also be used to measure flow measurements in piping and to monitor brine separators and steam scrubber efficiencies, etc. [18,19].

TABLE 9.1
Amorphous Silica Saturation Condensate Dilution of Brine

Condensate ^a Fraction	Mixture		Mixture SiO ₂		Final pH
	Temperature, °F	SiO ₂ (ppm _w)	Saturation	Salinity (ppm _w)	
0	405	1130	1.13	19,000	5.14
0.10	380	1017	1.13	17,100	4.66
0.20	354	904	1.13	15,200	4.47
0.30	328	791	1.12	13,300	4.35
0.40	302	678	1.09	11,400	4.26
0.50	275	565	1.05	9,500	4.18

^a Condensate temperature = 140°F.

B. Some geothermal fields utilize the dilution of the silica supersaturated geothermal water/brine with freshwater to reduce the silica concentration to below the saturation point. Steam condensate or potable hot water is typically used in these applications. Although cold dilution water may not have a significant net effect on silica saturation due to the opposing effects of cooling and dilution, it has been determined that adjusting the pH of the condensate, surface water, or cooling tower water to that of the brine will slow the precipitation kinetics sufficiently to mitigate deposition [20–22]. Table 9.1 lists the silica saturation as a function of cold condensate (60°C) dilution of hot brine (200°C) for a geothermal project in Hawaii. Even a 50% dilution of the brine with condensate results in only a minor decrease in silica supersaturation, but in a drop in pH of about 1 unit. The reduction in salinity and pH provides a substantial reduction in the silica deposition rate for this fluid.

C. Brine pH modification has been utilized at several fields to slow the polymerization kinetics of silicic acid. The acids that may be used in this application include HCl, H₂SO₄, H₂SO₃, HF, organic acids, and acid precursors such as urea-acid adducts or chlorinated hydrocarbons. The selection of the acid must be compatible with the water/brine to avoid forming by-product scales. One practice was to inject liquid acid downstream of the separator to modify brine pH to control silica scaling. Chevron® has also used acidic turbine off-gasses to inhibit silica scaling. Gallup [23] reported that 75–125 ppm HCl reduced the pH level of brine entering a pilot tester with a pH level of 5.8–5.9 at above 550 kPa and 170°C to 5.2–5.5, which limited scaling to less than 10 ppm. Below 550 kPa and 170°C, greater than 150 ppm HCl, which reduced the pH to around 4.6, was necessary to achieve acceptable scaling inhibition. The pH of brine typically needs to be lowered to the 5–6 range to slow the silica polymerization without detrimentally increasing corrosion.

Gallup [24] also studied the silica inhibition properties of H₂SO₃ and sulfite salts up to 392°F. H₂SO₃ inhibits silica scaling by slowing silica polymerization and forming soluble sulfite–silicate complexes, which results in increased amorphous silica solubility. In a comparative test with HCl and H₂SO₄, H₂SO₃ maintained the highest silica concentration in solution at each interval of the 72 h test. The use of H₂SO₄ in brine acidification is typically undesirable because of the secondary precipitation of alkaline-earth sulfates. On the other hand, the solubility of alkaline-earth sulfites increases with decreasing pH levels and the primary product of calcium/bisulfite interactions below a pH level of 5.5 is soluble calcium bisulfate. Consequently, H₂SO₃ can be used to treat most geothermal brines without the formation of by-product scales. Even though H₂SO₃ is more expensive than HCl or H₂SO₄, the costs can be mitigated by manufacturing H₂SO₃ onsite by incinerating H₂S or S, an easy and cheap process. Enough H₂S is available at most facilities to meet all acid requirements [25].

Hirowatari and Yamauchi [26] reported on the injection of exhausted gases into the brine to decrease the brine's pH level. The exhausted gases were 70% CO₂ and 2% H₂S. The pH level of

the brine decreased with increasing liquid to gas ratios up to a ratio of 15 after which the pH level remained constant with increasing ratios. Gas was injected at a ratio of 14.5 into Hatchobaru brine with a pH of 7. The gas injection lowered the pH to 5.2 and resulted in scale deposition approximately 1/30 of that prior to the gas injection. The brine pH level remained relatively constant after injection as long as the temperature did not decrease. The effects of the treatment are limited by the amount of gas. Only 10% of the brine can be treated with a once-through pass of the exhausted gases. However, circulating and reusing the gas can substantially increase the volume of treated brine.

The Salton Sea geothermal field suffers from iron-rich silica scaling at rates from 0.5 cm/year in production wells to over 50 cm/year in injection wells. Even though the brines contain mostly ferrous (Fe^{2+}) iron, the iron in the scales is primarily ferric (Fe^{3+}). A wide variety of commercial silica inhibitors have proven to be ineffective. Therefore, Gallup [27] investigated the use of iron-reducing agents to convert the ferric ions to ferrous ions, which are more soluble at geothermal temperatures. The reducing agents were tested on synthetic brine (pH 5.5) and actual field brine (pH 4.5). The agents were added at a several-fold stoichiometric excess, and the tests were carried out at 240°C. Most of the agents were effective at pH 5.5. However, only eight agents—sodium thiosulfate, sodium dithionite, sodium formaldehyde bisulfite, thioglycolic acid, ammonium thioglycolate, stannous chloride, iron, and aluminum—were effective at pH 4.5. Eight of the more promising and cheaper agents—formic acid, sodium formate, potassium iodide, sodium dithionite, thioglycolic acid, sodium thiosulfate, corn syrup, and dextrose—were then pilot-tested at Salton Sea. While most of these agents had performed poorly at pH 4.5, they all had over 60% efficiency at pH 5.5. In all the tests, the agent was applied at a threefold stoichiometric excess. Sodium formate, which exhibited the highest reduction rate, was selected for additional pilot tests to optimize the dosage for brines with varying scaling rates. Increasing the stoichiometric excess improved the inhibition efficiency for all brines. Due to the encouraging results of the sodium formate pilot tests, a 56 day field demonstration test was performed. Prior to the inhibitor test, a similar 60 day control test (no agent injection) was carried out. The injection of sodium formate at a 2.8 stoichiometric excess achieved up to 50% inhibition. Additionally, the sodium formate converted up to 99% of the ferric iron into ferrous iron. Gallup also compared the efficiency of HCl/reducing agent mixtures to HCl alone. The tests produced mixed results. For some brines, the mixtures increased efficiency by as much as 50% over the acid alone. In other brines, the mixtures were less efficient. In most cases, the acid alone provided adequate scale control. One benefit of the HCl/reducing agent mixtures, though, was a significant reduction in corrosion [28].

C–E. These scale control methods are relatively similar in that they utilize a controlled precipitation of silica from geothermal brine by various means. Silica deposition can be controlled by operating separators at pressures higher or equal to amorphous silica saturation. However, these pressures can often be quite high, which reduces the amount of power generated. Because hot injection of brine is less economic, cold injection methods, which control silica deposition without pressure modification, have been developed. Since colloidal precipitation is much slower, silica deposition can be controlled by placing the brines in storage ponds to allow the dissolved monomeric silica to convert to colloids. Candelaria [29] believes that neither adherent gel nor solid scale will form if the silica is in colloidal form. The hypothesis relies on the requirement of monomeric silica to cement silica colloids together. Application of this procedure at the Botong, Philippines field showed that the colloidal silica (30 nm each) formed a gelatinous, fluffy precipitate that did not settle in the ponds but, rather, was transported into the injection wells. After 3 years, though, the precipitate had not caused a serious decline in the injection capacity. Attempts to clear the settling ponds of deposited silica by removing baffles at the ends of the lanes to allow flow of the silica solids, though, resulted in a substantial decline in injection capacity within a week, most likely caused by the plugging of the reservoir formation. This result indicates that the effects of precipitate transport are related to particle size. Acid can act as a pseudo-inhibitor by delaying the precipitation until the deposition would no longer cause damage. The addition of acid to a supersaturated silica solution delays the polymerization by preventing the reaction

between ionized and nonionized silicic acid. This delay will allow the silica solution to travel long distances into the well bore before deposition occurs. Candelaria [29], believes that silica deposition within the huge volume of the reservoir will cause less damage than deposition in the wellbore. Additionally, higher reservoir temperatures will increase the solubility of silica, which will decrease the ultimate deposition amounts.

The Salton Sea, California field has also been notorious for massive scale deposition. As the hypersaline brine was flashed to produce steam, numerous scale types were precipitated. These included iron silicates, barite, fluorite, iron and silver antimonides, copper arsenide, heavy metal sulfides, and several other exotic deposits. Production engineering and chemistry efforts led to the development of crystallizer-clarifier technology, where iron silicates were purposely precipitated in surface equipment as sludge to prevent the fouling of pipelines, brine- and steam-handling equipment, and reinjection wells [30,31]. The crystallizer-clarifier technology not only precipitated the iron silicate, but due to reaching iron silicate saturation at the boiling point of the brine (109°C), Ra-rich BaSO_4 and CaF_2 also deposited. A scale inhibition system was developed to inhibit crystalline scale growth without adversely affecting the precipitation of the nanocrystalline hisingerite scale [i.e., $\text{Fe}_3^{2+}\text{Si}_2\text{O}_5(\text{OH})_4 \cdot 2\text{H}_2\text{O}$] [32].

9.5 CURRENT SCALE CONTROL TECHNIQUES AT HIGH SUPERSATURATION

A major advancement in the exploitation of “liquid-dominated” geothermal fields has been the application of “bottoming cycle” heat recovery systems to maximize the heat extraction and power generation from a given resource. Bottoming cycle heat recovery systems, as defined herein, are typically binary plants or multistage flash plants. In the case of binary plant cycles, the heat from a single phase water/brine is exchanged against a binary working fluid. This secondary working fluid is flashed, passed through a turbine to generate electricity, condensed, and recycled. Some binary plants are used as the sole source of electricity production, in which case the hot water, using electric submersible production well pumps, is maintained under pressure through the entire process from production to injection. This process has the advantage of not releasing gases (primarily CO_2 and H_2S) into the environment.

Binary bottoming cycles can result in very high levels of amorphous silica supersaturation, where the silica saturation index (SSI) is 2 or greater (silica concentration/solubility at given temperature). The successful processing of high silica fluids through binary cycle heat exchangers is attributed to the rapid quenching of temperature, which reduces the kinetics of silica deposition. Figure 9.5

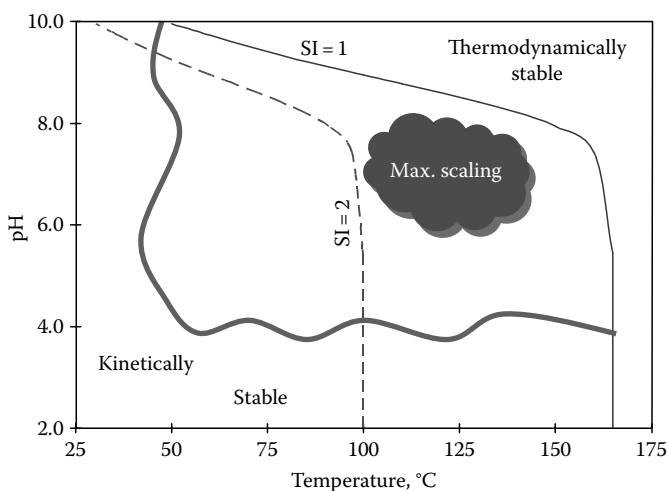


FIGURE 9.5 Silica stability map 700 ppm SiO_2 .

is a generic thermal stability map for amorphous silica. In this example, the amorphous silica is *thermodynamically* stable above 170°C and only at lower temperatures where the pH level is high (pH >8). The brine is *kinetically* stable at temperatures below about 50°C and when pH values are less than about 4 or 5 units. The maximum potential for scale deposition is marked by the region in red, which is the typical range of conditions resulting from a second-stage flash. *Thermodynamic* stability prevents any possibility of scale deposition, while *kinetic* stability results in an extended period of time before the deposition will occur. It is the kinetic stability that allows the successful operation of a binary bottoming cycle by taking advantage of the kinetic effects of both thermal quenching (inherent with the binary cycle) and low-pH (augmented by acid injection as needed).

The non-release of the acid-gases (CO₂ and H₂S) in the binary process maintains the brine pH at a lower level. Upon cooling in a binary heat exchanger, the brine pH will drop further due to the increased acidity of carbonic acid at the lower temperature (Figure 9.6). This often provides an advantage in silica scale control for binary cycles since the pH is lower than in a dual-flash process and the scale is kinetically inhibited to some extent. In other cases, a second flash will result in a very high pH level (pH 9 or more for dilute, alkaline brines) and the silica becomes thermodynamically inhibited due to the dissociation of silicic acid to the soluble silicate ions (above the blue line in the upper right region of Figure 9.5).

Whether a second- or third-stage flash system or a binary system is used as a bottoming cycle, amorphous silica usually becomes highly supersaturated at the outlet temperature of the process. Generally, only single-flash plants are operated at or below the silica saturation limit. Historically, single-flash geothermal plants were built for this reason, to prevent the possibility of silica scale, but at the expense of maximum resource utilization. Figure 9.7 shows the solubility of quartz and amorphous silica as a function of temperature. Also plotted (heavy red line) is the concentration “path” for a brine flashed from single-phase reservoir conditions in an equilibrium with quartz at 300°C to a typical first-stage power plant flash condition of 160°C, then in a second-stage to 110°C. The dashed blue line shows the path from the first flash to subcooling in a binary cycle as an alternate bottoming process to the second flash. The binary cycle does not further concentrate the silica but may involve cooling to a lower temperature than the second flash. Note that the concentration of silica in the brine begins to exceed the amorphous silica solubility at just under 200°C. A hybrid plant design in Hawaii, flashes 300°C reservoir brine to 200°C, where it is slightly undersaturated

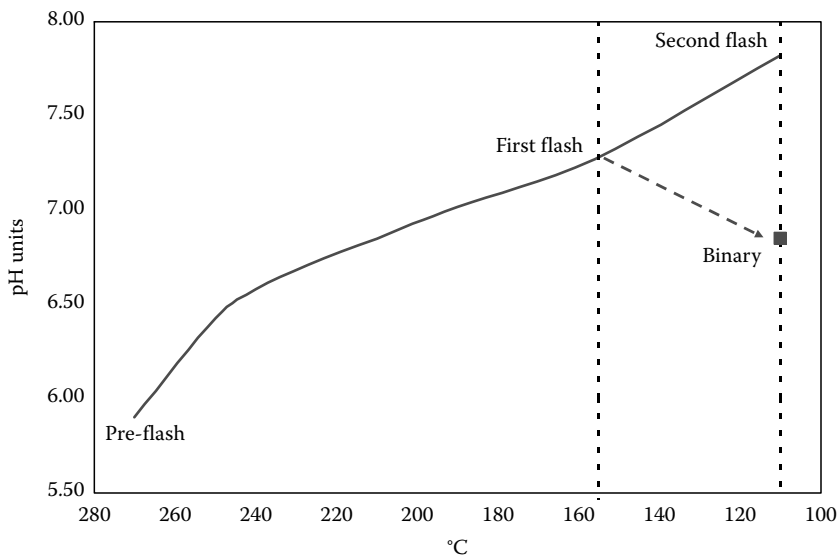


FIGURE 9.6 Brine pH as a function of flash temperature.

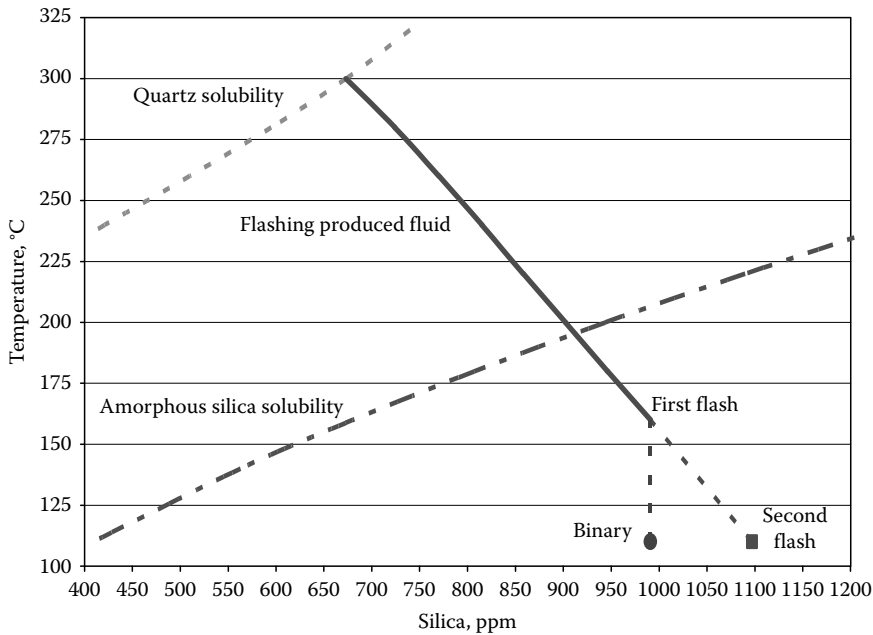


FIGURE 9.7 Silica concentration and solubility vs. flash temperature.

in silica, then passes that brine through a bottoming cycle where it becomes highly supersaturated (SSI~3.5) at about 100°C. The natural brine pH level is 5.5 and reduced to 4.5 with an acid injection to control the scale.

Binary bottoming cycle plants may use several types of silica scale control methods. Brine acidification is commonly used to prevent silica deposition in the heat exchanger tubes, the injection lines and wells, and the injection formation [33]. The inherent thermal quenching and low pH of subcooled brine have resulted in minimal scaling in some binary plants. At the Rotokawa, New Zealand field, a hybrid flash/binary plant allows the geothermal water to cool from 219°C to 150°C. Although silica in the water is supersaturated to an SSI of 1.6, no significant scaling has developed in the heat exchanger tubes. Prior to disposal by reinjection, the geothermal water is diluted with steam condensate and injected into the reservoir at 130°C. At the Kawerau, New Zealand field, a hybrid flash-binary process is also utilized. The binary plant rapidly cools the brine from 180°C to 120°C. Even at an SSI of 1.5, no significant scaling is observed due to the rapid quenching. The Los Azufres, Mexico field uses binary plants to generate electricity. The geothermal water is rapidly quenched in the binary exchanger from 174°C to 108°C. The heat exchanger tubes are cleaned once per year, even though the SSI is 2. At the Svartsengi, Iceland geothermal field, brine is flashed from 6 to 0.3 bar resulting in an instantaneous temperature decrease from 160°C to 70°C. While the silica in the brine is highly supersaturated with amorphous silica, the scaling is essentially mitigated by the rapid thermal quenching.

In several applications worldwide, binary-type heat exchangers are used for space heating where the geothermal hot water or brine is used to heat “clean” potable water for residential and commercial heating and domestic hot water. The hot “clean” water can also be used for deicing and agricultural applications [1]. If the geothermal fluid were used directly in these widely distributed applications, “radiator” type piping will eventually foul or corrode as the fluid cools. The Nesjavellir geothermal plant in Iceland cools geothermal water in a heat exchanger bottoming cycle to 55°C in the process of heating potable water for the city of Reykjavik. In the process, silica in the geothermal fluid becomes supersaturated to an SSI of 4. Due primarily to the rapid cooling and the low outlet temperature of the geothermal water, scaling is minimal and the heat exchanger tubes are only

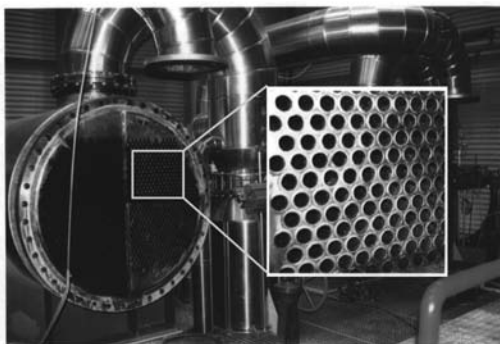


PHOTO 9.1 Nesjavellir power plant heat exchangers.

cleaned once per year (Photo 9.1). In the course of processing the geothermal fluid, it is aged prior to injection to control the silica precipitation and is diluted with steam condensate [34].

In the multiple flash processes, steam is generated in stages while brine concentrates and the fluid temperature drops in each stage. As described above, the binary cycle does not concentrate the brine but usually extracts more heat resulting in a lower outlet temperature. If amorphous silica or metal silicate saturation is exceeded, scaling is thermodynamically possible. Depending on factors such as the fluid temperature, pH, salinity, and concentration of certain cations (in the case of silicates), scale may deposit immediately or be kinetically delayed for a significant amount of time. Chemical treatment scale control methods may need to be employed, especially if the brine is to be reinjected. Injection pipelines, injection wells, and injection formations may be plugged or damaged if silica is precipitating therein (Photo 9.2). In the bottoming cycle, shell and tube heat exchangers are utilized; the shell side usually contains the binary working fluid. As a result, the small diameter tubes in the binary heat exchanger may become scaled, causing a drop in pressure and reduced heat transfer, if conditions yield silica/silicate supersaturation [2].

The most common chemical treatment option for silica scale control in both binary and multi-flash power cycles is acid treatment, known as “pH-modification” [23]. Although very effective, in some cases pH-modification can be difficult to control since the target pH is typically at the inflection point of the acid titration curve for the brine (pH 4.5–5), where bicarbonate is the dominant alkaline species being neutralized in the process. Substantial amounts of dissolved CO_2 in the brine (>200 ppm CO_2) can smooth the pH response curve to acid, resulting in more precise and stable pH control. Poor pH control (± 0.5 units or worse) can result in the corrosion of carbon steel pipelines and inadequate scale inhibition.

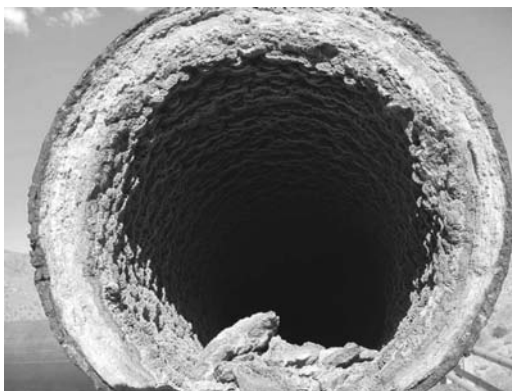


PHOTO 9.2 Dual-flash brine injection pipeline.

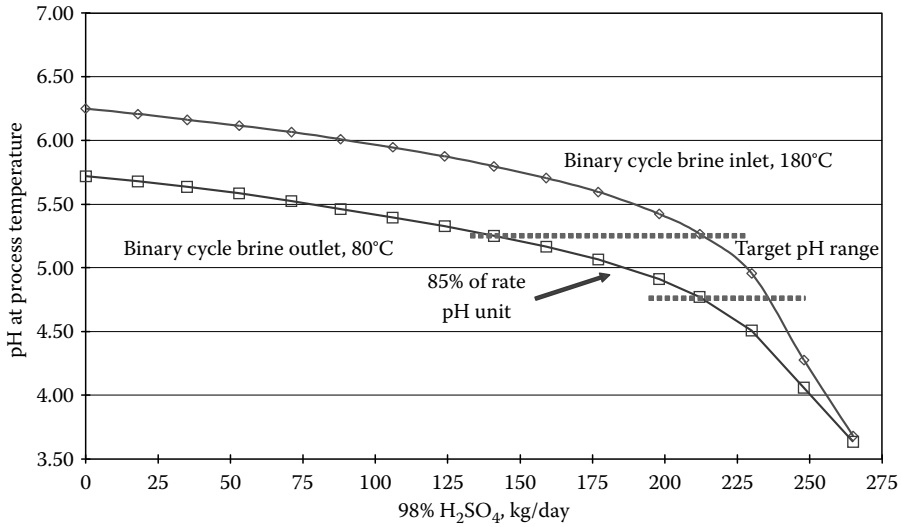


FIGURE 9.8 Characteristic pH modification curve for pumped well binary system.

Figure 9.8 shows the pH-modification dosing curve for a binary cycle process in Nevada, where the brine is pumped from the wells with no flashing and all the gases remain dissolved (>1000 ppm CO₂). The curve is quite flat near the target pH region where an 85% change in the total acid dosing rate only results in a 1 unit pH change. Note also that the outlet brine pH at 80°C is considerably lower than the inlet brine at 180°C due to the increased acidity at a lower temperature of the primary pH-controlling species; i.e., carbonic acid.

A typical pH-modification curve for a single-flash brine is shown in Figure 9.9. In this case, a 7% change in the total acid dosing rate results in a pH change of 1 unit. This is still a controllable process under steady flow conditions with accurate online pH monitoring and precise dosing pumps for the concentrated acid. Figure 9.10 shows the pH-modification curves for a dual-flash process in New Zealand. A change of only 1%–2.5% in the acid dosing rate results in a pH change of 1 unit.

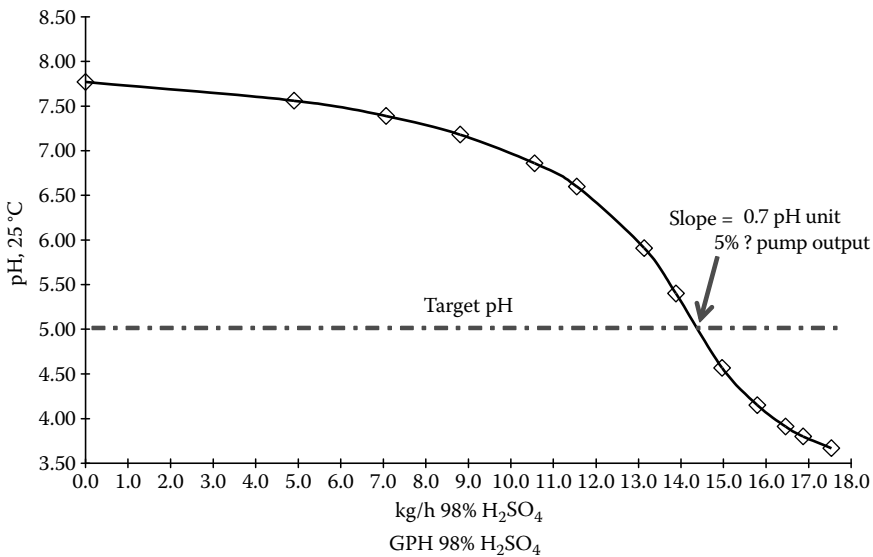


FIGURE 9.9 Characteristic first flash/brine bottoming cycle pH modification curve.

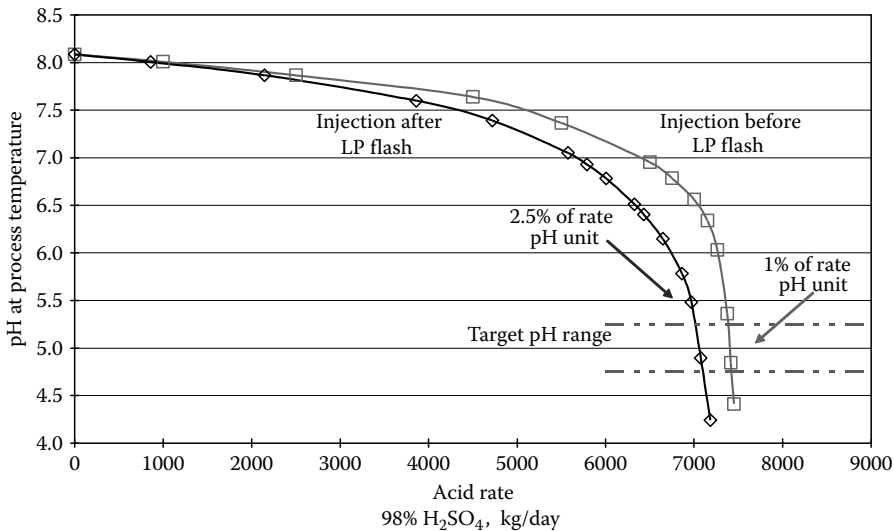


FIGURE 9.10 Characteristic pH modification curves for dual-flash brine.

This is a very difficult process to control and is not possible without highly stable brine flow. The control is more difficult when acid is injected upstream of the second flash vessel, which results in more total CO_2 lost from the brine than occurs with injection into the single-phase brine after the second flash. In many cases, acid must be injected upstream of the second flash to prevent the onset of rapid silica polymerization.

9.6 CASE STUDY FOR SCALE CONTROL IN A HYBRID PLANT DESIGN

A hybrid single-flash steam turbine with a binary bottoming cycle process was designed for a geothermal field in Reykjanes, Iceland [35]. The initial heat and mass balance, given in Figure 9.11, provides a first-stage flash and bottoming cycle design that will maintain the silica saturation index at or below 1.0 through the heat exchangers and injection system. The separated brine would have an SSI of 0.80, the second preheater outlet brine would have an SSI of 1.03, and the brine and condensate injection mixture would have an SSI of 0.96. These saturation indexes include the effects of pH on silicic acid dissociation and salinity on the overall solubility of amorphous silica. The produced brine pH is neutral to acidic and the salinity is moderately high, approximately that of seawater. The wells are produced from a single-phase brine reservoir in the range of 290°C – 320°C .

This initial design is conservative in that it will thermodynamically prevent amorphous silica deposition in the power cycle and injection system by maintaining temperatures at or above the silica saturation limits. The preheater outlet brine will be slightly supersaturated (by 3%), but will be immediately diluted with condensate to below saturation (Stage 1 Proposed Design).

In order to recommend the optimum process parameters for the Reykjanes binary bottoming cycle, a Stage 2 Proposed Design was developed that would kinetically inhibit silica scale deposition through maximum heat recovery from the brine and acidification with condensate and noncondensable gas. Chemical modeling was performed on the production fluid to determine the pH and silica saturation under various process conditions and to calculate the relative molecular deposition rates of silica vs. temperature and pH.

Figure 9.12 shows the heat and mass balance for the Stage 2 bottoming cycle configuration. At the flash condition of 220°C (same for Stages 1 and 2), silica is undersaturated by 20% and cannot deposit. The brine outlet temperature at the vaporizer is to be reduced to 195°C , where the silica is undersaturated by 3% and still will not deposit at this temperature. After the brine exits the

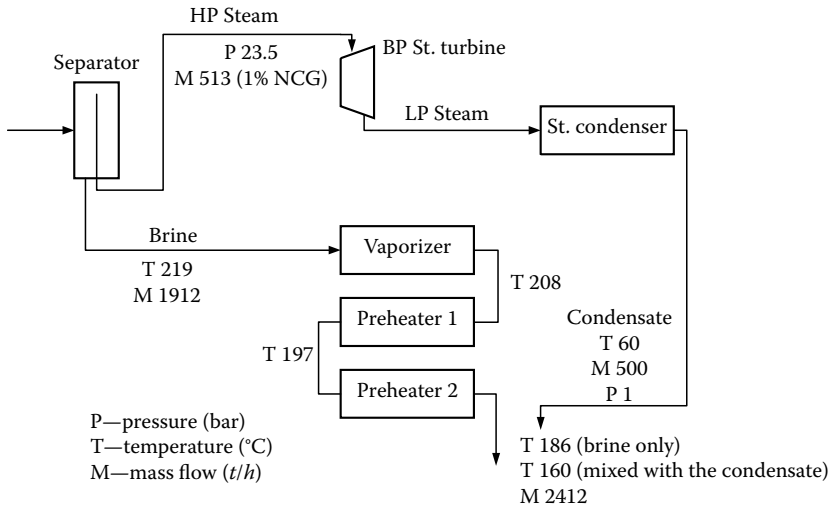


FIGURE 9.11 Stage 1 proposed bottoming cycle.

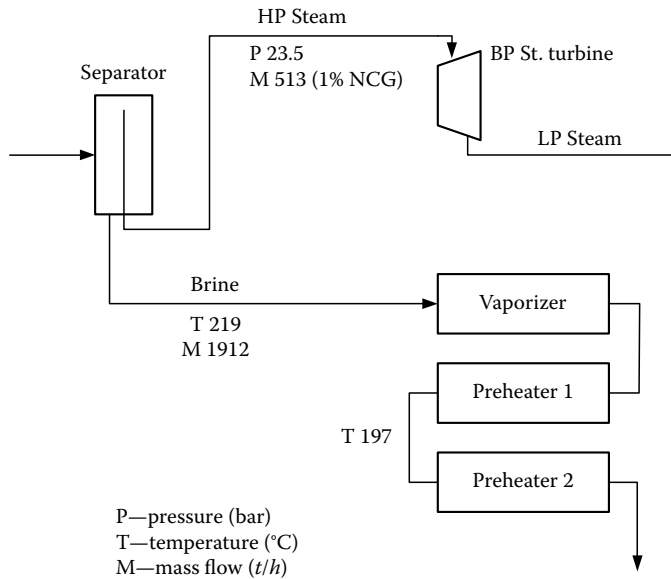


FIGURE 9.12 Stage 2 proposed bottoming cycle.

vaporizer, it is mixed with steam condensate and gas from the condenser. This immediately reduces the temperature to 167°C and the pH to 4.6 units. The silica remains undersaturated (SSI = 0.96) at this point due to dilution. The addition of condensate also reduces the salinity, which helps to increase the solubility of silica and reduce the kinetics of deposition later in the process. The main benefit of condensate and gas addition is the large reduction in pH. Successful processing of this fluid through the preheaters to low temperatures requires that the pH is reduced to below 5.0 units. Addition of the condensate alone without gas will result in a pH of 5.5 units.

In the Stage 2 design, the brine/condensate mixture at the outlet of the second preheater should be 80°C or less to maximize heat recovery and minimize scale. At an outlet temperature of 80°C, the silica saturation will be 2.5. Due to the thermal quenching effect on silica scale kinetics, an even lower temperature would be desirable. At 50°C, the saturation would be 3.8, but the deposition rate

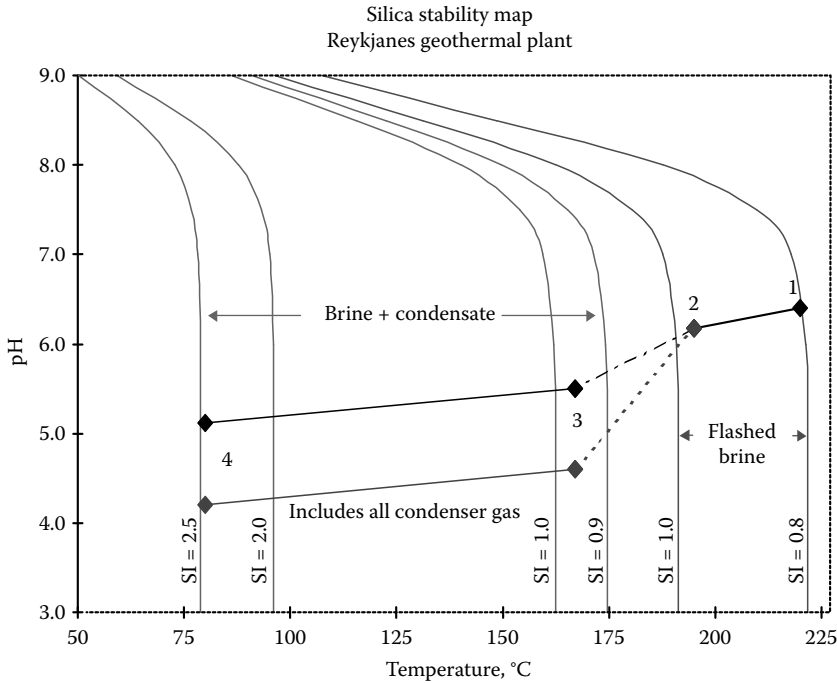


FIGURE 9.13 Stage 2 process.

is expected to be less than 80°C. With acidification to pH 4.5 or less, and cooling of the mixture to 80°C or less, significant silica scaling problems are not anticipated in the heat exchangers or injection pipelines over time intervals in the injection system on the order of 1–2 h.

Figure 9.13 is a thermal and pH stability map for amorphous silica under the conditions proposed for the Stage 2 design. Point 1 represents the separated brine and point 2 represents the brine after cooling through the vaporizer. Both points are below saturation. The silica is *thermodynamically* stable above 190°C, and at lower temperatures where the pH is high (pH >8), as indicated by the SI curves that tend to lower temperatures at a higher pH level. Point 3 represents the brine/condensate mixtures at the inlet to the first preheater, which are undersaturated at the lower temperature (167°C) due to dilution. Point 4 represents the mixtures exiting the last preheater, where the saturation is about 2.5. The brine is expected to be *kinetically* stable at temperatures of about 80°C or less, when the pH level is below about 5 units. *Thermodynamic* stability can be predicted precisely and will prevent any possibility of scale deposition. The limits of *kinetic* stability cannot be predicted precisely, but operating in this region does result in an extended period of time before significant deposition will occur. It is the kinetic stability that allows the successful operation of a binary bottoming cycle. In Reykjanes, significant silica scale problems can be prevented in a binary bottoming cycle by taking advantage of the kinetic effects of both thermal quenching and low pH levels.

Figure 9.14 is a plot of relative molecular deposition rates calculated for the Reykjanes brine and condensate mixture as a function of temperature. Bulk polymerization of silica can be neglected at these lower pH conditions. The maximum deposition rate occurs at a temperature of 100°C, and approaches a minimum at 50°C, even though the saturation is over 3.5 at this lower temperature. The rate is dependent on both saturation and temperature, but temperature overwhelms the saturation effect below 100°C. The relative effect of pH is also noted on the figure where the brine, condensate, and gas mixture are plotted at 80°C and pH 4.5, resulting in a deposition rate almost 10 times lower than the brine and condensate mixture at the same temperature. Note the Stage 1

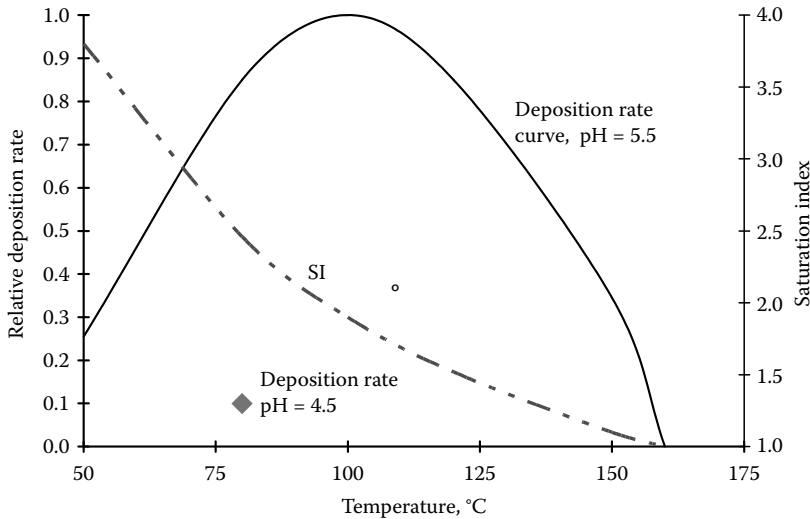


FIGURE 9.14 Relative silica deposition rate stage 2 process.

design brine/condensate injectate mixture plots on Figure 9.14 at 167°C and zero for the deposition rate because it will be undersaturated in silica.

The initial Stage 1 design is conservative in that it will thermodynamically prevent amorphous silica deposition in the power cycle and injection system. Although the preheater outlet brine will be slightly supersaturated (SSI = 1.03), it will immediately be diluted with condensate to below saturation (SSI = 0.96). This is essentially a zero risk design approach to silica scale issues, provided the process temperatures are maintained at or above the proposed design values.

As a modification to the initial Stage 1 design, the Stage 2 process would kinetically inhibit silica scale deposition through maximum heat recovery from the brine and acidification with condensate and noncondensable gas (or sulfuric acid). The Stage 2 design involves the addition of condensate, plus noncondensable gas or sulfuric acid, to the brine exiting the vaporizer. This mixture is then cooled to 80°C or less through the preheaters.

9.7 SCALE CONTROL USING NEW INHIBITORS AND DISPERSANTS

Ammonia can be used to control silica scaling. Laboratory tests have shown that ammonia, rather than inhibiting precipitation, promotes precipitation in solution rather than on equipment walls. The scale is then carried out of the wellbore by the produced fluids without adhering to the downhole equipment. The primary disadvantage to this technique is the possibility of metal hydroxide, carbonate, and sulfide precipitation at pH 6–9 [36].

Crane and Kenkeremath [37] reported the results of field testing of non-pH adjusting additives for geothermal silica scale control. The tested additives were divided into 11 groups: polyoxyethylenes, cellulose derivatives, other polymers, quaternary ammonium, imines, surfactants, organic acids, other organics, silanes, proprietary chemicals, and inorganics. Tests were performed at 90°C, 125°C, and 210°C. The polyoxyethylenes exhibited the most obvious inhibitive activity. The proprietary chemicals, on the other hand, were almost all ineffective. For all additives, inhibition effectiveness reduced as temperature increased. Overall, the best additives were the cationic nitrogen-containing compounds. No tests were conducted to verify the findings, but these authors suggested that silica scaling promotes sulfide scaling. Therefore, silica scaling inhibition should reduce sulfide scaling. The major uncertainty about the applicability of the tests results is the often unknown ratio between monomeric and colloidal silica at geothermal field operating locations.

9.7.1 EARLY STUDIES OF ORGANIC ADDITIVES

Harrar et al. [38,39] studied the use of organic compounds to stabilize colloidal solids instead of acid treatments to delay precipitation. Over 120 compounds were tested that included simple and polymeric alcohols, ethers, aldehydes, carboxylic acids, amines, amides, cellulose derivatives, detergents, surfactants, coupling agents, inorganics, and chelants. The compounds were tested for scale inhibition efficiency when injected at the front-end of a Salton Sea geothermal field test facility. Several compounds were immediately eliminated because they either were not sufficiently water soluble or immediately formed precipitates when added to the brine. Further testing was done on the compounds that maintained, for at least 24 h, a silica concentration 1.5 times higher than that in the HCl-treated brine.

Active compounds included compounds containing polymeric chains of oxyethylene moiety and nitrogen-containing cationic-functioning compounds. The cationic-functioning compounds, which are entirely hydrophilic, did not become insoluble at high temperatures. The attraction between the cationic compound and the silica creates a strong bond that inhibits the precipitation of silica. Most compounds were not reactive—polyacrylates, polymaleic acid, sulfonates, lignosulfonates, phosphate esters, phosphonates, nonethoxylated cellulose derivatives, technical proteins, and silanes. Unfortunately, none of the compounds reduced scale formation at the highest test temperature (220°C); only pH reduction was effective at this elevated temperature at the time. The best scale inhibition results were achieved by mixing compounds. The best combination was one of the active compounds with HCl, especially if the active compound also inhibited corrosion. The active compound/HCl combinations did not decrease pH as significantly as acid alone, which resulted in less corrosion. The combinations were more effective at removing the low temperature scales than the active compound alone.

9.7.2 LATER STUDIES OF ORGANIC ADDITIVES

Organic additives were revisited by Gallup [40] and Gallup and Barcelon [41]. They tested over 50 organic additives, whose ingredients included phosphonic acids, phosphonates, phosphinocarboxylic acids, acrylate polymers, polyacrylamides, oxyethylenes, poly-maleates, sulfonates, carboxylic acids, polyethyleneimines, caustic soda, and quaternary ammonium compounds. They concluded that organic additives will likely continue to see limited use in the geothermal industry. Organic additives disperse particles and/or modify crystal growth. These control mechanisms do not have a large impact on amorphous silica, which is the silica state typically found in geothermal operations. Rather, organic additives are more effective at controlling crystalline silicates. Additionally, they make the deposits softer and easier to remove, but do not prevent polymerization or increase solubility. This means that the silica exists in the solution as suspended solids, which have the potential to cause damage in the injection wells.

In the first series of tests by Gallup [40], only Geogard SX (GSX) had >50% efficiency in inhibiting pure amorphous silica scale in a laboratory-simulated tube blocking test. GSX achieved 70% efficiency so long as the dosage remained below 1.5 ppm. The brine displayed fluffy, dispersed silica upon treatment. However, the scope of the findings was limited because most of the additives were only tested at the vendor-recommended dosages. Some of the additives that showed moderate inhibition efficiencies might have been better at lower or higher dosages. It was shown that overdosing of the additives led to flocculation rather than dispersion. In subsequent field tests, none of the additives achieved the same efficiency as acidification (pH modification). Additionally, many of the additives that showed some efficiency in the lab increased scaling during the field tests. However, some additives did produce results in agreement with laboratory-determined efficiencies. Additives that were the same or similar to those tested by Harrar et al. [39] generally exhibited lower efficiencies in the laboratory and field tests. Gallup hypothesized that his harsher testing conditions of -200°C for 4 h possibly led to the decreased efficiencies [40].

Gallup and Barcelon [41] expanded on the original work by testing more organic additives in the laboratory tube-blocking protocol. Only six of the additives tested met the 75% efficiency requirement for field testing, which was based on previous experience. Again, many of the additives had minimal or even negative efficiencies. For additives displaying acceptable efficiencies, additional tests were performed to optimize the dosage. At the time of publication, no field tests had been performed with the six promising additives. However, lab testing of acid efficiency on the same brines suggested that the additives will not reach the level of inhibition activity that can be achieved by brine acidification used in several fields around the world. Gallup and Barcelon [41] planned to study the effectiveness of acid/organic additive combinations in the laboratory and field.

Since acidification has proven to be one of the optimal silica control methods, Gallup and Barcelon [41] also studied acid precursors as possible replacements for strong acid treatments. The tested precursors all performed as well or better than the organic additives. Urea-sulfuric acid and urea-hydrochloric acid exhibited 92% and 97% inhibition, respectively. Halogenated hydrocarbons were also field tested. Carbon tetrachloride reduced the brine pH by 1 unit and reduced scaling by 75%. Some precursors, such as urea-sulfuric acid and urea-hydrochloric acid, can reduce the environmental and handling concerns associated with the use of strong acids. Other precursors, such as halogenated hydrocarbons, though would still pose transportation and environmental concerns. Furthermore, fluorocarbons should only be used to treat brines with low calcium concentrations to avoid calcium fluoride precipitations. This concern can be mitigated if calcium fluoride inhibitors are added to the fluorocarbon treatment. The use of chloro- and fluoro-carbons to control siliceous scales could, however, reduce inventories of compounds known to harm the ozone layer. Table 9.2

TABLE 9.2
Comparison of Inhibitor Treatment Costs

Inhibitor	Unit Price (US\$/kg)	Dosage (ppm _w)	Cost to Treat 1000 t of Brine (US\$)
Chemlogis #1271	3.78	1	3.78
Chemlogis #1271	3.78	10	37.80
Chemlogis #1272	3.10	1	3.10
Chemlogis #1272	3.10	10	31.00
Chemlogis #1274	5.81	1	5.81
Chemlogis #1274	5.81	10	58.10
Chemlogis #1276	2.40	1	2.40
Chemlogis #1276	2.40	10	24.00
Polyethyleneimine	3.56	1	3.56
Polyethyleneimine	3.56	10	35.60
Wellon #1	3.48	5	17.40
Wellon #2	3.08	5	15.40
Wellon #3	7.08	5	35.00
Wellon #4	3.74	1	3.74
Urea sulfuric acid adduct	0.92	25	23.00
Urea sulfuric acid adduct	0.92	50	46.00
H ₂ SO ₄	0.25	25	6.25
H ₂ SO ₃	0.51	40	20.40
H ₂ NSO ₃ H	0.90	40	36.00
31% HCl	0.25	80	20.00
CCl ₄	0.88	25	22.00
CHCl ₃	0.92	35	32.20

lists the approximate treatment costs for these inhibitors and chemical treatments, where chemical cost data is available.

Additional recent laboratory studies have been conducted by several companies. Geothermal scale inhibitors have been patented for use in the oil field steam flooding operations [42] and have been examined for controlling silica/silicate scales in reverse osmosis and cooling water applications [43]. Testing and application of these inhibitors in geothermal operations are limited.

9.7.3 GEOGARD SX AND OTHER INHIBITORS

Research by PNOC (Energy Development Corporation of the Philippines) and Biolab (U.K. water additive company) on silica scale inhibitors led to the synthesis of a phosphino carboxylic copolymer, called GSX, in 1995. GSX, designed to control colloidal and monomeric silica deposition, is an aqueous solution based on a phosphino carboxylic acid copolymer. It includes a dispersant that prevents colloidal silica from agglomerating and a hydrate iron oxide sequestrant that limits monomeric silica reaction sites forcing the monomeric silica to polymerize to form colloidal silica, whose deposition is then controlled by the dispersant. GSX was tested to determine the inhibition efficiency as a function of dosing concentration at the Malitbog Pilot Test Facility of the Lyte Geothermal Power Project in 1995. The efficiency effects of atmospheric brine flashing and high fluid velocities were also tested. Under all conditions, GSX reduced the silica deposition with efficiencies ranging from 38% (5 ppm) to 99% (8 ppm with a topping spool). In 1996, GSX was tested at the Botong Pilot Test Facility. Excessive silica deposition stopped the flow in the untreated pipelines within 12 h. In contrast, a 10 ppm GSX treatment prevented silica deposition along the pipelines and in the formation material over the same test interval. GSX was first tested in a commercial application in 1998 at the Botong Fluid Collection and Disposal System. The inhibitor was injected in the two-phase flow line prior to steam separation. Silica deposition in the hot sections was minimal after 17 months of operation, but gel-type silica continued to deposit in the cold sections. In 2000, GSX was used to treat low-silica brines for the first time. Testing occurred at the Southern Negros Geothermal Production pilot test facility. At a dosing level of 1 ppm, GSX slowed the silica deposition and limited particle size, but was unable to disperse the scaling completely. At a dosing level of 0.5 ppm, however, deposition was reduced significantly, and the inhibitor had 70% efficiency [15].

GSX and perturbations of its formulations have been further tested in the field with mixed results. Some tests have yielded positive results, while others have dramatically increased silica scale deposition compared with pH modification (see Photos 9.3 and 9.4). Although cleanout of the deposited silica is still often required, avoiding high-pressure hydroblasting of deposits in heat exchanger tubes and pipelines has been beneficial [44-46]. Lastly, the authors are in the process of testing several new inhibitors in geothermal fields. Of four formulations tested to date, none have yielded significantly positive results (publication forthcoming).

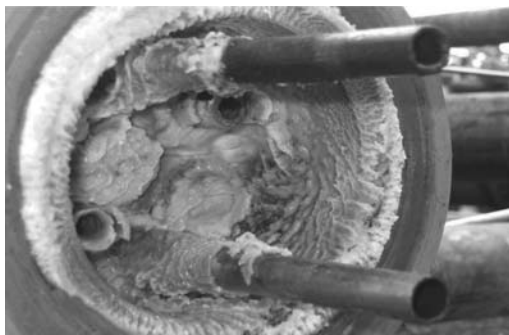


PHOTO 9.3 HX tubes after 30 day test at Puna, Hawaii PowerChem “CSX 5110” inhibitor.

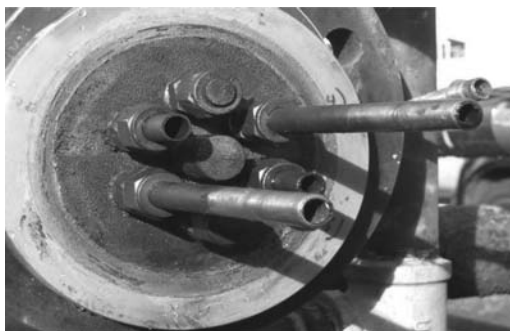


PHOTO 9.4 HX tubes after a 30-day test, at Puna, Hawaii pH-mod treatment.

9.8 SUMMARY

There is huge potential for geothermal energy development worldwide. Renewable geothermal energy is currently used to generate electric power in 24 countries, for a total of 9000 MWe. Geothermal energy has the potential to be the world's primary source of baseload renewable power. The Massachusetts Institute of Technology (MIT) and U.S. Department of Energy (DOE) have concluded that with a reasonable R&D investment, geothermal energy could provide 100,000 MWe of cost-competitive power for the United States within the next 50 years [47].

Since geothermal energy utilization involves direct heat transfer between water and rock in the reservoir, geothermal fluids are *always* saturated in silica with respect to the mineral quartz. But the kinetics of quartz dissolution/precipitation are slow, so in the time it takes to extract the energy on the surface and reinject the fluids, quartz precipitation does not normally occur. However, amorphous silica deposition is possible and does occur once the fluid is supersaturated due to cooling. Fortunately, the kinetics of amorphous silica deposition are relatively slow, but still can easily occur within the timeframe of fluid processing and handling.

In early geothermal development, silica scaling was a significant limiting factor in the amount of energy that could be extracted from a resource. Recent production engineering and chemistry advances have greatly reduced these barriers by implementing technology to control silica/silicate scaling and corrosion from geothermal produced fluids. Proven engineering strategies such as binary power cycles and pH modification are currently the primary means for mitigating silica scale, but few organic inhibitors have been successfully tested at commercial geothermal power plants. A wide range of new organic inhibitors and dispersants are available for evaluation, and with continued testing it is possible that a cost-effective alternative chemical treatment for silica scale will be found soon.

REFERENCES

1. Bertani, R. World geothermal power generation in the period, 2001–2005. *Geothermics*, 34, 651–690 (2005).
2. Gallup, D. L. Advances in geothermal production engineering in recent decades. *Geothermal Resources Council Transactions*, 31, 11–15 (2007).
3. Arnórsson, S. The quartz and Na/K geothermometers. 1. New thermodynamic calibration. In *Proceedings World Geothermal Congress*, Tohoku, Japan, pp. 929–934 (2000).
4. Weres, O., Yee, A., and Tsao, L. Equations and type curves for predicting the polymerization of amorphous silica in geothermal brines. *Society of Petroleum Engineering Journal*, February, 22(1), 9–16 (1982).
5. Fournier, R. O. The behavior of silica in hydrothermal solutions. In *Reviews in Economic Geology*, Vol. 2, eds. B. R. Berger and P. M. Bethke, pp. 45–61. Society of Economic Geologists, Littleton, CO (1985).
6. Fournier, R. O. and Marshall, W. L. Calculation of amorphous silica solubilities at 25°C to 300°C and apparent cation hydration numbers in aqueous salt solutions using the concept of effective density of water. *Geochimica et Cosmochimica Acta*, 47, 587–596 (1983).

7. Goto, K. Research on the state of silicic acid in water (Part 2): Solubility of amorphous silicic acid. *Journal of the Chemical Society of Japan, Pure Chemistry Section*, 76, 1364–1366 (1955).
8. Wahl, E. F. *Geothermal Energy Utilization*. John Wiley & Sons, New York (1977).
9. Manceau, A., Ildefonse, Ph., Hazemann, J. L., Flank, A. M., and Gallup, D. L. Crystal chemistry of hydrous iron silicate scale deposits at the Salton Sea geothermal field. *Clays & Clay Minerals*, 43, 304–317 (1995).
10. Gallup, D. L. Aluminum silicate scale formation and inhibition. *Geothermics*, 26, 483–499 (1997).
11. Manceau, A. and Gallup, D. L. Nanometer-sized divalent manganese-hydrous silicate domains in geothermal brine precipitates. *American Mineralogist*, 90, 371–381 (2005).
12. Gallup, D. L. Unusual adherence of manganese silicate scale to metal substrates. *Geothermal Resources Council Transactions*, 28, 529–532 (2004).
13. Kindle, C. H., Mercer, B. W., Elmore, R. P., Blair, S. C., and Myers, D. A. Geothermal injection treatment: Process chemistry, field experiences and design options. PNL-4767, UC-66d (1984).
14. Iler, R. K. *The Chemistry of Silica*. John Wiley & Sons, New York (1979).
15. Garcia, S. E. and Mejorada, A. V. Geogard SX: A silica scale inhibitor for geothermal brine. *Geothermal Resources Council Transactions*, 25, 15–21 (2001).
16. Gallup, D., Sugiaman, F., Capuno, V., and Manceau, A. Laboratory investigation of silica removal from geothermal brines to control silica scaling and produce usable silicates. *Applied Geochemistry*, 18, 1597–1612 (2003).
17. Sugiaman, F., Sunio, E., Molling, P., and Stimac, J. Geochemical response to production of the Tiwi geothermal field, Philippines. *Geothermics*, 33, 57–86 (2004).
18. Rose, P. E., Benoit, W. R., and Kilbourne, P. M. The application of the polyaromatic sulfonates as tracers in geothermal reservoirs. *Geothermics*, 30, 617–640 (2001).
19. Hirtz, P., Kunzman, R., Broaddus, M., and Barbita, J. Developments in tracer flow testing for geothermal production engineering. *Geothermics*, 30(6), 727–745 (2001).
20. Gallup, D. L. and Featherstone, J. L. Acidification of steam condensate for incompatibility control during mixing with geothermal brine. U.S. Patent 4,615,808 (1986).
21. Gallup, D. L. and Featherstone, J. L. Use of added water to achieve 100% injection weight in geothermal operations. U.S. Patent 5,413,718 (1995).
22. Hirtz, P., Thermochem, Inc. internal report to Puna Geothermal Venture (1998).
23. Gallup, D. L. Brine pH modification scale control technology. *Geothermal Resources Council Transactions*, 20, 749–752 (1996).
24. Gallup, D. L. The interaction of silicic acid with sulfurous acid scale inhibitor. *Geothermal Resources Council Transactions*, 21, 49–53 (1997).
25. Gallup, D. L. and Kitz, K. Low cost silica, calcite and metal sulfide scale control through on-site production of sulfurous acid from H₂S or elemental sulfur. *Geothermal Resources Council Transactions*, 21, 399–403 (1997).
26. Hirowatari, K. and Yamauchi, M. Experimental study on a scale prevention method using exhausted gases from geothermal power stations. *Geothermal Resources Council Transactions*, 14, 1599–1602 (1990).
27. Gallup, D. L. The use of reducing agents for control of ferric silicate scale deposition. *Geothermics*, 22, 39–48 (1993).
28. Gallup, D. L. and Jost, J. W. Use of reducing agents to control scale deposition from high temperature brine. U.S. Patent 4,830,765 (1989).
29. Candelaria, M. N. R. Methods of coping with silica deposition—the PNOC experience. *Geothermal Resources Council Transactions*, 20, 661–672 (1996).
30. Featherstone, J. L., Van note, R. H., and Pawlowski, B. S. A cost effective treatment system for the stabilization of spent geothermal brines. *Geothermal Resources Council Transactions*, 3, 201–204 (1979).
31. Featherstone, J., Butler, S., and Bonham, E. Comparison of crystallizer reactor clarifier and pH mod process technologies used at the Salton Sea geothermal field. In *Proceedings World Geothermal Congress*, Florence, Italy, pp. 2391–2396 (1995).
32. Gallup, D. L. and Featherstone, J. L. Control of NORM deposition from Salton Sea geothermal brine. *Geothermal Resources Council Transactions*, 17, 379–385 (1993).
33. Gallup, D. L. Combination flash-bottoming cycle geothermal power generation facility: A case history. In *Proceedings of IECEC*, Washington, DC, pp. 1622–1627 (1996).
34. Gestur, G. Reykjavik Energy, personal communication (2001).
35. Hirtz, P. Thermochem, Inc. internal report to Ormat (2004).

36. Phillips, S. L., Mathur, A. K., and Doebler, R. E. A survey of treatment methods for geothermal fluids. Society of Petroleum Engineering, Paper 6606 (1977).
37. Crane, C. H. and Kenkeremath, D. C. Field evaluation of chemical additives for scale control. *Geothermal Resources Council Transactions*, 5, 459–462 (1981).
38. Harrar, J. E., Lorensen, L. E., Otto, C. H. Jr., Deutscher, S. B., and Tardiff, G. E. Effects of organic additives on the formation of solids from hyper-saline geothermal brine. *Geothermal Resources Council Transactions*, 2, 259–262 (1978).
39. Harrar, J. E., Locke, F. E., Otto, C. H. Jr., Lorensen, L. E., Monaco, S. B., and Frey, W. P. Field tests of organic additives for scale control at the Salton Sea geothermal field. *Society of Petroleum Engineering Journal*, 22(2), 17–27 (1982).
40. Gallup, D. L. Investigations of organic inhibitors for silica scale control from geothermal brines. *Geothermics*, 31, 415–430 (2002).
41. Gallup, D. L. and Barcelon, E. Investigations of organic inhibitors for silica scale control from geothermal brines. II. *Geothermics*, 34, 756–771 (2005).
42. Gauthier, B., Garnier, O., Pedenaud, P., and Pottier, F. Procèdes d'extraction d'huiles Lourdes et de generation de vapeur d'eau comprenant l'utilisation d'inhibiteurs de depot de silice. France Patent 2,858,314-A1 (2003).
43. Amjad, Z. and Zuhl, R. W. An evaluation of silica scale control additives for industrial water systems. NACE/08, Paper No. 08368, National Association of Corrosion Engineers, Houston, TX (2008).
44. Gonzalez, W. J., Kellogg, N. L., Pelant, F. G., Reyes Briseno, E., Garibaldi, F., and Mora, O. Evaluations of various organic inhibitors in controlling silica fouling at the CFE Cerro Prieto geothermal field. *Geothermal Resources Council Transactions*, 27, 477–483 (2003).
45. Matlick, S. and Stapleton, M. Successful development of new silica inhibitor technology at Ormesa. *Geothermal Resources Council Transactions*, 28, 425–428 (2004).
46. Angcoy, E. C., Alcober, E. H., Mejorada, A. V., Gonzalez, R. C., Cabel, A. C. Jr., Magpantay, R. O., Ruaya, J. R., and Stapleton, M. Test results of another silica scale inhibitor for Malitbog geothermal brine, Tongonan, Leyte. *Geothermal Resources Council, Transactions*, 29, 681–686 (2005).
47. Tester, J. W. et al. The future of geothermal energy: Impact of enhanced geothermal systems (EGS) on the United States in the 21st century. Final Report to the U.S. Department of Energy Geothermal Technologies Program. Massachusetts Institute of Technology, Cambridge, MA (2006).

10 Recent Developments in Controlling Silica and Magnesium Silicate Foulants in Industrial Water Systems

Konstantinos D. Demadis

CONTENTS

10.1	Introduction.....	179
10.2	Formation and Growth of Amorphous Silica	180
10.3	Silica Scale Control.....	182
10.4	Silica Growth Inhibition by the Use of Chemical Additives	183
10.5	Mechanism of Silica Scale Inhibition	188
10.6	Magnesium Silicate in Geochemistry	188
10.7	Water-Formed “Magnesium Silicate” Deposits	189
10.8	The Role of Mg ²⁺ Level, Temperature, pH, and Supersaturation	191
10.9	Other Metal Silicate Scales.....	192
	10.9.1 Iron Silicate.....	192
	10.9.2 Aluminum Silicate.....	194
	10.9.3 Calcium Silicate.....	195
10.10	Effect of Other Cations	195
10.11	Magnesium Hydroxide and Its Role in Magnesium Silicate Formation.....	195
10.12	Effect of Additives on Metal Silicate Scale Control.....	195
10.13	Practical Guidelines for Control of Magnesium Silicate Scale.....	197
10.14	“Metal Silicates” in Biological Systems	198
10.15	Epilogue	199
	Acknowledgments.....	199
	References.....	200

10.1 INTRODUCTION

Fouling presents an enormous challenge in industrial process waters [1]. Often system operators are obligated to discard critical equipment components because of fouling and the inability to remove it. Even if mechanical or chemical cleaning are viable options, they require several hours, total system shutdowns, and high costs [2]. Foulants could be organic or inorganic, as illustrated in Figure 10.1. Organic foulants are a result of poor system biocontrol, or deposition of organic matter brought into the system from external sources (e.g., a river or lake) [3]. Inorganic foulants include crystalline sparingly soluble salts such as calcium carbonate(s), calcium sulfate(s), barium, and strontium sulfates, as well as amorphous and colloidal deposits, such as amorphous calcium phosphate, silica, magnesium silicate, and many others, depending on the particular water chemistry [4]. This chapter deals with silica and metal silicate scales and deposits (with an emphasis on magnesium silicate).

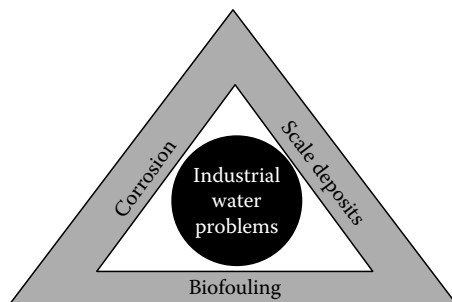


FIGURE 10.1 Schematic depiction of industrial water problems. (Reproduced from Demadis, K.D. et al., *Desalination*, 213, 38, 2007. With permission.)

Silica and magnesium silicate are poorly studied foulants and established methods for their control are not satisfactorily developed. Perhaps the reason for that is their scarcity in water systems; their presence is rather limited to those waters that satisfy one of the following three conditions: (a) contain high levels of silica, (b) contain high levels of magnesium, or (c) operate at high pH regions (>8.5). The purpose of this chapter is to review the “state of the art” of the formation and control of silica and magnesium silicate and to present efforts for their control using chemical additives. Throughout this chapter, the term “soluble silica” means “molybdate-reactive silica.”

10.2 FORMATION AND GROWTH OF AMORPHOUS SILICA

The formation, precipitation, and deposition of amorphous silica in process industrial waters have been a subject of intense interest. In parallel, there is also substantial focus on biosilica formation, due to the fact that silica is used by nature as a structural material for several organisms, such as diatoms [5]. Silica scale formation is a highly complex process [6]. It is usually favored at a pH level of less than 8.5, whereas magnesium silicate scale forms at a pH level of greater than 8.5. Available data suggest that silica solubility is largely independent of pH in the range of 6–8. This pH region of minimum silica solubility and silicic acid polymerization has a maximum rate, as shown in Figure 10.2. Silica exhibits normal solubility characteristics. Its solubility increases proportionally to temperature. In contrast, magnesium silicate exhibits inverse solubility. Other forms of silica, e.g., quartz (crystalline SiO_2) and glass also possess “normal” solubility, but they are both less soluble than amorphous silica. This is shown clearly in Figure 10.3.

Silica formation is actually a polymerization event. When silicic acid/silicate ions condense and polymerize, they form a plethora of structural motifs, including rings of various sizes, cross-linked polymeric chains of different molecular weights, oligomeric structures, etc. [7]. The resulting silica scale is a complex and amorphous product (colloidal silica)—a complicated mixture of the above components. Silicic acid polymerization starts with an attack of a deprotonated, negatively charged silicate ion to a silicic acid molecule, yielding an initial “dimer,” which then continues to undergo further attack. The initial stages of the silica dimerization/oligomerization/polymerization process are shown in Figure 10.4. This results in random polymer chain growth that produces silica nanoparticles. These, in turn, can further grow (by incorporation of silicic acid onto the silica particle surface) or agglomerate with other nanoparticles to give larger particles.

Operation in a high-pH regime is not necessarily a solution for combating silica scale. Water system operators must take into account the presence of magnesium (Mg^{2+}) and other scaling ions such as calcium (Ca^{2+}). As will be discussed later, other metal cations may aggravate metal silicate fouling. A pH adjustment to greater than 8.5 might result in the massive precipitation of magnesium silicate if high levels of Mg^{2+} are present or in calcium carbonate (CaCO_3) or calcium phosphate if high levels of these ions are overlooked.

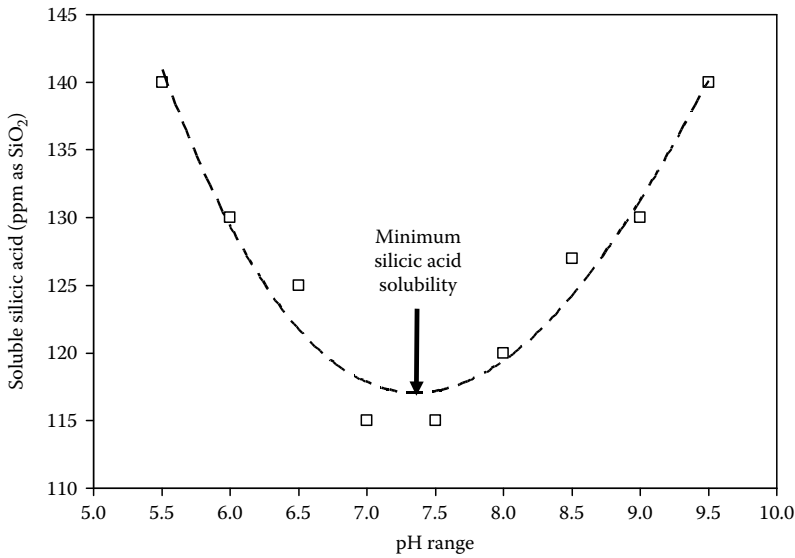


FIGURE 10.2 Dependence of silicic acid polymerization on pH based on experimental results [17j]. Starting level of silicic acid was 500ppm (as SiO₂) and pH of silica growth was 7.00. (Reproduced from Ketsetzi, A. et al., *Desalination*, 223, 487, 2008. With permission.)

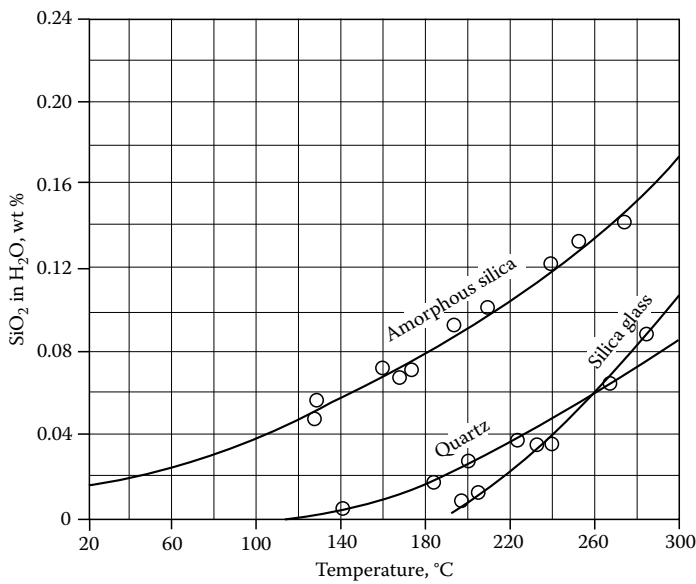


FIGURE 10.3 Dependence of different forms of silica solubility on temperature.

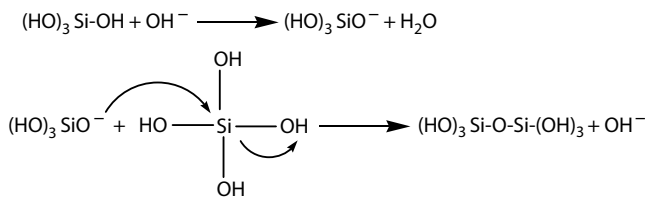


FIGURE 10.4 Initial steps in silicic acid polymerization. (Reproduced from Ketsetzi, A. et al., *Desalination*, 223, 487, 2008. With permission.)

Silica precipitation can also be aggravated by the presence of metal ions such as iron ($\text{Fe}^{2+/3+}$) or aluminum (Al^{3+}) and their hydroxides. Corroded steel surfaces (e.g., on pipes or heat exchangers) are prone to silica fouling. Iron oxides/hydroxides act as deposition matrices for silica (either soluble or colloidal) deposits.

There are three principal ways by which silica forms [8]: surface deposition, bulk precipitation, and in living organisms.

Surface deposition: This occurs as a deposit on a solid surface where silicic acid condenses with any solid surface possessing $-\text{OH}$ groups. If the surface contains $\text{M}-\text{OH}$ moieties ($\text{M} = \text{metal}$), this reaction is further enhanced. Such pronounced silica deposition phenomena in the water treatment industry are evident on metallic surfaces that have suffered severe corrosion on a surface covered with metal oxides/hydroxides. Once the receptive surface is covered with silica scale, additional silica is deposited on an already formed silica film.

Bulk precipitation: This occurs as colloidal silica particles grow through the aforementioned condensation reaction. The particles collide with each other and agglomerate, forming larger particles.

In living organisms: This form of silica is called biogenic or biosilica and appears in certain microorganisms such as diatoms that have the ability to remove and deposit silica from highly undersaturated solutions into precisely controlled structures of intricate design [9]. It should be mentioned that sessile microorganisms in a biofilm-fouled heat exchanger can entrap colloidal silica. The high affinity of soluble silica toward extracellular biopolymers such as polysaccharides has also been recognized.

10.3 SILICA SCALE CONTROL

The current practices for combating silica scale growth in industrial waters include operation at low cycles of concentration (The number of cycles of concentration indicated how many times the concentration of a certain water-soluble species has been increased.), prevention of “other” scale formation, pretreatment [10], and inhibitor or dispersant use. This section focuses on the inhibition of silica polymerization by the use of polymers.

Operation at low cycles of concentration is a common practice, but one that consumes large amounts of water. In a cooling tower operating at a pH level of less than 7.5, soluble silica generally should be maintained below 200 ppm (as SiO_2). For a pH level higher than 7.5, soluble silica should be maintained below 100 ppm (as SiO_2). One should bear in mind that Mg^{2+} levels also should be taken into account at a pH level greater than 7.5. In this case, the product (ppm Mg as CaCO_3) \times (SiO_2 as SiO_2) should be below 20,000.

Prevention of “other” scale formation indirectly interferes with the propensity of silica scale to co-precipitate with other scales [11]. The method is based on the prevention of other scaling species such as CaCO_3 or calcium phosphate and indirectly benefits the whole cooling tower operation. CaCO_3 precipitates provide a crystalline matrix in which silica can be entrapped and grown. In environments in which CaCO_3 or any other mineral precipitate is prevented completely, higher silica levels generally are tolerated in the process water as opposed to those environments in which other scales are controlled ineffectively.

Pretreatment involves reactive or colloidal silica removal in precipitation softeners through an interaction between silica and a metal hydroxide. Both iron hydroxide, $\text{Fe}(\text{OH})_3$, and aluminum hydroxide, $\text{Al}(\text{OH})_3$, have shown silica-removal capabilities, although magnesium hydroxide, $\text{Mg}(\text{OH})_2$, is considered to be more effective. In addition, silica can be removed through reverse osmosis (RO) and ion exchange techniques, as well as desilicizers. RO membranes are not immune to silica scale, which forms as a gelatinous mass on the membrane surface. It can then dehydrate, forming a cement-like deposit [12].

10.4 SILICA GROWTH INHIBITION BY THE USE OF CHEMICAL ADDITIVES

The use of inhibitors or dispersants to control silica scale generally follows two approaches: (a) inhibition and (b) dispersion. Inhibition is defined as the prevention of silicic acid oligomerization or polymerization. As a result, silicic acid remains soluble and, therefore, formation of colloidal silica is prevented. Dispersion, on the other hand, is the prevention of particle agglomeration to form larger-size particles and the prevention of the adhesion of these particles onto surfaces.

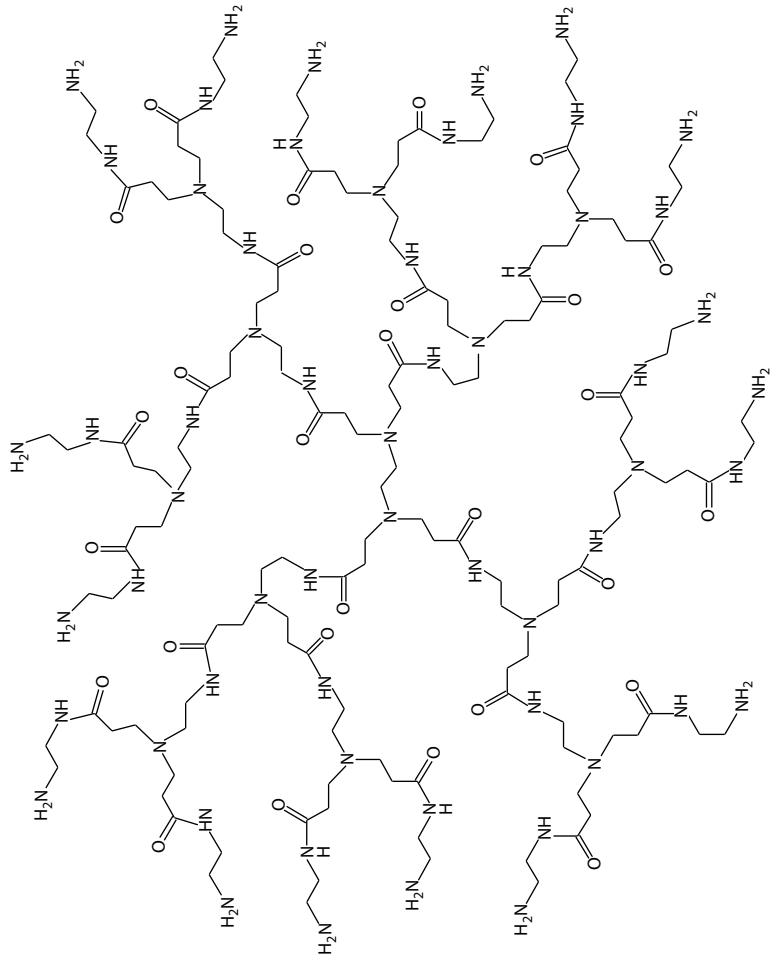
A number of products are available commercially for silica scale control in RO, geothermal, and evaporative cooling water applications. A detailed discussion of these commercial products is not the intent of this chapter. However, some promising chemistries will be discussed herein. Much information about commercial silica scale treatment can be found on the Internet through any of the popular search engines. In addition, several proprietary technologies can be found in patent literature.

Amjad et al. [13] have tested a number of polymers for silica inhibition with an emphasis on reverse osmosis systems. They discovered that a proprietary polymer at a polymer:silica ratio of 1:12 can maintain ~500 ppm of soluble silica in a pilot scale RO system for about 5 h. The conditions of the study were 600 ppm initial silica, 200 ppm Ca, 120 ppm Mg, and pH 7 at 40°C. A mixture containing molybdate (MoO_4^{2-}), phosphonate (diethylenetriamine-penta(methylene-phosphonic acid)), and a copolymer of acrylic acid and 2-acrylamido-2-methylpropane sulfonic acid (AA:SA) was found to be effective in preventing the formation and deposition of silica-containing deposits [14]. A carboxylate/sulfonate/balanced terpolymer was tested in the field [15]. This multipolymer contains balanced hydrophilic/hydrophobic functional groups that enhance adsorption of the dispersant onto colloidal silica and magnesium silicate composite scales when the temperature is raised. In addition, the multipolymer contains sulfonate and carboxylate groups that impart tolerance to soluble iron and superior dispersancy. The presence of the hydrophilic groups serves to induce steric repulsion between silica particles that have polymer chains adsorbed onto them. In another study, a polyanionic/neutral polymer at 12.5 ppm maintained soluble silica up to 370 ppm in RO systems [16].

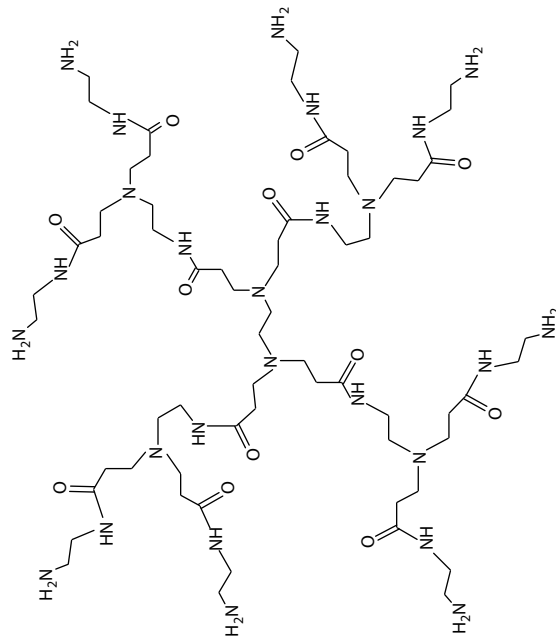
Recent research in our laboratories has shown that “small molecules” (cationic or anionic) are not active in silica scale inhibition under conditions and dosages pertinent to water treatment systems [17]. Furthermore, anionic polymers have also shown inactivity; one literature example showed that modified polyacrylates (at dosages >1000 ppm) have shown some inhibition [18]. Therefore, polymeric additives that contain some degree of cationic charge were sought. The schematic structures of some inhibitors are shown in Figure 10.5.

The selected polymers show a variety of structural features. All contain some degree of cationic charge. Some (PAMAM-1, PAMAM-2, PEI, PALAM, PAMALAM) possess cationic charge exclusively. Others (PPEI, PCH) are zwitterionic, i.e., they have cationic and anionic charge on the polymer backbone. Some polymers possess a positive charge by virtue of the protonated amine groups (PAMAM-1, PAMAM-2, PEI, PALAM), while others have a “pure” cationic charge due to a tertiary N group (PAMALAM). These additives have been extensively tested with varying dosages. Figure 10.6 presents silicic acid stabilization results with 40 ppm dosage for all polymers.

It is evident from Figure 10.6 that all polymers show inhibitory activity (higher soluble silicate levels than the “control” [17]). PAMAM-1 and PAMAM-2 (both have their surface amine groups protonated at pH 7) are very effective inhibitors at a dosage of 40 ppm. The presence of protonated amine groups is not the only necessary condition for good inhibition. Notice that polymers PEI and PALAM (also having their amine groups protonated at pH 7) show rather poor performance. This could be explained by the fact that excessive cationic charge causes the polymeric additive to be entrapped and hence deactivated within the colloidal silica matrix. PAMALAM, which is a polymer that possesses a tertiary N group, is a “medium” performance inhibitor. From the zwitterionic polymers (PPEI and PCH), PPEI is a very effective inhibitor. In this case, it appears that the negative charge ($-\text{PO}_3\text{H}^-$ for PPEI) “balances” the positive charge in such a way that the polymer continues to be active, but inhibitor entrapment and deactivation is stopped. For the PCH polymer, perhaps the anionic charge (due to $-\text{PO}_3\text{H}^-$) is too excessive and the cationic charge (necessary for inhibition) is “neutralized.”



PAMAM-2



PAMAM-1

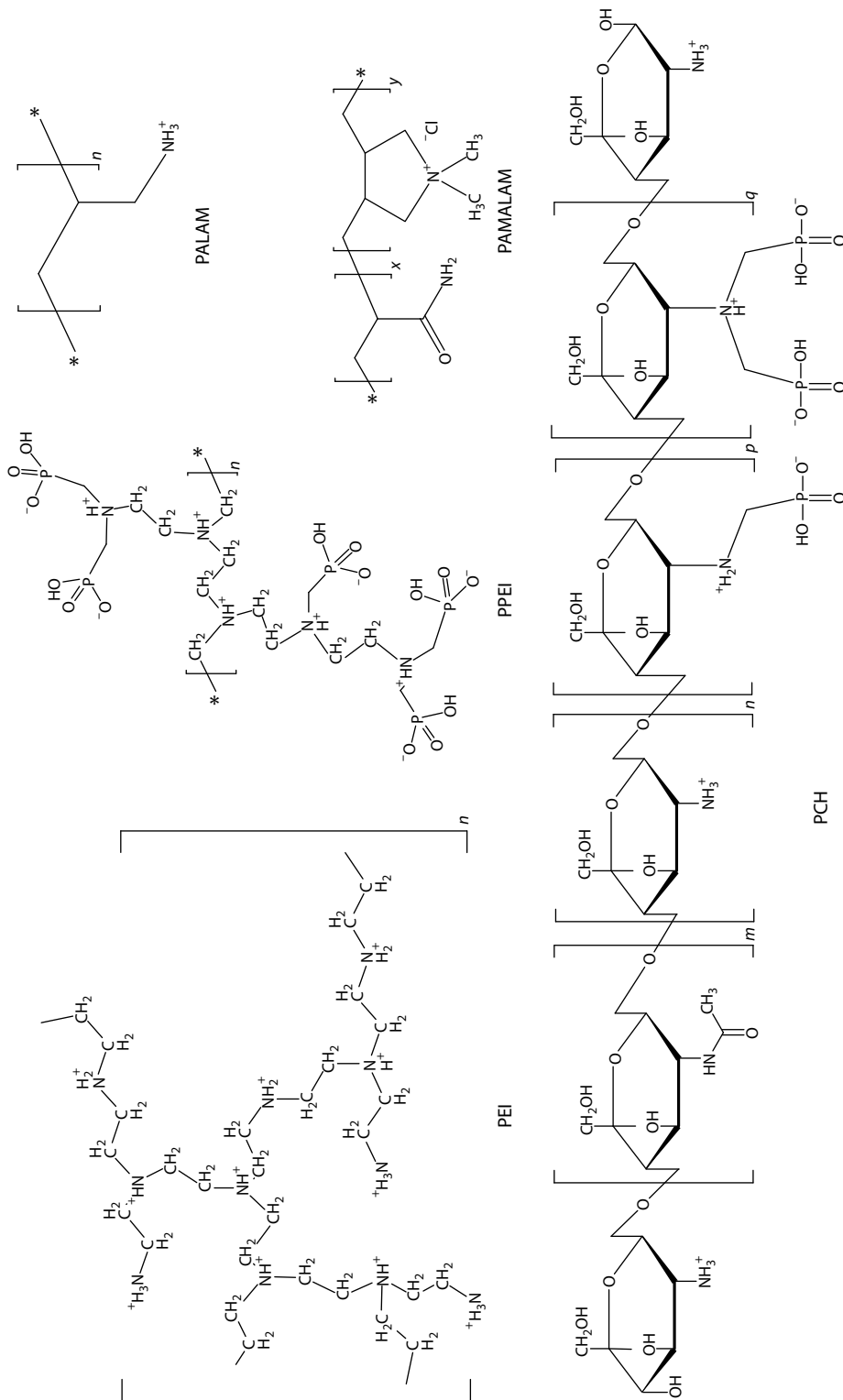


FIGURE 10.5 Schematic structures of the polymeric inhibitors. Abbreviations: PAMAM-1, polyaminoamide dendrimer of generation 1; PAMAM-2, polyaminoamide dendrimer of generation 2; PEI, polyethylenimine; PALAM, polyallylamine; PAMALAM, poly(acrylamide-co-diallyl-dimethylammonium chloride) ($x = 0.55, y = 0.45$); PPEI, phosphonated polyethylenimine; PCH, phosphonomethylated chitosan with $m = 0.16, n = 0.37, p = 0.24, q = 0.14$.

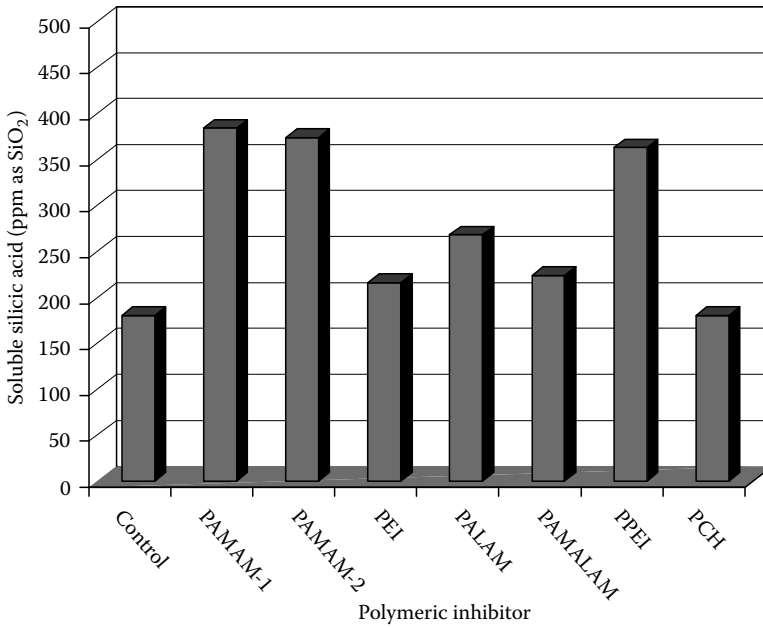


FIGURE 10.6 Silicate stabilization (starting silicate level = 500 ppm) in the presence of polymeric additives (at 40 ppm dosage). Experimental conditions: pH = 7.0, temperature = 2.5°C, polymerization time = 24 hours, filter pores 0.8 μm .

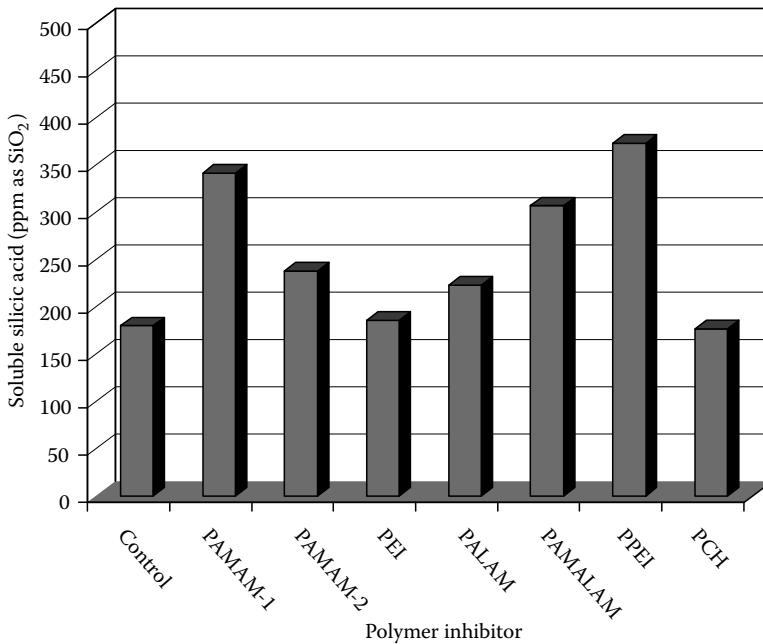


FIGURE 10.7 Silicate stabilization (starting silicate level = 500 ppm) in the presence of polymeric additives (at 80 ppm dosage) (The experimental conditions are the same as in Figure 10.6).

When the polymer dosage is doubled (an increase from 40 to 80 ppm), a number of interesting features appear in the inhibition activity (Figure 10.7). PAMAM-1 retains its inhibitory activity, in contrast to PAMAM-2, which substantially drops in performance (from 374 to 238 ppm soluble silicate). PEI, PALAM, PPEI, and PCH retain their previous inhibitory activity, with only minor alterations. The only polymer that increases its activity is PAMALAM. Further dosage increase, however, caused no further solubility enhancement (data not shown).

It is apparent that an increase in inhibitor dosage has detrimental effects on inhibitory activity. This has been observed before for other cationic inhibitors [17c]. It can be explained upon the examination of the possible silica inhibition mechanism. Experimental results from our group have supported the premise that anionic molecules (either monomeric or polymeric) have no effect on silicate polymerization [17c]. In contrast, cationic polymeric molecules are effective silica scale inhibitors [17]. When silicate polymerization takes place in the presence of a cationic polymeric additive, there are a number of competing reactions taking place concurrently: (a) polymerization of silicic acid. This occurs through an S_N2 -like mechanism that involves the attack of a monodeprotonated silicic acid molecule on a fully protonated silicic acid molecule. This pathway generates at first short-lived silicate dimers, which in turn continue to polymerize in a random way to eventually yield colloidal silica particles. (b) Silicate ion stabilization by the cationic additive. This is the actual inhibition step and occurs presumably through cation–anion interactions, and (c) flocculation between the polycationic inhibitor and the negatively charged colloidal silica particles (at pH 7) that are formed by the uninhibited silicate polymerization (Figure 10.8).

The cationic inhibitor is trapped within the colloidal silica matrix, based on process (c). This is demonstrated by the appearance of a light flocculent precipitate (or dispersion at times). Inhibitor entrapment causes its depletion from solution and its deactivation. Therefore, only a portion of the inhibitor is available to continue inhibition at much lower levels than initially added to the polymerization medium. Thus, soluble silicate levels continue to decrease because eventually there is not a sufficient amount of inhibitors to perform the inhibition. Inhibitor entrapment is directly

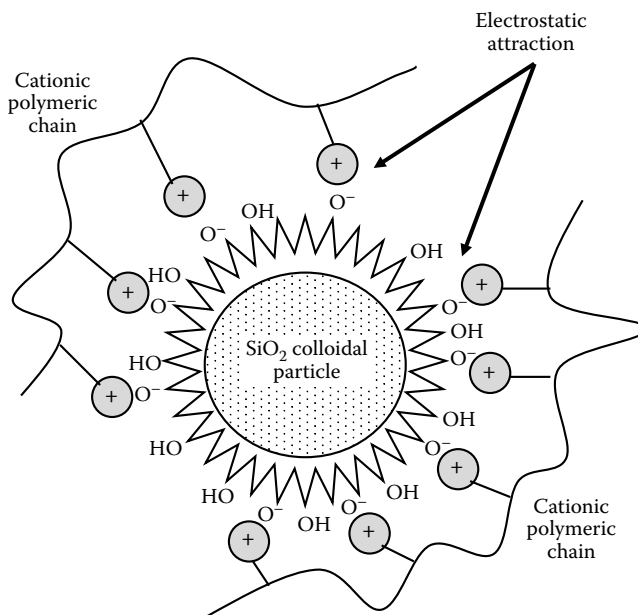


FIGURE 10.8 Cationic polymer–induced flocculation of silica particles that leads to inhibitor entrapment. (Reproduced from Ketsetzi, A. et al., *Desalination*, 223, 487, 2008. With permission.)

proportional to cationic charge density. For example, PEI (polyethyleneimine), a branched cationic polymer with high positive charge density, creates composite precipitates with colloidal silica rapidly [17f]. It is now certain that effective silica scale inhibition is dependent on the cationic charge on the polymer backbone (in an as of yet insufficiently quantified fashion). It has been demonstrated that certain cationic polymers are trapped in the colloidal silica matrix by FT-IR spectroscopy and elemental analyses [17c].

10.5 MECHANISM OF SILICA SCALE INHIBITION

Amorphous silica formation is governed by several important equilibria. Some of these are given in Figure 10.9.

As mentioned above, silica deposition results from silicic acid self condensation. This reaction is first order and is catalyzed by OH^- in the pH range of 5–10. Reports have shown that the reaction yielding a silicic acid dimer is kinetically slow in contrast to the reactions giving a trimer, tetramer, pentamer, etc., which are very fast [19]. All these equilibria are sensitive to pH and tend to be accelerated by metal ions that form hydroxides, e.g., $\text{Fe}^{2+/3+}$, Mg^{2+} , or Al^{3+} .

Polymerization of silicic acid is believed to occur through a $\text{S}_{\text{N}}2$ -like mechanism involving a deprotonated silicic acid monoanion ($(\text{HO})_3\text{Si-O}^-$) and the Si center of silicic acid, $\text{Si}(\text{OH})_4$. Inhibition of this step should be critical in the inhibition of silica scale formation. Some reports indicate that orthosilicates hydrolyze more rapidly than other silicate species such as disilicates, chain silicates, cross-linked oligomers, and polymers, suggesting that bridging oxygens are much more resistant to attack than non-bridging oxygens. Above a pH of 2, this mechanism involves polymerization with condensation, catalyzed by OH^- .

One can envision electrostatic interactions between a cationic polymeric inhibitor and monodeprotonated silicic acid. These interactions stabilize soluble silicate and prohibit the condensation reaction. Alternatively, a cationic polymer whose positive charge is primarily based on protonated amine moieties can stabilize silicic acid molecules and/or silicate ions by hydrogen bonds. Most likely, a combination of the above interactions occur simultaneously for polymeric inhibitors with protonated amine groups, whereas electrostatic interactions are responsible for the stabilizing effect for polymers that have no N–H moieties, but possess $-\text{NR}_4^+$ groups (e.g., PAMALAM).

To prove that cationic charges on the polymer backbone are responsible for the silicic acid stabilizing effect, experiments were performed in which a second, anionic polymer was added with the cationic polymeric inhibitor. If this second anionic polymer is added in sufficient excess to “blanket” the positive charge of the cationic inhibitor, inhibition performance deteriorates to virtually none [20]. This was proven for dendrimers PAMAM-1 and PAMAM-2 and PCH. The characteristics of the anionic polymer play a profound role in this “inhibition of inhibition” event.

The precise mechanism of silica formation is only partially understood. As a consequence, the exact mechanism of silica scale inhibition is not fully delineated. However, it is now certain that any interference with the condensation reaction could lead to silica scale growth inhibition. A relevant example is silica inhibition by orthoborate, which reacts with silicate ions to form borosilicates. These products are more soluble in water than are silica/metal silicates [21].

10.6 MAGNESIUM SILICATE IN GEOCHEMISTRY

Examination of the composition of the nine rock-forming minerals reveals that they all belong to the silicate group of minerals. The basic building unit of silicate minerals is the SiO_4^{4-} complex ion, the silicon tetrahedron. Oxygen and silicon are the most

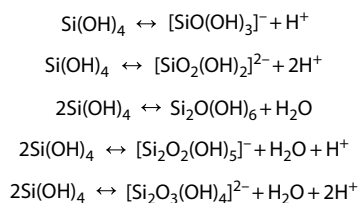


FIGURE 10.9 Silicic acid equilibria that occur in aqueous systems.

TABLE 10.1
Names and Compositions of
the Most Common Magnesium
Silicate Minerals

Magnesium Silicates	Molecular Formula
Chrysotile	$Mg_3Si_2O_5(OH)_4$
Clinoenstatite	$Mg_3Si_2O_6$
Enstatite	$Mg_2Si_2O_6$
Forsterite/chrysolite	Mg_2SiO_4
Magnesiosilica	$MgOSiO_2$
Olivine	$Mg_{1.6}Fe^{2+}(SiO_4)$
Orthochrysotile	$Mg_3Si_2O_5(OH)_4$
Parachrysotile/amianthus	$Mg_3Si_2O_5(OH)_4$
Pyrope	$Mg_3Al_2(SiO_4)_3$
Ringwoodite	Mg_2SiO_4
Saponite	$Ca_{0.1}Na_{0.1}Mg_{2.25}Fe_{0.75}^{2+}$ $Si_3AlO_{10}(OH)_2 \cdot 4H_2O$
Sepiolite	$Mg_4Si_6O_{15}(OH)_2 \cdot 6H_2O$
Serpentine/clinochrysotile	$Mg_3Si_2O_5(OH)_4$
Stevensite	$Ca_{0.15}Na_{0.33}Mg_{2.8}Fe_{0.2}^{2+}$ $Si_4O_{10}(OH)_2 \cdot 4H_2O$
Talc	$Mg_3Si_4O_{10}(OH)_2$
Wadsleyite	$Mg_{1.5}Fe_{0.05}^{2+}SiO_4$

abundant elements in the crust and mantle, and they form the strongly coordinating species SiO_4^{4-} over a wide range of conditions. This species is even stable in silicate melts, and because more than 90% of the Earth's crust is made of these two elements (more than 70% by weight), it is easy to understand why practically all the minerals in the crust (and mantle) are composed of silicate tetrahedra with a variety of other elements included among them.

Although the nine rock-forming minerals were mentioned above, they are really families of minerals with the same structural styles (in fact three of the rock-forming minerals, albite, orthoclase, and plagioclase are all from the feldspar family). In each of these "families" there is a basic framework/geometric arrangement of silicate tetrahedra, and the difference between "family members" is primarily in the types and abundances of other chemical elements that participate in the structure. Table 10.1 shows the most common magnesium silicate minerals.

10.7 WATER-FORMED "MAGNESIUM SILICATE" DEPOSITS

The term "magnesium silicate" is widely recognized in the water treatment industry. However, its definition differs from that in geology. In general, a deposit that contains both magnesium and silicon is called "magnesium silicate." In more harsh environments, such as in geothermal applications, the effect of high temperature favors the formation of geologically recognized magnesium silicates.

Precipitation of magnesium silicate can cause problems in a number of water treatment applications from truck radiators to geothermal wells and plants. Figure 10.10 shows a heat exchanger tube bundle fouled with magnesium silicate. The magnesium silicate system is highly pH-dependent. Below pH 7, there is essentially no chance of precipitation, because the silica exists in an unreactive, non-ionized form. Above pH 9, magnesium silicate is very likely to form because silica forms reactive silicate ions. Furthermore, the temperature is extremely important. Precipitation begins at a lower pH if the temperature is sufficiently high.

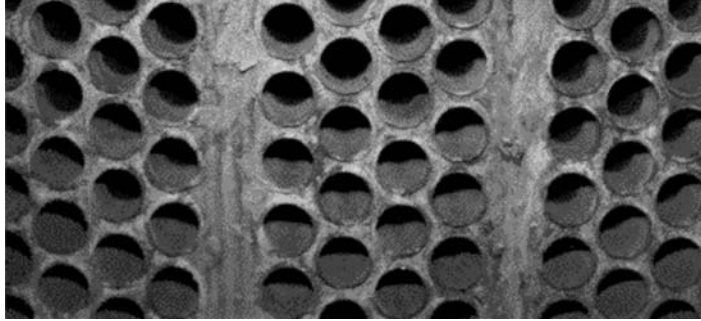


FIGURE 10.10 A magnesium silicate fouled heat exchanger tube bundle.

Scaling of magnesium silicates has been a problem in some of the Icelandic district heating systems [22]. This kind of scaling is not encountered in heating systems utilizing geothermal water directly but occurs by heating and deaerating fresh water. Two of the plants have heat exchangers to heat fresh water. The water in those systems is also discarded after a single use and not recirculated in the heating system. Scaling of a similar type occurred in a few other systems due to the mixing of cold water with the geothermal water. Magnesium silicates have low solubility in warm waters at a high pH level. The heating of groundwater depletes the magnesium concentration of geothermal waters mostly below 0.1 mg/kg. Magnesium silicate is amorphous based on x-ray diffraction (XRD) experiments whatever structure and it resembles that of chrysotile. It was also found that the Mg:Si ratio is close to 1 with small variations. An FT-IR spectrum of the above magnesium silicate deposits is shown in Figure 10.11.

The magnesium silicate sepiolite will precipitate from sea water at low temperatures (down to 25°C), as the dissolved silica concentration is increased. Increased temperature and high pH levels will enhance the rate of precipitation. The magnesium silicate talc will form easily in hydrothermal experiments and is frequently formed outside its stability field. Several other magnesium silicates such as stevensite, saponite, and chrysotile are known to be formed hydrothermally at relatively low temperatures. The heating of fresh water also initiates precipitation and it is well known that magnesium is one of the major components in “boilerstone.” The major factors controlling the

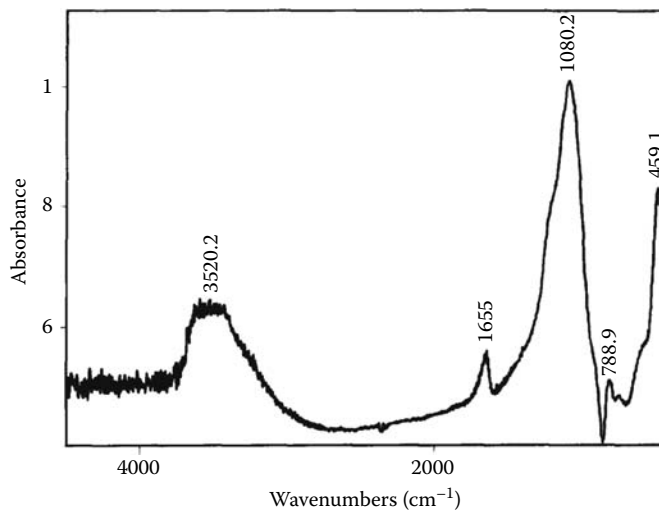


FIGURE 10.11 The FT-IR spectrum of a magnesium silicate deposit from Icelandic water used for heating applications. (Reproduced from Kristmannadóttir H. et al., *Geothermics*, 18, 191, 1989. With permission.)

degree of supersaturation are boiling temperature and pH, which in turn is mainly dependent on the deaeration process. Supersaturation is in all cases greater for talc than for chrysotile [23].

Co-precipitation of magnesium hydroxide, $\text{Mg}(\text{OH})_2$, and colloidal silica has also been observed [21]. One theory proposes that the formation of $\text{Mg}(\text{OH})_2$ occurs first, and then $\text{Mg}(\text{OH})_2$ subsequently reacts with monomeric silicate and/or polymeric silica to form magnesium silicate [24]. Ca^{2+} and Mg^{2+} salts were found to catalyze the silica polymerization reaction [25]. Higher concentrations of total hardness lead to a faster drop in dissolved silica in solution. In batch runs, Mg^{2+} was found to affect silica concentrations more than Ca^{2+} . For example, runs with a given hardness level but with lower ratios of Ca:Mg caused a faster decline in dissolved silica.

Magnesium silicate seems to be a “true” compound according to Young et al. [26]. According to their results, fairly consistent *amorphous* precipitate was obtained. The stoichiometric ratio of silicon to magnesium was found to be 1:1. This is the same whether the mother liquor contained a 1:2 or 2:1 mole ratio of silica to magnesium and whether the precipitation took place at room temperature or 75°C. Some comments on the possible mechanism of formation are warranted. If magnesium hydroxide precipitated out and silica simply absorbed, there should be little effect of silica on the precipitation point. By the same reasoning, the “opposite” mechanism of silica precipitation followed by magnesium absorption should be independent of magnesium concentration. In fact, increasing or decreasing silica concentration has an effect essentially equal to similar increases or decreases in magnesium concentration. The precipitate was found to contain significant amounts of adventitious water, presumably in the pores of the gel. This magnesium silicate precipitate dissolved in acid. Alternatively, ethylenediamine tetraacetic acid chelated the magnesium from the precipitate, leaving a loose flock of virtually pure colloidal silica, which did not redissolve in acid. It can be assumed that the magnesium silicate initially forms a loose, open gel structure with numerous hydroxide bridges. An alternative mechanism of magnesium silicate formation was proposed. According to this proposal, formation of magnesium silicate seems to be a two-step process. Under relatively high pH conditions, magnesium hydroxide is precipitated. Because magnesium hydroxide is inversely soluble with respect to temperature, the precipitation can take place near the surface of the heat transfer tubes and the maximum exchanger tube wall temperature should be ~80°C. Temperature has a greater influence upon the deposition than any of the variables. It was reported that a hydroxylated magnesium silicate forms in seawater in which SiO_2 concentration exceeds 26 ppm at pH 8.1 and clay minerals are found (kaolinite, glauconite, and montmorillonite) [27].

10.8 THE ROLE OF Mg^{2+} LEVEL, TEMPERATURE, pH, AND SUPERSATURATION

Magnesium silicate exhibits “inverse solubility” properties; its solubility decreases as the temperature increases [22,28]. The effect of pH is also profound. At pH regions <8, magnesium is rarely observed in deposits. This does not imply the absence of Si-containing scale deposits, it merely means that magnesium is not incorporated in the deposit structure. Figure 10.12 demonstrates that at pH > 8.5, analyses of several deposits showed that the Mg content increased with pH.

Several experiments performed in our laboratories demonstrated that Mg^{2+} ions actually act as a catalyst in silicic acid condensation reaction. In these experiments, the effect of Mg^{2+} level and pH were studied by following soluble levels of silicic acid. Figure 10.13 clearly shows that at pH 8, Mg^{2+} up to 100 ppm has virtually no effect in the silicic acid condensation reaction.

When pH is increased to 9.0 (Figure 10.14), the catalytic effects of Mg^{2+} start appearing, but Mg^{2+} dosage seems to have no measurable effect.

An increase in the operational pH level to 9.5 has a dramatic change on the catalytic effects of Mg^{2+} . Figure 10.15 demonstrates this dramatic effect. Another significant conclusion derived from Figure 10.15 is that at pH 9.5, the level of Mg^{2+} is now measurable and important. There seems to be a rapid decrease in soluble silicic acid levels as Mg^{2+} concentrations increase. At a level of 100 ppm Mg^{2+} , soluble silicic acid levels drop ~100 ppm lower than the “control.” This is convincing evidence that Mg^{2+} is an effective catalyst of silicic acid polymerization at pH regions > 9.0.

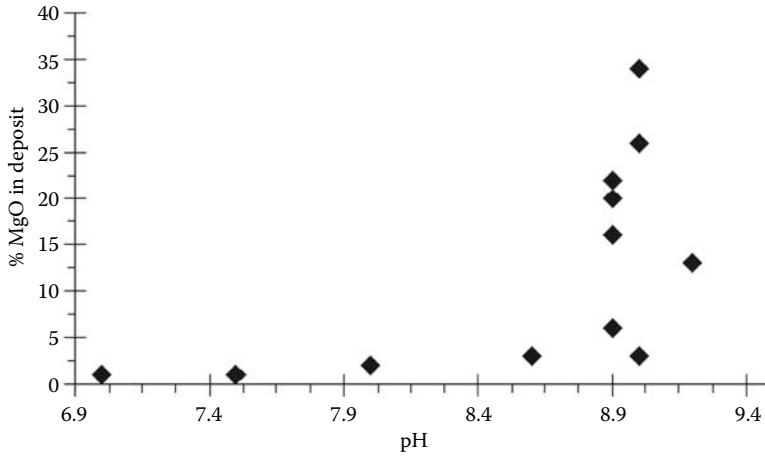


FIGURE 10.12 Magnesium content dependence on operational pH in a magnesium silicate scale deposit from pilot cooling tower tests. (Reproduced from Demadis, K.D. et al., *Desalination*, 179, 281, 2005. With permission.)

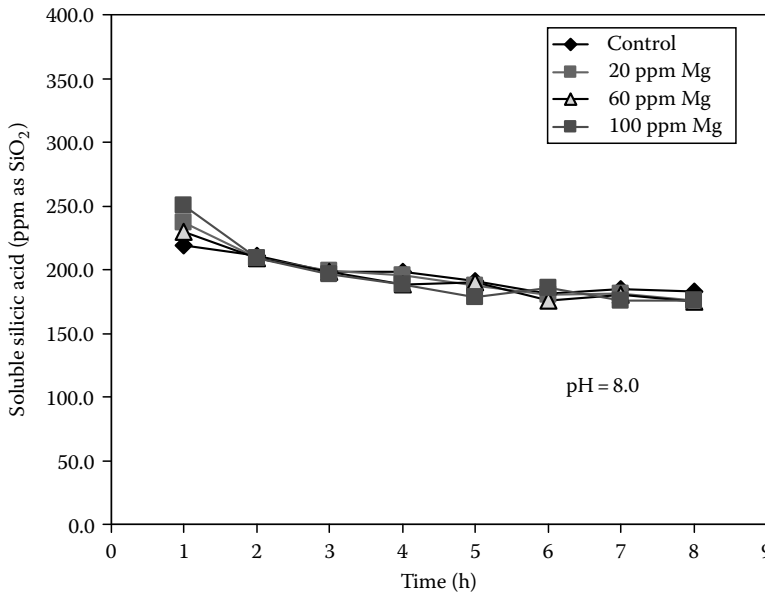


FIGURE 10.13 The effect of Mg level on silica polymerization at pH 8.0.

10.9 OTHER METAL SILICATE SCALES

10.9.1 IRON SILICATE

Qualitative evidence for the interaction of silicic acid with metal ions in aqueous solutions was observed as early as 1933 by Mattson [29], who suggested the existence of simple Al-silicate complexes in order to explain his soil experiments. This was followed by Hazel, who employed titrimetric procedures to study metal-silicate interactions with metals such as Al, Fe, and Cr [30]. No quantitative relationships were established for any of these interactions until the work of Weber and Stumm delineated the formation of a Fe(III)-silicate complex [31]:

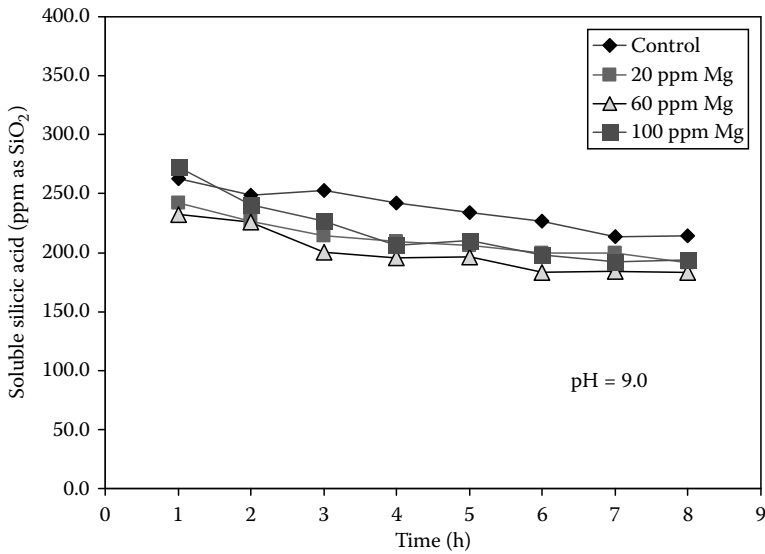


FIGURE 10.14 The effect of Mg level on silica polymerization at pH 9.0.

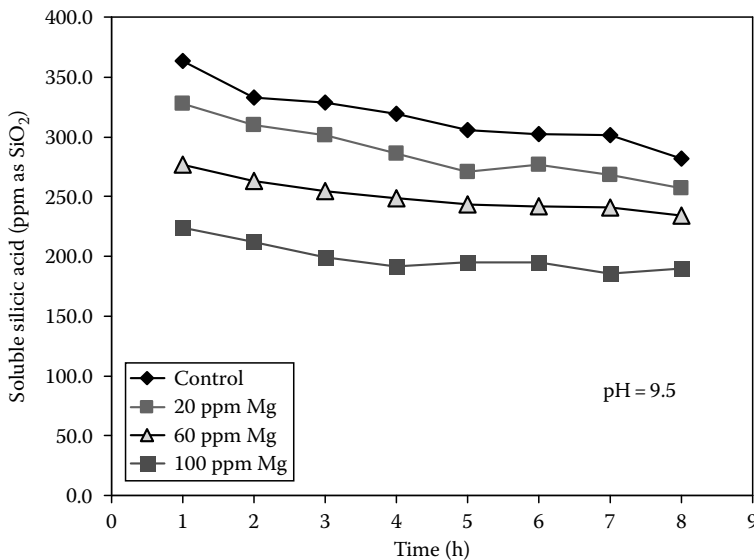
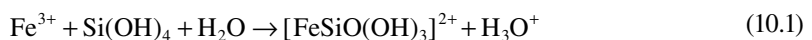


FIGURE 10.15 The effect of Mg level on silica polymerization at pH 9.5.



The experimental pH covered was 3.5, however it is expected that similar interactions take place in natural water pH. They found that the stability constant for the Fe(III)-silicate complex is 1.8×10^9 . Increased silica concentrations accelerated Fe(II) to Fe(III) oxidation in pH ranges 6.6–7.1 [32]. Fe(III) has a higher propensity for silicate or colloidal silica than Fe(II). This may create iron (III) silicate precipitates. Chan et al. studied the effect of Fe^{3+} on silica fouling of a pilot heat exchanger [33]. Experiments were performed at 125°C – 165°C , 1.58 MPa and under turbulent conditions. It was shown that the addition of a few ppm Fe^{3+} into a silica solution was sufficient to induce coagulation

and deposition of silica particles. These in turn caused a significant increase in fouling rates. Gallup studied iron silicate formation and its inhibition in geothermal systems [34].

10.9.2 ALUMINUM SILICATE

Siliceous scales deposited from geothermal brines often contain co-deposited Fe and Al. Fe and Al-rich amorphous silica scales have been reported to form from geothermal brines in Iceland; Japan; Greece; Djibouti; Salton Sea, California; Coso Hot Springs, California; and Dixie Valley, Nevada [35]. The concentrations of Al and SiO₂ in brines depositing scale range from 0.1 to 1 and 600 to 900 ppm, respectively. The scales consist primarily of Al-rich SiO₂. Al/Si molar ratios typically range from 0.1 to 0.2. Traces of Fe, alkalis, and alkaline earth metals were also found. Based on XRD, NMR, and FT-IR measurements, it was concluded that Al is four-coordinate in an opal-like framework [36]. Although Al retards *silicic acid* polymerization, in the near-neutral pH range [37], it is observed to concentrate in siliceous geothermal scales [38].

Amorphous aluminum-rich silica has been identified as a primary scale constituent deposited from certain geothermal brines. This scale is a non-stoichiometric compound exhibiting an empirical formula approaching Al₂O₃·(10–20)SiO₂, and consists of aluminum incorporated in an amorphous silica matrix. Spectroscopic studies indicate that aluminum is coordinated with silica in a three-dimensional array of corner-sharing tetrahedra. Aluminum in scale appears to derive from brine as a result of a reaction with silicic acid oligomers. There is no evidence to suggest that the scale is a simple mixture of amorphous alumina and silica, or a mixture of molecularly deposited silica and aluminosilicate minerals transported in brine from the reservoir. The Al-rich scale tends to deposit from brine at a higher temperature than that of pure amorphous silica. In laboratory experiments, aluminum reacts with supersaturated silicic acid solutions over the pH range 5–9 to precipitate aluminum and silica. The concentrations of aluminum and silica in the mixtures reach a minimum at near-neutral pH. Laboratory experiments indicate that aluminum-silica precipitation reactions are inhibited below pH 5 and above pH 9. A schematic presentation of the structural details of aluminum silicate is shown in Figure 10.16.

Amorphous aluminosilicate is one of the essential components in geochemical processes, such as weathering [39] and adsorption phenomena [40]. In natural systems, amorphous aluminosilicates are formed mainly by the co-precipitation of silicic acid and aluminum hydroxide [41]. There is a strong pH-dependent reaction between silica sols and Al³⁺ [42]. For example, 1 ppm of Al³⁺ is sufficient to reduce 45 ppm SiO₂ in the sol to 5 ppm in the pH range 4–5. Soluble SiO₂ requires considerably larger ratios of Al³⁺ to precipitate the silica at an optimum pH of 8–9 [43].

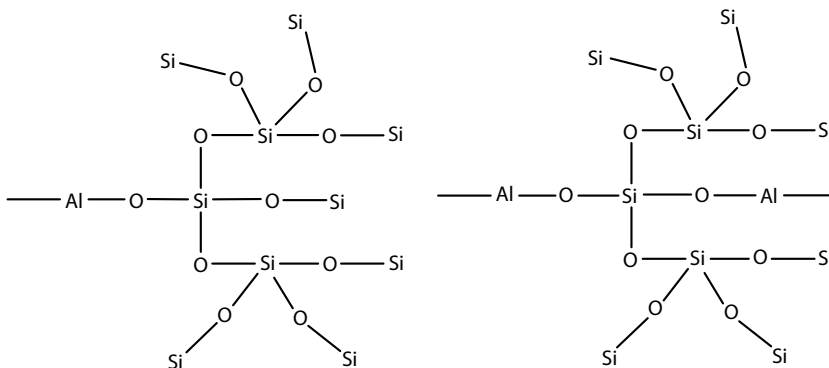


FIGURE 10.16 Schematic three-dimensional structures of aluminum silicate.

10.9.3 CALCIUM SILICATE

Calcium silicate hydrate (CSH) is the major product of Portland cement hydration, where it forms as an amorphous phase of variable composition. CSH is thought to form a layered structure related to tobermorite and jennite [44]. FT-IR of CSH is very similar to that of silica [45].

10.10 EFFECT OF OTHER CATIONS

Studies on the effects of Na^+ and K^+ on silica fouling of heat exchangers under turbulent flow conditions were carried out. It was found that the silica fouling rate in the presence of Na^+ is greater than that when K^+ is present [46]. The effect of cations on decreasing silica solubility follows the order $\text{Mg}^{2+} > \text{Ca}^{2+} > \text{Li}^+ > \text{Na}^+ > \text{K}^+$ [47,48]. At pH 7, Cu^{2+} ions are absorbed on a SiO_2 surface as polymeric hydroxide species [49]. The structure of these species is similar to that of the bulk amorphous $\text{Cu}(\text{OH})_2$. The amorphous state of the supported $\text{Cu}(\text{OH})_2$ is caused by a small size (11 Å) of the surface particles. In contrast, the overstoichiometric water molecules seem to have an effect of making bulk $\text{Cu}(\text{OH})_2$ more amorphous.

10.11 MAGNESIUM HYDROXIDE AND ITS ROLE IN MAGNESIUM SILICATE FORMATION

Our discussion on metal silicates also involves $\text{Mg}(\text{OH})_2$. This is because its role has been invoked before in the formation and growth of magnesium silicate [50]. The region of $\text{Mg}(\text{OH})_2$ insolubility is from pH 9.2 upward [51]. Aspects of magnesium hydroxide chemistry have been utilized in removing silica from process water streams. Other than anion resins, Mg^{2+} has been the most commonly used reagent to remove silica from water [52]. It was shown that for a saturated amorphous SiO_2 solution with about 140 ppm silica content, with an equivalent amount of MgCl_2 added, the maximum precipitation is at pH 11–11.5. About 35 ppm of SiO_2 remains in the solution [53]. Another report also showed that the addition of 100 ppm of “active” MgO can reduce silica content at 93°C from 22 to 1 ppm [54]. However, at 30°C the reduction is only 16 ppm. A common method of water “softening” is the hot-lime process in which lime (or dolomitic lime) and soda ash are added to water preheated with steam. Such a system is often used to remove silica. Temperature has a profound effect on silica removal [55]. A practical set of curves from Nordell shows the relation between silica present and magnesium added for removal. These curves include a 15% safety factor. Although this method seems to be effective, there are some disadvantages: (a) high temps are required for effective silica removal, (b) circulation of sludge and cold influent is required for maximum reaction with silica, and (c) high cost.

In the desalination of brackish water, silica is one of the major foulants that forms on the reverse osmosis membranes and limits the water recovery. In addition, it is a very adherent scale and once it forms, it is very difficult to clean and cleaning may damage the membrane. There are also complicating factors affecting silica fouling, such as the presence of cations (e.g., Ca, Mg, etc.) that usually promote silica polymerization. Pretreatment is used as a measure to reduce silica levels in the feed and hence mitigate silica fouling. Silica removal was also tested in the presence of sodium aluminate, lime, and soda ash in laboratory tests using field waters [56].

10.12 EFFECT OF ADDITIVES ON METAL SILICATE SCALE CONTROL

Since waterborne metal silicates are amorphous “binary systems,” the use of “traditional” threshold scale inhibitors is expected to be ineffective. However, control strategies that are based on either eliminating the metal cation or stabilizing silicic acid in its soluble form have a realistic

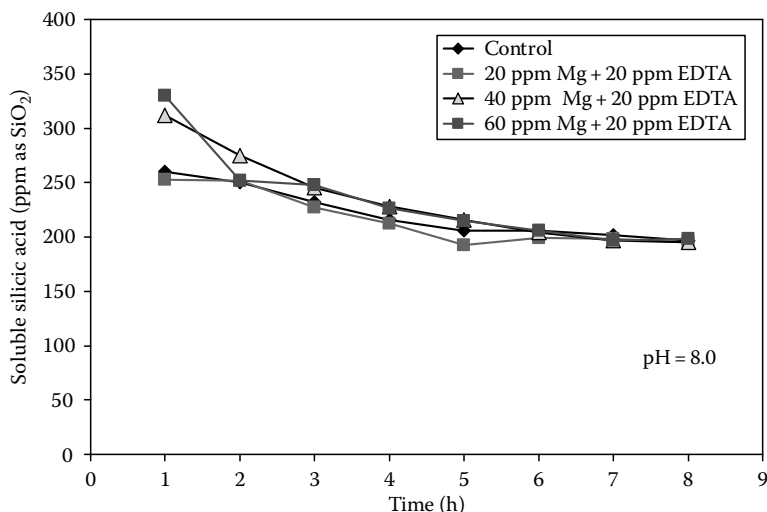


FIGURE 10.17 Influence of EDTA dosage on inhibiting the catalytic effect of Mg^{2+} on silicic acid polymerization at pH 8.0.

chance of being successful. Laboratory studies show that sequestering agents such as citric, acetic, and EDTA acids inhibit aluminum silicate scale formation in geothermal water systems [35]. Aluminum silicate scale deposition may be controlled at these pH extremes with precaution against corrosion and by-product scale formation. Low concentrations of complexing/sequestering agents with a carboxylate functionality maintain aluminum and silica in solution. These results imply that aluminum silicate scaling may be controlled by the treatment of brine with agents that form complexes with aluminum. Bulk silica precipitation can be successfully inhibited by brine pH adjustment alone. When residual aluminum-rich, amorphous silica scaling is to be prevented, the treatment of brines with low dosages of aluminum complexing agents may be necessary. Combinations of complexing agents and brine pH adjustment or the use of acidic complexing agents may prove useful in controlling amorphous aluminum-rich silica scale deposition from geothermal brines.

Magnesium silicate scale control was pursued in our laboratories by the use of EDTA as a Mg sequestering agent. Figure 10.17 shows that the addition of EDTA at a ppm level equal to that of Mg has no effect on soluble silicic acid. These experiments were performed by monitoring soluble silicic acid levels (starting concentration of silicic acid was 500 ppm as SiO_2). EDTA was proven to be ineffective at the dosages shown. Soluble silicic acid levels were the same as those without the presence of EDTA.

When the operational pH was increased to 9.0, the same situation was observed. As illustrated in Figure 10.18, no increase in soluble silicic acid levels is observed and these silicic acid values are the same as those without EDTA present.

When the pH was increased to 9.5, a profound, dosage-dependent effect of EDTA was observed (Figure 10.19). All three EDTA dosages (20, 40, and 60 ppm) caused soluble silicic acid above the control. An interesting observation warrants further discussion. The dosage dependence seems to have an inverse relationship. The higher the Mg/EDTA combination dosage, the lower soluble silica is observed. Therefore, the most effective Mg/EDTA combination for maximum soluble silica is 20/20 ppm. A possible explanation for this inverse effect may be that at increased Mg/EDTA levels (40/40 and 60/60 ppm), the possible precipitation of a Mg-EDTA complex may be occurring. EDTA is well known to be an effective chelator of Mg at high pH regions. A Mg-EDTA complex has been structurally characterized [57].

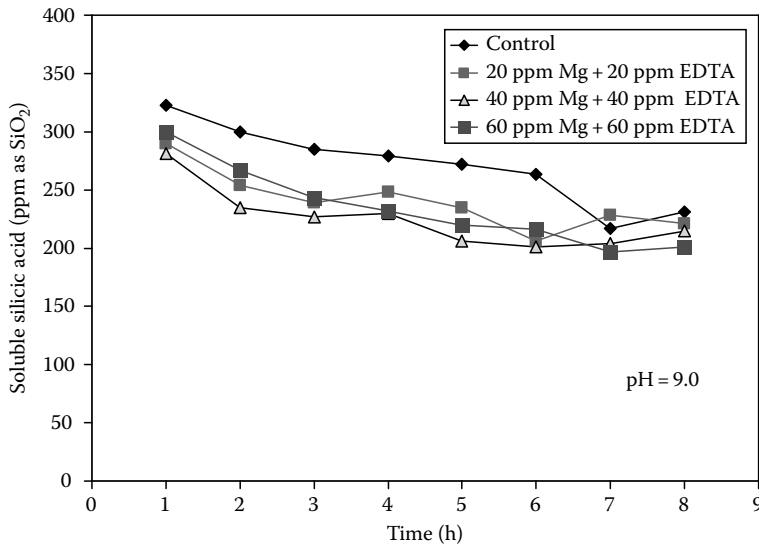


FIGURE 10.18 Influence of EDTA dosage on inhibiting the catalytic effect of Mg^{2+} on silicic acid polymerization at pH 9.0.

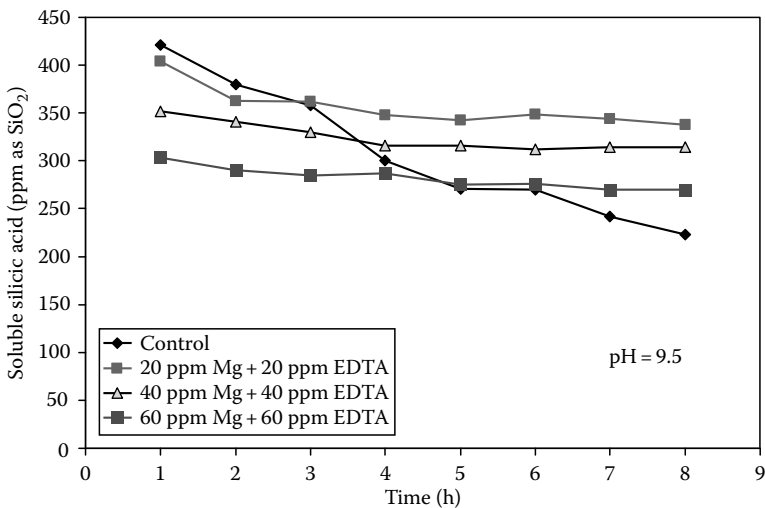


FIGURE 10.19 Influence of EDTA dosage on inhibiting the catalytic effect of Mg^{2+} on silicic acid polymerization at pH 9.5.

10.13 PRACTICAL GUIDELINES FOR CONTROL OF MAGNESIUM SILICATE SCALE

Previously, rough guidelines (summarized in Table 10.2) were based on multiplying the magnesium hardness with the silica concentration. If the product was below 20,000, the water was considered stable. A more advanced rule of thumb was to set the maximum at 40,000 when the pH was below 7.5. Even this was only an approximation, and did not account for the temperature effects. The magnesium silicate system is quite complicated. Several solid compounds of different stoichiometries and hydration states are well known. Magnesium also forms stable complexes with the $(OH)_3SiO^-$ anion as well as the hydroxide ion. This is an addition to the already complicated chemistry of silica

TABLE 10.2
Rough Guidelines for Magnesium Silicate Control

pH Region	Mg ^a × SiO ₂ ^a	SiO ₂ ^a	Comments
<7.5	Mg × SiO ₂ should be below 40,000 ppm ²	Reactive SiO ₂ should be below ~200 ppm	Magnesium silicate usually does not precipitate
>7.5–8.5	Mg × SiO ₂ should be below 12,000 ppm ²	Reactive SiO ₂ should be below ~150 ppm	Onset of magnesium silicate precipitation possible
>8.5	Mg × SiO ₂ should be below 3,000 ppm ²	Reactive SiO ₂ should be below ~100 ppm	“High-risk” pH region for magnesium silicate precipitation

^a Mg is expressed in ppm as CaCO₃ and SiO₂ as ppm SiO₂.

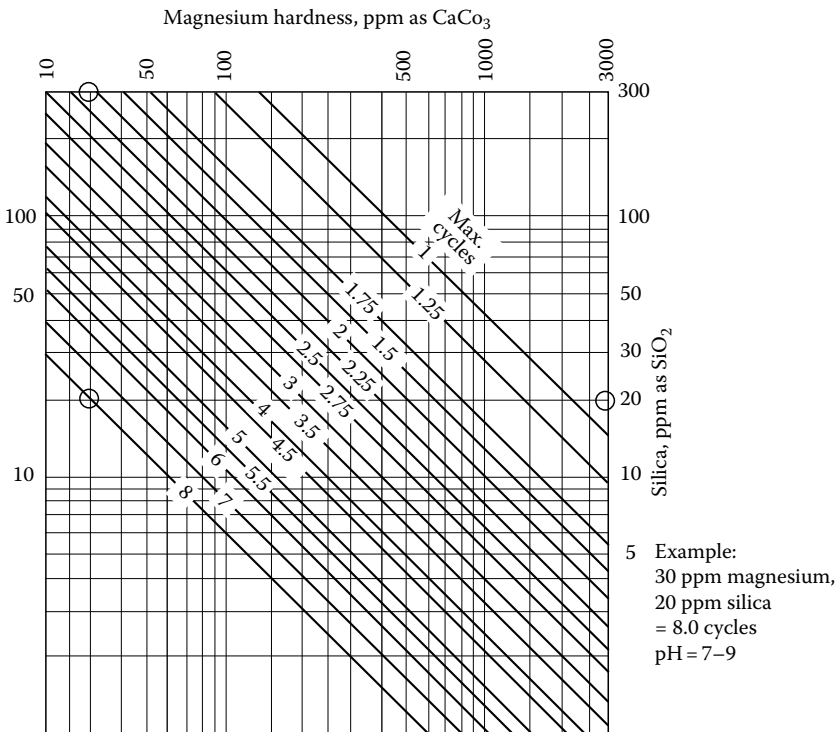


FIGURE 10.20 Correlation between magnesium hardness and silica in process waters in calculating maximum cycles of concentration.

alone. All these factors influence the precipitation of magnesium silicate. Guidelines for the proper operation of the cooling tower under high concentrations of magnesium and silica have been set (see Figure 10.20).

10.14 “METAL SILICATES” IN BIOLOGICAL SYSTEMS

Calcium and iron are found in mineral phases and biopolymers next to silica within biomineralized structures. Silicon can affect the mineralization of both iron oxide and calcium phosphate phases by solution or solid-state interactions. Silicon also appears to have a direct relationship

with aluminum in mineralized pathological deposits. In summary, it can be clearly seen that “silicon”–metal interactions not only occur, but they are an important part of biological processes. Significant studies have been published on the molecular nature of the silicon–metal interactions and in particular on which species (silicon-containing and metal-containing) are involved in such processes [58]. Results indicated that Al^{3+} and orthosilicic acid/silica are able to interact under conditions relevant to biological systems. The inclusion of aluminum in silica, even at the highest Si:Al ratio, also demonstrates the strong affinity between these elements. This is because silicic acid is able to compete successfully with other strong ligands for the metal cation. In a different paper, Perry et al. showed that the use of complexing/sequestering agents for aluminum to prevent the formation of the aluminum-rich silica scale may not be as feasible an option as originally thought [59].

It was reported that the complex formed between aluminum and oligomeric silica has a log K_{eff} of 11.70. This affinity for aluminum is at least 1 million times greater than that for monomeric silica). Another important observation is that aluminum stabilizes silica oligomers for several days under conditions in which depolymerization would otherwise be complete within 24 h. In contrast, oligomeric silica diluted in the absence of aluminum, fully deoligomerized by 24 h, and lost its aluminum binding capacity. Under physiological conditions, this soluble oligomeric silica competes effectively for aluminum with the endogenous chelator citrate. Clearly, the oligomeric-silica/aluminum interaction is of high affinity, and work demonstrating the biological activity of soluble silica should carefully distinguish between monomeric and oligomeric forms.

10.15 EPILOGUE

Silica polymerization is governed largely by pH. Unfortunately, silica is a recalcitrant foulant that is not easily mitigated by simple operational pH adjustments. For example, CaCO_3 scale can virtually be eliminated if a cooling tower system is operated at a lower pH. With water containing a high concentration of silica, operation at a higher pH generates the problem of magnesium silicate scale. Lowering the pH (by feeding acid) does not eliminate the problem, it just shifts the “high risk” from magnesium silicate to silica. In contrast to “traditional” mineral scales such as CaCO_3 , threshold inhibitors (usually phosphonates) are not active for silica scale [60].

An added requirement that is recently gaining a lot of attention is that chemical additives for scale inhibition must be nontoxic, environmentally friendly, and biodegradable. This approach is gaining more governmental and public approval, but is certainly a challenge for chemists and water technologies that are active in the field of chemical water treatment. In the quest for the discovery, application, and commercialization of new silica and metal silicate scale inhibitors, Nature may play an important role in revealing how high levels of silicic acid are stabilized within the diatom. New information may lead to novel synthetic polymers in a biomimetic approach [61]. Until then, research in this field will be active.

ACKNOWLEDGMENTS

A number of hardworking students and enthusiastic collaborators have greatly contributed to the research described herein. A sincere “thank you” goes to my past and current students Eleftheria Neofotistou, Eleftheria Mavredaki, Anna Tsistraki, Kostas Pachis, Stella Katarachia, Antonia Ketsetzi, Aggeliki Stathouloupoulou, Panos Lykoudis, and my collaborators Prof. Petros G. Koutsoukos (University of Patras, Greece), Dr. Viviana Ramos (Universidad Complutense, Spain), and Dr. Adriana Popa (Romanian Academy of Sciences, Romania). This research was funded by the General Secretariat of Science and Technology (Ministry of Development) under Grants GSRT 170c and PEPER-2006 (Crete Prefecture).

REFERENCES

- (a) Bott, T.R. *Fouling Notebook*, Institution of Chemical Engineers, Rugby, U.K. (1990); (b) Cowan, J.C. and Weintritt, D.J. *Water-Formed Scale Deposits*, Gulf Publishing Company, Houston, TX (1976); (c) Amjad, Z. *Mineral Scale Formation and Inhibition*, Plenum Press, New York (1995); (d) Bott, T.R. *Fouling of Heat Exchangers*, Elsevier Science, Amsterdam, the Netherlands (1995); (e) Chan, S.H., Heat and mass transfer in fouling, in *Annual Review of Heat Transfer*, Begell House, Inc., New York (1992), pp. 363–402.
- (a) Frenier, W. *Technology for Chemical Cleaning of Industrial Equipment*, NACE, Houston, TX (2000); (b) Demadis, K.D. and Mavredaki, E., Green additives to enhance silica dissolution during water treatment. *Environ Chem Lett* 3, 127–131 (2005); (c) Frenier, W.W. and Barber, S.J., Choose the best heat exchanger cleaning method. *Chem Eng Prog* 94, 37–44 (July, 1998).
- (a) Brözel, V.S. and Cloete, T.E. Resistance of bacteria from cooling waters to bactericides. *J Ind Microbiol* 8, 273–276 (1991); (b) Saad, M.A. Biofouling prevention in RO polymeric membrane systems. *Desalination* 88, 85–105 (1992); (c) Vrouwenvelder, J.S., Manolarakis, S.A., Veenendaal, H.R., and van der Kooij, D. Biofouling potential of chemicals used for scale control in RO and NF membranes. *Desalination* 132, 1–10 (2000).
- Demadis, K.D., Yang, B., Young, P.R., Kouznetsov, D.L., and Kelley, D.G. Rational development of new cooling water chemical treatment programs for scale and microbial control. In *Advances in Crystal Growth Inhibition Technologies*, Amjad, Z. (Ed.), Plenum Press, New York (2000), Chapter 16, pp. 215–234.
- (a) Mann, S. and Perry, C.C. In *Silicon Biochemistry*, Ciba Foundation Symposium 121, Evered, D. and O'Connor, M. (Eds.), John Wiley & Sons Ltd., New York (1986); (b) Tacke, R. Milestones in the biochemistry of silicon: From basic research to biotechnological applications. *Angew Chem Int E* 38, 3015–3018 (1999).
- (a) Iler, R.K. *The Chemistry of Silica (Solubility, Polymerization, Colloid and Surface Properties and Biochemistry)*, Wiley-Interscience, New York (1979); (b) Fournier, R.P. The solubility of amorphous silica in water at high temperatures and high pressures. *Am Mineral* 62, 1052–1056 (1977); (c) Weres, O., Yee, A., and Tsao, L. Kinetics of silica polymerization. *J Colloid Interface Sci* 84, 379–402 (1981); (d) Sjöberg, S. Silica in aqueous environments. *J Non-Cryst Solids* 196, 51–57 (1996).
- Bergna, H.E. In *The Colloid Chemistry of Silica*, Bergna, H.E. (Ed.), American Chemical Society, Washington DC (1994).
- Demadis, K.D., Water treatment's "Gordian Knot". *Chem Process* 66(5), 29–32 (2003).
- (a) Kroger, N., Lorenz, S., Brunner, E., and Sumper, M. Self-assembly of highly phosphorylated silaffins and their function in biosilica morphogenesis. *Science* 298, 584–586 (2002); (b) Morse, D.E. Silicon biotechnology: Harnessing biological silica production to construct new materials. *Trends Biotechnol* 17, 230–232 (1999); (c) Simpson, T.L. and Volcani, B.E. (Eds.), *Silicon and Siliceous Structures in Biological Systems*, Springer-Verlag, New York (1981).
- (a) Harfst, W. Treatment methods differ for removing reactive and unreactive silica. *Ultrapure Water*, 59–63 (April, 1992); (b) Den, W. and Wang, C.-J. Removal of silica from brackish water by electrocoagulation pretreatment to prevent fouling of reverse osmosis membranes. *Sep Purific Technol* 59, 318–325 (2008); (c) Sheikholeslami, R. and Bright, J. Silica and metals removal by pretreatment to prevent fouling of reverse osmosis membranes. *Desalination* 143, 255–267 (2002); (d) Drucker, J.R., Brodie, D., and Dale, J. Removal of colloids by the use of ion exchange resins. *Ultrapure Water* December, 14–17 (1988); (e) Nakamura, M., Kosaka, K., and Shimizu, H. Process for the removal of silica in high purity water systems. *Ultrapure Water* 31–37 (December, 1988).
- (a) Yu, H., Sheikholeslami, R., and Doherty, W.O.S. Mechanisms, thermodynamics and kinetics of composite fouling of calcium oxalate and amorphous silica in sugar mill evaporators—A preliminary study. *Chem Eng Sci* 57, 1969–1978 (2002); (b) Yu, H., Sheikholeslami, R., and Doherty, W.O.S. Composite fouling of calcium oxalate and amorphous silica in sugar solutions. *Ind Eng Chem Res* 42, 904–910 (2003).
- (a) Amjad, Z., Zibrida, J.F., and Zuhl, R.W. Silica control technology for reverse osmosis systems. *Ultrapure Water* 16(2), 35–41 (1999); (b) Amjad, Z. (Ed.), *Reverse Osmosis: Membrane Technology, Water Chemistry, and Industrial Applications*, Van Nostrand Reinhold Publishing Company, New York (1992); (c) Sheikholeslami R., *Fouling of Membrane and Thermal Units: A Unified Approach. Its Principles, Assessment, Control and Mitigation*, 1st edn., Balaban Publishers, Italy (2007); (d) Freeman, S.D.N. and Majerle, R.J. Silica fouling revisited. *Desalination* 103, 113–115 (1995).

13. Amjad, Z., Zibrida, J.F., and Zuhl, R.W. A new antifoulant for controlling silica fouling in reverse osmosis systems. In *International Desalination Association World Congress on Desalination and Water Reuse*, October 6–9, 1997, Madrid, Spain.
14. (a) Gill, J.S. Inhibition of silica-silicate deposit in industrial waters. *Coll Surf A Physicochem Eng Aspects* 74, 101–106 (1993); (b) Gill, J.S. Silica scale control. *Mater Perform* 37, 41–45 (1998).
15. (a) Hann, W.M. and Robertson, S.T., Control of iron and silica with polymeric dispersants, *International Water Conference* 1990, Paper No. 29, pp. 315–329; (b) Hann, W.M., Robertson, S.T., and Bardsley, J.H. Recent experiences in controlling silica and magnesium silicate deposits with polymeric dispersants. *International Water Conference* 1993, Paper No. 59, pp. 358–370; (c) Hann, W.M. and Robertson, S.T., Control of iron and silica with polymeric dispersants, *Ind Water Treatment* 23(6), 12–24 (November/December, 1991).
16. Weng, P.F. Silica scale inhibition and colloidal silica dispersion for reverse osmosis systems. *Desalination* 103, 59–67 (1995).
17. (a) Demadis, K.D. and Neofotistou, E. Inhibition and growth control of colloidal silica: Designed chemical approaches, *Mater Perform*, 38–42 (April, 2004); (b) Neofotistou, E. and Demadis, K.D., Silica scale growth inhibition by polyaminoamide STARBURST® dendrimers. *Coll Surf A Physicochem Eng Aspects* 242, 213–216 (2004); (c) Neofotistou, E. and Demadis, K.D. Use of antiscalants for mitigation of silica fouling and deposition: Fundamentals and applications in desalination systems. *Desalination* 167, 257–272 (2004); (d) Demadis, K.D., Neofotistou, E., Mavredaki, E., Tsiknakis, M., Sarigiannidou, E.M., and Katarachia, S.D. Inorganic foulants in membrane systems: Chemical control strategies and the contribution of “Green Chemistry”. *Desalination* 179, 281–295 (2005); (e) Demadis, K.D. A structure/function study of polyaminoamide dendrimers as silica scale growth inhibitors, *J Chem Technol Biotechnol* 80, 630–640 (2005), (f) Demadis, K.D. and Stathouloupoulou, A. Solubility enhancement of silicate with polyamine/polyammonium cationic macromolecules: Relevance to silica-laden process waters. *Ind Eng Chem Res* 45, 4436–4440 (2006); (g) Demadis, K.D. Focus on operation & maintenance: Scale formation and removal. *Power* 148(6), 19–23 (2004); (h) Stathouloupoulou, A. and Demadis, K.D. Enhancement of silicate solubility by use of “green” additives: Linking green chemistry and chemical water treatment. *Desalination* 224, 223–230 (2008); (i) Demadis, K.D., Ketsetzi, A., Pachis, K., and Ramos, V.M. Inhibitory effects of multicomponent, phosphonate-grafted, zwitter-ionic chitosan biomacromolecules on silicic acid condensation. *Biomacromolecules* 9, 3288–3293 (2008); (j) Ketsetzi, A., Stathouloupoulou, A., and Demadis, K.D. Being “green” in chemical water treatment technologies: Issues, challenges and developments. *Desalination* 223, 487–493 (2008).
18. Euvrard, M., Hadi, L., and Foissy, A. Influence of PPCA (phosphinopolycarboxylic acid) and DETPMP (diethylenetriaminepentamethylenephosphonic acid) on silica fouling. *Desalination* 205, 114–123 (2007).
19. (a) Kinrade, S.D. and Swaddle, T.W. Silicon-29 NMR studies of aqueous silicate solutions. 2. Transverse ²⁹Si relaxation and the kinetics and mechanism of silicate polymerization. *Inorg Chem* 27, 4259–4264 (1988); (b) Radzig, V.A. Reactive silica: A new concept of the structure of active sites. *Coll Surf A: Physicochem Eng Aspects* 74, 91–100 (1993); (c) Dove, P.M. and Rimstidt, J.D. Silica-water interactions. Physical behaviour, geochemistry and materials applications. *Rev Mineral* 29, 259–308 (1994); (d) Van Blaaderen, A., Van Geest, J., and Vrij, A. Monodisperse colloidal silica spheres from tetraalkoxysilanes: Particle formation and growth mechanism. *J Colloid Interface Sci* 154, 481–501 (1992).
20. Demadis, K.D. and Neofotistou, E. Synergistic effects of combinations of cationic polyaminoamide dendrimers/anionic polyelectrolytes on amorphous silica formation: A bioinspired approach. *Chem Mater* 19, 581–587 (2007).
21. (a) Dubin, L. Silica stabilization in cooling water systems, in *Surface Reactive Peptides and Polymers: Discovery and Commercialization*, Sikes, C.S. and Wheeler, A.P. (Eds.), American Chemical Society, Washington DC, (1991), pp. 355–379; (b) Meier, D.A. and Dubin, L.A. Novel Approach to silica scale inhibition, CORROSION/87, Paper No. 344, NACE International, Houston, TX (1987); (c) Dubin, L., Dammeier, R.L., and Hart, R.A. Deposit control in high silica water. *Mater Perform* 24(10), 27–33 (1985).
22. Kristmannsdóttir, H., Ólafsson, M., and Thórhallsson, S. Magnesium silicate scaling in district heating systems in Iceland. *Geothermics* 18, 191–198 (1989).
23. Kent, D.B. and Kastner, M. Mg²⁺ removal in the system Mg²⁺-amorphous SiO₂-H₂O by adsorption and Mg-hydroxysilicate precipitation. *Geochim Cosmochim Acta* 49, 1123–1136 (1985).
24. Smith, C.W., Usage of a polymeric dispersant for control of silica. *Ind Water Treat* 4, 20–26 (July/August, 1993).
25. Sheikholeslami, R. and Tan, S. Effects of water quality on silica fouling of desalination plants. *Desalination* 126, 267–280 (1999).

26. (a) Young, P.R. Magnesium silicate precipitation. CORROSION/93, Paper No. 466, NACE International, Houston, TX (1993); (b) Brooke, M. Magnesium silicate scale in circulating cooling systems. CORROSION/84, Paper No. 327, NACE International, Houston, TX (1984).
27. MacKenzie, F.T., Garrels, R.M., Bricker, O.P., and Bickley, F. Silica in sea water: Control by silica minerals. *Science* 155, 1404–1405 (1967).
28. Kristmannsdóttir, H. Types of scaling occurring by geothermal utilization in Iceland. *Geothermics* 18, 183–190 (1989).
29. Mattson, S. The laws of soil colloidal behavior. XI. Electrodialysis in relation to soil processes. *Soil Sci* 16, 149–156 (1933).
30. Hazel, F., Schock, R., and Gordon, M. Interaction of ferric ions with silicic acid. *J Am Chem Soc* 71, 2256–2257 (1949).
31. Weber, W.J. and Stumm, W. Formation of a silicato-iron (III) complex in dilute aqueous solution. *J Inorg Nucl Chem* 27, 237–239 (1965).
32. (a) Schenk, J.E. and Weber, W.J. Chemical interactions of dissolved silica with Fe(II) and Fe(III). *J Am Water Works Assoc* 60, 199 (February, 1968); (b) O'melia, C.R. and Stumm, W. Aggregation of silica dispersions by Fe(III). *J Colloid Interface Sci* 23, 437–447 (1967).
33. Chan, S.H., Chen, Z.J., and He, P. Effect of ferric chloride on silica fouling. *J Heat Transfer* 117, 323–328 (1995).
34. (a) Gallup, D.L. Iron silicate formation and inhibition at the Salton Sea geothermal field. *Geothermics* 18, 97–103 (1989); (b) Gallup, D.L. The influence of iron on the solubility of amorphous silica in hypersaline geothermal brines. In *Proceedings of 1991 Symposium on Chemistry in High-Temperature Aqueous Solutions*, Provo, UT.
35. (a) Yokoyama, T., Sato, Y., Maeda, Y., Tarutani, T., and Itoi, R. Siliceous deposits formed from geothermal water. I. The major constituents and the existing states of iron and aluminum. *Geochem J* 27, 375–384 (1993); (b) Yokoyama, T., Sato, Y., Nakai, M., Sunahara, K., and Itoi, R. Siliceous deposits formed from geothermal water in Kyushu, Japan: II. Distribution and state of aluminum along the growth direction of the deposits. *Geochem J* 33, 13–18 (1999); (c) Benevidez, P.J., Mosby, M.D., Leong, J.K., and Navarro, V.C. Development and performance of the Bulalo geothermal field. In *Proceedings of the 10th New Zealand Geothermal Workshop*, Auckland, New Zealand (1988), pp. 55–60; (d) Gunderson, R.P., Dobson, P.F., Sharp, W.D., Pudjianto, R., and Hasibuan, A. Geology and thermal features of the Sarulla contract area, North Sumatra, Indonesia. In *Proceedings of World Geothermal Congress*, Vol. 2, Florence, Italy (1995), p. 687; (e) Gallup, D.L. Aluminum silicate scale formation and inhibition (2): Scale solubilities and laboratory and field inhibition tests. *Geothermics* 27, 485–501 (1998); (f) Gallup, D.L. Aluminum silicate scale formation and inhibition: Scale characterization and laboratory experiments. *Geothermics* 26, 483–499 (1997).
36. Manceau, A., Ildephonse, P., Hazemann, J.-L., Flank, A.-M., and Gallup, D.L. Crystal chemistry of hydrous iron silicate scale deposits at the Salton Sea geothermal field. *Clays Clay Minerals* 43, 304–317 (1995).
37. (a) Yokoyama, T., Takahashi, Y., and Tarutani, T. Retarding and accelerating effects of aluminum on the growth of polysilicic acid particles. *J Colloid Interface Sci* 141, 559–563 (1991); (b) Yokoyama, T., Takahashi, Y., Yamanaka, C., and Tarutani, T. Effect of aluminum on the polymerization of silicic acid in aqueous solution and the deposition of silica. *Geothermics* 18, 321–326 (1989).
38. Yokoyama, T., Sato, Y., Maeda, Y., and Tarutani, T. Elements concentrated into siliceous deposit formed from geothermal water and their distribution. In *Proceedings of the 9th New Zealand Geothermal Workshop*, Auckland, New Zealand (1987), p. 69.
39. (a) Nugent, M.A., Brantley, S.L., Pantano, C.G., Maurice, P.A. The influence of natural mineral coatings on feldspar weathering. *Nature* 395, 588–591 (1998). (b) Ugolini, F.C. and Dahlgren, R.A. Weathering environments and occurrence of imogolite/allophane in selected Andisols and Spodosols. *Soil Sci Soc Am J* 55, 1166–1171 (1991).
40. Miyazaki, A. and Tsurumi, M. The H⁺/Zn²⁺ exchange stoichiometry of surface complex formation on synthetic amorphous aluminosilicate. *J Colloid Interface Sci* 172, 331–334 (1995).
41. (a) Ossaka, J. and Iwai, S. Transformation of allophane to kaolinite under low-grade hydrothermal conditions. *Nature* 201, 1019–1020 (1964); (b) Childs, C.W., Parfitt, R.L., and Newman, R.H. Structural studies of silica springs allophone. *Clay Minerals* 25, 329–341 (1990).
42. Okamoto, G., Okuna, T., and Goto, K. Properties of silica in water. *Geochim Cosmochim Acta* 12, 123–132 (1957).
43. Wohlberg, C. and Buchholz, J.R. Silica in water in relation to cooling tower operation, CORROSION/75, Paper No. 143, NACE International, Houston, TX (1975).
44. Taylor, H.F.W. *Cement Chemistry*, 2nd edn., Thomas Telford, London, U.K. (1997).

45. Matsuyama, H. and Young, J.F. Intercalation of polymers in calcium silicate hydrate: A new synthetic approach to biocomposites. *Chem Mater* 11, 16–19 (1999).
46. Chan, S.H., Chen, Z.J., and He, P. Effects of sodium and potassium chlorides on silica fouling. In *Winter Annual Meeting of the American Society of Mechanical Engineers*, Paper No. 90-WA/HT-1, Dallas, TX (1990).
47. Marshall, W.L. and Warakowski, J.M. Amorphous silica solubilities, II: Effect of aqueous salt solutions at 25°C. *Geochim Cosmochim Acta* 44, 915–917 (1980).
48. (a) Chan, S.H., Neusen, K.F., and Chang, C.T. The solubility and polymerization of amorphous silica in geothermal energy applications. In *Proceedings of 1987 ASME-JSME Thermal Engineering Joint Conference*, Vol. 3, Honolulu, HI (1987), p. 103; (b) Chan, S.H. A review on solubility and polymerization of silica. *Geothermics* 18, 49–56 (1989).
49. (a) Kriventsov, V.V., Kochubey, D.I., Elizarova, G.L., Matvienko, L.G., and Parmon, V.N. The structure of amorphous bulk and silica-supported copper(II) hydroxides. *J Colloid Interface Sci* 215, 23–27 (1999); (b) Zaporozhets, O., Gawer, O., and Sukhan, V. The interaction of Fe(II), Cu(II) and Ag(I) ions and their complexes with 1,10-phenanthroline adsorbed on silica gel. *Coll Surf A Physicochem Eng Aspects* 147, 273–281 (1999).
50. Young, P.R. Stuart, C.M., Eastin, P.M., and McCormick, M. Silica stabilization in industrial cooling towers: Recent experiences and advances. Cooling Technology Institute Annual Meeting Technical Paper TP93-11 (1993).
51. (a) Liu, S.-T. and Nancollas, G.H. The crystallization of magnesium hydroxide. *Desalination* 12, 75–84 (1973); (b) Chieng, C. and Nancollas, G.H. The crystallization of magnesium hydroxide, a constant composition study. *Desalination* 42, 209–219, (1982).
52. (a) Midkiff, W.S. and Foyt, H.P. Silica scale technology and water conservation. *Mater Perform* 39–42 (August, 1979); (b) Midkiff, W.S. and Foyt, H.P. Silica removal and prevention in high silica cooling waters. *Mater Perform* 17–22 (February, 1978).
53. (a) Nesterchuk, N.I. and Makarova, T.A. The formation of aqueous magnesium silicate in the interaction of solutions of magnesium chloride and sodium metasilicate. *Bull Acad Sci USSR, Div Chem Sci* 19, 2053–2055 (1970); (b) Chen, C.T.A. and Marshall, W.L. Amorphous silica solubilities IV. Behavior in pure water and aqueous sodium chloride, sodium sulfate, magnesium chloride, and magnesium sulfate solutions up to 350°C. *Geochim Cosmochim Acta* 46, 279–287 (1982).
54. Betz, L.D., Noll, C.A., and Maguire, J.J. Removal of silica from water by cold process, *Ind Eng Chem* 32, 1320–1323 (1940).
55. Nordell, E. *Water Treatment for Industrial and Other Uses*, 2nd edn., Reinhold Publishing Company, New York (1961).
56. Sheikholeslami, R., Al-Mutaz, I. S., Tan, S., and Tan, S.D. Some aspects of silica polymerization and fouling and its pretreatment by sodium aluminate, lime and soda ash. *Desalination* 150, 85–92 (2002).
57. Stezowski, J.J., Countryman, R., and Hoard, J.L. Structure of the ethylenediaminetetraacetato-aquomagnesate(II) ion in a crystalline sodium salt. Comparative stereochemistry of the seven-coordinate chelates of magnesium(II), manganese(II), and iron(III). *Inorg Chem* 12, 1749–1754 (1973).
58. Perry, C.C. and Keeling-Tucker, T. Aspects of the bioinorganic chemistry of silicon in conjunction with the biometals calcium, iron and aluminum. *J Inorg Biochem* 69, 181–191 (1998).
59. Perry, C.C. and Keeling-Tucker, T. Model studies of the precipitation of silica in the presence of aluminum; implications for biology and industry. *J Inorg Biochem* 78, 331–339 (2000).
60. (a) Demadis, K.D. Combating heat exchanger fouling and corrosion phenomena in process waters, in *Compact Heat Exchangers and Enhancement Technology for the Process Industries*, Shah, R.K. (Ed.), Begell House Inc., New York (2003); (b) Demadis, K.D. and Katarachia, S.D. Metal-phosphonate chemistry: Preparation, crystal structure of calcium-amino-tris-methylene phosphonate and CaCO₃ inhibition. *Phosphorus Sulfur Silicon* 179, 627–648 (2004); (c) Demadis, K.D. and Lykoudis, P. Chemistry of organophosphonate scale growth inhibitors: 2. Physicochemical aspects of 2-phosphonobutane-1,2,4-tricarboxylate (PBTC) and its effect on CaCO₃ crystal growth. *Bioinorg Chem Appl* 3, 135–149 (2005).
61. Demadis, K.D., Pachis, K., Ketsetzi, A., and Stathouloupoulou, A. Bioinspired Control of Colloidal silica in vitro by dual polymeric assemblies of zwitterionic phosphomethylated chitosan and polycations or polyanions. *Adv Coll Interf Sci* 151, 33–48 (2009).

11 Phosphate-Containing Scale Formation in Wastewater

Peter G. Koutsoukos and Aikaterini N. Kofina

CONTENTS

11.1	Introduction.....	205
11.2	Thermodynamics.....	206
11.3	Struvite Scale Formation in Wastewater	207
11.3.1	Use of $\text{MgSO}_4 \cdot 7\text{H}_2\text{O}$ as Magnesium Source	209
11.3.2	Use of $\text{MgCl}_2 \cdot 6\text{H}_2\text{O}$ as Magnesium Source	212
11.3.3	Comparison between the Two Magnesium Sources ($\text{MgCl}_2 \cdot 6\text{H}_2\text{O}$ and $\text{MgSO}_4 \cdot 7\text{H}_2\text{O}$).....	214
11.4	Summary.....	223
	References.....	223

11.1 INTRODUCTION

The presence of relatively high phosphorus concentrations in wastewater is responsible for both the deterioration of the water quality of natural water sources and for the formation of insoluble scale on the various equipment and parts of machinery used during wastewater treatment processes. Soil fertilization and domestic and/or industrial processes are responsible for the accumulation of high phosphorus concentrations in wastewater. The lack of water resources has resulted in a need for the use of treated wastewater. There are cases, however, in which phosphate levels may be high enough to cause the formation of undesirable crystalline scale formed through a combination of the orthophosphate ions with metals such as calcium, magnesium, and iron that may be present in excess in wastewater. Serious operational problems in wastewater treatment plants that have been in operation for a short time have been attributed to the formation of magnesium ammonium phosphate hexahydrate ($\text{MgNH}_4\text{PO}_4 \cdot 6\text{H}_2\text{O}$ or struvite, heretofore MAP) in pipes and aerators [1].

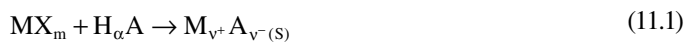
The presence of metal ions in excess in wastewater, including calcium and magnesium, is responsible for the formation of tenaciously adhering scale forming on various equipment parts (piping, pumps, heat exchanger, aerators, etc.). Moreover, the presence of iron or aluminum that is encountered in high concentrations due to the treatment of wastewater by the addition of sulfate salts of these metals as flocculants results in the formation of iron and aluminum phosphate scale deposits. The low solubility of the metal phosphate salts in combination with the formation of a number of metal phosphate phases involved in the system contribute to the complexity of the scale formation problem. The use of phosphate-containing products for the prevention of corrosion of metallic parts may also contribute to the formation of iron phosphate-containing scale deposits. The corrosion of metallic parts in wastewater plant equipment in combination with the presence of phosphate concentrations are the main factors responsible for the formation of iron phosphates. Carbonate and phosphate scale deposits are the most important priority for the maintenance of a wastewater treatment plant in the industry, especially in cases where elevated temperatures and alkaline pH are involved [2,3].

On the other hand, in municipal wastewater, the formation of MAP is the predominant problem. It is therefore evident that the prerequisite for the prevention of undesirable scale is the thorough understanding of the processes taking place in the aqueous phase and at the fouled solid surface/aqueous phase interface. Knowledge of the solution chemistry makes it possible to calculate the thermodynamic driving force for the formation of crystalline solids. These solids may adhere to the surfaces they are in contact with, depending on the surface charge of the particles and on the surface. Scale deposits of struvite have been reported to depend not only on the nature but also on the surface roughness of the substrate [4]. PVC and acrylic materials have been reported to have less tendency for the formation of struvite scale deposits [1]. Overall, irrespective of the substrate material, surface roughness enhances the deposition of struvite. It is evident from all reports that in the control of struvite scale formation the master variable is supersaturation with respect to this salt in the fluid phase. The addition of iron and/or aluminum to avoid struvite formation through the complex formation with orthophosphate ions is not always successful, as it results in the formation of the respective insoluble salts [5,6].

The kinetics of the formation of struvite or other phosphate-containing scale deposits is also of paramount importance for the assessment of the scaling problems encountered in wastewater treatment processes. In aqueous media, the positive supersaturation with respect to more than one salt and the presence of dissolved organic, water-soluble compounds poses the very important problem of competition of precipitation between the various potential scalants and the differences in the relative inhibition in the presence of water-soluble compounds [7–9]. It has been suggested that the magnitude of the relative supersaturation with respect to two different salts, which may form in an aqueous medium, is a decisive factor for the preferred formation of one crystalline material over the other [10,11]. The adsorption of phosphate on suspended particles, clays, and/or complexation with dissolved organic matter affects the ion activities of the lattice ions of the crystalline phosphate deposits and thus changes the supersaturation with respect to the forming solid [12].

11.2 THERMODYNAMICS

The precipitation of a sparingly soluble salt, including metal phosphates, may be represented as follows:



where

M is the metal cation of valency m^+

A is the anion of valency α^-

The supersaturation ratio, S , with respect to the solid forming is defined as

$$S = \left\{ \frac{(\alpha_{M^{m^+}})_{aq}^{v^+} (\alpha_{A^{\alpha^-}})_{aq}^{v^-}}{K_{S, M_{v^+} A_{v^-}}^0} \right\}^{1/v} \quad (11.2)$$

where $v = v^+ + v^-$ and $K_{S, M_{v^+} A_{v^-}}^0$ is the thermodynamic solubility product of the precipitating solid. For precipitation to take place, the necessary (but not sufficient) condition is that $S > 1$.

The most common metal phosphates identified in scale deposits of wastewater treatment plants and the respective thermodynamic solubility products are summarized in Table 11.1.

The solubilities of the scalant salts outlined in Table 11.1 are quite different, as shown in Figure 11.1.

TABLE 11.1
Phosphate Salts in Scale Deposits in Wastewater
Treatment and Their Respective Solubility Products;
25°C, Ionic Strength $\rightarrow 0$

Formula	Name	$\log K_s^0$	Ref.
$\text{FePO}_4 \cdot 2\text{H}_2\text{O}$	Strengite	-26.40	[52]
AlPO_4	Aluminum phosphate	-18.34	[52]
$\text{MgNH}_4\text{PO}_4 \cdot 6\text{H}_2\text{O}$	Struvite	-13.26	[53]
$\text{CaHPO}_4 \cdot 2\text{H}_2\text{O}$	Brushite or DCPD	-6.62	[52]
$\text{Ca}_4\text{H}(\text{PO}_4)_3 \cdot 2.5\text{H}_2\text{O}$	Octacalcium phosphate, OCP	-47.08	[52]
$\text{Ca}_5(\text{PO}_4)_3\text{OH}$	Hydroxyapatite, HAP	-58.33	[52]

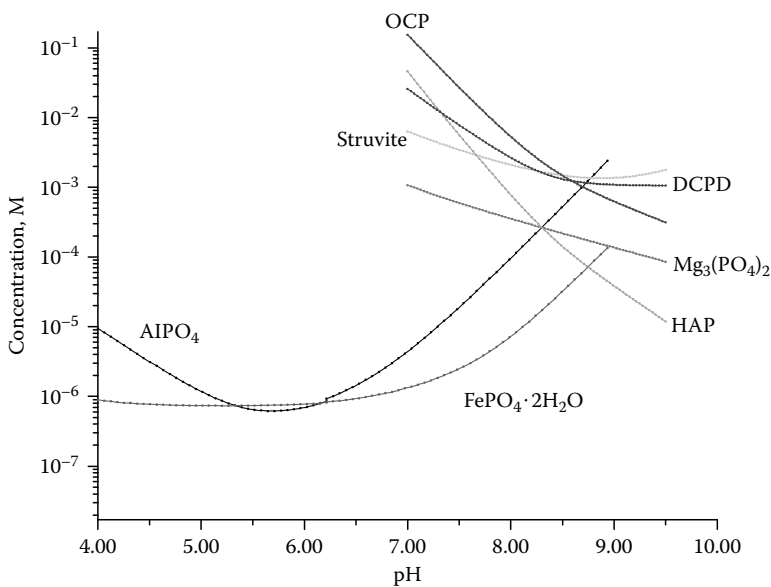


FIGURE 11.1 Solubility isotherms of scalants forming in wastewater treatment processes; 25°C, 0.1 M NaCl. (From Ketrick, B., Boiler system flow diagram, Guardian CSC, York, PA.)

11.3 STRUVITE SCALE FORMATION IN WASTEWATER

The investigation of the conditions for spontaneous precipitation of struvite from aqueous supersaturated solutions is necessary for the construction of the respective stability diagrams. A series of experiments were done in which the working solutions were prepared by rapidly mixing small volumes of stock solutions of salts of the lattice ions of the precipitated solid. The onset of precipitation was determined on the basis of the appearance of the first crystallites of the newly formed solid [13]. It should be noted, however, that true spontaneous precipitation takes place in absolute pure solutions in the absence of any foreign particle or any heterogeneous surface in it. In experiments of spontaneous precipitation in a laboratory room atmosphere, the process is heterogeneous due to suspended foreign particles and inhomogeneities in the reaction vessel.

In this chapter, the investigation of the kinetics of struvite precipitation was done by monitoring the pH value and the chemical composition of the supersaturated solutions. Precipitation experiments, in which no parameter is controlled after the preparation of the supersaturated solutions, and the achievement of threshold supersaturation value are known as free drift experiments [14,15]. In the case of spontaneous struvite precipitation, the solution pH and the chemical composition of

the reactants (calcium, ammonium, and phosphate) were reduced with time. However, the variable supersaturation may result in the stabilization of transient phases [16,17]. An improvement of this approach is the pH-stat experiments in which the pH of the supersaturated solutions is maintained through the addition of a standard alkali solution [18]. The constant supersaturation method in which the solution supersaturation is maintained by the addition of titrant solutions with the stoichiometry of the precipitating salt is a significant improvement of the pH stat method for the quantitative measurement of the precipitation and crystal growth kinetics [19]. The rates of precipitation and crystal growth can be accurately measured directly from the volume of the titrant solutions, added to maintain the supersaturation. The measurement of the kinetics can thus be done at pseudo steady-state conditions. The development of the particle number and size can thus be monitored throughout the process. The influence of other parameters, such as the presence of pollutants, can be measured accurately and over extended periods of crystal growth.

The stability domain of the struvite system was investigated at conditions of constant pH. The supersaturated solutions were prepared in simulated wastewater, with the composition shown in Table 11.2.

It should be noted that the concentration of the glucose included corresponds to a value for the chemical oxygen demand (COD) of 100 ppm. Supersaturation was achieved by the addition of small volumes of concentrated stock solutions of MgSO_4 and $\text{NH}_4\text{H}_2\text{PO}_4$.

The precipitation of struvite is described as



The induction time, preceding the onset of precipitation, was calculated from the plot of the added alkali volume needed to keep the pH constant as a function of time. The initial precipitation rates were calculated from the magnesium-time profiles and the phosphate-time profiles:

$$R = \frac{dn}{dt} = V \frac{dC_i}{dt} \quad (11.4)$$

where

V is the total volume of the working solution

C_i is the concentration of total magnesium or phosphate ions

The calculation of $\left. \frac{dC_i}{dt} \right|_{t \rightarrow 0}$ was determined by the polynomial fitting into the concentration–time profiles.

The driving force for the formation of struvite in aqueous supersaturated solutions is the difference between the chemical potentials of the salt in the supersaturated solution and the corresponding value at equilibrium. Assuming that the chemical potentials of the standard states in the supersaturated solution and at equilibrium are equal, the difference in chemical potentials is

TABLE 11.2
Chemical Composition of Simulated
Wastewater for the Investigation of the
Spontaneous Precipitation of Struvite
at Constant Solution pH

Component	Concentration, $\times 10^4 \text{ M}$
Glucose	5.17
NaHCO_3	178.60
NaCl	100.00
NaNO_3	5.88

$$\begin{aligned}\Delta\mu &= \mu_{\infty} - \mu_s \Rightarrow \\ \Delta\mu &= \left[\mu_{\infty}^0 + kT \ln(a_{\text{Mg}^{2+}} \cdot a_{\text{NH}_4^+} \cdot a_{\text{PO}_4^{3-}})_{\infty}^{1/3} \right] - \left[\mu_s^0 + kT \ln(a_{\text{Mg}^{2+}} \cdot a_{\text{NH}_4^+} \cdot a_{\text{PO}_4^{3-}})_s^{1/3} \right] \Rightarrow \\ \Delta\mu &= kT \ln \frac{(a_{\text{Mg}^{2+}} \cdot a_{\text{NH}_4^+} \cdot a_{\text{PO}_4^{3-}})_{\infty}^{1/3}}{(a_{\text{Mg}^{2+}} \cdot a_{\text{NH}_4^+} \cdot a_{\text{PO}_4^{3-}})_s^{1/3}} = \frac{kT}{3} \ln \Omega\end{aligned}\quad (11.5)$$

where

k is the Boltzmann constant

T is the absolute temperature

Ω is the supersaturation ratio given by the following equation

$$\Omega = \frac{a_{\text{Mg}^{2+}} \cdot a_{\text{NH}_4^+} \cdot a_{\text{PO}_4^{3-}}}{K_s^0} \quad (11.6)$$

where K_s^0 is the thermodynamic solubility product of struvite. The relative supersaturation is defined as

$$\sigma = \Omega^{1/3} - 1 \quad (11.7)$$

The concentrations of the ionic species in solution and the supersaturation ratio of struvite were calculated by the MINEQL+ software [20], a chemical equilibrium modelling system taking into account all chemical equilibrium together with mass balance and electroneutrality conditions. The source of magnesium is an issue for the development of the struvite scale. We have investigated two reagents as a source for Mg^{2+} ions: magnesium sulfate heptahydrate ($\text{MgSO}_4 \cdot 7\text{H}_2\text{O}$) and magnesium chloride hexahydrate ($\text{MgCl}_2 \cdot 6\text{H}_2\text{O}$).

11.3.1 USE OF $\text{MgSO}_4 \cdot 7\text{H}_2\text{O}$ AS MAGNESIUM SOURCE

The struvite spontaneous precipitation experiments were carried out at 25°C under conditions with constant pH values of 7.00, 8.50, 9.00, and 9.50 from supersaturated solutions prepared in a synthetic wastewater solution. The plots of the induction time as a function of solution supersaturation (stability diagrams) are shown in Figure 11.2.

As may be seen from the stability diagrams of struvite, the induction time was found to decrease with increasing solution supersaturation. At higher pH values, the spontaneous precipitation of struvite seems to take place at lower solution supersaturation values. The increase of the solution pH either by the addition of reactant solutions, aeration, or solution disorder may result in the reduction of the measured induction times in real aqueous wastewater solutions [21,22,23]. At lower pH values, the extent of struvite precipitation is limited [24]. Struvite scale formation is favored at higher solution pH values. According to the classical theory of nucleation [13], there is a linear relationship between the logarithm of induction time and the inverse of the square of supersaturation. The variation of the logarithm of induction time $\log \tau$, as a function of $1/\log^2 \Omega$ for the various pH values investigated is shown in Figure 11.3. The change of the slope of the straight lines at the corresponding solution supersaturation values is considered to reflect the transition from the predominantly homogeneous to the mainly heterogeneous nucleation process. The threshold supersaturation values were found to be $\Omega = 1.76$ for pH 9.50, $\Omega = 4.11$ for pH 9.00, and $\Omega = 3.21$ for pH 8.50.

The dependence of the measured induction time on the solution supersaturation in a logarithmic form is given by the expression

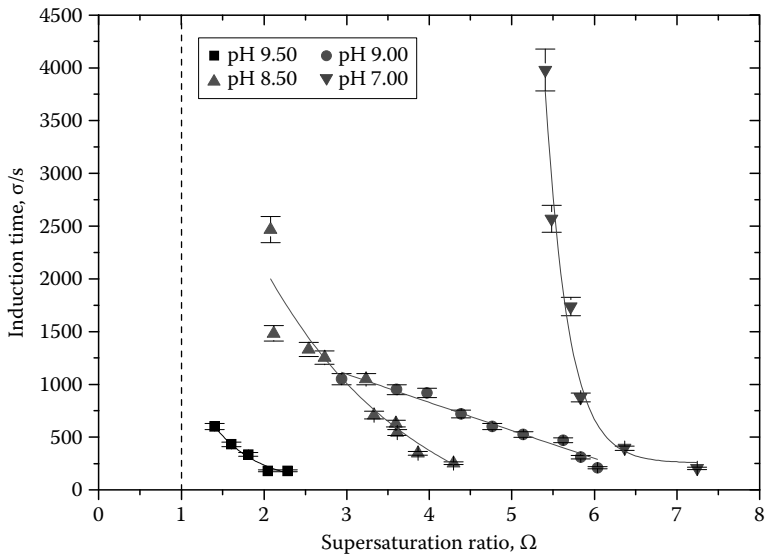


FIGURE 11.2 Plots of induction time, τ as a function of supersaturation, Ω for struvite spontaneous precipitation at conditions of constant pH for pH values 7.00 (∇), 8.50 (\blacktriangle), 9.00 (\bullet), and 9.50 (\blacksquare) at 25°C; simulated wastewater. (From Cotton, I., Clarification products AWT TRTM, Rockville, MD, pp. 2–16, 2001.)

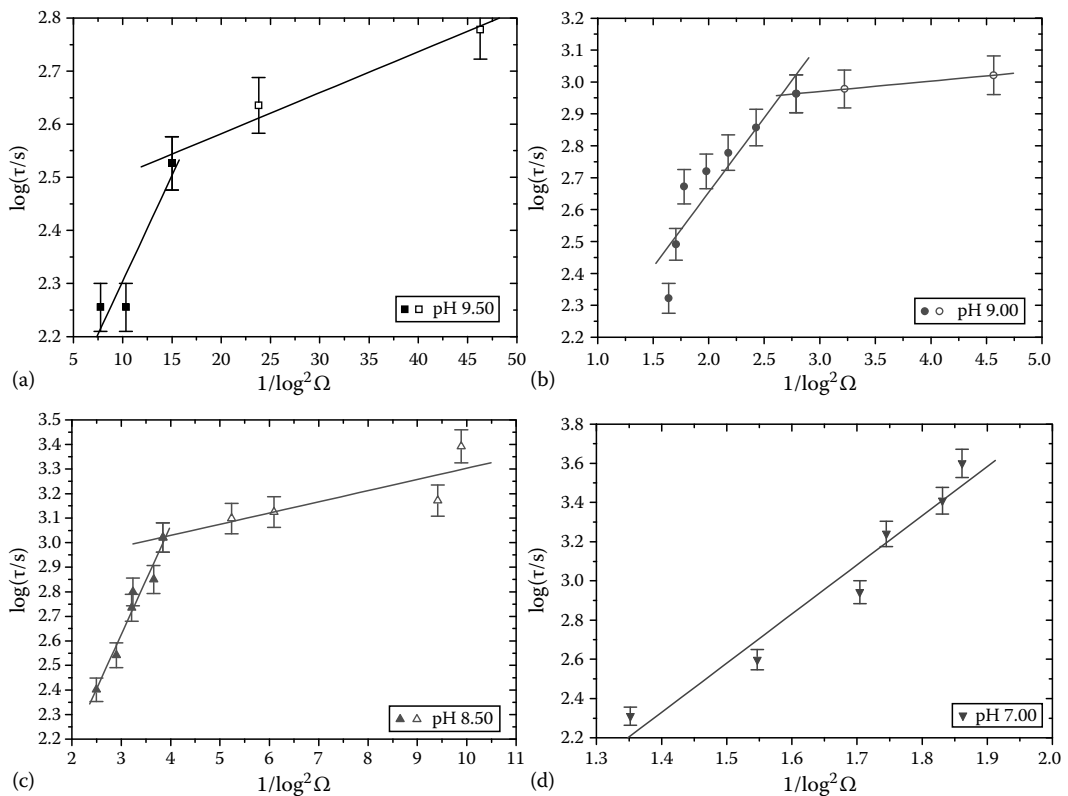


FIGURE 11.3 Plots of the logarithm of induction time, $\log \tau$ as a function of $1/\log^2\Omega$ for struvite spontaneous precipitation in simulated wastewater at conditions of constant pH; pH (a) 9.50, (b) 9.00, (c) 8.50, and (d) 7.00 at 25°C. (From Ketrick, B., Types of filters, Internal Training Program, Guardian CSC, York, PA.)

$$\log \tau = A + \frac{\beta V_m^2 \gamma_s^3}{(2.303kT)^3} \frac{1}{\log^2 \Omega} \quad (11.8)$$

where

A is a constant

γ_s is the surface energy of the solid that is forming

β is a shape factor for the crystals (≈ 32)

V_m is the molecular volume of the precipitated phase ($\approx 7.99 \times 10^{-23} \text{ cm}^3$) [25]

The surface energy of the formed solid, γ_s , was calculated from the slopes of the linear segments at the region of higher supersaturation values, corresponding to the mainly homogeneous precipitation and according to Equation 11.8. From the experimental results, the values of the surface energy for the struvite were: $\gamma_s = 5.5 \text{ mJ} \cdot \text{m}^{-2}$ at pH 9.50, $\gamma_s = 12.5 \text{ mJ} \cdot \text{m}^{-2}$ at pH 9.00, $\gamma_s = 12.3 \text{ mJ} \cdot \text{m}^{-2}$ at pH 8.50, and $\gamma_s = 21.8 \text{ mJ} \cdot \text{m}^{-2}$ at pH 7.00.

The dependence of the logarithm of induction time as a function of the logarithm of the free magnesium ion concentration is shown in Figure 11.4. The expression for the variation of the logarithm of induction time, $\log \tau$, as a function of the logarithm of the free magnesium ion concentration, $\log[\text{Mg}^{2+}]$ is

$$\log \tau = \log k_p + (1 - p) \log[\text{Mg}^{2+}] \quad (11.9)$$

where

p is a number indicative of the size of the critical nucleus

k_p is a constant

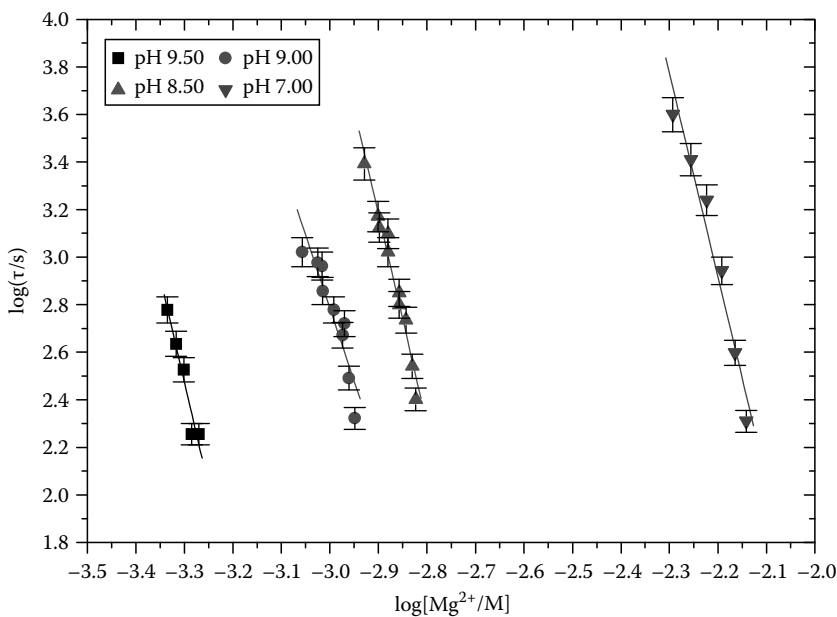


FIGURE 11.4 Plots of the logarithm of induction time, $\log \tau$ as a function of the logarithm of the free magnesium ion concentration, $\log[\text{Mg}^{2+}]$ for struvite spontaneous precipitation at conditions of constant pH in model; pH: 7.00 (\blacktriangledown), 8.50 (\blacktriangle), 9.00 (\bullet), and 9.50 (\blacksquare), 25°C, simulated wastewater. (From Ketrick, B., Resin beads, Internal Training Program, Guardian CSC, York, PA.)

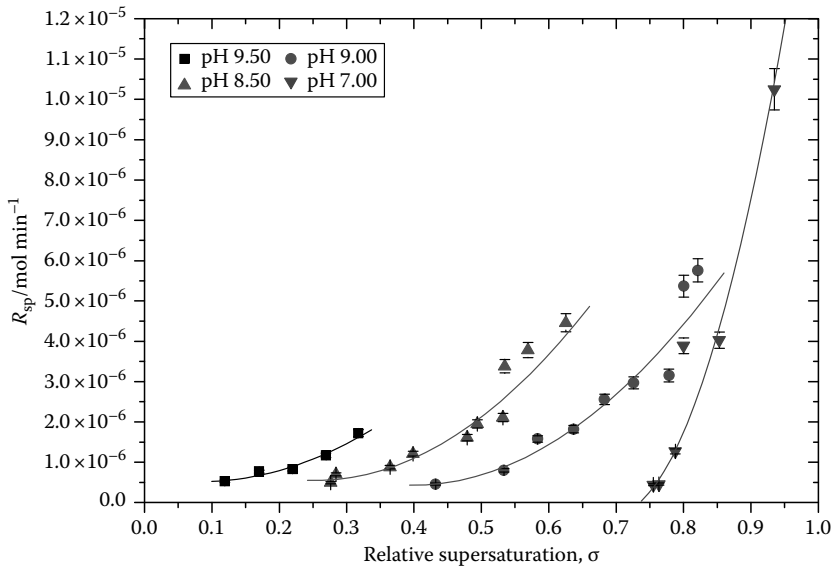


FIGURE 11.5 Plots of initial precipitation rate, R_{sp} as a function of relative supersaturation, σ for struvite spontaneous precipitation at conditions of constant pH in simulated wastewater at 25°C; pH: 7.00 (∇), 8.50 (\blacktriangle), 9.00 (\bullet), and 9.50 (\blacksquare). (From Ketrick, B., Resin comparative table, Internal Training Program, Guardian CSC, York, PA.)

As shown in Figure 11.5, a satisfactory linear fit was obtained for the experimental data according to Equation 11.7 and the value of the factor p was about 10 in all cases.

The dependence on the initial rates of the spontaneous precipitation of struvite on the solution relative supersaturation may be expressed by a power-law equation:

$$R_{sp} = k_{sp}\sigma^n \quad (11.10)$$

where

k_{sp} is the apparent rate constant

n is the apparent order of the precipitation

The value of the apparent order of the precipitation is indicative of the mechanism of the precipitation process.

The plots of the initial rates of precipitation as a function of the relative supersaturation showed a parabolic dependence over the range of supersaturations investigated, suggesting a surface diffusion controlled mechanism for the formation and further crystal growth of struvite.

11.3.2 USE OF $MgCl_2 \cdot 6H_2O$ AS MAGNESIUM SOURCE

A second series of struvite spontaneous precipitation experiments were done under conditions of a constant pH from supersaturated solutions prepared in a simulated wastewater solution using magnesium chloride hexahydrate ($MgCl_2 \cdot 6H_2O$) as the magnesium source.

From the stability diagrams shown in Figure 11.6, the induction time, τ , preceding the onset of precipitation was found to be inversely proportional to the solution supersaturation Ω ; while increasing the working solution pH decreased the induction times. There was no significant differentiation of the solutions with respect to their stability for precipitation at the pH values investigated.

The plots for the logarithm of induction time, $\log \tau$, as a function of $1/\log^2 \Omega$ for struvite spontaneous precipitation at the pH values tested is shown in Figure 11.7. The experimental data were fitted into two straight lines with different slopes, from which the supersaturation values were calculated

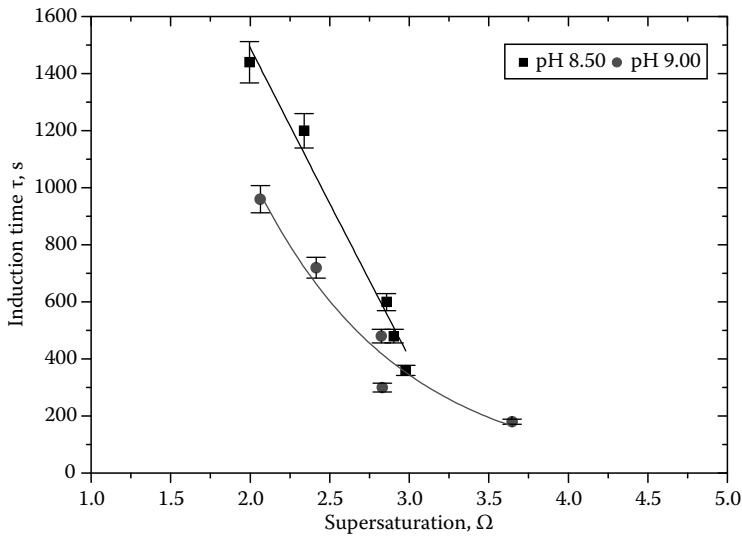


FIGURE 11.6 Plots of induction time, τ as a function of supersaturation, Ω for struvite spontaneous precipitation in simulated wastewater at constant pH at 25°C; pH: 9.00 (●), 8.50 (■). (From Ketrick, B., Reverse osmosis flow, Internal Training Program, Guardian CSC, York, PA.)

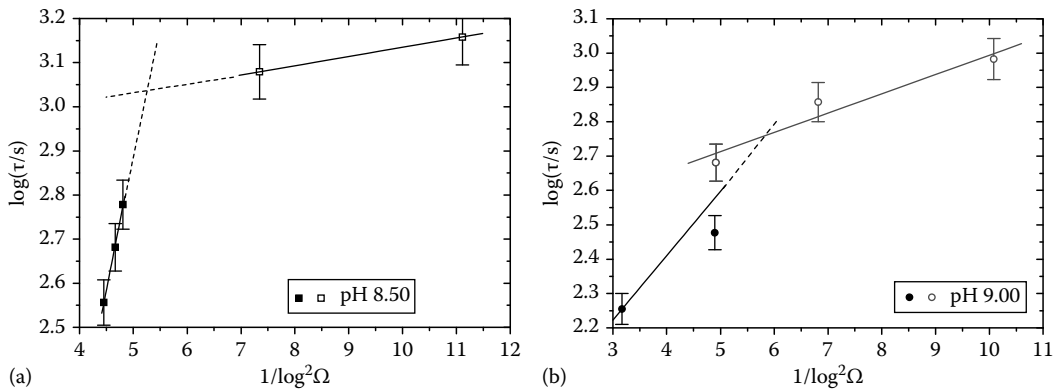


FIGURE 11.7 Plots of the logarithm of induction time, $\log \tau$ as a function of $1/\log^2\Omega$ for struvite spontaneous precipitation at conditions of constant pH for pH values (a) 8.50 and (b) 9.00 at 25°C simulated waste water. (From Ketrick, B., Feed water tank drawing, Internal Training Program, Guardian CSC, York, PA.)

where the transition from the predominantly homogeneous to the mainly heterogeneous nucleation process happened. The supersaturation ratio values were determined to be $\Omega = 2.60$ for pH 9.00 and $\Omega = 2.73$ for pH 8.50. The surface energy of the precipitated struvite γ_s was determined from the slopes of the linear segments corresponding to the mainly homogeneous precipitation and Equation 11.8. The values of the surface energy for the struvite were: $\gamma_s = 9.2$ and $13.7 \text{ mJ}\cdot\text{m}^{-2}$ at pH 9.00 and 8.50, respectively. The two values did not differ significantly suggesting as expected that there is no pH effect on the surface energy of the newly formed nuclei.

Plots for the logarithm of induction time as a function of the logarithm of the free magnesium ion concentration are shown in Figure 11.8. The values of parameter p , corresponding to the size of the new nuclei were about 8 for both pH values, which again suggested no difference between the two pH values tested.

As may be seen in Figure 11.9, the initial rates of precipitation as a function of the relative supersaturation showed a parabolic dependence for both pH values tested.

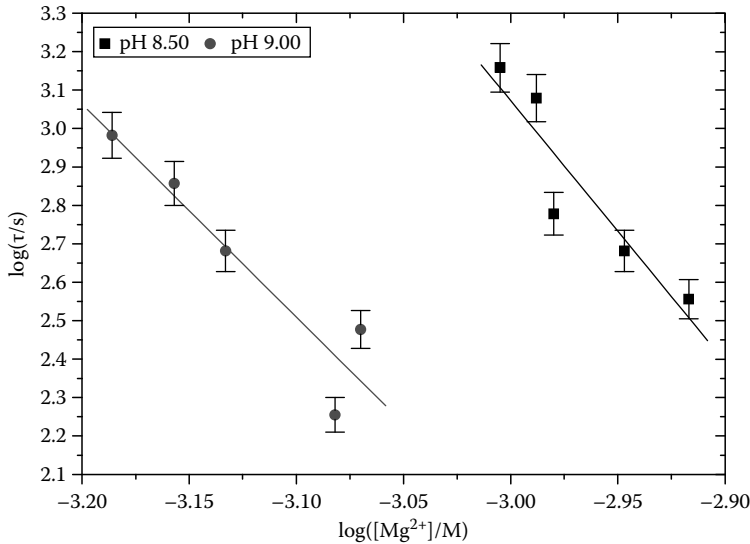


FIGURE 11.8 Plots of the logarithm of induction time, $\log \tau$ as a function of the logarithm of the free magnesium ion concentration, $\log[Mg^{2+}]$ for struvite spontaneous precipitation in simulated wastewater at constant pH at 25°C; pH: 9.00 (●), 8.50 (■).

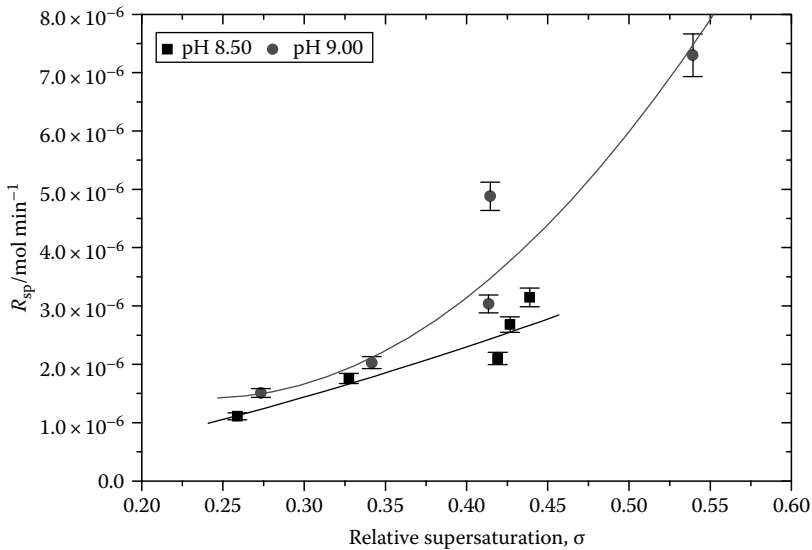


FIGURE 11.9 Plots of initial rate of precipitation, R_{sp} as a function of relative supersaturation, σ for the spontaneous precipitation of struvite in simulated wastewater at constant pH at 25°C; pH: 9.00 (●), 8.50 (■).

11.3.3 COMPARISON BETWEEN THE TWO MAGNESIUM SOURCES ($MgCl_2 \cdot 6H_2O$ AND $MgSO_4 \cdot 7H_2O$)

As shown in the plots in Figure 11.10 for the two pH values tested, it seems that for the same supersaturation value the precipitation reactions initiate faster when magnesium chloride hexahydrate ($MgCl_2 \cdot 6H_2O$) is used as a magnesium source. The values of the indicative numbers of the size of the critical nucleus and the values of the surface energies are not affected by the magnesium source used. On the other hand, the threshold supersaturation values where the transition from

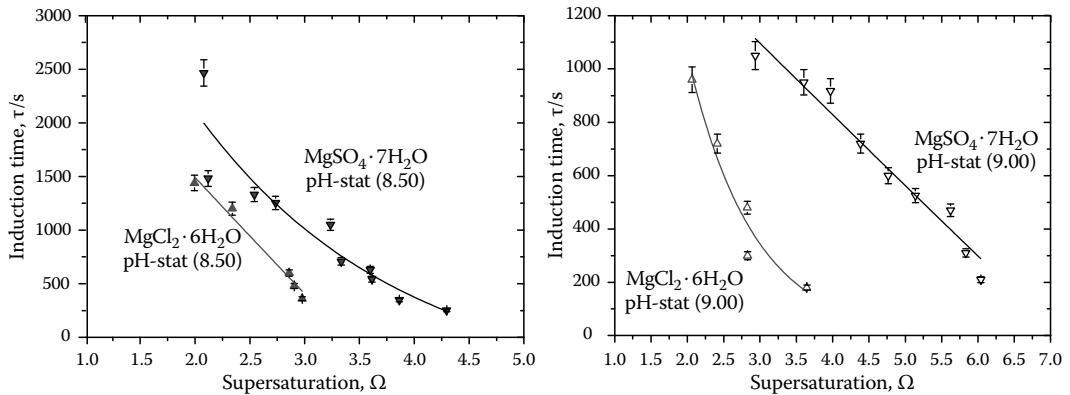


FIGURE 11.10 Plots of induction time, τ as a function of supersaturation, Ω for the spontaneous precipitation of struvite in simulated wastewater at constant pH at 25°C with $\text{MgCl}_2 \cdot 6\text{H}_2\text{O}$ as magnesium source for pH: 9.00 (Δ), 8.50 (\blacktriangle) and with $\text{MgSO}_4 \cdot 7\text{H}_2\text{O}$ for pH:9.00 (∇), 8.50 (\blacktriangledown). (From Frayne, C. Ketrick, B., Oxygen scavenger properties, AWT Training Course, Rockville, MD, Boiler water treatment, p. 56, 2009.)

the predominantly homogeneous to the mainly heterogeneous nucleation process takes place were determined to be lower when magnesium chloride hexahydrate ($\text{MgCl}_2 \cdot 6\text{H}_2\text{O}$) instead of magnesium sulfate heptahydrate ($\text{MgSO}_4 \cdot 7\text{H}_2\text{O}$) was used as a magnesium source.

From the comparison of the kinetics plots shown in Figure 11.11, it is shown that for the two pH values tested, it seems that for the same solution supersaturation, the initial precipitation rates were higher when magnesium chloride hexahydrate ($\text{MgCl}_2 \cdot 6\text{H}_2\text{O}$) was used as a magnesium source.

In the literature, the most commonly used magnesium ion sources are magnesium chloride hexahydrate ($\text{MgCl}_2 \cdot 6\text{H}_2\text{O}$) [26], which has the advantage of quick ion dissociation resulting in shorter reaction times and magnesium hydroxide, $\text{Mg}(\text{OH})_2$ [27,28], which raises the solution pH value. Furthermore, many cases reported that instead of magnesium chloride hexahydrate ($\text{MgCl}_2 \cdot 6\text{H}_2\text{O}$), seawater [29] and bittern (the salt left after seawater evaporation) [30] have been used to test the relative ability to cause struvite precipitation.

The characterization of the solid precipitates at a constant pH was done by x-ray powder diffraction and the analysis of their morphology was done by scanning electron microscopy. The x-ray powder diffraction patterns of the spontaneously precipitated solid in simulated wastewater and of synthetically prepared struvite [Joint Committee on Powder Diffraction Standards] (File no. 15-672) are shown in Figure 11.12. As may be seen from the agreement of the reflections, it may be concluded that the spontaneously precipitated solid in simulated wastewater is stoichiometric struvite. It should be noted particularly that in all cases the working solutions were supersaturated with respect to struvite, $\text{MgNH}_4\text{PO}_4 \cdot 6\text{H}_2\text{O}$, magnesium phosphate, $\text{Mg}_3(\text{PO}_4)_2$, and magnesite, MgCO_3 . They were, however, undersaturated with respect to newberyite, $\text{MgHPO}_4 \cdot 3\text{H}_2\text{O}$.

The specific surface area of the precipitated struvite crystals was measured with the N_2 adsorption BET method and was found to be between 2–4 $\text{m}^2 \cdot \text{g}^{-1}$, regardless of the method of precipitation and the experimental conditions examined. The morphology of the spontaneously precipitated crystals in model wastewater at a constant pH for pH values 7.00, 8.50, 9.00, and 9.50 is shown in the scanning electron micrographs in Figures 11.13 and 11.14, respectively. As may be seen in all received micrographs, slim prismatic crystals were formed with characteristic cracks on their surface and a mean size of approximately 30 μm .

It is interesting that at higher pH levels (pH 9.50), a distinctly different morphology of the precipitated crystals was observed. In this case, the size of the formed crystals was smaller and their shape was plate-like.

The precipitation kinetics and the characteristics of the precipitating solid depend, to a large extent, on the presence of organic soluble compounds, which may interact, e.g., through surface

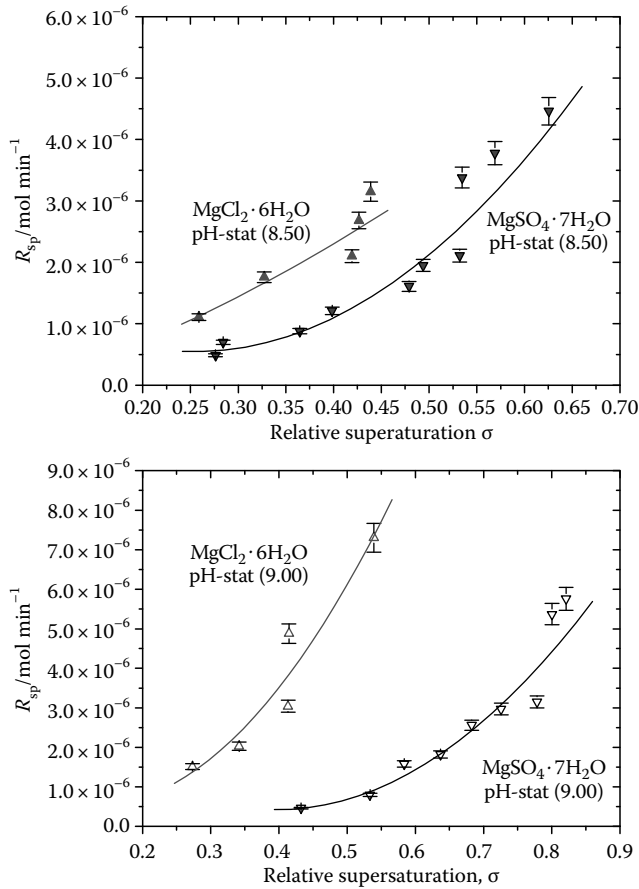


FIGURE 11.11 Plots of initial precipitation rate, R_{sp} as a function of relative supersaturation, σ for the spontaneous precipitation of struvite in simulated wastewater at constant pH; 25°C. $\text{MgCl}_2 \cdot 6\text{H}_2\text{O}$ as magnesium source pH: 9.00 (Δ), 8.50 (\blacktriangle). $\text{MgSO}_4 \cdot 7\text{H}_2\text{O}$ source. pH: 9.00 (∇); 8.50 (\blacktriangledown). (From Ketrick, B., Carbonic acid corrosion, Internal Training Program, Guardian CSC, York, PA.)

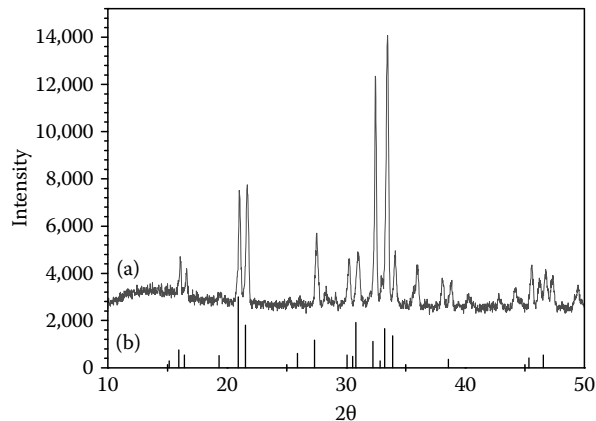


FIGURE 11.12 Powder x-ray diffraction spectra (a) for struvite precipitated spontaneously from simulated wastewater supersaturated solution at conditions of constant pH with $\text{MgSO}_4 \cdot 7\text{H}_2\text{O}$ as magnesium source at pH 8.50 and (b) reference pattern from JCPDS (file no. 15-762) for synthetic prepared struvite. (From Ketrick, B., Chemical feed points, Internal Training Program, Guardian CSC, York, PA.)

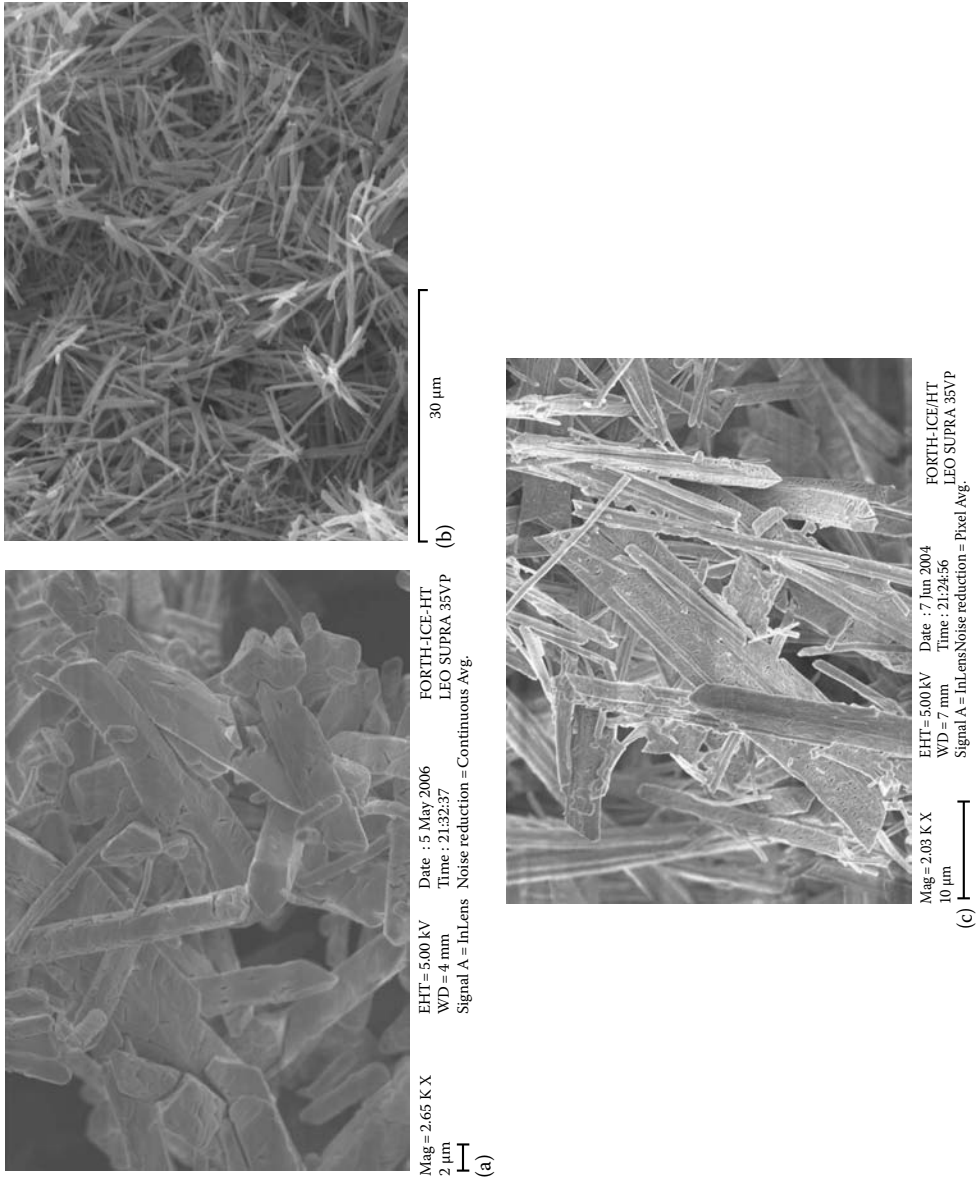


FIGURE 11.13 Scanning electron micrographs of struvite crystals precipitated spontaneously at constant pH: (a) 7.00, (b) 8.50, and (c) 9.00 at 25°C, simulated wastewater.

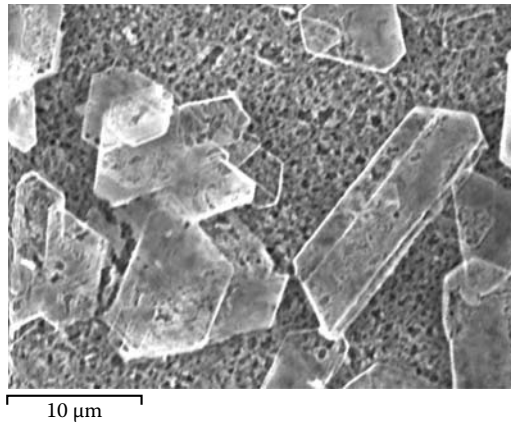


FIGURE 11.14 Scanning electron micrographs of struvite crystals precipitated spontaneously at conditions of constant pH 9.50 at 25°C in simulated water.

adsorption with the solid forming. The problems associated with struvite scale formation may be overcome through the use of a specific type of compounds that show an enhanced affinity for this solid. The use of inhibitors for scale prevention is widely practiced since the remediation of those parts most of the times is a costly and time-consuming process. The inhibition of scale formation involves the addition of very low concentrations of compounds in the aqueous medium in which scale is deposited, inhibiting the formation of a specific type of scale deposits [31–33]. In the present work, the effect of a series of compounds possessing carboxylic functional groups on the scale formation of struvite was investigated. At $\text{pH} > \text{p}K_a$ of the corresponding compounds, it is anticipated that they interact with struvite. Formic acid has $\text{p}K_a$ 3.74 for the one $-\text{COOH}$ group; for malonic acid $\text{p}K_{a1} = 2.85$ and $\text{p}K_{a2} = 5.70$ for the two $-\text{COOH}$ groups; and for citric the three $\text{p}K_a$ values are 3.13, 4.76, and 6.40, respectively corresponding to the three $-\text{COOH}$ groups. At pH 8.50, where all the experiments were carried out, formic, malonic, and citric acid are fully ionized and possess a 1-, 2-, and 3-charge, respectively [34]. Polyacrylic acid [35–37] is the most negatively charged because it has the larger number of $-\text{COOH}$ groups present in the molecule and is expected to interact strongly with the cationic sites of the struvite crystals.

The compounds tested are shown in Figure 11.15. More specifically, formic acid, malonic acid, and citric acid were used, having respectively one, two, and three carboxyl groups. A low molecular weight polymer (ca. 2000) polyacrylic acid was also tested.

These compounds have been suggested to be effective inhibitors of the crystal growth of several sparingly soluble salts including calcium phosphate (hydroxyapatite and octacalcium phosphate) [38–43], calcium pyrophosphate [44], calcium oxalate [45,46], calcite, and gypsum [46,47]. Doyle et al., who investigated a number of struvite scale inhibitors, suggested that significant scale formation reduction was achieved using chemical reagents with the ability to form strong complexes with ions Mg^{2+} [48].

In order to examine the effect of the presence of organic soluble compounds on the spontaneous precipitation of struvite, two sets of experiments were done: in the first set of experiments, the concentration of the organic soluble compound was kept constant for the different working solution supersaturation values tested. In the second set of experiments, the effect of increasing organic soluble compound concentration was examined at a given supersaturation value of the working solution. The concentrations of the tested organic soluble compound in this set of experiments were in the range between 1 and $10\mu\text{M}$. The induction times and the initial precipitation rates of struvite were estimated from the plots of the added volume of the titrant solutions as a function of time.

The kinetics results were obtained from experiments at conditions of a constant supersaturation at 25°C and at pH 8.50 from supersaturated solutions with respect to struvite, using the $\text{MgSO}_4 \cdot 7\text{H}_2\text{O}$ solution as a magnesium source and the simulated wastewater solution as the aqueous medium.

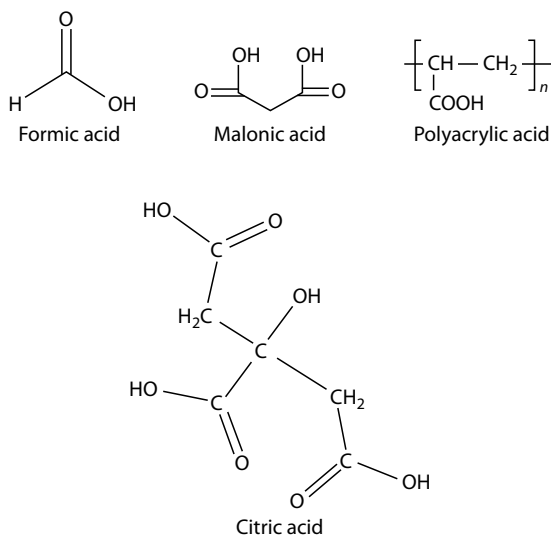


FIGURE 11.15 Chemical structures of the organic soluble compounds used for the study of their effect in spontaneous precipitation of struvite in simulated wastewater.

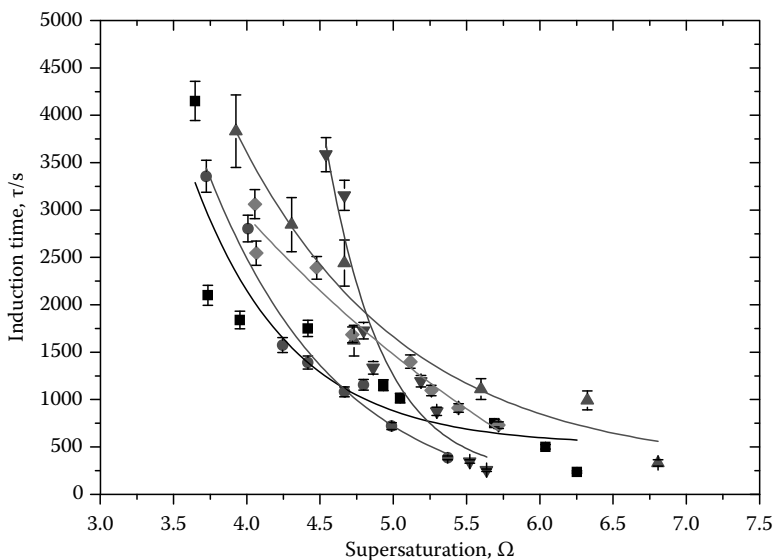


FIGURE 11.16 Plots of induction time, τ as a function of supersaturation ratio, Ω for struvite spontaneous precipitation in simulated wastewater at conditions of constant supersaturation pH 8.50, 25°C in the absence (■) and in the presence of 1 μM : formic (●), malonic (▲), citric (▼), and polyacrylic (◆) acids.

The induction times preceding the onset of precipitation were found to be inversely proportional to the solution supersaturation as can be seen from the plots presented in Figure 11.16. At lower solution supersaturation values, all the organic soluble compounds tested inhibit the onset of precipitation, while at higher solution supersaturation values the induction times do not present a considerable difference. The abatement of the effect from the presence of inhibitors with solution supersaturation increase is a general comment which is applied for almost all the salts. The presence of formic acid has a lower effect on the time lapsed until the initiation of the precipitation reaction. The effect of the presence of the carboxylic acids on the induction times of spontaneous precipitation of struvite

was found to be very small in agreement with reports for their effect on magnesium or calcium phosphate salts [49].

From the dependence of the induction times on solution supersaturation, the surface energy, γ_s , of the precipitated solid was calculated to be equal to 16.4, 25.7, 25.1, and 15.0 $\text{mJ} \cdot \text{m}^{-2}$ in the presence of 1 μM of formic acid, malonic acid, citric acid, and polyacrylic acid, respectively. These values are relatively low because of the contribution of heterogeneous nucleation and there is no practical differentiation of the values obtained. Moreover, there is no significant differentiation from the respective value (15.5 $\text{mJ} \cdot \text{m}^{-2}$) obtained in the absence of additives. Of more practical significance is the value of the supersaturation ratio corresponding to the transition between mainly homogeneous to mainly heterogeneous nucleation, which is obtained from plots of the logarithm of induction time $\log \tau$, as a function of $1/\log^2 \Omega$, shown in Figure 11.17. These threshold supersaturation ratio values were found to be equal to $\Omega = 4.60, 6.35, 5.25,$ and 4.48 in the presence of 1 μM formic, malonic, citric, and polyacrylic acids. Since the corresponding value obtained in the absence of additives was $\Omega = 4.78$, it seems that only malonic and citric acid had a significant effect on the shifting of the threshold to higher supersaturation ratio values.

The dependence of the measured initial precipitation rates of struvite as a function of the relative solution supersaturation is shown in the plots in Figure 11.18. In the presence of all carboxylic acids tested, with the exception of formic acid, the rates of precipitation measured were lower than in the absence of acid compounds. In all cases, the dependence of initial precipitation rates on relative solution supersaturation was parabolic suggesting that the rate determining step of the precipitation process is the surface diffusion of the growth units.

The presence of the inhibitors tested at different concentrations of the additive organic soluble compound on struvite precipitation was investigated. The experiments were performed at the same

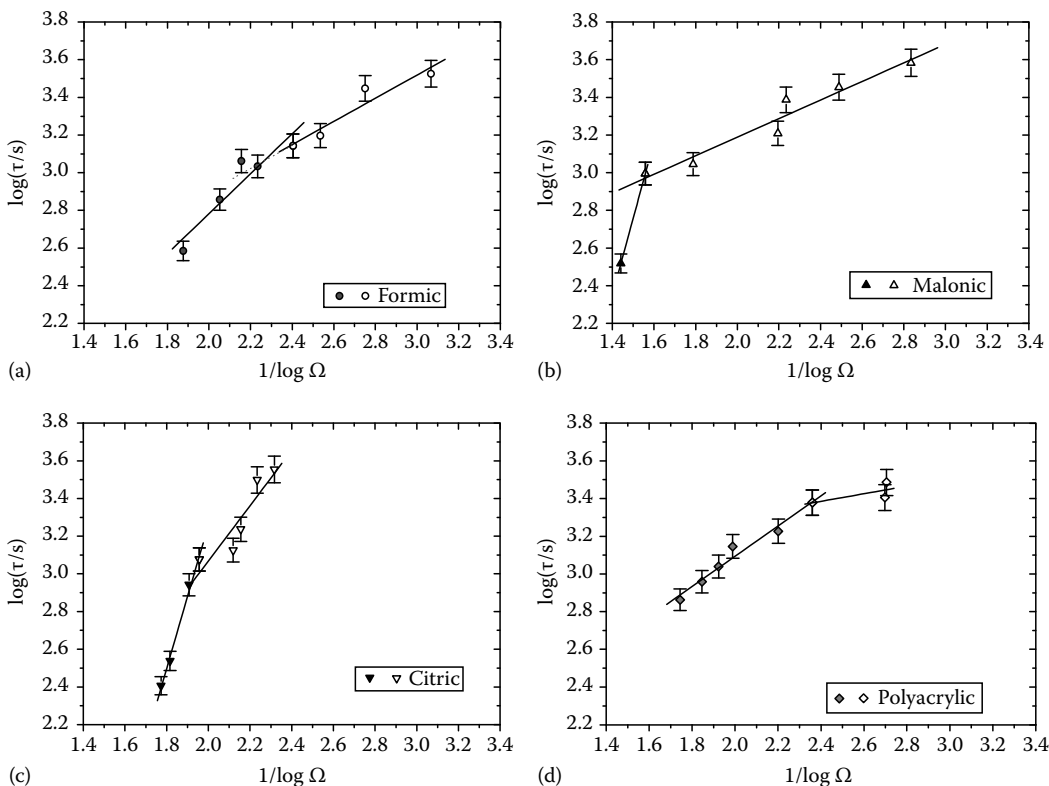


FIGURE 11.17 Plots of the logarithm of induction time, $\log \tau$ as a function of $1/\log^2 \Omega$ for spontaneous precipitation of struvite in simulated wastewater at conditions of constant supersaturation for pH 8.50 and at 25°C in the presence of 1 μM (a) formic, (b) malonic, (c) citric, and (d) polyacrylic acids.

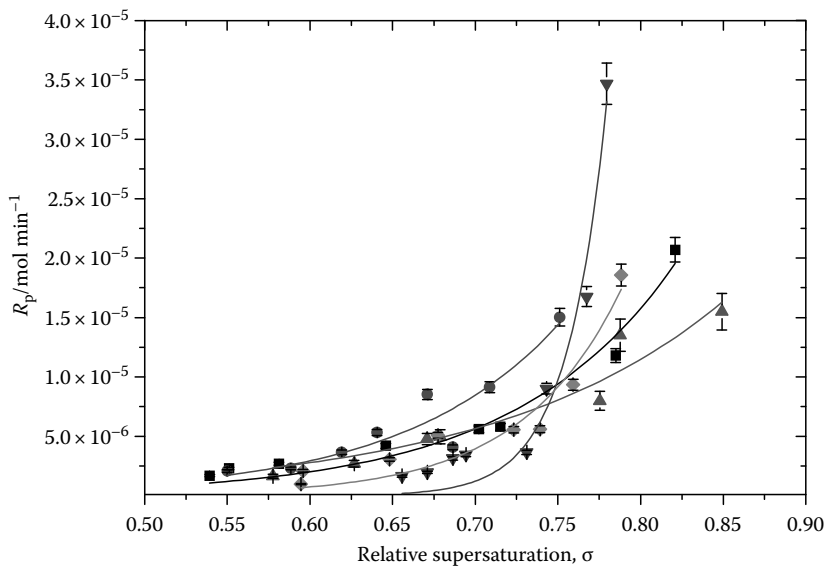


FIGURE 11.18 Plots of initial precipitation rate, R_p , as a function of relative supersaturation, σ for struvite spontaneous precipitation in simulated wastewater at conditions of constant supersaturation at 25°C pH 8.50 in the absence (■) and in the presence of 1 μM formic (●), malonic (▲), citric (▼), and polyacrylic (◆) acids.

supersaturation with respect to struvite, $\Omega = 4.86$, and the concentrations of the carboxylic acids tested was in the range of 1 and 10 μM . In all cases, the induction time preceding the onset of struvite precipitation increased with increasing additive concentration, as shown in Figure 11.19.

The acids tested affected not only the induction times but they also resulted in the reduction of the rates of precipitation, R_p , as shown in Figure 11.20. The relative inhibition was defined as

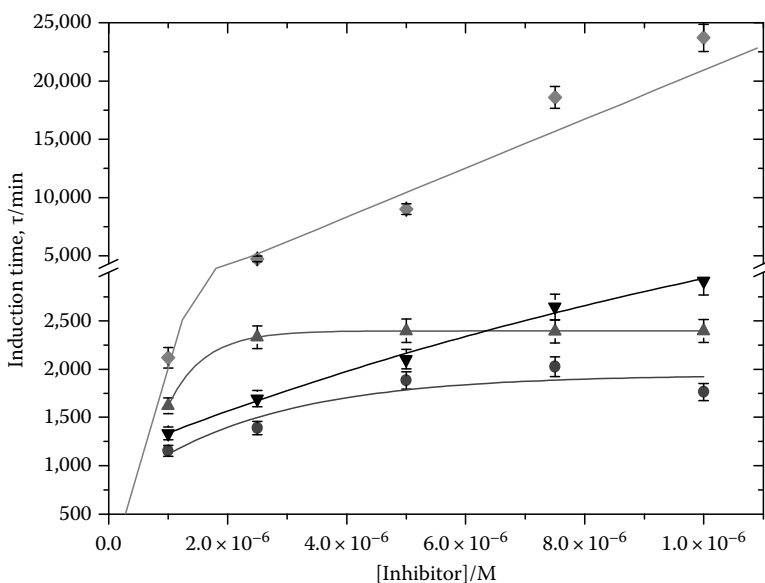


FIGURE 11.19 Dependence of the induction time, τ preceding spontaneous precipitation of struvite in simulated wastewater on the additive concentration at conditions of constant supersaturation, $\Omega = 4.86$; pH 8.50, 25°C in the presence of: formic acid (●); malonic acid (▲); citric acid (▼); polyacrylic acid (◆).

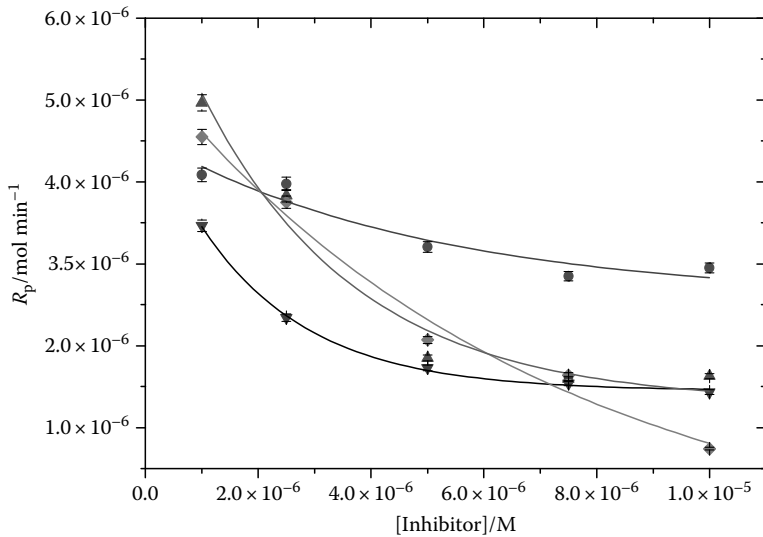


FIGURE 11.20 Dependence of the initial precipitation rate, R_p , of spontaneous precipitation of struvite in simulated wastewater on the additive concentration at conditions of constant supersaturation; $\Omega = 4.86$; pH 8.50, 25°C. Formic acid (●); malonic acid (▲); citric acid (▼); polyacrylic acid (◆).

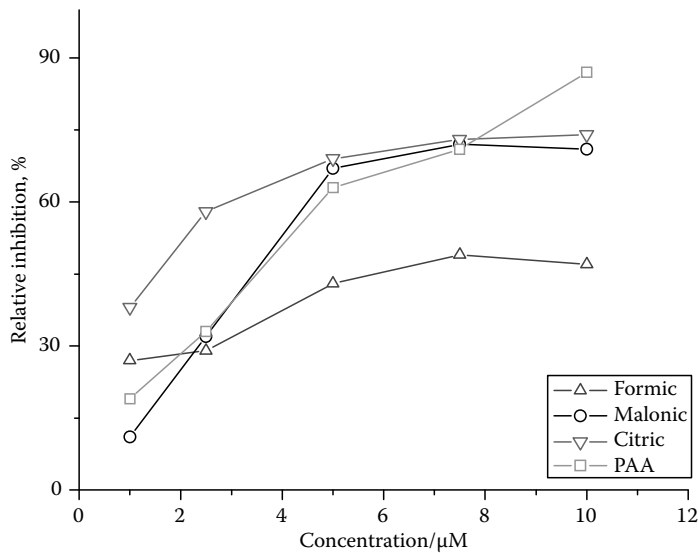


FIGURE 11.21 Relative inhibition of struvite precipitation in simulated wastewater in the presence of carboxylic acids; pH 8.50, 25°C, $\Omega = 4.86$. Citric acid (Δ); malonic acid (\circ); citric acid (∇); polyacrylic acid (\square).

$$\text{Relative inhibition} = \frac{R - R_{\text{inh}}}{R} 100\% \quad (11.11)$$

where R , R_{inh} are the precipitation rates in the absence and in the presence of the inhibitor, respectively.

The relative inhibition plot as a function of the inhibitor concentration is shown in Figure 11.21. As may be seen, with the exception of PAA, there is a concentration plateau above which the rate of struvite precipitation proceeds at a limiting value.

The reduction in initial crystal growth rates for several sparingly salts has been described by a kinetic Langmuir-type adsorption model. The model assumes a steady-state adsorption/ desorption in the absence of interactions between growth sites and the Langmuir adsorption isotherm [50]. According to this model, plots of $R/(R_{\text{inh}} - R)$ as a function of the inverse of the inhibitor concentration, $1/C_{\text{inh}}$, are expected to be linear. From the slopes of the linear fit of the data obtained for the organic acids tested, the affinity constants k_{aff} were calculated. They were found to be equal to 11×10^5 , 0.15×10^5 , 8.20×10^5 , and 1.73×10^5 for formic, malonic, citric acid, and polyacrylic acids, respectively. Affinity constants of the same order of magnitude have been reported for the effect of organic soluble compounds on the precipitation of calcium phosphate salts [40,51].

11.4 SUMMARY

The presence of inorganic orthophosphates and polyphosphates that may hydrolyze is responsible for phosphate-containing scale formation in equipment designed for wastewater treatment. Scale deposits are formed when metal (calcium, magnesium, iron, aluminum, and ammonium) concentrations are sufficiently high. Struvite formation is the scale deposit most often encountered phosphate scale in the domestic wastewater treatment processes. The stability domain and the kinetics of precipitation of struvite were investigated from simulated wastewater. The threshold for the spontaneous precipitation of struvite was investigated using the pH-stat method at 25°C and pH 8.50. The induction times preceding spontaneous precipitation were measured and the threshold for the transition from mainly heterogeneous to mainly homogeneous precipitation was determined. At the conditions tested, struvite was the only solid forming “winning” the competition over magnesium phosphate. The dependence of the rates of precipitation of struvite on the relative supersaturation showed that the process was controlled from the surface diffusion of the growth units. The presence of carboxylic acids containing one, two, three, and a large number of carboxylic groups resulted in the inhibition of the rates of struvite precipitation and in the increase of the induction times preceding the formation of the precipitate. The polymeric acid tested was found to inhibit efficiently the formation of struvite, while all inhibitors tested showed a high affinity for the solid. It is suggested that the ionized carboxyl groups promote adsorption onto the active sites of the crystals forming.

REFERENCES

1. Mohajit, K., Bhattarai, K., Taiganides, E. P., and Yap, B. C. Struvite deposits in pipes and aerators. *Biol Wastes* 30, 133–147 (1989).
2. Austine, A. M. B. Multifunctional calcium carbonate and calcium phosphate scale inhibitor, U.S. Patent 7R52, 770B2 Aug. 7, 2007, 13 pp.
3. Ferguson, J. F., Jenkins, D., and Stumm, W. Calcium phosphate precipitation in wastewater treatment. *Chem Eng Prog Symp Ser* 67, 279–287 (1971).
4. Doyle, J. D., Oldring, K., Churchley, J., and Parsons, S. A. Struvite formation and fouling propensity of different materials. *Water Res* 36, 3971–3978 (2002).
5. Strickland, J. Perspectives for phosphorus recovery offered by enhanced biological P removal. *Environ Technol* 20, 721–726 (1999).
6. Mamais, D., Pi, P. A., Cheng, Y. W., Locaino, J., and Jenkins, D. Determination of the ferric chloride dose to control struvite precipitation in anaerobic digesters. *Water Environ Res* 66, 411–416 (1994).
7. Ekama, G. A., Wentzel, M. C., and Lowenthal, R. E. Integrated chemical-physical processes kinetic modelling of multiple mineral precipitation problems. *Water Sci Technol* 53, 65–73 (2006).
8. van Renburg, P., Musvoto, E. V., Wentzel, M. C., and Ekama, G. A. Modelling multiple mineral precipitation in anaerobic digester liquor. *Water Res* 37, 3087–3097 (2003).
9. Yong, S., Hahn, H. H., and Hoffmann, H. The effect of carbonate on the precipitation of calcium phosphate. *Environ Technol* 23, 207–215 (2002).
10. Abbona, F., Lundager-Madsen, H. E., and Boistelle, R. Crystallization of two magnesium phosphates, struvite and newbeyerite: Effect of pH and concentration. *J Cryst Growth* 57, 6–14 (1982).
11. Cao, X. and Harris, W. Carbonate and magnesium interactive effect on calcium phosphate precipitation. *Environ Sci Technol* 42, 436–442 (2008).

12. House, W. A. The physico-chemical conditions for the precipitation of phosphate with calcium. *Environ Technol* 20, 727–733 (1999).
13. Mullin, J. W. *Crystallization*, 4th edn., Butterworths-Heinemann, Oxford, U.K. (2001).
14. Reddy, M. M. and Nancollas, G. H. The crystallization of calcium carbonate: I. Isotopic exchange and kinetics. *J Colloid Interface Sci* 36, 166–172 (1971).
15. Nancollas, G. H. The crystal growth of sparingly soluble salts. *Croat Chem Acta* 45, 225–232 (1973).
16. Kazmierczak, T. F., Schuttringer, E., Tomazic, B., and Nancollas, G. H. Controlled composition studies of calcium carbonate and sulfate crystal growth. *Croat Chem Acta* 54, 277–287 (1981).
17. De Rooij, J. F., Heughebaert, J. C., and Nancollas, G. H. pH study of calcium phosphate seeded precipitation. *J Colloid Interface Sci* 100, 350–358 (1984).
18. Nancollas, G. H. and Mohan, M. S. The growth of hydroxyapatite crystal. *Arch Oral Biol* 15, 731–745 (1970).
19. Tomson, M. B. and Nancollas, G. H. Mineralization kinetics: A constant composition approach. *Science* 200, 1059–1060 (1978).
20. Schecher, W. D. and McAvoy, D. C. MINEQL+ A chemical equilibrium modeling system: Version 4.0 for Windows user's manual. Environmental Research Software, Hallowell, ME (1998).
21. Ohlinger, K. N., Young, T. M., and Schroeder, E. D. Kinetics effects on preferential struvite accumulation in wastewater. *J Environ Eng* 125, 730–737 (1999).
22. Stratful, I., Scrimshaw, M. D., and Lester, J. N. Conditions influencing the precipitation of magnesium ammonium phosphate. *Water Res* 35, 4191–4199 (2001).
23. Nelson, N. O., Mikkelsen, R. L., and Hesterberg, D. L. Struvite precipitation in anaerobic swine lagoon liquid: Effect of pH and Mg:P ratio and determination of rate constant. *Bioresour Technol* 89, 229–236 (2003).
24. Battistoni, P., Fava, G., Pavan, P., Musacco, A., and Cecchi, F. Phosphate removal in anaerobic liquors by struvite crystallization without addition of chemicals: Preliminary results. *Water Res* 31, 2925–2929 (1997).
25. Bouropoulos, N. Ch. and Koutsoukos, P. G. Spontaneous precipitation of struvite from aqueous solutions. *J Cryst Growth* 213, 381–388 (2000).
26. Jaffer, Y., Clark, T. A., Pearce, P., and Parsons, S. A. Potential phosphorus recovery by struvite formation. *Water Res* 36, 1834–1842 (2002).
27. von Münch, E. and Barr, K. Controlled struvite crystallization for removing phosphorus for anaerobic digester sidestreams. *Water Res* 35, 151–159 (2000).
28. Uludag-Demirer, S., Demirer, G. N., and Chen, S. Ammonia removal from anaerobically digested dairy manure by struvite precipitation. *Process Biochem* 40, 3667–3674 (2005).
29. Kumashiro, K., Ishiwatari, H., and Nawamura, Y. A pilot plant study on using seawater as a magnesium source for struvite precipitation. In *Proceedings of Second International Conference on the Recovery of Phosphorus from Sewage and Animal Wastes*, Noordwijkerhout, the Netherlands, May 12–13 (2001).
30. Lee, S. I., Weon, S. Y., Lee, C. W., and Koopman, B. Removal of nitrogen and phosphate from wastewater by addition of bittern. *Chemosphere* 51, 265–271 (2003).
31. Sallis, J. D. Structure/performance relationships of phosphorus and carboxyl containing additives as calcium phosphate crystal growth inhibitors. In *Calcium Phosphates in Biological and Industrial Systems*. Amjad, Z. (Ed.), pp. 173–191, Kluwer Academic Publishers, New York (1998).
32. Demadis, K. D., Sallis, J. D., Raptis, R. G., and Baran, P. A crystallographically characterized nine-coordinate calcium phosphocitrate complex as calcification inhibitor in vivo. *J Am Chem Soc* 123, 10129–10130 (2001).
33. Demadis, K. D. Structure and in vivo anticalcification properties of a polymeric calcium-sodium-phosphocitrate organic-inorganic hybrid. *Inorg Chem Commun* 6, 527–530 (2003).
34. Aylward, G. and Findlay, T. *SI Chemical Data*, 5th edn., John Wiley & Sons, Australia (2002).
35. De Stefano, C., Gianguzza, A., Piazzese, D., and Sammartano, S. Polyacrylate protonation in various aqueous ionic media at different temperatures and ionic strengths. *J Chem Eng Data* 45, 876–881 (2000).
36. De Stefano, C., Gianguzza, A., Piazzese, D., and Sammartano, S. Polyacrylates in aqueous solution. The dependence of protonation on molecular weight, ionic medium and ionic strength. *React Funct Polymers* 55, 9–20 (2003).
37. De Stefano, C., Gianguzza, A., Piazzese, D., and Sammartano, S. Quantitative parameters for the sequestering capacity of polyacrylates towards alkaline earth metal ions. *Talanta* 61, 181–194 (2003).
38. Tew, W. P., Mahle, C., Benavides, J., Howard, J. E., and Lehninger, A. E. Synthesis and characterization of phosphocitric acid, a potent inhibitor of hydroxyapatite crystal growth. *Biochemistry* 19, 1983–1988 (1980).

39. Williams, G. and Sallis, J. D. Structural factors influencing the ability of compounds to inhibit hydroxyapatite formation. *Calcif Tissue Int* 34, 169–177 (1982).
40. Amjad, Z. The inhibition of dicalcium phosphate dihydrate crystal growth by polycarboxylic acids. *J Colloid Interface Sci* 117, 98–103 (1987).
41. Sharma, V. K., Johnsson, M., Sallis, J. D., and Nancollas, G. H. Influence of citrate and phosphocitrate on the crystallization of octacalcium phosphate. *Langmuir* 8, 676–679 (1992).
42. van der Houen, J. A. M., Cressey, G., Cressey, B. A., and Valsami-Jones, E. The effect of organic ligands on the crystallinity of calcium phosphate. *J Cryst Growth* 249, 572–583 (2003).
43. Tsortos, A. and Nancollas, G. H. The role of polycarboxylic acids in calcium phosphate mineralization. *J Colloid Interface Sci* 250, 159–167 (2002).
44. Cheung, H. S., Kurup, I. V., Sallis, J. D., and Ryan, L. M. Inhibition of calcium pyrophosphate dihydrate crystal formation in particular cartilage vesicles and cartilage by phosphocitrate. *J Biol Chem* 27(145), 28082–28085 (1996).
45. Wierzbicki, A., Sikes, C. S., Sallis, J. D., Madura, J. D., Stevens, E. D., and Martin, K. L. Scanning electron microscopy and molecular modeling of inhibition of calcium oxalate monohydrate crystal growth by citrate and phosphocitrate. *Calcif Tissue Int* 56, 297–304 (1995).
46. Sallis, J. D., Juckes, W., and Anderson, M. E. Phosphocitrate: Potential to influence deposition of scaling salts and corrosion. In *Mineral Scale Formation and Inhibition*, Amjad, Z. (Ed.), Plenum Press, New York (1995).
47. Lioliou, M. G., Paraskeva, C. A., Koutsoukos, P. G., and Payatakes, C. A. Calcium sulfate precipitation in the presence of water-soluble polymers. *J Colloid Interface Sci* 303, 164–170 (2006).
48. Doyle, J. D., Oldring, K., Churchley, J., Price, C., and Parsons, S. A. Chemical control of struvite precipitation. *J Environ Eng* 129, 419–426 (2003).
49. Golubev, S. V., Pokrovsky, O. S., and Savenko, V. S. Unseeded precipitation of calcium and magnesium phosphates from modified seawater solutions. *J Cryst Growth* 205, 354–360 (1999).
50. Nancollas, G. H. and Zawacki, S. J. Inhibitors of crystallization and dissolution. In *Industrial Crystallization 84*, Jancic, S. J. and DeJong, E. J. (Eds.), Elsevier, Amsterdam, the Netherlands (1984).
51. Amjad, Z., Koutsoukos, P. G., and Nancollas, G. H. The crystallization of hydroxyapatite and fluorapatite in the presence of magnesium ions. *J Colloid Interface Sci* 101, 250–256 (1984).
52. Martell, A. E. and Smith, R. M. NIST, Critically selected stability constants of metal complexes. Standard Reference Database 46 v. 60.
53. Kofina, A., Kanelloupolou, D. G., and Koutsoukos, P. Solubility of salts in water: key issue for crystal growth and dissolution processes. *Pure Appl Chem* 79, 825–850 (2007).
54. Ketrick, B. Resin comparative table. Internal Training Program, Guardian CSC, York, PA.
55. Cotton, I. Clarification products. AWT TRTM, Rockville, MD, pp. 2–16 (2001).
56. Ketrick, B. Types of filters. Internal Training Program, Guardian CSC, York, PA.
57. Ketrick, B. Resin beads. Internal Training Program, Guardian CSC, York, PA.
58. Ketrick, B. Resin comparative table. Internal Training Program, Guardian CSC, York, PA.
59. Ketrick, B. Reverse osmosis flow. Internal Training Program, Guardian CSC, York, PA.
60. Ketrick, B. Feed water tank drawing. Internal Training Program, Guardian CSC, York, PA.
61. Frayne, C. and Ketrick, B. Oxygen scavenger properties. AWT Training Course, Rockville, MD, Boiler water treatment, p. 56 (2009).
62. Ketrick, B. Carbonic acid corrosion. Internal Training Program, Guardian CSC, York, PA.
63. Ketrick, B. Chemical feed points. Internal Training Program, Guardian CSC, York, PA.

12 New Developments in Membrane-Based Processes for Industrial Applications

Peter S. Cartwright

CONTENTS

12.1	Introduction.....	228
12.2	History.....	228
12.3	Background.....	230
12.3.1	Microfiltration.....	230
12.3.2	Ultrafiltration.....	230
12.3.3	Nanofiltration.....	231
12.3.4	Reverse Osmosis.....	231
12.4	Device Configuration.....	233
12.4.1	Plate and Frame.....	233
12.4.2	Tubular.....	233
12.4.3	Capillary (Hollow) Fiber.....	233
12.4.4	Spiral Wound.....	234
12.5	System Performance.....	234
12.6	Applications.....	235
12.6.1	MBR Technology.....	235
12.7	System Design.....	236
12.8	Testing Background.....	238
12.8.1	Feed Water Chemistry.....	238
12.8.2	Membrane Element Configuration.....	239
12.8.3	Membrane Area.....	239
12.8.4	Membrane Polymer.....	239
12.8.5	Temperature.....	239
12.8.6	Applied Pressure.....	239
12.8.7	Recovery.....	239
12.8.8	Flow Conditions.....	240
12.8.9	Membrane Element Array.....	240
12.8.10	Pretreatment Requirements.....	240
12.9	Testing.....	240
12.9.1	Cell Test.....	240
12.9.2	Applications Testing.....	241
12.9.3	Pilot Testing.....	243
12.10	Summary.....	243
	Membrane Technology Glossary.....	243

12.1 INTRODUCTION

Water covers almost 75% of the earth's surface; however, less than 1% of this volume is of a quality sufficient to sustain life and maintain health. Due to the fact that fresh water supplies are unevenly distributed throughout the world, and because a financial investment is required to at least disinfect these supplies, over 1 billion people, primarily in the developing countries, do not have access to safe water supplies. As a result, some 2.2 million people die each year from contaminated water and poor sanitation. It is estimated that by 2025, one-half of the world's population will face serious shortages of potable water.

Water treatment involves the removal of contaminants from water. Whether the requirement is to treat a municipal or individual well water supply coming into a facility, or wastewater leaving it, is immaterial; the goal is to remove some (or most) of certain (or all) of the contaminants in that particular water stream. It is possible to group all of the contaminants into five specific classes, as indicated in Table 12.1.

The membrane separation technologies of microfiltration (MF), ultrafiltration (UF), nanofiltration (NF), and reverse osmosis (RO) possess characteristics that make them attractive as wastewater reuse processes. These include

- Continuous process, resulting in automatic and uninterrupted operation
- Low energy utilization involving neither phase nor temperature changes
- Modular design—no significant size limitations
- Minimal moving parts with low maintenance requirements
- No effect on the form or chemistry of contaminants
- Discreet membrane barrier to ensure the physical separation of contaminants
- No chemical addition requirements

In this chapter, the history of membrane technology is presented, the fundamentals of these technologies are introduced, engineering design requirements addressed, and testing details described.

12.2 HISTORY

Natural biological processes utilize membrane technologies to transport water and nutritional materials through cell walls; these technologies have been in use since the evolution of life. The interest of man in these processes is evidenced by writings and illustrations found in artifacts tracing back to ancient Chinese and early Mediterranean civilizations.

The following chronicles the more notable achievements in membrane technology research:*

1748—Abbe Nollet observed osmosis through semipermeable animal bladders. He placed “spirits of wine” in a vessel, the mouth of which was covered with an animal bladder and immersed in pure water. The bladder swelled and sometimes burst because of osmosis of water into the wine, an indication of semipermeability of the bladder material.

TABLE 12.1
Water Contaminants

Class	Examples
Suspended solids	Dirt, clay, colloidal materials, silt, dust, insoluble metal oxides, and hydroxides
Dissolved organics	Trihalomethanes, synthetic organic chemicals, humic acids, fulvic acids
Dissolved ionics (salts)	Heavy metals, silica, arsenic, nitrate, chlorides, carbonates
Microorganisms	Bacteria, viruses, protozoan cysts, fungi, algae, molds, yeast cells
Gases	Hydrogen sulfide, methane, radon, carbon dioxide

* A number of dates in Section 12.2 are from “Reverse Osmosis Membrane Milestones,” as published in the February 4, 2008 issue of *Water Desalination Report*, edited by Tom Pankratz, Global Water Intelligence (<http://www.globalwater-intel.com>).

1845—Matteuci and Cima noted asymmetric permeability differences. Using animal membranes for osmotic studies, they were the first researchers to report on permeability differences related to the asymmetry of pores in membranes. They observed higher flow rates in one direction than in the other.

1855—Fick developed the first synthetic membrane out of nitrocellulose by dipping ceramic thimbles into an ether alcohol solution of cellulose nitrate called collodion. The resulting membrane “sacs” were used for dialyzing solutions of biological fluids. Incidentally, it was also in 1855 that Fick published his phenomenological laws of diffusion which are still used today to describe diffusion through membranes.

1887—van Hoff formulated the osmotic pressure equation.

1906—Bechhold made the first UF membranes, developed the bubble point method for determining pore size, and produced graded pore sizes by varying collodion concentration. In addition, he developed membranes made from formalized gelatin with pore diameters of less than 0.01 microns. For these, he coined the term “ultrafiltration” which has stuck. Bechhold used his membranes to separate the mixtures of colloids and prepare sterile filtrates and liquids suitable for ultramicroscopic work. In addition, he compiled a list of substances in descending size of suspended particles, ranging from a true suspension to a real crystalloid.

1907—Bigelow and Gemberling regulated pore size by varying evaporation time. They used the ether alcohol solutions of collodion to form membranes sufficiently strong to be self-supporting by pouring a thin layer of the solution onto a leveled glass plate and regulating the pore size by varying the evaporation time before immersion into water. It is now clear that many of these early membranes were somewhat asymmetric, with the smallest pores on the air-dried surface.

1911—Schoep regulated pore size with nonvolatile additives in casting solutions. He added glycerol or castor oil to the casting solution resulting in larger pores. An extra bonus was the improved flexibility of the membrane due to the addition of the plasticizer.

1915–1917—Brown regulated pore size with alcohol in quench water. He controlled the pore size by drying the collodion films to a specific weight and then immersing them in an alcohol–water solution. The permeability was a function of the alcohol content in water. Brown was also the first to use cellulose acetate in preparing membranes and to recognize the asymmetric pore structure.

1921—Eggerth regulated pore size by varying alcohol/ether ratio in casting solutions. He was able to vary the pore size in this fashion while holding the drying time constant. He was also able to increase the pore size by adding lactic acid to the casting solution.

1925—Asheshov regulated pore size with volatile additives. He investigated additives such as acetone and amyl alcohol ether solutions of nitrocellulose and found that acetone tended to increase the pore diameter whereas amyl alcohol decreased it.

1930—Elford studied gel structure and produced highly permeable membranes using amyl alcohol, acetone, acetic acid, and water. He was the first to study the microscopic gel structure of membranes. Following the work of Asheshov, he found that acetone and amyl alcohol together were antagonistic, tending to precipitate the nitrocellulose. He took advantage of this phenomenon to prepare highly permeable membranes (3–10-micron pore size) with good tensile strength.

In the mid-1930s, theories were developed by Teorell, Meyer, and Seavers relating to electro dialysis. Pressure dialysis was first demonstrated by Wilhem Kolff in the 1940s, which led to the development of the artificial kidney.

World War II saw the initial development of an industry for the manufacture of MF membranes by the Germans to monitor drinking water supplies affected by air raids. The interest of the United States in these membranes for bacteriological water analysis led to the origins of MF manufacturing in the mid-1950s, and the field has grown rapidly since.

In 1955, Charles E. Reid at the University of Florida investigated cellulose acetate films for desalination applications. In 1958, Loeb and Sourirajan discovered a method to cast very thin cellulose acetate membranes, the first practical RO membranes. In the early 1960s, spiral wound membrane elements were developed, followed by the introduction of thin film composite membrane polymers in the early 1970s.

The commercial development of UF membranes follows a path similar to that of RO; however, the earliest membrane elements were of either hollow fiber or tubular construction. NF membranes are a later development related to RO membrane activity.

12.3 BACKGROUND

Membrane separation technologies are based on a process known as “crossflow” filtration which allows for the continuous processing of liquid streams. In this process, the bulk solution flows over and parallel to the membrane surface, and because the liquid is pressurized, water is forced through the membrane. The turbulent flow of the bulk solution over the surface minimizes the accumulation of particulate matter. Figure 12.1 illustrates crossflow filtration compared to conventional filtration.

The crossflow membrane separation technologies of MF, UF, NF, and RO are defined by some membrologists on the basis of pore size. Other experts prefer to use definitions based on the removal function, as described here.

12.3.1 MICROFILTRATION

MF is utilized to remove submicron suspended materials on a continuous basis. The size range is from approximately 0.01–1 micron (100–10,000 Å). By definition, MF does not remove dissolved materials. MF is illustrated in Figure 12.2.

12.3.2 ULTRAFILTRATION

UF is the membrane process that removes dissolved nonionic solute, typically organic materials (macromolecules). UF membranes are usually rated by *molecular weight cutoff* (MWCO), the maximum

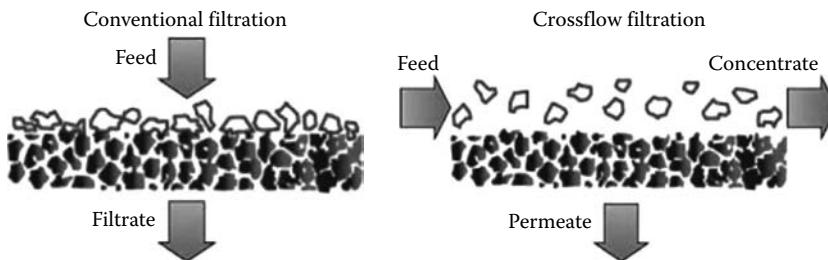


FIGURE 12.1 Convention vs. crossflow filtration.

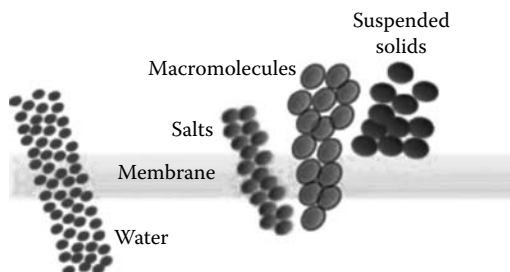


FIGURE 12.2 Microfiltration.

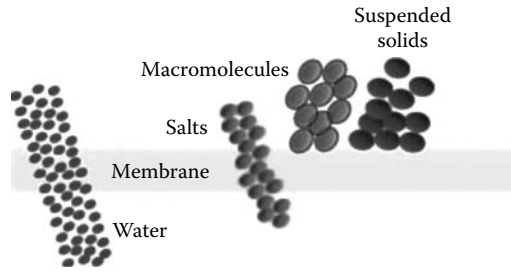


FIGURE 12.3 Ultrafiltration.

molecular weight of the compound that will pass through the membrane pores into the permeate stream. UF pore sizes are usually smaller than 0.01 micron (100 Å) in size. UF is depicted in Figure 12.3.

The above processes (MF and UF) separate contaminants on the basis of a “sieving” process; that is, any contaminant too large to pass through the pore is rejected and exits in the concentrate stream.

12.3.3 NANOFILTRATION

NF can be considered “loose” RO. It rejects dissolved ionic contaminants, but to a lesser degree than RO. NF membranes reject a higher percentage of multivalent salts than monovalent salts (e.g., 99% vs. 20%). These membranes have MWCOs for nonionic solids below 1000 Da. NF is illustrated in Figure 12.4.

12.3.4 REVERSE OSMOSIS

RO produces the highest quality permeate of any pressure-driven membrane technology. Certain polymers will reject over 99% of all ionic solids, and have MWCOs in the range of 50–100 Da. Figure 12.5 illustrates RO.

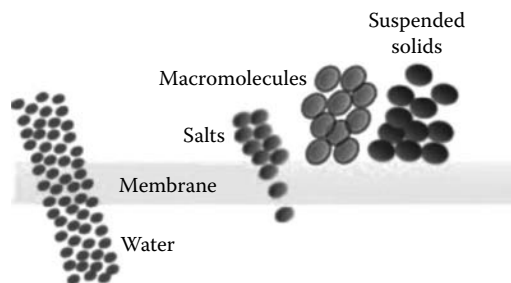


FIGURE 12.4 Nanofiltration.

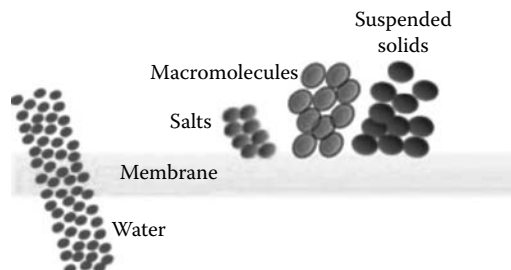


FIGURE 12.5 Reverse osmosis.

NF and RO membranes reject salts utilizing a mechanism that is not fully understood. Some experts endorse the theory of pure water preferentially passing through the membrane; others attribute it to the effect of the surface charges of the membrane polymer on the polarity of the water. Monovalent salts are not as highly rejected from the membrane surface as multivalent salts; however, the high rejection properties of the newer thin film composite RO membranes exhibit very little differences in salt rejection characteristics as a function of ionic valance. As indicated earlier, this difference is significant with NF membranes. In all cases, the greater the degree of contaminant removal, the higher the pressure requirement to affect this separation. In other words, RO, which separates the widest range of contaminants, requires an operating pressure typically an order of magnitude higher than MF, which removes only suspended solids.

The water passage rate through the membrane to generate treated water (permeate) is known as *flux rate*. It is a function of applied pressure, water temperature, and in the case of NF and RO (and to a limited extent, UF), the osmotic pressure of the solution under treatment. Flux rate is usually measured as GFD (gallons per square foot per day) or LMD (liters per square meter per day). Increasing the applied pressure will increase the permeate rate; however, a high flow of water through the membrane will promote more rapid fouling. Membrane element manufacturers usually provide limits with regard to maximum applied pressures to be used as a function of feed water quality. Heating the water will also increase the permeate rate, but this requires significant energy and is generally not considered practical. Table 12.2 summarizes the various properties and other features of these technologies.

TABLE 12.2
Membrane Technologies Compared

Feature	MF	UF	NF	RO
Polymers	Ceramics Sintered metals Polypropylene Polysulfone Polyethersulfone Polyvinylidene fluoride Polytetrafluoroethylene	Ceramics Sintered metals Polypropylene Polysulfone Polyethersulfone Polyvinylidene fluoride	Thin film composites Cellulosics	Thin film composites Cellulosics
Pore size range (μm)	0.01–1.0	0.001–0.01	0.0001–0.001	<0.0001
Molecular weight cutoff range (Da)	>100,000	1,000–100,000	300–1,000	50–300
Operating pressure range (psi)	<30	20–100	50–300	225–1,000
Suspended solids removal	Yes	Yes	Yes	Yes
Dissolved organics removal	None	Yes	Yes	Yes
Dissolved inorganics removal	None	None	20%–95%	95% to 99% +
Microorganism removal	Protozoan cysts, algae, bacteria ^a	Protozoan cysts, algae, bacteria, ^a viruses	All ^a	All ^a
Osmotic pressure effects	None	Slight	Moderate	High
Concentration capabilities	High	High	Moderate	Moderate
Permeate purity (overall)	Low	Moderate	Moderate–high	High
Energy usage	Low	Low	Low–moderate	Moderate
Membrane stability	High	High	Moderate	Moderate

^a Under certain conditions, bacteria may grow through the membrane.

12.4 DEVICE CONFIGURATION

To be effective, membrane polymers must be packaged into a configuration commonly called a *device* or *element*. The most common element configurations are

- Plate and frame
- Tubular
- Capillary allow fiber
- Spiral wound

The element configurations are described next and illustrated in Figure 12.6.

12.4.1 PLATE AND FRAME

This element incorporates sheet membrane stretched over a frame to separate the layers and facilitate the collection of the permeate which is directed to a collection tube. This design is similar to a plate and frame filter press.

12.4.2 TUBULAR

Manufactured from ceramics, carbon, stainless steel, or a number of thermoplastics, these tubes have inside diameters ranging from 1/4 in. up to approximately 1 in. (6–25 mm). The membrane is typically coated on the inside of the tube and the feed solution flows under pressure through the interior (lumen) from one end to the other, with the permeate passing through the wall and collected outside of the tube.

12.4.3 CAPILLARY (HOLLOW) FIBER

These elements are similar to the tubular element in design, but are smaller in diameter, and are usually unsupported membrane polymers or ceramics. In the case of polymeric capillary fibers, they

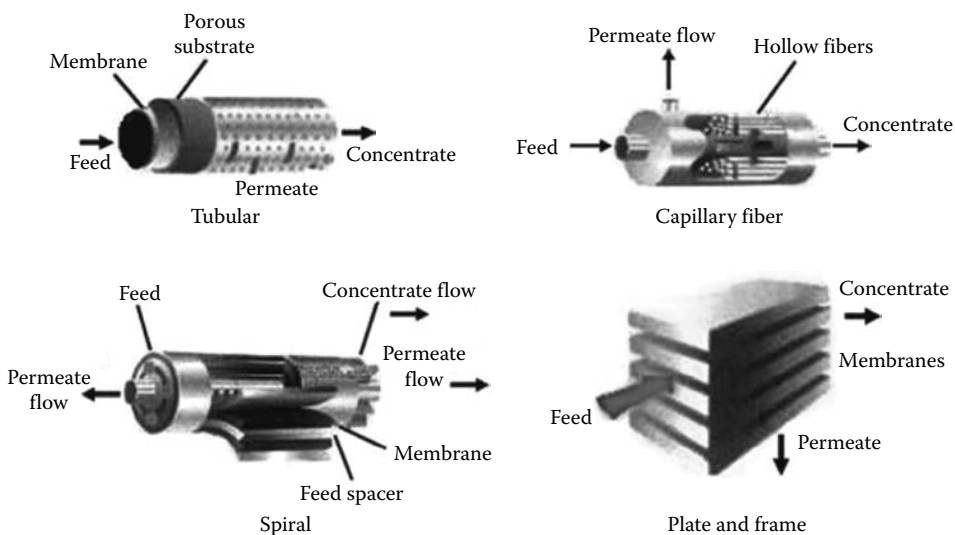


FIGURE 12.6 Membrane element configurations.

TABLE 12.3
Membrane Element Configuration Comparison

Element Configuration	Packing Density ^a	Fouling Resistance ^b
Plate and frame	Low	High
Capillary (hollow fiber)	Medium	High
Tubular	Low	Very high
Spiral wound	Medium	Moderate

^a Membrane area per unit volume.

^b Tolerance to suspended solids.

require rigid support on each end provided by an epoxy “potting” of a bundle of the fibers inside a cylinder. Feed flow is either down the interior of the fiber (“lumen feed”) or around the outside of the fiber (“outside-in”).

12.4.4 SPIRAL WOUND

This element is constructed from an envelope of sheet membrane wound around a permeate tube that is perforated to allow the collection of the permeate. Water is purified by passing through one layer of the membrane and, following a spiral pattern, by having it flow into the permeate tube. It is by far the most common configuration in water purification applications, but generally requires extensive pretreatment in wastewater applications.

From the perspective of cost and convenience, it is beneficial to pack as much membrane area into as small a volume as possible. This is known as *packing density*. The greater the packing density, the greater the membrane area enclosed in a certain sized device, and generally, the lower its cost. The downside of the high packing density membrane elements is their greater propensity for fouling. Table 12.3 compares the element configurations with regard to their packing densities.

12.5 SYSTEM PERFORMANCE

The vast majority of membrane system failures occur as a result of membrane fouling. This fouling is usually caused by one or more of the following mechanisms:

- Suspended solids in the feed stream resulting from incomplete feed water filtration
- Precipitation of insoluble salts or oxides resulting from concentration effects within the membrane device
- Biofilms resulting from microbiological activity

These mechanisms cause the membrane surface to become coated with fouling materials that build up in layers. As the layer thickness increases, the flow rate and resulting turbulence across the membrane surface (and immediately adjacent to it) is reduced, thereby encouraging more settling of suspended solids and increasing the fouling layer thickness, which further slows the rate of permeate flow through the membrane—a vicious cycle.

With NF and RO membranes which reject ionic contaminants, fouling usually creates a phenomenon known as *concentration polarization*. The fouling layers inhibit the free movement of contaminants in the feed stream away from the membrane surface via turbulent flow, and as salts are rejected from the membrane, their concentration at the surface is higher than in the

bulk solution (that portion above the fouling layer). Since ionic rejection is always a percentage of the salts, concentration at the surface of the membrane, the permeate quality decreases as a result of concentration polarization, and this phenomenon may actually indicate the presence of foulants before a reduction in permeate rate is detected. The increased salts concentration at the membrane surface also promotes the precipitation of those salts whose solubility limit is exceeded.

12.6 APPLICATIONS

A largely untapped resource to address water shortages is the reuse of wastewater, both residential/municipal and industrial. To recover acceptable quality water from these sources, advanced, innovative treatment technologies must be utilized.

12.6.1 MBR TECHNOLOGY

As the newest membrane technology application, and one with huge potential, membrane bioreactor (MBR) technology justifies special mention. For wastewaters containing biodegradable contaminants, the traditional treatment method is to encourage the use of bacteria to break down the contaminant (bioremediation). This encouragement can take the form of adding oxygen (in the case of aerobic treatment), a mechanical matrix (for bacterial attachment), mixing, and other approaches intended to maximize the metabolic activity of these microorganisms.

MBR involves utilizing an MF or UF membrane to filter the treated water to remove particles, microorganisms, and perhaps some dissolved organics. The permeate is recovered, and, if necessary, further purified with RO or another polishing process. The concentrate stream is returned to the bioremediation tank. Compared to other biological processes, MBR offers the following advantages:

- High-quality effluent, almost free from solids
- The ability to partially disinfect without the need for chemicals
- The complete independent control of hydraulic retention time (HRT) and sludge retention time (SRT)
- Reduced sludge production
- Process intensification through high biomass concentrations with mixed liquor suspended solids (MLSS) over 15,000 mg/L
- The treatment of recalcitrant organic fractions and the improved stability of processes such as nitrification
- Ability to treat high-strength wastes

The membrane device configurations most commonly used today are capillary fiber and plate and frame, although tubular and spiral wound devices are becoming more widely used. The most common biological treatment is aerobic and, typically, air is bubbled into the treatment tank. A very popular approach is to immerse the membrane element in the treatment tank and either allow the hydrostatic head of the solution to provide the driving force or to use a pump to pull the permeate through the membrane (or both). In this case, air bubbles are also directed over the surface of the membrane (air scouring) in an effort to reduce fouling. Another design involves pumping water through the membrane system external to the treatment tank, and yet another uses a separate tank for the membrane processing downstream of the biological treatment tank. Additional designs and configurations are sure to appear as MBR technology becomes more widely used. Figure 12.7 illustrates aerobic MBR applications for both “immersed” and “external” designs.

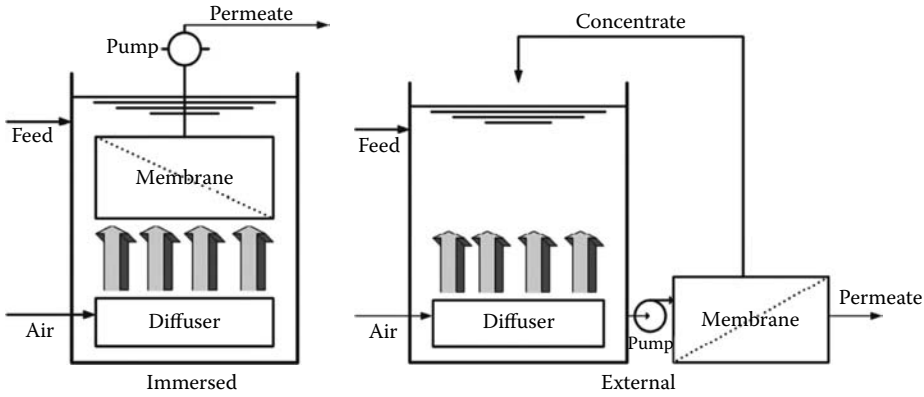


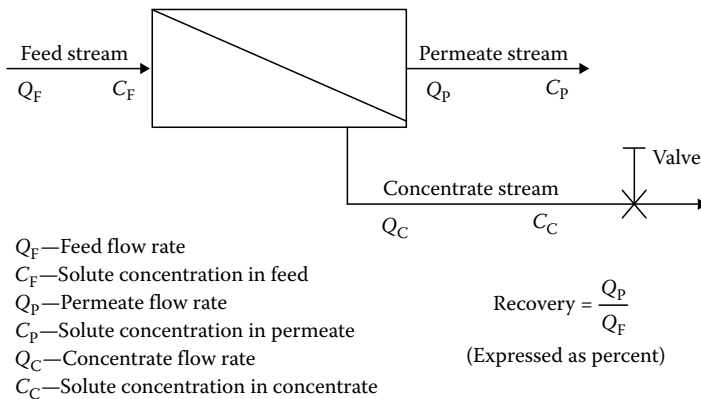
FIGURE 12.7 Aerobic MBR applications.

12.7 SYSTEM DESIGN

Figure 12.8 is a schematic of a complete membrane processing system (or a single membrane element).

Note that the “feed” stream enters the system (or membrane element), and as the stream passes along and parallel to the surface of the membrane under pressure, a percentage of the water is forced through the membrane polymer producing the permeate stream. Contaminants are prevented from passing through the membrane based on the polymer characteristics. This contaminant-laden stream exits the membrane system (or element) as the concentrate stream, also known as the brine or reject (see Glossary).

The permeate rate of a given membrane element cannot be changed without varying the applied pressure or temperature. Recovery, however, can be easily changed by varying the feed flow rate to the element, and this is one of the variables that is controlled by the system designer. The effect of recovery on system performance is important. As recovery is increased, the flow rate of the concentrate stream diminishes; all contaminants that are rejected by the membrane



TDS = Total dissolved solids: Usually considered the total of the ionic contaminants (salts) in solution.

mg/L (milligrams per liter) is the same as ppm (parts per million)

FIGURE 12.8 Membrane system schematic.

TABLE 12.4
Effect of Recovery
on Concentration

Recovery (%)	X
33	1.5
50	2
67	3
75	4
80	5
90	10
95	20
97.5	40
98	50
99	100

Note: $C_c \approx \frac{C_F}{1 - \text{recovery}} = XC_F$

where X ≡ concentration factor.

and concentrated in the concentrate stream become more concentrated. The effect of increasing recovery on the concentration of contaminants in the concentrate stream is illustrated in Table 12.4 and Figure 12.9. For wastewater treatment and water reuse applications, the minimum recovery is usually higher than 80%.

One way to understand concentration factor is to think in terms of the evaporation or distillation process. If half of a given volume of water is distilled and the condensate recovered as pure water (permeate), this is the same concept as operating a membrane system at 50% recovery. The evaporation of three-fourths of the water is 75% recovery, and so on.

The advantages of operating systems at high recoveries are that the volume of concentrate is small and the flow rate of the feed pump is smaller. The potential disadvantages are numerous:

- The higher concentration of contaminants can result in precipitation and greater propensity for fouling.
- In NF and RO applications, the concentrated salts will result in higher osmotic pressure, requiring a higher pressure pump and a more pressure-resistant system.
- Also with RO and NF, as recovery is increased, the ionic purity of the permeate decreases.
- As higher recoveries reduce the quantity of concentrate to be discharged, the higher concentration of this concentrate stream can itself present discharge problems.

The issue of recovery is definitely application specific: most water purification applications—those treating raw water to be purified for some downstream applications (drinking, product manufacturing, rinsing, and so on)—generally operate at relatively low recoveries, not exceeding 85%, even for the largest applications. In general, most water purification applications involve feed water conductivities that are relatively low so that osmotic pressure does not play a significant role; the one exception is seawater desalination. Usually, the larger the system, the higher its recovery.

It is possible to completely close off the concentrate line through the use of a valve, thereby using the membrane as a conventional or “dead-end” filter (forcing 100% of the water through

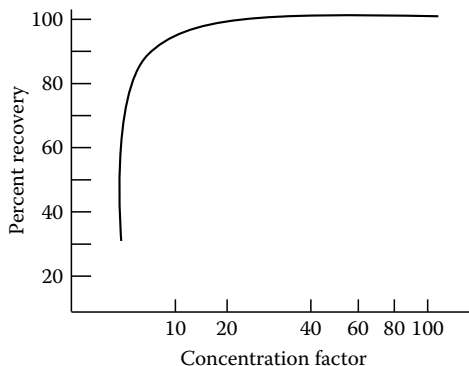


FIGURE 12.9 Effect of recovery on concentration.

the membrane), with occasional periods when the concentrate valve is opened to allow the crossflow feature to reduce the concentration of contaminants at the surface of the membrane. Some membrane elements of tubular, capillary (hollow) fiber, or plate and frame configuration can also be “backwashed,” which involves running permeate (or another high-quality water supply) backward into the element to dislodge suspended materials from the surface of the membrane.

12.8 TESTING BACKGROUND

It is virtually impossible to accurately design a wastewater treatment or water reuse system utilizing membrane technologies without a complete, thorough, and comprehensive testing program. This is required to identify the best membrane polymer and element configuration, and to optimize the system design and operating conditions. In general, every stream must be tested to develop the following design factors:

- Optimum membrane element configuration
- Total membrane area
- Specific membrane polymer
- Temperature effects
- Optimum pressure
- Maximum system recovery
- Flow conditions
- Membrane element array
- Pretreatment requirements

Specific parameters that influence these design factors are discussed next.

12.8.1 FEED WATER CHEMISTRY

The chemical composition of the feed water can affect the membrane element in a number of ways. The polymer itself (or components of the membrane element) can be degraded by certain chemicals. For example, cellulosic membrane polymers are subject to hydrolysis by high pH, thin film composite polymers are degraded by oxidizing agents such as chlorine, and most of the polymers are affected by chlorinated hydrocarbon solvents in concentrations above 5%. Water chemistry can also contribute to fouling problems, the bane of all membrane systems. Certainly, the suspended solids of any kind represent a potential problem, and the configuration of the membrane element plays a major role in its ability to resist fouling.

The most significant feed water parameters are

- Total solids content
- Suspended (TSS)
- Dissolved organic (TOC, MBAS, COD, and BOD)
- Dissolved inorganic (TDS)

Chemicals of concern include

- Oxidizing chemicals
- Organic solvents
- Saturated solutes
- Surfactants

Other factors include

- pH
- Operating temperature
- Osmotic pressure as a function of system recovery
- Variation in feed stream chemistry as a function of time

12.8.2 MEMBRANE ELEMENT CONFIGURATION

The particular way that the membrane polymer is configured in an element design has a direct bearing on the resistance of the membrane to fouling. It is usually most economical to pack as much membrane area into the device as possible without it becoming too large or heavy. Unfortunately, the element designs that provide the greatest packing density also have the lowest resistance to fouling as a result of the close spacing required to accomplish the high packing density. The selection of the optimum membrane element configuration is one of the most critical outcomes of testing.

12.8.3 MEMBRANE AREA

In general, the greater the membrane area, the higher the permeate rate, everything else being equal.

12.8.4 MEMBRANE POLYMER

As indicated in Table 12.2, many different membrane polymers are now in the market, with new ones frequently becoming available. Obviously, these are the key components with regard to effecting the separation, and each polymer has its particular strong and weak points; none is perfect. It is essential that the design engineer understands the particular characteristics of each polymer well enough to select the one(s) most appropriate for the testing.

12.8.5 TEMPERATURE

Because of its lower viscosity, warm water will flow more readily through membrane pores than cold water; therefore, as temperature is increased, permeate rate increases. Unfortunately, most membrane polymers are thermoplastic, and become more compressible when warmed. The combination of temperature and pressure can cause irreversible compaction in some polymers, resulting in premature failure. Certain plastic polymers as well as virtually all ceramic and metallic membranes exhibit excellent thermal stability and offer significant promise in those applications where it is considered desirable to process a stream at elevated temperatures. Each membrane element manufacturer provides data on temperature limits and the relationship of temperature to permeate rate for its products.

12.8.6 APPLIED PRESSURE

In general, the permeate rate of a membrane element is directly proportional to the net driving pressure. *Net driving pressure* is defined as the total pump pressure minus the osmotic pressure minus any back pressure in the permeate line. Net driving pressures range from as low as 30 psi (2 bar) for MF systems to as high as 1000 psi (68 bar) for RO systems.

12.8.7 RECOVERY

Of critical importance to solute concentration is the recovery. As defined, it is the percentage of feed water flow that exits the element or system as permeate. The relationship between concentration

factor and recovery is illustrated in Table 12.4 and Figure 12.9. As osmotic pressure is directly proportional to concentrate concentration (for polar solutes), this effect becomes critically important in many effluent treatment applications.

12.8.8 FLOW CONDITIONS

It has been shown that membrane elements are much less susceptible to fouling from suspended or precipitated solids if all of the flows through the element are turbulent. This is indicated by the term Reynolds number, which is a dimensionless number defined as:

$$\text{Reynolds number} = (\text{diameter} \times \text{mass velocity}) / \text{viscosity} \quad (12.1)$$

By definition, Reynolds numbers above 4000 indicate turbulent flow, and those below 2000 indicate laminar flow. Each membrane element manufacturer has determined the flow requirements for their elements which result in turbulent flow (if allowed), and all systems should be designed using these data.

12.8.9 MEMBRANE ELEMENT ARRAY

In order to maintain turbulent flow conditions, elements must be grouped according to specific criteria. Typically, the permeate from each element (or pressure vessel in the case of spiral wound configurations) is collected separately in a manifold, whereby the concentrate from one becomes the feed for the next element (or pressure vessel). Obviously, as permeate is removed from a feed stream, the total volume of concentrate available as feed to the next bank of elements decreases, so the total number of elements in parallel in each successive bank must decrease. With this design, turbulent flow conditions are maintained throughout the entire system.

12.8.10 PRETREATMENT REQUIREMENTS

One of the primary reasons for testing is to determine the optimum pretreatment technologies for this application.

12.9 TESTING

To generate the necessary design data, several testing options are available.

12.9.1 CELL TEST

Cell test devices are available for purchase (or used by a consulting engineering firm skilled in the art), which evaluate small sheets of membranes on the stream to be processed. Typically, the sheet is placed between two stainless steel plates, and the test stream pumped across the membrane surface at a selected pressure and flow rate. The permeate is collected and analyzed for the degree of separation, the possible effect of the stream on the test membrane, and other properties (Figure 12.10).

The cell test offers a number of advantages:

- Only the small areas of membranes are needed; excellent for screening membrane polymer candidates
- Can be run on small volumes of test stream
- Takes very little time
- Unit is simple to operate



FIGURE 12.10 Cell test unit.

The disadvantages of this testing approach are

- Cannot obtain engineering design data
- Cannot be used for long-term fouling study
- Is only useful with membranes available as flat sheet

The cell test approach is useful as an initial step, primarily to select one or more membrane candidates for further evaluation.

12.9.2 APPLICATIONS TESTING

Figure 12.11 illustrates an applications test schematic. Applications testing utilizes a membrane element in a test unit capable of operating similar to a production unit. Since the data from this testing will be used to scale up the design to full size, it is essential that the membrane element manufacturer supplies an element capable of this scale-up. The applications testing equipment should be designed so that very high recoveries can be achieved without compromising the flow rates required to produce turbulent flow, for example. This requires that the pump be capable of not only producing

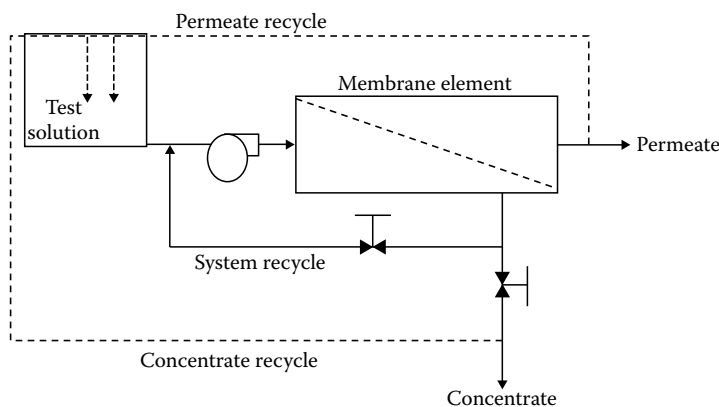


FIGURE 12.11 Applications test schematic.

the desired pressure, but also the flow rate to accomplish the minimum crossflow velocity across the membrane surface.

Because the system must be capable of testing at very high recoveries, the concentrate valving must be adjustable to accurately produce extremely low flow rates. This typically involves the assembly of a “valve nest” using micrometer valves. Additionally, the recycle line should be equipped with a diaphragm valve for the adjustment of flow and pressure. The most important feature for applications testing equipment is versatility. Different membrane elements have very specific operating parameters, and the equipment must accommodate these. To cover the entire gamut of membrane technologies, two different pieces of applications testing equipment are generally required: one for MF and UF, and the other for NF and RO. The latter must be capable of pressures up to 1000 psi (68 bar), and it is virtually impossible to find a single pump capable of supplying the flows and pressures required for all four technologies. For MF and UF applications, a variable speed drive centrifugal pump works fine, although the variable speed feature makes it expensive.

Materials of construction are an important consideration in testing considerations: 316L stainless steel (or equivalent) is essential for most applications requiring pressures in excess of 60 psi (4 bar); below that, schedule 80 PVC is sufficient. Applications testing is capable of generating complete design data for the full-sized system. An applications test can be run on as little as 50 gal (200L) of test stream, and after setup, can be completed in 1 h or less, for each membrane element tested.

A typical applications test is run as follows:

1. To establish “control conditions,” high-quality water [tap water or water treated with RO or deionization (DI)] is run into the system at low recovery to minimize any possible contaminant concentration effects. Control data are recorded.
2. Feed water is then run into the unit set at low recovery, and after stabilization (usually less than 5 min), the following data are taken:
 - a. Pressures
 - i. Prefilter
 - ii. Primary (feed)
 - iii. Final (concentrate line)
 - b. Flow
 - i. Recycle
 - ii. Permeate
 - iii. Concentrate
 - c. Temperature (recycle)
 - d. Quality (conductivity)
 - i. Feed
 - ii. Permeate
 - iii. Concentrate

The system recovery is then increased incrementally, while adjusting the recycle valve, to ensure that the correct crossflow velocity is maintained.

At each recovery, in addition to the collection of the above data, analytical samples should be taken for performance evaluation. Of course, the choice of parameters to be measured depends on the separation goals of the test. It is unusual for system recoveries to exceed 95%; however, that also depends on the goals of the testing, and it is possible to run a well-designed test unit up to 99% recovery.

Once the optimum conditions have been established, such as operating pressure and maximum system recovery, the normalized performance data will enable the test engineer to determine the total membrane area required for the full-sized system.

Applications testing provides the following advantages and disadvantages.

Advantages:

- Fast
- Provides scale-up data (flow, osmotic pressure as a function of recovery, pressure requirements, and so on)
- Can provide an indication of membrane stability

Disadvantages:

- Does not reveal long-term chemical effects
- Does not provide data on long-term fouling effects

12.9.3 PILOT TESTING

Usually, this involves placing a test machine (such as that used for the applications test) in the process, operating continuously on a “side-stream” for a minimum of 30 days.

Advantage:

- Accomplishes all of the functions of the applications test plus provides long-term membrane fouling and stability data

Disadvantage:

- Expensive in terms of monitoring and time requirements

12.10 SUMMARY

The opportunities for membrane separations technologies in wastewater reclamation and reuse are very bright. To realize this potential, it is imperative that all candidate streams be thoroughly tested. This requires knowledgeable, experienced personnel to run and interpret testing on well-designed testing equipment. Obviously, it is possible to retain the services of experienced and qualified consulting engineers to accomplish this.

MEMBRANE TECHNOLOGY GLOSSARY

Boundary layer: A very thin liquid layer immediately adjacent to the rejecting surface of membranes in which the concentration of suspended or dissolved solids is higher than it is in the main body of the water being processed. Also known as *gel layer*.

Brackish water: Water ranging from about 1000 ppm total dissolved solids to an arbitrary seawater concentration. In many cases, this upper level is defined as 25,000 ppm.

Brine: See concentrate.

Brine seal: A truncated cone of synthetic rubber attached to the upstream end of a spiral wound membrane element. Under water pressure, it forms a seal with the inner surface of the pressure vessel in which the element is placed to prevent water from bypassing around the outside of the element.

Channel: The opening or spacing between membrane layers, such as inside diameters of tubular or hollow fibers, or that resulting from netting in spirals, and so on. Also known as *bore*.

Concentrate: The stream exiting the membrane element which has not passed through the membrane, and, ideally, contains all the contaminants removed by the membrane. Concentrate is also known as: *brine, retentate, reject, effluent, and waste*.

Concentration factor (CF): Also abbreviated as VCF and VCR, this is the term that quantifies the effect of system recovery on the concentration of the rejected contaminants in a membrane element or operating system. It is mathematically related to recovery by the formula:

$$CF = \frac{1}{1 - \text{recovery}}$$

This equation results from a mass balance based on the assumption that the membrane provides complete rejection of the contaminant in question.

Concentration polarization: The formation of a more concentrated gradient of rejected material near the surface of the membrane (in the boundary layer), causing either increased resistance to solvent transport or an increase in local osmotic pressure, and possibly a change in rejection characteristics of the membrane.

Crossflow: The flow of solution tangentially or parallel to the surface of the membrane. This contrasts with “dead-end” flow seen in conventional filters, in which the liquid flows perpendicular to the surface of the filter. In crossflow, only a fraction of the crossflow solution passes through the membrane.

Crossflow membrane filtration: The separation of the components of a fluid by semipermeable membranes through the application of pressure and tangential flow to the membrane surface. This includes the processes of RO, UF, NF and MF.

Desalination: The general term applied to the removal of salts, particularly sodium chloride in seawater desalting applications. In actuality, it describes any act of removing ionic contaminants from water.

Diafiltration: A crossflow filtration process allowing for the transfer of low-molecular-weight species, water, and/or solvents through a membrane without changing the solution volume, accomplished by adding solvent (usually water) back into the feed. This process is used for purifying retained large molecular weight species, increasing the recovery of low-molecular-weight species, buffer exchange, or simply changing the properties of a given solution.

Effluent: See concentrate.

Feed: The feed water stream entering the membrane element. It is also known as *influent* or *feed water*.

Filtrate: See permeate.

Flux: The quantity of solution that passes through a unit of membrane area in a given amount of time. For example, a membrane element might have a flux of 10 LMD.

Fresh water: Water containing less than 500 parts per million (ppm) solids. Water above 1000 ppm is not recommended to be used for human consumption.

Influent: See feed.

Membrane element: The package containing the membrane and equipped with the necessary fittings to allow the feed stream to enter, and the permeate and concentrate streams to exit. The membrane element enables the membrane to effect separation. Synonyms are “membrane device” and “membrane module.” The general categories of membrane element configuration are: “spiral wound,” “capillary (hollow) fiber,” “tubular,” and “plate and frame.”

Molecular weight cutoff (MWCO): Referred to as the molecular weight above which a certain percentage (e.g., >90%) of the solute in the feed solution is rejected by the membrane. It is typically expressed in units of Daltons and used as an indication of the pore size of UF and NF membranes.

Net driving pressure: Applied (pump) pressure minus the sum of all back pressures [osmotic pressure, pipe pressure losses, head (elevation) losses, and so on].

Normalization: The calculations that allow performance data to be compared on a uniform basis. For example, flux should be corrected to a temperature of 25°C (77°F) and a constant pressure.

Permeate: The stream which has passed through the membrane (also known as “product” or *filtrate*).

Recovery: That percentage of the feed flow rate that passes through the membrane and becomes the permeate stream.

Reject: See concentrate.

Rejection rate: When pressure is applied to water in contact with a membrane, water passes through the membrane and the solids that were in the water are rejected. The degree to which they are repelled is the rejection rate. The overall rejection rate depends on the average concentration of dissolved solids in the entire unit, and is calculated from the following equation:

$$\% \text{ Rejection} = 100 \left(1 - \frac{\text{permeate concentration}}{\text{average feed concentration}} \right)$$

Although the average feed concentration is not actually the arithmetic average of the feed and the concentrate, but rather the integrated average composition, the arithmetic average provides a good approximation.

Retentate: See concentrate.

Seawater: The concentrations of dissolved solids in oceans and seas vary around the world. Typically, a level of 35,000 ppm total dissolved solids is considered average.

Specific flux: Flux rate divided by net driving pressure.

Tangential flow filtration (TFF): Filtration in which liquid flows tangential to (along) the surface of the membrane. Synonymous with the term crossflow. The sweeping action of fluid helps to minimize gel layer formation and surface fouling. Contrast with “dead-end” filtration.

Total dissolved solids (TDS): Although actually a measurement of both dissolved salts and organics, TDS is commonly equated with dissolved salts only, and is often expressed as conductivity (mmho/cm or ms/cm).

Transmembrane pressure (TMP): The force which drives liquid flow through a crossflow membrane. In crossflow devices, the TMP is calculated as an average related to the pressures of the inlet, outlet, and permeate ports. The TMP can be expressed as

$$\text{TMP} = \left(\frac{P_f + P_c}{2} \right) - P_p$$

where

P_f is the feed pressure

P_c is the concentrate pressure

P_p is the permeate pressure

Waste: See concentrate.

13 Reverse Osmosis Membrane Fouling Control

Jane Kucera

CONTENTS

13.1	Introduction	248
13.2	Membrane Fouling	248
13.2.1	Common RO Membrane Foulants.....	249
13.2.1.1	Colloids	249
13.2.1.2	Organics	250
13.2.1.3	Metals.....	250
13.2.1.4	Hydrogen Sulfide	251
13.2.2	Performance of fouled membranes.....	251
13.2.3	Concentration Polarization	252
13.3	Membrane Scaling.....	254
13.3.1	Common Species that Scale RO Membranes	254
13.3.1.1	Calcium Carbonate	254
13.3.1.2	Sulfate-Based Scales.....	254
13.3.1.3	Silica	254
13.3.2	Performance of Scaled Membranes.....	255
13.4	Membrane Degradation	255
13.5	Identifying Fouled, Scaled, and Degraded Membranes	256
13.5.1	Water Quality.....	256
13.5.2	Membrane Operations	257
13.5.2.1	Data Collection	257
13.5.2.2	Data Normalization.....	258
13.5.2.3	Membrane Autopsy.....	259
13.6	Controlling Membrane Fouling, Scaling, and Degradation	260
13.6.1	Water Analysis.....	260
13.6.2	Operating Conditions.....	260
13.6.2.1	RO System Recovery	260
13.6.2.2	Temperature	260
13.6.2.3	Velocity	261
13.6.2.4	Flux	261
13.6.3	Membranes	261
13.6.4	Pretreatment.....	261
13.6.4.1	Mechanical Pretreatment.....	261
13.6.4.2	Chemical Pretreatment	263
13.6.5	Membrane Cleaning	264
13.7	Recent Advances in RO Pretreatment Hybrid Membrane Systems	266

13.8 Case Studies.....	266
13.8.1 Data Normalization	266
13.8.2 High-Efficiency Filtration as RO Pretreatment	267
13.9 Summary	269
References.....	269

13.1 INTRODUCTION

Reverse osmosis (RO) has become an important demineralization technique. Since the development of the first commercially viable RO membranes in the late 1950s, improvements in performance and durability have resulted in membranes that are more efficient and cost less to operate. For example, low-energy membranes have succeeded in delivering high-quality permeate and high productivity with low pressure requirements. This advance has allowed RO membranes to operate on low-temperature feed water sources that otherwise would require prohibitively high operating pressure.

Other advances in membrane technology have addressed membrane fouling. “Low-fouling” membranes have been created by modifying surface properties of membranes, such as the charge, the hydrophilicity, and the roughness by applying a coating over the membrane and/or by changing the membrane polymer. These membranes have been somewhat successful in showing evidence of reduced fouling, but they have not completely eliminated the potential, and some come with the disadvantage of lower permeability [1,2]. Despite these advances in performance, RO membranes still suffer from membrane fouling, scaling, and degradation. Figure 13.1 shows the most common foulants and scales that were identified on RO membranes after conducting 150 membrane autopsies [3]. Nearly half of the materials found on the membrane were organics, followed by inorganic silica (reactive and colloidal), metal oxides, and sulfate and carbonate scales. Additionally, it is safe to add that microbes, which feed off organics, have most likely contributed to the fouling of membranes that exhibited fouling with organics.

Pretreatment is used along with improved membrane performance to offset fouling, scaling, and degradation. The objectives of pretreatment are to prevent or minimize membrane fouling, scaling, and degradation. Figure 13.2 is a process flow diagram that shows some of the most common mechanical and chemical techniques used to pretreat RO feed water in an effort to minimize membrane fouling, scaling, and degradation. These techniques are discussed later in the chapter after detailed discussions regarding the nature of membrane fouling, scaling, and degradation.

13.2 MEMBRANE FOULING

Membrane fouling occurs when suspended solids, soluble organics (including true color), or microbial material is deposited on the surface of the membrane or on the feed-channel spacer. The collection of foulants on the membrane and feed-channel spacer is primarily a physical filtration phenomenon,

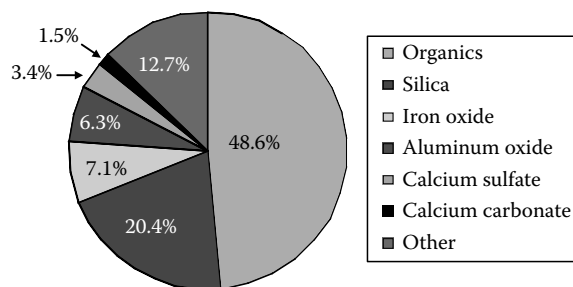


FIGURE 13.1 Common membrane foulants and scales identified in 150 membrane autopsies. (Courtesy of Engineering Society of Western Pennsylvania, Pittsburgh, PA.)

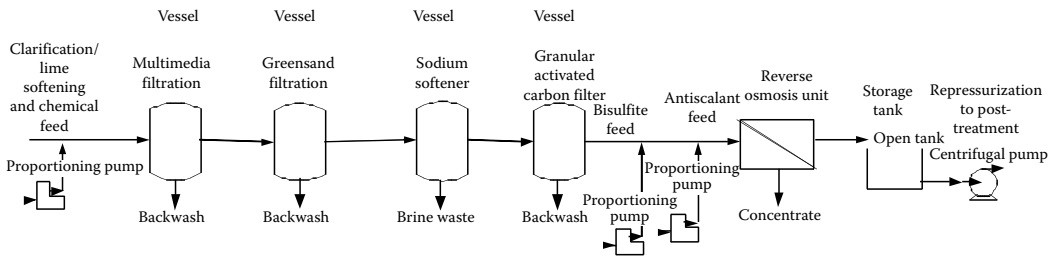


FIGURE 13.2 Common mechanical and chemical RO pretreatment techniques.

TABLE 13.1
Water Quality Guidelines to Minimize
Fouling of RO Membranes

Species	Measure	Guideline
Suspended solids	Turbidity	<1 NTU
Colloids (e.g., silicates)	SDI	<5
Microbes	Dip slides ^b	<1000 CFU/mL
Organics	TOC	<3 ppm
Color	Color units	<3 APHA
Metals (Fe, Mn, Al)	ppm	<0.05
Hydrogen sulfide	ppm	<0.10

Source: Kucera, J., *UltraPure Water*, 24, 18, 2007. With permission.

although other factors such as charge can affect the potential for a species to foul an RO membrane. As a result of this physical filtration, lead membranes in the first stage of an RO system are generally the membranes most affected by fouling. Biological fouling and organics are two exceptions as they both can be found in all stages of RO. Original microbial colonies can establish themselves anywhere in the membrane system where conditions favor growth. Satellite colonies then break off from the original colonies and further distribute microbes throughout the membrane system. Soluble organics will obviously deposit at any place in the system that they are swept to on the surface of the membrane.

Table 13.1 lists the common species that foul RO membranes [4]. Table 13.1 also lists the generally accepted feed water quality guidelines established to minimize fouling of membranes with these species. As the table shows, there are a variety of species that can foul an RO membrane.

13.2.1 COMMON RO MEMBRANE FOULANTS

13.2.1.1 Colloids

Colloids, such as alumino- and iron-silicates, are suspended solids that are directly filtered out by the lead RO membranes. When Al^{3+} and Fe^{3+} coexist with silica, alumino and iron silicates will form even when the concentration of silica is less than saturated [5].

Silt density index: The silt density index (SDI), along with turbidity, is used to measure the potential for fouling with colloids and other suspended solids. The advantage of SDI over turbidity alone is that SDI can be used on relatively low turbidity (<1 NTU) water, and as such, is a finer measure of suspended solids and colloids in water. The SDI test itself involves measuring the rate of plugging of a 0.45 micron filter. The test must be conducted online using RO feed water,

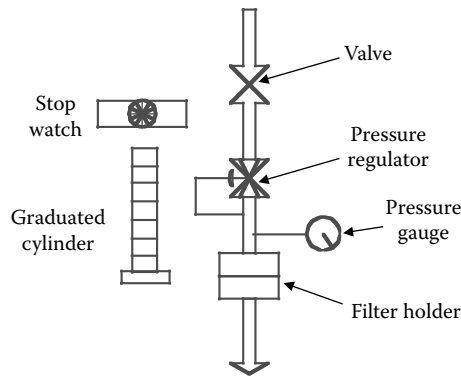


FIGURE 13.3 SDI test equipment.

with a slipstream of feed water taken as close to the RO membranes as possible (typically before or after the cartridge filters). Figure 13.3 shows the equipment required to run an SDI test. The procedures are as follows:

1. Open the ball valve and set the pressure to 30 psig.
2. Immediately start recording the time it takes to collect a 500 mL sample of water through the filter. Record this time as t_i .
3. Continue to run the feed water through the filter for a total of 15 min. Adjust the pressure to 30 psig as needed.
4. At the end of 15 min, record the time it takes to collect another 500 mL sample through the filter. Record this time as t_f .
5. Calculate the SDI_{15} using the following equation:

$$SDI_{15} = [(1 - (t_i/t_f)) \times 100] / 15 \quad (13.1)$$

The lower the SDI, the lower the potential for fouling an RO membrane. As part of their warranty, membrane manufacturers include conditions that the feed water SDI be <5 . (Note that SDI is a dimensionless number.)

13.2.1.2 Organics

Higher-molecular weight, straight-chained organics, such as humic and fulvic acids, are common foulants found in surface waters. These organics typically “blind” off sections of membrane so that water cannot permeate. Furthermore, organics provide nutrients that sustain microbial populations.

True color: True color can adsorb onto the polymer chain thereby irreversibly fouling an RO membrane.

13.2.1.3 Metals

Elemental metals such as iron and manganese can oxidize from soluble to insoluble forms within an RO membrane and precipitate on the membrane, thereby fouling it as a suspended solid. Oxidation is exacerbated by air leaking into the RO system, for example, through feed pumps. Aluminum is a problem when alum is used to pretreat RO water. Alum is typically overfed and can carry over to post-precipitate and foul a membrane as a suspended solid.

13.2.1.4 Hydrogen Sulfide

Hydrogen sulfide can oxidize and revert back to elemental species, in this case sulfur, a very sticky substance that once deposited on the membrane is virtually impossible to remove even with cleaning [6]. Oxidation is exacerbated by air leaking into the RO system, for example, through feed pumps. Since hydrogen sulfide is a gas, it readily permeates an RO membrane and can oxidize on the permeate side of the membrane. Fouling the backside of the membrane may result in the same performance problems as front-side fouling.

13.2.2 PERFORMANCE OF FOULED MEMBRANES

A fouled membrane exhibits two key performance problems: higher than normal operating pressure and higher than normal pressure drop. As the surface of the membrane becomes fouled with suspended solids, these solids form essentially another layer through which the feed water must penetrate to become permeate (see Figures 13.4 and 13.5). Higher feed water pressure is required to force water through this layer of foulants. This higher pressure naturally results in a higher drop in pressure. Additionally, the foulant layer, as well as the collection of foulants on the feed-channel spacer, increases the resistance to the cross-flow of feed water across the membrane. This increase in resistance is measured in terms of an additional drop in pressure.



FIGURE 13.4 Fouled membrane.



FIGURE 13.5 Fouled membrane. (From Kucera, J., *Ultrapure Water*, 22, 37, 2005. With permission.)

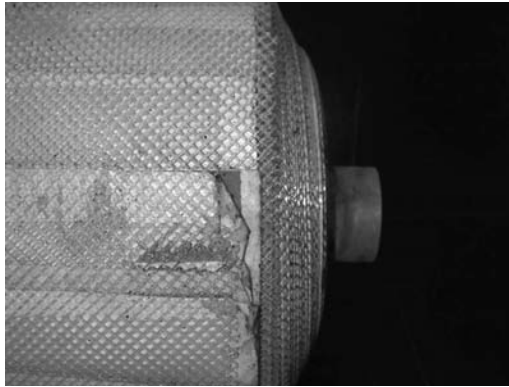


FIGURE 13.6 Telescoped membrane module. (From Kucera, J., *Ultrapure Water*, 22, 37, 2005. With permission.)

A high drop in pressure results in lower permeate productivity and can, together with high operating pressure, result in physical damage to the membranes. Lower productivity is particularly critical at lower feed water temperatures where higher pressure is naturally required to maintain productivity (every 1°C drop in feed water temperature leads to a 3% drop in productivity) [7]. If the pumping capacity of the RO feed water pump is to compensate for membrane fouling, there may be little or no capacity available when the feed water temperature decreases. Furthermore, there will come a point in time when the increase in pressure caused by fouling exceeds the pump capacity and RO will no longer maintain productivity, regardless of the feed water temperature. As the operating pressure and pressure drop increase, the drop in pressure is translated to an axial force on the membrane module. This physical force can crack the module's fiberglass outer shell and "telescope" the membranes and spacers to the point where the membranes fail, and feed water mixes with permeate (see Figure 13.6).

13.2.3 CONCENTRATION POLARIZATION

Deposition is a function of the feed water concentration of suspended solids and is exacerbated under certain operating conditions, such as high-operating flux and low cross-flow velocity. These two conditions result in a phenomenon called concentration polarization, a boundary layer where the concentration of solids is higher at the membrane surface than in the bulk solution. In the case of high operating flux, water is removed through the membrane at a quicker pace leaving more solid-laden feed water behind in the boundary layer. In the case of low cross-flow velocity, the thickness of the concentration polarization boundary layer expands. Because the concentration polarization boundary layer is characterized as supporting convective flow to the membrane, but only diffusional flow back from the membrane, solids within the boundary layer have more time to settle down on the membrane itself [8]. The concentration at the membrane surface becomes greater than the concentration in the bulk feed water. Figure 13.7 depicts the concentration polarization phenomenon.

Table 13.2 lists the recommended maximum feed water cross-flow velocities as a function of feed water quality to minimize fouling of RO membranes [9]. The higher the velocity, the faster the membrane becomes exposed to feed water contaminants, and the quicker the membrane will foul. Table 13.3 lists the recommended average flux as a function of feed water quality to minimize fouling with suspended solids [9]. Higher flux means that more water with contaminants is being forced to the surface of the membrane, and as more water goes through the membrane, solids are left behind at a faster rate. As these two tables show, higher quality feed water allows for operation at more aggressive (e.g., higher permeate flux and higher feed water cross-flow velocity) conditions. In most cases, however, RO feed water quality is not ideal and operating in the lower end of the ranges listed in Table 13.3 is recommended to reduce fouling potential and to reduce the maintenance of the RO system.

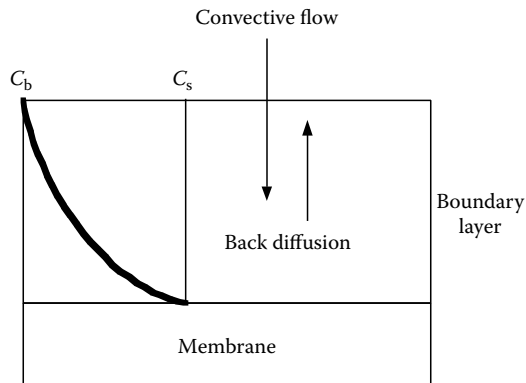


FIGURE 13.7 Concentration polarization.

TABLE 13.2
Maximum Feed Flow Rate as a Function of Feed Water Quality for 365 and 400 ft² Membrane Modules

Feed Water Quality	365 ft ² Membrane Module (gpm)	400 ft ² Membrane Module (gpm)
RO permeate	65	75
Well water	65	75
Surface water, SDI < 3	63	73
Surface water, SDI < 5	58	67
Municipal wastewater	52	61

Source: FilmTec Reverse osmosis membrane technical manual, Dow Liquid Separations, Form No. 609-00071-0705, 83, 2007. With permission.

TABLE 13.3
Recommended Average Flux as a Function of Feed Water Quality to Minimize Fouling with Suspended Solids

Feed Water Quality	Recommended Flux (gfd) ^a
RO permeate	21–25
Well water	16–20
Surface water, SDI < 3	13–17
Surface water, SDI < 5	12–16
Municipal wastewater, MF pretreatment	10–14
Municipal wastewater, conv. pretreatment	8–12

Source: FilmTec Reverse osmosis membrane technical manual, Dow Liquid Separations, Form No. 609-00071-0705, 83, 2007. With permission.

^a Gallons per square foot per day.

13.3 MEMBRANE SCALING

Membrane scaling involves the precipitation of saturated salts onto the membrane surface and feed-channel spacer material. Precipitation is a function of the feed water concentration and is controlled by the recovery of the RO system. As the percentage of recovery of the RO system increases, the feed water becomes more concentrated; in many cases meeting or exceeding the saturation limits for several species, which results in the precipitation of these species. The formation of scale on an RO membrane is a concentration phenomenon, and therefore occurs at the last stage in the RO system where the concentration of salts is the highest. To determine the potential for scaling, one needs to compare the ion product of the salt in question (in the concentrate stream) with the solubility product for the salt under conditions in the concentrate. In general, scaling will occur when the ion product is greater than the solubility product. For sulfate-based scales, scaling can occur when the ion product is greater than 80% of the solubility product.

Table 13.4 lists the common species that scale RO membranes [4]. Table 13.4 also lists generally accepted feed water quality guidelines established to minimize scaling with these species. As the table shows, there are a variety of species that can scale a membrane.

13.3.1 COMMON SPECIES THAT SCALE RO MEMBRANES

13.3.1.1 Calcium Carbonate

Calcium carbonate is perhaps the most common scale that affects RO membranes. The potential for forming this scale is typically measured using the Langelier saturation index (LSI). A positive index favors the formation of calcium carbonate scale.

13.3.1.2 Sulfate-Based Scales

Sulfate-based scales are scales of calcium and trace metals that are typically sparingly soluble. It should be noted that sulfuric acid typically used to drop the LSI for calcium carbonate scale will exacerbate sulfate-based scales of calcium, barium, and strontium, and this option should be carefully evaluated if these cations are present in the RO feed water.

13.3.1.3 Silica

The formation of silica scale is a function of pH and temperature; silica is most soluble at high temperature and at either low (<6) or high (>9) pH levels. Note, however, that as the pH level exceeds neutral, silica is present in the form of silicate anion (SiO_3^{2-})_n, which readily reacts with metals such

TABLE 13.4
Water Quality Guidelines to Minimize
Scaling of RO Membranes

Species	Measure	Guideline
Calcium carbonate	LSI	<0 ^a
Sulfate-based compounds (calcium, barium, strontium)	ppm	<0.05 ^b
Silica	ppm	<200 ^c

Source: Kucera, J., *UltraPure Water*, 24, 18, 2007. With permission.

^a Can be up to 1.5 with antiscalant.

^b For barium and strontium.

^c Measured in the RO concentrate stream—varies with temperature and pH.



FIGURE 13.8 Scaled spiral wound membrane module feed spacer.

as aluminum and iron to form insoluble silicates [5]. Furthermore, it has been shown that silica can precipitate as scale at concentrations below saturation in the presence of aluminum or iron [10].

13.3.2 PERFORMANCE OF SCALED MEMBRANES

A scaled membrane exhibits two key performance problems: higher than normal operating pressure and low salt rejection. Higher feed pressure is required to force water through a layer of scale, in a manner similar to that described for fouled membranes (see Figure 13.8). The interesting feature of scaled membranes is that the apparent rejection of the membrane decreases. This is a result of concentration polarization, in that the concentration of the scaled species is higher at the membrane surface than in the bulk solution. Since the membrane rejection is based on the concentration that the membrane actually “sees,” the rejection may still be 98%, but 98% rejection of a higher concentration than compared with the bulk concentration results in more salt passing into the permeate. Hence, the rejection appears to go down. The increase in permeate concentration is real and it can have many repercussions for downstream processing. For example, polishing of RO permeate with a mixed-bed ion exchange will require more frequent regeneration of the ion exchange units, and boilers operating on RO permeate will operate at lower cycles of concentration.

As with membrane fouling, concentration polarization plays a role in precipitation. As the recovery of the RO system increases, the concentration difference between that at the membrane surface and that in the bulk solution becomes greater. Diffusion within the boundary layer enhances the potential for forming scale. Lower cross-flow velocity can further enhance the scaling of membranes by affecting the thickness of the boundary layer. Table 13.5 lists the minimum concentrate cross-flow velocities as a function of feed water quality [9].

13.4 MEMBRANE DEGRADATION

Membrane degradation occurs when the membrane is exposed to water conditions that damage the membrane. Hydrolysis and oxidation are the two major causes of membrane failure. While hydrolysis and oxidation can affect all membranes in a system, typically, the lead membranes in the first stage are most affected by oxidation. This is because the lead membranes are exposed to the oxidizer first, and as the oxidizer is itself reduced, it no longer oxidizes the trailing membranes. However, if given enough time, the trailing membranes will be exposed and degraded by the oxidizer.

Table 13.6 lists the degradation conditions for RO membranes [4]. Note that temperature is included in this table. However, temperature effects are limited to the materials of construction for the membrane module rather than related to the degradation of the membrane polymer itself. A degraded membrane exhibits two key performance problems: higher than normal water flux (after a

TABLE 13.5
Water Quality Guidelines to Minimize
Scaling of RO Membranes

Species	Measure	Guideline
Calcium carbonate	LSI	<0 ^b
Silica (reactive)	ppm ^a	200 ^b
Trace metals (Ba, Sr)	ppm	<0.05
Other calcium-based scales (e.g., SO ₄ , F ₂)	ppm	None established

Source: Kucera, J., *UltraPure Water*, 24, 18, 2007. With permission.

^a Measured in RO concentrate stream.

^b Limit can change depending on temperature, pH, and anti-scalant used.

TABLE 13.6
Minimum Concentrate Flow Rate as a Function
of Feed Water Quality for 365 and 400 ft² Membrane
Modules

Feed Water Quality	365 ft ² Membrane Module (gpm)	400 ft ² Membrane Module (gpm)
RO permeate	10	10
Well water	13	13
Surface water, SDI < 3	13	13
Surface water, SDI < 5	15	15
Municipal wastewater, MF	16	18
Municipal wastewater, conv.	18	20

Source: FilmTec Reverse osmosis membrane technical manual, Dow Liquid Separations, Form No. 609-00071-0705, 83, 2007. With permission.

Note: MF, microfiltration pretreatment; conv., conventional pretreatment.

short initial period of reduced flux, in the case of oxidation) and higher than normal salt passage. The degraded membrane essentially springs a leak(s), which leads to the higher water and salt passage.

13.5 IDENTIFYING FOULED, SCALED, AND DEGRADED MEMBRANES

There are several techniques that can be used to help identify when membranes are fouled, scaled, or degraded. These techniques are discussed in detail.

13.5.1 WATER QUALITY

A comprehensive understanding of RO feed water quality is key to identifying potential foulants, scale formers, and agents of degradation in RO feed water. The water analysis can be scanned for species in Tables 13.1, 13.4, and 13.6 that are known to foul, scale, or degrade RO membranes, respectively. Table 13.7 lists the must-have species when requesting a water analysis for potential foulants and scale.

TABLE 13.7
Species That Should Be Included
in a Comprehensive Water Analysis

Species	Problem
pH	Scaling
Conductivity	N/A
Alkalinity	Scaling
Metals—Ca, Mg, Na, K	Scaling
Trace Metals—Al, Ba, Sr, Fe, Mn	Scaling, fouling
Fluoride	Scaling
Temperature	Scaling
TOC	Fouling
True color	Fouling
Silt density index	Fouling
Turbidity	Fouling
Anions—Cl, SO ₄ , NO ₃	Scaling
Phosphate	Scaling
Silica	Fouling, scaling
Hydrogen sulfide	Fouling

Projections can be used to determine the potential for scaling an RO membrane within a particular system. Projections can take the form of system projections using software provided by the membrane manufacturers (e.g., FilmTec™'s ROSA projection program—FilmTec is a trademark of Dow Chemical Company, Midland, Michigan). These programs project the potential for scaling based on the specific feed water analysis for the application in question, and the specific system design and operating conditions. There are also chemical projection programs that will project potential for scaling given a water analysis and the recovery of the RO system (e.g., Nalco's RO-12 projection program).

To determine whether a membrane has already been scaled or fouled, a mass balance should be conducted around the membrane. Feed, reject, and permeate samples should be taken and each species of interest should be analyzed to determine whether some of this species has deposited on the membrane. If the mass out through the reject plus the mass out through the permeate is less than the mass in through the feed, the remainder has most likely deposited on the membrane as either scale or fouling material. The source of the feed water also plays a role in determining the potential for membrane fouling, scaling, and degradation. For example, surface water may be more likely to foul with suspended solids, microbes, and organics than well water. Well water, on the other hand, may be more likely to scale a membrane than surface water.

13.5.2 MEMBRANE OPERATIONS

13.5.2.1 Data Collection

Operation of the membrane system can many times reveal the condition of the membranes. To that end, proper collection of data and correct interpretation is a key to understanding the condition of the membranes. Table 13.8 lists the essential data points necessary for determining the condition of membranes in an RO system [11]. Data are collected from the influent to the first stage of the RO unit and from the effluent to the last stage of the unit. Data should also be collected between the stages of the RO unit. Inter-stage data can be used to clarify whether fouling is occurring in the first stage or scaling is occurring in the last stage. However, many manufacturers of RO equipment fail to include the necessary probes to conduct complete inter-stage data collection. Because a loss of

TABLE 13.8
Essential RO System Monitoring Variables
and Locations

	Feed	Interstage	Product	Reject
Pressure	X	X	X	X
Flow rate	X	X	X	
Conductivity	X	X	X	X
Temperature	X			
pH	X			X
Chlorine, free	X			

Source: Kucera-Gienger, J., Successful application of reverse osmosis in the chemical process industries, Technical Paper, presented at the 1995 AIChE Summer National Meeting, Boston, MA, August 1, 1995. With permission.

performance due to fouling can exhibit symptoms similar to scaling, it can be difficult to distinguish between the two when interstage data is not available. Under these circumstances, operators will need to rely upon the other techniques, such as water analysis, mass balances, and projections to distinguish between membrane scaling and fouling.

13.5.2.2 Data Normalization

Once collected, the best way to interpret data is to normalize it. Normalized data are the only true measures of the condition of the membranes, be they fouled or scaled (or even degraded). Normalized product flow rate and normalized salt passage, along with pressure drop (feed to concentrate side) are the three major performance variables typically tracked to evaluate the true performance of RO membranes. The normalized product flow rate is used to track membrane fouling, scaling, and degradation; normalized salt passage is used to track membrane scaling and degradation; and pressure drop is used to track membrane fouling and membrane scaling.

Normalization of data is necessary because performance parameters, such as product flow rate (expressed in gpm) and salt passage (expressed as a percent), are functions of several variables that change with time, thereby making it impossible to compare the actual RO performance at one point in time to that at another point in time. For example, RO product flow rate is a function of the following variables: water temperature, dissolved solids concentration (as osmotic pressure), operating pressure, and the degree of membrane fouling, membrane scaling, and membrane degradation. If there is a difference in the product flow rate from one point in time to another point in time without normalization, it would be impossible to determine if the change is due to membrane fouling, scaling, or degradation or if it is due to a change in the feed water temperature (the flow rate increases by 3% for every 1°C increase in feed water temperature) or the operating pressure (there is a direct relationship between product flow rate and applied pressure) [12]. To eliminate the influences of temperature, concentration, and pressure on membrane performance, actual operating data is standardized or “normalized” to a given set of operating conditions (temperature, pressure, and osmotic pressure at system start-up) so that any changes in “normalized” performance would be due only to changes in membrane fouling, membrane scaling, and membrane degradation.

Figure 13.9 shows normalized product flow as functions of time and the degree of membrane fouling, membrane scaling, and membrane degradation [13]. As the graph shows, a negative slope indicates that less water is passing through the membrane than did under initial conditions, thus indicating that the membrane is fouling and/or scaling. A positive slope indicates that more water is

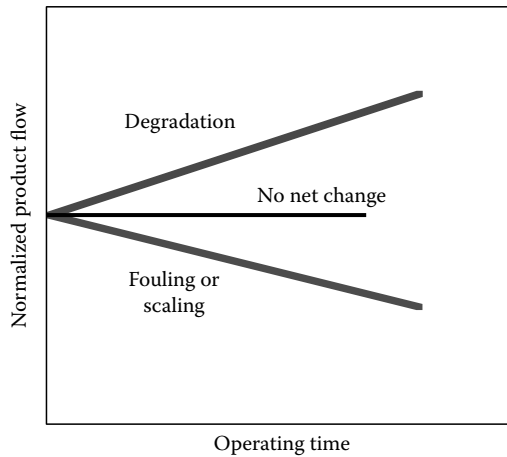


FIGURE 13.9 Normalized product flow as functions of time and degree of membrane fouling, scaling, and degradation. (Courtesy of Hydrocarbon Processing, Houston, TX.)

passing through the membrane than under initial conditions, and is indicative of a membrane that is degraded. A neutral slope indicates either nothing is happening (no scaling, fouling, or degradation) or that any fouling or scaling is being offset by membrane degradation.

13.5.2.3 Membrane Autopsy

Membrane autopsy, in most cases, offers the definitive answer to what is causing a loss in membrane performance. Because an autopsy is a destructive test, it should be considered as a last resort when other means of investigation have failed to identify the reasons for loss in performance.

The membrane(s) selected for autopsy should be based on a suspicion of what may be causing performance failure. If membrane fouling with suspended solids is suspected, the lead membrane(s) should be selected; whereas if scaling is suspected, the last membrane module in the system should be selected. Membranes selected for autopsy should be sealed in a plastic bag (preferably the bag the membrane was shipped in) and sent in for testing within 48 h of removal from the RO skid. The membrane should not be cleaned prior to removal from the skid. No membrane preservatives are needed for shipping.

Several tests are conducted on the membrane to determine the cause of failure. These tests include visual inspection, a pressure dye test, the Fujiwara test, spectroscopy, and microbial analysis.

13.5.2.3.1 Visual Inspection

The membrane module is visually inspected upon arrival in the autopsy facility. Cracks in the outer fiberglass skin of the module are investigated. Also, the feed and concentrate ends of the module are inspected for the accumulation of debris.

13.5.2.3.2 Pressure Dye Test

The pressure dye test is used to determine whether membrane damage by exposure to oxidizing chemicals or physical attack has occurred. After the autopsy, a sheet of membrane is placed in autopsy flat-sheet test rig. The feed side of that sheet of membrane is exposed to a solution of methylene blue. Areas of damage show dye soaking through the membrane to the permeate side.

13.5.2.3.3 Fujiwara Test

This test determines the exposure of a membrane to halogens by measuring the concentration of halogenated organics in a membrane sample. This test requires a small piece of suspect membrane be placed in a test tube and be exposed to sodium hydroxide and pyridine. The tube is then placed in a hot water bath for about 30 s. A positive test for halogenated organics is indicated by the appearance of a red or pink color in the pyridine layer in the tube.

13.5.2.3.4 Spectroscopy

Several spectroscopy tests are used to identify the nature of species that have fouled or scaled a membrane. A scanning electron microscopy (SEM), along with stereo or standard light microscopes, is used to determine the morphology of deposits on the membrane. An energy dispersive x-ray fluorescence (EDXRF) spectroscopy is used to determine which chemicals are in the deposit on the membrane. Inductively coupled plasma emission (ICP) spectroscopy and electron spectroscopy for chemical analysis (ESCA) are used to identify impurities that have been organically bound to the membrane surface.

13.5.2.3.5 Microbial Analysis

Slimy deposits removed from the membrane are analyzed for the type of microorganisms present. The results of this examination could lead to a chemical program capable of minimizing microbial fouling of membranes in the given application.

13.5.2.3.6 Membrane Cleaning

Membrane cleaning studies can also be conducted on sections of autopsied membranes to not only help determine what has led to the membrane failure, but also to develop a cleaning protocol to successfully clean the membranes out in the field.

13.6 CONTROLLING MEMBRANE FOULING, SCALING, AND DEGRADATION

Once the cause(s) for membrane loss of performance has been identified, it becomes necessary to address the set of circumstances that have led to this condition with the intent of minimizing the potential for continued membrane fouling and/or scaling. If a new installation is being considered, it is prudent to investigate the potential for fouling and scaling prior to deciding on the final system design.

13.6.1 WATER ANALYSIS

The first place to begin investigating the control of membrane fouling and scaling is the water analysis. A comprehensive analysis, including turbidity and silt density index is required to develop a full picture of potential foulants and scale [14]. Table 13.7 lists the species that should be included in the comprehensive water analysis. Once a water analysis has been obtained, it should be compared with the generally accepted guidelines for RO systems, as shown in Tables 13.1 and 13.4.

13.6.2 OPERATING CONDITIONS

The conditions under which the RO system is operated can have a significant influence on the degree of membrane fouling and scaling that may occur. For example, the recovery of the RO has a direct impact on the degree of scaling that can be expected.

13.6.2.1 RO System Recovery

Recovery defines how much water is removed from the feed stream to become permeate or product. As more water is removed or recovered, the remaining water becomes more concentrated in dissolved solids. Once the ion product (IP) of a salt equals its solubility constant, K_{sp} , the salt in question is ready to form scale. Note that for some species, such as sulfate salts, scale will form when the $IP > 0.8K_{sp}$.

13.6.2.2 Temperature

The temperature has an effect on the solubility of several species, including silica and calcium carbonate. While the temperature of an RO system is rarely adjusted to accommodate calcium carbonate, it is often increased to allow for higher recovery when a higher concentration of silica is present in the feed water. The solubility of silica is about 95 ppm at 10°C, while the solubility is about 160 ppm at 45°C. Continuous operation of up to 45°C at a neutral pH is tolerable for most membranes (check the membrane specifications for temperature/pH tolerance for specific membrane modules).

13.6.2.3 Velocity

As previously discussed, the feed water and concentrate velocities have significant effects of the fouling potential for a given feed water composition (see Tables 13.2 and 13.5 for the recommended limits). A higher feed water velocity forces more water to the membrane faster, thereby increasing the rate of fouling. A lower concentrate velocity thickens the concentration polarization boundary layer, thereby increasing the potential for fouling the membrane.

13.6.2.4 Flux

Membrane flux has a great influence on the degree of membrane fouling and scaling. Higher flux means that more water (and solids) are being forced to the membrane more rapidly, as well as more water being removed from the feed side of the membrane more rapidly. This results in more solids being “trapped” in the concentration polarization boundary layer, increasing the potential for fouling and scaling of the membrane. See Table 13.3 for the recommended fluxes as a function of feed water quality.

13.6.3 MEMBRANES

Low-fouling membranes have been available only since the mid-1990s. There are three primary techniques used to create low-fouling membranes: (a) modified membrane surface characteristics [15], (b) coating of the membrane [16], and (c) changes in the membrane chemistry itself [17].

The objectives are to change the charge, roughness, and hydrophilicity of the membrane surface. Polyamide membranes, perhaps the most common type of RO membrane used commercially, are known for negatively charged surfaces and rough surface morphology. The negative surface charge attracts positively charged materials, commonly cationic coagulants used to aid in the removal of suspended solids from RO feed water. An overfeed of cationic coagulant can lead to irreversible fouling of the negatively charged polyamide membranes. Furthermore, the rough surface makes it easy for the membrane to trap materials such as microbes, suspended solids, and long-chained dissolved organics, resulting in a fouled membrane. While low-fouling membranes have demonstrated efficiency in minimizing membrane fouling, evidence has shown that they can still foul [3]. Hence, this type of RO membrane should be used in conjunction with good design and operating methods as well as with appropriate pretreatment.

13.6.4 PRETREATMENT

By far the most common way to minimize membrane fouling and scaling involves the proper pretreatment of RO feed water, including both chemical and mechanical treatments. While the array of unit operations and chemical treatment is vast, the most common treatments are described herein.

13.6.4.1 Mechanical Pretreatment

13.6.4.1.1 Depth Filters

Depth filters, also called multimedia filters, are used to remove suspended solids, turbidity, and species contributing to SDI from RO feed water. Multimedia filters contain (from top to bottom) anthracite, sand, and garnet with each medium being of a different size. Solids are removed from the water using a sieving action; the largest particles are removed at the surface and the smaller particles are removed at the bottom of the filter bed. Multimedia filters should be operated at 5 gpm/ft² for optimum performance prior to on RO system.

Polymer coagulants are sometimes used prior to the filter to help with “bridging” and removal of smaller particles. Dosages of polymers are typically less than 1 ppm. Increasing the dosage and watching SDI of the filter effluent can determine the optimum dosage. After plotting the SDI as a function of the polymer dose, there will be a minimum in SDI at the optimum dosage of the polymer.

13.6.4.1.2 Carbon Filters

Carbon filters are used to remove organics (as TOC) and free chlorine from RO feed water. Bituminous carbon is used for industrial RO pretreatment applications. Organics are adsorbed on carbon particles for removal from water. Removal of chlorine involves an oxidation/reduction reaction with the carbon particles, where a transfer of electrons occurs from the activated carbon to the chlorine (the carbon acts as a reducing agent). Design flow rates should be 1 gpm/ft³ for TOC removal and 2 gpm/ft³ for chlorine removal when used for RO pretreatment. The expected TOC removal efficiency ranges from 25% to 80%, depending on the nature of the organics. Chlorine can be removed to less than 0.05 ppm. Activated carbon can also be used to remove chloramines in the same manner as chlorine, however, the contact time must be greater than for chlorine removal. For a 12 × 40 mesh carbon, contact times up to 30 min are required. Catalytic activated carbon can also be used to reduce the contact time for chloramine removal.

Care should be used when applying activated carbon for chlorine removal only. Because the carbon removes organics, there are plenty of nutrients for microbes to grow, and so carbon filters are known to harbor microbes [18]. Microbes travel with carbon fines from the filter bed into the downstream piping and into the RO membrane modules, thereby inoculating all the piping and the membranes. Other means of dechlorination, such as a chemical feed of metabisulfite, should be considered when organic removal is not a priority.

13.6.4.1.3 Iron-Removal Filters

Iron-removal filters such as manganese greensand filters are used to remove soluble iron and manganese (and some hydrogen sulfide) from RO feed water. The metals are oxidized to insoluble species by the media and then filtered out by mechanical filtration. Manganese greensand is simply glauconite particles coated with manganese oxide and dioxide. This coating acts as a catalyst in the oxidation of the iron and manganese. An oxidizer, such as chlorine or potassium permanganate is required. If iron alone is present, feed chlorine at a rate of 1 ppm per ppm of iron. If manganese is present, potassium permanganate is required at a dosage rate of 1 ppm per ppm of iron plus 2 ppm per ppm of manganese. Manganese greensand will remove hydrogen sulfide from RO feed water, but as the compound oxidizes into elemental sulfur, which is a sticky substance, it will coat and deactivate the media. The recommended design flow rate is 5 gpm/ft². Better iron removal media (BIRM) filters are also used to remove iron and manganese from RO feed water. BIRM is a man-made material consisting of granular zeolite with an inert center and a fine coating of manganese dioxide on the exterior. BIRM requires the presence of an oxidizer, such as chlorine or potassium permanganate. There are a variety of other iron-removal media available that rely on a form of manganese dioxide.

13.6.4.1.4 Sodium Softeners

Sodium softeners are designed to remove hardness and trace cations, including iron, from RO feed water. Calcium, magnesium, and other cations are removed via “exchange” with sodium sites on sodium-form cation resin. For every monovalent cation exchanged, one part of sodium is added to the softener effluent; for every divalent cation exchanged, 2 parts of sodium are added. Thus, the overall total dissolved solids (TDS) does not change through a softener, but the hardness can be reduced to a few ppm or less (depending on the feed water quality, the amount of regenerate used, and whether the bed is regenerated concurrently or countercurrently). The exchange process is reversible. Brine is used to regenerate the resin. Typically, 6, 10, or 15 lb of salt per cubic foot of resin is used to regenerate the beds. The resin capacity is about 20,000, 25,000, and 30,000 grains per cubic foot for the 6, 10, and 15 lb regenerate used, respectively. The affinity for various cations is shown in Figure 13.10. As the figure shows, if sodium were to have an affinity of 1, softener resin has the highest affinity for barium at 5.8 relative to sodium.

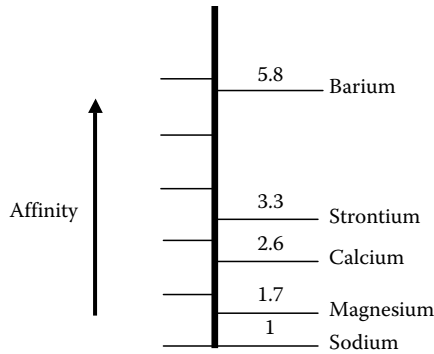


FIGURE 13.10 Sodium-form cation resin affinity for various cations.

13.6.4.2 Chemical Pretreatment

13.6.4.2.1 Lime

Lime is used in a lime softening process to reduce hardness, alkalinity, silica, and other constituents from RO feed water. Lime and sometimes soda ash together with lime are used to precipitate out insoluble species containing hardness and natural alkalinity. Specifically, noncarbonated hardness is removed chemically with lime and soda ash, along with coagulant and flocculent. Temperature also plays a role in the efficiency of the lime softening process. Cold lime softening is conducted at ambient temperatures, warm lime softening is conducted at 120°F–140°F, and hot process softening is conducted at 220°F–240°F. Table 13.9 shows the projected effluent from the lime softening process as a function of temperature for cold and hot processes [19].

Silica is very well removed using the hot process softener by adsorption onto the magnesium hydroxide precipitate. If there is not enough magnesium hydroxide, magnesium compounds such as magnesium chloride, magnesium oxide, magnesium sulfate, magnesium carbonate, or dolomitic lime can be used.

13.6.4.2.2 Antiscalant

Antiscalants are used to prevent scaling of RO membranes with species such as calcium carbonate, barium sulfate, and silica. Antiscalants work by crystal inhibition or by surface modification of crystals. Crystal inhibition antiscalants prevent the formation of crystals larger than the critical

TABLE 13.9
Typical Lime-Soda Softener Effluent Analysis
for Cold and Hot Processes

CaCO ₃ (ppm)	Raw Water	Cold Lime-Soda	Hot Lime-Soda
		Softening	Softening
Total hardness	250	81	20
Calcium hardness	150	35	15
Magnesium hardness	100	46	5
P alkalinity	0	37	23
M alkalinity	150	55	40
Silica (ppm as ion)	20	18	1–2
pH	7.5	10.6	10.5

Source: *Betz Handbook of Industrial Water Conditioning*, 9th edn., Betz Publisher, Philadelphia, PA, 1991, p. 41. With permission.

size necessary for nucleation. Modification of the surface of crystals that have already grown causes the crystal to distort as it continues to grow, thereby slowing or even stopping further growth of the crystal.

Antiscalants are composed of polyphosphates, phosphonate, and polymers such as polyacrylic acid (PAA), polymethacrylic acid (PMAA), and polymaleic acid (PMA) [20]. Polyphosphates prevent the precipitation of calcium carbonate scale using what is known as “threshold treatment.” Threshold treatment involves scale inhibition at substoichiometric ratios where the inhibitor adsorbs onto the crystal, thereby interfering with future crystal growth. Phosphonates are also a good inhibitor for calcium carbonate, barium sulfate, and calcium fluoride. HEDP or 1-hydroxyethylidene-1,1-diphosphonic acid is a common phosphonate used today for threshold treatment. However, there is a potential for calcium phosphonate precipitation. Finally, PAA is recognized as a good antiscalant for calcium carbonate, calcium sulfate, barium sulfate, and calcium fluoride scale control.

Good control of the addition of antiscalant is critical to the success of this scale-prevention technique. Feeding too much antiscalant can result in fouling of the membrane, particularly if there is an overfeed of coagulant to the RO. Overfeed also increases the cost of operations, due to the wastage of product and the need to deal with any fouling issues that may arise. An underfeed of antiscalant results in scaling of the membrane and contributes to higher operating costs because of the need to clean the membrane more often to remove the scale (if it indeed can be removed). Most RO systems rely on the feed flow rate to adjust the feed rate of the antiscalant. This is an inherently inexact technique for feeding antiscalant. The Trasar[®] technology was developed by a chemical supplier in which a fluoro-marker is bound to the antiscalant, making it possible to actually measure the amount of antiscalant being feed. This allows for greater precision in the feeding of antiscalants.

13.6.4.2.3 Acid/Caustic

Acid and caustic can be used to adjust the pH of RO feed water in an effort to make a given species more soluble and less likely to scale. Acid is used to lower the pH level making calcium carbonate more soluble. Hydrochloric acid should be used preferably over sulfuric acid, as the latter will result in enhanced sulfate-based scale. Caustic has been traditionally added to increase the solubility of silica. The HERO[™] (high efficiency RO) process relies upon high pH levels together with weak-acid cation pretreatment to treat water with high concentrations of silica. Whereas the typical ambient saturation of silica at pH 6.5–7.5 is 120 ppm, the HERO process allows for concentrations as high as 820 ppm at a pH level of 11.0 [21,22].

13.6.4.2.4 Bisulfite

Sodium bisulfite is a common reducing agent typically used to reduce free chlorine used for biological control in RO feed water into hydrochloric acid. About 1.8 ppm of sodium bisulfite is required for each ppm of free chlorine. Typically, the sodium bisulfite is obtained by using sodium metabisulfite. If sodium metabisulfite is used, a stoichiometric rate of 1.34 ppm is required for each ppm of free chlorine. In practice, however, 3 ppm of metabisulfite is fed per ppm of free chlorine. The product used should be feed-grade quality and NOT cobalt-activated (cobalt catalyzes the oxidation of the RO membrane). Control is typically attained by oxidation reduction potential (ORP). Each system must be calibrated because the background interference varies from water source to water source. Sometimes, chlorine monitors are used for control of the bisulfite feed. Free chlorine should be reduced to less than 0.02 ppm, as chlorine will degrade RO membranes. Degradation of more RO membranes will occur after 200–1000 ppm/h of exposure to free chlorine [23].

13.6.5 MEMBRANE CLEANING

Membrane cleaning can be an important part of the program to control membrane fouling and scaling. Membranes that are cleaned on time will exhibit longer membrane life than they would if there were a

TABLE 13.10
The Relationship between
Temperature and pH for
Preventing Hydrolysis of RO
Membranes

Temperature, °C (°F)	pH
25 (77)	10.5
35 (95)	12
45 (113)	13

Source: FilmTec Reverse Osmosis Membrane Technical Manual, Dow Liquid Separations, Form No. 609-961071-0705, 126, 2007. With permission.

delay in cleaning. Cleaning the membranes on time will ensure that foulants and scale do not become irreversibly bound to the membranes or feed spacers. Membranes should be cleaned when the normalized permeate flow drops 10%–15% from start-up, or when pressure drop (feed to concentrate) increases by 10%–15% from start-up.

Cleaning formulas can be categorized as high pH, neutral pH, and low pH; each is designed to remove specific foulants and/or scale. Specific recipes are provided by membrane manufacturers and include the following [24]: (a) caustic with tetrasodium salt of ethylene diamine tetracetic acid (Na₄-EDTA) at pH 12, 95°F max. for sulfate scales, (b) caustic with sodium salt of dodecylsulfate (Na-DSS) at pH 12, 95°F max for silt, silica, biofilms, and organics, hydrochloric acid at pH 1–2, 77°F max, for calcium carbonate, and (c) sodium hydrosulfite (Na₂S₂O₄) at pH 5, 77°F for metal oxides.

If multiple foulants and scale are present such that two or more cleaning solutions at different pH levels are required, the high-level pH cleaner should be used first. This is because acid sets biofilm, making it virtually impossible to remove after acid treatment.

Recent studies have shown that cleaning solutions are more effective the higher the pH level [25,26]. For example, recovery of productivity after biofouling can be up to 10 times greater when the membranes are cleaned at pH 12 rather than at pH 11 [26]. However, the pH is also temperature dependent. Higher pH levels require a lower temperature to prevent hydrolysis of the membranes. In general, cleaning protocols should follow the pH/temperature guidelines listed in Table 13.10 to maximize cleaning efficiency and minimize membrane hydrolysis [27]. It is recommended that RO skids be cleaned one stage at a time. That way, foulants removed from the first stage do not contaminate the second stage and scale from the second stage does not contaminate the first stage.

Cleaning of the membranes can be conducted *in situ* (known as clean-in-place or CIP) or offsite. Table 13.11 lists the advantages and limitations for each option [28]. Typically, smaller installations tend to go with offsite cleaning while larger installations find it easier to go with CIP.

TABLE 13.11
The Advantages and Limitations of CIP and Off-Site
Membrane Cleaning

	Advantages	Limitations
CIP	Onsite Fast	Less efficient cleaning Capital cost of CIP skid Chemical handling
Off-site cleaning	Expert service Documentation Ability to try various cleaners, conditions	More costly per cleaning Requires back-up modules

Source: Kucera, J., Reverse osmosis operations, Presented at the 65th Annual International Water Conference, Pittsburgh, PA, Paper No. 04-39, 10, 2004. With permission.

13.7 RECENT ADVANCES IN RO PRETREATMENT HYBRID MEMBRANE SYSTEMS

Hybrid membrane systems in which RO is preceded by another membrane technique has become very popular over the last few years. The most common processes are microfiltration (MF), ultrafiltration (UF), and nanofiltration (NF) each followed by RO. Microfiltration is generally used to remove bacteria from RO feed water. Microfiltration, with membrane pore sizes of 0.1 μm , can provide 4 log removal of bacteria such as *Guardia* and *Cryptosporidium*. Because of this, the MF–RO hybrid system is commonly used for municipal drinking water applications and for recovery of tertiary effluent. Microfiltration also removes suspended solids and has been used in place of clarification when the RO feed source is surface water.

UF is a finer filtration medium than MF, with pore sizes ranging from 0.0001–0.1 microns. Hybrid UF–RO systems are typically found in high-purity and food-and-beverage applications, for example, or the production of bottled drinking water. UF membranes are used to remove very fine suspend solids, micro-organisms, and organics from RO feed water.

NF is essentially a “leaky” RO process. NF membranes are characterized in a similar manner to RO membranes by offering the removal of dissolved ions and organics. The difference between the two technologies is that the rejection of solutes by NF membranes is lower than by RO membranes. For example, while the rejection of sodium is on the order of 96%–98% for RO membranes, the rejection by NF membranes can be as low as 50%, depending on the polymer used to create the NF membrane. However, the rejection of divalent ions, such as calcium and magnesium, is in the mid-1990s, such that NF membranes are now used in water “softening” applications for drinking water. Hence, NF membranes are sometimes referred to as “softening” membranes. Nanofiltration has also shown particular abilities to remove color from RO feed water without the fouling that plagues RO membranes.

13.8 CASE STUDIES

13.8.1 DATA NORMALIZATION

This case study involves a power generation facility located on the Delaware River in New Jersey [29]. This facility used a combination of cooling-tower blow down and Delaware River water as make up to a 2-pass RO system. The pretreatment consisted of lime softening followed by acidification and multimedia filtration, and finally sodium softening. Hydrochloric acid was used to adjust the pH. Figure 13.11 shows the observed product flow from the first-pass RO system [29]. The first-pass RO was designed

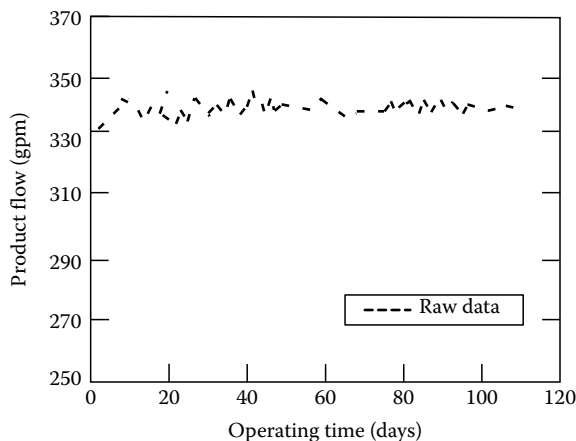


FIGURE 13.11 Observed RO product flow rate as a function of time. (Courtesy of UltraPure Water, Littleton, CO.)

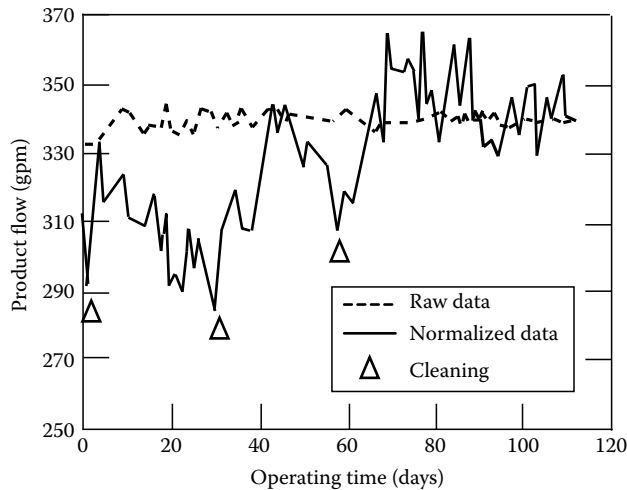


FIGURE 13.12 Normalized RO product flow rate superimposed on observed product flow rate as functions of time. (Courtesy of UltraPure Water, Littleton, CO.)

to yield 340gpm of product water. As the figure shows, the operators did a good job in keeping the observed product flow rate right on the design flow rate. However, the RO system had trouble keeping up with the design flow rate, and a higher operating pressure was required to maintain the 340gpm design flow rate. The observed flow rate, however, gave no hint of the difficulties with the RO system.

Figure 13.12 shows the normalized product flow superimposed on the observed product flow [29]. The normalized product flow curves reveal a different story than the observed product flow line. From start-up, the system experienced problems. Due to the negative slope of the normalized flow curve, the membranes were fouling and/or scaling. Subsequent investigations determined that the membranes were most likely fouling due to the following issues: (a) carry over of alum and suspended solids from the clarifier, (b) channeling through the multimedia filters, and (c) iron oxide products from hydrochloric acid addition into stainless steel piping.

As Figure 13.12 shows, normalized product flow dropped off over 10% during the first 30 days of operation. Since guidelines call for cleaning after a 10%–15% loss in normalized product flow, the membranes were cleaned on day 30. Some performance was recovered due to the efficiency of cleaning as well as improvements that were being made to the pretreatment system. However, normalized product flow continued to drop after the first cleaning, dropping 10% again over the next 29 days. Hence, the membranes were cleaned on day 59. After this cleaning, the performance improved significantly, and it began to stabilize. After about 90 days, the normalized product flow and observed product flow tracked well, indicating that the membranes had been sufficiently cleaned and the pretreatment system improved to the point where there was no loss in normalized product flow.

In this case study, the observed product flow gave no indication that the membranes were seriously fouling. Only by monitoring the normalized product flow did the fouling issues become evident. By monitoring only the observed product flow, it might have taken weeks for the fouling issues to become evident. Frequently, the only way fouling is noticed is that the RO feed pumps run out of available head, being unable to overcome the additional barrier to flow posed by the layer of foulants on the membrane. By that time, some of the foulants may already have become irreversibly attached to the membrane or feed spacer, hindering performance for the remainder of the life of the membranes.

13.8.2 HIGH-EFFICIENCY FILTRATION AS RO PRETREATMENT

This case study involves a power-generation facility located on the East Coast of the United States. Water from an aquifer provided feed water to the system. Pretreatment consisted of 5 micron

cartridge filters and electro dialysis reversal (EDR) membrane equipment. This system worked well until 2000–2001, when the chemistry of the aquifer changed resulting in a major increase in iron.

The iron and some other metals were oxidizing to particulates that plugged the cartridge pre-filters as well as fouled both the EDR and RO membranes. The plugging was so severe that it became necessary to change all 32 cartridge filters in the system every 18 h. The EDR membranes required hand cleaning to remove the iron particulates. Furthermore, the RO system operated at very high feed pressure to try to overcome the high degree of iron suspended solids deposited on the surface of the RO membranes. Eventually, the RO membrane modules were crushed and the RO feed pump failed due to the high pressure required.

The facility evaluated several pretreatment options including iron oxidation and precipitation followed by filtration with manganese greensand and filtration with conventional multimedia filters (MMF). The facility tried conventional MMF for removal of the iron particulates. The MMF option was plagued with a few significant challenges to success including: (a) particle-size analysis of the feed water indicating that greater than 99% of the particles in the feed water were smaller than 1 micron in size, while the MMF typically offers filtration down to about 10 microns without the use of coagulants, (b) the use of coagulant would get the removal efficiency down to about 1–2 microns, but would run the risk of under or overfeeding of the product, resulting in no removal or fouling of the membranes with overfed coagulant, and (c) the service flow rate is 5 gpm/ft², which would necessitate rather large vessel diameters to meet the flow 400 gpm demands of the system, and space was a premium at the facility.

Manganese greensand filters were not considered for this application due to the need for chemical addition, the slow service flow rate of about 2–5 gpm/ft², and the plant personnel naiveté with operation and regeneration of this type of filter. A decision was made after 4 years of plugging cartridge filters, hand-cleaning EDR membranes, and emergency RO membrane replacements to try high-efficiency filtration (HEF). High-efficiency filters are commonly used in side-stream filtration applications for cooling water systems. They are capable of removing particles down to the 0.25–0.5 micron level. An additional advantage of the HEF for this application was that the service flow rate for these filters is 10–15 gpm/ft², meaning that the footprint for the HEF filter system would be significantly smaller than that for either the MMF or greensand filter systems.

Figure 13.13 shows the cross section of an HEF. These filters operate in a top-over-bottom flow design. Feed water enters from the side of the bed and an area of turbulence is created over the bed,

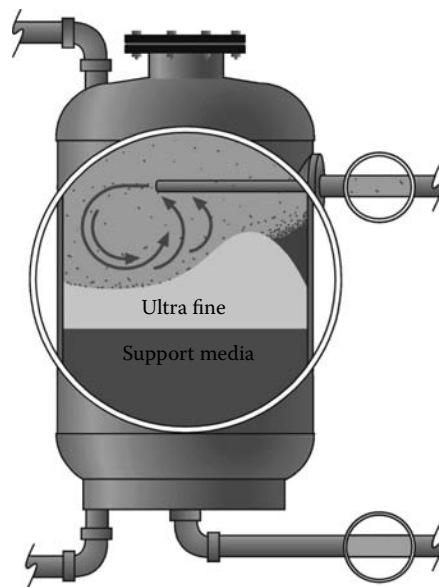


FIGURE 13.13 High efficiency filter system.

with a tangential force supplied by the influent water that scrubs the particle off the surface of the bed. This tangential force carries particles back toward the filter inlet, while at the same time pushing the sand toward the filter inlet, creating a “camel hump.” Behind this “hump” is an area of low turbulence that allows for the deposition of particles that have been scrubbed off the sand. This area behind the hump keeps filling with particles until they begin to cover the hump and collect on the turbulence-side of the hump, adding to the particle loading of the influent water onto the surface of the sand. This results in an increase in differential pressure through the bed, signaling time to backwash the filter.

A pilot test of an HEF was conducted at the facility with the following results: (a) the cartridge filters exhibited no increase in differential pressure while the HEF was online, (b) the EDR effluent quality improved by 20%, and (c) 60 days after the start-up, the HEF was removing 96%–99% of the incoming particulate iron. After a full-scale HEF was installed in March 2006, the cartridge filter replacement dropped from every 18 h to once per month. As of April 2008, there have been no RO membrane replacements since the start-up of the full-scale HEF.

This case study highlights how a new-to-RO pretreatment technology can be used to significantly reduce the concentration of suspended solids, in this case particulate iron, in the membrane feed water. High-efficiency filters should be considered a viable alternative to multimedia filtration and manganese greensand filtration for removal of small, submicron particles from RO feed water.

13.9 SUMMARY

Proper monitoring and analysis of operating data is critical to determine the health of a RO system. Despite advances in the technology, membranes still foul and scale. To meet this challenge, pretreatment and data normalization are critical. Pretreatment is used to reduce or eliminate potential foulants, scale-forming species, and agents of membrane degradation from RO feed water. Normalized flow and normalized salt passage, along with pressure drop, needs to be tracked as a function of time to monitor in real time the condition of the membranes. When the condition of the membranes deteriorates to the point where performance begins to decline, it is time to clean the membranes as well as investigate more appropriate pretreatment techniques.

REFERENCES

1. Recent advances and research needs in membrane fouling. Committee Report, *Journal AWWA* 97(8), 80 (August 2005).
2. Alexander, K. L. et al. Low-fouling reverse osmosis membranes: Evidence to the contrary on microfiltered secondary effluent. *Journal AWWA* (March 5, 2003).
3. Fazel, M. and Darton, E. D. Statistical review of 150 membrane autopsies. In Paper Presented at the *62nd Annual International Water Conference*, Pittsburgh, PA (2001).
4. Kucera, J. Troubleshooting: Methods to improve system performance—Part 1. *UltraPure Water* 24, 18–25 (2007).
5. FilmTec Reverse Osmosis Membrane Technical Manual, Dow Liquid Separations, Form No. 609-961071-0705, 47 (2007).
6. FilmTec Reverse Osmosis Membrane Technical Manual, Dow Liquid Separations, Form No. 609-961071-0705, 67 (2007).
7. Bersillon, J. and Thompson, M. A. Field evaluation and piloting. In *Water Treatment Membrane Processes*, American Water Works Association Research Foundation, Lyonnaise des Eaux, and Water Research Commission of South Africa, McGraw Hill, New York (1996).
8. Kucera, J. Studies on halogen interactions with polyamide-type reverse osmosis membranes, Master's thesis, University of California at Los Angeles, Los Angeles, CA (1984).
9. FilmTec Reverse Osmosis Membrane Technical Manual, Dow Liquid Separations, Form No. 609-00071-0705, 83 (2007).
10. Dudley, L. Combating the threat of silica fouling in RO plant-practical experiences. *Desalination & Water Reuse* 12, 28 (2003).
11. Kucera-Gienger, J. Successful application of reverse osmosis in the chemical process industries. Technical Paper, Presented at the 1995 AIChE Summer National Meeting, Boston, MA (August 1, 1995).

12. Singh, R. *Hybrid Membrane System for Water Purifications*, Elsevier Ltd., Oxford, U.K. (2006).
13. Kucera, J. Understanding reverse osmosis as a vital water treatment. *Hydrocarbon Processing* 85, 113 (2006).
14. Standard Test Method for Silt Density Index (SDI) of Water. ASTM International, Designation D4189-07 (2007).
15. Takeharu, I. et al. Low fouling RO membranes. *Membrane* 27, 209–212 (2002).
16. Duraslick membrane literature, GE-Osmonics-Desal, P/N 1232264 rev. A.
17. X-20 membrane literature, TriSep Corporation web site, <http://www.trisep.com/x-20%20low%20fouling.htm>
18. Activated carbon for drinking water filtration. Doulton USA, Southfield, MI, http://www.doultonusa.com/HTML/pages/activated_carbon_water_filtration.htm (2008).
19. Inc Betz laboratories. *Betz Handbook of Industrial Water Conditioning*, 9th edn., Betz Publisher, Philadelphia, PA, p. 41 (1991).
20. Amjad, Z. Scale inhibition in desalination applications: An overview. In *CORROSION/96, NACE International Annual Conference and Exposition*, Houston, TX, Paper No. 230 (1996).
21. HERO™. Aquatech International Corporation, Canonsburg, PA, sales flyer.
22. Moftah, K. High pH RO for wastewater treatment. *Pollution Engineering* Web site, issued Thursday, 1 (2004) (original print date October, 2002).
23. FilmTec Reverse Osmosis Membrane Technical Manual, Dow Liquid Separations, Form No. 609-961071-0705, 61 (2007).
24. FilmTec Reverse Osmosis Membrane Technical Manual, Dow Liquid Separations, Form No. 609-961071-0705, 129 (2007).
25. FilmTec Reverse Osmosis Membrane Technical Manual, Dow Liquid Separations, Form No. 609-961071-0705, 128 (2007).
26. Broden, C. Pushing the limits: Improved RO membrane cleaning recommendations. Paper presented at the *68th Annual International Water Conference*, Orlando, FL, Paper No. 07-43 (2007).
27. FilmTec Reverse Osmosis Membrane Technical Manual, Dow Liquid Separations, Form No. 609-961071-0705, 126 (2007).
28. Kucera, J. Reverse osmosis operations. Paper presented at the *65th Annual International Water Conference*, Pittsburgh, PA, Paper No. 04-39, 10 (2004).
29. Kucera, J. Membrane Part 2: The role of product flow normalization and membrane cleaning in RO operations, *UltraPure Water* 22, 37–40 (2005).

14 Scale Formation and Control in Thermal Desalination Systems

Faizur Rahman and Zahid Amjad

CONTENTS

14.1	Introduction.....	272
14.2	Thermal Desalination Systems.....	273
14.2.1	Multiple-Effect Distillation Process	273
14.2.2	Multistage-Flash Distillation Process.....	273
14.3	Mechanism of Scale Formation	275
14.3.1	Solubility and Its Importance in the Precipitation.....	278
14.3.2	Maximum Supersaturation and Supersolubility	278
14.4	Types of Scales.....	279
14.5	Scale Prediction	280
14.5.1	Scaling Index Determination	280
14.5.2	Solubility Method.....	281
14.5.3	Chemical Equilibrium Method	284
14.5.4	Kinetics and Transport Phenomena Considerations	284
14.6	Scale Control Methods.....	285
14.7	Acid Treatment.....	285
14.7.1	pH Control Method.....	286
14.7.2	Proportional Flow Control Method	286
14.7.3	Case Studies.....	286
14.7.3.1	Jeddah-I.....	286
14.7.3.2	Jeddah-II	286
14.8	Additive Treatment.....	287
14.8.1	Low-Temperature Additives Treatment	287
14.8.2	High-Temperature Additives Treatment	287
14.9	Hybrid Treatment (Acid + Additive).....	287
14.9.1	Case Studies of Hybrid Treatment.....	288
14.10	Survey on Scale Control Methods	289
14.10.1	Input from Consultants	290
14.10.2	Plant Suppliers.....	290
14.10.3	Plant Operators	291
14.11	Concluding Remarks on Scale Control Methods.....	291
14.12	Development of Scale Control Inhibitors	291
14.13	Summary	294
	Acknowledgment	294
	References.....	294

14.1 INTRODUCTION

Water is the most important liquid in the world to maintain human, plant, and animal life. Moreover, high population growth, rapid urbanization, phenomenal industrial growth, and agricultural development make water one of the most precious resources in the world. Of the entire globe's water, 94% is salt water present in the oceans and 6% is freshwater. Of the latter, about 27% is in glaciers and 72% is underground. While this water is important for transportation and fisheries, it is too salty to sustain human life or farming [1]. Besides salinity, other impurities in water come from many sources. It is important to understand the role of these impurities in desalination processes. Water may be purified by a number of desalination techniques in which the dissolved impurities are removed from water or pure water is removed from the impurities. The desalination process to be employed for given saline water depends on its impurities, level of salinity, colloidal matter, biological content, and its economics. Various desalination processes that are commonly in use are as follows:

- Thermal desalination—multi-stage-flash distillation, multi-effect distillation, solar evaporation or distillation, crystallization, or freeze distillation
- Membrane—reverse osmosis, electrodialysis, membrane distillation
- Ion exchange

The economics of desalination process suggest that the more pure water that can be recovered from a stream, the higher the efficiency of the process. The recovery of pure water from saline water results in the increased concentration of brine, thus increasing the potential for fouling due to the precipitation of scale-forming salts/coagulation and the deposition of colloidal matter from brine. The fouling of heat exchangers and RO membranes is a complex phenomenon involving the deposition of several different types of foulants on the surfaces. The development of such deposits on heat exchanger surfaces in distillation plants leads to inferior thermal performance, decreased production, unscheduled shutdowns, poor product quality, and premature heat exchanger failure [2]. Figure 14.1 shows the fouling of a heat exchanger in a multistage flash desalination plant.

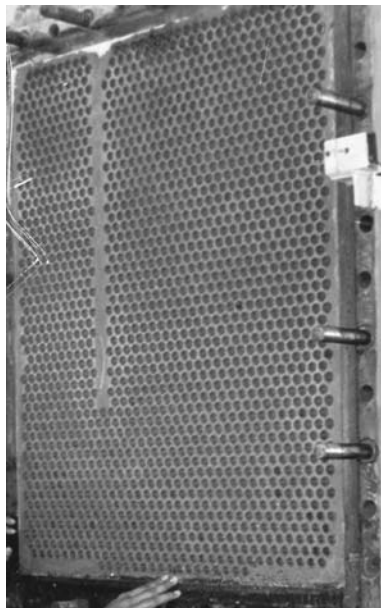


FIGURE 14.1 Fouled heat exchanger.

Commonly encountered foulants in desalination processes fall into the following three basic categories: (a) scale, (b) suspended/colloidal matter, and (c) biological matter. This chapter presents scale prediction methods and techniques to control scale formation in distillation plants.

14.2 THERMAL DESALINATION SYSTEMS

Thermal desalination processes cover a wide range of processes and are very robust methods of producing freshwater from seawater. However, these processes are energy intensive and well suited for regions where energy is cheap. Distillation is a process for seawater desalination and is an effective method of producing freshwater from seawater along with the power commonly known as dual-purpose desalination. In this process, most of the constituents are nonvolatile at temperatures encountered. The main steps involved [3] in distillation process are (a) the formation of vapor from seawater by the addition of heat, (b) the separation of vapor from seawater, and (c) the condensation of vapor by the removal of heat. When seawater is heated, the scale formation takes place inside the tubes based on the concentration of chemical constituents present in the seawater and prevailing temperature. The popular methods among distillation processes are multiple-effect distillation (MED) and multistage-flash distillation (MSF).

14.2.1 MULTIPLE-EFFECT DISTILLATION PROCESS

This process consists of two or more evaporator effects, which operate at successively lower temperatures and pressures. The first effect is heated by either exhaust steam or extraction steam from a turbine in the case of dual-purpose desalination plants. The heat source may be prime steam also. The vapors from the first effect are directed to the second effect and serve as heat input to evaporate the brine. In each effect, the vapors are condensed on the shell side of the tubes, and the brine receives the heat inside the tubes and evaporates. Brine that is not evaporated is pumped to the next effect for further evaporation, and vapors are separated by passing through demisters. The repetition of this process several times (4–12) provides MED. A process flow diagram of three-effect MED plant is shown in Figure 14.2. The detailed description of the MED process is available elsewhere [3,4].

In MED process, scale formation potential depends on the upper limit of the brine temperature. This temperature limit can be fixed based on the scale control treatment methods such as acid treatment, low-temperature additives, or high-temperature additives. Limiting the maximum brine temperature affects the thermal efficiency of the desalination plant. It should be noted that, in MED process, feed at its lowest concentration encounters maximum temperature, thereby reducing the risks of scale formation.

14.2.2 MULTISTAGE-FLASH DISTILLATION PROCESS

In the conventional distillation process, the heating of seawater and boiling takes place in the same vessel. In the flash evaporation process, seawater is heated in the tubes, and then it passes through a number of chambers (or stages) at progressively lower pressures. In each chamber or stage, “flashing” occurs instantly by producing vapor due to the sudden release of pressure until the water temperature is again in thermodynamic equilibrium with the vapor pressure in that stage. The brine is transferred to the next stage, which is maintained at a lower pressure. When the pressure is reduced, the boiling temperature is correspondingly decreased. Flashing occurs again, and the temperature of the brine decreases in an amount proportional to the amount of vapor generated, while the salt concentration of seawater increases. The pressure in each stage is lower than the pressure in the preceding stage. In each stage, distillate is produced and the amount of distillate produced is dependent on the following parameters: (a) temperature drop in each stage, (b) total flash range, and (c) stage heat-transfer coefficient. To increase the thermal efficiency of the process, the number of flash stages is increased. The efficiency of the process is defined by the performance ratio (PR),

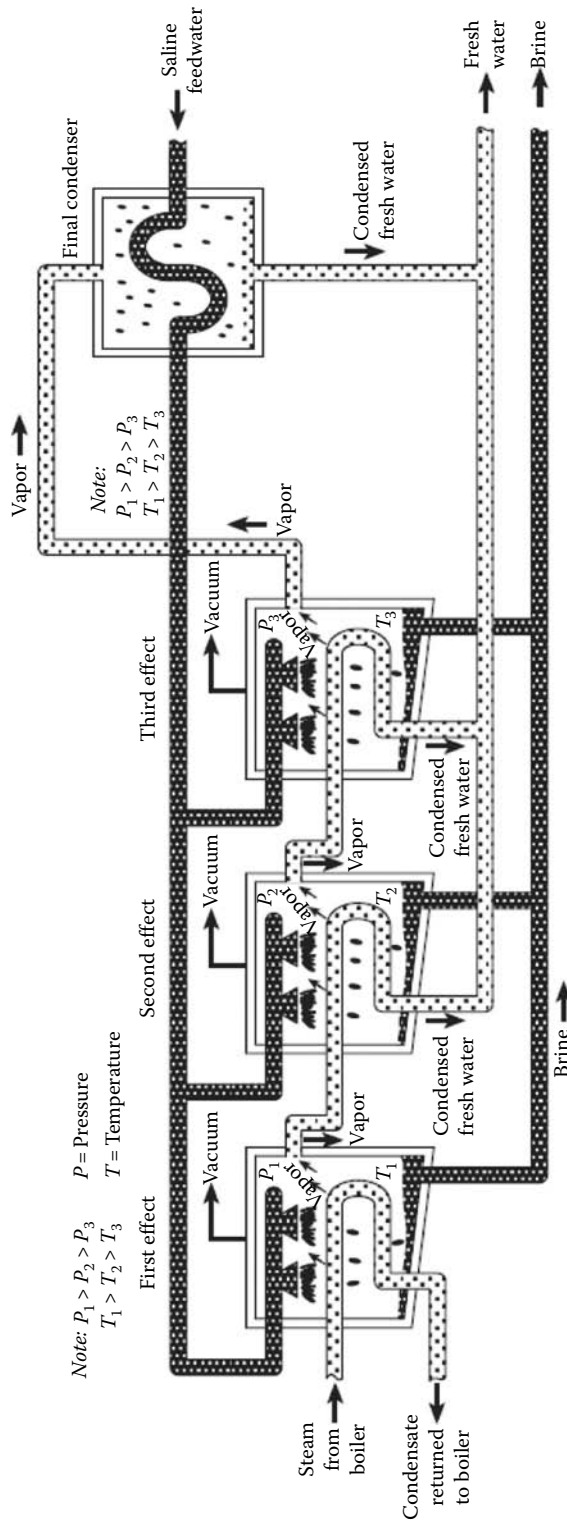


FIGURE 14.2 Process flow diagram of a three-effect MED plant. (From Buros, O. K., *The Desalting ABC's*, Prepared for International Desalination Association, Topsfield, MA, 1990. With permission.)

which is the distillate (in pounds) produced per 1000 Btu of heat input [3]. Alternatively, gain output ratio (GOR) is equal to the amount of distillate produced divided by the amount of heating steam supplied to the first effect [4]. The number of stages controls the amount of heat recovery possible, and this determines the quantity of external energy required. This process has three main sections: heat input section, heat recovery section, and heat rejection section. The design and operation details of MSF process are presented by several experts [3–5]. A typical process flow diagram is illustrated in Figure 14.3.

Other important process characteristics are water recovery and brine concentration ratio. The water recovery is the ratio of product water quantity to the seawater taken as feed. In Saudi Arabia, these values range from 9% to 14%. The brine concentration ratio is simply the ratio of the maximum brine concentration in the last stage to that of feed water. It usually varies from 1.3 to 2 [4]. The scale deposition process is dependent on the concentration ratio and maximum temperature selected for the flashing brine.

14.3 MECHANISM OF SCALE FORMATION

Scale is defined as the deposit of certain sparingly soluble salts from the brine onto the tubing and other process surfaces. It is one of the most serious problems in any desalination process, especially in distillation. When a sufficiently large amount of solute is maintained in contact with a limited amount of solvent, dissolution occurs continuously till it reaches a state when the reverse process becomes increasingly important. This is the return of dissolved species (atoms, ions, or molecules) to the undissolved state, a process called *precipitation*. When dissolution and precipitation occur continuously, and at the same rate, the amount of dissolved solute present in a given amount of solvent remains constant with time. The process is one of dynamic equilibrium and the solution in this state of equilibrium is known as a *saturated solution*. The concentration of the saturated solution is referred to as the solubility of the solute in the given solvent. Thus, the *solubility* of a solute is defined as its maximum concentration which can exist in solution under a given set of conditions of temperature, pressure, and the concentration of solution. A solution that contains less solute than required for saturation is called an *unsaturated solution*. A solution whose concentration is higher than that of a saturated solution due to any reason(s), such as change in solvent concentration, temperature, and so on, is said to be supersaturated. When the temperature or concentration of a solvent is increased, the solubility may increase, decrease, or remain constant, depending on the nature of the system. For example, if the dissolution process is exothermic, the solubility decreases with increased temperature; if endothermic, the solubility increases with decreased temperature [6,7]. The degree of supersaturation can be defined in two ways. One method is to measure the absolute supersaturation (AS), which can be represented as

$$AS = C - C_{eq} \quad (14.1)$$

where

C is the concentration of the dissolved substances in a given supersaturated solution

C_{eq} is its normal equilibrium saturation concentration

The other method of expressing the degree of supersaturation is by defining in terms of percent supersaturation (%PS) as

$$\%PS = [(C - C_{eq})/C_{eq}] \times 100 \quad (14.2)$$

and supersaturation ratio as

$$SR = C/C_{eq} \quad (14.3)$$

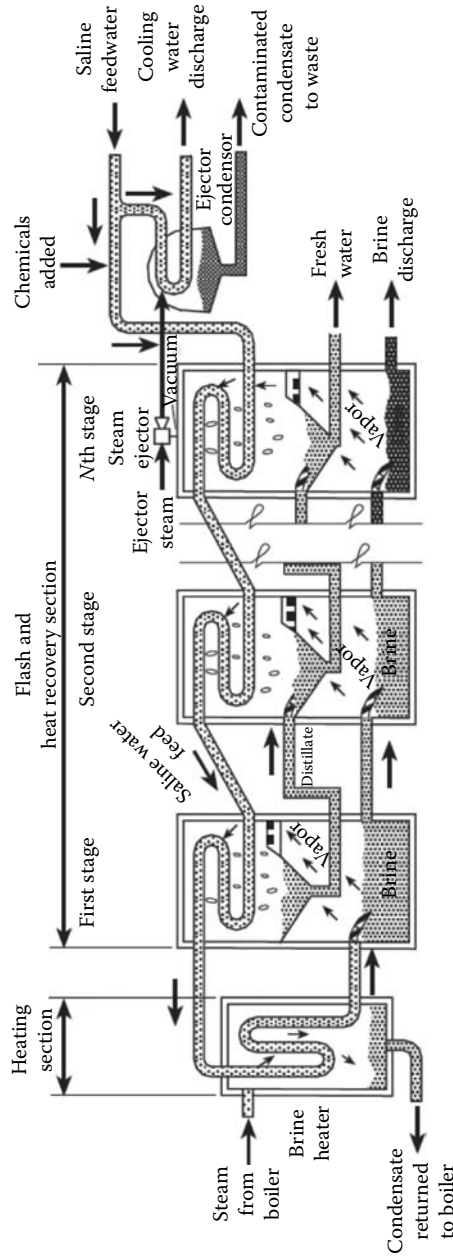


FIGURE 14.3 Process flow diagram of a multistage-flash plant. (From Buros, O. K., *The Desalting ABC's*, Prepared for International Desalination Association, Topsfield, MA, 1990. With permission.)

Solubility data of solutes provide a basis to establish saturation concentration. A convenient method of discussing the solubility (S) of a solute is by means of a solubility product (K_{sp}). Consider the addition of a solute $\text{MX}(\text{s})$ to distilled water. At the limit of solubility, there is a dynamic equilibrium which can be represented as



and the equilibrium constant, K_{sp}° , for the solubility process is given as

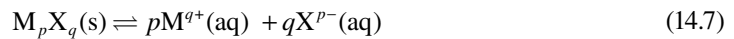
$$K_{sp}^{\circ} = [a(\text{M}^+)a(\text{X}^-)]/a(\text{MX}) \quad (14.5)$$

Since the activity of pure solid $\text{MX}(\text{s})$ is unity, the equilibrium expression simplifies to

$$K_{sp}^{\circ} = a(\text{M}^+)a(\text{X}^-) \quad (14.6)$$

K_{sp}° is known as *solubility product* or sometimes *thermodynamic solubility product*, and it is a function of temperature and invariant with the ionic strength of the solution [8]. In any aqueous solution containing M^+ and X^- ions, as long as the activities $a(\text{M}^+)$ and $a(\text{X}^-)$ are such that their product is greater than K_{sp}° , then some solid $\text{MX}(\text{s})$ should precipitate until the product of $a(\text{M}^+)$ and $a(\text{X}^-)$ becomes equal to K_{sp}° .

For a general case:



$$K_{sp}^{\circ} = a(\text{M}^{q+})^p a(\text{X}^{p-})^q \quad (14.8)$$

$$K_{sp}^{\circ} = [C(\text{M}^{q+})^p C(\text{X}^{p-})^q][\gamma(\text{M}^{q+})^p \gamma(\text{X}^{p-})^q] \quad (14.9)$$

where $\gamma(\text{M}^{q+})^p$ and $\gamma(\text{X}^{p-})^q$ are the activity coefficients of species M and X. If $C(\text{M}^{q+})$ and $C(\text{X}^{p-})$ are the concentrations, the mean activity coefficient of M_pX_q is denoted as γ^{p+q} , then

$$K_{sp}^{\circ} = [C(\text{M}^{q+})^p C(\text{X}^{p-})^q] \gamma^{p+q} \quad (14.10)$$

The solubility product expression now can be modified as follows:

$$K_{sp} = [C(\text{M}^{q+})^p C(\text{X}^{p-})^q] \quad (14.11)$$

where K_{sp} is known as the apparent solubility product and is related to thermodynamic solubility product as follows:

$$K_{sp} = K_{sp}^{\circ} / \gamma^{p+q} \quad (14.12)$$

If the ionic strength of the aqueous environment is low, the activity coefficient (γ) is unity (i.e., the ideal behavior of solution is approached, in which activities and concentration can be equated) and the above expression reduces to an approximate form.

$$K_{sp}^{\circ} \sim K_{sp} \quad (14.13)$$

$$K_{sp} \sim [C(M^{q+})]^p [C(X^{p-})]^q \quad (14.14)$$

This form is frequently used in practice, in which the true solubility product is expressed simply in terms of concentration of the ions. However, it should be noted that in aqueous systems of significant ionic strength, the activity coefficient is not equal to 1, and thus K_{sp} is not equal to K_{sp}^o . Then K_{sp} is a function of both temperature and ionic strength, while K_{sp}^o is invariant with ionic strength. In such circumstances, the use of Equation 14.13 is likely to introduce significant errors. The calculation of activity coefficients (γ_{\pm}) becomes necessary at higher ionic strengths. A number of correlations are available in the literature to estimate activity coefficients, and Horvath [9] has given an excellent review of these. Pytkowicz [10] suggested the following form for high ionic strength solutions:

$$\log \gamma = A\sqrt{I}/(1 + Ba\sqrt{I}) + C_1 + C_2I^{1.5} + C_3I^2 \quad (14.15)$$

where

$I = 1/2\sum m_i Z_i^2$ ionic strength

m_i is the molal concentration of ion i in the solution

Z_i is the ionic charge of ion i in the solution

a is the ion size parameter

A, B are the Debye–Huckel coefficients

C_1 – C_3 are the regression constants

Substituting Equation 14.15 in Equation 14.12, after taking log on both sides and assuming $p = q = 1$, will give the following equation for K_{sp} :

$$\log K_{sp} = \log K_{sp}^o + 2A\sqrt{I}/(1 + Ba\sqrt{I}) + 2C_1I + 2C_2I^{1.5} + 2C_3I^2 \quad (14.16)$$

14.3.1 SOLUBILITY AND ITS IMPORTANCE IN THE PRECIPITATION

The solubility of a salt, as discussed earlier, is defined as its maximum concentration which can exist in solution under given solution concentration, temperature, and pressure. At this condition of saturation, the solution is said to be in equilibrium with respect to the salt. As long as the salt concentration in the solution is equal to or below its saturation concentration, it will not precipitate out of the solution, and no scale will form. If, however, the concentration of the salt exceeds its saturation concentration due to any reason(s), such as change in solution concentration, temperature, pressure, and so on, the solution is said to be supersaturated. The excess salt in the saturated solution tends to precipitate and probably deposit as scale. The higher the degree of supersaturation, the greater is the driving force for precipitation to occur. Therefore, the basic condition required for scale formation is the attainment of supersaturation [2]. As a consequence of supersaturation, nuclei will form and lead to crystal growth and precipitation or scale formation. The solubility of the scale-forming salts is, therefore, like a border between the scale and no-scale regimes, and its knowledge is fundamental to the prediction and control of scale. So, the knowledge of solubility data is of vital importance for the prediction of scaling.

14.3.2 MAXIMUM SUPERSATURATION AND SUPERSOLUBILITY

It is important to know the maximum supersaturation of a substance and the stability of the solution that can be achieved under given conditions. The maximum supersaturation represents the limit at which spontaneous crystallization begins [7]. The value of maximum supersaturation can be measured either in terms of absolute supersaturation or percent supersaturation. The value of maximum supersaturation depends primarily on the nature of solute and the solvent. However, other factors such as

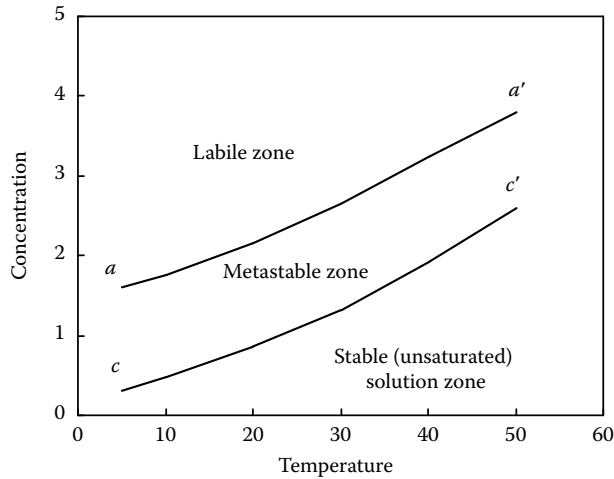


FIGURE 14.4 A typical diagram showing states of solution. (From Cowan, J. and Weintritt, D. J., *Water formed scale deposits*, Gulf Publishing Company, Houston, TX, 1976. With permission.)

temperature, impurities, the rate of cooling of a solution, and various other mechanical effects (filtration, stirring, irradiation with ultrasound, and so on) have a significant influence on the value of maximum supersaturation. In view of the above mentioned factors, the method of preparation of a solution and the degree of its purity may be very important in achieving a high level of supersaturation.

The phenomenon of maximum supersaturation is closely related to the stability of supersaturated solutions, which is governed by the metastability limit, also known as supersolubility. The *supersolubility* represents the maximum concentration, obtained at a given set of conditions of temperature, ionic strength, and so on, at which spontaneous crystallization begins [11]. The supersolubility (metastability limit) separates the region of supersaturated solutions into two parts. The supersaturated solutions with concentrations above the supersolubility limit crystallize instantaneously, while those whose concentrations are below the limit can be stored without inducing crystallization for sometime. The first mentioned region is known as *labile region* or *unstable zone*; the second region as the *metastable zone*, as shown in Figure 14.4 [12].

Miers and Isaac [13] have defined the supersolubility as the maximum concentration at which large-scale crystallization of a solution begins. The supersolubility curve resembles the solubility curve, and the two are usually almost parallel to each other. Tovbin and Kransnova [14] plotted the solubility and supersolubility data of three salts, as shown in Figure 14.5. For KNO_3 and KClO_3 , these curves are practically parallel while in the case of KCl , the solubility curve is steeper than the supersolubility curve. However, the difference between the two curves is relatively small and the two curves are in fact straight lines. In contrast to the solubility curve, the supersolubility curve does not depend just on the temperature and composition of the solution but also on the elapsed time, other conditions being equal. The period during which the concentration of a solution remains constant is known as the *induction period* or *latent period* [7]. The duration of the induction period depends on the degree of supersaturation of a solution, the nature of the solute and the solvent, the vigor of stirring of the solution, the presence of impurities, and other factors.

14.4 TYPES OF SCALES

In distillation processes, the scales formed can be divided into two types: (a) alkaline scales—mainly calcium carbonate and/or magnesium hydroxide, and are soft in nature; and (b) sulfate scales—mainly calcium sulfate. Calcium sulfate scales are hard and generally form at temperatures above 121°C when higher concentrations of calcium and sulfate ions are prevalent.

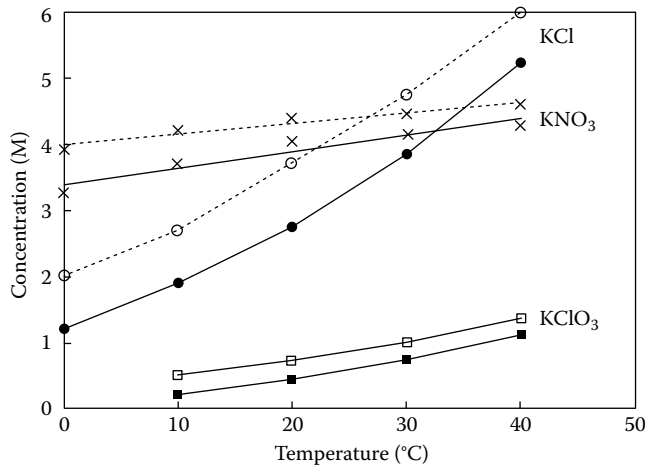


FIGURE 14.5 Supersolubility (dashed) and solubility (solid) curves of solutions of three salts (1) KNO₃; (2) KCl; (3) KClO₃. (From Tovbin, M. V. and Kransnova, S. I., *Zh. Fiz. Khim.*, 25, 161, 1951. With permission of Springer Science and Business Media.)

14.5 SCALE PREDICTION

The ability to predict scale formation is essential for its prevention and mitigation. There are a number of different methods that are used for predicting scale formation. They are generally divided into three categories: (a) scaling index determination, (b) scale prediction based on solubility data, and (c) chemical equilibrium calculations. These methods ignore the effect of kinetics and transport phenomena and are mainly based on thermodynamic concepts, which merely predict scaling tendency. It is not possible to predict how fast scale will form and how much. The scale prediction methods developed for predicting scaling potential in oil wells may be utilized for predicting scaling in seawater desalination by distillation method as the concentration and temperature range in the desalination plants are within the limits.

14.5.1 SCALING INDEX DETERMINATION

Ryzner [15] presented stability index to predict scaling tendency of CaCO₃ for waters at temperatures below 200°F (93°C) and low total dissolved solids (TDS). He defined the stability index (SI) as follows:

$$SI = 2pH_s - pH_a \quad \begin{array}{l} >7 \text{ Scaling tendency} \\ <7 \text{ Corrosion tendency} \end{array}$$

where

pH_a is the actual pH as determined

pH_s is the saturation pH determined by measuring the methyl orange alkalinity, the calcium hardness, total dissolved solids, and temperature

Langelier saturation index (LSI) proposed the following model to prevent scale and corrosion in municipal water systems:

$$SI = pH_s - pH_a \quad \begin{array}{l} >0 \text{ Scaling tendency} \\ <0 \text{ Corrosion tendency} \end{array}$$

LSI is applicable for waters with relatively low salt concentrations (around 4000 ppm) and in the pH range of 6.5–9.5. Stiff and Davis extended the Langelier equation to waters of TDS up to

200,000 ppm, temperatures less than 194°F (90°C), and pH of 5.5–8.5. The Stiff–Davis stability index may be defined as

$$SI = \text{pHa} - \text{p}(\text{Ca}) - \text{p}(\text{Alk}) - K \quad \begin{array}{l} >0 \text{ Scaling tendency} \\ <0 \text{ Corrosion tendency} \end{array}$$

where

pHa is the actual pH as determined

p(Ca) is the negative logarithm of calcium concentration

p(Alk) is the negative logarithm of the total alkalinity (based on bicarbonate content)

K is the constant which depends on temperature and total brine concentration

The detailed procedure of using Stiff–Davis index is presented by Cowan and Weintritt [2]. The main limitation of this index is that it does not consider pressure changes in predicting the scaling potential. In additive-treated desalination plants, CO₂ is not in significant quantities and Stiff–Davis index can be used. However, in acid-treated plants where CO₂ is released, it might give slight errors in predicting scaling potential. Oddo and Tomson [16], Valone and Skillern [17], and Kline [18,19] have proposed methods for calculating carbonate scale-forming potential using CO₂ partial pressures and the rate of precipitation.

14.5.2 SOLUBILITY METHOD

The solubility method is used to predict scaling potential based on the information of the solubility data of scaling species and its actual concentrations in the brine. This method may be used to mainly predict CaSO₄ scale formation in distillation plants. Stiff and Davis [20] developed a correlation for the solubility of CaSO₄ in a mixture with a view to simulate natural brines:

$$S = S_T F_1 F_2 F_3$$

where

S_T is the solubility of CaSO₄ in water at the given temperature

F₁ is a factor to take care of common ion effect (excess of Ca⁺⁺ or SO₄²⁻ ions);

$$F_1 = \frac{\text{Solubility of CaSO}_4 \text{ in presence of excess common ion}}{\text{Solubility in water}}$$

F₂ is the sodium ion factor; $\frac{\text{Solubility in NaCl}}{\text{Solubility in water}}$

F₃ is the magnesium ion factor; $\frac{\text{Solubility in Mg}^{2+} \text{ salt}}{\text{Solubility in water}}$

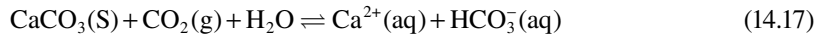
This correlation has many limitations, the most important being that it is based on the assumption that the contributions of excess common ions and ionic strength are independent, and hence can be accounted for separately. This correlation may only be used for low ionic strength brines.

The scaling potential of various brines can be determined using the scaling index (SI):

$$SI = \left(\frac{IP}{K_{sp}} \right) \quad \begin{array}{l} >1 \text{ Scaling tendency} \\ \leq 1 \text{ No scale} \end{array}$$

In general, the solubility of CaSO₄·2H₂O and CaCO₃: (a) decreases with temperature, (b) increases with pressure, and (c) increases with salt concentration up to a certain point and then tends to decrease.

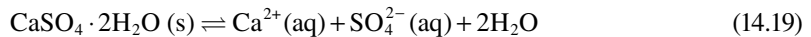
In the case of CaCO_3 , there is an additional parameter that has a strong influence on its solubility—partial pressure of CO_2 ($p\text{CO}_2$). The CaCO_3 solubility increases dramatically with $p\text{CO}_2$ according to the following reaction:



Unlike CaSO_4 , the solubility of CaCO_3 is very strongly dependent on the $\text{CO}_2 - \text{HCO}_3^- - \text{CO}_3^{2-}$ equilibria. The models that govern its solubility in saline waters are different from those for CaSO_4 . Raju and Atkinson [21,22] proposed empirical correlations to estimate the thermodynamic solubility product K_{sp}° and the mean activity coefficient γ_{\pm} for the sulfate-scale-forming compounds. The solubility can be determined with the following equation:

$$S = \sqrt{K_{\text{sp}}^{\circ}} / \gamma_{\pm} \quad (14.18)$$

The estimated solubility can then be used in determining the scaling potential of CaSO_4 scale in distillation plants. Considering MSF plants, the predominant scale is gypsum and the solubility of solid $\text{CaSO}_4 \cdot 2\text{H}_2\text{O}$ (gypsum) in aqueous electrolyte solutions may be related to the following reaction:



$$K_{\text{sp}}^{\circ} = m_{\text{Ca}^{2+}} \cdot m_{\text{SO}_4^{2-}} \cdot \gamma_{\pm}^2 \cdot a_{\text{H}_2\text{O}}^2$$

$$K_{\text{sp}}^{\circ} = K_{\text{sp}} \cdot \gamma_{\pm}^2 \cdot a_{\text{H}_2\text{O}}^2$$

where $a_{\text{H}_2\text{O}}$ is the activity of H_2O .

Following are the examples of equimolar and nonequimolar systems:

CaSO_4 -in- NaCl	Equimolar system
CaSO_4 -in- MgCl_2	Equimolar system
CaSO_4 -in- CaCl_2	Nonequimolar system

In equimolar systems, the molar concentrations of Ca^{2+} and SO_4^{2-} are equal, that is,

$$m_{\text{Ca}^{2+}} = m_{\text{SO}_4^{2-}}$$

and the K_{sp} is calculated from the solubility (S) data using the following equation:

$$K_{\text{sp}} = S^2$$

In the case of nonequimolar system (CaSO_4 -in- CaCl_2), the following condition is applicable:

$$m_{\text{Ca}^{2+}} > m_{\text{SO}_4^{2-}}$$

and the K_{sp} is calculated from the CaSO_4 -in- CaCl_2 solubility (S) data using the following equation:

$$K_{\text{sp}} = (S + X)S$$

where X is the excess common ion given by

$$X = m_{\text{Ca}^{2+}} - m_{\text{SO}_4^{2-}} = m_{\text{CaCl}_2}$$

Real brines are the complex mixtures of many salts. It is true that most brines (geothermal, oilfield, seawater, and brackish waters) are simulated using NaCl to determine solubility data. But there are other ions such as Ca^{2+} and Mg^{2+} which are present in appreciable quantities and have significant influence on solubility.

Suitable mixing rules can be used to estimate solubilities. There are many mixing rules available [23] for predicting the properties of the mixtures. A reasonable mixing rule to predict solubility in mixtures of salts and in the real brines is as follows:

$$\log S_m = \sum_{i=1}^N \left(\frac{I_i}{I} \right) \log S_i \quad (14.20)$$

$$\log K_{\text{sp}}(m) = \sum_{i=1}^N \left(\frac{I_i}{I} \right) \log K_{\text{sp}}(i) \quad (14.21)$$

Here, it is assumed that the solubility (or K_{sp}) in the mixtures of salts can be calculated from the sum of ionic strength fractions of single salt solubilities. Assuming the mixture (or brine) to consist of mainly three salts, NaCl, MgCl_2 , and CaCl_2 , the above equations can be written as

$$\log S_m = \left(\frac{I_1}{I} \right) [\log S_1] + \left(\frac{I_2}{I} \right) [\log S_2] + \left(\frac{I_3}{I} \right) [\log S_3] \quad (14.22)$$

$$\log K_{\text{sp}}(m) = \left(\frac{I_1}{I} \right) [\log K_{\text{sp}}(1)] + \left(\frac{I_2}{I} \right) [\log K_{\text{sp}}(2)] + \left(\frac{I_3}{I} \right) [\log K_{\text{sp}}(3)] \quad (14.23)$$

where

- 1 = NaCl
- 2 = MgCl_2
- 3 = CaCl_2

To determine the scaling potential of a particular system of brine, SI can be defined for the mixture as

$$\text{SI} = \log [IP(m)/K_{\text{sp}}(m)] \quad (14.24)$$

where $IP(m)$ = the product of ionic species of CaSO_4 present in a given mixture or brine

$$\text{(e.g., } IP(m) = m_{\text{Ca}^{2+}} \cdot m_{\text{SO}_4^{2-}} \text{)}$$

Ca^{2+} , SO_4^{2-} are obtained from the analysis of brine.

To summarize

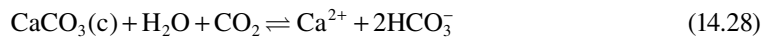
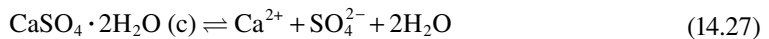
$$\begin{aligned} \text{SI} = \log[IP(m)/K_{\text{sp}}(m)] &< 0 \text{ No scale} \\ &= 0 \text{ Saturated} \\ &> 0 \text{ Scaling tendency} \end{aligned} \quad (14.25)$$

The models based on solubility data have some limitations. In most cases, the effect of ion pairs is not considered, and the solubility data used may be limited to low temperature and in sodium chloride solutions. The presence of ions such as magnesium that are known to have significant influence on solubility are often ignored. Thus, the models based on solubility data predict only scaling tendency and with a high degree of uncertainty. This means that a positive scaling potential does not

necessarily imply scale formation. Kinetics and transport phenomena considerations are required to predict actual precipitation and deposition.

14.5.3 CHEMICAL EQUILIBRIUM METHOD

Another method for predicting scale formation is by performing *equilibrium calculations* for a given system of brine. This method uses the analysis of brine, and based on mass balance and mass action equations for a set of possible reactions in the brine, equilibrium compositions of various species are estimated [24]. These equilibrium compositions will indicate the scaling potential of possible compounds. Some computer programs are available in the literature like WATEQ [25] and SOLMINEQ [26] that can perform equilibrium calculations by considering the analysis of particular brine. The basic philosophy is to define a system of reactions for the recycle brine of distillation plant. A simplified system for the precipitation of gypsum may be defined as



The set of reactions can be increased according to the requirement based on the analysis of the brine. The equilibrium constant method can be used to estimate the equilibrium concentrations of solute components. The free energy of the formation of all the species present in the above system can be estimated using methods available in the literature [27–29]. The activity coefficients of various species can be calculated using the Bromley or Pitzer method [9].

The mass action equations for the system, the mass balance equations, and the charge balance equation need to be written. These equations will form a set of nonlinear algebraic equations that can be solved by developing a FORTRAN program or using MATLAB®, and so on. The equilibrium composition obtained by solving the above mentioned set of equations will indicate the possibility of the scale formation of certain species.

14.5.4 KINETICS AND TRANSPORT PHENOMENA CONSIDERATIONS

Scale prediction can be done based on thermodynamics and solubility data. However, these methods only predict scaling tendency with high uncertainty. Precipitation may not occur even though the solution is supersaturated, as mentioned earlier, in the metastable region. In the metastable supersaturation region, spontaneous crystallization is not likely to occur whereas in labile region, spontaneous crystallization is possible. The kinetics of precipitation has to be investigated to determine actual precipitation phenomena and the rate of precipitation. Thus, a certain level of supersaturation must be exceeded for both thermodynamics and kinetics to result in actual precipitation. Unfortunately, the supersaturation level at which spontaneous precipitation occurs is not well defined and it is difficult to predict as it depends on a number of variables such as temperature, agitation, pH, ionic strength, and the presence of suspended matter which can act as nucleation site, and so on [30].

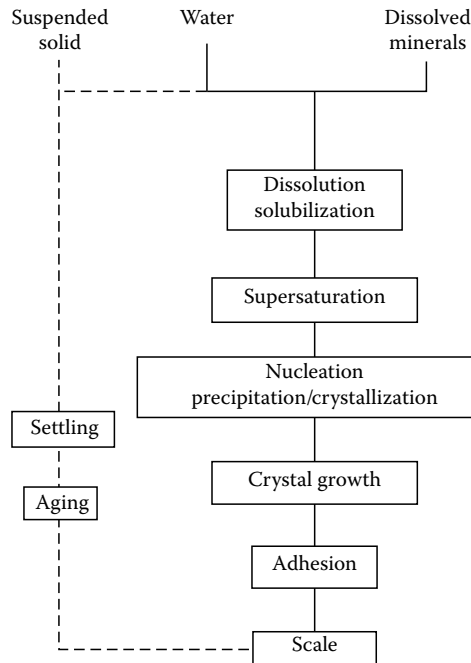


FIGURE 14.6 Steps involved in scale deposition process. (From Cowan, J. and Weintritt, D. J., *Water formed scale deposits*, Gulf Publishing Company, Houston, TX, 1976. With permission.)

Once precipitation begins, it may or may not deposit. This also depends on the hydrodynamics, like velocity and turbulence, temperature, sharp bends, the nature of substrate surface, and surface roughness, particularly surface homogeneities—such as grain boundaries, scratches, and regions of high residual strain. The corrosion of substrate plays an important role in an early stage of the deposition of precipitate. The mechanism of deposition after precipitation has been discussed by Cowan and Weintritt [2] in detail. Figure 14.6 illustrates the steps involved in the scale deposition process which are: dissolution of mineral salts in water, supersaturation of dissolved salts, nucleation, precipitation, adherence, and crystal growth on substrate.

14.6 SCALE CONTROL METHODS

Desalination plants based on distillation process generally use seawater as feed water, with salinity around 35,000–50,000 ppm. With appropriate concentration factor, the recycle brine concentration is around 1.2–1.5 times that of feed. Its various constituents can cause scaling or corrosion, and hence pretreatment is needed to prevent frequent interruptions in plants operation. Pretreatment comprises filtration, chlorination, dosing of antiscalants, and deaeration/decarbonation. The following paragraphs will focus mainly on scale control methods. There are a number of methods to control scale formation in desalination plants such as softening, seeding, the use of complexing agents, pH control, and threshold agents' treatment. The widely used methods for scale control are acid treatment or additive treatment.

14.7 ACID TREATMENT

The control of scale by acid treatment method is meant to prevent alkaline scale formation. The calcium sulfate scale is usually avoided in this case by operating the plant at temperatures and concentrations of brine below its supersaturation limit. Temperatures below 121°C and brine blowdown concentrations of 75,000 ppm are regarded as safe operating limits. When acid (HCl or H₂SO₄) is

injected to the makeup of the feed seawater, it kills the alkalinity, the very scale-forming constituent (HCO_3^-) by neutralizing reaction, and CO_2 is evolved. To remove this CO_2 , a decarbonator (DC) is installed before the deaerator in the acid-treated distillation plants. In principle, if acid is injected strictly according to stoichiometric quantities, scale will not form and thermal performance will be maintained for indefinite period. The correct dosing of acid needs skilled operators with the full understanding of the water chemistry of scale formation and prevention. Because the incorrect dosing of acid will either lead to scale formation or corrosion, the correct dosing of acid is very important and it can be done by two methods.

The dosage of acid does not depend on top brine temperature (TBT), while in additive dose plants the additive dosage is dependent on TBT. The additive dose has to be increased sharply with increase in TBT.

14.7.1 pH CONTROL METHOD

The pH of makeup feed seawater is adjusted to a predetermined value by acid injection based on the alkalinity and pH of feed. pH is measured after feeding acid but before DC to regulate the acid-dosing pump. pH meters need to be calibrated frequently to provide reliable readings and avoid any malfunctioning of pH meters. pH adjustments are done in different manners: (a) acidification based on stoichiometry to a pH of 4.4. The alkalinity is completely neutralized and the CO_2 released is removed through DC; however, a small amount of caustic is added to adjust pH; (b) overacidification to a pH of 3.8–4.0. Acid injection is more than the stoichiometric quantity required and caustic injection is necessary to adjust pH. This method eliminates scale-forming constituents completely, but poses the danger of severe corrosion if caustic injection malfunctions; and (c) underacidification to a pH of 5.0. Acid injection is less than the stoichiometric quantity required, leaving some alkalinity (15–20 ppm) in the makeup [31]. This method allows some scale formation, but the residual alkalinity is considered as buffer against corrosion and no caustic injection is necessary.

14.7.2 PROPORTIONAL FLOW CONTROL METHOD

In this method, the acid injection is based on the alkalinity and flow rate of makeup feed. Alkalinity is assumed to be constant, and acid dosing is regulated proportional to the flow of makeup feed so as to neutralize the total alkalinity. However, pH is measured regularly to make sure correct acid dosing is carried out. Alkalinity also has to be measured to make sure the acid injection is according to stoichiometry.

14.7.3 CASE STUDIES

14.7.3.1 Jeddah-I

Jeddah-I is a dual-purpose power and desalination plant with capacity of $2 \times 9500 \text{ m}^3/\text{day}$ and $2 \times 25 \text{ MW}$, and started operation in 1970. This plant was the first major MSF plant started in Saudi Arabia with little experience. With respect to scaling, Maadhah and Wojcik [32] reported that it suffered from both scaling and corrosion problems in brine heater and flash chambers. The reason was the incorrect dosing of acid due to inaccurate reading of pH and flow rates. Also, the TBT reached above design value of 120°C occasionally, which caused the formation of calcium sulfate scale in the brine heater tubes. The performance ratio was around 8.3 (designed value 9.5).

14.7.3.2 Jeddah-II

Jeddah-II is also a dual-purpose power and desalination plant, with a total desalination capacity of $38,000 \text{ m}^3/\text{day}$ and power production of 80 MW , and started operation in 1977. This plant was well operated based on acid injection less than the stoichiometric quantity, leaving alkalinity of 15–20 ppm in the makeup [31]. The performance ratio was around 9.9 compared to the design value of 9.3.

14.8 ADDITIVE TREATMENT

The additive treatment or threshold treatment comprises the injection of very small quantities of additives to the seawater makeup feed. Elliott [33] has extensively reviewed the early work on threshold agents. The mode of action of these threshold agents has not yet been fully explained but would appear to be due to the adsorption of the additive on the growing crystal nuclei which inhibits growth at the preferred nucleation sites and results in the formation of irregular, distorted crystals. Addadi [34] noticed that the required dosages of these additives vary from 5 wt.% in solution for the objective of habit modification up to 10 wt.% for total inhibition. Harris [35] discussed the effect of various additives in retarding the precipitation of alkaline scale (e.g., calcium carbonate and magnesium hydroxide) and sulfate scale in desalination plants. In the water treatment industry, these additives have been used successfully to control carbonate as well as sulfate scales.

14.8.1 LOW-TEMPERATURE ADDITIVES TREATMENT

Among the different types of additives to control scale formation in distillation plants, polyphosphates can be used for desalination plants up to the TBT of about 90°C. Above this temperature, the thermal degradation of polyphosphates begins and the additive will become ineffective. Proper additive dosage has to be determined to be able to utilize it effectively; otherwise lower dosage will increase scale problem and excessive dosage will form sludge and impair the thermal performance of the heat transfer tubes in the brine heater. However, the polyphosphates are susceptible to hydrolysis, and the rate of hydrolysis increases with temperature.

14.8.2 HIGH-TEMPERATURE ADDITIVES TREATMENT

The high-temperature additives (HTA) are organic polyelectrolytes that are stable at higher temperatures between 90°C and 112°C. Polymaleic acid (PMA) was found to overcome the disadvantage of polyphosphate and has the ability to withstand high temperatures and prevents the formation of alkaline scales. Low-molecular-weight polymeric carboxylic acid and phosphorous base alkaline antiscalants were developed as HTAs. It has become a common belief that these chemicals distort the lattice structure and, when adsorbed on a scale crystal, interfere either with the nucleation or the crystal growth process [36]. Polyphosphonate “phosphorous base alkaline group” does not hydrolyze as easily as the polyphosphate group due to the greater stability of the c-p bond in phosphonates as compared with the p-o bond in phosphates [37].

In a seeded crystal growth study on the evaluation of poly(acrylic acid) PAA of varying molecular weight, Amjad and Masler [38] reported that the molecular weight of polymers plays an important role in the inhibition of gypsum crystal growth from solution. The optimum effectiveness, determined by the induction time, occurred with a PAA molecular weight of 2100. Amjad [39], in another study, reported that the amount of gypsum scale deposited on the heat exchanger was found to be higher in the case of high-molecular-weight polyacrylates (240,000) compared to that obtained in the presence of lower molecular weight (2100) PAA.

Although effective in many applications, synthetic polymers such as PAA, PMA, polymethacrylic acid PMAA, like other scale control chemicals (e.g., polyphosphates and phosphonates, and so on), have low calcium tolerance, that is, they react with calcium ion to form the insoluble calcium-polymer salt.

14.9 HYBRID TREATMENT (ACID + ADDITIVE)

The hybrid scale control treatment method consists of a combination of acid and additive injection. The philosophy is to inject less than stoichiometric amount of acid to neutralize a substantial portion of total alkalinity (e.g., 80%–85%) in the seawater makeup feed followed by the appropriate quantities

of additive injection to prevent scale formation arising from residual alkalinity as well as from sulfates, depending on the TBT. The hybrid method is considered to provide the advantages of both acid treatment and additive treatment methods. In hybrid method, the underdosing of acid is employed that provides buffering action and protects against corrosion, as discussed earlier. Thus, the threat of corrosion of heat transfer tubes and other steel structures due to the accidental overdose of acid is greatly minimized, the chances of serious scale problem are avoided in the case of additive injection pump failure accidentally, and the thermal performance is better than additive-only plant and close to acid treatment plant. The hybrid method also reduces the frequency of acid cleaning and increases the plant life. Cox [40] described the technical and economic benefits of hybrid method.

14.9.1 CASE STUDIES OF HYBRID TREATMENT

Spanhaak et al. [41,42] presented the encouraging results of hybrid method at Texel and Terneuzen MSF plants. They reported that, at Texel plant, hybrid treatment with acid dose corresponding to neutralize 80% alkalinity and 3.5 ppm Belgard EV reduced iron losses by a factor of 10. At Terneuzen plant, acid dose corresponding to neutralize 90% alkalinity and 2.5 ppm Belgard EV reduced copper losses by a factor of five and iron losses by a factor of seven and operated for 18 months without any interruption and scaling [43].

Butt et al. [44] performed a systematic hybrid treatment trial on Desal Unit A of Ghazlan Power Plant. The units (three units produce 10,000 m³/day) were designed to operate at 112.8°C (235°F) TBT and use acid for the control of scale. Due to the nonavailability of well-trained and skilled operators, the plant management believed that the use acid might pose the danger of corrosion, so the units were switched to additive treatment. However, it took some time and effort, and after testing a number of additives, a suitable additive formulation (Albrivap-G) was identified that was successful and effective against the relatively high levels of iron in the makeup feed. The TBT temperature was brought down to 107.2°C, and Albrivap-G allowed operating the plant for 30 days after which acid cleaning was required. On-line acid cleaning was carried out at a recycle brine pH of 6.2–6.5.

The comparative field trials of additive-only and hybrid treatment were conducted on Desal Unit A under identical conditions. Albrivap-G trial was initiated using 12 ppm to the makeup feed, while hybrid trial used acid injection to neutralize 80% of alkalinity in the makeup along with Albrivap DSB at the rate of 3.0 ppm. Both Albrivap-G and Albrivap DSB were polyphosphate-based additives. Figure 14.7 shows the relative effectiveness of additive-only and the hybrid treatment in terms of heater shell pressure.

It can be observed that the scale buildup during additive-only trial was fast and reached the limiting value of 37 psia in 19 days. In hybrid trial, dramatic results were observed. The heater shell pressure barely reached the design value of 28.8 psia (far below the limiting value of 37 psia) even after 164 days.

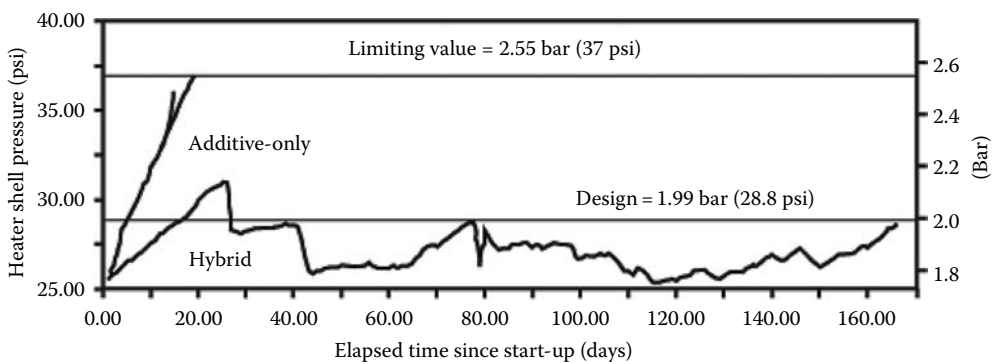


FIGURE 14.7 Variation in brine heater shell pressure with time during additive-alone and hybrid trials. (From Butt, F. et al., *Desalination*, 54, 307, 1985. With permission.)

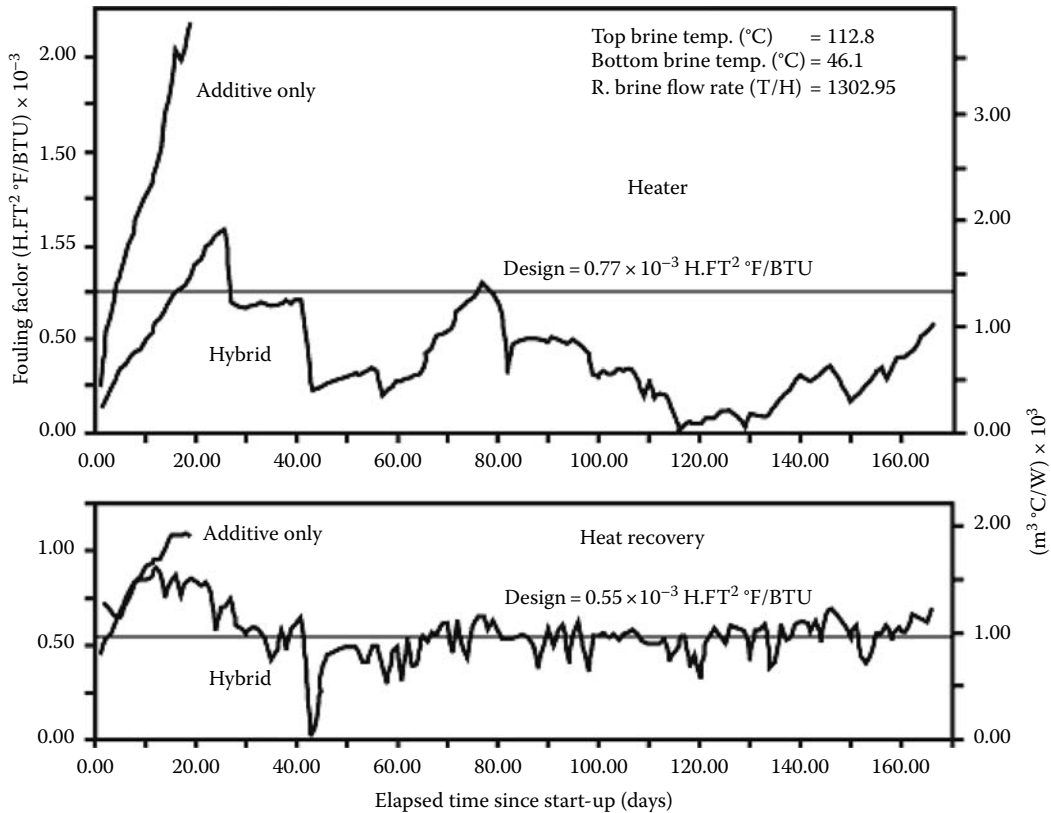


FIGURE 14.8 Variation in fouling factor with time during additive-only and hybrid trials. (From Butt, F. et al., *Desalination*, 54, 307, 1985. With permission.)

The thermal performance of both the trials is presented in Figure 14.8 in terms of fouling factors (FFs). In the case of additive-only trial, the brine heater FF reached design value of 3.9×10^{-4} $\text{m}^3\text{C/W}$, exceeding the design value by a factor of three in just 19 days and the FF of heat recovery section exceeded by a factor of two. In the case of hybrid trial, the heater FF increased rapidly in first 26 days and exceeded the design value. The sudden shutdown on day 27 brought the FF significantly below the design value, and further shutdowns intermittently maintained the FF below design value even after 164 days. The FF of heat recovery section was also found to be around design value after 164 days, demonstrating the superior performance of hybrid trial over additive-only treatment.

The hybrid trial provided adequate protection against the corrosion of copper alloy tubes and other plant internals as compared to additive-only trial. Upon the inspection of brine heater tubes, the soft and nonadherent type of white- to muddy-colored scale was observed which can be removed by wiping with fingers easily when wet. Beneath the soft scale deposit, a very thin but hard iron-rich layer was evident. However, the magnesium-based scale was predominant in the case of additive-only treatment compared to hybrid trial. The unit chemical treatment cost for hybrid treatment was about 50% lower than that of additive-only treatment besides superior thermal performance, resulting in the energy cost savings.

14.10 SURVEY ON SCALE CONTROL METHODS

A survey of scale control techniques was performed by contacting consultants, plant suppliers, and plant operators in the Arabian Gulf region, and also by searching published literature. A brief description of opinions provided by various organizations is presented here.

14.10.1 INPUT FROM CONSULTANTS

According to Wade [45] of Preece, Cardew, and Rider (PCR), the acid injection permits the TBT to be raised to about 115°C, “but at the risk of much greater corrosion rates.” He highlights that for a scale-free and corrosion-free operation, the recycle brine pH needs to be maintained in the narrow range of 7.7–7.8, which is difficult to achieve, “particularly where skilled operators are at a premium.” However, the acid-designed plants are thermally efficient as evident from the fouling factor allowance for heat recovery tubes, which is around $0.07 \times 10^{-3} \text{ m}^2\text{C/W}$. In the additive-dosed plants, the HTA allow the TBT to be raised up to 110°C. The pH of recycle brine is typically in the range of 8.5–9.0, resulting in low corrosion rates. Also, the fouling factor for the heat recovery section of an additive plant is in the range of $0.1\text{--}0.15 \times 10^{-3} \text{ m}^2\text{C/W}$. El-Saie [46], a consultant, always favors additive injection and he credits himself for having introduced Hagevap (a polyphosphate-based proprietary scale control chemical) in the MSF plants of Kuwait.

Fichtner Consulting Engineers favors the dual temperature design, such that a minimum production can be assured by operating the plant at 90°C, while the advantage of HTA can be realized by operating at higher temperatures. In Barba’s opinion [47], both acid and additive treatments are the safe and reliable methods of scale control. However, he is concerned about pollution caused by additives and corrosion due to dissolved oxygen which should be eliminated from recycle brine. He suggests that repeated shutdowns and startups should be avoided to prevent plant corrosion.

14.10.2 PLANT SUPPLIERS

Envirogenics has built several plants, both acid and additive dosed. Based on a survey [48] Envirogenics responded that, “as a company we are generally bound by the client or consultants specifications as to the type of scale control method.” The trend is to specify additive-dosed system probably because (a) additives are safe to handle and (b) the plants can operate with the recycle brine pH of more than 8, thereby eliminating the threat of corrosion. However, they mentioned that if intelligent and concerned operators are available, the acid dosing has the following advantages: (a) lower cost, (b) the possibility of operating at higher TBT, and (c) in the case of the malfunctioning of additive injection system, some scale will form, but the recycle brine pH can be easily adjusted to remove the scale formed in few hours. The preferred method of acid injection is less than stoichiometric amount of acid so as to leave 10–15 ppm of residual alkalinity in the makeup. This method minimizes chemical injection cost and greatly reduces the risk of plant corrosion.

Sasakura reported an interesting case of switch over from polyphosphate to acid dosing. Sasakura built a polyphosphate-dosed 2650 ton/day plant for Matsushima Mine Co. at Nagasaki, Japan. The unit was operated for about 2 years and it was observed that the design output and GOR could not be sustained and acid cleaning was frequently needed. After installing decarbonator, deaerator, and acid injection system in 1969, the plant was switched to acid-dosing system. Sasakura reported that the plant was operated nonstop with only 2 weeks of scheduled shutdown every year. Sidem clearly favors additive injection instead of acid-dosing system. Their response is as follows: although acid treatment allows a lower investment cost, but it is very difficult to control proper acid injection. If acid injection is more than stoichiometric amount, serious corrosion problems will be encountered, and if it is less than stoichiometric quantity, serious scale problems will occur. The continuous accurate measurement of pH in large flows is not easy and electrodes are generally not reliable. Additive dosing allows minimizing the risks associated with an underdosing or overdosing of acid.

Most of the plants in Italy built by Fraco Tosi are based on acid dosing while those built in the Middle East are additive dosed. Franco Tosi believes that if a plant is to be located in an area where skilled operators are available, acid treatment is preferable. However, if the skilled operators are scarce, and the plant is to be operated at TBT in the range of 90°C–100°C, additive treatment is more suitable.

14.10.3 PLANT OPERATORS

The response received from plant operators based on the survey conducted by contacting agencies responsible for the operation and maintenance of thermal desalination plants mainly within the Arabian Gulf region [48] is summarized here. The plants in Bahrain, Abu Dhabi, and Kuwait are mostly based on low-temperature additive—polyphosphate. The reason for opting additive treatment method is due to safe operation with available operators in the region. Consultant Dr. El-Saie has also supported additive treatment for the plants in that region (Arabian Gulf) mainly because of the lack of skilled operators and no acid manufacturing facilities. The operation and maintenance personnel of Bahrain remarked that the liberal lining of water boxes and flash chambers with superior metals was necessary to ensure trouble-free acid treatment operation. The initial operation of MSF plants was on Hagevap at the rate of 4.5 ppm, but the thermal performance was poor. In 1981, high-temperature additive Belgard EVN was used that increased the production by 17%. Qatar was one of the first Gulf countries to adopt seawater desalination based on MSF process in 1959. The two units of capacity 0.15 MIGD (million imperial gallons per day) were based on acid treatment. Diamond [49] reported that the handling and dosing of imported acid presented enormous problems and caused the serious corrosion of plant internals. The next generation of MSF plants was based on polyphosphate injection for the control of alkaline scale. But the polyphosphate operation was also found to be unsatisfactory. The units had to be acid-cleaned every 1–2 months which contributed to costly tube leakages and plant downtime [49]. In another study, Diamond [50] reported that a 10-month trial of Belgard EV at 5 ppm dosage was carried out in 1975–1976 at 105°C–110°C in a newly installed MSF unit at Ras Abu Fontas and was found to be highly satisfactory. Various additives evaluated by the team at Ras Abu Fontas station were: Belgard EV-100, Flocon 247, Calgon, and Albrivap. At Dubai, the consultant specified Albrivap-A and Belgard EV for low- and high-temperature operations, respectively, on their Wier-Westgarth units. Albrivap-A at 4.0 ppm gave reasonable performance; however, it was found to have two undesirable features: (1) Albrivap-A being in powder form, its mixing was difficult and (2) being polyphosphate based, it is good only for low-temperature operation. In 1982, Albrivap-A was completely replaced by Albrivap DSB. This new additive has three advantages: (1) it is in liquid form and therefore easy to inject, (2) at 2.0–2.5 ppm dose level, it is competitive with Albrivap-A, and (3) it permits high-temperature operation.

14.11 CONCLUDING REMARKS ON SCALE CONTROL METHODS

Each method of scale control has its own advantages and disadvantages. In the case of acid treatment, if the dosage of acid injection is adjusted properly, it neutralizes the total alkalinity and renders the operation practically scale free. But additive-alone treatment cannot eliminate scale formation, it can only minimize. Since no alkaline scale will form in properly acid-dosed plants, the need for acid cleaning is reduced and the thermal performance is improved, consequently lowering the operating cost. However, if any malfunctioning of acid-dosed system happens, the plant suffers from serious corrosion. In acid-dosed plants, acid injection can be monitored by measuring the pH of the recycle brine, whereas in additive-alone treatment, the monitoring of additive present in the system is difficult.

14.12 DEVELOPMENT OF SCALE CONTROL INHIBITORS

The performance of additives in relation to their chemical structure and functional groups has been investigated extensively. Buehrer [51] discussed the effect of small quantities of sodium-hexa-metaphosphate (SHMP) and mentioned that 2 ppm of SHMP can completely prevent the precipitation of 200 ppm of calcium carbonate at room temperature. Much work was carried out [52–54] with the homo- and copolymers of acrylic acid, which were used for the prevention of scale in industrial water recirculation systems. Scale formation was prevented to a certain extent but none of the additives tested had a greater activity than polyphosphate. Reddy and Nancollas [55] studied several

phosphonates to inhibit the crystal growth of calcite in evaporative desalination processes. The growth rate of inhibition was found to be a function of phosphonate dosage at levels.

Busch [56] developed a formulation to control scale buildup on metallic surfaces. The principle components of the formulation include a chelant, polymeric conditioners, a gluconate, a triazole, and sodium sulfate. The relationship between the structure and performance of high-temperature MSF plant scale control additives was studied by Walinsky et al. [57]. They evaluated low-molecular-weight polymers (MW = 500–10,000) of maleic, fumaric, itaconic, methacrylic, acrylic, and vinyl-sulfonic acid to prevent alkaline scale formation. The major findings are as follows: (a) the overall scale control was most effectively demonstrated by low-molecular-weight maleic-based polymers, (b) monomeric antiscalants and polyvinylsulfonic acids were mostly ineffective against magnesium hydroxide, and (c) hydroxyethylidene diphosphonic acid and polyitaconic acid (MW-7000) formed insoluble calcium and sodium complexes which precipitated out from seawater probably due to poor compatibility or temperature-dependent solubility in seawater.

Davey [58] presented an excellent review on the role of additives in precipitation processes. He pointed out that most of the literature available is regarding the precipitation inhibition of sparingly soluble inorganic substances. He classified the various additives studied into the following four groups: (1) low-molecular-weight organic substances, for example, citric, succinic, tartaric acids, and nitrilotrimethylene phosphonic acid; (2) low-molecular-weight inorganic materials, such as sodium triphosphate and sodium pyrophosphate; (3) long-chain polymeric materials with acidic and hydroxylic side groups, for example, polyacrylic acid, polyglutamic acid (PGA), and alginic; and (4) proteinaceous materials, for example, gelatin, statherin, phosphoproteins, and polyribonucleotides. He reviewed the effect of various additives (polyacrylic acid, sodium triphosphate, polymethacrylic acid, and sodium pyrophosphate) on the precipitation behavior of different supersaturated solutions (strontium sulfate, gypsum, and calcium oxalate) and concluded that the active additives invariably extend the induction time. He explains that the presence of active additive in the system may result in adsorption onto embryos that reduce the speed at which they pass through the critical size barrier, and thus reduces the rate of nucleation. Leung and Nancollas [59] reported the results of adsorption of nitrilotrimethylenephosphonic acid on barium sulfate crystals and concluded that only 5% surface coverage is necessary for the complete inhibition of crystal growth.

Gill and Varsanik [60] pointed out that a close comparison of the inhibitors and the mineral they inhibit or regulate shows some structural correlation. Various inhibitors have differing degrees of effectiveness even for different hydration forms of the same scale. Two crystallographic forms of calcium sulfate, dihydrate, and hemihydrate have been shown to have markedly distinct interactions with inhibitors like polyvinyl sulfonate (PVS) and polyglutamic acid (PGA) with respect to the change of the crystal habit. PGA is more effective than PVS for dihydrate phase, while the reverse is true for the hemihydrate phase. They attributed the changes in morphologies and inhibition to the close association of the negatively charged groups on the inhibitor and positively charged calcium ions in the crystal lattice of calcium sulfate hemihydrate/dihydrate.

It has been reported that structural matching between the functional groups of the additives and the cations at the crystal surface plays an important role in determining the effectiveness of the additives [39,58]. The molecular structures of some antiscalants are shown in Figure 14.9.

Amjad [61] examined a variety of polymeric inhibitors to prevent gypsum scale formation on heat exchange surfaces. He reported that scale growth experiments in the presence of low levels of acrylic acid-based copolymers clearly indicate that acrylic acid copolymer showed excellent inhibitory property compared to acrylic acid/acrylate ester, acrylic acid/2-acrylamido-2-methyl propane sulfonic acid, maleic acid copolymer, and maleic anhydride/sulfonated styrene.

Polycarboxyl-type antiscalants, in general, have a tendency to become less effective in the presence of multivalent metal ions such as Ca^{++} and Mg^{++} in sea water. Fukumoto et al. [62] developed a new antiscalant AQUAKREEN KC-550 by the copolymerization technology and has much higher stability against such multivalent ions. Amjad [63], in another study, presented a comprehensive overview of scale inhibition in desalination applications. The study covers a general discussion on

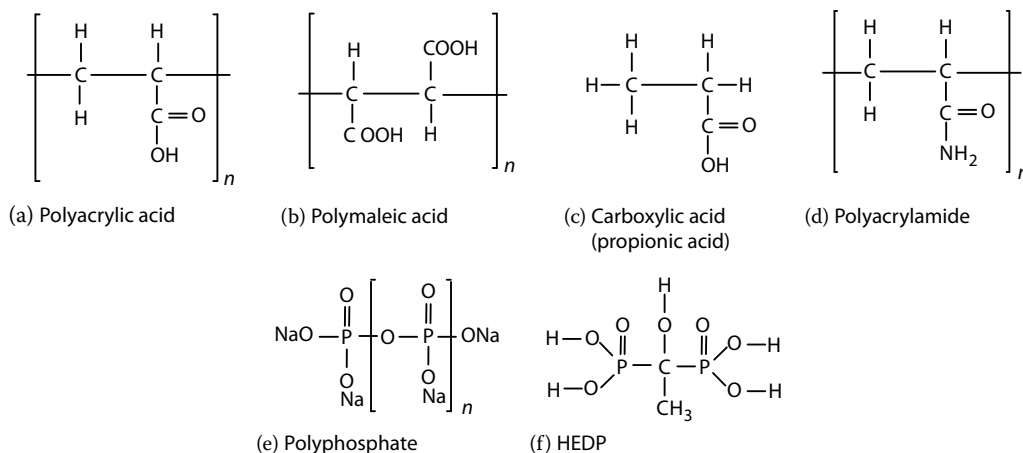


FIGURE 14.9 Structural characteristics of antiscalants. (From Amjad, Z. Scale inhibition in desalination applications: An overview CORROSION 1996, Paper No. 230, NACE International, Houston, TX, 1996. With permission.)

major desalination processes, performance comparisons, and problems encountered in each process along with advantages and disadvantages. The main focus was on the fouling by mineral scales, colloidal matter, and metal hydroxides, and the role of the foulant control agent in the desalination industry. He concluded that various types of antiscalants are employed to control fouling such as polyphosphates, phosphonates, acrylic, maleic homopolymers, copolymers, and blended products containing phosphonates and copolymers. The blended products demonstrated the best overall performance in preventing the deposition of foulants on heat exchanger and membrane surfaces. Gill [64] presented a novel chemical, polyamino polyether methylenephosphonate (PAPEMP), an additive that can reduce or eliminate acid injection and can control both calcium carbonate and calcium sulfate scales besides showing effectiveness against fouling by silica and iron hydroxides. PAPEMP has also indicated high tolerance for calcium ions.

Benchtop screening tests on various silica inhibition chemistries are reported, with emphasis on additives with dendrimeric or polymeric structure and backbone by Neofotistou [65]. The inhibition performance of STARBURST polyaminoamide (PAMAM) dendrimers of generations 0.5, 1, 1.5, 2, and 2.5 were studied. Experimental results show that inhibition efficiency mainly depends on structural features of PAMAM's and dose levels. Poly(2-ethyl-2-oxazoline) polymers of a variety of molecular weights were also investigated as potential SiO_2 inhibitors.

Euvrard et al. [66] discussed the silica formation, deposition, and its inhibition in desalination applications by conducting the kinetic investigation of silica formation and the morphometric characteristics of deposits. The inhibition performance of chemical inhibitors [phosphinopolycarboxylic acid (PPCA) and diethylenetriaminepentamethylenephosphonic acid (DETPMP)] were investigated. Experimental results indicated that the deposition of silica was highly delayed and the morphological characteristics of the deposit such as size were affected by the presence of inhibitors. An improved method of inhibiting corrosion and calcium sulfate and calcium carbonate scaling in thermal and membrane desalination processes has been invented by Dave et al. [67]. This method includes adding a composition having an oligomeric phosphinosuccinic acid to seawater or recirculation brine in a desalting process to produce water for drinking and industrial applications. The method also includes adding a composition, including mono-, bis-, and oligomeric phosphinosuccinic acid adducts, to the desalting process.

Martinod et al. [68] presented the understanding of scaling phenomena in seawater and the effects of green inhibitors. In order to understand the processes occurring at the liquid surface interface, a procedure has been developed to follow in situ and in real time the growth of scale particles in the micrometer size range and to quantify the effects of inhibitor on the crystal evolution. Experiments

were carried out with a green additive, PMA, at a concentration of 1 and 4 ppm and with PPCA (commercial phosphonate inhibitor) used as inhibitor reference. On the one hand, results showed that PMA reduces the formation of scale by acting on the nucleation and growth process namely at a concentration of 4 ppm. In this study, a comprehensive description of the inhibitor/surface interactions was presented. The role of the green additive in affecting the interface was discussed in relation to the principal mechanisms by which the inhibitors function.

14.13 SUMMARY

An overview on scale formation and control in thermal desalination processes has been presented. It describes the mechanism of scale formation and scale prediction techniques for brines at temperatures encountered in thermal desalination plants such as MSF and MED. The scale control methods utilized in the desalination industry were highlighted along with the opinion of different stakeholders (like desalination plant operators, consultants, and plant suppliers) on the choice of scale control method. Each type of scale control method is discussed with case studies. At the end, a brief discussion on the development of scale control inhibitors and their effectiveness with reference to thermal desalination systems is presented.

ACKNOWLEDGMENT

The authors acknowledge support from the Center for Refining and Petrochemicals, Research Institute of King Fahd University of Petroleum and Minerals, Dhahran, Saudi Arabia.

REFERENCES

1. Buros, O. K. *The Desalting ABC's*. Prepared for International Desalination Association, Topsfield, MA (1990).
2. Cowan, J. and Weintritt, D. J. *Water Formed Scale Deposits*. Gulf Publishing Company, Houston, TX (1976).
3. Howe, E. D. *Fundamentals of Water Desalination*. Marcel Dekker Inc., New York (1974).
4. Khan, A. H. *Desalination Processes and Multi-Stage-Flash Distillation Practice*. Elsevier, Amsterdam, the Netherlands (1986).
5. Spiegler, L. *Principles of Desalination*. Academic Press, New York (1980).
6. Mullin, J. W. *Crystallisation*. Butterworths, London, U.K. (1972).
7. Khamskii, E. V. *Crystallisation from Solutions*. Consultants Bureau, New York (A Division of Plenum Publishing Corporation) (1969).
8. Atkins, P. W. *Physical Chemistry*, 4th edn. Oxford University Press, London, U.K. (1995).
9. Horvath, A. L. (Ed.). *Handbook of Aqueous Electrolyte Solutions, Physical Properties Estimation and Correlation Methods*. Ellis Horwood Publishers, U.K. (1985).
10. Pytkowicz, R. M. *Thermodynamics of Aqueous Systems with Industrial Applications*, Newman, S. A. (Ed.). American Chemical Society Symposium Series No. 133, pp. 561–567, Washington, DC (1980).
11. Mullin, J. W. (1961). *Crystallisation*. Butterworths, London, U.K. (1980).
12. Ostwald, W. The formation and changes of solids. *Z. Phys Chem*, 34, 493 (1900).
13. Miers, H. A. and Isaac, F. J. The refractive indices of crystallising solutions, with a special reference to the passage from the metastable to the labile condition. *J Chem Soc*, 89, 413–454 (1906).
14. Tovbin, M. V. and Kransnova, S. I. Stability of super saturated solutions of salts. *Zh Fiz Khim*, 25, 161–166 (1951).
15. Ryzner, J. W. A new index for determining amount of calcium carbonate scale formed by a water. *J Am Waste Water Assoc*, 36, 472–478 (1944).
16. Oddo, J. E. and Tomson, M. B. Simplified calculation of CaCO₃ saturation at high temperatures and pressures in brine solutions. *J Petro Tech*, 34(7), 1583–1590 (July 1982).
17. Valone, W. F. and Skillern, K. R. A improved technique for predicting the severity of calcium carbonate. *SPE of AIME International Oil Field and Geothermal Chemistry Symposium*, Dallas, TX (1982).
18. Kline, W. E. Evaluating tendencies of calcium carbonate scale in wet oil producers. Exxon Production Research Co. Report, Houston, TX, March (1988).

19. Kline, W. E. Field testing of a method for predicting calcium carbonate scale. Exxon Production Research Co. Report, Houston, TX, March (1989).
20. Stiff, H. A. Jr. and Davis, L. E. A method for predicting the tendency of oilfield waters to deposit calcium sulfate. *Petro Trans*, 195, 25–28 (1952).
21. Raju, K. U. G. and Atkinson, G. Thermodynamics of scale mineral solubilities—1, BaSO₄ in H₂O and aqueous NaCl. *J Chem Eng Data*, 33, 490–499 (1988).
22. Raju, K. U. G. and Atkinson, G. Thermodynamics of scale mineral solubilities—1, SrSO₄ in H₂O and aqueous NaCl. *J Chem Eng Data*, 34, 361–370 (1989).
23. Nielson, L. E. *Predicting the Properties of Mixtures: Mixing Rules in Science and Engineering*. Marcel Dekker Publishers, New York (1978).
24. Ting-Po, I. and Nancollas, G. H. EQUIL—A general computational method for the calculation of solution equilibria. *Anal Chem*, 44, 1940–1950 (1972).
25. Truesdell, A. H. and Jones, A. H. WATEQ, A computer program for calculating chemical equilibria of natural waters. U.S. Department of Commerce, National Technical Information Service, PB 220 464 (1974).
26. Kharaka, Y. K., Gunter, W. D., Agarwal, P. K., Perkins, E. H., and Debraall, J. D. SOLMINEQ 88: A computer program for geothermal modeling of water rock interactions. U.S. Geological Survey, Water Resources Investigations Report No. 88-4227, Menlo Park, CA (1988).
27. Criss, C. M. and Cobble, J. W. The thermodynamic properties of high temperature aqueous solutions. *J Am Chem Soc*, M86, 5390–5393 (1961).
28. Naumav, G. B., Ryzhenko, B. N., and Khoda-Kovey, I. L., *Handbook of Thermodynamic Data*. U.S. Department of Commerce, NTIS, Springfield, VA (1974).
29. Barner, H. E. and Scheuerman, R. V. *Handbook of Thermochemical Data for Compounds and Aqueous Species*. John Wiley & Sons, New York (1978).
30. Yeboah, Y. D., Somuah, S. K., and Saeed, M. R. A new and reliable model for predicting oilfield scale formation. SPE 25166, *SPE International Symposium on Oilfield Chemistry*, New Orleans, LA (March 2–5, 1993).
31. Nada, N. Operating experience of MSF plants in Saudi Arabia. Presented at *the International Congress on Desal and Water Re-Use*, Bahrain Saudi Arabia (November–December, 1981).
32. Maadhah, A. G. and Wojcik, C. K. Performance study of water desalination methods in Saudi Arabia. *Desalination*, 39, 205–217 (1981).
33. Elliot, M. N. Scale control by threshold treatment. *Desalination*, 8, 231–236 (1970).
34. Addadi, L., Weinstein, S., Gati, E., Weissbuck, I., and Lahov, M. Resolution of conglomerates with the assistance of tailor-made impurities. Generality and mechanistic aspects of the “Rule of reversal”. A new method for assignment of absolute configuration. *J Am Chem Soc*, 104, 4610–4617 (1982).
35. Porteous, A. *Desalination Technology: Developments and Practice*. Applied Science Publishers, London, U.K. (1983).
36. Shams El Din, A. M. and Mohammed, R. A. Brine and scale chemistry in MSF distillers. *Desalination*, 99, 73–111 (1994).
37. Hamed, O. A., Al-Sofi, M. A., Mustafa, G. M., and Dalvi, A. G. The performance of different antiscalants in multi-stage-flash distillers. Presented in *Second Acquired Experience Symposium*, Al-Jubail, Saudi Arabia (1997).
38. Amjad, Z. and Masler, W. F. Inhibition of calcium sulfate dihydrate crystal growth by polyacrylates. CORROSION/1985, Paper No. 357, NACE International, Houston, TX (1985).
39. Amjad, Z. Calcium sulfate dehydrate (gypsum) scale formation on heat exchanger surfaces: The influence of scale inhibitors. *J Colloid Interface Sci*, 123, 523 (1988).
40. Cox, B. The chemical treatment of seawater feed for MSF plants. *Pure Water Magazine of IDEA*, Jul.–Aug. (1982).
41. Spanhaak, G., Finan, M. A., and Harris, A. Extended operation experience of the use of acid and a high temperature scale control additive in a European MSF plant. In *Proceedings of the 6th International Symposium on Fresh Water from Sea*, Vol. 2, pp. 289–298, Las Palmas, Spain (1978).
42. Spanhaak, G. The application of a high temperature scale control additive to a European MSF plant. *Desalination*, 23, 455–464 (1979).
43. Romeijn, A. A. Belgard EV field trials in the multi-stage-flash evaporators in Terneuzen, Holland. In *Proceedings of the 6th International Symposium on Fresh Water from Sea*, Vol. 2, pp. 241–256, Las Palmas, Spain (1978).
44. Butt, F., Rahman, F., Al-Abdallah, A., Al-Zahrani, H., Maadhah, A., and Amin, M. B. Field trials of hybrid acid-additive treatment for control of scale in MSF plants. *Desalination*, 54, 307–320 (1985).
45. Wade, N. M. A review of scale control methods. *Desalination*, 31, 309–320 (1979).

46. El-Saie, M. H. A. Secret of success using Hagevap (Polyphosphate) treatment and deaeration of seawater feed in flash distillation plants. In *Proceedings of the 3rd International Symposium on Fresh Water from Sea*, Vol. 1, pp. 405–416, Dubrovnik, Yugoslavia (1970).
47. Barba, D. et al. Porto Torres desalting plants. In *Proceedings of the 5th International Symposium on Fresh Water from Sea*, Vol. 2, pp. 33–48, Alghero, Italy (1976).
48. KFUPM-RI, Survey of the state-of-the-art of scale control techniques in MSF desalination plants. The Research Institute, King Fahd University of Petroleum & Minerals, Dhahran, Saudi Arabia (1983).
49. Diamond, M. D. Problems relating to the operation and maintenance of large MSF desalination plants. Presented at the *International Congress on Desal and Water Re-Use*, Bahrain Saudi Arabia (November–December, 1981).
50. Diamond, M. D. and Lee, W. S. Antiscalant additives at high temperature operation. Presented at the *10th Annual Conference of WSIA*, Vol. 1, Session IV, Hawaii (1982).
51. Buehrer, T. F. and Reitemeier, C. F. The inhibiting action of minute amounts of Sodium hexametaphosphate. *J Phys Chem*, 44, 535–551 (1940).
52. Herbert, L. S., Rolfe, P. E., and Sterns, U. J. Scale prevention by polymer additives. In *Proceedings of the 1st International Symposium on Water Desalination*, pp. 39–52, Washington, DC (1965).
53. Hanson, D., Ram, A., Porck, M., and Carmon, S. Characterization of additives inhibiting scale formation in desalination plants. Advances in desalination. In *Proceedings of the 7th National Symposium on Water Desalination*, pp. 39–52, Ayelet Hashahar, Israel (1970).
54. Flesher, D., Streatfield, E. L., Pearce, A. S., and Hydes, O. D. Polymeric additives as scale preventatives. In *Proceedings of the 3rd International Symposium on Fresh water from the Sea*, Vol. 1, pp. 493–504, Dubrovnik, Yugoslavia (1970).
55. Reddy, M. M. and Nancollas, G. H. Calcite crystal growth inhibition by phosphonates. *Desalination*, 12, 61–73 (1973).
56. Busch, B. D. U.S. Patent 4,279,768, 21, July (1981).
57. Walinsky, S. W., Morton, B. J., and O'Neill, J. J. Structure-performance relationship of high-temperature MSF scale control additives. In *Proceedings of the International Congress on Desalination and Water Re-use*, Vol. 1, p. 203, Manama, Bahrain (1981).
58. Davey, R. J. The role of additives in precipitation processes. In *Industrial Crystallisation*, Jancic, S. J. and De Jong, E. J. (Eds.), pp. 123–135. North-Holland Publishing Co., Amsterdam, the Netherlands (1982).
59. Leung, W. H. and Nancollas, G. H. Nitrotrifluoromethylphosphonic acid adsorption on barium sulfate crystals and its influence on crystal growth. *J Cryst Growth*, 44, 163–167 (1978).
60. Gill, J. S. and Varsanik, R. G. Computer modelling of the specific matching between scale inhibitors and crystal structure of scale forming minerals. *J Crystal Growth*, 76, 57–62 (1986).
61. Amjad, Z. Calcium sulfate dihydrate scale formation on heat exchanger surfaces in the presence of inhibitors. *Mater Perform*, 28, 52–55 (1989).
62. Fukumoto, Y., Isobe, K., Moriyama, N., and Pujadas, F. Performance test of a new antiscalant Aquakreen KC-550 under high temperature conditions at the MSF desalination plant in Dubai. *Desalination* 83, 65–75 (1991).
63. Amjad, Z. Scale inhibition in desalination applications: An overview. CORROSION/1996, Paper No. 230, NACE International, Houston, TX (1996).
64. Gill, J. S. A novel inhibitor for scale control in water desalination. *Desalination*, 124, 43–50 (1999).
65. Neofotistou, E. and Demadis, K. D. Use of antiscalants for mitigation of silica (SiO₂) fouling and deposition: Fundamentals and applications in desalination systems. *Desalination*, 167, 257–272 (2004).
66. Euvrard, M., Hadi, L., and Foissy, A. Influence of PPCA (phosphinopolycarboxylic acid) and DETPMP (diethylenetriaminepentamethylenephosphonic acid) on silica fouling. *Desalination*, 205, 114–123 (2007).
67. Dave, B. B., Rao, N., Yang, M., Grattan, D. A., and Blokker, P. Method of inhibiting scale formation and deposition in desalination systems. U.S. Pat. Appl. Publ. (2008), 9pp. Application: US 2007-622054 20070111.
68. Martinod, A., Euvrard, M., Foissy, A., and Neville, A. Progressing the understanding of chemical inhibition of mineral scale by green inhibitors. *Desalination*, 220, 345–352 (2008).

15 Boiler Water Treatment

Bruce T. Ketrick, Sr.

CONTENTS

15.1	Boiler System.....	298
15.1.1	Pretreatment	298
15.1.1.1	Clarification	298
15.1.1.2	Filtration	299
15.1.2	Ion Exchange.....	301
15.1.3	Reverse Osmosis	305
15.2	Boiler Water Treatment Programs.....	306
15.2.1	Feed Water System.....	306
15.2.1.1	Feed Water Tank	306
15.2.2	Oxygen Scavengers	308
15.3	Scale and Deposit Control	310
15.3.1	Precipitating Program.....	310
15.3.2	Chelant Program.....	311
15.3.3	Dispersant Program.....	312
15.3.4	Dispersants	312
15.3.5	Condensate Treatment.....	313
15.4	Chemical Feed Points	316
15.5	Summary	317
	References.....	317

Boiler water treatment encompasses the beneficial conditioning, both mechanical and chemical, of water used to generate steam or hot water in a boiler. The treatment process begins with the initial step of water preparation (pretreatment) and continues up to the final step of condensate return blending with makeup water to become feed water. Therefore, the boiler water treatment program has to consider the impurities in the water, the design of the boiler system, the pretreatment equipment, the boiler design, the steam purpose, the steam contact, the condensate return line system design, the chemical feed system, chemical feed points, chemical treatment products, and plant capabilities. All of these come into play in determining the parameters of the boiler water treatment program.

Paramount to all of this is economics. The insufficient treatment of boiler water is extremely costly, both in terms of fuel costs and in equipment maintenance. The two most important economic issues for the owner of a boiler are efficiency (fuel and water usage) and equipment longevity (maintaining internal surfaces clean of scale, deposits, and corrosion). As the quality of the makeup water to the boiler is improved, the potential for the formation of scale and deposits is reduced. This, in turn, maintains a cleaner internal surface, which reduces the potential for fuel loss. By minimizing corrosion in the system, water loss is also minimized, while maintaining the integrity of the boiler system metal. The minimization of scale and corrosion, therefore, equates into maximizing both efficiency and system integrity. This chapter addresses the various aspects of boiler water treatment, including pretreatment, treatment programs, and product applications.

15.1 BOILER SYSTEM

Figure 15.1 shows the flow diagram of a typical boiler system. The detailed description of the various parts of the boiler system is presented next.

15.1.1 PRETREATMENT

Pretreatment encompasses the process by which the water used as makeup to the boiler is conditioned to improve its quality. Therefore, this can include any or all of the following: clarification, filtration, ultrafiltration, water softening, dealcalization, reverse osmosis (RO), and demineralization.

15.1.1.1 Clarification

The first step in pretreatment is clarification. Where a municipal water supply is used as the makeup water source, clarification is performed by the municipality. As such, this is usually not a concern for the boiler water treatment program. However, numerous systems collect makeup water from surface and well water sources. These systems may have to consider the use of clarification to remove suspended solids from the water. Suspended solids from water that is not clarified will contribute a considerable amount of sludge to the boiler. Clarification is usually accomplished by adding a primary coagulant to the water that combines with the solids in the water to form either larger particles (flocs) or precipitates followed by mechanical removal. Table 15.1 lists the primary coagulants used in clarification.

The primary coagulants listed in Table 15.1 combine with suspended solids in the water, which then settle out of the water and are mechanically collected in clarifiers as sludge. This reduces the solids loading in the water. Problems with clarification are overfeed of the coagulant and insufficient solids removal. Overfeed of the coagulant can occur during periods when the water temperature drops below 50°F. The reaction time for most aluminum salts is directly related to the water temperature. When the water temperature drops, the reaction time increases. The usual result is an overfeed of aluminum salts in order to achieve the desired water clarity.

Excess aluminum salts can then continue to react as the water travels down the pipes and precipitate in the lines, eventually either causing flow restrictions or sloughing off and creating line blockages. Excess aluminum ions can pass through the system to the water softener and bind to the resin bead, diminishing ion exchange capacity. Reduced ion exchange capacity is also a problem where iron salts are overfed, as iron ions will also attach to the resin bead, blocking sites for the desired ion exchange.

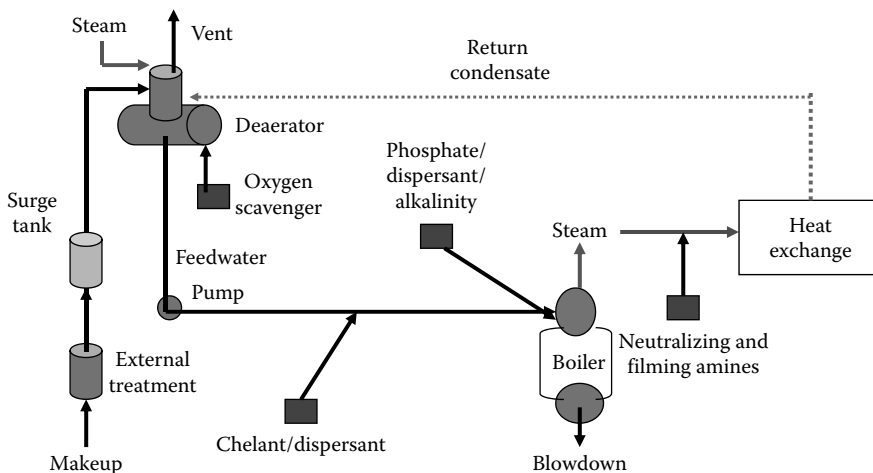


FIGURE 15.1 Boiler system flow diagram. (Courtesy of Guardian CSC, York, Pennsylvania, Water Processing Training Program.)

TABLE 15.1
List of Primary Coagulant Used in Clarification

Name	Formula	Commercial Strength	Grades Available
Aluminum sulfate	$Al_2(SO_4)_3 \cdot 18H_2O$	71% Al_2O_3 (liquid is 17%)	Lump, powder, granules, liquid
Sodium aluminate	$Na_2Al_2O_4$	55% Al_2O_3	Crystals
Ammonium alum	$Al_2(SO_4)_3(NH_4)_2SO_4 \cdot 24H_2O$	11% Al_2O_3	Lump, powder
Copperas	$FeSO_4 \cdot 7H_2O$	55% $FeSO_4$	Crystals, granules
Ferric sulfate	$Fe_2(SO_4)_3$	90% $Fe_2(SO_4)_3$	Powder, granules
Ferric chloride	$FeCl_3 \cdot 6H_2O$	60% $FeCl_3$	Crystals
Magnesium oxide	MgO	85% MgO	Powder
Bentonite	$Al_2O_3 \cdot 4SiO_2 \cdot H_2O$	—	Powder
Sodium silicate	$Na_2O \cdot 3SiO_2$	38° Bé	Liquid solution

Source: Cotton, I., Clarification products - AWT TRTM, Rockville, MD, pp. 2–16, 2001.

A solution to this problem obviously is not to overfeed the coagulant. However, this may mean that the clarity of the water is also compromised. In this case, the addition of a second coagulant aid, such as a low-molecular-weight cationic polymer, DADMAC (poly-diallyldimethylammonium chloride), or other polymer that can improve clarity in cold water and allow the reduction of the primary coagulant feed, is the solution. The key again is to make sure that excess metal ions have been reduced in the water. Coagulation does not remove all of the suspended solids in the water. Filtration is usually the next step in water preparation.

15.1.1.2 Filtration

Filtration is the mechanical removal of suspended solids from a fluid by means of a pressurized flow through a permeable medium. The amount and size of particles removed is based on the type of filtration media. Consider that clarification takes out the larger solids from the water. Filtration then removes more of the remaining suspended solids from the water. The degree of removal of the suspended solids is based on the size, type, and design of the filter. Boiler water treatment programs for boilers that operate under 300 psi (per square inch) usually only require the removal of suspended solids down to between 1 and 5 micron (micron (μ) = 10^{-6} m). Table 15.2 lists various types of filtration used in boiler pretreatment process.

The selection of the type of filtration is based on the remaining solids or water impurities that need to be removed. The following section presents discussion on the advantages and disadvantages of filtration process.

TABLE 15.2
Filtration Types

Types of Filtration

Aggregate: Media is a nonhydrous aluminum silicate.

Multilayered: Multiple layers of media distinctively layered with the coarsest media on the top.

Sand: Sand media where filtration is done on the surface.

Carbon: Activated carbon is used as the media for the removal of organics.

Cartridge filtration: Cartridge is designed to remove a specific size or type of particle.

Cyclonic: Centrifugal force separates solids down to approx. 50 μ .

Source: Ketrick, B., Types of filters, Internal Training Program, Guardian CSC, York, PA.

Aggregate filtration uses a magnesium-silicate-based media. The media is very light and porous. It has an appearance similar to a gray pumice. This media is housed in a tank similar to a water softener. The pros are that the aggregate filter is able to remove solids down to $1\ \mu$, takes a small footprint, and removes solids over the entire volume of the bed. The disadvantages are that the media is very light and can easily be backwashed out of the tank. If the flow regulator is removed, the bed can plug easily; it does not remove either organics or chlorine and the media will physically break down over time, requiring replacement every few years, based on backwash demand cycles. Aggregate filters are installed instead of or just after raw water clarification and before a water softener. Multilayered filtration is a series of layers of media, each layer being smaller in size than the layer preceding it. This allows a higher flow rate than using a single media size for filtration. It also allows the filter to be designed to remove solids down to a specific size. Multilayered filters perform the same function as the aggregate filter, but are more expensive to install and require a large footprint.

Sand filtration is a common filter media. Solids removal is based on the sand size used in the filter. Some of the pros of sand filtration are that the units are forgiving and the sand media is inexpensive to replace. The problems with sand filtration are filtration is only on the surface of the filter, sand filters require a large footprint for the unit, sand is easily fouled by oils and fats, and sand does not usually remove solids down to $1\ \mu$ in size. Sand filtration can be used as initial filtration to remove silt and debris and then followed by finer filtration as carbon filtration. This is common as pretreatment for RO systems.

Carbon filtration is used for the removal of (a) chlorine, (b) sediment, and (c) organics, phenols, pesticides, surfactants, colors, and so on. The carbon filter bed is backwashed with the aforementioned filters to remove suspended solids. The removal of organics that are captured in the carbon media requires the application of steam. Steaming the media drives off the organics and extends the use cycle of the carbon media. Carbon filters are housed in stainless steel, iron, and fiberglass tanks. Stainless steel is recommended as the tank media where carbon is to be steamed. Fiberglass cannot be used in steaming operations and the iron tanks tend to corrode under steaming conditions, resulting in shorter equipment life spans than the stainless steel.

One of the problems with using carbon filtration is that it is a good growth media for bacteria. When carbon filtration is used before RO or demineralization, it is important to run bacteria tests on the filter effluent. If bacteria are present, remove the carbon media from the filter, disinfect the vessel, and use new carbon media as a replacement. Bacteria can attack membranes and resin, causing media failure and should be avoided. If the carbon media cannot be easily replaced and a quick fix for bacteria is required, the addition of hydrogen peroxide to the system can effectively kill the bacteria while doing minimal damage to the carbon media.

Chlorine in the water will damage water softener resin beads. It is a common practice to place carbon filtration after the media filter and before the water softener. Run daily chlorine residual tests on the effluent of the carbon filter. When chlorine breakthrough occurs, backwash the unit. If this does not reduce the chlorine breakthrough, replace the carbon media. Carbon filtration is always recommended in front of a RO system. Chlorine can attack membranes similar to the attack on resin beads, and organics will foul the membranes.

Cyclonic filtration is the least common filtration method for boiler water pretreatment. Cyclonic filters use centrifugal movement to separate solids from the water. Each unit is designed to operate between two flow rate parameters and at a specific pressure drop. If the flow to the filter is above or below the design flow rate, the efficiency of the filter is dramatically reduced. Cyclonic filtration will effectively remove solids that are $75\ \mu$ or larger, and is able to remove solids down to $50\ \mu$ when operating within design parameters. Therefore, it is not effective for the removal of the smaller suspended solids that could result in deposit formation in the boiler if not removed with pretreatment.

A significant benefit of choosing cyclonic filtration is that a cyclonic filter has very few, if any, moving parts. This means that the filter does not require significant maintenance. In regard to application, cyclonic filters are used to remove high levels of large solids. A field verification method to determine if a cyclonic filter will perform in the designated application is to run a settling test on

the water to be filtered. Take a sample of water to be treated and let it sit for 30 s. Cyclonic filtration should be able to remove the solids in the water down to this level. Follow the cyclonic filter with either sand, aggregate, cartridge bag, or carbon, and the system should be able to achieve the desired water quality.

Cartridge filtration is the use of a manufactured cartridge media that filters solids down based on the micron size specific to the cartridge. The cartridge sizing varies, but industry standards are $1\ \mu$ absolute, 0.35, 1.0, 5, 20, 50, 100, and $150\ \mu$. The advantage of using this type of filtration is that one can filter very effectively to the specific particle size that is desired for the application. The disadvantage is that the filter cartridge will have to be replaced on a somewhat frequent basis, and that the cartridge must be made of a material that is compatible with the impurities in the water. The use of cartridge filtration allowed for less than $1\text{-}\mu\text{m}$ quality filtration and can be expanded into ultrafiltration and membrane technologies.

As quality water becomes scarce, the use of filtration technology will become more important for boiler water makeup. Waste streams from plant wastewater systems, cooling tower bleed, and contaminated water systems will be conditioned and used for boiler makeup. Suspended solids, oils, and other contaminants will be removed with clarification. Organics, surfactants, and volatile organic compounds (VOC) will be removed with carbon filtration. Ion exchange is now and will be used to remove ions that are harmful to the boiler.

15.1.2 ION EXCHANGE

Ion exchange is the substitution of ions in the water for ions that are attached to the resin bead. The type of resin bead used in this method of water conditioning dictates the ions that will be available in the water that enters the boiler. Figure 15.2 shows beads of ion exchange resin.

The primary ions that ion exchange removes from the makeup water to the boiler are the hardness ions, that is, Ca^{2+} and Mg^{2+} . The carbonate salts of these cations exhibit inverse solubility behaviors with increasing temperature. In short, as the water in the boiler is boiled to make steam, these solids will readily precipitate out of the water and form hard scale in the boiler. Hard scale acts as an insulator which results in fuel losses and metal fatigue. The removal of these cations is important for the prevention of scale in the boiler. The resin used for water softening and exchange of calcium and magnesium is strong acid/strong cation resin. Table 15.3 presents applications of various ion exchange resins commonly used in boiler water pretreatment process.

The process of ion exchange in water softening is basically: Ca^{2+} and Mg^{2+} ions pass through the resin bed and are ionically attracted to the sites in the resin beads. Since Ca^{2+} and Mg^{2+} have a higher charge than the sodium (Na^+) ion that is resident on the resin bead, there is a substitute reaction where one ion of Ca^{2+} and Mg^{2+} occupies the sites that were occupied by two Na^+ ions. The Na^+ ions are then released into the water as replacement for the Ca^{2+} and Mg^{2+} ions. The term *soft water*

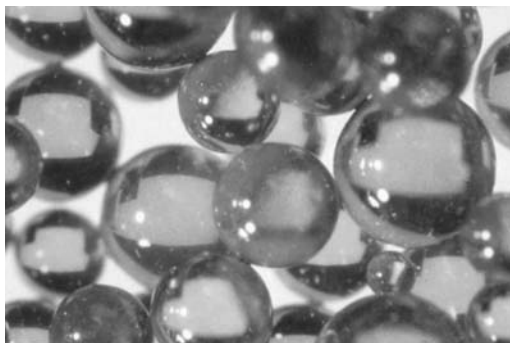


FIGURE 15.2 Resin beads. (Courtesy of Guardian CSC, York, Pennsylvania, External Water Processing Training Program.)

TABLE 15.3
Resin Applications

Resin Types	Strong Acid/Strong Cation	Weak Acid/Weak Cation
Application	Water softener.	Cation removal in deionization/demineralization.
Function	Due to its ability to convert neutral salts into their corresponding acids, this resin is called strong acid resin.	Weak acid or weak cation resin is used for removing the cations associated with alkalinity (Ca, Mg, and Na).
Regeneration	Normal regeneration is with NaCl. In the hydrogen cycle (using acid for regeneration instead of salt), virtually all of the raw water cations can be removed.	Resin is regenerated in the hydrogen cycle with acid. Weak cation resin will regenerate more efficiently than the strong cation resin.
Exchange group	This resin uses sulfonic acid as the exchange group.	This resin uses the carboxylic group (–COOH) as the exchange group.

Source: Ketrick, B., Resin application table, Internal Training Program, Guardian CSC, York, PA.

refers to water where the cations of calcium and magnesium have been replaced by the sodium ions. The importance of supplying quality soft water to the boiler is that the potential for scale and deposit formation are reduced or eliminated. Therefore, the boiler water treatment program relies heavily on the performance of the water softener. With water softener performance in mind, it is important to consider the potential issues related to unit operation.

Mechanically, the water softener allows water to pass over the resin bed. As the water passes over the resin bed, the ion exchange process occurs; this is called the *service cycle*. Eventually, the sites available for ion exchange on the resin bead are filled. At this point, regeneration of the resin bead is required. This process backwashes the resin bead to remove solids and broken beads; injects a brine, sodium chloride, solution over the resin beads where the calcium and magnesium ions are rejected to waste and sodium ions attach to the resin bead sites; and the resin bed is rinsed to settle the resin bed down and flush off any excess brine.

The steps in the water softener cycle are listed below.

- *Service*: The unit is in operation. Hardness is being removed from the water as it passes over the resin beads.
- *Regeneration*: The resin is exhausted.
 - *Backwash*: Initial regeneration step, where the resin is backwashed by the reversal of the water flow. Resin bed expands up to 50% of its height.
 - *Brining*: The longest part of the cycle, where the brine solution (salt solution) is slowly drawn over the resin beads. This is where the sodium forces the calcium and magnesium off the bead.
 - *Slow rinse*: The slow rinsing of the brine solution out of the resin bed, settling the bed.
 - *Fast rinse*: Rinses the excess brine off the resin beads, after the regeneration of the resin bead is completed.
 - *Brine refill*: Water refills the brine tank. This allows sodium chloride salt in the brine tank to dissolve in the refill water and form saturated brine for use in the next regeneration.
 - *Service*: The unit is ready to be returned to service.

The problems that can occur during the mechanical phases of the water softener cycle are as follows

Problem: Water softener does not pull brine. With insufficient brine draw, the water softener resin cannot regenerate. The result is a shortened run time failing to have any ion exchange capacity.

Solution: Check brine eduction valve. This valve sees corrosive brine with each regeneration and will either fail or build up solids in the educator. Clean the valve or replace it. This is the most common part on the unit to fail.

Solution: Check the foot valve in the brine tank. This is a float-activated valve that is used to prevent the brine tank from overflowing during the brine refill step. It can become plugged with dirt from the brine or hang in the up position. If this occurs, the water softener cannot pull brine, and it cannot refill to make a saturated brine. Clean or replace the foot valve assembly.

Solution: Manually put the water softener into the brine cycle. Remove the brine suction tube where it enters the water softener head. This is the brine educator. Press your finger over the hole in the educator valve where the tube was attached. If there is significant suction on your finger, the educator is working properly and the foot valve is the problem. If there is very little or no suction, the educator valve is the problem and needs to be replaced.

Problem: Resin is suddenly showing up in the drain after regeneration.

Solution: If the water temperature has suddenly dropped due to cold weather and the resin is less than a coffee cupful, then the bed expansion from colder water is the problem. This is only a temporary problem and usually will only occur once or twice in cold weather.

Solution: Each water softener has a flow-restricting valve or fixed-flow orifice that is installed in the line that discharges from the water softener head to the drain. This is installed to prevent the water flow during backwash from flushing the resin out of the water softener to the drain. It can wear over time and should be replaced every 5–7 years.

Solution: The water temperature, approximately room temperature, and the flow restriction valve are in place. At this point, if you also see resin in the feed water, the internal distributor is cracked and must be replaced. This is done by taking the water softener off-line. Remove the head of the water softener. Then pump the resin bed into empty plastic drums; this can be done by educting the resin or pulling it out with a wet vac. Pull the distributor and check the laterals on the distributor. Replace any part that shows any impairment. Replace the distributor, add the resin back into the unit, and reassemble the unit.

Problem: Water is hard when the water softener is put on line, then becomes soft after it runs.

Solution: When you have multiple units and a unit is allowed to sit after regeneration with no water flow for up to a week, the resin, which is only ever 50% regenerated, will allow all of the sodium to migrate to the top resin and all of the remaining calcium and magnesium to migrate to the lower resin. Once water begins to flow, the ions balance out and the water softener starts to allow ion exchange. To prevent this problem, always flush at least three times the volume of the water softener tank to drain when the unit is to be put on-line and before sending the effluent from the unit to the boiler.

These are the most common mechanical problems; the ion exchange resin also has to be understood to make sure that the boiler receives quality water.

To start with, the ion exchange occurs on the inside of the resin bead. Looking back at Figure 15.2, you see a smooth round plastic ball. The reality is that the bead is actually a multitude of minute fibers similar to a ball of yarn. The resin bead is formed by adding divinylbenzene (DVB) to the monomers that make up the resin bead. The DVB causes the bead to cross-link. The higher the DVB content of the resin bead, the more resistant the bead is to the degradation, but that is traded for a tighter bead which has less porosity and less capacity.

The bead being formed by DVB and the structure of the bead cause two potential problems. The first is that DVB is susceptible to oxidation. This is usually caused by the chlorine residual in the water. As the DVB is broken down, the integrity of the bead is lost. Eventually the bead becomes spongelike and soft. At this point, the resin bead is useless for ion exchange. The second problem is structure. Ion exchange occurs on the inside of the resin bead. Looking at Figure 15.2 again, you notice that in spite of the magnification, the fibers of the bead are not visible. This means that fine silt and micron-sized particles can impinge on the resin bead and block the flow of water through the resin bead. No flow, no ion exchange.

The solutions to these problems are filtration and cleaning. Where filtration is not installed before the water softener unit, fine particles impact on the resin bead and the resin bed becomes the filtration media. When used for this purpose, the ion exchange is affected. So, filtration before the water softener is recommended. Where chlorine is present in the water, carbon filtration should be used before the water softener. Carbon filtration will filter the solids and remove the chlorine from the water. This protects the resin bed from particle impaction and the breakdown of the DVB cross-linking.

The cleaning of the resin can be done as a part of maintenance or can be accomplished as an off-line procedure. The maintenance cleaning of the resin bed can be done by adding the resin cleaner to the brine tank. Cleaning occurs during the brining cycle of regeneration. Off-line cleaning is usually a last effort to save the resin rather than to replace the resin. This process is performed by taking the water softener off-line and opening the top of the unit. Resin cleaner is added to the unit. An air lance is inserted down to the base of the unit and air is added very slowly. This allows the resin to move and contact the cleaner. Too much air will cause excessive foaming, and too little will not allow the resin to make contact with the cleaner. This process usually takes 2–4 h to complete cleaning.

There are a number of different types of resin cleaners. The three basic formulas are

- 10% 1-Hydroxy ethylidene-1,1-diphosphonic acid (HEDP)—good general cleaner
 - 1 quart/10 ft³ of resin as a maintenance dosage
 - 1 gal for every 10 ft³ of resin for off-line cleanup
- Sodium bisulfite—inexpensive, watch for fumes
 - 1 lb/10 ft³ of resin for maintenance
 - 1 lb/2.5 ft³ for off-line cleaning
 - Be careful where iron is the main contaminant, as this can form with heavy iron to bind up the resin bed
- 10% Citric acid/20% HEDP—most effective general cleaner
 - 0.3–0.6 gal/10 ft³ of resin for maintenance
 - 0.3–0.6 gal/ft³ of resin for off-line cleaning

Up to this point, ion exchange has focused on water softener resin that removes cations; however, salts are formed from both cations and anions. Anions, carbonates in particular, contribute to problems in the boiler. Carbonates (HCO_3^- bicarbonate, CO_3^{2-} carbonate) break down in the boiler and form carbon dioxide (CO_2) which leaves the boiler with the steam and then reacts with the condensate to form carbonic acid (H_2CO_3). Sulfates (SO_4^{2-}) are anions that combine with calcium to form hard scale in the boiler. The reduction or removal of anions can be considered where these problems are prevalent, or where the cost to treat these problems chemically is sufficient to justify the cost of mechanical removal of the anions with dealkalization.

A dealkalizer used strong base/strong anion resin to remove anions. The unit can be regenerated with sodium hydroxide (NaOH) where the hydroxide ion (OH^-) is the ion that is attached to the resin, or with sodium chloride (NaCl) brine, where the chloride (Cl^-) ion is used on the resin. In the chloride cycle, the anion removal will only be a maximum of 90% removal from ion exchange. The use of the hydroxide cycle is far more efficient.

Problem: Water softener is leaking hardness, allowing to enter the dealkalizer.

Solution: Bypass the dealkalizer. Calcium hardness entering a dealkalizer will form calcium sulfate which will deposit on the resin bead and cannot be removed through regeneration. If hard water is allowed to pass into the dealkalizer for any length of time, the resin will have to be replaced.

Solution: The water flow should always be through the water softener and then to the dealkalizer. Never place the dealkalizer upstream of the water softener.

Problem: Dealkalizer using hydroxide cycle is not regenerating.

Solution: The sodium hydroxide used for regeneration of a dealkalizer has to be textile grade or better. Contaminants in less-expensive grades will plug the educator preventing regeneration.

Solution: 50% Sodium hydroxide will begin to form crystal as the temperature of the solution drops to 54°F. These crystals will cause the same fouling problem with the educator as impurities. The sodium hydroxide must maintain a temperature above 60°F to prevent this problem from occurring.

Classic pretreatment is filtration followed by water softening and then when applicable, dealkalization. The future of pretreatment will also see the widespread use of RO.

15.1.3 REVERSE OSMOSIS

Reverse osmosis is a pressure-driven process used to remove dissolved ions from the feed water by the use of semipermeable membrane, as shown in Figure 15.3. The resultant is approximately 98% removal of the salts found originally in the water. The permeate is the water that has been processed through the RO membrane, which contains approximately 2% of the original solids level. The reject is the concentrated solution containing the rejected salts and the quantity of water that did not process through the membrane. Note that gases in the water, as oxygen and carbon dioxide, will pass through the membrane into the permeate. If the presence of these gases is potentially detrimental to the quality of the process water, then they need to be dealt with either through deaeration or gas scrubbing.

The components of a RO unit are: prefilters, high-pressure pump, RO membrane, and storage tank. The prefilters are used to remove suspended solids and contaminants that would cause membrane fouling. This system usually consists of suspended solids filtration, either sand, aggregate, or cartridge, and carbon filtration to remove chlorine and organics. The high-pressure pump is used to create the RO process and force the water through the membrane. The membrane is the heart of the process. It is a multilayered cartridge that is designed to filter out the salts in the water. The storage tank is used to store permeate after it has been processed in the RO unit. Since the process is very slow, it is prudent to operate the RO unit continuously and to store any excess production for use at a later time. The life of the membrane depends on various factors, including operation parameters and water chemistry.

Filtration, as mentioned earlier, is used to remove total suspended solids (TSS), which is measured as the silt density index (SDI). The filter should be 1–5- μ filters, and they should be capable of reducing the silt index to less than 5 and preferably less than 3. Otherwise, these solids can rapidly foul a membrane. RO can remove up to 98% of salts from the feed water, so the higher the total dissolved solids (TDS), the greater the potential for forming insoluble salts on the membrane surface. For example, 98% removal of 100 ppm produces water with 2 ppm of salt content in the permeate, and 98% of feed water containing 400 ppm will produce permeate with 8 ppm of salt content.

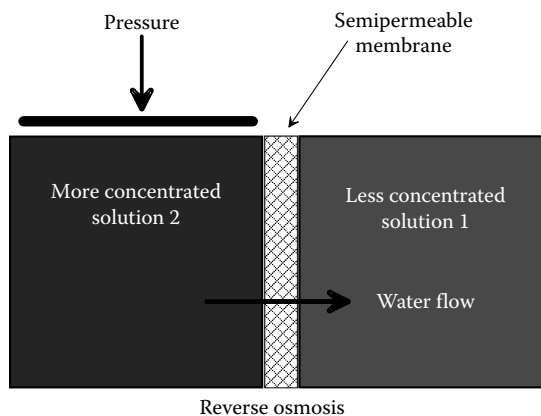


FIGURE 15.3 Reverse osmosis flow drawing. (Courtesy of Guardian CSC, York, Pennsylvania, External Water Processing Training Program.)

Chlorine used as a biocide in RO system may damage the semipermeable membrane, a key component of RO system. Chlorine attack causes the membrane to break down. Thin film composite membranes are not very tolerant to chlorine and have up to 98% rejection rate for salts. Cellulose acetate membranes are more tolerant to chlorine, but only have up to 95% rejection rate. Carbon filtration is therefore important in the pretreatment train to prevent chlorine attack on the membrane. The greatest operational problems with RO membrane fouling are: microbiological, mineral scale, iron, and suspended solids. These are handled by adding scale inhibitors to prevent mineral scale, biocides for the control of microbiological growth, pH adjustment to remove carbon dioxide, and iron and cleaners to keep the membrane surfaces as clean as possible.

Even with proper pretreatment and chemical cleaning, membranes should be cleaned off-line every 3–6 months. Always perform cleaning if there is a 10%–15% increase in the differential pressure or a 10%–15% reduction in the permeate flow. Cleaning is performed by acid cleaning the membrane to remove mineral scales; this is followed by caustic cleaning to remove organics, biocides, or surfactants for microbiological cleaning and chelating agents for special circumstances.

RO should be monitored to verify the water quality. The points to monitor include (a) differential pressure between feed, concentrate, and permeate; (b) permeate and concentrate flow rates and recovery rates; (c) temperature; (d) pH; and (e) SDI. It is important to note that softened water is very critical for the proper operation of the boiler. In cases where RO process is used for boiler water makeup, the RO unit must be placed prior to water softener.

15.2 BOILER WATER TREATMENT PROGRAMS

15.2.1 FEED WATER SYSTEM

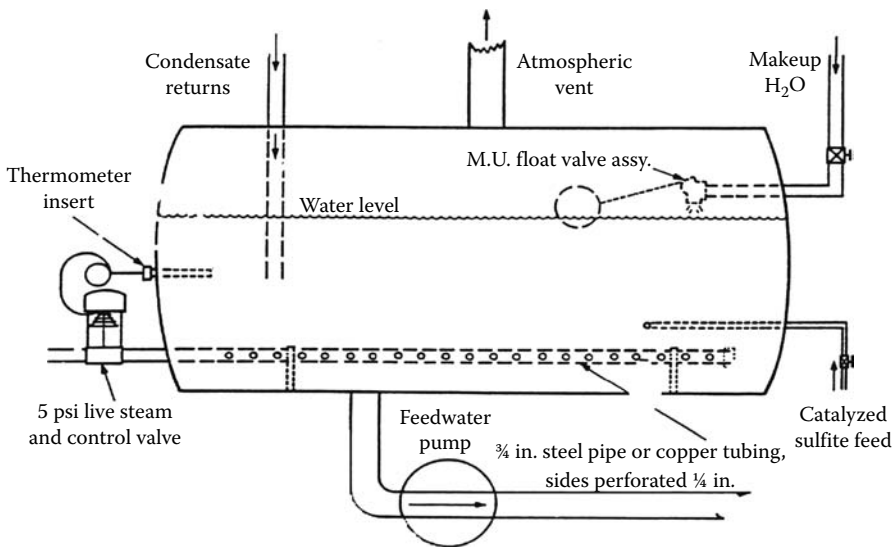
Once the makeup water has been processed in the pretreatment system, it becomes the feed water for the boiler. Feed water is the water that is fed to the boiler. It can be a combination of the condensate return and the makeup, or where there is no condensate return, the makeup is the feed water. Feed water is heated before it is fed to the boiler. This is done to prevent thermal shock to the boiler metal and to reduce the gases found in the makeup water. Thermal shock occurs when cold water is fed to a boiler. The temperature difference causes the boiler metal to contract. The process causes metal fatigue which reduces the life of the boiler.

By heating up the feed water to prevent thermal shock, we also cause the water to deaerate. As water temperature approaches the boiling point, both carbon dioxide and oxygen solubility is dramatically reduced. These gases escape from the water and can be vented out of the system. This is accomplished with the use of either a feed water tank or a deaerator. The importance of deaeration is that as the oxygen in the water is heated, its ability to react with boiler metal to create pitting corrosion also increases by doubling every 10°C. If the oxygen in the water is not removed by either mechanical and/or chemical means, then rapid pitting will occur in the feed water system. The result would be pinhole leaks in tanks and pipes.

15.2.1.1 Feed Water Tank

A feed water tank is most commonly found in use with fire tube boilers below 500hp. The feed water tank is not a pressurized system and it is open to the atmosphere. Figure 15.4 shows the picture of a feed water tank. The water in the feed water tank is heated with a steam sparging line that feeds steam to the tank based on the setting on a thermal couple. The water temperature should be controlled 200°F–205°F to allow as much oxygen release as possible. Operating the feed water tank at temperatures above 205°F may cause pump cavitation. Pump cavitation will result in damage to the feed water pump. A feed water tank cannot remove all of the oxygen in the water, so a reducing agent is added to the water to combine with the oxygen. The addition of sufficient reducing agent to the feed water neutralizes the ability of the oxygen to cause pitting in the feed water system. The oxygen solubility as a function of temperature is shown in Figure 15.5.

Open feedwater tank heating



Sketch for automatic steam heating of boiler feedwater, oxygen venting
 (Note: Metal tanks should be lined with corrosion resistant material)

FIGURE 15.4 Feed water tank drawing. (Courtesy of AWT, Rockville, MD, Technical Training Course, Boiler Water Treatment, Bruce Ketrick.)

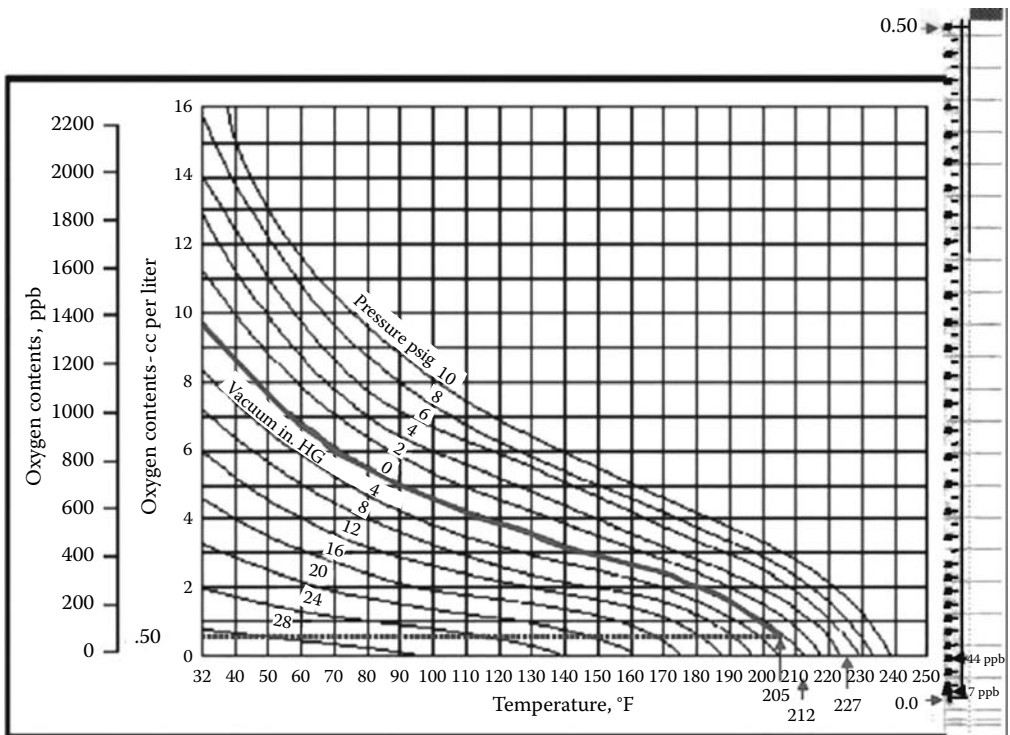


FIGURE 15.5 Oxygen solubility chart. (Courtesy of Guardian CSC, York, Pennsylvania, Training Course, Boiler Water Treatment.)

TABLE 15.4
Saturated Steam Pressure versus
Feed Water Temperature

Pressure, lb/sq in.	Temperature of Feed Water, °F	Btu per lb Feed Water
0	212	180
2	218	187
4	224	190
6	230	198
8	235	203

A deaerator differs from a feed water tank in that it uses pressure to raise the temperature of the feed water. This improves the efficiency of oxygen removal. The deaerator is also located at a height above the boiler. The elevation of the deaerator creates head pressure (1 psi for every 2.31 ft of elevation) which assists in preventing pump cavitation. The efficiency of the deaerator is based on holding the temperature of the feed water within 3°F of the saturation temperature based on the pressure. When the feed water in the deaerator is within 3°F of saturation, the feed water will only hold 5–7 ppb of dissolved oxygen. Most deaerators operate at approximately 5 psi and 234°F (Table 15.4).

15.2.2 OXYGEN SCAVENGERS

The reducing agents added to the feed water to remove the oxygen are also referred to as *oxygen scavengers*. The most commonly used oxygen scavenger for boilers operating under 300 psi is sodium sulfite. Sodium sulfite (Na_2SO_3) combines with oxygen (O_2) to form sodium sulfate (Na_2SO_4). A solid combines with a gas to form a solid. The reaction theoretically requires 7.88 ppm of sodium sulfite to react with 1 ppm of oxygen. In practical application, it requires 10 ppm of sodium sulfite to react with 1 ppm of oxygen. The reaction time is reduced dramatically by adding 0.01/100% sodium sulfite of a metal catalyst. The catalyst frequently used is cobalt sulfate. Sodium sulfite is controlled in the boiler 20–60 ppm as sodium sulfite. Table 15.5 references additional boiler water oxygen scavengers.

All oxygen scavengers should be fed to the system at the point that the feed water is initially heated. Some installations have a tank installed that mixes the makeup water and the condensate, downstream of the deaerator. Where this is the system design, the injection point for the oxygen

TABLE 15.5
Oxygen Scavenger

Oxygen Scavenger	Feed Rate	Control	Comments
DEHA, Diethylhydroxylamine	1.24 ppm/ppm O_2	0.5–1.0 ppm in condensate	Strong reducing agent; will volatilize and leave the boiler, protecting steam and condensate
Erythorbic acid	11 ppm/ppm O_2	30–60 ppm	GRAS food grade; used to passivate iron
Hydroquinone	6.9 ppm/ppm O_2	0.1–0.3 ppm	Works well in cold water; used in high pressure
Carbohydrazide	1.4 ppm/ppm O_2	0.05–0.3 ppm	Hydrazine substitute
Hydrazine	0.05–0.1 ppm	0.05–0.1 ppm	Known carcinogen; good in high pressure
Methylethylketoxime	5.4 ppm/ppm O_2	0.8–1.2 ppm	Volatilizes with steam, good in long-run systems; not for layup
Sodium Sulfite	10 ppm/ppm O_2	20–60 ppm	Reacts as a reducing agent to form sodium sulfate

Source: Ketrick, B., Oxygen scavenger, AWT Training Course, Rockville, MD, Boiler water treatment, pp. 47–55, 2009.

scavenger should be to that tank instead of to the deaerator. Where the mixing of condensate and makeup is in the deaerator, the injection should be in the storage section of the deaerator at a point that is 6 in. below the operating water level. Injection above that level will cause product waste as the product reacts with gases that are being liberated from the feed water.

The injection of oxygen scavengers, in particular sodium sulfite, should always use a stainless steel injection quill. Concentrated treatment products are very erosive and can be very reactive. In the case of sodium sulfite, as the solution is heated, it will react with a black iron injection quill to form soluble ferric sulfate. This rapidly eats away the black iron injection quill. Therefore, the injection quill, nipple, and valve located at the point of injection should be made of stainless steel. The rest of the chemical feed line, where it is not subjected to the heat of the deaeration system, can be made of black iron; heat is the driving factor. Table 15.6 presents the properties of oxygen scavengers.

Diethylhydroxylamine, DEHA, is effective at reducing red ferric oxide into passive black magnetite in the boiler and the condensate system. DEHA acts as a reducing agent, oxygen scavenger, in the boiler. DEHA is also a volatile amine, so a portion of the product fed to the boiler will volatilize

TABLE 15.6
Properties of Oxygen Scavengers

Oxygen Scavenger	Combined Ratio (Practical)	Maximum Pressure, psig	Volatility/ Distribution Ratio	Passivation Ability
Sodium sulfite, solid or 10%. Catalyst—cobalt or erythorbate	10:1 rapid scavenger	950 max. Risk of SO ₂ /H ₂ S	Not volatile/ DR = Nil	Limited only over 300 psig
Sodium bisulfite, 40% soln. Catalyst—cobalt or erythorbate	7:1 rapid scavenger	950 max. Risk of SO ₂ /H ₂ S	Not volatile/ DR = Nil	Limited only over 300 psig
Sodium metabisulfite 100% pwr. Catalyst—cobalt or erythorbate	5:1 rapid scavenger	950 max. Risk of SO ₂ /H ₂ S	Not volatile/ DR = Nil	Limited only over 300 psig
Hydrazine, 15 or 30% soln. Catalyst—hydroquinone	3:1 rapid scavenger	2,500 + produces NH ₃	Poor volatility/ DR = 0.1	Excellent for all systems
Diethylhydroxylamine, DEHA, 17.5–30% soln. Catalyst—HQ or copper	3:1 rapid scavenger	2,500 + some NH ₃	Good volatility/ DR = 1.3	Excellent for all systems
Erythorbate, 10–20% soln. Catalyst—Cu/Ni/Fe	10:1 good scavenger	1,500 + nothing harmful	Not volatile/ DR = Nil	OK, but only in the boiler
Hydroquinone, 15/25% soln. Catalyst—pyrogallol	7:1 scavenger enhancer	1,500 + produces CO ₂	Volatile only at 1500 psig/ DR = 0.15	Acts as an enhancer only
MEKO (poor solubility). Catalyst—erythorbate	6:1 weak scavenger	1,250 + risk of charring	Highly volatile/ DR = 2.2	No true ability to passivate
Carbohydrazide, 6.5% soln. Catalyst—Cu or Co	1.5:1 slow enhancer	2,500 + produces CO ₂ /NH ₃	Some volatility over 130 psig DR = 0.0	Excellent, but only for utilities
1-Aminopyrrolidine, 30% soln. Catalyst—hydroquinone	2:1 OK scavenger	1,250 + risk of charring	Some volatility/ DR = 0.7	OK, but not special
Tannins, 25–50% soln. Catalyst—none	10:1 good for cold FW	650 Max. Product then fails	Not volatile/ DR = Nil	Excellent, but only in the boiler

Source: Frayne, C. and Ketrick, B., Properties of oxygen scavengers, AWT Training Course, Rockville, MD, Boiler water treatment, p. 56, 2009.

Note: CR is for 100% scavenger.

and leave the boiler with the steam. This allows the product to remove oxygen from the boiler, steam, and the condensate system. DEHA residual is measured in the condensate, and as little as 150–300 ppb has been found effective in protecting metal surfaces from oxygen attack. Note that, on a use basis, DEHA is usually less expensive than the use of sodium sulfite. The downside to DEHA is that it is not approved for food contact under 21CFR 173.310.

Erythorbic acid, on the other hand, is generally recognized as safe (GRAS) approved for use where there may be food contact. It is an isomer of vitamin C. The areas that erythorbic acid is used for oxygen scavenging would be food applications, pharmaceuticals, and where iron corrosion byproducts are present in the feed water. Erythorbic acid is effective at transporting iron. The problems with this product are that the use rate is 10% higher than sodium sulfite, and the cost of the material is higher than that of sodium sulfite.

15.3 SCALE AND DEPOSIT CONTROL

Boiler internal treatment, once oxygen has been scavenged, is the prevention of the formation of scale and deposit on the boiler surface. Scale is usually described as the formation of calcium-based salts on the metal surfaces of the boiler. Deposits are the agglomeration of solids that settle on the metal surface. The problem with the formation of deposits is that they are insulative. This prevents efficient heat transfer across the boiler metal to the water that is fed to the boiler to form steam. The process also causes the boiler metal to heat to high temperatures. This overheating causes metal fatigue and eventual tube loss.

As little as 1/32 in. of calcium carbonate scale deposit can require approximately 8%/5% increase in fuel usage to develop the same quantity of steam as a clean boiler. Repeated over the heating of the boiler metal causes the carbon in the steel to migrate away from the grain of the metal. This results in the metal becoming brittle. Once the metal is brittle, both tube ends and tube sheets will form cracks at the points of stress. The end result is extensive repairs or replacement.

Both scale and deposits can be dramatically reduced by the reduction of the calcium and magnesium ions that are introduced to the boiler and the reduction of solids to the boiler. The importance of pretreatment to filter out solids and ion exchange to remove calcium and magnesium ions is as important as or more important than the chemistries used to control deposition. If these contaminants are removed before the boiler, they are not present to form deposits.

The programs used to prevent scale formation generally fall into three categories: precipitating, chelant, and dispersant.

15.3.1 PRECIPITATING PROGRAM

In this approach, phosphates are used to form a desirable precipitate. Phosphate combines with calcium to form a soft voluminous particle that can be suspended in the boiler water and removed through the blowdown. Table 15.7 lists the types of phosphates used in the precipitating programs. The key to this reaction is to have sufficient alkalinity in the form of the hydroxyl ion (OH^-). Where the hydroxyl ion is above 200 ppm and preferably 250 ppm, phosphate will combine with the calcium that is in the boiler to form hydroxyapatite [$\text{Ca}_{10}(\text{PO}_4)_6(\text{OH})_2$]. This is the preferred chemistry. If there is insufficient hydroxyl ion present, the calcium reacts with the phosphate to form tricalcium phosphate [$\text{Ca}_3(\text{PO}_4)_2$]. Tricalcium phosphate is a very dense, hard gray deposit that forms a tenacious scale on boiler metal surfaces.

As you can see, having enough hydroxyl ion is important for precipitating chemistry to work. Hydroxyl ions are lost when hard water is fed to the boiler. In the case of a water softener failure, calcium can enter the boiler. The calcium will combine with the hydroxyl ion and form calcium hydroxide $\text{Ca}(\text{OH})_2$. This ties up the hydroxyl ion and it is no longer available for use in forming hydroxyapatite. In addition, the calcium combines with the phosphate present and forms tricalcium phosphate. At this point, the normal reaction is to see that the phosphate residual is reduced in the boiler and the operator

TABLE 15.7
Types of Phosphates Used in Precipitating Programs

Phosphates Used in Precipitating Programs	Formula	P ₂ O ₅ %	PO ₄ %
Sodium hexametaphosphate	(NaPO ₃) ₆	68	93
Tetra potassium pyrophosphate	K ₄ P ₂ O ₄ ·3H ₂ O	36.9	59
Sodium tripolyphosphate	Na ₅ P ₃ O ₁₀	58	78
Sodium metaphosphate	NaPO ₃	69	94
Tetrasodium pyrophosphate	Na ₄ P ₂ O ₄	52	71
Monosodium phosphate	NaH ₂ PO ₄	58	79
Disodium phosphate	Na ₂ HPO ₄	48	66

Source: Ketrick, B., Types of phosphates, AWT Training Course, Rockville, MD, Boiler water treatment, p. 126, 2009.

adds phosphate to bring it back up. However, since the hydroxyl ion is not present, the only thing that the operator is doing is forming more tricalcium phosphate scale. It is recommended that in the phosphate treatment program, if a water softener failure occurs, stop the phosphate feed and add caustic soda (NaOH) until the hydroxyl alkalinity is 250 ppm or above. Then begin adding the phosphate product. Most importantly, the water softener must be returned to proper operating status.

Phosphate programs should be controlled at 20–80 ppm as orthophosphate (PO₄). Below 20 ppm, the phosphate is not a primary factor in the formation of hydroxyapatite. Above 80 ppm, the phosphate residual will combine with the magnesium in the boiler and form an undesirable sludge that will adhere to the tubes. The normal reaction for magnesium in the boiler would be to form magnesium hydroxide or magnesium silicate, both of which are small precipitating particles that do not readily form deposits. The overfeed of phosphate interrupts that reaction and forms a magnesium phosphate sludge [Mg₃(PO₄)₂]. It is therefore recommended not to ever overfeed phosphate.

15.3.2 CHELANT PROGRAM

This approach differs from precipitating chemistry in that chelant chemistry combines with scale-forming ions to form a soluble salt instead of a precipitant. This reduces the amount of sludge formed; precipitating chemistry increases the amount of sludge. The benefits are that with reduced sludge, there is a reduced demand for additional dispersant feed and a reduced requirement for blowdown. Reducing blowdown reduces fuel loss, water loss, and chemical loss from the boiler.

The chelants most commonly used in boiler water treatment are EDTA (ethylenediaminetetraacetic acid) and NTA (nitrilotriacetic acid). EDTA has gained popularity since NTA has been identified as a potential carcinogen. The primary functional difference between the two chelants is that EDTA can attack boiler metal and gouge the metal when overfed, while NTA will not aggressively attack boiler metal. EDTA is to be fed to the boiler, using a stainless steel quill, into the feed water line preferably or to the boiler if that is not available. When fed to the feed water line, EDTA should be fed downstream of the feed water check valve and at least 5 ft upstream of any elbow in the line to prevent erosion in the feed water system.

EDTA feed rate is based on the cations present in the feed water. Analyze the feed water for calcium, magnesium, and iron. Then multiply the cations in the feed water by the chelating factors for each: Calcium × 10.59, magnesium × 8.69, Fe²⁺ × 14.33, and Fe³⁺ × 25.1. Add the chelant demand together and multiply the ppm of chelant demand by the millions of pounds of feed water to determine the pounds of EDTA required. To prevent chelant attack, take the EDTA requirement and multiply it by 0.8. You are now feeding approximately 80% of the chelant demand. This would assist in preventing excess chelant feed. EDTA, as all chelants, will also react as oxygen scavengers.

Therefore, in order to have the benefit of the chelant for deposit prevention, it is important to always have sufficient oxygen scavenger in the boiler. Maintain a minimum of 30 ppm of sodium sulfite as sodium sulfite in the boiler or the EDTA may become tied up in oxygen removal and it will not be available for deposit control.

Since EDTA testing is easily interfered within the field, it is difficult to adequately measure EDTA residual in boiler water. The accepted control range for free chelant in a boiler is 1–3 ppm. Considering the difficulty of running an accurate field test and the low residual control range, it is usually easier to feed EDTA based on feed water usage. To check if there is excess EDTA in a boiler qualitatively, take a sample of the cooled boiler water and add the hardness buffer and hardness indicator to the sample. If the sample turns blue, excess EDTA is present and you should reduce the feed rate. If the sample turns purple, excess EDTA is not present.

A common approach to product development where EDTA is to be used in the boiler is to blend an orthophosphate-based product with the EDTA and a dispersant. The product level in the boiler is controlled using the orthophosphate test, which is accurate and easy to run on-site. This makes testing for the product level easier for the facility. The product can be formulated so that the proper chelant level is achieved with 5–15 ppm of orthophosphate in the boiler water. The wide range makes it easy to control the product level. The phosphate residual is below 20 ppm, so there is a minimal formation of phosphate sludge. The presence of orthophosphate ion in the boiler water will buffer the ability of EDTA to attack boiler metal when the EDTA residual is in excess. This product should be fed to the boiler, as the product contains phosphate, which as noted, requires hydroxyl ions to form a preferred sludge. The advantages include easy testing and buffering against metal attack. However, the disadvantages are increased sludge formation, increase in dispersant requirement, and a reduction in the ability for the EDTA to chelate deposit-forming ions.

EDTA can also be used to clean up old deposits in fouled boilers. Analyze the deposit before the cleanup and use the composition of the deposit to control the cleanup. Where phosphate is present in the scale, initiate EDTA feed at ten times the maintenance level and run orthophosphate residuals in the boiler water. As the deposit breaks down, phosphate is liberated, usually only a few ppm. Adjust the feed rate of the EDTA as the orthophosphate residual changes. When orthophosphate residual is not present, stop EDTA feed for a week and increase the dispersant feed. Since most deposits are layered, the program may have encountered a layer with high iron content instead of phosphate. Continue the EDTA feed after a week and look for the orthophosphate residual. EDTA cleanup in a boiler should be done slowly over months.

15.3.3 DISPERSANT PROGRAM

The program uses dispersant polymers and does not use either EDTA or phosphates. In this approach, the constituents in the feed water or in the boiler water side deposit will dictate the type of dispersant or types of dispersants that will be used. The program is used based on feed water usage. Organic programs can be fed to the deaerator, feed water line, or directly to the boiler. It would be recommended to feed the products to the feed water line for the best results. The concept is to disperse the solids in the boiler before nucleation (formation of a crystal) can occur. These minute particles are then dispersed in the boiler water. Without the ability to agglomerate or form crystals, the solids are then removed through blowdown. Organic programs are becoming more popular and will become more widely used once there is a quick and accurate method of measuring product levels in the boiler water. The key to selecting the type of deposit control program is to realize that they are all effective and they can all fail if misapplied.

15.3.4 DISPERSANTS

Dispersant chemistry has been discussed in detail in other chapters, so this section focuses on application. The basic function of a dispersant is to use a long-chain organic polymer that is a polyanion

to disrupt crystal formation and to change the phase chemistry of the boiler water from cationic (+) to anionic (-). Negatively charged polyanions are attracted to the cations in the boiler water (calcium, magnesium, iron, and so on). This disrupts the formation of the crystal lattice pattern of the corresponding salt, preventing crystal growth. The prevention of crystal growth means prevention of hard scale formation. The polyanion is fed to a slight excess, which results in the colloidal particle in the boiler water having a slight negative charge. In that like charges repel one another, the electronegative colloidal particles tend to disperse. These dispersed particles are then removed from the boiler water with blowdown. Dispersant molecular weight determines the potential particle size. A molecular weight of 2000–5000 MW is preferable in a boiler water treatment program. The smaller the dispersed particles, the less likely for these particles to form deposit. Polymeric dispersants are an integral part of all of the deposit prevention programs. When using a phosphate program, it is important to have a substantial amount of dispersant fed to the boiler. This is required to offset the high amount of sludge formation found with a phosphate program. When using a chelant program, the dispersant requirement is reduced due to the reduction in the formation of sludge. In that iron ties up more than 50% more EDTA than calcium, it is prudent to use a sulfonated iron dispersant as part of the dispersant product in the program to assist the EDTA. Organic programs are all dispersant programs. A dispersant is fed to the boiler system in the same manner as the organic program to the feed water line based on feed water usage preferably. If that is not possible, it is fed to the boiler and as a last resort to the deaerator.

The caution of feeding dispersant to the deaerator is due to the potential of eliminating the cobalt sulfate catalyst from the sodium sulfite. Dispersants come as a raw material with an acidic pH. Either sodium hydroxide or potassium hydroxide is added to the dispersant with some water to make a product with a pH of 10 or above. If a product with a pH above 8.0 is added directly to the sodium sulfite mixture, the cobalt sulfate catalyst will precipitate out. This plugs the chemical feed line and affects the ability of the oxygen scavenger to remove oxygen from the system. Whenever adding dispersant to the deaerator, do not feed it into the same chemical feed line as the oxygen scavenger; feed it to the opposite side of the deaerator as you feed the oxygen scavenger.

15.3.5 CONDENSATE TREATMENT

The boiler is used to make steam for process. Once the steam has been used in the process, it is condensed back into water. This water or condensate is then returned to the boiler for use in making more steam. This is hot, approximately 190°F–195°F, distilled water. It is valuable in that the more condensate a system can return to the boiler, the less makeup water is required. The requirement for all of the boiler water treatment products, with the exception of oxygen scavengers, as well as the amount of blowdown needed to remove the constituents from the makeup water are based on the amount of makeup water used to make steam. Reducing makeup usage reduces chemical, fuel, and water usage. So, condensate is very valuable and a system should bring back as much as possible. However, there are problems. The problems are carbon dioxide and oxygen. Both are gases and both will cause corrosion, metal loss, pipe failure, and excess iron in the boiler water that results in either excessive treatment costs or deposition.

The carbon dioxide is formed in the boiler. Carbon dioxide that was dissolved in the makeup water is virtually all removed by deaeration. However, hard water entering a water softener enters as calcium or magnesium in either the carbonate or bicarbonate form (CaCO_3 or MgCO_3 carbonate, CaHCO_3 or MgHCO_3). Ion exchange replaces the calcium and the magnesium with the sodium ion (Na^+). This water enters the boiler and the heat reverts any bicarbonate to a carbonate. The carbonate then breaks down to carbon dioxide (CO_2), which is a gas that evolves out of the boiler with the steam.

The carbon dioxide travels with the steam and then is converted to carbonic acid when it contacts the condensate ($\text{CO}_2 + \text{H}_2\text{O} \rightarrow \text{H}_2\text{CO}_3$). Acids are heavier than water, so the acid drops to the bottom of the condensate return pipe and corrodes the pipe, eating away the metal.



FIGURE 15.6 Carbonic acid corrosion. (Courtesy of Guardian CSC, York, Pennsylvania.)

The method of treatment for condensate carbonic acid corrosion is to use a neutralizing amine. Neutralizing amines are chemicals that are volatile and being amines, they are alkaline in nature. The function is for the amine to volatilize with the steam and then to condense with the condensate in sufficient amount to neutralize the carbonic acid. The carbonic-acid-induced corrosion of pipe is illustrated in Figure 15.6.

The control of the neutralizing amine is accomplished by running a pH at various points in the condensate return system. Control ranges may vary, but usually 7.6–8.4 is the recommended control range, with pH of 8.0 being the optimum. At a pH of 8.0, the carbon dioxide in the steam is not free to form carbonic acid. A pH controlled above 8.0 can give the system a cushion of safety, but a pH above 8.8 is a waste of product. Avoid going above a pH of 9.0. At 9.2, the amphoteric metals in the system, as all copper-bearing metals, will begin to solubilize in the condensate. Above 9.5, this occurs at a rapid rate.

Measure the pH at different points in the condensate return system. Some condensate return systems may have considerable length, referred to as “long runs.” It is not uncommon to find a significantly lower pH at the end of long runs than would normally be found in the rest of the system. In this instance, it is better to place a small satellite feed system in the low pH area to boost the pH of the system than it is to increase the feed rate of the neutralizing amine at the initial feed point. It is not recommended to have a pH above 9.0 at the beginning of the system in order to protect the end of the system with a pH of 7.6. This practice wastes product and will cause copper loss. To protect the system, more than one satellite feed may have to be used. The use of satellite system will allow the program to keep the pH more uniform throughout the system.

Table 15.8 lists the characteristics of commonly used neutralizing amines. The selection of neutralizing amines is also important. Neutralizing amines have different boiling points, which result in their ability to travel through the condensate system to also differ. The distribution ration is the method used to determine the ability of a neutralizing amine to travel through the system. The lower the distribution ration, the shorter the run; the quicker the amine will drop out of the steam, the higher the distribution ratio, and the farther the neutralizing amine will carry through the system.

The practice of blending two or more amines together so that the product will have the benefits of each is a common practice. The combination of diethylaminoethanol (DEAE) and cyclohexylamine in a ratio of 3:2 is widely used to get both the medium and the long-run abilities of both amines and to stay in the 15 ppm:10 ppm range for FDA food contact of steam regulation.

Ammonia as ammonia hydroxide is also used as a neutralizing amine in the food industry. It can be used in dairy facilities as well as in other food processing applications. The distribution ratio is higher than the distribution ratio for cyclohexylamine, so it is not always effective in short and

TABLE 15.8
Characteristics of Neutralizing Amines

Common Name	Diethylaminoethanol,			
	Morpholine	Cyclohexylamine	DEAE	AMP-95
Boiling point 100% amine	264°F	273°F	325°F	329°F
Boiling point amine/water	Nonazeotrope	Azeotrope 205°F	Azeotrope 210°F	Nonazeotrope
Decomposition temperature	644°F	626°F	794°F	660°F
Liquid vapor distribution ratio	0.4:1	4.7:1	1.7:1	0.3:1
Comments	Min. 40 psig, short runs and turbines	Low pressure and long run	Medium to long runs	Min. 75 psi short to med. runs
Regulatory 21CFR 173.310	Approved to 10 ppm	Approved to 10 ppm	Approved to 15 ppm	Not approved

Source: Ketrick, B., Characteristics of neutralizing amines, AWT Training Course, Rockville, MD, Boiler water treatment, p. 174, 2009.

medium runs in the facility. The product is also difficult to handle both from the point of dermal contact and odor. Control is the same as the other neutralizing amines.

The preferred feed point for neutralizing amines is through a stainless steel injection quill into the steam header. Neutralizing amines can be fed to the boiler effectively, but some of the product is lost as it combines to form a carbonate by-product. Never feed neutralizing amines to the deaerator. With boiling points of 205°F and 210°F, respectively, for cyclohexylamine and DEAE, feeding them to a deaerator that operates at 234°F would cause a high level of loss of these products. Where a feed water tank (operating below 195°F) open to atmosphere is being used, neutralizing amines may be added to the feed water tank. Feed to the steam header is always the preferred point of application.

Along with carbon dioxide, oxygen can reenter the condensate system. In this case, the neutralizing amines mentioned so far do not have the ability to react with the oxygen. The result of oxygen present in a neutralizing amine program is oxygen pitting. Oxygen can enter from leaking seals, vacuum breakers on heating systems, or condensate return tanks. The control of oxygen in the condensate return system can be accomplished by adding either a filming amine or DEHA. DEHA, as already discussed, will carry with the steam and is then available to control oxygen in the condensate system. This is one of the reasons that the control limit for DEHA is measured in the condensate. Residual DEHA in the condensate indicates that there is sufficient DEHA in the boiler and that oxygen is not present in the condensate.

The other alternative is the use of either a primary or a tertiary filming amine. These amines are long-chain aliphatic hydrocarbons and coat the internals of the pipes. The coating prevents contact with either carbonic acid or oxygen.

Octadecylamine (ODA) is the primary amine used in boiler water treatment. The material is thick and wax like, making it difficult to pump. It must be added to the steam header. In boilers operating under 300 psi, it will not volatilize out of the boiler. ODA is fed based on steam load. The percentage of makeup or condensate return does not factor into the feed rate.

ODA has both a hydrophobic and a hydrophilic end. The hydrophobic end attaches to the metal surface, displacing corrosion byproducts. The corrosion byproducts then carry with the condensate back to the feed water system. The overfeed of ODA will cause the condensate return line to close off, and the film builds onto itself in layers.

Chemical feed points

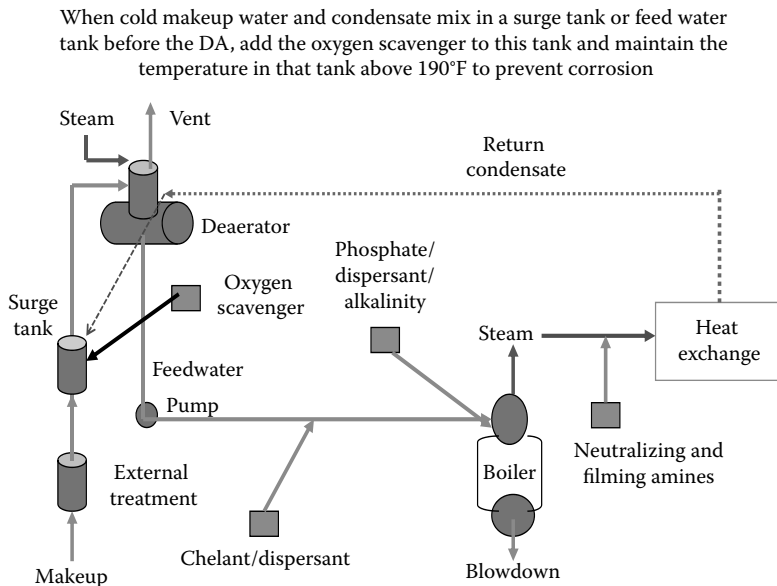


FIGURE 15.7 Chemical feed points. (Courtesy of Guardian CSC, York, Pennsylvania, Boiler Water Training Course.)

For these reasons, whenever an ODA program is initiated, begin at 25% of the maintenance feed rate for at least the first 30 days. Once the condensate has cleared, increase the feed rate of the ODA to 50% for the next 30 days and so on until the feed rate is at 100% of the recommended maintenance feed rate. It may take up to 6 months to reach the recommended feed rate. Caution: feeding the product at a more rapid rate will cause fouling and plugging of traps, strainers, and lines.

The tertiary amines are made from soy bean, tallow, and other organics. They function the same as the ODA, but tertiary amines are easier to feed due to a much lower viscosity. Tertiary amines carry the same as the primary amines, so they must be fed directly to the steam header. Tertiary amines tend to attach with multiple hydrophobic ends, so the attachment to the metal surface causes the tertiary amine to lay at an angle. This reduces the potential for the amine to cause line plugging the way the ODA does.

Neutralizing amine can be added to a filming-amine-treated system and the neutralizing amine will act similar to a paint stripper to thin the film. This process is beneficial where some fouling has occurred. A word of warning: the neutralizing amine, if fed at a sufficient level, can also act as a paint stripper. Picture all of the filming amine and the corrosion byproducts coming back to the feed water system at one time. Always act with caution when using neutralizing amines in a system treated with filming amines. Keep the pH low (around 8.0), and look for black sticky material plugging everything, including the continuous blowdown line.

15.4 CHEMICAL FEED POINTS

The feed point for the boiler water treatment product is as important as the product itself. Figure 15.7 presents the drawing showing the recommended feed points for the boiler water treatment programs discussed in this chapter.

15.5 SUMMARY

Boiler water treatment has to be considered as a program. The program consists of how to combine pretreatment, chemical treatment products, and application knowledge. When the program is implemented correctly, the result is a clean, fuel-efficient boiler system. However, boiler failures will occur if a mistake is made in any part of the program. Mistakes result in scale, corrosion, fuel loss, and mechanical failure in part or all of the boiler system.

Therefore, it is important to understand the relationships between water quality and boiler water treatment. The proactive maintenance of pretreatment equipment yields quality conditioned water for the boiler. Higher quality water requires less chemical conditioning and allows for reduced blowdown from the boiler. The reduction of blowdown reduces fuel usage. Chemical reduction reduces costs and minimizes the introduction of chemical back into the environment.

A major portion of this chapter has dealt with pretreatment, the mechanical conditioning of water impurities which appears to be the future of the boiler water treatment industry. Water scarcity, green technology, and fuel costs are changing the chemical water treatment industry toward minimizing chemical usage. This means that the future of boiler water treatment will see an increased use of filtration, ion exchange, and membrane technology.

The chemical treatment portion of the program will focus on oxygen scavenging and dispersant technology. With improved water purity, boiler scale and condensate corrosion potential will be reduced. Application knowledge will then become even more important. With higher quality makeup water, there will always be the potential for greater catastrophic failures, should a failure or misapplication occur in the pretreatment system.

REFERENCES

1. Freedman, A., Cotton, I., and Hollander, O. *Association of Water Technologies Technical Reference and Training Manual*. Association of Water Technologies, Rockville, MD (2001).
2. Ketric, B. *External Treatment*. Association of Water Technologies Technical Training Course, Rockville, MD (2008).
3. Ketric, B. *Boiler Water Training*. Association of Water Technologies Technical Training Course, Rockville, MD (2008).
4. Ketric, B. Field determination of deposits, *Association of Water Technologies*, Analyst, March (1990).
5. Ketric, B. Neutralizing amines, *Association of Water Technologies*, Analyst, Spring (1994).
6. Colin, F. *Boiler Water Treatment: Principles and Practice*, Volumes 1 and 2. Chemical Publishing Company, New York (2002).
7. Alco's Answers, *A Practical Guide to Every Day Engineering and Scientific Problems*. Alco Chemical, Chattanooga, TN.
8. Cotton, I. Clarification products. AWT TRTM, Rockville, MD, pp. 2–16 (2001).
9. Ketric, B. Types of filters. Internal Training Program, Guardian CSC, York, PA.
10. Ketric, B. Resin application table. Internal Training Program, Guardian CSC, York, PA.
11. Ketric, B. Oxygen scavenger. AWT Training Course, Rockville, MD, Boiler water treatment, pp. 47–55 (2009).
12. Frayne, C. and Ketric, B. Properties of oxygen scavengers. AWT Training Course, Rockville, MD, Boiler water treatment, p. 56 (2009).
13. Ketric, B. Types of phosphates. AWT Training Course, Rockville, MD, Boiler water treatment, p. 126 (2009).
14. Ketric, B. Characteristics of neutralizing amines. AWT Training Course, Rockville, MD, Boiler water treatment, p. 174 (2009).

16 Corrosion Control in Industrial Water Systems

Mel J. Esmacher

CONTENTS

16.1	Introduction.....	320
16.2	Corrosion Fundamentals.....	320
16.2.1	General Corrosion.....	320
16.2.2	Galvanic Corrosion.....	320
16.2.3	Crevice Corrosion.....	322
16.2.4	Pitting.....	322
16.2.5	Intergranular Corrosion.....	323
16.2.6	Dealloying.....	324
16.2.7	Erosion Corrosion.....	324
16.2.8	Stress-Corrosion Cracking.....	325
16.3	Water-Based Industrial Water Systems: Cooling and Boiler Systems.....	327
16.4	Corrosion Control in Cooling Water.....	327
16.4.1	Once-Through Cooling Water Systems.....	327
16.4.2	Closed Loop Cooling Water Systems.....	327
16.4.3	Open Recirculation Systems.....	328
16.5	Cooling Water Treatment.....	328
16.5.1	Barrier Film (Precipitating/Cathodic) Inhibitors.....	329
16.5.2	Passivating (Anodic) Inhibitors.....	329
16.5.3	Organic Inhibitors.....	329
16.5.4	Copper-Based Alloys Inhibitors.....	330
16.5.5	Treatment for Microbiological Control.....	330
16.6	Corrosion Control in Boiler Systems.....	330
16.6.1	General Corrosion Control in Boilers.....	331
16.6.2	Boiler Corrosion: Role of Dissolved Gases and Dissolved Solids.....	331
16.6.3	Boiler Water Treatment.....	332
16.6.4	Underdeposit Corrosion.....	332
16.6.5	Other Localized Corrosion/Cracking Mechanisms in Boilers.....	333
16.6.6	Erosion Corrosion.....	333
16.6.7	Steam Condensate Treatment.....	334
16.6.8	Steam Purity.....	335
16.7	Corrosion Control in Desalination Systems.....	335
16.8	Corrosion Control in Geothermal Systems.....	337
16.8.1	Corrosion Monitoring Techniques/Field Testing.....	339
16.8.2	Corrosion Coupons.....	339
16.8.3	Instantaneous Corrosion Rate Meters.....	339
16.9	Summary.....	339
	References.....	340

16.1 INTRODUCTION

Industrial water systems play a vital role in plant operation by facilitating heat transfer via heat exchangers and condensers, and enabling boiler operations to produce steam for process and electrical power generation. In addition to minimizing deposit fouling, avoiding scale buildup, and reducing microbiological growth, corrosion control in water systems can be the most important factor to avoid premature failure of the heat exchanger, boiler, or process equipment. Desalination and geothermal systems also represent unique challenges in controlling corrosion. Unfortunately, corrosion in water systems can take many forms, and unless precautions are taken to mitigate the potential causes of metal loss in an operating system, premature failure in the form of general attack, pitting, cracking, or other specialized degradation mechanisms can create a forced outage for repairs.

16.2 CORROSION FUNDAMENTALS

Corrosion can be defined as the generalized deterioration of a metal or engineered material in reaction with its environment via a chemical, an electrochemical, or a physical process. There are several classifications for the types of corrosive attack or degradation that can be encountered in an industrial water system, which historically have been identified by Fontana as “the eight forms of corrosion” [1]. These include

- General corrosion
- Galvanic corrosion
- Crevice corrosion
- Pitting
- Intergranular corrosion
- Dealloying
- Erosion corrosion
- Stress-corrosion cracking

16.2.1 GENERAL CORROSION

With industrial water systems, general corrosion is frequently the most common deterioration mechanism encountered, with the resultant failure mode in a piece of equipment being manifested as a generalized wastage away or thinning via an electrochemical process. A most common example is carbon steel that develops a porous, nonprotective rust corrosion product layer on the metal surface that increases over time at the expense of the base metal thickness, resulting in general corrosion failure via thinning. This process in aqueous environments takes place by the frequent switching of anodic and cathodic half-cell reactions on the metal surface, thereby causing an overall even loss of metal, as shown in Figure 16.1.

Another example is the generalized thinning of metal surfaces in contact with condensed steam containing unneutralized carbonic acid, where metal loss is typically distributed rather evenly across the surface wetted by condensate.

16.2.2 GALVANIC CORROSION

Galvanic corrosion, sometimes referred to as dissimilar metal corrosion, involves the direct contact of two different metal types in a water system, whereby one of the metals behaves in a preferred anodic dissolution region, while the second metal acts as a cathodic area where electron reduction reactions occur predominately, as shown in Figure 16.2.

In water systems, a specialized form of dissimilar corrosion can sometimes be termed *microgalvanic corrosion*, whereby dissolved metal cations become reduced on anodic metal surfaces [such as copper cations be cathodically reduced on steel, zinc-plated (galvanized) steel, or aluminum alloys] with severe general corrosion or rapid pitting attack developing.

16.2.3 CREVICE CORROSION

During electrochemical corrosion, general dissolution develops when anodic and cathodic half-cell reactions are randomized on metal surfaces, and gradually switch locations over time. However, the localized intensity of corrosion can develop when anodic regions reside in discrete locations such as that induced by fouling deposits or sedimentation on a metal surface, or under gasket joints (as shown in Figure 16.3), or under bolt heads or washers, and so on.

This is referred to as crevice corrosion or a crevice concentration cell. The anodic dissolution process in a crevice is thought to initially propagate due to differential concentration cells involving dissolved gases, such as oxygen, or variable concentration of corrosive anions, such as chlorides, for example. Once initiated, a secondary, autocatalytic process can accelerate corrosion, whereby the hydrolysis of metal salts formed underneath a deposit or occluded (trapped) space on a metal surface produces free mineral acidity. This markedly reduces the pH in the bottom of a crevice cell site (to less than 3.0).

16.2.4 PITTING

Similar to the localized intensity developed by crevice cell concentration effects, pitting can produce perforation and metal failure via generation of a hole or cavity that is deeply penetrating without any appreciable general corrosion. Thus, pitting is regarded as one of the most insidious forms of metal deterioration (as shown in Figure 16.4).

Because casual observations fail to detect pinholes as they develop, and generalized measurements (such as weight loss of corrosion coupons) do not adequately monitor the progress of pitting attack, leaks in water-based systems due to pitting tend to be severe when finally discovered. Unfortunately, there are a multitude of factors that can stimulate initiation and propagation of corrosion pits, which further complicates the predictability of whether corrosion pits will form or intensify with time. Because pitting tends to be more prevalent in stagnant or low-flow conditions and grow where water can pool or debris can build up on a surface, some generalizations can be made to reduce the impact of pitting by guiding corrective action. Such corrective actions include keeping metal surfaces clean, evacuating water used following the hydrotesting of new equipment, or using a corrosion inhibitor to mitigate corrosion pitting tendencies during wet storage or “layup” of equipment.

TABLE 16.1
Galvanic Series of Metals and Alloys

Corroded end (anodic, or least noble)
Magnesium
Magnesium alloys
Zinc
Aluminum
Cadmium
Aluminum alloys
Steel or iron
Cast iron
Chromium-iron (active)
Ni-resist
18–8 Cr-Ni-Fe (active)
18–8–3 Cr-Ni-Mo-Fe (active)
Lead-tin solders
Lead
Tin
Nickel (active)
Brasses
Copper
Bronze alloys
Copper-nickel alloys
Monel
Silver solder
Nickel (passive)
Inconel (passive)
Chromium-iron (passive)
18–8 Cr-Ni-Fe (passive)
18–8–3 Cr-Ni-Mo-Fe (passive)
Hastelloy C
Silver
Titanium
Graphite
Gold
Platinum
Protected end (cathodic, or most noble)

Source: *Betz Handbook of Industrial Water Conditioning*, 9th edn., Trevoise, PA, Betz Laboratories, 1991.

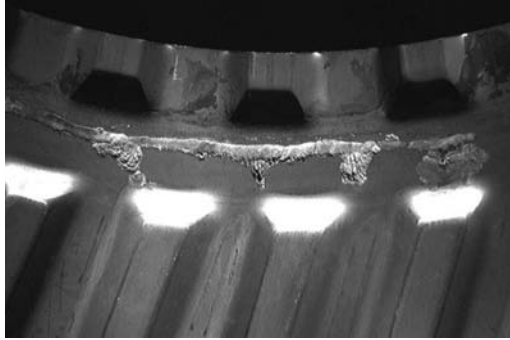


FIGURE 16.3 Crevice corrosion on stainless steel, after the removal of rubber gasket.

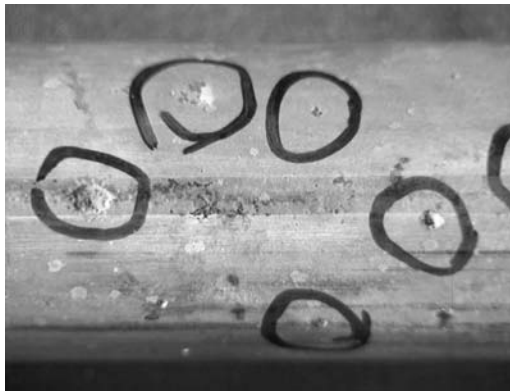


FIGURE 16.4 Pitting corrosion on a stainless steel tube surface.

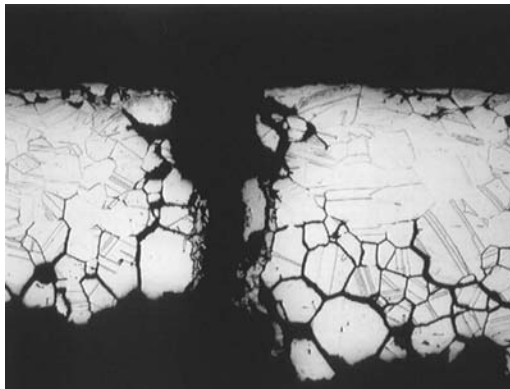


FIGURE 16.5 Intergranular corrosion in brass.

16.2.5 INTERGRANULAR CORROSION

Another form of localized corrosion is intergranular corrosion (as shown in Figure 16.5), which is often dependent on the metallurgical condition of the metal or alloy.

A classic example is the sensitization of welded 304-grade stainless steel in the heat affected zone (HAZ), which leads to intergranular corrosion due to chromium depletion within grain boundary regions of the metal via chromium carbide precipitation. The use of 304L (lower carbon grade where the carbon content does not exceed 0.03 wt.%) or niobium/titanium additions in austenitic

stainless steel alloys helps minimize grain boundary chromium carbide precipitation in welded regions, and thereby reduces the susceptibility to intergranular corrosion.

16.2.6 DEALLOYING

Another corrosion mechanism that is dependent on the alloy type being used in a water application is *dealloying*, which is sometimes referred to as *selective leaching* or “*parting*” corrosion. Specific dealloying terms have been used over the years that correspond to certain alloys, for example: dezincification for brass (copper-zinc) alloys, denickelification for copper-nickel, graphitic corrosion for damage that develops on cast iron alloys, and so on. A common feature of a dealloying mechanism is the difficulty to evaluate the damage based on the visual examination of the deteriorated region. This is due to the gradual dissolving and reprecipitation of the various alloy components and/or corrosion product. Thus, the part impacted by the dealloying may appear dimensionally intact and serviceable until cut and inspected in cross-section (as shown in Figure 16.6).

16.2.7 EROSION CORROSION

The term *erosion corrosion* is a broad term meant to encompass related metal loss conditions that include erosion, impingement, cavitation, and flow-accelerated corrosion (FAC). The action of water flow across a metal surface can produce patterns of directionalized metal loss elongated in the direction of flow, which can resemble horseshoe-shaped pits or divots (as shown in Figure 16.7). The erosive nature of the flow may involve excessive flow velocity, turbulence, sudden changes

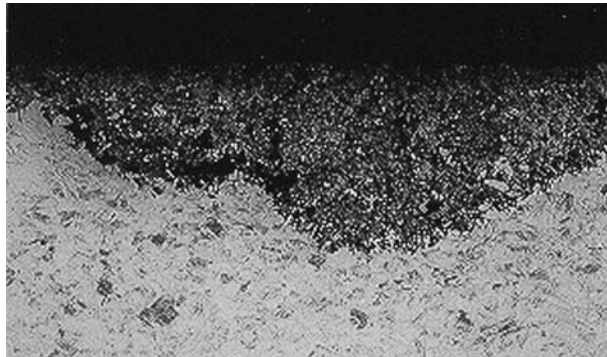


FIGURE 16.6 Dezincification corrosion in brass; microscopic cross-section view.



FIGURE 16.7 Erosion in brass. Note the horseshoe-shaped pits. Flow is from right to left.

in pressure that cause vapor-filled bubbles (or cavities) to violently collapse, and/or film-stripping of protective oxide layers required to maintain general corrosion resistance in a given water environment.

16.2.8 STRESS-CORROSION CRACKING

Stress-corrosion cracking (SCC), sometimes referred to as *environmental cracking*, involves the generation and propagation of cracks on a metal surface, which ultimately results in brittle fracture of a component. Classic examples in water systems include “caustic embrittlement” in boilers which involves carbon steel under high residual tensile stress in the presence of hot, concentrated caustic salts (as shown in Figures 16.8 and 16.9), “season cracking” which involves the cracking of brass alloys in stressed regions in contact with ammonia (from heavy “seasonal” rainfall and decomposition of organic matter), and chloride-SCC of austenitic stainless steel, such as 304 and 316 grades (as shown in Figures 16.10 and 16.11).

The theory of why finely branched cracks can grow on a metal surface with little to no general corrosion or pitting taking place is complex. What is clear is that the process that generates SCC damage is electrochemical in nature, with hydrogen evolution at advancing crack tips being confirmed as integral to the embrittlement phenomenon. In addition, only specialized alloy-environment-stress combinations will yield conditions sufficient to generate and propagate SCC damage. Thus, the ability to predict and protect equipment from SCC can usually be achieved through empirical evaluation of water characteristics and alloy/fabrication/material selection options.

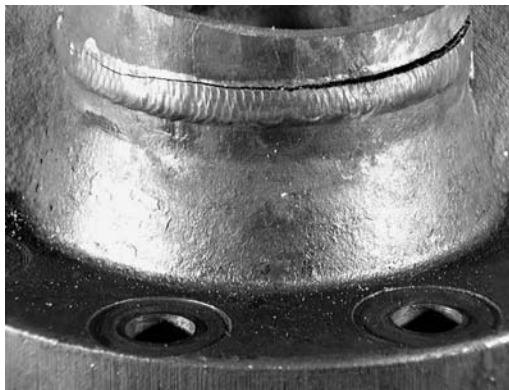


FIGURE 16.8 SCC due to caustic concentration at a welded steam line flange; macro view.

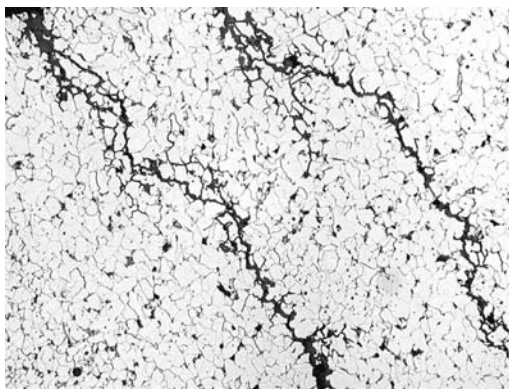


FIGURE 16.9 SCC due to caustic concentration at a welded steam line flange; microstructure view.

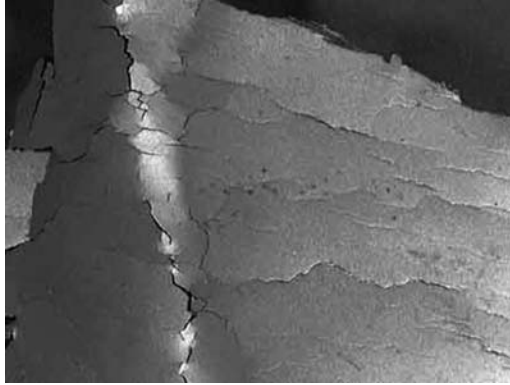


FIGURE 16.10 SCC of stainless steel due to chlorides; macro view.



FIGURE 16.11 SCC of stainless steel due to chlorides; microstructure view.



FIGURE 16.12 Hydrogen damage in a boiler tube.

A related environmental cracking mechanism is hydrogen embrittlement (or hydrogen-induced cracking) in water systems stemming from the absorption of nascent hydrogen in cathodic areas, especially in sour-water conditions where hydrogen sulfide is present. In boiler tubing, cracking from hydrogen damage can cause brittle fracture in regions where fine cracks grow from subsurface fissures that develop at the base (or periphery) of localized corrosion gouge sites (as shown in Figures 16.12 and 16.13).



FIGURE 16.13 Hydrogen damage in a boiler tube; microstructure view.

16.3 WATER-BASED INDUSTRIAL WATER SYSTEMS: COOLING AND BOILER SYSTEMS

With the various categories of potential failure mechanism defined, the evaluation of practical measures for corrosion control and prevention can be reviewed. The methodology of corrosion control is dependent on the type of water-based operating system being evaluated. For example, cooling water usage can be segmented into three broad categories: (a) once-through cooling water, (b) closed loop systems, and (c) open recirculating systems that employ a cooling tower for evaporative heat rejection. In addition, boiler water and related steam condensate return in utility plants represent a large usage of water in an industrial plant, but have different makeup and treatment conditions than cooling water. Each of these major areas of water use and treatment to mitigate corrosion will be covered in the later sections.

16.4 CORROSION CONTROL IN COOLING WATER

16.4.1 ONCE-THROUGH COOLING WATER SYSTEMS

Assuming ready access to abundant freshwater sources nearby, and limited difficulties with discharge issues (thermal or chemical pollution from water discharge), there are advantages to routing cooling water “once-through” heat exchanger tube bundles for absorbing waste heat. A key advantage of these systems is that little to no chemical treatment is typically required. Some natural water sources are not very corrosive in once-through applications, and cleanliness can be high so that there is no significant driving force for mineral scale formation, unlike open recirculating cooling systems that concentrate the mineral components via cycling. However, in once-through systems, consideration should be given to the use of intermittent biocide application to control microbiological growth. In once-through systems, more corrosion-resistant alloys such as copper–nickel, titanium, or specialized stainless steel alloys are required because the large volume of water processed does not allow for less corrosion-resistant materials of construction to be used for example, it is not feasible to feed corrosion inhibitors that lower-cost materials require if they are not retained in once-through cooling water system [2].

16.4.2 CLOSED LOOP COOLING WATER SYSTEMS

In contrast to once-through cooling systems, closed loop recirculating systems are operated with a high concentration of corrosion inhibitors, as long as system water losses are minimal (i.e., no significant uncontrolled leaks). This can create a tremendous advantage in terms of corrosion control,

with the only significant cost being during the initial commissioning of the system in which the inhibitor is dosed.

Conventional water treatment for corrosion control in closed loop systems includes nitrites and molybdate-based corrosion inhibitors for steel corrosion control, now that past chromate treatments are obsolete due to environmental concern. Most corrosion problems in closed loop cooling water systems that employ nitrite or molybdate-based inhibitor chemistry are related to dilution of concentration over time (in conjunction with inadequate monitoring), which can be critically important as these are both considered to be anodic inhibitors. When anodic corrosion inhibitors are not maintained at sufficient concentrations, the result can be manifested as severe pitting corrosion, as not enough inhibition of anodic dissolution sites are achieved, leaving unfavorable anode to cathode area effects on the corroding metal surface. In the case of nitrite-based treatment programs, microbiological activity by nitrifying bacteria can result in nitrite depletion via oxidation to nitrate, resulting in the acceleration of corrosion. The addition of a biocide may be necessary with nitrite-based corrosion programs or systems subject to organic contamination.

16.4.3 OPEN RECIRCULATION SYSTEMS

Open recirculation systems allow a more economic reuse of cooling water to be achieved by heat removal via evaporative cooling, ponds, cooling towers, and so on, and employing corrosion inhibitors, deposit control agents, and biocides (chlorine, bromine, and nonoxidizing biocides) to keep surfaces clean and free from corrosion. Open recirculation cooling water systems reuse water by an evaporation and concentration scheme. As the system evaporates water, the ions in the makeup water concentrate. The degree to which the water is concentrated is referred to as *cycles of concentration*, and is a multiple of ion concentration in the makeup water. Whether or not a specific cycled water source has inherent fouling or corrosive characteristics, based on the concentration of dissolved solids, temperature, and so on, it can be evaluated by various indexes, including the Langelier saturation index (LSI) or the Ryznar stability index, RSI [3]. These indexes are typically based on the relative degree of the supersaturation of the cycled water with respect to the formation of calcium carbonate deposits.

To avoid deposition and resultant underdeposit crevice corrosion from water-formed deposits in cooling systems, it is essential to understand the limits of the cycle of concentration of the makeup water and the impact of treatment chemicals that modify crystalline precipitation reactions in water systems. Likewise, attention must be directed at controlling the formation and buildup of microbiological deposits (i.e., biomass formation, algae, fungi, slime, and bacterial species that can metabolize corrosion by-products). In the case of the latter, both aerobic and anaerobic bacteria can be problematic, even for corrosion-resistant stainless steels, such as 304SS and 316SS, especially in conjunction with stagnant solutions [4]. In open recirculating systems, the buildup of potentially corrosive anions due to high cycle operation can also pose the risk of pitting corrosion or stress-corrosion cracking (i.e., chloride cracking of austenitic stainless steels).

16.5 COOLING WATER TREATMENT

As indicated above, the selection of appropriate water treatment chemicals to achieve corrosion control depends on the quality of cooling water makeup, the nature of the cooling water usage (once-through, closed, and open recirculation), and other design/operational parameters (such as cycles of concentration, heat load, water velocity, and so on). The goal of corrosion control is to maintain a clean surface, thus avoiding underdeposit concentration cells, and having achieved that, working toward maintaining a passivation layer on the metal surface via the use of water treatment chemicals that optimize passive films or retards dissolution of protective oxide films.

16.5.1 BARRIER FILM (PRECIPITATING/CATHODIC) INHIBITORS

Steel corrosion protection can be achieved with the application of inhibitors capable of forming an inert film on the metal surface that retards both the anodic and cathodic reactions. The film is the result of the local precipitation of inorganic compounds at the high pH cathodic sites. Inorganic phosphates (orthophosphate, as shown in Figure 16.14, and polyphosphate, like hexametaphosphate, as shown in Figure 16.15) and zinc salts are the most commonly used materials.

The solubility of the salts of the inhibitors (zinc hydroxide, zinc phosphate, calcium phosphate, and calcium carbonate) is pH dependent, decreasing with increasing pH. The success of this approach depends on limiting film formation to the cathodic sites and not allowing uncontrolled precipitation that would result in scale formation. Although inorganic phosphate acts primarily as a cathodic inhibitor, increasing cathodic polarization, it also provides anodic corrosion inhibition. High levels of inorganic phosphate will passivate steel in the presence of oxygen at near neutral pH (pH < 8). Another anodic characteristic is that corrosion is localized in the form of pitting when insufficient amounts of phosphate are present or high salinity conditions exist.

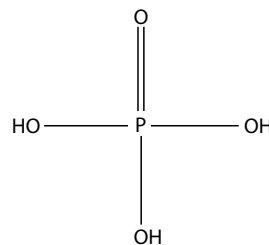


FIGURE 16.14 Orthophosphate—steel corrosion inhibitor.

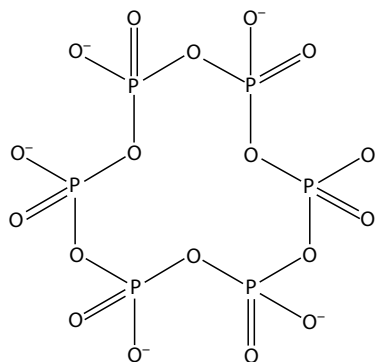


FIGURE 16.15 Hexametaphosphate—steel corrosion inhibitor.

16.5.2 PASSIVATING (ANODIC) INHIBITORS

In addition to precipitating inhibitors, passivating inhibitors (anodic inhibitors) are widely used, and include chromate, nitrite, molybdate, and orthophosphate. Although chromate is an excellent overall corrosion inhibitor, health, environmental, and regulatory concerns has all but eliminated this inhibitor from modern applications. Nitrite is an effective inhibitor at proper dosage levels and does not require dissolved oxygen to be present, which makes it ideal for closed systems. The downside to nitrite inhibitor usage is the potential to oxidize to nitrate via nitrifying bacteria. Nitrite is not utilized for open recirculation system because of both bacterial concerns and its incompatibility with oxidizing biocides use for microbial control. In some circumstances, the use of nitrite along with molybdate can be very effective and reduces the cost of the treatment program. With the increased cost of molybdate, this can be an important consideration. Lastly, although orthophosphate is widely used due to low costs, there can be a tendency to precipitate with calcium hardness present in makeup water, which requires the use of specific deposition control agents to prevent fouling.

16.5.3 ORGANIC INHIBITORS

Organic inhibitors work as a result of adsorption of inhibitor on the entire metal surface. The film formed by the adsorption of soluble organic inhibitors is very thin. Cationic organic inhibitors carry a net positive charge and anionic organic inhibitors a net negative charge. Organic inhibitors are adsorbed according to the ionic charge of the inhibitor and the charge on the metal surface. Cationic inhibitors (positively charged), such as amines, or anionic inhibitors (negatively charged), such as sulfonates, will be adsorbed preferentially, depending on whether the metal is charged

negatively or positively [5]. Very recently, newer programs using organic corrosion inhibitors to replace traditional nitrite and molybdate treatment programs have been introduced with promising results [6].

16.5.4 COPPER-BASED ALLOYS INHIBITORS

The most effective corrosion inhibitors for copper and its alloys are the aromatic triazoles, such as benzotriazole (BZT) and tolyltriazole (TTA) (see Figures 16.16 and 16.17).

These compounds bond directly with cuprous oxide (Cu_2O) at the metal surface, forming a “chemisorbed” film. In addition to bonding with the metal surface, triazoles bond with copper ions in solution. Thus, dissolved copper represents a “demand” for triazole, which must be satisfied before surface filming can occur. Although the surface demand for triazole filming is generally negligible, copper corrosion products can consume a considerable amount of chemical treatment, especially if high chlorination rates result in “copper throw” and cause a high level of dissolved copper to be in the cooling water. In addition, excessive chlorination will deactivate the triazoles and significantly increase copper corrosion rates. One successful approach to counteract this tendency in chlorinated systems is to utilize a halogen-resistant azole (HRA), which resists the chemical deactivation of the azole by chlorination [7].

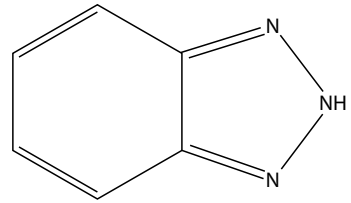


FIGURE 16.16 BZT—copper corrosion inhibitor.

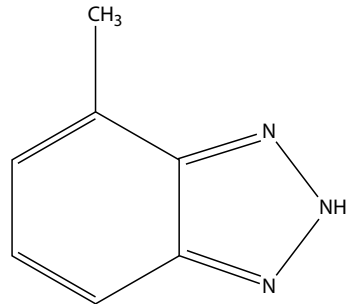


FIGURE 16.17 TTA—copper corrosion inhibitor.

16.5.5 TREATMENT FOR MICROBIOLOGICAL CONTROL

Microorganisms that form a biofilm on a metal surface can block corrosion inhibitor transport or create localized corrosion via indirect and direct microbiological growth processes. Some microbes in a biofilm layer can produce waste products such as organic acids and hydrogen sulfide that are directly aggressive to metal substrates or create crevices that can promote localized pitting via concentration cell action.

Basic chemical treatment preventative measures to limit bacterial growth and the establishment of biofilms include maintaining a sufficient residual halogen (chlorine, bromine, chlorine dioxide, etc) level and the periodic application of a nonoxidizing biocide or biofilm detergent. In addition to the measurement of residual chemical levels that are required to limit microbiological growth in a water system, the presence of microorganisms within the system may be monitored directly by enumerating microbes using growth- or culture-based methods. Examples of such methods include plate counts, dip slides, or serial dilution vials. The levels of bioactivity can also be monitored indirectly using specific biochemical markers [e.g., adenosine triphosphate (ATP)].

16.6 CORROSION CONTROL IN BOILER SYSTEMS

Corrosion control in boiler systems has historically been focused on the methodology to reduce explosions and improve reliability. In the 1880s, boiler explosions were so common that one industry journal had a regular column called “The Month’s Accidents” [8]. In addition to manufacturing and construction practices that were conducive to mechanical failure or leaks, boiler water chemistry often played a role (albeit unidentified at the time) with the generation and growth of stress corrosion cracks from caustic embrittlement at riveted joints or leaking tube joints. Although

presently forgotten, boiler explosions due to cracked drums created by caustic embrittlement have been largely minimized by modern practices in boiler construction (welding replacing riveted joints) and in boiler water treatment (such as the use of sodium nitrite as a SCC inhibitor or coordinated pH-phosphate treatment to eliminate free caustic alkalinity in boiler water systems), as well as advances in water purification technology, specifically ion exchange and more recent membrane pretreatment systems.

In reviewing methodologies to control corrosion in boiler systems, the type of approach to mitigate attack is dependent on the source water and external treatment characteristics. In most cases, the pretreatment of incoming boiler makeup water via softeners, demineralizers, and/or reverse osmosis (RO) systems has greatly reduced fouling tendencies in boiler systems, which directly impacts underdeposit corrosion tendencies boiler tubing. Unfortunately, softener upsets, demineralizer exhaustion, and RO system fouling can promote unexpected boiler feedwater quality upsets, as can unanticipated condensate return contamination issues. With the proper treatment and monitoring of boiler feedwater and steam condensate return, boiler water systems can be kept clean, which is conducive to minimizing localized underdeposit crevice corrosion tendencies.

16.6.1 GENERAL CORROSION CONTROL IN BOILERS

Unlike cooling water systems that frequently operate with high dissolved gases and high total dissolved solids levels, external treatment involving deaeration, softening/demineralization of water sources, and other techniques to purify boiler feedwater are typically required for economic boiler operation. With sufficient water purity, the maintenance of appropriate boiler water alkalinity and pH, and the elimination of dissolved oxygen, the protective magnetite (Fe_3O_4) layer on carbon steel surfaces typically proceeds. At temperatures below 250°C , the oxidation of iron in water creates iron hydroxide, which converts to hematite, and at higher temperatures (250°C – 350°C), direct oxidation to magnetite occurs [9]. Between an approximate pH of 8.5 and 12.7, the reaction of steel surfaces in contact with boiler water rapidly produces a thin, adherent, and highly protective magnetite film and is self-limiting [10]. Once established and maintained within a safe pH range, the thickness of magnetite film will tend to increase slightly over time, but with a limited transport of contaminants, tends to stabilize and protect the steel substrate from general corrosion and pitting.

16.6.2 BOILER CORROSION: ROLE OF DISSOLVED GASES AND DISSOLVED SOLIDS

Dissolved gases (such as dissolved oxygen, carbon dioxide, and so on) can play a key role in boiler and steam condensate corrosion. A principal corrosion threat to carbon steel components is dissolved oxygen, which becomes increasingly corrosive in closed systems as a function of temperature. Accordingly, dissolved oxygen in boiler feedwater is typically removed or reduced to low parts-per-billion levels through a combination of mechanical and chemical deaeration. Despite these precautions to preclude dissolved oxygen in boiler feedwater, the majority of corrosion pitting failures in boiler systems can be attributed to differential oxygen concentration cells that lead to perforation, especially in the absence of suitable precautions in the wet storage of units, or from inadequate on-line dissolved oxygen control.

In a similar manner to dissolved oxygen control, corrosion control in steam condensate return systems can be achieved by reducing carbonate alkalinity in the boiler feedwater makeup or using condensate treatment chemicals (such as neutralizing or filming amines) to protect equipment from low-pH carbonic acid attack. The aggressiveness of low-pH condensate due to the presence of carbonic acid is pronounced and should not be overlooked. For example, the mild steel corrosion rate induced by a pH of 4.7 carbonic acid solution has the equivalent corrosive effect on steel (30 mils per year) as a hydrochloric acid solution at a pH of 2.9. This is attributed to the fact that the carbonic acid formed by CO_2 is only partially dissociated, and thus its acidic strength is greater than the pH reading [11].

16.6.3 BOILER WATER TREATMENT

There are three general types of internal boiler chemical treatment options to be considered for industrial boiler water treatment: polymers, chelants, and phosphates. Polymers control the deposition of contaminants via complexation, crystal distortion, or dispersion. With complexation, the polymer combines with boiler feedwater contaminants, such as calcium, and the resultant polymer-contaminant complex remains soluble, and is removed via boiler blowdown. With crystal distortion, contaminants that form crystalline precipitate phases are the modified (or stunted) interaction of the polymer with the growing, or incipient crystals (often called crystal “nuclei”), thereby keeping the size of the particle within a range that encourages dissolution. In this mechanism, the crystals are maintained in the unstable size range where formation and dissolution are in a proportion that favors the latter, namely dissolution. In the dissolution mechanism, stable deposit particles that form (like particulate iron oxide that can be transported from the feedwater system, condensate return, or corrosion in the preboiler circuit or economizer) are effectively coated by the polymer adsorbing to their surfaces. Polymer adsorption enhances the natural repulsive electrostatic surface charges that effectively prevent coalescence or agglomeration into larger particles, as well as the attachment of particles to boiler internal surfaces (the polymer also adsorbs to internal tube and boiler surfaces). The dispersed particles are maintained in colloidal suspension in the boiler water, facilitating their removal via blowdown or the bleed of concentrated boiler water.

Chelants, such as ethylenediaminetetraacetic acid (EDTA), as shown in Figure 16.18, like polymers, can form highly stable complexes with calcium and magnesium contamination in boiler feedwater, which prevents the precipitation of these potentially scale-forming constituents. Low-level chelant additions are usually combined with polymeric dispersants to provide a very effective approach to maintaining boiler cleanliness.

Phosphate additions are used to control both deposition and corrosion. For example, with boiler water makeup containing hardness salts, inorganic orthophosphate can be used to precipitate feedwater calcium in boiler water, and also assists in the precipitation of magnesium contamination, which can then be removed from the system as a sludge rather than having calcium and magnesium form harder, highly insulating scales in steam generation areas. In higher quality boiler feedwater makeup free of calcium and magnesium, phosphate is frequently fed to control corrosion via the application of a “congruent” or “coordinated” phosphate-pH program, which can be especially effective in higher-pressure boiler systems. With this phosphate “buffer” approach, coordinated phosphate-pH treatment programs can capture or control acidic or alkaline contamination based on control limit guidelines [12].

16.6.4 UNDERDEPOSIT CORROSION

As discussed above, the use of boiler water treatment additives such as polymeric dispersants can greatly reduce the buildup of deposits and scale in a boiler. In addition, following good boiler layup

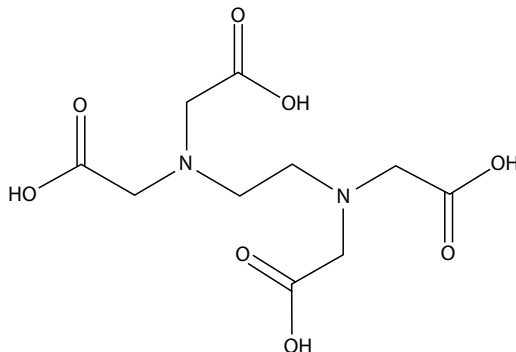


FIGURE 16.18 EDTA chelant—for boiler deposit control.

practices can reduce the ingress of iron oxides and copper alloy corrosion products from the pre-boiler circuit in conjunction with an outage [13]. However, when deposit control methods fail, the use of deposit-weight density (DWD) calculations to determine the amount of deposit accumulation per surface area, expressed in grams/square foot (or milligrams/square centimeter), is one way to quantify the buildup of deposits, sediments, or scales [14]. Of course, when evaluating a boiler deposit formation, it is imperative to also record deposit thickness and analyze for elemental weight percent composition in order to understand the severity of deposit accumulation and the origin of the deposit based on the elemental composition of the various layers that may be present [15].

There are strategies for boiler water chemistry and boiler water alkalinity treatment methodologies that can limit underdeposit corrosion. The use of a coordinated pH-phosphate control regime in higher-pressure boilers allows for the buffering of underdeposit acidic or caustic contamination to limit the corrosive impact of off-specification quality boiler feedwater or condensate return. For example, assuming an excursion in boiler feedwater or condensate contamination that causes chloride intrusion into the boiler water, a coordinated pH-phosphate treatment program would be anticipated to be twice as effective in preventing corrosion than a free-caustic control program against acid ingress and several orders of magnitude better than an all-volatile treatment (AVT) program [16].

Despite the best attempts to keep boiler watersides surfaces clean, boiler tube failure due to underdeposit corrosion can develop. During failure analysis, a careful diagnosis of the types of deposit layers that form within the corrosion gouge can often point to key causative factors that, in turn, can direct corrective action in troubleshooting water chemistry issues, boiler water, or steam condensate treatment [17]. For example, acidic underdeposit corrosion tends to leave behind distinctive layers as viewed in metallographic cross-sectional analysis, which tend to be absent in caustic underdeposit corrosion gouges [18]. In addition, with acidic phosphate corrosion gouging, the layers of maricite can be produced that help in identification that the pH range in coordinated pH-phosphate treatment program is in the low range of the control box or below the prescribed sodium to phosphate ratio [19].

16.6.5 OTHER LOCALIZED CORROSION/CRACKING MECHANISMS IN BOILERS

As indicated previously, the lack of deposit control can lead to various localized failure mechanisms in boiler equipment such as underdeposit corrosion, but other localized failure can develop due to overheating, hydrogen damage, thermal/corrosion fatigue, or stress-assisted corrosion (SAC) [20]. Tube metal overheating is frequently cited as the most common form of boiler tube failure, with deposit fouling, excessive heat flux, and inadequate circulation being the main causes for creep rupture due to overheating. In higher-pressure boilers, fouled regions that develop underdeposit concentration cells, can foster conditions conducive to the generation of hydrogen as a by-product of the cathodic half-cell reaction. This nascent hydrogen can migrate into the steel in the gouged areas to produce brittle fracture by forming a network of intergranular microfissures [21].

16.6.6 EROSION CORROSION

The destruction or dissolution of a protective metal oxide resulting in directional metal wastage or thinning can be referred to as *erosion corrosion* (EC) or *flow-accelerated corrosion* (FAC). The variance in the terminology is subject to some debate, but generally EC is thought to be more dependent on mechanical or impingement action that removes a protective film, whereas FAC is more often associated with a chemical dissolution process that thins or destroys the protective film on the metal surface, thereby rendering the substrate vulnerable to accelerated wastage. Thus, the interplay of design and operational characteristics of boiler water chemistry and treatment can influence the development of EC or FAC. For example, if the design geometry of a bend, tee joint, or header connection creates excessive localized velocity or turbulence, the mechanical impact

will produce a “wash-out” on the regions subject to the location where the change of flow direction is most pronounced [22]. In most cases, the metal surface left behind will feature sculpted or directional wastage patterns, with horseshoe-shaped pits sometimes seen [23]. In some cases, the polishing effective of the erosive water flow will leave a very thin, black magnetite layer that will have a shiny luster.

Although the design of tubing or piping configurations versus the water velocity is typically a controlling factor, the effect of pH in boiler water and steam condensate systems can also have a contribution to EC or FAC deterioration. For example, in boiler tubing, a change in boiler water pH from 9 to 10 can produce a 10-fold decrease in erosion corrosion metal loss [24]. In a similar fashion, controlling pH above 9.0 in steam condensate systems using a proper blend of neutralizing amines, the amount of material wear rate via erosion corrosion can be significantly minimized, but may require a computer-based condensate modeling system to account for basicity, neutralizing capacity, and distribution ratios [25].

In addition to pH dependence, temperature can have a significant effect on the FAC of steel, with the greatest wastage rate observed between 220°F and 320°F (104°C and 160°C) [26]. In situations where pH or temperatures are difficult to adjust in a particular application, the use of chromium and other alloying additions to steel can produce a substantial reduction in EC or FAC tendencies. As little as 0.1% Cr can arrest FAC damage, and with 1% Cr addition, the elimination of FAC in steel in boiler waterside environments can be achieved [27]. There are occasions where iron transport is documented to be high due to erosion corrosion in boiler feedwater systems, and in addition to increasing pH, the application of a filming polymer or reducing agent can provide other alternatives to reduce high feedwater iron contents from entering the boiler system [28].

16.6.7 STEAM CONDENSATE TREATMENT

Dissolved gases in condensed steam, such as oxygen and carbon dioxide (CO₂), can be controlled by minimizing air ingress into a steam condensate system, but the primary source of aggressive low-pH condensate related to CO₂ is the thermal decomposition in the boiler of carbonate and bicarbonate alkalinity that occurs naturally in the boiler feedwater. The carbon dioxide produced flashes off with the steam, and at the point of condensation, a portion becomes dissolved in the liquid phase and forms a dilute, carbonic acid solution. Reducing the carbonate/bicarbonate alkalinity in boiler water makeup streams via external pretreatment processes (i.e., dealkalization, reverse osmosis, demineralization, and so on) can reduce the amount of chemical treatment additive required to control or reduce condensate system corrosion [29].

Chemical treatment options for carbonic acid that may be present in condensed steam include the use of volatile organic amines, which are commonly referred to as *neutralizing amines*. Neutralizing amines hydrolyze in aqueous conditions and generate the hydroxide ions required for the neutralization of acidic species in the steam condensate, such as carbonic acid. There are several types of neutralizing amines used in steam condensate systems, and the ability of a specific neutralizing amine to protect a system effectively depends on its neutralizing capacity, recycle/recovery ratio, basicity, distribution ratio, as well as the thermal stability of the particular amine at the temperature and pressure of the system [12].

Another class of corrosion inhibitors, referred to as *filming amines*, work by establishing a protective monomolecular, barrier-type film. The long-chain aliphatic amines used in a typical filming application comprises a hydrophilic nitrogen group that absorbs onto the metal surface, and an attached hydrophobic, hydrocarbon chain that prevents the condensate and corrosive agents in the condensate from contacting the metal surface [30]. When properly applied, filming amine corrosion inhibitors can be both economical and effective. However, their practical application has been greatly limited due to the difficulty in preparing and injecting viscous feed solutions, as well as the tendency of certain filming amines to combine with hardness contaminant and/or iron oxide and other condensate corrosion products to form tacky or adherent deposits. Under some conditions,

these deposits can foul steam-condensate surfaces and components, such as steam traps, pressure control valves, and so on. These deposits can also accumulate in boilers when condensate is returned.

More recently, a new generation of nonamine filming corrosion inhibitors have been developed that overcome a number of the limitations of the older, filming amine technology. These products are effective corrosion inhibitors, are much easier to feed, and have a much lower tendency to combine with contaminants or corrosion products to form deposits. In addition, a newly introduced technology utilizing a unique phospholipid corrosion inhibitor shows significant promise as a steam-condensate corrosion inhibitor for use in systems such as applications where steam contacts food products, where volatile amines or nitrogen-containing steam treatments are either not permitted by the governing regulatory agencies or not desired by the steam user [31].

16.6.8 STEAM PURITY

Corrosion or metal failure in the steam path will be minimized by strict adherence to water makeup and condensate return quality, as well as total dissolved solids (TDS) limits in the steam, in accordance with the American Society for Testing and Materials (ASTM) guidelines [32]. Using these guidelines as a starting basis, additional consideration should be given to heat flux, boiler water circulation and load, and consistency for control. Thus, when higher heat flux is part of a design or operational scenario, the higher-pressure water chemistry guidelines for the boiler system should be followed to ensure that proper steam purity is achieved [33].

When proper guidelines are not followed and/or mechanical issues with water/steam separation equipment or level control develop, the carryover of water droplets into the steam phase can develop that creates severe operational problems in downstream steam lines, superheaters, turbine equipment, and other steam path components. Thus, carryover salts in steam systems can accumulate on hot metal surfaces via the evaporation concentration of water droplets, and cause the blockage of tubes, corrosion, overheating, and stress-corrosion cracking (SCC) [34]. In some cases, a single carryover upset can rapidly damage stainless steel components within hours or days of the event, and cause continued damage to replacement components until the steam system is properly flushed out of any residual caustic salt contamination in the steam line, header, and so on. [35].

16.7 CORROSION CONTROL IN DESALINATION SYSTEMS

The desalination of seawater accounts for a total global production of 24.5 million cubic meters of water per day [36]. There are several large-scale processes that can be employed in desalination, including multistage flash (MSF), multieffect distillation (MED), and seawater reverse osmosis (SWRO). The main corrosion control methodology employed in these systems is material selection, coordinated with the unique aspects of design and operational challenges in each type and stage of the individual desalination process being considered. For example, pitting corrosion has been estimated to account for 41% of all the corrosion failures in MSF plants, with crevice corrosion under deposits being most troublesome [37]. Accordingly, efforts to model the corrosion performance of a range of alloys in simulated MSF conditions that emulate behavior in both vapor and fully wetted conditions at various temperature stages have been attempted to better predict suitability for actual field conditions [38]. A variety of stainless steels and corrosion-resistant alloys (CRAs) can be utilized in the construction of desalination plant equipment. These include four major types of stainless steels: martensitic, ferritic, austenitic, and duplex. Within these major types, there are higher alloy content choices, typically referred to as super-ferritic, super-austenitic, and super-duplex.

Early desalination plants relied upon austenitic stainless steel, such as 316L, as a cost-effective material of construction, only to find pitting and severe crevice corrosion in high chloride service developing after the first several years of operation [39]. Over time, experience has now shown that super-austenitic containing 6% molybdenum (254 SMO, Al-6XN, and so on) and duplex-type

stainless steel alloys (that have a mixture of ferrite and austenite in the steel microstructure, such as 2205, 2507, Zeron 100, and so on) are more suitable for crevice corrosion and pitting applications. These alloys can be ranked to identify suitable candidates for the material of construction via the pitting resistance equivalent number (PREn), along with critical pitting temperature (CPT) and critical crevice temperature (CCT) parameters [40]. In addition, electrochemical polarization studies to produce values for corrosion and pitting potential via potentiodynamic polarization curves are often conducted to supplement PREn, CPT, and CCT test results [41].

Basically, the addition of molybdenum and nitrogen to a chromium-based stainless steel and the impact of metal alloy composition on pitting/crevice corrosion can be estimated by PREn, defined as:

$$\text{PREn} = \% \text{Cr} + 3.3\% \text{Mo} + 16\% \text{N} \quad (16.1)$$

In selected alloys, a higher multiple of 30 for nitrogen rather than 16 has been utilized to reflect a greater impact on localized corrosion resistance [42]. These relative performance rankings based on PREns of the candidate alloys, while not absolute in predicting actual field performance, can guide alternative material selection by approximating anticipated CPT and/or CCT values by the influence of alloy content, with a PREn value above 38 as indicative of good resistance to marine corrosion [43]. Thus, material selection based on alloy composition, coupled with comprehensive laboratory tests on metal samples to evaluate pitting or crevice temperature characteristics, can help guide anticipated engineering performance versus chloride concentration and temperature. An example of the typical chemical composition, strength, and corrosion performance values for alloys used in desalination plants has been recently compiled [44]. Material selection utilizing lower cost duplex stainless steels (via lower nickel content and higher strength) with corrosion performance that approaches the various austenitic stainless alloys also makes them a cost-efficient alternative to coated carbon steels [45]. In more recent approaches, a dual duplex material approach has been advocated to utilize lean duplex stainless steels in the less corrosive parts of the desalination and higher alloy duplex stainless steel in areas exposed to more harsh conditions [44]. In this regard, a key advantage of the lean duplex grades is the markedly lower nickel content (1.5% Ni), with pitting and crevice resistance on par with 300 series stainless steels, and strength values that could allow a reduction in gauge thickness up to 50% in comparison. At the next level, 2205 has similar pitting and crevice corrosion resistance to austenitic alloys, like 904L, but is not as resistant as super-duplex grades, which have a better performance record in SWRO. For example, the pitting corrosion and crevice resistance of the super-duplex, like 2507 approaches that of 254 SMO, with PREn values estimated to be equivalent (approximately 43), but having the cost advantage of lower nickel content (7% versus 18% Ni) [46].

Other alloys considered to be effective in various components in desalination service include copper-based alloys (aluminum brass, copper-nickel, and so on), titanium, super-ferritic stainless steels (SeaCure), and more expensive specialty high-nickel alloys (Hastelloy C-276, C-22, Inconel and Incoloy alloys, and so on). The key advantages to copper-based alloys are excellent heat transfer and inherent antifouling characteristics, which must be balanced with the negative impact of discharge limitations on heavy metals concentration (as by-products of corrosion), susceptibility to erosion corrosion, and sensitivity to ammonia and sulfide contamination. In certain applications, a higher strength alloy (i.e., duplex stainless steel alloys, super-ferritic stainless steel alloys like SeaCure, and titanium alloys) can be used with a thinner-wall configuration as compared to traditional copper alloys, allowing excellent corrosion resistance and comparable overall heat transfer characteristics (due to the thinner wall configuration). Lastly, nickel-based alloys, although superior in performance with regard to pitting, crevice corrosion, and stress-corrosion cracking in seawater service, can be cost-justified in only specific niche applications, such as bolting/fasteners, pump shafts, valve components, and other specialized circumstances.

Piping components in desalination systems and distribution networks represent a considerable proportion of capital expenditure and present frequent challenges in terms of failure prevention and inspection/repairs. Connection points in piping can be prone to intense localized corrosion, especially in threaded, flanged, or compression fittings (i.e., Victaulic-type) that use O-rings or gaskets to effectively seal the joint, but in turn create crevices. In SWRO plants, crevice corrosion in piping connections has been documented not only in the lower grade 316L stainless steel, but also 317L, 2205, and higher alloy austenitic 904L piping connections [47]. Care also must be taken when making connections between dissimilar metal components, because brackish and seawater environments can drive the galvanic corrosion of the less-corrosion-resistant alloy in the couple [47].

The evaluation of crevice corrosion pitting in marine environments is a function of several parameters in the bulk water environment conditions, such as pH levels, deaeration, chloride concentration, velocity, temperature, and microbiological fouling tendencies [47]. For example, the lower oxygen content in deaerated seawater helps retard the establishment of an oxygen differential concentration cell and reduces a cathodic depolarizing reaction, allowing lower alloy content stainless steel grades to be used in desalination operations via the use of deaeration [48]. Deaerated seawater, reduced from a normal level of 8 ppm down to 10 ppb, will show an order of magnitude decrease in anodic dissolution and pitting in stainless steel alloys [49]. However, in practice, deaerated solutions in desalination environments can be difficult to maintain in certain stages or locations, particularly around seals where air ingress can be problematic or in conjunction with outage periods during which aeration could develop. Thus, it is advisable to consider the option to drain and flush with fresh water in conjunction with longer duration outage periods to help mitigate the risk of stagnant, aerated brines or seawater solutions causing pitting of 300 series stainless steel alloys [50].

In certain areas, bulk water conditions can become more aggressive due to chemical treatment or unique operating conditions. For example, the presence of residual chlorination in the pretreatment of feed in the low-pressure section of a SWRO plant (as well as in high-pressure piping) can promote pitting and crevice corrosion. Also, higher temperatures and higher chloride concentrations found in energy recovery systems can cause similar corrosion challenges. The upgrading of piping and other components to 6-moly grade stainless steels such as 254 SMO, Al-6XN, or 2507 super-duplex stainless steels has proven to be successful in these types of circumstances [46].

16.8 CORROSION CONTROL IN GEOTHERMAL SYSTEMS

Similar to corrosion control in desalination systems, material selection guidelines have been developed in the past for geothermal power systems based on the specific resource characteristics [51]. Materials of construction (MOC) choices are typically dictated by the presence of key corrosive parameters in geothermal fluids, such as dissolved oxygen, pH, chlorides, sulfates, carbon dioxide, hydrogen sulfide, and ammonia content [52]. In addition, material selection choices (mild/low-alloy steels, stainless steels, titanium, nickel-based alloys, copper-based alloys, and other metallic materials) are dependent on the design of the specific process that involves either (a) a vapor-dominated geothermal resource where dry steam from a geological formation is produced at the wellhead, (b) a liquid-dominated water-based system where two-phase flow from the wellhead is processed via liquid/steam flash separators, and so on, or (c) binary systems in which the geothermal liquid heats another working fluid [53].

The individual geothermal process stream characteristics (chemical composition, pH, temperature, and velocity) can vary, depending on the geographical location of the source and on the point within the power generation cycle (from the well bore to collection at the wellhead, transfer piping, at separators, turbine, condenser, and so on). For example, the previous field studies of various alloys in Salton Sea geothermal brines with extreme total dissolved solids content (25–30 wt.%) confirmed the poor performance of copper alloys, aluminum, and ferritic steels with less than

18% chromium content, as well as most austenitic stainless steels, but satisfactory performance with high chromium/high nickel alloys and titanium [54]. In addition, the prediction of the corrosion performance of materials can be further complicated by the formation of scale and the presence of noncondensable gases, which varies significantly with the location of the geothermal fluid source and the geological makeup of the formation.

In steam-dominated geothermal systems, the role of noncondensable gases is often the most significant factor in evaluating the corrosion potential of system components, with carbon dioxide, hydrogen sulfide, ammonia, and hydrogen chloride gases being the most problematic. Given its relative abundance, the pH of geothermal fluids and process streams is largely controlled by CO₂, which can drive carbon steel corrosion via the formation of carbonic acid. Significant H₂S content can create conditions conducive to sulfide stress-corrosion cracking in hardened, high-strength steels, as well as promote attack on copper and nickel alloys. In addition, the oxidation of H₂S in aerated geothermal process streams increases the acidity of the stream. The combination of ammonia and hydrochloric gases is thought to drive acid dew-point corrosion via ammonia chloride formation, resulting in a pH as low as 3.0 and requiring neutralization approaches with caustic injection near the wellhead of these acid-chloride-producing wells [55]. The presence of dissolved gases, along with dissolved solids, is thought to provide nutrition to microbiological growth in geothermal-sourced steam condensate used for cooling water applications, which in turn creates biofilm fouling and corrosion [56].

In direct liquid-dominated geothermal systems, much more complicated process fluid compositions that provide a multitude of challenges in terms of material selection and corrosion control are encountered. With this type of system, the hot liquid is simply separated (flashed) to steam that spins a turbine that drives a power-plant electric generator. The liquid may also be double-flashed in order to provide additional steam to the turbine and increase efficiency [57]. Following along the flash steam path, a key challenge is to minimize erosion/corrosion impact by reducing droplet carryover, along with the inherent transport of acid gases (H₂S, CO₂, and HCl) in the steam and steam condensate. These conditions are typically not found in a nongeothermal-sourced steam power plant system. Accordingly, specialized methods have been attempted to control corrosion in the steam and steam condensing system, including the use of CRAs or more cost-effective measures such as injection of filming amine/corrosion inhibitors, and the use of protective coatings. For example, corrosion rate reduction via amine/inhibitor treatment has been estimated to reduce corrosion 90–95% in carbon steel, saving considerable cost avoidance versus utilization of CRAs [58]. In addition, coatings utilizing polyphenylene sulfide (PPS), with proprietary fillers (marketed under the trade name, CurraLon?), have been shown to protect carbon steel in condensed acidic steam in geothermal applications. PPS-derived coating formulations also show promise in extremely high-temperature geothermal brines and/or heat exchanger applications (reducing costs by approximately 80% compared to high-grade stainless steel or titanium) [59].

The additional materials challenge in a single- or double-flash steam power plant operation is that the originating geothermal fluid may be at elevated temperatures (over 200°C) and involve concentrated brine solutions that have 11%–15% chlorides, such as that utilized in the Salton Sea, California, geothermal brine resource area. In this regard, carbon steel piping was noted to corrode at a rate of 410 mils per year (10.4 mm/yr), leading to the evaluation and use of 2507 super-duplex stainless steel [60].

In a binary geothermal plant configuration, use of lower-temperature geothermal systems typically routes a mixture of corrosive brine, hot water, and/or a water/steam mix from the formation into a heat exchanger application. In a binary process, a working fluid (such as isopentane or isobutene) is heated by the geothermal resource, and the heated working fluid in turn vaporizes and expands across a turbine to drive electrical generation. Thus, the geothermal fluid is not flashed within this closed system, and is able to be completely reinjected back into the formation. This reduces corrosive gas release and simplifies the power generation side of the process in terms of materials of construction (MOC) [61].

16.8.1 CORROSION MONITORING TECHNIQUES/FIELD TESTING

When establishing a baseline to determine the relative corrosivity of an aqueous system, various methodologies are available to help quantify the corrosion rate. Once a baseline corrosion performance has been established, corrective action (such as injecting a corrosion inhibitor into the stream) can be properly evaluated.

16.8.2 CORROSION COUPONS

Common tools used for corrosion monitoring include *corrosion coupons*, which are preweighed metal strips exposed for a set length of time that is determined to be representative within the system. Based on the weight loss of the coupon after the removal of corrosion products, measured per surface area and exposure time, a mils per year (MPY) calculation can be used to estimate the average thickness loss based on the density of the metal being tested. In addition to weight loss, metal coupons can be viewed for the patterns of corrosion (pitting, microbiological corrosion, discoloration related to dealloying, and so on), which can guide corrective actions in terms of corrosion inhibitor feed in the field or the adjustment of microbiological control parameters. Corrosion coupons can also be configured to evaluate susceptibility to crevice corrosion (CC), or stress-corrosion cracking (SCC), based on the manipulation of attachment points to the surface (crevice washers) or stresses (U-bend or c-ring coupons).

The disadvantage of using corrosion coupons is the lack of heat transfer on the metal surface as compared to an actual heat exchanger in the system. In addition, the flow rate in the bypass rack that is typically optimized for uniform results and may not actually mimic low-flow conditions that may be prevalent within the system. In addition, only time-weighted averages are compiled for general corrosion and pit rates; there is no ability to ascertain the impact of a single upset or series of upsets on the accumulated total metal loss within the exposure period.

16.8.3 INSTANTANEOUS CORROSION RATE METERS

A key advantage of measuring the corrosion rate at any particular moment in time via electrical resistance probe or electrochemical measurements (such as linear polarization) is that sudden changes in corrosion propagation in a system can be detected, quantified, and recorded to correlate to episodic events in the system being evaluated. For example, the impact of a consistent pattern of repeated acid ingress or overdosing during a chlorination cycle in cooling water treatment are upsets that can produce significant metal loss that could be detected based on evaluating electrode probe characteristics in the system. There are many other electrochemical techniques that can be evaluated for the real-time estimation of corrosion performance, including potentiodynamic cyclic polarization studies, electrochemical noise (ECN) monitoring, use of a multielectrode array device, and so on.

16.9 SUMMARY

In summary, corrosion control in heat exchangers and steam generation systems is dependent on system design and the cost-effective use of suitable corrosion inhibitors, and keeping cooling water and boiler systems free of deposits and scale. In desalination systems, effective corrosion control is achieved by the evaluation of the actual process conditions (pH, chlorides, total dissolved solids, chlorination, temperature, velocity, the frequency of stagnant conditions, and so on) versus predictive material selection parameters for candidate materials (such as utilizing PREn, CPT, CCT, electrochemical studies, and so on). Lastly, as operating experience in geothermal energy applications continues to confirm advances in scale/corrosion inhibition treatment and materials or coatings are optimized for geothermal process fluids, geothermal power plants are anticipated to demonstrate improved reliability and cost-effective operation.

REFERENCES

1. Fontana, M. G. *Corrosion Engineering*, New York: McGraw-Hill (1986).
2. Dillon, C. P. *Materials of Construction for Once-Through Water Systems*, MTI Publication No. 43, St. Louis, MO: Materials Technology Institute of the Chemical Process Industries, Inc. (1998).
3. Dillon, C. P. *Corrosion Control in the Chemical Process Industries*, MTI Publication No. 45, St. Louis, MO: Materials Technology Institute of the Chemical Process Industries, Inc. (1997).
4. Perry, R. H. and Green, D. W. *Perry's Chemical Engineer's Handbook*, 7th edn., New York: McGraw Hill, (1997).
5. Methods of corrosion control, Chapter 6. In: *NACE Basic Corrosion Course*, May 2004, NACE International, Houston, TX (2004).
6. Beer, W. and Corvetto, R. A new closed system treatment program for industrial applications. In: *Cooling Tower Institute Annual Conference*, Corpus Christi, TX (2007).
7. May, R. C., Cheng, L., and Shao, F. Second generation, halogen resistant copper corrosion inhibitors. In: *CORROSION/02, Paper No. 02413, NACE International*, Houston, TX (2002).
8. Kuehn, S. E. Power for the industrial age: A brief history of boilers. *Power Engineering* 100, 15–19 (1996).
9. Gibbon, D. L., Seels, F. H., and Simon, G. C. Magnetite and water-formed deposits in steam boilers: SEM and EDX observations. *Scanning Electron Microscope Conference*, 641–649 (1981).
10. Johnston, N. N. Formation and prevention of boiler water side corrosion are detailed. *Pulp & Paper* 64, 138–142 (1990).
11. Kirby, G. N. Corrosion performance of carbon steel. *Chemical Engineering*, 86, 72–84 (1979).
12. Betz Laboratories Inc. *Betz Handbook of Industrial Water Conditioning*, 9th edn. Trevese, PA: Betz Laboratories (1991).
13. Daniels, D. Follow good layup practice to prevent cycle corrosion. *Power*, 142, 37–40 (1998).
14. Esmacher, M. J. Deposit weight density methodology for industrial boilers. *Materials Performance* 28, 74–78 (1988).
15. Esmacher, M. J. and Bodman, G. H. Use of comprehensive deposit analysis techniques to evaluate boiler deposits prior to chemical cleaning. In: *International Water Conference, IWC-00-33*, Pittsburg, PA (2000).
16. Stodola, J. Review of boiler water alkalinity control. In: *International Water Conference, IWC-86-27*, Pittsburg, PA (1986).
17. Esmacher, Mel J. Avoiding potential problems in diagnosing boiler tube failure mechanisms. In: *International Water Conference, IWC-98-03 Report*, Pittsburg, PA (1998).
18. Esmacher, Mel J. The impact of water chemistry on boiler tube failures. In: *25th Annual Electric Utility Chemistry Workshop*, University of Illinois at Champaign-Urbana, Champaign and Urbana IL, May (2005).
19. Dooley, B. and McNaughton, W. P. Don't let those boiler tubes fail again. *Power Engineering* 101, 55–61 (1997).
20. Sylvester, W. R. Waterside corrosion fatigue cracking—Is there a single cause and solution? In: *CE Canada Power Systems 4th Availability Workshop*, Ottawa, Ontario, Canada, October (1987).
21. Hendrix, D. The influence of water cycle chemistry in the failure of waterwall tubes in a high pressure boiler due to hydrogen attack. In: *CORROSION/95, Paper No. 613, NACE International*, Houston, TX (1995).
22. Weed, R. H., Tvedt, T. J., and Cotton, I. J. Erosion corrosion in utility systems. In: *Power-Generation Conference*, Orlando, FL, December (1995).
23. Kotwica, D. Analysis of heat recovery steam generator tube failures. In: *CORROSION/03, Paper No. 03487, NACE International*, Houston, TX (2003).
24. Heltmann, H. G. and Kastner, W. Erosion-corrosion in water-steam cycles – causes and countermeasures. *VGB. Kraftwerkstechnik* 62, 180–187, March (1982).
25. Robinson, J. O. New computer modeling system improves condensate treatment. In: *Corrosion Asia*, Singapore, September (1994).
26. Lopriore, R. P. How utilities monitor pipe-wall thinning at nuclear plants. *Power* 32, 67–70 (1988).
27. Thailer, H. J., Dala, K. J., and Goyette, L. F. Flow-accelerated corrosion in steam generators. In: *PVP Vol. 316, Plant Systems/Components Aging Management*, New York, NY, ASME, p. 134 (1995).
28. Drews, T. and Robinson, J. O. Resolving flow accelerated corrosion problems in the industrial steam plant. In: *CORROSION/99, Paper No. 346, NACE International*, San Antonio, TX (1999).
29. Dilcer, S. B. Making condensate treatment successful. In: *CORROSION/84, Paper No. 226, NACE International*, Houston, TX (1984).

30. Robinson, J. O. Effective condensate treatment: A key to improving mill operation. *Paper Trade Journal* 169, 51–55 (1985).
31. Crovetta, R. and Murtagh, E. Novel boiler condensate corrosion inhibitor with FDA approval. In: *NACE/2007, Paper No. 07073, NACE International*, Houston, TX (2007).
32. ASME. *Consensus on Operating Practices for the Control of Feedwater and Boiler Water Quality in Modern Industrial Boilers*, New York: ASME (1994).
33. Dyer, D. B. Internal water treatment for industrial steam plants. *Internal Technical Paper*. GE Water & Process Technologies, TP-415, June (2002).
34. Kotwica, D. J. Deposit related failures of boiler superheater tubing and steam piping. In: *CORROSION/95, Paper No. 615, NACE International*, Houston, TX (1995).
35. Esmacher, M. J. Stress corrosion cracking of stainless steel components in steam service. In: *CORROSION/01, Paper No. 01496, NACE International*, Houston, TX (2001).
36. Lattemann, S. and Hopner, T. Environmental impact and impact assessment of seawater desalination. *Desalination* 220, 1–15 (2008).
37. Malik, K. Corrosion and material selection in desalination plants. In: *SWCC, O&M Seminar*, Al Jubail, Saudi, Arabia, April (1992).
38. Essam E. F., El-Sayed, Ali Al-Odwani, Mansour, A., and Mohamed, Al-Tabtabaei. Process design and performance of an MSF distillation test unit for corrosion studies. *Desalination* 201, 23–34 (2006).
39. Olsson, C. Stainless steels for SWRO plants high-pressure piping, properties and experience. IDA, BAH03-041.
40. Nordstrom, J. and Olsson, J. Stainless steel for high pressure piping in SWRO plants: Are there any options. *Desalination* 97, 213–220 (1994).
41. Malik, A., Andijani, U., Ismail, N., and Siddiqi, N. A. Corrosion behavior of some conventional and high alloy stainless steels in gulf seawater. Technical Report No. SWCC RCC-20, September (1992).
42. Malik, A. U., Siddiqi, N. A., Ahmad, S., and Andijani, I. N. The effect of dominant alloy additions on the corrosion behavior of some conventional and high alloy stainless steels in seawater. *Corrosion Science* 37, 1521–1535 (1991).
43. Malik, A. U., Ahmad, S., and Andijani, I. Corrosion behavior of steels in gulf seawater environment. *Desalination* 123, 205–213 (1999).
44. Olsson, J. and Sinis, M. Duplex – A new generation of stainless steels for desalination plants. *Desalination* 205, 104–113 (2007).
45. Sinis, M. and Olsson, J. Reduced cost for storage and distribution of desalted water – Use of duplex stainless steel. *Desalination* 223, 476–486 (2008).
46. Olsson, J. Stainless steels for desalination plants. *Desalination* 183, 217–225 (2005).
47. Al Hossani, H. I., Saber, T. M. H., Mohammed, R. A., and Shams El Din, A. M. Galvanic corrosion of copper-base alloys in contact with molybdenum-containing stainless steels in Arabian gulf water. *Desalination* 109, 25–37 (1997).
48. Abu-Safiah, A. Failure of sections and components in seawater RO plants. *Desalination* 84, 309–333 (1991).
49. Glover, T. J. Recent developments in corrosion-resistant metallic alloys for construction of seawater pumps. *Materials Performance* 27, 51–56, July (1988).
50. Oldfield, T. Corrosion consideration in selecting metals for flash chambers, water for life. In: *Proceedings of the International Congress on Desalination and Water Re-use*, Nice, France, October 21–27 (1979).
51. DeBerry, D., Ellis, P. F., and Thomas, C. C. *Material Selection Guidelines for Geothermal Power Systems*, 1st edn. US Dept of Energy (DOE). Document No. ALO/3904-1, Radian Corp., Austin, TX, September (1978).
52. Ellis, P. F. and Anliker, D. M. Geothermal power plant corrosion experience-A global survey. In: *CORROSION/81, Paper No. 235, NACE International*, Houston, TX (1981).
53. Conover, M., Ellis, P., and Curzon, A. Material selection guidelines for geothermal power systems – An overview. In: *Geothermal Scaling and Corrosion – Symposium* New Orleans, LA. ASTM Special Publication 717 (1979).
54. Carter, J. P. and Cramer, S. D. Materials of construction for Salton sea geothermal brines. In: *CORROSION/89, Paper No. 535, NACE International*, Houston, TX (1989).
55. Hirtz, P., Buck, C., and Kunzman, R. Current techniques in acid-chloride corrosion control and monitoring at the geysers. In: *Proceedings, Sixteenth Workshop on Geothermal Reservoir Engineering*, Stanford University, Stanford, CA, January 23–25 (1991).
56. Pryfogle, P. A. *Monitoring Biological Activity at Geothermal Power Plants*, Idaho National Laboratory, Idaho Falls, Idaho, DOE Contract DE-AC-07-99ID13727 (2005).

57. Duchane, D. Geothermal energy, In: *Kirk-Othmer, Encyclopedia of Chemical Terminology*, 4th edn., Vol. 12. pp. 521–525 (1994).
58. Stapleton, M. Helping power plants run better. In: *Geothermal Resources Council, 2005 Annual Meeting*, Reno, NV, September 25–28 (2005).
59. Geothermal today, coating technology improves performance, US-DOE (2003).
60. Furmanski, G., Kaiser, S. D., and Shoemaker, L. E. A. NiCrMo welding product provides optimum weldments in superduplex pipeline for geothermal power serviced. In: *CORROSION/08, Paper No. 08177, NACE International*, Houston, TX (2008).
61. Kagel, A. GEA, The state of geothermal technology, Part II. *Surface Technology* January (2008).

17 Interactions of Polyelectrolytes with Particulate Matter in Aqueous Systems

P. Somasundaran and Venkataramana Runkana

CONTENTS

17.1	Introduction.....	343
17.2	Characteristics of Particulate Matter and Polyelectrolytes.....	344
17.3	Polymer Adsorption	345
17.4	Polymer-Induced flocculation	348
17.5	Modeling of Polymer Adsorption, Interaction Forces, and Flocculation	352
	17.5.1 Polymer Adsorption	353
	17.5.2 Interaction Forces between Polymer-Covered Particles	353
	17.5.3 Polymer-Induced Flocculation.....	354
17.6	Summary and Suggestions for Future Research.....	359
	Acknowledgments.....	360
	References.....	360

17.1 INTRODUCTION

Water is the most precious natural resource as it impacts the health and survival of the people, agriculture, industrial productivity, as well as the generation of power. According to estimates, more than 1.2 billion people lack access to safe drinking water and nearly 4000 children die daily due to diseases transmitted through unsafe water or human excreta [1,2]. Water treatment plants have to meet not only stringent regulations on quality of produced water but also changing demands from consumers in terms of suspended particulate matter, color, odor, taste, and residual concentrations of chemicals employed during water purification. Water is also an important process medium and a solvent in many industries. For example, practically all industrial manufacturing operations require water as boiler feed and all semiconductor fabricators require an enormous amount of water for washing silicon. Water is also an essential ingredient in many food and beverage products and pharmaceutical formulations [3].

Coagulation and flocculation are key unit operations in water treatment as efficiency of subsequent clarification and filtration steps is linked critically with the manner, effectiveness, and rate of flocculation [4,5]. Polymers and polyelectrolytes have become favorable flocculation and filtration aids in water treatment due to several reasons [6]. For example, the required polymer dosage is relatively lower than that for the commonly employed inorganic coagulant, alum. The resultant sludge generated is also relatively low and the concentrations of dissolved inorganics such as aluminum in treated water are minimal. The strength of flocs obtained through polymer-induced flocculation is also high because polymeric flocculants provide many links between particles due to the attachment of a number of segments with surface groups on particles. Moreover, it is not always possible to control the stability of colloidal suspensions efficiently and obtain the desired

results by manipulating just pH and concentrations of coagulants such as alum. Even small amounts of dissolved electrolyte ions, particularly those of multivalent species, can change the stability of a suspension drastically. Similarly, depending on the pH, mineral and metal oxide particles can partially dissolve in solution and the dissolved species can adsorb onto particle surfaces and modify their electrochemical and other surface characteristics [7,8]. Due to these reasons, polymers and polyelectrolytes have become standard favorite flocculation additives for effluent treatment. The efficiency of water purification and quality of effluent water depend strongly on the interactions between polyelectrolytes and constituents of raw water such as particulate matter, natural organic matter, and dissolved chemical species. Hence, it is possible to control the flocculation by engineering the polymer adsorption density and importantly the conformation at the solid–solution interface by varying process variables such as pH, ionic strength, polyelectrolyte type, dosage, and temperature. Indeed, such engineering depends on an accurate understanding of the mechanisms by which a polymer adsorbs on particles and affects the interaction between particles.

The focus of this chapter is on interactions of polyelectrolytes with particulate matter that affect coagulation and flocculation. The discussion involves relevant characteristics of particulate matter and polyelectrolytes, principles of polymer adsorption on particles, and polymer-induced flocculation. Mathematical modeling is now an important tool for any new process or product development, and for the optimization and control of existing processes. Hence, modeling of polymer adsorption and flocculation is discussed subsequently.

17.2 CHARACTERISTICS OF PARTICULATE MATTER AND POLYELECTROLYTES

Water from natural resources such as rivers consists of particulate matter, natural organic matter (NOM), dissolved chemical species, and, due to environmental pollution, toxic industrial or domestic waste products. Industrial wastewaters too contain similar constituents, in varying proportions. Water is essentially a multicomponent mixture of solid and liquid species along with bubbles and droplets. The particulate matter includes clay, minerals or metal oxides, metal carbonates, algae, protozoa, bacteria, and viruses. The NOM consists of fulvic acids, humic acids, tannins and polysaccharides, etc. [9]. The characteristics of NOM are described in detail by Bolto [10]. NOM has a strong influence on the stability and removal of inorganic particles. It can not only complex with other chemical species present in water but also adsorb on particles and drastically change their surface characteristics. This will in turn influence the effectiveness of the polyelectrolyte used for flocculation and may lead to higher coagulant/flocculant dosages.

The suspended particulate matter is a critical component of the raw water, as higher concentrations of particles not only lead to high turbidity but also provide high surface area for adsorption of dissolved chemical species, micropollutants, pathogens, and natural organic matter. The particle size distribution varies from more than 100 μm to less than 10 nm. The solid concentration usually ranges from 2 mg/L to more than 200 mg/L, but can go up to more 50,000 mg/L during floods [6]. As compared to raw water from rivers, municipal wastewater contains a wide variety of contaminants and pathogens and has high organic matter content. The metal oxides and carbonates present in water include kaolinite ($\text{Al}_2\text{Si}_2\text{O}_5(\text{OH})_4$), hematite (Fe_2O_3), quartz or silica (SiO_2), corundum (Al_2O_3), rutile (TiO_2), calcite (CaCO_3), magnesia (MgO), hydroxyapatite ($\text{Ca}_5(\text{PO}_4)_3\text{OH}$), etc. The point of zero charge (PZC) of these materials has a strong influence on operating conditions to be employed during coagulation and flocculation, especially operating pH and the type of polyelectrolytes to be employed. Experimental data for PZC as well as zeta potentials of a number of materials can be found elsewhere [11,12].

Most commercial flocculants are polyelectrolytes based on polyacrylamide polymer [13,14]. The two most important properties of a polymer as a flocculant are its molecular weight distribution and charge density distribution. As compared to the neutral or nonionic polymers, polyelectrolytes are highly soluble in water and adsorb strongly on oppositely charged surfaces. High molecular weight polymers that are often used in water clarification can be produced through aqueous polymerization

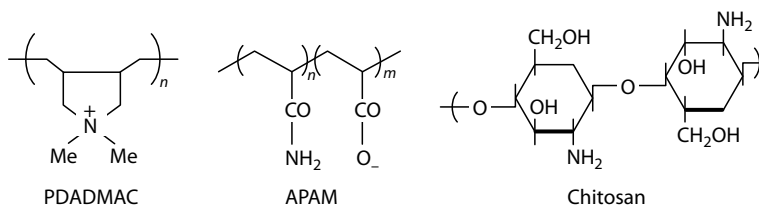


FIGURE 17.1 Structures of some commonly used polyelectrolytes in water treatment. PDADMAC, poly(diallyldimethyl ammonium chloride); APAM, anionic polyacrylamide.

of acrylamide. The charge density of a polyelectrolyte can be modified by introducing anionicity through controlled hydrolysis or cationicity through copolymerization of acrylamide with a suitable cationic monomer or through incorporation of functional groups. It is dependent on the fraction of cationic or anionic groups present. Both natural and synthetic cationic, anionic, and nonionic polymers are used in water treatment as flocculation and filtration aids. Chemical formulae, structure, and charge densities of several polyelectrolytes are provided elsewhere [4,10,15]. The structures of a few commonly used polyelectrolytes are shown in Figure 17.1. The molecular weights and charge densities of synthetic polyelectrolytes can range from a few thousands to more than 10^6 Da and 1.2–10 meq/g, respectively [6].

Since it is difficult to decipher interactions between different types of metal oxides or carbonates and polyelectrolytes in a multicomponent particulate mixture, experimental studies have focused mainly on model systems such as kaolin clay [16], hematite [17], alumina [18], calcite [19], and silica [20] and their interactions with various types of polyelectrolytes employed for flocculation. While polyelectrolytes are essentially charged polymers and the term polymer refers to neutral or nonionic polymers, both are used interchangeably in this chapter. Interactions between polyelectrolytes and particles and resultant flocculation involve adsorption of polyelectrolyte chains and accompanying repulsion or aggregation depending on the net energy of interaction between particles covered with polyelectrolyte chains.

Flocculation by polymers is a complex phenomenon, which involves several steps or sub-processes occurring sequentially or concurrently. These include (a) mixing; (b) dissolution of polymers in the suspension; (c) diffusion of the polymer species to the particle surface; (d) adsorption of polymer chains on the particles; (e) reformation of adsorbed chains on the surface; (f) desorption/readsorption of the polymer species; (g) aggregation between primary particles; (h) aggregation between primary particles and clusters; (i) aggregation among clusters; (j) restructuring of flocs; (k) fragmentation/reflocculation of flocs; and (l) subsidence, or sedimentation of flocs [21,22]. Changes in flocculation and clarification can be brought about effectively by altering polymer adsorption and conformation at the solid–solution interface by manipulating a number of variables such as pH, ionic strength, temperature, polymer combination, dosage, addition mode, and sequence of addition. Many of these events and even scission of polymer chains can be seriously affected by shear applied to improve the rate of flocculation. In any case, the first important step in the overall flocculation process is the interaction between polymers and particles leading to polymer adsorption, which is discussed next.

17.3 POLYMER ADSORPTION

Adsorption of polymers at the solid–liquid interface depends on various factors such as polymer type (pellets, powder, liquid), mode of addition (continuous or step-wise), concentration in solution and at the interface, polymer molecular weight distribution, charge density of the polymer and the surface, surface heterogeneity, nature of the solvent, pH, temperature, salinity, and multivalent ions in solution [23–25]. Polymer adsorption on particles occurs by collisions between particles and polymer chains. These collisions also take place under Brownian motion or due to fluid velocity

gradients in sheared suspensions. The process essentially involves diffusion of polymer chains from bulk solution to the interface, attachment of polymer segments to surface sites and reorientation of polymer chains at the interface, and possibly desorption and readsorption subsequently. Polyelectrolyte adsorption is the result of a subtle balance between electrostatic attraction and repulsion. It is promoted by electrostatic attractions between the charged polyelectrolyte segments and the surfaces bearing charges and short-range forces of van der Waals attraction, hydrophobic attraction, and hydrogen bonding. Entropic effects due to the release of counterions from both the surface and the polyelectrolyte can also enhance adsorption. On the other hand, there will be electrostatic repulsions between charged monomers, which results in chain stiffening, and long-range repulsion between similar charges on the polyelectrolyte chain and the surface. Adsorption of polyelectrolytes on oppositely charged surfaces is generally fast, strong, and irreversible. Polymer relaxation times could, however, range from a few seconds [26] to days and months. It is generally assumed that polymer chains attain equilibrium conformation before particles undergo any meaningful number of collisions. However, this is not the case always as experimental studies on polymer conformation [27] and interparticle forces [28] have indicated that adsorption does not reach equilibrium within the time scales of flocculation/dispersion. There are also other studies which suggest that kinetics of polymer adsorption can affect the process and result in nonequilibrium flocculation [26,29,30]. Polymer conformation in solution has an important role in this as diffusion of polymer chains as well as collisions between solid particles and polymer chains can depend on the conformation or shape of polymer chains. For example, diffusion of a spherical particle is significantly different from that of a cylindrical particle. Similarly, the nature and frequency of collisions between two spherical particles is different from that between two cylindrical particles or between a spherical particle and a cylindrical particle. Moreover, collisions between individual particles and polymer chains occur only during the initial stages of flocculation. As flocculation proceeds, the collisions will mainly involve clusters and polymer chains.

Depending on the affinity of the polymer to the surface, polymer chains can have any one or a combination of the three conformations: trains or thin layers (stretched flat on the surface), loops or coils, and dangling tails that are stretched into the solution, at some angle to the surface [25,31]. A schematic representation of different polymer conformations at the solid–liquid interface is shown in Figure 17.2. Polymer conformation at the solid–liquid interface is a function of polymer adsorption density, charge density of the polymer and particle surface, nature of the solvent, pH, salt concentration, etc. The conformation can be determined using fluorescence and electron spin resonance spectroscopy [32]. This involves measuring monomer (I_m) and excimer (I_e) emission peaks, for example, of the pyrene-labeled polymer. The coiling index, defined as the ratio of the excimer to monomer peak, I_e/I_m , gives a measure of the conformation. A high ratio indicates coiled conformation while a low ratio indicates dangling or flat conformation. Polymer conformation can also be estimated by neutron scattering and ellipsometry.

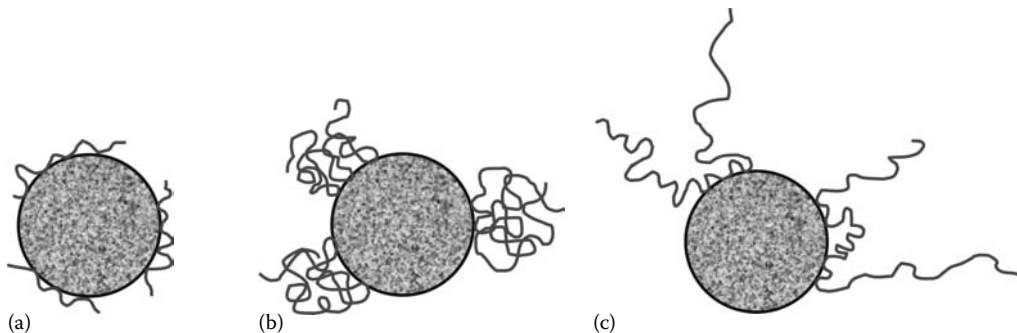


FIGURE 17.2 Polymer conformation at the solid–liquid interface (a) thin layers, low δ , (b) coils, moderate δ , and (c) trains, loops and tails, high δ . δ is the adsorbed layer thickness.

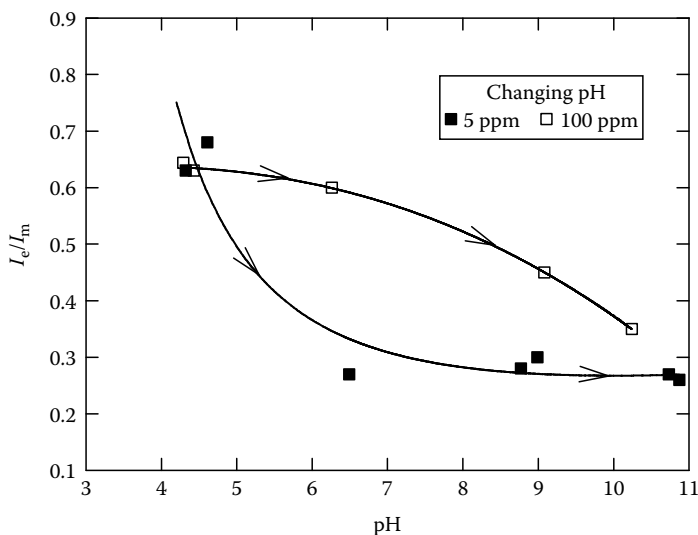


FIGURE 17.3 Coiling index (excimer-to-monomer ratio, I_e/I_m) of polyacrylic acid at the alumina–liquid interface as a function of pH (changing pH conditions) and polymer concentration (ionic strength = 0.03 M NaCl, $S/L = 10$ g/200 mL). (Reproduced from Tjipangandjara, K. and Somasundaran, P., *Colloids Surf. A*, 55, 245, 1991.)

The two most critical variables that influence polymer adsorption and flocculation are polymer concentration and pH. The solution pH influences not only the electrochemical nature of particle surfaces but also the dissociation of polyelectrolytes and hence their conformation in solution and at the interface. Natural waters contain inorganic materials such as hematite and silica, which are positively charged below their isoelectric point (IEP) and become negatively charged at a pH above the IEP. Similarly, polyelectrolytes remain in compact coiled form below their dissociation pH and attain stretched conformation at higher pH due to the repulsion between charged polymer segments. For example, polyacrylic acid (PAA) has a relatively high coiling index of about 0.7 at pH 4 and a low value of about 0.2–0.3 at pH 10.5 [33]. Polyelectrolyte adsorption is a dynamic process and adsorption density and conformation of a polyelectrolyte can be controlled by manipulating pH. For example, adsorption of polyelectrolytes such as polyacrylic acid (PAA), polyacrylamide (PAM), and a linear anionic polysaccharide, polygalacturonic acid (PGAU), on hematite was found to be high under acidic pH than under basic pH conditions [34–36]. The conformation of PAA, represented in terms of coiling index defined above, obtained at two different polymer concentrations under changing pH conditions is shown in Figure 17.3 [33]. In this study, PAA was first adsorbed on alumina at pH 4 and then the pH was increased incrementally. As a result, PAA conformation at the alumina–water interface changed from coiled to stretching conformation as the pH increased from 4 to 10. The sensitivity to pH shifting was more at the lower PAA concentration than at the higher concentration. This could be because the space available at the interface for polymer stretching was lower at higher PAA concentration than that at lower concentration. These results clearly indicate the importance of pH control in water purification. The influence of polymer conformational changes due to perturbed pH on the efficiency of flocculation is discussed in the next section.

Polymer conformation can also change in the presence of another polymer due to complexation [37,38]. Depending on the nature of complexation and application, this could be detrimental or beneficial for flocculation. The effect of a commercial polymer, Percol, on PAA conformation in solution and at the interface is shown in Figure 17.4. The coiling index of PAA in solution increases initially with Percol concentration due to charge neutralization of PAA by Percol. But as Percol

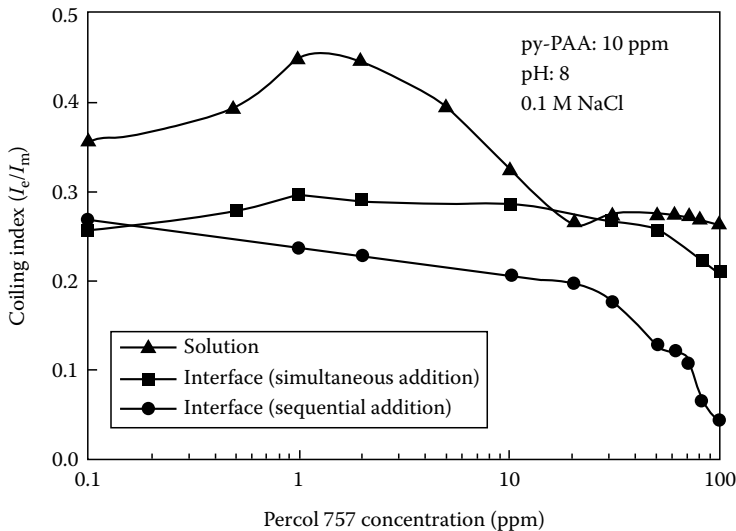


FIGURE 17.4 Effect of Percol 757 concentration on pyrene-labelled polyacrylic acid conformation in solution and at the alumina–water interface under simultaneous and sequential addition modes. (Reproduced from Fan, A. et al., *Colloids Surf. A*, 162, 141, 2000.)

concentration is increased further, the coiling index decreases because the complex is now more positively charged with the resultant electrostatic repulsion between Percol segments. The mode of addition of the second polymer also influences polymer conformation. When the two polymers, PAA and Percol, are added sequentially, the coiling index decreases with Percol concentration because of increased Percol concentration at the interface which causes stretching of the PAA chains. In the case of simultaneous addition, the coiling index at the interface does not change significantly with Percol concentration because PAA is already complexed with Percol before adsorption. These observations have important implications for water treatment. It would be necessary to select a combination of polyelectrolytes judiciously to enhance the rate of flocculation and dewatering, as discussed in the next section.

17.4 POLYMER-INDUCED FLOCCULATION

Flocculation of colloidal suspensions is essentially an aggregation process and can be induced by adsorbing as well as nonadsorbing polymers. The size distribution and strength of flocs produced by polymer-induced flocculation depend on properties of solids (size, shape, apparent density, and surface charge density of particles), properties of the system (temperature, pH, solids concentration, polyelectrolyte concentration, and type and concentrations of multivalent ions and dissolved chemical species), properties of polyelectrolyte (average molecular weight or molecular weight distribution, charge density distribution, and branching or nature of functional groups) and flocculation tank, and stirrer geometry (tank shape, height and diameter, number and dimensions of baffles, impeller type and diameter, number of blades/paddles, and impeller speed). Aggregation can occur by particle–particle, particle–cluster, and cluster–cluster collisions followed by the formation of flocs. Collisions take place due to Brownian motion of particles (perikinetic aggregation), fluid velocity gradients (orthokinetic aggregation), and differential sedimentation of particles and flocs. As aggregation proceeds, flocs develop as porous objects with highly irregular and open structure. They are usually referred to as fractal aggregates and are characterized by their mass fractal dimension because the aggregate mass scales with its size. Highly open and branched flocs have high porosities and are characterized by low fractal dimensions, and closely

packed flocs have low porosities and are characterized by high fractal dimensions. The fractal dimension is a function of flocculation process variables like electrolyte concentration, temperature, pH, and polymer concentration [39,40].

The collision volume of a particle or a floc increases due to the adsorbed polymer and its magnitude depends on the adsorbed layer thickness, which is determined by polymer conformation at the solid–liquid interface. It is generally accepted that flocculation by adsorbing polymers occurs through one of the three mechanisms: charge neutralization, charge patch neutralization, and bridging [41]. When an oppositely charged polyelectrolyte is added to a colloidal suspension, it reduces or neutralizes the charge density on the particle surface by adsorption and induces flocculation. This is usually the case with simple charge neutralization. Bridging flocculation occurs when a single polyelectrolyte chain adsorbs on more than one particle and induces aggregation. Charge patch neutralization takes place when the polyelectrolyte adsorbs in the form of discrete patches on the particle surface and the charge density of the adsorbed polyelectrolyte chain is higher than that on the particle surface. It is difficult to ascertain which mechanism is responsible for flocculation because more than one mechanism may be operational during flocculation, depending on the nature of the particle surface and polymer conformation at the solid–liquid interface. Bridging flocculation by large molecular weight polymers usually results in large as well as strong flocs [13]. The rate of flocculation obtained by charge patch neutralization is about two to three times greater than that by simple charge neutralization [42], which is comparable to that obtained in the presence of inorganic electrolytes [17]. It is essentially a function of the frequency of collisions between particles if the forces of attraction dominate those due to repulsion.

The frequency of collisions is a function of the effective collision radii of interacting particles. When the polymer adsorbs in the form of trains (stretched in the form of a thin layer on the particle surface), the number of contacts between the polymer backbone and the surface is high and the thickness of the adsorbed layer is low. Under these conditions, the rate of flocculation is comparable to that obtained with inorganic electrolytes. This is the situation in the case of flocculation by simple charge neutralization. In the case of charge patch neutralization, it has been proposed [20,42,43] that the polymer chains adsorb in the form of electrostatic patches of high charge density. The higher rate of flocculation compared to simple charge neutralization was attributed to patchy or mosaic-type surface charge distribution of polymer-covered particles. In the case of bridging flocculation, which occurs mainly due to the long dangling tails, the adsorbed layer thickness is quite high and results in high collision radii and high rates of flocculation observed with high molecular weight polymers [37]. It should be noted that flocs obtained with polymers are stronger than those produced with salts because the strength of polymer–surface bond is high and also because an adsorbed polymer chain has attachments at multiple sites on the surface.

Polymer conformation can have a strong influence on flocculation. It is possible to control the rate of flocculation by manipulating polymer conformation at the interface, which, in turn, is manipulated using variables such as pH and ionic strength (see Figure 17.3). Results obtained for flocculation of colloidal alumina suspensions by PAA [33] are shown in Figure 17.5. The percent of settled solids increases as the pH is increased at two different polymer concentrations. It is to be noted that flocculation can be affected markedly by perturbing pH during flocculation. For example, at lower pH values, the percent of solids settled under fixed pH conditions was slightly superior to that under shifted pH, after initial flocculation. At 100 ppm PAA (Figure 17.5b), the percent of solids settled was always higher under shifted pH conditions than that obtained under fixed pH, except at high pH. At 5 ppm PAA (Figure 17.5a), flocculation appears to be occurring in stages. At low pH, PAA adsorbs in the coiled form and the surface coverage is low. Flocculation occurs by charge neutralization and results in the formation of microflocs. As pH is increased, PAA stretches into the solution and results in what can be considered as macroflocculation through bridging. As the pH is raised further, PAA conformation does not change as it is already in the stretched form. However, because the surface coverage is low, flocculation progresses further by the bridging of macroflocs leading to the formation of superflocs.

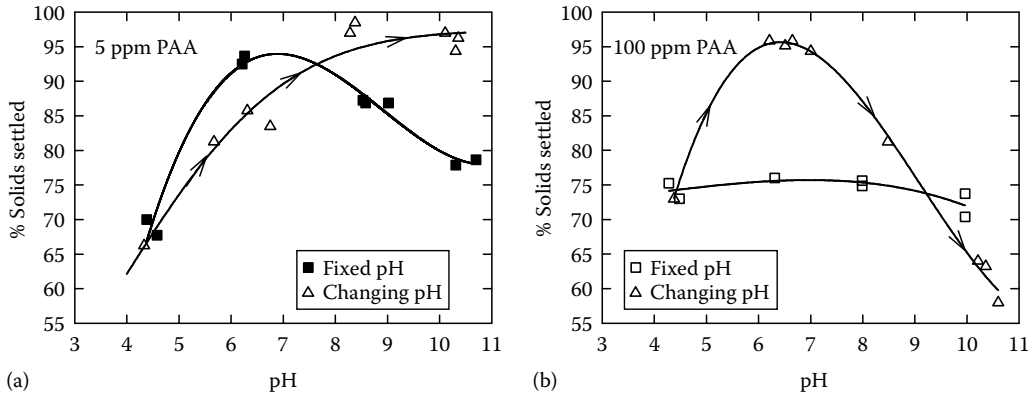


FIGURE 17.5 (a) Percent alumina settled with 5 ppm polyacrylic acid as a function of pH (fixed and changing pH conditions) (ionic strength = 0.03 M NaCl, $S/L = 10 \text{ g}/200 \text{ mL}$). (b) Percent alumina settled with 100 ppm polyacrylic acid as a function of pH (fixed and changing pH conditions) (ionic strength = 0.03 M NaCl, $S/L = 10 \text{ g}/200 \text{ mL}$). (Reproduced from Tjipangandjara, K. and Somasundaran, P., *Colloids Surf. A*, 55, 245, 1991.)

In certain cases, use of two or three polymers may result in desired flocculation than with a single polymer [27,38,44–47]. It is to be noted that the conformation of a polymer can change in the presence of another due to complexation between the two [48] and this can result in different degrees of flocculation. Turbidity of alumina suspensions without the addition of any polymer and in the presence of 5 ppm Percol 757 alone, 5 ppm PAA alone, and their mixtures (Percol and PAA added simultaneously or sequentially) is shown in Figure 17.6 [38]. It can be seen that the combination of Percol and PAA leads to a larger reduction in suspension turbidity than that with individual polymers. Alumina is positively charged at pH 8. Since Percol is also positively charged (80% charge density), it does not lead to any flocculation. On the other hand, PAA is negatively charged at this pH and results in better flocculation than that obtained in the presence of Percol. Flocculation is enhanced when both the polymers are used because PAA adsorbs first on alumina and acts as an anchor for

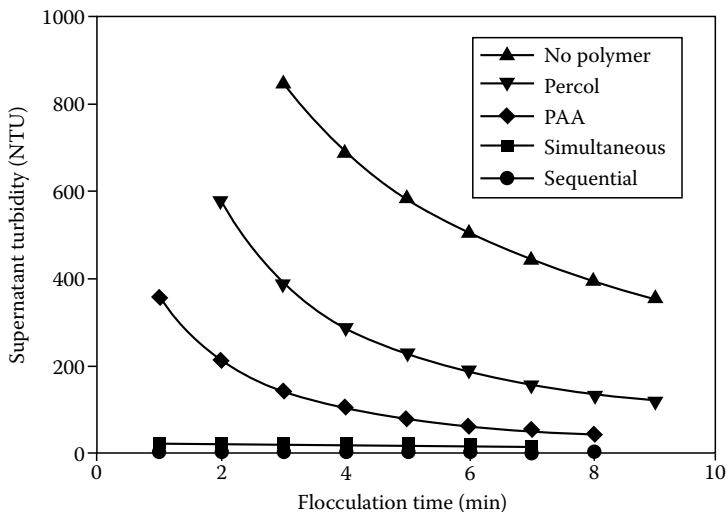


FIGURE 17.6 Supernatant turbidity of alumina suspensions without any polymer and in the presence of $1.8 \times 10^6 \text{ g/mol}$ Percol 757 (5 ppm), $10,000 \text{ g/mol}$ PAA (5 ppm) and their combinations (simultaneous addition and sequential addition of Percol followed by PAA, each 5 ppm) (pH: 8 and 0.1 M NaCl). (Reproduced from Fan, A. et al., *Colloids Surf. A*, 162, 141, 2000.)

Percol, which has a higher capture radius due to its higher molecular weight. Moreover, sequential mode of addition seems to be better than simultaneous addition because of both, the complexation between PAA and Percol that can modify the PAA conformation and competition between PAA and Percol for adsorption sites on alumina.

Dual polymer flocculation occurs by a combination of two mechanisms: charge or patch neutralization by the oppositely charged polymer followed by bridging by the long chain polymer. In the case of sequential addition, the first polymer not only results in the formation of primary flocs, but also acts as an anchor for subsequent adsorption of the long chain polymer, which can lead to enhanced floc growth by bridging. Clearly, it is possible to achieve optimum flocculation performance by choosing a combination of polymers with appropriate charge densities and molecular weights judiciously. Lee and Liu [49] have employed two commercial polyelectrolytes, cationic KP-201C and nonionic NP-800, for the treatment of waste activated sludge and found that dewatering is enhanced by using the same total concentration of polymers that was used with individual polymers. They also found that preconditioning the sludge with the cationic polyelectrolyte followed by the nonionic polyelectrolyte is more efficient than preconditioning with the nonionic polyelectrolyte followed by the cationic polyelectrolyte.

The water to be treated may also contain surfactants because of their widespread industrial and domestic applications. Presence of surfactants in water will influence not only the polymer conformation and adsorption at the interface but also the degree of flocculation, which will affect the turbidity of suspensions [50]. Similarly, the presence of dissolved ionic species, such as Ca^{2+} , Li^+ , Cs^+ , Mg^{2+} , will have a profound influence on polyelectrolyte adsorption, solid–liquid interface potential, as well as electrochemical characteristics of particle surfaces. This will, in turn, affect the nature of interactions between particles, NOM, and the polyelectrolytes and hence the rate of flocculation [23,51].

While aggregation is desirable in the case of flocculation in potable water and wastewater treatment processes, it is undesirable in the case of applications such as cooling, steam generation in boilers, distillation processes, power generation, paints, chemical mechanical polishing, and detergency. In the case of cooling and boiler applications [52], it is undesirable because particulate matter present in untreated water can deposit on equipment surfaces and lead to scale formation and fouling, which in turn, can result in poor heat transfer, corrosion and, in some situations, pipeline or nozzle blockage. Scale formation will ultimately lead to equipment failure, especially of heat exchanger tubes. Hence, natural (for example, starch, sodium alginate, and lignosulfonate) as well as synthetic (for example, polyacrylic acid, polymaleic acid, and polyaspartic acid) polymers are employed to act as dispersants in these industrial applications to prevent scale formation and equipment fouling. The particulate matter consists of mud or silt, microbial mass, mineral scales such as CaCO_3 , CaSO_4 , and CaF_2 , and corrosion products such as Fe_2O_3 , Fe_3O_4 , ZnO , and CuO [53]. One of the main challenges here is to prevent or reduce the deposition of iron-based foulants because dispersion of iron oxide is relatively difficult. The polymer molecular architecture, for example, the functional groups present, plays a critical role in the dispersion of iron oxide. Amjad [54] found that natural additives containing phenolic, carboxyl, and sulfonic acid groups, that is, lignosulfonate, fulvic acid, and tannic acid, are better than starch and sodium alginate in dispersing iron oxide. Similarly, it was also found that synthetic copolymers and terpolymers containing carboxyl and sulfonic acid groups are better iron oxide dispersants than homopolymers containing carboxyl groups. The state of dispersion of iron oxide in the absence of any additive and in the presence of a terpolymer made of acrylic acid, sulfonic acid, and sulfonated styrene [55] is shown in Figure 17.7. It can be seen that the terpolymer was effective in finely dispersing the iron oxide particles where extensive aggregation occurs in the absence of the polymer.

Thermal and irradiation degradation characteristics of polymers is another important parameter to be considered for high temperature applications as exposure to such environments for prolonged periods leads to loss of molecular weight, which will result in poor dispersion efficiency. It was found that both natural and synthetic polymers degrade due to exposure to high temperature and

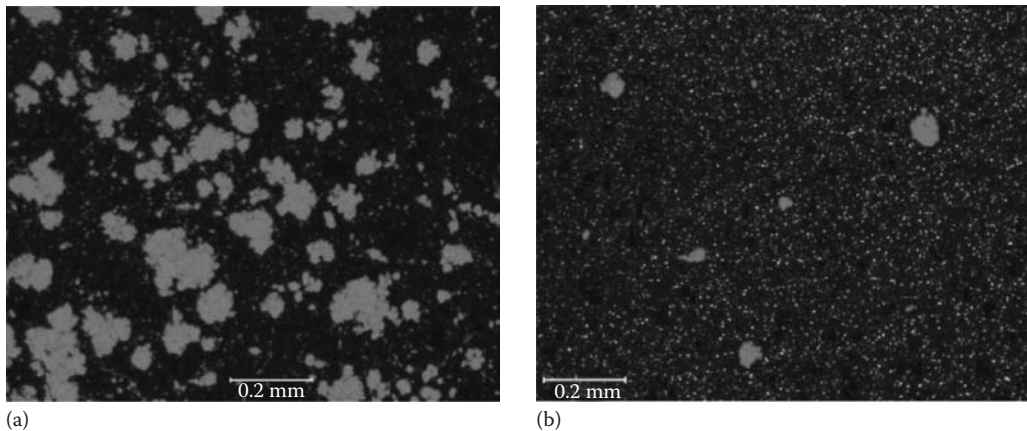


FIGURE 17.7 State of dispersion of iron oxide (a) in the absence of any additive and (b) in the presence of a terpolymer made of acrylic acid, sulfonic acid, and sulfonated styrene. (Reproduced from Amjad, Z., *Tens. Surf. Deterg.*, 43, 242, 2006.)

pressure environments. The extent of degradation depends on polymer architecture, temperature, pressure, and duration of exposure. Experimental results indicated that deterioration of the performance of a dispersant depends more on the degradation of functional groups than on the cleavage of the polymer backbone [55].

Depending on the molecular weight, a polyelectrolyte can act as a dispersant as well as a flocculant. For example, it was found [35] that a low molecular weight (MW) (5000 g/mol) PAA resulted in complete dispersion of hematite suspensions over a wide pH range while a high molecular weight PAA (10⁶ g/mol) lead to complete flocculation over the same pH range. Dispersion due to low MW PAA occurred mainly because of the coverage of iron oxide particles with PAA and steric repulsion. On the other hand, flocculation by high MW PAA occurred due to charge patch neutralization as well as polymer bridging. These results clearly indicate that a polymer can be employed as a dispersant in one application and as a flocculant in another by manipulating its molecular weight and conformation.

17.5 MODELING OF POLYMER ADSORPTION, INTERACTION FORCES, AND FLOCCULATION

Mathematical modeling is a proven tool for the simulation, analysis, optimization, and control of complex physicochemical and transport-based processes. Mathematical models for polymer adsorption [25] and flocculation [56,57] have been developed and tested with experimental data for ideal systems under laboratory experimental conditions. Additionally, since interaction forces between polymer-covered particles play an important role in many natural and industrial processes, models have also been developed for surface forces [58] such as van der Waals attraction, electrical double layer repulsion, and forces due to adsorbed polymer chains. However, it must be noted that to date no model exists that takes into account all the complex phenomena that occur in real flocculation systems. Polymer adsorption models do not account for the effect of charge density distribution, functionalization, polydispersity, relaxation or rearrangement of polymer segments at the solid-liquid interface, and desorption. More seriously, there will be competition between polymers in the case of multipolymer schemes that are used in practical applications. Similarly, in the case of flocculation models, rearrangement, fragmentation or reaggregation, as well as dependence of all these adsorption and flocculation processes on shear or shear gradients are yet to be incorporated. Nevertheless, the state-of-the-art models are described here, first for polymer adsorption, followed by those for interaction forces and flocculation.

17.5.1 POLYMER ADSORPTION

Polymer movement in solution is usually modeled as random walks in the continuous space or on a lattice. Polymer adsorption models can be broadly classified as [59] models based on conformational statistics, which can calculate the contributions of trains, loops, and tails and models starting from the overall density profile, where all the properties of the adsorbed layer are expressed as a function of local concentration. The self-consistent mean field lattice model developed by Scheutjens and Fleer [60–62] belongs to the first kind whereas the model based on scaling concepts, proposed by de Gennes [63–65] belongs to the second kind.

Mathematical models for polyelectrolyte adsorption are generally extensions of the models for neutral polymers. van der Schee and Lyklema [66] extended the polymer adsorption models of Roe [67] and Scheutjens and Fleer [60,61] to model polyelectrolyte adsorption by including an additional term for the electrostatic contribution to the total free energy of the system. This model was later extended by Evers et al. [68] and Bohmer et al. [69] for weak polyelectrolytes. The model predictions have been tested with experimental data [70], and the features of polyelectrolyte adsorption predicted by the model are generally in agreement with those observed experimentally. This model was later extended for variable charge surfaces [71]. A continuum mean-field model was developed by Borukhov et al. [72] for polyelectrolyte adsorption, but this model does not take into account the train-loop-tail conformation. Juvekar et al. [73] developed a continuum mean-field model for polymer adsorption that is computationally less intensive than the Scheutjens–Fleer model. These models assume that polymer adsorption is much faster than particle aggregation and the polymer molecule attains an equilibrium conformation. As mentioned earlier, adsorption does not reach equilibrium within the time scales of flocculation [27,28], and kinetics of polymer adsorption can affect the process and result in nonequilibrium flocculation [26,29,30]. Hogg [74] proposed a simple model for polymer adsorption dynamics, treating polymer molecules as spherical particles, and suggested collision kernels similar to those used for particle–particle interactions. Such an approach would be applicable only when the polymer chains are in a coiled or globular conformation. It becomes necessary to modify the theoretical treatment of interactions between spherical particles and rodlike polymers and also of the diffusion of cylindrical- or elliptical-shaped polymer chains in solution.

17.5.2 INTERACTION FORCES BETWEEN POLYMER-COVERED PARTICLES

When particles are suspended in solution, they acquire a net negative or positive charge on their surfaces due to (a) defective lattice structure, (b) dissolution of surface species, and (c) adsorption of specific ions, polymers, or surfactants from solution. To maintain electroneutrality at the interface, a layer of counterions forms at the interface. The two layers of opposite charges at the interface are normally referred to as the electric double layer. There will be an electrostatic repulsion between two similarly charged particles due to the presence of this double layer. The electrochemical nature of particle surface changes due to the adsorption of polyelectrolytes. The adsorbed polymer chains introduce steric and bridging forces in addition to perturbing the van der Waals attraction and electrostatic repulsion. The van der Waals attraction is affected because dielectric constant and refractive index of the polymer are different from those of the solvent. The surface potential increases or decreases depending on polymer charge density distribution. Moreover, the range over which particle–particle interaction occurs also changes depending on the thickness of the adsorbed layer, especially tail length in the case of dangling polymer chains in the solution. The total interaction energy between particles with adsorbed polymer layers is normally computed by applying the usual assumption of additivity. It is generally acknowledged that the assumption of each force acting individually, neither influencing nor getting influenced by other forces present, is a gross simplification. However, in the absence of sufficient understanding of how the forces influence each other, the simple addition assumption is generally invoked.

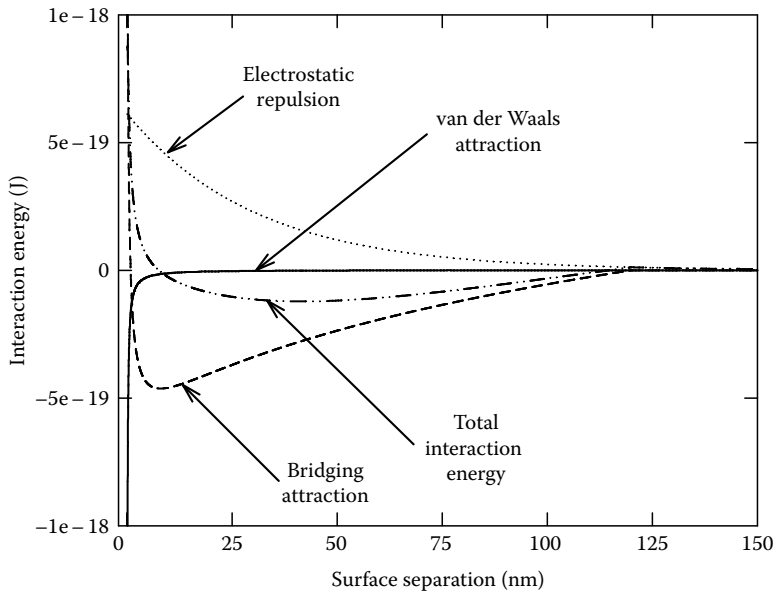


FIGURE 17.8 van der Waals attraction, electrostatic repulsion, bridging attraction, and total interaction energy between identical spherical polystyrene latex particles of radius 165 nm with adsorbed polymer layers. (Reproduced from Runkana, V. et al., *Chem. Eng. Sci.*, 61, 182, 2006.)

Vold [75] derived an equation for van der Waals attraction between two identical particles having adsorbed layers of the same polymer. Subsequently, Vincent [76] generalized Vold's expression for two dissimilar solids and polymers. The interaction energy due to electrical double layers around colloidal particles can be calculated accurately by the rigorous solution of the Poisson–Boltzmann equation. Since this is a difficult task, approximate expressions have been proposed in the literature [77–79]. Either the self-consistent field theory of Scheutjens and Fleer [60–61] or the scaling theory [63–65] can be used to calculate forces due to adsorbed polymer. Intermolecular and surface forces are described in detail elsewhere [58].

Runkana et al. [80] computed interaction energy profiles (Figure 17.8) for two polymer-covered spherical polystyrene latex particles undergoing bridging flocculation. The interaction energy curves are typical of the force–distance profiles measured between polymer-covered surfaces. Due to the low electrolyte concentration, the double layer thickness is quite large. However, bridging attraction is also present due to the adsorbed polymer. It is weakly attractive at long distances and becomes progressively stronger as the particles approach closer. The particle surfaces repel each other at very short distances due to the compression of the adsorbed layer. Even though electrostatic repulsion is present, bridging attraction dominates and results in net attraction. The interaction energy–surface separation diagrams are useful to ascertain how various surface forces contribute to suspension stability and to determine, at least qualitatively, parameters such as ionic strength, polymer molecular weight, and concentration that can lead to net attraction or repulsion between particles in the presence of polymers.

17.5.3 POLYMER-INDUCED FLOCCULATION

The effectiveness of coagulation or flocculation is usually represented in terms of readily measurable parameters such as settling rate of flocs, percent solids settled, supernatant turbidity, sediment volume or weight, moisture content, and strength of flocs. These parameters are indirect measures of flocculation efficiency and a majority of them are actually functions of aggregate or floc size distribution (FSD), which is the direct and explicit indicator because flocculation is essentially an

aggregation phenomenon. Population balance models have been developed, starting from the classical work of Smoluchowski [81], to predict the time evolution of aggregate size distribution during flocculation. Since the process is complex, several assumptions are usually made to simplify the mathematical treatment [57]. For example, it was assumed earlier that both primary particles and flocs are spherical in shape. However, with the advent of fractal geometry [82] and the recognition that flocs are fractal in nature, the open and irregular structure of flocs is routinely represented in terms of their mass fractal dimension in flocculation models now. Similarly, kinetics of floc fragmentation was not included in the population balance initially. However, later models incorporated simultaneous colloid aggregation and floc fragmentation [56,83,84]. Population balance models were also developed for flocculation of colloidal suspensions encountered in water treatment [85–87].

Apart from polymer adsorption, flocculation can be visualized as a two-step process: particle transport leading to collision and subsequent attachment upon collision. Accordingly, these steps are represented by two parameters, the collision frequency factor and the collision efficiency factor, in the population balance model (PBM) for flocculation. Particle collisions are governed mainly by suspension hydrodynamics at the macroscopic level and by short range interaction or surface forces on the microscopic scale. However, the majority of flocculation models either assume that all particle collisions lead to aggregation or treat particle collision efficiency as an adjustable parameter. The probability or efficiency of colloid aggregation upon collision is actually a function of the surface forces between interacting particles. Taking note of the various phenomena and the parameters that influence flocculation, it can be stated that it is necessary to combine the basic principles of chemical engineering with those of surface and colloid science to develop a realistic model for flocculation. Recognizing this, we have incorporated fundamental theories of surface forces into the population balance framework to model flocculation [80,88–91]. The general population balance framework for flocculation incorporating simultaneous aggregation–fragmentation kinetics and influence of surface forces is shown in Figure 17.9. It will be noticed that several phenomena related to flocculation are incorporated except the heterogeneous structure of fluid flow in stirred

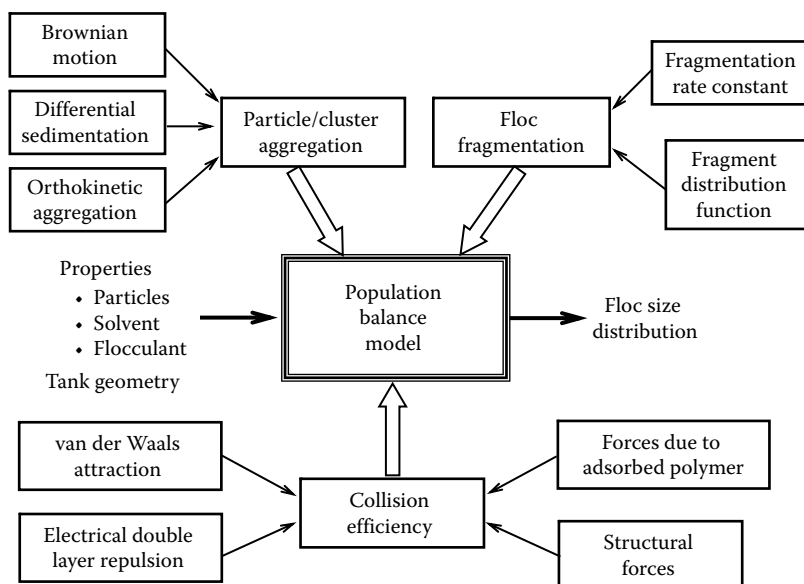


FIGURE 17.9 General population balance framework for flocculation incorporating simultaneous aggregation-fragmentation kinetics and influence of surface forces. (Reproduced from Runkana, V. and Somasundaran, P., *Mathematical modeling of coagulation and flocculation of colloidal suspensions incorporating the influence of surface forces*, in *Colloid Stability and Application in Pharmacy*, Tadros, Th. F., Ed., Wiley-VCH Verlag GmbH & Co. KGaA, Weinheim, Germany, 2007, pp. 91–118.)

suspensions and dynamics of polymer adsorption. The model can readily be extended by combining a suitable fluid dynamics model for fluid flow and a model for polymer adsorption dynamics.

Industrial scale coagulation and flocculation processes involve application of shear as it enhances the rate of aggregation, which, in turn, helps in improving the rate of sedimentation of aggregates. However, application of shear results in the fragmentation of aggregates concurrently. The population balance equation for simultaneous aggregation and fragmentation is given by [92]

$$\begin{aligned} \frac{\partial n(v,t)}{\partial t} = & - \int_0^{\infty} \alpha(v,u)\beta(v,u)n(v,t)n(u,t)du + \frac{1}{2} \int_0^v \alpha(v-u,u)\beta(v-u,u)n(v-u,t)n(u,t)du \\ & - S(v)n(v,t) + \int_v^{\infty} S(u)\gamma(v,u)n(u,t)du \end{aligned} \quad (17.1)$$

where

- n is number concentration of aggregates (or particles)
- v and u denote aggregate volume
- t is aggregation time
- β is collision frequency factor
- α is collision efficiency factor
- γ is breakage distribution function
- S is specific rate constant of floc fragmentation

The first two terms on the right hand side account for aggregation. The third term accounts for the loss of aggregates due to fragmentation while the last term represents the generation of primary particles or smaller aggregates due to breakage or erosion of larger aggregates. The rate of fragmentation has a first order dependence on the solid concentration unlike the rate of aggregation which has a second order dependence. Analytical solutions do not exist for the above equation and several techniques for its discretization have been proposed in the literature [93]. The discretized population balance equation for simultaneous aggregation and fragmentation is obtained by applying discretization procedures for the aggregation and fragmentation terms separately. The rate of change of particle number concentration during simultaneous aggregation and fragmentation is given by the following discretized population balance equation [84]:

$$\begin{aligned} \frac{dN_i}{dt} = & N_{i-1} \sum_{j=1}^{i-2} 2^{j-i+1} \alpha_{i-1,j} \beta_{i-1,j} N_j + \frac{1}{2} \alpha_{i-1,i-1} \beta_{i-1,i-1} N_{i-1}^2 \\ & - N_i \sum_{j=1}^{i-1} 2^{j-i} \alpha_{i,j} \beta_{i,j} N_j - N_i \sum_{j=i}^{\max_1} \alpha_{i,j} \beta_{i,j} N_j - S_i N_i + \sum_{j=i}^{\max_2} \gamma_{i,j} S_j N_j \end{aligned} \quad (17.2)$$

where

- N_i is number concentration of particles or aggregates in a section i
- \max_1 is maximum number of sections used to represent the complete size spectrum
- \max_2 is the largest section from which aggregates in the current section are produced by fragmentation

The first and second terms on the right hand side account for growth while the third and fourth terms represent loss by aggregation, respectively. The fifth and sixth terms represent loss and growth of flocs by fragmentation, respectively.

To introduce the effect of polymer adsorption on flocculation, it is necessary to know the net interaction energy between polymer-covered particles, which is a function of adsorption density, interface potential, and polymer conformation as well as thickness of the adsorbed layer. These parameters can be predicted, in principle, using the polymer adsorption models discussed earlier. But the applicability of these models for practical systems has been rather limited because the models involve a large number of adjustable parameters and the predictions are sensitive to these parameters. However, parameters such as adsorption density and adsorbed layer thickness can be measured experimentally. The surface potential is commonly assumed to be close to the zeta potential, which can also be measured readily. Hence, if experimental data for these parameters are available for a system, one could utilize such data for computing interaction forces between particles in the presence of polymers without the need for a theoretical polymer adsorption model.

The probability of attachment, when two aggregates collide, depends mainly on the interaction between primary particles in the colliding surfaces rather than on particles residing in the interior. This is because forces between particles drop rapidly with distance and, as such, the interaction between aggregates can be approximated by the interaction between the primary surface particles [94,95]. The collision efficiency factor for aggregates is computed as the reciprocal of the modified Fuchs' stability ratio, W , for two primary particles, k and l [96–99]:

$$W_{k,l} = \frac{\int_{r_{0k}+r_{0l}}^{\infty} D_{k,l} \frac{\exp(V_T/k_B T)}{s^2} ds}{\int_{r_{0k}+r_{0l}}^{\infty} D_{k,l} \frac{\exp(V_{vdW}/k_B T)}{s^2} ds} \quad (17.3)$$

where

k_B is Boltzmann constant

T is temperature

$D_{k,l}$ is hydrodynamic correction factor [100]

V_T is total energy of interaction

V_{vdW} is van der Waals energy of attraction between two primary particles of radii r_{0k} and r_{0l} (assumed spherical)

s is distance between particle centers ($s = r_{0k} + r_{0l} + h_0$)

h_0 is distance of closest approach between particle surfaces

Runkana et al. [80,88] developed population balance models (PBMs) for polymer-induced flocculation by two well-known mechanisms, simple charge neutralization [88] and bridging [80]. They assumed that polymer adsorption on oppositely charged particle surfaces is fast and equilibrium conformation is achieved before collisions between particles take place. It was also assumed that the polymer adsorbs uniformly and polymer surface coverage and adsorbed layer thickness are the same for all particles. The composite polymer-coated particle radius was estimated by adding adsorbed layer thickness to the solid particle radius. Runkana et al. [88] incorporated Vincent's expression [76] for van der Waals attraction between particles with adsorbed layers into the population balance and simulated the aggregation of hematite suspensions in the presence of PAA. In Figure 17.10, their simulation results for evolution of mean aggregate diameter with flocculation time at some typical PAA concentrations are compared with the experimental data of Zhang and Buffle [17]. In the cases of aggregation by charge patch neutralization or bridging, it is necessary to include steric or bridging forces. Bridging flocculation takes place when polymer chains adsorb on more than one particle and act as bridges. Runkana et al. [80] simulated bridging flocculation by solving the discretized population balance equation and assuming the total interaction energy to be a sum of van der Waals attraction, electrical double layer repulsion, and bridging attraction or steric repulsion due

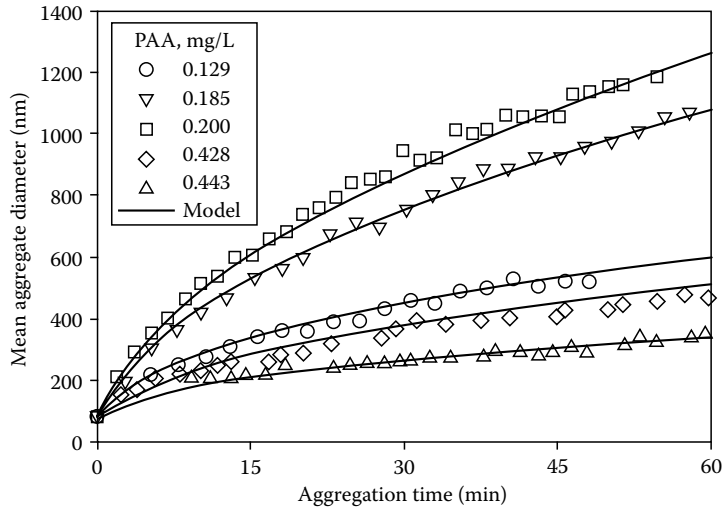


FIGURE 17.10 Simulated and experimental time evolution of mean diameter of hematite aggregates at different PAA concentrations. (Reproduced from Runkana, V. and Somasundaran, P., Mathematical modeling of coagulation and flocculation of colloidal suspensions incorporating the influence of surface forces, in *Colloid Stability and Application in Pharmacy*, Tadros, Th. F., Ed., Wiley-VCH Verlag GmbH & Co. KGaA, Weinheim, Germany, 2007, pp. 91–118.)

to adsorbed polymer. Their model was tested with experimental data published by Biggs et al. [101] for flocculation of anionic polystyrene latex particles by a cationic quaternary ammonium based derivative of polyacrylamide. Later, Somasundaran et al. [91] extended the model for flocculation by polymers in shear environments. Their model was tested qualitatively with experimental data for flocculation of colloidal alumina suspensions in the presence of PAA and was found to reproduce the observed experimental trends [102] reasonably well. Typical simulation results for flocculation kinetics of alumina suspensions in a stirred tank are shown at different values of polymer surface coverage in Figure 17.11. The rate of flocculation increases as polymer concentration increases in sheared suspensions also. However, as polymer concentration increases further, the fractional

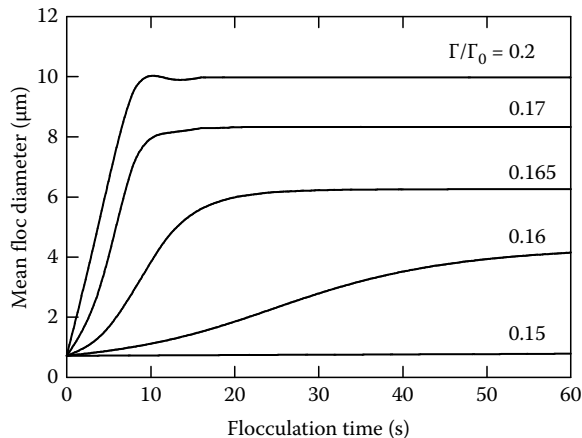


FIGURE 17.11 Simulation of effect of polymer surface coverage on evolution of mean floc diameter with time in stirred suspensions (Γ/Γ_0 , fractional surface coverage). (From Somasundaran, P. et al., Population balance modeling of flocculation of mineral suspensions by polymers, Paper presented at *International Mineral Processing Congress (IMPC-2006)*, Istanbul, Turkey, September 3–9, 2006.)

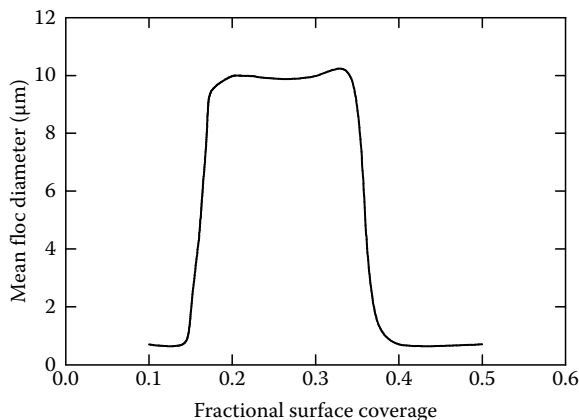


FIGURE 17.12 Simulation of effect of polymer surface coverage on mean floc diameter in stirred suspensions. (From Somasundaran, P. et al., Population balance modeling of flocculation of mineral suspensions by polymers, Paper presented at *International Mineral Processing Congress (IMPC-2006)*, Istanbul, Turkey, September 3–9, 2006.)

surface coverage increases and results in restabilization (Figure 17.12) as observed experimentally in general. This was attributed to the change in net interaction energy between polymer-covered particles due to changes in fractional surface coverage.

One of the important issues in modeling flocculation in shear environments is how to incorporate the inhomogeneous nature of fluid flow. In general, the global average shear rate is employed to compute the rate constants of aggregation and fragmentation. The local rates of shear are significantly different from the global average [103,104] and the local turbulent energy dissipation rate depends not only on the impeller type and surface but also on the tank dimensions [103]. Besides, the number of impellers and baffles also affects the shear rate distribution. Complete description of flocculation in turbulent environments requires simultaneous solution of basic balance equations for mass, momentum, energy, and concentration of species present along with population balances for particles/aggregates of different size classes. Recently, a number of developments have been made to couple population balance (PB) model for size distribution with computational fluid dynamics (CFD) model for fluid flow [105–107]. One of the important applications of such coupled PB-CFD models is in identifying the correct location for polymer addition, which is otherwise a difficult task. Secondly, these models will be useful in designing new flocculation tanks in terms of size and shape of the vessel, type and number of impellers to be installed, number of baffles, etc., which have a strong influence on effectiveness of mixing polymers and particles and hence on the rate of flocculation.

17.6 SUMMARY AND SUGGESTIONS FOR FUTURE RESEARCH

The suspended particulate matter is one of the key components in natural waters and in industrial wastewaters. Interactions between the suspended particles and the natural or synthetic polyelectrolytes play a critical role in coagulation and flocculation as well as in the subsequent clarification and filtration operations in water treatment processes. Hence, complete characterization of suspended particles and natural organic matter is essential not only for understanding the complexity of interactions between polyelectrolytes and particles but also for designing new flocculants and flocculation equipment.

Besides the characteristics of particles and polyelectrolytes, water chemistry and other important constituents of water, such as natural organic matter and dissolved chemical species, have a significant influence on the effectiveness of flocculation. Hence, future research is warranted to

develop an understanding of the interactions between complexation of NOM with polyelectrolytes in the presence of dissolved chemical species and their effect on polyelectrolyte adsorption and flocculation.

Since it is difficult to study interactions between polyelectrolytes and various components of the multicomponent system that is water, experimental and theoretical studies have been focused mostly on interactions between pure component systems. Although there have been studies on heteroflocculation of two component systems and dual polymer flocculation, more research is required on polyelectrolyte adsorption in a multicomponent system of mineral or metal oxide particles and subsequent flocculation.

Mathematical models for polyelectrolyte adsorption, interaction forces between polymer-covered particles, and flocculation of single component systems have been developed. These models require extensive testing with data from both laboratory scale and industrial flocculation units to find practical applications. There is a dire need to refine current models to take into account various complexities of real systems, such as charge density distribution, functionalization, polydispersity, and relaxation or rearrangement of polymer segments, desorption, competition between polymers, fragmentation and reaggregation of clusters, as well as distribution of shear gradients. Further research is also required in this direction for the development of coupled multidimensional population balance—fluid dynamics models, incorporation of coagulant/flocculant adsorption dynamics, influence of surface forces, and the evolution of aggregate structure during flocculation.

ACKNOWLEDGMENTS

This work was supported by the National Science Foundation (NSF Grants # INT-96-05197 and INT-01-17622) and the NSF Industry/University Cooperative Research Center (IUCRC) for Advanced Studies in Novel Surfactants at Columbia University (NSF Grant # EEC-98-04618). We thank the management of Tata Research Development and Design Centre for the permission to publish this chapter. We thank Prof. E. C. Subbarao, Prof. Mathai Joseph, Prof. P. C. Kapur, and Dr. Pradip for their advice and encouragement. Sathish Ponnurangam is appreciated for his help during the manuscript preparation.

REFERENCES

1. Montgomery, M. and Elimelech, M. Water and sanitation in developing countries: Including health in the equation. *Environmental Science & Technology*, 41, 17–24 (January 1, 2007).
2. Shannon, M. A., Bohn, P. W., Elimelech, M., Georgiadis, J. G., Marinas, B. J., and Mayes, A. M. Science and technology for water purification in the coming decades. *Nature*, 452, 301–310 (2008).
3. Sutherland, K. Water extraction: Pure water production. *Filtration + Separation*, 44(5), 33–35 (June 2007).
4. Farinato, R. S., Huang, S.-Y., and Hawkins, P. Polyelectrolyte-assisted dewatering. In *Colloid-Polymer Interactions: From Fundamentals to Practice*, Farinato, R. S. and Dubin, P. L. (Eds), pp. 3–50, John Wiley & Sons, Inc., New York (1999).
5. Hogg, R. Flocculation and dewatering. *International Journal of Mineral Processing*, 58, 223–236 (2000).
6. Bolto, B. and Gregory, J. Organic polyelectrolytes in water treatment. *Water Research*, 41, 2301–2324 (2007).
7. Amankonah, J. O. and Somasundaran, P. Effects of dissolved mineral species on the electrokinetic behavior of calcite and apatite. *Colloids and Surfaces A*, 15, 335–353 (1985).
8. Laarz, E., Meurk, A., Yanez, J. A., and Bergstrom, L. Silicon nitride colloidal probe measurements: Intersurface forces and the role of surface-segment interactions in poly(acrylic acid) adsorption from aqueous solution. *Journal of the American Ceramic Society*, 84, 1675–1682 (2001).
9. Pernitsky, D. J. and Edzwald, J. K. Selection of alum and polyaluminium coagulants: Principles and applications. *Journal of Water Supply: Research and Technology—AQUA*, 55, 121–141 (2006).
10. Bolto, B. A. Soluble polymers in water purification. *Progress in Polymer Science*, 20, 987–1041 (1995).
11. Hunter, R. J. *Zeta Potential in Colloid Science: Principles and Applications*. Academic Press, New York (1981).

12. Kosmulski, M. and Rosenholm, J. B. High ionic strength electrokinetics. *Advances in Colloid and Interface Science*, 112, 93–107 (2004).
13. Gregory, J. Flocculation by polymers and polyelectrolytes. In *Solid-Liquid Dispersions*. Tadros, Th. F. (Ed), pp. 163–181, Academic Press, New York (1987).
14. Pefferkorn, E. Polyacrylamide at solid/liquid interface. *Journal of Colloid and Interface Science*, 216, 197–220 (1999).
15. Schwoyer, W. L. K. (Ed). *Polyelectrolytes for Water and Wastewater Treatment*. CRC Press, Boca Raton, FL (1981).
16. Addai-Mensah, J. and Ralston, J. Investigation of the role of interfacial chemistry on particle interactions, sedimentation and electroosmotic dewatering of model kaolinite dispersions. *Powder Technology*, 160, 35–39 (2005).
17. Zhang, J. and Buffle, J. Kinetics of hematite aggregation by polyacrylic acid: Importance of charge neutralization. *Journal of Colloid and Interface Science*, 174, 500–509 (1995).
18. Das, K. K. and Somasundaran, P. Ultra-low dosage flocculation of alumina using polyacrylic acid. *Colloids and Surfaces A*, 182, 25–33 (2001).
19. Heath, A. R., Parisa A. B., Fawell, P. D., and Farrow, J. B. Polymer flocculation of calcite: Relating the aggregate size to the settling rate. *American Institute of Chemical Engineering Journal*, 52, 1987–1994 (2006).
20. Mabire, F., Audebert, A., and Quivoron, C. Flocculation properties of some water-soluble cationic copolymers toward silica suspensions: A semiquantitative interpretation of the role of molecular weight and cationicity through a “Patchwork” model. *Journal of Colloid and Interface Science*, 97, 120–136 (1984).
21. Runkana, V. and Somasundaran, P. Mathematical modeling of coagulation and flocculation of colloidal suspensions incorporating the influence of surface forces. In *Colloid Stability and Application in Pharmacy*, Tadros, Th. F. (Ed), pp. 91–118, Wiley-VCH Verlag GmbH & Co. KGaA, Weinheim, Germany (2007).
22. Gregory, J. Polymer adsorption and flocculation in sheared suspensions. *Colloids and Surfaces A*, 31, 231–253 (1988).
23. Atesok, G., Somasundaran, P., and Morgan, L. J. Adsorption properties of Ca^{+2} on Na-kaolinite and its effect on flocculation using polyacrylamides. *Colloids and Surfaces A*, 32, 127–138 (1988a).
24. Atesok, G., Somasundaran, P., and Morgan, L. J. Charge effects in the adsorption of polyacrylamides on sodium kaolinite and its flocculation. *Powder Technology*, 54, 77–83 (1988b).
25. Fleer, G. J., Cohen Stuart, M. A., Scheutjens, J. M. H. M., Cosgrove, T., and Vincent, B. *Polymers at Interfaces*. Chapman & Hall, Inc., New York (1993).
26. van de Ven, T. G. M. Kinetic aspects of polymer and polyelectrolyte adsorption on surfaces. *Advances in Colloid and Interface Science*, 48, 121–140 (1994).
27. Yu, X. and Somasundaran, P. Kinetics of polymer conformational changes and its role in flocculation. *Journal of Colloid and Interface Science*, 178, 770–774 (1996).
28. Pedersen, H. G. and Bergstrom, L. Stabilizing ceramic suspensions using anionic polyelectrolytes: Adsorption kinetics and interparticle forces. *Acta Materialia*, 48, 4563–4570 (2000).
29. Adachi, Y. Dynamic aspects of coagulation and flocculation. *Advances in Colloid and Interface Science*, 56, 1–31 (1995).
30. Cohen Stuart, M. A. and Fleer, G. J. Adsorbed polymer layers in nonequilibrium situations. *Annual Review of Materials Science*, 26, 463–500 (1996).
31. Tjipangandjara, K., Huang, Y.-B., Somasundaran, P., and Turro, N. J. Correlation of alumina flocculation with adsorbed polyacrylic acid conformation. *Colloids and Surfaces A*, 44, 229–236 (1990).
32. Chander, P., Somasundaran, P., Turro, N. J., and Waterman, K. C. Excimer fluorescence determination of solid–liquid interfacial pyrene-labeled polyacrylic acid conformations. *Langmuir*, 3, 298–300 (1987).
33. Tjipangandjara, K. and Somasundaran, P. Effects of changes in adsorbed polyacrylic acid conformation on alumina flocculation. *Colloids and Surfaces A*, 55, 245–255 (1991).
34. Au, K.-K., Yang, S., and O’Melia, C. R. Adsorption of weak polyelectrolytes on metal oxide surfaces: A hybrid SC/SF approach. *Environmental Science & Technology*, 32, 2900–2908 (1998).
35. Somasundaran, P., Das, K. K., and Pradip, Polymer induced flocculation/dispersion of colloidal iron oxide and alumina suspensions. In *Proceedings of the XXI International Mineral Processing Congress*, Rome, Italy. Elsevier, Amsterdam, the Netherlands, pp. A5:62–68 (2000).
36. Chibowski, S. and Wisniewska, M. Study of electrokinetic properties and structure of adsorbed layers of polyacrylic acid and polyacrylamide at Fe_2O_3 —Polymer solution interface. *Colloids and Surfaces A*, 208, 131–145 (2002).

37. Yu, X. and Somasundaran, P. Role of polymer conformation in interparticle-bridging dominated flocculation. *Journal of Colloid and Interface Science*, 177, 283–287 (1996).
38. Fan, A., Turro, N. J., and Somasundaran, P. A study of dual polymer flocculation. *Colloids and Surfaces A*, 162, 141–148 (2000).
39. Klimpel, R. C. and Hogg, R. Effects of flocculation conditions on agglomerate structure. *Journal of Colloid and Interface Science*, 113, 121–131 (1986).
40. Bushell, G. C., Yan, Y. D., Woodfield, D., Raper, J., and Amal, R. On techniques for the measurement of the mass fractal dimension of aggregates. *Advances in Colloid and Interface Science*, 95, 1–50 (2002).
41. Levine, S. and Friesen, W. I. Flocculation of colloid particles by water-soluble polymers. In *Flocculation in Biotechnology and Separation Systems*, Attia, Y. A. (Ed), pp. 3–20, Elsevier Science Publishers B.V., Amsterdam, the Netherlands (1987).
42. Gregory, J. Rates of flocculation of latex particles by cationic polymers. *Journal of Colloid and Interface Science*, 42, 448–456 (1973).
43. Das, K. K. and Somasundaran, P. Flocculation-dispersion characteristics of alumina using a wide molecular weight range of polyacrylic acids. *Colloids and Surfaces A*, 223, 17–25 (2003).
44. Petzold, G. and Lunkwitz, K. The interaction between polyelectrolyte complexes made from poly(dimethyldiallylammonium chloride) (PDMDAAC) and poly(maleic acid-co-c-methylstyrene) (P(MS-c-MeSty)) and cellulosic materials. *Colloids and Surfaces A*, 98, 225–233 (1995).
45. Petzold, G., Buchhammer, H.-M., and Lunkwitz, K. The use of oppositely charged polyelectrolytes as flocculants and retention aids. *Colloids and Surfaces A*, 119, 87–92 (1996).
46. Yu, X. and Somasundaran, P. Enhanced flocculation with double flocculants. *Colloids and Surfaces A*, 81, 17–23 (1993).
47. Glover, S. M., Yan, Y., Jameson, G. J., and Biggs, S. Dewatering properties of dual-polymer-flocculated systems. *International Journal of Mineral Processing*, 73, 145–160 (2004).
48. Sivadasan, K., Somasundaran, P., and Turro, N. J. Fluorescence and viscometric study of complexation of polyacrylic acid with polyacrylamide with hydrolyzed polyacrylamide. *Colloid and Polymer Science*, 269, 131–137 (1991).
49. Lee, C. H. and Liu, J. C. Enhanced sludge dewatering by dual polyelectrolytes conditioning. *Water Research*, 34, 4430–4436 (2000).
50. Fan, A., Somasundaran, P., and Turro, N. J. Role of sequential adsorption of polymer/surfactant mixtures and their conformation in dispersion/flocculation of alumina. *Colloids and Surfaces A*, 146, 397–403 (1999).
51. Chen, K. L., Mylon, S. E., and Elimelech, M. Aggregation kinetics of alginate-coated hematite nanoparticles in monovalent and divalent electrolytes. *Environmental Science & Technology*, 40, 1516–1523 (2006).
52. Amjad, Z. Factors to consider in selecting a dispersant for treating industrial water systems. *UltraPure Water*, 16, 17–24 (1999).
53. Amjad, Z. Dispersion of iron oxide particles in industrial waters. *Tenside Surfactants Detergents*, 36, 50–56 (1999).
54. Amjad, Z. Factors influencing the performance of natural and synthetic additives as iron oxide dispersants. *Tenside Surfactants Detergents*, 44, 88–93 (2007).
55. Amjad, Z. Role of heat treatment on the performance of polymers as iron oxide dispersants. *Tenside Surfactants Detergents*, 43, 242–250 (2006).
56. Somasundaran, P. and Runkana, V. Modeling flocculation of colloidal mineral suspensions using population balances. *International Journal of Mineral Processing*, 72, 33–55 (2003).
57. Thomas, D. N., Judd, S. J., and Fawcett, N. Flocculation modeling: A review. *Water Research*, 33, 1579–1592 (1999).
58. Israelachvili, J. N. *Intermolecular and Surface Forces*. Academic Press, New York (1991).
59. Fleer, G. J. and Scheutjens, J. M. H. M. Modeling polymer adsorption, steric stabilization, and flocculation. In *Coagulation and Flocculation: Theory and Applications*, Dobias, B. (Ed), pp. 209–263, Marcel Dekker, Inc., New York (1993).
60. Scheutjens, J. M. H. M. and Fleer, G. J. Statistical theory of the adsorption of interacting chain molecules. 1. Partition function, segment density distribution, and adsorption isotherms. *The Journal of Physical Chemistry*, 83, 1619–1635 (1979).
61. Scheutjens, J. M. H. M. and Fleer, G. J. Statistical theory of the adsorption of interacting chain molecules. 2. Train, loop, and tail size distribution. *The Journal of Physical Chemistry*, 84, 178–190 (1980).
62. Scheutjens, J. M. H. M. and Fleer, G. J. Interaction between two adsorbed polymer layers. *Macromolecules*, 18, 1882 (1985).

63. de Gennes, P. G. Polymer solutions near an interface. 1. Adsorption and depletion layers. *Macromolecules*, 14, 1637–1644 (1981).
64. de Gennes, P. G. Polymer solutions near an interface. 2. Interaction between two plates carrying adsorbed polymer layers. *Macromolecules*, 15, 492–500 (1982).
65. de Gennes, P. G. Polymers at an interface: A simplified view. *Advances in Colloid and Interface Science*, 27, 189–209 (1987).
66. van der Schee, H. A. and Lyklema, J. A lattice theory of polyelectrolyte adsorption. *The Journal of Physical Chemistry*, 88, 6661–6667 (1984).
67. Roe, R. Multilayer theory of adsorption from a polymer solution. *The Journal of Chemical Physics*, 60, 4192–4207 (1974).
68. Evers, O. A., Flerer, G. J., Scheutjens, J. M. H. M., and Lyklema, J. Adsorption of weak polyelectrolytes from aqueous solution. *Journal of Colloid and Interface Science*, 111, 446–454 (1986).
69. Bohmer, M. R., Evers, O. A., and Scheutjens, J. M. H. M. Weak polyelectrolytes between two surfaces: Adsorption and stabilization. *Macromolecules*, 23, 2288–2301 (1990).
70. Blaakmeer, J., Bohmer, M. R., Cohen Stuart, M. A., and Flerer, G. J. Adsorption of weak polyelectrolytes on highly charged surfaces. Poly (acrylic acid) on polystyrene latex with strong cationic groups. *Macromolecules*, 23, 2301–2309 (1990).
71. Vermeer, A. W. P., Leermakers, F. A. M., and Koopal, L. K. Adsorption of weak polyelectrolytes on surfaces with a variable charge. Self-consistent-field calculations. *Langmuir*, 13, 4413 (1997).
72. Borukhov, I., Andelman, D., and Orland, H. Effect of polyelectrolyte adsorption on intercolloidal forces. *The Journal of Physical Chemistry B*, 103, 5042–5057 (1999).
73. Juvekar, V. A., Anoop, C. V., Pattanayek, S. K., and Naik, V. M. A continuum model for polymer adsorption at the solid-liquid interface. *Macromolecules*, 32, 863–873 (1999).
74. Hogg, R. The role of polymer adsorption kinetics in flocculation. *Colloids and Surfaces A*, 146, 253–263 (1999).
75. Vold, M. J. The effect of adsorption on the van der Waals interaction of spherical colloidal particles. *Journal of Colloid Science*, 16, 1–12 (1961).
76. Vincent, B. The van der Waals attraction between colloid particles having adsorbed layers. II. Calculation of interaction curves. *Journal of Colloid and Interface Science*, 42, 270–285 (1973).
77. Hogg, R., Healy, T. W., and Fuerstenau, D. W. Mutual coagulation of colloidal dispersions. *Transactions of Faraday Society*, 62, 1638–1651 (1966).
78. Bell, G. M., Levine, S., and McCartney, L. N. Approximate methods of determining the double-layer free energy of interaction between two charged colloidal spheres. *Journal of Colloid and Interface Science*, 33, 335–359 (1970).
79. Sader, J. E., Carnie, S. L., and Chan, D. Y. C. Accurate analytic formulas for the double-layer interaction between spheres. *Journal of Colloid and Interface Science*, 171, 46–54 (1995).
80. Runkana, V., Somasundaran, P., and Kapur, P. C. A population balance model for flocculation of colloidal suspensions by polymer bridging. *Chemical Engineering Science*, 61, 182–191 (2006).
81. Smoluchowski, M. v. Versuch einer mathematischen theorie der koagulationskinetik kolloider losungen. *Zeitschrift fur Physikalische Chemie*, 92, 129–168 (1917).
82. Mandelbrot, B. B. *The Fractal Geometry of Nature*. Freeman, New York (1983).
83. Lu, C. F. and Spielman, L. A. Kinetics of floc breakage and aggregation in agitated liquid suspensions. *Journal of Colloid and Interface Science*, 103, 95–105 (1985).
84. Spicer, P. T. and Pratsinis, S. E. Coagulation and fragmentation: Universal steady-state particle-size distribution. *American Institute of Chemical Engineers Journal*, 42, 1612–1620 (1996).
85. Biggs, C. A. and Lant, P. A. Modelling activated sludge flocculation using population balances. *Powder Technology*, 124, 201–211 (2002).
86. Nopens, I., Koegst, T., Mahieu, K., and Vanrolleghem, P. A. PBM and activated sludge flocculation: From experimental data to calibrated model. *American Institute of Chemical Engineers Journal*, 51, 1548–1557 (2005).
87. Ding, A., Hounslow, M. J., and Biggs, C. A. Population balance modeling of activated sludge flocculation: Investigating the size dependence of aggregation, breakage and collision efficiency. *Chemical Engineering Science*, 61, 63–74 (2006).
88. Runkana, V., Somasundaran, P., and Kapur, P. C. Mathematical modeling of polymer-induced flocculation by charge neutralization. *Journal of Colloid Interface Science*, 270, 347–358 (2004).
89. Runkana, V., Somasundaran, P., and Kapur, P. C. Reaction-limited aggregation in presence of short-range structural forces. *American Institute of Chemical Engineers Journal*, 51, 1233–1245 (2005).

90. Somasundaran, P., Runkana, V., and Kapur, P. C. A population balance model for flocculation of colloidal suspensions incorporating the influence of surface forces. In Paper presented at *5th World Congress on Particle Technology (WCPT5-2006)*, Orlando, FL (April 23–27, 2006).
91. Somasundaran, P., Kapur, P. C., and Runkana, V. Population balance modeling of flocculation of mineral suspensions by polymers. In Paper presented at *International Mineral Processing Congress (IMPC-2006)*, Istanbul, Turkey (September 3–9, 2006).
92. Ramkrishna, D. *Population Balances: Theory and Applications to Particulate Systems in Engineering*. Academic Press, New York (2000).
93. Vanni, M. Approximate population balance equations for aggregation–breakage processes. *Journal of Colloid and Interface Science*, 221, 143–160 (2000).
94. Firth, B. A. and Hunter, R. J. Flow properties of coagulated colloidal suspensions I. Energy dissipation in the flow units. *Journal of Colloid and Interface Science*, 57, 248–256 (1976).
95. Kusters, K. A., Wijers, J. G., and Thoenes, D. Aggregation kinetics of small particles in agitated vessels. *Chemical Engineering Science*, 52, 107–121 (1997).
96. Fuchs, N. Ueber die stabilität und aufladung der aerosole. *Zeitschrift für Physik*, 89, 736–743 (1934).
97. Derjaguin, B. V. and Muller, V. M. Slow coagulation of hydrophobic colloids. *Doklady Akademii Nauk SSSR* 176, 738–741 (1967).
98. McGown, D. N. and Parfitt, G. D. Improved theoretical calculation of the stability ratio for colloidal systems. *The Journal of Physical Chemistry*, 71, 449–450 (1967).
99. Spielman, L. A. Viscous interactions in Brownian coagulation. *Journal of Colloid and Interface Science*, 33, 562–571 (1970).
100. Honig, E. P., Roeberson G. J., and Wiersema P. H. Effect of hydrodynamic interaction on the coagulation rate of hydrophobic colloids. *Journal of Colloid and Interface Science*, 36, 97–109 (1971).
101. Biggs, S., Habgood, M., Jameson, G. J., and Yan, Y.-d. Aggregate structures formed via a bridging flocculation mechanism. *Chemical Engineering Journal*, 80, 13–22 (2000).
102. Das, K. K. and Somasundaran, P. A kinetic investigation of the flocculation of alumina with polyacrylic acid. *Journal of Colloid and Interface Science*, 271, 102–109 (2004).
103. Ducoste, J. J., Clark, M. M., and Weetman, R. J. Turbulence in flocculators: Effects of tank size and impeller type. *American Institute of Chemical Engineers Journal*, 43, 328–338 (1997).
104. Kramer, T. A. and Clark, M. M. Influence of strain-rate on coagulation kinetics. *Journal of Environmental Engineering*, 123, 444–452 (1997).
105. Heath, A. R. and Koh, P. T. L. Combined population balance and CFD modeling of particle aggregation by polymeric flocculant. In Paper presented at *3rd International Conference on CFD in Minerals and Process Industries*, Melbourne, Australia (2003).
106. Marchisio, D. L., Pikturna, J. T., Fox, R. O., Vigil, R. D., and Barresi, A. A. Quadrature method of moments for population-balance equations. *American Institute of Chemical Engineers Journal*, 49, 1266–1276 (2003).
107. Prat, O. and Ducoste, J. J. Modeling spatial distribution of floc size in turbulent processes using the quadrature method of moment and computational fluid dynamics. *Chemical Engineering Science*, 61, 75–86 (2006).

18 Mechanistic Aspects of Heat Exchanger and Membrane Biofouling and Prevention

Luis F. Melo and Hans-Curt Flemming

CONTENTS

18.1	Introduction.....	365
18.2	Biofilms	367
18.3	Heat Exchanger Biofouling	371
18.4	Membrane Biofouling	374
18.5	Strategies to Combat Biofouling in Heat Exchangers and Membranes	377
18.6	Summary.....	378
	References.....	379

18.1 INTRODUCTION

Microbial films (hydrated layers of microorganisms and their extracellular products) develop in practically all natural and engineered aqueous systems. Often they are unwanted and, in such cases, the formation of biofilms is called biofouling. Biofouling is an operational definition, referring to that amount of biofilm development that interferes with technical, aesthetic, or economical requirements. From the economic and environmental point of view, two of the most important examples of industrial biofouling occur in heat exchangers and membrane systems.

Heat exchangers are commonly used in industry (e.g., chemical, food, pharmaceutical, oil refining, thermal power plants, nuclear power stations, paper production, and desalination), in buildings (e.g., hospitals, hotels, shopping malls, and office buildings), and in transportation vehicles (e.g., airplanes, cars, trains, and ships) to cool or heat fluids to the required process temperatures, recover heat from hot fluids, condense vapors, pasteurize/sterilize food and biological fluids, refrigerate computer systems, and provide proper climatization. Although the following may not be the most general definition of a heat exchanger, the latter is often seen as an equipment where two fluids at different temperatures, separated by a solid wall, exchange heat. Each fluid flows in its own channel, tube, or chamber and the wall that separates the two fluids is usually made of a good thermal conducting material (almost always a metal such as stainless steel, copper, copper–nickel alloy, and titanium), as thin as possible in order to minimize wall thermal resistance.

In a significant number of processes, water and/or aqueous solutions are used either as process or as auxiliary liquids. Sometimes, water is used in the same equipment both as a heat source and a cold source, as it occurs in the different sections of plate heat exchanger units where milk is pasteurized/sterilized and, subsequently, cooled down to ambient temperatures. Therefore, most heat exchangers that process aqueous liquids (including simple water) offer a set of optimal conditions for the development of microbial films (biofilms): surfaces where bacteria and other microbes are keen to attach to, temperatures in a suitable range for microbial growth (15°C–40°C), and appropriate nutrients in the water [1]. In heat exchangers, biofilms are predominantly formed by bacteria,

although other types of microorganisms can be present (e.g., algae, filamentous fungi, and yeasts) together with protozoa.

Membrane technology in water systems is a separation process based on semipermeable surfaces that allow water to flow through their pores while soluble compounds and suspended solids are retained on the membrane surface. The membrane flux is enhanced by applying pressure or concentration gradients between the two sides of the membrane or, in some cases, by imposing an electric potential.

When the goal is to remove larger particles from the water, micro- and ultrafiltration membranes are used. To remove ions and small molecules, nanofiltration and reverse osmosis (RO) systems are applied with higher pressure gradients. RO is the more commonly used membrane technology in drinking water, industrial water, and wastewater treatment systems. However, the operating efficiency of membranes (flux and solute rejection capacity) and the integrity of the materials that constitute such systems are severely damaged by fouling/biofouling phenomena. Biofilms grow both on the feedwater and the permeate surfaces of RO membranes. In potable/drinking water production, this contributes highly to the degradation of the water quality. Although abiotic layers (scaling, particle deposition) also form on the membrane surfaces, they usually come together with biofouling. Studies were carried out on 70 industrial plants where more than half of these systems were clearly affected by biofilm formation, representing nearly 30% of the plant operating costs [2].

Biofouling is, in fact, a costly problem [3,4]. It causes:

- Reduction in heat transfer efficiency due to the thermal insulating effect that they introduce
- Reduction in the membrane flux and in the solute rejection efficacy
- Increase in the pressure drop across the heat exchanger or the membrane surfaces due to the irregular topography of the biofilm and the reduction of the flow area
- Increased corrosion of metallic surfaces due to differential aeration microzones next to the microbial colonies and/or to the acidic metabolites produced by the attached bacteria (pitting corrosion)
- Contamination of the fluids flowing through the tubes/channels by the microbial species as a consequence of biofilm detachment from the wall
- Contamination of potable water produced in membrane systems due to the formation of biofilms on the permeate side
- Increased costs of equipment cleaning and disinfection, which is commonly based on the use of biocides such as chlorine, ozone, and quaternary ammonium salts, together with detergents/dispersants
- Increased environmental costs associated to the need to treat the wastewater containing the chemicals used in the cleaning processes
- Significant costs due to production breaks (product losses, manpower) to perform cleaning, disinfection, and maintenance operations (replacement of membrane modules and of heat exchanger tubes)
- Radioactive leaks to the water due to corrosion in nuclear power plant cooling units

Several estimates for fouling costs (of which biofouling represents possibly 20%–30%) point out to 0.25% of the GNP (gross national product) in industrialized countries [5]. Biofouling costs in specific cases such as power and desalination plants were calculated as being over \$15 billion per year [6,7]. In power plants around the world, thousands of tons of chlorine are spent each day to combat biofilms, which amounts to very high values in terms of biocide and wastewater treatment costs. Capital costs are also directly affected by the oversizing of the heat exchanger transfer area obtained through the introduction of the so-called fouling factor, which is an additional thermal resistance due to the unwanted attached layer.

Data collected from a membrane system at Water Factory 21, Orange County, CA in 1994 [8], showed that the biofouling costs by that time were about \$750,000 per year, approximately 30% of the entire plant operating costs. This estimate considered not only the costs for membrane cleaning itself and labor costs, but also for off-time during cleaning, pretreatment costs including biocides and other additives, as well as an increased energy demand due to higher transmembrane and tangential hydrodynamic resistance, and shortened lifetime of the membranes. This assessment reflects how complex and essentially arbitrary such numbers are, but it certainly shows that including indirect costs of biofouling reveals surprisingly high overall values.

Collectively, the costs of biofouling are very substantial and support a healthy antifouling industry offering everything from antifouling surfaces and materials to biocides, cleaners, and consulting—this market is worth billions of dollars annually worldwide. Probably the cheapest factor is the cost for biocides and cleaners (if cleaners are employed at all). The treatment of wastewater contaminated with antifouling additives will represent an emerging cost factor as the release of biocides is increasingly restricted and will require more effort in removal—a problem that will come further into focus in Europe when new EU guidelines limit the biocide content in effluents

18.2 BIOFILMS

Microbial films are strategically organized and highly hydrated (often, with 90%–99% of water) communities of microorganisms attached to surfaces. These biological structures contain polymers excreted by the microbes, known as extracellular polymeric substances or EPS [9], as well as adsorbed molecules and small particles captured from the surrounding liquid. Natural and process waters are habitats for a vast number of different microbial species, from heterotrophic bacteria and nitrifiers to algae, fungi, and protozoa. Bacteria usually predominate in biofilm layers [1,7,8]. Some of them are more prone to produce extracellular polymers and easily attach to solid surfaces (e.g., *Pseudomonas aeruginosa*, *Pseudomonas fluorescens*, and *Escherichia coli*); others imbed themselves in biological layers formed by the first ones (e.g., *Helicobacter pylori* in drinking water systems). The EPS composition is based on polysaccharides and glycoproteins [9]. The resulting biological layer is of viscoelastic (slimy) nature with thicknesses that can vary from a few microns to some millimeters or, in less common situations, centimeters. On account of the very large fraction of water present in these biolayers, their density is practically equal to the water density, but the EPS produced by the bacteria create a complex polymeric network of pores and channels with high tortuosity, which in some cases limit the rate of diffusion of nutrients, metabolites, and toxic compounds (e.g., biocides and antibiotics) through the matrix.

Figure 18.1 shows a scanning electron micrograph of the surface of a (dried) biofilm formed in contact with the water flowing under a turbulent regime, where a significant amount of EPS can be seen together with groups of bacteria (here they appear as small round entities just below the surface) imbedded in the polymeric matrix.

The processes involved in the buildup of biofilms can be divided into two main categories: those that promote biomass production and those that tend to oppose the development of such biolayers, as shown in Figure 18.2. The former include the transport of bacteria/microorganisms, nutrients, and oxygen to the walls of the equipment (during biofouling start-up) or to the liquid–biofilm interface (in later stages), the diffusion of nutrients/substrates inside the microbial film, and their consumption by the active cells within the biofilm structure. Mechanistically, these phenomena occur in series and, as such, the slowest of them all will control the rate of this set of processes [10].

In heat exchangers, due to the relatively high external mass transfer coefficients in turbulent flows (the most common flow regime in this type of equipment, at least when operating with Newtonian liquids), the processes occurring inside the microbial matrix (diffusion of nutrients/oxygen or the internal biological kinetics) are usually the ones that limit the overall rate of biomass production. This argument can also be applied to the penetration of biocides to combat biofilms.

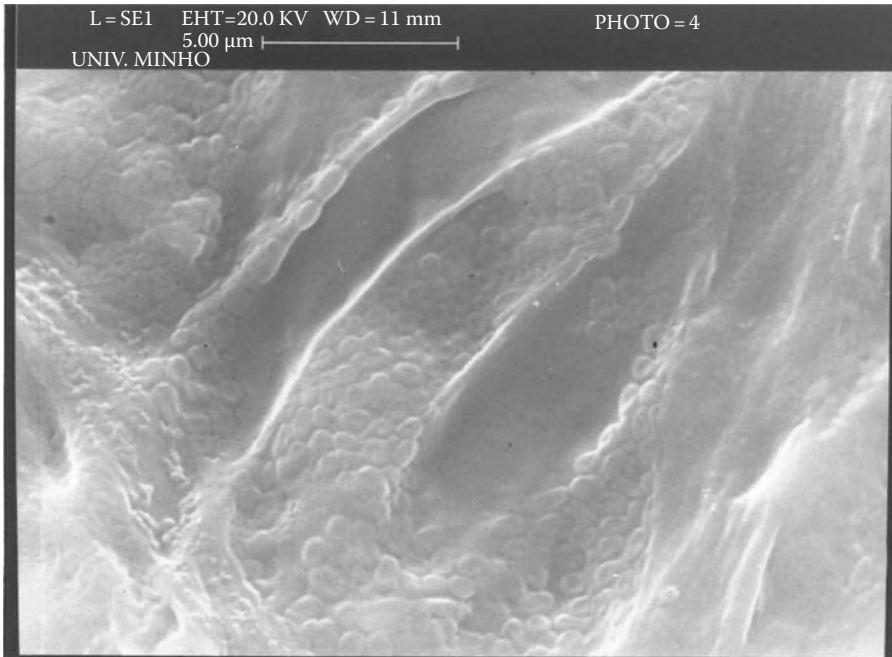


FIGURE 18.1 Scanning electron microscopy (SEM) image of the surface of a biofilm formed by *Pseudomonas fluorescens* in contact with water in turbulent flow regime (Reynolds number = 12,000).

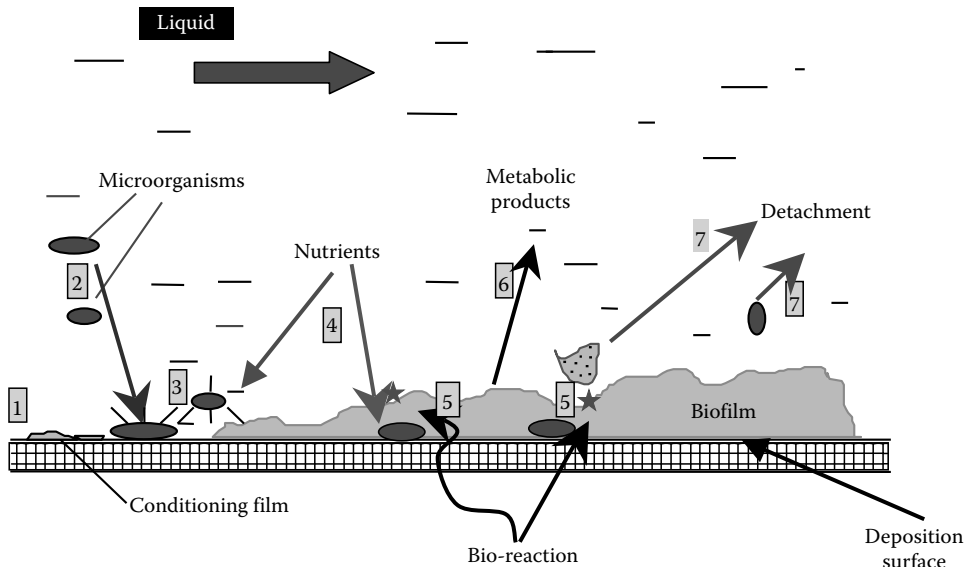


FIGURE 18.2 Main macroscopic processes involved in biofilm buildup: (1) Initial formation of a conditioning organic layer on the surface; (2) attachment of microorganisms to the deposition surface; (3) production of extracellular polymers; (4) mass transfer of nutrients and oxygen to the biofilm–liquid interface and inside the biofilm layer; (5) consumption of nutrients/oxygen; (6) formation and release of metabolic products; (7) removal/detachment of biomass from the biofilm.

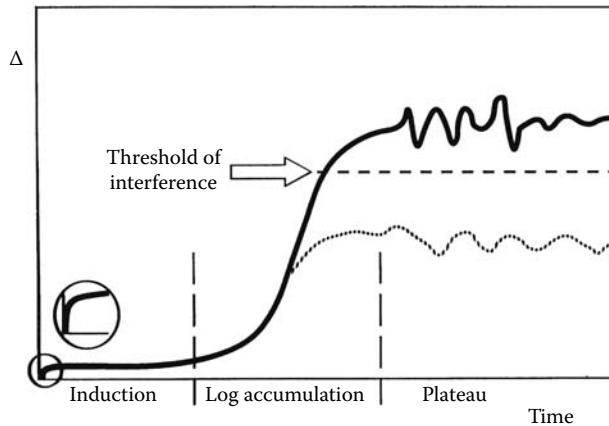


FIGURE 18.3 Schematic biofilm development. Dashed straight line: arbitrary threshold of interference. (Adapted from Flemming, H.-C. and Ridgway, H.F., *Biofilm control: Conventional and alternative approaches*, in *Marine and Industrial Biofouling*, Flemming, H.-C., Murthy, P.S., Venkatesan, R., and Cooksey, K.C. (Eds.), Springer, New York, 2008.)

In parallel, a second type of process (removal of the biofilm from the surface) is activated when some biomass is already adhered to the deposition surfaces. Such processes occur through two main mechanisms: erosion, which is basically the continuous detachment of small amounts of biomass/cells from the biofilm surface; and sloughing off, which is the stochastic detachment of macroscopic amounts of biofilm, sometimes leaving the surface locally bare. The removal of biomass is reinforced by the hydrodynamic forces of the liquid flowing over the biofilm surface, but sloughing-off events can also be observed in stagnant media, possibly due to the formation of thick biofilms that do not allow nutrients to fully penetrate the biological layer and feed the bacteria in the deeper zones.

As may be seen in Figure 18.3, the biofilm tends to reach a maximum thickness that may vary from a few microns to some millimeters in heat exchangers and membranes. The balance between the two sets of processes (biofilm production and biofilm removal) determines the overall rate of biofilm buildup and the maximum thickness reached by the microbial layer. Several authors observed that shear stress effects are predominant when the adjacent liquid flows at high velocities (high Reynolds numbers, usually in the turbulent flow regime) over the biofilm surface, controlling the thickness of the microbial layer [1,11]. As such, higher shear stresses lead to thinner and more cohesive microbial layers, while lower shear stresses lead to thicker and fluffier biofilms. The reason is that only those EPS molecules that are strongly enough connected to withstand the actual shear conditions will be retained, which inevitably leads to higher cohesion.

Table 18.1 shows the effects of the fluid velocity on the amount and structural characteristics of a biofilm attached to a metallic surface, under turbulent flow conditions [12]. Increasing the liquid velocity, the maximum mass of attached biofilm decreases, which reveals the dominant effects of shear stress. The authors also reported that when the nutrients were totally suppressed from the water flowing in contact with the biofilm, the fraction of biomass that subsequently detached from the surface increased significantly with the liquid velocity to which the biofilm had been previously subjected (see Table 18.1). This suggests that the thinner biofilms, formed under conditions of higher shear stresses, were more dependent on the substrate (glucose in the reported case), that is, were almost completely penetrated by the substrate, while the thicker ones were only partially penetrated by the substrate.

By extrapolating these findings to the penetration of other chemicals (biocides, detergents), it may be concluded that the biofilm structure formed at higher liquid velocities is not only thinner but also allows the penetration of antimicrobial compounds. This explains the “rules of practice”

TABLE 18.1
Effects of External Liquid Velocity and
Nutrient Depletion on Biofilm Properties

Liquid Velocity (m/s)	Maximum Biofilm Mass (kg/m ²)	Fraction of Biofilm Mass Detached after Nutrient Depletion (%)
0.34	2.0	21.4
0.54	1.8	79.4
0.72	1.5	90.7

Source: Melo, L.F. and Vieira, M.J., *Bioprocess Eng.*, 20, 363, 1999.

applied to the design of heat exchangers, which recommend higher liquid velocities during equipment operation. There are, however, upper limits for the recommended water velocity, which are dictated by other type of considerations, such as keeping the pressure drop within an adequate range of values, surface material wear (corrosion is enhanced at higher fluid velocities), and allowing sufficient residence time for the fluids to heat, cool, or condense according to the process requirements.

The understanding of biofilm phenomena significantly improved in the last decade by novel information obtained through the development and application of molecular biology approaches that brought important insights into the metabolic and genetic issues related to the growth and behavior of these microbial layers.

Biofilms are now seen as the predominant *modus vivendi* of bacteria on our planet [4], a kind of habitat they build to protect their communities and improve the exchange of useful chemicals/nutrients and information to support microbial development and survival. It has been found that bacteria communicate between them by chemical signaling through molecules such as acyl-homoserine lactones (in gram-negative species) and modified peptides (in gram-positive species). They excrete these molecules either when they are dispersed in a suspension or more close together in aggregates and they use those tools to manage their survival strategy [13–15], because they are able to recognize/detect the much higher concentration levels that such molecules reach inside biofilms or flocs (*quorum sensum* phenomenon), as compared to dispersed aqueous suspensions.

Some researchers [16] sought to explain the effects of increased shear stress on bacterial metabolism and biofilm density, and they reported that such effects were related to the increase in dehydrogenase activity within the microbial cells. As a consequence, the translocation of protons to the outer wall of the cells is enhanced and the cells become more hydrophobic, favoring their mutual adhesion, that is, reinforcing the cohesiveness and mechanical strength of the biofilm. This is in accordance with the experimental data obtained by other authors at the macroscopic level [11,12,17] who measured higher densities and resistances to removal by hydrodynamic forces in cases where the biofilms had been previously formed under higher liquid velocities. Enhanced production of EPS polysaccharides was shown to be the response of biofilms when subject to higher shear stresses [17].

However, it seems that such a sudden increase in shear stress may have different consequences depending on the particular history of formation of each biofilm. For example, a biofilm that was formed in contact with water flowing at 0.35 m/s lost 40% of its mass when the fluid velocity was increased up to 1 m/s; however, a biofilm of the same microbial species formed in contact with water flowing at 0.62 m/s did not lose any mass when the fluid velocity was changed to 1 m/s [12].

Is there a contradiction between these results and the conclusions drawn from Table 18.1? No, because the phenomena under discussion are completely different: in Table 18.1, last column, the

relevant process is the penetration of chemicals (nutrients/substrates or biocides), while the examples given in the last paragraph are related to the mechanical strength of the biofilm. The overall conclusion is that higher velocities promote the buildup of thinner and more stable biofilms that, at the same time, are more easily penetrated by either nutrients or biocides.

The effects of nutrient type and concentration can be also of some importance due to the variety of aqueous solutions that may flow through heat exchangers in different processes. Work carried out in a paper mill water stream [18] revealed that by increasing nutrient content (nitrogen and phosphorous) in a paper mill water stream, the biofilm amount also increased. Other researchers [19] observed also an increase in biofilm thickness when increasing glucose concentration up to a certain limit (around 0.5 g/L), above which an additional increase of substrate (e.g., to 1 g/L) resulted in a very thick microbial film that lost its cohesiveness and detached easily, reducing the final amount of attached biomass. These authors found also that low nitrogen contents favor the regular erosion mechanism, while high nitrogen concentrations promote the stochastic sloughing off of macroscopic biofilm portions. Therefore, it can be said that, in general, detachment mechanisms seem to control biofilm accumulation as regards the effects of nutrients or fluid velocity. However, there is not yet an established in-depth explanation for the predominant role of detachment. To reach a better understanding of these phenomena, one should look at the principles of transport phenomena, in particular the effects of fluid velocity on the various biofilm formation mechanisms: (a) external mass transfer of nutrients to the biofilm surface increases with the liquid velocity to a power of around 0.8 in turbulent flow; (b) higher fluid velocities promote thinner and denser biofilms that will affect internal diffusion and substrate consumption kinetics (the quantitative effects in this case are not clearly determined, but they are, acceptably, not higher than the effects on external mass transfer); (c) simultaneously, the opposite mechanisms of detachment are regulated mostly by shear stress, which increases with the fluid velocity up to a power of around 2. Since the rate at which the internal mechanisms occur prevails within the biomass production processes and, simultaneously, the opposite processes (detachment) are much more affected by the fluid velocity, it is not surprising that the effect of velocity on the detachment rate will control the overall processes of biofilm formation.

18.3 HEAT EXCHANGER BIOFOULING

Simple microbial layers containing only one species and no abiotic material are almost never found in practical situations outside the research laboratories. In industrial systems, biofouling appears together with other types of fouling, namely, inorganic precipitation, particulate deposition, and corrosion deposits, which interact with biofilm formation and properties [20]. Scaling (undesired precipitation of inorganic salts) occurs frequently, mainly in those systems using hard waters such as those containing high concentrations of calcium and magnesium salts and it depends very much on temperature and pH. Calcium cation (Ca^{2+}) is known for its ability to bind proteins [21], which contributes to reinforce the cohesion of the gelatinous biofouling layer, particularly in polyanionic EPS matrices. Additionally, some microorganisms promote or intensify the nucleation of calcium carbonate within the extracellular polymeric matrix, resulting in calcification on the deposition surface [22].

Depending on their dimension, concentration, and local hydrodynamic patterns, inorganic particles (sand, clay) suspended in the water may either reduce biofouling by producing a scouring action on the microbial films or become incorporated in the biological matrix and modify its properties [23,24]. In particular, the effects of small clay particles (10–20 micron) on the survival of biofilm formed under turbulent flow conditions were studied by assessing the thickness of the microbial layer after suppressing the substrate (glucose) from the water: biofilms containing clay material kept their thickness constant during 2 to 3 days, while biolayers without any clay particles resisted only for 1 day before their structure collapsed [25].

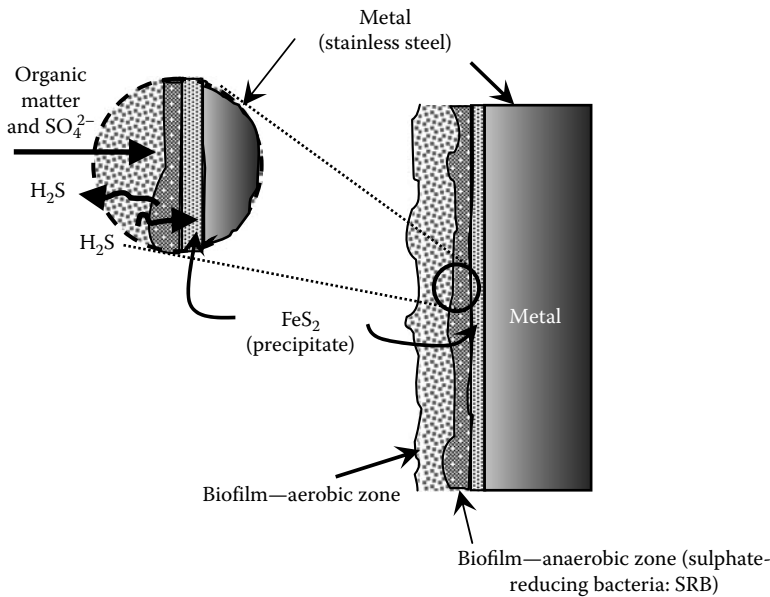


FIGURE 18.4 Simplified biocorrosion mechanism by sulfate reducing bacteria.

Both in cooling water systems and in process water streams (e.g., in paper mills), the biofilm matrix (biological layer and abiotic debris) may become thick enough to prevent oxygen to reach the deeper layers of the deposit, especially because aerobic organisms in the surface layers consume oxygen faster than it can diffuse. Since industrial biofilms contain mixed microbial populations (and may favor the growth of certain species over others, if the proper conditions are established), the lack of oxygen promotes the development of anaerobic bacteria in the inner zones of the biofilm, some of which (e.g., sulfate reducing bacteria, SRB) produce metabolites that electrochemically attack the metallic surface and cause corrosion as shown in Figure 18.4.

Biofilms *per se* are the focus of numerous problems in industry, independent of the presence of other types of fouling. One of the more relevant economical impacts of biofouling in heat exchangers occurs in thermal power plants for electricity production. These plants may use steam coming from a furnace to impart mechanical energy to the turbines in order to keep them rotating and producing electricity. This steam has to be condensed downstream to maintain a low pressure at the turbine outlet, since the efficiency of electricity production relies much upon the pressure differential between the inlet and outlet of the turbine ($P - P'$, in Figure 18.4). The temperatures of the cooling water in the condenser may range from 15°C (at the inlet) to 35°C (at the outlet), which are quite favorable to microbial growth and, therefore, promote biofilm formation inside the tubes. As a consequence, the condensation rate is reduced due to the additional thermal resistance introduced by the attached layer, and the steam pressure at the condenser inlet (turbine outlet) increases, affecting the kinetic energy of the rotating turbine. Electricity production efficiency is thus reduced in the power plant (Figure 18.5).

Biofouling effects on the heat transfer rate are quite impressive in these processes. Considering a biofilm of only 0.1 mm (100 microns), its thermal resistance per unit surface area is $1.7 \times 10^{-4} \text{ m}^2 \text{ K/W}$ (assuming that the thermal conductivity of biofilms and water are similar and around 0.6 W/m K). Since the overall heat transfer coefficient in the condenser may be in the range of $2500 \text{ W/m}^2 \text{ K}$ when the tubes are still clean, the thermal resistance of a 0.1 mm thick biofilm will cause a decrease of this coefficient down to $1750 \text{ W/m}^2 \text{ K}$, that is, a 30% loss in the condensation rate. Taking into account that such condensers may have 5,000–10,000 tubes and that the total flow rate of the cooling water is therefore very large, the occurrence of biofouling represents enormous costs related to energy production inefficiencies.

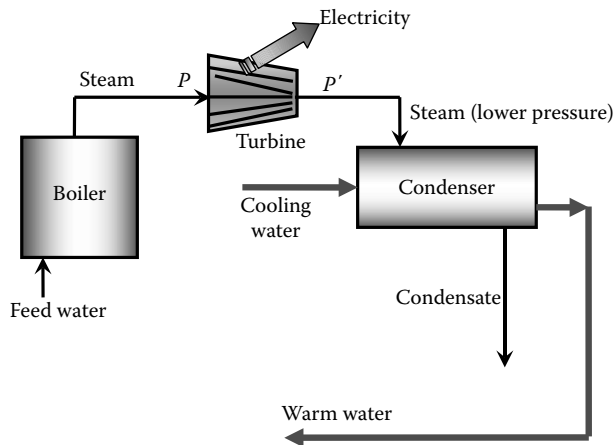


FIGURE 18.5 Thermal power plant to produce electricity (schematic). Biofouling in the condenser causes (a) decrease in condensation rate; (b) increase in pressure P' ; (c) decrease in turbine efficiency and in electricity production.

To tackle these problems, biocides (often chlorine compounds) are periodically introduced in the cooling water, making the whole process much more expensive and causing environmental and corrosion problems. Some condensers contain a mechanical cleaning system (Taprogge System) consisting of small rubber balls that are periodically (e.g., once a day) injected through the tubes to remove the attached biofilm by abrasion. This represented at the time an important practical advance that reduces the amount of biocides, and, thus, the costs, although it is difficult to ensure (due to different hydrodynamic flow pattern) that the sponge rubber balls pass through all the tubes, mainly those that are more distant from the central zone of the tube bundle. Furthermore, above a given thickness of the deposit, the sponge balls may remove only part of it and glide on the remaining layer.

Sometimes, improper design of heat exchangers results in quite low water velocity in localized zones (dead zones), where the buildup of thick biofilm layers, often with a rather loose consistence, will be favored. Biomass lumps will tend to detach easily from the equipment surfaces at these places and promote severe fouling and environmental problems downstream. Additionally, those “dead zones” are also difficult to reach by biocides carried in the water stream used when cleaning and disinfecting the equipment.

When designing heat exchangers, an allowance is always considered in order to compensate for the negative impact of biofilms on the heat transfer rate. This is usually achieved by oversizing the equipment, that is, by introducing a “fouling factor” (an additional thermal resistance) that results in a larger heat transfer area of the exchanger [3]. Therefore, when the operation of a clean heat exchanger is started up, the heat transfer rate during the first period will be higher than desired, and operators may tend to bypass part of the cooling water stream in order to reduce the cooling effect to the desired level. This is not an appropriate solution, because it leads to lower water velocities and, consequently, to faster buildup of fouling layers. The recommended operating measure in such cases would be to recycle part of the cooling water at the heat exchanger outlet, thereby increasing the inlet water temperature and decreasing the heat transfer rate during the initial period of operation. Figure 18.6 presents the adequate approach to overcome this problem.

The development of novel surface materials to build heat exchangers has been given much attention in the last decade [26–28]. The role of the deposition surface on microbial attachment is associated with its roughness and with its chemical composition (particularly, its surface tension). However, apart from high costs, practical problems are still hampering the introduction of new materials and coatings, one of them being abiotic fouling that masks original anti-biofouling

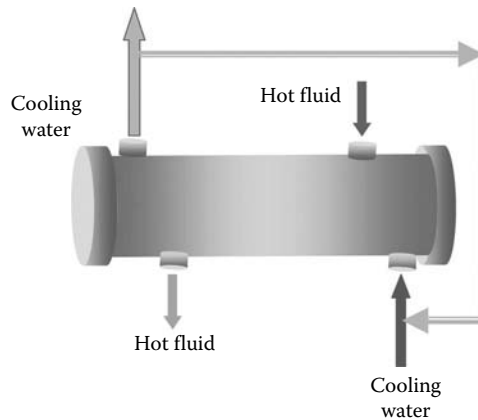


FIGURE 18.6 Cooling water recycling to avoid excessive heat transfer rate in the initial period of biofilm formation, after the start-up of a clean heat exchanger.

properties. Some authors concluded that surface topography containing irregularities with dimensions around 5 times the bacteria size favor microbial attachment [29]. Others showed that smooth surfaces such as electropolished stainless steel and some polymers were less subject to biofouling than 316 stainless steel [30]. A report on biofouling tests carried out with copper–nickel alloy and titanium tubes in seawater systems [31] indicates that the former fouled to a greater thickness than the latter. However, a major part of the fouling layer on the copper–nickel alloy was composed by corrosion products, while the biological material prevailed on the fouled titanium surface.

Clean smooth surfaces as well as materials or coatings containing fluorinated compounds (low surface energy) are known to reduce or prevent fouling [27]. Quite important is the fact that the deposits formed on some of these new surfaces were found to be more easily removed during cleaning operations [32–35]. This can have a significant impact in reducing the costs of cleaning/disinfection operations (less water, less chemicals, less time to clean, less production losses).

Although the production of novel antifouling surfaces is one of the most promising developments to mitigate biofouling effects, preliminary practical studies should be carried out in order to answer a few relevant questions: (a) Do these coatings add an unacceptable heat transfer resistance that offsets the advantageous effects of reduced biofouling rate? (b) Are these coatings able to resist peeling off from the surface during longer periods of operation? (c) How long will such surfaces maintain their smoothness in an industrial water environment where deposition of small particles or corrosion tend to occur (thereby modifying their roughness and surface tension to the benefit of biofouling)?

18.4 MEMBRANE BIOFOULING

Research on RO membrane biofouling revealed that biofilms commence development within the first moments of operation, thereby contributing to the demise of the separation process without any knowledge or forewarning that such processes are at work [36]. Only after observing a certain reduced membrane permeability is the “level of interference” passed and biofouling is said to have occurred (see Figure 18.3). This motif can be transferred to other water systems—they practically all carry biofilms, but not all of them suffer from biofouling. What are the options to keep biofilm development in a system below the individual level of interference? Basically, the extent of biofilm growth is grossly ruled by the availability of nutrients and the shear forces. Thus, nutrients must be considered as potential biomass. This is an important issue as, usually, biocidal approaches do not take this aspect into account and do not limit nutrients; on the contrary, some biocides increase the nutrient content by oxidizing recalcitrant organics and rendering them more bioavailable. Nutrient

limitation has been demonstrated successfully as a countermeasure to biofouling [36]. By using biological sand filters prior to RO membranes, it was possible to suppress the extent of biofilm growth below the threshold of interference although the membrane was not completely free of a biofilm. Figure 18.7a and b show thin cuts of membrane samples before and after the filter. Table 18.2 shows the flux decline data.

Obviously, this approach cannot be applied in all cases. However, there remain still plenty of opportunities where it provides a suitable and realistic alternative to adding biocides for the prevention of biofouling. This approach would certainly reduce the burden of wastewater with environmentally problematic substances and certainly deserves more attention. In the meantime, it is widely applied, not only for membrane systems but for others as well, e.g., for heat exchangers. As a consequence, we will have to live with the fact that most surfaces can and will be colonized by microorganisms that will cause fouling given the right conditions. Nevertheless, surfaces susceptible to biofouling may be “reengineered” to discourage fouling. For example, some authors [37] recently demonstrated that thin-film composite RO membranes could be coated with a polyether–polyamide

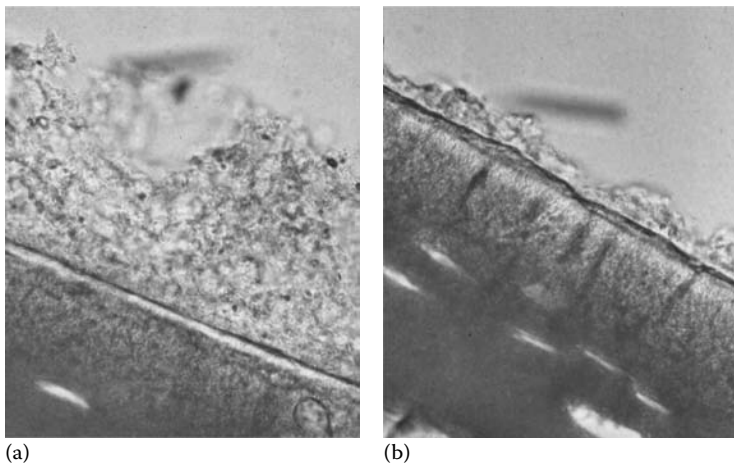


FIGURE 18.7 (a) Micrograph of a thin cut of a reverse osmosis membrane fed with river water after flocculation and sedimentation; (b) after additional sand filter; see decrease of fouling layer. (From Flemming, H.-C. and Griebe, T., unpublished data.)

TABLE 18.2
Deposit and Flux Decline Data before and after Sand Filter

Parameter	Unit	Before Filter	After Filter
Cell number	#/cm ²	1.0 × 10 ⁸	5.5 × 10 ⁶
Colony-forming units	cfu/cm ²	1.0 × 10 ⁷	1.2 × 10 ⁶
Protein	μg/cm ²	78	4
Carbohydrates	μg/cm ²	26	3
Uronic acids	μg/cm ²	11	2
Humic substances	μg/cm ²	41	12
Biofilm thickness	μm	27	3
Flux decline	%	35	<2

Source: Griebe, T. and Flemming, H.-C., *Desalination*, 118, 153, 1998.

copolymer (PEBAX 1657), which penetrated deeply into the membrane surface resulting in a smoother hydrophilic surface. Compared to uncoated controls, the coated RO membranes displayed a significant reduction in fouling by an oil/surfactant/water emulsion in trials lasting more than 100 days.

A more novel approach to designing low-fouling surfaces that is still in its early stages of development involves the application of molecular simulations to observe and measure *in silico* the dynamics of surface fouling by macromolecular substances [38]. An example of this approach is illustrated in Figure 18.8 in which a hydrated oligomer of bacterial alginate is shown undergoing rapid adsorption to the “surface” of an aromatic cross-linked polyamide RO membrane. The system potential energy is shown to decline substantially in this molecular dynamics simulation (inset) suggesting this type of adsorption interaction is energetically favorable. The aim of such modeling exercises is to introduce chemical modifications into the (polyamide) surface that will inhibit or impede such rapid macromolecular fouling.

The alginate oligomer is positioned initially (at $t = 0$) above the membrane surface fragment (left vertical panel). The $t = 0$ positions are viewed from three spatial perspectives: side view (top), oblique view (middle), and top-down view (lower). Water and sodium counterions have been hidden in the $t = 0$ images to better observe the alginate and membrane atoms. The right-hand side upper panel indicates that alginate adsorption occurred relatively rapidly over a period of about 300 ps. As indicated by a decline in the system potential energy (inset graph), alginate adsorption was thermodynamically favorable. Alginate and membrane bonds are represented as sticks, water atoms are given as dark or light gray depending whether they were initially associated with membrane or alginate, respectively.

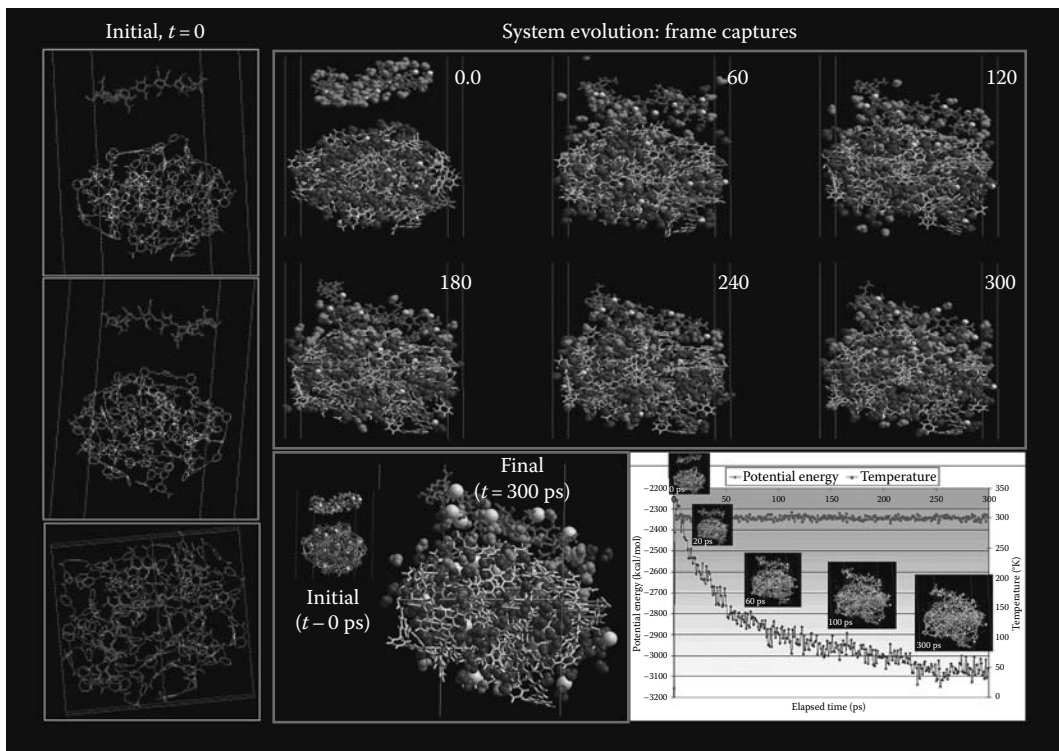


FIGURE 18.8 Molecular dynamics simulation of bacterial alginate adsorption to a polyamide RO membrane “surface” fragment. (From Ridgway, H., AquaMem Scientific Consultants and Stanford University, unpublished data; Flemming, H.-C. and Ridgway, H.F., Biofilm control: Conventional and alternative approaches, in *Marine and Industrial Biofouling*, Flemming, H.-C. Murthy, P.S., Venkatesan, R., and Cooksey, K.C. (Eds.), Springer, New York, 2008.)

18.5 STRATEGIES TO COMBAT BIOFOULING IN HEAT EXCHANGERS AND MEMBRANES

It is generally accepted that biofilms are quite difficult to prevent, since they occur even in distilled ultrapure water with extremely low levels of nutrients and bacteria. Therefore, most realistically, many engineers accept the fact that biofouling will always occur in industrial plants using water and in drinking water systems, with very few exceptions. The challenge here is thus to devise appropriate strategies to mitigate the undesired effects of such phenomena, that is, to reduce overall costs using environmentally friendly approaches.

At the present moment, the trends in biofouling combat in heat exchangers are focused on a few important issues:

1. Good design, namely, improved hydrodynamic patterns. This means designing the exchanger to operate at relatively high water velocities (always above 1 m/s, preferably around 1.5–2 m/s) to reinforce the detachment mechanisms over the deposition ones [10] and conceiving geometries that avoid or minimize dead zones along the water flow pathway in order to reduce biofilm development and favor the access of biocide solutions and detergents to every spot within the heat exchanger during cleaning/disinfection operations. Optimizing the balance between thin biofilms (that are less deleterious in terms of heat transfer efficiency, but can be more resistant to chemical attack, due to their higher compactness) and biocide/dispersant penetration through the biological matrix is the goal to pursue as regards the choice of flow velocity.
2. More efficient and environmentally intelligent chemicals to inactivate bacteria or break down the microbial polymeric matrix. Use of enzymes to hydrolyze proteins and peptides or to break down polysaccharides of the EPS matrix can be an important tool in biofilm removal, since they may be able to remove the polymeric slime from the biofilm and expose the microorganisms to biocide attack [35]. Nevertheless, the specificity and complexity of the chemical composition of microbial films may require the use of a cocktail of enzymes in order to achieve the desired anti-biofouling goals [39], but such chemical blends are usually costly. The application of biocides and dispersants should be optimized taking into account each particular case under study, namely, the biocide dose (concentration \times time of application) [40,41].
3. Development of antifouling, possibly “self-cleaning” surfaces. An increasing number of recent studies has focused on the creation of novel surfaces, often stainless steel modified surfaces that seem capable to reduce adhesion of foulants and simultaneously to improve cleaning efficiency [42]. Reports have been published on self-cleaning surfaces [43] such as those using titanium oxide coatings activated by ultraviolet radiation, that minimize or avoid biofouling. The practical application of such surfaces is still under scrutiny, although it seems difficult to foresee their use in heat exchanger tubes at short term, mainly those that require activation by UV radiation. The consequences of nanostructured surfaces on bacterial adhesion and removal are also being studied, and a clear consensus has not yet been reached on the advantages and disadvantages of these technologies [44].
4. Online monitoring tools to control fouling buildup and minimize cleaning cycles and biocide consumption. This is becoming a mandatory approach to optimize biofouling impacts in industrial plants. In fact, by monitoring the development of biofilms on surfaces and/or by detecting the cleaning endpoint during disinfection operations, it will be possible to assess the efficacy of antifouling measures during biofilm growth and to control the cleaning cycles in order to minimize the use of anti-biofouling agents, the consumption of water, and the production breaks. In industry, biofouling is usually monitored by measuring the pressure drop along tubes or across membranes and, in the case of heat exchangers, by following the evolution of outlet temperatures and calculating the decline of the heat

transfer rate. These techniques do not have enough resolution to detect biofilms in the early stages of development and, furthermore, they do not distinguish biological from abiotic deposits.

In recent decades, many new measurement techniques have been proposed [45,46]. Most of the modern online monitoring methods reported in the literature are either too sophisticated and expensive or not robust enough for industrial application. Two of them seem to offer some practical advantages against the others, on account of their cost and easiness of operation. The fiber-optics sensor (FOS), based on light scattering caused by the contamination of surfaces with particles or bacteria, is able to detect small numbers of bacteria adhering on a transparent surface [45] and is particularly useful for following the initial steps of bacterial adhesion and detachment in units with low biofouling propensity (e.g., ultrafiltration membranes in drinking water systems). The mechatronic surface sensor (MSS), which measures the effect of the deposited layers on nanovibrations induced on the surface [47], can be used to monitor biofilm buildup and removal on practically any type of rigid surface (stainless steel, PVC, copper, etc.) since its actuator and sensor are located on the external face (not in contact with the flowing water) of the surface being monitored.

18.6 SUMMARY

Biofouling has been for many decades mainly associated to the important problem of (bio)corrosion. Gradually, scientists and engineers became fully aware of the much wider effects of unwanted biofilm formation on the process plant efficiency (energy costs, contamination risks, etc.) and external environmental impacts. The search for solutions to this problem that can be applied to improve the operation of heat exchangers, cooling water circuits, RO, and ultrafiltration membranes is nowadays part of a significant business sector. What clearly makes more sense is putting more effort in the prevention of biofouling by advanced strategies and moving away from traditional remediation techniques that often bring undesirable side effects.

At the moment, scientists are trying to overcome the limitations of the present practices by looking at the following.

1. The deposition surface: How to design new industrial surfaces that reduce the adhesion of microbes and nonliving material and facilitate the removal or cleaning of the biofouling deposit? How does the initial surface affect the spatial structure and cohesiveness of the final biofilm layer?
2. The water phase: There is already a well established background on the effects of water velocity and hydrodynamic patterns on biofilm formation and detachment, but better insights are needed on the relationships between the history of the biofilm and the efficacy of disinfection procedures. Novel processes of biofilm cleaning/disinfection with much less environmental impacts (namely, the discharge of biocides) and with acceptable costs are still needed.
3. The biofilm composition, architecture, and microbial community behavior: In the last 15 years significant advancements were obtained, through confocal laser microscopy, molecular biology, and modeling, on the understanding of the three-dimensional spatial distribution of the microbial layers and of the way microbes act/react in aggregates (their metabolism). There is still a gap to fill in terms of translating such findings to practical solutions, such as controlling/predicting the response of biofilms to antimicrobial measures.
4. Online monitoring: This tool is an indispensable complement to the other ones mentioned above. The optimization of preventive and cleaning measures, including the need to stop operation of heat exchangers, depends much on the availability of sensitive, robust, easy-to-use and cost-effective monitoring systems.

REFERENCES

1. Bott, T. R. Biological growth on heat exchanger surfaces. In *Fouling of Heat Exchangers*, Bott, T. R. (Ed), Chapter 12, pp. 223–267, Elsevier, Amsterdam, the Netherlands (1995).
2. Hardörfer, F. and Härtel, G. Bacteriophobic membranes for decreasing biofilm formation in wastewater treatment. *Chemical Engineering & Technology* 21(4), 313–316 (1999).
3. Pritchard, A. M. The economics of fouling. In *Fouling Science and Technology*, Melo, L. F., Bott, T. R., and Bernardo, C. A. (Eds.), pp. 31–45, Kluwer Academic Publishers, Dordrecht, the Netherlands (1988).
4. Flemming, H.-C. Why microorganisms live in biofilms and the problem of biofouling. In *Industrial and Marine Biofouling*, Flemming, H.-C., Murthy, P. S., Venkatesan, R., and Cooksey, K. C. (Eds.), pp. 3–12, Springer, New York (2008).
5. Muller-Steinhagen, H., Malayeri, M. R., and Watkinson, A. P. Fouling of heat exchanger—new approaches to solve an old problem. *Heat Transfer Engineering* 25(9), 1–6 (2005).
6. Azis, P. K. A., Al-Tisan, I., and Sasikumar, N. Biofouling potential and environmental factors of seawater at a desalination plant intake. *Desalination* 135, 69–82 (2001).
7. Cloete, T. E. Biofouling—What we know and what we should know. *Materials and Corrosion* 54, 520–526 (2003).
8. Flemming, H.-C., Schaule, G., McDonogh, R., and Ridgway, H. F. Effects and extent of biofilm accumulation in membrane systems. In *Biofouling and Biocorrosion in Industrial Water Systems*, Geesey, G. G., Lewandowski, Z., and Flemming, H.-C. (Eds.), pp. 63–89, CRC Press Inc., Boca Raton, FL (1994).
9. Flemming, H.-C., Neu, T. R., and Wozniak, D. The EPS matrix: The house of biofilm cells. *Journal of Bacteriology* 189, 7945–7947 (2007).
10. Melo, L. F. and Bott, T. R. Biofouling in water systems. *Experimental Thermal and Fluid Science* 14, 375–381 (1997).
11. Vieira, M. J., Melo, L. F., and Pinheiro, M. M. Biofilm formation—Hydrodynamic effects on internal diffusion and structure. *Biofouling* 7, 67–80 (1993).
12. Melo, L. F. and Vieira, M. J. Physical stability and biological activity of biofilms under turbulent flow and low substrate concentration. *Bioprocess Engineering* 20, 363–368 (1999).
13. Welch, M., Mikkelsen, H., Swatton, J. E. et al. Cell–cell communication in Gram-negative bacteria. *Molecular BioSystems* 1, 196–202 (2005).
14. Nadell, C. D., Xavier, J. B., Levin, S. A., and Foster, K. R. The evolution of quorum sensing in bacterial biofilms. *PLoS Biology* 6(1), 0171–0179 (2008).
15. Kirisits, M. J. and Parsek, M. R. Does *Pseudomonas aeruginosa* use intercellular signalling to build biofilm communities? *Cellular Microbiology* 8(12), 1841–1849 (2006).
16. Liu, Y. and Tay, J. H. Metabolic response of biofilm to shear stress in fixed-film culture. *Journal of Applied Microbiology* 90, 337–342 (2001).
17. Ramasamy, P. and Zhang, X. Effects of shear stress on the secretion of extracellular polymeric substances in biofilms. *Water Science and Technology* 52(7), 217–223 (2005).
18. Klahre, J. and Flemming, H.-C. Monitoring of biofouling in paper mill process waters. *Water Research* 34(14), 3657–3665 (2000).
19. Rochex, A. and Lebeault, J. M. Effects of nutrients on biofilm formation and detachment of a *Pseudomonas putida* strain isolated from a paper machine. *Water Research* 41, 2885–2892 (2007).
20. Flemming, H.-C. Biofouling in water treatment. In *Biofouling and Biocorrosion in Industrial Water Systems*, Flemming, H.-C. and Geesey, G. C. (Eds.), pp. 47–80, Springer Verlag, Berlin, Germany (1991).
21. Mayer, C., Moritz, R., Kirschner, C., Borchard, W., Maibaum, R., Wingender, J., and Flemming, H.-C. The role of intermolecular interactions: Studies on model systems for bacterial biofilms. *International Journal of Biological Macromolecules* 26, 3–16 (1999).
22. Braissant, O., Cailleau, G., Dupraz, C., and Verrecchia, E. P. Bacterially induced mineralization of calcium carbonate in terrestrial environments: The role of exopolysaccharides and amino acids. *Journal of Sedimentary Research* 73(3), 485–490 (2003).
23. Lowe, M. J., Duddridge, J. E., Pritchard, A. M., and Bott, T. R. Biological particulate fouling interactions: Effects of suspended particles on biofilm development. In *Proceedings of the First UK National Heat Transfer Conference*, pp. 391–400, Leeds, U.K. (1984).
24. Bott, T. R. and Melo, L. F. Particle-bacteria interactions in biofilms. In *Biofilms—Science and Technology*, Melo, L. F., Bott, T. R., Fletcher, M., and Capdeville, B. (Eds.), pp. 199–206, Kluwer Academic Publishers, Dordrecht, the Netherlands (1992).

25. Vieira, M. J. and Melo, L. F. Effect of clay particles on the behaviour of biofilms formed by *Pseudomonas fluorescens*. *Water Science and Technology* 32(8), 45–52 (1995).
26. Müller-Steinhagen, H. and Zhao, Q. Investigation of low fouling surface alloys made by ion implantation technology. *Chemical Engineering Science* 52(19), 3321–3332 (1997).
27. Pereni, C. I., Zhao, Q., Liu, Y., and Abel, E. Surface free energy effect on bacterial adhesion. *Colloids and Surfaces B* 48(2), 143–147 (2006).
28. Zettler, H. U., Weiss, M., Zhao, Q., and Müller-Steinhagen, H. Influence of surface properties and characteristics on fouling in plate heat exchangers. *Heat Transfer Engineering* 26(2), 13–17 (2005).
29. Messing, R. A. and Oppermann, R. A. Pore dimensions for accumulating biomass. I. microbes that reproduce by fission or by budding. *Biotechnology and Bioengineering* 21, 49–58 (1979).
30. Mott, I. E. C. and Bott, T. R. The adhesion of biofilms to selected materials of construction for heat exchangers. In *Proceedings of the Ninth International Heat Transfer Conference*, vol. 5, pp. 21–26, Jerusalem, Israel (1991).
31. Christensen, B. E. and Characklis, W. G. Physical and chemical properties of biofilms. In *Biofilms*, Characklis, W. G. and Marshall, K. C. (Eds.), pp. 93–130, John Wiley & Sons, Inc., New York, (1990).
32. Rosmaninho, R. and Melo, L. F. Calcium phosphate deposition from simulated milk ultra-filtrate (SMUF) on different stainless steel-based surfaces. *International Dairy Journal* 16, 81–87 (2006).
33. Bott, T. R. Heat exchanger cleaning. In *Fouling of Heat Exchangers*, Bott, T. R. (Ed.), pp. 357–407, Elsevier, Amsterdam, the Netherlands (1995).
34. Rosmaninho, R., Rocha, F., Rizzo, G., Müller-Steinhagen, H., and Melo, L. F. Calcium phosphate fouling on TiN coated stainless steel surfaces: Role of ions and particles. *Chemical Engineering and Science* 62(14), 3821–3831 (2007).
35. Olsen, S. M., Pedersen, L. T., Laursen, M. H., Kiil, S., and Dam-Johansen, K. Enzyme-based antifouling coatings: A review. *Biofouling* 23(5), 369–383 (2007).
36. Griebe, T. and Flemming, H.-C. Biocide-free antifouling strategy to protect RO membranes from biofouling. *Desalination* 118, 153–156 (1998).
37. Louie, J. S., Pinnau, I., Ciobanu, I., Ishida, K. P., and Reinhard, M. Effects of polyether–polyamide block copolymer coating on performance and fouling of reverse osmosis membranes. *Journal of Membrane Science* 280, 762–770 (2006).
38. Flemming, H.-C. and Ridgway, H. F. Biofilm control: Conventional and alternative approaches. In *Marine and Industrial Biofouling*, Flemming, H.-C., Murthy, P. S., Venkatesan, R., and Cooksey, K. C. (Eds.), Springer, New York (2008).
39. Wiatr, C. L. Enzyme blend containing cellulase to control industrial slime. U.S. Patent 4,994,390 (1991).
40. Stewart, P. S., Hamilton, M. A., Goldstein, B. R., and Schneider, B. T. Modeling biocide action against biofilms. *Biotechnology and Bioengineering* 49(4), 445–455 (1996).
41. Eguía, E., Trueba, A., Girón, A., Rfo-Calonge, B., Otero, F., and Bielva, C. Optimization of biocide dose as a function of residual biocide in a heat exchanger pilot plant effluent. *Biofouling* 23(4), 231–247 (2007).
42. Santos, O., Nylander, T., Rosmaninho, R. et al. Modified stainless steel surfaces targeted to reduce fouling—Surface characterization. *Journal of Food Engineering* 64(1), 63–79 (2004).
43. Blossey, R. Self cleaning—Virtual realities. *Nature Materials* 2, 301–306 (2003).
44. Li, X., Liu, T., and Chen, Y. The effects of the nanotopography of biomaterial surfaces on *Pseudomonas fluorescens* cell adhesion. *Biochemical Engineering Journal* 22, 11–17 (2004).
45. Flemming, H.-C. Role and levels of real-time monitoring for successful anti-fouling strategies—An overview. *Water Science and Technology* 47(5), 1–8 (2003).
46. Janknecht, P. and Melo, L. F. Online biofilm monitoring. *Reviews in Environmental Science and Bio/Technology* 2, 269–283 (2003).
47. Pereira, A., Mendes, J., and Melo, L. F. Using nanovibrations to monitor biofouling. *Biotechnology and Bioengineering* 99(6), 1407–1415 (2008).

19 Biocides: Selection and Application

Christopher J. Nalepa and Terry M. Williams

CONTENTS

19.1	Introduction.....	382
19.2	Microbial Growth and Biofouling in Industrial Systems.....	382
19.2.1	Microorganisms Present in Industrial Systems.....	383
19.2.2	Problems Caused by Microbial Growth.....	383
19.3	Biocide Regulation.....	384
19.4	Biocide Selection—Oxidizing Biocides.....	385
19.4.1	General Overview.....	385
19.4.1.1	Gas Systems.....	385
19.4.1.2	Liquid Systems.....	386
19.4.1.3	Solid Systems.....	386
19.4.2	Principles of Chlorine Chemistry.....	386
19.4.3	Properties of Selected Chlorine-Based Biocides.....	387
19.4.3.1	Chlorine Gas.....	388
19.4.3.2	Sodium Hypochlorite (Industrial Bleach).....	388
19.4.3.3	Sodium Dichloroisocyanurate (Dichlor) and Trichloroisocyanuric Acid (Trichlor).....	389
19.4.3.4	Calcium Hypochlorite (Cal Hypo).....	389
19.4.4	Principles of Bromine Chemistry.....	389
19.4.4.1	Activated Sodium Bromide.....	389
19.4.4.2	Stabilized Bromine Chloride.....	390
19.4.4.3	Stabilized Sodium Hypobromite.....	390
19.4.4.4	Bromochlorodimethylhydantoin (BCDMH).....	390
19.4.4.5	Dibromodimethylhydantoin (DBDMH).....	391
19.4.4.6	Bromine-Releasing Isocyanurate Compositions.....	391
19.4.5	Principles of Chlorine Dioxide Chemistry.....	391
19.4.5.1	Machine-Based Activation.....	392
19.4.5.2	Acid Activation.....	392
19.4.5.3	In Situ Chemical Activation.....	393
19.4.5.4	Unactivated Sodium Chlorite.....	393
19.4.5.5	Sodium Chlorate Methods.....	393
19.4.6	Hydrogen Peroxide.....	393
19.4.7	Peracetic Acid.....	393
19.4.8	Ozone.....	394
19.5	Biocide Selection—Nonoxidizing Biocides.....	394
19.5.1	Aldehydes.....	396
19.5.2	Dithiocarbamates.....	396
19.5.3	Organobromines.....	396

19.5.4	Isothiazolones.....	397
19.5.5	Quaternary Compounds	397
19.5.6	Miscellaneous Types	398
19.6	Biocide Mechanisms of Action and Resistance	398
19.6.1	Electrophilic Biocides: Oxidants (Extreme Electrophiles)	398
19.6.2	Electrophilic Biocides: Moderate Electrophiles.....	399
19.6.3	Membrane Active—Lytic Biocides.....	400
19.6.4	Membrane Active Biocides—Protonophores.....	400
19.6.5	Resistance to Biocides.....	400
19.7	Strategies for Successful Biocide Application.....	401
19.7.1	Cooling System Design.....	402
19.7.2	Water Quality	402
19.7.3	Using Combinations and Synergistic Blends for Increasing Biocide Efficacy	403
19.7.4	Enhancing Biocide Efficacy with Adjuvants and Biodispersants	403
19.7.5	Biocide and Microbiological Monitoring.....	404
19.8	Summary.....	404
	References.....	405

19.1 INTRODUCTION

Biocide programs work together with scale and corrosion inhibitor programs to optimize cooling system performance. Biocides, for the purpose of this chapter, represent chemical agents and formulations to control harmful microorganisms that colonize industrial cooling systems. Biocides function to kill or inhibit the growth of microorganisms such as bacteria, fungi, and algae. Left unchecked, microbial growth can result in higher energy costs, increased maintenance procedures, shortened equipment life, and increased health risks. The objectives of this chapter are (a) reviewing the problems caused by microbial growth, (b) discussing the wide variety of biocides available to the industrial water treatment community, and (c) providing guidelines for proper biocide selection and application. It is not intended to be a thorough review, but rather to serve as a practical guide based on years of direct experience by the authors in the development, application, and service of oxidizing and nonoxidizing biocide chemistries. It should be recognized that a good biocide program is an important part, but not the sole part, of a cooling system maintenance program. Good engineering practices (i.e., minimizing system dead legs and reducing cooling tower drift), good water treatment practices (i.e., minimizing scale and corrosion of system surfaces), and good preventative practices (i.e., regular inspections and system cleanouts) are also necessary to promote efficient system operation, prolong system service life, and minimize the impact of problem microorganisms.

Many common treatment programs employ nonoxidizing biocides in conjunction with standard oxidizing biocides for a broad-based approach to microbial control. The overall efficacy of any given treatment program is a function of its activity versus the problem organisms, correct use level and dosing strategy, stability under environmental conditions, microbial load, overall system dynamics (pH, temperature, and residence time), and compatibility with other cooling water treatment additives[1–3].

19.2 MICROBIAL GROWTH AND BIOFOULING IN INDUSTRIAL SYSTEMS

Industrial recirculating systems represent an ideal environment for microbial growth. The combination of warm temperatures, aeration, nutrients, diverse construction materials, and water flow sets the stage for the exponential growth of microorganisms. The following section reviews the key organisms of concern and the problems associated with their growth in both the liquid phase (planktonic) as well as when they are attached to surfaces (sessile or biofilm) [4–9].

19.2.1 MICROORGANISMS PRESENT IN INDUSTRIAL SYSTEMS

The most diverse group organisms in cooling water are bacteria, which include general slime-forming organisms (*Pseudomonas*, *Enterobacter*, *Klebsiella*, *Flavobacterium*), health-related species (*Legionella pneumophila*), sulfate reducers (*Desulfovibrio*, *Desfulomaculum*), iron reducers (*Vibrio*, *Shewanella*), acid producers (*Thiobacillus*, *Clostridium*, *Enterobacter*), and filamentous types (*Sphaerotilus*, *Leptothrix*). These bacteria include both aerobic and anaerobic organisms, which utilize the organic matter in the water for growth.

Photosynthetic organisms (green algae and cyanobacteria, formerly known as blue-green algae) utilize sunlight and CO₂ for growth and produce visible amounts of slime visible in cooling tower waters. This causes cosmetic issues and also blocks key surfaces on tower decks and the interior fill. Many genera of cyanobacteria (*Phormidium*, *Anabaena*, *Oscillatoria*, and *Anacystis*) and green algae (*Chlorella*, *Scenedesmus*, *Chlorococcum*, *Ulothrix*, and *Spirogyra*) are commonly reported in cooling systems. Fungal contaminants (*Aspergillus*, *Saccharomyces*, and *Rhodoturula*) occur less frequently, but are still considered problematic in wooden cooling towers. Fungi produce viscous slimes and may also cause structural problems by the degradation of the cellulose in the wood, a process known as *delignification*.

Larger (single-cell) life forms such as protozoa are also found in cooling water in instances where microbial contamination is more severe. These various types of protozoa include amoebae (*Acanthamoeba*, *Cochliopodium*, *Hartmannella*, *Dictyostelium*, *Naegleria*, and *Vanella*) and ciliates (*Tetrahymena* and *Colpoda*). These protozoan hosts may provide protection for *Legionella*, allowing for intracellular growth (amplification) and increased resistance to biocides (via poor biocide penetration within the host cell). Due to the prevalence and adaptive nature of microorganisms, it is impractical to maintain industrial cooling systems under sterile or near-sterile conditions. Industrial biocide programs necessarily focus instead on the regular control or “knock-down” of problem microorganisms. Studies in sterile model cooling towers, for example, indicate that bacteria rapidly recolonize recirculating systems within a few days [10].

19.2.2 PROBLEMS CAUSED BY MICROBIAL GROWTH

Microbial growth is a major concern in water treatment applications affecting a variety of operational and system problems, including microbially influenced corrosion (MIC), reduction in process efficiency (heat transfer and evaporative cooling), system cleanliness, and potential health concerns. The various types of microbial groups discussed earlier are well recognized as major causes of these problems. Such microorganisms also assemble together into complex communities termed biofilms.

Biofilm can be defined as a collection of microorganisms attached to a surface, the metabolic products they produce, and associated entrained debris (silt, scale, iron, and so on) [11]. Figure 19.1 shows the impact of biocide treatment on a simple, 24 h laboratory-grown biofilm consisting of *Pseudomonas aeruginosa*, a common fouling organism in industrial water systems [12]. Note that the relatively low levels of hypobromous acid (0.6 ppm residual, as Cl₂) effectively deactivate the biofilm organisms, that is, only a few intact microorganisms were observed. High levels of this relatively strong oxidizing biocide (5 ppm residual, as Cl₂) completely destroy the biofilm microorganisms, but have little impact on the extracellular material remaining in the biofilm. Thus, biofilms and associated material, once developed, can be difficult to completely remove from the system and are best prevented from forming in the first place. Although biofilms can be beneficial, as the microbial sludge that breaks down waste material in sewage plants, they are a nuisance in industrial water treatment [13]. Problems posed by biofilms fall into three broad categories: cooling tower efficiency, system integrity, and health risk.

Biofilms decrease cooling system efficiency by insulating cooling tower heat exchangers and tower fill surfaces. The thermal conductivity of a biofilm can be just 25% that of a calcium carbonate

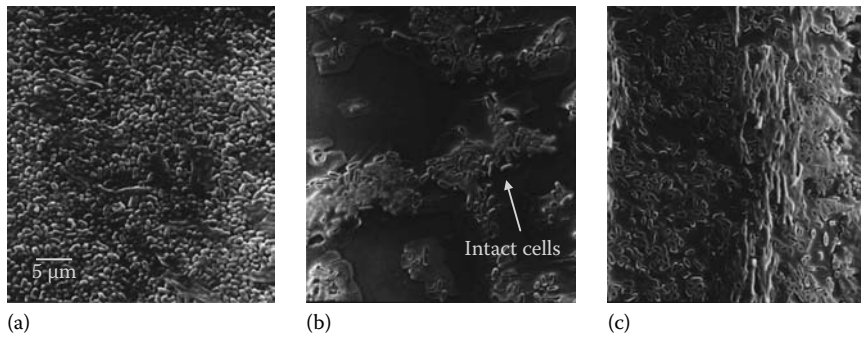


FIGURE 19.1 Biofilms of *Pseudomonas aeruginosa* treated with: (a) no biocide (control), (b) sublethal dose of HOBr (0.6 ppm as Cl₂), and (c) lethal dose of HOBr (5 ppm as Cl₂).

scale of equivalent thickness, giving rise to increased compressor energy consumption [14,15]. In addition, biofilms can entrain silt and other debris, resulting in “astounding” weight gain and even plugging of cooling tower fill [16].

The colonization of surfaces by microorganisms and the products associated with microbial metabolic processes (biomineralization) can compromise the integrity of the cooling system [17]. Low oxygen environments at the biofilm/substrate surface, for example, provide conditions where highly destructive anaerobic organisms, such as sulfate-reducing bacteria (SRB), can thrive. This leads to MIC (microbially induced corrosion), a particularly insidious form of corrosion, which can result in localized, pitting corrosion rates 1000-fold higher than that experienced for the rest of the system [18]. In extreme cases, MIC leads to perforations, equipment failure, and expensive reconditioning operations within a short period of time [19].

As pointed out in a Chapter 20, cooling systems can harbor pathogenic microorganisms such as *L. pneumophila* [20]. This bacterium can infect man-made water systems such as cooling towers and evaporative condensers, whirlpool baths and spas, domestic hot water/shower systems, and grocery misters. Guidelines and recommended practices for biocide application and sampling have been published by various industry groups and government organizations [21–27]. In addition, summary reports are available on the efficacy of industrial biocides versus *Legionella* [10,28,29]. Although many outbreaks have been attributed to industrial cooling systems, recent studies have shown that building (potable) water distribution systems are considered as the primary sources of the disease and that the route of infection is via “aspiration” of this water from the mouth into the lungs (not via aerosols directly) [30,31]. As a result, cooling towers may not represent the main source for *Legionella* bacteria associated with the disease [32]. More information on this mode of transmission is available online [33]. In addition to *Legionella*, other pathogenic microorganisms, such as nontuberculosis mycobacteria (NTM) may also be found in cooling water systems [34]. In summary, the excessive growth of microorganisms in industrial water treatment systems may significantly reduce the efficiency of the specific process, shorten equipment life, and result in potential health concerns. Several years ago, the economic impact of biofouling in the United States alone was estimated at \$60 billion dollars [35].

19.3 BIOCIDES REGULATION

The manufacture, storage, and applications of biocides are highly regulated. The typical biocide formulation consists of an active ingredient, for example, the basic chemical entity that possesses the antimicrobial activity, together with inert ingredients, for example, additional components added for various purposes—enhanced product shelf-life, improved formulation stability, increased tablet

strength, and so on. Biocide manufacturers must submit a data package to regulatory agencies to demonstrate efficacy against claimed microorganisms at label dosages, disclose information on toxic effects, identify degradation products and by-products, and provide procedures (label directions) for proper biocide application, handling, and storage.

In the United States, the Environmental Protection Agency (EPA) regulates biocides as pesticides under federal law contained under FIFRA (Federal Insecticide, Fungicide, and Rodenticide Act) [36,37]. The European Union has a different set of regulations, referred to as the Biocidal Products Directive (BPD) [38]. In Canada, the Pest Management Regulatory Agency (PMRA) of Health Canada functions to register and approve products for biocidal uses [39]. EPA, PMRA, and the BPD incorporate the concept of reregistration in which biocidal products already in commerce must undergo a periodic review. Although somewhat onerous to the manufacturers and formulators of biocidal products, such reregistration activity of individual pesticide products and formulations provides for a thorough review by all biocide stakeholders (manufacturers, distributors, end-users, and the general public) of application and use patterns, environmental fate of active and degradation products, and consequences of misapplication and exposure. A very useful Web resource for searching EPA-approved biocide product labels and use directions is available from the National Pesticide Information Retrieval System (NPIRS) [40]. Information on the specific biocides approved by the California Department of Pesticide Regulation (DPR) is also available online [41].

19.4 BIOCIDES SELECTION—OXIDIZING BIOCIDES

19.4.1 GENERAL OVERVIEW

Biocides are often categorized in two broad classes: oxidizers and nonoxidizers. The mechanisms of action, principles of application, monitoring methods, and responses to system contamination differ significantly between the two groups.

Oxidizing biocides demonstrate broad-spectrum activity across a wide range of microorganisms such as bacteria, fungi, algae, and protozoa. They are typically fast acting and feature multiple modes of action for microbial deactivation [42,43]. For this reason, few reported cases of acquired microbial resistance (selection for resistant microorganisms through repeated applications) have been reported in the annals of the water treatment literature. Slight resistance toward chlorine was demonstrated in a 30-generation study of *E. coli* exposed to low levels (0.2 ppm) at short contact time (1 min) [44]. Oxidizing biocides are generally effective at low ppm levels in industrial water treatment, which makes them cost effective. They also have proven effectiveness against biofilms and problem microorganisms such as *Legionella* [10,20,28,45–48].

The disadvantages of oxidizers include susceptibility to system demand and process contaminants due to their high reactivity. Corrosion issues may result as well since most of the oxidizers result in a significant increase in ORP (oxidation-reduction potential) and slowly degrade certain corrosion and scale inhibitor programs, for example, phosphonates, when applied at label dosages [49]. Oxidizer formulations for industrial water treatment are also highly reactive so care must be taken not to mix or accidentally contaminate them with other chemicals.

Oxidizing biocides come in all forms of matter—solid, liquid, and gas—and specific delivery systems have been developed for all of the various forms. Generators have also been developed to provide for the on-site generation of the active ingredient by various means—chemical reaction, electrolysis, plasma ionization, or UV activation.

19.4.1.1 Gas Systems

This category includes gases such as chlorine, chlorine dioxide (generated via chemical reaction or electrolysis), and ozone (generated via plasma discharge or UV). In general, the systems in this category often require rather specialized equipment and maintenance procedures and are often

more appropriate for the heavy industrial setting. In this case, the capital cost of the equipment and increased maintenance requirements are offset by the lower costs of raw materials that is, 1-t cylinders for chlorine gas, solutions of sodium chlorite and hydrochloric acid for chlorine dioxide, and dry air for ozone.

19.4.1.2 Liquid Systems

These systems represent the staple of biocidal systems in the industrial water treatment market. Products in this category include industrial bleach, activated sodium bromide (bleach and sodium bromide solution), and stabilized forms of bromine (stabilized sodium hypobromite, stabilized bromine chloride). A common method of dosing liquids is via a diaphragm pump. Such pumps are readily available, are low in cost, and allow the precise control of product delivery by adjusting the stroke length and stroke frequency. Self-degassing designs allow the trouble-free application of materials that may off-gas during storage.

19.4.1.3 Solid Systems

Solid biocide products provide a high percentage of active halogen per volume of product. For example, a 50 lb pail of solid biocide often packs the same activity as a 500 lb drum of a liquid product such as bleach. These products are used to advantage in applications where space is at a premium or access is limited, such as cooling towers located on roofs and other difficult-to-reach areas. Solid biocides also maintain activity for long periods of time (in their dry form) and can be compacted into various shapes (pucks, tablets, granules, and so on) to control product delivery based on particular application requirements. Solid products are typically dosed using flow-through feeders but other feed methods include the slow dissolution of pucks or granules into the system via floaters, mesh bags, or other containment systems.

19.4.2 PRINCIPLES OF CHLORINE CHEMISTRY

Under proper conditions, the addition of chlorine into water leads to the formation of hypochlorous acid (HOCl). HOCl is a very effective and economical general-purpose biocide. It is a weak acid with $pK_a = 7.4$ [50]. At the alkaline pH conditions generally encountered in cooling towers today (pH 8–9 and above), HOCl converts to the hypochlorite anion (OCl^-), which is not as effective a biocide. Some studies, in fact, indicate that OCl^- is 100 times less effective than HOCl [51].



At pH 7.5, about equal amounts of HOCl and OCl^- are present. At pH 8.5, the split is about 10% HOCl–90% OCl^- (Figure 19.2). What this means in practice is that a cooling tower operating at pH 8.5 may require more chlorine feed to maintain overall cleanliness than a comparable system operating at pH 7.5.

Several common cooling system impurities react with HOCl, including nitrogen compounds such as ammonia or urea (e.g., fertilizer plants), hydrocarbons such as olefins and aromatics (e.g., refineries), iron (especially ferrous form, Fe^{2+}), manganese (Mn^{2+}), and sulfides (e.g., H_2S). Nitrogen compounds convert “free” forms of chlorine (HOCl and OCl^-) into combined forms (NH_2Cl and $NHCl_2$). The combined forms are generally less effective biocides by a factor of 10 or more [52]. This difference in effectiveness led to the development of simple laboratory and field tests such as the diethylphenylene diamine (DPD) method to distinguish between the free and combined forms of chlorine.

The high levels of impurities in the system may require the use of less reactive, nonoxidizing biocides for auxiliary treatment during the periods of high chlorine demand to ensure effective biocidal control. Other conditions to note include high levels of silt, algae, and slime. Such highly fouled

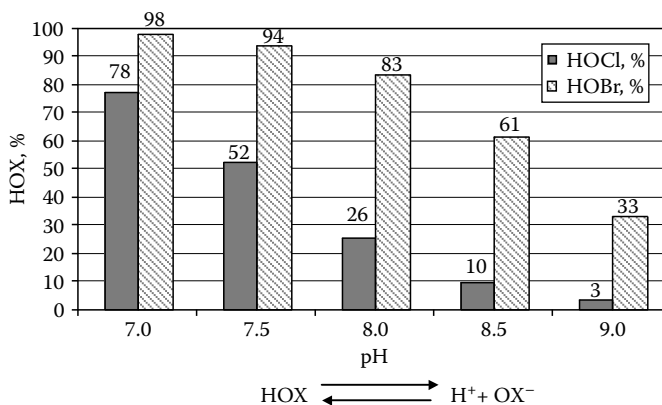


FIGURE 19.2 Effect of pH on hypochlorous and hypobromous acid.

systems may require mechanical or chemical pretreatment. Cooling towers and decks exposed to full sunlight may require additional treatment for algae or slime since free chlorine residuals degrade rapidly on exposure to UV light and heat [53].

Chlorine species are reactive to common cooling tower treatment chemicals such as phosphonates [e.g., aminotris(methylene phosphonic acid) (AMP), 1-hydroxyethylidene,1-diphosphonic acid (HEDP)], tolyltriazole (TTA), and some polymeric scale and corrosion inhibitors [54,55]. Several halogen-resistant chemistries have been developed to mitigate the impact of reactive chlorine species on industrial water treatment programs. These include 2-phosphonobutane-1,2-4 tricarboxylic acid (PBTC), and chlorobenzotriazole (CBT) [56].

19.4.3 PROPERTIES OF SELECTED CHLORINE-BASED BIOCIDES

This section presents some of the important properties and chemistries of the individual chlorine-based biocides available to the industrial water treatment community. Much information is available in this area since chlorine is the historic workhorse compound in many areas of water treatment. It is recommended to consult Clifford White's book for details regarding gas chlorine and sodium hypochlorite (bleach) and other chlorine compounds [57]. Some of the data presented here first appeared several years ago in a more detailed, modular format [58].

Table 19.1 presents the key properties and aspects of individual chlorine-based chemistries. Available chlorine (Av. Cl_2) represents a method of comparing the activity of different chlorine-containing biocides on a per-weight basis. The value for chlorine is 100% by definition. Note that only one of the two chlorine atoms in the chlorine molecule winds up as the biocidally active HOCl. The other is essentially wasted as HCl.

The solubility and pH data in Table 19.1 allow selection of biocides based on criteria such as water chemistry. For example, gas chlorine leads to a decrease in system pH due to the HCl byproduct. This is normally not a problem in cooling systems with normal levels of alkalinity—above 40 ppm or so. However, some refinery cooling systems on gas chlorine using low alkalinity river water for makeup have found the need to install caustic addition systems to neutralize the acid byproduct and maintain the system at greater than pH 7. Conversely, the use of sodium hypochlorite will provide a slight increase in system pH. Solubility and pH represent distinguishing features for the solid chlorine-based biocides as well. Trichloroisocyanuric acid, for example, can decrease system pH and saturated solutions (e.g., solutions found in flow-through feeders) can have a pH of 3. Such a solution may have a distinct chlorine odor.

Although several different forms of chlorine are represented in Table 19.1, it is important to point out that, in most cases, free chlorine residuals between 0.2 and 1 ppm continuous or 0.5 and 2 ppm

TABLE 19.1
Important Properties of Chlorine-Based Biocides

Biocide	Gas Chlorine	Bleach	E-Bleach	Dichlor	Trichlor	Cal Hypo
Formula	Cl ₂	NaOCl	NaOCl	C ₃ N ₃ O ₃ Cl ₂ Na	C ₃ N ₃ O ₃ Cl ₃	Ca(OCl) ₂
Mol. wt.	70.91	74.44	74.44	198.0	232.4	143.0
Av. Cl ₂	100	12	Varies	60	90	70
pH (1% soln.)	1	11	High, varies	6	2.8	10.4
Solubility, %	Miscible	Miscible	Miscible	25	1.2	Miscible
Density ^a	11.7 lb/gal	10 lb/gal	Varies	55 lb/ft ³	64 lbs/ft ³	
CAS #	7782-50-5	7681-52-9	7681-52-9	2893-78-9	87-90-1	7778-54-3
EPA code	20501	14703	14703	81404	81405	14701
Product forms	1-t cylinders	Liquid	Batch; in situ	Granules	Tablets	Tablets; granules

^a 20°C, 6.9 atm.

on a slug-dose or intermittent basis often lead to good microbiological control in industrial cooling towers. The biocide dose can be adjusted up or down based on results of visual, chemical, and microbiological monitoring methods.

The CAS (Chemical Abstracts Service) number can be searched for more information on the basic properties and chemistry of the active ingredients. The EPA chemical code represents a convenient entry into the large amount of pesticide data found on the EPA Web site [36]. The individual pesticide labels, with specific dosing instructions, can be retrieved from the National Pesticide Information Retrieval System Web site, as indicated previously [40]. Here are some additional features of the chlorine-based biocides.

19.4.3.1 Chlorine Gas

This biocide is low in initial cost but effective application requires specialized equipment (e.g., vacuum eductor system), frequent monitoring, and care in handling the product, which is extremely irritating to mucous membranes [59].

19.4.3.2 Sodium Hypochlorite (Industrial Bleach)

The common industrial grade contains between 10 and 12.5 wt.% sodium hypochlorite [60]. Thus, 1 gal of bleach contains about the same amount of active ingredient as 1 lb of chlorine gas. The product degrades rapidly (Figure 19.3) and should be consumed within 6 months. Stability issues can be avoided by on-site generation via the electrolysis of salt solutions [61].

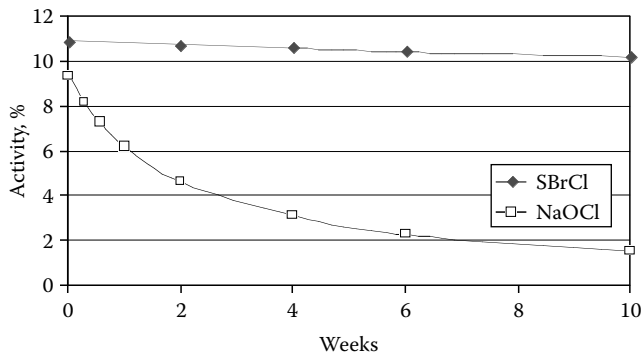


FIGURE 19.3 Long-term storage of stabilized BrCl (BrCl basis) vs. bleach (Cl₂ basis) at 40°C.

19.4.3.3 Sodium Dichloroisocyanurate (Dichlor) and Trichloroisocyanuric Acid (Trichlor)

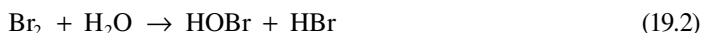
These solid biocides are often used in recreational water treatment but enjoy use in smaller industrial cooling systems as well. Dichlor is highly water soluble and suitable for shock dosing. Trichlor is relatively insoluble [62]. A by-product of these biocides is cyanuric acid, which functions as an effective UV stabilizer [63].

19.4.3.4 Calcium Hypochlorite (Cal Hypo)

This is a popular recreational biocide as well. It is readily soluble but slow-dissolving forms have been developed for application using flow-through feeders. A by-product is calcium hydroxide that can increase scaling potential and generally lead to the increased maintenance of chemical feed systems [41].

19.4.4 PRINCIPLES OF BROMINE CHEMISTRY

The addition of bromine into water generates hypobromous acid (HOBr) and hydrogen bromide (HBr). Unlike chlorine, elemental bromine is not offered as a biocide. Rather, different product forms and delivery systems have been developed that provide convenient access to HOBr for industrial water treatment [64].



At the pH conditions generally encountered in cooling towers (pH from 8 to 9+), HOBr shows less of a tendency to convert to the less-effective anion (OBr^-) than in the case with HOCl (Figure 19.2). This is because HOBr is a weaker acid ($\text{p}K_a = 8.7$) than HOCl ($\text{p}K_a = 7.5$) [65]. What this means in practice is that a cooling tower operating at pH 8.5 on activated sodium bromide may require less biocide feed to maintain overall cleanliness than a comparable system operating on chlorine.

Many of the same impurities and environmental conditions that reduce chlorine effectiveness also impact bromine effectiveness with a few important exceptions. In contrast to chlorine species, bromine species typically perform well at elevated pH and in the presence of nitrogen compounds such as amines or urea, which produce “combined” forms of bromine [62,66]. It is not usually necessary to distinguish between the free (e.g., HOBr and OBr^-) and combined (e.g., NH_2Br and NHBBr_2) forms. The monitoring of bromine residuals is thus typically accomplished by running the total DPD test, which determines all forms of oxidizing bromine species. Bromine residuals in the 0.5–1 ppm range (continuous application) and 1–4 ppm (slug dose) are typically sufficient for good microbiological control. Some of the stabilized forms have recommended residuals higher than this (see the following discussion).

It is important to note that residuals in the case of bromine biocides are variously expressed relative to chlorine (ppm residual, as chlorine) or relative to bromine (ppm residual, as bromine). The residuals are related by a factor of 2.25 (the ratio of the molecular weight of bromine and chlorine). That is:

$$\text{Chlorine residual, ppm} \times 2.25 = \text{Bromine residual, ppm} \quad (19.3)$$

Table 19.2 summarizes the key properties and aspects of selected bromine-based biocides. Some additional comments are described next.

19.4.4.1 Activated Sodium Bromide

Sodium bromide is not a biocide itself but must be used together with an activating agent such as chlorine gas, bleach, calcium hypochlorite, ozone, and so on. A typical installation will feed bromide into the side stream, then oxidant, and then pass the mixture through a static mixer to ensure thorough mixing and conversion to HOBr [67]. The sodium bromide to oxidant ratio should be

TABLE 19.2
Important Properties of Bromine-Based Biocides

Biocide	Act. NaBr	Stabilized BrCl	Stabilized NaOBr	BCDMH	DBDMH	Br-isocyanurates
Formula	NaBr, 40%	Proprietary	Proprietary	C ₅ H ₆ N ₂ O ₂ BrCl	C ₅ H ₆ N ₂ O ₂ Br ₂	NaBr + iso
Mol. wt.	102.9	115.4 (BrCl)	118.9 (NaOBr)	241.5	285.9	Varies ^a
Av. Br ₂ , %	NA	15	14	128	111	
pH (conditions)	7–9 (1:10 dilution)	12 (1% soln.)	12 (1% soln.)	3.5 (0.2% soln.)	6.6 (0.1% soln.)	6 (1% soln.); 3 (1% soln.)
Solubility	Miscible	Miscible	Miscible	0.2%	0.1%	25%; 1.2%
Density	11.8 lb/gal	11 lb/gal	11 lb/gal	57 lb/ft ³	68 lb/ft ³	63 lb/ft ³
CAS #	7647-15-6	13863-41-7	7647-15-6; 7681-52-9	16079-88-2	77-48-5	NA
EPA code	13907	20504	13907; 14703	6315	6317	13907; 81404; 81405
Product forms	Solutions of 40%–44%; Solid	Solutions of 15%, 18%, 21% Av. Br ₂	Solutions of 14%, 23% Av. Br ₂	Granules and tablets	Granules	Tablets

^a Two products are available. One is based on NaBr + dichlor; another is based on NaBr + trichlor.

maintained in the range of 0.5:1.0–2.0:1.0 on a molar basis, based on label directions. In practice, sodium bromide to oxidant ratios <1 are almost always used. Sodium bromide solutions can also be activated by electrolysis [68].

19.4.4.2 Stabilized Bromine Chloride

Stabilized bromine chloride features good storage stability and handling properties. These alkaline solutions contain 11% bromine chloride as the active ingredient, equivalent to 15.2% active on a bromine (Br₂) basis [69]. Recently, higher active ingredient formulations have been introduced into the marketplace [70]. The product is significantly more stable than industrial bleach for long-term storage (Figure 19.3). This means that in many applications, the continual adjustment of biocide feed is unnecessary. Stabilized bromine chloride is relatively unreactive toward other water treatment chemicals such as phosphonates, triazoles, and polymeric scale and corrosion treatments [71]. These treatment chemicals often represent the highest cost of the treatment program. Product application consists of shock doses to 4–10 ppm as Br₂ total halogen residual (2–4 ppm as Cl₂) or continuous dosages in the initial range of 4 ppm as Br₂. The product is registered as an effective biofilm control agent.

19.4.4.3 Stabilized Sodium Hypobromite

Stabilized sodium hypobromite, like stabilized bromine chloride, enjoys good storage stability and handling properties. These alkaline solutions contain sodium hypobromite, derived from sodium bromide and sodium hypochlorite, equivalent to 14.3% active on a bromine (Br₂) basis [72]. Higher active ingredient formulations are also available [73]. Application consists of shock doses to 4–10 ppm as Br₂ as total halogen residual (2–4 ppm as Cl₂) or continuous dosages in the initial range of 4 ppm as Br₂. This product won a Green Chemistry award [74].

19.4.4.4 Bromochlorodimethylhydantoin (BCDMH)

This biocide is a white to off-white solid in both granule or tablet forms. It has been used in industrial water treatment for over 25 years [75]. The specific chemical composition varies between

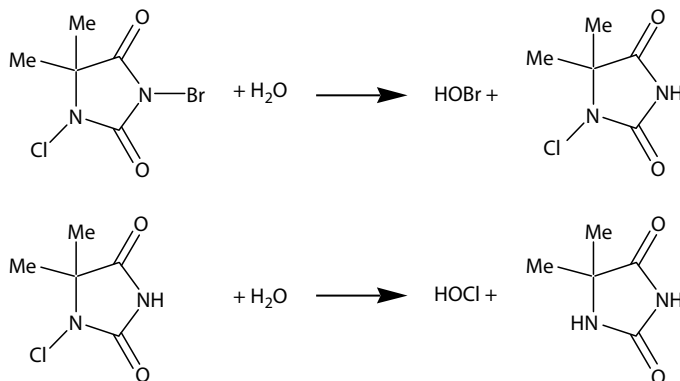


FIGURE 19.4 Release of halogen from BCDMH.

manufacturers. Several years ago, a gel-type form was introduced [76]. BCDMH is sparingly soluble in water. The chemistry of BCDMH can be described as a facile release of HOBr followed by a slow release of HOCl (Figure 19.4). The analysis of BCDMH in demand-free waters by the free and total DPD methods indicate that about half of the oxidant value analyzes as free halogen (i.e., free HOBr) with the other half analyzing as combined halogen (i.e., combined chlorine as chloro-DMH) [77]. It is generally recommended to add product to achieve 1–2 ppm residuals (as Cl_2) for shock or intermittent dosing or 0.2–0.5 ppm (as Cl_2) for continuous dosing. The distinction between free and total residual is often not clear with this product based on label directions.

19.4.4.5 Dibromodimethylhydantoin (DBDMH)

DBDMH is a white to off-white solid sold primarily as granules. This product is also sparingly soluble in water. The product contains more bromine activity than bromine itself—111% for DBDMH versus 100% for elemental bromine [78]. Almost all of the halogen residual from DBDMH analyzes as free as determined by the DPD method, in contrast to other hydantoin products. In many applications, this property leads to lower relative product consumption than other hydantoin products, and thus less product inventory and handling. Another property of DBDMH is that saturated solutions are near-neutral in pH and low in halogen odor.

19.4.4.6 Bromine-Releasing Isocyanurate Compositions

Two products are available based on a blend of a solid chlorine source and solid bromide source. One product features the combination of sodium dichloroisocyanurate (dichlor) and sodium bromide. A second product is based on the combination of trichloroisocyanuric acid (trichlor) and sodium bromide. When either composition is added to water, it effectively generates HOBr through the reaction of HOCl (liberated from the chlorinated isocyanurate) and sodium bromide. The application of these products with chemical feeders requires special precautions [79].

19.4.5 PRINCIPLES OF CHLORINE DIOXIDE CHEMISTRY

Chlorine dioxide (ClO_2) is a yellow-green gas with a pungent, irritating odor similar to that of chlorine. ClO_2 is readily soluble in water but, unlike chlorine, does not undergo hydrolysis. It is a powerful oxidizing agent with 2.6 times the oxidizing ability of chlorine. Unlike chlorine, the bactericidal efficacy of ClO_2 is little affected by changes in pH [80]. See Table 19.3 for the additional properties of ClO_2 .

ClO_2 can be a more effective biocide than chlorine. The product can be added directly into the cooling tower sump or into a cooling tower side stream. Target residuals of as low as 0.1 ppm

TABLE 19.3
Important Properties of Chlorine Dioxide and Oxygen-Based Biocides

Biocide	Chlorine Dioxide	Sodium Chlorite	Sodium Chlorate	Hydrogen Peroxide	Peracetic Acid	Ozone
Formula	ClO ₂	NaClO ₂	NaClO ₃	H ₂ O ₂	CH ₃ CO ₃ H	O ₃
Mol. wt.	67.4	90.4	106.4	34.0	76.0	48.0
Typical conc., %	100	25, eq. to 18% ClO ₂	40, eq. to 18% ClO ₂	35	15.2, PAA; 11.2, H ₂ O ₂	100%
pH (cond.)	7 (1% soln.)	13 (neat soln.)	7–9 (neat soln.)	5–6 (1% soln.)	2–3 (1% soln.)	NA
Solubility	Miscible	Miscible	Miscible	Miscible	Miscible	0.001% (32°F)
Density	NA	10.2lb/gal	11.6lb/gal	9.2lb/gal	9.4 lb/gal	NA
CAS #	10049-04-4	7758-19-2	7775-09-9	7722-84-1	79-21-0	10028-15-6
EPA code	20503	20502	73301	595	63201	NA
Product forms	Generated in situ	Solutions, packs, pouches of 0.8%–80% NaClO ₂	Solutions of 25%–50% NaClO ₃	Solutions of 20%–50% H ₂ O ₂	Solutions of 5%–15% PAA (with H ₂ O ₂)	Generated in situ

continuous or 0.25–5.0 ppm residual on a slug-dose basis have been found to lead to good microbiological control in industrial cooling towers. ClO₂ does not typically react with nitrogen compounds and organics. It is also effective over a wide pH range. It is thus compatible with the following situations: systems containing nitrogen compounds such as ammonia or urea (e.g., fertilizer plants), systems containing organics such as olefins and aromatics (e.g., refineries), and high pH conditions (>8.0).

ClO₂ is subject to UV degradation and is volatile. It is easily lost through evaporation in recirculating cooling systems. Several methods exist for the generation of biocidally active solutions containing ClO₂. The most common precursor material is sodium chlorite (NaClO₂). NaClO₂ is typically sold as a 25% solution, although a wide variety of solutions, packs, and pouches ranging from about 0.8% to 80% NaClO₂ content are available. Here are brief descriptions of the methods used to prepare biocidal solutions from NaClO₂ precursors.

19.4.5.1 Machine-Based Activation

Large amounts of ClO₂ can be produced via the reaction of NaClO₂ with either (a) chlorine alone, (b) bleach plus acid, or (c) electrolysis of salt solutions. It is a common practice to employ commercial generators to carry out this activation process. Such generators typically achieve conversion efficiencies of 90%–95%.

19.4.5.2 Acid Activation

Solutions of ClO₂ can be generated by acidifying sodium chlorite solutions to pH 2–3, with appropriate amounts of organic or inorganic acids such as citric, acetic, phosphoric, sulfuric, or hydrochloric. Although it is said that conversions of up to 80% (the theoretical amount) can be obtained by this method, this method is generally not indicated to produce large amounts of ClO₂. The activation process takes time and is dependent on the relative concentrations of NaClO₂/acid and environmental conditions such as temperature. Some use directions indicate activation periods (reaction times before use) of 30 min–15 h. Acid activation can also produce chlorous acid (HClO₂), also referred to as acidified sodium chlorite. Some suppliers of acidified sodium chlorite actually make a point that ClO₂ generation between pH 2.3 and 3.2 is very low, in support of the view that this technique generates lower levels of ClO₂ than the chlorine/bleach/electrochemical methods indicated above.

19.4.5.3 In Situ Chemical Activation

A recent development consists of tablets based on the combination of sodium chlorite and sodium dichloroisocyanurate [81]. One product is based on a combination of 20.0% NaClO₂ and 8.0% dichlor active ingredient. It is recommended to add between 2 and 10 tablets (10 g each) per 10,000 gal of system volume to maintain ClO₂ residuals between 0.1 and 0.5 ppm.

19.4.5.4 Unactivated Sodium Chlorite

While not technically a chlorine dioxide technology, EPA labels associated with NaClO₂ as a precursor material sometimes include directions for the use of unactivated material for the control of algae or the inhibition of slime-forming bacteria. Typical dosages range from 8 to 16 ppm NaClO₂.

19.4.5.5 Sodium Chlorate Methods

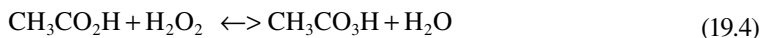
Another method of chlorine dioxide generation employs sodium chlorate. Sodium chlorate is available as solutions up to 50 wt.%, although lesser concentrations of 25% are also available. Over 95% of the chlorine dioxide produced is actually used for bleaching operations in the pulp and paper industry and most of it is generated by this method [80].

19.4.6 HYDROGEN PEROXIDE

Hydrogen peroxide (H₂O₂) is a clear, colorless liquid. Additional properties appear in Table 19.3. Hydrogen peroxide enjoys moderate usage in industrial water treatment for the prevention of biofouling and removal and control of biofilms [82]. Typical label application rates range widely from 10–500 ppm H₂O₂ for highly fouled systems to 3–100 ppm levels for cooling system maintenance. One study found that the low levels of hydrogen peroxide (2–3 ppm) gave a 2-log reduction in sessile bacteria in a laboratory cooling system operating at pH 9 [83]. Interestingly, the efficacy of hydrogen peroxide is not greatly affected by pH. Lab results indicate a slight increase in killing time of 6–8 h versus *Bacillus* spores over the pH range of 3–9 units (1% solution, 50°C) [84].

19.4.7 PERACETIC ACID

Peracetic acid, CH₃CO₃H, PAA, like hydrogen peroxide, is a clear, colorless solution with an acrid odor. It is actually an equilibrium mixture prepared by blending hydrogen peroxide, acetic acid, and, optionally, an acid catalyst such as sulfuric acid [64]. Additional properties of peracetic acid are shown in Table 19.3.



A survey of FIFRA labels indicates several peracetic acid formulations approved for cooling tower use that differ in relative amounts of peracetic acid and hydrogen peroxide (Table 19.4). Typical

TABLE 19.4
Peracetic Acid Formulations for Cooling Tower Use

Formulation	Peracetic Acid, %	Hydrogen Peroxide, %
1	4.5	27.0
2	5.6	26.5
3	15.0	22.0
4	15.2	11.2

label directions for peracetic acid formulations call for dosing in the range of 2–10 ppm based on PAA content. Severely fouled systems may require addition of 5–25 ppm based on PAA. The effectiveness of PAA begins to be impacted at pH 8.0 and is greatly affected at pH 9.

19.4.8 OZONE

Ozone is a bluish gas with a characteristic, pungent odor. The important properties of ozone are shown in Table 19.3. Ozone is unstable and reverts back to oxygen. It therefore must be generated on-site just prior to use. Two general methods are used to produce ozone: ultraviolet radiation and corona discharge [85]. Generation by corona discharge is the preferred method for industrial water treatment and consists of exposing dry oxygen or air to a high-voltage or high-frequency electrical field. This method produces heat, which can degrade the ozone produced. Commercial generators are designed to efficiently remove heat and ensure high yields.



Ozone is only partially soluble in water and is volatile [86]. The half-life of ozone in cooling tower applications is typically short (5–20 min) due to its reactive nature and volatility. In some cooling tower applications, ozone residuals of 0.05–0.2 ppm have proved adequate for microbiological control. To maintain sufficient residuals, it may be necessary to apply ozone at several different points in the cooling system. Ozone is very reactive and can degrade chemicals used for corrosion or deposit control (e.g., phosphonates). It is also aggressive to typical cooling tower materials (seals, pumps, metals, and so on) so these must be suitable for ozone service. Ozone degradation is pH-dependent, being fairly stable under certain conditions at pH 6 and instantaneous at pH 10.

19.5 BIOCIDES SELECTION—NONOXIDIZING BIOCIDES

There is a wide range of biocides used in cooling water treatment that are classified as nonoxidizers [1,2,3,9]. In general, they are broad-spectrum biocides which are effective across the range of pH and temperatures typical of cooling water systems. With some exceptions, they are typically small organic molecules, compatible with process additives, and less affected by the presence of organic matter or system contaminants (relative to oxidizers). Nonoxidizers are generally liquid products, which may be easily metered into systems or dispensed by hand, as needed. The products are typically stable, as provided, for 1 year or longer. Some of the limitations of nonoxidizers may include concerns for effluent discharge (environmental toxicity), reactivity with additives (e.g., cationic biocides), higher use costs, and safe handling of corrosive or sensitizing products.

Unlike the oxidizing biocides, these biocides are typically slower killing (hours vs. minutes), significantly longer lasting (persistent) in the recirculating water, less corrosive at use levels, and contain more complex organic molecules. These biocides typically interact with the metabolism of the cell or affect its structural integrity. The various biocides are grouped by basic class and described in the following sections. Note that all biocide use levels in the following discussion are on an active ingredient basis, since varying concentrations of the different products are often available.

A summary of the various nonoxidizing biocide major application areas, efficacy characteristics, and physical-chemical properties are summarized in Tables 19.5 through 19.7, respectively. Individual groups of each class of nonoxidizers are discussed next.

TABLE 19.5
Major Applications for Nonoxidizing Biocides

Biocide	CAS #	Application		
		Cooling	Oilfield	Paper
Alkyldimethylbenzylammonium chloride	68424-85-1	+	+	+/-
Didecyldimethylammonium chloride	7173-51-5	+	+	+/-
Bronopol	52-51-7	+	-	+/-
CMIT/MIT	26172-55-4	+	+/-	+
	2682-20-4	+	+/-	+
DBNPA	10222-01-2	+	+/-	+
DCOIT	64359-81-5	+	-	+
DGH	13590-97-1	+/-	-	+
Potassium dimethyldithiocarbamate	128-03-0	+	-	+
Disodium ethylenebisdithiocarbamate	142-59-6	+	-	+
Glutaraldehyde	111-30-8	+	+	+
MBT	6317-18-6	-	-	+
MIT	2682-20-4	+	-	-
Poly Quat	31512-74-0	+	-	-
TBZ	5915-41-3	+	-	-
TCMTB	21564-17-0	-	-	+
THPS Quat	55566-30-8	+	+	+/-
TTPC Quat	81741-28-8	+	+	+/-
TN	126-11-4	+/-	-	-

Note: Product rating key: +, primary application; +/-, minor application; -, not significant application.

TABLE 19.6
Comparative Efficacy Properties of Nonoxidizing Biocides

Biocide	Bacteria	SRBs	Algae	Zebra Mussels	Fungi	Quick Kill	Long-Lasting Efficacy
ADBAC Quat	+	+	+	+	+/-	+	+
Bronopol	+	+	-	?	-	-	-
CMIT/MIT	+	+/-	+	+/-	+	-	+
DBNPA	+	?	-	-	-	+	-
DCOIT	+/-	?	+	+	+	-	+
DGH	+	?	?	+	+	?	?
Dithiocarbamates	+/-	+/-	+/-	?	+	-	+
Glutaraldehyde	+	+	-	?	-	+	+
MBT	+	?	+/-	-	+/-	-	-
MIT	+	+/-	-	?	+/-	-	+
Poly Quat	+	?	+	+	+/-	+	+
TBZ	-	-	+	-	-	-	+
TCMTB	+/-	?	-	+	+	-	+
THPS Quat	+	+	+	?	-	+	+
TN	+	+	?	?	-	-	+

Note: Product rating key: +, high efficacy; -, low efficacy; +/-, variable efficacy; ?, characteristic unknown.

TABLE 19.7
Comparative Physical and Chemical Properties of Nonoxidizing Biocides

Biocide	Highly Water Soluble	No Salts	No/Low Odor	Nonfoaming	Stable at pH 8	Compact. with Anionics	No Formaldehyde
ADBAC Quat	+	–	+	–	+	+	+
Bronopol	+	+	+	+	–	+	–
CMIT/MIT	+	–	+	+	+	+	+
DBNPA	+	+	+	+	–	+	+
DCOIT	+/-	+	+	+/-	+	+	+
DGH	+	–	+	+/-	+	–	+
Dithiocarbamates	+	+	–	+	+	+	+
Glutaraldehyde	+	+	–	+	+	+	+
MBT	–	+	+	+	–	+	+
MIT	+	+	+	+	+	+	+
Poly Quat	+	–	+	+/-	+	+/-	+
TBZ	–	+	+	+	+	+	+
TCMTB	+	+	+	+	+	+	+
THPS Quat	+	–	+	+/-	+	+/-	–
TN	+	+	+	+	+	+	–

Note: Product rating key: +, yes; –, no; +/-, variable feature within the group or condition.

19.5.1 ALDEHYDES

Glutaraldehyde (1,5-pentanedial) is used for various water treatment applications. It is quick killing and especially effective versus bacteria, including sulfate-reducing bacteria (SRB) [87,88]. Glutaraldehyde is typically used at 20–100 ppm and is formulated in water at 15% and 45% active concentrations. Studies have shown that glutaraldehyde is effective across a pH range of 6.5–9.0, readily biodegradable, and effective versus *Legionella* [10]. It is deactivated by ammonia and primary amines.

19.5.2 DITHIOCARBAMATES

The two main groups of carbamates products used in cooling systems are potassium or sodium salts of dimethyldithiocarbamate (DMDC) and ethylene-bis-dithiocarbamate (EBDC) [1]. These biocides are primarily fungicides with some antibacterial activity, especially versus SRBs. They are available as standalone products at 20%–25% active or may be blended together. Carbamates are dosed at 5–90 ppm in systems at pH 7–8.5. They are not compatible with oxidizers, aldehydes, metals, and strong acids. The degradation of EBDC may result in ethylene thiourea.

19.5.3 ORGANOBROMINES

2-Bromo-2-nitropropane-1,3-diol (BNPD; bronopol) is a broad-spectrum bactericide, with efficacy versus aerobic and anaerobic microorganisms, including SRBs [1]. It is formulated in a water-glycol mixture and typically used at 20–100 ppm active in system below pH 8.0. Bronopol is deactivated by reducing agents. It is available as a solid powder or in a 20%–40% solution. Alkaline decomposition can result in formaldehyde release.

2,2-Dibromo-3-nitropropionamide (DBNPA) is a quick killing and rapidly degrading biocide. It is used at 0.24–24 ppm and is primarily effective versus bacteria [1]. Studies have shown that it is

effective versus strains of *Legionella* [10]. It is not persistent in alkaline waters above pH 8 (due to rapid hydrolysis) and is degraded by reducing agents. DBNPA is available as a solid product, but is mainly sold as a liquid at 5%–20% active in a water-glycol formulation.

19.5.4 ISOTHIAZOLONES

Several isothiazolone biocides are used in industrial water treatment applications [1,89]. They are slower killing biocides, but rapidly inhibit microbial metabolism within minutes. They are generally deactivated by reducing agents, but compatible with other biocides and process additives, including low levels of halogens. All isothiazolone biocides are biodegradable and produce nontoxic metabolites that do not persist or bioaccumulate in the environment.

The most widely used isothiazolone biocide is a 3:1 ratio of 5-chloro-2-methyl-4-isothiazolin-3-one (CMIT) and 2-methyl-4-isothiazolin-3-one (MIT). It is available as a 14% active liquid concentrate and formulated at 1.5%–4% levels for end-use applications. CMIT/MIT has broad-spectrum efficacy versus bacteria, algae, and fungi, including various strains of *Legionella* and associated protozoa species [10,89]. It is typically dosed at 1–5 ppm active and has good stability in waters up to pH 9.

4,5-Dichloro-*n*-octyl-isothiazolin-3-one (DCOIT) is used in cooling water as an algicide and a fungicide for paper making. It is formulated as a 4.25% microemulsion and is used at 0.25–6 ppm active [1,89,90]. The active ingredient, DCOIT, received the first EPA Green Chemistry biocide award in 1996 for its use in replacing tin-based antifouling products.

The newest isothiazolone biocide recently approved by EPA for water treatment is MIT alone. It is a water-based formulation at 9.5% active and is most effective versus bacteria. It is dosed at 25–100 ppm active and provides long-term preservative efficacy in systems with high pH and temperature ranges.

19.5.5 QUATERNARY COMPOUNDS

Various types of quaternary compounds are used in water treatment [1]. As a group, these cationic biocides typically show (a) broad-spectrum efficacy versus bacteria, algae, fungi, and macrofouling organisms (Asiatic clams and zebra mussels); (b) varying degrees of foaming; (c) varying reactivity with salinity, organics, and anionic scale, corrosion, and surfactant additives; and (d) less influence by the pH of the cooling water. Efficacy studies have indicated that quats have poor activity versus *Legionella* [10].

Several types of quaternary ammonium biocides are used in water treatment. The original quats were based on alkyldimethylbenzylammonium chloride (ADBAC) with C₈–C₁₆ chain lengths. Second-generation dialkyl quats have recently been developed, including didecyldimethylammonium chloride (DDAC). More recently, branched dialkyl quats are used. In general, alkyl ammonium quats are used at 5–50 ppm. They are often provided as 50%–80% active water-based formulations [91].

Two types of phosphonium quats are used for water treatment. These include tetrakis-hydroxymethyl-phosphonium sulfate (THPS) and tributyltetradecyl-phosphonium chloride (TTPC) [92,93]. These materials are used at 20–100 ppm and 5–30 ppm active, respectively. THPS has been shown to generate formaldehyde during decomposition in water and may be inactivated by high levels of halogens, iron, or anionics. THPS also received a Green Chemistry award in 1997. Both phosphonium quats are highly effective versus anaerobic SRBs. They are available as 50%–75% concentrates and 5%–50% end-use formulations.

Polymeric quats include the ionene polyquat, poly[oxyethylene(dimethyliminio)ethylene-(dimethyliminio) ethylene dichloride] [94]. It is used at 1.2–12 ppm active and is significantly less foaming than ADBAC quats. Similar levels are used for typical cooling water microorganisms as well as macrofouling organisms. The products are typically 10%–60% active formulations in water.

19.5.6 MISCELLANEOUS TYPES

Dodecylguanidine hydrochloride (DGH) is a broad-spectrum (bacteria, fungi, and algae) cationic biocide which is dosed at 5–35 ppm [1]. It is a positively charged, surface-active molecule which can react with anionic compounds, including anionic polymers and surfactants, bicarbonates, and so on. Typical products are 5%–35% active formulations.

Methylenebisthiocyanate (MBT) is also a broad-spectrum biocide and is used at 2–9 ppm. It is not compatible with sulfides or oxidizing agents and is often used in combination with other biocides [1]. It is produced as a solid and may be formulated as a 10% active dispersion due to its low water solubility. Degradation in alkaline water (pH >8) may result in the release of cyanide.

The following is a list of additional biocides which are also used in industrial water treatment systems: the algicide terbutylazine (TBZ: 0.5–3 ppm, which is effective when activated with halogens); the fungicide 2-(thiocyano-methylthio)benzothiazole (TCMTB: 5–40 ppm); 2-nitro-2-hydroxymethyl-1,3-propanediol (TN: 50–75 ppm); and tetrahydro-3,5-dimethyl-2H,1,3,5-thiadiazine-2-thione (DMTT), both of which release formaldehyde; bis(trichloromethyl)sulfone; β -bromo- β -nitrostyrene (BNS); *N*-coco-trimethylenediamine; and 4,5-dichloro-1,2-dithiol-3-one (dithiol) [1,2,3,9].

19.6 BIOCIDES MECHANISMS OF ACTION AND RESISTANCE

The mode of action of industrial biocides is an important aspect in optimizing their use in systems and combating the development of resistance. Traditionally, biocide mechanisms have been classified as either being membrane active or electrophilic [42]. These may be further divided as oxidants (extreme electrophiles), electrophiles (moderate), lytic (membrane active) agents, and protonophores (affecting membrane energy processes). Nonoxidizers fall into one of the latter three categories [95]. The specific mechanisms of action and target sites of attack on microbial cells by various biocides are illustrated in Figure 19.5 and are discussed next.

The overall rate and extent of damage to the cell is a function of (a) the presence or absence of critical sites within an organism, (b) the rate of access of the antimicrobial to critical sites, (c) the rate of reaction with the critical site, and (d) the rate of reaction with noncritical sites. The overall rate and extent of repair is affected by the rate at which a cell can physically repair the damage or synthesize new sites, and the relationship of the site to energy and precursor generation.

Most industrial biocides affect functional groups such as thiols or amines that reside on many different types of macromolecules (e.g., proteins and enzymes). Access to critical sites is also an important factor that determines the range and types of organisms that are affected by a biocide. Differences in the structure of the cell walls in Gram-negative and Gram-positive bacteria are key factors. Generally, because of the presence of an outer membrane and lipopolysaccharide layer in Gram-negative bacteria, there is less access for large and hydrophobic antimicrobials to reach critical sites inside the cell [42,95,96].

19.6.1 ELECTROPHILIC BIOCIDES: OXIDANTS (EXTREME ELECTROPHILES)

Oxidizing biocides that function by halogenating macromolecules within a cell, including chlorine, bromine, and many different types of halogenated compounds (e.g., sodium bromide, chlorinated isocyanuric acids, stabilized bromine products, and halogenated hydantoin) are widely used in industrial water treatment. Other oxidants that do not release active halogens may function by generating toxic free radicals within cells (e.g., chlorine dioxide, hydrogen peroxide, and peracetic acid). This class of biocides is very effective against most problem organisms and exhibits rapid speed of kill. The moderate-to-high concentrations of oxidants can “burn” through most biological material, reacting nonspecifically with the nucleophilic functional groups (nitrogen and sulfur) on critical cell components, including proteins, lipids, adenosine triphosphate (ATP), carbohydrates, and nucleic acids. Although oxidizing biocides are effective at disrupting the metabolic

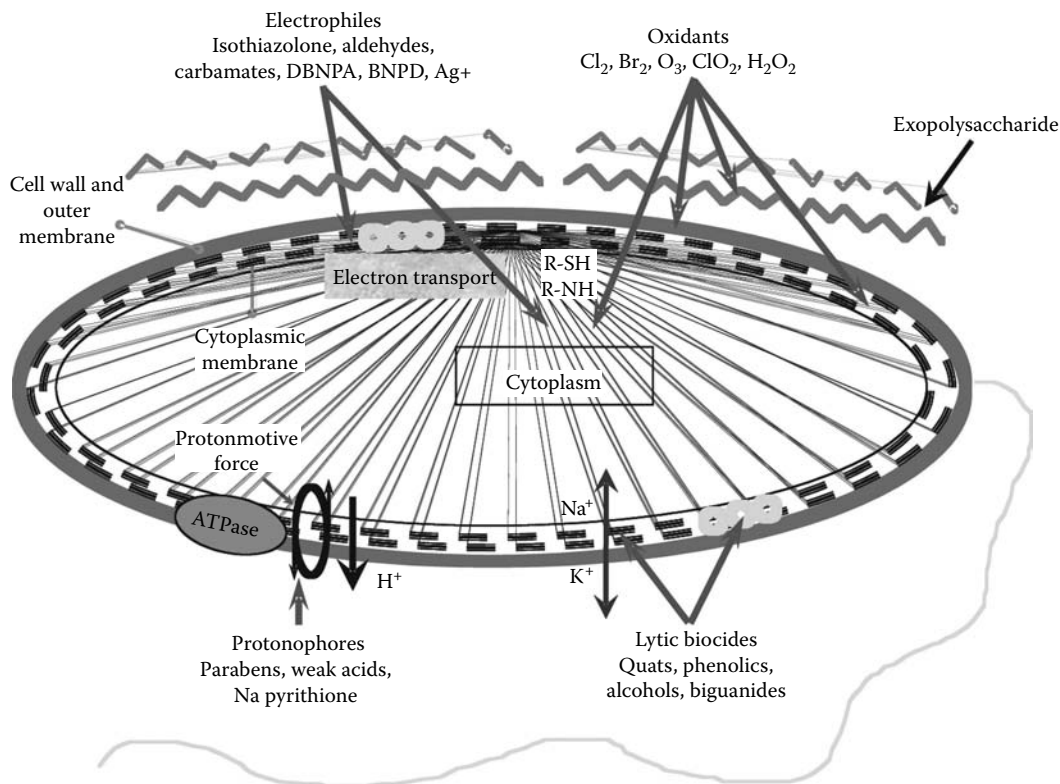


FIGURE 19.5 Schematic view of biocide mechanisms of action and sites of interaction with microbial cell components.

and biosynthetic machinery of a microorganism, their highly reactive nature also can be a disadvantage. To react with the intracellular machinery, the oxidant must pass through the outer layer of exopolysaccharide (EPS), cell wall, and internal membrane. Oxidant species will readily react with these outer layers of the cell, creating a reaction barrier that prevents penetration of the oxidant species into the cell.

19.6.2 ELECTROPHILIC BIOCIDES: MODERATE ELECTROPHILES

Most of the nonoxidizing biocides fall into this category. Isothiazolones are perhaps the best-studied electrophilic biocides with respect to the mechanism of action. They interact primarily with thiol groups in proteins and critical enzymes. Isothiazolones inhibit dehydrogenase enzymes in the respiratory pathways that affect metabolism and growth. Cell respiration is rapidly inhibited after treatment with isothiazolone, and the microorganism begins to die after several hours. During this period, intracellular thiols are destroyed and radicals are formed which contribute to the cidal effect of the biocide [97].

Formaldehyde, glutaraldehyde, formaldehyde-releasers, and formaldehyde condensates are moderate electrophiles that react nonspecifically with cellular nucleophiles. In the case of formaldehyde-releasers, the active electrophile is typically formaldehyde; however, some of the antimicrobial activity of bronopol has been attributed to the bromine functional group. Glutaraldehyde contains two aldehyde groups that can interact with amino groups in proteins, causing cross-linking within and between proteins [98].

Less is known about the mechanism of other electrophilic, nonoxidizing biocides such as DBNPA, bronopol, and MBT. Generally, the mechanism of action described earlier also pertains to

these biocides with regard to reactivity with thiols and radical formation. However, some biocides exhibit more than one mechanism of reaction with intracellular macromolecules. For example, MBT and carbamates may react specifically with the metal-containing (Fe) centers of some coenzymes, destroying their functionality within the cell.

19.6.3 MEMBRANE ACTIVE—LYTIC BIOCIDES

The cytoplasmic membrane, or cell membrane, is an attractive target for membrane-active biocides. The examples of membrane-active, lytic biocides include quaternary ammonium compounds, polymeric quats, phosphonium quats, and biguanides. These biocides disrupt the structure and function of the cell membrane, leading to changes in membrane permeability, leaking of intracellular material, osmotic lysis, and the inhibition of membrane-associated metabolism. Lower concentrations can cause the leakage of cellular components and disrupt metabolic functions, and higher concentrations can cause a lysis of the entire cell [42,96].

The membrane-active biocides interact with cell membranes as a function of their amphiphilic structure. The presence of a positive electrostatic charge and hydrophobic functional groups enables these chemicals to pass through the cell wall and interact with the cytoplasmic membrane. After penetration through the cell wall, membrane-active biocides associate with negatively-charged phospholipids in the cell membrane, followed by insertion of the hydrophobe. As more and more of these molecules insert themselves into the membrane, the structure of the membrane becomes more disturbed until it loses integrity.

19.6.4 MEMBRANE ACTIVE BIOCIDES—PROTONOPHORES

Protonophores interact with components of the cell wall and cell membrane, but generally do not cause a rapid catastrophic lysis of the cell at use levels. They act as proton conductors, which dissipate the transmembrane proton-motive force and affect the gradient of protons (H^+) across the cytoplasmic membrane involved in energy (ATP) generation. When the proton-motive force is disrupted, the cell cannot produce enough energy to maintain its functions. Once the energy reserves within the cell are exhausted, the microorganism will begin to die [42,96]. These biocides are typically not used in water treatment, because of their slow speed of kill, high use level, use at low pH, and poor activity against Gram-negative bacteria. Some examples of this class of biocides include parabens and weak acids such as benzoic acid, citric acid, and sorbic acid.

19.6.5 RESISTANCE TO BIOCIDES

It is well known that microorganisms have developed the potential to become resistant to antibiotics and many commonly used industrial biocides. *Biocide resistance* can be defined as a reduction in the susceptibility of an organism to an antimicrobial agent as a result of physiological or genetic changes. Thus, a previously effective level of biocide no longer provides the same level of biological control. Microorganisms do have the innate potential to develop resistance to any biocide, although this is largely a function of the use rate, environmental conditions, and microbial population density. Resistance is most likely to occur as a result of underdosing biocides at levels below the minimum effective dose, poor stability of the biocide, extensive biofilm development, cross-contamination by resistant strains, and efficacy gaps against certain groups of microorganisms [42,95,96,98,99–101].

Overall, antimicrobial resistance can be separated into two major types: *acquired* and *intrinsic*. *Acquired resistance* is a decrease in susceptibility or the lack of susceptibility due to specific changes in the genetic composition of the cell through natural mutation or the transfer of genetic elements (plasmids) from one organism to another. *Intrinsic resistance*, a more common occurrence, involves a decrease in susceptibility or a lack of susceptibility to an antimicrobial by an already existing or inherent property of the organism. This may be permanent, as in the case of

TABLE 19.8
Biocides Reported as Resistant to One
or More Microorganisms

Benzalkonium chloride	Imidazolidinyl urea
Benzisothiazolone	Iodine
Benzoic acid	Methylenebischlorophenol
Bromonitropropanediol (bronopol)	Methylchloro/methyl isothiazolone
Chloroallyltriazine-azoniadamantane	Methyl paraben
Chlorhexidine	Orthophenylphenol
Chlorophenol	Phenoxyethanol
Dibromonitropropionamide (DBNPA)	Phenylethyl alcohol
Dibromodicyanobutane	Phenylmercuric acetate
Dimethylloxazolidine	Propyl paraben
Dimethyldithiocarbamate	Povidone iodine
Dimethyloldimethylhydantoin	Quaternary ammonium compounds
Formaldehyde	Sorbic acid
Glutaraldehyde	Tetrahydrothiadiazinethione
Hexahydrotriethyltriazine	Triclosan
Hypochlorite/chloramine	Trifluoromethyl dichlorocarbaniide
Hypobromite	

the Gram-negative bacteria where the natural cell wall provides inherent resistance to quaternary biocides, or temporary, due to adaptation to the low levels of biocide, the development of biofilms, growth phase, and inoculum level.

Antimicrobials with the documented instances of resistance are shown in Table 19.8 and include hypochlorite, hypobromite, quaternary ammonium compounds (quats), glutaraldehyde, chlorhexidine, formaldehyde, chlorine, peroxide, thiones, hydantoins, parabens, bronopol, carbamates, triazines, alcohols, organic acids, pyriithones, DBNPA, and isothiazolones. Antimicrobial resistance is typically due to modifications in the uptake of the biocide by the cell. The mechanisms of inherent resistance are known to occur in microorganisms and include altering in the permeability of the cell wall or membrane to prevent the biocide from entering the cell (e.g., loss of porin proteins), deactivation or degradation of the antimicrobial agent by biochemical reactions (e.g., catalase degrading peroxide), and transport of the agent outside the cell (via multidrug efflux pumps).

If true resistance is observed in use, remedial treatments may include: (a) applying the biocide at the maximum dose level and frequency of addition, (b) adding an additional biocide to broaden the spectrum of efficacy and/or provide different mechanisms of action, (c) switching or alternating to another product, and (d) adding an adjuvant material (e.g., chelator or surfactant) which may improve biocide penetration and efficacy [97].

For water treatment service companies and end-users, the mechanism of biocides should be considered along with other properties when determining the best and most cost-effective biocide treatment program for a given system. A greater understanding of the mechanism of action can lead to more effective programs to control biofouling and prevent resistance from developing.

19.7 STRATEGIES FOR SUCCESSFUL BIOCIDES APPLICATION

The correct use of industrial biocides is critical to the performance of successful water treatment programs to reduce microbial populations on surfaces and in the recirculating bulk water. Optimizing and improving biocide programs will allow the most efficient use of the products to gain the highest degree of microbial control. Many treatment programs typically employ the routine use of oxidizing

biocides as the primary product and supplement periodic dosing with nonoxidizers to achieve a broad-based approach to microbial control. Using this dual biocide dosing provides a very complete program. The correct choice of the individual biocides will depend on the spectrum of organisms of interest, environmental variables, system dynamics, and process concerns. The biocide selection criteria must include compatibility with scale and corrosion additives, system pH and temperatures, residence times in the water circuit, process leaks and other sources of contaminants, and discharge limitations. The choice of a biocide for a particular application can depend on a number of factors—cooling system design, cooling system location, water chemistry, operating conditions, environmental factors, system contaminants, and potential upset conditions [1–3].

19.7.1 COOLING SYSTEM DESIGN

The basic design of the cooling system can greatly impact biocide performance. Although system design is generally outside the scope of the water treatment professional, here are a few factors to consider.

It is important to minimize low flow areas or “dead legs” in cooling systems. Laboratory studies and field experience indicate that high flow rates increase the susceptibility of microorganisms to biocides, that is, enhance biocidal activity. Interestingly, biofilms grown under high flow rates are also inherently more susceptible to biocides. The effect of flow is generally attributed to better mass transport of the biocide into the biofilm. Several examples of improved efficacy with peracetic acid or glutaraldehyde with high flow have been reported [88,102]. Lower rates of flow or shear can lead to inherently tougher, more difficult to control biofilms [103].

The effect of temperature appears more complex than flow velocity. Warm temperatures tend to promote microbial activity while at the same time tend to promote biocidal efficacy. It is probable that the impact of temperature is that systems under a poor biocide program tend to spiral out of control more quickly at higher operating temperatures where bacterial metabolism and populations are at their peak. Also, keep in mind that higher operating temperatures and environmental temperatures place additional stresses on the biocide delivery system and lead to decreased biocide shelf-life and residence time in the cooling system. Laboratory studies indicate that microbial populations and metabolic activity peak in the range of 30°C–40°C (86°F–104°F). Specific examples demonstrating this concept for *Legionella*, total bacteria, protein, and carbohydrate in biofilms have been reported [72,104,105]. Other investigators have shown that the efficacy of chlorine compounds and peracetic acid increased with temperatures for various microorganisms [102,106,107].

The cycles of concentration can impact biocide performance. High cycles result in longer resident times (increased half-life) for all treatment chemicals, including biocides, and increased impurities in the system (higher system demand, see later). Long residence times (half-life) in such systems may favor the use of slower-acting oxidizing or nonoxidizing biocides. The increased concentrations of salts and organic matter may negatively affect certain biocides, such as quats.

19.7.2 WATER QUALITY

Water quality plays a big role in biocide selection. The different biocides, both oxidizers and non-oxidizers, often have a pH range for optimum efficacy. In the case of chlorine or bromine chemistry, pH impacts the relative amount of hypohalous acid available—the protonated form (HOX)—which is more effective at microbial deactivation than the nonprotonated form (OX⁻) [108]. In the case of nonoxidizing chemistries, some of the active ingredients, such as DBNPA and MBT undergo appreciable decomposition above pH 7.5 [109].

Oxidizing biocides are also sensitive to many extraneous components present in cooling systems. Ozone, due to its highly reactive nature, is greatly impacted by system impurities such as organic matter. Impurities have much less effect on the performance of chlorine dioxide. Chlorine and bromine represent the intermediate case relative to reactivity.

The high level of cooling tower impurities may require the use of less reactive, nonoxidizing biocides for treatment during periods of high chlorine demand to ensure effective biocidal control. Other conditions to avoid include high levels of silt, algae, and slime. Such highly fouled systems may require mechanical or chemical pretreatment. Cooling towers and decks exposed to full sunlight may require additional biocide treatment for algae or slime. Nitrogen-containing impurities can impact the efficacy of chlorine treatment relative to bromine chemistry. Nonoxidizers are generally less affected by nitrogenous contaminants, with the exception of glutaraldehyde, which may be deactivated by free ammonia or complexed amines.

Reduced sulfur species (sulfides) may be encountered in industrial water treatment systems from process leaks or anaerobic bacteria (SRB). Sulfites may also be encountered through process contamination. Reduced sulfur compounds will deactivate all of the oxidizing biocides and many of the nonoxidizers, including DBNPA, isothiazolones, bronopol, MBT, glutaraldehyde, and so on [1].

19.7.3 USING COMBINATIONS AND SYNERGISTIC BLENDS FOR INCREASING BIOCIDAL EFFICACY

Individual biocides cannot always provide complete control of microorganisms, even at high use concentrations, due to weak activity against certain microorganisms or chemical compatibility. The combinations of different microbicides are often used to provide the overall control of microorganisms in industrial water treatment systems. Cooling water systems will often use an oxidizing biocide supplemented with a nonoxidizing biocide as the standard treatment program. In some situations, only one type of product may be used, due to either cost, environmental, or other factors. Other systems may employ rotation or combinations of nonoxidizers.

Using combinations of biocides may provide different types of antimicrobial effects on microbial populations. These may be measured as inhibition (of growth or activity) or kill (cell death). One desired effect of biocide combinations is termed *synergy*, where the effect of two biocides is greater than the sum of the activity of both products alone. This results in enhanced efficacy and improved control for the system. Synergy may be measured mathematically, as described by Kull et al., by the use of the standard biocide efficacy measurement techniques [110]. The synergistic effect of two biocides acting together is often a result of two different mechanisms of action attacking the cell. For example, biocides that act on the cell membranes (quats, alcohols, and aldehydes) would be good candidates when combined with biocides that function by interacting with the cells enzymatic (metabolic) activity (isothiazolones, bronopol, carbamates, and DBNPA). A key to using biocide combinations is to assure the products are compatible. For example, do not use oxidizers with reducing biocides, such as carbamates or thiones, and do not dose oxidizers and nonoxidizers in the same location at the same time.

Numerous examples of synergistic combinations of two or more biocides have been described over the past 25 years for industrial water treatment applications, including chlorine, bromine, peroxides, isothiazolones, glutaraldehyde, bronopol, DBNPA, carbamates, thiones, quats, peracetic acid, chlorine dioxide, and others [111–118]. These combination treatments may provide effective and beneficial treatment programs to improve the spectrum of activity of each biocide, provide different modes of action, and prevent resistance from either biocide alone.

19.7.4 ENHANCING BIOCIDAL EFFICACY WITH ADJUVANTS AND BIODISPERSANTS

A variety of different classes of compounds have been used in water treatment as biodispersants or adjuvants to enhance the activity of biocide for microbial control and biofouling on surfaces. Surface-active materials which have been used as biodispersants to reduce microbial fouling include ethylene oxide-propylene oxide block copolymers, fatty acid amides, sulfosuccinates, terpenes, linear alkylbenzene sulfonates, alkylphenoethoxylates, modified polyethoxylated alcohols, alkylthioamines, alkylpolyglycosides, and enzymes [119–122]. Surfactants are known to affect the integrity of bacterial cell wall/membrane complex by interfering with the structure and function

of the various lipids and fatty acid components of the membrane, thus increasing the uptake of the biocide into the cell [89]. Cationic materials also destabilize bacterial cell walls and membranes of microorganisms, which may improve microbial control. Limitations with certain classes of biodispersants or surfactants involve foaming and charge. Low foaming products are available, and defoamers may be employed as needed. Surfactants may include nonionic, anionic, and cationic varieties so that interactions with anionic system additives, such as acrylates, phosphonates, and so on, need to be taken into account. In addition, the compatibility of amine-based additives with halogens should be understood prior to use.

19.7.5 BIOCIDES AND MICROBIOLOGICAL MONITORING

Biocide performance is critically dependent on accurate dosing, which in turn relies on knowing the total volume, recirculation rate, and half-life for a given system. Monitoring the level of biocides can optimize treatment programs to prevent overdosing and underdosing, and assuring that the right frequency of biocide addition is occurring. Monitoring is also an important tool in troubleshooting problems or for starting up new systems.

Oxidizing biocides are routinely measured in the field directly using DPD-based colorimetric test kits or indirectly using oxidation-reduction (redox) electrodes. It is a common practice to monitor chlorine residuals using the “free” DPD test, which is specific for the uncombined forms of chlorine residuals (HOCl and OCl^-). Bromine residuals are most commonly monitored using the “total” DPD test, which measures contributions from both the free (HOBr and OBr^-) and combined (haloamine) forms [123]. Residuals for other oxidizing biocides can be determined via modifications of the DPD test and other colorimetric methods. Lab-based methods for oxidizers include amperometric or iodometric titration [124].

Nonoxidizers are most accurately measured using complicated lab methods involving high-pressure liquid chromatography or gas chromatography. These are not suitable for use in the field and require trained personnel to operate. Colorimetric field test kits are available for nonoxidizers, including glutaraldehyde, quats, bronopol, DBNPA, and isothiazolone.

Biofilm growth, activity, and system cleanliness have been measured by a variety of methods, including (a) viable counts of total bacteria, fungi, and algae; (b) photosynthetic pigments such as chlorophyll a; (c) total and volatile dry solids; (d) adenosine triphosphate (ATP); (e) total protein; (f) total carbohydrate; and (g) specific bacterial populations, such as *Legionella*, sulfate reducers, slime formers, and iron-reducing bacteria [45–47,105,109,118,125–128]. Methods such as ATP monitoring have the advantage of providing rapid (minutes) results of microbial populations in the field. Many of the fouling and corrosion monitoring devices may be coupled with online access so the system may be monitored from remote locations in real-time and treatment programs may be automatically or manually adjusted to reflect the status of the systems [129,130]. The integration of the concepts of monitoring biocide concentrations and the parameters of system performance (efficacy) will continue to provide new insights into approaches to improve and optimize biocide treatment programs for various industrial applications.

19.8 SUMMARY

Much knowledge has been gained over the past 20 years to improve and optimize biocide performance in water treatment systems, and many approaches have been utilized. Many new oxidizing biocide products have emerged, with a major focus on bromine chemistry. New products based on nonoxidizing biocides have also been introduced for water treatment for both niche and broad-spectrum microbial control. The use of biodispersants or biopenetrants has become a common practice for improved killing of planktonic bacteria and biofilm control. Many different types of materials have been evaluated and implemented, demonstrating the value of this type of improved treatment program.

Enhanced microbial control may also be achieved by the combinations of certain biocides that display a synergistic effect on the mixed populations of organisms. These combinations have gained acceptance over the years, with blends of actives including halogens, glutaraldehyde, quats, bronopol, isothiazolones, MBT, and others. Studies have also shown the benefit of rotating or alternating biocides for overall microbial control and to prevent the development of resistant organisms, which may develop following the use of low doses of a single biocide.

Other approaches to provide additional knowledge on biocide dosing and microbial control may be achieved through the use of model biofilm systems designed to simulate key environmental parameters of industrial systems. Many variations of biofouling models have been used to evaluate biocide dosing strategies; however, these systems are complicated and time-consuming to operate. Newer methods using microtiter plates and drip-flow reactors are available for evaluating biocide efficacy against biofilm populations on surfaces.

Future biocide development in water treatment will likely encompass the use of advanced monitoring systems for online feedback and control, combination products, novel delivery systems, and enhanced microbial detection for common microorganisms and pathogens. A better knowledge of biofilm structure and function and new methods for biofouling control will provide improved operation and efficiency for a wide variety of industrial water treatment applications.

REFERENCES

1. Biocide monitoring and control in cooling towers. Item No. 24230, Publication 11206, NACE International, Houston, TX (2006).
2. Frayne, C. *Cooling Water Treatment: Principles and Practice*. Chemical Publishing Company, New York (1999).
3. *Water Treatment Strategies*. Report 1009598. Electric Power Research Institute, Palo Alto, CA (2004).
4. Mittleman, M. W. and Geesey, G. G. (Eds.). *Biological Fouling of Industrial Water Systems: A Problem Solving Approach*. Water Micro Associates, San Diego, CA (1987).
5. Fleming, H. C. and Geesey, G. G. *Biofouling and Biocorrosion in Industrial Water Systems*. Springer-Verlag, New York (1991).
6. Geesey, G. G., Lewandowski, Z., and Flemming, H. C. (Eds.). *Biofouling and Biocorrosion in Industrial Water Systems*. Lewis Publishers, Ann Arbor, MI (1994).
7. Pope, D. H. Microbiologically influenced corrosion in the twentieth century and where do we go from here. CORROSION/2000, Paper No. 00402, NACE International, Houston, TX (2000).
8. McIlwaine, D. B. Oilfield application of biocides. In *Directory of Microbicides for the Protection of Materials a Handbook*, Paulus, W. (Ed.), pp. 157–175, Springer, Dordrecht, the Netherlands (2005).
9. Ludensky, M. Microbiological control in cooling systems. In *Directory of Microbicides for the Protection of Materials a Handbook*, Paulus, W. (Ed.), pp. 121–139, Springer, Dordrecht, the Netherlands (2005).
10. Thomas, W. M., Eccles, J., and Fricker, C. Laboratory observations of biocide efficiency against legionella in model cooling tower systems. Paper No. SE-99-3-4, ASHRAE Transactions (1999).
11. Characklis, W. G. and Marshall, K. C. Biofilms: A basis for an interdisciplinary approach. In *Biofilms*, Characklis, W. E. and Marshall, K. C. (Eds.), pp. 3–15, John Wiley & Sons, New York (1990).
12. Costerton, J. W. and Anwar, H. *Pseudomonas aeruginosa*: The microbe and pathogen. In *Pseudomonas Aeruginosa Infections and Treatment*, Baltch, A. L. and Smith, R. P. (Eds.), pp. 1–17, Marcel Dekker, New York (1994).
13. Introduction to biofilms section 1: What are biofilms? In *Center for Biofilm Engineering's Hypertextbook*. http://www.erc.montana.edu/biofilmbook/MODULE_01/Mod01_IntroPage.htm
14. Zelter, N., Characklis, W. G., and Roe, F. L. Discriminating between biofouling and scaling in a deposition monitor. Paper TP239A, Cooling Tower Institute, Houston, TX (1981).
15. Monitoring energy efficiency in electric drive air conditioning systems. Paper presented at *APPA 67th Annual Meeting*, Toronto, Canada (1996).
16. Mortensen, K. P. and Conley, S. N. Film fouling in counterflow cooling towers: Experimental & field results and "Generation II" low-clog pack design. Paper TP98-14, Cooling Tower Institute, Houston, TX (1998).
17. Little, B. J., Wagner, P. A., and Lewandowski, Z. The role of biomineralization in microbial influenced corrosion. CORROSION/1998, Paper No. 294, NACE International, Houston, TX (1998).

18. Licina, G. L. Monitoring biofilm on metallic surfaces in real time. CORROSION/2001, Paper 01442, NACE International, Houston, TX (2001).
19. Bly, A. J. Personal discussions. U.S. Water Services, Edna, MN (May 2000).
20. Miller, J. and Simpson, G. D. Chemical control of *Legionella*. Paper presented at the *Association of Water Technologies (AWT) Annual Conference*, Palm Springs, CA (1999).
21. Minimizing the risk of legionellosis associated with building water systems, ASHRAE Guideline 12-2000. American Society of Heating, Refrigerating and Air-Conditioning Engineers, Atlanta, GA (2000).
22. Legionellosis guideline: Best practices for control of *Legionella*. Cooling Tower Institute, Houston, TX (2006).
23. Guidelines for control of legionnaires' disease. Health Department Victoria, Melbourne, Australia (1989; reprinted in 1999).
24. Control of *Legionella* in cooling towers: Summary guidelines. Wisconsin Division of Health, Wisconsin (August 1987).
25. Freije, M. R. *Legionellae* Control in Health Care Facilities: A Guide for Minimizing Risk. HC Information Resources, Inc., Indianapolis, IN (1996).
26. Utility systems management, Standard EC 1.7. Joint Commission on Accreditation of Healthcare Organizations. <http://www.ashe.org/ashe/codes/jcaho/pdfs/regadv050512legionella.pdf>
27. *Legionella* 2003: An update and statement by the association of water technologies (AWT). Association of Water Technologies, McLean, VA (2003).
28. Kim, B. R., Anderson, J. E., Mueller, S. A., Gaines, W. A., and Kendall, A. M. Literature review: Efficacy of various disinfectants against *Legionella* in water systems. *Water Research*, 36: 4433–4444 (2002).
29. Stout, J. E. New and emerging technologies for legionella control: A multi-step approach to evaluating efficacy. *International Water Conference*, Paper No. IWC-02-02, Engineers' Society of Western Pennsylvania, Pittsburgh, PA (2002).
30. Pukorius, P. R. Cooling tower systems & *Legionella* bacteria: Recent use incidents/outbreaks/causes/corrective actions methods are we making progress? What action should be taken? *International Water Conference*, Paper IWC-99-17, Engineers' Society of Western Pennsylvania, Pittsburgh, PA (1999).
31. Stout, J. E., Yu, V. L., Muraca, P., Joly, J., Troup, N., and Tompkins, L. S. Potable water as a cause of sporadic cases of community acquired Legionnaires' disease. *New England Journal of Medicine*, 326: 151–155 (1992).
32. Sabria, M. and Yu, V. L. Hospital-acquired legionellosis: Solutions for a preventable infection. *The Lancet Infectious Diseases*, 2: 368–373 (2002).
33. For a good website on Legionella issues, see: <http://www.legionella.org/>
34. Bardouniotis, E., Huddleston, W., Ceri, H., and Olson, M. E. Characterization of biofilm growth and biocide susceptibility testing of *Mycobacterium phlei* using the MBEC assay system. *FEMS Microbiology Letters*, 203: 263–267 (2001).
35. Von Rège, H., Sand, W., Bixer, S., et al. Monitoring of biofilm development in process water. CORROSION/2000, Paper No. 00346, NACE International, Houston, TX (2000).
36. Environmental Protection Agency, <http://www.epa.org>.
37. Oxford, A. M. An overview of FIFRA: Regulating the manufacture, sales, and application of biocides. *The Analyst*, 12(1): 35–37 (Winter 2007).
38. For more information, see the following website: <http://ec.europa.eu/environment/biocides>
39. For more information, see the following website: <http://www.hc-sc.gc.ca/cps-spc/pest/index-eng.php>
40. National Pesticide Information Retrieval System, <http://ppis.ceris.purdue.edu/>
41. California Department of Pesticide Regulation, <http://www.cdpr.ca.gov/>
42. Denyer, S. P. Mechanisms of action of antibacterial biocides. *International Biodeterioration and Degradation*, 36: 227–245 (1995).
43. Gerba, C. P. Disinfection. In *Environmental Microbiology*, Maier, R. M., Pepper, I. P., and Gerba, C. P. (Eds.), pp. 543–556, Academic Press, San Diego, CA (2000).
44. Keswick, B. H. Bromine chloride as an alternative disinfectant to chlorine of human enteric viruses and other pathogens in water and wastewater. Doctoral dissertation, University of Hawaii, Ann Arbor, MI (1979).
45. Rusznak, L. H. and Pidane, K. W. Dynamic simulation of biofouling and corrosion recovery. CORROSION/2000, Paper 01275, NACE International, Houston, TX (2000).
46. Ludensky, M. L., Himpler, F. J., and Sweeny, P. G. Control of biofilms with cooling water biocides. CORROSION/1998, Paper No. 522, NACE International, Houston, TX (1998).

47. Nalepa, C. J., Ceri, H., and Stremick, C. A. novel technique for evaluating the activity of biocides against biofilm bacteria. CORROSION/2000, Paper 00347, NACE International, Houston, TX (2000).
48. Nalepa, C. J. and Howarth, J. N. Strategies for effective control of surface-associated microorganisms: A literature perspective, Paper IWC 02-01, Engineers' Society of Western Pennsylvania, Pittsburgh, PA (2002).
49. Tvedt, Jr., T. J. and Wilson, D. A. Effect of chlorination of phosphonates used for scale inhibition in cooling water. CORROSION/1985, Paper No. 126, NACE International, Houston, TX (1985).
50. Ingham, J. W. and Morrison, J. The dissociation constant of hypochlorous acid: Glass-electrode potential determination. *Journal of Chemical Society*, 1200–1205 (1933).
51. Fair, G. M., Morris, J. C., Chang, S. L., Weil, I., and Burden, R. P. The behavior of chlorine as a water disinfectant. *Journal of American Water Works Association*, 40: 1051–1061 (1948).
52. Weber, G. R. and Levine, M. Factors affecting germicidal efficiency of chlorine and chloramines. *American Journal of Public Health*, 32: 719–728 (1944).
53. Nowell, L. A. and Hoigné, J. Photolysis of aqueous chlorine at sunlight and ultraviolet wavelengths—I. Degradation rates. *Water Research*, 26: 593–598 (1992).
54. Scerbo, L., Charkhutian, K., and Go, W. Stability of cooling water treatment chemicals in the presence of alternative oxidants. CORROSION/1993, Paper No. 471, NACE International, Houston, TX (1993).
55. Amjad, Z., Zuhl, R. W., and Zibrida, J. F. The Effect of biocides on deposit control performance. Paper presented at the *Association of Water Technologies (AWT) Annual Conference*, Honolulu, HI (2000).
56. Kessler, S. M. and Kurt, G. Halogen compatible treatment programs for open recirculating cooling water systems. CORROSION/1999, Paper No. 300, NACE International, Houston, TX (1999).
57. White, G. C. *Handbook of Chlorination and Alternative Disinfectants*, 4th edn., John Wiley & Sons, New York (1999).
58. Nalepa, C. J. Oxidizing biocides: Properties and applications. Paper presented at the *Association of Water Technologies (AWT) Annual Conference*, Charlotte, NC (2006).
59. White, G. C. Chemistry of chlorination. In *Handbook of Chlorination and Alternative Disinfectants*, 4th edn., pp. 212–287, John Wiley & Sons, New York (1999).
60. White, G. C. Hypochlorination. In *Handbook of Chlorination and Alternative Disinfectants*, 4th edn., pp. 103–166, John Wiley & Sons, New York (1999).
61. White, G. C. On-site generation of chlorine. In *Handbook of Chlorination and Alternative Disinfectants*, 4th edn., pp. 167–211, John Wiley & Sons, New York (1999).
62. Wojtowicz, J. A. Chloramines and bromamines. In *Kirk-Othmer Encyclopedia of Chemical Technology*, 4th edn., Vol. 5, pp. 911–922, John Wiley & Sons, New York (1993).
63. Fuchs, R. J. and Lichtman, I. A. Stabilization of active chlorine containing solutions. U.S. Patent 2,988,471. FMC Corporation (1961).
64. Nalepa, C. J. 25 years of bromine chemistry in industrial water treatment: A review. CORROSION/2004, Paper No. 04087, NACE International, Houston, TX (2004).
65. Shilov, E. A. and Gladtschikova, J. N. On the calculation of the dissociation constants of hypohalous acids from kinetic data. *Journal of American Chemical Society*, 60: 490–491 (1938).
66. Johannesson, J. K. Anomalous bactericidal action of bromamines. *Nature*, 181: 1799–1800 (1958).
67. White, G. C. Bromine, bromine chloride, and iodine. In *Handbook of Chlorination and Alternative Disinfectants*, 4th edn., pp. 103–166, John Wiley & Sons, New York (1999).
68. Keister, T. Electrolytic bromine: A green biocide for cooling towers. Paper presented at the *80th Annual Water Environment Federation Technical Exhibition and Conference*, Alexandria, VA (2007).
69. Nalepa, C. J., Howarth, J. N., and Moore, R. M. First field trials of a single-feed liquid bromine-based biocide for cooling towers, Paper TP00-09, Cooling Technology Institute Houston, TX (2000).
70. Nalepa, C. J. and Azarnia, F. D. Development of a high activity liquid biocide for industrial water treatment. CORROSION/2006, Paper No. 06096, NACE International, Houston, TX (2006).
71. Nalepa, C. J., Howarth, J. N., and Azarnia, F. D. Factors to consider when applying oxidizing biocides in the field. CORROSION/2002, Paper 02223, NACE International Houston, TX (2002).
72. McCoy, W. F., Allain, E. J., Dallmier, A. W., and Yang, S. Strategies used in nature for microbial fouling control: Application for industrial water treatment. CORROSION/1998, Paper No. 520, NACE International, Houston, TX (1998).
73. Howarth, J. N. and Harvey, M. S. Practical and economic aspects of using highly concentrated liquid bromine biocides. Paper presented at the *Association of Water Technologies (AWT) Annual Conference*, Charlotte, NC (2006).

74. The Presidential Green Chemistry Awards Challenge Program: Summary of 1999 Award Entries and Recipients, EPA744-R-00-001, p. 44, United States Environmental Protection Agency, Washington, DC (March 2000).
75. Spurrell, C. and Clavin, J. S. Solid halogen donor economically answers the challenge of SARA Title III and corrosion concerns. CORROSION/1993, Paper No. 474, NACE International, Houston, TX (1993).
76. Sook, B. R., Ling, T. F., and Harrison, A. D. A new thixotropic form of bromochlorodimethylhydantoin: A case study. CORROSION/2003, Paper No. 03715, NACE International, Houston, TX (2003).
77. Zhang, Z. and Matson, J. V. Organic halogen stabilizers: Mechanisms and disinfection efficiencies. Paper TP89-05, Cooling Tower Institute, Houston, TX (1989).
78. Howarth, J. N. and Nalepa, C. J. A new, bromine-releasing solid for microbiological control of cooling water. Paper IWC-01-05, Engineers' Society of Western Pennsylvania, Pittsburgh, PA (2001).
79. Kuechler, T. C. A Towerbrom[®] progress report. Paper presented at the *Association of Water Technologies (AWT) Annual Conference*, McLean, VA (2007).
80. Chlorine Dioxide. In *Alternate Disinfectants and Guidance Manual*, Document EPA 815-R-99-014. United States Environmental Protection Agency, Washington, DC (April 1999).
81. Byrne, J. and Speronello, B. Biocide controls microbes for water towers beyond target levels. *Industrial Waterworld*, May/June: 41–42 (2006).
82. Block, S. S. Peroxygen compounds. In *Disinfection, Sterilization, and Preservation*, Block, S. S. (Ed.), pp. 167–181, Lea & Febiger, Philadelphia, PA (1991).
83. Coughlin, M. F. and Steimel, L. Performance of hydrogen peroxide as a cooling water biocide and its compatibility with other cooling water inhibitors. CORROSION/1997, Paper No. 397, NACE International, Houston, TX (1997).
84. Curran, H. R., Evans, F. R., and Leviton, A. The sporicidal action of hydrogen peroxide and the use of crystalline catalase to dissipate residual peroxide. *Journal of Bacteriology*, 40: 423–434 (1940).
85. Wichramanayake, G. B. Disinfection and sterilization by ozone. In *Disinfection, Sterilization, and Preservation*, 4th edn., Block, S. S. (Ed.), pp. 182–190, Lea & Febiger, Philadelphia, PA (1991).
86. Peroxone (Ozone/Hydrogen Peroxide). In *Alternate Disinfectants and Guidance Manual*, Document EPA 815-R-99-014. United States Environmental Protection Agency, Washington, DC (April 1999).
87. Grab, L. A. and Theis, A. B. Comparative biocidal efficacy versus sulfate reducing bacteria. CORROSION/1992, Paper No. 9284, NACE International, Houston, TX (1992).
88. Ganzer, G. A., McIlwaine, D. B., Diemer, J. A., Freid, M., and Russo, M. Applications of glutaraldehyde in the control of MIC. CORROSION/2001, Paper 01281, NACE International, Houston, TX (2001).
89. Williams, T. M. Review of isothiazolone biocides in water treatment applications. CORROSION/2004, Paper No. 04083, NACE International, Houston, TX (2004).
90. Wiencek, K. M., Williams, T. M., and Semet, R. F. A new biocide for control of algal biofouling in cooling towers. *Cooling Tower Institute Journal*, 19(2): 56–65 (1998).
91. Sweeny, P. Anionic compatible quats. Paper 07-17, Cooling Technology Institute, Houston, TX (2007).
92. Kramer, J. F., O'Brien, F., and Strba, S. F. A new high performance quaternary phosphonium biocide for microbiological control in oilfield water systems. CORROSION/2008, Paper 08660, NACE International, Houston, TX (2008).
93. Downward, B. L., Talbot, R. E., and Haack, T. K. Tetrakis(hydroxymethyl)phosphonium sulfate (THPS)—A new industrial biocide with low environmental toxicity. CORROSION/1997, Paper No. 97401, NACE International, Houston, TX (1997).
94. Wiatr, C. Control of resistant bacteria in recirculating water systems. Paper TP-05-16, Cooling Technology Institute, Houston, TX (2005).
95. Wiencek, K. M. and Chapman, J. S. Water treatment biocides: How they work and why should you care? CORROSION/1999, Paper 308, NACE International, Houston, TX (1998).
96. Russell, A. D. Antiseptics and disinfectants: Activity, action, and resistance. *Clinical Microbiology Reviews*, 12: 147–179 (1999).
97. Williams, T. M. The mechanism of action of isothiazolone biocides. CORROSION/2006, Paper 06090, NACE International, Houston, TX (1998).
98. Gorman, S. P., Scott, E. M., and Russell, A. D. Antimicrobial activity, uses and mechanism of action of glutaraldehyde. *Journal Applied Bacteriology*, 48(20): 161–190 (1980).
99. Russell, A. D. Antibiotic and biocide resistance in bacteria. *Microbios*, 85: 45–65 (1996).
100. Bienzel, M. Phenomena of biocide resistance in microorganisms. *International Biodeterioration and Biodegradation*, 41: 225–234 (1998).
101. Brözel, V. S., Pietersen, B., and Cloete, T. E. Resistance of bacterial cultures to non-oxidising water treatment bactericides by adaptation. *Water Science and Technology*, 31: 169–175 (1995).

102. Blanchard, A. P., Bird, M. R., and Wright, J. L. Peroxygen disinfection of pseudomonas aeruginosa biofilms on stainless steel disks. *Biofouling*, 13: 233–253 (1998).
103. Willcock, L., Gilbert, P., Holah, J., Wirtanen, G., and Allison, D. G. A new technique for the performance evaluation of clean-in-place disinfection of biofilms. *Journal of Industrial Microbiology*, 25: 235–241 (2000).
104. Rogers, J., Dowsett, A. B., Dennis, P. J., Lee, J. V., and Keevil, C. W. Influence of temperature and plumbing material selection on biofilm formation and growth of *Legionella pneumophila* in a model potable water system containing complex microbial flora. *Applied and Environmental Microbiology*, 60: 1585–1592 (1994).
105. Williams, T. M. and Holz, J. W. Biofouling studies with methylchloro-methylisothiazolone in model cooling systems. CORROSION/1998, Paper 298, NACE International, Houston, TX (1998).
106. Dychdala, G. R. Chlorine and chlorine compounds. In *Disinfection, Sterilization, and Preservation*, 4th edn., Block, S. S. (Ed.), pp. 131–151, Lea & Febiger, Philadelphia, PA (1991).
107. Weber, G. R. and Levine, M. Factors affecting germicidal efficacy of chlorine and chloramines. *American Journal of Public Health*, 32: 719–728 (1944).
108. Rudolph, A. S. and Levine, M. Factors affecting the germicidal efficiency of hypochlorite solutions. Bulletin 150, Engineering Experimental Station. Iowa State College, Ames, IA (1941).
109. McCoy, W. F., Ridge, J. E., and Lashen, E. S. Efficacy of biocides in a laboratory model cooling tower. CORROSION/86, Paper No. 12, NACE International, Houston, TX (1986).
110. Kull, F. C., Eisman, P. C., Sylwestrowicz, H. D., and Mayer, R.L. Mixtures of quaternary ammonium compounds and long-chain fatty acids as antifungal agents. *Applied Microbiology*, 9: 538–541 (1961).
111. Hsu, J. C. Biocide Composition. U.S. Patent 5,028,620 (1991).
112. Lazonby, J. G. Method and composition for inhibiting growth of microorganisms including peracetic acid and a second biocide. U.S. Patent 5,494,589 (1996).
113. Donofrio, D. K. and Whitekettle, W. K. Biocidal compositions and use thereof containing a synergistic mixture of 2-bromo-2-nitropropane-1,3,-diol and a mixture of 5-chloro-2-methyl-4-isothiazolin-3-one and 2-methyl-4-isothiazolin-3-one. U.S. Patent 4,732,905 (1988).
114. Shema, B. F. and Brink, R. H. Synergistic compositions containing 2,2-dibromo-3-nitrilopropionamide and their use. U.S. Patent 3,929,562 (1975).
115. Clifford, R. P. and Birchall, G. A. Biocide. U.S. Patent 4,539,071 (1985).
116. Lukanich, J. T. A new registered combination of microbicidal actives: Mixed isothiazolinones and a polymeric ionene. Paper presented at the *Association of Water Technologies (AWT) Annual Conference*, Traverse City, MI (1997).
117. Haack, T. K. and Greenley, D. G. Controlling sulfate reducing bacteria by slug dosing with quick kill antimicrobials and by continuous dosing with isothiazolones. U.S. Patent 5,025,491 (1991).
118. Kleina, L. G., Czechowski, M. H., Clavin, J. S., and Whitekettle, W. K. Performance and monitoring of a new nonoxidizing biocide: The study of BNPD/ISO and ATP. CORROSION/1997, Paper No. 403, NACE International, Houston, TX (1997).
119. Wright, J. B. and Michaelopoulis, D. L. Method for inhibiting microbial adhesion on surfaces. U.S. Patent 5,736,058 (1998).
120. Yu, F. P. and McCoy, W. F. Use of linear alkylbenzene sulfonates as a biofouling control agent. U.S. Patent 5,670,055 (1997).
121. Czechowski, M. H. and Whitekettle, K. W. Unique biocidal dispersant removes biofilms and increases biocide efficacy. Paper TP99-16, Cooling Tower Institute, Houston, TX (1999).
122. Beardwood, E. S. and Therrien, J. K. Implications of various dispersants on biofilm clean up processes. CORROSION/1997, Paper No. 301, NACE International, Houston, TX (1999).
123. *Water Analysis Handbook*, 5th edn., Hach Company, Loveland, CO (2008).
124. *Standard Methods for the Examination of Water and Wastewater*, 21th edn., American Public Health Association, Washington, DC (2005).
125. Chalut, J., Small, G., and Peyton, J. Control and monitoring the effectiveness of different biocides with the use of free ATP. CORROSION/1996, Paper No. 276, NACE International, Houston, TX (1996).
126. Borchardt, S. A., Wetegrove, R. L., and Martens, J. D. New approaches to biocide effectiveness monitoring using on-site biocide active analysis, ATP analysis, and on-line dosage monitoring control. CORROSION/1997, Paper No. 466, NACE International, Houston, TX (1997).
127. McCoy, W. M., Downes, E. L., Lasko, T. M., and Neville, M. J. A new field method for enumerating viable *Legionella* and total heterotrophic aerobic bacteria. Paper presented at the *Association of Water Technologies (AWT) Annual Conference*, Colorado Springs, CO (2007).

128. Murga, R., Foster, T. S., Brown, E., Pruckler, J. M., Fields, B. S., and Donlan, R. M. Role of biofilms in the survival of *Legionella pneumophila* in a model potable-water system. *Microbiology*, 147: 3121–3126 (2001).
129. Licina, G. J. Optimizing biocide additions via real time monitoring of biofilms. CORROSION/2004, Paper No. 582, NACE International, Houston, TX (2004).
130. Chatteraj, M., Fehr, M. J., Hatch, S. R., and Allain, E. J. On-line measurement and control of microbiological activity in industrial water systems. CORROSION/2001, Paper 01453, NACE International, Houston, TX (2001).

20 *Legionella* in Water Systems

Yusen E. Lin

CONTENTS

20.1	Introduction.....	411
20.2	<i>Legionella</i> and Infection	412
20.2.1	Source of <i>Legionella</i> Infection.....	412
20.2.2	Minimum Contaminant Level for <i>Legionella</i>	413
20.2.3	Growth-Promoting Conditions for <i>Legionella</i>	413
20.2.4	<i>Legionella</i> in Biofilms.....	413
20.2.5	Water Constituents and Plumbing Materials.....	414
20.2.6	<i>Legionella</i> in Hot Water Storage Tanks.....	414
20.2.7	<i>Legionella</i> and Amoebae	415
20.3	Control of <i>Legionella</i> Colonization in Water Systems	415
20.3.1	Water Safety Plan.....	415
20.3.2	Criteria for Selecting a Disinfection Method.....	416
20.3.3	Monitoring Control Measures.....	416
20.4	Disinfection Methods for <i>Legionella</i> in Water Systems	416
20.4.1	Superheat-and-Flush	416
20.4.2	Hyperchlorination	417
20.4.3	Copper–Silver Ionization	418
20.4.4	Chlorine Dioxide.....	419
20.5	Summary.....	420
	References.....	420

20.1 INTRODUCTION

Safe water is taken for granted in Western industrialized societies. The right to a safe and abundant supply of drinking water for all U.S. communities is ensured in the Safe Drinking Water Act. The monitoring of microbiological and physicochemical quality indicators according to the U.S. Environmental Protection Agency (EPA) or other standards provides the certainty that the water has sufficient quality for human consumption. This standard for drinking water quality remains unchallenged until recently, when drinking water was linked to outbreaks of infectious diseases. Man-made water systems have created public health problems, such as the sick building syndrome and Legionnaires' disease. Numerous studies suggested that large plumbing fixtures found in hospitals, office buildings, apartment complexes, and hotels, provided a reservoir with favorable growth conditions for waterborne pathogens. As water quality and distribution systems deteriorate, on-site supplemental disinfection systems may be required. Environmental engineers are often in a position to design disinfection processes for institutional water systems. This is a challenge for environmental engineers, and will require cooperation between engineers and facility managers for the successful control of these waterborne pathogens.

Since its discovery, Legionnaires' disease has been in the headlines of news media and draws extensive public attention. Extensive research efforts have been invested in cooling towers'

disinfection and maintenance, and the efficacy of biocides has been documented elsewhere [1–4]. Thus, this chapter focuses on *Legionella* in potable water systems that now appears to have more clinical significance.

20.2 LEGIONELLA AND INFECTION

20.2.1 SOURCE OF *LEGIONELLA* INFECTION

Legionnaires' disease (Legionellosis) is a lung infection, or pneumonia, caused by a bacterium named *Legionella pneumophila*. The name *L. pneumophila* was derived from the original outbreak at the 1976 American Legion Convention in Philadelphia [5]. *Legionella* is an aerobic Gram-negative bacterium. The colony is usually glistening and transparent with an internal structure that resembles a moldy cotton ball, and has a cut-glass appearance (Figure 20.1). The rod-shaped cells can be observed under a fluorescent microscope using direct fluorescent antibody (DFA) staining (Figure 20.2). Several studies have ranked *Legionella* among the top four microbial causes of community-acquired pneumonia [6]. Moreover, *Legionella* is responsible for 10%–50% of hospital-acquired pneumonia when a hospital's water system is colonized with the *L. pneumophila*

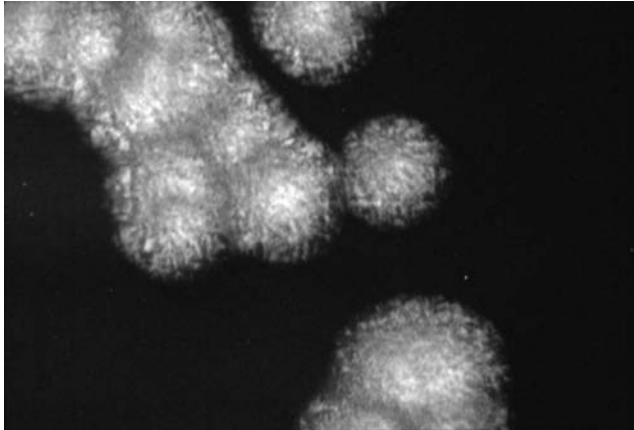


FIGURE 20.1 *Legionella* morphology under 10× microscope.



FIGURE 20.2 *Legionella* under DFA stain.

bacteria [7]. Cases associated with traveling and long-term care facilities are increasingly reported worldwide [8–10]. Community-acquired Legionnaires' diseases have also been described, but the risk of contracting Legionnaires' disease in this setting seems to be very low [6]. Aspiration is now known to be the major mode of transmission, although aerosolization may also occur [7]. The risk factors of acquiring Legionnaires' disease include cigarette smoking, receipt of immunosuppressive therapy, receipt of prior antibiotics, and receipt of a transplant organ. Underlying diseases include chronic obstructive pulmonary diseases.

Legionnaires' disease is not contagious. No special precautions for care providers are necessary. The disease is transmitted via contaminated water, not by infected individuals; unlike SARS and influenza, where masks must be worn. Many antibiotics are highly effective against *Legionella* infection. The two most potent classes of antibiotics are macrolides and quinolones [11,12].

20.2.2 MINIMUM CONTAMINANT LEVEL FOR *LEGIONELLA*

The minimum contaminant level (MCL) for *Legionella* has been proposed by various agencies. For example, the United Kingdom and Netherlands posted a target limit of 100 cfu/L in potable water. Germany and France posted a target limit of 1000 cfu/L in potable water systems for general public. However, there is no clear-cut MCL or infective dose of *Legionella* in humans. For cooling towers, no such dose has been validated based on evidence-based studies. Currently, neither the U.S. CDC nor the U.S. EPA specifies an MCL for *Legionella*. For water distribution systems, the quantitative counts of *Legionella* (i.e., cfu/mL) from the distal fixtures (faucets) do not correlate with the incidence of the disease in hospitals [13,14]. On the other hand, several studies have found that when distal site positivity is 30% or higher, cases of hospital-acquired Legionnaires' disease are likely to occur [15,16]. The complete eradication of *Legionella* from the water system is not necessary to eliminate cases of Legionnaires' disease [16].

20.2.3 GROWTH-PROMOTING CONDITIONS FOR *LEGIONELLA*

Legionella can be found in natural environments [17–20] and man-made environments [17, 21–32]. Water systems in hospitals [27,29,32–40], hotels [41], nursing homes [42], industrial plants [43–45], and homes [20,46,47] have been linked to disease. Although cooling towers were initially reported to be an important reservoir, virtually all of those reports were published in an era prior to the discovery that potable water could also be the source [48].

Legionnaires' disease emerged because of the human alteration of the environment, since *Legionella* species are found in aquatic environments, and grow in warm water and warm, damp places, such as cooling towers and hot water recirculating systems. *Legionella* organisms are readily found in natural aquatic bodies, and some species have been recovered from soil [49]. The organisms can survive in widely varying conditions, including temperatures of 0°C–63°C, a pH of 5.0–8.5, and dissolved oxygen concentrations as low as 0.2 ppm in water. Temperature is a critical determinant for *Legionella* proliferation. Colonization of hot water tanks is more likely if temperatures are between 40°C and 50°C (104°F–122°F). *Legionella* and other microorganisms become attached to surfaces in an aquatic environment forming a biofilm. *Legionella* has been shown to attach to and colonize various materials found in water systems, including plastics, rubber, and wood. Organic sediment scales and inorganic precipitates provide *Legionella* with a surface for attachment and a protective barrier.

20.2.4 *LEGIONELLA* IN BIOFILMS

Legionella and other microorganisms can attach to surfaces submerged in an aquatic environment, which forms a biofilm. The biofilm facilitates nutrient and gaseous exchange, and protects microorganisms not only from biocides but also from periodic increases in temperature and attempts at

physical removal, especially in areas where surfaces are scaled or corroded. These biofilms are found on the surface of pipes, distal sites, and stagnant areas of any water distribution system. *Legionella* has been documented to colonize the surfaces of plumbing materials in concentrations up to 10^5 cfu/cm² [50]. A disruption to the biofilm after water pressure changes associated with construction may cause brown water and dramatically increase the *Legionella* concentration [51]. In addition to facilitating growth, the presence of a biofilm can also interfere with the disinfection process. Bacteria in biofilms are more resistant to biocides than planktonic (freely suspended) bacteria. For example, *Legionella* attached to a stainless-steel surface were 135 times more resistant to iodine than freely suspended *Legionella*, and 210,000 times more resistant than agar-grown strains [52]. Biofilms can also protect microorganisms from disinfectants and harsh environmental conditions, such as elevated water temperatures. Some chemical disinfectants such as chlorine are even rendered inactive by the organic constituents of biofilms. The presence of *Legionella* in the biofilms throughout building water systems may explain the rapid recolonization despite the application of the superheat-and-flush procedure or shock hyperchlorination [53].

20.2.5 WATER CONSTITUENTS AND PLUMBING MATERIALS

The presence of *Legionella* in hot water systems has been associated with the physicochemical constituents of the water and certain plumbing materials. Higher concentrations of calcium and magnesium in water, the main components of scales and sediments, were found to be associated with the presence of *L. pneumophila* in hot water tank samples in a prospective study among 15 hospitals [54]. Higher iron concentration is also associated with lower *Legionella* colonization from a 16-hospital study [23].

Various materials found in water systems may support or promote the growth of *Legionella*. Shock absorbers installed within water lines can be a reservoir for *Legionella*. After removal of these shock absorbers, the percent of tap water samples that were positive for *Legionella* dropped from 20% to 5%. Investigators suggested that the presence of *L. pneumophila* in hot water distribution systems was due to the designs of shower and tap fittings, which allowed water to be trapped behind rubber washers and gaskets. These rubber fittings were shown to support the growth of *Legionella* [55]. The replacement of these rubber materials with suitable alternatives was reported to have eradicated *Legionella* from the fittings [55]. In a model cooling tower system, higher counts of biofilm-associated *Legionella* were recovered from galvanized steel surfaces than plastic polymer surfaces [56].

However, there are reports that contradict these findings. Biofilm formation would eventually build up on the surfaces where microorganisms are not affected by the surface of the materials. For example, *Legionella* was still recovered in a water system that replaced rubber washers with nitrile washers [57]. It is unclear that the simple removal of rubber washers or gaskets or a change of plumbing materials can eliminate the growth of *Legionella*, since *Legionella* can colonize a variety of plumbing materials, including plastics such as polyvinyl chloride (PVC); stainless steel; wood; and, to a lesser degree, copper [50]. The maximum accumulation of *Legionella* occurred on plastics at 40°C [50].

20.2.6 LEGIONELLA IN HOT WATER STORAGE TANKS

Early investigations found higher concentrations of *Legionella* in hot water lines compared to cold water lines. The highest concentrations of *Legionella* were recovered from water collected from the bottom of hot water storage tanks [54]. This led to the early investigation of *Legionella* in hot water storage tanks. Since then, various factors were defined that promoted the growth of *Legionella* in water distribution systems, including hot water temperatures less than 60°C, physicochemical factors, water system materials and design, and commensal microflora. Since the current understanding now includes the concept of biofilms, hot water tanks are only one component of a distribution system, which is a niche for many microorganisms, including *Legionella*.

The large water distribution systems and high-volume hot water storage tanks of hospitals provide *Legionella* with optimal conditions for growth: warm temperatures, nutrients in the form of sediments and biofilms, and commensal microorganisms. In vivo studies using a model plumbing system, *L. pneumophila* was able to survive and/or grow at temperatures of 20°C, 40°C, and 50°C, but was not recovered at 60°C [58]. Plouffe et al. found that hot water tank samples with temperatures of 50°C or less were significantly more likely to be positive for *Legionella* [59]. Similar associations with temperatures less than 60°C were also demonstrated in surveys of hospitals in Quebec [60] and western Pennsylvania [54]. These studies suggested that the average hot water storage temperature (45°C–50°C) in hospitals is ideal for *L. pneumophila* colonization.

The configuration of hot water storage tanks has also been predictive of *L. pneumophila* contamination. Vertical tanks were more likely to be contaminated than horizontal tanks; 79% of vertical hot water tanks were contaminated with *L. pneumophila* while only 29% of horizontal tanks were contaminated with *L. pneumophila* [54]. Furthermore, older tanks were found to be contaminated with *L. pneumophila* while newer tanks (less than 5 years) were generally free of *L. pneumophila* [54,60]. This may be the result of the accumulation of scales and sediments in the older systems after years of service. However, cases of Legionnaires' disease have also been diagnosed in newly constructed hospitals [61].

20.2.7 LEGIONELLA AND AMOEBAE

Other bacteria and protozoa also colonize plumbing surfaces, some of which have been shown to promote *Legionella* replication. Rowbotham was the first to report the relationship between amoebae and *Legionella* [62]; it has subsequently been confirmed that *Legionella* are facultative intracellular parasites. Amoebae and other ciliated protozoa are natural hosts for *Legionella* [63]. *Legionella* are known to infect five different genera of amoebae, most notably, *Hartmannella vermiformis* and *Acanthamoeba* spp. *Legionella* can also multiply within the ciliated protozoa *Tetrahymena* spp. [64]. Bacterial species that appear to provide *Legionella* with growth-promoting factors include *Pseudomonas* spp., *Acinetobacter* spp., *Flavobacterium*, and *Alcaligenes* spp. Amoebae also help to protect *Legionella* from the effects of biocides [65] and heat eradication [66].

20.3 CONTROL OF LEGIONELLA COLONIZATION IN WATER SYSTEMS

20.3.1 WATER SAFETY PLAN

If cases of Legionnaires' disease can be epidemiologically linked to a source of *Legionella*, the control of *Legionella* in such a source can prevent further cases. The World Health Organization (WHO) [67] and the U.S. CDC [68] both provide guidelines on preventive measures for *Legionella* control. WHO promotes the idea of water safety plan (WSP) [69]. WSP is an approach to manage specific health risks due to exposure to *Legionella* from water systems. This plan includes the following three components [69]:

1. Assessment: to determine whether the water supply chain (up to the point of consumption) can deliver water of a quality that meets health-based targets. This also includes the assessment of the design criteria of new systems.
2. Monitoring: to identify the control measures in a drinking water system that will collectively control identified risks and ensure that health-based targets are met. For each control measure identified, the appropriate means of monitoring should be defined (e.g., biocide levels, temperature, and pH), which ensure that any deviation from the required performance is rapidly detected.
3. Management: to list the actions to be taken during routine operation or incident conditions, and for documenting the system assessment (including upgrading and improvement), monitoring and communication plans, and supporting programs.

The primary objectives of a WSP are the minimization of contamination of source waters, the reduction or removal of contamination through treatment processes, and the prevention of contamination during storage, distribution, and handling of drinking water. The Allegheny County Health Department, Pennsylvania, provides the most comprehensive guidelines, which are a template for many state guidelines [70]. In a study of 110 hospitals and long-term care facilities in western Pennsylvania, investigators found a significant decrease in the number of health care–acquired cases between the pre-guideline (33%) and post-guideline (9%) periods in hospitals [71].

20.3.2 CRITERIA FOR SELECTING A DISINFECTION METHOD

Using the evidence-based approach, Stout and Yu have postulated the evaluation criteria for recommending the disinfection methods. The criteria include: (a) demonstrated efficacy of *Legionella* eradication in vitro using laboratory assays, (b) anecdotal experiences in preventing Legionnaires' disease in individual hospitals, (c) controlled studies in individual hospitals, and (d) validation in confirmatory reports from multiple hospitals for a prolonged time [72]. These objective criteria for the demonstration of efficacy will assist building engineers and facility managers in making cost-effective choices based on scientific criteria.

20.3.3 MONITORING CONTROL MEASURES

Routine environmental surveillance for *Legionella* is the only method to determine if a control measure for *Legionella* eradication is successful. A number of methods have been used to detect *Legionella* in the environment. These include culture on selective media with or without acid pretreatment, DFA, enzyme immunoassay (EIA), immunochromatographic test (ICT), and polymerase chain reaction (PCR). Culture has been shown to be the most sensitive method for the detection of *Legionella* in environmental samples. One apparent disadvantage of DFA, EIA, ICA, and PCR tests is that they detect both viable and nonviable *Legionella* bacteria. These tests can be positive even though the *Legionella* bacterium has been inactivated by chemical biocides or heat [73,74]. False-positive readings could lead to the implementation of unnecessary and expensive emergency decontamination procedures by the engineering and management staff.

20.4 DISINFECTION METHODS FOR *LEGIONELLA* IN WATER SYSTEMS

Four major disinfection methods for *Legionella* in potable water systems, as summarized in Table 20.1, are discussed in this section in the chronological order of their application. These methods provide residual protection throughout the water system. They are superheat-and-flush, hyperchlorination, copper–silver ionization, and chlorine dioxide.

20.4.1 SUPERHEAT-AND-FLUSH

Superheat-and-flush was the first documented method used for the eradication of *Legionella* in water systems. This method requires no special equipment, so it can be conducted as an emergency decontamination procedure in an outbreak situation. Disinfection is only temporary, and the recolonization of *Legionella* has been reported followed by new cases of Legionnaires' disease [75,76].

Superheat-and-flush requires that hot water tank temperatures be elevated to 70°C (158°F), followed by flushing of all water outlets, faucets, and showerheads with a hot water temperature of ≥60°C for a minimum of 30 min to kill *Legionella* [77]. If this temperature is not achieved and maintained, the procedure is likely to fail. After the flush, selected sites are required to re-culture to validate the efficacy; if no *L. pneumophila* is recovered, the procedure is considered completed. If *L. pneumophila* is isolated, the entire heat and flush protocol needs to be repeated. Scalding can

TABLE 20.1
Summary of Disinfection Methods for *Legionella* in Potable Water Systems

Hyperchlorination	Condition	Superheat-and-Flush	Copper-Silver Ionization	Chlorine Dioxide
2–4 ppm as free chlorine	Concentration	60°C for 30 min	Cu = 0.2–0.8 ppm Ag = 0.02–0.08 ppm	0.5–1 ppm as ClO ₂
Residuals decrease as temperature increases	Water temperature	Not applicable	Residuals unaffected	Residuals decrease as temperature increases
Elevated pH (>8.0) affects efficacy	pH	No effect	Elevated pH (>8.5) may affect efficacy	No effect
Trihalomethanes (THMs)	Disinfection by-product	None	None known	Chlorate and chlorite
Yes	Taste and odor	No	None	Minimal at high concentrations
Carcinogenic by-products	Environmental and health concerns	Scalding possible	Resistance to ions ^a	High chlorite may cause congenial defects
Corrosion control, chlorine storage, concentration control and monitoring	Maintenance issues	Labor intensive	Scale control, routine electrode cleaning, routine ion monitoring	Concentration control, chlorate and chlorite monitoring

^a Mietzner, M. et al., Reduced susceptibility of *Legionella pneumophila* to the antimicrobial effects of copper and silver ions. In: *45th Interscience Conference on Antimicrobial Agents and Chemotherapy*, Washington, DC, 2005.

occur with hot tap water at 60°C, although it has not been reported by hospitals using this method. Posted signs and newsletters may prevent scalding incidents.

Maintaining the hot water temperature at 60°C after the superheat-and-flush disinfection has been successful in minimizing *Legionella* recolonization with a subsequent disappearance of hospital-acquired Legionnaires' disease. Two hospitals reported that after maintaining the hot water temperature at 60°C, only two cases of hospital-acquired Legionnaires' disease were diagnosed in the subsequent 2 years [78,79]. A follow-up study showed that maintaining the hot water temperature above 55°C was satisfactory in controlling hospital-acquired Legionnaires' disease; only four cases of Legionnaires' disease were diagnosed over a 10 year prospective surveillance [80]. Some states regulate the temperature for water discharged from the hospital and prohibit water temperatures above 43.3°C (110°F) at the outlet. Institutions should consult local and state water authorities before implementing this method.

20.4.2 HYPERCHLORINATION

Hyperchlorination is a method recommended by the U.S. CDC to control *Legionella* [68]. Chlorine is a strong oxidizing agent that has been successfully used for a number of years as a disinfectant for controlling pathogens in domestic drinking water. Two approaches have been applied with regard to *Legionella* disinfection: shock hyperchlorination and continuous hyperchlorination. Shock hyperchlorination is used by a pulse injection of chlorine in water to achieve a concentration of chlorine at 20–50 ppm throughout the system [81]. After a period of time, the water is drained and the system is mixed with the incoming water so that the residual chlorine level returns to its normal concentration (0.5–1 ppm). Continuous hyperchlorination is accomplished by a continuous injection of additional chlorine, which may be introduced via calcium hypochlorite, sodium hypochlorite, or gas chlorination. Residual chlorine levels will fluctuate because of changes in the



FIGURE 20.3 Pipe corrosion due to hyperchlorination.

incoming water quality and flow rate variation. If the system has areas of stagnation or low usage, or if there are recirculation problems within the water distribution system, chlorine will not inactivate *Legionella* in these areas. Qualified maintenance personnel are needed to conduct monitoring programs and perform residual disinfectant analysis.

However, continuous hyperchlorination has been used with variable success to control the growth of *Legionella* [76,82]. *Legionella* attached to a pipe surface are more resistant to chlorine. Inactivation and suppression of *L. pneumophila* requires chlorine levels of greater than 3 ppm, while the residual level in domestic water is usually less than 1.0 ppm [58]. In addition, chlorine is unstable at elevated water temperatures and undergoes spontaneous decomposition to chloride ions. The major disadvantage of hyperchlorination is that chlorine is highly corrosive and causes significant pipe damage (Figure 20.3). The average number of pipe leaks can increase from 30 times pre-chlorination to 3 years post-chlorination [82]. Although the rate of pipe leaking can be lowered by chemically coating all hot water pipes with a sodium silicate precipitate, the initial and yearly maintenance costs are high (e.g., \$10,000/year). Furthermore, leaks continued to occur at a rate of one to three leaks per month even after the pipes were coated with silicates at a university hospital in Iowa [82].

In addition, high residual chlorine may react with organic materials and accelerate the production of trihalomethanes and other disinfection by-products, some of which are known carcinogens. Numerous epidemiological studies found a positive association between the consumption of chlorinated water and cancer. For example, results derived from 10 epidemiological studies [83] show a higher risk estimate for cancer with exposure to chlorinated water as compared to controls. These studies also showed a significant association between neoplastic diseases and consumption of water containing chlorination by-products. In summary, hyperchlorination may not be an ideal disinfection method for *Legionella* in water systems.

20.4.3 COPPER–SILVER IONIZATION

Copper–silver ionization is the only disinfection method with documented consistent efficacy from multiple field evaluations. The efficacy of copper–silver ionization in eradicating *Legionella* from hospital water distribution systems has been documented by numerous investigators worldwide [72]. The ions are generated from a flow cell containing copper–silver alloy electrodes. The flow cells are usually installed in the hot water return line proximal to the hot water tank for hot water treatment, or in the cold water storage tank for both hot and cold water treatments. The concentration of



FIGURE 20.4 Scale built up on copper–silver electrodes in a poorly maintained flow cell.

copper and silver ions ($\text{Cu} = 0.2\text{--}0.8\text{ mg/L}$; $\text{Ag} = 0.02\text{--}0.08\text{ mg/L}$) is controlled by a programmable power supply. A minimum quarterly maintenance of flow cells is required to remove scales from the electrodes for optimal performance (Figure 20.4).

The first controlled evaluation in a water distribution system was in a hospital in Pittsburgh, Pennsylvania [84]. When copper and silver ion concentrations were above 0.4 and 0.04 mg/L , respectively, the distal site colonization of *Legionella* declined to zero within 3 months; however, lower ion concentrations have been effective, as documented by other investigators [85,86]. A 16-hospital survey also documented the long-term efficacy and the robustness of copper–silver ionization with 5–11 years of experience [72]. After the installation of ionization systems, distal site positivity was well controlled and no new cases of hospital-acquired Legionnaires’ disease had occurred in any of these hospitals since 1995. Furthermore, the efficacy of ionization has also been documented in a long-term care facility [61], an office building [87], and an apartment building [88]. Today, more than 200 hospitals worldwide have adopted copper–silver ionization as the primary *Legionella* disinfection control measure. Thirty-two percent (12/38) of the 1998 U.S. National Nosocomial Infections Surveillance hospitals had instituted ionization as a disinfection measure [89].

The EPA has a maximum containment level for copper in drinking water of 1.3 mg/L . Silver has a secondary (nonenforceable) limit of 0.1 mg/L . Monitoring for ions on a prescribed schedule has been mandated by the State of Texas. Furthermore, a recent ruling by the U.S. EPA requires the manufacturers of copper–silver ionization systems to “register” the ions as an approved biocide for use in potable water [90]. The EPA will allow ionization manufacturers to continue to offer the system while waiting for the approval [90].

20.4.4 CHLORINE DIOXIDE

Chlorine dioxide is a soluble gas and a known biocidal disinfectant against waterborne pathogens. Unlike chlorine, its low oxidation potential allows chlorine dioxide to penetrate biofilms without loss of biocidal activity. The use of chlorine dioxide for the control of *Legionella* in hospital water systems is relatively new. Although chlorine dioxide has been used for potable water treatment in Europe since the 1940s, it was not widely adopted because the generation of chlorine dioxide involved the mixture of chlorite (as NaClO_2), and a strong acid (HOCl), which posed a danger of explosion as it quickly dissociates into chlorine gas, oxygen gas, and heat. Since the 1990s, a new electrolytic process has allowed the on-site generation of chlorine dioxide to be safe in smaller

quantities. More recently, alternatives to on-site generation of chlorine dioxide are available for direct injection. Consequently, disinfection of water systems using chlorine dioxide has now become a viable option and is being increasingly applied worldwide.

The first controlled evaluation of chlorine dioxide in the United States to control *L. pneumophila* was conducted in a hospital that had cases of hospital-acquired Legionnaires' disease [91]. Chlorine dioxide was injected into a 500,000 gallon reservoir that provided water to 23 adjacent buildings. A period of 1.7 years was necessary to demonstrate complete eradication of *L. pneumophila*. Residual chlorine dioxide in the hot water was below the concentration required for efficacy; the average residual chlorine dioxide in hot water taps (0.08 mg/L) was significantly less than that measured in the reservoir (0.68 mg/L). Nevertheless, no new cases of hospital-acquired Legionnaires' disease were detected [91].

Based on studies from Europe and the United States, complete eradication of *Legionella* (0% site positivity) has not been reported when the study duration was less than 6 months [92–94]. Two studies, with longer periods of use (3–6 years), also failed to eradicate *Legionella* from the water distribution systems [95,96]. It is clear that maintaining a sufficient residual concentration of chlorine dioxide (ClO_2) in hot water systems is challenging. Elevated water temperatures accelerate the conversion of chlorine dioxide to chlorite (ClO_2 to ClO_2^-) by reactions with organic compounds in the water system, as observed in a control study.

The use of chlorine dioxide in potable water is highly regulated because chlorine dioxide and its disinfection by-products, chlorite (ClO_2^-) and chlorate (ClO_3^-) ions, may pose a health risk to consumers. Chlorite may cause congenital cardiac defects and hemolytic anemia through oxidative damage to the red blood cell membrane. The U.S. EPA has set the maximum residual disinfectant level (MRDL) for ClO_2 of 0.8 mg/L and the MCL for ClO_2^- of 1.0 mg/L [97]. Chlorate is currently not regulated due to the lack of health data to set the MCL. The United Kingdom Drinking Water Inspectorate specifies a maximum value of 0.5 mg/L for the total oxidants in drinking water that is the combined concentration of chlorine dioxide, chlorite, and chlorate. Chlorine dioxide is considered a safe and promising method; however, it has not yet fulfilled all the four criteria required for the validation of efficacy [72,98]. Based on numerous studies, a minimum chlorine dioxide residual of approximately 0.5–0.8 mg/L must be maintained throughout the water systems to effectively control *Legionella*.

20.5 SUMMARY

Prevention of Legionnaires' disease can be achieved by disinfecting water systems. A successful WSP can assist facility managers to assess, monitor, and manage the risk associated with *Legionella* in water systems. If disinfection is necessary, copper–silver ionization appears to be the best available technology today given its documented efficacy. Chlorine dioxide is undergoing multicenter evaluation for *Legionella* eradication, and may be promising. Superheat-and-flush can be used in outbreak situations to halt the nosocomial transmission. Hyperchlorination is no longer the preferable method due to its various limitations, as discussed in this chapter.

REFERENCES

1. Ozlem Sanli-Yurudu, N., Kimiran-Erdem, A., and Cotuk, A. Studies on the efficacy of chloramine t trihydrate (n-chloro-p-toluene sulfonamide) against planktonic and sessile populations of different *Legionella pneumophila* strains. *Int J Hyg Environ Health* 210, 147–153 (2007).
2. Bentham, R. H. and Broadbent, C. R. Field trial of biocides for control of *Legionella* in cooling towers. *Curr Microbiol* 30, 167–172 (1995).
3. Bartolome, M. C. and Sanchez-Fortun, S. Effects of selected biocides used in the disinfection of cooling towers on toxicity and bioaccumulation in artemia larvae. *Environ Toxicol Chem* 24, 3137–3142 (2005).
4. Turetgen, I. Comparison of the efficacy of free residual chlorine and monochloramine against biofilms in model and full scale cooling towers. *Biofouling* 20, 81–85 (2004).

5. Fraser, D. W., Tsai, T. R., Orenstein, W., et al. Legionnaires' disease: Description of an epidemic of pneumonia. *N Engl J Med* 297, 1189–1197 (1977).
6. Pedro-Botet, M. L., Stout, J. E., and Yu, V. L. Legionnaires' disease contracted from patient homes: The coming of the third plague? *Eur J Clin Microbiol Infect Dis* 21, 699–705 (2002).
7. Sabria, M. and Yu, V. L. Hospital-acquired legionellosis: Solutions for a preventable infection. *Lancet Infect Dis* 2, 368–373 (2002).
8. Anonymous. Legionnaires disease associated with potable water in a hotel—Ocean City, Maryland, October 2003–February 2004. *MMWR Morb Mortal Wkly Rep* 54, 165–168 (2005).
9. Ricketts, K. D., McNaught, B., and Joseph, C. A. Travel-associated legionnaires' disease in Europe: 2004. *Euro Surveill* 11, 107–110 (2006).
10. Seenivasan, M. H., Yu, V. L., and Muder, R. R. Legionnaires' disease in long-term care facilities: Overview and proposed solutions. *J Am Geriatr Soc* 53, 875–880 (2005).
11. Yu, V. L., Greenberg, R. N., Zadeikis, N., et al. Levofloxacin efficacy in the treatment of community-acquired legionellosis. *Chest* 125, 2135–2139 (2004).
12. Plouffe, J. F., Breiman, R. F., Fields, B. S., et al. Azithromycin in the treatment of *Legionella* pneumonia requiring hospitalization. *Clin Infect Dis* 37, 1475–1480 (2003).
13. Kool, J. L., Bergmire-Sweat, D., Butler, J. C., et al. Hospital characteristics associated with colonization of water systems by *Legionella* and risk of nosocomial legionnaires' disease: A cohort study of 15 hospitals. *Infect Control Hosp Epidemiol* 20, 798–805 (1999).
14. Boccia, S., Laurenti, P., Borella, P., et al. Prospective 3-year surveillance for nosocomial and environmental *Legionella pneumophila*: Implications for infection control. *Infect Control Hosp Epidemiol* 27, 459–465 (2006).
15. Stout, J. E., Muder, R. R., Mietzner, S., et al. Role of environmental surveillance in determining the risk of hospital-acquired legionellosis: A national surveillance study with clinical correlations. *Infect Control Hosp Epidemiol* 28, 818–824 (2007).
16. Yu, V. L. Resolving the controversy on environmental cultures for *Legionella*: A modest proposal. *Infect Control Hosp Epidemiol* 19, 893–897 (1998).
17. Zinecker, H., Gutjahr, R., Maucher, H., and Breitenstein, A. Detection and identification of *Legionella* spp. From man-made water systems and aquatic environments. *Int J Med Microbiol* 297, 15–15 (2007).
18. Lin, Y. E., Lu, W. M., Huang, H. I., and Huang, W. K. Environmental survey of *Legionella pneumophila* in hot springs in Taiwan. *J Toxicol Environ Health A* 70, 84–87 (2007).
19. Gast, R. J., Moran, D. M., Dennett, M. R., Rocca, J., and Amaral-Zettler, L. Amoebae from saline environments harbor *Legionella* species. *J Phycol* 43, 6–6 (2007).
20. Chen, Y. S., Lin, W. R., Liu, Y. C., et al. Residential water supply as a likely cause of community-acquired legionnaires' disease in an immunocompromised host. *Eur J Clin Microbiol Infect Dis* 21, 706–709 (2002).
21. Leoni, E., Legnani, P. P., Bucci Sabattini, M. A., and Righi, F. Prevalence of *Legionella* spp. In swimming pool environment. *Water Res* 35, 3749–3753 (2001).
22. Stout, J. E., Yu, V. L., Yee, Y. C., et al. *Legionella pneumophila* in residential water supplies: Environmental surveillance with clinical assessment for legionnaires' disease. *Epidemiol Infect* 109, 49–57 (1992).
23. Yu, P. Y., Lin, Y. E., Lin, W. R., et al. The high prevalence of *Legionella pneumophila* contamination in hospital potable water systems in Taiwan: Implications for hospital infection control in Asia. *Int J Infect Dis* 12 (4), 416–420 (2008).
24. Veronesi, L., Capobianco, E., Affanni, P., et al. *Legionella* contamination in the water system of hospital dental settings. *Acta Biomed* 78, 117–122 (2007).
25. Tanzi, M. L., Capobianco, E., Affanni, P., et al. *Legionella* spp. In hospital dental facilities. *J Hosp Infect* 63, 232–234 (2006).
26. Fujimura, S., Oka, T., Tooi, O., et al. Detection of *Legionella pneumophila* serogroup 7 strain from bathwater samples in a Japanese hospital. *J Infect Chemother* 12, 105–108 (2006).
27. Perola, O., Kauppinen, J., Kusnetsov, J., et al. Persistent *Legionella pneumophila* colonization of a hospital water supply: Efficacy of control methods and a molecular epidemiological analysis. *APMIS* 113, 45–53 (2005).
28. Leoni, E., De Luca, G., Legnani, P. P., et al. *Legionella* waterline colonization: Detection of *Legionella* species in domestic, hotel and hospital hot water systems. *J Appl Microbiol* 98, 373–379 (2005).
29. Darelid, J., Bernander, S., Jacobson, K., and Lofgren, S. The presence of a specific genotype of *Legionella pneumophila* serogroup 1 in a hospital and municipal water distribution system over a 12-year period. *Scand J Infect Dis* 36, 417–423 (2004).
30. Abdul Samad, B. H., Suhaili, M. R., Baba, N., and Rajasekaran, G. Isolation of *Legionella pneumophila* from hospital cooling towers in Johor, Malaysia. *Med J Malaysia* 59, 297–304 (2004).

31. Kusnetsov, J., Torvinen, E., Perola, O., Nousiainen, T., and Katila, M. L. Colonization of hospital water systems by *Legionellae*, mycobacteria and other heterotrophic bacteria potentially hazardous to risk group patients. *APMIS* 111, 546–556 (2003).
32. Legnani, P. P., Leoni, E., and Corradini, N. *Legionella* contamination of hospital water supplies: Monitoring of private healthcare facilities in Bologna, Italy. *J Hosp Infect* 50, 220–223 (2002).
33. Triassi, M., Di Popolo, A., Ribera D’Alcala, G., et al. Clinical and environmental distribution of *Legionella pneumophila* in a university hospital in Italy: Efficacy of ultraviolet disinfection. *J Hosp Infect* 62, 494–501 (2006).
34. Qasem, J. A., Mustafa, A. S., and Khan, Z. U. *Legionella* in clinical specimens and hospital water supply facilities: Molecular detection and genotyping of the isolates. *Med Princ Pract* 17, 49–55 (2008).
35. Garcia-Nunez, M., Sopena, N., Ragull, S., et al. Persistence of *Legionella* in hospital water supplies and nosocomial legionnaires’ disease. *FEMS Immunol Med Microbiol* 52, 202–206 (2008).
36. Scaturro, M., Dell’eva, I., Helfer, F., and Ricci, M. L. Persistence of the same strain of *Legionella pneumophila* in the water system of an Italian hospital for 15 years. *Infect Control Hosp Epidemiol* 28, 1089–1092 (2007).
37. Galli, M. G., Tesauro, M., Bianchi, A., Pregliasco, F., and Consonni, M. 5-Year surveillance for *Legionella pneumophila* and comparison of disinfection methods in two hospitals of Milan. *Ann Ig* 19, 533–540 (2007).
38. Johansson, P. J., Andersson, K., Wiebe, T., Schalen, C., and Bernander, S. Nosocomial transmission of *Legionella pneumophila* to a child from a hospital’s cold-water supply. *Scand J Infect Dis* 38, 1023–1027 (2006).
39. Ditommaso, S., Biasin, C., Giacomuzzi, M., et al. Colonization of a water system by *Legionella* organisms and nosocomial legionellosis: A 5-year report from a large Italian hospital. *Infect Control Hosp Epidemiol* 27, 532–535 (2006).
40. Tercelj-Zorman, M., Seljak, M., Stare, J., et al. A hospital outbreak of *Legionella* from a contaminated water supply. *Arch Environ Health* 59, 156–159 (2004).
41. Cowgill, K. D., Lucas, C. E., Benson, R. F., et al. Recurrence of legionnaires disease at a hotel in the united states virgin islands over a 20-year period. *Clin Infect Dis* 40, 1205–1207 (2005).
42. Loeb, M., McGeer, A., McArthur, M., et al. Surveillance for outbreaks of respiratory tract infections in nursing homes. *CMAJ* 162, 1133–1137 (2000).
43. Nygard, K., Werner-Johansen, O., Ronsen, S., et al. An outbreak of legionnaires disease caused by long-distance spread from an industrial air scrubber in Sarpsborg, Norway. *Clin Infect Dis* 46, 61–69 (2008).
44. O’Keefe, N. S., Heinrich-Morrison, K. A., and McLaren, B. Two linked cases of legionellosis with an unusual industrial source. *Med J Aust* 183, 491–492 (2005).
45. Fry, A. M., Rutman, M., Allan, T., et al. Legionnaires’ disease outbreak in an automobile engine manufacturing plant. *J Infect Dis* 187, 1015–1018 (2003).
46. Luck, P. C., Schneider, T., Wagner, J., et al. Community-acquired legionnaires’ disease caused by *Legionella pneumophila* serogroup 10 linked to the private home. *J Med Microbiol* 57, 240–243 (2008).
47. Den Boer, J. W., Nijhof, J., and Friesema, I. Risk factors for sporadic community-acquired legionnaires’ disease. A 3-year national case-control study. *Public Health* 120, 566–571 (2006).
48. Yu, V. L. Cooling towers and legionellosis: A conundrum with proposed solutions. *Int J Hyg Environ Health* 211, 229–234 (2008).
49. Wallis, L. and Robinson, P. Soil as a source of *Legionella pneumophila* serogroup 1 (lp1). *Aust N Z J Public Health* 29, 518–520 (2005).
50. Rogers, J., Dowsett, A. B., Dennis, P. J., Lee, J. V., and Keevil, C. W. Influence of temperature and plumbing material selection on biofilm formation and growth of *Legionella pneumophila* in a model potable water system containing complex microbial flora. *Appl Environ Microbiol* 60, 1585–1592 (1994).
51. Mermel, L. A., Josephson, S. L., Giorgio, C. H., Dempsey, J., and Parenteau, S. Association of legionnaires’ disease with construction: Contamination of potable water? *Infect Control Hosp Epidemiol* 16, 76–81 (1995).
52. Cargill, K. L., Pyle, B. H., Sauer, R. L., and McFeters, G. A. Effects of culture conditions and biofilm formation on the iodine susceptibility of *Legionella pneumophila*. *Can J Microbiol* 38, 423–429 (1992).
53. Levin, A. S., Gobara, S., Scarpitta, C. M., et al. Electric showers as a control measure for *Legionella* spp. In a renal transplant unit in Sao Paulo, Brazil. Legionellosis study team. *J Hosp Infect* 30, 133–137 (1995).
54. Vickers, R. M., Yu, V. L., Hanna, S. S., et al. Determinants of *Legionella pneumophila* contamination of water distribution systems: 15-hospital prospective study. *Infect Control* 8, 357–363 (1987).

55. Colbourne, J. S., Pratt, D. J., Smith, M. G., Fisher-Hoch, S. P., and Harper, D. Water fittings as sources of *Legionella pneumophila* in a hospital plumbing system. *Lancet* 1, 210–213 (1984).
56. Turetgen, I. and Cotuk, A. Monitoring of biofilm-associated *Legionella pneumophila* on different substrata in model cooling tower system. *Environ Monit Assess* 125, 271–279 (2007).
57. Ribeiro, C. D., Burge, S. H., Palmer, S. R., Tobin, J. O., and Watkins, I. D. *Legionella pneumophila* in a hospital water system following a nosocomial outbreak: Prevalence, monoclonal antibody subgrouping and effect of control measures. *Epidemiol Infect* 98, 253–262 (1987).
58. Muraca, P., Stout, J. E., and Yu, V. L. Comparative assessment of chlorine, heat, ozone, and UV light for killing *Legionella pneumophila* within a model plumbing system. *Appl Environ Microbiol* 53, 447–453 (1987).
59. Plouffe, J. F., Webster, L. R., and Hackman, B. Relationship between colonization of hospital building with *Legionella pneumophila* and hot water temperatures. *Appl Environ Microbiol* 46, 769–770 (1983).
60. Alary, M. and Joly, J. R. Factors contributing to the contamination of hospital water distribution systems by *Legionellae*. *J Infect Dis* 165, 565–569 (1992).
61. Stout, J. E., Brennen, C., and Muder, R. R. Legionnaires' disease in a newly constructed long-term care facility. *J Am Geriatr Soc* 48, 1589–1592 (2000).
62. Rowbotham, T. J. Preliminary report on the pathogenicity of *Legionella pneumophila* for freshwater and soil amoebae. *J Clin Pathol* 33, 1179–1183 (1980).
63. Lasheras, A., Boulestreau, H., Rogues, A. M., et al. Influence of amoebae and physical and chemical characteristics of water on presence and proliferation of *Legionella* species in hospital water systems. *Am J Infect Control* 34, 520–525 (2006).
64. Kikuhara, H., Ogawa, M., Miyamoto, H., Nikaido, Y., and Yoshida, S. Intracellular multiplication of *Legionella pneumophila* in *Tetrahymena thermophila*. *J UOEH* 16, 263–275 (1994).
65. Barker, J., Brown, M. R., Collier, P. J., Farrell, I., and Gilbert, P. Relationship between *Legionella pneumophila* and acanthamoeba polyphaga: Physiological status and susceptibility to chemical inactivation. *Appl Environ Microbiol* 58, 2420–2425 (1992).
66. Storey, M. V., Ashbolt, J., and Stenstrom, T. A. Biofilms, thermophilic amoebae and *Legionella pneumophila*—a quantitative risk assessment for distributed water. *Water Sci Technol* 50, 77–82 (2004).
67. Bartram, J., Chartier, Y., Lee, J. V., Pond, K., and Surman-Lee, S. *Legionella and the Prevention of Legionellosis*. World Health Organization, Geneva, Switzerland (2007).
68. Tablan, O. C., Anderson, L. J., Besser, R., Bridges, C., and Hajjeh, R. Guidelines for preventing health-care-associated pneumonia, 2003: Recommendations of cdc and the healthcare infection control practices advisory committee. *MMWR Recomm Rep* 53, 1–36 (2004).
69. Davison, A., Howard, G., Stevens, M., et al. *Water Safety Plans: Managing Drinking-Water Quality from Catchment to Consumer*. World Health Organization, Geneva, Switzerland (2005).
70. Allegheny County Health Department. *Approaches to Prevention and Control of Legionella Infection in Allegheny County Health Care Facilities*. Allegheny County Health Department, Pittsburgh, PA (1997).
71. Squier, C. L., Stout, J. E., Krsyotfiak, S., et al. A proactive approach to prevention of health care-acquired legionnaires' disease: The Allegheny County (Pittsburgh) experience. *Am J Infect Control* 33, 360–367 (2005).
72. Stout, J. E. and Yu, V. L. Experiences of the first 16 hospitals using copper-silver ionization for *Legionella* control: Implications for the evaluation of other disinfection modalities. *Infect Control Hosp Epidemiol* 24, 563–568 (2003).
73. Lin, Y. E., Sidari, F. P., and Stout, J. E. Comparison of culture and equate water test for detecting *Legionella* in cooling towers. In: *Third International Water Congress*, Melbourne, Australia (2002).
74. Shih, H. Y. and Lin, Y. E. Caution on interpretation of *Legionella* results obtained using real-time PCR for environmental water samples. *Appl Environ Microbiol* 72, 6859 (2006).
75. Heimberger, T., Birkhead, G., Bornstein, D., Same, K., and Morse, D. Control of nosocomial legionnaires' disease through hot water flushing and supplemental chlorination of potable water. *J Infect Dis* 163, 413 (1991).
76. Snyder, M. B., Siwicki, M., Wireman, J., et al. Reduction in *Legionella pneumophila* through heat flushing followed by continuous supplemental chlorination of hospital hot water. *J Infect Dis* 162, 127–132 (1990).
77. Best, M., Goetz, A., and Yu, V. L. Heat eradication measures for control of nosocomial legionnaires' disease. Implementation, education, and cost analysis. *Am J Infect Control* 12, 26–30 (1984).
78. Colville, A., Crowley, J., Dearden, D., Slack, R. C., and Lee, J. V. Outbreak of legionnaires' disease at University Hospital, Nottingham. Epidemiology, microbiology and control. *Epidemiol Infect* 110, 105–116 (1993).

79. Darelid, J., Bengtsson, L., Gastrin, B., et al. An outbreak of legionnaires' disease in a Swedish hospital. *Scand J Infect Dis* 26, 417–425 (1994).
80. Darelid, J., Lofgren, S., and Malmvall, B. E. Control of nosocomial legionnaires' disease by keeping the circulating hot water temperature above 55 degrees C: Experience from a 10-year surveillance programme in a district general hospital. *J Hosp Infect* 50, 213–219 (2002).
81. Lin, Y. E., Vidic, R. D., Stout, J. E., and Yu, V. L. *Legionella* in water distribution systems. *J A W W A* 90, 112–121 (1998).
82. Grosserode, M., Wenzel, R., Pfaller, M., and Helms, C. Continuous hyperchlorination for control of nosocomial legionnaires' disease: A ten year follow-up of efficacy, environmental effects, and cost. In: *Legionella-Current Status and Emerging Perspectives*. Barbaree, J. M., Breiman, R. F., and Dufour, A. P. (Eds.), American Society for Microbiology, Washington, DC (1993).
83. Villanueva, C. M., Fernandez, F., Malats, N., Grimalt, J. O., and Kogevinas, M. Meta-analysis of studies on individual consumption of chlorinated drinking water and bladder cancer. *J Epidemiol Community Health* 57, 166–173 (2003).
84. Liu, Z., Stout, J. E., Tedesco, L., et al. Controlled evaluation of copper-silver ionization in eradicating *Legionella pneumophila* from a hospital water distribution system. *J Infect Dis* 169, 919–922 (1994).
85. Biurrun, A., Caballero, L., Pelaz, C., Leon, E., and Gago, A. Treatment of a *Legionella pneumophila*-colonized water distribution system using copper-silver ionization and continuous chlorination. *Infect Control Hosp Epidemiol* 20, 426–428 (1999).
86. Chen, Y. S., Lin, Y. E., Liu, Y. C., et al. Efficacy of point-of-entry copper-silver ionisation system in eradicating *Legionella pneumophila* in a tropical tertiary care hospital: Implications for hospitals contaminated with *Legionella* in both hot and cold water. *J Hosp Infect* 68, 152–158 (2008).
87. Liu, Z., Stout, J. E., Boldin, M., et al. Intermittent use of copper-silver ionization for *Legionella* control in water distribution systems: A potential option in buildings housing individuals at low risk of infection. *Clin Infect Dis* 26, 138–140 (1998).
88. Lin, Y. E., Vidic, R. D., Stout, J. E., and Yu, V. L. Legionnaires' disease in an apartment building: Disinfection methods and recommendations. In: *World Water Congress of the International Water Association*. International Water Association, Paris, France (2000).
89. Fiore, A. E., Butler, J. C., Emori, T. G., and Gaynes, R. P. A survey of methods used to detect nosocomial legionellosis among participants in the national nosocomial infections surveillance system. *Infect Control Hosp Epidemiol* 20, 412–416 (1999).
90. Environmental Protection Agency. *Pesticide Registration: Clarification for Ion-Generating Equipment*. EPA-HQ-OPP-2007-0949. Federal Register. Environmental Protection Agency, Washington, DC (2007).
91. Sidari, F. P., Stout, J. E., Vanbriesen, J. M., et al. Keeping *Legionella* out of water systems. *J A W W A* 96, 111–119 (2004).
92. Hamilton, E., Seal, D. V., and Hay, J. Comparison of chlorine and chlorine dioxide disinfection for control of *Legionella* in a hospital potable water supply. *J Hosp Infect* 32, 156–160 (1996).
93. Smith, A. J., Bagg, J., and Hood, J. Use of chlorine dioxide to disinfect dental unit waterlines. *J Hosp Infect* 49, 285–288 (2001).
94. Srinivasan, A., Bova, G., Ross, T., et al. A 17-month evaluation of a chlorine dioxide water treatment system to control *Legionella* species in a hospital water supply. *Infect Control Hosp Epidemiol* 24, 575–579 (2003).
95. Hood, J., Cheape, G., Mead, A., and Curran, E. Six years' experience with chlorine dioxide in control of *Legionella pneumophila* in potable water supply of Glasgow royal infirmary. *Am J Infect Control* 28, 86 (2000).
96. Ricci, M. L., Dell'Eva, I., Scaturro, M., et al. A four-year experience of a chlorine dioxide treatment for the control of *Legionella* in a hospital water system. *ISTISAN Congressi* 05, 18 (2005).
97. USEPA. National primary drinking water rules: Disinfectants-disinfection by-products. Final Rule. Federal Register (1998).
98. Zhang, Z., McCann, C., Stout, J. E., et al. Safety and efficacy of chlorine dioxide for *Legionella* control in a hospital water system. *Infect Control Hosp Epidemiol* 28, 1009–1012 (2007).

21 Analytical Techniques for Identifying Mineral Scales and Deposits

Valerie P. Woodward, Robert C. Williams, and Zahid Amjad

CONTENTS

21.1	Introduction.....	425
21.2	Analytical Techniques for Identifying Mineral Scales and Deposits.....	426
21.2.1	Optical Microscopy	427
21.2.2	Scanning Electron Microscopy.....	428
21.2.3	Energy Dispersive X-Ray Spectrometry Analysis.....	430
21.2.4	Wide Angle X-Ray Diffraction	432
21.3	Particle Size Analysis.....	435
21.4	Other Analytical Techniques.....	435
21.5	Infrared Spectroscopy	436
21.5.1	Transmission Spectroscopy	437
21.5.2	ATR-IR Spectroscopy	439
21.6	Applications to Water-Treatment Problems	441
21.6.1	Metal-Inhibitor Salt Formation.....	441
21.6.2	Cationic Polymer-Anionic Polymer Coacervate Formation.....	442
21.6.3	Thermal Treatment of Deposit Control Polymers.....	443
21.7	Summary.....	445
	References.....	445

21.1 INTRODUCTION

In many industrial processes, the feed water used contains mixtures of dissolved ions that are unstable with respect to precipitation. Various factors such as pH, temperature, the type and concentration of dissolved ions, flow velocity, equipment metallurgy, and so on contribute to the precipitation and deposition of sparingly soluble salts on equipment surfaces. The class of crystalline and amorphous compounds formed in industrial water systems, generically known as scale and deposits, has a widespread importance across a variety of disciplines, as can be seen from other chapters in this book and from other books [1–3]. *Scale* is defined as the deposit of certain sparingly soluble salts such as calcium carbonate, calcium phosphate, calcium oxalate, magnesium hydroxide, and calcium sulfate from the process fluids after precipitation onto the tubing and other process surfaces. The commonly encountered deposits in industrial water systems include carbonates, sulfates, and phosphates of alkaline earth metals, silica, magnesium silicate, corrosion products, microbiological mass, and suspended matter. These deposits, especially on heat-transfer surfaces in thermal distillation, cooling, and boiler systems, lead to overheating, loss of system efficiency, unscheduled shutdown, and untimely heat exchanger failure. In desalination by reverse osmosis (RO) process,

the deposition of unwanted precipitates may result in poor water quality and premature membrane failures. The deposition of scale in some cases may be beneficial as in the case of drinking water transmission lines wherein the layer of scale deposit protects the piping from corrosion by isolating it from the water. However, in most cases, scale is undesirable as it adversely affects the overall efficiency of the process.

Over the last three decades, considerable experience has been gained through the examination of failed heat exchangers and RO membranes; in that process, deposit characterization has been performed on the heat exchangers of different metallurgies and nearly every type of RO membranes, including spiral-wound, tubular, and hollow fiber configurations. In addition, the autopsies of the membranes of different compositions such as cellulose acetate, cellulose triacetate, and thin-film composite polyamide have been carried out using different analytical techniques for identifying the possible cause(s) of membrane failure and deposit composition. The information collected through deposit characterization has enabled the academic researchers and industrial technologists to develop new scale inhibitors, dispersants, and membrane cleaners. This chapter addresses the use of several analytical techniques to characterize the type, crystalline structure, and the composition of mineral scales and deposits. In addition, these techniques can also be used to identify the cause(s) of heat exchanger and membrane failures in the industrial water systems.

21.2 ANALYTICAL TECHNIQUES FOR IDENTIFYING MINERAL SCALES AND DEPOSITS

A number of methods may be employed to characterize mineral scales (i.e., calcium carbonate, calcium sulfate, barium sulfate, calcium fluoride, and so on) and deposits (i.e., rust, clay, zinc oxide, and so on). Some of these methods are listed in Table 21.1, along with the type of information and their advantages and disadvantages.

TABLE 21.1
Analytical Methods for Water Treatment Precipitates and Deposits

Technique	Information	Advantages	Disadvantages
Optical microscopy	M	Cost, time	Limited information
Scanning electron microscopy (SEM)	M, S	Time, sample size	Cost
Inductively coupled plasma	E	LDL	Sample size, prep time
Infrared	C	LDL, time, cost	Interpretation
Transmitted	C	LDL, time, sample size	Prep, sample must be homogenous
Reflected	C	Time, sample prep	Flat smooth surfaces, must be homogeneous
Energy dispersive x-ray spectrometry (EDS)	E	Time, sample size	LDL
X-ray photoelectron spectroscopy (XPS)	E, C	LDL, surface sensitivity, chemical states	Cost, interpretation
Wide angle x-ray diffraction (WAXD)	C	Time, phase identification	Cost, sample size
Particle size analysis (PS)	S	Time, cost	Size range limitations per instrument type, particles must stay suspended

Note: E, elemental; M, morphology; C, composition; S, size; LDL, lower detectable limit.

The following sections discuss various analytical techniques used to characterize commonly encountered scales and deposits. There is also a brief description of the other methods used in support of the deposit characterization, although it will not be as extensive as those listed above. These analytical techniques include:

- Optical microscopy
- Scanning electron microscopy and energy dispersive x-ray (SEM/EDS)
- Wide angle x-ray diffraction (WAXD)
- Particle size analysis
- Infrared spectroscopy

21.2.1 OPTICAL MICROSCOPY

Optical microscopy can be used to obtain color, size, crystalline structure, refractive index, and other information about water-formed deposits. The sample can be examined using a stereomicroscope or a compound optical microscope, both of which can have transmitted and reflected light sources. One of the most powerful tools in optical microscopy is polarized light illumination for particle classification. Many materials have distinct properties in polarized light—color, brightness, refractive index, and crystalline habits are only a few. These properties can be unique to specific materials and can serve as benchmarks for the experienced microscopist. Figures 21.1 and 21.2 illustrate the unique appearance of calcium carbonate and iron oxide. The brightness (birefringence) and high refractive index of calcium carbonate and the color of iron oxide are distinctive benchmarks that can guide the microscopist in identifying deposits.

Transmitted light observation can also be used to do microchemical spot tests to identify cations and anions if one does not have immediate access to SEM/EDS. A very common test for calcium carbonate is the addition of a droplet of 10% aqueous hydrochloric acid to a dry deposit sample to determine the presence of carbonate salts. The carbon dioxide evolution from carbonates occurs in the form of bubbles. Some disadvantages of optical microscopy include limited depth of focus, especially in reflected illumination, magnification limitations ($\sim 1 \mu\text{m}$ resolution), and lack of direct elemental information. When these limitations are encountered, SEM/EDS is the next step in the analytical scheme. Currently, most optical microscopes are equipped with digital cameras specifically designed for microscopic use. The cameras are accompanied by powerful capture and processing software, making acquisition, manipulation, storage, and usage of high-quality photomicrographs rather commonplace.

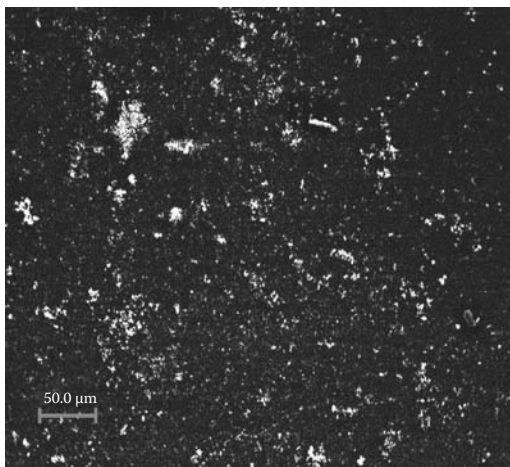


FIGURE 21.1 Transmitted polarized light micrograph of calcium carbonate (nominal 130 \times).

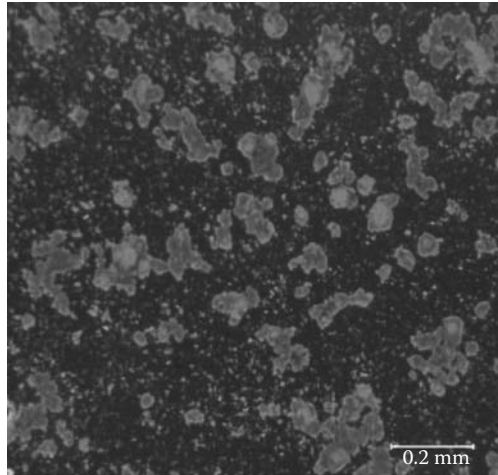
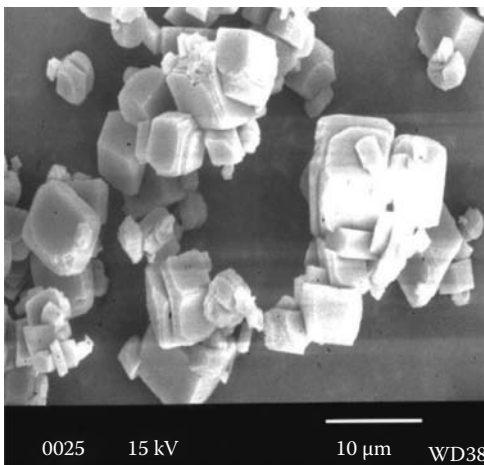


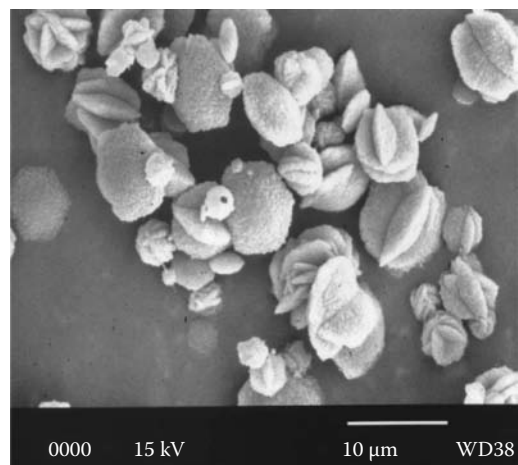
FIGURE 21.2 Transmitted polarized light micrograph of iron oxide (nominal 130 \times).

21.2.2 SCANNING ELECTRON MICROSCOPY

The scanning electron microscope (SEM) is the next logical tool in the microscopy analysis scheme after optical microscopy. The SEM provides an excellent depth of field, a very large magnification range, several detection modes and flexible analysis environments, as well as a means to elemental analysis. Particle size, shape, crystal habits, packing tendencies, and the degree of agglomeration are all characteristics that can be elucidated via SEM imaging. A particularly informational usage of the SEM is tracking the morphology changes of mineral scale such as calcium carbonate. A series of standalone deposit particles or particles collected on filters during the laboratory evaluation of water treatment products can be compared for all of the previously noted attributes as well as for changes in particle population. Figures 21.3 and 21.4 are typical secondary electron images of Ca-containing deposits formed in the absence and presence of inhibitor.



(a)



(b)

FIGURE 21.3 SEM micrographs of two different calcium carbonate polymorphs; (a) vaterite and (b) calcite.

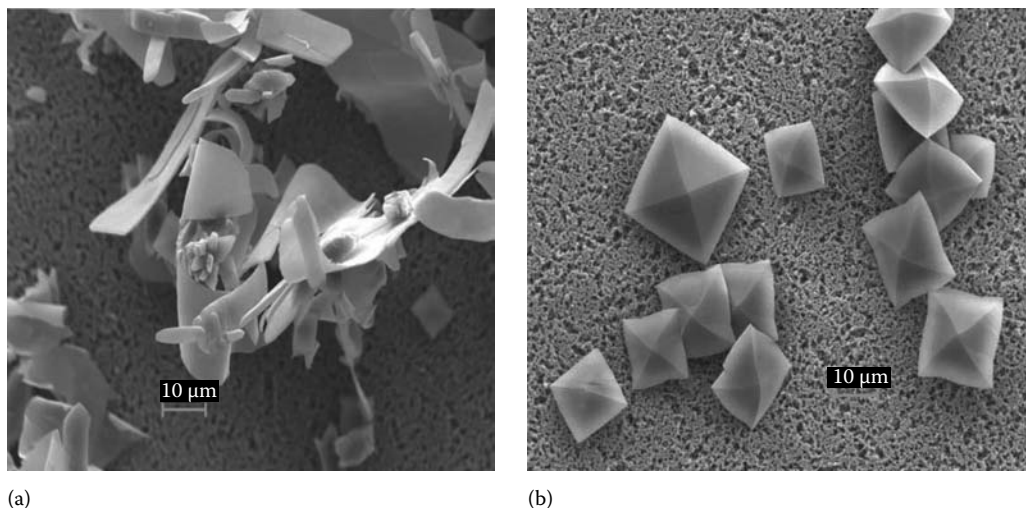


FIGURE 21.4 SEM micrographs of calcium oxalate monohydrate (a) and calcium oxalate dihydrate (b) crystals formed in the absence and presence of inhibitor.

Figure 21.3a and b is an example of two different CaCO_3 polymorphs, namely, vaterite and calcite. Figure 21.4a and b shows the different morphologies of calcium oxalate crystals resulting from the absence or presence of an inhibitor. In the absence of an inhibitor, the crystals formed are calcium oxalate monohydrate ($\text{CaC}_2\text{O}_4 \cdot \text{H}_2\text{O}$); however, the presence of 1 ppm Carbosperse™ K-732, a low-molecular-weight poly(acrylic acid), favors the formation of calcium oxalate dihydrate ($\text{CaC}_2\text{O}_4 \cdot 2\text{H}_2\text{O}$). Calcium oxalate scale, also known as “beerstone,” is generally encountered in the brewing industry.

Current SEMs are entirely digital and allow the simple acquisition and storage of electronic images. Electronic image formats also allow ease of postprocessing, embedded annotation, and simple transfer to electronic documents. Another important aspect of the digital SEM is that the majority or all of the operations are performed via software. Until about 15 years ago, commercial SEMs were only available in the high-vacuum mode. High-vacuum SEMs required that the samples were dry and coated with a conductive metal or carbon to prevent charging (the poor conduction of the electron beam). Current SEMs are also available in high-pressure modes (also called variable pressure, low vacuum, and so on, depending on the manufacturer) and “environmental” modes (ability to image liquid water at room temperature). Both of these modes allow the analyst to observe uncoated samples or materials that are not completely dry.

SEM imaging and EDS elemental analysis are made possible by the interaction of a high-energy electron beam with a sample. Numerous types of interactions occur, mostly in the top-most 10 or so micrometers (μm) of a sample in 3D. The interactions of importance are those which allow the emission of secondary or backscattered electrons (imaging and atomic number contrast) and primary x-rays (elemental analysis). Most morphology imaging is performed in the secondary electron (SE) mode. The actual depth of penetration of the electron beam is dependent on the accelerating voltage of the electron beam and the atomic number of the specimen, with higher accelerating voltage and lower specimen atomic number yielding greater depth of penetration. The accelerating voltage relationship can be exploited to obtain surface information (lower voltage) or subsurface information (higher voltage). Secondary electron imaging can be performed in high-pressure modes as well as high vacuum with the advent of improved detectors made specifically for the collection of secondary electrons in the high-pressure environment. The majority of the images presented in this chapter were obtained between 15 and 25 kV accelerating voltage on metallized specimens in a high-vacuum mode.

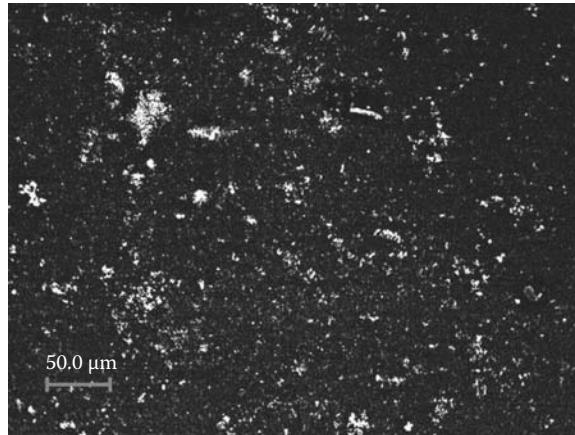


FIGURE 21.5 SEM micrograph in backscattered electron contrast (BSE) mode to facilitate locating small particles on filter substrate.

The backscattered electron (BSE) mode provides information from depths below that from which secondary electrons are generated and is sensitive to the average atomic number of the specimen if there is not much surface topography. BSE mode can be helpful in imaging samples that charge in high vacuum even when coated, and in locating higher atomic number particles on lower atomic number substrates. The former use of BSE is not so important if one has a high-pressure microscope. The latter method is extremely helpful when attempting to locate small particles in a low concentration on filters. Many times, the particles of interest and filtration debris cannot be distinguished from each other morphologically and can only be confirmed using energy dispersive x-ray spectrometry (EDS); however, performing EDS analysis on a number of tiny particles can be tedious. In the BSE mode, S-, Ca-, and Fe-containing particles will present themselves as brighter spots or areas on the darker filter background and make isolation for EDS analysis rather facile. Figure 21.5 illustrates typical BSE imaging of the mixed particles of calcium carbonate and iron oxide on a filter for the purpose of particle location. There are times when particle populations are quite sparse and manually searching the filter surface in the SE mode is time consuming. Using BSE to “light up” the particles that have significant average atomic number differences from the filter allow the analyst to go directly to a brighter spot and then spend quality analysis time to determine the particle morphology and elemental composition.

21.2.3 ENERGY DISPERSIVE X-RAY SPECTROMETRY ANALYSIS

One of the more valuable assets of the scanning electron microscopy is the ability to obtain elemental composition information from materials. Characteristic x-rays from elements are generated at a depth below that from which backscattered electrons are generated; as in the imaging method, that depth can be affected by the accelerating voltage of the electron beam and the density of the specimen. EDS analysis can be used to obtain compositional information on quasi-bulk specimens (low SEM magnification and high accelerating voltage) or on specific particles, morphologies, or isolated areas on filters or within deposits.

Historically, detectors were protected from the SEM chamber environment with a thin window of beryllium, which limited the detection of elements to atomic number 10 (sodium) and above. Most current EDS detectors are able to detect boron, and in some cases beryllium, by the use of a thin polymer window between the chamber environment and the detector crystal. In addition to qualitative identification of the very low atomic number (low Z) elements, the thin window detectors also allow improved quantitative analysis of elements such as sodium and magnesium by virtue of

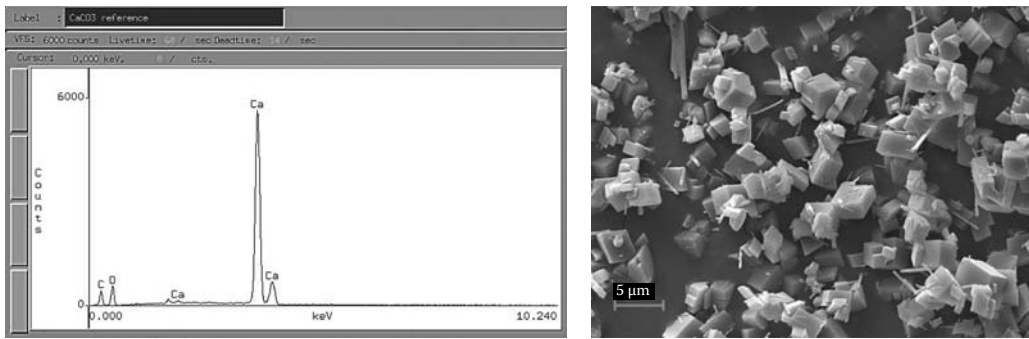


FIGURE 21.6 Typical EDS spectrum of calcium carbonate and SEM micrograph of sample from which EDS spectrum was generated.

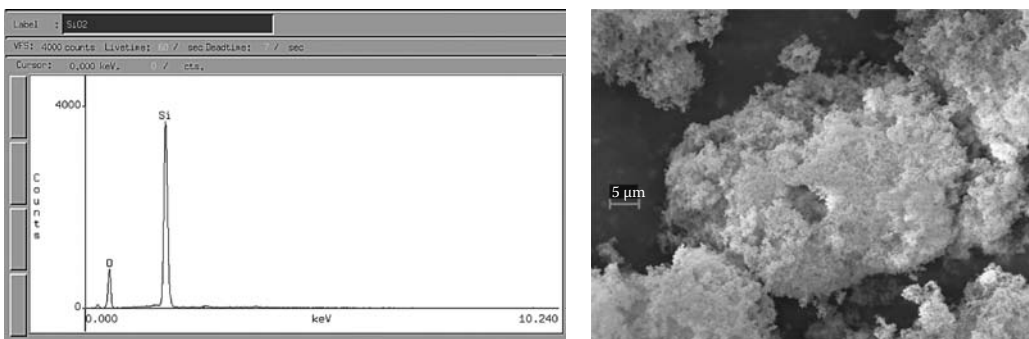


FIGURE 21.7 Typical EDS spectrum of silica and SEM micrograph of sample from which spectrum was generated.

improved signal-to-noise ratio in that area of the spectrum. Detection and quantification of lower atomic number elements can also be improved by the use of lower accelerating voltages, which confines excitation to elements in that range of energies. Figures 21.6 and 21.7 are typical EDS spectra and accompanying SEM images of CaCO₃ and SiO₂ collected with a thin window detector. Figure 21.6 illustrates CaCO₃ with a very crystalline morphology and its typical EDS spectrum at 20kV accelerating voltage. Figure 21.7 illustrates an amorphous SiO₂ and its typical EDS spectrum. The ~200 nm primary particle size of the SiO₂ particles is the contributing factor to the amorphous nature of the material. In both EDS spectra, the peak intensity for oxygen is not intuitively as high as one would conjecture, considering that oxygen is ~48 wt.% of CaCO₃ and ~53 wt.% of SiO₂; however, the x-ray yield for very low-Z elements is low. If one were doing quantitative analysis, the algorithms used would take into account the x-ray line properties and the SEM conditions to correct for the low-Z yield.

Under certain conditions, EDS analysis can be quantitative as well as qualitative. For routine use, those conditions include homogeneous specimens, specimen thickness that is “infinite” to the beam penetration, relatively flat surfaces, and beam geometries that favor optimum collection of x-rays by the EDS detector. SEM column conditions are used by the EDS analysis programs in the correction algorithms; modern EDS analyzers can be integrated with digital SEMs so that information can be collected and stored automatically with the spectra; older instruments require the analyst to store the acquisition information manually with the spectra. There are also special conditions and programs that are required for quantitative analysis of individual particles, extremely small phases, and thin films, but those are not typically used in the characterization of water treatment precipitates and deposits.

21.2.4 WIDE ANGLE X-RAY DIFFRACTION

While EDS analysis in the SEM can provide elemental information about scales and/or deposits, there are times when it is necessary to know the form in which the materials exist. As an example, an EDS spectrum alone can indicate that there is C, O, and Ca in a deposit; however, it is necessary to know whether that is CaCO_3 , CaO on carbon, or even an organic salt of Ca. WAXD of deposits, either removed from heat exchanger or RO membrane or on filters collected during precipitation experiments, provides crystalline phase information about those materials.

The theory of WAXD is based on the interactions of x-rays with the crystalline planes in materials. X-rays are generated. The resulting pattern takes the form of peaks of varying intensities, with the x -axis measured in either analysis angles (degrees 2θ) or d -spacing (\AA) and the y -axis measured in counts per second. A typical crystalline low-background WAXD pattern for $\text{CaSO}_4 \cdot 2\text{H}_2\text{O}$ is shown in Figure 21.8, and a typical noncrystalline, mostly amorphous pattern, for silica is shown in Figure 21.9. A crystalline WAXD pattern, as illustrated in Figure 21.8, typically allows the analyst

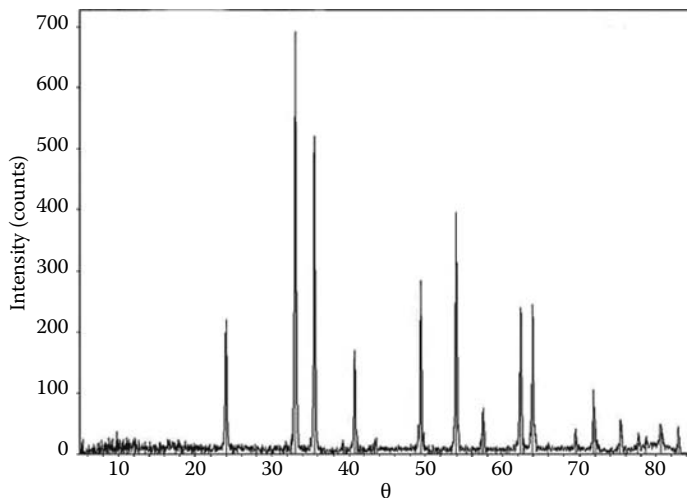


FIGURE 21.8 Low-background WAXD pattern of crystalline calcium sulfate.

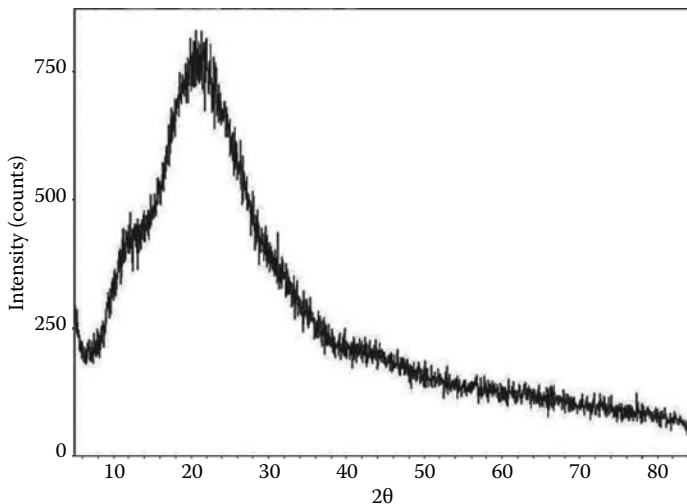


FIGURE 21.9 High-background WAXD pattern of amorphous silica.

to obtain a rather unambiguous identification of phase(s) using search-match programs with a high degree of certainty, given the pattern's well-formed reflections, excellent resolution, and low background. On the other hand, an amorphous pattern, such as that illustrated in Figure 21.9, makes phase identification nearly impossible; the best that can be achieved on this type of pattern is to determine the d -spacings of the approximate centroids of the broad reflections and to combine the EDS information with the d -spacings to manually search for sensible matches. The broad reflections can also be caused by very small (submicrometer) particle size; in this case, the material was the ~ 200 nm SiO_2 .

Current WAXD acquisition is entirely computer-based and essentially automated. The sample preparation is the most labor-intensive portion of the analysis; if working with freestanding particles, they must be placed in the sample holder in a way that does not impart preferential orientation, and if working with particles on filters, the filters must be mounted in or on a holder in a way that does not change the sample height with respect to the incident x-rays. Preferred orientation can change a pattern such that it may not match known references, and the sample height above or below the incident beam level of the sample holder can lead to 2θ shifts in reflection positions. Both of these pattern changes can confuse the computer-based interpretation of the patterns and must be considered.

WAXD application programs are also completely computer-driven and their operations range from the basic marking of reflections to full quantitative analysis. Phase identification can be performed manually or automatically. Manual identification requires a general idea of phases that may be present in a material and the use of commercially available databases that one can search by chemistry, strongest reflections, phase name, and so on. Once reasonable candidates are identified, they can be visually applied to a pattern to check for fit. Automatic phase identification also uses the databases, but allows the analyst to tailor the searches for chemistry, statistical fit, preferred orientation, and many other aspects.

One of the more common applications of WAXD in the study of mineral scales and deposits is the determination of the polymorphs of CaCO_3 . The polymorphs of most interest are the calcite, vaterite, and aragonite forms of the calcium carbonate. These forms have distinct WAXD patterns whose strongest reflections are well resolved from each other. Figure 21.10 illustrates a typical WAXD pattern of CaCO_3 with the different polymorphs indicated.

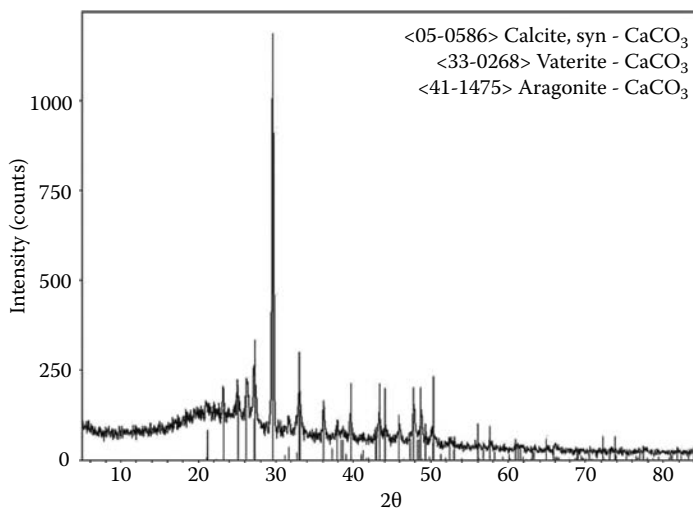


FIGURE 21.10 WAXD pattern of a mixture of calcium carbonate polymorphs—calcite, vaterite, and aragonite.

If deposits are directly on filters, it is important to acquire a reference pattern of an unadulterated filter under identical conditions to the deposits. The reference filter pattern can be used for qualitative comparison to (via overlays) or quantitative subtraction from the analysis patterns. A type of semiquantitative analysis of crystalline patterns can be accomplished if the phase identification is robust, the strongest reflections for those phases are well resolved from each other, and the background can be reasonably removed. For each element in the periodic table, mass absorption coefficients for various x-ray sources have been determined and are available in various reference tables. To determine the mass absorption coefficient of a compound, the elemental fractional composition of the compound is determined, each fraction is multiplied by the mass absorption coefficient for that particular element, and those products are summed to obtain the compound coefficient. The exercise for determining the mass absorption coefficient for CaCO_3 using Cu K- α radiation is illustrated as follows:

1. Determine weight fraction (f) of elements in CaCO_3 :
 MW (CaCO_3) \cong $100(1 \text{ mol Ca} \times 40 \text{ g/mol}) + (1 \text{ mol C} \times 12 \text{ g/mol}) + 3 \text{ mol O} \times 16 \text{ g/mol}$
 Wt. fraction Ca $\cong 40/100 = 0.40$
 Wt. fraction C $\cong 12/100 = 0.12$
 Wt. fraction O $\cong 28/100 = 0.48$
2. Mass absorption coefficients μ/ρ for elements Ca K- α (see note in optical microscopy microchemical tests section):
 μ/ρ Ca = 162
 μ/ρ C = 4.60
 μ/ρ O = 11.5
3. Mass absorption coefficient μ/ρ for compound CaCO_3 is shown in Table 21.2.

Once the mass absorption coefficients are determined for the compounds of interest, the next step in the semiquantitative analysis is to determine the net (background-subtracted) counts in the strongest reflections for each compound. The modeling of backgrounds and their subsequent subtraction and the determination of the net counts are reasonably facile procedures in current WAXD interpretation programs. Then, the net counts for each compound are multiplied by the mass absorption coefficient for the compounds and those products are summed. Finally, the individual products are divided by the sum and compositional fractions are obtained for a well-resolved, robust mix of CaCO_3 , CaSO_4 , and CaO , as illustrated in Table 21.3. If the pattern consists of the polymorphs of the same compound, there is no need to incorporate the mass absorption coefficients as they will be the same for each polymorph. In that case, a simple determination of the fractions based only on the net counts in the strongest reflection for each polymorph is indicated.

TABLE 21.2
Mass Absorption Coefficient μ/ρ
Calculation for Compound CaCO_3

Element	Wt. Fraction (f)	μ/ρ	$f \times \mu/\rho$
Ca	0.40	162	64.80
C	0.12	4.60	0.55
O	0.48	11.5	5.52
Compound			
CaCO_3			70.87

TABLE 21.3
Determination of Approximate Phase Composition in a WAXD
Pattern Using Net Areas under the 100% Reflections and
Compound Mass Absorption Coefficients

Compound	μ/ρ (Rounded)	Net Counts	$\mu/\rho \times$ Net Counts	~Fraction Compound
CaCO ₃	71	15,000	1,065,000	0.3
CaSO ₄	74	24,000	1,776,000	0.5
CaO	118	6,200	731,600	0.2
			3,572,600 (total)	

21.3 PARTICLE SIZE ANALYSIS

For particles deposited on filters or substrates, SEM or reflected light optical microscopy can be used to obtain various size measurements, including average size and size distribution. For the suspension of particles (i.e., calcium carbonate, iron oxide, and clay) in aqueous medium, automated particle analyzers are commonly used to provide many types of particle information. The modern analyzers are of several types, including x-ray sedimentation, electrical sensing zone, and laser light scattering. The particle size ranges and the analytical basis for each method are listed in Table 21.4.

Figure 21.11 illustrates the typical output from a laser light scattering instrument, with particle diameter on the *x*-axis and volume % on the *y*-axis. Figure 21.12 presents an excellent example of the particle size distribution of iron oxide in the absence and presence of a polymeric dispersant. As may be seen, the presence of 1 ppm Carbosperse™ K-781 exhibits a significant effect on the particle size distribution and causes a reduction of larger particles to smaller size particles. This type of information is useful in benchmarking the dispersants of different polymer architecture.

21.4 OTHER ANALYTICAL TECHNIQUES

Inductively coupled plasma, or ICP, analysis is a wet-chemical method for the quantitative determination of most metallic elements from the percent level to parts per trillion (ppt). This method requires that the sample can be taken up in a solution (some samples may require ashing and/or acid digestion) so that it can be aspirated into a plasma. The resulting atomic vapor emits light that is detected; the wavelengths are element-specific so that their intensities are proportional to the amount of analyte in the liquid sample. The method requires the analysis of the standard concentrations of the analytes in matrix-matched solutions to determine the response of the detection system. This method is particularly helpful when it is necessary to determine very low concentrations of metals in solutions from water treatments.

TABLE 21.4
Particle Size Analysis Ranges for Three Most Common Techniques

Technique	Particle Size Range (μm)	Theory
X-ray sedimentation	0.1–300	Natural size separation upon settling; mass fractions sensed by soft x-ray absorption
Electrical sensing zone	0.5–1000	Electrical signal proportional to volume of particles swept through an orifice; counts particles and determines concentration
Laser light scattering	0.02–2000	Mie and Fraunhofer theories to determine particle size distribution from a light-scattering pattern

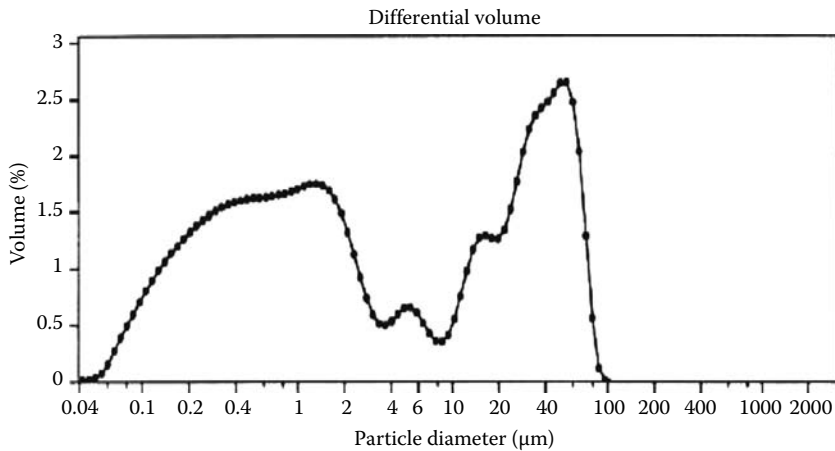


FIGURE 21.11 Typical output from laser light scattering particle size analyzer.

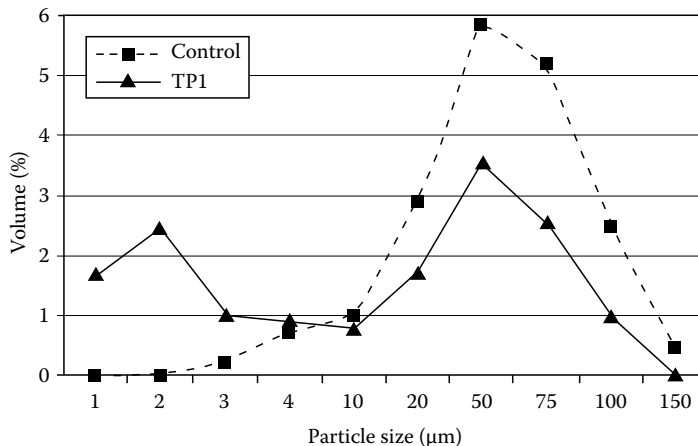


FIGURE 21.12 Comparison of particle size distributions of iron oxide in the absence and presence of Carbosperse™ K-781 terpolymer (TP1).

X-ray photoelectron spectroscopy, XPS (or colloquially ESCA, electron spectroscopy for chemical analysis), is a surface-sensitive elemental analysis technique. Electrons are ejected from inner or outer shells when excited by x-rays (the converse of EDS analysis, whence electron excitation causes ejection of x-rays). Each element has a specific binding energy that is affected by its atomic number and its coordination with other atoms. The position of the resulting peaks and their shifts from literature values aid the analyst in determining what analytes are present and if (and how) they are bonded to other atoms. XPS is sensitive to the first 10–50 Å of a surface and is particularly valuable when analyzing the thin deposits of the films of materials on substrates.

21.5 INFRARED SPECTROSCOPY

Infrared (IR) spectroscopy provides information that is complementary to the other methods that have been discussed. As the previous examples have illustrated, optical microscopy provides information on morphology, while ICP and the x-ray methods generally provide elemental information. However, with the exception of WAXD and XPS, none of these other methods provide any

information about chemical bonding or the specific chemical formula (although joint element mapping can sometimes provide some inferential information). Because IR spectroscopy usually detects bonds between atoms in a molecule, IR can often provide information regarding various functional groups in, and the chemical structure of, the analyte. However, just as the other methods have some limitations, so too does IR. Specifically, IR is the most sensitive to highly polar molecular bonds, is insensitive to nonpolar bonds between like atoms in diatomic molecules such as N_2 , O_2 , and Cl_2 , and so on, and is relatively insensitive to molecular sulfur (S_8) and similar materials. Moreover, IR cannot usually detect materials based on purely ionic bonds, including many of the common, two-element salts, especially the common metal halides. Although a detailed discussion of the physics of IR and the associated instrumentation is beyond the scope of this chapter, the references include several works that do an excellent job of this [4–9].

However, the common IR limitations are really quite minute, when compared with the overall power of the method. IR can provide a “fingerprint” from pure materials, and a list of functional groups in mixture spectra from which the total composition can often be inferred. Moreover, the cost of a modern, benchtop IR is generally significantly lower than many of the SEM, x-ray, and ICP instruments; sample preparation issues are minimal; and results can be obtained very quickly. For these reasons, IR is often the first technique used, after initial microscopic screening, in the analysis of boiler scale deposits.

As was noted above, IR spectroscopy is complementary to the x-ray/ICP methods. In particular, IR is sensitive to and can usually identify organic components to which these other techniques are largely insensitive. In addition, it can often see the “other half” of some inorganic materials containing constituents to which the x-ray/ICP methods are blind. One such example is calcium carbonate, a commonly observed boiler scale material. Although the other methods can detect the calcium component, they are usually blind to the carbonate anion, and as was previously noted, even when all the elements are detected, it is still difficult to unambiguously determine the molecular formula. Conversely, the carbonate anion is unequivocally identified by IR, but this technique is relatively insensitive to the metal cation component, due to the ionic nature of the metal carbonate bond. The specific cation can often be inferred from the positions of several of the carbonate bands, but a confirming metals analysis is usually necessary for absolute certainty. In addition, because IR spectroscopy is sensitive to molecular bonds, it can often yield an indication of chemical changes in the analyte material, as will be shown in later examples. For the most part, these chemical changes might only be hinted at by changes in morphology in microscopic observation, and would not be detected at all by most x-ray and ICP methods.

The two most commonly used IR spectroscopic techniques in most laboratories are transmission spectroscopy and attenuated total reflectance (ATR) analysis [10–11]. (The latter is also sometimes referred to as frustrated multiple internal reflectance or FMIR.) The overlaid transmission and ATR spectra of calcium carbonate, plotted in absorbance mode, are shown in Figure 21.13. The pattern created by the three strongest peaks (i.e., the very strong, broad band in the region $1530\text{--}1320\text{ cm}^{-1}$, accompanied by two weaker sharp bands in the regions $890\text{--}800$ and $745\text{--}670\text{ cm}^{-1}$) is diagnostic for carbonate anion; the specific cation can often be inferred from the exact positions of all the three bands [12]. Differences between these spectra will be explained in the ensuing discussions of these two techniques.

21.5.1 TRANSMISSION SPECTROSCOPY

Transmission spectroscopy is an older technique, and was for many years by far the most commonly used infrared technique for a wide variety of samples. However, transmission spectroscopy also suffers from several disadvantages, especially when analyzing mineral scale and scale-inhibition materials. Aqueous media are difficult to analyze, both because many IR windows are water soluble and because it is difficult to prepare aqueous samples sufficiently thin for transmission spectroscopy. Similarly, solid samples need to be both relatively dry and very

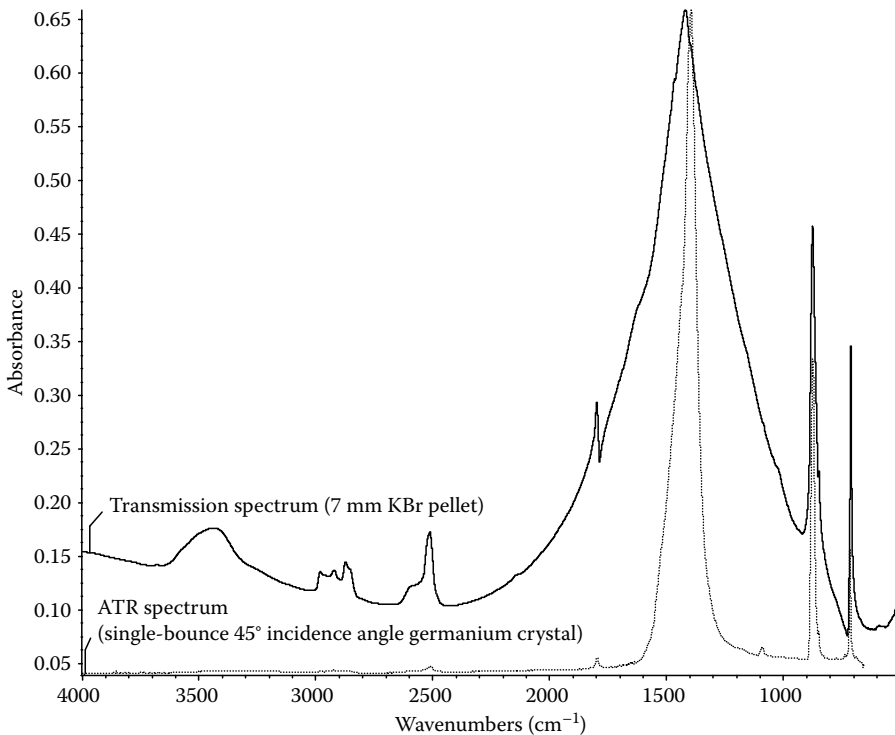


FIGURE 21.13 Infrared transmission and ATR spectra of calcium carbonate.

dilute in order to avoid exceeding the spectrometer's operating limits: typically approximately 10 microns thick for pressed polymer or cast organic films, and sometimes less for inorganic materials. Solid samples that can neither be pressed nor dissolved are commonly prepared either as very dilute (typically less than 1 wt.%) suspensions in a pressed potassium bromide pellet matrix or as dispersions in Nujol[®] mineral oil. The IR transmission spectrum of calcium carbonate, shown in Figure 21.13, was acquired as a KBr pellet. Unfortunately, this technique can be moderately labor intensive and is not suitable for aqueous liquids or wet solids. In addition, the interaction of the analyte material with the KBr-pelletizing matrix can cause band frequency shifts and other artifacts, including occasional spurious bands. The mineral oil dispersion technique is no longer commonly used, since it has been superseded by other newer techniques, including ATR.

Another application of transmission spectroscopy is the use of an IR microscope (which, in many instances can also acquire reflectance and micro-ATR, as well as transmission spectra) [13]. This application is best suited for heterogeneous samples, where several compositionally different (but preferably, spatially separated) materials are present on the same substrate, and/or for very small samples, where there is insufficient material to use one of the other techniques. However as in the case of ordinary transmission spectroscopy, there is an upper limit on the sample thickness that can be analyzed using transmission IR microscopy. In addition, it can be difficult to sort out all the constituents in a heterogeneous sample. Ideally, for transmission IR microscopy, each of the individual particles should be homogeneous, but there can be different spatially dispersed particle species present; for ATR, it is desirable that all of the particles be compositionally similar (although it is sometimes possible to obtain useful information when several different particle species are present). For most of the applications in our laboratory, the samples were sufficiently homogeneous (and sufficiently large) that macro-ATR was a more appropriate choice.

21.5.2 ATR-IR SPECTROSCOPY

In contrast to the various transmission techniques, ATR spectra can be collected very quickly for a wide variety of liquid and solid samples with essentially no sample preparation. In addition, the accessories now in use are capable of analyzing samples as small as 300 microns in diameter. While this is still considerably larger than the lower limit for a good IR microscope (around 10–20 microns), it is often sufficient for a wide variety of samples. Moreover, the cost of a good ATR unit can be one-tenth or less than the cost of a good IR microscope. These advantages generally render ATR more appropriate as the first-choice approach for the initial screening of boiler scale and water treatment samples.

ATR-IR spectroscopy is normally presented by invoking quantum mechanical tunneling [10]; however, an alternate conceptual approach which does not require any knowledge of or familiarity with quantum mechanics is presented here. Visual information associated with this explanation is shown in Figure 21.14. The physics associated with the ATR technique is the same one involved when a person underwater in a swimming pool looks up out of the water. If the swimmer looks straight up, he or she will see the ceiling of the swimming pool. However, if that same swimmer begins to look toward the end of the pool, at some point, instead of seeing the ceiling, he/she will see the floor at the far end of the swimming pool. This is a practical illustration of *Snell's law*. When a light ray in an optically dense medium (in this case, water) strikes an interface between that medium and a less optically dense medium (in this case, air) at any angle other than zero degrees (i.e., perpendicular to the interface), it will normally be refracted away from the perpendicular. As the angle of incidence increases from zero, at some point, it will reach a critical angle, beyond which the incident ray is *totally internally reflected* back into the denser medium. This critical angle is defined by the two indices of refraction and can be calculated using Snell's law. Although there may be some reflective loss, rays striking the interface at less than the critical angle (i.e., more nearly perpendicular to the interface) will always be at least partially transmitted; however, rays striking the interface at anything greater than the critical angle (i.e., more nearly parallel to the interface) will always be totally internally reflected.

Now, replace water in the example above with a high-index material such as germanium, zinc selenide, or diamond, and replace the air with a water treatment sample. Suppose that there is some means of monitoring the internally reflected ray, and consider a ray that is incident at a value very close to, but slightly greater than, the critical angle. It has already been stated that this ray is normally totally internally reflected. Now, examine what happens if that rarer medium is a material that has an absorption band occurring at the same energy as the incident ray. Around a strong absorption

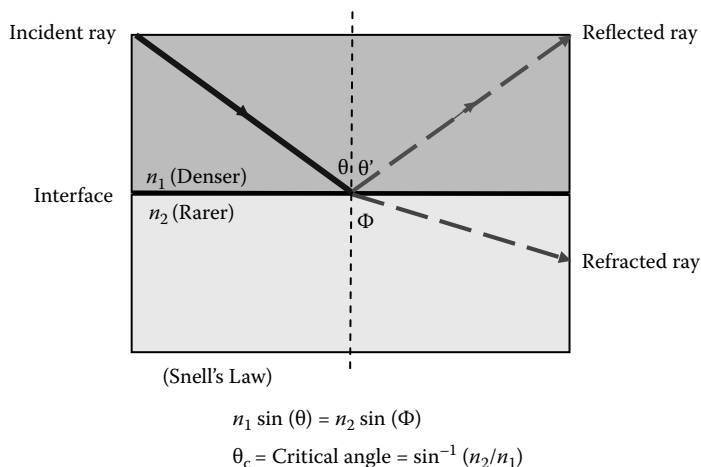


FIGURE 21.14 Schematic illustrating principles underlying the ATR technique.

band, the index of refraction increases drastically. This increased index of refraction means that in the region of this absorption band, there is now a different critical angle, which is greater than the absorption-free critical angle. If conditions have been chosen appropriately, the net effect is that the incoming ray is now incident at *less than* the new critical angle, and that there will be at least some transmission from the denser to the rarer medium. The ray that was formerly totally internally reflected is now said to be *attenuated* by the portion that was transmitted. If an infrared spectrometer is used to scan the spectral range and to measure the intensity of the internally reflected refracted ray, the result is a spectrum that is qualitatively similar to the conventional transmission spectrum of the rarer medium. The effective sampling depth of this technique (which can be calculated using quantum mechanics) is dependent on the denser medium and analyte indices of refraction and varies as a function of the incident wavelength, but is typically on the order of a few microns. The effective penetration depths for several commonly used crystal materials at a variety of incidence angles are shown in Table 21.5.

To some extent, the effective sampling depth at any given wavelength can be altered either by adjusting the angle of incidence and/or by choosing an alternate substrate medium that has a different optical density. There have been papers on “spectroscopic microtoming,” where successively deeper penetration depths would sometimes reveal layers below the surface [11,14]; however, in more recent times, this technique has essentially been superseded by the IR microscopic analysis of sample cross sections.

As previously noted, one of the major advantages of ATR is the minimal sample preparation involved. Figure 21.15 is a schematic of one commonly used ATR configuration. This is a single-bounce unit that utilizes a 45° incidence angle; the crystal material can be germanium ($n = 4$), zinc selenide, or diamond ($n \sim 2.4$ for both). Because the working surface of the ATR crystal is less than 1 mm in diameter, only minimal sample quantities are required. Acceptable spectra have been acquired from sample spot sizes as small as 0.3 mm in diameter. For solid samples (including deposits on filter paper), it is merely necessary to use some form of clamp to press the sample into intimate contact with the ATR crystal. (Best results are obtained if the surfaces are flat and moderately smooth; good results have also been obtained for many powders.) Liquid samples can be run neat, in a sample cup. Wet solids can be run as received, although better results can usually be achieved if the sample is dried first; otherwise, the strong water bands will often obscure some of the analyte bands of interest. In addition, this technique is nondestructive; analyzed samples can usually be recovered for use in subsequent tests.

Because the ATR method interrogates only the first several microns of the material in contact with the crystal, it is ideally suited for the analysis of coatings as well as material deposited on the surface of filter media (although it is sometimes necessary to digitally subtract the spectrum of the filter substrate). However, the surface sensitivity of ATR is significantly worse than what can be achieved with SEM-EDS.

TABLE 21.5
Effective Penetration Depth (Microns)
into a 1.50 Index Medium

Crystal	Incidence Angle	Wave Numbers (cm ⁻¹)			
		3000	2000	1000	500
Ge	30	0.40	0.60	1.20	2.40
Ge	45	0.22	0.33	0.66	1.33
Ge	60	0.17	0.25	0.51	1.02
ZnSe and diamond	45	0.67	1.00	2.00	4.00
ZnSe and diamond	60	0.37	0.55	1.11	2.21

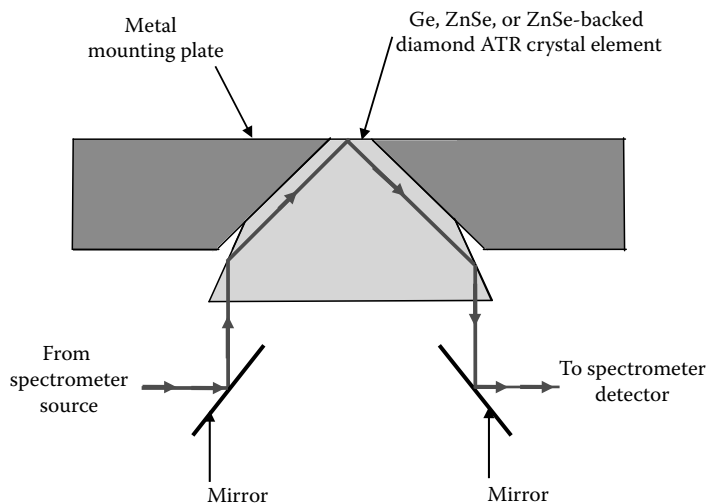


FIGURE 21.15 Generalized schematic of a single-bounce ATR accessory.

One of the primary limitations of the ATR technique is the necessity of good surface contact between the analyte and the crystal window in order to obtain an acceptable spectrum. Although this issue has been minimized by the advent of ATR accessories that utilize much smaller contact areas, badly abraded or etched surfaces or very coarse powders may not yield sufficiently good contact to acquire useful spectra. However, the flatness required is still significantly less than that necessary for backscattered SEM imaging.

Other limitations are dictated by the basic physics inherent in this technique. Because the effective sampling depth (and hence, apparent sample thickness) is a function of wavelength, ATR spectra show diminished band intensities in the high-frequency region, and enhanced intensities in the low-frequency region, relative to what is observed in a normal transmission spectrum. The peak frequency values can also shift by up to 20 (but usually less than 10) cm^{-1} , relative to the transmission values, but often will not shift at all. Some of these differences are illustrated by the calcium carbonate transmission and ATR spectra overlaid in Figure 21.13. ATR-induced artifacts can also make searching an ATR spectrum against transmission libraries problematic; however, several instrument companies now provide proprietary software that does a relatively good job of converting an ATR spectrum to a "pseudotransmission" spectrum in order to facilitate such searches.

Another potential issue with the ATR technique is that very thin (less than 0.5 micron thick) coatings may not be detected, especially if there are no strong coating bands in the high-frequency portion of the spectrum, where the penetration depth is smallest. Moreover, it must always be remembered that ATR is a surface technique that may not accurately reflect the composition of materials below the surface. Finally, as in the case of transmission spectroscopy, in a complex mixture, it may be difficult to completely characterize all of the constituents; however, the technique can be quite useful for simple mixtures, especially ones that are primarily inorganic.

21.6 APPLICATIONS TO WATER-TREATMENT PROBLEMS

21.6.1 METAL-INHIBITOR SALT FORMATION

Scale inhibitors (polymeric and nonpolymeric) used in water treatment formulations may form insoluble salts with metal ions (e.g., Fe, Ca, Ba, and Sr) under conditions frequently encountered in cooling water systems. The trend toward the operation of cooling water systems under increasingly severe operating conditions (e.g., high hardness, high alkalinity, and increased pH and temperature) has favored the formation of insoluble calcium-inhibitor salt. For this reason, the metal ion tolerance

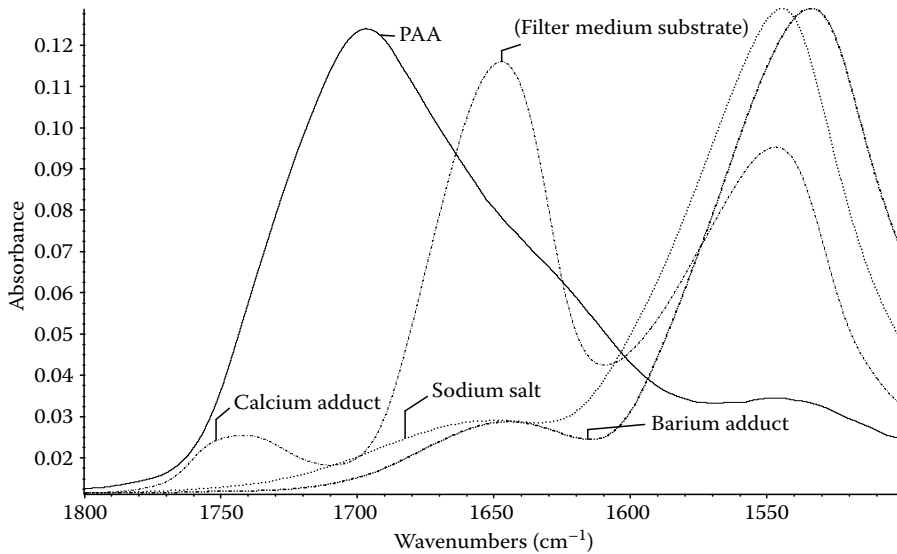


FIGURE 21.16 IR spectra of PAA and several metal salts. All salts were vacuum-dried. PAA and sodium salt spectra were acquired from neat powders. Calcium and barium adducts were on filter media. The band near 1647 cm^{-1} on the calcium adduct spectrum is from the underlying filter medium.

or the ability of the inhibitor to remain soluble in the presence of metal ions is of increasing importance. The precipitation of metal-inhibitor salt on heat exchanger and RO membrane surfaces lead to poor system performance. A typical application of ATR to metal-polymer scaling problem is shown in Figure 21.16 [15]. In this figure, the diamond ATR spectra of poly(acrylic acid) (PAA), a common boiler scale inhibitor, and its sodium, calcium, and barium salts are shown in the $1800\text{--}1500\text{ cm}^{-1}$ region. In this case, the PAA and its sodium salt were supplied as aqueous solutions, which were vacuum-dried, following which the spectra of the dried powders were acquired. The calcium and barium precipitates were isolated on a 0.22 micron cellulose nitrate filter, and then vacuum-dried. Spectra were acquired directly from the filter, with no subtraction or other correction. For the barium precipitate, coverage was sufficiently complete that most of the filter bands are masked by the barium salt. For the calcium salt, however, there was apparently less material on the filter, and the underlying cellulose nitrate band near 1650 cm^{-1} is evident. In Figure 21.16, the chemical change occurring as the acid is converted to salt is clearly evident with the loss of the acid carbonyl band near 1700 cm^{-1} , and the corresponding growth of the carboxylate salt carbonyl band near 1547 , 1543 , and 1533 cm^{-1} , respectively, for the calcium, sodium, and barium salts. Note that the calcium and sodium salt bands occur at almost the same frequency. Moreover, it is also known that these frequencies can vary slightly as a function of concentration, and the calcium salt precipitate is known to be a relatively diffuse coating on the filter medium. If these samples had not been lab specimens whose compositions were well known, this would be an example of the possible need for x-ray/ICP analysis to distinguish between two possible cation possibilities. Further discussion on metal-inhibitor salts is presented in Chapter 5.

21.6.2 CATIONIC POLYMER-ANIONIC POLYMER COACERVATE FORMATION

As discussed in Chapter 5, the role of anionic polymers such as PAA in water treatment formulations is to prevent the precipitation of mineral scaling salts such as calcium carbonate and calcium sulfate. Cationic polymers such as diallyldimethyl ammonium chloride (*p*-DADMAC) and copolymers of acrylic acid:acrylamide are commonly used as flocculating agents to help in removing suspended and colloidal matter from the feed water. It has been reported that the low levels ($<1\text{ ppm}$)

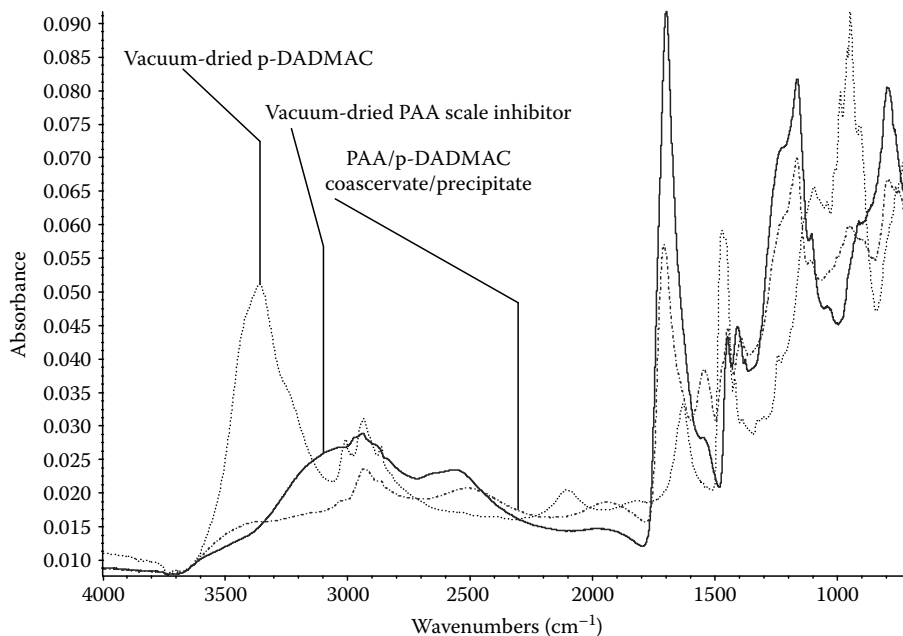


FIGURE 21.17 IR spectra of PAA/*p*-DADMAC coacervate/precipitate.

of cationic polymer interferes with the performance of anionic polymer used in the water treatment formulation. A second ATR application example is shown in Figure 21.17, in this instance using a zinc selenide crystal. These spectra come from a study of anionic polymer-cationic polymer coacervate precipitation. In this instance, an approximately 5000-MW PAA was mixed with *p*-DADMAC. The overlaid spectra (all of vacuum-dried materials) include the PAA, the *p*-DADMAC, and the coacervate precipitate resulting from the mixture of the concentrated solutions of the first two ingredients. Although the bands attributable to the PAA dominate the precipitate spectrum (albeit with some small frequency shifts), the shoulders near 3400, 1470, and 950 cm^{-1} suggest the presence of the *p*-DADMAC salt, and correspond roughly to bands seen in the neat *p*-DADMAC spectrum. These data were used to confirm a hypothesis developed during the turbidity studies of PAA-*p*-DADMAC solutions. Additional information on polymer-polymer interaction is presented in Chapter 5.

21.6.3 THERMAL TREATMENT OF DEPOSIT CONTROL POLYMERS

Figures 21.18 and 21.19 present the results from several time-temperature stability studies of 10% solutions of PAA and some common co- and terpolymer constituents [16]. The spectra of the actual solutions (not shown) consisted mainly of water-solvent bands which masked out the information of interest. In order to avoid inducing any additional thermal history to the heat-aged samples, several drops of solution were deposited in the ATR liquid sample cup, and dried with an impinging room-temperature nitrogen stream for in excess of 10 min. The spectra of the residues remaining after drying were acquired using a germanium ATR crystal.

Figure 21.18 shows the spectra of a terpolymer of acrylic acid:2-acrylamido-2-methylpropane sulfonic acid:sulfonated styrene (AA:AMPS[®]:SS) monomer both before thermal treatment and after two different treatment times. (In order to avoid interference from residual water bands, these solutions used 99% pure deuterium oxide, rather than normal water.) The heat-aged sample spectra are quite similar; however, both exhibit significant differences from the original untreated PAA:AMPS:SS terpolymer, especially in the intensities of the bands near 1649 (amide carbonyl),

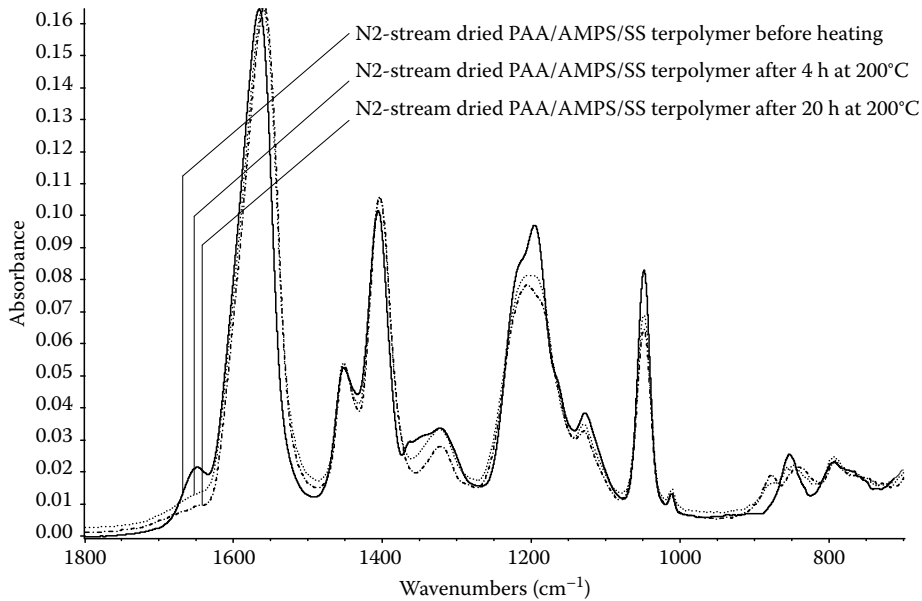


FIGURE 21.18 PAA/AMPS/SS terpolymer with and without heat treatment.

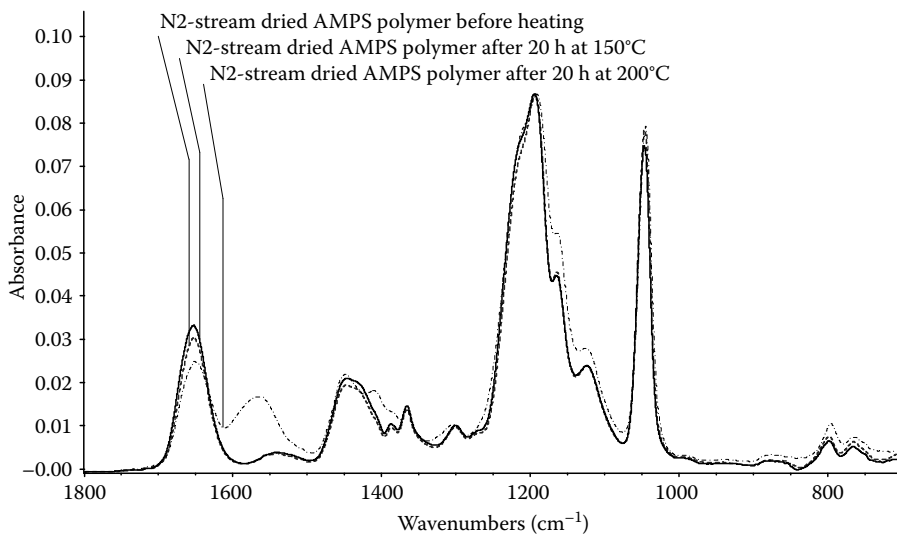


FIGURE 21.19 IR spectra of poly-AMPS with and without heat treatment.

1196 (asymmetric SO_3 stretch), and 1049 cm^{-1} (symmetric SO_3 stretch) and to a lesser extent, the band near 1405 cm^{-1} (asymmetric SO_2 stretch); in addition, there are small band shifts in three of these bands. The disappearance of the 1649 cm^{-1} correlates well with the expected loss of amide carbonyl band as this moiety is oxidized; the other differences are ascribed primarily to a suspected pH shift and other changes in molecular geometry caused by the degradation of the AMPS component. In any event, the similarity of the 4 and 20 h traces indicates that most of the decomposition in this formulation occurs within the first 4 h.

Figure 21.19 contains the spectra of poly-AMPS before heat treatment and after 20 h heat treatment at 150°C and 200°C , respectively. Although there are some small differences between the unheated

and 150°C spectra, they are quite similar; however, the 200°C spectrum differs significantly. These results suggest that poly-AMPS is relatively stable at 150°C, but degrades readily at 200°C.

The spectra shown in these examples represent a few of the IR analyses we have performed to obtain information on chemical changes that can occur to boiler water treatment chemicals due to precipitation with hard water cations or cationic polymers and during prolonged exposure at elevated temperatures. The results of these studies have been and will be used to design more stable and more effective water treatment packages.

21.7 SUMMARY

A variety of analytical techniques are available to analyze complex mineral scales and deposits commonly encountered in industrial water systems. In selecting a method of analysis, the important roles played by various microscopic methods, EDS, and WAXD, in identifying composition, crystalline structure, and crystal morphology of foulants should be considered. The utility of particle size analysis in studying changes in the particle size of foulants such as iron oxide, clay, calcium carbonate, and so on (especially in the presence of deposit control polymers) must also be kept in mind. In addition, IR spectroscopy is an excellent tool for detecting chemical changes in polymer architecture under conditions typically encountered in industrial water systems.

REFERENCES

1. Amjad, Z. *Reverse Osmosis: Membrane Technology, Water Chemistry, and Applications*, Van Nostrand Reinhold, New York (1993).
2. Schroeder, C. D. *Solutions to Boiler and Cooling Water Problems*, The Fairmont Press, Inc., Atlanta, GA (1986).
3. Cowan, J. C. and Weintritt, D. J. *Water-Formed Scale Deposits*, Gulf Publishing Company, Houston, TX (1976).
4. Colthup, N. B., Lawrence, H. D., and Wiberly, S. E. *Introduction to Infrared and Raman Spectroscopy*, 3rd edn., Academic Press, New York (1990).
5. Smith, B. *Infrared Spectral Interpretation*, CRC Press, Boca Raton, FL (1999).
6. Silverstein, R. M., Francis X. W., and Kiemle, D. *Spectrometric Identification of Organic Compounds*, 7th edn., Wiley, New York (2005).
7. Socrates, G. H. *Infrared and Raman Characteristic Group Frequencies: Tables and Charts*, 3rd edn., John Wiley & Sons, New York (2001).
8. Smith, B. *Fourier Transform Infrared Spectroscopy*, CRC Press, Boca Raton, FL (1996).
9. Griffiths, P. R. and de Haseth, J. A. *Fourier Transform Infrared Spectrometry*, 2nd edn., Wiley-Interscience, New York (2007).
10. Harrick, N. J. *Internal Reflection Spectroscopy*, Wiley-Interscience, New York (1967).
11. Urban, M. W. *Attenuated Total Reflectance Spectroscopy of Polymers: Theory and Practice*, American Chemical Society, Washington, DC (1996).
12. Nyquist, R. A. and Kagel, R. O. *Infrared Spectra of Inorganic Compounds*, Academic Press, New York (1971).
13. Messerschmidt, R. G. and Harthcock, M. A. (Eds). *Infrared Microspectroscopy: Theory and Applications*, Marcel Dekker, New York (1988).
14. Hirshfeld, T. Subsurface layer studies by attenuated total reflection Fourier transform spectroscopy. *Appl Spectrosc* 31(4), 239–292 (1977).
15. Amjad, Z. Interactions of hardness ions with polymeric scale inhibitors in aqueous systems. *Tens Surf Deterg* 42, 71–77 (2005).
16. Amjad, Z. and Zuhl, R. W. The impact of thermal stability on the performance of polymeric dispersants for boiler water systems. In: Paper presented at the Association of Water Technologies, Inc. Annual Convention, Palm Springs, CA (2005).

22 Deposit Control Polymers: Types, Characterization, and Applications

Zahid Amjad, Robert W. Zuhl, and Strong Huang

CONTENTS

22.1	Introduction.....	448
22.2	Polymer Types.....	448
22.2.1	Natural Polymers.....	448
22.2.2	Synthetic Polymers.....	449
22.2.3	Polymerization Methods.....	449
22.2.3.1	Precipitation Polymerization.....	450
22.2.3.2	Solution Polymerization.....	450
22.2.3.3	Suspension Polymerization.....	450
22.2.3.4	Emulsion Polymerization.....	450
22.2.3.5	Inverse Emulsion Polymerization.....	450
22.2.3.6	Bulk Polymerization.....	450
22.2.4	Polymerization Processes.....	450
22.2.5	Polymer Characteristics.....	451
22.2.5.1	Molecular Weight.....	451
22.2.5.2	Tacticity.....	452
22.2.5.3	End Groups.....	452
22.2.5.4	Branching.....	452
22.2.5.5	Residual Monomers.....	452
22.2.5.6	Homogeneity and Heterogeneity.....	452
22.2.6	Parameters Typifying Polymer Properties and Specifications.....	452
22.2.6.1	Form.....	452
22.2.6.2	Appearance.....	452
22.2.6.3	Total Solids.....	453
22.2.6.4	Active Solids.....	453
22.2.6.5	Molecular Weight.....	453
22.2.6.6	pH.....	454
22.2.6.7	Viscosity.....	454
22.2.6.8	Acid Number.....	454
22.2.6.9	Specific Gravity.....	455
22.2.6.10	Color.....	455
22.2.6.11	Other Parameters.....	455
22.2.7	Differences between Water Treatment Polymers.....	455
22.3	The Evolution and Role of Deposit Control Polymers in Water Treatment Applications...	456
22.3.1	Historical Perspective.....	456
22.3.2	Current Environment.....	457

22.3.3	Deposit Control Polymers in Cooling and Boiler Water	
	Treatment Applications	457
22.3.3.1	Cooling Water Treatment Programs	457
22.3.3.2	Boiler Water Treatment Programs	457
22.3.4	Deposit Control Polymer Mechanisms.....	459
22.3.4.1	Scale Inhibition	459
22.3.4.2	Dispersion	460
22.3.4.3	Metal Ions Stabilization	461
22.3.4.4	Crystal Modification	462
22.4	Summary.....	462
	References.....	463

22.1 INTRODUCTION

Industrial water technologists use a variety of chemical additives to control corrosion, scaling and deposition, and microbiological growth. The chemical selection largely depends on various factors including water chemistry, system metallurgy, system operating conditions, and chemical compatibility with other formulation components as well as with cations present in the recirculating water. Typical deposit control additives including polyphosphates, organophosphonates, poly(acrylic acid) (P-AA), poly(maleic acid), and acrylic/maleic acid-based copolymers are used to prevent the precipitation and deposition of unwanted materials (e.g, mineral scales, corrosion products, biomass, and suspended matter). A variety of corrosion control chemicals (e.g., polyphosphates, organophosphonates, tolyltriazole, benzotriazole, filming amines, and oxygen scavengers) are used to prevent the deterioration of metal-based equipment such as heat exchangers, pipes, and pumps. In addition, oxidizing and nonoxidizing biocides are also used to control the formation and deposition of microbiological films on heat exchangers.

Currently, a large variety of polymers are commercially available, and they possess a wide range of physical and chemical properties including composition, molecular weight, solids (total and active) level, degree of neutralization, residuals (e.g., residual monomers, polymerization process by-products, etc.) For example, P-AAs, even those with the same “reported” molecular weights produced by different manufacturers can have distinctly different properties. Thus, the selection of polymer should be based on technical/business needs and customer requirements. This chapter reviews synthetic polymers, and specifically those used for deposit control in the water treatment industry. The parameters by which polymers may be characterized are discussed. The history and role of polymers in cooling water treatment (CWT) and boiler water treatment (BWT) applications are also reviewed. Several examples of applications of laboratory screening tests (discussed in Chapter 5) to evaluate deposit control polymers are included as a means to explain how different types of polymers perform.

22.2 POLYMER TYPES

The word “polymer” is derived from the Greek words “poly” (many) and “mer” (part). A polymer is a substance made of many small molecules (monomers) connected into long chains. Polymers can be categorized as either inorganic or organic (natural and synthetic) as discussed below.

22.2.1 NATURAL POLYMERS

Natural polymers include sodium alginates tannins, starches, lignosulfonates, sodium polyphosphates, and silica. Sodium alginate is a form of carbohydrate that is extracted from the cell walls of kelp. The alginates function by adsorbing onto the surfaces of the precipitated particles preventing them from agglomerating by keeping the particles fluidized and nonadherent. Therefore, the alginates act principally as dispersants and crystal modifiers. Alginates and lignosulfonates are rarely used today because of the marginal performance and temperature stability problems.

Sodium polyphosphate (a well-recognized detergent builder and corrosion and scale inhibitor) is an inorganic polymer containing P–O–P units that are made by the dehydration of phosphate ions. Although polyphosphate exhibits good corrosion and scale inhibiting properties, it hydrolyzes or reverts to orthophosphate ions. Polyphosphate reversion results in the loss of all their corrosion and scale control properties. In addition, the orthophosphate ions that form from the hydrolysis process combine with the available calcium ions to form calcium orthophosphate deposits. In many cases where polyphosphates have been used, they may have been the principal source of calcium phosphate deposits.

22.2.2 SYNTHETIC POLYMERS

Synthetic deposit control polymers include P-AA, poly(maleic acid), and (meth)acrylic acid or maleic acid–based copolymers. Synthetic polymers may be classified as homopolymers or copolymers depending on the number of monomers used in the polymerization recipe. For example, homopolymers contain repeating units of only one monomer. Table 22.1 shows the list of homo-, co-, and terpolymers commonly used in water treatment formulations (a more detailed description of structures of various polymers is presented in Chapter 5, Table 5.1). As indicated, the monomers used to make these polymers contain different functional groups (e.g., COOH, SO₃H, CONH₂), as well as different ionic charges (i.e., anionic, nonionic, cationic). The copolymers are produced by polymerization of two or more monomers of different compositions. Some monomers such as acrylamide and acrylate ester may not be hydrolytically stable and therefore polymers containing these monomers may not be suitable for high pH formulations.

22.2.3 POLYMERIZATION METHODS

Polymerization refers to the bonding of two or more monomers to produce a polymer. Polymerization is also any chemical reaction that produces such a bonding. Polymerization methods for synthetic polymers include precipitation, solution, suspension, emulsion, and bulk as discussed below. All of these polymerization methods have the advantage of heat and viscosity control during the polymerization. The desired product properties dictate the choice of polymerization process.

TABLE 22.1
Deposit Control Polymer Types

Polymer	Acronym(s)	Functional Group(s)
Homopolymers		
Poly(acrylic acid)	P-AA	COOH
Poly(methacrylic acid)	P-MAA	COOH
Poly(maleic acid)	P-MA	COOH
Copolymers of AA and/or MAA and monomers such as		
Acrylamide or substituted acrylamide	Am or SAm	CONH ₂ or CONR ₁ R ₂
Acrylate esters	AE	COOR
Maleic acid or maleic anhydride	MA	COOH
Sulfonic acid or sulfonated styrene	SA or SS	SO ₃ H or Styrene–SO ₃ H
Copolymers of MA and monomers such as		
Acrylic acid and/or methacrylic acid	AA or MAA	COOH
Acrylate esters	AE	COOR
Sulfonic acid or sulfonated styrene	SA or SS	SO ₃ H or Styrene–SO ₃ H
Alkenes	—	(R ₁ , R ₂)C = C(R ₃ , R ₄)

22.2.3.1 Precipitation Polymerization

In precipitation polymerization, all reactants are initially soluble in the polymerization solvent. Polymerization proceeds in the solution until the polymer reaches a critical molecular weight when the precipitation of the polymer occurs due to polymer insolubility in the solvent. Polymerization then proceeds in the heterogeneous medium by absorption of monomer and initiator into the polymer particles.

22.2.3.2 Solution Polymerization

In solution polymerization, all reagents, including the polymeric product remain soluble in the polymerization solvent throughout the reaction.

22.2.3.3 Suspension Polymerization

In suspension polymerization, droplets (50–500 μm) of a water-insoluble monomer are suspended in water by means of a suspending agent (usually less than 0.1 wt% of the aqueous phase). Both the suspending agent and agitation are necessary in order to keep the monomer droplets from coalescing. By reusing large amounts of dispersing agent (>1 wt%), very small monomer droplets can be produced that give polymer particle size ranging from 0.5 to 10 μm . The process is then called dispersion polymerization.

22.2.3.4 Emulsion Polymerization

In emulsion or latex polymerization, the polymerization of monomer only occurs with monomer that is contained within the micelles (colloidal dispersion) that are formed in water by means of a surfactant. These colloidal dispersions are generally stable, and once formed do not need agitation to maintain the colloidal state. A hydrophilic monomer is emulsified in water and polymerization is initiated with a water-soluble initiator.

22.2.3.5 Inverse Emulsion Polymerization

In inverse emulsion, a hydrophilic monomer is emulsified in a nonpolar organic solvent.

22.2.3.6 Bulk Polymerization

Bulk polymerization is the polymerization of the neat monomer(s).

22.2.4 POLYMERIZATION PROCESSES

Reportedly, there are over 50 P-AA manufacturers in the United States. Many of these products are used internally in applications that do not demand the consistent high quality and performance requirements of the deposit control polymers used by the water treatment industry. Less than a dozen manufacturers are actively supplying the water treatment industry. Not surprisingly, there are wide variations in the manufacturing processes as well as the product appearance consistency and physical properties of the P-AAs offered.

Deposit control polymer manufacturers that supply the water treatment formulators use a variety of manufacturing techniques. The choice of a polymerization process depends on several considerations including technology alternatives, product performance and application requirements, and economics. Solution polymerization is the primary method for manufacturing scale and deposit control polymers. Solution polymerization process variables include polymerization medium (water, solvent), initiator/catalyst, chain transfer agent, monomer(s), temperature, time of reaction, and agitation. For brevity, these variables are not discussed herein. However, it is important to note that polymer manufacturing complexity increases proportionately to the number of monomers in part because of the different properties and reaction rates of individual monomers.

22.2.5 POLYMER CHARACTERISTICS

Polymers may be characterized by several parameters including molecular weight, tacticity, end groups, branching, residual monomers, and homogeneity or heterogeneity, as discussed below.

22.2.5.1 Molecular Weight

A polymer sample consists of varying (short and long) chain lengths as opposed to a monomer sample where all molecules have the same length. Hence, a polymer sample does not have a unique molecular weight, unlike a monomer sample that has a precisely defined molecular weight. A polymer sample is typically characterized by an average molecular weight and molecular weight distribution. The actual number depends on the molecular weight measurement method, and there may be considerable associated bias. Table 22.2 provides a listing of molecular weight measurement methods among which gel permeation chromatography (GPC) and viscosity are the two most frequently used by water treatment polymer manufacturers. Table 22.3 summarizes the major measurements used to characterize the molecular weight of deposit control polymers. Figure 22.1 illustrates typical

TABLE 22.2
Polymer Molecular Weight Measurement Methods

Freeze point depression
Boiling point elevation
Osmotic pressure
Vapor pressure lowering
Viscosity
Light scattering
Ultra centrifugation
Sedimentation
Gel permeation chromatography

TABLE 22.3
Measurements Used to Characterize the Molecular Weight of Polymers

M_n	Number-average molecular weight. Emphasizes the low molecular weight fraction.
M_v	Viscosity-average molecular weight. Used to compare data from GPC to data obtained by viscosity methods. Close to the weight-average molecular weight.
M_w	Weight-average molecular weight. Emphasizes the central portion of the molecular weight distribution.
M_z	High molecular weight fraction. The larger this is compared to M_w , the more high molecular weight fraction is present.
M_w/M_n	Polydispersity. Measures the breadth of the molecular weight distribution. The smaller this number, the narrower the distribution.

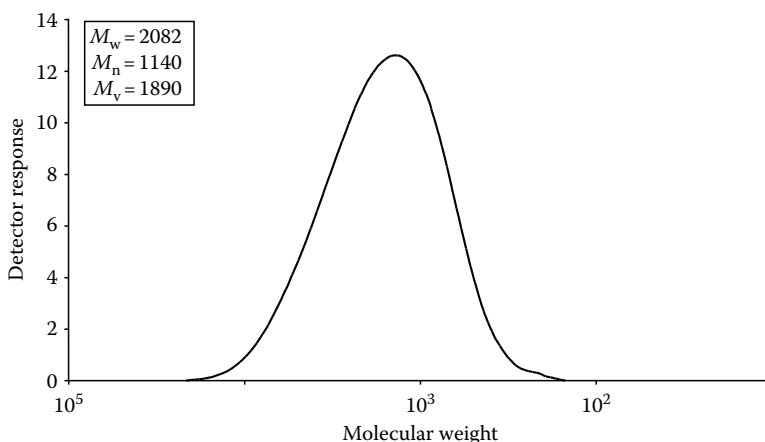


FIGURE 22.1 Typical molecular weight distribution of deposit control polymer.

aqueous GPC molecular weight distribution of a commercial P-AA. Other than composition, molecular size is the most important factor that gives the characteristic of polymeric material.

22.2.5.2 Tacticity

Monomers may contain atomic groups that are not involved in the polymerization reaction that forms the polymer backbone. These groups become pendant to the main chain. The pendant groups may be arranged in a regular manner about the polymer backbone. This gives rise to polymer tacticity. When all the pendant groups are on one side of the planar zigzag polymer chain, the polymer is isotactic. When the pendant groups are located alternatively on the opposite side of the plane of the polymer chain, the polymer is syndiotactic. If the distribution of the pendant groups is random, the polymer is atactic.

22.2.5.3 End Groups

Initiator molecules are used to commence the polymerization process. A fragment from the initiator will bond with the monomer to start a chain. The initiator fragment is then attached to one end of the polymer chain, thus becoming an “end group.” When the polymer chain stops growing due to the chemical reactions that prevent monomer addition to the chain end, another “end group” is formed.

22.2.5.4 Branching

During the polymerization process, chemical reactions take place on the backbone of a polymer chain causing the formation of a new polymer chain attached to the original one. This phenomenon is known as branching.

22.2.5.5 Residual Monomers

Polymerization reactions or the linking of monomers to form large chains are subject to chain termination reactions. Thus, at the end of a polymerization reaction, unreacted monomers or residual monomers will be left admixed with the polymeric product.

22.2.5.6 Homogeneity and Heterogeneity

When only one monomer is involved in the polymerization process, the product is homogeneous. For example, if two monomers A and B are copolymerized, and both A and B are equally reactive in the polymerization reactions, then monomer A and B will be randomly distributed in all of the polymer chains, and the product is homogeneous. However, a heterogeneous polymer is made if monomer B is less reactive than monomer A. In this case, the initially formed polymer chains contain larger amounts of monomer A compared to monomer B. As the concentration of monomer A decreases, the polymer chains formed later in the reaction will contain more of the copolymerized monomer B. Further, within each chain, the distribution of monomers A and B would not be random.

22.2.6 PARAMETERS TYPIFYING POLYMER PROPERTIES AND SPECIFICATIONS

Most deposit control polymers used by water treatment formulators are supplied as liquid solutions. The polymers may be characterized by a variety of parameters as shown in Table 22.4 and discussed below.

22.2.6.1 Form

Water treatment polymers are typically water solutions. However, some powdered sodium salts are supplied typically for use in applications where dry product dosing systems are desired.

22.2.6.2 Appearance

Deposit control polymer appearance is an aesthetic rather than a performance issue. The goal of manufacturers and formulators should be consistent product quality: batch to batch, lot to lot, and

TABLE 22.4
Parameters Typifying Deposit Control
Polymer Properties and Specifications

Form
Appearance ^a
Total solids (%) ^a
Active solids (%)
Weight-average molecular weight (Mw)
pH ^a
Viscosity (cP at 25°C) ^a
Acid number (mg KOH/g dry polymer) ^b
Specific gravity (or bulk density for powders)
Color

^a Recommended specification parameter for copolymers.

^b Recommended specification parameter for copolymers.

shipment after shipment. The polymer manufacturer should have procedures in place to ensure that the product meets a visual appearance specification and is free from any contamination. The appearance of one polymer compared to another may differ greatly. Examples of the product literature descriptions for the “appearance” of several commonly used water treatment polymers supplied as liquids are shown in Table 22.5.

22.2.6.3 Total Solids

“Total solids” measures the non-water component of a deposit control polymer. The higher the total solids, the greater a deposit control polymer’s specific gravity and viscosity. The total solids for a particular polymer are normally limited by product stability during storage conditions and/or handling considerations. Total solids measurements are used to verify that the proper level of ingredients has been used to manufacture the polymer. A deposit control polymer manufacturer’s product approval should be based on a specification that includes an acceptable total solids range; typically the midpoint $\pm 1\%$. Polymer manufacturers use a variety of test methods for determining product total solids. Ideally, a total solids test procedure should be based on removing the volatile or liquid component from the product without burning or degrading the polymer. A microwave-based drying method has been reported to give highly reproducible total solids measurements [1].

22.2.6.4 Active Solids

A polymer’s “active solids” content is the difference between the total solids and the counter ions added by post-polymerization neutralization typically with sodium hydroxide. Post-polymerization neutralization is frequently not the only source of sodium ions in a polymer. Thus, active solids cannot be measured directly. Therefore, active solids values are normally reported as a typical value (calculated) rather a measurement. It is important to remember that only the synthetic polymeric component of a product, not the counter ions from neutralization, provides value added performance. Unfortunately, most deposit control polymer manufacturers still do not publish active solids values.

22.2.6.5 Molecular Weight

A consistent molecular weight is critical to a polymer’s performance. Unfortunately, the test procedures for molecular weight determinations are very expensive and time consuming and are therefore not well suited for use as quality control tests. Molecular weight test methods are likely to be run by the analytical department of a polymer manufacturer’s research and development organization but

TABLE 22.5
Appearance of Competitive Deposit Control Polymers
Supplied as Liquids

Polymer Type	Appearance
Solvent polymerized P-AAs	Clear to hazy, colorless to amber colored Light amber with a slight haze Light straw
Water polymerized P-AAs	Water white to amber, slightly hazy Light to amber colored Clear to slightly hazy Clear straw colored
P-AA with phosphinate groups	Colorless Clear to slightly turbid yellow
Sodium P-MAA	Clear amber Clear pale yellow
P-MA	Amber Clear amber
P-AA/Am copolymer	Straw colored
MA/EA/VoAc terpolymer	Clear to slightly turbid amber
Maleic anhydride copolymer	Amber with a slight haze
SS/MA copolymer	Clear amber
AA/MA copolymer	Pale yellow and clear
Acrylate ester copolymer	Clear to cloudy, amber to slightly pink
Sulfonate copolymer	Clear, dark brown
AA/SA copolymers	Clear yellow Clear Clear to slightly hazy Water white to amber, clear to slightly hazy
AA/SA terpolymers	Clear yellow Water white to amber, clear to slightly hazy

Note: P-AA, poly(acrylic acid); AA, acrylic acid; MA, maleic acid or maleic anhydride; EA, ethyl acrylate; SS, sulfonated styrene; VoAc, vinyl acetate; SA, sulfonic acid.

are not typical for manufacturing operations. Polymer manufacturers typically define a product by total solids and viscosity specifications that are closely related to a polymer's molecular weight.

22.2.6.6 pH

Measurement of pH is used to verify that a product has been produced to established specifications and is a direct indication of the extent to which a polymer is neutralized.

22.2.6.7 Viscosity

A polymer's viscosity, as discussed previously, is directly related to molecular weight. Therefore, viscosity measurements are a means to verify that a product is within established specifications. Product approval is based on the established specifications and the specific test procedure (e.g., 25°C, RVF # spindle, and rpm) for each product.

22.2.6.8 Acid Number

Acid number measurements are a means to verify that deposit control copolymers are within the established tolerances for ratios of co-monomers and the degree of neutralization.

22.2.6.9 Specific Gravity

Specific gravity provides a measurement of a product's density. Although specific gravity is a relatively easy test to run, the information it provides pertaining to a product's composition vs. water is redundant to the total solids measurement.

22.2.6.10 Color

Color measurement such as Gardner (yellow), Lovibond yellow, and Lovibond red may be used as an indicator of a product's appearance.

22.2.6.11 Other Parameters

There are a variety of other parameters such as turbidity, haze, iron, and residual monomer levels that may be of interest for specific water treatment polymers and/or for particular applications. A brief discussion of each of these parameters follows.

Turbidity and haze measurements are not typical quality control parameters. However, turbidity and/or haze measurements may provide a means to verify that a polymer meets an established criterion for appearance.

Deposit control polymers typically contain low levels of iron as a by-product of the manufacturing process or that are present in the raw materials. However, iron measurements are not a typical quality control test. Only in rare cases will deposit control polymer iron levels be a concern. A polymer may contain excessive iron levels if it turns black when fully neutralized with caustic soda.

Unreacted or residual monomer(s) or solvent(s) may be a health/safety work exposure, production process efficiency, or regulatory issue. Neither residual monomer nor residual solvent measurements are typically quality control tests. However, periodic testing of residual monomer and/or solvent (if applicable) levels may be used by a deposit control polymer manufacturer to ensure that the production process is operating properly or to meet a regulatory agency requirement for new chemical substances.

22.2.7 DIFFERENCES BETWEEN WATER TREATMENT POLYMERS

Acrylic acid based water treatment polymers are normally polymerized as acid but not all polymerization processes are the same. Polymers are typically neutralized with sodium hydroxide after polymerization to various degrees in order to (a) provide pH values above the DOT limit for corrosive materials, (b) ensure product stability in the drum, and (c) meet specific customer requirements. However, polymer neutralization adds inactive solids and thus, higher pH values (a) imply greater gaps between total and active solids and (b) necessitate lower total solid levels in order to supply products with manageable viscosities. Accordingly, in addition to molecular weight properties, it is important to examine the pH, total solids, and active solids of the competitive polymers in order to ensure "an apple to apple comparison." Another way to understand the differences between water treatment polymers supplied at different pH values is to obtain or develop neutralization curves for deposit control polymers such as shown in Figure 22.2 for Carbosperse™* K-7028 and Carbosperse™ K-7058 (≈3000 and ≈6000 molecular weight, respectively). Extending the discussion above, it is logical and in practice has been found that concentrated polymers (those supplied at higher total solids and lower pH values) more readily facilitate the preparation of more concentrated water treatment formulations. In addition, deposit control polymers supplied at higher total solids and lower pH values mean less packaging materials and freight costs per active pound of product supplied.

Most deposit control polymer manufacturers use aqueous polymerization processes. However, solvent polymerization process results in the manufacture of polymers, and P-AAs, in particular, with performance characteristics that are superior to P-AAs made in aqueous medium. The

* Carbosperse is a registered trademark of The Lubrizol Corporation.

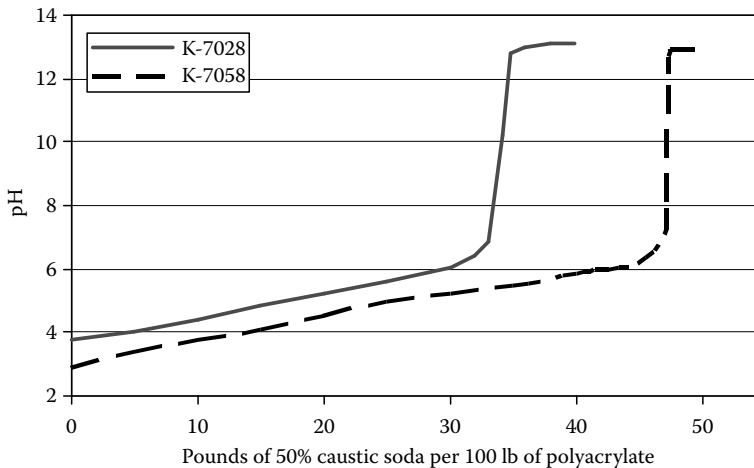


FIGURE 22.2 Pounds of 50% caustic soda per 100 lb of polymer.

distinguishing properties of solvent-based P-AAs (e.g., Carbosperse K-752 and Carbosperse K-732) compared to P-AAs of similar MW, made by aqueous polymerization processes (e.g., K-7028 and K-7058, respectively) include (a) exceptional calcium ion tolerance (facilitating the operation of cooling systems at higher cycles of concentration), (b) greater thermal stability, (c) better silt/clay dispersion, and (d) greater formulating flexibility.

Dubin and Fulks [2] concluded that “polymer structure, molecular weight and even the method of manufacture and choice of solvent will strongly influence the activity of a polymer. The practical significance of this is that gross descriptions of polymers such as polyacrylate or copolymers do not accurately describe a polymer accurately or define its performance, especially under different water conditions.”

Lubrizol believes that “it is often desirable to use a polymer product in which the molecules are as similar as possible” or to have a polymer with a narrow molecular weight distribution. However, others [3] have found that polyacrylates with broad molecular weight ranges are generally more cost effective than polyacrylates with narrow molecular weight ranges. Regardless of whether broad or narrow molecular weight distributions are optimal, there is a consensus that molecular weight is a key factor in determining the optimal polymer(s) for a particular application [2–5].

22.3 THE EVOLUTION AND ROLE OF DEPOSIT CONTROL POLYMERS IN WATER TREATMENT APPLICATIONS

22.3.1 HISTORICAL PERSPECTIVE

The use of synthetic water treatment polymers dates back to the 1950s [6]. The early synthetic polymers used were high MW (>100,000 Da) P-AAs. With the passage of time, lower MW P-AAs as well as poly(methacrylic acids), P-MAs, and poly(maleic acids), P-MAs, were found to be more efficacious. Researchers have shown that P-AA molecular weight is an important consideration relative to performance [3–5]. Eventually, copolymers of acrylic acid, methacrylic acid, and maleic acid were found to provide improved performance characteristics for specific applications.

In the late 1970s, Betz Laboratories introduced the Dianodic II® stabilized phosphate CWT program, which incorporated the use of acrylic acid/hydroxypropyl acrylate (AA/HPA) copolymer [7]. Reportedly, the AA/HPA technology which Betz patented and used for this application was not originally intended for use in CWT but in the pulp and paper industry. The Dianodic program dominated the heavy industrial CWT market place for a number of years as it provided an environmentally acceptable alternative to chromate-based water treatment programs.

In the mid-1980s, Calgon Corporation introduced its pHreeGUARD® CWT program based on acrylic acid/2-acrylamido-2-methylpropane sulfonic acid (AA/SA) copolymer called TRC-233™. This copolymer technology [8] was touted as having “improved operating conditions by eliminating or minimizing acid feed, removed the potential for deposit formation, and increased cycles of concentrations.” Subsequently, a barrage of technical papers touted successful applications of non-chromate CWT programs including alkaline all-organic [9,10], phosphate-based [10], molybdate-based [13], and alkaline-zinc [14] CWT programs. These papers and several others [15–18] point out that the secret to the successful application of non-chromate CWT programs was the evolution of copolymer technology that is capable of supporting the alternative corrosion inhibitors programs.

The success of the Betz Dianodic II program is largely responsible for triggering efforts by other water service companies and merchant market polymer manufacturers to develop alternative polymer technology. The rapid research and development period occurred in the 1980s and led to the introduction of a variety of merchant market polymers. These proprietary deposit control copolymers as a class have been targeted to provide specific performance properties in some cases for niche applications, and typically have been progressively more expensive.

22.3.2 CURRENT ENVIRONMENT

The use of synthetic deposit control polymers in water treatment applications has increased dramatically since the 1950s. The demands on deposit control polymer performance have increased significantly due to trends toward operating cooling water systems using more environmentally friendly corrosion inhibitors and under more severe operating conditions to increase process efficiency, safety, and water conservation. Modern deposit control polymers have multifunctional properties that are typically the key to successful water treatment program application/performance. The multifunctional properties of deposit control polymers are precipitation prevention for scale forming salts (i.e., calcium carbonate, calcium sulfate, calcium phosphate, calcium phosphonate, etc.), stabilizing metal ions (i.e., Fe, Mn, Zn), and dispersing suspended matter that collectively prevent and/or control the deposition of unwanted materials on heat exchangers and equipment surfaces. It is generally agreed that these polymers operate by adsorption onto submicroscopic crystallites, thereby preventing further crystal growth and deposition.

Most of the commercially available deposit control polymers used today are acrylic acid or maleic acid based homo- or copolymers. Table 22.6 provides an overview of the types of deposit control polymers used by the water treatment industry.

22.3.3 DEPOSIT CONTROL POLYMERS IN COOLING AND BOILER WATER TREATMENT APPLICATIONS

The functions of deposit control polymers as components of CWT and BWT programs are summarized in Table 22.7. Wilkes [6] provides a review of the functions and mechanisms. Other papers [10,11,15–17,19] outline the generic components used in non-chromate CWT programs and how these programs should be selected and applied [11,17,19].

22.3.3.1 Cooling Water Treatment Programs

The major non-chromate CWT programs used today and the functions performed by the deposit control polymer components are summarized in Table 22.8.

22.3.3.2 Boiler Water Treatment Programs

BWT programs in use today and the treatment objectives are described in Table 22.9. Collectively, this information indicates that the roles of polymers in BWT programs include sludge conditioning, particulate dispersion, and hardness stabilization.

TABLE 22.6
Types of Commercially Available Deposit Control Polymers

Product/ Acronym	Description	Supplier
K-752	Solvent polymerized ≈ 2 k M_w P-AA	Lubrizol Advanced Materials
K-732	Solvent polymerized ≈ 6 k M_w P-AA	Lubrizol Advanced Materials
K-7028	Water polymerized ≈ 2 k M_w P-AA	Lubrizol Advanced Materials
K-7058	Water polymerized ≈ 7 k M_w P-AA	Lubrizol Advanced Materials
K-765	Water polymerized ≈ 30 k M_w P-MAA	Lubrizol Advanced Materials
K-766	Water polymerized ≈ 5 k M_w P-MAA	Lubrizol Advanced Materials
BC200	P-MA	BWA water additives
V-TL4	P-SS/MA	Alco chemical
K-775	P-AA/SA (75/25) < 10 k M_w	Lubrizol Advanced Materials
K-776	P-AA/SA (60/40) > 10 k M_w	Lubrizol Advanced Materials
AC3100	P-AA/SA/NI < 10 k M_w	Rohm and Haas
K-781	P-AA/SA/SS < 10 k M_w	Lubrizol Advanced Materials
K-797	P-AA/SA/SS < 15 k M_w	Lubrizol Advanced Materials
K-798	P-AA/SA/SS < 15 k M_w	Lubrizol Advanced Materials

Note: AA, acrylic acid; MA, maleic acid; MAA, methacrylic acid; SS, sulfonated styrene; SA, 2-acrylamido-2-methylpropane sulfonic acid; NI, nonionic monomer.

TABLE 22.7
**Roles of Deposit Control Polymers
 in CWT and BWT Programs**

Deposit Control Function	CWT	BWT
Scale inhibitors for		
Carbonate and sulfate scales	X	X
Calcium phosphate	X ^a	X ^a
Calcium phosphonate	X ^a	—
Particulate dispersants for		
Silt, mud, etc.	X	—
Iron oxide	X ^a	X ^a
Sludge conditioners	—	X

^a Copolymers are required.

TABLE 22.8
**Major Non-Chromate CWT Programs and Deposit
 Control Polymer Functions**

CWT Program	Deposit Control Polymer Functions
All-organic	Ca-phosphonate inhibitor, dispersant
Stabilized-phosphate	Ca-phosphate inhibitor, dispersant
Molybdate-based	Ca-phosphonate inhibitor, Ca-phosphate inhibitor, Zn stabilizer, dispersant
Alkaline zinc	Ca-phosphonate inhibitor, Zn stabilizer, dispersant

TABLE 22.9
BWT Program Types and Descriptions/Objectives

Program Type/Name	Description/Objective
Precipitation Carbonate cycle	Depend upon the dispersion of calcium carbonate as boiler sludges. Normally, natural organic polymers such as starch and lignin derivatives are used in carbonate cycle programs.
Precipitation Phosphate cycle	Rely upon the precipitation and dispersion of calcium phosphate sludge (ideally calcium hydroxyapatite) to minimize accumulations on heat transfer surfaces. Synthetic polymers are used to ensure that the sludge remains fluid until removed via blowdown.
Precipitation Coordinated phosphate	Typically used in boilers operating at ≥ 800 psig. Alkaline and acid phosphates (e.g., mono-, di-, and trisodium) are used to control the free caustic that accumulates in restricted flow areas. Neutralizing amines and oxygen scavengers are used (usually fed separately) as appropriate. Synthetic polymers are used to disperse iron-containing suspended solids and stray calcium compounds.
Chelant	Typically use chelating agents such as ethylenediamine tetraacetic acid (EDTA) or nitrilotriacetic acid (NTA) to complex feed water calcium or magnesium so it cannot form boiler scale. Synthetic polymers are required to disperse suspended iron compounds and any salts that precipitate as a result of the fluctuations in feed water hardness ions and/or treatment programs upsets.
All polymer	Rely on the stabilizing properties of polymers as alternatives to EDTA and NTA in chelant programs. Polymers also disperse iron and other suspended solids in these programs.

22.3.4 DEPOSIT CONTROL POLYMER MECHANISMS

The mechanisms for deposit control polymers in CWT and BWT applications include (a) scale inhibition, (b) dispersion, (c) metal ions stabilization, and (d) crystal modification. The following sections present discussions on the performance of deposit control polymers as scale inhibitors, crystal modification agents, dispersion agents, and metal ions stabilization agents.

22.3.4.1 Scale Inhibition

In most industrial water systems, the dissolved salts in the feed water are concentrated. If supersaturation occurs and their solubility limits are exceeded due to increased cycles of concentration (or increased system recovery in reverse osmosis (RO) processes), precipitation or scaling will occur. The precipitation and deposition of sparingly soluble salts results in scaling on heat exchanger, RO membranes, and other equipment surfaces. Among the methods used to prevent scaling are the acidification of the water and the use of chemical additives (polymeric and non-polymeric). These methods prevent and/or retard markedly the precipitation and deposition of scale forming salts on various surfaces. The acidification method has the disadvantage of exposing metal surfaces to a corrosive environment, while the use of chemical additives seems promising since only very low concentrations are needed to extend the time required for the initiation of scale formation. Also, if the acid feed system shuts down, an increase in pH can cause immediate precipitation of calcium carbonate and calcium phosphates. Due to more stringent regulations and from a worker-safety perspective, addition of chemical additives seems to be the only reliable solution to the scaling problem. Figure 22.3 presents the performance data for the inhibition of barium sulfate (BaSO_4) in the presence of P-AAs of varying MW. It is evident that under similar experimental conditions the BaSO_4 inhibition value increases with decreasing MW (from 20,000 to 2,000), reaches a maximum at an MW about 2,000, and thereafter decreases with decreasing MW (from 2000 to 800). Similar correlations of deposit control polymer MW and precipitation inhibitor efficacy has been reported and/or observed for calcium carbonate, calcium sulfate, and calcium phosphate systems [3,5,6].

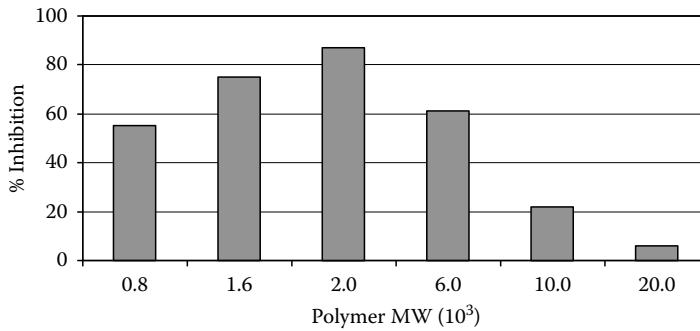


FIGURE 22.3 Barium sulfate inhibition by P-AAs of varying molecular weights ($\text{BaSO}_4 = 5.00 \times 10^{-4} \text{ M}$, pH 7.00, $T = 35^\circ\text{C}$, 24 h).

22.3.4.2 Dispersion

The fouling of heat exchangers and RO membranes by suspended matter is a critical concern to water technologists and plant operators. Certain feed waters, especially surface waters, require far more extensive pretreatment than sources such as deep wells. Changes in feed water composition can occur because of seasonal variations of the water supply. Cooling water is generally contaminated with various forms of oxidized iron due to the corrosion of steel equipment, and/or its introduction with the feed water. Maintaining this oxidized iron in soluble and in dispersed forms can prevent the fouling of heat exchanger surfaces. Although iron-based deposits are common in industrial water systems, there are no prognostic methods such as those for calcium carbonate, calcium sulfate, or barium sulfate. Magnetite (Fe_3O_4) and hematite (Fe_2O_3) are the two most common iron oxide deposits encountered in industrial water systems. Other suspended matter that can contribute to deposit buildup include clay, debris, biomass, carbonate and sulfate salts of alkaline earth metals, etc.

The suspended particles typically encountered in industrial water applications generally carry a slightly negative charge. Therefore, anionic polymers are normally the most efficient dispersants because they increase negative surface charge and help keep particles suspended. Cationic polymers can be used as dispersants, but this requires relatively high polymer concentrations in order to first neutralize the negative surface charges and then to transfer cationic charge to particles for efficient dispersion. Figure 22.4 shows iron oxide dispersion data as a function of the deposit control

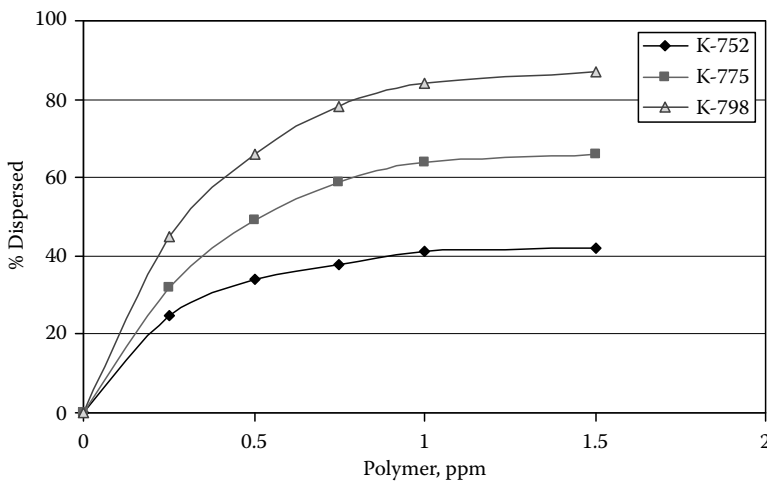


FIGURE 22.4 Iron oxide dispersion by homo-, co-, and terpolymers (100 ppm Ca, 30 ppm Mg, 314 ppm Na, 571 ppm Cl, 200 ppm SO_4 , 60 ppm HCO_3 , pH 7.8, 23°C , 1 ppm polymer).

polymer dosage for homo-, co-, and terpolymers. It can be seen that terpolymer compared to co- and homopolymers exhibits superior performance in terms of dispersing iron oxide in aqueous systems. In addition, the data also show that the dispersion value increases with increasing polymer concentration.

22.3.4.3 Metal Ions Stabilization

Among the various dissolved impurities present in the natural waters, iron-based compounds present the most serious problems in many domestic and industrial applications. In the reduced state, iron (II) or ferrous (Fe^{2+}) ions are very stable and pose no serious problems, especially at low pH values. However, upon contact with air, ferrous ions are oxidized to higher valence state and readily undergo hydrolysis to form insoluble hydroxides.

Manganese (Mn) ions like Fe^{3+} and Al^{3+} ions also cause serious fouling problems in industrial water systems. In cooling water applications, Mn-based foulants have been identified in both once-through and recirculating systems. In these cases various factors such as the presence of oxidizing agents (e.g., oxygen, chlorine), pH, temperature, and natural organics appear to influence the precipitation of manganese oxides. Manganese solution chemistry is very complex. Manganese exists in several oxidation states among which Mn^{2+} and Mn^{4+} are the most important with respect to water problems. Mn^{2+} is soluble and less susceptible to oxidation at $\text{pH} \leq 7$. In alkaline pH conditions, Mn^{2+} readily oxidizes to less soluble Mn^{4+} (e.g., MnO_2). Manganese-based deposits typically encountered in cooling water systems contain MnO_2 . Ferrous ion oxidation occurs at a somewhat lower pH than a Mn^{2+} oxidation, and this is perhaps the reason that iron and manganese salts are typically encountered together in domestic and industrial applications. Additionally, it has been reported that soluble metal ions (i.e., Cu, Fe, Mn, Zn) interfere with the performance of scale inhibitors. Thus, from a practical application point of view it is of paramount importance to keep these metal ions stabilized by polymeric additives. Figure 22.5 presents performance data on the stabilization of Mn ions by several homo-, co-, and terpolymers. Based on the performance data, the effectiveness of the polymers as Mn stabilizing agents follows the following ranking (from best to worst): terpolymers > copolymers > homopolymers. Figure 22.6 shows the optical micrographs of manganese oxide particles collected on the filter papers at the end of the experiments for K-7058 (P-AA), K-775 (P-AA/SA), and K-798 (a terpolymer of acrylic acid/2-acrylamido-2-methylpropane sulfonic acid/sulfonated styrene or P-AA/SA/SS). As shown, Carbosperse K-798 is an excellent manganese ions stabilizing agent (the darker the brown color, the more manganese oxide precipitated from the solution).

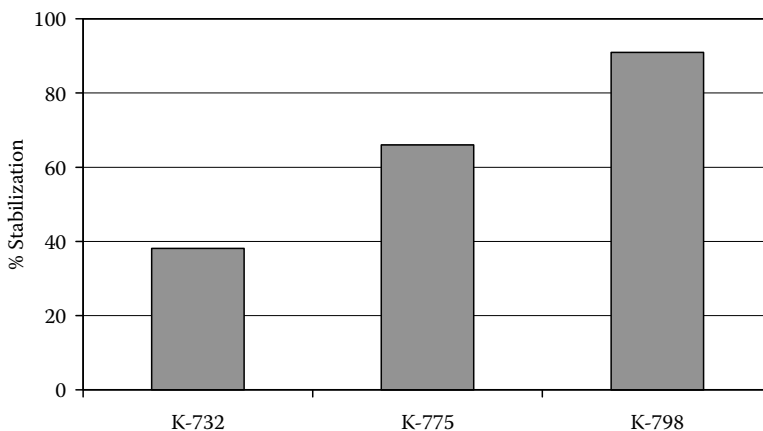


FIGURE 22.5 Stabilization of Mn^{4+} by homo-, co-, and terpolymers (104 mg/L Ca, 31 mg/L Mg, 361 mg/L Na, 202 mg/L SO_4 , 600 mg/L Cl, 146 mg/L HCO_3 , 3 ppm Mn^{4+} , pH 7.5, 23°C, 3 h, 10 ppm Cl_2 , 2 ppm polymer).

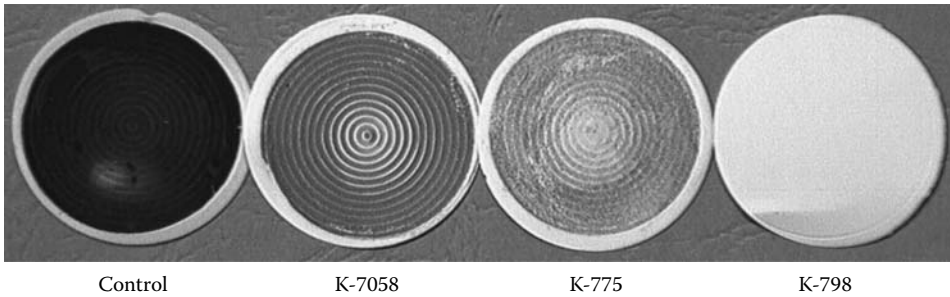


FIGURE 22.6 Manganese hydroxide precipitates formed in the absence and the presence of homopolymer (K-7058), copolymer (K-775), and terpolymer (K-798).

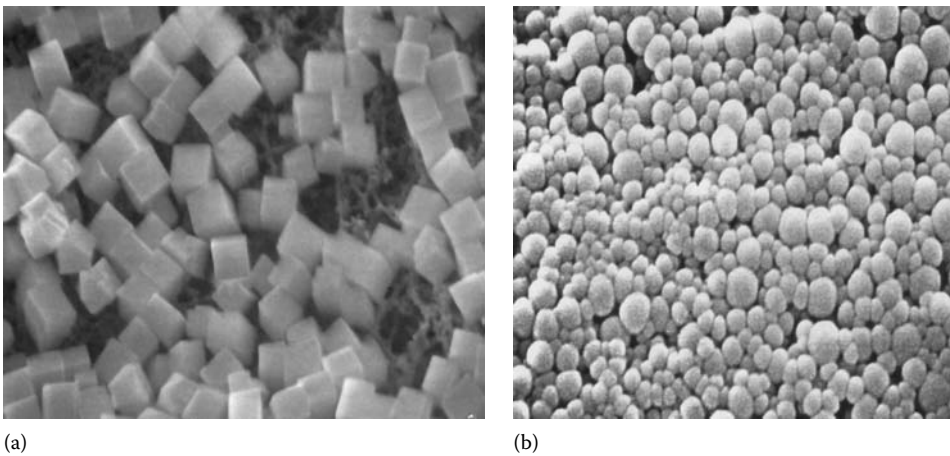


FIGURE 22.7 CaF_2 crystals grown (a) in the absence of polymer and (b) in the presence of K-798.

22.3.4.4 Crystal Modification

It has been reported that the presence of low levels of scale inhibitors influences the growth rate and morphology of crystals as well as the nature of the hydrated phase that forms [18–20]. This may be of particular importance in industrial water systems because the presence of certain inhibitors may influence the nature of the scaling mineral(s). Figure 22.7 presents scanning electron micrographs of calcium fluoride crystals grown in the absence and presence of 1.0 ppm P AA/SA/SS and clearly shows the contrast between crystals grown in the absence of inhibitor (Figure 22.7a) and highly modified crystals grown in the presence of inhibitor (Figure 22.7b). The observed change in morphology may be explained in terms of surface adsorption of K-798 on the growing calcium fluoride crystals.

22.4 SUMMARY

The information herein indicates that synthetic polymers have important roles in BWT and CWT programs. It has been shown that not all polymers are created equal, and the performance of the polymer depends on the composition, molecular weight, type, and charge of the functional groups. Polymer selection should be based on performance criteria reflecting use conditions, regulatory considerations, system metallurgy, water chemistry, and operating conditions.

REFERENCES

1. The Lubrizol Corporation, Microwave Total Solids Test Procedure for Carbosperse™ K-700 Polymers, Technical Bulletin Microwave TSTP, Cleveland, OH (October 2007).
2. Dubin, L. and Fulks, K. E. The role of water chemistry on iron dispersant performance. CORROSION/84, Paper No. 118, NACE International, Houston, TX (1984).
3. Libutti, B. L., Knudsen, J. G., and Mueller, R. W. The effects of antiscalants on fouling by cooling water. CORROSION/84, Paper No. 119, NACE International, Houston, TX (1984).
4. Thomas, P. A. and Mullins, M. A. A current review of polymeric structures and their practical significance in cooling water treatment. CORROSION/85, Paper No. 130, NACE International, Houston, TX (1985).
5. Amjad, Z. and Masler, W. F. The inhibition of calcium sulfate dihydrate crystal growth by polyacrylates and the influence of molecular weight. CORROSION/85, Paper No. 357, NACE International, Houston, TX (1985).
6. Wilkes, J. F. A historical perspective of scale and deposit control. CORROSION/93, Paper No. 458, NACE International, Houston, TX (1993).
7. Godlewski, I. T., Schuck, J. J., and Libutti, B. L. Polymers for use in water treatment. U. S. Patent No. 4,029,577 (1977).
8. Boffardi, B. C. and Schweitzer, G. W. Advances in the chemistry of alkaline cooling water treatment. CORROSION/85, Paper No. 132, NACE International, Houston, TX (1985).
9. Little, D. A., Waller, J. E., and Soule, C. Alkaline all-organic cooling water treatment. Cooling Technologies Institute, 1987 Annual Meeting, Paper No. TP 87-5, Houston, TX (1987).
10. Masler, W. F. and Amjad, Z. Advances in the control of calcium phosphonate with a novel polymeric inhibitor. CORROSION/88, Paper No. 11, NACE International, Houston TX, (1988).
11. Zuhl, R. W., Amjad, Z., and Masler, W. F. A novel polymeric material for use in minimizing calcium phosphate fouling in industrial cooling water systems. Cooling Tower Institute, 1987 Annual Meeting, Paper No. TP 87-7, Houston, TX (1987).
12. Crucil, G. A., Macdonald, J. R., and Smyk, E. B. Role of polymers in the mechanisms and performance of phosphate-based cooling water treatment programs. *International Water Conference*, Paper No. IWC-87-40, Pittsburgh, PA (1987).
13. Soeder, K. F. and Roti, J. S. Molybdate-based cooling water treatment: New developments which expand their application areas. *International Water Conference*, Paper No. IWC-87-12, Pittsburgh, PA (1987).
14. Crucil, G. A. and Schild, R. H. An alternative cooling water treatment program for the replacement of chromates. Cooling Technologies Institute, 1988 Annual Meeting, Paper No. TP 87-11, Houston, TX (1988).
15. Smyk, E. B., Hoots, J. E., Fulks, K. E., and Fivazzani, K. P. The design and application of polymers in cooling water treatment programs. CORROSION/88, Paper No. 14, NACE International, Houston, TX (1988).
16. Terry, J. P. and Yates, C. W. Current cooling water corrosion control technology. *International Water Conference*, Paper No. IWC-90-13, Pittsburgh, PA (1987).
17. Young, T. J. The proper use of modern polymer technology in cooling water programs. *AWT, Third Annual Convention*, Lake Buena Vista, FL (1990).
18. Young, T. J. The use of zinc for corrosion control in open cooling systems. Association of Water Technologies, Spring Conference, San Antonio, TX (1991).
19. Macdonald, J. R. Choosing the correct cooling water treatment programs. In *Chemical Engineering*, New York, (January 19, 1987).

23 Applications of Cationic Polymers in Water Treatment

Logan A. Jackson

CONTENTS

23.1	Introduction.....	465
23.2	Mechanisms of Coagulation and Flocculation.....	466
23.2.1	Introduction.....	466
23.2.2	Bridging Flocculation Mechanism	466
23.2.3	Charge Neutralization and the Electrostatic Patch Flocculation Mechanism.....	467
23.3	Cationic Polymers—Polyelectrolytes	468
23.3.1	Naturally Occurring Cationic Polymers	468
23.3.1.1	Cationic Starch	468
23.3.1.2	Chitosan.....	469
23.3.2	Synthetic Cationic Polymers.....	470
23.3.2.1	Polyvinylamine.....	470
23.3.2.2	Polyethyleneimines	470
23.3.2.3	Polydiallyldimethylammonium Chloride.....	471
23.3.2.4	Polyamines	472
23.3.2.5	Cationic Polyacrylamides.....	472
23.4	Manufacture of Cationic Polyacrylamides.....	472
23.4.1	Aqueous Solution Polymerization	472
23.4.2	Dry Powders and Beads.....	473
23.4.3	Inverse Emulsions	473
23.4.4	Postreaction of Polyacrylamide	474
23.4.5	Copolymerization of Acrylamide with Cationic Vinyl Monomers.....	475
23.5	Applications—Wastewater Treatment.....	475
23.5.1	Introduction.....	475
23.5.2	Potable Water Treatment (Drinking Water)	476
23.5.3	Municipal Wastewater Treatment	477
23.5.4	Industrial Raw Water Treatment	477
23.6	Summary	477
	References.....	477

23.1 INTRODUCTION

The global market for coagulants and flocculants used in water treatment in 2004 was estimated at \$2.75 billion dollars annually, with a growth rate of ~5.5% per year [1]. This includes inorganic and polymeric organic coagulants and flocculants. Synthetic cationic polymers (polyelectrolytes) and, to a much lesser degree, naturally occurring cationic polymers constitute approximately 30% of the wastewater treatment market and are used in a wide range of industries and applications.

Cationic polymers are extremely important materials used in the removal of suspended and dissolved solids from wastewaters via processes known as coagulation and flocculation. Wastewaters requiring treatment can come from a wide range of sources. This can be as simple as water from the local reservoir scheduled for clarification for drinking and domestic use to complex industrial and municipal wastewaters. Industrial wastewaters include wastewater from the manufacture of paper, industrial manufacturing, and food processing and that generated during the extraction and refining of petroleum. In general, wastewater comprises either singly or a combination of suspended solid particles (organic biological solids and inorganic materials such as mineral, clays, coal fines, aggregate washings, etc.), dissolved organic matter, and dissolved inorganic salts [2].

For the most part, the suspended and dissolved colloidal materials in wastewater bear a negative (anionic) charge and can be removed using cationic polymers via coagulation and flocculation mechanisms. The mechanisms that produce coagulation and flocculation include surface charge neutralization, complexation/precipitation, charge-patch formation, and polymer bridging [3]. In this chapter, the processes of coagulation and flocculation will be reviewed, followed by a discussion of the industrially useful cationic polymer classes. In discussing the cationic polymers, the focus will be on the polymer structure, useful molecular weight regimes, and the general manufacturing processes and applications.

23.2 MECHANISMS OF COAGULATION AND FLOCCULATION

23.2.1 INTRODUCTION

To remove small colloidal particles from water, the particles must be induced to form larger aggregates that can then be removed using physical processes (sedimentation, flotation, and filtration). The terms coagulation and flocculation are used to describe the collection of processes that can be used to aggregate smaller particles into larger structures that will allow for economical solid removal. The terms are often used interchangeably in the literature, therefore there is no well-defined, widely accepted definition [4,5]. There are at least two conventions that are in widespread use [5]. The first comes from the colloid science community and restricts coagulation to situations where particles are destabilized by simple salts or by charge neutralization. The aggregates formed are small and densely packed. Flocculation is the situation where bridging between destabilized particles occurs to form larger agglomerates. In the wastewater treatment industry, coagulation refers to the destabilization of particles by charge neutralization using an oppositely charged additive (usually a high charge density, low molecular weight polymer). Flocculation occurs by mixing to induce the aggregation of the destabilized particles. This is often accomplished by the addition of a high molecular weight polymer of opposite charge of the coagulating additive [6]. The bridging model and the charge-patch model are the two most common mechanisms used to describe the aggregation processes of coagulation and flocculation. These two mechanisms are discussed briefly in the following sections.

23.2.2 BRIDGING FLOCCULATION MECHANISM

Bridging flocculation is the process whereby a single polymer chain adsorbs and becomes attached to two or more suspended particles, as illustrated in Figure 23.1. This flocculation mechanism is dominant at low to medium polymer concentrations. The effectiveness of polymers as bridging flocculants is highly dependent on molecular weight, with higher molecular weight polymers being more effective. There is generally an optimum polymer charge and molecular weight for a particular substrate.

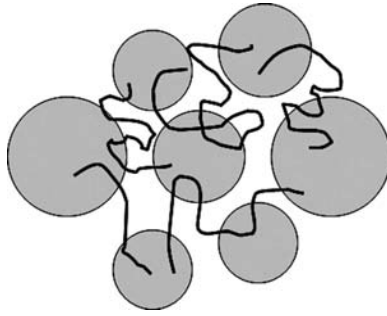


FIGURE 23.1 Illustration of bridging flocculation showing polymer chains attached to particles.

23.2.3 CHARGE NEUTRALIZATION AND THE ELECTROSTATIC PATCH FLOCCULATION MECHANISM

Charge neutralization occurs when the negative charge of the colloidal particles is equally balanced by the cationic charge of the polymer. (There is an optimum dosage required to achieve the most effective flocculation.) This destabilizes the particles and induces aggregation by coagulation and/or flocculation. Highly charged, low molecular weight polymers tend to adsorb and spread out more in flat conformations. Thus, the tendency for interparticle bridging is small. The charge density of the polymer is more important than the polymer molecular weight. This is indeed the case for low molecular weight, highly charged cationic polymers, such as polyamines and poly(diallyldimethylammonium) chloride (poly-DADMAC) polymers, which are often called coagulants in the wastewater treatment industry.

In reality, when a highly charged cationic polyelectrolyte adsorbs on particles with a weakly charged negative surface, it is not possible for all of the surface charge to be neutralized by the cationic segment of an absorbed chain. The distance between negative surface charges may be significantly different than the distance between positive charges on the cationic polymer chain. This leads to overall charge neutralization but will leave patches of charge on the surface of the particle. This is known as the electrostatic patch mechanism and is shown in Figure 23.2.

Obviously, if patches of charge exist on the surface of the particle, even though the net charge on the particle is zero, patch regions can still show strong electrical attraction to oppositely charged patch regions on other particles. The attraction between two oppositely charged regions between two patches is responsible for coagulation and flocculation. Flocculated aggregates formed by the

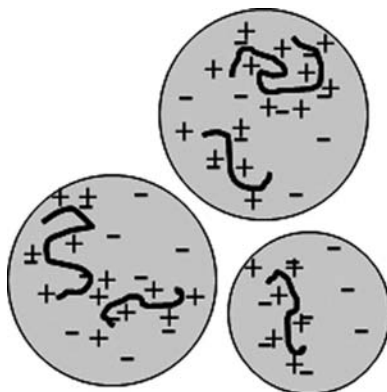


FIGURE 23.2 Electrostatic patch model for cationically charged polymers and negatively charged particles.

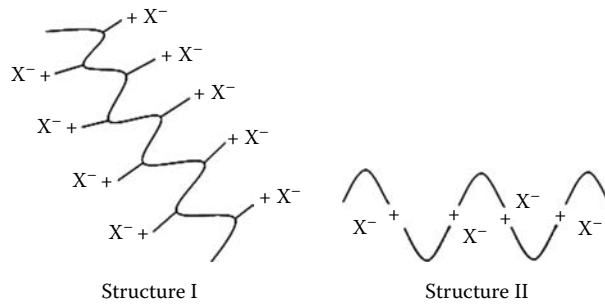


FIGURE 23.3 Schematic of types of cationic polymer backbones showing pendant cationic charges attached along the backbone (structure I) and within (structure II) the polymer backbone.

electrostatic patch mechanism are known to be quite reversible in nature when exposed to high shear and can be easily broken up to smaller aggregates by mixing.

23.3 CATIONIC POLYMERS—POLYELECTROLYTES

Numerous definitions for the term polyelectrolytes (charged polymers) can be found in the literature [7,8]. Simply put, polyelectrolytes are charged, polymeric materials that have either anionic or cationic charge placed along the polymer backbone or charged pendant groups placed along the polymer chain. In the case of cationic polyelectrolytes, the polymers are positively charged, with the charge being contained within the backbone or pendant of the polymer chain, as shown in Figure 23.3.

Cationic polymers (cationic polyelectrolytes) can be derived from natural, biological sources or can be synthetic in nature, prepared from the appropriate monomers. Not all of the materials described in the following sections are used extensively in wastewater treatment. However, they are industrially valuable cationic polymers in their own right and their areas of application are mentioned. A discussion of the two basic classes of cationic polymers (natural and synthetic) with their industrial value is given in the following sections.

23.3.1 NATURALLY OCCURRING CATIONIC POLYMERS

Naturally occurring cationic polymers have long been used as coagulants and flocculants [9]. The key advantage with naturally occurring polymers is that, in general, they are nontoxic, biodegradable, and often locally available. However, naturally occurring materials are often not as cost effective as synthetic polymers, mostly because of the low degree of cationic substitution achievable versus synthetic polymers. This type of polymers tend to be used in niche markets, where their low toxicity and biodegradability are more important than the cost of the materials.

23.3.1.1 Cationic Starch

Starch is a highly polymerized carbohydrate and its use in treating water dates back thousands of years [9]. Cationic starch is prepared by the reaction of a natural starch (nonionic) with a quaternizing agent [10,11]. An example of cationic starch is shown in Figure 23.4. The degree of substitution is typically low, being 0.02–0.03 [12]. The use of cationic starch in the papermaking industry is very well known. It is used to enhance paper strength and as a sizing agent [13,14]. Cationic starch can be sold as dry solids and as liquid dispersions in water. In wastewater treatment, cationic starch is used as a clarifying agent for the treatment of drinking water and in the treatment of some industrial wastes owing to its natural biodegradability. However, cationic starch is rarely used in municipal wastewater treatment due to the sludge volumes generated and the cost and performance in comparison to synthetic cationic polymers.

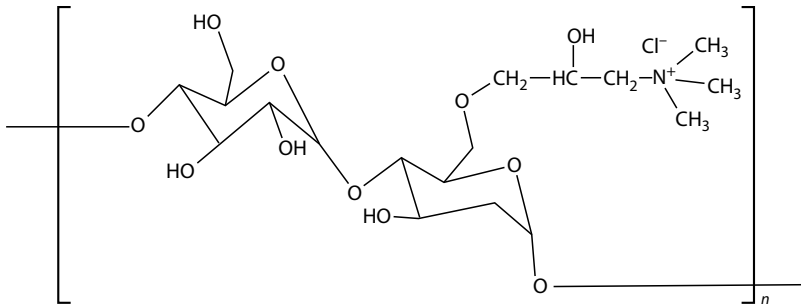


FIGURE 23.4 General structure of a cationic starch.

23.3.1.2 Chitosan

Chitosan (poly-D-glucosamine) is another naturally occurring cationic polymer of note and is produced commercially by the deacetylation of chitin (chitin is the primary structural element in the exoskeleton of crustaceans and the most abundant naturally occurring polymer after cellulose) [15,16]. This polysaccharide is composed of randomly distributed, deacetylated *N*-acetylglucosamine units. At low pH, the amine groups of the polymer backbone are cationically charged and the polymer is water soluble. The general preparation of chitosan from chitin is shown in Figure 23.5. These materials are of great importance from the aspects of low toxicity, biodegradability, and source. Although chitosan has numerous uses in the food industry [17] and is a biocide in medical, textile, and agricultural applications [18,19], it has found little use in general wastewater treatment. Again, this is due to the cost–performance disadvantage in comparison to synthetic cationic polymers.

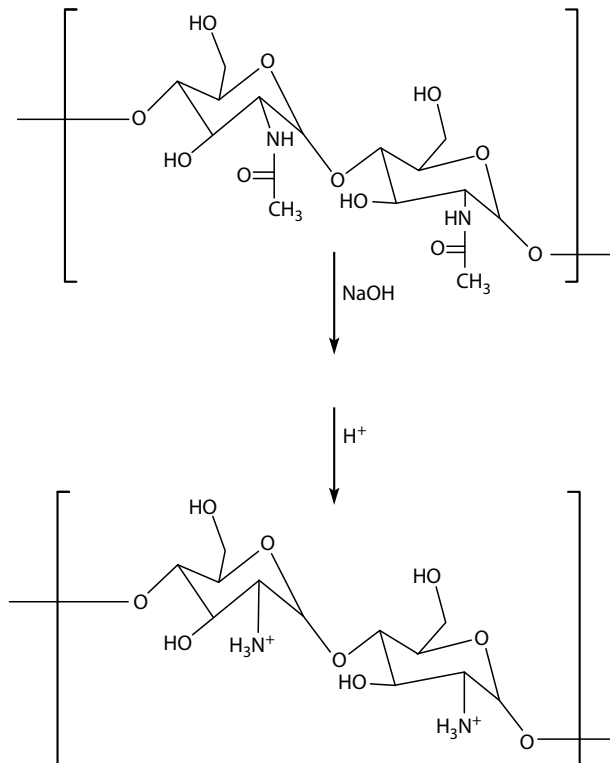


FIGURE 23.5 Production of Chitosan from Chitin by deacetylation of Chitin followed by protonation to yield the cationic chitosan polymer.

23.3.2 SYNTHETIC CATIONIC POLYMERS

Classes of synthetic organic cationic polymers that have significant industrial value include the typically lower molecular weight polyvinylamines (PVA), polyethyleneimine, (PEI), poly-DADMAC and copolymers, and dimethylamine/epichlorohydrin addition polymers (EPI/DMA) and the generally higher molecular weight cationic polyacrylamide (PAM) copolymers. The PVA, PEI, poly-DADMAC, and EPI/DMA polymers are lower molecular weight materials ranging from 1,000 to 500,000 g/mol while the PAM copolymers can have molecular weights ranging from a few thousands to tens of millions g/mol. The lower molecular weight materials (<500,000 g/mol) are often described as coagulants (PVA, PEI, poly-DADMAC, and EPI/DMA) for their ability to aggregate suspended material into small tight particles. The higher molecular weight materials (cationic PAM) are termed flocculants for their ability to aggregate suspended material into large flocculated aggregates by bridging flocculation that can easily be dewatered. However, keep in mind, as mentioned above, the terms, coagulant or flocculant, are well defined by any particular convention, but for our purposes here these definitions will suffice.

23.3.2.1 Polyvinylamine

Polyvinylamine is prepared commercially by free-radical polymerization of *N*-vinylformamide, followed by hydrolysis as shown in Figure 23.6 [20,21]. If acid hydrolysis is used for conversion, then the resulting polyvinylamine is cationic [21]. Processes to manufacture polyvinylamine in dry powder, aqueous solution, emulsion, and dispersion have been described in the literature [22]. Polyvinylamine has found utility in numerous areas; however, its greatest value has been in the paper industry, where it is used as various forms of papermaking additives [23,24].

23.3.2.2 Polyethyleneimines

The polyethyleneimines constitute a large family of water-soluble polyamines of varying molecular weight and degree of modification [25,26]. Unmodified polyethyleneimine (PEI) is produced by the ring-opening cationic polymerization of ethyleneimine and has been shown to be highly branched, containing primary, secondary, and tertiary amines in the polymer backbone [27,28]. When protonated (under acidic conditions), these materials are cationic and water soluble. The protonated form of PEI is shown in Figure 23.7. The degree of protonation varies as a function of the pH of the aqueous solution. At a pH of 10.5, approximately 1 in 40 nitrogen atoms are protonated, at pH 7, 1 in 10 and at pH 4, 1 in 2 are charged.

PEI is useful in a broad range of applications requiring cationic charge that include papermaking, oil production, textile manufacture, water clarification (coagulation/flocculation), agriculture, and mining. Papermaking is one application where PEI and modified PEIs are used extensively. Although the starting material, ethyleneimine monomer, is extremely toxic, its thermodynamic

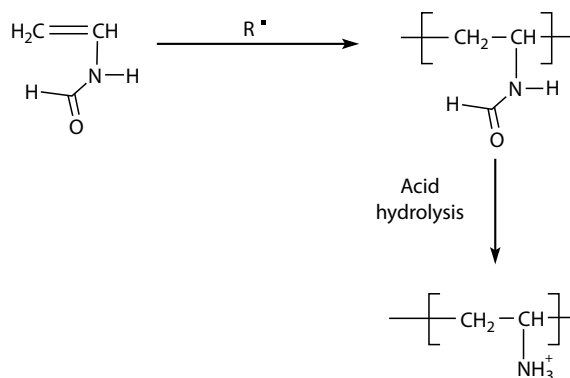


FIGURE 23.6 Process for the preparation of polyvinylamine.

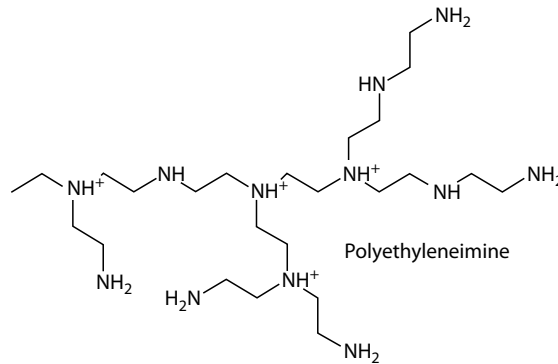


FIGURE 23.7 Basic structure of polyethyleimine showing the various types of branching that can occur.

instability and high chemical reactivity yield PEI polymers with essentially no monomer residuals (<50 ppb). However, due to the cost of PEI compared to metal salts and other less expensive synthetic cationic polymers, PEI is not used to a great degree in wastewater treatment but has a strong position in the papermaking industry and is widely accepted.

23.3.2.3 Polydiallyldimethylammonium Chloride

Aqueous polymerization of diallyldimethylammonium chloride (DADMAC) yields one of the earliest known and least expensive cationic polyelectrolytes used in wastewater treatment [6,29]. The DADMAC monomer can be produced in high concentration (60–70 wt.%) by reaction of allylchloride with dimethylamine and sodium hydroxide in aqueous solution without further purification [30–33]. poly-DADMAC is manufactured by the polymerization of an aqueous solution of DADMAC using free radical methods [34,35]. The polymerization yields a five-membered ring structure, with the quaternary ammonium group situated away from the polymer backbone [36]. The structure for the polymer is shown in Figure 23.8. Molecular weights are low due to chain transfer to the allyl groups and typically range between 10,000 and 500,000 g/mol [6]. The polymers are supplied as viscous solutions with concentrations ranging from 20 to 50 wt.% of the active polymer.

Copolymerization of DADMAC with acrylamide (AMD) yields low molecular weight polymer due to chain transfer to the allyl group of the DADMAC as well as poor incorporation of the DADMAC into the polymer chain due to the large difference in reactivity of the two monomers [29]. Due to the low molecular weight and poor cationic monomer incorporation, DADMAC/PAM copolymers have found little utility in wastewater treatment application, and few commercial products exist.

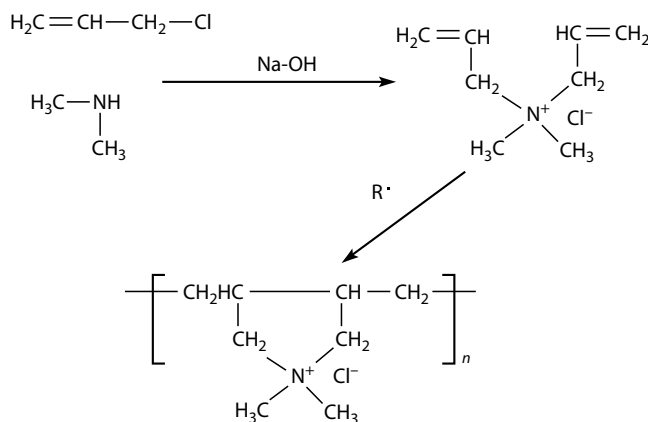


FIGURE 23.8 Synthesis scheme for the preparation of homopolymers of DADMAC.

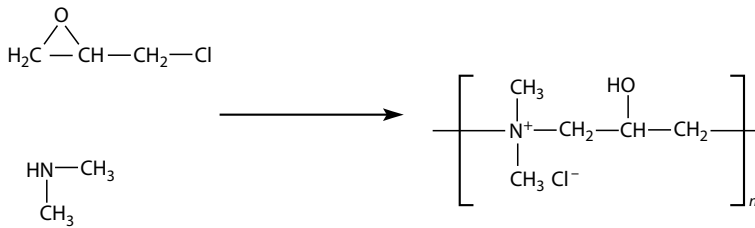


FIGURE 23.9 General synthesis of typical linear polyamine (poly(dimethylamine-*co*-epichlorohydrin)) used on the industrial scale.

23.3.2.4 Polyamines

The ring opening condensation polymerization of a primary or secondary alkylamine and an epoxide compound allows for the synthesis of a group of polyquaternary flocculants generally termed polyamines in the wastewater treatment industry [37,38]. On the commercial scale, the polymerizations are carried out at high temperatures (70°C–100°C) by the addition of the epoxide to an alkylamine. These polymers were first developed and commercially manufactured in the early 1970s and can be prepared as both linear and branched copolymers with molecular weights ranging from 10,000 to 300,000 g/mol. The workhorse of this group is the copolymers of dimethylamine (or less commonly methylamine) and epichlorohydrin. The general synthesis and structure for poly(dimethylamine-*co*-epichlorohydrin) is shown in Figure 23.9.

The presence of a quaternary ammonium group within the backbone of this molecule ensures that it maintains its cationic charge throughout the pH range of the application. Polyamines have many uses in different applications and are widely used in wastewater treatment. These materials have been noted to be used in both coagulation and flocculation applications [39,40] and are delivered as aqueous solutions of concentrations up to 50 wt.% of the active polymer. Polyamines are also known to be useful for the control of microorganisms (algae and bacteria) [41,42].

23.3.2.5 Cationic Polyacrylamides

By far the largest group of cationic polymers is that derived from acrylamide monomers [29]. Very high molecular weights can be achieved, which are usually on the order of 5–10 million g/mol when used in wastewater treatment. Cationic polyacrylamide copolymers are manufactured in four different general product forms. These are aqueous solutions, dry polymer powders and beads, water-in-oil inverse emulsions and microemulsions, and aqueous brine dispersions [29]. The polymer molecular weight required, cost–performance benefit, and ease of use in the application are the primary driving factors for a particular product form. Cationic polyacrylamides can be produced via post reaction of the homopolymer of acrylamide or by copolymerization with a cationically charged vinyl monomer. Of the two, the copolymerization route is the most widely used across all of the product forms. General methods of manufacture of cationic polyacrylamide copolymers as well as the routes to imparting cationic charge via postreaction are described in the following sections.

23.4 MANUFACTURE OF CATIONIC POLYACRYLAMIDES

Cationic polyacrylamide copolymers are manufactured in four different forms. A brief description of each is given in the following section.

23.4.1 AQUEOUS SOLUTION POLYMERIZATION

The earliest method for the manufacture of cationic polyacrylamide was polymerization in solution. The advantage with solution polymerization is the simplicity of reacting the AMD monomer or comonomers in aqueous solution generally using free radical initiation systems (azo, peroxy,

persulfate, redox, or combinations thereof) [29]. The polymerization reactions can be carried out either adiabatically or isothermally with the aim of controlling the molecular weight and fluid bulk viscosity of the final product. The main limitation to solution polymerization method is achieving an economical balance between polymer molecular weight, active polymer solids, and handling characteristics (fluid viscosity) in the final product. For example, in the case of the case of cationic polyacrylamide derived via the Mannich reaction described in a later section, high molecular weight polyacrylamide backbones are required. Thus, low active solid (6–10 wt.%) products are the result of the high solution viscosities developed due to the high molecular weight of the PAM backbone used [29]. Conversely, high active solid products can only be achieved by polymerization to low molecular weight.

23.4.2 DRY POWDERS AND BEADS

Dry cationic polyacrylamide powders are manufactured using both batch and continuous processes. In a batch process, the comonomers are placed in a reactor and polymerized isothermally. Control of the temperature is achieved by setting the comonomer concentrations and initiator levels appropriately to achieve the desired maximum temperature and residual monomer levels. After polymerization, the polymer gel is removed from the reactor vessel, sliced up, and then chopped to smaller size and dried via conventional processes. Finally the dried cationic polyacrylamide is ground to the desired particle size, packaged, and sold.

A number of continuous processes have been developed for the manufacture of cationic polyacrylamides. The method generally consists of polymerization of an aqueous solution of acrylamide and comonomer on a moving belt [43,44]. The speed of the moving belt can be controlled so that polymerization is completed prior to cutting the gel formed into smaller granules. The gel granules can then be dried, ground to the desired size, and packaged.

Processes for manufacturing dry cationic polyacrylamide beads have also been developed, having the ability of producing bead sizes ranging from about 100–2000 μm [45,46]. The polymer beads are produced by polymerization of monomer or comonomers in inverse suspension using a surfactant in an acceptable nonsolvent, followed by azeotropic distillation of water. The polymer beads are collected by filtration and dried. The bead size is controlled by surfactant type and amount, additives, and polymer stabilizers.

23.4.3 INVERSE EMULSIONS

The manufacture of high molecular weight cationic polyacrylamides can be carried out in inverse emulsion and inverse microemulsion. Of the two technologies, the standard inverse emulsion (water-in-oil) process first described by Vander Hoff is by far the most common process due to the higher active polymer solids achievable and lower surfactant amounts required [47]. However, microemulsion-based systems have also found utility [48,49]. The advantages of the manufacture of polyacrylamide in emulsion form include low fluid bulk viscosities, facile management of the heat of polymerization, and the ease of dispersal in water for dissolution of the polymer. The primary disadvantage is the length of shelf life since emulsions are prone to settle with time and remixing of the emulsion is required. Note that this is not true for the microemulsions as they are thermally dynamically stable and the polymer particle will remain suspended indefinitely.

In both cases, the process involves preparation of an oil phase containing low HLB ionic surfactant and a high boiling point paraffin oil. In a second vessel, an aqueous phase is assembled that contains the comonomers, water, and other additives required. The aqueous phase is then added to the oil phase to form the crude emulsion followed by homogenization. In the case of microemulsion products, the emulsion forms thermodynamically. The monomer emulsion and microemulsion are then polymerized using well-known vinyl-free radical polymerization processes.

23.4.4 POSTREACTION OF POLYACRYLAMIDE

The first process of industrial value to be discussed here is the postreaction equilibrium reaction of polyacrylamide with formaldehyde and dimethylamine to yield aminomethylated polyacrylamide (Mannich base) as shown in Figure 23.10 [50]. A wide range of substitutions can be achieved, up to about 80 mol % conversion. The polymer is made cationic by protonation of the Mannich base with an acid (lowering the pH) or by quaternization of the Mannich base with a quaternizing agent (Figure 23.10). High molecular weight Mannich-reacted polyacrylamides are almost always produced as low active polymer solid solutions (6–10 wt.%). This is due to the fact that continued reaction with residual formaldehyde leads to severe cross-linking of the polymer and gelation of the polymer solution in short periods of time (as little as a few weeks). The rate of cross-linking and gelation is a function of polymer concentration [51]. The addition of formaldehyde scavengers has been described for increasing the shelf-life of Mannich PAMs [52]. Due to the ease of manufacture and the low cost of the raw material, significant quantities of this type of materials are in use in wastewater treatment. Manufacturing facilities for Mannich polyacrylamides are often sited near the application to reduce shipping costs.

The Mannich reaction process can be extended by the addition of a quaternizing agent (for example, methyl chloride) to yield a cationic polymer that is not sensitive to pH. Although quaternized Mannich polyacrylamides can be manufactured as low solid solutions, advances in emulsion and microemulsion technology have yielded higher solid products. The use of emulsion and microemulsion technology allows for the manufacture of very high molecular weight polymers in liquid form that can be easily handled and dispersed in water for use [53,54]. Again, the manufacturing scheme involves postreaction of a high molecular weight polyacrylamide emulsion, followed by the reaction with an adduct of formaldehyde and dimethylamine, followed by quaternization with a quaternizing agent. The emulsion product can be further stabilized by treatment with a buffering acid, formaldehyde scavenger, and heat [55,56].

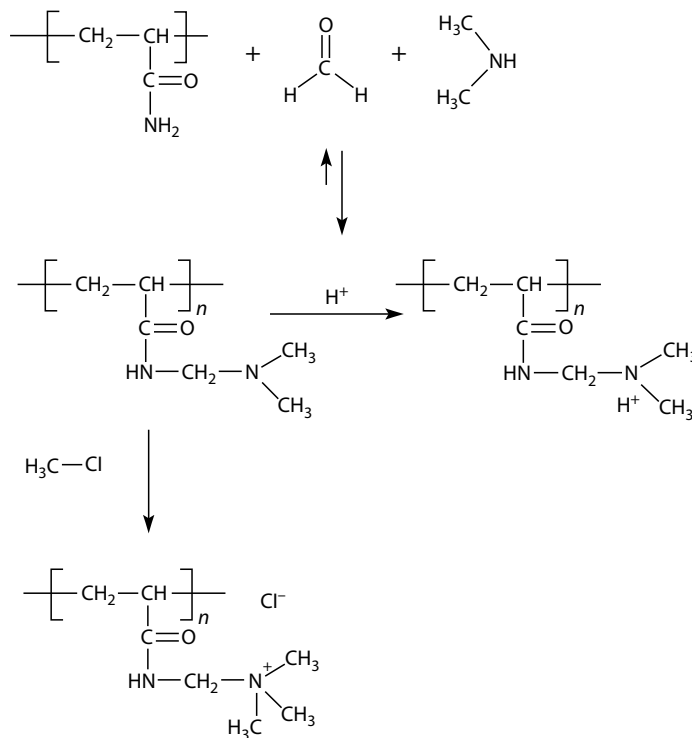


FIGURE 23.10 Reaction of dimethylamine (DMA) and formaldehyde with acrylamide (AMD) to yield the Mannich base. The cationic charge is induced by either protonation with an acid or quaternization with a quaternizing agent.

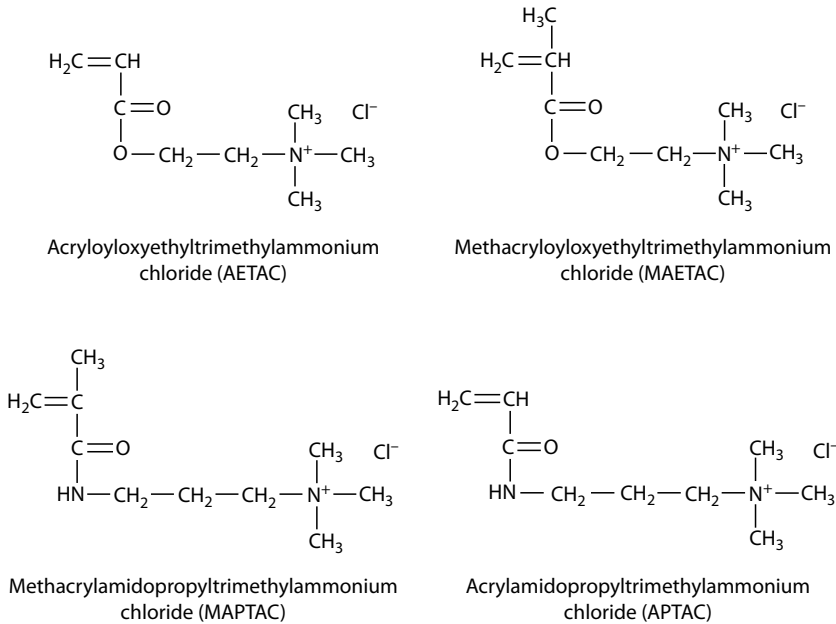


FIGURE 23.11 Comonomers used for the preparation of cationic polyacrylamide copolymers for use in commercial wastewater treatment.

23.4.5 COPOLYMERIZATION OF ACRYLAMIDE WITH CATIONIC VINYL MONOMERS

Copolymerization of acrylamide with a cationic vinyl comonomer yields one of the most important groups of flocculants to the wastewater treatment industry. The literature abounds with examples of various monomers; however, only a handful have found their way to industrial success. A collection of monomers of industrial utility are shown in Figure 23.11. The workhorse of this collection is the acryloyloxyethyltrimethylammonium chloride (AETAC). This is due to its favorable reactivity with AMD, and the polymers prepared using this monomer in combination with AMD yield polymers that have a uniform sequence distribution and low cost [57,60]. High molecular weight linear polymers as well as structured polymers have been described and are used extensively [58,59]. However, it must be pointed out that quaternary aminoesters are susceptible to base hydrolysis, but are stable under acidic conditions. The mechanism of this hydrolysis has been thoroughly studied and discussions can be found elsewhere [60].

Copolymers of methacrylamidopropyltrimethylammonium chloride (MAPTAC) and acrylamidopropyltrimethylammonium chloride (APTAC) are hydrolytically stable and yield polymers with reasonably random distributions [29]. However, they are more expensive and only very low charge (~3–10 mol %) materials have found significant place in the wastewater treatment market. Figure 23.12 presents the structure of copolymers of acrylamide with acryloyloxyethyltrimethylammonium chloride.

23.5 APPLICATIONS—WASTEWATER TREATMENT

23.5.1 INTRODUCTION

Cationic polymers find their primary use in wastewater treatment in the areas of potable water clarification, municipal sewage treatment, industrial raw water treatment, and treatment of paper wastes. The cationic polymers described above are, generally, divided into two groups based on molecular weight and charge density. The terms used in the wastewater treatment industry to describe the two classes

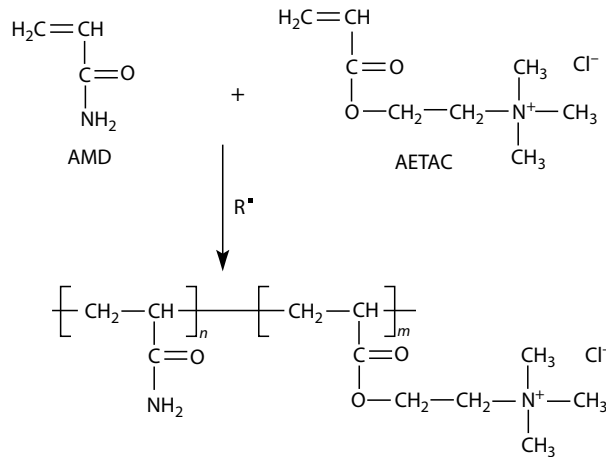


FIGURE 23.12 Copolymerization of acrylamide (AMD) with acryloyloxyethyltrimethylammonium chloride.

of cationic polymers are coagulants and flocculants. Each description is based on the physical characteristics of the polymer (charge density and molecular weight). Again, the boundary between what is termed coagulant and flocculant is a gray area, and there is considerable overlap in the definitions.

The first group, coagulants, consists of low molecular weight polymers with very high charge density (prime examples are the polyamines, poly-DADMAC, and PEI classes of polymers). Molecular weights are less than 1,000,000 g/mol and most often less than 500,000 g/mol. The high charge density allows for charge neutralization while the low molecular weight results in small tight aggregates (due to the reduced degree of bridging that can occur), which can be easily separated from the wastewater stream. Coagulants are especially useful in settling applications where suspended solids' levels are low and high levels of water clarity are desired.

The second group, called flocculants, are much higher in molecular weight and generally lower in charge density (the cationic polyacrylamides constitute the largest group of flocculants). The polymer molecular weights are greater than 1,000,000 g/mol and are often in the tens of millions. The high molecular weights are favorable to the bridging mechanism for floc formation, creating larger, more open floc. The floc that are formed are stronger and more resistant to shear than those produce by coagulants. This is important in high shear applications where high speed centrifuges, belt presses, or filter presses are used [4].

23.5.2 POTABLE WATER TREATMENT (DRINKING WATER)

Potable drinking water generally comes from natural raw water sources. These include streams, rivers, lakes, and reservoirs. The purpose of treatment is to remove suspended colloidal solids (particles <1 μm in size) that are responsible for color, odor, taste, etc. The suspended solids include clays, metal oxides, proteins, microorganisms, and organic substances (all negatively charged species). The bulk of potable water treatment is done using inorganic metal salts to destabilize the colloidal particles and induce coagulation and flocculation, the most common being aluminum and iron salts with the metal being present as Al³⁺ and Fe³⁺ [2,4,5]. The disadvantages with the use of metal salts are the corrosive nature of the salts, the requirement of an optimum operational pH, followed by posttreatment pH adjustment of the product water, and the high sludge volumes generated by use of the metal salts. However, the metal salts can be augmented or even replaced with a low to medium molecular weight cationic polymer (i.e., polyamine or poly-DADMAC). This reduces sludge volumes (cationic polymers have 10%–20% lower dosage optimum compared to metal salts [6]) and allows for a more effective pH regime (not requiring posttreatment pH adjustment). The separation of the solids from the liquid in potable water treatment is done using a sedimentation process.

23.5.3 MUNICIPAL WASTEWATER TREATMENT

Municipal wastewater treatment is defined as the process of removing solids and contaminants. Municipal wastewater includes water from baths, showers, sinks, dishwashers, washing machines, toilets, hospitals, and sometimes even small businesses. However, it does not generally include industrial or agricultural wastewater. Most treatment plants have three stages of treatment: primary treatment (physical removal of solids), secondary treatment (the biological removal of dissolved solids), and tertiary treatment (effluent polishing). Cationic polymers play a role in the first two stages (primary and secondary treatment) of the treatment process.

High molecular weight cationic polyacrylamide polymers are the workhorses of municipal wastewater treatment. They can be manufactured in high molecular weights over a wide range of charge densities. High charge, high molecular weight cationic polyacrylamides are used in both primary- and secondary-treated sludges to improve the dewatering characteristics of the sludge. Often, the molecular weight and charge density of the polymer are selected to match the treated sludge of a particular treatment plant with the aim of obtaining the highest possible cake solids after sludge dewatering. The sludge, once treated, can be dewatered via a variety of mechanical processes that include drying beds, vacuum filters, belt presses, filter press, and centrifuge.

23.5.4 INDUSTRIAL RAW WATER TREATMENT

Industrial raw water includes water from oil drilling and oil recovery, food industry, sugar processing, gravel washing, steel industry, and chemical industry, waste effluents generated during the manufacture of paper, and even waste from the nuclear industry. Most of the equipments used for the treatment of municipal wastes are used in industrial wastewater treatment. However, industrial sources of wastewater often require specialized treatment processes. As would be expected, cationic polymers find a variety of uses in industrial wastewater treatment.

23.6 SUMMARY

Cationic polymers are important materials in the treatment of wastewater. The areas of applicability range from potable water clarification and municipal sewage treatment to industrial raw water treatment, oil recovery and waste water treatment. The cationic polymers that have greatest industrial value are of low cost, are easily manufactured, and come in a variety of product forms such as simple solutions, inverse emulsions, aqueous dispersions, dry powders, and beads. Polymers can be manufactured across a wide range of molecular weights and cationic charges, so they can be tailored specifically to the demands of a particular application. The workhorse cationic polymers in the wastewater treatment industry include poly-DADMAC, polyamines (primarily poly(dimethylamine-*co*-epichlorohydrin), and the cationic copolymers of polyacrylamide. The other cationic polymers described above have also found application in wastewater treatment but these are usually in niche applications where their unique properties are required. It is expected that many of these polymers will continue to hold a place in the wastewater treatment industry.

REFERENCES

1. Deneen, M. A. and Gross, A. C. The global market for water treatment products. *Bus. Econ.* 40(1) 50–56 (2005). <http://www.nabe.com/publib/be/0501/deneen.html>
2. Gillberg, L., Hansen, B., Karlsson, I. et. al., *About Water Treatment*, pp. 50–56. Kemira Kemwater, Helsingborg Sweden (2003).
3. Gregory, J. and Finch, C. A. (Ed), *Industrial Water Soluble Polymers*, pp. 62–75. The Royal Society of Chemistry, Cambridge, U.K. (1996).
4. Bratby, J. *Coagulation and Flocculation in Water and Wastewater Treatment*, pp. 187–193. IWA Publishing, London, U.K. (2006).

5. Gregory, J. *Particles in Water, Properties and Processes*, pp. 133–147. Taylor & Francis, Boca Raton, FL (2006).
6. Mortimer, D. A. Synthetic polyelectrolytes—A review. *Polym. Int.* 25(1), 29–41 (1990).
7. Lyubartsev, A. P. and Nordenskiöld, L., *Handbook of Polyelectrolytes and Their Applications*. American Scientific Publishers, Stevenson Ranch, CA (2002).
8. Hodgson, D. F. and Amis, E. J. Polyelectrolyte dynamics. In *Polyelectrolytes: Science and Technology*, Hara, M. (Ed), pp. 127–181. CRC Press, Boca Raton, FL (2002).
9. Bratby, J. *Coagulation and Flocculation in Water and Wastewater Treatment*, pp. 52–57. IWA Publishing, London, U.K (2006).
10. Carlyle, G. C. and Wurzburg, O. B. Ungelatinized tertiary amino alkyl ethers of amylaceous materials, U.S. Patent No. 2,813,093 (1957).
11. Paschall, E. F. and Minkema, W. H. Flocculation by starch ethers, U.S. Patent No. 2,995,513 (1961).
12. Hubbe, M. Cationic Starch. In *Mini-Encyclopedia of Papermaking Wet-End Chemistry Additives and Ingredients, Their Composition, Functions, Strategies for Use*, <http://www4.ncsu.edu/~hubbe/CST.htm> (2008).
13. Meisel, H. Sizing cellulosic substances with starch derivatives, U.S. Patent No. 2,965,518 (1960).
14. Reynolds, W. F. and Sexsmith, D. R. Sizing paper, U.S. Patent No. 3,212,962 (1965).
15. Peniston, Q. P. Process for the manufacture of chitosan, U.S. Patent No. 4,195,175 (1980).
16. Mima, S., Miya, M., Yoshikawa, N., and Iwamoto, R. Chitosan, JP 55012109.
17. No, H. K., Meyers, S. P., Prinyawiwatkul, W., and Xu, Z. Applications of chitosan for improvement of quality and shelf life of foods: A Review. *J. Food Sci.* 72(5), R87–R100 (2007).
18. Lin, Y. Process for antimicrobial treating textiles, U.S. Patent No. 2,008,102,217.
19. Cardenas, G., Cabrera, G., Casals, P., Villar, A., and Galvez, G. Synthesis and agricultural applications of chitosan derivatives. In *Natural Polymers and Composites IV, Proceedings from the International Symposium on Natural Polymers and Composites*, pp. 324–331. Embrapa Instrumentacao Agropecuaria, Brazil (2002).
20. Burkert, H., Brunnmüller, F., Beyer, K. H., Kroener, M., and Mueller, H. Flocculants for sludges, U.S. Patent No. 4,444,667 (1984).
21. Brunnmüller, F., Schneider, R., Kroener, M., Mueller, H., and Linhart, F. Linear basic polymers, their preparation and their use, U.S. Patent No. 4,421,602 (1983).
22. Bonn, J., Ettl, R., and Lorenz, K. Aqueous dispersions of reactive gluing Agents, method for the production and the use thereof. PCT Int. Appl., WO2005083174 (2005).
23. Ito, K. Manufacture of paper showing good oil and water resistance, and high strength, and manufactured paper. Jpn. Kokai Tokkyo Koho, JP 2005042271 (2005).
24. Koch, O., Prechtel, F., Blum, R., and Kannengiesser, D. Microparticle dispersions of polymeric retention agent and inorganic filler in production of paper, cardboard and millboard. PCT Int. Appl., WO 2006069660 (2006).
25. Horn, D., *IUPAC International Symposium on Polymeric Amino and Ammonium Salts*, pp. 333–355, Ghent, Belgium (1979).
26. Rivas, B. L. and Geckler, K. E. Synthesis and metal complexation of poly(ethyleneimine) and derivatives. In *Advances in Polymer Science*, Hocker, H. (Ed), pp. 171–188. Springer-Verlag Berlin, Heidelberg, Germany (1992).
27. Ulrich, H. and Harz, W. Polymerization of ethylene-imines, U.S. Patent No. 2,182,306 (1939).
28. Dick, C. R. and Ham, G. E. Characterization of polyethylenimine. *J. Macromol. Sci. Chem.* A4(6), 1301–1314 (1970).
29. Huang, S. Y., Lipp, D. W., and Farinato, R. S., Acrylamide polymers. In *Encyclopedia of Polymer Science and Technology*, pp. 41–79. John Wiley & Sons, Inc., New York (2002).
30. Negi, Y., Harada, S., and Ishizuka, O., Part A-1, Preparation and cyclopolymerization of diallylamine derivatives. *J. Polym. Sci. Chem.* 5, 1951–1965 (1967).
31. Schuller, W. H. and Thomas, W. M. Linear copolymer of quaternary ammonium compounds, U.S. Patent No. 2,923,701 (1960).
32. Boothe, J. E. Dimethyl diallyl ammonium chloride, U.S. Patent No. 3,461,163 (1969).
33. Boothe, J. E. Purifying dialkyl diallyl ammonium chloride and dialkyl dimethylallyl ammonium chloride, U.S. Patent 3,472,740 (1969).
34. Butler, G. B. Water soluble quaternary ammonium polymers, U.S. Patent No. 3,288,770 (1966).
35. Welcher, R. P., Rabinowitz, R., and Cibulskas, A. S., Controlled polymerization of dimethyldiallylammonium halides by the use of alkali metal or ammonium bisulfites or metabisulfites, U.S. Patent 4,092,467 (1978).

36. Lancaster, J. E., Baccei, L., and Panzer, H. P. The structure of poly(diallyldimethylammonium) chloride by carbon-13 NMR spectroscopy. *J. Polym. Sci. Polym. Lett. Ed.* 14, 549–554 (1976).
37. Bock, L. H. and Houk, A. L. Polymeric quaternary ammonium salts, U.S. Patent No. 2,454,547 (1948).
38. Lobach, W., Lehmann, W., and Muller, F. Polyalkylenepolyamines containing quaternary dialkylammonium groups, U.S. Patent No. 4,250,112 (1981).
39. Priesing, C. P. and Mogelnicki, S. Dewtering aqueous suspensions of organic solids, U.S. Patent No. 3,259,570 (1966).
40. Panzer, H. P. and Dixon, K. W. Process for treating industrial wastes, U.S. Patent No. 3,894,947 (1975).
41. Shair, S. A., Stewart, N. P., and Cairns, J. E. Polyquaternary compounds for the control of microbiological growth, U.S. Patent No. 4,111,679 (1978).
42. Pera, J. D. Microbicidal compositions of dimethylamine-epichlorohydrin amines, U.S. Patent No. 5,051,124 (1991).
43. Gershberg, D. B. High molecular weight acrylamide polymer production by high solids solution polymerization, U.S. Patent No. 3,929,751 (1975).
44. Davies, W. B. High solids process for the production of water soluble polymers by exothermic polymerization, Eur. Patent No. 296311 (1988).
45. Flesher, P. and Allen, A. S. Inverse suspension polymerization process, U.S. Patent No. 4,506,062 (1985).
46. Allen, A. S. Polymeric stabilizers, their preparation and dispersions containing them, U.S. Patent No. 4,962,150 (1990).
47. Vanderhoff, J. W. and Wiley, R. M. Water-in-oil emulsion polymerization process for polymerizing water-soluble monomers, U.S. Patent No. 3,284,393 (1966).
48. Candau, F., Leong, Y. S., Kohler, N., and Dawans, F. Process for manufacturing a microlatex in a continuous oil phase by polymerization of a water-soluble monomer in a water-in-oil microemulsion, resultant microlatexes, and their use for enhanced oil recovery, U.S. Patent No. 4,521,317 (1985).
49. Buchert, P. and Candau, F. Polymerization in microemulsions: I. Formulation and structural properties of microemulsions containing a cationic monomer. *J. Colloid Interface Sci.* 136(2), 527–540 (1990).
50. McDonald, C. J. and Beaver, R. H. The Mannich reaction of poly(acrylamide). *Macromolecules* 12(2), 203–208 (1979).
51. Phillips, K. G., Ballweber, E. G., and Hurlock, J. R. Rapidly-producing amino methylated polymers and quaternary ammonium salts, U.S. Patent No. 4,179,424 (1979).
52. Witschonke, C. R. and Rabinowitz, R. Stabilized Mannich base solutions. U.S. Patent No. 3,988,277 (1976).
53. Phillips, K. G., Ballweber, E. G., Nordquist, K. A., and Miller, R. A. Quaternary modified acrylamide polymers, U.S. Patent No. 4,010,131 (1977).
54. Kozakiewicz, J. J. and Huang, S. Y. Emulsified Mannich acrylamide polymers, U.S. Patent No. 5,132,023 (1992).
55. Huang, S. Y., Leone-Bay, A., Schmitt, J. M., and Waterman, P. S. Quaternized tertiary aminomethyl acrylamide polymer microemulsions with improved performance, U.S. Patent No. 5,627,260 (1997).
56. Huang, S. Y., Leone-Bay, A., Schmitt, J. M., and Waterman, P. S. Quaternized tertiary aminomethyl acrylamide polymer microemulsions with improved performance, U.S. Patent No. 5,863,982 (1999).
57. Tanaka, H. Copolymerization of cationic monomers with acetyl-amido in aqueous solution. *J. Polym. Sci. Polym. Chem. Ed.* 24, 29 (1986).
58. Neff, R. E., Pellon, J. J., and Ryles, R. G. High performance cationic flocculating agents, U.S. Patent No. 5,945,494 (1999).
59. Neff, R. E., Pellon, J. J., and Ryles, R. G. High performance flocculating agents nonionic polymers, U.S. Patent No. 6,147,176 (2000).
60. Draney, D. R., Huang, S. Y., Kozakiewicz, J. J., and Lipp, D. W. Mechanism of cationicity loss in acrylamide/cationic ester copolymers. *Polym. Prep.* 31, 500 (1990).

24 Recent Development in Water Treatment Chemicals Monitoring

Vadim Malkov and Phil Kiser

CONTENTS

24.1	Introduction.....	482
24.2	Disinfection Monitoring.....	482
24.2.1	Chlorine Disinfection.....	483
24.2.1.1	Technology Limitations	485
24.2.2	Chlorine Dioxide Disinfection.....	486
24.2.2.1	High/Mid-Range Direct Read Method	488
24.2.2.2	DPD/Glycine Method	488
24.2.2.3	Chlorophenol Red Method	488
24.2.2.4	Other Methods: Amaranth and Lissamine Green B.....	488
24.2.2.5	Laboratory Chlorine Dioxide Amperometric Methods.....	488
24.2.3	Ozone Disinfection	488
24.2.4	Bromine Disinfection.....	489
24.2.5	Oxidation–Reduction Potential.....	489
24.3	On-Line Monitoring and Analysis of Cooling and Boiler Water Treatment Parameters	492
24.3.1	Pretreatment, Boiler, Steam, and Power System	492
24.3.1.1	Silica Analyzer	492
24.3.1.2	Dissolved Oxygen (Parts per Billion) Analyzer	492
24.3.1.3	Sodium Analyzer	492
24.3.1.4	Hardness Analyzer	493
24.4	Cooling Tower Control	493
24.4.1	Organic Contaminants	493
24.4.1.1	Chemical Oxygen Demand.....	493
24.4.1.2	Biochemical Oxygen Demand.....	494
24.4.1.3	Total Organic Carbon.....	494
24.4.2	On-Line Analysis	494
24.4.2.1	The UV Persulfate Technique for TOC	494
24.4.2.2	The High Temperature Oxidation Technique for TOC	495
24.4.2.3	TOC Test/Analyzer	495
24.4.3	pH Measurements and Control	496
24.4.3.1	Definition of pH.....	496
24.4.3.2	pH Electrode	496
24.4.4	Alkalinity	498
24.4.4.1	Chemical Reactions	498
24.4.5	Conductivity/Total Dissolved Solids	499
24.4.5.1	The Conductivity Spectrum	499

24.4.6	TDS Relationship to Conductivity and Resistivity	499
24.4.7	Turbidity and Suspended Solids	500
24.4.7.1	Turbidity and Total Suspended Solids	501
24.4.7.2	Four-Beam and Advanced Measurement Techniques for Suspended Solids.....	501
24.4.8	Control and Monitoring of Corrosion.....	502
24.5	Summary	503
	References.....	504

24.1 INTRODUCTION

There is no question as to whether or not it is necessary to monitor processes and specific chemicals in various water treatment applications. The question normally is which parameters of the treated water should be monitored continuously, which parameters should be monitored on a regular basis, and which parameters should be monitored only occasionally. To answer this question, each customer or water treater should fully understand the treatment process and the application specifics, because sometimes the monitoring of the same parameter results in completely different conclusions. Some applications require different chemicals to address the specific needs of the equipment and/or to achieve specific goals. Once the treatment agent is chosen, the next big task is to establish the right protocol for its monitoring.

The monitoring practices normally include two major approaches: laboratory methods and on-line (process, continual, or continuous) analyses. The major difference is obvious—the frequency of the analyses, while there may be some other differences between the laboratory and on-line methods and approaches. Another significant difference between these two approaches is in the accuracy of the results. Usually, lab methods are developed to achieve high accuracy of the analysis throughout the entire range, while the process control approach often does not need this feature. Therefore, many on-line instruments may not be extremely accurate throughout the entire range of concentration, but will accurately measure the analyte concentration around the calibrated set point. Thus, such lack of accuracy requires more frequent calibrations. Naturally, there are exceptions to this rule—some process analyzers use the same chemical methods as those developed for laboratory analyses. These major considerations, along with economic reasons (the cost of a single analysis is always lower with the use of process instrumentation), should always be taken into account when a decision on monitoring is being made.

Water treatment in various industrial applications may seem as different as the applications themselves; however, at a closer look it appears that many of the treatment practices are very similar in nature. Therefore, monitoring chemicals in these applications sometimes comes to the same techniques and methods. The majority of treated waters are routinely monitored for several basic parameters such as temperature, pressure, pH, conductivity, and disinfection. For example, the efficiency of disinfection is one of the most-often-monitored characteristics of any water, because it is hard to overestimate the importance of this parameter for ensuring the equipment working conditions, water reuse safety, and public health, to mention just a few. Depending on the application, there are plenty of parameters to be monitored specifically: silica, hardness, alkalinity, corrosion inhibitors, biocides, suspended solids, etc. Monitoring of these parameters is vital for controlling the treatment processes efficiently and in this chapter we review the modern techniques for monitoring both general and specific parameters relevant to major industrial applications, such as the power generation industry, cooling technology, and beverage production.

24.2 DISINFECTION MONITORING

The monitoring of treatment against microbial growth in water may be the most common application of various chemical methods and technologies and is very important to ensure the quality of processed water. Disinfection monitoring and control is often an area of water treatment that is

TABLE 24.1
Typical Applications for Disinfection Efficiency Monitoring
in Beverage Industry

Typical Applications	Common Disinfection Parameters
Influent water	Chlorine, UV, and ozone Turbidity, chlorine, conductivity, pH, alkalinity, sulfate, aluminum, and hardness are other commonly monitored parameters
In-process water	UV, ozone, and chlorine dioxide Alkalinity, chlorine, bromate, chlorite, conductivity, total hardness, calcium hardness, pH, DO, iron, color, and turbidity are other commonly monitored parameters
Clean-in-place (CIP)	Quaternary ammonia, peracetic acid, chlorine, ClO ₂ , ozone, and conductivity for the identification of product/CIP chemical/rinse water interfaces. Bacteria, coliforms, <i>E. coli</i> , and total plate counts may also be monitored
Effluent	Chlorine and UV BOD, COD, pH, TSS, chlorine, and nutrients are other commonly monitored parameters in beverage water effluent with high organics (beer, wine, fresh fruit juice, milk)

regulated both by internal drivers (cost optimization) and external regulations (EPA, FDA, etc.) For example, the beverage industry is subject to strict regulations on sanitation. Some typical applications for process monitoring at a beverage plant are presented in Table 24.1.

Some of the parameters listed in Table 24.1 may be covered by laboratory methods and do not require continuous analysis; however, the efficiency of on-line (process) monitoring has proven its implementation for process optimization and cost control. A case study [1] has been conducted and proved the efficiency of the on-line monitoring of CIP processes. Beside the CIP processes, one of the most challenging applications to monitor is the cooling water disinfection, because it provides ideal conditions for the growth and development of all kinds of harmful bacteria—moisture, warmth, and darkness. The most widely used disinfectants for cooling water are chlorine, chlorine dioxide, bromine, and ozone.

24.2.1 CHLORINE DISINFECTION

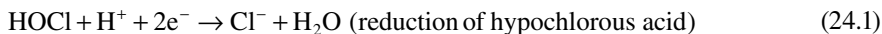
Chlorine is the most widely used disinfectant and may be applied in various states from gaseous (Cl₂) to solid (sodium or calcium hypochlorite) and is monitored in water in forms of free chlorine (HOCl—hypochlorous acid, OCl⁻—hypochlorite ion), or total chlorine (mono-, di-, and trichloramines in combination with free chlorine species). The monitoring of free and total chlorine species is usually conducted by an array of laboratory and on-line methods based on either colorimetric or amperometric technology. Colorimetric detection is a method based on the *N,N*-diethyl-*p*-phenylenediamine (DPD) reaction with active halogens. This reaction is a standard analytical approach for the analysis of residual chlorine species and is based on the formation of colored products with DPD proportional to the analyte concentration. In a laboratory, DPD analysis is conducted on various instruments commonly called spectrophotometers or colorimeters. Minimal training is required and the handheld colorimeters are specifically designed as portable devices for field use.

Laboratory amperometric analysis is performed using titration methodology and the procedure may be either manual or automated. The digital titrator requires an operator to manually add titrant to a sample and visually (subjectively) identify when the end point of the titration has been reached.

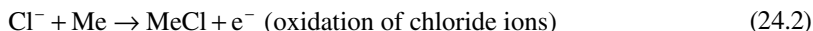
Process instruments for on-line chlorine monitoring have become essential tools for many and they employ the same two most common methods as used in the laboratory. There are instruments using the DPD technology available from HF Scientific (CLX), Hanna (PCA series), and Blue I (HG702).

Amperometry is an electrochemical technique that measures the change in current resulting from chemical reactions taking place as a function of the analyte concentration. A typical amperometric sensor consists of two dissimilar electrodes—an anode and a cathode (i.e., silver/platinum or copper/gold). Below is a general schematic of the reduction–oxidation reaction taking place in the amperometric system.

Cathode (working electrode):



Anode (reference electrode):



The anode may be split into two parts—a reference and an auxiliary (or counter) electrode making the measurement more stable. Such systems are called three-electrode sensors.

Typically, electrodes are covered with a membrane, which provides better selectivity of the analysis (Figure 24.1a). Additionally, a small electrical voltage is applied across the electrodes. In the case of no membranes, the system is called open cell or bare-electrode amperometric and in the case of no applied voltage, the system is called galvanic (Figure 24.1b). From a technical standpoint, many electrochemical methods fall under the amperometric measurement category, including systems, sometimes wrongly referred to as polarographic.

It is important to note that on-line amperometric sensors do not use the same methodology as the laboratory amperometric titration apparatus. Additionally, it should be considered that the DPD methodology and amperometric titration are standard measurement methods that provide adequate accuracy throughout the entire measurement range. In contrast, on-line amperometric sensors are designed for process control and, therefore, provide adequate accuracy only around the calibrated

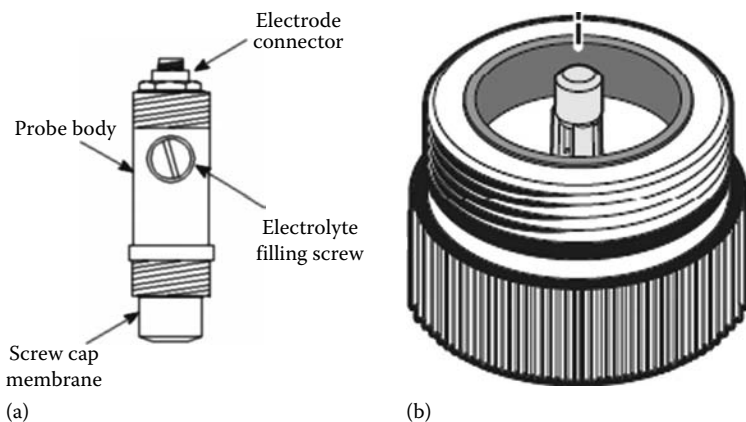


FIGURE 24.1 Two schematic examples of common amperometric systems. (a) Probe-type (membrane covered), closed amperometric cell and (b) bare electrode system (open amperometric cell).

set point (normally, within ± 1 ppm or $\sim 20\%$ of the set point). With this being said, the amperometric technology may be considered to be the main candidate for the monitoring and control of industrial water treatment given the analyte concentration within a specified frame.

24.2.1.1 Technology Limitations

Currently, no “ideal” method exists for quantifying chlorine and chloramines in water. Both chemical and amperometric methods suffer from interferences due to the presence of some specific compounds. The most significant interference to the amperometric method is provided by pH. In free chlorine applications, a pH level of 5.0–7.0 is the ideal operational range for an amperometric sensor, due to the high percentage of hypochlorous acid (HOCl) ($>80\%$) in the sample and the steepness of the free chlorine dissociation curve in this range (see Figure 24.2).

In the pH range of 7.0–8.0, the HOCl concentration is much lower versus the OCl^- (hypochlorite ion). Amperometric free chlorine sensors directly measure only HOCl, not OCl^- or Cl_2 , so any change in pH levels within this range will substantially affect the accuracy of the on-line unit. When pH influence is mathematically compensated, the instrument will read more consistently; however, there always exists a possibility of readings drift. In contrast, the DPD method is equally sensitive to all present chlorine species, plus, it is pH independent because the sample is buffered during the on-line measurement and the pH level of the reaction is under control. At a pH level of 8.0 or greater (often the operating range for facilities trying to minimize corrosion), the HOCl part of free chlorine concentration is very low ($<20\%$), therefore the accuracy of the amperometric probe suffers significantly with any slight changes in the pH level.

It has been demonstrated in the field that internal pH compensation greatly improves the potential accuracy of on-line amperometric sensors. However, having a changing and complex water matrix will lead to poor accuracy and more frequent changes of the electrolyte (sensor maintenance). In external pH compensation applications, a buffer from an external reservoir is added to the sample to adjust and control its pH. Although this approach provides improved accuracy, the on-line instrumentation often loses its “reagentless” appeal.

Design of the flow cell is a critical component to the overall performance of amperometric sensors. Due to the flow and pressure sensitivity of these sensors (Figure 24.3), a flow cell design that does not adequately compensate for these changes will allow for continued poor accuracy.

In some cases, amperometric sensors have been mounted in-pipe with no flow cell and it has been reported that the sensor’s accuracy is completely lost if the sample pressure changes more than ± 5 psi. In any membrane-based measurement system, varying sample pressure will change the thickness

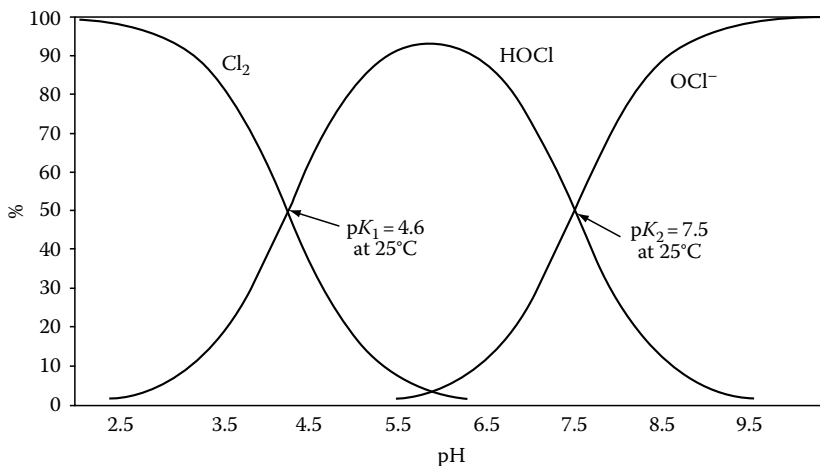


FIGURE 24.2 Free chlorine dissociation curve.

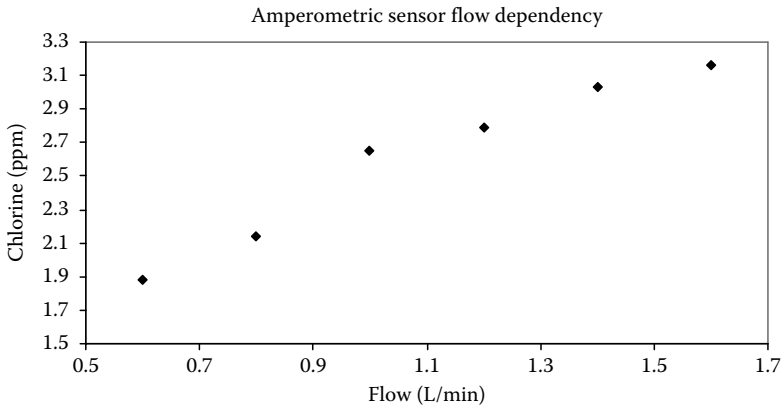


FIGURE 24.3 Dependency of an amperometric sensor readings on the sample flow rate (steady chlorine concentration ~2 ppm).

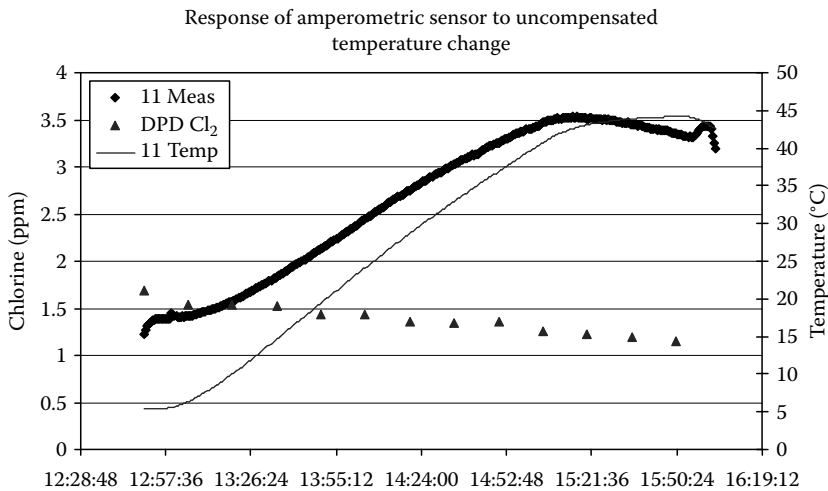


FIGURE 24.4 Response of an amperometric chlorine sensor to temperature change vs. DPD readings. The downward trend of the DPD measurements reflects evaporation of chlorine from the solution at elevated temperature.

of the micron-sized electrolyte layer between the membrane and electrode surface, which leads to erratic responses. Amperometric sensors are always sensitive to temperature changes, as illustrated in Figure 24.4. Two areas that are affected by temperature are the membrane permeability rate and the pH compensation, which is done by calculation. No mathematical algorithm can accurately reflect all the changes in the water matrix, and eventually the response of chlorine to those changes.

In summary, any essential changes to the water sample matrix may require the recalibration of the amperometric sensor. In contrast, DPD technology does not require calibration due to the established proportionality between chlorine concentration and light absorbance.

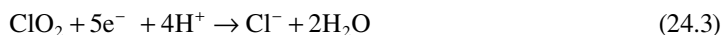
24.2.2 CHLORINE DIOXIDE DISINFECTION

Chlorine dioxide (ClO₂) is commonly used to control microbial growth in cooling water, because it can effectively penetrate biofilm and kill slime-forming organisms, which can diminish heat transfer efficiency. It is also an effective biocide at pH > 7. Chlorine dioxide is also used to sanitize

food-handling equipment in a variety of industries including vegetable processing, poultry chiller waters, and beverage industries. It is also approved for the treatment of flume water used in vegetable processing. Chlorine dioxide can be used to oxidize both iron and manganese, which may be more applicable to control the quality of source water for industrial application.

In pulp and paper bleaching processes, chlorine dioxide is by far the most prevalent agent. It is an oxidizer that can be used in delignification (lignin is the “glue” that holds wood fibers together) or in the final bleaching stages to obtain strong, stable high-brightness Kraft pulp. ClO_2 selectively destroys lignin without significant degradation of the pulp fibers, and preserves pulp strength while providing stable high brightness.

There are several manufacturers offering on-line instruments for ClO_2 measurements—Hach, Severn Trent, ATi, E&H, etc. All these sensors are built on the amperometric technology; therefore, as an example of such instrumentation, we will discuss the Hach 9187sc analyzer. The 9187sc chlorine dioxide analyzer is an on-line single-channel analyzer that measures chlorine dioxide in applications that require monitoring of chlorine dioxide at the 0–2 ppm range, especially at low levels (20–200 ppb). The molecules of chlorine dioxide contained in the sample diffuse through the membrane and are then found in an electrolyte zone of very slight thickness between the membrane and the cathode. A constant work potential is applied to the work electrode (cathode) where ClO_2 is reduced according to the reaction:



At the silver electrode (anode), the silver is oxidized:



The reduction in chlorine dioxide at the cathode generates a current that is directly proportional to the partial pressure of the analyte in the sample. The electrochemical reaction and diffusion through the membrane are dependent upon temperature; consequently the probe is fitted with a temperature sensor that enables the automatic compensation of measurement variations according to temperature. A diagram of the 9187sc amperometric electrode is given in Figure 24.5.

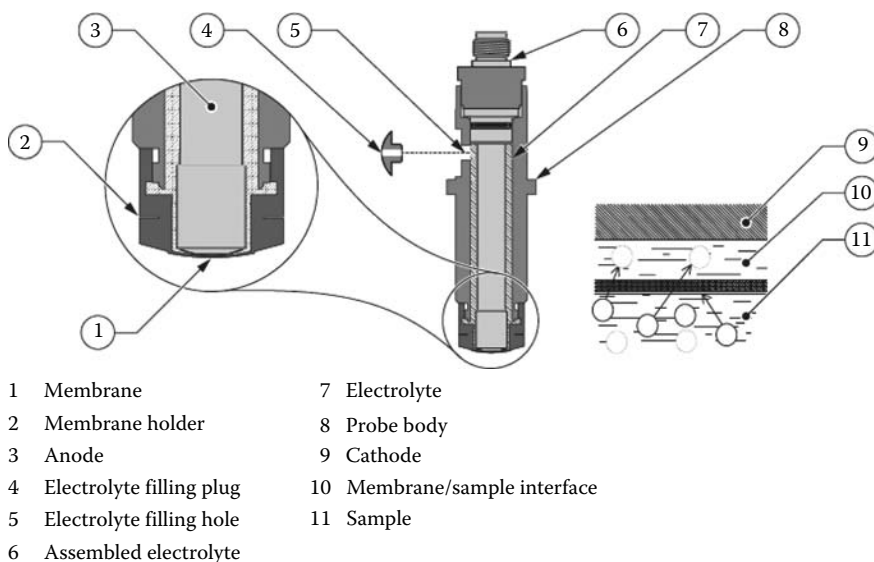


FIGURE 24.5 General schematic of the Hach 9187sc electrode. (Courtesy of Hach Company, Loveland, CO.)

There is a number of available laboratory methods for chlorine dioxide, both colorimetric and amperometric, for different concentration ranges. In addition, there are amperometric and chromatographic methods available for chlorite, which is the ClO_2 disinfection by-product.

24.2.2.1 High/Mid-Range Direct Read Method

Since chlorine dioxide at high concentrations imparts a yellow color to water, it can be measured directly without the use of reagents. The yellow color is linearly proportional to the chlorine dioxide concentration. The high-range (HR) test covers the range of 5–1000 mg/L, while the mid-range test covers the range of 1–50 mg/L. The HR test is in an appropriate range to test the chlorine dioxide generator output.

24.2.2.2 DPD/Glycine Method

The DPD/Glycine method is an Environmental Protection Agency (EPA)-accepted colorimetric method for chlorine dioxide (based on Standard Methods 4500 ClO_2 -D). Glycine is added prior to DPD and binds chlorine present in the sample, leaving the chlorine dioxide available to react with the DPD powder pillow. Because the method uses DPD chemistry, it is also subject to the same interferences as the DPD chlorine test (including other oxidants such as oxidized manganese).

24.2.2.3 Chlorophenol Red Method

The chlorophenol red (CPR) method is a low-range method applicable for 0.02–1.00 mg/L ClO_2 concentrations. The main benefit of this method over the DPD/glycine method is that the CPR method is not susceptible to interference from other oxidants such as free chlorine and chlorite.

24.2.2.4 Other Methods: Amaranth and Lissamine Green B

Chlorine dioxide is an effective bleaching agent for many dyes; therefore, there are numerous methods for chlorine dioxide using a variety of dyes. Some of these include Amaranth and Lissamine Green B (commonly referred to as the LGB method). The Amaranth method is particularly sensitive to low levels of chlorine dioxide, measuring concentrations of up to 500 ppb only. However, the Amaranth method reagent sets are available only in Europe. The LGB method includes a procedure for using horseradish peroxidase to convert chlorite into chlorine dioxide and determines the chlorite level by difference between two measurements of chlorine dioxide. This is an extremely complicated and time-consuming method requiring frequent calibrations. A newer simplified method based on this approach is currently being developed by Hach Company.

24.2.2.5 Laboratory Chlorine Dioxide Amperometric Methods

Chlorine dioxide and chlorite titration method is an EPA-approved method, based on Standard Methods 4500 ClO_2 -E. The method consists of four forward titrations. In the first titration, phosphate buffer and potassium iodide are added to the sample. The sample from the first titration is then acidified and left in the dark to react for 5 min before being titrated again. These titrations are repeated on a nitrogen-purged sample for the third and fourth titrations. The Hach AutoCAT 9000 guides the user step-by-step through all of the titrations involved in the analysis and calculates the chlorine dioxide, chlorite, and chlorine from the results of these four titrations.

24.2.3 OZONE DISINFECTION

Ozone is a strong oxidizer (Redox potential = 2.1 eV), stronger than chlorine (0.8–1.6 eV) or chlorine dioxide (1.5 eV). Beyond clean in place (CIP) processes in the food and beverage industries, primary applications of ozone are for the final disinfection of bottled water, for disinfection of fresh produce [3], and in fish hatcheries [4].

There are several major techniques for monitoring ozone levels in process water—on-line UV or amperometric methods and laboratory methods based on spectrophotometry. On-line amperometric instrumentation is offered by Hach Company (9185sc), ATi (Q45/64), Rosemount/Emerson (499AOZ), Orbisphere (Model 410), and some other manufacturers. Different technologies lie in the basis of the instrumentation manufactured by IN USA (dual-path UV absorbance) and Eco Sensors (heated metal oxide sensor technology [HMOS]). The latter instrumentation measures ozone levels in the gas phase after stripping it from the water sample. All instruments besides the Eco Sensors feature different measurement ranges, but similar technical specs such as accuracy and precision, while the HMOS-based technology has demonstrated poor accuracy and high sensitivity to airborne contaminants [5]. The most widely used industrial applications instruments employ amperometric technology and their operation is based on the same principles as discussed above.

The laboratory methods are based on bleaching chemistry and include the Indigo method (Standard Method 4500-O3 B), the DPD method (Hach, Palintest), and the Iodometric method. Hach offers the indigo trisulfonate method [6] for determining ozone residuals with a spectrophotometer, colorimeter, or color wheel. Because this is the only method based on the Standard Methods [7], it is considered to be a reference method for the calibration and verification of on-line instruments. The DPD compound used to determine chlorine, bromine, and iodine will also react with the ozone and may be used to determine ozone concentrations. Many manufacturers offer this method for determining ozone. The major drawback of using the DPD method is that the method is not specific for just ozone, therefore chlorine or other oxidizers present in the sample will bias the results.

24.2.4 BROMINE DISINFECTION

Disinfection with bromine is often used in cooling tower applications to reduce the risk of corrosion. A reaction with DPD is a common method for analysis of this disinfectant. Although bromine is a common oxidizer, its potential is significantly lower than the potential of ozone, chlorine, or chlorine dioxide, therefore, the DPD method is subject to interference from all these oxidizers. This method is offered by almost all manufacturers for laboratory analysis and there is currently no on-line instrumentation designed specifically for bromine. The following question often comes from customers who wish to measure this parameter on-line—is it possible to use a DPD process analyzer for measuring bromine? There is no simple answer and therefore we suggest asking the manufacturer for specific recommendations. Being a common oxidizer, and also being fed along with chlorine compounds, bromine can also be monitored by the oxidation–reduction potential measurement that is discussed in Section 24.2.5.

24.2.5 OXIDATION–REDUCTION POTENTIAL

Oxidation–reduction (redox) potential (ORP) is a measure of the state of oxidation of a system. The ORP sensors are often used for the control of disinfection processes based on treatment with oxidizing biocides such as the ones listed in the previous section. The sensors measure the chemical equilibrium potential of the water system, which is generated by the relative concentration (ratio) of chemical oxidants and reductants in the sample.

Using ORP for chlorine control has been done successfully in many plants; however, there are several considerations that must be taken into account. Among these are chlorine dissociation (Figure 24.2), pH level and temperature, mV variations, verification with direct chlorine measurements, placement of sensors in water streams, and instrument options. We know that HOCl is a much more powerful oxidant than OCl⁻ (1.6eV vs. 0.8eV), so with any change in pH, the percentage of HOCl to OCl⁻ changes (Figure 24.2). Samples with pH levels below 5.5 will not have a large change in ORP. Samples above pH levels of 9.5 will be impossible to control based on the very low percentage of HOCl. Additionally, the curve is slightly affected by temperature. As the temperature increases, the curve shifts to the right, and as the temperature decreases, the curve shifts to the left.

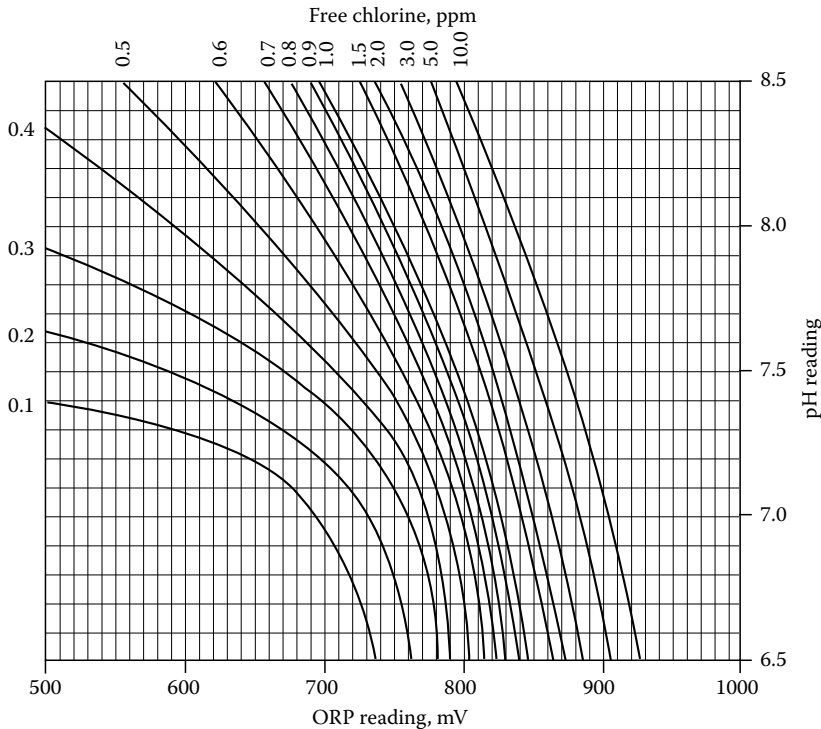


FIGURE 24.6 Empirical dependency between pH, ORP, and chlorine concentration.

The graph [8] presented in Figure 24.6 shows the general relationship of ORP, pH, and chlorine concentration. The purpose is to demonstrate how the pH levels affect different chlorine set points.

Other variables in this measurement are the difference in probes and drift. It is important to establish a chlorine baseline with each ORP probe because a different probe might yield an ORP difference of up to 25 mV. This is usually explained by pH levels or temperature variations, but changes in metal concentrations, specifically manganese, dissolved oxygen, or other redox reactions may influence the ORP even at constant chlorine feed rates. Since the ORP measurement is not specific to any parameter, disinfection with any oxidizing biocide may potentially be controlled with this method because the potential provides a strong correlation between the bacteria kill rate and the mV value. The Nernst equation has been used for many years to control cooling tower disinfection:

$$E = E_0 + kT \log ([\text{Oxidants}][\text{H}^+][\text{Reductants}]) \quad (24.5)$$

Therefore, the presence of either will contribute to the overall ORP value and the relationship is expressed on the chart below (Figure 24.7).

The general working principle of an ORP sensor is of any potentiometric electrode, such as a pH sensor, for example, and will be discussed in Section 24.4.3.2. The difference between pH and ORP sensors is that the pH-electrode is covered with a glass membrane that provides selectivity for protons penetrating the membrane, while the ORP electrode is a bare electrode (Figure 24.8a). An example of the ORP sensor is displayed in Figure 24.8b.

As discussed above with regard to the example of chlorine disinfection control, ORP technology and sensors have their drawbacks and limitations that do not allow this method to be the universal one for every application. Other technology limitations include variations in background potential known as “poise.” Poise refers to the amount of potential existing in the natural water from

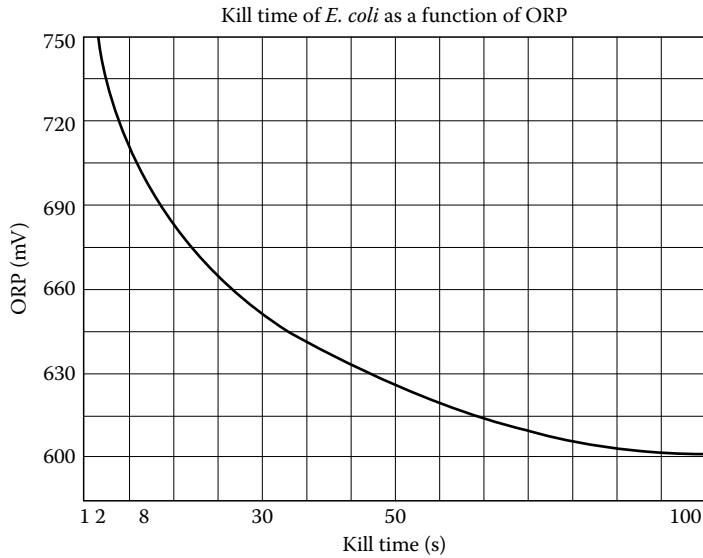


FIGURE 24.7 Expanded ORP vs. bacteria kill time.

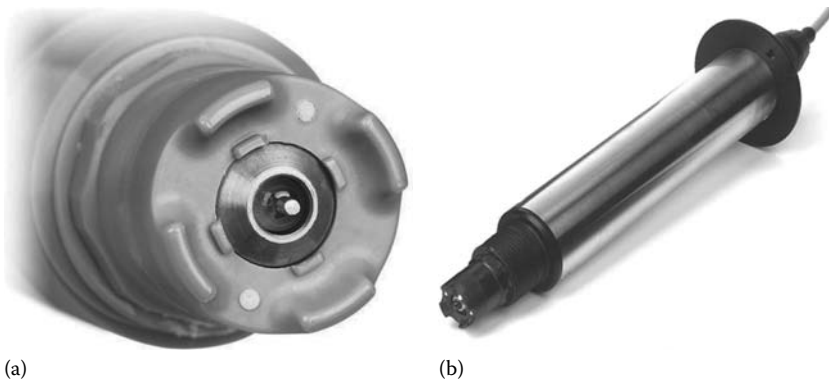


FIGURE 24.8 Examples of ORP electrode (a) and sensor (b). (Courtesy of Hach Company, Loveland, CO.)

existing or introduced chemicals that will exert a small redox potential. For example, water with no oxidants is not zero mV. It may be anywhere from 100 to 300 mV. This background potential must be accounted for and considered when determining the actual mV control range for the system. Commonly, this is achieved by comparing the expected mV range to the accepted microbiological test results such as plate counts and/or ATP results. From a series of side by side comparisons, an mV control range can be determined that is acceptable for the system.

Along with oxidizing chemicals commonly used in a majority of disinfection applications, there are several compounds known as nonoxidizing biocides, which are used in conjunction with oxidizers and mostly in cooling tower applications. These compounds are represented by gluteraldehyde, isothiazolines, triazine (triazone), and quaternary ammonium compounds (QAC), to name a few [9], and their use is aimed at enhancing disinfection in some specific applications, normally, for cooling water. The concentration of these chemicals is commonly monitored off-line by gas or liquid chromatography (GC, GC/MS, LC/MS) or by using the NMR method. These analyses are usually provided by well-equipped specialized off-site laboratories. Currently, only gluteraldehyde and QAC can be analyzed on-site by simpler colorimetric methods [10,11].

24.3 ON-LINE MONITORING AND ANALYSIS OF COOLING AND BOILER WATER TREATMENT PARAMETERS

In today's challenging financial environment, utility sections of the plant are required to tighten control and realize cost savings. Accurate and consistent blowdown control optimizes the cycles in the boiler without jeopardizing the integrity of the equipment and minimizes fuel costs. A reduction in the blowdown requires less makeup, saves water and energy, and reduces wastewater expenses. The effective use of on-line monitors and process analyzers allows to achieve these results.

24.3.1 PRETREATMENT, BOILER, STEAM, AND POWER SYSTEM

24.3.1.1 Silica Analyzer

A silica analyzer should be used for the early detection of deionized filter breakthroughs in boiler water pretreatment to decrease potential contamination in boiler-feed water resulting in increased cycles. Traditionally, resistivity is used to detect a breakthrough in anion or mixed bed deionizers and condensate polishing systems. Silica is weakly ionized, and resistivity does not register an anion breakthrough until approximately 50 ppb of silica is detected. Continuous on-line silica analyzers with lower detection limits (LDL) of 0.5 ppb, therefore, detect cation breakthrough 100 times sooner than resistivity.

Continuous monitoring of condensate return percentage for process control requires flows of various parameters like feed water, makeup water, and/or condensate return. If some of these parameters are not monitored for flow, an on-line silica analyzer with a sample sequencer could be utilized to detect silica in feed water, makeup water, and condensate return, and a mass balance calculation could determine the total condensate return. Carryover and in some cases boiler cycles based on silica (systems > 1000 psi) could also be detected and optimized using this approach. This allows operators to maximize boiler cycles while maintaining the integrity of the system.

24.3.1.2 Dissolved Oxygen (Parts per Billion) Analyzer

Industrial steam systems often are most susceptible to dissolved oxygen excursions due to the varying condensate return quality. Makeup water entering the deaerator contains 7000 ppb dissolved oxygen (DO), and as makeup needs change from 20% to 30% based on the grade produced, the DO could vary greatly. This is often negated through the use of chemical oxygen scavengers fed to the drop-leg of the deaerator to remove the oxygen not removed through mechanical means. In order to compensate for the varying condensate feed quality, these scavengers are often fed at rates high enough to accommodate the maximum possible oxygen level in order to protect the system. This can result in the excessive use of chemicals, and can also reduce the pH level of the feed water, requiring the addition of chemicals (caustic) to raise the pH level back to the operating pH level.

Dissolved oxygen monitors are not new to the industry. Historically however, DO sensors (generally electrochemical sensors) were often installed, only to be taken out of service as a result of maintenance complexity, stable flow requirements, and the continuous need for recalibration to maintain accurate readings. The latest technology for oxygen sensors uses luminescent technology, eliminating the need for membrane replacement, eliminating flow requirements, and drastically reducing the maintenance requirement. The automatic calibration feature allows for a consistent and accurate DO readout, and requires 5 min of maintenance annually.

24.3.1.3 Sodium Analyzer

Due to the high energy and steam demands, many large industrial plants today are equipped with steam generators that also produce electricity. These cogeneration boilers receive condensates from the steam turbine, as well as from the steam used in the process. As discussed earlier, returning the maximum amount of condensate is imperative to optimizing energy savings in the steam/power circuit. Returning poor quality condensates places the turbine and boiler in jeopardy. Conductivity is

still used as an indicator of the quality of the condensate to either recover this high quality water or reject the polluted condensate. Due to the high content of sodium salts in most of the process steps where the steam is used (phosphate/sodium blend boiler chemicals, caustic soda in some processes), the sodium represents a better alternative for detecting condensate contamination.

Sodium analyzers have been labor intensive, requiring regular etching and recalibration of probes. The latest sodium analyzers offer automatic calibration and auto regeneration of the ISE probe without the use of harsh chemicals. An LDL of 30 ppt, compared with the best estimation of 0.1 ppm (100 ppb) expected from a good conductivity measurement, makes today's sodium analyzers about 300 times more sensitive than conductivity probes.

24.3.1.4 Hardness Analyzer

Many plants use sodium zeolite softeners for pretreatment to reverse osmosis, for low pressure boiler applications, or for chemical makeup. Hardness monitors can also be used to prompt the regeneration of softeners instead of throughput. This increases the longevity of ion exchange resins, while offering alarm conditions for hardness detection in water. Using a hardness monitor for regeneration reduces water, wastewater, and energy costs, while freeing operator time. A hardness monitor in the condensate in return protects the boiler from hardness intrusion by alerting operators in a timely fashion, while reducing testing frequency and offering maximum boiler protection. Hardness excursion could severely impair heat transfer efficiency and reduce energy consumption while attributing to potential tube failure.

24.4 COOLING TOWER CONTROL

For efficient cooling, the heat transfer surfaces must be protected from corrosion and scale. After the water is cooled, it is collected in a sump and pumped back through the process piping. Proper control of key parameters will keep the tower operating efficiently and prevent damage to the vital parts from scale, corrosion, and biological growth. As air flows through the tower, airborne contaminants are picked up by the water/air interface and pH is one of many parameters that control the water chemistry of the tower. Maintaining a pH level between 6.0 and 8.0 is fairly common. Depending on the pH level of the supply water to the tower (lake, stream, or municipal water supply), an acid control scheme is often used to maintain the pH level in this range. Blowdown from the cooling tower is concentrated from three times up to ten or more times. This concentrated stream goes to the waste treatment plant, if it exists, for additional treatment and discharge.

24.4.1 ORGANIC CONTAMINANTS

The presence of any organic chemical in the reuse stream makes the water unusable for any reuse purpose without further treatment. Acceptable organic levels are essentially near zero. Laboratory tests for organics include an oil and grease test, plus tests for biochemical oxygen demand (BOD), chemical oxygen demand (COD), and total organic carbon (TOC). The oil and grease test is used less often than the others. A description of the testing and on-line instruments for COD, BOD, and TOC are presented in the following sections.

24.4.1.1 Chemical Oxygen Demand

The COD test uses a strong chemical oxidant in an acid solution and heat to oxidize organic carbon to CO_2 and H_2O . By definition, COD is "a measure of the oxygen equivalent of the organic matter content of a sample that is susceptible to oxidation by a strong chemical oxidant" [12]. Oxygen demand is determined by measuring the amount of oxidant consumed using titrimetric or photometric methods. Toxic substances do not adversely affect the test, and test data is available in 1–1/2 to 3 h, providing water quality assessment and process control. COD test results can also be used to estimate the BOD of a given sample. An empirical relationship exists between BOD, COD, and

TOC; however, the specific relationship must be established for each sample. Once a correlation has been established, the test is useful for monitoring and control.

24.4.1.2 Biochemical Oxygen Demand

BOD is the amount of oxygen, expressed in mg/L or ppm, that bacteria take from water when they oxidize organic matter. The carbohydrates (cellulose, starch, sugars), proteins, petroleum hydrocarbons, and other materials that comprise organic matter get into water from natural sources and from pollution. To determine BOD, the amount of oxygen is calculated by comparing the amount left at the end of 5 days with the amount known to be present at the beginning. During the 5 day period of a BOD test, the bacteria oxidize mainly the soluble organic matter present in the water. Very little oxidation of the solid (insoluble) matter occurs in that short time.

Two methods are widely used for BOD measurement. One method, the dilution method, is a standard method of the American Public Health Association (APHA) and is approved by the U.S. Environmental Protection Agency (USEPA). The other method, the manometric method, has been used for over 75 years in many sewage plants and other installations throughout the world. The dilution method involves putting incremental portions of the sample into bottles and filling the bottles with dilution water. The dilution water contains a known amount of dissolved oxygen, a portion of inorganic nutrients, and a pH buffer. The bottles are completely filled, freed of air bubbles, sealed, and allowed to stand for 5 days at a controlled temperature of 20°C (68°F) in the dark. At the end of the 5 day period, the remaining dissolved oxygen is measured. The relationship of the oxygen that was consumed during the 5 days and the volume of the sample increment are then used to calculate the BOD.

Measurement of BOD using the manometric method is easier because the consumed oxygen is measured directly rather than with chemical analysis. Because the sample is usually tested in its original state (not diluted), its behavior more closely parallels that of the waste in an actual treatment plant. As the oxygen in the sample is used up, more will dissolve into the water from the air space over it. The manometer measures the drop in air pressure in the bottle. This continuous indication of the amount of oxygen uptake by the sample is an important feature of the manometric method. By graphing the results one can find the rate of oxygen uptake at any time and thereby gain considerable insight into the nature of the sample.

24.4.1.3 Total Organic Carbon

The total organic carbon (TOC) test uses a strong chemical oxidant with either heat or ultraviolet light (or a combination of these three) to oxidize organic compounds to CO₂ and H₂O. Oxygen demand is measured indirectly by determining the amount of CO₂ produced using infrared spectroscopy, conductivity, or coulometry (an electrochemical technique). The CO₂ is measured and reported as mg/L of TOC. Because BOD and COD tests directly measure the amount of oxygen required to stabilize a waste sample, the results reflect the original oxidation state of the chemical pollutants.

24.4.2 ON-LINE ANALYSIS

On-line analyzers exist for all three tests—COD, BOD, and TOC. The largest installed base for on-line analyzers of this group is for TOC analyzers. The TOC analysis will measure all natural/biodegradable organic carbon and all synthetic organic carbon. There are two key oxidation techniques: the UV persulfate oxidation technique and the high-temperature oxidation technique.

The on-line TOC analyzer is considered to be the simplest and cheapest approach for obtaining this information.

24.4.2.1 The UV Persulfate Technique for TOC

The UV persulfate oxidation technique utilizes high-energy ultraviolet radiation to catalyze the chemical oxidation of a liquid sample in the presence of a strong oxidizer, sodium persulfate. Due to

the oxidation, the organic carbon in the sample is converted to CO_2 gas, and then the gas is separated from the liquid and analyzed with a nondispersive infrared detector (NDIR). The CO_2 concentration is directly proportional to the carbon concentration in the sample. Total inorganic carbon (TIC) will cause interference and it is removed from the sample by adding an acid to lower the pH and sparging the CO_2 produced from the TIC in the sample.

24.4.2.2 The High Temperature Oxidation Technique for TOC

In this technique, a furnace at 680°C or higher and an oxidative catalyst (generally a mixture of platinum and palladium) are employed to convert all the carbon in a liquid sample to CO_2 gas. The gas is separated from the liquid and analyzed with a NDIR (Figure 24.9). The CO_2 concentration is directly proportional to the carbon concentration in the sample. In the same manner as in the UV persulfate technique, TIC must be removed by acidifying the sample and by sparging the CO_2 .

24.4.2.3 TOC Test/Analyzer

The TOC test is the most widely accepted test for quick results. TOC analysis time for both laboratory analyzers and on-line instrumentation may be as short as 4–5 min. This gives a plant the ability to make quick decisions about whether to use a water stream or divert it to a holding pond or for further treatment. The best recommendation for a plant wanting to compare BOD/COD/TOC is to

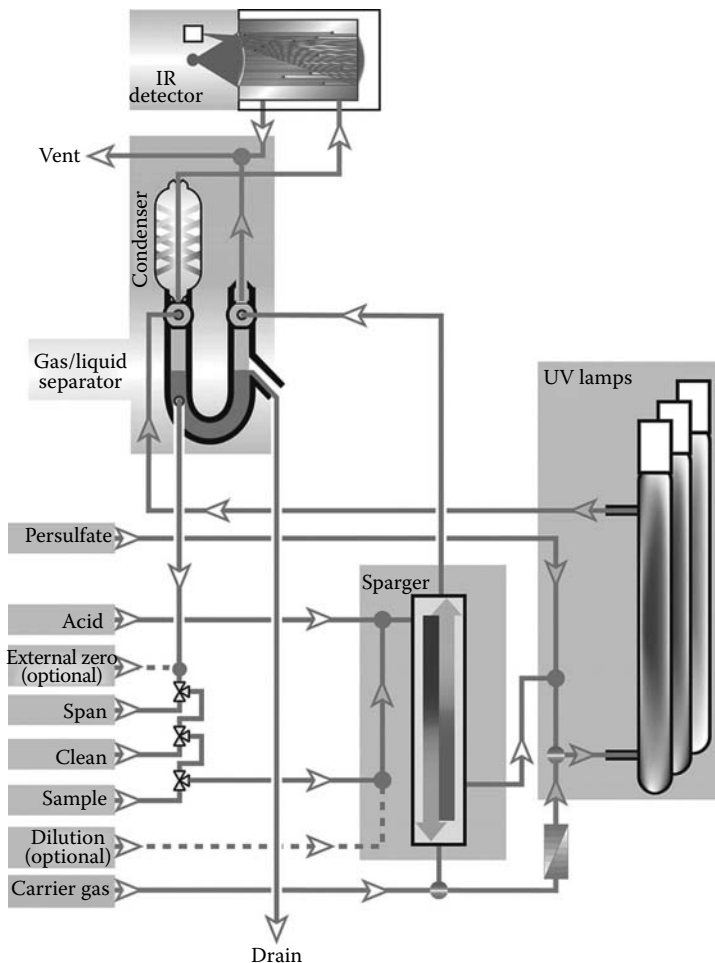


FIGURE 24.9 Typical flow diagram of an on-line UV persulfate TOC analyzer.

run a side-by-side analysis for several months and compare the results. In this way, an empirical relationship can be determined for each stream.

24.4.3 pH MEASUREMENTS AND CONTROL

Almost all processes containing water have a need for pH measurement. All human beings and animals rely on internal mechanisms to maintain the pH level of their blood, which must have a pH level between 7.35 and 7.45 and exceeding this range by as little as one-tenth of a pH unit could prove fatal. The pH level of wastewater leaving manufacturing plants and wastewater purification plants, as well as potable water from municipal drinking water plants, must be within a specific pH control limit as set forth by local, state, or federal permits. This value is typically between 5 and 9 pH, but can vary from area to area.

24.4.3.1 Definition of pH

pH is the measurement of the hydrogen ion concentration $[H^+]$ in a solution and is defined as the negative logarithm of the hydrogen ion concentration. This definition of pH was introduced in 1909 by the Danish biochemist, Soren Peter Lauritz Sorensen. It is expressed mathematically as

$$\text{pH} = -\log [H^+] \quad (24.6)$$

where $[H^+]$ is the hydrogen ion concentration in mol/L

The pH value is an expression of the ratio of $[H^+]$ to $[OH^-]$ (hydroxide ion concentration). If the $[H^+]$ is greater than $[OH^-]$, the solution is acidic. Conversely, if the $[OH^-]$ is greater than the $[H^+]$, the solution is basic. At pH 7, the ratio of $[H^+]$ to $[OH^-]$ is equal and, therefore, the solution is neutral. Because pH is a logarithmic function, a change of one pH unit represents a 10-fold change in the concentration of the hydrogen ion. In a neutral solution, the $[H^+] = 1 \times 10^{-7}$ mol/L. This represents a pH of 7.

$$\text{pH} = -\log (1 \times 10^{-7}) = -(\log 1 + \log 10^{-7}) = -(0.0 + (-7)) = 7.0 \quad (24.7)$$

Since the concentration of hydrogen ions and hydroxide ions are constant in a stable solution, either one can be quantified if the value of the other is known. Therefore, when determining the pH of a solution, (even though the hydrogen ion concentration is being measured), the hydroxide ion concentration can be calculated from:

$$[H^+][OH^-] = 10^{-14} \quad (24.8)$$

24.4.3.2 pH Electrode

A pH electrode is constructed with two types of glass as shown in Figure 24.10. The stem of the electrode is a nonconductive glass. The tip, which is most often bubble-shaped, is a specially formulated "pH sensitive" lithium ion-conductive glass consisting of the oxides of silica, lithium, calcium, and other elements. The structure of the pH glass allows lithium ion electrons to be exchanged by hydrogen ions in aqueous solutions, forming a hydrated layer. A millivolt potential is created across the interface between the pH glass and the external aqueous solution. The magnitude of this potential is dependent on the pH value of the solution. The difference of potentials ($V_1 - V_2$) created at the outer and inner hydrated layers of the pH glass can be measured using silver/silver chloride electrodes.

Since the internal solution of the glass electrode is buffered, its pH value is kept constant, making the measured potential difference dependent only upon the pH value of the external solution being measured. Differential pH systems drastically reduce drift associated with traditional pH

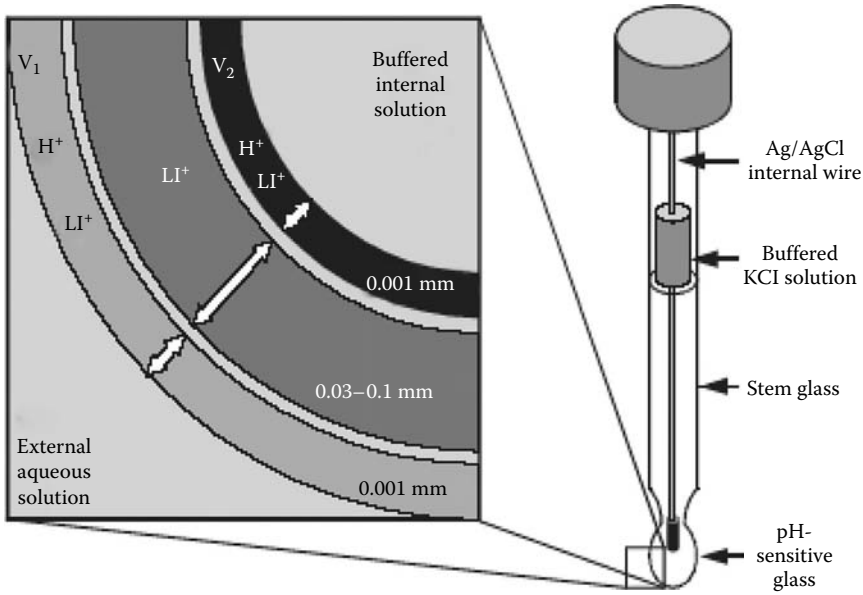


FIGURE 24.10 pH glass electrode details.

for increased accuracy and reduced calibration requirements. The following depicts the difference between traditional pH and differential pH (Figure 24.11).

The potassium chloride fill solution is not buffered from the process and contamination will result in measurement error over time (drift). Complete sensor dismantling is required to replace the reference electrode (E2), which is time consuming and costly. Ground loops flow through the reference electrode causing a measurement error. Contamination from the process coats the low-impedance reference electrode, altering the resistance of the electrode and the overall pH measurement.

A double-junction salt bridge minimizes the contamination from entering the inner chamber of the reference electrode (E2), thus providing a physical barrier, but allowing an electrical pathway to maintain measurement accuracy over time (Figure 24.12). A concentrated pH 7 buffer protects the reference electrode and minimizes the dilution effects from any contamination, which significantly minimizes the measurement error and drift. The double-junction salt bridge and the pH 7 buffer

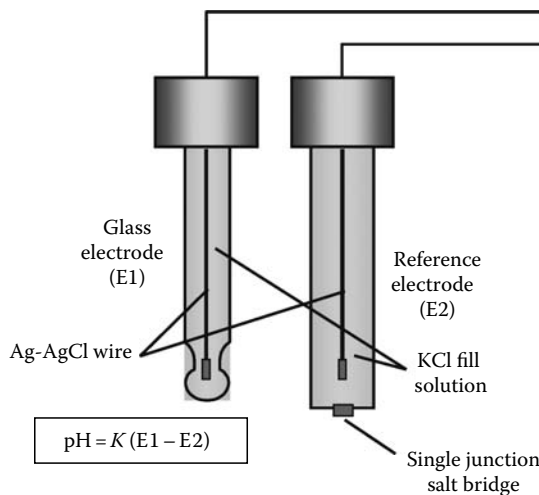


FIGURE 24.11 Traditional pH system.

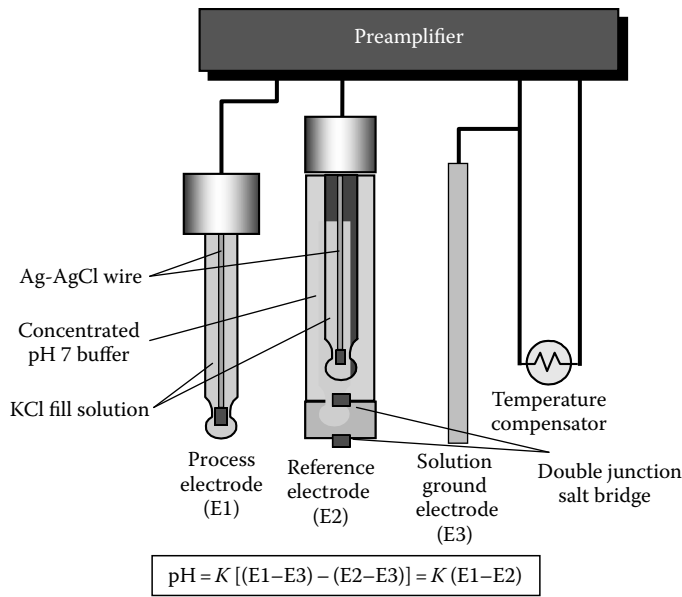


FIGURE 24.12 Differential pH system.

solution can be replaced in the field, making the sensor economical to maintain. Ground loops pass through the ground electrode (E3) instead of the reference electrode, preventing measurement errors. A high-impedance reference electrode minimizes the effects of contaminant coating.

24.4.4 ALKALINITY

Alkalinity is a measure of the capacity of water to neutralize acids. The alkalinity of water is due primarily to the presence of bicarbonate, carbonate, and hydroxide ions. Salts of weak acids, such as borates, silicates, and phosphates, may also contribute. Salts of certain organic acids may contribute to alkalinity in some waters, but their contribution usually is negligible. Bicarbonate is the major form of alkalinity. Carbonates and hydroxide may be significant when algal activity is high, and in certain industrial water and wastewater, such as boiler water.

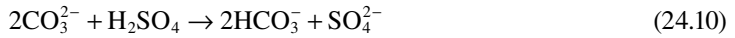
Alkalinity is expressed as phenolphthalein alkalinity or total alkalinity. Both types of alkalinity can be determined by titration with a standard sulfuric acid solution to an endpoint pH, shown by the change in color of a standard indicator solution. The pH also can be determined with a pH meter. Phenolphthalein alkalinity is determined by titration to a pH of 8.3 (the phenolphthalein endpoint) and gives the total hydroxide and one half the carbonate present. Total alkalinity is determined by titration to a pH of 4.9, 4.6, 4.5, or 4.3, depending on the amount of carbon dioxide present. The total alkalinity includes all carbonate, bicarbonate, and hydroxide alkalinity.

24.4.4.1 Chemical Reactions

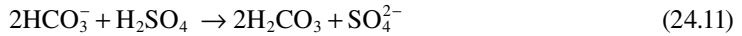
Sulfuric acid (hydrochloric acid may be used) reacts with the three forms of alkalinity, converting them to water directly or carbonic acid as an intermediate. If hydroxide is present, it reacts to form water:



This conversion usually is complete at a pH level of about 10. Phenolphthalein alkalinity is determined by titration to an endpoint pH level of 8.3, which corresponds to the conversion of carbonate to bicarbonate.



If hydroxide is present, titration to pH 8.3 will indicate the alkalinity due to all of the hydroxide plus one-half of the carbonate. Continued titration to pH 4.5 completes the conversion of carbonate plus any bicarbonate present to carbonic acid. This value is termed total alkalinity.



The color indicator traditionally used is methyl orange, hence, total alkalinity is referred to as methyl orange alkalinity. Some procedures use a mixed indicator solution, bromcresol green-methyl red, for a more distinct endpoint change in color. The mixed indicator goes through a series of color changes from blue to pink in the pH region of interest. A pH meter is required to titrate to the alternative pH endpoints of 4.9, 4.6, and 4.3.

There are several process analyzers designed to measure alkalinity on-line and the measurements are based on either colorimetric or potentiometric titration and both technologies have their advantages and drawbacks, such as different accuracy/precision, reagent consumption, etc. However, in order to find the right instrument for the application, we recommend contacting the manufacturer in every specific case.

24.4.5 CONDUCTIVITY/TOTAL DISSOLVED SOLIDS

Electrolytic conductivity is the measure of the ability of a solution to conduct an electric current and is sometimes referred to as “specific conductance.” Electrolytic conductivity is defined as the inverse or reciprocal of electrical resistance (ohms) and uses measurement units called mhos where one millionth of a Siemens unit equals one microSiemens ($\mu\text{S}/\text{cm}$). Resistivity as the inverse of conductivity is defined as the measure of the ability of a solution to resist an electric current flow. Conductivity is an indication of the quantity of ions contained in a solution. In ultrapure water, for example, minute amounts of ions affecting the conductivity measurement by as little as $0.05 \mu\text{S}/\text{cm}$ can produce unwanted deposits on plated parts; can cause significant problems in manufacturing semiconductors, and can damage turbine components used in the power industry. The conductivity of the solutions used in various applications must be measured and kept within acceptable limits. For all cooling and reuse water, a conductivity range can be set to be appropriate for that stream. Since the measurement and monitoring of conductivity or total dissolved solids (TDS) can be done by handheld or on-line instrumentation, the control of conductivity is relatively straightforward.

24.4.5.1 The Conductivity Spectrum

If all salts and free ions are removed from water, what remains is referred to as theoretically pure water. Theoretically pure water has, at 25°C , a specific conductance of $0.056 \mu\text{S}/\text{cm}$ and a resistivity of $18.21 \text{ M}\Omega \cdot \text{cm}$. High-quality condensed steam and distilled or demineralized water have a specific conductance of $1.0 \mu\text{S}/\text{cm}$ or less. This value is caused by about 0.5 ppm of dissolved salts. Table 24.2 shows the typical conductivity ranges.

24.4.6 TDS RELATIONSHIP TO CONDUCTIVITY AND RESISTIVITY

TDS is the amount of solids dissolved in a water sample. Suspended solids (SS) is the amount of solids that have not dissolved into a water sample, or solids that are insoluble in water. Total solids (TS) is the sum of TDS and SS. In laboratory analysis, measurements of these parameters are made by filtering and weighing to determine the amount of SS, then drying and weighing to determine

TABLE 24.2
Conductivity Ranges of Common Solutions

Pure water	0.05 $\mu\text{S}/\text{cm}$
Demineralized water	0.1–1.0 $\mu\text{S}/\text{cm}$
Distilled water	1–10 $\mu\text{S}/\text{cm}$
Tap water	100–1000 $\mu\text{S}/\text{cm}$
Polluted water	1000–10,000 $\mu\text{S}/\text{cm}$
Sea water	30,000–50,000 $\mu\text{S}/\text{cm}$
5% sodium chloride solution	70,000 $\mu\text{S}/\text{cm}$
10% sulfuric acid solution	40,000 $\mu\text{S}/\text{cm}$

TABLE 24.3
Conductivity/Resistivity/TDS Conversions

Conductivity ($\mu\text{S}/\text{cm}$) at 25°C	Resistivity ($\Omega \text{ cm}$) at 25°C	Dissolved Solids (ppm)
Pure Water		
1.110	900,000	0.566
1.250	800,000	0.625
1.430	700,000	0.714
1.670	600,000	0.833
2.000	500,000	1.000
2.500	400,000	1.250
3.330	300,000	1.670
5.000	200,000	2.500
10.00	100,000	5.000

the TDS. In a process stream, TDS is commonly measured with a conductivity analyzer. However, this measurement is only an approximation because it is based on a multiplication factor of 0.4–0.75 times the raw conductivity value. The variation is due to the type of dissolved solid(s) that are in the sample. The conversion between conductivity, resistivity, and TDS is shown in Table 24.3.

24.4.7 TURBIDITY AND SUSPENDED SOLIDS

An important water quality indicator for almost any use is the presence of dispersed, suspended solids—particles not in true solution. These often include silt, clay, algae, and other microorganisms, organic matter, and other minute particles. The extent to which suspended solids can be tolerated varies widely, as do the levels at which they exist. Industrial cooling water, for example, can tolerate relatively high levels of suspended solids without significant problems. In modern high pressure boilers, however, water must be virtually free of all impurities. In almost all water supplies, high levels of suspended matter are unacceptable for aesthetic reasons and can interfere with chemical and biological tests. Suspended solids obstruct the transmittance of light through a water sample and impart a qualitative characteristic, known as turbidity, to water. The APHA defines turbidity as an “expression of the optical property that causes light to be scattered and absorbed rather than transmitted in straight lines through the sample.” Turbidity can be interpreted as a measure of the relative clarity of water. Turbidity is not a direct measure of suspended particles in water but, instead, a measure of the scattering effect such particles have on light.

24.4.7.1 Turbidity and Total Suspended Solids

TSS include all particles suspended in water that will not pass through a filter. Traditional solids analysis, usually completed by gravimetric methods in the laboratory, is time-consuming and technique sensitive. Generally, it takes from 2–4 h to complete an analysis. Therefore, it is important as a lab result but not as a process control tool. On-line analyzers for either turbidity or suspended solids are in wide use for continuous control and monitoring. Since the properties of suspended solids in different applications may vary (size, shape, color, etc.), the effect on the light transmission or turbidity may vary. For example, a stream of municipal wastewater, with a suspended solid concentration of 50 mg/L could have a different turbidity than a stream of coal plant effluent also carrying 50 mg/L of suspended solids. The makeup of the suspended solids differs and will scatter and absorb light differently.

24.4.7.2 Four-Beam and Advanced Measurement Techniques for Suspended Solids

Most on-line TSS analyzers use a backscatter measurement or a light-absorbance measurement to determine suspended solids concentration. A typical four-beam style sensor emits light from two LED light sources and measures incident light by two receivers (Figure 24.13). Light measurement is correlated to a laboratory TSS determination to calibrate the analyzer. The system will need to be calibrated occasionally to compensate for any color changes in the sample or fouling of the system. Operators clean the system automatically with a self-cleaning air or water blast or manually by removing the system and wiping the sensor off.

The latest suspended solids system uses a different measurement technique, measuring the backscattered light with two detectors—one at 140° and one at 90°. The measurement of turbidity only involves a measurement at 90°. The sensor controller reads this light measurement as a suspended solids value based on the calibration against a laboratory grab sample reading. A self-cleaning sensor significantly reduces maintenance (Figure 24.14).

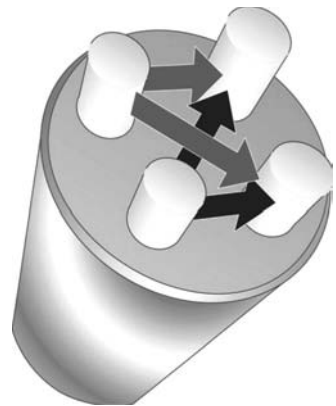


FIGURE 24.13 Four beam suspended solids measurement.

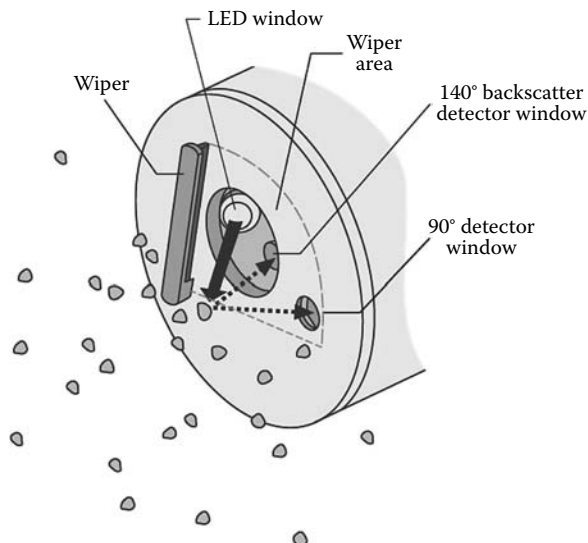


FIGURE 24.14 Advanced suspended solids sensor.

24.4.8 CONTROL AND MONITORING OF CORROSION

In most open-loop cooling water systems, corrosion is controlled through the addition of water treatment formulations containing scale and corrosion inhibitors. Although molybdates or rather molybdenum-based compounds are recognized as highly effective inhibitors, lately they are seldom used as the primary means of corrosion control, partly for economic reasons and partly due to environmental compliance concerns. Therefore, open loop cooling towers do not typically use molybdate for corrosion control. To reduce cost and environmental impact, polymers have largely replaced molybdate and other heavy metal treatments.

As with all treatment programs, close monitoring is required to ensure effective polymer concentrations are maintained in the system. Phosphonate and polymer field test methods used for determining the treatment dosages are often inaccurate and difficult to use, which can result in costly overtreatment or undertreatment, incurring higher potential for scaling, corrosion, fouling, or the unnecessary loss of water in blowdown. The inability or impracticality to effectively test for these inhibitors is why molybdate continues to play an active role in cooling water treatment programs. Molybdate at very low concentrations is often used as a tracer in these products. Low levels of molybdate are included in the polymer to provide a means to more easily determine the polymer concentration in a cooling water system (i.e., a 0.2–0.5 ppm molybdate [as Mo^{6+}] level may indicate 100 ppm of the product).

With the molybdate tracer, dosage rates of water treatment inhibitors are typically controlled based on intermittent measurements (from grab samples) of the molybdenum concentration in the system water. Because this method is intermittent, the results are variable and can bring lengthy lag-times between concentration adjustments. A case study [13] has been conducted to prove the performance of a process analyzer designed to measure the molybdenum concentration in the ranges of both tracer and corrosion inhibition applications.

However, there are other tracing technologies based on the same principle, but using different tracing agents and methods of monitoring. The control of cooling water and boiler water chemicals is now commonly provided by using fluorescent dyes as tracers. This technique was introduced by Nalco Company approximately 10 years ago. The fluorescent dye programs are called TRASAR® with the latest version called 3D TRASAR. This technique involved blending various specific proprietary fluorescent dyes into the various water treatment chemicals at a predetermined concentration. The treated water sample is then fed into a sample chamber in a device containing a fluorometer. The test results in the detection of the fluorescent species in the analyzer is then considered proportional to the treatment chemical much like any other tracer, such as molybdate discussed in detail above.

Another modern approach for process monitoring, control, and optimization involves a more sophisticated methodology of combining the results of several relevant measurements in an algorithm to see the trends of the treatment process. This approach involves either several on-line instruments sending their readings to a “central brain” (i.e., SCADA) or a multiparameter analyzer able to process the data. These systems sometimes allow predictability in the behavior of the process, especially when the “brain” knows the historic trends.

A new approach utilizing an online multicomponent analyzer for use in industrial water treatment has recently been developed. The analyzer is capable of measurement and control of multiple active key treatment components, including polymeric dispersants, corrosion inhibitors, and oxidizing biocides. The MultiTrak™ analyzer (Figure 24.15) has the following major performance characteristics [14]:

- The MultiTrak analyzer measures the active ingredients using reagent-based colorimetric methods rather than measuring product tracers.
- A large number of readily available and well-documented reagent-based methods can be adapted.

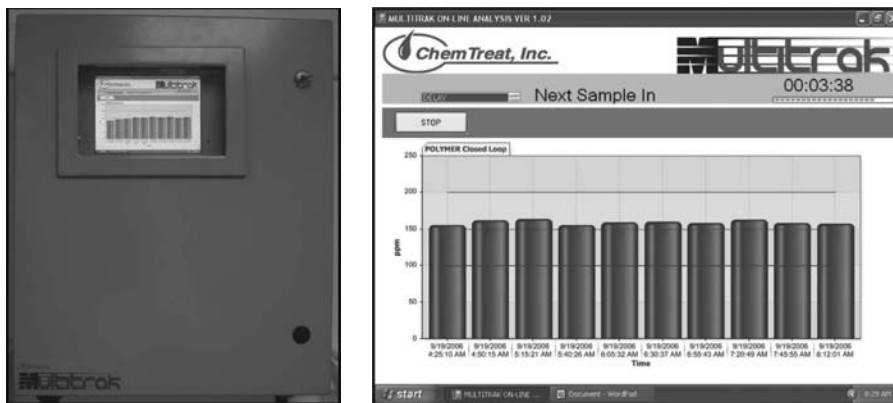


FIGURE 24.15 ChemTreat Multitrak analyzer. (From Richardson, J. et al., On-line analysis of water treatment programs, in *Proceedings of the 67th Annual International Water Conference, IWC-06-08*, Pittsburgh, PA, 2006.)

- The MultiTrak analyzer is capable of measuring more than one component at a time, such as active polymer and free chlorine.
- Unit results can be verified using readily available grab sample/bench top methods.
- Historical data can be plotted and trended.
- The MultiTrak analyzer has internal data logging with a 40 GB hard drive that is capable of maintaining years of data.
- The MultiTrak analyzer has a computer-based control board that enables the unit to be programmed with an unlimited variety of methods.
- Downloading data, upgrading software, or adding new methods can be performed easily through a USB port with a jump drive.

One of the main differences from regular process analyzers is the ability of this instrument to compare active ingredient levels to theoretical concentrations, which leads to the determination of the product functionality and performance. For example, if the corrosion inhibitors are below specifications and polymeric dispersants are not, it may indicate that a product with different inhibitor ratios is needed. This ability provides some degree of intelligence to the process analysis at the point of measurement and may, therefore, shorten the time for decision making and help further process control automation.

24.5 SUMMARY

No matter what technique and methodology is chosen for monitoring of a water treatment process, the ultimate goal is always to optimize the process and cut costs. Thus, employing of on-line analyzers provides for a faster response to the changes occurring in the process, compared with the use of laboratory analyses. The next step in monitoring and control is to use the process instrumentation to distinguish between the reasons for the observed changes in the process—is it due to the process itself or because of malfunctioning instrumentation? The analyzers equipped with self-verification functions and the ability to track and analyze historical and multiparametrical data provide additional benefits for the customers helping to automate the system response by minimizing the involvement of the operators.

The ultimate future vision of the water treatment process control is the intelligent information management (IIM) systems, where the role of on-line instrumentation is not only to provide data for a central brain, but to ensure the reliability of the data. This function of on-line analyzers seems to be vital to ensure the overall performance of an IIM system, which will provide a completely

automated process control even in an emergency situation and will eventually eliminate the need for multiple operators working in multiple shifts.

REFERENCES

1. Malkov, V. B. and Tocio, J. Inductive conductivity for control of CIP processes. In *Proceedings of the 53rd ISA Analytical Division Symposium*, Calgary, Alberta, Canada, AD2008 S12 (October 20–23, 2008).
2. Courtesy of Hach Company, Loveland, CO.
3. Suslow, T. V. Ozone applications for postharvest disinfection of edible horticultural crops. Division of Agriculture and Natural Resources, University of California, Oakland, CA, Publication 8133 (2004).
4. Eugster, U. and Stanley, B. The use of ozone as a disinfectant in fish hatcheries and fish farms. www.ozomax.com/pdf/article-seafood-hatchery.pdf
5. Courtesy of Ozone Solutions, Inc., Hull, IA (<http://www.ozonesupplies.com>), http://www.ozoneapplications.com/products/o3sensors/electrochemical_HMOS_ozone.htm
6. *Water Analysis Handbook*, 5th edn., Method 8311, pp. 1043–1046, Hach Company (2008).
7. Method 4500-O₃ B, *Standard Methods for Examination of Water and Wastewater*, 19th edn., APHA, AWWA, WEF, pp. 4–104 (1995).
8. Courtesy of Sensorex Corporation, Garden Grove, CA (<http://www.sensorex.com>)
9. Frayne, C. The selection and application of nonoxidizing biocides for cooling water systems. *The Analyst*, 1–14 (Spring 2001).
10. *Water Analysis Handbook*, 5th edn., Method 8337, pp. 1193–1198, Hach Company (2008).
11. Hach Gluteraldehyde Test Kit Model GT-1, Cat. No. 25872–00 (www.hach.com)
12. Method 5220 COD, *Standard Methods for Examination of Water and Wastewater*, 19th edn., by APHA, AWWA, WEF, pp. 5–12, 5–16 (1995).
13. Malkov, V. B., Kiser, P., Nagao, B., and Dumpler, S. Tracking molybdate in cooling water. *CTI Journal*, 29, 8–24 (Summer 2008).
14. Richardson, J., Richard, H., Geisler, R. E., Stuart, D. P., and Trulear, M. G. On-line analysis of water treatment programs. *Proceedings of the 67th Annual International Water Conference*, IWC-06-08, Pittsburgh, PA (2006).

Index

A

Absolute supersaturation (AS), 275
Acid treatment method
 pH control, 286
 procedure, 285–286
 proportional flow control, 286
Acquired resistance, 400
Activated sodium bromide, 389–390
Adenosine triphosphate (ATP)-based biomonitoring, 123–124
Aggregate filtration, 300
Alkalinity monitoring, 498–499
Alkyl epoxy carboxylate (AEC) inhibitor, 115
Aluminum silicate scale
 amorphous aluminosilicate, 194
 biological systems, 199
 control, brine pH adjustment, 196
 formation, 194
 three-dimensional structures, 194
Amaranth method, 488
Analytical techniques, *see* Scale identifying techniques
Anionic polyelectrolytes, 23
Anodic inhibitors, *see* Passivating corrosion inhibitors
Antiscalants, 263–264, 292–293
Aqueous solution polymerization, 472–473
ATR-IR spectroscopy
 advantages, 440
 calcium carbonate, 438
 effective penetration depth, 440
 limitations, 441
 principles, 439

B

Backscattered electron contrast (BSE) mode, 430
Bare electrode amperometric systems, 484
Barrier film corrosion inhibitors, 329
Benzotriazole (BZT) inhibitor, 117, 330
Binary plant cycles
 amorphous silica supersaturation, 163
 pH modification (*see* pH-modification)
 rapid thermal quenching, 165
 silica concentration and solubility, 164–165
 thermal and kinetic stability, 164
Biochemical oxygen demand (BOD), 494
Biocides, 120–121; *see also* Biological growth control
 application strategies
 adjuvants and biodispersants, 403–404
 cooling system design, 402
 monitoring, 404
 synergistic blends, 403
 water quality, 402–403
 mechanisms
 membrane active, 400
 moderate electrophiles, 399–400

 oxidants or extreme electrophiles, 398–399
 protonophores, 400
 resistance, 400–401
 microbial growth problems, 383–384
 microorganisms, industrial systems, 383
 regulation, 384–385
 resistance, 400
 selection
 nonoxidizers, 394–398
 oxidizers, 385–394
Biofilms, 118–121, 123
Biofouling, 17
 causes, 366
 costs, 366–367
 definition, 365
 heat exchangers
 biofilm formation, 365
 cooling water recycling, 374
 corrosion, 371–372
 design consideration, 373–374
 heat transfer rate, 372–373
 membrane systems
 biofilm formation, 366
 flux decline data, sand filter, 375
 molecular dynamics simulation,
 alginate oligomer, 375
 permeability, 374–375
 microbial films
 bacterial metabolism, 370
 buildup processes, 367, 368
 development processes, 369
 fluid velocity, 369–370
 nutrient depletion, 370–371
 optimization factors, 378
 prevention strategies, 377–378
Biological growth control
 algae growth, 120–121
 biodispersants, 123
 biofilms, 118
 biomonitoring
 biochemical markers, 123–124
 culture-based method, 123
 performance indicators, 124
 cooling towers, 120–121
 fungi attack, 120
 Legionella bacteria control, 119
 macroscopic life forms, 118
 microscopic life forms, 119
 nonoxidizing biocide
 activity and types, 122
 biofilms, 121–122
 dosage and frequency, 122–123
 shot feed, 122
 oxidizing biocide, 121
 planktonic organisms, 119
 plenum, 120

- purpose, 118
 - sulfate-reducing bacteria (SRB), 119, 125
 - Bishexamethylenetriaminepenta (methylenephosphonic acid) (BHPMP), 140
 - Bisphosphonates
 - HAP growth inhibition, 110, 111
 - osteoporosis, 110–111
 - Boiler system
 - ion exchange process
 - cleaning procedure, 304
 - dealkalizer, 304–305
 - mechanical problems, 302–303
 - resin beads and applications, 301–302
 - water softener cycle, 302
 - pretreatment process
 - clarification, 298–299
 - filtration, 299–301
 - reverse osmosis method, 305–306
 - scale control
 - chelant approach, 311–312
 - chemical feed points, 316
 - condensate, 313–316
 - dispersants, 312–313
 - precipitating approach, 310–311
 - treatment
 - feed water tank, 306–308
 - oxygen scavengers, 308–310
 - Boiler water treatment (BWT)
 - deposit control polymers
 - crystal modification, 462
 - dispersion, 460–461
 - metal ions stabilization, 461–462
 - roles, 458
 - scale inhibition, 459–460
 - types and descriptions, 459
 - monitoring (*see* Cooling water treatment (CWT))
 - Bottoming cycle heat recovery system, 163–168
 - Bridging attraction force, 354
 - Bridging flocculation, 349, 466–467
 - Bromine-based biocides
 - activated sodium bromide, 389–390
 - bromine-releasing isocyanurate, 391
 - bromochlorodimethylhydantoin (BCDMH), 390–391
 - dibromodimethylhydantoin (DBDMH), 391
 - disinfection monitoring, 489
 - properties, 390
 - stabilized bromine chloride and hypobromite, 390
 - Bromochlorodimethylhydantoin (BCDMH), 390–391
 - 2-Bromo-2-nitropropane-1,3-diol (BNPD), 396
 - Bulk polymerization, deposit control polymers, 450
- C**
- Calcium carbonate polymorphs
 - aragonite crystals, 62–63
 - calcite crystals, 63
 - crystallographic description, 62
 - DETPMP effect
 - crystal morphology, 71–72
 - scale kinetics, 71, 72
 - supersaturated solutions, 76
 - synchrotron radiation, 75–76
 - wide-angle X-ray scattering (WAXS)
 - measurement, 73–74
 - X-ray diffractogram (XRD) analysis, 72–73, 74
 - dissolved iron ion effect, 63
 - magnesium ion effect
 - crystal morphology, 64, 65
 - Mg²⁺ concentration, 64–66
 - surface deposition, 63–64
 - surface roughness, 66–67
 - organic phosphonates, 67
 - PPCA effect
 - crystal morphology, 68–70
 - kinetics, 67–68
 - surface deposit, 68, 69
 - XRD analysis, 69, 71
 - scale composition, 68
 - scale inhibitors, 63
 - scanning electron microscope (SEM), 428
 - vaterite crystals, 62–63
 - Calcium carbonate scale
 - amorphous, 39
 - control
 - calcite dissolution, 55–56
 - 1-hydroxy ethylidene-1,1-diphosphonic acid (HEDP), 52
 - mineral acids, 50
 - phosphonate, 52, 54
 - polymers, 52–54
 - polyphosphates, 51
 - surface-diffusion-controlled crystal growth, 51–52
 - threshold inhibition, 51
 - crystallization fouling, 39
 - kinetics
 - concentration profile, 49–50
 - crystal growth from solution, 48–49
 - encrustation, 46
 - equation, 48
 - induction time, 46, 47
 - nucleation, 44–45
 - pH-stat method, 47–48
 - rate expression, 50
 - surface charge, 50
 - physical processes, in aqueous media, 40, 41
 - polymorphism, 39
 - scale inhibition
 - co- and terpolymer heat treatment, 94–95
 - crystal morphology, 98, 99
 - deposit control polymers, 97
 - DETPMP inhibitors, 144–145
 - homopolymer heat treatment, 93–94
 - phosphonates, 95–96
 - polymer dosage, 93
 - polymeric and nonpolymeric, 92–93
 - polymer/phosphonate blends, 97–98
 - PPCA inhibitors, 144
 - temperature effect, 95
 - water chemistry, 97
 - thermodynamics
 - Langelier index (LI), 43, 44
 - mixed substrate products, 42–43
 - Ryznar solubility index (RSI), 43, 44
 - seeded growth technique, 42
 - solution distance, 40–41
 - Stiff and Davis index (SDI), 43–44
 - supersaturation, 42
 - water-carrying pipes, 39–40

- Calcium hypochlorite, 389
- Calcium oxalate; *see also* Crystal growth inhibition
 - additives effect, 34–35
 - biomineralization, 32–33
 - crystal habits, 33
 - hydrated forms, 33–34
 - mono and dihydrates, SEM, 429
 - uroolithiasis, 33
- Calcium oxalate dihydrate (COD), 32–34
- Calcium oxalate monohydrate (COM), 32–34
- Calcium oxalate trihydrate (COT), 33–34
- Calcium phosphate scale
 - bisphosphonate inhibitor, 110–111
 - brushite
 - dissolution rate *vs.* step length, 107, 108
 - pit formation, 107
 - constant composition (CC) experiment, 107
 - critical pit size, 107–110
 - crystallization/dissolution theory
 - nucleation process, 106
 - supersaturation, 105–106
 - undersaturation, 107
 - hydroxyapatite, CC dissolution
 - dissolution termination, 108–110
 - titrant volume *vs.* time, 108, 109
- Calcium–phosphonate inhibitor interaction
 - Ca-HEDP inhibition, 88
 - turbidity *vs.* phosphonate concentration, 87
- scale inhibition
 - CWT programs, 90
 - iron (III) effect, 91–92
 - polymer composition, 90–91
 - polymer dosage, 91
 - polymer solution temperature, 91, 92
- Calcium–polymer inhibitor interaction
 - Ca ion compatibility, 86
 - Ca ion tolerance, 85
 - heat treatment effect, 86–87
 - turbidity *vs.* P3 concentration, 85–86
- Calcium silicate scale
 - biological systems, 198
 - formation, 195
- Calcium sulfate; *see also* Crystal growth inhibition
 - equipment failure, 29–30
 - kinetics and mechanism, 30–32
 - nitrilotrismethylene phosphonic acid (NTMP), 30
 - phosphonates, 30
 - polyelectrolytes, 30
- Cal Hypo, *see* Calcium hypochlorite
- Carbon filters, 262
- Carbonic acid corrosion, 313–314
- Carboxy methyl inulins (CMIs), 132–133
- Cationic polyelectrolytes, 88
- Cationic polymers
 - applications, water treatment
 - coagulants and flocculants, 475–476
 - industrial raw water, 477
 - municipal wastewater, 477
 - potable drinking water, 476
 - mechanisms
 - bridging flocculation, 466–467
 - charge neutralization, 467
 - electrostatic patch flocculation, 467–468
 - natural type
 - cationic starch, 468–469
 - chitosan, 469
 - polyacrylamides
 - aqueous solution polymerization, 472–473
 - copolymerization method, 475, 476
 - dry powders and beads, 473
 - inverse emulsions, 473
 - postreaction method, 474–475
 - synthetic type
 - manufacture methods, 472–475
 - polyacrylamides, 472
 - polyamines, 472
 - polydiallyldimethylammonium chloride, 471
 - polyethyleneimines (PEI), 470–471
 - polyvinylamine (PVA), 470
- Cationic starch, 468–469
- Charge neutralization, 349, 467
- Charge patch neutralization, 349
- Chelant, 311–312
- Chemical diverters, 130
- Chemical equilibrium method, 284
- Chemical feed points, 316
- Chemical oxygen demand (COD), 493–494
- Chemical pretreatment
 - acid/caustic, 264
 - antiscalant, 263–264
 - bisulfite, 264
 - lime, 263
- ChemTreat Multitrak analyzer, 502–503
- Chitosan, 469
- Chlorine-based biocides
 - calcium hypochlorite, 389
 - chlorine gas, 388
 - disinfection monitoring
 - amperometric titration method, 484
 - colorimetric method, 483
 - limitations, 485–486
 - on-line amperometric method, 484–485
 - oxidation–reduction potential (ORP), 489–491
 - properties, 387–388
 - sodium dichloroisocyanurate and trichloroisocyanuric acid, 389
 - sodium hypochlorite, 388
- Chlorine dioxide biocide
 - Amaranth and Lissamine Green B (LGB), 488
 - amperometric method, 488
 - chlorophenol red method, 488
 - DPD/glycine method, 488
 - food-handling equipment sanitization, 486–487
 - Hach 9187sc analyzer, 487
 - high/mid-range direct read method, 488
 - Legionella* disinfectant, 419–420
 - preparation methods, 392–393
 - properties, 392
 - pulp and paper bleaching process, 487
- Chlorine gas, 388
- 5-Chloro-2-methyl-4-isothiazolin-3-one (CMIT), 397
- Chlorophenol red (CPR) method, 488
- Clarification
 - coagulant, 299
 - procedure, 298
- Closed loop cooling water systems, 327–328
- Coagulants, cationic polymers, 476

- Coiling index, 347–348
 - Collision efficiency factor, 357
 - Collision volume, 349
 - Colloidal fouling, 17
 - Concentration factor (CF), 244
 - Concentration polarization, 234–235, 252–253
 - Condensate treatment
 - carbonic acid corrosion, 313–314
 - filming amine, 315–316
 - neutralizing amine, 314–315
 - Constant composition (CC) crystal growth
 - and dissolution, 107
 - Continuum mean field lattice model, 353
 - Cooling tower monitoring
 - alkalinity, 498–499
 - biochemical oxygen demand (BOD), 494
 - chemical oxygen demand (COD), 493–494
 - conductivity/total dissolved solids, 499–500
 - pH, 496–498
 - total organic carbon (TOC), 494
 - high temperature oxidation technique, 495
 - test/analyzer, 495–496
 - UV persulfate technique, 494–495
 - turbidity, 500–501
 - Cooling water treatment (CWT), 82
 - applications
 - chemical feed control, 124
 - data management, 126
 - monitoring system, 124–126
 - calcium carbonate inhibition, 97
 - deposit control polymers
 - crystal modification, 462
 - dispersion, 460–461
 - metal ions stabilization, 461–462
 - roles and evolution, 456–458
 - scale inhibition, 459–460
 - design treatment
 - biological control, 118–124
 - corrosion control, 116–118
 - deposit control, 114–116
 - formulation components, 89
 - iron (III) effect, 91–92
 - monitoring
 - hardness, 493
 - silica and dissolved oxygen, 492
 - sodium, 492–493
 - phosphonates, 87, 90
 - system performance and cost optimization, 113, 126
 - Copper-based alloys corrosion inhibitors, 330
 - Copper–silver ionization method, 418–419
 - Corrosion control
 - boiler systems
 - dissolved gases and solids, 331
 - erosion corrosion, 333–334
 - general corrosion, 331
 - localized corrosion and cracking, 333
 - polymers, chelants, and phosphates, 332
 - steam condensate, 334–335
 - steam purity, 335
 - underdeposit corrosion, 332–333
 - cooling water
 - barrier film inhibitors, 329
 - closed loop systems, 327–328
 - copper-based alloys inhibitors, 330
 - microbiofilm treatment, 330
 - once-through systems, 327
 - open recirculation systems, 328
 - organic inhibitors, 329–330
 - passivating inhibitors, 329
 - desalination systems, 335–337
 - design
 - HRA inhibitor, copper corrosion, 117
 - metallurgy type, 116–117
 - microbiologically induced corrosion (MIC), 118
 - phosphate inhibitor, mild steel corrosion, 117–118
 - geothermal systems, 339
 - monitoring, 502–503
 - Corrosion coupons, 339
 - Corrosion-related fouling, 17–18
 - Cross flow membrane filtration, 244
 - Crystal growth inhibition
 - calcium oxalate crystallization
 - additives effect, 34–35
 - biomineralization, 32–33
 - crystal habits, 33
 - hydrated forms, 33–34
 - uroolithiasis, 33
 - calcium sulfate crystallization
 - equipment failure, 29–30
 - kinetics and mechanism, 30–32
 - nitrilotris(methylene phosphonic acid) (NTMP), 30
 - phosphonates, 30
 - polyelectrolytes, 30
 - mechanism
 - additives, 23–24
 - crystal morphology modification, 25–26
 - growth rate retardation, 24
 - nucleation delay, 24–25
 - scale
 - formation, 22
 - inhibitors, 23
 - problems, 22–23
 - theory
 - impurities, 27–28
 - kink blocking, 27
 - Kossel model, 26–27
 - step edge adsorption, 28–29
 - step pinning, 27
 - Cyclonic filtration, 300–301
- ## D
- DBNPA, *see* 2,2-Dibromo-3-nitrilopropionamide (DBNPA)
 - Deaerator, 308
 - Dealkalizer, 304–305
 - Dealloying, 324
 - DEHA, *see* Diethylhydroxylamine (DEHA)
 - Deposit control design
 - alkyl epoxy carboxylate (AEC) inhibitor, 115
 - phosphonates-based treatment, 114–115
 - stress-tolerant polymer (STP)
 - efficacy, 116, 117
 - performance, 115–116
 - water analysis, 114
 - Deposit control polymers
 - BWT and CWT programs
 - mechanisms, 459–462
 - roles and functions, 456–459

- characteristics
 - end groups and branching, 452
 - homogeneity and heterogeneity, 452
 - molecular weight, 451–452
 - residual monomers, 452
 - tacticity and residual monomers, 452
 - commercial types, 458
 - comparison, 455–456
 - deposits
 - category, 81
 - control, 81–82
 - dispersing particulate matter
 - iron oxide dispersion, 99–100
 - iron (III) stabilization, 100–101
 - suspended and colloidal matter, 98–99
 - industrial water system, 82
 - laboratory screening tests, 82, 85
 - molecular weight distribution, 451
 - performance evaluation
 - calcium carbonate, 92–98
 - calcium phosphate, 90–92
 - calcium–phosphonate interaction, 87–88
 - calcium–polymer interaction, 85–87
 - polymer–polymer interaction, 88–89
 - pilot testing, 82, 85
 - polymeric and nonpolymeric additives, 83–84
 - scale identifying techniques, 443–445
 - specification parameters
 - appearance, 452–453, 454
 - form, 452
 - molecular weight, 453–454
 - pH, viscosity and acid number, 454
 - specific gravity and color, 455
 - total and active solids, 453
 - turbidity, haze, iron, and residual monomer levels, 455
 - types
 - natural polymers, 448–449
 - synthetic polymers, 449
 - Depth filters, 261
 - DETPMP, *see* Diethylenetriaminepenta (methylenephosphonic acid) (DETPMP) inhibitor
 - Dezincification corrosion, 324
 - Diafiltration, 244
 - Diallyldimethyl ammonium chloride homopolymer (P17), 88–89
 - Dibromodimethylhydantoin (DBDMH), 391
 - 2,2-Dibromo-3-nitrilopropionamide (DBNPA), 396–397
 - Dichlor, *see* Sodium dichloroisocyanurate
 - 4,5-Dichloro-*n*-octyl-isothiazolin-3-one (DCOIT), 397
 - Diethylenetriaminepenta (methylenephosphonic acid) (DETPMP) inhibitor
 - calcium carbonate, 67
 - crystal morphology, 71–72
 - scale kinetics, 71, 72
 - supersaturated solutions, 76
 - synchrotron radiation, 75–76
 - wide-angle X-ray scattering (WAXS) measurement, 73–74
 - X-ray diffractogram (XRD) analysis, 72–73, 74
 - with carbonate rock interaction, 148
 - molecular formulae, 68
 - oilfield scale inhibitors, 144
 - vs. PVS inhibitor, 145
 - Diethylhydroxylamine (DEHA), 309–310
 - Differential pH electrode system, 498
 - Dimethyldithiocarbamate (DMDC), 396
 - Disinfection
 - Legionella*
 - chlorine dioxide, 419–420
 - comparison, 417
 - copper–silver ionization, 418–419
 - hyperchlorination, 417–418
 - selection criteria, 416
 - superheat-and-flush, 416–417
 - monitoring
 - bromine, 489
 - chlorine, 483–486
 - chlorine dioxide (ClO₂), 486–488
 - ozone, 488–489
 - parameters and applications, 483
 - Dispersants, 312–313
 - Dissolved oxygen analyzer, 492
 - Dodecylguanidine hydrochloride (DGH), 398
 - Dual polymer flocculation, 351
- E**
- EDTA, *see* Ethylenediamine tetra acetic acid (EDTA)
 - Electrical sensing zone technique, 435
 - Electrophilic biocides, 398–399
 - Electrostatic patch flocculation, cationic
 - polymers, 467–468
 - Electrostatic repulsion force, 354
 - Emulsion polymerization, deposit control
 - polymers, 450
 - Energy dispersive x-ray spectrometry (EDS) analysis
 - calcium carbonate and silica, 431
 - operating procedure, 430–431
 - Environmental cracking, *see* Stress corrosion cracking (SCC)
 - Environmentally acceptable inhibitors, 132–133
 - Erosion corrosion (EC), 333–334
 - Erythorbic acid, 310
 - Ethylene-bis-dithiocarbamate (EBDC), 396
 - Ethylenediamine tetra acetic acid (EDTA), 311–312
 - Extracellular polymeric substances (EPS), 367
- F**
- Feed water tank system, 306–308
 - Field testing, 339
 - Flocculants, 344–345, 476
 - Flocculation model, *see* Population balance model (PBM)
 - Flow-accelerated corrosion (FAC), *see* Erosion corrosion (EC)
 - Fluorocarbon treatment, 173
 - Flux rate, 232
 - Fouling; *see also* Scaling
 - biofouling, 17 (*see also* Biofouling)
 - colloidal fouling, 17
 - corrosion-related fouling, 17–18
 - membrane, 234–235 (*see also* Reverse osmosis (RO) membrane fouling)
 - Four beam suspended solids analyser, 501
 - Fujiwara test, 259

G

- Geogard SX (GSX) inhibitor, 174–175
- Geothermal silica scale
 - ammonia, 171
 - common scale inhibition method
 - brine dilution with freshwater, 161
 - brine pH modification, 161–162
 - controlled silica precipitation, 162–163
 - water/brine processing, saturation, 160
 - Geogard SX (GSX) inhibitor, 174–175
 - geothermal power generation, 155–156
 - hybrid plant design
 - heat and mass balance, stage 1, 168, 169
 - heat and mass balance, stage 2, 168–170
 - relative silica deposition rates, 170–171
 - thermal and pH stability, stage 2, 170
 - limiting factor, geothermal energy, 175
 - organic additives
 - crystalline silicate control, 172
 - early studies, 172
 - fluorocarbon treatment, 173
 - inhibition efficiency, 172–173
 - inhibitor treatment costs, 173–174
 - urea-sulfuric and urea-hydrochloric acid, 173
 - polyoxyethylenes, 171
 - scale control techniques, supersaturation
 - binary-type heat exchangers, 165–166
 - brine acidification, 164, 165
 - multiple flash processes, 166
 - pH-modification, 166–168
 - rapid thermal quenching, 165
 - silica concentration and solubility vs. flash
 - temperature, 164–165
 - silica stability, 163–164
 - silica deposition, 158–159
 - silica precipitation kinetics, 159–160
 - silica solubility
 - amorphous silica and quartz, 156–157
 - NaCl effect, 157
 - pH effect, 157–158
 - silicates, 158
- Glutaraldehyde, 396
- Green rust, 16
- Green scale inhibitors (GSI), *see* Environmentally acceptable inhibitors

H

- Hach 9187sc analyzer, 487
- Halogen-resistant azole (HRA) inhibitor,
 - copper corrosion, 117
- Hardness analyzer, 493
- Heat exchanger biofouling
 - biofilm formation, 365
 - cooling water recycling, 374
 - corrosion, 371–372
 - design consideration, 373–374
 - heat transfer rate, 372–373
- HEDP, *see* Hydroxyethylidene diphosphonic acid (HEDP)
- Hexametaphosphate–steel corrosion inhibitor, 329
- High/mid-range direct read method, 488
- High-temperature additives treatment, 287
- High temperature oxidation technique, 495

- Hybrid treatment method
 - advantages, 287–288
 - case studies, 288–289
- Hydrogen peroxide (H₂O₂), 393
- Hydrologic cycle, 2–3
- Hydroxyapatite (HAP)
 - CC dissolution, 111
 - dissolution termination, 108–110
 - titrant volume vs. time, 108, 109
 - precipitating program, 310
- Hydroxyethylidene diphosphonic acid (HEDP)
 - CaCO₃ inhibition, 96–98
 - Ca-HEDP inhibition, 87–88
 - chemical structure, 110
- Hyperchlorination, 417–418

I

- Inductively coupled plasma (ICP), 435
 - Industrial bleach, *see* Sodium hypochlorite
 - Industrial water systems
 - cooling and boiler systems, 327
 - crevice corrosion, 322
 - dealloying, 324
 - erosion corrosion, 324–325
 - galvanic corrosion, 320–322
 - general corrosion, 320, 321
 - intergranular corrosion, 323–324
 - pitting, 322, 323
 - stress-corrosion cracking (SCC), 325–327
 - Infrared (IR) spectroscopy
 - ATR-IR spectroscopy
 - advantages, 440
 - calcium carbonate, 438
 - effective penetration depth, 440
 - limitations, 441
 - principles, 439
 - PAA/AMPS/SS terpolymer, 443–444
 - PAA/p-DADMAC coacervate, 443
 - poly(acrylic acid) (PAA), 442
 - poly-AMPS, 444–445
 - transmission spectroscopy, 437–438
 - In situ* chemical activation, 393
 - Instantaneous corrosion rate meters, 339
 - Interaction energy profile, 354
 - Intergranular corrosion, 323–324
 - Intrinsic resistance, 400–401
 - Inverse emulsion method, 473
 - Inverse emulsion polymerization, deposit control
 - polymers, 450
 - Ion exchange process, boiler system
 - cleaning procedure, 304
 - dealkalizer, 304–305
 - mechanical problems, 302–303
 - resin beads and applications, 301–302
 - water softener cycle, 302
 - Iron-removal filters, 262
 - Iron silicate scale
 - biological system, 198
 - formation, 192–194
- J**
- Jeddah-I and II power and desalination plant, 286

K

Kink blocking, 27
Kossel model, 26–27

L

Laboratory chlorine dioxide amperometric methods, 488
Langelier saturation index (LSI), 280
Laser light scattering technique, 435
Legionella
 colonization control
 disinfection criteria, 416
 monitoring control measures, 416
 water safety plan (WSP), 415–416
 disinfection methods
 chlorine dioxide, 419–420
 comparison, 417
 copper–silver ionization, 418–419
 hyperchlorination, 417–418
 selection criteria, 416
 superheat-and-flush, 416–417
 infection
 amoebae, 415
 biofilms, 413–414
 growth-promoting conditions, 413
 hot water storage tanks, 414–415
 minimum contaminant level (MCL), 413
 source, 412–413
 water constituents and plumbing materials, 414
 water quality, 411
Legionellosis, *see* Legionella
Legionnaires' disease, *see* Legionella
Lissamine Green B (LGB) method, 488
Localized corrosion and cracking, 333
Low-temperature additives treatment, 287
Lytic biocides, 400

M

Machine-based activation, 392
Magnesium ammonium phosphate hexahydrate (MAP), 205; *see also* Struvite scale
Magnesium ion effect, calcium carbonate
 crystal morphology, 64, 65
 Mg²⁺ concentration, 64–66
 surface deposition, 63–64
 surface roughness, 66–67
Magnesium silicate scale/foulant control, *see* Silica
 and magnesium silicate foulants
Maximum supersaturation, 278–279
Mean field lattice model, 353
MED, *see* Multiple-effect distillation process
Membrane active biocides, 400
Membrane biofouling, *see* Reverse osmosis (RO)
 membrane fouling
Membrane bioreactor (MBR) technology, 235–236
Membrane cleaning, 260
 efficiency vs. membrane hydrolysis, 265
 formulas, 265
 membrane life, 264–265
 off-site and clean-in-place (CIP) cleaning, 265
Membrane fouling, *see* Reverse osmosis (RO) membrane
 fouling

Membrane operations

 data collection, 257–258
 data normalization, 258–259
 membrane autopsy, 259–260

Membrane technology

 boundary layer, 243
 brackish water, 243
 brine (*see* concentrate)
 characteristics, 228
 chronicles
 asymmetric permeability differences, 229
 electrodialysis, 229
 Fick's laws of diffusion, 229
 membrane gel structure, 229
 microfiltration (MF) membrane, 229
 nanofiltration (NF) membranes, 230
 osmosis, semipermeable materials, 228
 pore size regulation, 229
 pressure dialysis, 229
 reverse osmosis (RO) membranes, 229
 synthetic membrane, 229
 ultrafiltration membrane, 229
 concentrate, 243
 crossflow filtration, 230
 flux rate, 232
 membrane bioreactor (MBR) technology, 235–236
 membrane element configurations
 capillary (hollow) fiber, 233–234
 packing density, 234
 plate and frame, 233
 spiral wound, 234
 tubular, 233
 membrane fouling, 234–235
 membrane processing system design, 236–238
 microfiltration (MF), 230
 nanofiltration (NF), 231, 232
 properties and features, 232
 reverse osmosis (RO), 231–232
 system performance, 234–235
 testing
 applications testing, 241–243
 applied pressure, 239
 cell test, 240–241
 design factors, 238
 feed water chemistry, 238–239
 flow conditions, 240
 membrane area, 239
 membrane element array, 240
 membrane element configuration, 239
 membrane polymer, 239
 pilot testing, 243
 pretreatment requirement, 240
 recovery, 239–240
 temperature, 239
 ultrafiltration (UF), 230–231
 water contaminant, 228
Methylenebisthiocyanate (MBT), 398
2-Methyl-4-isothiazolin-3-one (MIT), 397
Microbial analysis, 260
Microbiologically induced corrosion (MIC), 118
Microgalvanic corrosion, 322
Mineral scales and deposits, *see* Fouling; Scaling; Water
Minimum inhibition concentration (MIC), 140
Molecular weight cutoff (MWCO), 230, 244

Monitoring system

- biofouling tube tracking device, 126
 - biomonitoring methods, 123–124, 125
 - chemical tests, 124–125
 - continuous performance monitoring, 124
 - corrosion-monitoring techniques, 125
 - DAT and MonitAll units, 125
 - flow meters, 125
- MSF, *see* Multistage-flash distillation process
- Multimedia filters, *see* Depth filters
- Multiple-effect distillation process, 273, 274
- Multistage-flash distillation process, 273, 275, 276

N

- Nano-filtration membranes, 134; *see also* Membrane technology
- Natural organic matter (NOM), 344
- Natural polymers
- cationic polymers
 - cationic starch, 468–469
 - chitosan, 469
 - deposit control polymers, 448–449
- Neutralizing amine, 314–315
- Nitrilotrimethylene phosphonic acid (NTMP), 30
- N, N*-diethyl-*p*-phenylenediamine (DPD) analysis, 483
- N, N*-diethyl-*p*-phenylenediamine (DPD)/glycine method, 488
- Nonoxidizing biocides
- aldehydes and dithiocarbamates, 396
 - application areas, 395
 - efficacy properties, 395
 - isothiazolones and quaternary compounds, 397
 - limitations, 394
 - organobromines, 396–397
 - vs.* oxidizing biocides, 394
 - physical and chemical properties, 396
- Nucleation inhibitor index, 52

O

- Octadecylamine (ODA), 315–316
- Oilfield scale control
- brine mixing, ion exchange, and scale precipitation, 136–137
 - environmentally acceptable inhibitors, 132–133
 - hydrate inhibitor impact
 - barite nucleation, 138–139
 - barite solubilities, 137–138
 - halite solubilities, 138, 139
 - model, 138–139
 - in salt solutions, 137–138
 - scale inhibitor efficiency, 140
- inhibitor interactions and reactions, rock substrates
- adsorption/precipitation mechanism, 146–147
 - calcite and NTMP reactions, 147–148
 - carbonate rocks–DETPMP inhibitor interactions, 148
 - inhibitor/core material reactions, 147
 - surface poisoning, 147–148
- low dosage hydrate inhibitors (LDHIs), 137
- mineral scales, 129
- nonaqueous inhibitor solutions, squeeze treatment, 131–132

- oil and gas production, 148–149
- polymeric scale inhibitor, 133
- scale formation, precipitation, and deposition
- barite kinetics, 143
 - RDC technique, 141–142
 - SXRD technique, 142–143
- scale inhibition
- diethylenetriaminepenta (methylenephosphonic acid) (DETPMP), 144–145
 - phosphinopolycarboxylic acid (PPCA), 143–144
 - polyvinylsulfonic acid (PVS), 145–146
- sulfate removal, injection seawater
- barium sulfate scales, 133–134
 - Ba²⁺ *vs.* SO₄²⁻ concentration, 135, 136
 - cost-effectiveness, 135–136
 - desulfation, barium concentration, 135
 - nano-filtration membranes, 134
 - reverse osmotic process, 134
 - thermodynamic hydrate inhibitors (THIs), 137–138
 - viscosified fluids, chemical placement, 130–131
- Once-through cooling water systems, 327
- On-line amperometric sensor
- chlorine flow rate, 486
 - free chlorine dissociation curve, 485
 - temperature change, 486
- Open recirculation systems, 327–328
- Optical microscopy
- calcium carbonate, 427
 - iron oxide, 428
- Organic corrosion inhibitors, 329–330
- Organophosphonate, 87
- Orthophosphate–steel corrosion inhibitor, 329
- Oxidation–reduction potential (ORP), 489–491
- Oxidizing biocides
- bromine-based biocides, 389–391
 - chlorine-based biocides, 386–389
 - chlorine dioxide, 391–393
 - disadvantages, 385
 - gas systems, 385–386
 - hydrogen peroxide, 393
 - liquid and solid systems, 386
 - ozone, 394
 - peracetic acid, 393–394
- Oxygen scavengers
- operating procedure, 308–309
 - properties, 310
- Oxygen solubility chart, 307
- Ozone, 394
- Ozone disinfection monitoring, 488–489

P

- PAA, *see* Peracetic acid
- Packing density, 234
- Particle size analysis (PS), 435, 436
- Parting corrosion, *see* Dealloying
- Passivating corrosion inhibitors, 329
- 1,5-Pentanediol, *see* Glutaraldehyde
- Peracetic acid, 393–394
- Percent supersaturation (PS), 275
- Permeate, 245
- pH control method, 286, 497–498
- pH-modification method
- acid treatment, 166

- brine pH vs. flash temperature, 164
 - dosing curve, 167
 - dual-flash brine, 168
 - single-flash brine, 167
 - Phosphate-containing scales
 - inorganic orthophosphates and polyphosphates, 223
 - MAP formation, 206
 - phosphorus concentrations, wastewater, 205
 - solubility isotherms, 207
 - struvite scale
 - chemical composition, 208
 - inhibitors, 218–223
 - magnesium source, 209–214
 - $\text{MgCl}_2 \cdot 6\text{H}_2\text{O}$ vs. $\text{MgSO}_4 \cdot 7\text{H}_2\text{O}$, 214–215
 - morphology, 215, 217–218
 - precipitation kinetics, pH stat method, 207–208
 - spontaneous precipitation, 207
 - supersaturation ratio, 209
 - thermodynamics, 206–207
 - thermodynamic solubility products, 207
 - Phosphate inhibitor, mild steel corrosion, 117–118
 - Phosphinopolycarboxylic acid (PPCA) inhibitor
 - calcium carbonate scale inhibition, 143–144
 - surface and bulk scaling, 146
 - Phosphonates; *see also* Calcium–phosphonate inhibitor
 - CWT programs, 87
 - types, 87
 - Pitting corrosion, 117–118, 322, 323
 - Pitzer theory, 139
 - Poly(dimethylamine-co-epichlorohydrin), 472
 - Polyacrylamides, 472
 - Polyadsorption
 - collisions, 345–346
 - conformation
 - complexation, coiling index, 347–348
 - concentration and pH, 347
 - schematic representation, 346
 - dependent factors, 345
 - mean field lattice model, 353
 - Polyadsorption model, *see* Mean field lattice model
 - Polyamines, 472
 - Polyaspartates, 133
 - Poly-D-glucosamine, *see* Chitosan
 - Poly diallyldimethylammonium chloride (DADMAC), 471
 - Polyelectrolyte–particulate matter interactions
 - adsorption, 345–348
 - characteristics
 - floculants, 344–345
 - NOM and suspended particulate matter, 344
 - flocculation, 348–352
 - mathematical modeling
 - flocculation, 354–359
 - interaction forces, 353–354
 - polymer adsorption, 353
 - Polyelectrolytes, 88; *see also* Cationic polymers
 - Polyethyleneimines (PEI), 470–471
 - Polymer conformation
 - adsorption
 - complexation, coiling index, 347–348
 - concentration and pH, 347
 - schematic representation, 346
 - flocculation
 - collision volume, mechanisms, 349
 - complexation, supernatant turbidity, 350–351
 - pH and ionic strength, 349–350
 - Polymeric calcium phosphonate inhibitor, *see* Calcium–phosphonate inhibitor
 - Polymer-induced flocculation
 - collision volume, 349
 - conformation, 349–351
 - cooling and boiler applications, 351
 - fractal aggregates, 348–349
 - molecular weight, 352
 - population balance model (PBM)
 - aggregation rate, 356
 - collision efficiency factor, 357
 - fluid flow, shear rate, 359
 - framework, 355
 - mechanisms, 357–358
 - particle number concentration, 356
 - surface coverage vs. mean floc diameter, 358, 359
 - steps, 345
 - surfactants, 351
 - thermal and irradiation degradation, 351–352
 - Polymer–polymer inhibitor interaction
 - anionic-cationic polymer interaction, 89
 - polyelectrolytes, 88
 - water chemistry, 89
 - Poly[oxyethylene(dimethyliminio)ethylene-(dimethyliminio) ethylene dichloride], 397
 - Polyphosphonocarboxylic acid (PPCA)
 - calcium carbonate, 67
 - crystal morphology, 68–70
 - kinetics, 67–68
 - surface deposit, 68, 69
 - synchrotron radiation (WAXS), 75–76
 - XRD analysis, 69, 71, 74
 - oilfield scale inhibitors, 144–145
 - Polyvinylamine (PVA), 470
 - Polyvinylsulfonic acid (PVS) inhibitor, 145–146
 - Population balance model (PBM)
 - aggregation rate, 356
 - collision efficiency factor, 357
 - framework, 355
 - mechanisms, 357–358
 - particle number concentration, 356
 - shear rate, 359
 - surface coverage vs. mean floc diameter, 358, 359
 - PPCA, *see* Phosphinopolycarboxylic acid (PPCA) inhibitor
 - Precipitating/cathodic inhibitors, *see* Barrier film corrosion inhibitors
 - Precipitation polymerization, deposit
 - control polymers, 450
 - Pressure dye test, 259
 - Probe-type amperometric systems, 484
 - Proportional flow control method, 286
 - Protonophores, 400
 - PVS, *see* Polyvinylsulfonic acid (PVS) inhibitor
- ## R
- Recovery, 236–237, 239, 245
 - Reverse osmosis (RO) membrane fouling
 - biofouling
 - biofilm formation, 366
 - boiler system, 305–306
 - flux decline data, sand filter, 375

- molecular dynamics simulation, alginate
 - oligomer, 375
 - permeability, 374–375
 - concentration polarization, 252–253
 - control
 - chemical pretreatment, 263–264
 - low-fouling membranes, 261
 - mechanical pretreatment, 261–263
 - membrane cleaning, 264–265
 - membrane flux, 261
 - RO system recovery, 260
 - temperature, 260
 - velocity, 261
 - water analysis, 260
 - data normalization, 266–267
 - demineralization technique, 248
 - feed water quality guidelines
 - flow rate, membrane module, 253
 - fouling, 249
 - recommended flux, 253
 - scaling, 254, 256
 - foulants, 248
 - colloids, 249–250
 - elemental metals, 250
 - hydrogen sulfide, 251
 - organics, 250
 - high-efficiency filter system (HEF)
 - cross section, 268–269
 - electrodialysis reversal (EDR) membrane, 267–268
 - multimedia filters (MMF), 268
 - pilot test, 269
 - hybrid membrane systems, 266
 - identification
 - membrane operations, 257–260
 - water quality, 256–257
 - mechanical and chemical pretreatment techniques, 248, 249
 - membrane degradation, 255–256
 - membrane scales, 248
 - calcium carbonate, 254
 - performance, 255
 - precipitation, 254
 - silica, 254–255
 - sulfate-based scales, 254
 - occurrence, 248–249
 - performance problems, 251–252
 - proper monitoring and analysis, 269
 - Reverse osmosis system, 183
 - Reverse osmotic process, 134
 - RO, *see* Reverse osmosis (RO) membrane fouling
 - Rotating disk crystallizer (RDC) technique, 141–142, 144
 - Rotating disk electrode (RDE), *see* Rotating disk crystallizer (RDC) technique
- S**
- Sand filtration, 300
 - Saturated solution, 275
 - Scale control inhibitors, 51–52, 63
 - boiler system
 - chelant approach, 311–312
 - chemical feed points, 316
 - condensate, 313–316
 - dispersants, 312–313
 - phosphate precipitating approach, 310–311
 - calcium carbonate polymorphs, 63
 - thermal desalination systems
 - additives, classification, 292
 - antiscalants, 292–293
 - green additive, PMA, 293–294
 - silica inhibition, 293
 - sodium-hexa-metaphosphate (SHMP), 291
 - Scale control survey, thermal desalination system
 - consultants, 290
 - plant operators, 291
 - plant suppliers, 290
 - Scale identifying techniques
 - advantages and disadvantages, 426
 - applications
 - coacervate formation, 442–443
 - metal-inhibitor salt formation, 441–442
 - thermal treatment, deposit control polymers, 443–445
 - EDS analysis, 430–431
 - inductively coupled plasma (ICP), 435
 - infrared (IR) spectroscopy
 - ATR-IR spectroscopy, 439–441
 - transmission spectroscopy, 437–438
 - optical microscopy, 427–428
 - particle size analysis, 435
 - scanning electron microscope (SEM), 428–430
 - wide angle x-ray diffraction, 432–435
 - X-ray photoelectron spectroscopy, 436
 - Scale squeeze treatment
 - barium ion concentrations, 137
 - downhole, 133
 - nonaqueous scale inhibitors, 131–132
 - polymeric scale inhibitor, 133
 - Xanthan viscosified scale inhibitor, 131
 - Scaling; *see also* Fouling
 - boiler scale deposits, 10
 - calcium carbonate deposits, 11
 - calcium fluorides, 14
 - calcium oxalates, 14
 - calcium phosphate scale deposits, 13–14
 - definition, 22
 - hard scale, 22
 - iron-based scales, 16
 - metal sulfate scale deposits, 11–13
 - periodic descaling, 23
 - silica/metal silicates, 14–15
 - Scaling index, 280–281
 - Scanning electron microscope (SEM)
 - BSE mode, small particles, 430
 - calcium carbonate polymorphs, 428
 - calcium oxalate mono and dihydrates, 429
 - Selective leaching, *see* Dealloying
 - Self-consistent mean field lattice model, 353
 - Shear-thinning fluids, 130
 - Siderite, 16
 - Silica analyzer, 492
 - Silica and magnesium silicate foulants; *see also*
 - Geothermal silica scale
 - aluminum silicate scale
 - amorphous aluminosilicate, 194
 - biological systems, 199
 - control, brine pH adjustment, 196

- formation, 194
 - three-dimensional structures, 194
 - amorphous silica formation and growth
 - bulk precipitation, 182
 - in living organisms, 182
 - pH level, 180, 181
 - polymerization, 180–181
 - silica precipitation, 182
 - solubility characteristics, 180, 181
 - surface deposition, 182
 - calcium silicate scale
 - biological systems, 198
 - formation, 195
 - inhibition and dispersion, 183
 - iron silicate scale
 - biological system, 198
 - formation, 192–194
 - magnesium silicate
 - composition, 188–189
 - EDTA effect, 196–197
 - formation mechanism, 191
 - FT-IR spectrum, 190
 - heat exchanger, 189–190
 - inverse solubility, 191
 - magnesium hydroxide influence, 191, 195
 - pH effect, 191–193
 - practical scale control guidelines, 197–198
 - precipitation, 190–191
 - Na⁺ and K⁺ effects, 195
 - organic and inorganic foulants, 179–180
 - pH effect, 199
 - polymeric additives
 - cationic polymer-induced flocculation, 187
 - detrimental effects, inhibitory activity, 186–187
 - reverse osmosis system, 183
 - schematic structures, 183–185
 - silicate polymerization, 187
 - silicic acid stabilization, 183, 186
 - zwitterionic and cationic polymers, 183, 187
 - scale inhibition mechanism, 188
 - silica scale control, 182
 - Silica scale control, *see* Geothermal silica scale; Silica and magnesium silicate foulants
 - Silt density index (SDI), 249–250
 - Sodium analyzer, 492–493
 - Sodium chlorate methods, 393
 - Sodium dichloroisocyanurate, 389
 - Sodium-hexa-metaphosphate (SHMP), 291
 - Sodium hypochlorite, 388
 - Sodium softeners, 262–263
 - Sodium trichloroisocyanuric acid, 389
 - Solubility scale prediction method, 281–284
 - Solution polymerization, deposit control polymers, 450
 - Squeeze treatment, *see* Scale squeeze treatment
 - Stability index (SI), 280
 - Step edge adsorption, 28–29
 - Step pinning, 27
 - Stiff–Davis stability index, 281
 - Stress corrosion cracking (SCC), 118, 325–327
 - Stress-tolerant polymer (STP)
 - efficacy, 116, 117
 - performance, 115–116
 - Struvite scale
 - chemical composition, 208
 - induction time vs. Mg²⁺ concentration
 - MgCl₂·6H₂O, 213, 214
 - MgSO₄·7H₂O, 211
 - induction time vs. supersaturation
 - MgCl₂·6H₂O, 212–213
 - MgSO₄·7H₂O, 209–211
 - initial precipitation rates vs. relative supersaturation
 - MgCl₂·6H₂O, 213–214
 - MgSO₄·7H₂O, 212
 - kinetics, pH stat method, 207–208
 - MgCl₂·6H₂O vs. MgSO₄·7H₂O
 - nucleation process, 214–215
 - precipitation kinetics, 215, 216
 - precipitation reactions, 214
 - scanning electron micrographs, 215, 217–218
 - x-ray powder diffraction patterns, 215, 216
 - organic soluble compound inhibitors
 - chemical structure, 218, 219
 - concentration and struvite precipitation, 220–221
 - induction time and initial precipitation rate, 218–220
 - Langmuir-type adsorption model, 223
 - relative inhibition, 221–222
 - supersaturation, 220, 221
 - spontaneous precipitation, 207
 - stability diagrams
 - MgCl₂·6H₂O, 212, 213
 - MgSO₄·7H₂O, 209, 210
 - supersaturation ratio, 209
 - Sulfate-reducing bacteria (SRB), 118, 119
 - Superheat-and-flush disinfection methods, 416–417
 - Supernatant turbidity, 350–351
 - Supersolubility, 279
 - Surface poisoning effects, 147–148
 - Suspended particulate matter, 344
 - Suspension polymerization, deposit control polymers, 450
 - Synchrotron XRD (SXRD) technique, 142–144
 - Synthetic polymers
 - cationic polymers
 - manufacture methods, 472–475
 - polyacrylamides, 472
 - polyamines, 472
 - polydiallyldimethylammonium chloride, 471
 - polyethyleneimines (PEI), 470–471
 - polyvinylamine (PVA), 470
 - deposit control polymers
 - polymerization methods, 449–450
 - polymerization processes, 450
 - types, 449
- ## T
- Tangential flow filtration (TFF), 245
 - Tetrakis-hydroxymethyl-phosphonium sulfate (THPS), 397
 - Thermal desalination systemic scale control
 - absolute and percent supersaturation, 275
 - inhibitors
 - additives, classification, 292
 - antiscalants, 292–293
 - green additive, PMA, 293–294
 - silica inhibition, 293
 - sodium-hexa-metaphosphate (SHMP), 291
 - maximum supersaturation, 278–279

- methods
 - acid treatment, 285–286
 - additive treatment, 287
 - hybrid treatment, case studies, 287–289
 - multiple-effect distillation process, 273, 274
 - multistage-flash distillation process, 273, 275, 276
 - prediction techniques
 - chemical equilibrium method, 284
 - kinetics and transport phenomena, 284–285
 - scaling index, 280–281
 - solubility, precipitation, 278
 - solubility product, 277
 - survey, 289–291
 - types, 279
 - Threshold inhibitors, 51
 - Tolyltriazole (TTA) inhibitor, 117, 330
 - Total organic carbon (TOC) analysis
 - high temperature oxidation technique, 495
 - test analyzer, 495–496
 - UV persulfate oxidation technique, 494–495
 - Traditional pH electrode system, 497
 - Transmembrane pressure (TMP), 245
 - Trichlor, *see* Sodium trichloroisocyanuric acid
 - True color, 250
 - Turbidity monitoring, 500–501
- U**
- Unactivated sodium chlorite, 393
 - Underdeposit corrosion, 332–333
 - Unsaturated solution, 275
 - Urea-hydrochloric acid, 173
 - Urea-sulfuric acid, 173
 - Urolithiasis, 33
 - UV persulfate oxidation technique, 494–495
- V**
- Van der Waals attraction force, 354
 - Viscosified self-diverting treatment, 130–131
- W**
- Water
- characteristics
 - aluminum, 6
 - barium, 6
 - bicarbonate, 8
 - calcium, 7
 - carbonate, 8
 - carbon dioxide, 9
 - chloride, 8
 - chromium, 7
 - color, 5
 - copper, 7
 - detergency, 5
 - fluoride, 8
 - hydrogen sulfide, 9
 - iron, 7
 - magnesium, 7
 - manganese, 7
 - odor, 5
 - organic chemicals, 9
 - oxygen, 9
 - potassium, 7
 - selenium, 8
 - silica, 7–8
 - sodium, 7
 - strontium, 8
 - sulfate, 8
 - temperature, 5
 - turbidity, 5–6
 - zinc, 8
 - feed water
 - analysis, 9–10
 - classification, 6
 - quality, industrial application, 18
 - resources
 - ground water, 4
 - lake water, 4
 - seawater, 3–4
 - surface water, 4
 - reverse osmosis (RO), 2
 - universal solvent, 2
 - water cycle, 2–3
- Water safety plan (WSP), 415–416
- Water softener cycle, 302
- Water-soluble inhibitors, 51, 56
- Water treatment chemicals monitoring
- cooling tower
 - alkalinity, 498–499
 - biochemical oxygen demand (BOD), 494
 - chemical oxygen demand (COD), 493–494
 - conductivity, total dissolved solids, 499–500
 - pH, 496–498
 - total organic carbon (TOC), 494
 - turbidity, 500–501
 - corrosion, 502–503
 - CWT and BWT parameters
 - hardness, 493
 - silica and dissolved oxygen, 492
 - sodium, 492–493
 - disinfection
 - bromine, 489
 - chlorine, 483–486
 - chlorine dioxide (ClO₂), 486–488
 - ozone, 488–489
 - parameters and applications, 483
 - oxidation–reduction potential (ORP), 489–491
- Wide angle x-ray diffraction (WAXD)
- calcium carbonate polymorphs, 433
 - calcium sulfate and silica, 432
 - mass absorption coefficient, 434
 - phase composition, 435
- X**
- Xanthan viscosified scale inhibitor, 131
 - X-ray photoelectron spectroscopy (XPS), 436
 - X-ray sedimentation technique, 435

THE SCIENCE AND TECHNOLOGY OF INDUSTRIAL WATER TREATMENT

Mineral scale deposits, corrosion, suspended matter, and microbiological growth are factors that must be controlled in industrial water systems. Research on understanding the mechanisms of these problems has attracted considerable attention in the past three decades as has progress concerning water treatment additives to ameliorate these concerns. **The Science and Technology of Industrial Water Treatment** provides a comprehensive discussion on the topic from specialists in industry and academia.

Topics discussed include:

- The basics of water chemistry
- The characteristics, formation, and control of common mineral scales
- Membrane-based separation processes
- Reverse osmosis systems and scale control in thermal distillation processes
- Corrosion control in cooling, boiler, geothermal, and desalination systems
- The interactions of polyelectrolytes with suspended matter
- Bacterial species commonly encountered in water supplies, including *Legionella*
- Analytical techniques for identifying mineral scales and deposits
- Polymers for treating industrial and wastewater systems
- Monitoring operational parameters and chemicals in water treatment

A valuable addition to the library of academic researchers, this volume will also prove useful to those working not only in the water treatment industry, but also to those in petroleum, textiles, pharmaceuticals, and other areas where purity processes are a significant concern.



Co-published by IWA Publishing, Alliance House, 12 Caxton Street, London SW1H 0QS, UK
Tel. +44 (0) 20 7654 5500, Fax +44 (0) 20 7654 5555
publications@iwap.co.uk
www.iwapublishing.com



CRC Press
Taylor & Francis Group
an informa business

www.crcpress.com

6000 Broken Sound Parkway, NW
Suite 300, Boca Raton, FL 33487
270 Madison Avenue
New York, NY 10016
2 Park Square, Milton Park
Abingdon, Oxon OX14 4RN, UK

71440

ISBN: 978-1-4200-7144-3

